

VOLUME 11, 1960

BRITISH JOURNAL OF

Applied Physics

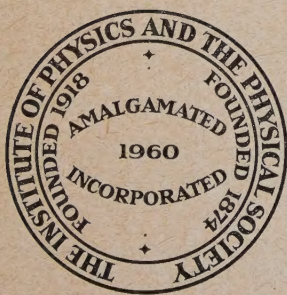
EDITOR: H. R. LANG, A.R.C.S., Ph.D., F.Inst.P.

Secretary of The Institute of Physics

Succeeded on amalgamation by

A. C. STICKLAND, M.Sc., Ph.D.

*Editor and Deputy Secretary of
The Institute of Physics and the Physical Society*



THE INSTITUTE OF PHYSICS AND
THE PHYSICAL SOCIETY
LONDON

THE INSTITUTE OF PHYSICS AND THE PHYSICAL SOCIETY

OFFICERS AND MEMBERS OF THE COUNCIL, 1960-61

PRESIDENT	Sir John Cockcroft, O.M., K.C.B., C.B.E., D.Sc., F.Inst.P., F.R.S.
IMMEDIATE PAST-PRESIDENTS OF THE INSTITUTE AND OF THE SOCIETY	Sir George Thomson, M.A., LL.D., Sc.D., Hon.F.Inst.P., F.R.S. J. A. Ratcliffe, C.B.E., M.A., F.R.S.
VICE-PRESIDENTS	Prof. R. W. Ditchburn, M.A., B.Sc., Ph.D., F.Inst.P. A. J. Philpot, C.B.E., M.A., B.Sc., F.Inst.P. W. H. Taylor, M.A., D.Sc., F.Inst.P. J. Topping, M.Sc., Ph.D., F.Inst.P.
HONORARY TREASURER	J. Taylor, M.B.E., D.Sc., F.R.I.C., F.Inst.P.
HONORARY SECRETARY	C. G. Wynne, B.A., Ph.D., F.Inst.P.
ORDINARY MEMBERS OF COUNCIL	Prof. C. C. Butler, B.Sc., Ph.D., A.Inst.P. E. R. Davies, O.B.E., B.Sc., F.Inst.P. Prof. B. H. Flowers, M.A., D.Sc. J. M. A. Lenihan, M.Sc., Ph.D., A.M.I.E.E., F.Inst.P. G. R. Noakes, M.A., F.Inst.P. Prof. C. F. Powell, M.A., Sc.D., F.R.S. F. A. Vick, O.B.E., Ph.D., A.M.I.E.E., F.Inst.P. Prof. D. A. Wright, D.Sc., F.R.A.S., F.Inst.P.
REPRESENTING BRANCHES	M. R. Hopkins, M.Sc., Ph.D., F.Inst.P. Prof. H. Lipson, M.A., D.Sc., F.Inst.P., F.R.S.

EXECUTIVE OFFICERS

SECRETARY	H. R. Lang, B.Sc., Ph.D., A.R.C.S., F.Inst.P.
EDITOR AND DEPUTY SECRETARY	Miss A. C. Stickland, M.Sc., Ph.D.
DEPUTY SECRETARY	N. Clarke, B.Sc., F.Inst.P.

British Journal of Applied Physics

SUB-COMMITTEE

J. M. A. Lenihan, M.Sc., Ph.D., A.M.I.E.E., F.Inst.P. (*Chairman*)
 Prof. R. W. Ditchburn, M.A., B.Sc., Ph.D., F.Inst.P. (*Ex-officio member*)
 W. Hirst, B.Sc., Ph.D., F.Inst.P.
 C. A. Hogarth, B.Sc., Ph.D., F.Inst.P.
 J. W. Menter, M.A., Ph.D., F.Inst.P.
 A. C. G. Menzies, M.A., D.Sc., F.Inst.P.
 Prof. D. A. Wright, D.Sc., F.R.A.S., F.Inst.P.

INDEX TO VOLUME 11

SUBJECTS

(SA) denotes special article, (CR) conference report, (C) correspondence, and (NC) notes and comments.

- Aberration, Fifth order spherical, of magnetic lenses 521
 Aberrations, instrumental, on the Schultz technique for the measurement of pole figures, Influence of 96
 Absorption coefficient, effective X-ray, of heterogeneous slabs, Variation with particle size of the 43
Abstracts, Instrument 136 (NC)
 Accelerator, linear, Stroboscopic radiography with a 132
 Adhesion of zinc sulphide films to glass and silica, Effects of oil vapour contamination on the 382
 Adiabatic demagnetization 449 (CR)
 Aerosols, Deposition of 535
 Air
 bubbles in water containing a small dissolved air content, Change of size of 38
 content, Change of size of air bubbles in water containing a small dissolved 38
 content of water, low dissolved-, New technique for measurement of 228
 Airborne dust samples from British coalmines, Size distribution of 1
 Alkaline-earth oxides, Evaporation and diffusion rate measurements on cathodes of sintered nickel containing 73
 Alloy steels, High, for use as a thermal conductivity standard 195
 Alloys, columnar crystal, Variation of permanent-magnet properties with crystal orientation in 279
 Alloys, High resistivity nickel-iron, with rectangular hysteresis loops 58
 Alumina, water/, Dielectric properties of (*erratum*) 264
 Aluminium
 mirrors, Annealing silicon monoxide films on 167 (C)
 X-ray K-lines, carbon and, Absolute intensity measurements of the, with a proportional counter 64
 X-ray microbeam study of deformation bands in 162
 Amalgamation of The Institute of Physics and The Physical Society, The 392 (NC)
 Analogue, electrical, Use of an, for the solution of a variety of torsion problems 461
 Analogue networks, Finite-difference 437
 Analysis
 Chemical 525 (CR)
 Isotopic 525 (CR)
 Radioactivation 525 (CR)
 Spectrochemical 525 (CR)
 X-ray, Summarized proceedings of a conference on,—London, November 1959 393 (CR)
 X-ray, Summarized proceedings of a conference on the borders of,—Reading, April 1960 481 (CR)
 Annealing silicon monoxide films on aluminium mirrors 167 (C)
 Annual Report of The Institute of Physics, 1959 447 (NC)
 Anode surface effects in diodes containing oxide-coated cathodes 124
 Apparatus, Scientific Instruments and, Annual Exhibition of 556 (NC)
 Arc initiation, Importance of insulating inclusions in 468
 Arc velocity, enhanced, on magnetic electrodes, Explanation of the 385
 Argon mixtures, helium—, Glow-discharge characteristics of 305 (C)
 A.S.T.M. Powder Data File-5, Comments on the 306 (C)
 Atomic differential scattering cross-sections, Measurement of (*erratum*) 448 (NC)
 Austenitic steel
 Measurement of surface stress in 242
 X-ray stress determination in 523 (C)
Automatic control in Soviet industry 264 (NC)
 Background structure in platinum/carbon shadowing deposits, Study in 506
 Back-reflexion technique, Determination of orientation of bismuth single crystals, using 229
 Bayard-Alpert gauge 433
 Beryllium detectors 525 (CR)
 Beryllium, X-ray microscopy of 498
 Bimetallic brake drum, Temperatures reached in a 445
 Biological applications of electron microscopy 22 (CR)
 Bismuth single crystals, Determination of orientation of, using back-reflexion technique 229
 Bistable element, Thermal propagation of a normal region in a thin superconducting film and its application to a new type of 292
 Bodies in contact 67
 Bombardment, electron, of metal targets, Image formation by 547
Books, New
 Absorption and dispersion of ultrasonic waves 108
 Acta Imeko 1958: Proceedings of the International Measurements Conference, Budapest 24-30 November 1958. 5 Vols. 424
 Adhesives guide 117
 Advanced propulsion systems 413
 Advances in cryogenic engineering. Vol. 5 417
 Advances in electronics and electron physics. Vol. X 235
 Advances in mass spectrometry 232
 Analysts' pocket book 425
 Annual reports on the progress of chemistry. Vol. LV 114
 Applications of finite groups 111
 Atlas of γ -ray spectra from radiative capture of thermal neutrons 238
 Atomic radiation and polymers 421
 Basic data of plasma physics 418
 Beam and wave electronics in microwave tubes 418
 Beryllium 415
 Bibliography of the stable isotopes of oxygen (^{17}O and ^{18}O) 114
 Chemical engineering practice. Vol. 11. *Works, design, etc.* 425
 Circuit theory of linear noisy networks 110
 Classification and indexing in science. 1st edn. 236
 Classification and indexing in science. 2nd edn. 425
 Control system components 111
 Course of theoretical physics. Vol. 7. *Theory of elasticity* 112
 Crystal chemistry of simple compounds of uranium, thorium, plutonium, neptunium 427
 Deformation, strain and flow: An elementary introduction to rheology 413
 Dendritic crystallization 118
 Der Raman-Effekt 239
 Der Transistor 418
 Directory of nuclear reactors. Vol. 1. *Power reactors* 115
 Directory of nuclear reactors. Vol. II. *Research, test and experimental reactors* 421
 Dynamische Vorgänge in lineären Systemen der Nachrichten- und Regelungstechnik 112
 Einführung in die Physik der Leiterwerkstoffe 415
 Electrical impedance plethysmography 418
 Electrical noise: Fundamentals and physical mechanism 419
 Electronic flash photography 424
 Elektronenmikroskopische Untersuchungs- und Präparationsmethoden 239

Books, New—continued

- Encyclopedia of physics.* Vol. VIII/1. *Fluid dynamics.* 1 427
- Encyclopaedia of physics.* Vol. XXXVIII/2. *Neutrons and related gamma ray problems* 115
- Evaporation and droplet growth in gaseous media* 425
- Experimental techniques in low-temperature physics* 108
- Exploding wires* 232
- Flames: Their structure, radiation and temperature* 417
- Formation and trapping of free radicals* 417
- Fracture* 232
- Friction in textiles* 425
- Gas chromatography abstracts* 1958 426
- Glossaria interpretum: Nuclear physics and atomic energy. Terms of nuclear physics and nuclear technology in English, French, German and Russian* 421
- Glossary of atomic terms* 422
- Grundlagen der Selbsttätigen Regelung* 240
- Grundlagen der Selbsttätigen Regelung. Band II. Einige Probleme aus der Theorie der nichtlinearen Regelungssysteme* 112
- Guide de thermométrie: Méthodes—réalisations des mesures* 417
- Handbook of chemical microscopy.* Vol. 1 117
- Handbuch der Kältetechnik.* Vol. III 417
- Handbuch der Kältetechnik. Band 7. Sorptions-Kältemaschinen* 109
- High-speed aerodynamics and jet propulsion.* Vol. 5. *Turbulent flows and heat transfer* 414
- Hypersonic flow* 414
- Instationäre Wärmespannungen* 109
- International conference on high-energy accelerators and instrumentation—CERN 1959* 238
- International directory of radio-isotopes.* Vol. 1. *Unprocessed and processed radio-isotope preparations and special radiation sources* 422
- Introduction to the theory of quantized fields* 240
- Ionization phenomena in gases.* Vols. 1 and 2 419
- Lectures on Fourier integrals. Annals of mathematics studies No. 42* 428
- Magnetodynamics of conducting fluids, The* 236
- Manual of mathematical physics* 240
- Many body problem, The* 419
- Masers. Microwave amplification and oscillation by stimulated emission* 236
- Mechanical design of laboratory apparatus* 236
- Metallurgy of the rarer metals. No. 6. Tantalum and niobium* 232
- Méthodes générales d'essai et de contrôle en laboratoire. Vol. 1. Mesures géométriques et mécaniques* 233
- Methods of experimental physics. Vol. 1. Classical methods* 117
- Methods of experimental physics. Vol. 6. Solid state physics. Part A* 426
- Millimicrosecond pulse techniques* 419
- Moisture in textiles* 426
- New method in the theory of superconductivity, A* 110
- Non-homogeneity in elasticity and plasticity* 233
- Non-linear wave mechanics* 428
- Non-Newtonian fluids* 414
- Nuclear engineering monographs, No. 7. Nuclear reactor materials* 422
- Nuclear engineering monographs, No. 5. Nuclear reactor control and instrumentation.* 115
- Nuclear engineering monographs, No. 4. Nuclear reactor shielding.* 115
- Nuclear engineering monographs, No. 6. Steam cycles for nuclear power plant.* 116
- Optics of thin films* 420
- Organisation et fonctionnement des machines arithmétiques* 428
- Penetration of charged particles in matter. (Nuclear Science Series No. 29)* 423

Books, New—continued

- Photomicrography* 239
- Physical chemistry of steel making, The* 114
- Physical methods of investigating textiles* 233
- Physikalische Kernchemie* 423
- Physicochemical measurements at high temperatures* 234
- Plansee proceedings 1958: High melting metals* 233
- Plasma physics and the problem of controlled thermonuclear reactions. Vol. 3* 116
- Principles of radiation dosimetry* 116
- Problems of low temperature physics and thermodynamics* 235
- Problems of metallography and the physics of metals* 416
- Proceedings of the fifth annual computer application symposium* 241
- Proceedings of the first national biophysics conference* 233
- Proceedings of the fourth national conference on tube techniques* 110
- Proceedings of the international conference on nuclear physics. Low energy nuclear interactions and nuclear structure, Paris, 1958* 116
- Proceedings of an international symposium on the theory of switching. Parts I and II* 236
- Proceedings of the third national congress of applied mechanics* 112
- Progress in cryogenics. Vol. 1* 109
- Progress in cryogenics. Vol. 2* 418
- Progress in dielectrics. Vol. 2* 420
- Progress in metal physics* 7 114
- Progress in non-destructive testing. Vol. 2* 416
- Progress in nuclear energy. Series XI. Plasma physics and thermonuclear research. Vol. 1* 423
- Progress in solid mechanics. Vol. 1* 414
- Progress in vacuum science and technology* 114
- Property measurements at high temperatures* 235
- Quantum chemistry integrals and tables* 117
- Radiation biology* 234
- Radiation hygiene handbook* 423
- Radio stations: installation, design and practice* 237
- Radioisotopes for industry* 116
- Recent research in molecular beams: A collection of papers dedicated to Otto Stern on the occasion of his 70th birthday* 114
- Reciprocals of the integers from 1000 to 9999* 428
- Regression analysis* 428
- Rheology. Theory and applications. Vol. III* 415
- Robertson guide to world screw thread standards, The* 237
- Rocket propulsion* 237
- Sampling inspection tables. Single and double sampling* 113
- Scattering and diffraction of waves, The* 420
- Scientific Russian* 237
- Solid state magnetic and dielectric devices* 110
- Solid state physics. Advances in research and application. Vol. 9* 427
- Solid state physics. Advances in research and applications. Vol. 10* 427
- Solid state physics in electronics and telecommunications. Vol. I. Semiconductors. Part 1* 427
- Statistical methods in radio wave propagation* 241
- Structural damping* 426
- Structure and properties of thin films* 420
- Structure reports for 1952. Vol. 16* 416
- Studies in crystal physics* 237
- Supplement to "Helium", A* 108
- Teaching of mathematics to physicists, The* 108
- Technische Kunstgriffe bei physikalischen Untersuchungen* 118
- Telemetering systems* 421
- Theorie der Stabilität einer Bewegung* 113
- Theory of elementary particles, The* 238
- Theory of storage, The* 241
- Theory of thin shells, The* 429
- Uranium production technology* 424

Books, New—continued

- Vacuum metallurgy* 234
- Vector space and its application in crystal-structure investigation* 118
- Vibration engineering* 241
- Wärme-und Stoffaustausch in Arbeitsdiagrammen auf projektiver Grundlage* 429
- Wave propagation and group velocity* 429
- Werkstoffkunde der Hochvakuumtechnik. Band 1. Metalle und metallischleitende Werkstoffe* 416

- Boron trifluoride, liquid, Viscosity and thermal conductivity of 60
- Brake drum, bimetallic, Temperatures reached in a 445
- Breakdown, Electrical 468
- British Standards Institution, Publications of the 448 (NC)
- Brushless generating magnetometer, a TIM, 448 (NC)
- Bubbles, air, in water containing a small dissolved air content, Change of size of 38

- Cadmium sulphide crystals, Etch pits and dislocations in 296
- Calibration of manganese and gold foils for relative neutron flux measurements 342
- Carbide, cobalt-bonded tungsten, Wear of the hard and soft phases in 517
- Carbon and aluminium X-ray K-lines, Absolute intensity measurements of the, with a proportional counter 64
- Carbon, platinum/, shadowing deposits, Study in background structure in 506

- Cathodes
 - of sintered nickel containing alkaline-earth oxides, Evaporation and diffusion rate measurements on 73
 - oxide-coated, Anode surface effects in diodes containing 124
 - oxide-coated, Charge localization on the surfaces of 223
 - oxide-coated, Emission of negative ions of oxygen during the activation of 430
 - sintered nickel matrix, Some electrical and surface properties of 513

- Cavitation 38
- Ceramics, Q of low-Q piezoelectric, coupling coefficient and, Measurement of 390 (C)

- Charge localization on the surfaces of oxide-coated cathodes 223
- Coalmines, British, Size distribution of airborne dust samples from 1

- Cobalt-bonded tungsten carbide, Wear of the hard and soft phases in 517

- Coefficient, coupling, and Q of low-Q piezoelectric ceramics, Measurement of 390 (C)

- Coke and chemistry, U.S.S.R.* 264 (NC)

- Cold-worked metals, annealed and heavily, Microcracks, and the static and dynamic elastic constants of 81

- Columnar crystal alloys, Variation of permanent-magnet properties with crystal orientation in 279

- Computers, Application of 408

- Conduction current in insulating liquids, Some remarks on the 539

- Conduction, Pre-breakdown, in continuously-pumped vacuum systems 454

- Conductivity
 - standard, thermal, High alloy steels for use as a 195
 - Thermal 60
 - Viscosity and thermal, of liquid boron trifluoride 60

- Conference
 - on applied spectroscopy, Summarized proceedings of a,—Sea-scale, June 1960 525 (CR)
 - on electron microscopy—Exeter, July 1959, Summarized proceedings of a 22 (CR)
 - on irreversibility and statistical mechanics 524 (NC)
 - on solid state physics, Summarized proceedings of a,—Melbourne, August 1959 137 (CR)
 - on some aspects of magnetism, Summarized proceedings of a,—Sheffield, September 1959 307 (CR)

Conference—continued

- on the borders of X-ray analysis, Summarized proceedings of a,—Reading, April 1960 481 (CR)
- on X-ray analysis, Summarized proceedings of a,—Leeds, April 1959 89 (CR)
- on X-ray analysis, Summarized proceedings of a,—London, November 1959 393 (CR)

- Constants, Static and dynamic elastic 522 (C)

- Constants, static and dynamic elastic, of annealed and heavily cold-worked metals, Microcracks, and the 81

- Contact
 - electrification and polarization of nylon threads 202
 - electrification of semiconductors 324

- Hertz theory of, Investigation into one of the assumptions of the 67

Contacts

- Electrical, Symposium on 556 (NC)
- graphite-copper, Thermal transients in 389 (C)

- Contemporary physics* 447 (NC)

- Content, air, Change of size of air bubbles in water containing a small dissolved 38

- Contrast of electron micrographs 486

- Control in Soviet industry, Automatic* 264 (NC)

- Convective heat transfer, Measurement of, by means of the Reynolds analogy 471

- Copper contacts, graphite-, Thermal transients in 389 (C)

- Corrosion 22 (CR)

- Counter, proportional, Absolute intensity measurements of the carbon and aluminium X-ray K-lines with a 64

- Counting, dust, Some statistical aspects of 13

- Counting levels, Thermal precipitator 119

- Creep information centre 136 (NC)

- Creep, Power law for 281

- Critical porosity, Skeleton strength and, in set sulphate plasters 338

- Cross-sections, atomic differential scattering, Measurement of 259 (erratum) 448 (NC)

- Crystal alloys, columnar, Variation of permanent-magnetic properties with crystal orientation in 279

- Crystal orientation in columnar crystal alloys, Variation of permanent-magnet properties with 279

- Crystallinity in drawn polyethylene terephthalate fibres by X-ray diffraction, Measurement of 353 (erratum) 448 (NC)

- Crystallinity in polyethylene terephthalate, Comparison of X-ray and nuclear magnetic resonance measurements of 543

- Crystallographic supplies, Index of* 136 (NC)

Crystals

- bismuth single, Determination of orientation of, using back-reflexion technique 229

- cadmium sulphide, Etch pits and dislocations in 296

- tin single, Determination of the elastic moduli of, and their variation with temperature 254

- Current, Passage of, through the glass envelope of a receiving-type valve 440

- Currents, direct, Sensitive method for measurement of magneto-resistance effect with, and with microwaves 35

- Cycles, duty, Fourier series associated with 103

- Cylinder viscometer, oscillating, for Newtonian liquids, Experimental and theoretical investigations on the 283

- Data File-5, A.S.T.M. Powder, Comments on the 306 (C)

- Deformation bands in aluminium, X-ray microbeam study of 162
- Delay line, Variable ultrasonic water 358

- Delineation 177 (SA)

- Densitometry, photoelectric, Application of, to the assessment of respirable dust samples 371

- Density integrator, Smoke 509

- Deposition of *Lycopodium* spores upon glass slides exposed in a wind tunnel 535

- Deposits, platinum/carbon shadowing, Study in background structure in 506

- Detonation waves in hydrogen-oxygen mixtures, Vibration phenomena in 190
- Devices, thermoelectric, Principles of 209 (SA)
- Dielectric properties of water/alumina (*erratum*) 264
- Differential scattering cross-sections, atomic, Measurement of 259 (*erratum*) 448 (NC)
- Diffracted electrons, Reflexion electron microscopy using 158
- Diffraction, Selected-area, in the electron microscope 504
- Diffraction, X-ray, Measurement of crystallinity in drawn polyethylene terephthalate fibres by 353 (*erratum*) 448 (NC)
- Diffusion, Gaseous, in porous media.
- Part 1—A non-steady state method 314
- Part 2—Dry granular materials 318
- Diffusion rate measurements, Evaporation and, on cathodes of sintered nickel containing alkaline-earth oxides 73
- Diodes containing oxide-coated cathodes, Anode surface effects in 124
- Dioxide rods, solid uranium, Temperatures, thermal stresses and displacements in 33
- Direct currents, Sensitive method for measurement of magneto-resistance effect with, and with microwaves 35
- Discharge tubes of non-circular cross-section, Production of resonance radiation in 492
- Discharges, Electrical, in vacuo 454
- Dislocations, Etch pits and, in cadmium sulphide crystals 296
- Dissolved-air content of water, low, New technique for measurement of 228
- Distribution, Size, of airborne dust samples from British coal-mines 1
- Drawn and undrawn nylon, irradiated, Strength of 277
- Droplet getter-ion pump, titanium, Pumping characteristics of a 401
- Drum, bimetallic brake, Temperature reached in a 445
- Dust
- concentrations, Measurement of, with the thermal precipitator 13
- counting, Some statistical aspects of 13
- samples, airborne, from British coalmines, Size distribution of 1
- samples, respirable, Application of photoelectric densitometry to the assessment of 371
- Duty cycles, Fourier series associated with 103
- Dynamic
- elastic constants, Static and 522 (C)
- elastic constants, static and, of annealed and heavily cold-worked metals, Microcracks, and the 81
- measurement of elasticity using resonance methods 478 (C)
- testing machine, Simple rotary 165
- Earth oxides, alkaline-, Evaporation and diffusion rate measurements on cathodes of sintered nickel containing 73
- Eddy-current tube testing, Choice of frequency for 218
- Eddy impaction 535
- Effective diffraction camera length 504
- Elastic
- constants, Static and dynamic 522 (C)
- constants, static and dynamic, of annealed and heavily cold-worked metals, Microcracks, and the 81
- moduli of tin single crystals, and their variation with temperature, Determination of the 254
- Elasticity using resonance methods, Dynamic measurement of 478 (C)
- Elections to The Institute of Physics 447 (NC), 524 (NC)
- Elections to The Institute of Physics and The Physical Society 555 (NC)
- Electrical
- Contacts, Symposium on 556 (NC)
- breakdown 468
- resistivity of high alloy steels 195
- Electrification, Contact, and polarization of nylon threads 202
- Electrode contamination 547
- Electrodes, magnetic, Explanation of the enhanced arc velocity on 385
- Electrolysis, Valve envelope 440
- Electron
- bombardment of metal targets, Image formation by 547
- diffraction 481 (CR)
- diffraction, Effect of specimen thickness on background intensities in 259
- lenses 521
- lenses, unipotential, Numerical investigation of a range of 408
- micrographs, Contrast of 486
- microscope, Accuracy of selected-area microdiffraction in the 185
- microscope, Selected-area diffraction in the 504
- microscopy, Reflexion, using diffracted electrons 158
- microscopy, Summarized proceedings of a conference on, Exeter, July 1959 22 (CR)
- optics 185
- probe methods of X-ray microanalysis 169 (SA)
- probe techniques 22 (CR)
- stereomicroscopy, Correction of errors in 199
- Electronic Guide, The* 264 (NC)
- Electrons, diffracted, Reflexion electron microscopy using 158
- Element, bistable, Thermal propagation of a normal region in a thin superconducting film and its application to a new type of 292
- Elements, storage, lead film, superconductive, Relaxation times in 78
- Emission, Spectral, of radiation by glass 151
- Envelope, glass, of a receiving-type valve, Passage of current through the 440
- Errors in electron stereomicroscopy, Correction of 199
- Etch pits and dislocations in cadmium sulphide crystals 296
- Evaluating thermal precipitator slides, Inter-observer checks on standards of performance in 119
- Evaluation of thermal precipitator samples 119
- Evaporated films of niobium 304 (C)
- Evaporation and diffusion rate measurements on cathodes of sintered nickel containing alkaline-earth oxides 73
- Exhibition, Annual, of Scientific Instruments and Apparatus 556 (NC)
- Fair Copying Declaration, The Royal Society's 136 (NC), 480 (NC)
- Ferrites, Energy concentration in 69
- Ferromagnetic resonance?, What is 69
- Fibres 543
- Fibres, drawn polyethylene terephthalate, Measurement of crystallinity in, by X-ray diffraction 353 (*erratum*) 448 (NC)
- Figures, pole, Influence of instrumental aberrations on the Schultz technique for the measurement of 96
- Film, lead, superconductive, storage elements, Relaxation times in 78
- Film, thin superconducting, and its application to a new type of bistable element, Thermal propagation of a normal region in a 292
- Films
- adhesion of zinc sulphide, to glass and silica, Effects of oil vapour contamination on the 382
- Annealing silicon monoxide, on aluminium mirrors 167 (C)
- Evaporated, of niobium 304 (C)
- thin, of nickel-iron, Observations of the magnetization reversal process in, using the Kerr magneto-optic effect 335
- Finite-difference analogue networks 437
- Fission events, New technique for the direct investigation of 555 (C)
- Fission-product mixtures, Interpretation of γ -ray scintillation spectra from 346
- Flames in turbulent pre-mixed gas streams, Optical methods for the study of 269
- Flow of lubricating greases in plunger viscometers, Wall effect in the 363

- Fluctuation records and its application to electrical noise, Photo-electric method for the analysis of 377
- Fluorescent X-rays excited by a radioactive source, Measurement of tinplate thickness using 49
- Foils, polycrystalline metal, Determination of preferred orientation in, using a sputtering technique 475
- Fourier series associated with duty cycles 103
- Frequency for eddy-current tube testing, Choice of 218
- Frictional electrification 324
- Fuel elements 33
- γ -ray scintillation spectra from fission-product mixtures, Interpretation of 346
- γ -spectrometry 525 (CR)
- Gas
- discharge 305 (C)
 - Sorption and desorption of, in a hot-cathode ionization gauge 433
 - streams, turbulent pre-mixed, Optical methods for the study of flames in 269
- Gaseous diffusion in porous media
- Part 1—A non-steady state method 314
 - Part 2—Dry granular materials 318
- Gauge, hot-cathode ionization, Sorption and desorption of gas in a 433
- Generating magnetometer, a brushless, TIM 448 (NC)
- Generation 209 (SA)
- Generation of temperatures below 1° K, Summarized proceedings of a symposium on the 449 (CR)
- Generator, compact surge, Design and performance of a 265
- Getter-ion pump, titanium droplet, Pumping characteristics of a 401
- Glass
- and silica, the adhesion of zinc sulphide films to, Effects of oil vapour contamination on 382
 - envelope of a receiving-type valve, Passage of current through the 440
 - Spectral emission of radiation by 151
 - technology; *Physics and chemistry of glasses* 264 (NC)
 - Temperature measurement of 151
- Glow-discharge characteristics of helium-argon mixtures 305 (C)
- Gold foils, manganese and, for relative neutron flux measurements, Calibration of 342
- Grain-oriented silicon-iron, Rotational hysteresis loss in 46
- Granular materials, Dry, Part 2—Gaseous diffusion in porous media 318
- Graphite-copper contacts, Thermal transients in 389 (C)
- Greases, lubricating, in plunger viscometers, Wall effect in the flow of 363
- Gyromagnetic resonance 69
- Half-life of iridium 192 302
- Hardness, Measurement of, at very high temperatures 551
- He³ 449 (CR)
- Heat flow 389 (C), 445
- Heat transfer, convective, Measurement of, by means of the Reynolds analogy 471
- Helium-argon mixtures, Glow-discharge characteristics of 305 (C)
- Hertz theory of contact, Investigation into one of the assumptions of the 67
- Heterogeneous slabs, Variation with particle size of the effective X-ray absorption coefficient of 43
- High alloy steels for use as a thermal conductivity standard 195
- High polymers, Static on 202
- High temperatures, very, Measurement of hardness at 551
- Hot-hardness 551
- Hydrogen-oxygen mixtures, Vibration phenomena in detonation waves in 190
- Hysteresis, Rotational, loss in grain-oriented silicon-iron 46
- Ice 522 (C)
- Image formation by electron bombardment of metal targets 547
- Inclusions, Importance of insulating, in arc initiation 468
- Institute
- of Physics and The Physical Society, Elections to The 555 (NC)
 - of Physics and The Physical Society, The amalgamation of The 392 (NC)
 - of Physics, Annual Report of The, 1959 447 (NC)
 - of Physics, Elections to The 447 (NC), 524 (NC)
- Instrument abstracts* 136 (NC)
- Instrumental aberrations on the Schultz technique for the measurement of pole figures, Influence of 96
- Instruments and Apparatus, Scientific, Annual Exhibition of 556 (NC)
- Insulating inclusions in arc initiation, Importance of 468
- Insulating liquids, Some remarks on the conduction current in 539
- Integrator, Smoke density 509
- Interaction between two equal-sized equal-settling spheres moving through a viscous liquid 87 (C)
- Ion pump, titanium droplet getter-, Pumping characteristics of a 401
- Ionization gauge, hot-cathode, Sorption and desorption of gas in a 433
- Ions of oxygen, negative, Emission of, during the activation of oxide-coated cathodes 430
- Iridium 192, Half-life of 302
- Iron
- alloys, High resistivity nickel-, with rectangular hysteresis loops 58
 - grain-oriented silicon-, Rotational hysteresis loss in 46
 - nickel-, Observations of the magnetization reversal process in thin films of, using the Kerr magneto-optic effect 335
- Irradiated drawn and undrawn nylon, Strength of 277
- Isotope Information Bureau 524 (NC)
- Isotope tracer techniques 525 (CR)
- Junctions, *p-n* and *l-h*, Location of, in semiconductors 177 (SA)
- Kerr magneto-optic effect, Observations of the magnetization reversal process in thin films of nickel-iron, using the 335
- K-lines, carbon and aluminium X-ray, Absolute intensity measurements of the, with a proportional counter 64
- l-h* junctions, *p-n* and, Location of, in semiconductors 177 (SA)
- Laboratory and Workshop Notes*, 1956-58 556 (NC)
- Ladder networks containing non-linear resistances, Solution of 437
- Lamps, Fluorescent 492
- Lattice parameters 498
- Lead film, superconductive, storage elements, Relaxation times in 78
- Lenses, magnetic, Fifth order spherical aberration of 521
- Lenses, unipotential electron, Numerical investigation of a range of 408
- Line, delay, Variable ultrasonic water 358
- Linear accelerator, Stroboscopic radiography with a 132
- Liquid, viscous, Interaction between two equal-sized equal-settling spheres moving through a 87 (C)
- Lorenz function of high alloy steels 195
- Low-angle X-ray scattering when intensity scattered by specimen changes rapidly with time, Method of recording 287
- Low dissolved-air content of water, New technique for measurement of 228
- Low temperatures 449 (CR)
- Low temperatures, Resistance-temperature relationship of platinum at, and its influence on precision thermometry 205
- Lubricating greases in plunger viscometers, Wall effect in the flow of 363

- Luminescence, zinc sulphide, Influence of temperature on the spectral composition of the 289
- Magnet properties, permanent-, with crystal orientation in columnar crystal alloys, Variation of 279
- Magnetic electrodes, Explanation of the enhanced arc velocity on 385
lenses, Fifth order spherical aberration of 521
resonance measurements, X-ray and nuclear, of crystallinity in polyethylene terephthalate, Comparison of 543
- Magnetism, Summarized proceedings of a conference on some aspects of,—Sheffield, September 1959 307 (CR)
- Magnetization reversal process in thin films of nickel-iron, Observations of the, using the Kerr magneto-optic effect 335
- Magnetometer, a brushless generating, TIM 448 (NC)
- Magneto-optic effect, Kerr, Observations of the magnetization reversal process in thin films of nickel-iron, using the 335
- Magneto-resistance effect, Sensitive method for measurement of, with direct currents and with microwaves 35
- Manganese and gold foils for relative neutron flux measurements, Calibration of 342
- Materials, organic, Purification of, by zone refining 128
- Matrix cathodes, Properties of 513
- Matrix cathodes, sintered nickel, Some electrical and surface properties of 513
- Measurement
Dynamic, of elasticity using resonance methods 478 (C)
of atomic differential scattering cross-sections 259 (erratum) 448 (NC)
of convective heat transfer by means of the Reynolds analogy 471
of coupling coefficient and Q of low-Q piezoelectric ceramics 390 (C)
of crystallinity in drawn polyethylene terephthalate fibres by X-ray diffraction 353 (erratum) 448 (NC)
of low dissolved-air content of water, New technique for 228
of magneto-resistance effect with direct currents and with microwaves, Sensitive method for 35
of pole figures, Influence of instrumental aberrations on the Schultz technique for the 96
of surface stress in austenitic steel 242
of tinplate thickness using fluorescent X-rays excited by a radioactive source 49
- Measurements
Absolute intensity, of the carbon and aluminium X-ray K-lines with a proportional counter 64
relative neutron flux, Calibration of manganese and gold foils for 342
X-ray and nuclear magnetic resonance, of crystallinity in polyethylene terephthalate, Comparison of 543
- Mechanics, irreversibility and statistical, Conference on 524 (NC)
- Media, porous, Gaseous diffusion in,
Part 1—A non-steady state method 314
Part 2—Dry granular materials 318
- Metal
foils, polycrystalline, Determination of preferred orientation in, using a sputtering technique 475
physics 22 (CR)
targets, Image formation by electron bombardment of 547
- Metallurgical applications of electron microscopy 22 (CR)
- Metallurgy 229
- Metals, annealed and heavily cold-worked, Microcracks, and the static and dynamic elastic constants of 81
- Meter, Smoke density 509
- Microanalysis, X-ray, Electron probe methods of 169 (SA)
- Microbeam, X-ray, study of deformation bands in aluminium 162
- Microcracks, and the static and dynamic elastic constants of annealed and heavily cold-worked metals 81
- Microdiffraction, selected-area, in the electron microscope, Accuracy of 185
- Micrographs, electron, Contrast of 486
- Microradiography 498
- Microscope, electron, Accuracy of selected-area microdiffraction in the 185
- Microscope, electron, Selected-area diffraction in the 504
- Microscopy, electron, Summarized proceedings of a conference on,—Exeter, July 1959 22 (CR)
- Microscopy, X-ray, of beryllium 498
- Microwaves, Sensitive method for measurement of magneto-resistance effect with direct currents and with 35
- Minerals, Electron microscopy of 22 (CR)
- Mirrors, aluminium, Annealing silicon monoxide films on 167 (C)
- Moduli, elastic, of tin single crystals, and their variation with temperature, Determination of the 254
- Moiré fringes, a geometric demonstration by means of; Analogy between the slow motion of a viscous fluid and the extension and flexure of plates 244
- Monoxide films, Annealing silicon, on aluminium mirrors 167 (C)
- Mössbauer effect 525 (CR)
- Multiplex splitting of arbitrary periodic function 103
- Networks, ladder, containing non-linear resistances, Solution of 437
- Neutron diffraction 481 (CR)
- Neutron flux measurement, relative, Calibration of manganese and gold foils for 342
- Newtonian liquids, Experimental and theoretical investigations on the oscillating cylinder viscometer for 283
- Nickel
cathodes of sintered, containing alkaline-earth oxides, Evaporation and diffusion rate measurements on 73
-iron alloys, High resistivity, with rectangular hysteresis loops 58
-iron, Observations of the magnetization reversal process in thin films of, using the Kerr magneto-optic effect 335
matrix cathodes, sintered, Some electrical and surface properties of 513
- Niobium, Evaporated films of 304 (C)
- Noise, electrical, Photoelectric method for the analysis of fluctuation records and its application to 377
- Noise problems, Recent studies of 53 (CR)
- Nuclear, X-ray and, magnetic resonance measurements of crystallinity in polyethylene terephthalate, Comparison of 543
- Nuclei (Cavitation) 38
- Nylon, irradiated drawn and undrawn, Strength of 277
- Nylon threads, Contact electrification and polarization of 202
- Oil vapour contamination on the adhesion of zinc sulphide films to glass and silica, Effects of 382
- Omegatron 433
- Optical methods for the study of flames in turbulent pre-mixed gas streams 269
- Organic materials, Purification of, by zone refining 128
- Organic skin theory (Air bubbles) 38
- Orientation of bismuth single crystals, Determination of, using back-reflexion technique 229
- Orientation, preferred, Determination of, in polycrystalline metal foils using a sputtering technique 475
- Oriented, grain-, silicon-iron, Rotational hysteresis loss in 46
- Oscillating cylinder viscometer for Newtonian liquids, Experimental and theoretical investigations on the 283
- Oxidation 22 (CR)
- Oxide-coated cathodes
Anode surface effects in diodes containing 124
Charge localization on the surfaces of 223
Emission of negative ions of oxygen during the activation of 430
- Oxides, alkaline-earth, Evaporation and diffusion rate measurements on cathodes of sintered nickel containing 73
- Oxygen, Emission of negative ions of, during the activation of oxide-coated cathodes 430
- Oxygen mixtures, hydrogen-, Vibration phenomena in detonation waves in 190

- p - n and i - h junctions in semiconductors, Location of 177 (SA)
- Parallel plate viscometer, Theory of the 85
- Particle shape, Effect on diffusion of 318
- Particle size of the effective X-ray absorption coefficient of heterogeneous slabs, Variation with 43
- Particles, Deposition of 535
- Permanent-magnet properties with crystal orientation in columnar crystal alloys, Variation of 279
- Petrol engine, Dynamic valve behaviour of a 132
- Phases, hard and soft, in cobalt-bonded tungsten carbide, Wear of the 517
- Photoconductivity 296
- Photoelectric densitometry, Application of, to the assessment of respirable dust samples 371
- Photoelectric method for the analysis of fluctuation records and its application to electrical noise 377
- Physical Society, The amalgamation of The Institute of Physics and The 392 (NC)
- Physics and chemistry of glasses; Glass technology* 264 (NC)
- Physics, solid state, Summarized proceedings of a conference on,—Melbourne, August 1959 137 (CR)
- Piezoelectric ceramics, low- Q , coupling coefficient and Q of, Measurement of 390 (C)
- Pits, Etch, and dislocations in cadmium sulphide crystals 296
- Plasma physics 265
- Plasters, set sulphate, Skeleton strength and critical porosity in 338
- Plastimeters 85
- Plate viscometer, parallel, Theory of the 85
- Plates, the extension and flexure of, Analogy between the slow motion of a viscous fluid and; a geometric demonstration by means of moiré fringes 244
- Platinum
- at low temperatures and its influence on precision thermometry, Resistance-temperature relationship of 205
 - /carbon shadowing deposits, Study in background structure in 506
 - resistance thermometry 205
- Plunger viscometers, Wall effect in the flow of lubricating greases in 363
- Pneumoconiosis, Airborne dust hazard in coalworkers' 1
- Poisson's ratio, A study of large strains and the effect of different values of 273
- Polarization microscope 229
- Polarization of nylon threads, Contact electrification and 202
- Pole figures, Influence of instrumental aberrations on the Schultz technique for the measurement of 96
- Polycrystalline metal foils, Determination of preferred orientation in, using a sputtering technique 475
- Polyethylene terephthalate, Comparison of X-ray and nuclear magnetic resonance measurements of crystallinity in 543
- Polyethylene terephthalate fibres, drawn, Measurement of crystallinity in, by X-ray diffraction 353 (*erratum*) 448 (NC)
- Polymer* 524 (NC)
- Porosity, critical, Skeleton strength and, in set sulphate plasters 338
- Porous media, Gaseous diffusion in,
- Part 1—A non-steady state method 314
 - Part 2—Dry granular materials 318
- Powder Data File-5, A.S.T.M., Comments on the 306 (C)
- Power law for creep 281
- Precipitator slides, thermal, Inter-observer checks on standards of performance in evaluating 119
- Pre-mixed gas streams, turbulent, Optical methods for the study of flames in 269
- Probe methods, Electron, of X-ray microanalysis 169 (SA)
- Proceedings
- of a conference on applied spectroscopy, Summarized,—Seascale, June 1960 525 (CR)
 - of a conference on solid state physics, Summarized,—Melbourne, August 1959 137 (CR)
 - of a conference on the borders of X-ray analysis, Summarized,—Reading, April 1960 481 (CR)
- Proceedings—*continued*
- of a conference on X-ray analysis, Summarized,—Leeds, April 1959 89 (CR)
 - of a conference on X-ray analysis, Summarized,—London, November 1959 393 (CR)
 - of a symposium on the generation of temperatures below 1° K, Summarized,—London, December 1959 449 (CR)
 - Summarized, of a conference on some aspects of magnetism,—Sheffield, September 1959 307 (CR)
 - Summarized, of a conference on electron microscopy—Exeter, July 1959 22 (CR)
- Propagation, Thermal, of a normal region in a thin superconducting film and its application to a new type of bistable element 292
- Properties, Some electrical and surface, of sintered nickel matrix cathodes 513
- Proportional counter, Absolute intensity measurements of the carbon and aluminium X-ray K-lines with a 64
- Pump, titanium droplet getter-ion, Pumping characteristics of a 401
- Pumping characteristics of a titanium droplet getter-ion pump 401
- Purification of organic materials by zone refining 128
- Q of low- Q piezoelectric ceramics, coupling coefficient and, Measurement of 390 (C)
- Radiation by glass, Spectral emission of 151
- Radiation, resonance, Production of, in discharge tubes of non-circular cross-section 492
- Radioactive source, Measurement of tinplate thickness using fluorescent X-rays excited by a 49
- Radiography, Stroboscopic, with a linear accelerator 132
- Ratio, Poisson's, A study of large strains and the effect of different values of 273
- Recording low-angle X-ray scattering when intensity scattered by specimen changes rapidly with time, Method of 287
- Rectangular hysteresis loops, High resistivity nickel-iron alloys with 58
- Refining, zone, Purification of organic materials by 128
- Reflexion electron microscopy using diffracted electrons 158
- Reflexion technique, back-, Determination of orientation of bismuth single crystals, using 229
- Refrigeration 209 (SA)
- Relaxation times in lead film, superconductive, storage elements 78
- Resistance
- effect, magneto-, Sensitive method for measurement of, with direct currents and with microwaves 35
 - network, Application of 408
 - temperature relationship of platinum at low temperatures and its influence on precision thermometry 205
- Resistances, non-linear, Solution of ladder networks containing 437
- Resistivity, High, nickel-iron alloys with rectangular hysteresis loops 58
- Resonance
- ferromagnetic, What is 69
 - measurements, X-ray and nuclear magnetic, of crystallinity in polyethylene terephthalate, Comparison of 543
 - methods, Dynamic measurement of elasticity using 478 (C)
 - radiation, Production of, in discharge tubes of non-circular cross-section 492
- (Resonant) cavities 69
- Respirable dust samples, Application of photoelectric densitometry to the assessment of 371
- Reynolds analogy, Measurement of convective heat transfer by means of the 471
- Rolling-sphere viscometer for structured liquids 332
- Rotary dynamic testing machine, Simple 165
- Royal Society's Fair Copying Declaration, The 136 (NC) 480 (NC)

- Rubber, Energy dissipation of 165
 Rubber, Hysteresis of 165
- Sanded plasters 338
- Scattering cross-sections, atomic differential, Measurement of 259
 (erratum) 448 (NC)
- Scattering, low-angle X-ray, when intensity scattered by specimen changes rapidly with time, Method of recording 287
- Schultz technique for the measurement of pole figures, Influence of instrumental aberrations on the 96
- Scintillation spectra, γ -ray, from fission-product mixtures, Interpretation of 346
- Selected-area diffraction in the electron microscope 504
- Selected-area microdiffraction in the electron microscope, Accuracy of 185
- Semiconductor noise 377
- Semiconductors 209 (SA)
 Contact electrification of 324
 Location of *p-n* and *l-h* junctions in 177 (SA)
- Shadowing deposits, platinum/carbon, Study of background structure in 506
- Silica, glass and, Effects of oil vapour contamination on the adhesion of zinc sulphide films to 382
- Silicon-iron, grain-oriented, Rotational hysteresis loss in 46
- Silicon monoxide films, Annealing, on aluminium mirrors 167 (C)
- Single crystals 498
 bismuth, Determination of orientation of, using back-reflexion technique 229
 tin, Determination of the elastic moduli of, and their variation with temperature 254
- Sintered nickel containing alkaline-earth oxides, cathodes of, Evaporation and diffusion rate measurement on 73
- Sintered nickel matrix cathodes, Some electrical and surface properties of 513
- Size distribution of airborne dust samples from British coalmines 1
- Skeleton strength and critical porosity in set sulphate plasters 338
- Skin friction 471
- Slabs, heterogeneous, Variation with particle size of the effective X-ray absorption coefficient of 43
- Slides, thermal precipitator, Inter-observer checks on standards of performance in evaluating 119
- Slip, Effect of, in plunger viscometers 363
- Smoke density integrator 509
- Solid-state electronics* 447 (NC)
- Solid state physics, Summarized proceedings of a conference on,—Melbourne, August 1959 137 (CR)
- Source, radioactive, Measurement of tinplate thickness using fluorescent X-rays excited by a 49
- Soviet industry, Automatic control in* 264 (NC)
- Spectra, γ -ray scintillation, from fission-product mixtures, Interpretation of 346
- Spectral composition of the zinc sulphide luminescence, Influence of temperature on the 289
- Spectral emission of radiation by glass 151
- Spectroscopy, applied, Summarized proceedings of a conference on,—Seascale, June 1960 525 (CR)
- Sphere viscometer, Rolling-, for structured liquids 332
- Spheres, two equal-sized equal-settling, moving through a viscous liquid, Interaction between 87 (C)
- Spherical aberration, Fifth order, of magnetic lenses 521
- Spinning detonation 190
- Spores, *Lycopodium*, Deposition of, upon glass slides exposed in a wind tunnel 535
- Sputtering technique, Determination of preferred orientation in polycrystalline metal foils using a 475
- State method, A non-steady, Gaseous diffusion in porous media. Part 1— 314
- Static 202
 and dynamic elastic constants 522 (C)
 and dynamic elastic constants of annealed and heavily cold-worked metals, Microcracks, and the 81
- Static electrification 324
- Steel, austenitic, X-ray stress determination in 523 (C)
- Steels, High alloy, for use as a thermal conductivity standard 195
- Stereomicroscopy, electron, Correction of errors in 199
- Storage elements, lead film, superconductive, Relaxation times in 78
- Strains, large, and the effect of different values of Poisson's ratio, A study of 273
- Strength of irradiated drawn and undrawn nylon 277
- Strength, Skeleton, and critical porosity in set sulphate plasters 338
- Stress, surface, Measurement of, in austenitic steel 242
- Stresses, thermal, Temperatures, and displacements in solid uranium dioxide rods 33
- Stroboscopic radiography with a linear accelerator 132
- Structured liquids, Rolling-sphere viscometers for 332
- Sulphate plasters, set, Skeleton strength and critical porosity in 338
- Sulphide
 crystals, cadmium, Etch pits and dislocations in 296
 films, adhesion of zinc, to glass and silica, Effects of oil vapour contamination on the 382
 luminescence, zinc, Influence of temperature on the spectral composition of the 289
- Superconducting film, thin, and its application to a new type of bistable element, Thermal propagation of a normal region in a 292
- Superconducting phase transition 292
- Superconductive, storage elements, lead film, Relaxation times in 78
- Surface
 effects, Anode, in diodes containing oxide-coated cathodes 124
 pitot tubes (Preston probe) 471
 stress, Measurement of, in austenitic steel 242
- Surge generator, compact, Design and performance of a 265
- Switching mechanism 335
- Symposium on electrical contacts 556 (NC)
- Symposium on the generation of temperatures below 1° K, Summarized proceedings of a 449 (CR)
- Targets, metal, Image formation by electron bombardment of 547
- Temperature
 Determination of the elastic moduli of tin single crystals, and their variation with 254
 of discharges 525 (CR)
 on the spectral composition of the zinc sulphide luminescence, Influence of 289
 relationship of platinum, Resistance-, at low temperatures and its influence on precision thermometry 205
- Temperatures
 below 1° K, Summarized proceedings of a symposium on the generation of 449 (CR)
 low, Resistance-temperature relationship of platinum at, and its influence on precision thermometry 205
 reached in a bimetallic brake drum 445
 thermal stresses and displacements in solid uranium dioxide rods 33
- Terephthalate fibres, drawn polyethylene, Measurement of crystallinity in, by X-ray diffraction 353 (erratum) 448 (NC)
- Terephthalate, polyethylene, Comparison of X-ray and nuclear magnetic resonance measurements of crystallinity in 543
- Terylene, Measurement of crystallinity 353 (erratum) 448 (NC)
- Testing machine, Simple rotary dynamic 165
- Theory of contact, Hertz, Investigation into one of the assumptions of the 67
- Thermal
 conduction 445
 conductivity 78
 conductivity standard, High alloy steels for use as a 195
 conductivity, Viscosity and, of liquid boron trifluoride 60
 precipitator slide evaluation 13

- Thermal—*continued*
 precipitator slides, Inter-observer checks on standards of performance in evaluating 119
 propagation of a normal region in a thin superconducting film and its application to a new type of bistable element 292
 stresses, Temperatures, and displacements in solid uranium dioxide rods 33
 transients in graphite-copper contacts 389 (c)
 Thermoelectric devices, Principles of 209 (SA)
 Thermometry, precision, Resistance-temperature relationship of platinum at low temperature and its influence on 205
 Thickness, tinplate, Measurement of, using fluorescent X-rays excited by a radioactive source 49
 Thin films of nickel-iron, Observations of the magnetization reversal process in, using the Kerr magneto-optic effect 335
 Thin superconducting film and its application to a new type of bistable element, Thermal propagation of a normal region in a 292
 Threads, nylon, Contact electrification and polarization of 202
 TIM: a brushless generating magnetometer 448 (NC)
 Tin single crystals, Determination of the elastic moduli of, and their variation with temperature 254
 Tinplate thickness, Measurement of, using fluorescent X-rays excited by a radioactive source 49
 Titanium droplet getter-ion pump, Pumping characteristics of a 401
 Torsion problems, Use of an electrical analogue for the solution of a variety of 461
 Transients, Thermal, in graphite-copper contacts 389 (c)
 Triboelectrification 324
 Trifluoride, liquid boron, Viscosity and thermal conductivity of 60
 Tube testing, eddy-current, Choice of frequency for 218
 Tubes, discharge, of non-circular cross-section, Production of resonance radiation in 492
 Tungsten carbide, cobalt-bonded, Wear of the hard and soft phases in 517
 Turbulent pre-mixed gas streams, Optical methods for the study of flames in 269
 Ultrasonic, Variable, water delay line 358
 Ultrasonics, Very high energy 143 (SA)
 Undrawn nylon, irradiated drawn and, Strength of 277
 Unipotential electron lenses, Numerical investigation of a range of 408
 Uranium 304
 Uranium dioxide rods, solid, Temperatures, thermal stresses and displacements in 33
 Vacuum breakdown 454
 Vacuum systems, continuously pumped, Pre-breakdown conduction in 454
 Valve, receiving-type, Passage of current through the glass envelope of a 440
 Vapour contamination, oil, on the adhesion of zinc sulphide films to glass and silica, Effects of 382
 Vibration phenomena in detonation waves in hydrogen-oxygen mixtures 190
 Viscometer
 oscillating cylinder, for Newtonian liquids, Experimental and theoretical investigations on the 283
 parallel plate, Theory of the 85
 Rolling-sphere, for structured liquids 332
 Viscometers, plunger, Wall effect in the flow of lubricating greases in 363
 Viscosity and thermal conductivity of liquid boron trifluoride 60
 Viscous fluid, slow motion of a, and the extension and flexure of plates, Analogy between the; a geometric demonstration by means of moiré fringes 244
 Viscous liquid, Interaction between two equal-sized equal-settling spheres moving through a 87 (c)
 Wall effect in the flow of lubricating greases in plunger viscometers 363
 Water
 alumina, Dielectric properties of (*erratum*) 264
 delay line, Variable ultrasonic 358
 New technique for measurement of low dissolved-air content of 228
 Waveguide containing ferrites 69
 Waves, detonation, in hydrogen-oxygen mixtures, Vibration phenomena in 190
 Wear 22 (CR)
 Wear of the hard and soft phases in cobalt-bonded tungsten carbide 517
 Whiskers, On the nature of 477 (c)
 Wind tunnel, Deposition of *Lycopodium* spores upon glass slides exposed in a 535
 Work function 124
 X-ray
 absorption coefficient, effective, of heterogeneous slabs, Variation with particle size of the 43
 analysis, Summarized proceedings of a conference on,—Leeds, April 1959 89 (CR)
 analysis, Summarized proceedings of a conference on,—London, November 1959 393 (CR)
 analysis, Summarized proceedings of a conference on the borders of,—Reading, April 1960 481 (CR)
 and nuclear magnetic resonance measurements of crystallinity in polyethylene terephthalate, Comparison of 543
 diffraction, Measurement of crystallinity in drawn polyethylene terephthalate fibres by 353 (*erratum*) 448 (NC)
 emission spectroscopy 481 (CR)
 fluorescence analysis 22 (CR)
 K-lines, carbon and aluminium, Absolute intensity measurements of the, with a proportional counter 64
 Method of surface stress measurement by 242
 microanalysis 481 (CR)
 microanalysis, Electron probe methods of 169 (SA)
 microbeam study of deformation bands in aluminium 162
 microscopy of beryllium 498
 scattering, low-angle, when intensity scattered by specimen changes rapidly with time, Method of recording 287
 stress determination in austenitic steel 523 (c)
 X-rays 229
 X-rays, fluorescent, excited by a radioactive source, Measurement of tinplate thickness using 49
 Zinc sulphide films, adhesion of, to glass and silica, Effects of oil vapour contamination on the 382
 Zinc sulphide luminescence, Influence of temperature on the spectral composition of the 289
 Zone refining, Purification of organic materials by 128

AUTHORS

(SA) denotes special article, (CR) conference report and (c) correspondence.

- Agar, A. W., Accuracy of selected-area microdiffraction in the electron microscope 185
- Allison, J. W., Half-life of iridium 192 302
- Archard, G. D., Fifth order spherical aberration of magnetic lenses 521
- Archenhold, W. F., Sandham, W. F., and Thompson, J. E., Rotational hysteresis loss in grain-oriented silicon-iron 46
- Arridge, R. G. C., Contact electrification and polarization of nylon threads 202
- Ashford, J. R., Some statistical aspects of dust counting 13
- Ashford, J. R., *see under* Fay, J. W. J.
- Assenheim, J. G., *see under* Clark, D. E.
- Baker, F. A., and Giorgi, T. A., Sorption and desorption of gas in a hot-cathode ionization gauge 433
- Ball, R., *see under* Holland, L.
- Bareham, F. R., Choice of frequency for eddy-current tube testing 218
- Barker, J. R., *see under* Kovattana, T.
- Bateman, S. K., *see under* Holland, L.
- Beattie, J. R., and Coen, E., Spectral emission of radiation by glass 151
- Beynon, J. H., and Saunders, R. A., Purification of organic materials by zone refining 128
- Birks, F. T., *see under* Bovey, L.
- Bovey, L., and Birks, F. T., Summarized proceedings of a conference on applied spectroscopy—Seascale, June 1960 525 (CR)
- Boxall, G., *see under* Granville, R. A.
- Bradfield, G., Dynamic measurement of elasticity using resonance methods 478 (c)
- Bradley, D. E., Study in background structure in platinum/carbon shadowing deposits 506
- Bramhall, A. D., and Hutton, J. F., Wall effect in the flow of lubricating greases in plunger viscometers 363
- Bristow, J. R., Microcracks, and the static and dynamic elastic constants of annealed and heavily cold-worked metals 81
- Broom, R. F., and Rhoderick, E. H., Thermal propagation of a normal region in a thin superconducting film and its application to a new type of bistable element 292
- Broom, R. F., and Simpson, O., Relaxation times in lead film, superconductive storage elements 78
- Bugden, A. R., Hamilton, R. J., and Jones, G. H. S., Application of photoelectric densitometry to the assessment of respirable dust samples 371
- Buhl, P. A., *see under* Kelsch, J. J.
- Bullen, G. J., and Mackay, A. L., Summarized proceedings of a conference on X-ray analysis—London, November 1959 393 (CR)
- Cameron, J. F., and Rhodes, J. R., Measurement of tinplate thickness using fluorescent X-rays excited by a radioactive source 49
- Cayless, M. A., Production of resonance radiation in discharge tubes of non-circular cross-section 492
- Chapman, J. A., and Whelan, M. J., Summarized proceedings of a conference on electron microscopy—Exeter, July 1959 22 (CR)
- Clark, D. E., and Assenheim, J. G., Sensitive method for measurement of magneto-resistance effect with direct currents and microwaves 35
- Coen, E., *see under* Beattie, J. R.
- Cooper, W. M., *see under* Stephens, K. G.
- Coppen, P. J., *see under* Iles, P. A.
- Currie, J. A., Gaseous diffusion in porous media. Part 1—A non-steady state method 314
- Currie, J. A., Gaseous diffusion in porous media. Part 2—Dry granular materials 318
- Daglish, H. N., Passage of current through the glass envelope of a receiving-type valve 440
- Das, Y. C., *see under* Hsiao, C. C.
- Davies, C. N., Deposition of *Lycopodium* spores upon glass slides exposed in a wind tunnel 535
- Davies, W., *see under* Greenwood, J. A.
- Dolby, R. M., Absolute intensity measurements of the carbon and aluminium X-ray K-lines with a proportional counter 64
- Duncumb, P., Electron probe methods of X-ray microanalysis 169 (SA)
- Edwards, D. H., and Jones, T. G., Vibration phenomena in detonation waves in hydrogen-oxygen mixtures 190
- Ellington, J. P., Temperatures, thermal stresses and displacements in solid uranium dioxide rods 33
- Eveson, G. F., *see under* Matthews, H. W.
- Fane, R. W., Some electrical and surface properties of sintered nickel matrix cathodes 513
- Farrow, G., and Preston, D., Measurement of crystallinity in drawn polyethylene terephthalate fibres by X-ray diffraction 353
- Farrow, G., and Ward, I. M., Comparison of X-ray and nuclear magnetic resonance measurements of crystallinity in polyethylene terephthalate 543
- Fay, J. W. J., and Ashford, J. R., Size distribution of airborne dust samples from British coalmines 1
- Fay, J. W. J., Ashford, J. R., and Smith, P. H., Inter-observer checks on standards of performance in evaluating thermal precipitator slides 119
- Ferrier, R. P., and Willis, B. T. M., Summarized proceedings of a conference on the borders of X-ray analysis—Reading, April 1960 481 (CR)
- Fessler, H., and Lewin, B. H., A study of large strains and the effect of different values of Poisson's ratio 273
- Fitzgerald, L. M., Measurement of hardness at very high temperatures 551
- Fox, M. D., and Weinberg, F. J., Optical methods for the study of flames in turbulent pre-mixed gas streams 269
- Gale, B., and Griffiths, D., Influence of instrumental aberrations on the Schultz technique for the measurement of pole figures 96
- Gent, A. N., Simple rotary dynamic testing machine 165
- Gent, A. N., Theory of the parallel plate viscometer 85
- Giorgi, T. A., *see under* Baker, F. A.
- Glaister, R. M., Measurement of coupling coefficient and Q of low-Q piezoelectric ceramics 390 (CR)
- Gold, L., Static and dynamic elastic constants 522 (c)
- Golden, J., and Rowe, G. W., Wear of the hard and soft phases in cobalt-bonded tungsten carbide 517
- Goldsmid, H. J., Principles of thermoelectric devices 209 (SA)
- Granville, R. A., and Boxall, G., Measurement of convective heat transfer by means of the Reynolds analogy 471
- Greenwood, J. A., and Williamson, J. B. P.; Davies, W., Thermal transients in graphite-copper contacts 389 (c)
- Griffiths, D., *see under* Gale, B.
- Grohnman, A., and Krylow, J., On the nature of whiskers 477 (c)

- Halliday, J. S., Measurement of atomic differential scattering cross-sections 259
- Halliday, J. S., and Newman, R. C., Reflexion electron microscopy using diffracted electrons 158
- Halliday, J. S., and Quinn, T. F. J., Contrast of electron micrographs 486
- Hamilton, R. J., *see under* Bugden, A. R.
- Iancox, R., Importance of insulating inclusions in arc initiation 468
- Harper, A. F. A., *see under* Lowenthal, G. C.
- Harper, W. R., Contact electrification of semiconductors 324
- Hart, A., High resistivity nickel-iron alloys with rectangular hysteresis loops 58
- Haynes, A., *see under* Hsiao, C. C.
- Head, J. W., *see under* Mayo, C. G.
- Hirsch, E. H., Image formation by electron bombardment of metal targets 547
- Holland, L., and Bateman, S. K., Effects of oil vapour contamination on the adhesion of zinc sulphide films to glass and silica 382
- Holland, L., and Laurenson, L., Pumping characteristics of a titanium droplet getter-ion pump 401
- Holland, L., Putner, T., and Ball, R., Annealing silicon monoxide films on aluminium mirrors 167 (c)
- Hopkins, B. J., Anode surface effects in diodes containing oxide-coated cathodes 124
- Hopkins, B. J., and Vick, F. A., Charge localization on the surfaces of oxide-coated cathodes 223
- House, D. G., and Vernon, E. V., Determination of the elastic moduli of tin single crystals and their variation with temperature 254
- Hsiao, C. C., Das, Y. C., and Haynes, A., Strength of irradiated drawn and undrawn nylon 277
- Hughes, J. W., Lewis, Isabel E., and Wilson, A. J. C., Comments on the A.S.T.M. Powder Data File-5 306 (c)
- Hutton, J. F., *see under* Bramhall, A. D.
- Ibrahim, Ali Abdel Kerim, and Kabiell, Abdel Monem I., Experimental and theoretical investigations on the oscillating cylinder viscometer for Newtonian liquids 283
- Iles, P. A., and Coppen, P. J., Location of *p-n* and *I-h* junctions in semiconductors 177 (SA)
- Jones, G. H. S., *see under* Bugden, A. R.
- Jones, T. G., *see under* Edwards, D. H.
- Kabiell, Abdel Monem I., *see under* Ibrahim, Ali Abdel Kerim
- Kammerer, O. F., *see under* Kelsch, J. J.
- Kelsch, J. J., Kammerer, O. F., and Buhl, P. A., New technique for the direct investigation of fission events 555
- Kovattana, T., and Barker, J. R., Solution of ladder networks containing non-linear resistances 437
- Krylow, J., *see under* Grohman, A.
- Laurenson, L., *see under* Holland, L.
- Lewin, B. H., *see under* Fessler, H.
- Lewis, D., X-ray microbeam study of deformation bands in aluminium 162
- Lewis, Isabel E., *see under* Hughes, J. W.
- Lowenthal, G. C., and Harper, A. F. A., Resistance-temperature relationship of platinum at low temperatures and its influence on precision thermometry 205
- McCaig, M., and Wright, W., Variation of permanent-magnet properties with crystal orientation in columnar crystal alloys 279
- Mackay, A. L., *see under* Bullen, G. J.
- Mallon, H. D., and Wilson, C. G., Determination of orientation of bismuth single crystals using back-reflexion technique 229
- Manley, D. M. J. P., Change of size of air bubbles in water containing a small dissolved air content 38
- Manley, D. M. J. P., New technique for measurement of low dissolved-air content of water 228
- Mansfield, W. K., Pre-breakdown conduction in continuously-pumped vacuum systems 454
- Matthews, H. W., Smith, F. B., and Eveson, G. F., Interaction between two equal-sized equal-settling spheres moving through a viscous liquid 87 (c)
- Mayo, C. G., and Head, J. W., Fourier series associated with duty cycles 103
- Mitra, G. B., and Wilson, A. J. C., Variation of particle size of the effective X-ray absorption coefficient of heterogeneous slabs 43
- Moore, J. C., Measurement of surface stress in austenitic steel 242
- Neilson, J. H. S., X-ray stress determination in austenitic steel 523 (c)
- Nelson, R. S., Determination of preferred orientation in polycrystalline metal foils using a sputtering technique 475
- Neppiras, E. A., Very high energy ultrasonics 143 (SA)
- Newcomb, T. P., Temperatures reached in a bimetallic brake drum 445
- Newman, R. C., *see under* Halliday, J. S.
- Nicholas, J. F., Summarized proceedings of a conference on solid state physics—Melbourne, August 1959 137 (CR)
- Oosthuizen, J. C., *see under* Scott Blair, G. W.
- Parfitt, G. G., Recent studies of noise problems 53 (CR)
- Parkinson, D. H., Summarized proceedings of a symposium on the generation of temperatures below 1° K—London, December 1959 449 (CR)
- Peirson, D. H., Interpretation of γ -ray scintillation spectra from fission-product mixtures 346
- Phillips, R., Selected-area diffraction in the electron microscope 504
- Powell, R. W., and Tye, R. P., High alloy steels for use as a thermal conductivity standard 195
- Preston, D., *see under* Farrow, G.
- Prutton, M., Observations of the magnetization reversal process in thin films of nickel-iron, using the Kerr magneto-optic effect 335
- Putner, T., *see under* Holland, L.
- Quinn, T. F. J., *see under* Halliday, J. S.
- Redshaw, S. C., Use of an electrical analogue for the solution of a variety of torsion problems 461
- Rhoderick, E. H., *see under* Broom, R. F.
- Rhodes, J. R., *see under* Cameron, J. F.
- Richards, T. H., Analogy between the slow motion of a viscous fluid and the extension and flexure of plates; a geometric demonstration by means of moiré fringes 244
- Richardson, J. F., and Vick, F. A., Evaporation and diffusion rate measurements on cathodes of sintered nickel containing alkaline-earth oxides 73
- Rigby, B. J., Poor law for creep 281
- Rowe, G. W., *see under* Golden, J.
- Sandham, W. F., *see under* Archenhold, W. F.
- Sato, T., *see under* Sugita, K.
- Saunders, R. A., *see under* Beynon, J. H.
- Sawkill, J., and Schwarzenberger, D. R., X-ray microscopy of beryllium 498
- Schiller, K. K., Skeleton strength and critical porosity in set sulphate plasters 338

- Schwarzenberger, D. R., *see under* Sawkill, J.
- Scott, J., Photoelectric method for the analysis of fluctuation records and its application to electrical noise 377
- Scott Blair, G. W., and Oosthuizen, J. C., Rolling-sphere viscometer for structured liquids 332
- Secker, P. E., Explanation of the enhanced arc velocity on magnetic electrodes 385
- Shaw, D., and Watts, B. N., Evaporated films of niobium 304 (c)
- Simpson, O., *see under* Broom, R. F.
- Skertchly, A., and Steadman, R., Summarized proceedings of a conference on X-ray analysis—Leeds, April 1959 89 (CR)
- Smith, F. B., *see under* Matthews, H. W.
- Smith, P. H., *see under* Fay, J. W. J.
- Soudek, I., Influence of temperature on the spectral composition of the zinc sulphide luminescence 289
- Spencer, A. N., and Todd, M. C. J., Viscosity and thermal conductivity of liquid boron trifluoride 60
- Steadman, R., *see under* Skertchly, A.
- Stephens, K. G., and Cooper, W. M., Calibration of manganese and gold foils for relative neutron flux measurements 342
- Storey, C., Investigation into one of the assumptions of the Hertz theory of contact 67
- Storey, R. M., Smoke density integrator 509
- Sugita, K., Sato, T., and Toriyama, Y., Some remarks on the conduction current in insulating liquids 539
- Surplice, N. A., Emission of negative ions of oxygen during the activation of oxide-coated cathodes 430
- Teare, P. W., Method of recording low-angle X-ray scattering when intensity scattered by specimen changes rapidly with time 287
- Tebble, R. S., and Williams, D. E. G., Summarized proceedings of a conference on some aspects of magnetism—Sheffield, September 1959 307 (CR)
- Thompson, J. E., *see under* Archenhold, W. F.
- Thornton, E., Design and performance of a compact surge generator 265
- Todd, M. C. J., *see under* Spencer, A. N.
- Toriyama, Y., *see under* Sugita, K.
- Tye, R. P., *see under* Powell, R. W.
- Vernon, E. V., *see under* House, D. G.
- Vick, F. A., *see under* Hopkins, B. J.
- Vick, F. A., *see under* Richardson, J. F.
- Vincent, B. J., Stroboscopic radiography with a linear accelerator 132
- Vine, J., Numerical investigation of a range of unipotential electron lenses 408
- Waldron, R. A., What is ferromagnetic resonance? 69
- Ward, I. M., *see under* Farrow, G.
- Watts, B. N., *see under* Shaw, D.
- Weinberg, F. J., *see under* Fox, M. D.
- Wells, O. C., Correction of errors in electron stereomicroscopy 199
- Weston, G. F., Glow-discharge characteristics of helium-argon mixtures 305 (c)
- Whelan, M. J., *see under* Chapman, J. A.
- Williams, D. E. G., *see under* Tebble, R. S.
- Williams, G. W., Variable ultrasonic water delay line 358
- Williamson, J. B. P., *see under* Greenwood, J. A.
- Willis, B. T. M., *see under* Ferrier, R. P.
- Wilson, A. J. C., *see under* Hughes, J. W.
- Wilson, A. J. C., *see under* Mitra, G. B.
- Wilson, C. G., *see under* Mallon, H. D.
- Woods, J., Etch pits and dislocations in cadmium sulphide crystals 296
- Wright, W., *see under* McCaig, M.

CONTENTS OF VOLUME 11

iii

Contact electrification and polarization of nylon threads. By R. G. C. ARRIDGE	202
Resistance-temperature relationship of platinum at low temperatures and its influence on precision thermo- metry. By G. C. LOWENTHAL and A. F. A. HARPER	205

JUNE 1960

SPECIAL ARTICLE

Principles of thermoelectric devices. By H. J. GOLDSMID	209
---	-----

PAPERS

Choice of frequency for eddy-current tube testing. By F. R. BAREHAM	218
Charge localization on the surfaces of oxide-coated cathodes. By B. J. HOPKINS and F. A. VICK	223
New technique for measurement of low dissolved-air content of water. By D. M. J. P. MANLEY	228
Determination of orientation of bismuth single crystals using back-reflexion technique. By H. D. MALLON and C. G. WILSON	229

NEW BOOKS SECTION

Reviews and notices	231-241
---------------------	---------

PAPERS (continued)

Measurement of surface stress in austenitic steel. By J. C. MOORE	242
Analogy between the slow motion of a viscous fluid and the extension and flexure of plates; a geometric demon- stration by means of moiré fringes. By T. H. RICHARDS	244
Determination of the elastic moduli of tin single crystals, and their variation with temperature. By D. G. HOUSE and E. V. VERNON	254
Measurement of atomic differential scattering cross- sections. By J. S. HALLIDAY	259

NOTES AND NEWS

Notes and comments	264
--------------------	-----

JULY 1960

PAPERS

Design and performance of a compact surge generator. By E. THORNTON	265
Optical methods for the study of flames in turbulent pre- mixed gas streams. By M. D. FOX and F. J. WEINBERG	269
A study of large strains and the effect of different values of Poisson's ratio. By H. FESSLER and B. H. LEWIN	273
Strength of irradiated drawn and undrawn nylon. By C. C. HSIAO, Y. C. DAS and A. HAYNES	277
Variation of permanent-magnet properties with crystal orientation in columnar crystal alloys. By M. McCAIG and W. WRIGHT	279
Power law for creep. By B. J. RIGBY	281
Experimental and theoretical investigations on the oscil- lating cylinder viscometer for Newtonian liquids. By ALI ABDEL KERIM IBRAHIM and ABDEL MONEM I. KABIEL	283
Method of recording low-angle X-ray scattering when intensity scattered by specimen changes rapidly with time. By P. W. TEARE	287
Influence of temperature on the spectral composition of the zinc sulphide luminescence. By I. SOUDEK	289
Thermal propagation of a normal region in a thin super- conducting film and its application to a new type of bistable element. By R. F. BROOM and E. H. RHODERICK	292
Etch pits and dislocations in cadmium sulphide crystals. By J. WOODS	296
Half-life of iridium 192. By J. W. ALLISON	302

CORRESPONDENCE

Evaporated films of niobium. From D. SHAW and B. N. WATTS	302
Glow-discharge characteristics of helium-argon mixtures. From G. F. WESTON	305
Comments on the A.S.T.M. Powder Data File—5. From J. W. HUGHES, ISABEL E. LEWIS and A. J. C. WILSON	300

AUGUST 1960

CONFERENCE REPORT

Summarized proceedings of a conference on some aspects of magnetism—Sheffield, September 1959. By R. S. TEBBLE and D. E. G. WILLIAMS	307
--	-----

PAPERS

Gaseous diffusion in porous media. Part 1—A non- steady state method. By J. A. CURRIE	312
Gaseous diffusion in porous media. Part 2—Dry granular materials. By J. A. CURRIE	318
Contact electrification of semiconductors. By W. R. HARPER	324
Rolling-sphere viscometer for structured liquids. By G. W. SCOTT BLAIR and J. C. OOSTHUIZEN	332
Observations of the magnetization reversal process in thin films of nickel-iron, using the Kerr magneto-optic effect. By M. PRUTTON	335
Skeleton strength and critical porosity in set sulphate plasters. By K. K. SCHILLER	338
Calibration of manganese and gold foils for relative neutron flux measurements. By K. G. STEPHENS and W. M. COOPER	342
Interpretation of γ -ray scintillation spectra from fission- product mixtures. By D. H. PEIRSON	346
Measurement of crystallinity in drawn polyethylene terephthalate fibres by X-ray diffraction. By G. FARROW and D. PRESTON	351
Variable ultrasonic water delay line. By G. W. WILLIAMS	358
Wall effect in the flow of lubricating greases in plunger viscometers. By A. D. BRAMHALL and J. F. HUTTON	361
Application of photoelectric densitometry to the assess- ment of respirable dust samples. By A. R. BUGDEN, R. J. HAMILTON and G. H. S. JONES	37
Photoelectric method for the analysis of fluctuation records and its application to electrical noise. By J. SCOTT	37
Effects of oil vapour contamination on the adhesion of zinc sulphide films to glass and silica. By L. HOLLAND and S. K. BATEMAN	382
Explanation of the enhanced arc velocity on magnetic electrodes. By P. E. SECKER	383

CORRESPONDENCE

Thermal transients in graphite-copper contacts. From J. A. GREENWOOD and J. B. P. WILLIAMSON; W. DAVIES	389
Measurement of coupling coefficient and Q of low-Q piezoelectric ceramics. From R. M. GLAISTER	390

NOTES AND NEWS

Notes and comments	392
--------------------	-----

SEPTEMBER 1960

CONFERENCE REPORT

Summarized proceedings of a conference on X-ray analysis—London, November 1959. By G. J. BULLEN and A. L. MACKAY	39
--	----

	PAGE		PAGE
PAPERS		PAPERS	
Pumping characteristics of a titanium droplet getter-ion pump. By L. HOLLAND and L. LAURENSEN	401	Contrast of electron micrographs. By J. S. HALLIDAY and T. F. J. QUINN	486
Numerical investigation of a range of unipotential electron lenses. By J. VINE	408	Production of resonance radiation in discharge tubes of non-circular cross-section. By M. A. CAYLESS	492
NEW BOOKS SECTION		X-ray microscopy of beryllium. By J. SAWKILL and D. R. SCHWARZENBERGER	498
Reviews and notices	412-429	Selected-area diffraction in the electron microscope. By R. PHILLIPS	504
PAPERS (continued)		Study of background structure in platinum/carbon shadowing deposits. By D. E. BRADLEY	506
Emission of negative ions of oxygen during the activation of oxide-coated cathodes. By N. A. SURPLICE	430	Smoke density integrator. By R. M. STOREY	509
Sorption and desorption of gas in a hot-cathode ionization gauge. By F. A. BAKER and T. A. GIORGI	433	Some electrical and surface properties of sintered nickel matrix cathodes. By R. W. FANE	513
Solution of ladder networks containing non-linear resistances. By T. KOVATTANA and J. R. BARKER	437	Wear of the hard and soft phases in cobalt-bonded tungsten carbide. By J. GOLDEN and G. W. ROWE	517
Passage of current through the glass envelope of a receiving-type valve. By H. N. DAGLISH	440	Fifth order spherical aberration of magnetic lenses. By G. D. ARCHARD	521
Temperatures reached in a bimetallic brake drum. By T. P. NEWCOMB	445	CORRESPONDENCE	
LETTERS AND NEWS		Static and dynamic elastic constants. From L. GOLD	522
Notes and comments	447	X-ray stress determination in austenitic steel. From J. H. S. NEILSON	523
OCTOBER 1960		NOTES AND NEWS	
REFERENCE REPORT		Notes and comments	524
Summarized proceedings of a symposium on the generation of temperatures below 1° K—London, December, 1959. By D. H. PARKINSON	449	DECEMBER 1960	
CONFERENCE REPORT		CONFERENCE REPORT	
Breakdown conduction in continuously pumped vacuum systems. By W. K. MANSFIELD	454	Summarized proceedings of a conference on applied spectroscopy—Seascale, June 1960. By L. BOVEY and F. T. BIRKS	525
Use of an electrical analogue for the solution of a variety of torsion problems. By S. C. REDSHAW	461	PAPERS	
Importance of insulating inclusions in arc initiation. By R. HANCOX	468	Deposition of <i>Lycopodium</i> spores upon glass slides exposed in a wind tunnel. By C. N. DAVIES	535
Measurement of convective heat transfer by means of the Reynolds analogy. By R. A. GRANVILLE and G. BOXALL	471	Some remarks on the conduction current in insulating liquids. By K. SUGITA, T. SATO and Y. TORIYAMA	539
Determination of preferred orientation in polycrystalline metal foils using a sputtering technique. By R. S. NELSON	475	Comparison of X-ray and nuclear magnetic resonance measurements of crystallinity in polyethylene terephthalate. By G. FARROW and I. M. WARD	543
CORRESPONDENCE		Image formation by electron bombardment of metal targets. By E. H. HIRSCH	547
On the nature of whiskers. From A. GROHMAN and J. KRYLOW	477	Measurement of hardness at very high temperatures. By L. M. FITZGERALD	551
Dynamic measurement of elasticity using resonance methods. From G. BRADFIELD	478	CORRESPONDENCE	
NOTES AND NEWS		New technique for the direct investigation of fission events. From J. J. KELSCH, O. F. KAMMERER and P. A. BUHL	555
Notes and comments	480	NOTES AND NEWS	
NOVEMBER 1960		Notes and comments	555
CONFERENCE REPORT		SUBJECT INDEX TO VOLUME 11	557
Summarized proceedings of a conference on the borders of X-ray analysis—Reading, April, 1960. By R. P. FERRIER and B. T. M. WILLIS	481	AUTHOR INDEX TO VOLUME 11	566

Size distribution of airborne dust samples from British coalmines

by J. W. J. FAY, Ph.D., D.I.C., and J. R. ASHFORD, M.A., Ph.D., National Coal Board, Scientific Department, London

[Paper first received 16 June, and in final form 23 August, 1959]

Abstract

This paper is concerned with the size-distribution analysis of samples of airborne dust from British coalmines, taken with the thermal precipitator and evaluated using the optical microscope. It is shown that many of the particles of less than $1\ \mu$ in diameter present underground are probably associated with atmospheric pollution, and do not arise directly from mining operations. Consideration is then given to the size distribution of the above- $1\ \mu$ component of the dust. The results recorded on special samples by the Pneumoconiosis Field Research Unit, together with some published size-analyses of airborne dust in British and South African mines, are examined, and it is shown that a single-component exponential distribution provides a reasonably good fit to the observed data. The size distributions reported during routine sampling work at the 26 collieries associated with the research are then analysed in terms of the exponential distribution. It appears that within any given colliery there is no considerable variation in size distribution between facework on the coal-getting and preparation shifts and non-facework underground, although there is a suggestion that the airborne dust encountered in hard headings may contain a higher proportion of smaller particles than in other parts of the same colliery. There are, however, marked variations from coalfield to coalfield, the coarsest dust being reported in South Wales and the finest in Scotland. The implications of these results are discussed and it is shown that the $1\text{--}5\ \mu$ particle number count is a satisfactory parameter for the measurement of the hazard associated with airborne dust.

Introduction

IN the course of the environmental sampling programme undertaken as part of the National Coal Board's Pneumoconiosis Field Research Programme,⁽¹⁾ many thousands of samples of airborne dust have been collected with the thermal precipitator on coal faces, elsewhere underground and on the surface at twenty-six selected collieries throughout coalfields in England, Scotland and Wales. The analysis of such samples of "respirable" dust from this wide variety of sources provides an excellent opportunity for examining the size distribution of samples of airborne dust in British coalmines.

The evaluation of the samples is carried out using the optical microscope, the particles being sized in terms of the diameters of circles of equivalent projected areas. In view of the doubts which have been expressed about the validity of optical methods for sizing particles of less than $1\ \mu$ in diameter,⁽²⁾ the size distribution of the below- $1\ \mu$ particles

is not considered in detail in this paper. The counts recorded in the $0\cdot5\text{--}1\ \mu$ range do, however, enable consideration to be given to the original "2-component" hypothesis of dust concentrations which was put forward, particularly by workers at the Safety in Mines Research Establishment.⁽³⁾ According to this hypothesis, the particle number count can be expressed as a function containing two exponential terms, one applicable to the dust particles of less than about $1\ \mu$ in diameter, and the other to the particles of diameter greater than about $1\ \mu$. Subsequent work at S.M.R.E.⁽⁴⁾ suggested that the dust below $1\ \mu$ in diameter arose largely from atmospheric pollution and confirmed that the simple exponential relationship held good for the dust above- $1\ \mu$ and up to at least $10\ \mu$.⁽⁵⁾ The latest work at S.M.R.E. has, however, modified this hypothesis to the extent of postulating two exponential terms, one applicable from $1\ \mu$ to about $6\ \mu$ and the other above $6\ \mu$.⁽⁶⁾ Other workers^(7,8) have put forward alternative models to describe the size distribution, and these hypotheses have also been examined in the light of the data available.

Experimental data

The procedures adopted by the N.C.B.'s Pneumoconiosis Field Research Unit (P.F.R.) for the measurement of individual dust exposures are based on the principle of sampling randomly selected individual workmen throughout a complete shift. The first thermal-precipitator sample is started at the beginning of the shift (generally when the selected workman arrives at pit bottom) and subsequent samples are taken continuously throughout the shift. A size-distribution analysis is carried out on one randomly selected cover glass from each sampling shift, a count being made of the numbers of particles in the $0\cdot5\text{--}1$, $1\text{--}2\cdot5$, $2\cdot5\text{--}5$ and above- $5\ \mu$ ranges. For the purposes of the present analysis, each sample on which the size-distribution counts were carried out has been assigned to one or other of seven broad classes of environment—coal face (coal-getting shift), coal face (preparation shift), development in coal, hard heading, elsewhere underground, surface ("dusty" occupations) and surface ("non-dusty" occupations). All concentrations have been expressed in terms of particles per cm^3 of air sampled (p.p.c.c.).

To investigate the general laws concerning size distributions, special samples have been taken at P.F.R. collieries in the Northumberland, Nottinghamshire and Lancashire Coalfields, covering respectively the operations of machine-cutting in stone (four shifts), power-loading with the Anderton Disc Shearer (two shifts), and hand-filling with pneumatic picks (three shifts). The samples were collected and the detailed size-distribution analyses made by a single,

experienced microscopist,* using a Patterson-Cawood graticule. To minimize errors arising from the relatively rare occurrence of particles in the larger size ranges, a modification of the method of "Truncated Multiple Traversing" described by Sichel⁽⁷⁾ was employed, at least 10 particles in each size range up to 10μ being counted. In addition to these results obtained within the Research unit, the detailed size distributions of airborne dust samples from British coalmines published by Wynn and Dawes⁽³⁾ and from South African mines by Sichel,⁽⁷⁾ Tucker,⁽⁹⁾ and Kerrich⁽¹⁰⁾ have also been used in the analyses described.

The below- 1μ component of the dust

A measure of the general form of the size distribution of an airborne dust sample is provided by the ratio of the number

of particles of less than 1μ in the sample. The distribution of the p -ratios in terms of the seven broad classes of general environment at the twenty-six collieries associated with the P.F.R. programme is given in Table 1. It will be seen that the lowest p -ratios are, in general, recorded at the coal face during the coal-getting shift. The ratio tends to be slightly higher on the coal face during the preparation shifts and increases progressively as the samples are located farther away from the coal face, being highest (and most variable) on the surface. Because this order of placing the different environments corresponds inversely with their relative levels of dustiness, it appears that the data are not inconsistent with the presence of a substantial proportion of 0.5 – 1μ dust not associated with the mining activities.

Further support is given to this conclusion by a few simple calculations which show that the measured 0.5 – 1μ concen-

Table 1. *Distribution of the p -ratio in terms of general environment*

The figures given in brackets denote the numbers of thermal-precipitator samples on which the results are based.

Coalfield	Colliery	Coal face (Longwall C.G.S. and Arcwall)	Coal face (Longwall preparation)	Development (in coal)	Coal face (all shifts)	Hard heading	Elsewhere underground	Surface "dusty"	Surface "non-dusty"	Surface (all occupations)
Scottish	SC1	2.8 ₍₁₇₉₎	2.7 ₍₁₆₈₎	2.4 ₍₁₅₎	2.7 ₍₃₆₂₎	3.6 ₍₂₀₎	4.3 ₍₂₃₃₎	4.5 ₍₂₀₎	7.5 ₍₁₁₎	5.6 ₍₃₁₎
	SC2	1.9 ₍₁₉₁₎	2.2 ₍₂₈₄₎	1.4 ₍₆₎	2.1 ₍₄₈₁₎	2.8 ₍₁₅₎	2.4 ₍₁₁₅₎	— ₍₀₎	5.9 ₍₁₈₎	5.9 ₍₁₈₎
	SC3	1.8 ₍₄₅₎	2.0 ₍₇₄₎	1.5 ₍₃₎	1.9 ₍₁₂₂₎	2.0 ₍₉₎	2.0 ₍₈₉₎	1.5 ₍₁₎	4.0 ₍₁₂₎	3.8 ₍₁₃₎
	SC4	1.9 ₍₁₀₆₎	2.0 ₍₁₁₇₎	1.9 ₍₂₃₎	1.9 ₍₂₄₆₎	2.1 ₍₉₎	2.6 ₍₆₉₎	— ₍₀₎	7.3 ₍₁₀₎	7.3 ₍₁₀₎
	SC5	2.2 ₍₇₅₎	2.3 ₍₅₉₎	1.9 ₍₂₀₎	2.2 ₍₁₅₄₎	1.8 ₍₂₎	2.4 ₍₅₀₎	2.5 ₍₄₎	— ₍₀₎	2.5 ₍₄₎
Northumberland	NH1	2.6 ₍₁₁₆₎	3.2 ₍₈₀₎	3.8 ₍₁₈₎	2.9 ₍₂₁₄₎	1.9 ₍₃₎	7.2 ₍₁₁₁₎	6.5 ₍₇₎	9.3 ₍₇₎	7.9 ₍₁₄₎
	NH2	1.7 ₍₂₀₂₎	1.9 ₍₁₈₂₎	1.7 ₍₁₆₎	1.8 ₍₄₀₀₎	4.9 ₍₈₎	2.6 ₍₁₄₇₎	2.0 ₍₅₎	5.9 ₍₁₂₎	4.7 ₍₁₇₎
Cumberland	C1	1.5 ₍₁₅₆₎	1.5 ₍₁₆₇₎	1.5 ₍₁₉₎	1.6 ₍₃₄₂₎	1.4 ₍₁₎	2.2 ₍₁₆₆₎	3.3 ₍₈₎	6.2 ₍₁₄₎	5.1 ₍₂₂₎
Durham	D1	1.7 ₍₁₆₁₎	1.9 ₍₈₅₎	1.6 ₍₂₄₎	1.7 ₍₂₇₀₎	2.1 ₍₂₎	2.2 ₍₁₃₉₎	3.4 ₍₁₂₎	5.2 ₍₆₎	4.0 ₍₁₈₎
	D2	1.8 ₍₁₂₃₎	2.2 ₍₇₈₎	1.7 ₍₃₃₎	1.9 ₍₂₃₄₎	2.2 ₍₂₎	2.3 ₍₁₄₂₎	3.5 ₍₈₎	7.7 ₍₁₂₎	6.0 ₍₂₀₎
Yorkshire	Y1	2.2 ₍₁₅₃₎	2.2 ₍₁₅₃₎	2.0 ₍₆₎	2.2 ₍₃₁₂₎	— ₍₀₎	4.5 ₍₁₅₂₎	5.1 ₍₇₎	9.1 ₍₁₉₎	8.0 ₍₂₆₎
	Y2	2.1 ₍₇₆₎	2.2 ₍₄₈₎	3.6 ₍₃₎	2.1 ₍₁₂₇₎	2.7 ₍₂₎	2.4 ₍₁₇₁₎	2.2 ₍₅₎	4.1 ₍₁₅₎	3.6 ₍₂₀₎
	Y3	1.5 ₍₁₀₅₎	1.6 ₍₁₁₇₎	1.6 ₍₄₎	1.6 ₍₂₂₆₎	2.0 ₍₇₎	3.1 ₍₁₀₈₎	3.6 ₍₇₎	4.0 ₍₁₀₎	3.8 ₍₁₇₎
Lancashire	L1	1.7 ₍₇₅₎	2.2 ₍₃₇₎	— ₍₀₎	1.8 ₍₁₁₂₎	1.8 ₍₅₎	3.7 ₍₉₉₎	3.4 ₍₁₇₎	6.0 ₍₂₅₎	4.9 ₍₄₂₎
North Wales	NW1	2.4 ₍₁₂₈₎	2.6 ₍₁₀₄₎	2.7 ₍₃₎	2.5 ₍₂₃₅₎	2.7 ₍₃₎	2.9 ₍₁₈₇₎	7.0 ₍₃₅₎	9.1 ₍₁₃₎	7.5 ₍₄₈₎
Nottinghamshire	NT1	2.0 ₍₉₂₎	1.8 ₍₅₀₎	1.6 ₍₂₎	1.9 ₍₁₄₄₎	2.1 ₍₅₎	2.5 ₍₆₆₎	4.7 ₍₆₎	6.0 ₍₁₃₎	5.6 ₍₁₉₎
Staffordshire	ST1	1.4 ₍₂₂₎	1.4 ₍₁₆₎	— ₍₀₎	1.4 ₍₃₈₎	— ₍₀₎	1.8 ₍₁₄₎	4.4 ₍₃₎	4.0 ₍₂₎	4.2 ₍₅₎
	ST2	1.7 ₍₁₆₎	1.9 ₍₂₄₎	1.4 ₍₅₎	1.8 ₍₄₅₎	— ₍₀₎	3.6 ₍₄₅₎	8.0 ₍₅₎	9.0 ₍₉₎	8.7 ₍₁₄₎
Warwickshire	W1	1.6 ₍₁₀₅₎	1.6 ₍₁₂₄₎	1.8 ₍₂₀₎	1.6 ₍₂₄₉₎	2.2 ₍₃₎	2.2 ₍₁₁₃₎	2.8 ₍₆₎	2.9 ₍₅₎	2.8 ₍₁₁₎
South Wales (Anthracite)	SWA1	1.5 ₍₄₅₎	1.6 ₍₄₁₎	1.9 ₍₅₎	1.6 ₍₉₁₎	2.0 ₍₁₎	2.1 ₍₅₃₎	1.5 ₍₃₎	6.1 ₍₇₎	4.7 ₍₁₀₎
	SWA2	1.4 ₍₇₄₎	1.5 ₍₄₁₎	1.4 ₍₆₎	1.4 ₍₁₂₁₎	1.5 ₍₂₎	1.8 ₍₇₇₎	7.9 ₍₅₎	6.4 ₍₆₎	7.1 ₍₁₁₎
South Wales (Steam Coal)	SWS1	1.4 ₍₁₁₆₎	1.5 ₍₃₇₎	1.2 ₍₂₎	1.4 ₍₁₅₅₎	1.6 ₍₅₎	1.6 ₍₈₂₎	2.1 ₍₄₎	3.6 ₍₆₎	3.0 ₍₁₀₎
	SWS2	1.4 ₍₁₇₉₎	1.5 ₍₉₃₎	1.3 ₍₁₃₎	1.4 ₍₂₈₅₎	1.6 ₍₆₎	1.5 ₍₁₂₂₎	2.1 ₍₁₈₎	2.5 ₍₈₎	2.3 ₍₂₆₎
	SWS3	1.5 ₍₁₂₇₎	1.8 ₍₉₇₎	1.9 ₍₁₎	1.6 ₍₂₂₅₎	1.3 ₍₂₎	2.4 ₍₁₂₆₎	3.2 ₍₆₎	4.2 ₍₆₎	3.7 ₍₁₂₎
South Wales (Bituminous)	SWB1	2.1 ₍₁₄₁₎	2.7 ₍₁₂₃₎	5.3 ₍₆₎	2.5 ₍₂₇₀₎	2.8 ₍₁₁₎	5.6 ₍₁₀₈₎	7.0 ₍₂₁₎	5.0 ₍₁₂₎	6.3 ₍₃₃₎
Kent	K1	1.7 ₍₁₂₆₎	1.8 ₍₆₀₎	2.1 ₍₂₎	1.7 ₍₁₈₈₎	1.8 ₍₁₎	2.2 ₍₁₃₉₎	7.2 ₍₁₄₎	6.9 ₍₁₂₎	7.1 ₍₂₆₎

of particles between 0.5 and 5μ to the number between 1 and 5μ , which will be referred to as the " p -ratio". Although the exact size range covered by the particles classed as 0.5 – 1μ by optical microscopy is problematical, it is nevertheless evident that the higher the p -ratio, the greater the proportion

of particles of less than 1μ in the sample. The distribution of the p -ratios in terms of the seven broad classes of general environment at the twenty-six collieries associated with the P.F.R. programme is given in Table 1. It will be seen that the lowest p -ratios are, in general, recorded at the coal face during the coal-getting shift. The ratio tends to be slightly higher on the coal face during the preparation shifts and increases progressively as the samples are located farther away from the coal face, being highest (and most variable) on the surface. Because this order of placing the different environments corresponds inversely with their relative levels of dustiness, it appears that the data are not inconsistent with the presence of a substantial proportion of 0.5 – 1μ dust not associated with the mining activities.

Further support is given to this conclusion by a few simple calculations which show that the measured 0.5 – 1μ concen-

* Mr. B. SKOROBHATYJ, Regional Investigator, P.F.R.

Table 2. *Average dust concentration in terms of general environment*

 (p.p.c.c. 0.5–1 μ)

The figures given in brackets denote the numbers of sampling shifts on which the results are based.

Coalfield	Colliery	Coal face (Longwall C.G.S. and Arcwall)	Coal face (Longwall preparation)	Development (in coal)	Coal face (all shifts)	Hard heading	Elsewhere underground	Surface "dusty"	Surface "non-dusty"	Surface (all occupations)
Scottish	SC1	340 ₍₁₇₉₎	190 ₍₁₆₈₎	220 ₍₁₅₎	270 ₍₃₆₂₎	310 ₍₂₀₎	230 ₍₂₃₃₎	280 ₍₂₀₎	200 ₍₁₁₎	250 ₍₃₁₎
	SC2	170 ₍₁₉₁₎	180 ₍₂₈₄₎	80 ₍₆₎	170 ₍₄₈₁₎	230 ₍₁₅₎	100 ₍₁₁₅₎	— ₍₀₎	100 ₍₁₈₎	100 ₍₁₈₎
	SC3	80 ₍₄₅₎	130 ₍₇₄₎	170 ₍₃₎	110 ₍₁₂₂₎	110 ₍₉₎	70 ₍₈₉₎	20 ₍₁₎	60 ₍₁₂₎	60 ₍₁₃₎
	SC4	120 ₍₁₀₆₎	80 ₍₁₁₇₎	100 ₍₂₃₎	100 ₍₂₄₆₎	260 ₍₉₎	60 ₍₆₉₎	— ₍₀₎	130 ₍₁₀₎	130 ₍₁₀₎
	SC5	200 ₍₇₅₎	160 ₍₅₉₎	120 ₍₂₀₎	170 ₍₁₅₄₎	90 ₍₂₎	110 ₍₅₀₎	80 ₍₄₎	— ₍₀₎	80 ₍₄₎
Northumberland	NH1	340 ₍₁₁₆₎	240 ₍₈₀₎	560 ₍₁₈₎	320 ₍₂₁₄₎	90 ₍₃₎	310 ₍₁₁₁₎	220 ₍₇₎	250 ₍₇₎	240 ₍₁₄₎
	NH2	190 ₍₂₀₂₎	180 ₍₁₈₂₎	200 ₍₁₆₎	190 ₍₄₀₀₎	620 ₍₈₎	180 ₍₁₄₇₎	70 ₍₅₎	200 ₍₁₂₎	160 ₍₁₇₎
Cumberland	C1	140 ₍₁₅₆₎	100 ₍₁₆₇₎	160 ₍₁₉₎	120 ₍₃₄₂₎	80 ₍₁₎	140 ₍₁₆₆₎	180 ₍₈₎	260 ₍₁₄₎	230 ₍₂₂₎
Durham	D1	250 ₍₁₆₁₎	160 ₍₈₅₎	200 ₍₂₄₎	220 ₍₂₇₀₎	110 ₍₂₎	140 ₍₁₃₉₎	120 ₍₁₂₎	130 ₍₆₎	120 ₍₁₈₎
	D2	300 ₍₁₂₃₎	320 ₍₇₈₎	340 ₍₃₃₎	310 ₍₂₃₄₎	500 ₍₂₎	120 ₍₁₄₂₎	180 ₍₈₎	200 ₍₁₂₎	190 ₍₂₀₎
Yorkshire	Y1	300 ₍₁₅₃₎	260 ₍₁₅₃₎	220 ₍₆₎	280 ₍₃₁₂₎	— ₍₀₎	380 ₍₁₅₂₎	250 ₍₇₎	320 ₍₁₉₎	300 ₍₂₆₎
	Y2	310 ₍₇₆₎	260 ₍₄₈₎	470 ₍₃₎	290 ₍₁₂₇₎	800 ₍₂₎	250 ₍₁₇₁₎	130 ₍₅₎	120 ₍₁₅₎	120 ₍₂₀₎
	Y3	220 ₍₁₀₅₎	190 ₍₁₁₇₎	170 ₍₄₎	200 ₍₂₂₆₎	60 ₍₇₎	380 ₍₁₀₈₎	210 ₍₇₎	120 ₍₁₀₎	160 ₍₁₇₎
Lancashire	L1	380 ₍₇₅₎	190 ₍₃₇₎	— ₍₀₎	320 ₍₁₁₂₎	210 ₍₅₎	320 ₍₉₉₎	170 ₍₁₇₎	300 ₍₂₅₎	250 ₍₄₂₎
North Wales	NW1	350 ₍₁₂₈₎	320 ₍₁₀₄₎	220 ₍₃₎	340 ₍₂₃₅₎	420 ₍₃₎	210 ₍₁₈₇₎	300 ₍₃₅₎	320 ₍₁₃₎	310 ₍₄₈₎
Nottinghamshire	NT1	660 ₍₉₂₎	400 ₍₅₀₎	410 ₍₂₎	570 ₍₁₄₄₎	600 ₍₅₎	390 ₍₆₆₎	330 ₍₆₎	100 ₍₁₃₎	170 ₍₁₉₎
Staffordshire	ST1	160 ₍₂₂₎	70 ₍₁₆₎	— ₍₀₎	120 ₍₃₈₎	— ₍₀₎	120 ₍₁₄₎	170 ₍₃₎	30 ₍₂₎	110 ₍₅₎
	ST2	150 ₍₁₆₎	130 ₍₂₄₎	70 ₍₅₎	130 ₍₄₅₎	— ₍₀₎	160 ₍₄₅₎	210 ₍₅₎	240 ₍₉₎	230 ₍₁₄₎
Warwickshire	W1	80 ₍₁₀₅₎	70 ₍₁₂₄₎	80 ₍₂₀₎	80 ₍₂₄₉₎	110 ₍₃₎	60 ₍₁₁₃₎	70 ₍₆₎	20 ₍₅₎	50 ₍₁₁₎
South Wales (Anthracite)	SWA1	60 ₍₄₅₎	70 ₍₄₁₎	120 ₍₅₎	70 ₍₉₁₎	20 ₍₁₎	40 ₍₅₃₎	10 ₍₃₎	50 ₍₇₎	40 ₍₁₀₎
	SWA2	70 ₍₇₄₎	40 ₍₄₁₎	50 ₍₆₎	60 ₍₁₂₁₎	20 ₍₂₎	60 ₍₇₇₎	140 ₍₅₎	110 ₍₆₎	120 ₍₁₁₎
South Wales (Steam coal)	SWS1	100 ₍₁₁₆₎	60 ₍₃₇₎	100 ₍₂₎	90 ₍₁₅₅₎	50 ₍₅₎	50 ₍₈₂₎	80 ₍₄₎	70 ₍₆₎	70 ₍₁₀₎
	SWS2	80 ₍₁₇₉₎	40 ₍₉₃₎	60 ₍₁₃₎	70 ₍₂₈₅₎	60 ₍₆₎	40 ₍₁₂₂₎	90 ₍₁₈₎	30 ₍₈₎	70 ₍₂₆₎
	SWS3	240 ₍₁₂₇₎	150 ₍₉₇₎	200 ₍₁₎	200 ₍₂₂₅₎	300 ₍₂₎	170 ₍₁₂₆₎	40 ₍₆₎	30 ₍₆₎	40 ₍₁₂₎
South Wales (Bituminous)	SWB1	180 ₍₁₄₁₎	170 ₍₁₂₃₎	520 ₍₆₎	180 ₍₂₇₀₎	230 ₍₁₁₎	320 ₍₁₀₈₎	240 ₍₂₁₎	80 ₍₁₂₎	180 ₍₃₃₎
Kent	K1	120 ₍₁₂₆₎	100 ₍₆₀₎	150 ₍₂₎	110 ₍₁₈₈₎	70 ₍₁₎	110 ₍₁₃₉₎	620 ₍₁₄₎	120 ₍₁₂₎	390 ₍₂₆₎

at any particular colliery, invariably highest on the coal face, decreasing to a minimum on the surface.

The results are further illustrated in Figs. 1, 2 and 3. In Fig. 1(a), the 0.5–1 μ concentrations recorded at the coal face on the coal-getting shift at each of the twenty-six collieries are plotted against the corresponding data for the preparation shifts. If anything, the preparation-shift concentrations in this size and range might be expected to be higher, because more work in stone is usually performed than on the coal-getting shift, and the hard-heading results (Table 2) tend to support the general view that stone dust often (but not always) has a finer size distribution than coal dust. In fact, however, there is a fairly good one-to-one correspondence for most of the collieries, with a tendency towards the reverse effect. The corresponding relationship for the 1–5 μ size range is illustrated in Fig. 1(b), which shows that the differences in 1–5 μ concentrations between the coal-getting and preparation shifts are generally more marked than the differences in the 0.5–1 μ concentrations. The implication of these two sets of results is that a high proportion of the 0.5–1 μ fraction of the dust is not produced on the coal face.

Figs. 2(a) and 2(b) respectively compare the 0.5–1 μ and 1–5 μ concentrations on the coal face (all shifts) and else-

where underground, and similarly support the contention that a comparatively small proportion of the 0.5–1 μ dust is actually produced in the course of the mining operations. Indeed, at certain collieries, a lower concentration of 0.5–1 μ dust is present at the coal face than elsewhere underground, and the differences between the 0.5–1 μ and the 1–5 μ dust fractions are even more marked.

In Figs. 3(a) and 3(b) the corresponding results are shown, comparing elsewhere underground with "non-dusty" surface occupations, that is, the environment on the surface in the vicinity of the colliery where the dust concentrations are the result of atmospheric pollution. Here the data show a wider scatter and the results at a few pits appear to be anomalous. In general, however, the 0.5–1 μ concentrations lie reasonably evenly distributed around the 45 degree line, contrasting very strongly with the 1–5 μ concentrations. It must be noted that the numbers of results for surface measurements are much smaller than those for the underground samples and, in addition, the surface concentrations themselves are lower.

The variation in the reported dust concentrations along the underground roadways is illustrated in Table 3, which refers to the results obtained at five selected collieries in different coalfields. The concentrations recorded in the 1–5 μ size

SIZE DISTRIBUTION OF AIRBORNE DUST SAMPLES FROM BRITISH COALMINES

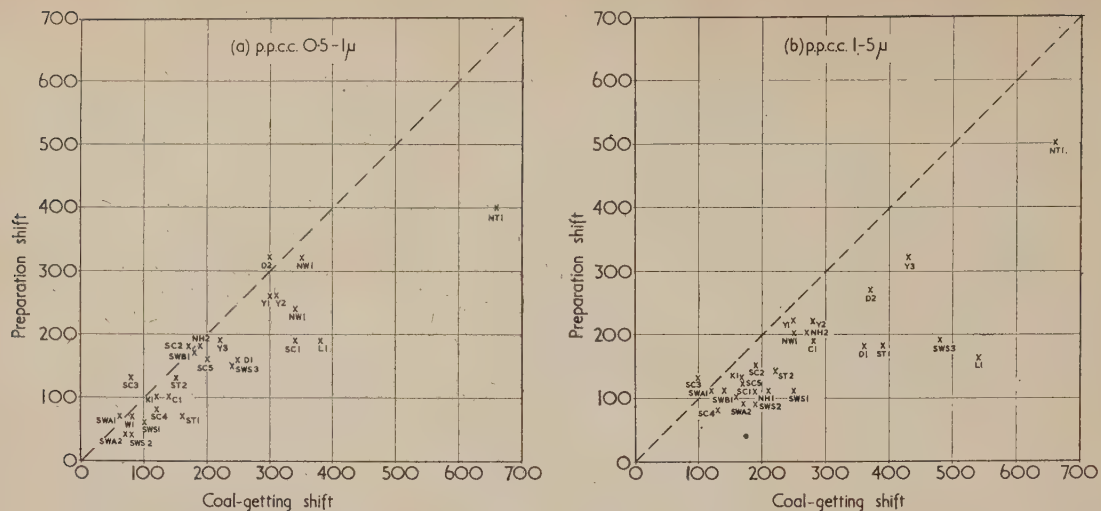


Fig. 1. Comparison of concentrations reported on coal face during coal-getting and preparation shifts (key: see tables)

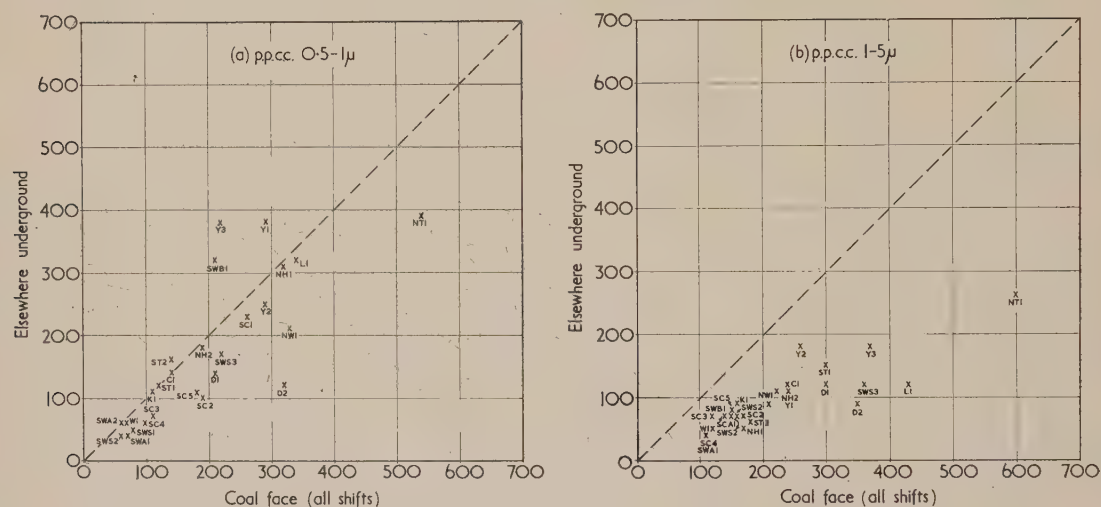


Fig. 2. Comparison of concentrations reported on coal face (all shifts) and elsewhere underground (key: see tables)

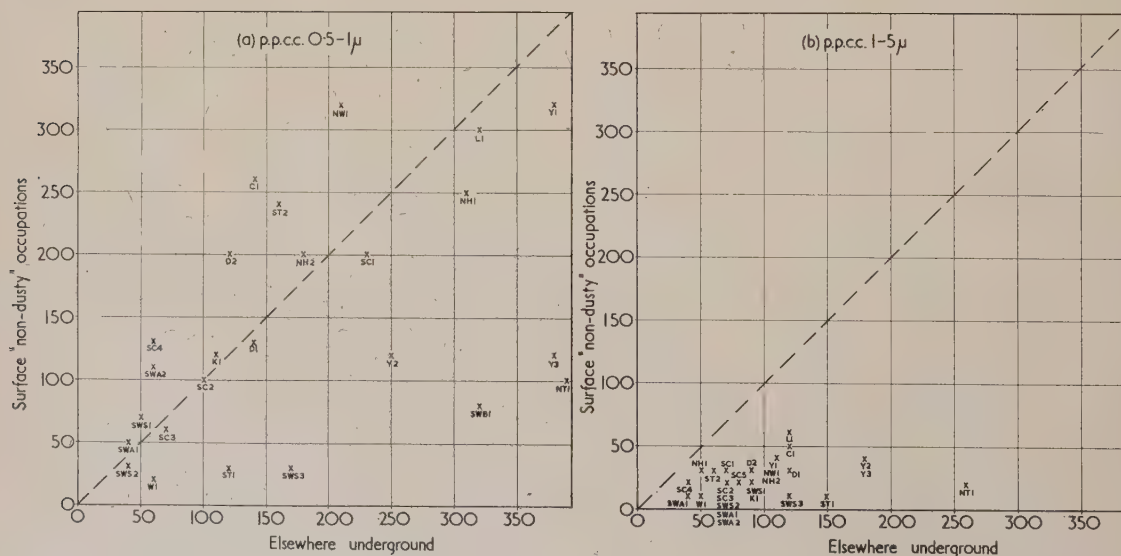


Fig. 3. Comparison of concentrations reported elsewhere underground and for "non-dusty" surface occupations (key: see tables)

range (Table 3a) show a general increase between the downcast pit bottom and the intake roadways and between the intake and return roadways, falling again at the upcast pit bottom. The 0.5–1 μ concentrations (Table 3b) show a similar trend, but the differences between the various locations are very much less marked.

Table 3. *Average dust concentrations in underground roadways*

The figures given in brackets denote the numbers of sampling shifts on which the results are based.

<i>a—p.p.c.c. 1–5 μ</i>					
<i>Coalfield</i>	<i>Colliery</i>	<i>Downcast pit bottom</i>	<i>Intake roadways</i>	<i>Return roadways</i>	<i>Upcast pit bottom</i>
Scottish	SC4	15 (4)	25 (17)	60 (14)	25 (7)
Durham	D1	40 (6)	120 (86)	200 (8)	70 (6)
Nottinghamshire	NT1	90 (6)	250 (44)	360 (9)	110 (6)
Warwickshire	W1	30 (14)	55 (112) (a)	60 (14) (a)	40 (1)
South Wales (Steam coal)	SWS3*	(a) 30 (16)	70 (16) (b) 130 (11)	110 (8) (b) 300 (7)	(b) 100 (21)
<i>b—p.p.c.c. 0.5–1 μ</i>					
<i>Coalfield</i>	<i>Colliery</i>	<i>Downcast pit bottom</i>	<i>Intake roadways</i>	<i>Return roadways</i>	<i>Upcast pit bottom</i>
Scottish	SC4	50 (4)	60 (17)	65 (14)	25 (7)
Durham	D1	125 (6)	120 (86)	245 (8)	130 (6)
Nottinghamshire	NT1	260 (6)	220 (44)	350 (9)	300 (6)
Warwickshire	W1	50 (14)	55 (112) (a)	50 (14) (a)	40 (1)
South Wales (Steam coal)	SWS3*	(a) 80 (16)	70 (16) (b) 55 (11)	130 (8) (b) 120 (7)	(b) 80 (21)

* At this colliery, two seams are worked in one of which [denoted (a)] the coal haulage is located in the intake airways and in the other [denoted (b)] the coal haulage is located in the return airway.

These results, which are based on an extensive sampling programme at a number of collieries covering all the major coalfields in the United Kingdom, are consistent with the hypothesis that many of the particles of less than 1 μ in diameter found in airborne dust in coalmines are present as a result of atmospheric pollution and do not arise in the main from mining operations. This leads to an interesting possibility. Since pneumoconiosis is not found amongst coal-workers whose working history has been confined to "non-dusty" surface work, it may be that the hazard associated with atmospheric pollution so far as radiological pneumoconiosis is concerned is negligible compared with that from the dust generated underground. The concentration of dust particles of less than 1 μ in size would thus appear to be of little importance from this point of view. However, further evidence of a more direct nature is required before other possible explanations can be ruled out. For example, the nature of the below-1 μ component of the airborne dust may vary from one part of the pit to another, and investigations on these lines are to be carried out.

Distribution of the above-1 μ component of the dust

From the results described in the previous section, it is apparent that the presence of atmospheric pollution makes it

desirable to confine detailed optical-microscope studies of the size distribution of the dust clouds associated with mining operations to the above-1 μ component. It should be borne in mind that the data examined represent the size distribution of the particles actually deposited on the thermal-precipitator cover glass, as opposed to the distribution of particles in the breakage products which give rise to the dust cloud being sampled. Watson⁽¹¹⁾ has shown that there is a selective reduction in the sampling efficiency of the thermal precipitator as the particle size increases, and that the losses become appreciable for particles of above about 10 μ . Gravity settlement in the dust cloud will lead to a further reduction in the number of larger particles, so that it is likely that the samples examined will be deficient in the larger particles compared with the actual dust cloud being sampled.

The size distribution of an airborne dust may conveniently be described in terms of the "number-size" distribution, denoted $f_N(x)$, where x represents the particle diameter. The proportion of particles having diameters lying between x_1 and x_2 is then given by the expression:

$$P(x_1, x_2) = \int_{x_1}^{x_2} f_N(x) dx \quad (1)$$

As consideration is to be restricted to the above-1 μ component, then:

$$\int_1^{\infty} f_N(x) dx = 1 \quad (2)$$

Associated with the number-size distribution are the "area-size" distribution, denoted $f_A(x)$, and the "weight-size" distribution, denoted $f_W(x)$. On the assumption that particle shape and density are independent of size, these distributions may be derived from the number-size distribution by the following relationships:

$$f_A(x) \propto x^2 f_N(x) \quad (3)$$

and

$$f_W(x) \propto x^3 f_N(x) \quad (4)$$

As the greater part of the data concerning the size distribution of samples of airborne dust available in the literature, and all the data obtained by the P.F.R. Unit, refer to the number-size distribution, the subsequent analysis will be carried out in these terms. This has the advantage of avoiding complicating factors such as the possible variations of particle shape and density (coal has a specific gravity of about 1.4 and rock about 2.4) with size.

In the search for a suitable mathematical law to represent the number-size distribution, three factors must be borne in mind. First, and most important, the theoretical relationship must agree with the experimental data. Second, it should be consistent with some physical explanation of the processes of breakage and collection by which the dust cloud is generated and sampled. Third, the mathematical calculations associated with the estimation of the parameters of the distribution in any particular case should be as simple as possible, consistent with the first two requirements.

The size distribution of airborne dust samples from British coalmines was investigated in a systematic manner by Wynn and Dawes,⁽³⁾ who proposed a two-component number-size distribution of the form:

$$f_N(x) = C_1 \exp(-\alpha x) + C_2 \exp(-\beta x) \quad (5)$$

where the first term represents the component of the dust cloud covering the majority of the particles of less than about 0.5–1 μ and the second term represents the component of

the dust cloud covering the majority of the particles of about $0.5\text{--}1\text{ }\mu$ and over. These authors emphasized that there was no direct justification for the assumption that the below- $0.5\text{ }\mu$ cloud was exponential in form. Work by Weinstein,⁽²⁾ which suggests that the sizing of particles of less than $1\text{ }\mu$ with the optical microscope is open to considerable doubt, emphasizes the importance of this reservation. More recently, Dawes and Maguire⁽⁶⁾ have proposed that the above- $1\text{ }\mu$ fraction of the dust may be divided into two exponential components, one of which covers the distribution up to about $6\text{ }\mu$ and the other the distribution above about $6\text{ }\mu$.

A critical study of the laws governing the size distribution of airborne dust has been made by Sichel,⁽⁷⁾ who was particularly concerned with conditions in South African mines. After considering the application of the Wynn-Dawes relationship to the size distributions of some thermal precipitator samples taken during a drilling test in a gold mine, Sichel concluded that it did not provide a satisfactory fit to the data. He also suggested that the Wynn-Dawes relationship did not fit their own data if the particles of greater than about $10\text{ }\mu$ were taken into consideration. The size-distribution law proposed by Sichel is a two-component function of the form:

$$f_N(x) = C_1 \exp(-\alpha\sqrt{x}) + C_2 \exp(-\beta\sqrt{x}) \quad (6)$$

where the first component covers the range $0.13\text{--}0.80\text{ }\mu$ and the second the range $0.80\text{ }\mu$ and above. It will be noted that equations (5) and (6) are very similar in form, the only point of difference being that x in equation (5) is replaced by \sqrt{x} in equation (6). Sichel's work has been criticized (by Lambrecht,⁽⁷⁾ for example) on the grounds that the experimental data considered were not representative.

A third relationship to describe the number-size distribution has been proposed by Hamilton and Knight,⁽⁸⁾ as a result of their work on the size distribution of fine disintegration products produced by the breakage of coal and various coal measure rocks. This is the "power-law", which takes the form:

$$f_N(x) = Cx^{-\beta} \quad (7)$$

The above considerations, taken in conjunction with the assumption that the below- $1\text{ }\mu$ dust consists mainly of atmospheric pollution, suggest that the above- $1\text{ }\mu$ dust may be described in terms of a single-component, one-parameter law, which may take one of the following forms:

$$f_N(x) = C \exp(-\beta x) \quad (8)$$

$$f_N(x) = C \exp(-\beta\sqrt{x}) \quad (9)$$

$$f_N(x) = Cx^{-\beta} \quad (10)$$

Alternatively, the above- $1\text{ }\mu$ dust may be described in terms of a two-component exponential-law of the form:

$$f_N(x) = C_1 \exp(-\beta_1 x) + C_2 \exp(-\beta_2 x) \quad (11)$$

when β_1 and β_2 cover the distributions below and above about $6\text{ }\mu$ respectively.⁽⁶⁾

To determine which of these four relationships is the most appropriate, it is necessary to examine the fit of the experimental data. This can conveniently be done by plotting the logarithm of the observed number of particles per unit interval of particle size against (in turn) particle size, the square root of particle size and the logarithm of particle size. If the one-component exponential, Sichel, or power-law relationship holds good, then either the first, second, or third

of these plots will be linear. If the two-component exponential law is applicable the plot will consist of two straight lines intersecting at about $6\text{ }\mu$.

The detailed size analyses obtained in the special investigation at the P.F.R. collieries in the Northumberland, Nottinghamshire and Lancashire coalfields are plotted

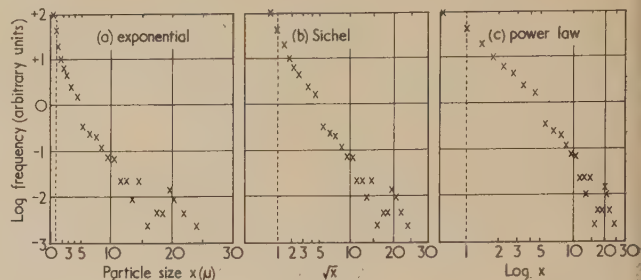


Fig. 4. Number-size distribution. P.F.R. data Northumberland colliery, coal face (preparation shift) machine cutting in floor (4 shifts).

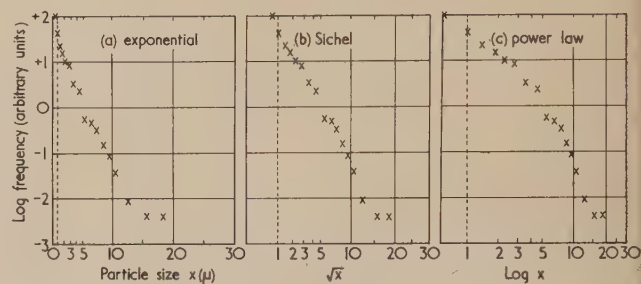


Fig. 5. Number-size distribution. P.F.R. data Nottinghamshire colliery, coal face (filling shift) power loading with Anderton shearer (2 shifts).

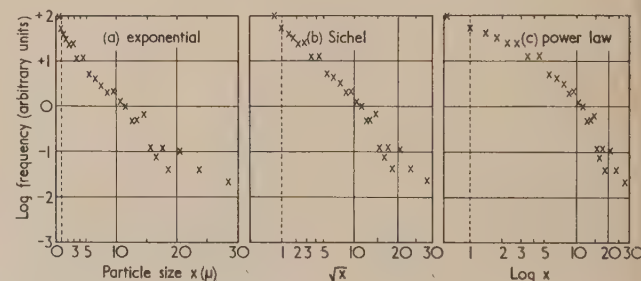


Fig. 6. Number-size distributions. P.F.R. data Lancashire colliery, coal face (filling shift), hand-got using air-picks, ripping in gates (3 shifts).

respectively at Figs. 4, 5 and 6. In Figs. 5 and 6, which cover coal-getting operations, the simple exponential relationship gives at least as good a fit as the others, but in Fig. 4, which refers to machine cutting in stone, the Sichel relationship is slightly more linear, and there is a suggestion that the exponential plot consists of two distinct components. The data presented by Wynn and Dawes⁽³⁾ are illustrated at Figs. 7-9 (Medical Research Council, M.R.C.) and Figs. 10-12 (S.M.R.E.). The particles in excess of $10\text{ }\mu$ (S.M.R.E.) and $11.52\text{ }\mu$ (M.R.C.) have been included in these plots. On the M.R.C. data, which represent coal-getting operations at collieries in Glamorgan, Cumberland and North Staffordshire, the simple exponential relationship is again at least as

good as the others. None of the three one-component laws provides a completely satisfactory fit to the S.M.R.E. data and there is evidence of two distinct components in the exponential plots of these particular distributions.

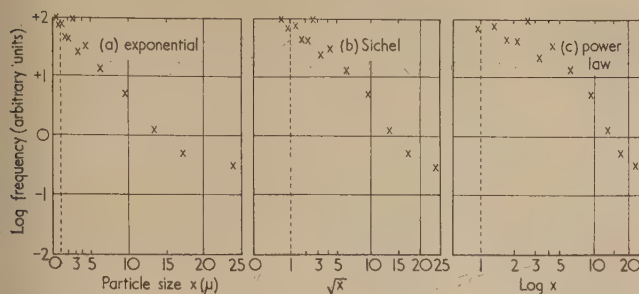


Fig. 7. Number-size distributions. M.R.C. (Watson) data Cumberland colliery, coal face (filling shift).

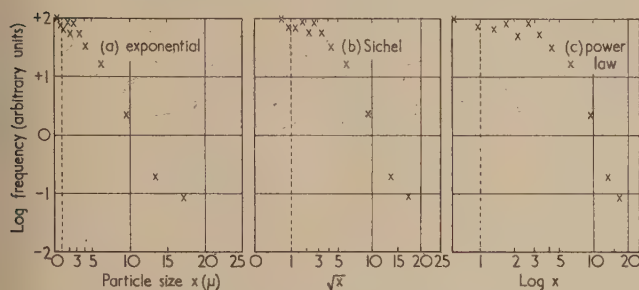


Fig. 8. Number-size distributions. M.R.C. (Watson) data Glamorgan colliery, coal face (filling shift).

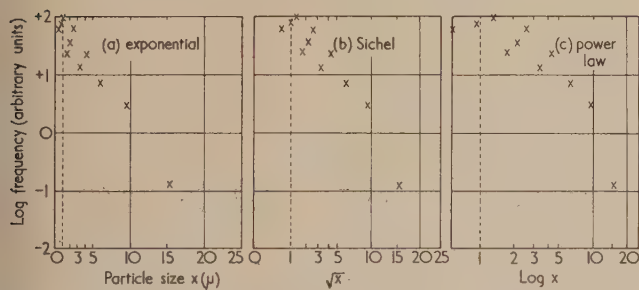


Fig. 9. Number-size distributions. M.R.C. (Watson) data Staffordshire colliery, coal face (filling shift).

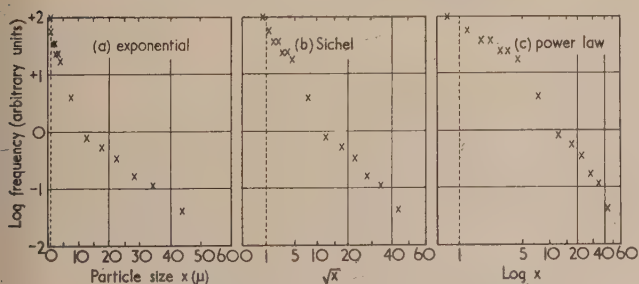


Fig. 10. Number-size distributions. S.M.R.E. data Glamorgan colliery, coal face (filling shift), hand-got using air-picks.

Some information about the size distribution of airborne dust in South African mines is also available in the literature. Tucker⁽⁹⁾ quotes the detailed size analysis up to 4μ of some 1100 thermal-precipitator samples taken during the course of

underground drilling tests between 1939 and 1943. Details are given in Fig. 13, which refers to the samples after ignition and acid treatment. Although there is evidence of a discontinuity in the size-distribution curve at about 2μ , it is apparent that the exponential distribution provides the best fit to the above- 2μ component. The size-distribution analysis quoted by Sichel, which refers to 48 thermal-precipitator slides taken during a drilling test in a gold mine,

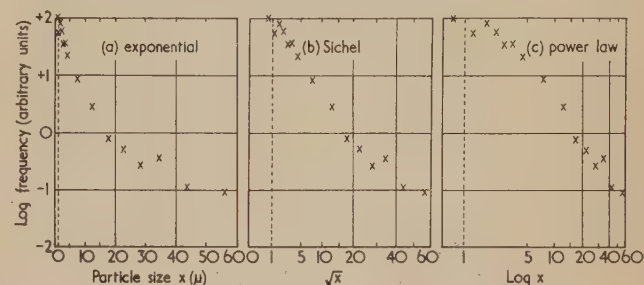


Fig. 11. Number-size distributions. S.M.R.E. data Yorkshire colliery, coal face (filling shift) stripping with experimental machine.

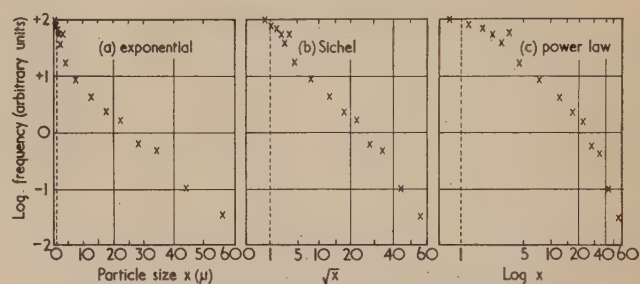


Fig. 12. Number-size distributions. S.M.R.E. data Staffordshire colliery, coal face (preparation shift) machine cutting.

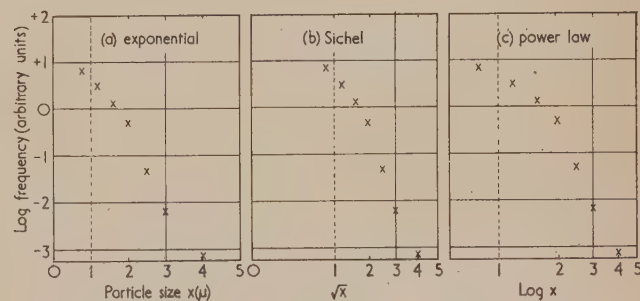


Fig. 13. Number-size distributions. S. African data "Jackhammer" drilling tests, wet-drilling in rock, slides ignited and acid-treated (Tucker).

is illustrated in Fig. 14. Not surprisingly, Sichel's function provides the best agreement with his own data, but the fit is only slightly better than that of the exponential distribution. The data quoted by Kerrich⁽¹⁰⁾ in a paper directed primarily towards illustrating a mathematical technique, are shown in Fig. 15. This size distribution, which refers to a dust cloud in a gold mine, is also best represented by the one-component exponential function.

It appears, therefore, that the simple exponential distribution of Wynn and Dawes gives at least as good a fit as the others to all the size analyses considered, except the S.M.R.E.

data, which are best represented by the two-component exponential distribution, and a few samples associated predominantly with work in stone, for which the Sichel distribution is the most appropriate. In every case, the power law is inadequate to describe the samples of dust collected on the thermal precipitator, the actual numbers of larger particles recorded being lower than the numbers

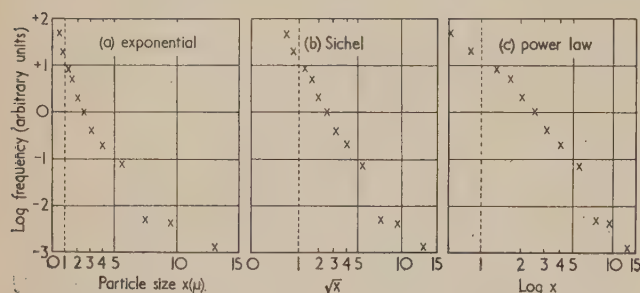


Fig. 14. Number-size distributions. S. African data
Blyvooruitzicht drilling tests, drilling in rock, slides ignited (Sichel).

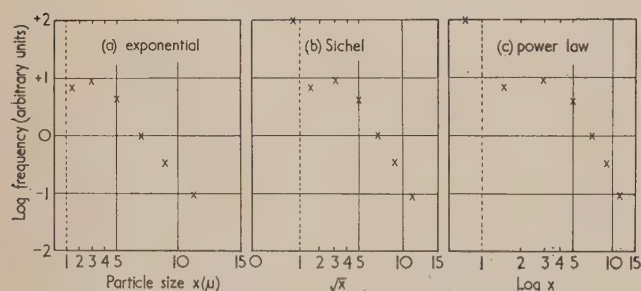


Fig. 15. Number-size distributions. S. African data
Gold mine dust (Kerrich).

predicted, and the difference between the observed and expected frequencies increasing with particle size. This is, perhaps, to be expected. Thus, the theoretical processes involved in the breakage of coal have been considered by Evans and Pomeroy,⁽¹²⁾ who show that the "weakest link" theory is applicable and that the probability of breakage at any particular stress is related to specimen size. Hamilton and Knight⁽⁸⁾ have demonstrated that the size distribution of fine-breakage products (smaller than 100μ) follows the power law and that this law is consistent with the "weakest link" theory. The dust deposit on a thermal-precipitator slide cannot be expected to be entirely representative of the products produced by breakage, in view of the selective removal of the larger sizes because of gravity settlement in the airborne dust cloud and of the sampling characteristics of the instrument. It is, therefore, not surprising that the basic power-law distribution of the breakage products will be modified in the sample and the proportion of larger particles correspondingly decreased. The Sichel distribution represents a "half-way" stage between the power-law and the exponential distribution. It is interesting to note that this distribution provides the best fit to the samples obtained during cutting in stone (Fig. 4) and drilling in rock (Fig. 13). Possibly the instruments concerned were sited in close proximity to these localized sources of dust production and the effect of the gravitational fall-out of the larger particles was thereby reduced.

Of all the results considered, only the S.M.R.E. data give

any real support for the hypothesis of a two-component distribution above 1μ . On all three sets of S.M.R.E. data, the exponent (β_1) of the $1-6 \mu$ dust is larger than that (β_2) of the dust above 6μ . This difference is confirmed by Dawes and Maguire,⁽⁶⁾ who quote average values of about 0.5 and 0.3 for β_1 and β_2 respectively. Thus, their hypothesis of a two-component distribution involves, in general, the assumption that the proportion of particles above 6μ is greater than would be expected on the basis of the one-component exponential distribution for the whole range of particles of 1μ and above. There appears to be no physical justification or other obvious reason for a sudden break in the size distribution at about 6μ , and the question arises whether or not the observed effects in these particular results are due to some artifact of the sampling or counting procedures. Various factors could contribute to the peculiarities observed. For instance, if a sample is taken very close to a source of dust production, the proportion of coarser particles may be unduly high because of "fall-in" through the sampling orifice. Adventitious contamination of the thermal-precipitator slides is also a possibility. Another potential source of error, already mentioned, is the fact that the proportion of particles of above 5μ is relatively small, and it can be shown⁽⁷⁾ that, unless special precautions are taken, the counts of particles recorded in any particular interval of size range may be subject to considerable errors. Finally, it must be remembered that the majority of routine counting is done in the size range $0.5-5 \mu$, and detailed size analyses above 5μ may therefore be subject to error, because of lack of practice by, and checking of, the observers, unless special precautions are taken to standardize and monitor their counting levels. Any one or more of these factors may have contributed to these anomalous results, but whatever the reason, the fact remains that the observed effect is essentially limited to these particular sets of data.

On balance, therefore, the one-component exponential distribution is considered to provide a satisfactory description of the samples of airborne dust clouds obtained with the thermal precipitator during normal mining operations. It provides a good fit to a wide range of experimental results, and agrees at least as well with the bulk of the observations as either of the alternative distributions. It also has the advantage of being more tractable mathematically than the Sichel and power-law distributions. On these grounds it seems reasonable to describe the number-frequency distribution of dust samples obtained with the thermal precipitator by a function of the form:

$$f_N(x) = \beta \exp \beta(1 - x) \quad (12)$$

The term $\beta \exp \beta^*$ is introduced in this expression to satisfy the requirement of a probability distribution that the chance of the occurrence of any particle size within the range under consideration (in this case $1 \mu - \infty$) should be unity. The associated area-size distribution, assuming that shape is independent of size,⁽⁴⁾ is given by the expression:

$$f_A(x) = \frac{\beta^3 x^2}{(\beta^2 + 2\beta + 2)} \exp \beta(1 - x) \quad (13)$$

The corresponding weight-size distribution can be written:

$$f_W(x) = \frac{\beta^4 x^3}{(\beta^3 + 3\beta^2 + 6\beta + 6)} \exp \beta(1 - x) \quad (14)$$

* In this context, β has the dimensions of reciprocal length, and is expressed in μ^{-1} .

The derivation of equation (14) from the number-frequency distribution implies that density is independent of size. In the case of a dust cloud consisting of a single component this is probably true. However, many of the dust clouds encountered in coalmines are of "mixed" composition, and if the density and size-frequency distributions of the coal and non-coal components are very different the assumption will not necessarily apply rigidly.

Variation of the above-1 μ component

The validity of the exponential distribution having been established on the basis of the detailed size analyses, it is possible to examine the variation of the above-1 μ component

the results (given in Table 4) are considered it should be borne in mind that the higher values of β correspond to the less-coarse dust clouds.

The values of β obtained from the coal face during the coal-getting shift vary from 0.77 to 0.40, although most of the results lie between 0.45 and 0.65. In general the highest values are recorded in Scotland and the lowest in South Wales.* These figures may be compared with the results given by Burdekin and Dawes,⁽⁵⁾ who quote an average value for β of 0.475 for coal-face samples taken in the Scottish, Northern, South Western and South Eastern Divisions of the National Coal Board, and an average value of 0.690 for samples in the Durham, West Midlands and East Midlands Divisions. Here, again, the S.M.R.E. data do not follow

Table 4. Size-distribution of the above-1 μ component of the airborne dust samples in terms of general environment (Values of β)

The figures given in brackets denote the numbers of thermal-precipitator samples on which the results are based.

Coalfield	Colliery	Coal face (Longwall C.G.S. and Arcwall)	Coal face (Longwall preparation)	Development (in coal)	Coal face (all shifts)	Hard heading	Elsewhere underground	Surface "dusty"	Surface "non-dusty"	Surface (all occupations)
Scottish	SC1	0.68 ₍₈₄₎	0.68 ₍₅₂₎	0.71 ₍₇₎	0.68 ₍₁₄₃₎	0.60 ₍₄₎	0.82 ₍₃₄₎	0.58 ₍₇₎	0.60 ₍₅₎	0.59 ₍₁₂₎
	SC2	0.58 ₍₂₂₎	0.58 ₍₄₉₎	0.37 ₍₃₎	0.57 ₍₇₄₎	— ₍₀₎	0.52 ₍₂₀₎	— ₍₀₎	0.68 ₍₂₎	0.68 ₍₂₎
	SC3	0.68 ₍₇₎	0.55 ₍₁₃₎	0.47 ₍₁₎	0.59 ₍₂₁₎	0.68 ₍₂₎	0.99 ₍₉₎	— ₍₀₎	0.60 ₍₂₎	0.60 ₍₂₎
	SC4	0.52 ₍₂₂₎	0.60 ₍₃₇₎	0.55 ₍₈₎	0.57 ₍₆₇₎	0.58 ₍₄₎	0.68 ₍₁₃₎	— ₍₀₎	0.77 ₍₅₎	0.77 ₍₅₎
	SC5	0.77 ₍₁₂₎	0.86 ₍₁₃₎	0.77 ₍₈₎	0.81 ₍₃₃₎	1.60 ₍₃₎	1.12 ₍₂₈₎	0.77 ₍₅₎	1.12 ₍₂₎	0.87 ₍₇₎
Northumberland	NH1	0.63 ₍₁₇₎	0.63 ₍₁₆₎	0.68 ₍₇₎	0.64 ₍₄₀₎	— ₍₀₎	0.77 ₍₉₎	0.86 ₍₃₎	1.06 ₍₁₎	0.91 ₍₄₎
	NH2	0.55 ₍₂₉₎	0.55 ₍₂₇₎	0.71 ₍₄₎	0.56 ₍₆₀₎	— ₍₀₎	0.58 ₍₁₅₎	0.37 ₍₃₎	1.20 ₍₁₎	0.58 ₍₄₎
Cumberland	C1	0.55 ₍₃₂₎	0.55 ₍₃₄₎	— ₍₀₎	0.55 ₍₆₆₎	— ₍₀₎	0.50 ₍₂₀₎	0.40 ₍₁₎	0.92 ₍₅₎	0.83 ₍₆₎
Durham	D1	0.58 ₍₂₀₎	0.60 ₍₁₂₎	0.66 ₍₅₎	0.60 ₍₃₇₎	0.86 ₍₁₎	0.66 ₍₁₁₎	0.52 ₍₁₎	0.86 ₍₁₎	0.69 ₍₂₎
	D2	0.52 ₍₂₉₎	0.55 ₍₁₉₎	0.55 ₍₈₎	0.53 ₍₅₆₎	— ₍₀₎	0.52 ₍₁₂₎	0.37 ₍₁₎	0.55 ₍₂₎	0.49 ₍₃₎
Yorkshire	Y1	0.60 ₍₂₈₎	0.58 ₍₁₆₎	0.96 ₍₃₎	0.62 ₍₄₇₎	— ₍₀₎	0.74 ₍₃₀₎	— ₍₀₎	0.86 ₍₃₎	0.86 ₍₃₎
	Y2	0.52 ₍₄₁₎	0.52 ₍₁₉₎	0.47 ₍₂₎	0.52 ₍₆₂₎	0.60 ₍₃₎	0.52 ₍₄₆₎	0.63 ₍₂₎	0.86 ₍₁₎	0.71 ₍₃₎
	Y3	0.55 ₍₂₀₎	0.68 ₍₄₄₎	0.86 ₍₁₎	0.64 ₍₆₅₎	0.89 ₍₂₎	0.66 ₍₂₇₎	0.63 ₍₁₎	1.99 ₍₁₎	1.31 ₍₂₎
Lancashire	L1	0.47 ₍₁₅₎	0.50 ₍₉₎	— ₍₀₎	0.48 ₍₂₄₎	0.71 ₍₁₎	0.50 ₍₁₀₎	— ₍₀₎	— ₍₀₎	— ₍₀₎
North Wales	NW1	0.40 ₍₁₂₎	0.45 ₍₇₎	0.42 ₍₂₎	0.42 ₍₂₁₎	0.50 ₍₁₎	0.47 ₍₁₈₎	0.71 ₍₁₎	0.71 ₍₃₎	0.71 ₍₄₎
Nottinghamshire	NT1	0.66 ₍₃₅₎	0.63 ₍₁₁₎	0.86 ₍₂₎	0.66 ₍₄₈₎	0.77 ₍₂₎	0.63 ₍₁₄₎	1.02 ₍₄₎	0.71 ₍₂₎	0.92 ₍₆₎
Staffordshire	ST1	0.55 ₍₁₅₎	0.47 ₍₈₎	— ₍₀₎	0.52 ₍₂₃₎	0.50 ₍₁₎	0.50 ₍₁₇₎	— ₍₀₎	1.31 ₍₁₎	1.31 ₍₁₎
Warwickshire	W1	0.45 ₍₂₂₎	0.40 ₍₂₀₎	0.47 ₍₆₎	0.43 ₍₄₈₎	— ₍₀₎	0.45 ₍₂₅₎	0.63 ₍₂₎	— ₍₀₎	0.63 ₍₂₎
South Wales (Anthracite)	SWA1	0.45 ₍₅₎	0.50 ₍₁₄₎	0.96 ₍₁₎	0.51 ₍₂₀₎	0.45 ₍₁₎	0.45 ₍₁₁₎	— ₍₀₎	0.63 ₍₁₎	0.63 ₍₁₎
	SWA2	0.45 ₍₂₃₎	0.50 ₍₉₎	0.63 ₍₄₎	0.48 ₍₃₆₎	— ₍₀₎	0.58 ₍₂₀₎	0.71 ₍₁₎	0.63 ₍₁₎	0.67 ₍₂₎
South Wales (Steam coal)	SWS1	0.40 ₍₂₄₎	0.52 ₍₃₎	0.40 ₍₂₎	0.41 ₍₂₉₎	0.50 ₍₃₎	0.37 ₍₁₆₎	0.45 ₍₂₎	0.58 ₍₁₎	0.49 ₍₃₎
	SWS2	0.42 ₍₁₇₎	0.37 ₍₈₎	0.47 ₍₂₎	0.41 ₍₂₇₎	— ₍₀₎	0.42 ₍₁₀₎	0.35 ₍₅₎	0.89 ₍₁₎	0.44 ₍₆₎
	SWS3	0.42 ₍₃₅₎	0.47 ₍₂₂₎	0.63 ₍₁₎	0.44 ₍₅₈₎	0.71 ₍₁₎	0.55 ₍₁₈₎	1.47 ₍₁₎	0.52 ₍₂₎	0.84 ₍₃₎
South Wales (Bituminous)	SWB1	0.45 ₍₂₈₎	0.45 ₍₁₆₎	0.45 ₍₁₎	0.45 ₍₄₅₎	0.71 ₍₁₎	0.47 ₍₁₆₎	0.40 ₍₁₎	0.42 ₍₂₎	0.41 ₍₃₎
Kent	K1	0.45 ₍₃₉₎	0.45 ₍₁₇₎	0.55 ₍₂₎	0.45 ₍₅₈₎	0.45 ₍₃₎	0.50 ₍₂₄₎	0.52 ₍₃₎	0.86 ₍₁₎	0.60 ₍₄₎

from colliery to colliery and from place to place at the same colliery. This can be done in terms of the routine P.F.R. size analyses, which cover the ranges 1–2.5 μ , 2.5–5 μ and above 5 μ . The mathematical procedures required for the estimation of β from these data are given at Appendix I. The necessary computations involve the calculation of the root lying between zero and unity of an eighth-degree equation, the coefficients of which are simple functions of the numbers of particles assigned to the three size groups. When

the same pattern as those obtained in the P.F.R. programme, but, as the authors themselves point out, their results were collected from several different sources, with no direct control over possible biases, and were grouped together

* This effect is not caused by counting biases of the different operators involved. In general, the variations in levels of the counters are small and not systematically distributed with geographical location. The standard deviation for β in Table 4 is of the order of 0.03 for coal-face samples.

"whenever there was no evidence . . . that the populations amalgamated were not homogeneous, and whenever similar operations were in progress". Their emphasis was therefore on operations and not locality.

It will be seen from Table 4 that at the majority of the P.F.R. collieries, the results obtained on the coal face on the preparation shifts are very similar to those on the filling shift. This suggests that there is little difference in the size distributions, in spite of the fact that a greater amount of stone work is generally carried out on the preparation shift. The values of β reported for development in coal and hard-heading work tend to be higher than those on the coal face, but the majority of these figures are based on a small number of sampling shifts and must therefore be treated with reserve. In this connexion, it is interesting to note that Burdekin and Dawes⁽⁵⁾ quote a value of about 0.9 for β associated with samples taken in a hard heading, corresponding to a finer dust than that encountered in their coal-face samples. The size distributions of the P.F.R. samples taken elsewhere underground are similar to those on the coal face, and there is no evidence of any consistent difference between the surface and underground distributions. In summary, therefore, there appear to be marked regional variations in the size distributions of the component of the airborne dust samples associated with mining operations. The differences between the various classes of environment at the same colliery are, however, comparatively small and do not follow any systematic pattern.

Reference to Appendix I shows that it is possible to examine the fit of the data to the exponential distribution by comparing the observed number of particles in the various size ranges with the numbers predicted, and it has been found that for all collieries and classes of environment the agreement between the two sets of figures is good. There is, however, a tendency for the observed numbers of particles in the 1-2.5 μ and the above 5 μ ranges to be slightly higher than expected, and for the observed numbers in the 2.5-5 μ range to be slightly lower. This divergence could well result from the fact that a proportion of the atmospheric pollution consists of particles of aggregates of above 1 μ . In the above-5 μ range, the average difference between the observed and expected numbers of particles is only about 2% of the total. This suggests that if there are, in fact, two exponential components of the above-1 μ dust in the samples obtained at the P.F.R. collieries, the difference between them is very much smaller than that reported by Dawes and Maguire.⁽⁶⁾ Indeed, the difference is so small as to be negligible, and for practical purposes they might, if real, nevertheless be regarded as effectively one and the same distribution.

An estimate of the variation of β in coalmine dust having thus been obtained, it is of some interest to compare the associated number-size, area-size, and weight-size distributions. To do this directly it is, of course, necessary to make the assumption that the shape-factor of the particles is constant in the relevant size range. Work by Cartwright at S.M.R.E. with the optical and electron microscopes has shown that the shape-factors of particles of respirable size do not vary greatly with particle size,⁽⁶⁾ and the effect of such variations has therefore been neglected in the calculations illustrated in Figs. 16, 17 and 18. These plots show the relevant distributions corresponding to values of β of 0.3, 0.4, 0.5, 0.6, 0.7 and 0.8. Although the data considered in this paper refer only to the above-1 μ component of the dust associated with mining operations, there is no reason to suspect a sudden discontinuity in the distribution at about 1 μ and it therefore seems reasonable to interpolate the

exponential distribution curves into the below-1 μ region. There is obviously a lower limit to the particle size, depending on the molecular structure of the material, but it is considered that the errors introduced by taking this limit as zero in the present context will not be appreciable. Table 5 shows the proportion of the dust sample lying in the size ranges 0-0.5 μ , 0.5-1 μ , 1-2.5 μ , 2.5-5 μ and above 5 μ , so calculated and expressed as a percentage of the above-1 μ component, for the number-size, area-size and weight-size distributions.

Reference to Fig. 16 and Table 5a shows that there are wide variations in the number-size distributions as β ranges

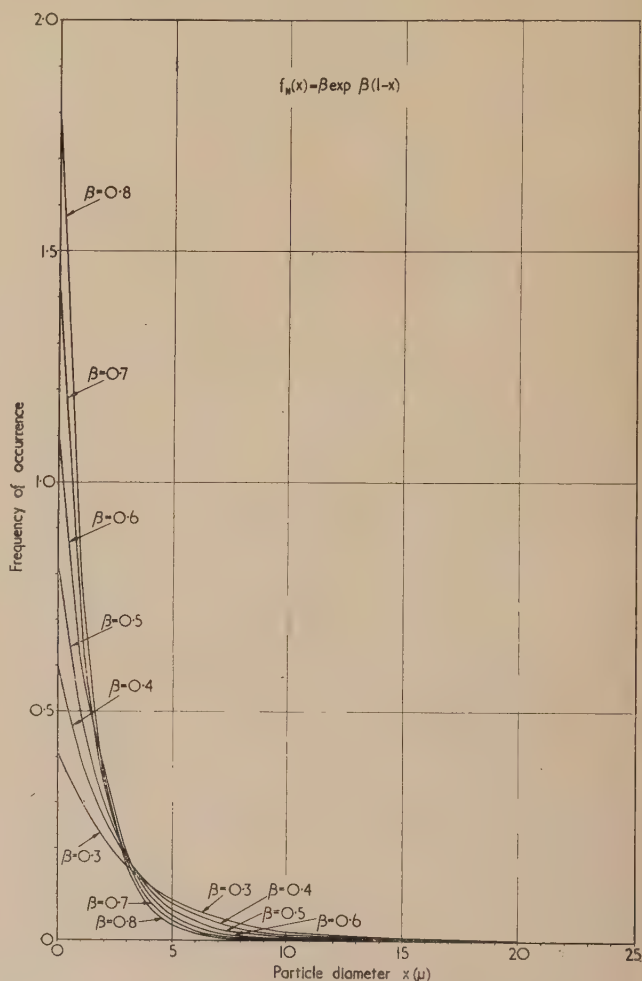


Fig. 16. Number-size distribution of the component of airborne dust associated with mining operations

from 0.3 to 0.8. For example, the proportion of the above-1 μ dust which is in excess of 5 μ varies from about 20% when β equals 0.4 to 6% when β equals 0.7. The corresponding figures for the 0.5-1 μ range are about 22% when β equals 0.4 and 42% when β equals 0.7. There are considerable variations in the numbers of particles in the vicinities of 1 μ and 5 μ , but, at about 3 μ , the numbers are only slightly affected by the value of β .

The area-size distributions (Fig. 17 and Table 5b) show even greater variations with β . The above-5 μ dust represents nearly 70% of the total area of the above-1 μ dust when β equals 0.4, but the corresponding figure when β equals 0.7 is only 33%. It is interesting to note that for none of the values of β considered does the area of the below-1 μ dust

Table 5. Proportions of the dust associated with mining operations in various size ranges, expressed as percentages of the above-1 μ component

a—Number-size distribution

Size range (β)	0-0.5 μ	0.5-1 μ	1-2.5 μ	2.5-5 μ	Above 5 μ
0.3	18.8	16.2	36.2	33.6	30.1
0.4	27.0	22.1	45.1	34.7	20.2
0.5	36.5	28.4	52.8	33.7	13.5
0.6	47.2	35.0	59.3	31.6	9.1
0.7	59.5	41.9	65.0	28.9	6.1
0.8	73.4	49.2	69.9	26.0	4.1

b—Area-size distribution

Size range β	0-0.5 μ	0.5-1 μ	1-2.5 μ	2.5-5 μ	Above 5 μ
0.3	0.0	0.3	3.7	15.1	81.2
0.4	0.1	0.7	7.3	24.5	68.2
0.5	0.2	1.2	11.9	33.0	55.2
0.6	0.4	2.0	17.2	39.5	43.3
0.7	0.6	3.0	23.0	43.8	33.2
0.8	0.8	4.1	29.0	46.0	25.0

c—Weight-size distributions

Size range β	0-0.5 μ	0.5-1 μ	1-2.5 μ	2.5-5 μ	Above 5 μ
0.3	0.0	0.0	0.7	5.8	93.5
0.4	0.0	0.1	1.8	12.4	85.8
0.5	0.0	0.2	3.6	20.5	75.9
0.6	0.0	0.3	6.2	28.8	64.9
0.7	0.0	0.5	9.6	36.5	54.0
0.8	0.1	0.8	13.5	42.7	43.8

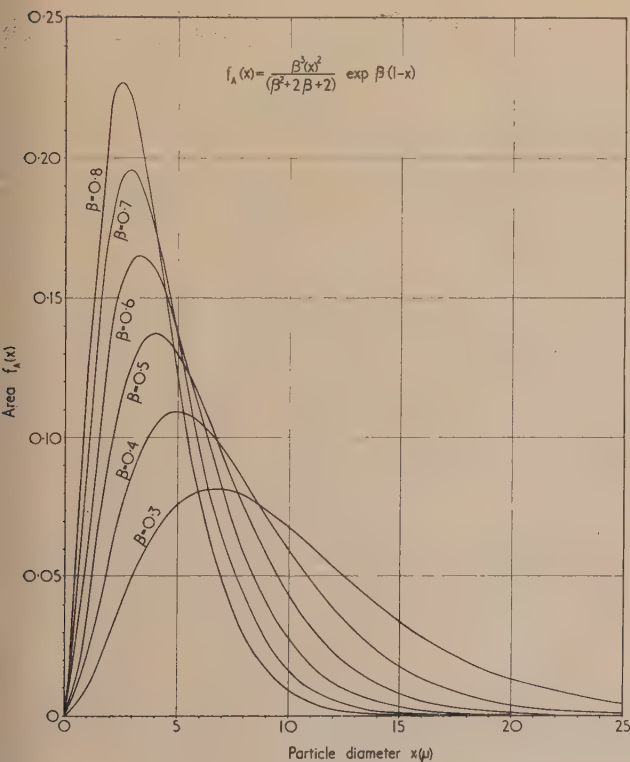


Fig. 17. Area-size distribution of the component of airborne dust associated with mining operations

amount to more than 5% of the total area of the above-1 μ component. There is approximately a 5:1 difference between the total area of the particles in the vicinity of 1 μ as β varies from 0.4 to 0.7.

The effect of the larger particles is further accentuated when the weight-size distribution is considered (Fig. 18 and

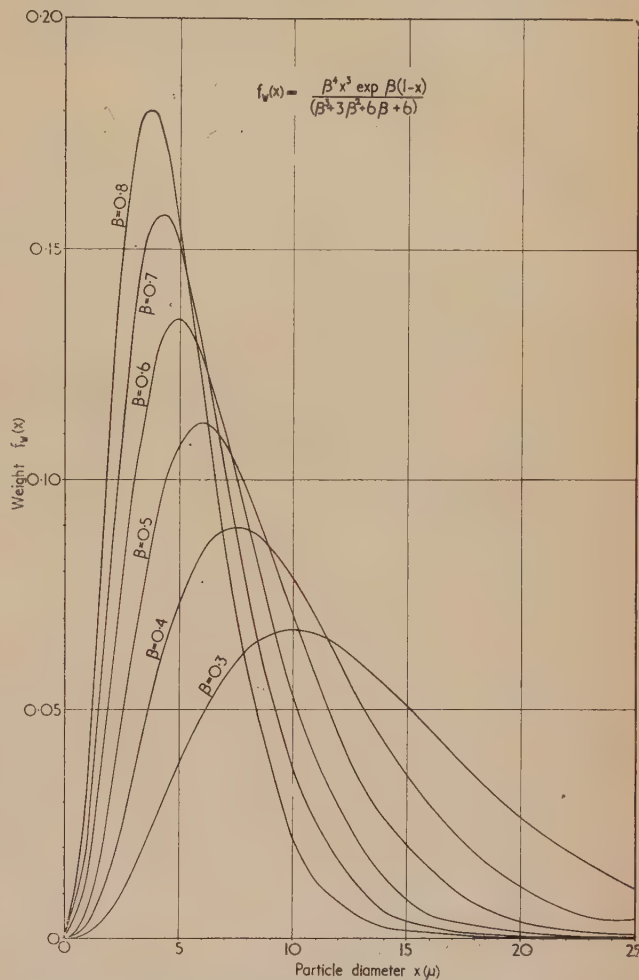


Fig. 18. Weight-size distribution of the component of airborne dust associated with mining operations

Table 5c). The weight of the above-5 μ dust represents more than 85% of the total weight of the above-1 μ component when β equals 0.4, falling to 54% when β equals 0.7. The contribution of the below-1 μ dust to the total weight is negligible for all values of β considered.

The mean particle size is sometimes used as a measure of the size distribution of a dust sample. For the above-1 μ particles in the exponential distribution, this is given by the expression $(1 + \beta)/\beta$. The mean particle sizes when β equals 0.3, 0.4, 0.5, 0.6, 0.7 and 0.8 are thus 4.3, 3.5, 3.0, 2.7, 2.4 and 2.2 μ respectively.

Discussion and conclusions

From the analysis of the results described, four general conclusions can reasonably be drawn regarding thermal-precipitator samples of airborne dust obtained on the coal faces and in the roadways. The data for hard-heading work are insufficient to justify any generalizations.

- (1) The below- $1\ \mu$ particles appear to arise largely from atmospheric pollution and may be negligible from the point of view of the hazard represented by radiological pneumoconiosis.
- (2) The above- $1\ \mu$ dust obeys a simple exponential size-distribution law.
- (3) The average β -values for the exponential function vary with locality.
- (4) At any one colliery, the average β -value is reasonably constant regardless of location and shift.

The evidence quoted in this paper in support of the first conclusion is largely of an indirect nature, but it is in complete accord with previous results reported by the workers at S.M.R.E., and there seems no reason to doubt its validity. An attempt is, however, now being made within the Research programme to collect further evidence of a more direct kind, for instance, by sampling immediately upwind and downwind of sources of dust production on coal faces at different collieries.

The other three conclusions, relating to the size distribution of the above- $1\ \mu$ component, seem well established, and sufficiently convincing to be accepted as generalizations. Nevertheless, it is intended as time and opportunity permit to submit the mass of data available from the P.F.R. environmental studies to a more detailed analysis. For example, it will be possible to investigate the existence of small variations between seams and even faces at the same colliery, as well as differences between collieries. As the result of such more detailed examination of the results, it may be possible to assign reasons for the observed differences. At the present time, the variation of β with locality is not to be explained in terms of obvious factors, such as rank of coal or underground ventilation velocities, and it may well be that some other property, such as the hardness of the coal, is of importance.

The implications of these four general conclusions in respect of a sampling programme such as that involved in the P.F.R. programme are quite wide. The present sampling procedures are based on the assessment of the airborne dust in terms of the $1\text{--}5\ \mu$ particle number concentrations. To a great extent, this policy has been dictated by practical considerations, in that this property has been measured on a routine basis for several years, whereas no suitable alternative means are available, for example, to measure the mass of respirable dust routinely on the required scale. Nevertheless, there is a good case on both theoretical and practical grounds for using the $1\text{--}5\ \mu$ count.

Even if suitable instruments had been available, there is no reliable evidence on which to base the choice of an alternative parameter, such as surface area or mass. The uncertainty is increased because of a further lack of reliable experimental data from which to assess the hazardous size range of airborne dust. It is, of course, possible to calculate theoretically the size ranges of particles which are likely to enter and to be retained by the lung,⁽¹³⁾ and experimental work on human and animal subjects has been reported,^(14, 15) but the value of this information is severely limited by the fact that short-term retention is of relatively little interest. It is much more important to know the long-term retention of dust in the human lung, that is, the dust which remains there in spite of the body's defence mechanism for elimination.

Some information on this latter point is available from the post-mortem examination of lungs of pneumoconiosis sufferers⁽¹⁶⁾ and the implication of the evidence available is that particles larger than about $5\ \mu$ (certainly those larger than $10\ \mu$) are of little importance in radiological pneumo-

coniosis. This immediately sets an upper limit of size for the particles which need to be measured and explains why those larger than $5\ \mu$ have been ignored in measurements of dust concentrations in British coalmines. The arguments set out in the present paper have shown that, whatever the method of assessment (number count, area or mass), the particles below $1\ \mu$ are likely to be of relatively little account. Hence the particles in the size range between 1 and $5\ \mu$ are quite properly those which are routinely estimated.

One final problem which remains to be solved is that concerning which parameter is the best one to use as a measure of risk. If the data analysed in this paper had produced a constant value of β for the above- $1\ \mu$ dusts at the collieries in all the coalfields, then the number count now being carried out would have been immediately interchangeable with either of the other parameters, surface area or mass. As it is, however, there is some variation in the values of β (albeit small, mostly ranging from about $0\cdot45$ to $0\cdot65$) between the various collieries, although fortunately β remains reasonably constant within any one colliery.

This means that the present procedure of recording the $1\text{--}5\ \mu$ number-concentration, together with the knowledge of the β -values, is sufficient to cover any eventualities which are likely to arise. In other words, if the correlations between particle-number counts and progression of pneumoconiosis show local fluctuations it will be possible to investigate them in terms of area and mass concentrations for particles above $1\ \mu$ and up to any reasonable size. In fact, it is an interesting thought that the present measurements being made in the course of the P.F.R. programme may well provide a quite useful, if indirect, contribution to the solution of the problem, so long outstanding, of whether number, surface area or mass of respirable dust is the important factor in coal workers' pneumoconiosis.

Acknowledgements

The authors wish to express their thanks to Mr. B. Skorobohatyj and the Senior Investigators of the P.F.R. team, who collected and evaluated the samples on which much of this analysis is based, and to Mr. D. Hicks, who directed the work, for his constant encouragement and advice. The paper is published by permission of the National Coal Board.

References

- (1) FAY, J. W. J. *Nature (London)*, **180**, p. 309 (1957).
- (2) WEINSTEIN, W. J. *Queckett Microscopical Club*, Series 4, IV, No. 7a (1957).
- (3) WYNN, A. H. A., and DAWES, J. G. *S.M.R.E. Research Report*, No. 28 (1951).
- (4) CARTWRIGHT, J., and SKIDMORE, J. W. *S.M.R.E. Research Report*, No. 139 (1957).
- (5) BURDEKIN, J. T., and DAWES, J. G. *S.M.R.E. Research Report*, No. 149 (1958).
- (6) DAWES, J. G., and MAGUIRE, B. A. *S.M.R.E. Research Report*, No. 150 (1958).
- (7) SICHEL, H. S. *J. South African Institute of Mining and Metallurgy*, **60**, p. 171 (1957).
- (8) HAMILTON, R. J., and KNIGHT, G. *Proceedings of a Conference on the Mechanical Properties of Non-Metallic Brittle Materials*, Paper 21 (London: Butterworths Scientific Publications, 1958).
- (9) TUCKER, H. ST. G. *Brit. J. Appl. Phys.*, **9**, p. 98 (1957).
- (10) KERRICH, J. E. *Biometrika*, **45**, p. 270 (1958).
- (11) WATSON, H. H. *Brit. J. Appl. Phys.*, **9**, p. 78 (1958).

- (12) EVANS, I., and POMEROY, C. D. *Proceedings of a Conference on the Mechanical Properties of Non-Metallic Brittle Materials*, Paper 1 (London: Butterworths Scientific Publications, 1958).
- (13) DAVIES, C. N. *Brit. J. Industr. Med.*, **6**, p. 245 (1949).
- (14) BROWN, J. H., *et al.* *Amer. J. Pub. Health*, **40**, p. 450 (1950).
- (15) WILSON, H. B., *et al.* *Arch. Industr. Hyg. and Occupational Medicine*, **6**, p. 93 (1952).
- (16) BEDFORD, T., and WARNER, C. G. *Brit. J. Industr. Med.*, **7**, p. 187 (1950).

Appendix

Estimation of the Size Distribution Parameter from the Counts in the 1-2.5, 2.5-5 and above-5 μ Ranges

The numbers of particles in the 1-2.5, 2.5-5 and above-5 μ ranges are denoted, respectively, r_1 , r_2 and r_3 . As the number-size distribution is given by the expression $f_N(x) = \beta \exp \beta(1-x)$, the corresponding probabilities are:

$$P_1 = \left\{ \exp \beta(1-x) \right\}_{x=0}^{x=2.5} = 1 - \exp \left(-\frac{3}{2}\beta \right) = 1 - z^3,$$

$$P_2 = \left\{ \exp \beta(1-x) \right\}_{x=2.5}^{x=5} = \exp \left(-\frac{3}{2}\beta \right) - \exp \left(-4\beta \right) = z^3(1 - z^5),$$

$$P_3 = \left\{ \exp \beta(1-x) \right\}_{x=5}^{\infty} = \exp \left(-4\beta \right) = z^8,$$

where $z = \exp \left(-\frac{1}{2}\beta \right)$.

The logarithm L of the likelihood of any particular set of observations may be written:

$$L = \text{constant} + \sum_{i=1}^3 r_i \log P_i.$$

Hence, the maximum-likelihood estimate of the parameter z is given by the expression:

$$g(z) = \frac{dL}{dz} = \sum_{i=1}^3 \frac{r_i}{P_i} \left(\frac{dP_i}{dz} \right) = 0.$$

That is:

$$g(z) = (3r_1 + 8r_2 + 8r_3)z^8 - (8r_2 + 8r_3)z^5 + (3r_1 + 3r_2 + 8r_3)z^3 - (3r_2 + 8r_3) = 0.$$

Now because β is greater than zero, the physically interesting root of the above equation lies between $z = 0$ and $z = 1$. By a consideration of the values of $g(z)$, $g'(z)$ and $g''(z)$ it can be shown that there always exists one such root, which can be determined by the application of Newton's method. Hence the value of β may be obtained from any particular set of data. The asymptotic variance of this estimate is given by the expression:

$$\text{var } \hat{\beta} = -\frac{1}{E} \left(\frac{d^2 L}{d\beta^2} \right) = \frac{1}{n} \sum_{i=1}^3 \frac{1}{P_i} \left(\frac{dP_i}{d\beta} \right)^2.$$

Some statistical aspects of dust counting

by J. R. ASHFORD, M.A., Ph.D., National Coal Board, Scientific Department, London

[Paper first received 16 June, and in final form 26 August, 1959]

Abstract

This paper is concerned with the application of statistical methods to the problem of evaluating samples of airborne dust obtained with the thermal precipitator. A brief description is given of the nature of the dust sample, followed by an outline of the techniques employed to estimate the number of particles deposited. The three main sources of counting variation—systematic differences between observers, basic counting error and random distribution of particles in the dust deposit—are then considered. The effect of size distribution on counting errors is examined and it is shown that this factor may lead to appreciable variation in the recorded counts. Following a short description of various properties of the dust deposit which, although not strictly associated with the counting process, have a bearing on the reported concentration, recommendations are made about optimum procedures for counting thermal-precipitator samples.

Introduction

IT has long been recognized that exposure to airborne dust may be a serious hazard to the health of the men employed in many industrial undertakings. To ensure that environmental conditions are maintained at an acceptable level, there is an obvious need to measure the dust concentration

at the place of employment of all men exposed to a potential risk. In this country, the greatest problem of dust measurement probably occurs in the coal-mining industry, with its many thousands of different working places and wide variation in mining conditions.

The main instrument used by the National Coal Board for the measurement of airborne dust concentrations is the standard thermal precipitator (Green and Watson⁽¹⁾). This instrument is based on the phenomenon of the dust-free space surrounding a hot body. A measured quantity of dust-laden air is drawn past a heated wire and the dust is deposited on to a pair of microscope cover slips placed in the vicinity of the wire. The corresponding dust concentration is then calculated by evaluating a proportion of the dust deposit, using the optical microscope.

The errors involved in measuring the quantity of air sampled by the thermal precipitator are relatively small (Beadle and Kerrich⁽²⁾) but the evaluation of the dust deposit, which involves the subjective assessment by a particular observer of a small fraction of the total sample, leads to a considerable degree of uncertainty in the final estimate of the dust concentration. The purpose of this paper is to examine and assess the main sources of error involved in the evaluation of the dust deposit. Mention is also made of various complicating factors, such as the overlapping of

particles on the cover glass, which although not strictly associated with the counting process have a bearing on the accuracy of the reported dust concentrations. The numerical results quoted in the paper are based on the counts recorded on samples of coalmine dust taken as part of the National Coal Board's Pneumoconiosis Field Research (P.F.R.) programme.⁽³⁾

Evaluation of the dust sample

When any particular sample has been taken with the standard thermal precipitator, the two cover glasses on to which the dust is deposited are mounted on a microscope slide for evaluation. The dust deposit on each cover glass is rectangular in shape and is generally between 9 and 10 mm in length and about 1 mm wide, the exact dimensions depending on the characteristics of the particular instrument used to obtain the sample and on the density of the deposit. The first stage in the evaluation of the dust strip involves the examination of the deposit, using a low-power (16 mm) microscope objective, to check that there are no irregularities. If this preliminary inspection is satisfactory, the length and position of the deposit are determined by reference to the stage vernier on the microscope. The sample is then evaluated using a high power (2 mm) oil-immersion objective.

The total number of particles deposited in the dust strip is so large that it would be an impossibly laborious task for a human observer to evaluate the whole deposit, and counting is normally confined to a series of "traverses", of known width, perpendicular to the length of the deposit. It is the general practice to examine three such traverses on each cover glass, one being located in the centre of the deposit and the others 2 mm from either end, although in certain circumstances the number of traverses may be regulated according to the density of the deposit. By convention, the counts on each traverse are extended to a distance of 1 mm on either side of the centre of the deposit. The total number of particles contained in the volume v of air sampled is estimated by multiplying the number counted n by the ratio of the total area of the deposit A to the area evaluated a . The corresponding dust concentration C is then calculated in terms of particles per cm^3 of air sampled (p.p.c.c.), by means of the expression:

$$C = \frac{nA}{av} \quad (1)$$

The appearance of some typical samples of airborne dust obtained during underground sampling in coalmines, when viewed under the high-power objective, is illustrated in Fig. 1. A frame of reference is provided by the rectangular graticule fitted to the microscope eye-piece, and it is the standard practice in the National Coal Board for the magnification of the microscope to be adjusted so that the graticule represents a rectangle with sides of 30 and 50 μ . The graticule also includes reference circles which represent diameters of 0.5, 1, 2.5, and 5 μ respectively under this magnification. When a particular traverse is evaluated, the dust deposit is moved in a direction perpendicular to its length across the field of view of the microscope, and the number of particles in the particular size range under consideration which lie within the traverse 2 mm in length and 30 μ wide formed by the top and bottom edges of the graticule is recorded. The majority of the counts is made in the 1–5 μ size range, although other size ranges (for example, 0.5–5 μ) are also considered in certain circumstances. Each particle is compared by the observer with the circles on the graticule and is included in the count if its area is considered to lie between the areas of the two circles which define the size

range. In addition to counts of the total number of particles, the observer may also be required to make a visual assessment of the composition of the deposit, each particle being classified as "coal" or "non-coal" according to an agreed set of criteria.

Reference to Fig. 1 shows that there may be considerable differences in the shape, size, and appearance of the particles in the dust deposit. Provided the sampling instrument is in a serviceable condition there is no appreciable variation in these factors, nor in the density of the deposit, along the length

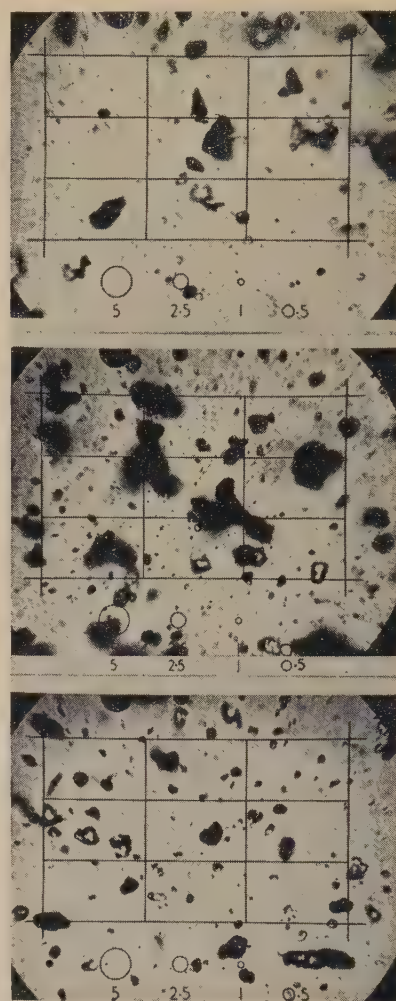


Fig. 1. Typical examples of appearance of samples of coalmine dust under 2 mm oil-immersion objective

of the strip. However, when the variation across the deposit is considered, there is a marked tendency for the density to be greatest in the middle and to decrease towards the edges. A typical density distribution is illustrated in Fig. 2, which shows the counts of the particles lying within the size ranges 0.5–1, 1–2.5, 2.5–5, and above 5 μ , as the field of view of the microscope is moved in 50 μ stages across the dust deposit. It will be noted that there is evidence of a slight systematic difference in size distribution across the strip.

Sources of variation in dust counting

The process of evaluating the dust deposit consists of the measurement of the length of the strip under the low-power

objective, followed by the counting of the particles in the selected traverses under the high-power objective. Experiments carried out by the Pneumoconiosis Field Research (P.F.R.) unit have shown that measurements of strip length made by experienced observers are virtually free from errors

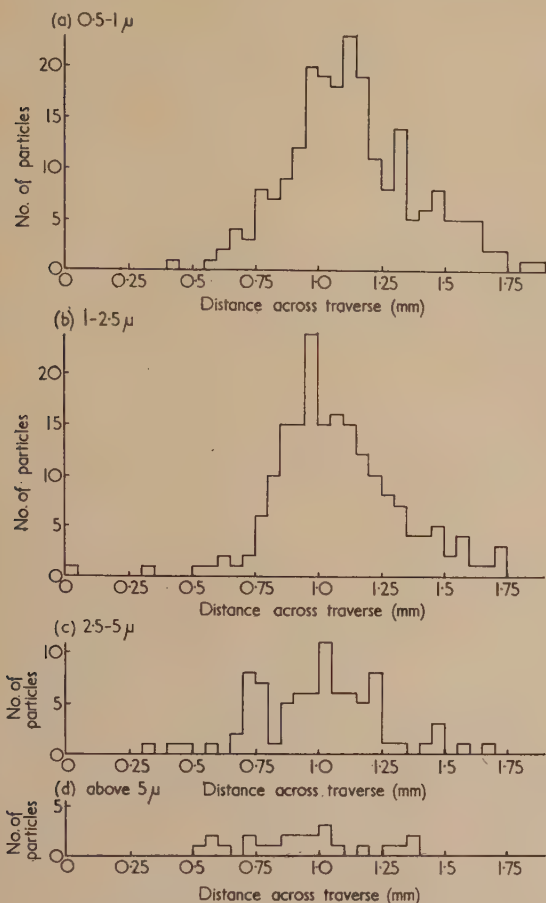


Fig. 2. Distribution of particles across typical dust deposit

of observation and that this factor does not contribute appreciably to the uncertainty of the results. The main sources of error are associated with the counting of the particles in the deposit. The first of these is the random distribution of particles in the dust strip which, as only a small proportion of the total deposit can be examined, leads to sampling variations in the number of particles counted. The second source of variation is the basic error of the counter, as revealed by differences between repeated counts by the same observer on the same traverse. This results from the difficulty of deciding whether or not any particular particle lies within the size range considered, and of "marking-off" particles already counted. As counts of coalmine dust are generally restricted to particles greater than 0.5μ in diameter (which is well within the resolving power of the optical microscope) errors resulting from particular particles being invisible to certain observers do not normally arise. The third factor leading to the uncertainty of the reported dust concentrations is the presence of systematic differences in counting levels between different observers, as revealed when the same deposit is counted many times by different observers. In spite of the existence of the reference circles on the graticule, it is found that some observers may count consistently more or less particles in a given size range than others.

Methods of statistical analysis

It is the accepted practice for the statistical analysis of dust records to be carried out in terms of the logarithm of the actual number of particles counted. One of the main reasons for the use of this transformation is that the variability of the counts tends to increase with increasing numbers of particles examined. This is illustrated in Fig. 3, which gives a comparison of the counts by a particular observer with the average of the counts by six observers on a batch of 36 cover glasses. It will be noted that the variation appears to be relatively constant at all points on the logarithmic scales used in this figure. A further argument in support of the logarithmic transformation is the fact that the characteristic counting level of a particular observer is more likely on

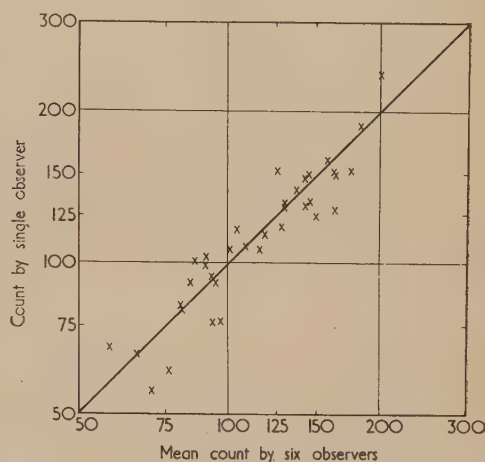


Fig. 3. Comparison of counts by single observer with mean of counts by six observers on a batch of cover glasses ($1-5 \mu$ size range)

general grounds to take the form of a multiplicative, rather than an additive, bias. If a man tends to count "high" or "low" the effect will be to include or exclude from the count a certain proportion of the particles examined, rather than a fixed number of particles however many are considered.

Corresponding to each thermal-precipitator sample, two cover glasses are obtained for evaluation. It is found that, although there is no appreciable difference in size distribution or composition, the density of the dust deposits on corresponding cover glasses belonging to the same sample may differ widely. For this reason it is necessary to consider, each cover glass separately. Thus, it is assumed for the purpose of the statistical analysis that the logarithm of the count x by an observer on a particular traverse can be expressed in the form;

$$\log x = \log m + b + \xi \quad (2)$$

where m represents the average count per traverse of the dust deposit on the cover glass, b the systematic counting bias of the observer at the time the count was made and ξ the random error associated with the non-uniformity of the dust strip and with the basic counting variation. As the statistical analysis is carried out in terms of the logarithm of the actual counts, the random error is most conveniently described by the coefficient of variation, that is, the standard deviation expressed as a percentage of the mean. For similar reasons the systematic bias associated with a particular counter is best expressed as a multiplicative factor.

Systematic variation between counters

The process of evaluating a dust sample involves an element of subjective judgment, and it is not possible to obtain an absolute measure of the true count corresponding to a particular sample. It has been found, however, that the mean count of a number of experienced observers remains stable over a considerable period of time and can therefore be taken as a convenient reference standard. The performance of an individual counter can thus be assessed by circulating a batch of test samples amongst a group of observers and by comparing the counts returned by the individual with the average for the group as a whole.

The variation in the average counting levels of experienced observers with time may be illustrated by the results of one of the counting checks carried out by the P.F.R. unit. This check (Fay, Ashford, and Smith⁽⁴⁾) consisted of a basic design which was repeated at monthly intervals for a period of sixteen months. In this way, an estimate was obtained,

tends to have a characteristic average counting level at any given point in time. It is therefore correct to represent the component of the variability due to systematic differences in counting standards by a constant multiplicative factor, as indicated in equation (2). However, the presence of appreciable systematic bias can only be regarded as unsatisfactory, and it has been found that, by means of regular check counts and training courses, differences between individual counting levels amongst a large group of counters can be reduced to negligible proportions.

Basic counting error

The basic counting variation is represented by the difference between repeat counts on the same particles by a particular observer. The magnitude of this effect can be estimated by making a series of counts by one or more observers, on the same (fixed) traverses. Details of some typical results obtained in this way during the training courses in counting for the

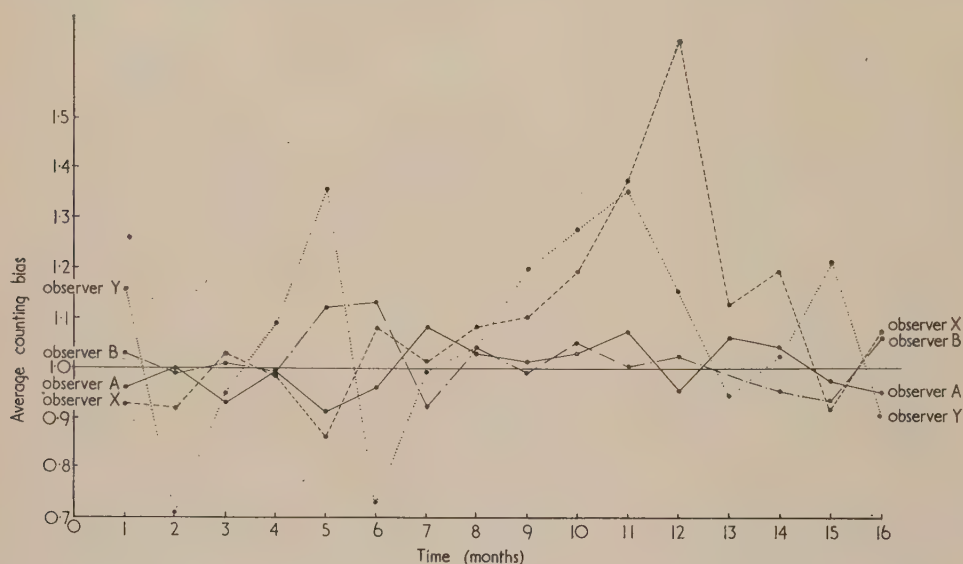


Fig. 4. Variation of counting biases with time (1–5 μ size range)

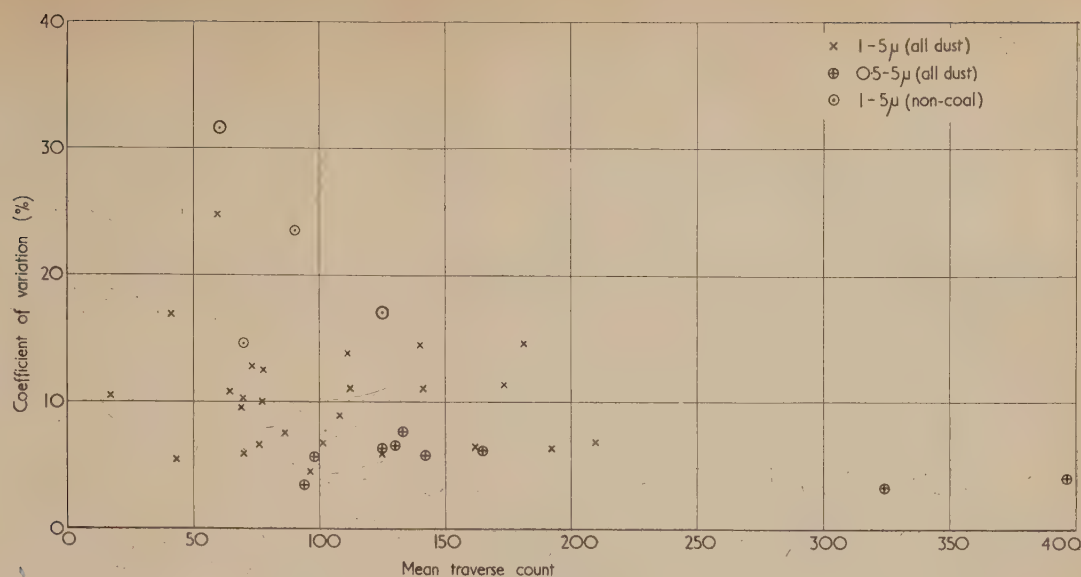
month by month, of the average counting levels of each of the observers taking part. Although the results obtained for any one month in this check are subject to some random variation, because of the comparatively small number of slides involved, the average over two or three months can be taken as a reliable index of the observer's performance. The monthly biases in the 1–5 μ range of four of these observers, referred to the mean counting level for the group as a whole, are shown in Fig. 4. Observers A and B are very experienced counters and their levels were close to the average throughout the whole period. The performances of observers X and Y, on the other hand, were less satisfactory and their counting levels showed systematic deviations from the group average for several months at a time.

By designing the counting checks in such a way that each batch of slides is counted in a pre-assigned order, it is possible to determine whether or not there is any systematic variation in the average counting level of an observer during the course of a single counting session. The results reported on a number of counting trials showed no evidence of any such change, even when a whole day was spent at the evaluation of dust samples.

These results illustrate experience in the P.F.R. unit, based on a study of a hundred different observers over a period of more than five years, that a particular observer

P.F.R. observers are given in Fig. 5. Each of the points shown in this figure is based on the evaluation of a batch of four cover glasses by a group of four or more observers, each traverse being specially set up on the microscope and counted by each of the observers in turn. For counts of all particles in the 1–5 μ size range on a single traverse the coefficient of variation appears to be independent of the number of particles counted, and lies between about 5 and 15%, with an average of about 10%. Counts of all particles in the 0.5–5 μ size range appear to be slightly less variable, with an average coefficient of variation of about 7%. These results are considered to underestimate the normal variability of the 0.5–5 μ counts, which is more usually found to be higher than that of the 1–5 μ counts in the same sample. When the counts of non-coal particles in the 1–5 μ range are considered, the need to decide whether a particular particle should be classed as "coal" or "non-coal" provides an additional source of variability and the coefficient of variation tends to be considerably higher than for counts of all particles.

Experience in the P.F.R. unit has shown that amongst experienced observers who are continuously engaged on the evaluation of slides, there is little variation from person to person in the basic counting error. Amongst observers with little recent counting experience, however, the basic counting error may be considerably higher.



The combined counting errors

The nature of the dust deposit is such that the number of particles contained in a traverse of given width cannot be absolutely uniform along the whole length of the strip. Different traverses will therefore contain different numbers of particles, and the choice of the position of the traverse to be counted will introduce an additional source of variability. On general grounds it is considered that any particular particle of respirable dust in the quantity of air sampled by the thermal precipitator is equally likely to fall in any particular traverse. The number of particles per traverse may therefore be expected to follow a Poisson distribution and, if this is so, the coefficient of variation will be of the same order as 100 times the reciprocal of the square root of the average number of particles in the traverse.

If the counts are made by a particular observer on a number of different traverses on the same cover glass, the variation between the results recorded on the various traverses will provide an estimate of the combined errors of counting. These combined errors represent the summation of the basic counting error and the error arising from the random distribution of particles in the dust deposit. During one of the P.F.R. counting checks a large number of cover glasses, selected at random from the samples obtained during routine survey work, were evaluated in turn by groups of four counters. A separate analysis of variance was carried out on the counts of particles in the 1-5 μ size range recorded on three traverses on each cover glass. The results obtained are illustrated in Fig. 6, where the coefficient of variation on a single traverse has been plotted against the average traverse density. A solid line has been drawn in to show the average trend of these results. For comparison the diagram also shows the coefficient of variation of the errors arising from the random distribution of particles, as predicted by the Poisson theory.

The salient feature of these results is that, in spite of the large differences in the combined counting errors on slides with the same traverse density, there is a general tendency for the variability to decrease with increasing numbers of particles counted, in a similar way to the errors arising from the random distribution of particles predicted by the Poisson theory. The average coefficient of variation decreases from 22% at a mean traverse count of 50 particles to 19% at 75 particles, 17% at 100 particles, 14% at 150 particles, 12%

at 200 particles, and 11% at 250 particles. There is a suggestion that the variability tends to increase again for densities above about 300 particles per traverse but this is not very marked. Most of the results illustrated in Fig. 6 refer to counts on strips with less than about 150 particles per traverse, but the general order of magnitude of the variability of the combined counting errors for higher strip densities is confirmed by the analysis of two further P.F.R. counting checks. In each of these checks the test slides were divided into groups according to their reputed mean traverse count and were evaluated by a number of observers in turn. On the first check there were four traverse density groups, with average traverse counts of about 70, 120, 150, and 270 particles in the 1-5 μ range, and the corresponding coefficients of variation for the combined error based on the counts on the centre traverse only were 20, 15, 15, and 16%. On the second check, there were three traverse density groups with average traverse counts of 90, 120, and 150 particles in the 1-5 μ size range, and the corresponding coefficients of variation for the counts on the centre traverse were 20, 19, and 17%.

The latter results are based on a comparison of the counts recorded by different observers on the centre traverse of each cover glass, each observer following the standard procedures to determine the position of the traverse. If exactly the same traverse had been examined by each observer the coefficient of variation would represent only the basic counting error which, from previous experience, would be of the order of 10%. In fact, however, the observed coefficients of variation tend to be slightly higher than those based on a comparison of counts by the same observer on three different traverses on the same cover glass. This suggests that, in spite of the fact that each observer has tried to locate the same (centre) traverse in accordance with the standard procedures, the errors of measurement are appreciable in comparison with the traverse width (30 μ) and the selection of the "standard" traverses is effectively random.

If the coefficient of variation of the basic counting errors is denoted by C_1 and the coefficient of variation of the errors arising from the non-uniformity of the dust deposit is denoted C_2 , it can be shown (Beadle and Kerrich⁽²⁾) that the coefficient of variation of the combined errors (denoted C_3) is given by the expression,

$$C_3^2 = C_1^2 + C_2^2 \quad (3)$$

On the assumption that the Poisson theory holds good,

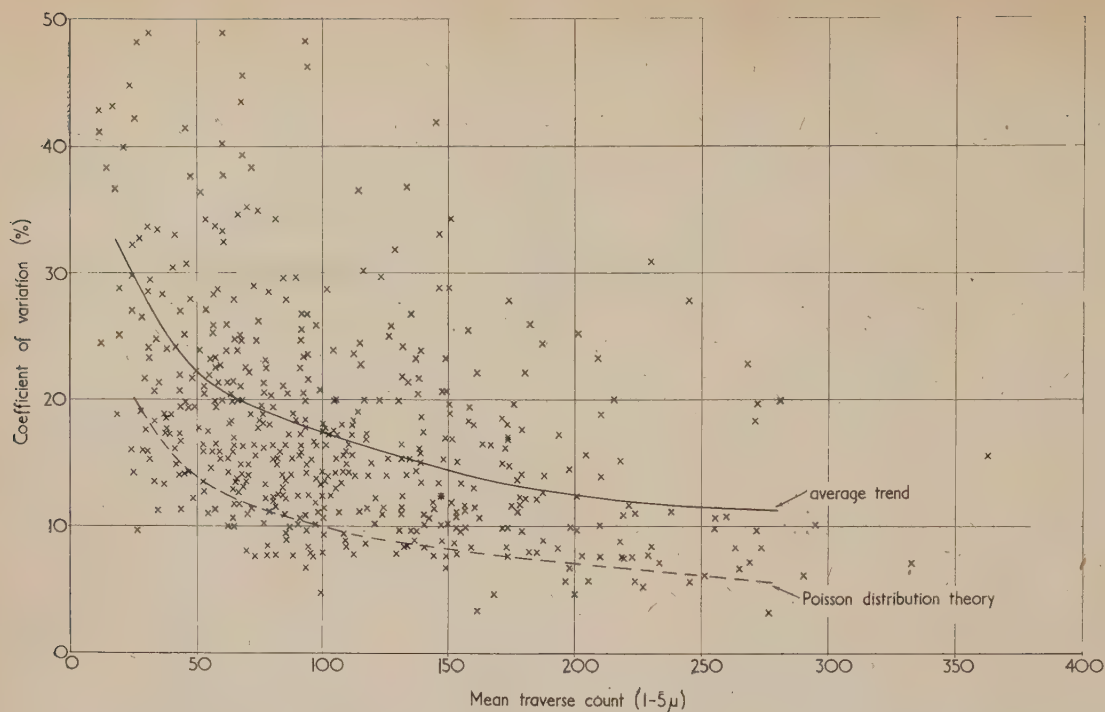


Fig. 6.
Combined
counting
error (1–5 μ
size range)

this means that the average coefficient of variation of the basic counting error in the 1–5 μ size range decreases from about 16% for mean traverse counts of 50 particles to 13.5% for 100 particles, 12% for 150 particles and 10% for 200 and 250 particles. Taken in conjunction with the results described in the previous section, which suggest that the average coefficient of variation of the basic counting error is of the order of 10% for all strip densities, these results indicate that the errors arising from the random distribution of particles in the dust deposit tend to be slightly higher than would be expected by the Poisson theory, particularly for the lower strip densities. This difference is consistent with the existence of a tendency for the deposition of particles to show some departure from randomness. Possibly the particles tend to “attract each other” as they are deposited.

One of the main problems of dust counting is determining what proportion of the total deposit should be evaluated. From the point of view of errors of evaluation the criterion should be to reduce the coefficient of variation of the counts to the lowest practicable value. It appears that, mainly because of the effect of the random distribution of particles in the dust deposit, the coefficient of variation of counts of all particles in the 1–5 μ size range decreases with increasing numbers of particles counted up to a limit of 250–300 particles. On general grounds it is likely that counts in other size ranges, whether of all dust or of “non-coal” particles, will follow the same pattern as counts in the 1–5 μ range, although because of possible differences in the basic counting error the amount of variation may be different. The tendency for the coefficient of variation to reach a minimum value for counts of about 250 particles is confirmed by the work reported by Beadle and Kerrich,⁽²⁾ which is based on counts of all visible particles on dust samples taken in the Witwatersrand gold mines. Similar results have also been reported by Roach.⁽⁵⁾

Effect of size distribution

The results described previously show that there may be considerable differences in the accuracy of the counts by

experienced observers on different slides. Apart from the broad relationship between the combined counting errors and the number of particles examined, it is apparent that other properties of the dust deposit must have a bearing on the variability of the counts. One of the most obvious factors of this kind is the size distribution, as it is to be expected on general grounds that the smaller the proportion of particles whose area is on the borderline of the size range considered the greater will be the counting accuracy.

A detailed study of the size distribution of airborne dust samples from British coalmines (Fay and Ashford⁽⁶⁾) has shown that the number-size distribution of the above 1 μ component of the dust deposit as measured by the standard thermal precipitator may be expressed in the form:

$$f(x) = \beta \exp \beta(1 - x) \quad (4)$$

where x is the particle diameter and β is a variable parameter having the dimensions of reciprocal length. At any one colliery, the value of β corresponding to samples taken on the coal face, elsewhere underground and on the surface are relatively uniform, but there are considerable variations between collieries in different coalfields. The observed values of β vary from about 0.40 in South Wales to about 0.80 in Scotland. The majority of the particles below about 1 μ are associated with atmospheric pollution, although some are represented by the extension of the exponential distribution which covers the dust produced by mining operations. The effect of atmospheric pollution on the size distribution of the below-1 μ dust will depend on the relative proportions of the dust cloud derived from this source and from mining operations. However, the majority of the pollution consists of particles which are considerably smaller than 1 μ and the distribution given by equation (4) provides a reasonable approximation in the vicinity of 1 μ .

The number-size distributions corresponding to β values of 0.4 and 0.8, which represent the extreme values of the size-distribution parameter likely to be encountered in British coalmines, are shown in Fig. 7. The main point to be noted about these distributions is the sharp decrease in the number

of particles with increasing size. When β equals 0.4, there are about five times as many particles in the vicinity of $1\ \mu$ as in the vicinity of $5\ \mu$, and when β equals 0.8, there are about twenty-five times as many. There are also considerable differences between the two distributions, except in the vicinity of $2.5\ \mu$.

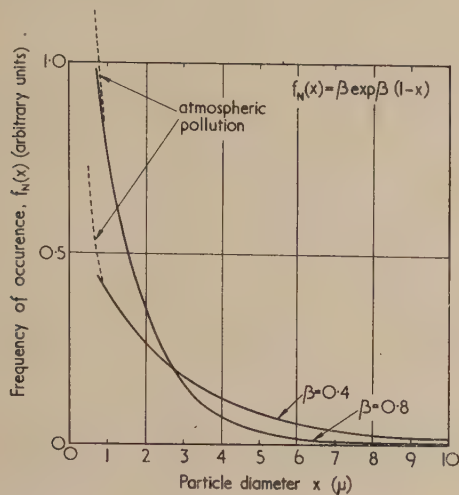


Fig. 7. Number-size distribution of the above- $1\ \mu$ component of airborne dust samples in British coalmines

The basic errors of counting are derived from two main sources. The first of these is associated with the failure to include in the count all the particles of the appropriate size or to count some of these particles more than once. If the observer is experienced and reasonably conscientious, it is unlikely that errors of this kind will depend on the size distribution of the sample or indeed that they will contribute appreciably to the total. The second, and probably the more important, source of error is associated with the difficulty of deciding whether or not a particular particle lies within the appropriate size range. Each particle must be compared in turn with each of the two reference circles which define the boundaries of the size range and a decision taken (possibly after repeated focusing and re-focusing of the microscope) as to whether the projected area of the particle is greater or less than that of the circle. The idea of a systematic counting level in a particular size range is therefore a reflexion of the more fundamental concept of a separate bias on each of the boundaries. In view of the differences between repeat counts on the same particles, it is reasonable to suppose that a random sizing error will be superimposed upon this systematic variation. Thus, if the true area of a particle is denoted x , the sizes attributed to the particle on repeated examinations by a particular observer will be distributed about x with a characteristic "error" distribution, $b(x, t)$, with mean $\{x + b(x)\}$ and variance $\sigma^2(x)$. The probability that the particle will be classed as lying within any given size range (S_1, S_2) is given by the expression:

$$p(x, S_1, S_2) = \int_{S_1}^{S_2} \phi(x, t) dt \quad (5)$$

If the number-size distribution of the dust deposit is denoted $f_N(x)$, the number of particles classed as between S_1 and S_2 will be proportional to the expression:

$$P(S_1, S_2) = \int_0^\infty \int_{S_1}^{S_2} f_N(x) \cdot \phi(x, t) dx dt \quad (6)$$

which relates the counting bias in a given size range to the more fundamental error distributions. It is thus apparent that, for any given error distribution, the conventional counting bias depends on the size distribution of the dust deposit as well as on the performance of the observers.

In general, the bias and variance of the error distribution will be small in comparison with the width of the size range and the only errors of sizing will occur in the immediate vicinity of the boundaries. In view of the shape of the number-size distributions (which are decreasing functions of particle size) the majority of these errors will appear on the lower boundary of the size range, provided the errors of sizing on the two boundaries are of the same order of magnitude. It is thus possible to obtain a rough estimate of the effect of size distribution on counting errors by considering the lower boundary only. For example, if an observer has a bias of $0.25\ \mu$ on the $1\ \mu$ boundary (that is, if he classifies all particles greater than $0.75\ \mu$ as "above $1\ \mu$ ") his true $1-5\ \mu$ count will be increased, on average, by 13% when β equals 0.4 and by 23% when β equals 0.8, assuming that there is no bias on the $5\ \mu$ boundary. Thus, the same fundamental bias can lead to very different estimates of the conventional $1-5\ \mu$ counting level for different size distributions.

If there is no systematic bias on a particular boundary and if, as seems reasonable, the error distribution is symmetrical, the effect of random sizing variations will be to classify some of the "below the boundary" particles as "above the boundary" and an equal proportion of "above the boundary" particles as "below the boundary". However, the number-size distribution is a decreasing function of particle size and there will always be more particles just below the boundary than just above. The random sizing errors will then lead to an over-estimate of the number of particles lying above the boundary and an under-estimate of the number lying below. This effect will be increased as the variance of the error distribution becomes larger.

A practical illustration of the effect of size distribution on counting levels may be obtained from the results of a counting trial in which a batch of 32 cover glasses were evaluated in turn by four observers. On each cover glass, a count was made of the number of particles in the $1-2.5$, $2.5-5$ and above- $5\ \mu$ size ranges, and an estimate of the size distribution parameter β was obtained on the basis of the average results.

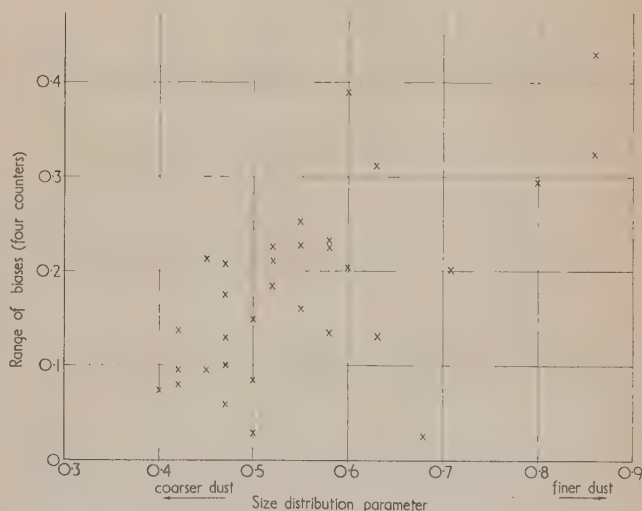


Fig. 8. Effect of size distribution on counting levels ($1-5\ \mu$ size range)

If the four observers each have different sizing errors on the $1\ \mu$ boundary, it is to be expected that the range of the $1\text{--}5\ \mu$ counting biases on any particular cover glass will increase with increasing proportions of particles of about $1\ \mu$ in size. This is confirmed by the results given in Fig. 8, where the range of the four biases is plotted against the size distribution parameter. It will be seen that there is a very marked tendency for the variation in individual biases to increase as the dust deposit becomes finer.

The effect of size distribution on the variability of the counts is illustrated at Fig. 9, where the coefficient of variation of the combined counting errors on each cover glass has been

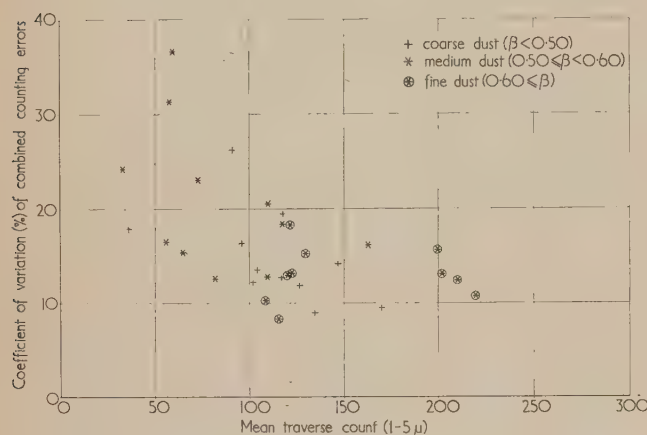


Fig. 9. Effect of size distribution on counting errors ($1\text{--}5\ \mu$ size range)

plotted against the mean traverse count for the three ranges of the size distribution parameter: $\beta < 0.50$ (coarser dust), $0.50 \leq \beta < 0.60$ (medium dust) and $\beta \geq 0.60$ (finer dust). The general tendency for the combined counting errors to decrease with increasing number of particles counted is again apparent and, on the whole, the variability of the counts tends to increase with increasing proportions of small particles. The effect is, however, obscured by the fact that the combined errors include the variability arising from the non-uniformity of the dust deposit, which depends mainly on the number of particles counted.

Complicating factors

Apart from the errors associated with the counting process, there are several other factors which influence the accuracy of the concentrations reported as a result of sampling with the standard thermal precipitator, the most important of which are the overlapping of particles in the deposit, the presence of background contamination on the cover glass and the fall-off of particles from the dust strip. Although a full consideration of these problems would be inappropriate in the present paper, their general effect must be taken into account in any realistic appraisal of counting procedures.

Overlapping. When the dust strip is being formed, some particles may be deposited in such close proximity to others that their images overlap when they are examined under the microscope. In these circumstances, it is normally impossible to determine whether one or more particles is involved or, indeed, whether the aggregate occurred before or after deposition. A standard practice has therefore been adopted whereby an apparent aggregate is regarded as a single particle unless it is possible to separate completely the constituent particles at some stage in the focusing. This means that two

or more overlapping particles may be regarded as a single larger particle and the apparent count will differ from the actual number of particles present in the deposit.

The main factor having a bearing on the overlapping of particles is the density of the dust deposit. If the number of particles in the strip is small, the chance that two will fall sufficiently close together for their images to overlap will be remote. At the opposite extreme, it is conceivable that the dust deposit could be so dense that the whole of the traverse would be obscured and the count reduced to zero. When the effect on counting a whole traverse is considered, it must, of course, be borne in mind that there is a systematic variation in density across the dust strip. Size distribution will also have a direct effect on the amount of overlapping which, for a given density of particles, will increase as the dust becomes coarser. A further relevant factor, although of less practical importance than deposit density and size distribution, is the shape of the dust particles. The least amount of overlapping will take place when the projected area of the particles is circular. Finally, there is at present no conclusive evidence as to whether or not particles tend to "attract" each other as they are deposited. It is apparent that any such effect would tend to increase the amount of overlapping.

The theoretical study of the effect of overlapping resolves itself into a consideration of the problem in terms of the deposition of laminae of known size and shape distribution onto a flat plate, the field of view of the microscope being effectively two-dimensional. Even if it is assumed that there is no tendency towards clustering, the problem is an extremely difficult one and no solution dealing with the effect of overlapping on the counts in a given size range, even in approximate terms, is available in the literature. Empirical studies of the effect have been reported by Roach,⁽⁷⁾ but the universal application of his results is open to doubt because the dust described in his experiments contains an abnormally high proportion of large particles in comparison with samples taken in British coalmines generally. Roach suggests that for an observed $1\text{--}5\ \mu$ count of 50 particles per $30\ \mu$ traverse, the loss from overlapping is about 20%, that for an observed count of 100 particles the loss is about 80%, and that with more than about 120 particles, the correction is infinite (that is, a density greater than about 120 particles in the $1\text{--}5\ \mu$ range per $30\ \mu$ traverse is impossible). On the other hand, studies of the problem by the P.F.R. team (Fay *et al.*)⁽⁸⁾ suggest that for more typical thermal-precipitator samples ($\beta = 0.55$) there is a loss of the order of 20% for an observed count ($1\text{--}5\ \mu$) of 50 particles per $30\ \mu$ traverse, about 40% for observed counts of 100 particles per traverse and about 90% for counts of 150 particles per traverse. It is, however, apparent that whatever the shape and size distributions of the dust being sampled, the lower the density of the dust deposit the smaller will be the effect of overlap.

Contamination. Examination of large numbers of thermal-precipitator samples shows that, in addition to the clearly-defined dust strip, there may also be a background of particles distributed over the whole area of the cover glass. The origin of this background contamination is obscure and even when stringent precautions are taken during sampling, the effect may still occur. As there appears to be no systematic variation in the density of the contamination on the area off the cover glass in the vicinity of the dust strip, it seems reasonable to infer that the same level of contamination is also present in the deposit, and since it is not possible to discriminate between the contamination and the remainder of the dust strip, particles associated with contamination will be included in the count if they lie within the limits of

the traverse. Thus, the effect of contamination will be to lead to an over-estimate of the number of particles deposited in the dust strip.

The effect of contamination shows marked variation from colliery to colliery and from sample to sample at the same colliery. On the routine samples obtained by the P.F.R. unit, the average amount by which the count in the $1\text{--}5\ \mu$ size range on the standard $2\text{ mm} \times 30\ \mu$ traverse is increased is of the order of 10 particles. This will represent an appreciable proportion of the total deposit for mean traverse counts of less than, say, 100 particles.

Fall-off particles. It is the normal practice to separate the cover glass from the micro-slide on which it is mounted by means of a paper ring or a layer of paraffin wax. The dust deposit is thus suspended on the under-surface of the cover glass and any particles dislodged from the strip will fall on to the upper surface of the slide, forming a "lower field" which can be viewed under the microscope by re-focusing, but which is not normally counted. Examination of a large number of slides has shown that an appreciable number of particles may fall from the dust deposit on to the lower field, leading to a corresponding under-estimation of the number of particles deposited. These fallen particles tend to be larger than the average in the deposit, and almost all that are likely to fall seem to be removed as the result of an initial shock. When slides which have already been evaluated are circulated by post to a number of different counters there is, in general, no tendency for the number of particles to change as the result of repeated counting and handling.

It has been found that if the focusing of the 2 mm oil-immersion objective is carried out carelessly and if, for example, the cover glass is compressed by the close contact of the lens, the fall-off of particles from the strip is encouraged. This means that the amount of focusing should be curtailed as much as possible to avoid the loss of particles and consequent under-estimation of the true count. As the main chance of distorting the cover glass occurs when focusing at the beginning of a traverse, it follows that the number of traverses evaluated should be kept to a minimum.

Conclusions

Optimum density of dust deposit. To obtain a coefficient of variation for counting errors of less than about 14%, the number of particles counted on the two cover glasses corresponding to any particular sample should be between 150 and 300 particles, or, say, about 75–150 particles on each cover glass. These particles may be examined in one or more traverses depending on the density of the dust deposit, which can be controlled to within relatively narrow limits by varying the duration of the sample. From the point of view of reducing the effect of overlapping, it is desirable that the deposit should be relatively light and, therefore, that more than one traverse should be counted. On the other hand, the presence of background contamination will have a greater effect on the reported concentration the lower the density of the deposit. A further consideration is that the number of traverses should be kept as small as possible to reduce the effect of fall-off from the dust strip. These requirements are conflicting, and the choice of the optimum sampling technique must represent a compromise between them. On balance, it is considered that the aim should be to obtain deposit densities of 75–125 particles in the $1\text{--}5\ \mu$ size range and that one traverse only should be evaluated. As it is sometimes found that the dust deposit is wedge-shaped instead of rectangular, because of the displacement of the cover glasses

in the thermal precipitator while the sample is being taken, this traverse should be located at the centre of the dust strip. The deposit density of samples taken in collieries where the dust is particularly coarse, such as in South Wales, should be at the lower limit of the recommended range. In this way the coefficient of variation of the counting errors will be, on average, between 11 and 14%.

Size distribution counts. The high variability of counts of small numbers of particles emphasizes the need when carrying out detailed size-distribution analyses to examine a reasonable number of particles in each size range. Apart from the question of variability, it has been shown by Sichel⁽⁹⁾ that, if particles lying within a particular size range occur infrequently, there may be a tendency to under-estimate the surface area and mass of a dust cloud if a fixed number of traverses is counted in all size ranges. Sichel recommends a technique known as "Truncated Multiple Traversing" to overcome this difficulty, whereby the number of traverses counted in a particular size range is adjusted in accordance with the frequency of occurrence of particles in that range, in such a way that at least ten particles occur in each size range. The results of the present investigation support this procedure.

The effect of size distribution on counting levels. Consideration of the effect of the size distribution of the dust deposit on counting levels has demonstrated that the same basic sizing errors may give rise to very different apparent counting levels, depending on the proportion of particles on the boundaries of the size range. Thus, the apparent performance of a group of counters on slides with a high proportion of finer particles may be expected to be worse than on slides with a smaller proportion of fine particles. This observation is consistent with the general experience that closer agreement can be obtained in counts of dust samples from South Wales than on samples from other coalfields. The effect of size distribution should also be taken into account in counting trials which are designed in such a way that all observers do not count the same slides. This is especially important when the majority of the samples evaluated by a particular observer is obtained from his local collieries. Under these conditions, the best apparent levels of performances will be achieved by the observers who count the highest proportions of coarser samples.

Acknowledgements

The author's thanks are due to Dr. J. W. J. Fay for helpful discussions and advice. The paper is published by permission of the National Coal Board.

References

- (1) GREEN, H. L., and WATSON, H. H. *Medical Research Council Special Report Series*, No. 199 (1935).
- (2) BEADLE, D. G., and KERRICH, J. E. *J. Chem. Met. Min. S.A.*, **56**, p. 219 (1955).
- (3) FAY, J. W. J. *Nature (London)*, **180**, p. 309 (1957).
- (4) FAY, J. W. J., ASHFORD, J. R., and SMITH, P. H. Accepted for *Brit. J. Appl. Phys.*
- (5) ROACH, S. A. *Brit. J. Industr. Med.*, **16**, p. 104 (1959).
- (6) FAY, J. W. J., and ASHFORD, J. R. *Brit. J. Appl. Phys.*, **11**, p. 1 (1960).
- (7) ROACH, S. A. *Brit. J. Industr. Med.*, **15**, p. 250 (1958).
- (8) FAY, J. W. J., *et al.* Errors in Thermal Precipitator Dust Counts due to the Overlapping of Particles. To be published (1960).
- (9) SICHEL, H. S. *J.S.A. Inst. Min. Met.*, **58**, p. 171 (1957).

Summarized proceedings of a conference on electron microscopy—Exeter, July 1959

Abstract

The annual conference of the Electron Microscopy Group of The Institute of Physics was held in the Washington Singer Laboratory, University of Exeter, from 7 to 10 July, 1959. The papers presented are summarized in this report.

Metal physics and metallurgy

ON the first two days of the conference, papers on metallurgical applications of the electron microscope were read. Mr. E. C. H. SILK and Mr. R. S. BARNES (A.E.R.E., Harwell), described observations on annealed mica prepared by cleaving. Rotational moiré patterns from loose superimposed sheets were useful in describing dislocations lying in the field of the patterns. Tracks of fission fragments were also observed in mica irradiated in a pile next to uranium foils (Fig. 1).

Mr. R. L. SEGALL and Mr. P. G. PARTRIDGE (Cavendish Laboratory, Cambridge University) then discussed experiments on dislocation distributions produced by fatigue in face centred cubic metals, such as aluminium and copper and also in stainless steel. Comparisons were made with the distributions produced by unidirectional deformation. Polygonization was not observed in aluminium fatigued at low stresses, despite a dislocation density comparable with that in well polygonized tensile specimens. A high density of dislocation loops found in some areas suggested the formation of point defects during fatigue.

Mr. R. PHILLIPS and Mr. O. P. HARTREE (Aeon Laboratories, Egham, and Associated Electrical Industries Ltd., Aldermaston) described dislocation arrangements in germanium as a function of deformation temperature. At temperatures below 700° C the distribution of dislocations was complex and contained a high density of dislocations running in [110] directions for distances of up to a few microns. Dislocation loops were also observed in these specimens. Above 700° C increasing amounts of polygonization occurred.

Dr. D. McLEAN and Mr. K. F. HALE (N.P.L., Teddington) then described observations of precipitation at and around dislocations in iron (< 0.01% carbon). After quenching from 690° C and ageing at room temperature and 100° C, dendritic forms of precipitates running in [100] directions were visible at dislocations. Fine particles also precipitated in the matrix away from dislocations. Dislocation loops emitted by incoherent precipitates and inclusions were also observed. Dr. McLean and Mr. Hale also reported on dislocation arrangements in α -iron in the annealed state and after cold work, creep and polygonization. Hexagonal networks of dislocations have been analysed in terms of [111] dislocations with [100] junction pieces and in terms of [100] dislocations with [110] junction pieces.

Mr. D. G. BRANDON (Metallurgy Department, Cambridge University) described the arrangement of dislocations observed in α -iron after deformation in tension. At small deformations (< ~ 1%) irregular pile-ups were formed and

at larger deformations complex networks predominated. After about 7% extension distinct subgrains appeared. The dislocation arrangement in a single crystal foil was found to bear little relation to the slip traces on the surface of the specimen.

Dr. D. W. PASHLEY and Mr. A. E. B. PRESLAND (Tube Investments Research Laboratories, Saffron Walden) described observations of superlattices of ordered alloys. Thin single crystals of Cu–Au alloy were prepared by an evaporation technique. The foils were annealed on a high temperature stage during examination and the ordering process was observed directly. A continuous change was found to occur in the arrangement of domain boundaries (Fig. 2) from the irregular CuAu I structure to the regular periodic CuAu II structure. A study was also made of the influence of dislocations on the ordering process and on the final arrangement of domain boundaries in the CuAu II structure.⁽¹⁾

Mr. P. KELLY and Dr. J. NUTTING (Metallurgy Department, Cambridge University) went on to discuss results obtained from studies of shear type transformations in 20% Ni, 0.8% C steels quenched to martensite. Examination of thin foils revealed that the martensite plates were internally twinned on a very fine scale, the widths of the twins being about 20 Å (Fig. 3). This suggests that the “second” (inhomogeneous) shear occurs on the (112) twinning plane in the “anti-twinning” direction, while twinning of the adjacent portion results in zero overall distortion.^(2, 3)

Mr. M. J. ARROWSMITH (Metallurgy Department, Cambridge University) described results on precipitation of NbC on dislocations in stainless steels. The austenitic steel (0.4% C, 13% Ni, 13% Cr, 10% Co) showed a Widmanstätten precipitation of Cr₂₃C₆ after ageing at 700° C. The presence of 3% Nb was sufficient to cause all the precipitation at 700° C to occur at dislocations. The precipitates consisted of cubes of Cr₂₃C₆ and ellipsoids of NbC. The dislocations appear to be generated by thermal contraction stresses⁽⁴⁾ set up by the NbC particles which are only partially dissolved at the solution treatment temperature of 1300° C.

Mr. H. J. BLACKBURN (Metallurgy Department, Cambridge University) then discussed the problem of the “475 embrittlement” of chromium steels.

Mr. F. B. PICKERING (United Steel Co. Ltd., Rotherham, Yorks.) described an electron microscopical examination of the ageing characteristics of 25% Cr, 4% Ni stainless steels containing aluminium contents up to 3%.⁽⁵⁾ Precipitation hardening occurred with the formation of an ordered NiAl precipitate. At small Al content after ageing at high temperatures the sigma phase was formed but this was suppressed by increasing the Al content. The lattice parameter of the NiAl precipitate was measured and the degree of misfit with the ferritic matrix was assessed. Similarities were drawn between the crystallography of the precipitation of NiAl in ferritic steels and that of Ni₃Al in nimonic alloys.

Dr. G. THOMAS and Dr. M. J. WHELAN (Metallurgy Department and Cavendish Laboratory, Cambridge University) then reported experiments on direct observations of

precipitation in thin foils of quenched Al-4% Cu alloys using a high temperature stage. Angular precipitates, about 500 Å in diameter, were observed to form in about 30 seconds at 250 to 300° C. Much of the initial precipitation may have been a surface effect. On raising the temperature the precipitates coarsened and eventually went into solution at 500° C. A ciné-film illustrating the effects observed was shown.

Mr. M. WHITE (Metallurgy Department, Imperial College, London) described similar experiments on an Al-3.8% Cu-0.51% Mg alloy.

Dr. G. THOMAS (Metallurgy Department, Cambridge University) reported results on quenching defects in aluminium alloys containing various amounts of copper, silver, zinc and magnesium. In all the alloys dislocation loops and complex dislocations were observed. The results suggested that many vacancies remain quenched-in in concentrated alloys. The magnitude of this effect increased in the order zinc-magnesium-silver-copper, suggesting that the binding energy between a vacancy and a solute atom increased in this order. This was also the order of decreasing mobility of these elements in aluminium. The migration of vacancies (to form loops) was thought to be accompanied by solute clustering in Al-Cu, Al-Ag and Al-Zn alloys. In Al-Mg alloys it was thought that most of the vacancies were held by solute atoms even after ageing. These ideas could account qualitatively for preferential precipitation at dislocations and at grain boundaries.

Electron diffraction effects from thin foils containing precipitates were discussed by Mr. R. B. NICHOLSON⁽⁶⁾ (Metallurgy Department, Cambridge University). The growth of γ^1 precipitates in an Al-Ag alloy was studied. The precipitates contained stacking faults and measurements of the frequency of faulting were made. The thickness of the precipitate was measured on the micrograph and calculated from the length of the streak through (000) on the diffraction pattern. The frequency of faulting was measured from the lengths of streaks from planes whose periodicity was affected by the faulting. The results showed that the faults are only 10 Å apart in small precipitates, but that during growth the faults are removed leaving a perfect ordered hexagonal structure.

Mr. K. H. WESTMACOTT, Dr. D. HULL, Mr. R. S. BARNES (A.E.R.E., Harwell) and Dr. R. E. SMALLMAN (Department of Physical Metallurgy, Birmingham University) went on to discuss evidence for dislocation sources in Al-3 and 4% Cu alloys quenched into acetone from 425 and 525° C.⁽⁷⁾ Concentric dislocation rings were observed around an isolated source not associated with the dislocation network. The source appeared to consist of a dislocation loop, one segment of which had bowed out in another (111) plane thereby generating new dislocations (Fig. 4). Inside the dislocation rings rows of loops were visible. These were explained by climb of the dislocation rings into spirals by condensation of vacancies and subsequent dissociation.

Experiments using a high temperature stage in the electron microscope to observe directly the annealing of prismatic dislocation loops in quenched aluminium were discussed by Mr. J. SILCOX and Dr. M. J. WHELAN (Cavendish Laboratory, Cambridge University). The loops were observed to shrink and eventually to disappear in a few minutes in the temperature range 170 to 200° C. The results have been interpreted in terms of the behaviour of the loops as vacancy sources and provide direct evidence of the correctness of the hypothesis of dislocation climb. A ciné-film was shown demonstrating clearly the effects observed.

Mr. K. F. HALE and Mr. B. GALE (N.P.L., Teddington)

reported on temperature and stress distributions in thin metal foils. When operating the Siemens Elmiskop 1 electron microscope at 100 kV and 60 μ A with a 600 μ diameter condenser aperture and with an illumination spot diameter of 17 μ , the temperature of an iron foil 3000 Å thick reached a maximum of about 900° C. However, for normal operation with an illumination diameter of about 4 μ the maximum temperature was about 75° C. Corresponding normal maximum temperatures for aluminium and gold were 30° C and 20° C. The maximum shear stress at the centre of the foil was found to be about G/1500 (G, shear modulus). However, the actual stress would have been somewhat smaller since the foils could buckle.

Dr. J. E. BAILEY (Cavendish Laboratory, Cambridge University) went on to describe observations on recovery and recrystallization of deformed silver. Observations on partially annealed foils, cold rolled to 95% reduction, showed that subgrains were formed in the heavily rolled silver prior to annealing. Annealing produced more subgrains which were slightly larger than those formed during deformation. High temperature stage experiments confirmed that the subgrains form by a polygonization process. The growth of these subgrains was also observed directly at high temperatures. The observations showed that recrystallization occurred by the migration of boundaries. However, it was not known whether the mechanism involves the migration of original grain boundaries or the growth of subgrains.

The tempering of a uranium steel containing 0.2% C and 2.0% U was investigated by Mr. A. J. BAKER (Metallurgy Department, Cambridge University) using carbon replica and thin foil methods. The replica work indicated that the presence of uranium in solid-solution delayed softening on tempering but produced no secondary hardening. This was subsequently confirmed by thin-foil methods.

Dr. P. LUCASSON (Metallurgy Department, Cambridge University) reported observations of radiation damage in thin foils of stainless steel. The thin foils were irradiated by α -particles from Po²¹⁰ in a hydrogen atmosphere. A very fine structure, thought to be associated with the radiation damage introduced by α -particles, was observed. This structure appeared as small spots less than 60 Å in size. The density of the structure was less than that of the primary knocked-on atoms by a factor of 15. All the small spots in the thinnest regions of the specimen disappeared during examination.

Mr. J. SILCOX (Cavendish Laboratory, Cambridge University) then described observations of neutron irradiation damage in copper. The bulk specimens were irradiated in the Harwell piles Bepo (at $\sim 35^\circ$ C) and Dido (at $\leq 60^\circ$ C). Specimens irradiated to a dose of 6.7×10^{17} n cm⁻² (at 35° C) contained $\sim 3 \times 10^{15}$ defects per cubic centimetre in the form of small regions of strain (average diameter ~ 75 Å). Some of the defects could be resolved as dislocation loops. At high irradiation doses (1.4×10^{20} n cm⁻²) most of the defects were resolvable as loops. The stability of the loops and their behaviour on annealing were in accordance with that from prismatic loops. The loops were considered to form by collapse of disks of vacancies formed at displacement spikes⁽⁸⁾ (see Fig. 5).

Oxidation, wear and corrosion

Mr. P. R. SWANN and Dr. J. NUTTING (Metallurgy Department, Cambridge University) reported observations on alloys susceptible to stress corrosion cracking. Several single phase copper alloys were examined and stacking faults were observed

in all cases. Examination of the edges of the foils showed that these faults dissolved at a different rate to the matrix. A mechanism of discontinuous stress corrosion cracking in these alloys was proposed, in which preferential dissolution of a stacking fault creates a small crack. The stress concentration at the tip of this crack is raised further by the presence of piled-up dislocations against the original fault. This leads to a short brittle crack and the process repeats itself across the material.

Mr. S. O'HARA and Mr. J. W. SHARPE (Royal College of Science and Technology, Glasgow) described a replica technique based on the softening of Perspex at 110° C and secondary carbon evaporation for studying fatigue. The localization of slip movement during fatigue to produce both broad and narrow extrusions and intrusions has been observed in the case of annealed 99.8% pure aluminium and annealed O.F.H.C. copper. In higher purity material (annealed 99.99% aluminium) Forsyth⁽⁹⁾ did not observe narrow extrusions after fatigue. Observations have also been made on fracture surfaces of fatigued steel and the appearance of conchoidal rings noted.

Mr. F. B. PICKERING (United Steel Co. Ltd., Rotherham, Yorks.) then mentioned some aspects of oxidation of steels. Pfefferkorn⁽¹⁰⁾ showed that, when metals are oxidized, whisker- or needle-like growths occur on the surface. One of the recurrent problems in power plant industry is the build-up of flue dust on superheater tubes.⁽¹¹⁾ The size of oxide whiskers which form on typical superheater tube steels in their normal working temperature ranges has been examined. The growths are capable of trapping particles of flue dust. Examination of the flue dust indicated that the particles were probably electrostatically charged and in addition to entrapment, electrostatic precipitation might also occur.

Miss J. S. STEEL (Fulmer Research Institute, Stoke Poges) also discussed oxide growth on steels. The growth of oxide needles on metals during high temperature oxidation is of interest since their location corresponds to weak spots in the oxide film where the oxidation rate is considerably greater than the mean rate over the whole surface. Reflexion electron microscopy, electron diffraction and X-ray methods were used to identify oxide needles on mild steel and Si-Al sheet, oxidized in air and steam for various periods at 700° C.

Mr. R. H. SEEBOHM and Mr. J. W. MARTIN (Metallurgy Department, Oxford University) described observations on internally oxidized dilute alloys of copper with aluminium and beryllium. Carbon extraction replicas of the dispersed oxide particles were shown (Fig. 6). Grain boundary precipitates and the associated grain denudation effects were discussed. Replicas of tensile fracture surfaces showed both grain boundary surfaces, where precipitated oxides had caused brittleness, and areas of transgranular failure where the dispersed particles had affected the deformation process. The distribution of slip lines on deformed polished surfaces was also modified by the presence of oxide particles. Some results on internally oxidized sintered powder alloys were also mentioned.

Physical and chemical changes on silicon surfaces during heat treatment at diffusion temperatures were then described by Dr. R. C. NEWMAN and Mr. J. WAKEFIELD (Associated Electrical Industries Ltd., Aldermaston). On heating silicon to 1250° C in argon, surface migration occurred and etch pits with {111} facets were formed. An overgrowth of β -SiC, which was partially orientated, also formed, the carbon originating both as an internal and external impurity.⁽¹²⁾ The carbide particles were between 50 and 500 Å in diameter,

and an enhanced density was found near etch pits. Rows of carbide particles along [110] directions were found; these probably initiated the formation of the pits. A mass of SiC particles was sometimes found embedded in pits on a (100) surface.

Dr. V. D. SCOTT (A.W.R.E., Aldermaston) discussed the dispersion of beryllium oxide in beryllium and the surface oxidation of the metal. Electron microscopy and diffraction techniques were used to locate and identify a high temperature form of oxide (>800° C) in hot worked beryllium. Extraction replica micrographs were compared with optical micrographs. The surface oxidation of beryllium in air was also mentioned. The protective nature of the oxide formed at 300 to 400° C was indicated by the epitaxial growth on (001) cleavage faces, while the non-protective nature of the oxide above 600° C was evident from the growth of BeO whiskers and flakes on the metal surface. Electron diffraction showed the whisker axis to be [110] with a screw dislocation parallel to the axis.

Mr. D. SCOTT and Mrs. H. M. SCOTT (National Engineering Laboratory, Thorntonhall, Glasgow) described how the electron microscope has been used to study the initiation of wear and how this was affected by the type of material and the nature of the lubricant used. Investigations of fretting corrosion, the study of oxide fibres and the investigation of metallographic changes due to sliding, rolling, rubbing and abrasive action were also discussed.

The formation of transferred graphite layers was discussed by Dr. J. S. HALLIDAY (Associated Electrical Industries Ltd., Aldermaston). The successful operation of electrical generators and other electrical machinery depends upon the build-up of suitable graphite layers on the metal slip rings and commutators, the layers being transferred from graphite brushes. The structure and mode of formation of graphite layers on steel surfaces was investigated using a high voltage electron diffraction camera and a reflexion electron microscope.

Dr. J. S. HALLIDAY and Mr. D. A. S. ROSE (Associated Electrical Industries Ltd., Aldermaston) also described the direct observation of wear processes. The specimen manipulator of a reflexion electron microscope was modified so that the wear of sliding contacts could be observed during examination. The results illustrated the initiation and growth of fragments transferred from one specimen to the other.

Instrumental

A new approach to the correction of spherical aberration was suggested by Dr. G. D. ARCHARD, Mr. T. MULVEY and Mr. D. P. R. PETRIE (Associated Electrical Industries Ltd., Aldermaston). Previous systems for correcting spherical aberration have used electrostatic elements but these are difficult to build and to operate. The authors proposed the use of magnetic quadrupole and octupole fields, with no axially symmetric lens. Three quadrupoles would be needed to form an image free from first order astigmatism and distortion; three octupoles should counteract the primary aberration. As the primary spherical aberration of these astigmatic systems is greater than that of conventional lenses, it would be advantageous to choose a system with the least possible aberration, before correcting. The main application envisaged at present is to electron probe techniques.

Dr. W. C. NIXON (Cavendish Laboratory, Cambridge University) discussed the operation of the Metropolitan-Vickers EM 6 electron microscope at low kilovoltages. With minor modifications the instrument could be used in the

(See pages 22–24 and 28–32)

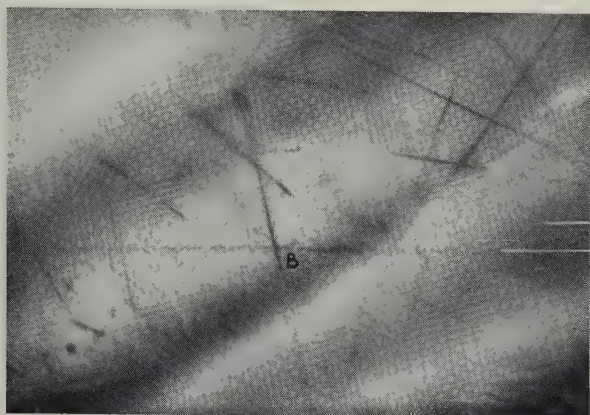


Fig. 1. Tracks of fission fragments in mica irradiated near uranium. An energetic collision has occurred along one track at B. The structure of the tracks is observable with a higher resolution than that obtained in nuclear emulsions or cloud chambers ($\times 20\,000$, Silk and Barnes)

Fig. 2. CuAu during the I \rightarrow II transition ($\times 300\,000$, Pashley and Presland)

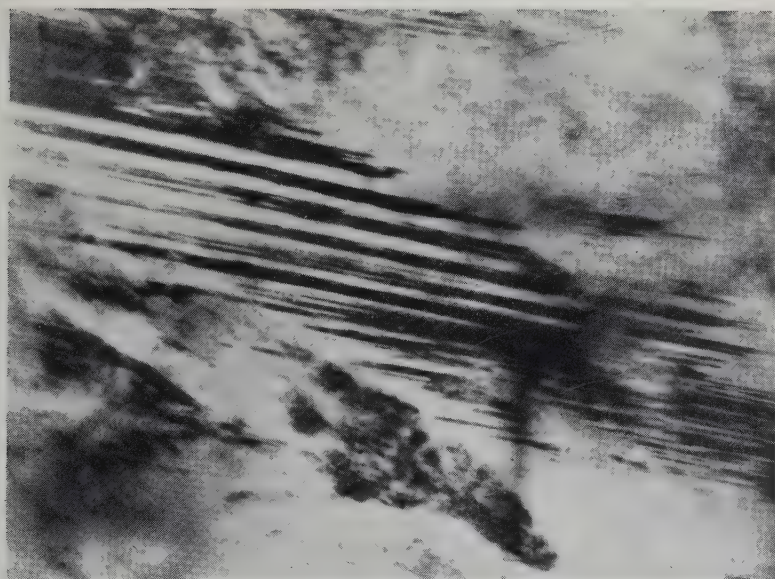
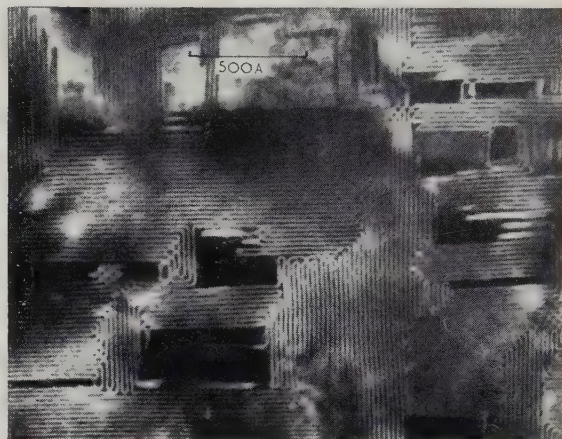


Fig. 3. 0.985% C steel quenched from 900° C showing narrow twins within a single martensite plate ($\times 80\,000$, Kelly and Nutting)



Fig. 4. Al-4% Cu quenched from 525° C into acetone. Dislocations symmetrically arranged about a source with associated rows of loops ($\times 20\,000$, Westmacott, Hull, Barnes and Smallman)

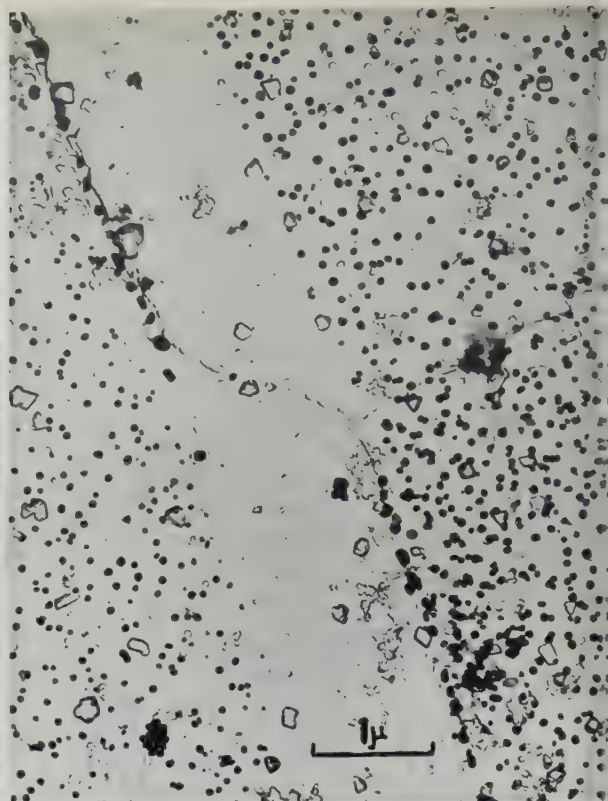


Fig. 6. Grain boundary of internally oxidized Be-Cu, showing effect of twin band (right) on denudation. Etched. Carbon replica ($\times 16\,000$, Seebohm and Martin)

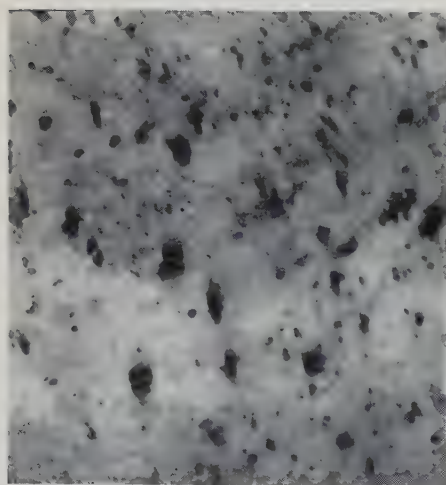


Fig. 5. Dislocation loops in neutron-irradiated copper. Total neutron flux $\sim 5.6 \times 10^{18} \text{ n cm}^{-2}$ ($\times 100\,000$, Silcox and Whelan)



Fig. 7. Moiré pattern from overlapping (111) gold films. Dark field ($\times 2\,200\,000$, Bassett and Pashley)

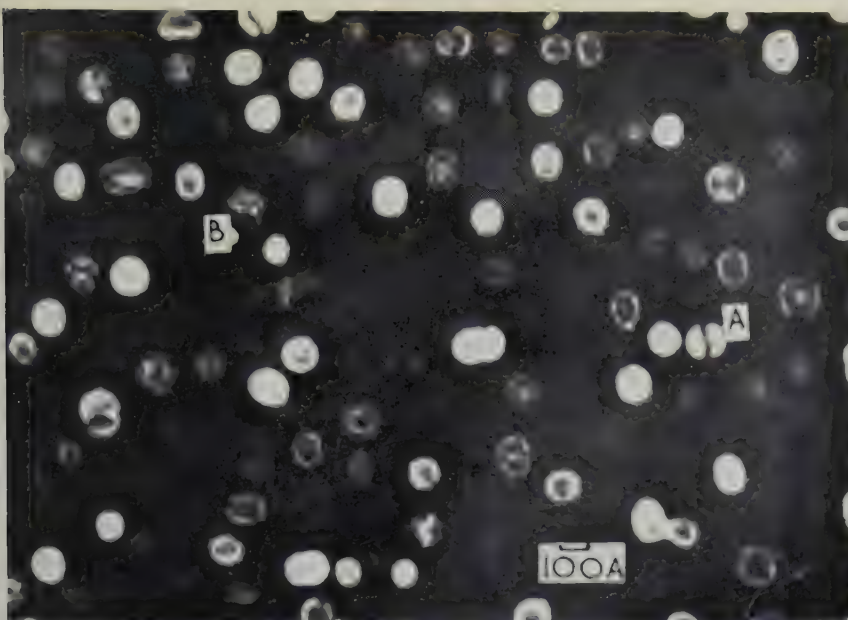


Fig. 8(a). Dark field micrograph of oriented gold from a rocksalt substrate. 15 Å thick deposit ($\times 400\,000$, Bassett and Pashley)

Fig. 8(b). Bright field micrograph of the same field of view as Fig. 8(a) ($\times 400\,000$, Bassett and Pashley)

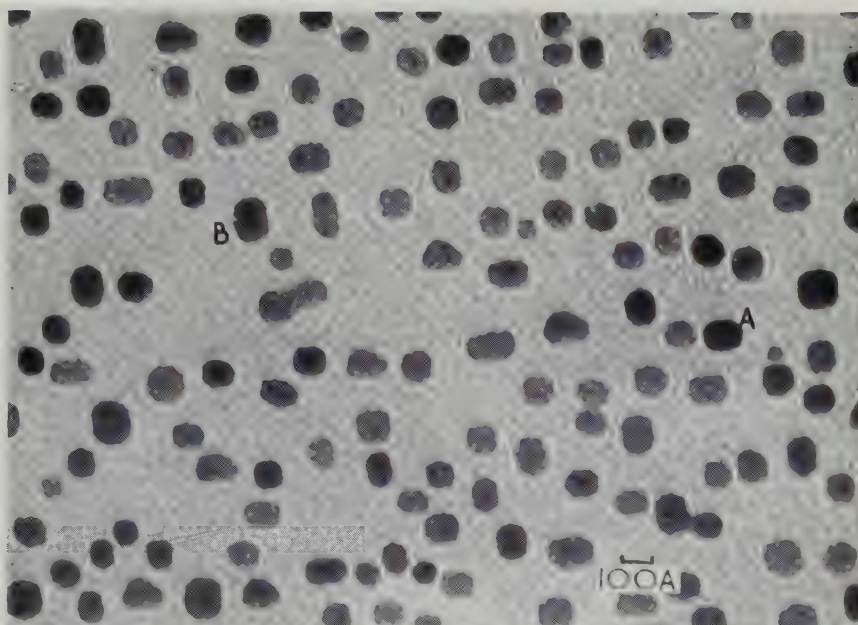
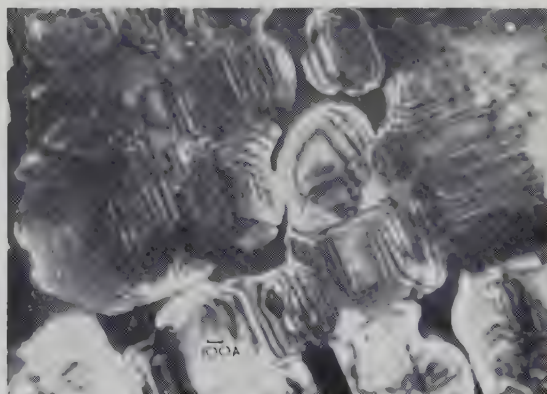


Fig. 9. Moiré fringes in a polyethylene crystal showing a dislocation ($\times 76\,000$, Keller, taken in conjunction with A. W. Agar)



Below:

Fig. 10. Oriented gold, 500 Å thick, from rocksalt substrate ($\times 200\,000$, Bassett)



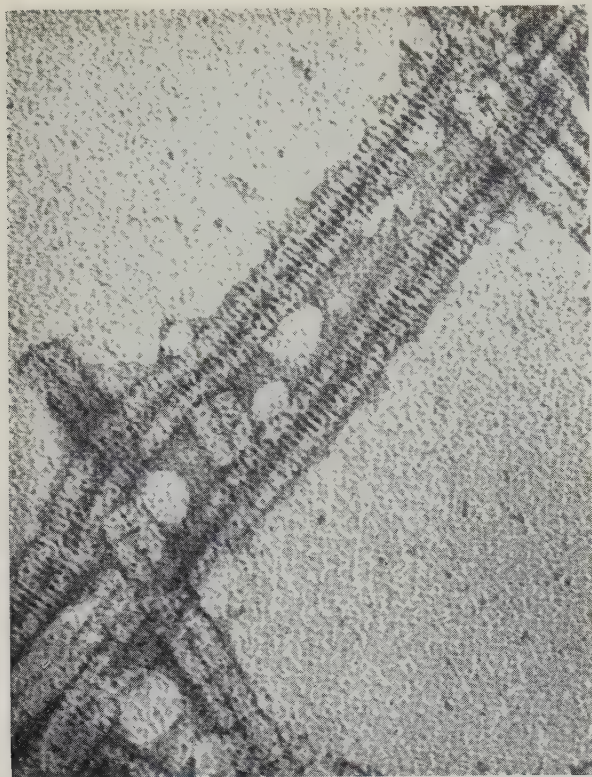


Fig. 11. Tobacco mosaic virus stained with phosphomolybdic acid ($\times 400\,000$, Nixon)

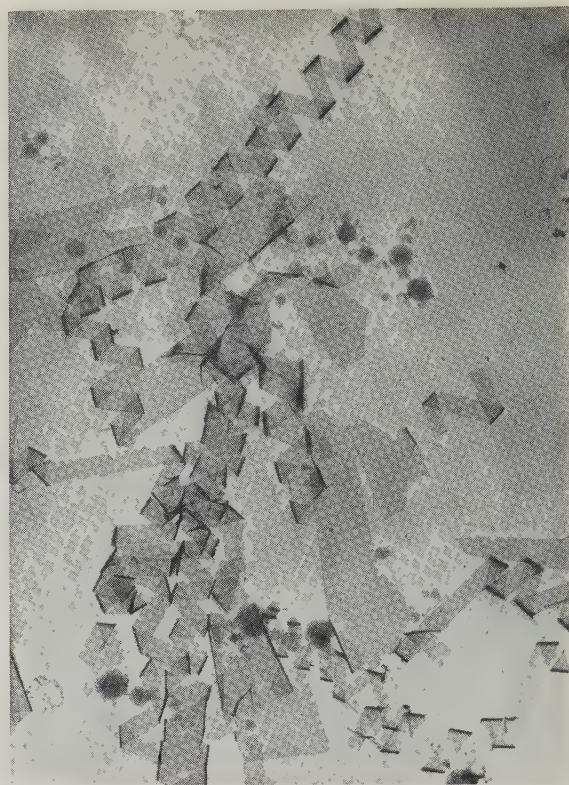


Fig. 12. Allevardite (a clay mineral) ($\times 4000$, Weir, Nixon and Woods)

4 kV to 15 kV range. It was necessary to replace the electron gun by one with a much smaller anode to grid spacing and with a separate high voltage and filament current supply. The electron lens currents were reduced by series and parallel dropping resistors. A different photographic plate (Ilford Q 1) was used. At 7 kV to 10 kV the brightness was sufficient for a 4-s exposure at $16\,000\times$. Micrographs demonstrating the improved contrast at these low kilovoltages were shown.

Dr. D. W. PASHLEY and Mr. A. E. B. PRESLAND (Tube Investments Research Laboratories, Saffron Walden) described a hot stage for the Siemens Elmiskop I.⁽¹⁾ The stage was constructed to allow direct observation of transmission specimens at any temperature up to about 600°C . To avoid introducing stray magnetic fields the heater element consisted of a single coiled-coil of wire heated by direct current. The hot stage could not be inserted through the air-lock, but was incorporated in a modified specimen stage which was removable for all specimen changes. Very high resolution micrographs (an example of 8 \AA was given) could be obtained with the specimen hot, because thermal drift had been reduced to a very small amount (less than 0.5 \AA s^{-1}). Above 200°C exceptionally high contrast micrographs were obtainable due to the elimination of carbon contamination.

Mr. A. C. VAN DORSTEN (Philips Electrical Ltd., Eindhoven, Holland) then described the latest Philips 100 kV electron microscope (E.M.200) which had now reached the production stage. Noteworthy features included high mechanical and electrical stability, a double condenser lens system giving a spot size down to $1.5\text{ }\mu$, a stigmator and a $10\times$ viewing binocular. Specimen and objective aperture contamination was reduced by seating the specimen between two cooled plates.

Electron probes and fluorescence analysis

In a survey lecture on electron probe techniques Dr. V. E. COSSLETT (Cavendish Laboratory, Cambridge University) gave an account of present trends in the application of these techniques to X-ray microscopy and X-ray microanalysis and reviewed the recent Stockholm Symposium⁽¹³⁾ on this subject.

Mr. T. MULVEY (Associated Electrical Industries Ltd., Aldermaston) described an X-ray micro-analyser for routine spectro-chemical analysis.^(13, 14, 15) In this instrument a finely focused electron probe is directed on to a chosen part of the specimen and the resulting characteristic X-rays are analysed by a suitable spectrometer. Mr. Mulvey described how the micro-analyser could be incorporated in an electron microscope or electron diffraction camera and gave examples of its use in this way. A reasonable counting rate was obtained with specimens as thin as 500 \AA .

Dr. R. G. BAKER (Metallurgy Department, Cambridge University) showed how the technique of X-ray fluorescence analysis could be used to follow quantitatively the changes in composition of carbides during the tempering of steels. The carbides were extracted in carbon extraction replicas and were examined by electron microscopy, electron diffraction, X-ray diffraction and X-ray fluorescence analysis. The analysis apparatus was calibrated by preparing comparable specimens of known composition so that absolute analyses (with a known statistical error) could be obtained. The method was applied to a study of the carbides in Ni-Cr type steels during tempering; the results agreed with those obtained on similar steels by workers using conventional methods of chemical analysis.

Techniques—instrumental

Dr. J. A. CHAPMAN (Manchester University) discussed the procedure for correcting astigmatism in the Siemens Elmiskop I. The rule for compounding two astigmatisms (magnitudes A_1 , A_2 and directions α_1 , α_2) is to add the corresponding vectors (magnitudes A_1 , A_2 and directions $2\alpha_1$, $2\alpha_2$). This rule provides a simple graphical method which can be used to predict the change in setting of the stigmator controls required to correct an observed degree of astigmatism.

Electron microscopists have tended to neglect the technique of dark field working, with its advantages of high contrast, easier image interpretation and, in some instances, increased detail. Mr. G. A. BASSETT and Dr. D. W. PASHLEY (Tube Investments Research Laboratories, Saffron Walden) discussed these advantages and showed that, in dark field electron microscopy of crystalline specimens, high resolution could be retained by tilting the illuminating system so that a diffracted beam passed down the axis of the objective lens. With the Siemens Elmiskop I the tilting operation should be carried out using condenser II only and re-aligning for double condenser operation after tilting. (It is also advisable to remove the large aperture above the specimen air-lock.) Illustrations of the method included a moiré pattern of 7 Å from two overlapping (111) gold films (Fig. 7), a 20 Å periodic spacing from gold-copper alloy, and oriented gold nuclei removed from a rocksalt substrate. In some of these nuclei (e.g. *A* and *B*) detail visible in dark field [Fig. 8(*a*)] cannot be seen in bright field [Fig. 8(*b*)].

Another approach to the study of crystals, with particular reference to crystalline organic polymers, was put forward by Dr. A. KELLER (Bristol University). He showed that diffraction effects (in diffraction patterns and also in the electron image) could provide valuable structural information. Thus selected area diffraction from single crystals of polymers enabled the direction of the chain molecules to be deduced and indicated a folded molecular configuration. In electron images of these polymer crystals moiré patterns (Fig. 9) and Bragg extinction fringes could be observed, using suitable operational techniques (developed in collaboration with Mr. A. W. AGAR). These observations confirmed that the apparent single crystals consisted of structurally different regions, distinguished by different fold directions and satisfying different diffraction conditions. This was evident from the appearance of moiré patterns and Bragg fringes. The Bragg fringes were most conveniently identified by using a large objective aperture and recording the displacement of the ghost images. (This displacement arises from the spherical aberration error between the direct and the diffracted beams.) In all this work a very low intensity electron beam was essential as the crystallinity of organic polymers disappeared at normal intensities.

The method of selected area micro-diffraction is being increasingly used in electron microscopy, but little attention has hitherto been paid to the accuracy with which a chosen area of the object can be selected for diffraction. In discussing the factors governing this accuracy Mr. A. W. AGAR and Mr. R. PHILLIPS (Aeon Laboratories, Egham) showed that, owing to spherical aberration in the objective lens, the area defined by the selector aperture does not correspond exactly to those parts of the specimen contributing to the diffraction pattern. Thus reflexions may appear from object points outside the chosen area. Other errors may arise through incorrect lens settings (particularly the objective lens strength). It is evident that special care is required in, for example, studies of mis-orientation between grains in thin metal films.

Techniques—applications

In preparing single stage positive carbon replicas of powders and surfaces it is not always desirable (or possible) to etch away the sample after deposition of the carbon film. An ingenious method of overcoming this difficulty was put forward by Mr. G. L. MACDONALD (Mullard Radio Valve Co. Ltd., Mitcham). In this method the carbon rods are used as a heat source to evaporate other materials prior to the evaporation of carbon. In particular, if aluminium foil was placed between vertical carbon rods, the lower one flat-ended and the upper one pointed, a thin, easily dissolved layer of aluminium could be formed between the sample and the carbon replica without apparently obscuring any surface detail. Powders partially embedded in plastic were replicated by this method. High resolution amorphous metal-carbon replicas showing 20 Å details were produced by placing platinum/rhodium foil and aluminium between the carbons, the former evaporating simultaneously with the carbon.

A method for the successive replication of the same area of a fabric was described by Mr. M. CAMP (Unilever Ltd., Port Sunlight). A piece of cotton fabric was partially embedded in "Marco" resin as described by Dlugosz.⁽¹⁶⁾ Successive replicas were taken from the surface in "Triafol" plastic which was then shadowed with gold/palladium alloy. Carbon was evaporated on top of the alloy and the specimen grid was fixed to the selected area of the replica with paraffin wax, using a specially constructed device. Dissolving away the "Triafol" and then the wax left the correctly positioned carbon replica ready for examination.

In a critical survey of replica techniques used in both light and electron microscopy of paper surfaces Mr. D. H. PAGE and Mr. N. S. HORSEY (British Paper and Board Industry Research Association, Kenley) pointed out that a disparity frequently existed between conclusions that would be drawn from a separate examination of light and electron micrographs, even though the replica techniques were largely identical. They drew attention to the need for care in the interpretation of micrographs and to the need in certain cases for co-ordinating different microscopical methods.

When isolating included material from a metal matrix by the extraction replica method, it is necessary to select an etchant and give the specimen an "optimum etch". Dr. G. R. BOOKER and Dr. J. NORBURY (Richard Thomas and Baldwins Ltd., Aylesbury) described experiments showing how the "optimum etch" depended on the size and distribution of the included particles in the matrix.

Mr. A. M. ADAMS (Central Electricity Research Laboratory, Leatherhead), Mr. M. A. SILVA, Mr. A. W. AGAR and Miss V. M. SPIERS (Aeon Laboratories, Egham) outlined a technique for sampling oxide layers and brittle materials for microdiffraction. Ordinary etchants do not attack oxide layers on steel and, as the layers are often single-phase, material cannot be attacked differentially to free particles which could then be removed in an extraction replica. In this technique a lightly-loaded diamond point was drawn across the area of interest. The debris from the scratch was removed by a normal replica stripping process and examined by electron microscopy and microdiffraction. The method was capable of precise location and could be applied to brittle materials.

Thin evaporated films used in shadow-casting for the electron microscope possess a background structure. In metal films this arises from aggregation but in amorphous films, such as those formed by the simultaneous evaporation of platinum and carbon,⁽¹⁷⁾ the origin of this structure is not known. Mr. D. E. BRADLEY (Associated Electrical

Industries Ltd., Aldermaston) suggested that the uneven building up of a film was due to the random distribution of the impinging atoms and was therefore an inherent property of evaporated films in general. This idea was supported by electron micrographs of the background structure in films of silicon monoxide and carbon, both of which have a finer structure than platinum/carbon films. The effect on the background structure of varying the angle of deposition was studied and it was shown that the optimum angle for platinum/carbon shadowing is about 45° . Further electron micrographs of specimens shadowed with platinum/carbon revealed that the background was not always present and was not as serious a limitation as might have been expected. In the discussion following this paper Mr. G. SIDDALL (Edwards High Vacuum Ltd.) pointed out that platinum-carbon rods were now available commercially.

The use of the ultra-microtome in metallurgical applications of the electron microscope was then considered by Mr. R. PHILLIPS (Aeon Laboratories, Egham). Metal sections thin enough for transmission microscopy and diffraction could now be cut with a diamond knife. Mr. Phillips discussed the scope of the method, together with recent improvements and applications and difficulties that have yet to be eliminated. Attention was directed to a second important aspect of the sectioning of metals. After sections had been cut from a block of metal, the surface of the block was very clean and strain-free. Apart from the usefulness that such a surface might have in other fields it appeared to be ideal for reflexion electron diffraction and for taking replicas from specimens where chemical preparation had to be avoided, for example cavitated and α -bombarded specimens.

Mr. B. A. IRVING (Associated Electrical Industries Ltd., Aldermaston) described the preparation of thin films of germanium and silicon. Slices of germanium with (111) faces were mounted and one side ground and polished conventionally. The specimen was removed, cleaned and this side etched in warm dilute sodium hypochlorite solution. The prepared surface was mounted against a polishing jig and the bulk of the crystal was ground away. A final thinning by polishing gave slices 5 to $10\ \mu$ thick and these were further thinned by floating on the etchant. For silicon specimens 4% sodium hydroxide solution containing sufficient sodium hypochlorite to prevent hydrogen liberation was used. The final specimens showed no preparational damage.

To obtain thin films of steel and other hard ferrous alloys, suitable for direct examination by transmission electron microscopy, relatively thick material must be thinned (to about 0.05 mm thickness) without destroying or modifying the structure of the metal in any way. Mr. P. M. KELLY and Dr. J. NUTTING (Metallurgy Department, Cambridge University) described an electrolytic jet machining apparatus for producing these uniform thin sheets of steel and showed electron micrographs of thin films prepared from these sheets by controlled electropolishing.

Mr. G. A. BASSETT (Tube Investments Research Laboratories, Saffron Walden) gave an account of recent work on the growth of oriented metal films on single crystal substrates. The preparation of an oriented film of gold by vacuum evaporation on (1) a cleavage surface of rocksalt to give a (100) film and (2) a (111) silver surface prepared on mica to give a (111) gold film, were followed by removal of the gold deposit on a carbon film for examination in the electron microscope. With a substrate temperature of 270°C parallel orientation occurred. On rocksalt a step decoration process, similar to that already described for a room temperature substrate,⁽¹⁸⁾ was found to operate. As the thickness of the

deposit was increased complex internal structures in the nuclei developed due to a combination of internal faults and external shape (Fig. 10). The cube gold film did not become continuous until a thickness of about 800 Å had been reached; in contrast, the (111) gold film grown on silver/mica became continuous at a thickness of about 50 Å.

Mr. P. G. PARTRIDGE and Mr. R. L. SEGALL (Cavendish Laboratory, Cambridge University) described a preparative technique permitting the simultaneous observation of the surface and the immediately adjacent interior layer of a metal in the transmission electron microscope. The specimens were thinned by electropolishing from one side only so that slip steps and other surface contours were preserved on the other surface. Using this technique it was possible to observe dislocations associated with surface slip steps.

Biological applications

Biological applications of electron microscopy presented at this conference were restricted to studies of virus structure and the use of specialized preparative techniques.

Mr. H. L. NIXON (Rothamsted Experimental Station, Harpenden) gave an account of recent studies of the structure of tobacco rattle virus^(19, 20) and tobacco mosaic virus. Specimens were prepared either by shadow-casting partly degraded virus particles or by mounting particles on carbon films and treating with solutions of lanthanum nitrate, uranyl acetate, osmium tetroxide, phosphotungstic acid (PTA) or phosphomolybdic acid (PMA). Tobacco rattle virus was shown to have a structure similar to that of tobacco mosaic virus; the particles were tubular, with a central hole, but long and short particles occurred, only the long ones being active. The staining reactions of the various heavy metal reagents were investigated and it was found that treatment with PMA and PTA revealed transverse bands 25 Å apart. Recent pictures of tobacco mosaic virus stained with PMA now showed similar transverse bands (Fig. 11), in good agreement with the helical structure determined by X-ray diffraction.

The beet yellows virus has been studied by Mr. G. E. RUSSELL and Mr. A. R. TRIM (Plant Breeding Institute, Cambridge). Partially purified preparations were examined in the electron microscope, using the negative staining technique.⁽²¹⁾ The loose internal structure of this virus (which also accounts for the flexibility of the filaments) allows PTA to penetrate readily and micrographs showed filaments with a pronounced banded structure. This structure was compared with that of tobacco mosaic virus, potato virus X and several other plant viruses.

Dr. K. M. SMITH and Mr. G. J. HILLS (Agricultural Research Council Virus Research Unit, Cambridge) described studies of the cytoplasmic polyhedral viruses of insects.⁽²²⁾ Bulk preparations of cytoplasmic virus particles were obtained by alkali treatment of the polyhedral inclusion bodies. The infectivity of the virus particle was tested and its shape was determined by shadow analysis. The digestion of the polyhedral inclusion bodies with alkali was investigated and the best method of extraction from the larvae was deduced.

Mr. R. W. HORNE, Dr. S. BRENNER, Dr. P. WILDY and Dr. A. P. WATERSON (Cavendish Laboratory, Cambridge University) described the application of the negative staining technique to studies of virus structure^(21, 23) and showed that the technique apparently preserved the three-dimensional structure at the molecular level. Electron micrographs of Adenovirus Type 5, Herpes Simplex, Fowl Plague and

Influenza virus showed clear sub-unit structures forming the components associated with the outer protein layer.

Mr. R. W. HORNE and Dr. S. BRENNER also described recent work on the injection mechanism of T2 bacteriophage.⁽²⁴⁾ A previous study of intact phage and isolated components forming the protein structure failed to explain the injection mechanism of the tail core into the bacterial cell. Further investigations have now revealed the existence of a complex hexagonal plate at the base of the core. The function of the core, sheath, plate and tail fibres isolated from T2 phage and the means of attachment to the cell wall were discussed.

Dr. Audrey M. GLAUERT, Dr. E. M. BRIEGER and Dr. Jennifer M. ALLEN (Strangeways Research Laboratory, Cambridge University) considered the development of techniques for the preparation of thin sections of bacteria, using the large bacterium, *Caryophanon latum*, as a test organism. The effect of different fixation and embedding procedures and the results of staining the sections were described. The most satisfactory results were obtained using Araldite as an embedding medium⁽²⁵⁾ and uranyl acetate as an electron stain.

In the ensuing discussion Dr. W. van ITERSOM (Amsterdam University) gave a short account of results she had obtained using similar techniques on *Bacillus cereus* and a *Tetracoccus* species. These results showed evidence of filamentous structures in the nucleus.

Some of the advantages of Araldite embedding were also stressed by Mr. J. M. DAVIS (Radiotherapy Department, Cambridge University). Methacrylate embedding revealed little structure in the mammalian nucleus, but the use of Araldite enabled high resolution pictures of the fibrous structure of chromosomes and nucleoli to be obtained.

Mrs. Barbara G. BARNES (Cavendish Laboratory, Cambridge University) described techniques used to study the structure of the acidophilic cells in the anterior pituitary of the mouse. Blocks fixed in isotonic osmium tetroxide were stained with a saturated solution of phosphotungstic acid in absolute alcohol and embedded in Araldite. Ribbons of adjacent serial sections were examined without a supporting film to obtain increased contrast. When carefully cured in the electron beam, such ribbons were stable enough to permit high magnification photography. From the serial sections three-dimensional reconstructions of various structures in the acidophilic cell were prepared.

Minerals

Dr. J. A. CHAPMAN and Dr. J. ZUSSMAN (Manchester University) discussed the electron optical fringe systems observable in micrographs of some serpentine minerals.⁽²⁶⁾ In picrolite, a fibrous antigorite, fringes with spacings of approximately 17 Å and 19 Å were found in adjacent regions of the same crystal. Possible explanations of such variable fringe spacings in terms of crystal structure were suggested.

Dr. J. A. GARD, Dr. J. W. HOWISON and Dr. H. F. W. TAYLOR (Chemistry Department, Aberdeen University) described an investigation of synthetic compounds related to tobermorite, as a background to the study of cement hydration. Specimens in the tobermorite group with various calcium: silicon ratios were synthesized at 25° C and hydrothermally at 140° C. The 25° C specimens were aggregates of crumpled foils while the autoclaved ones comprised mixtures of platy crystals and fibrous aggregates. These observations assisted the interpretation of the dehydration data and permitted speculation on the nature of the products.

Mr. J. CARTWRIGHT and Mr. J. W. SKIDMORE (Safety in Mines Research Establishment, Sheffield) described how the penetration and long-term retention of mineral particles in human lungs could be estimated by combined optical and electron microscopy. Mineral dusts were recovered by ashing and acid washing, and dust from coalminers' lungs by refluxing the lung material in hydrochloric acid. By comparing the size distributions of the residues with those of the environmental airborne dusts an estimate was made of the variation with particle size of the penetration and retention of dust particles in the lung. Although particles up to 15 μ in projected diameter were found in miners' lung residues, such particles were of extreme shapes and the results suggested that there was negligible alveolar penetration of particles exceeding 5 μ in Stokes's diameter.

The morphology of three expanding lattice clays, beidellite (from Idaho) and two alleverdites (from Allevard and Baluchistan), was studied by Mr. A. WEIR, Mr. H. L. NIXON and Mr. R. D. WOODS (Rothamsted Experimental Station, Harpenden). When fully dispersed, each sample was composed of very thin flakes, those of the Allevard alleverdite being in the form of zig-zag folded ribbons, probably existing as helices in suspension (Fig. 12). By measuring shadow lengths it was demonstrated that these minerals could exist in suspension as flakes of unit cell thickness.

Scattering, contrast and resolution

Dr. D. W. PASHLEY (Tube Investments Research Laboratories, Saffron Walden) discussed the factors limiting the resolution of periodic structures in the electron microscope. The formation of a periodic line image was considered in terms of the combination of a diffracted beam with the undeviated beam and it was shown that the resolution limit is controlled by the phase difference across the wave front of the diffracted beam. This phase difference arises from spherical aberration (involving the divergence of the illumination and the crystal size) and chromatic aberration (involving the stability of the accelerating voltage and of the objective lens current). It was deduced that the best available electron microscopes had a resolution limit of about 5 Å for periodic structures. Some improvement (considerable in the case of chromatic aberration) should be obtainable by tilting the illumination to bring the two interfering beams into symmetry with respect to the objective lens axis.

Dr. P. B. HIRSCH, Mr. A. HOWIE and Dr. M. J. WHELAN (Cavendish Laboratory, Cambridge University) discussed contrast effects from dislocations in thin metal foils. To explain some of these effects the authors have developed a kinematical theory of diffraction contrast.⁽²⁷⁾ The theory predicts that dislocations should appear as dark lines about 100 Å wide on bright field micrographs and that the contrast should be one-sided, i.e. that the dark line should lie to one side of the centre of the dislocation. The contrast may also appear as two parallel dark lines on opposite sides of the dislocation when two Bragg reflexions are excited. The contrast also changes sides by crossing higher order extinction contours. The theory was found to hold for thin regions, where absorption is unimportant, and for angles not too close to the Bragg angle. Examples of the observed effects were described.

Mr. A. HOWIE and Dr. M. J. WHELAN also presented a paper on anomalous absorption effects in metal foils. Experiments by transmission electron microscopy on metal foils have revealed certain interesting contrast effects in the form of dark bands in thicker regions (greater than about 0.1 μ

in thickness), thought to be due to an anomalous absorption effect similar to the well-known Borrmann effect^(28, 29) observed with X-rays. The bands appeared dark and showed poor resolution, suggesting absorption of electrons, whereas regions just outside the bands showed very good electron transmission and resolution. Selected area diffraction experiments showed that a dark band with its light borders was associated with Bragg reflexions $\{hkl\}$ and $\{\bar{h}\bar{k}\bar{l}\}$. The bands showed no fringe structure as for extinction contours, but merged into extinction contours in thin regions. A theory for these bands was outlined; the effect may account for the very high electron transmission of thick foils close to the Bragg angle.

The last paper, dealing with electron scattering and the contrast of electron micrographs, was given by Dr. J. S. HALLIDAY and Mr. T. F. J. QUINN (Associated Electrical Industries Ltd., Aldermaston). The contrast produced by electron scattering in an amorphous film, thickness t , is given by $C = t(1-p)/\lambda_T$, where λ_T is the electron mean free path when elastic and inelastic scattering occurs and $p = \int_0^{\omega_0} d\sigma_T$, σ_T being the total scattering cross section and ω_0 the solid angle of the objective aperture. This equation is the quantitative equivalent of that proposed by Hall⁽³⁰⁾ and, unlike that of Zeitler and Bahr,⁽³¹⁾ should apply in plural scattering conditions. Experiments with evaporated iron films confirmed that C was proportional to t/λ_T and dependent on ω_0 , but the theoretical values, calculated from data given by Lenz,⁽³²⁾ were about four times smaller. This discrepancy, which also occurred with other elements, may be due to under-estimation of the differential scattering cross-section at the very smallest angles.

J. A. CHAPMAN and M. J. WHELAN

References

- (1) PASHLEY, D. W., and PRESLAND, A. E. B. *J. Inst. Metals*, **4**, p. 419 (1959).
- (2) BILBY, B. A., and CHRISTIAN, J. W. *Institute of Metals Monograph and Report Series*, No. 18, p. 121 (London: Institute of Metals, 1956).
- (3) KELLY, P. M., and NUTTING, J. *J. Inst. Metals*. To be published.
- (4) JONES, D. A., and MITCHELL, J. W. *Phil. Mag.*, **3**, p. 1 (1958).
- (5) NORDHEIM, R., and GRANT, R. *Trans. A.I.M.E.*, p. 211 (1954).
- (6) NICHOLSON, R. B., and NUTTING, J. *Acta Metallurgica*. To be published.
- (7) WESTMACOTT, K. H., HULL, D., BARNES, R. S., and SMALLMAN, R. E. *Phil. Mag.* To be published.
- (8) SILCOX, J., and HIRSCH, P. B. *Phil. Mag.* To be published.
- (9) FORSYTH, P. J. E. *J. Inst. Metals*, **80**, p. 181 (1951-2).
- (10) PFEFFERKORN, J. *Naturwissenschaften*, **21**, p. 551 (1953).
- (11) GUNZ, W. *Steam Eng.*, p. 222 (May, 1956).
- (12) NEWMAN, R. C., and WAKEFIELD, H. *Proceedings of the International Conference on Solid State Physics in Electronics and Telecommunications* (Brussels, 1958).
- (13) *Proceedings of the Second International Symposium on X-Ray Microscopy and X-Ray Microanalysis* (Stockholm, June 15-17, 1959). To be published.
- (14) MULVEY, T. *J. Sci. Instrum.*, **36**, p. 350 (1959).
- (15) MULVEY, T. *Mémoires Scientifiques Rev. Metallurg.*, **56** (part 2), p. 163 (1959).
- (16) DLUGOSZ, J. *Proc. Stockholm Conf. on Electron Microscopy*, p. 283 (Stockholm: Almqvist and Wiksell, 1956).
- (17) BRADLEY, D. E. *Brit. J. Appl. Phys.*, **10**, p. 198 (1959).
- (18) BASSETT, G. A. *Phil. Mag.*, **3**, p. 1042 (1958).
- (19) HARRISON, B. D., and NIXON, H. L. *J. Gen. Microbiol.* To be published.
- (20) NIXON, H. L., and HARRISON, B. D. *J. Gen. Microbiol.* To be published.
- (21) BRENNER, S., and HORNE, R. W. *Biochem. Biophys. Acta*, **34**, p. 103 (1959).
- (22) SMITH, K. M., and HILLS, G. J. *J. Insect Pathology*. To be published.
- (23) HORNE, R. W., BRENNER, S., WATERSON, A. P., and WILDY, P. *J. Molec. Biol.*, **1**, p. 84 (1959).
- (24) BRENNER, S., STREISINGER, G., HORNE, R. W., CHAMPE, S. P., BARNETT, L., and BENZER, S. *J. Molec. Biol.* To be published.
- (25) GLAUERT, A. M., and GLAUERT, R. H. *J. Biophys. Biochem. Cytol.*, **4**, p. 191 (1958).
- (26) CHAPMAN, J. A., and ZUSSMAN, J. *Acta Cryst.*, **12**, p. 550 (1959).
- (27) HIRSCH, P. B., HOWIE, A., and WHELAN, M. J. *Proc. Roy. Soc.* To be published.
- (28) BORRMANN, G. *Phys. Z.*, **42**, p. 157 (1941).
- (29) BORRMANN, G. *Z. Phys.*, **127**, p. 297 (1950).
- (30) HALL, C. E. *J. Appl. Phys.*, **22**, p. 655 (1951).
- (31) ZEITLER, E., and BAHR, G. F. *Exptl. Cell Research*, **12**, p. 44 (1957).
- (32) LENZ, F. *Z. Naturforsch.*, **9a**, p. 185 (1954).

Temperatures, thermal stresses and displacements in solid uranium dioxide rods

by J. P. ELLINGTON, B.Sc., A.M.I.Mech.E., United Kingdom Atomic Energy Authority, Development and Engineering Group, Risley, Warrington, Lancashire

[Paper first received 16 June, and in final form 5 August, 1959]

Abstract

Expressions are derived for the temperatures, stresses and displacements in a solid uranium dioxide fuel rod, the thermal conductivity of which decreases exponentially with temperature. Graphs of the temperatures and displacements are given, and calculation shows that the rod will fracture when the centre-to-surface temperature drop exceeds 80–90° C.

Introduction

THE calculation of temperatures, thermal stresses and dilations in fuel rods is necessary for design purposes, but it is rendered difficult with uranium dioxide fuel by the wide variation of thermal conductivity of the substance with temperature. However, it is possible, with a suitable expression representing this variation of conductivity, to derive equations for the required temperatures, stresses and expansions and to obtain graphs showing the relationships between these quantities and the rating, diameter and surface temperature of the fuel.

Thermal conductivity of uranium dioxide

Measurements of the thermal conductivity of uranium dioxide have been reported by several investigators, the results exhibiting a large scatter attributed to experimental difficulties and to fracture of the specimens. Two expressions have been suggested to represent the thermal conductivity k , Scott⁽¹⁾ giving:

$$k = \frac{10(\rho/\rho_0)}{T + 400} \text{ W/cm } ^\circ\text{C},$$

and Rose⁽²⁾ giving:

$k = 0.024(\rho/\rho_0) \exp \{-1.2 \times 10^{-3}(T + 273)\} \text{ cal/cm s } ^\circ\text{C}$, where (ρ/ρ_0) is the ratio of the material density to the theoretical density of uranium dioxide, and T is the temperature in deg. C.

The latter expression has been found easier to use, and, noting that

1 cal/cm s °C is equivalent to $2.419 \times 10^2 \text{ CHU/ft h } ^\circ\text{C}$,

it can be rewritten as,

$$k = 4.20(\rho/\rho_0) \exp(-1.2 \times 10^{-3} \times T) \text{ CHU/ft h } ^\circ\text{C} \quad (1)$$

Temperatures in a solid rod

For radial heat flow in a solid rod of outer radius R with internal heat generation of density H , the equation of conduction is:

$$\pi r^2 H = -k(2\pi r) \frac{dT}{dr}$$

and equation (1) can be rewritten as:

$$k = A \exp(-BT) \quad (2)$$

where for uranium dioxide, $A = 4.20(\rho/\rho_0) \text{ CHU/ft h } ^\circ\text{C}$ and $B = 1.2 \times 10^{-3}/^\circ\text{C}$. Integration gives:

$$\frac{HB}{4A}(R^2 - r^2) = \exp(-BT_0) - \exp(-BT),$$

or:

$$T = -\frac{1}{B} \ln \left\{ \exp(-BT_0) - \frac{HB}{4A}(R^2 - r^2) \right\} \quad (3)$$

where T_0 is the surface temperature. The centre temperature T_i is then:

$$T_i = -\frac{1}{B} \ln \left\{ \exp(-BT_0) + \frac{HBR^2}{4A} \right\} \quad (4)$$

If h is the rating of the fuel in megawatts per tonne of uranium {MW/Te(U)}, the rating of the uranium dioxide is $(238/270)h \text{ MW/Te(UO}_2\text{)}$, or, with a theoretical density of 10.97 gm/cm^3 , the rating is

$$10.97 \times (238/270)(\rho/\rho_0) \times 10^{-6} h \text{ MW/cm}^3(\text{UO}_2).$$

1 MW $\equiv 1.896 \times 10^6 \text{ CHU/h}$ and $1 \text{ cm}^3 \equiv 3.531 \times 10^{-5} \text{ ft}^3$.

Thus, the density of internal heat generation H is given by:

$$H = 10.97 \times \frac{238}{270} \times \frac{1.896 \times 10^6}{3.531 \times 10^{-5}} \times \frac{\rho}{\rho_0} \times 10^{-6} h,$$

$$\text{or: } H = 5.19 \times 10^5 (\rho/\rho_0) h \text{ CHU/ft}^3 \text{ h} \quad (5)$$

Then, if D is the diameter of the rod, in inches:

$$T_i = -\frac{1}{B} \ln \{ \exp(-BT_0) - 0.0645hD^2 \} \quad (6)$$

It will be noted that, as both H and A are proportional to (ρ/ρ_0) for a given rating, h and diameter D the temperatures are independent of the density. Fig. (1) gives values of the centre temperature T_i , and shows the rapid increase of centre temperature with small changes in surface temperature at higher ratings and diameters. The temperature distribution across the fuel may also be found from this figure by reading off the value of surface temperature, at a given centre temperature corresponding to the required hD^2 value.

Thermal stresses and expansions

For a brittle material, such as a sintered form of uranium dioxide, the criterion of failure is that the maximum tensile stress exceeds the fracture strength. In the case under consideration, the maximum tensile stress is the circumferential stress occurring at the outer radius of the cylinder, and failure will occur by cracks propagating along radial planes

towards the centre of the cylinder. Timoshenko⁽³⁾ gives the following expression for the circumferential stress in a long cylinder:

$$\sigma_{\theta} = \frac{\alpha E}{1-\nu} \left(\frac{1}{R^2} \int_0^R T r dr + \frac{1}{r^2} \int_0^r T r dr - T \right),$$

the maximum stress at $r = R$ being:

$$\sigma_{max} = \frac{\alpha E}{1-\nu} \left(\frac{2}{R^2} \int_0^R T r dr - T_0 \right) \quad (7)$$

Here α is the coefficient of linear expansion, E is Young's modulus and ν is Poisson's ratio, all taken as being constant

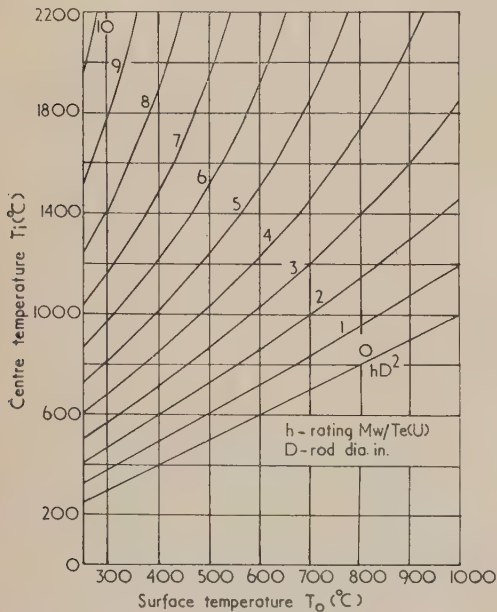


Fig. 1. Values of centre temperature

over the temperature range concerned. Substitution in equation (7) from equations (3) and (4) gives:

$$\sigma_{max} = \frac{\alpha E}{1-\nu} \left[\frac{1}{R^2} \int_0^R \ln \left\{ \exp(-BT_i) + \frac{HB}{4A} r^2 \right\} d(r^2) - T_0 \right],$$

or

$$\sigma_{max} = \frac{\alpha E}{(1-\nu)B} \left[1 - \frac{B(T_i - T_0)}{\exp \{B(T_i - T_0)\} - 1} \right] \quad (8)$$

If $(T_i - T_0)$, the centre-to-surface temperature drop, is fairly small then the exponential term can be expanded as:

$$\frac{x}{\exp(x) - 1} \approx \frac{x}{x + \frac{1}{2}x^2}$$

which is approximately $1 - \frac{1}{2}x$. Thus equation (8) becomes:

$$\sigma_{max} = \frac{\alpha E(T_i - T_0)}{2(1-\nu)} \quad (9)$$

Nichols⁽⁴⁾ gives an average figure of 17000 lb/in.² for the fracture strength of uranium dioxide at 1000°C, so that with values of $E = 27.5 \times 10^6$ lb/in.², $\nu = 0.25$ and $\alpha = 11 \times 10^{-6}/^\circ\text{C}$:

$$(T_i - T_0)_{max} = \frac{1.5 \times 17000}{11 \times 27.5} ^\circ\text{C},$$

or 84°C.

As the fracture strength seems to decrease with temperature, it can thus be said that cracking will occur when the centre-to-surface temperature drop exceeds 80–90°C. For temperature drops below this value, the radial expansion u can be calculated from the hoop strain as:

$$(u/r) = (\sigma_{\theta} - \nu\sigma_z)/E.$$

From Reference (3), for a long cylinder with free ends, the longitudinal stress σ_z at the outer radius equals the hoop stress σ_{θ} giving the maximum radial displacement δ as:

$$\delta = R(1 - \nu)\sigma_{\theta}/E = R\alpha(T_i - T_0)/2 \quad (10)$$

To this, of course, must be added the thermal expansion in raising the rod from room temperature to the surface temperature T_0 . To calculate the radial expansion in the case where the fuel is cracked, it is assumed that the material has no coherence and that each element is free to expand unrestrainedly. In this case:

$$\delta = \alpha \int_0^R T dr,$$

or by substitution from equation (3):

$$\delta = \alpha \int_0^R \left\{ T_i - \frac{1}{B} \ln(1 + \beta^2 r^2) \right\} dr \quad (11)$$

where $\beta^2 = HB/[4A \exp(-BT_i)]$.

Integration then gives:

$$\delta = \alpha R \left\{ T_i - \frac{1}{B} \ln(1 + \beta^2 R^2) + \frac{2}{B} \left(1 - \frac{\tan^{-1} \beta R}{\beta R} \right) \right\},$$

or:

$$\delta = \alpha R \left\{ T_0 + \frac{2}{B} \left(1 - \frac{\tan^{-1} [\exp \{B(T_i - T_0)\} - 1]^{1/2}}{[\exp \{B(T_i - T_0)\} - 1]^{1/2}} \right) \right\} \quad (12)$$

A useful approximation valid for values of centre-to-surface temperature drop up to about 300°C can be found by expanding the term in large parentheses as:

$$(\tan^{-1} x)/x \approx 1 - (x^2/3).$$

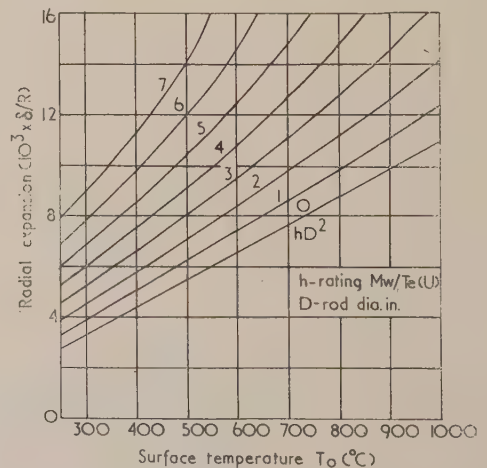


Fig. 2. Values of δ/R calculated from equation (12)

Equation (12) then becomes:

$$\delta \simeq \alpha R \left(T_0 + \frac{2}{3B} [\exp \{B(T_i - T_0)\} - 1] \right)$$

or

$$\delta \simeq \alpha R \left\{ T_0 + \frac{2}{3}(T_i - T_0) \right\}, \text{ for } (T_i - T_0) < 300^\circ \text{ C} \quad (13)$$

Fig. 2 gives values of δ/R calculated from equation (12), based on an average value of α of $11 \times 10^{-6}/^\circ\text{C}$.

References

- (1) SCOTT, R. *Thermal conductivity of UO_2* , AERE M/R. 2526 (1958).
- (2) ROSE, R. G. *A note on thermal conductivity of UO_2* , IGR-TM/R. 0175 (1958).
- (3) TIMOSHENKO, S., and GOODIER, J. N. *Theory of Elasticity* (New York: McGraw-Hill, 1951).
- (4) NICHOLS, R. W. *Nuc. Eng.*, 3 (29), p. 327 (1958).

Sensitive method for measurement of magneto-resistance effect with direct currents and with microwaves

by D. E. CLARK, Ph.D., A.Inst.P., and J. G. ASSENHEIM, B.Sc., A.M.I.E.E., The Northern Polytechnic, London

[Paper first received 26 June, and in final form 19 August, 1959]

Abstract

An experimental investigation is made of the magneto-resistance effect in bismuth at frequencies of 9.2×10^9 , 1.5×10^9 and 1.1×10^9 c/s, in magnetic fields of intensities up to 6270 oersteds. Some results were also obtained using direct current. The method developed for the measurements is one of high sensitivity. In general form the results are in agreement with the theoretical predictions of Donovan.⁽¹⁾

Introduction

CONSIDERABLE attention has, in the past, been devoted to measurements on the magneto-resistance effect, that is, the change in the electrical resistance of a conductor resulting from a magnetic field applied either perpendicularly to the current lines (the transverse effect), or parallel to the current lines (the longitudinal effect). Most of the early work was undertaken by measuring the change in the direct-current resistance of the specimen, though some measurements have been made with high-frequency currents. If ΔR is the change in the resistance of a specimen resulting from an increase of magnetic field from zero intensity to a value of H oersted, and if R is the resistance in zero field, then for most materials:

$$\frac{\Delta R}{R} = \alpha - aH^n \quad (1)$$

The index n is a constant usually found to be about 2. For bismuth, which was the material used throughout the present set of measurements, the experimental values obtained by using direct currents are $\alpha = 0.12$ and $a = 0.32$ in transverse fields of intensities equal to 4000 and 8000 oersteds respectively.⁽²⁾ In 1948 Blunt⁽³⁾ made observations on bismuth at a frequency of 3.5×10^6 c/s, and his results agreed closely with those obtained with direct currents. In 1950 Heaps⁽⁴⁾ showed that at the microwave frequency of 3×10^9 c/s, α is about one-half of its direct-current value but that it depends, to a marked degree, on the nature of the surface. Donovan,⁽¹⁾ in a theoretical treatment of the subject, applied the electron theory of metals to the problem, and showed that at suffi-

ciently high frequencies, the magneto-resistance effect should become too small to be detected. For a model in which the electrons occupy two overlapping, partially filled bands, the nature of the frequency variation of the magneto-resistance effect was calculated to be similar to that of Fig. 1, where

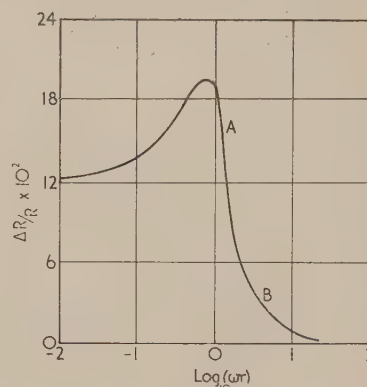


Fig. 1. Variation of magneto-resistance effect with frequency (Theoretical curve for $H = 1.1 \times 10^5$ oersteds.)

$\omega/2\pi$ is the frequency of observation and τ is the relaxation time of the electrons. No appreciable decrease in the effect should occur until the frequency exceeds $\omega_1/2\pi$, which is given approximately by:

$$\omega_1\tau = 1. \quad (2)$$

On this theory, the results of Heaps indicate that, for bismuth, the relaxation time is about 3×10^{-11} s, though from the observations of Pippard and Chambers⁽⁵⁾ on the determination of the mean free path of electrons in bismuth, the relaxation time should be about 5×10^{-12} s. Mead⁽⁶⁾ has recently made observations on the magneto-resistance effect in bismuth at a frequency of approximately 10^{10} c/s, and found that, in fields of intensities up to 10000 oersteds, α was too small to be detected—that is, it was less than 0.001.

The main purpose for undertaking the present series of

observations was that of obtaining further experimental results over the portion of the curve *AB* of Fig. 1, with the view to verifying experimentally the predictions of Donovan.⁽¹⁾ By devising a method which is considered to be of greater sensitivity than those which had previously been used by other experimenters, it was hoped to be able to detect a resistance change at the frequency of 10^{10} c/s in a field of intensity about 6000 oersteds, that is, under conditions which, from previous work, might be expected to yield values of α possibly as low as 1×10^{-3} or less. By making observations also at frequencies lower than that used by Heaps⁽⁴⁾ the general shape of the curve *AB* was investigated. In order to assess the validity of the method used at these high frequencies, observations were also made with direct currents using a fundamentally similar arrangement.

Experimental methods

The experiments of Heaps⁽⁴⁾ basically comprised the measurement of the *Q*-factors of a cylindrical wave-guide cavity, both with and without a steady magnetic field applied in a suitable direction, the cavity being made entirely from the specimen of bismuth under investigation. In the present series of observations a rectangular wave-guide cavity was used at the highest frequency investigated, and coaxial line resonators were used at the other frequencies. In each of these resonators, to facilitate construction, only part of the system was of bismuth, the remainder being of brass. The details of the coaxial line resonators are illustrated in Fig. 2.

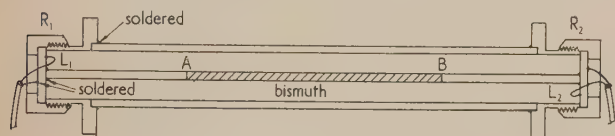


Fig. 2. Resonant line construction

Each resonator was of electrical length equal to half the wavelength at the frequency for which it was designed. The portion *AB* of the centre conductor was a rod of bismuth turned to the requisite diameter. The remainder of this conductor, the outer conductor, and the end plates were of brass. For some measurements, *AB* was replaced by a length of brass rod of the same diameter as the bismuth rod. Energy was coupled into and out of each resonator by loops *L*₁ and *L*₂, formed by soldering to the end plates the ends of the centre conductor of the coaxial cables, as indicated. The sections of the resonators were securely held together by threaded rings *R*₁ and *R*₂ which were tightened firmly to reduce the effect of contact resistance. A separate experiment was conducted using a specimen of half the length of the one on which the measurements were made, and from the readings obtained a determination of the contact resistance between the brass sections of the centre conductor and the test material was made. The main components used in the observations are indicated in Fig. 3. The electromagnet was operated from the 50 c/s mains supply, and the frequency of the oscillator was adjusted to the resonant frequency *f* of the resonator. The *Q* factor of any coaxial line resonator is a function of the resistance of the central conductor, that is, on the strength of the magnetic field if the coefficient α of equation (1) is not zero. The resonance curves of a resonator obtained, for example, by frequency variation of the applied signal using a source of constant current output, are as indicated in Fig. 4, for the conditions of (a) an applied

magnetic field and (b) zero field. Though the difference between these two curves is greatly exaggerated for normal values of the field intensity, such a difference is present if the magneto-resistance effect is not zero. That is, the *Q*-factor obtained from curve (b) is greater than that obtained from curve (a). As the field of the electromagnet, which can be assumed to have a sinusoidal variation with time, varies in the manner indicated in Fig. 5(a), the resistance of the bismuth specimen, which depends on the intensity of the magnetic

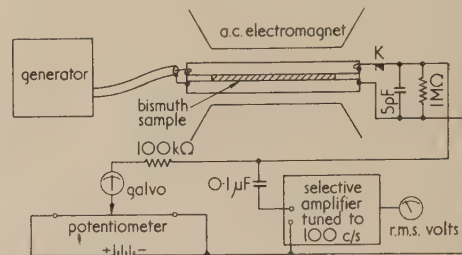


Fig. 3. Resonant line and components

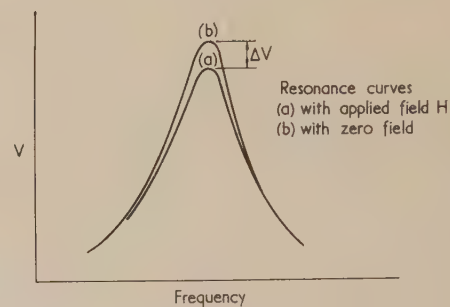


Fig. 4. Effect of magnetic field on *Q*-factor of resonator

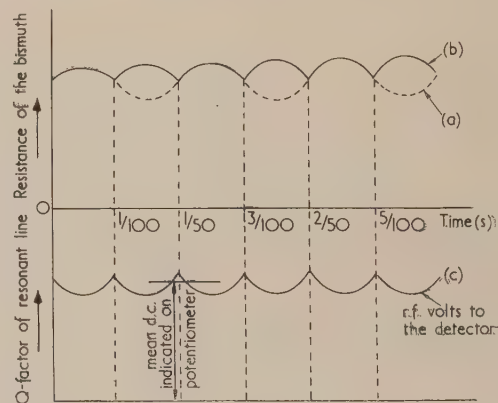


Fig. 5. Modulation of r.f. voltage by alternating magnetic field

field, varies in the manner indicated in Fig. 5(b). A reversal of the direction of the field does not alter the sign of the resistance change. This resistance variation causes the *Q*-factor of the tuned line to vary with time in the manner shown in Fig. 5(c), which is effectively equivalent to a modulation of the radio-frequency signal in the resonant line. Reference to Fig. 3 shows that this modulation depth can be determined quite simply by measuring the amplitude of the 100 c/s component of the output voltage from the crystal detector *K* by means of a selective amplifier, while the d.c. component may be measured by means of the potentiometer shown. The small change in *Q* as the bismuth changes its

resistance can thus be calculated by means of a simple Fourier analysis. The selective amplifier was tuned to receive the 100 c/s component rather than the 50 c/s one in order to eliminate the effects of the large 50 c/s stray field around the a.c. electromagnet, which would otherwise render the method impracticable. With conventional methods, using steady magnetic fields, in which it is necessary to measure a small change in a large current reading, sensitivity is not very high. The system described above is capable of considerably higher sensitivity mainly because the small change in current, produced by the application of the magnetic field and which alternates with a fundamental frequency equal to the field frequency, is readily separable from the much larger main current. The amplifier responds only to this alternating current which is proportional to the coefficient α . The limit of sensitivity attainable is set mainly by the characteristics of the amplifier.

The method adopted for the measurements at a wavelength of 3 cm was basically similar to that described above, the only difference being that, instead of a coaxial line, the resonator was a rectangular wave-guide cavity of which one end wall was constructed of bismuth, the remainder being of brass. The cavity was placed in such a position that the bismuth wall was situated in the field of the electromagnet. Microwave energy was coupled into the cavity by means of the input probe, and the output was taken by a second probe as indicated in Fig. 6.

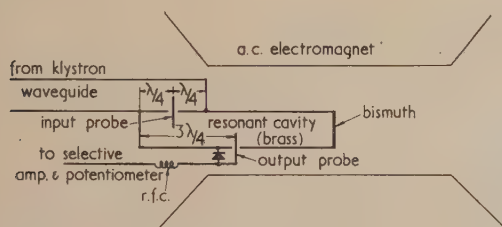


Fig. 6. Wave-guide resonator and components

In addition to the microwave measurements, a similar set of observations was made using direct current, the specimen being a length of bismuth wire through which was passed a direct current from a constant-current source. The field of the electromagnet was applied perpendicularly to the axis of the wire. For this set of observations, the e.m.f. across the specimen consisted of two components—a d.c. one caused by the current flowing through it, and an alternating one caused by the magnetic field producing an alternating change in the resistance of the bismuth. By determining the magnitudes of these components, as with the microwave measurements, the magneto-resistance effect was evaluated for direct currents.

Calculation of results

It is assumed that Q_1 is the Q -factor of the coaxial line resonator when the inner conductor is of brass, that Q_2 is this quantity when the inner conductor is of bismuth and no magnetic field applied, and that Q_3 is the value in a magnetic field H . If R_1 is the resistance per unit length of the outer conductor, and R_2 and R_3 are resistances per unit length of the brass and bismuth sections of the inner conductor, and if R_{3H} is the resistance per unit length of the bismuth section in a magnetic field H (see, for example, reference 7), then:

$$\frac{1}{Q_1} = \frac{R_1 + R_2}{\omega L} + \frac{8R_e}{\lambda\omega L} + R_a + R_{b1} \quad (3)$$

$$\frac{1}{Q_2} = \frac{R_1 + bR_2 + (1-b)R_3}{\omega L} + \frac{8R_e}{\lambda\omega L} + R_a + R_{b2} \quad (4)$$

$$\frac{1}{Q_3} = \frac{R_1 + bR_2 + (1-b)R_{3H}}{\omega L} + \frac{8R_e}{\lambda\omega L} + R_a + R_{b2} \quad (5)$$

where b depends on the fraction of the total length of the inner conductor occupied by brass, R_e is the resistance of each end plate, R_{b1} and R_{b2} are terms dependent on the contact resistances between the different sections of the inner conductor, and R_a is a term dependent on the effect of coupling loops, etc.

It is assumed that:

$$R_{b2} - R_{b1} = \delta \quad (6)$$

where δ is a small quantity determined experimentally by making a separate set of observations with a different length of bismuth in the centre conductor.

Then, from equations (3), (4), (5) and (6):

$$\frac{\frac{1}{Q_3} - \frac{1}{Q_2}}{\left(\frac{1}{Q_2} - \frac{1}{Q_1}\right) - \delta} = \frac{R_{3H} - R_3}{R_3 - R_2}$$

or:

$$\frac{\Delta Q}{(Q_1 - Q_2)} \cdot \frac{Q_1}{Q_3} \left\{ 1 + \frac{\delta Q_1 Q_2}{(Q_1 - Q_2)} \right\} \approx \frac{\Delta R}{R},$$

where ΔQ is the change in Q , and ΔR is the change in R produced by the magnetic field of intensity H . The last equation may be written:

$$\frac{\Delta R}{R} = \frac{Q_1}{(Q_1 - Q_2)} \cdot \frac{\Delta v}{v} \left\{ 1 + \frac{\delta Q_1 Q_2}{(Q_1 - Q_2)} \right\} \quad (7)$$

where v and Δv are determined experimentally. The value of v is obtained from the potentiometer readings after calibration, and Δv is obtained from the output readings of the

Table of α -values

Frequency = 9.2×10^9 c/s		Frequency = 1.5×10^9 c/s		Frequency = 1.1×10^9 c/s		D.C. measurements	
H (oersteds)	α	H (oersteds)	α	H (oersteds)	α	H (oersteds)	α
1030	0.0019	1030	0.0089	1030	0.022	1030	0.027
1424	0.0028	1424	0.0132	1424	0.036	2172	0.077
1612	0.0036	1612	0.0193	1612	0.037	3002	0.113
2172	0.0062	2172	0.0312	2172	0.065	4125	0.154
2736	0.0077	2736	0.041	2736	0.071	6270	0.23
3405	0.0105	3405	0.061	3405	0.097		
4125	0.0135	4125	0.073	4125	0.128		
4390	0.019	4390	0.088	4390	0.128		
6270	0.028	6270	0.130	6270	0.189		

selective amplifier, allowance being made for the fact that the 100 c/s component of the output signal is chosen.

Equation (7) was derived for the line resonator, and was the one used for all the microwave calculations. An identical equation can be derived for the wave-guide resonator.

Tabulated results

The values of α , in equation (1), obtained with bismuth at a temperature of approximately 20° C in a transverse magnetic field are given in the accompanying table.

From this table, it is seen that, over the frequency range investigated, the magneto-resistance effect falls off rapidly between 1.1×10^9 c/s and 9.2×10^9 c/s, the values at the lower of these frequencies being not greatly different from the d.c. values. However, there still appears to be an appreciable effect at the highest frequency of observation which is not in agreement with the results of Mead.⁽⁶⁾ It is considered that, though several difficulties occur if simple apparatus is used in measurements of this kind, the method is very sensitive

for the determination of small changes in the Q -factor of an electrical resonator. The method lends itself to measurements in fields other than the one investigated.

The results obtained in the present investigation lend support to the theoretical predictions of Donovan,⁽¹⁾ though further experimental work in this field seems desirable.

References

- (1) DONOVAN, B. *Proc. Phys. Soc. A*, **67**, p. 305 (1954).
- (2) *International Critical Tables*, Vol. VI (New York: McGraw-Hill Inc., 1929).
- (3) BLUNT, R. F. *Phys. Rev.*, **73**, p. 654 (1948).
- (4) HEAPS, C. W. *Phys. Rev.*, **80**, p. 892 (1950).
- (5) PIPPARD, A. B., and CHAMBERS, R. G. *Proc. Phys. Soc. A*, **65**, p. 955 (1952).
- (6) MEAD. Unpublished work.
- (7) JACKSON, W. *High Frequency Transmission Lines*. (London: Methuen, 1945).

Change of size of air bubbles in water containing a small dissolved air content

by D. M. J. P. MANLEY, B.Sc., Ph.D., A.Inst.P.,* Department of Mathematics and Physics, The Polytechnic, Regent Street, London, W.1

[Paper received 24 June, 1959]

Abstract

The rates of growth and collapse of air bubbles in distilled degassed water are studied. Experimental results show that the effective diffusion coefficient for air through the bubble walls is low at very small bubble diameters. These results are interpreted by the organic skin effect, and the physical qualities of this skin surrounding the bubble walls are discussed.

Introduction

IN order to acquire information concerning the stability of the nuclei or discontinuities that help to produce cavitation in water under tension, it is necessary to study the change of size of air bubbles. The change of volume of air bubbles in water at static pressure will depend entirely on the diffusion rate of air through the bubble walls into or out of solution of the surrounding liquid.

The water can be placed in a supersaturated or undersaturated state by the variation of the superincumbent pressure, and it is found that the most advantageous state of the water for experimental work is when the dissolved air content is about 5 to 10% of that corresponding to distilled water at atmospheric air pressure.

The change of size of bubbles in water which is either under-saturated or supersaturated with air has been studied theoretically by Epstein and Plesset.⁽¹⁾ The change of

diameter D with time t of an air bubble of initial diameter D_0 is given by the relation:

$$\frac{D^2}{D_0^2} = 1 + \frac{8k(c_i - c_s)t}{\rho' D_0^2} \quad (1)$$

where c_i is the initial dissolved air concentration in solution in the water, c_s is the saturated gas concentration in solution corresponding to the pressure P in the water in the neighbourhood of the bubble concerned, ρ' is the density of air in the bubble and k is the diffusion coefficient of the air through water.

Equation (1) shows that the change of the square of the diameter of a bubble divided by the time t will be a constant i.e.

$$\frac{D^2 - D_0^2}{t} = \frac{8(c_i - c_s)k}{\rho'} \quad (2)$$

In degassed water, $c_i \ll c_s$, and equation (2) will become:

$$(D^2 - D_0^2)/t = -8c_s k/\rho' \quad (3)$$

For an air bubble in degassed water at which the pressure P is one atmosphere, values⁽²⁾ are $8c_s/\rho'$ equal to 0.16, and k is 2×10^{-5} cm² s⁻¹; therefore $(D^2 - D_0^2)/t$ is 3.2×10^{-6} cm² s⁻¹.

Air bubbles in undersaturated water

The study of the change of diameters of bubbles with time has been undertaken using a simple apparatus constructed o

* Now at Royal Aircraft Establishment, Farnborough, Hampshire.

Perspex (Fig. 1a), the bubble resting underneath the top Perspex plate. A bright annulus is seen on the outside of the bubble as shown in Fig. 2(a). Let x be the inner radius of the bright ring and R be the radius of the bubble, then the contact angle θ of water with the Perspex is given by the equation:

$$\sin \theta = x/R \quad (4)$$

The volume of the bubble (Fig. 2b) is:

$$(\pi R^3/3)\{2 + \cos \theta (2 + \sin^2 \theta)\} \quad (5)$$

The area of the air-water boundary is:

$$2\pi R^2(1 + \cos \theta) \quad (6)$$

From the solution of the diffusion equation (Epstein and Plesset), it can be shown that:

$$dV/dt = Ak(\partial c/\partial r)R \quad (7)$$

where V is the volume of the bubble, A is the area of the water boundary, and $(\partial c/\partial r)_R$ is the dissolved gas concentration gradient at the bubble boundary. Equation (1) is therefore modified to:

$$\left(\frac{D^2}{D_0^2} - 1\right) \left\{ \frac{2 + \cos \theta (2 + \sin^2 \theta)}{32(1 + \cos \theta)} \right\} = \frac{k(c_i - c_s)t}{\rho' R_0^2} \quad (8)$$

for a bubble with contact angle θ against Perspex.

Experimental results

Air bubbles in undersaturated water. Fig. 3(a) shows the square of the diameter (D^2) plotted against time t for a typical bubble resting under Perspex, and Fig. 3(b) shows the change of contact angle θ {as determined by equation (4)} plotted against diameter D . Curve (a) of Fig. 3(a) was plotted taking no account of the Perspex boundary; curve (b) shows the correction due to contact angle only. Owing to the presence of the Perspex surface, however, the concentration distribution of dissolved gas around the bubble will not be uniform, and this factor reduces the gas transport rate. Liebermann⁽³⁾ has evaluated a correction term applicable for a plane boundary next to the bubble, and equation (1) therefore becomes:

$$1.45 \frac{D^2}{D_0^2} = 1 + \frac{8k(c_i - c_s)t}{\rho' D_0^2} \quad (9)$$

The gradient of curve (b) in Fig. 3(a) gives a calculated value for the diffusion coefficient of air through water as $1.46 \times 10^{-5} \text{ cm}^2 \text{ s}^{-1}$. Using the correction factor of Liebermann, the diffusion coefficient of air through water is $2.1 \times 10^{-5} \text{ cm}^2 \text{ s}^{-1}$. This value compares very favourably with other existing data.⁽⁴⁾

Air bubbles in supersaturated water. The growth of single bubbles was observed against the inner cylindrical surface of a vertical Perspex tube. Fig. 1(b) shows the simple apparatus used to place the water in the vertical Perspex tube in a supersaturated state by the reduction of the air

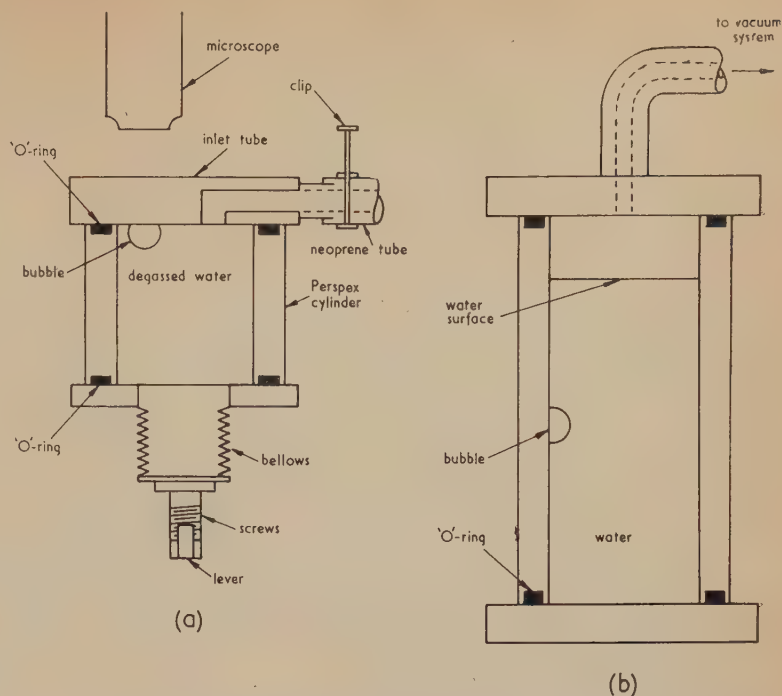


Fig. 1. Apparatus for the observation of the change of size of air bubbles in (a) undersaturated water and (b) supersaturated water

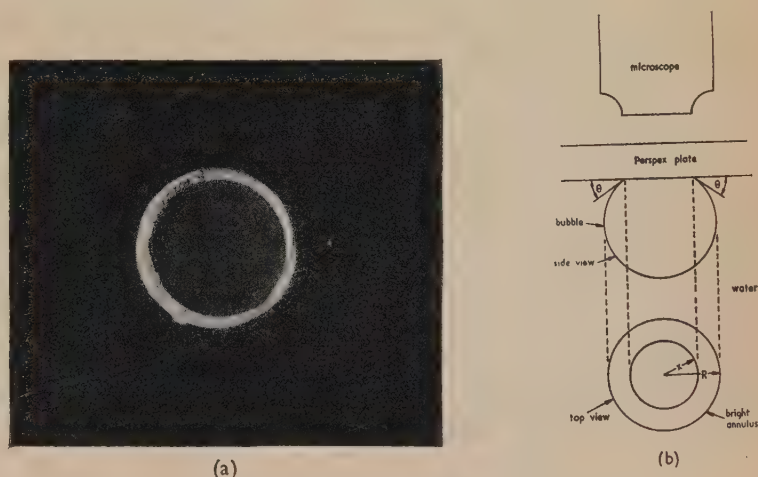


Fig. 2. (a) Photograph of air bubble under the Perspex plate. (b) Diagram of the air bubble under the Perspex plate

pressure above the water surface. The water is initially at atmospheric pressure containing only about 20 cm^3 of dissolved air per litre.

The square of the diameter of a typical bubble is plotted against time (Fig. 4) for water, and from the gradient of the linear section of the graph it is calculated that the supersaturation ratio c_i/c_s is 63 using equation (1). The bubble was at a depth of 3.7 cm in the water.

Similar experiments to investigate the growth of a large number of bubbles in water showed that the growth rate was very similar to that given in Fig. 4, although the instant at which the bubble first appeared was a function of depth in the water.

Low diffusion rates associated with very small bubbles. Fig. 3(a) for diminishing bubbles in undersaturated water shows that the square of the diameter of the bubble no longer

changes in proportion with time when the bubble is very small. However it is difficult to measure with any accuracy the apparent reduction in the coefficient of diffusion of air associated with these small bubbles. On the other hand, Fig. 4, for the case of growing bubbles in supersaturated water, does show clearly the reduction in the diffusion coefficient of air into the bubble when the diameter is less than 0.4 mm. More accurate measurements are therefore possible on reduced diffusion rates with growing bubbles.

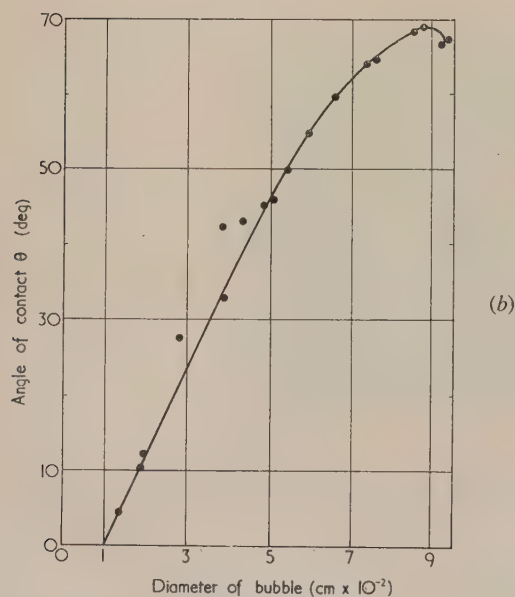
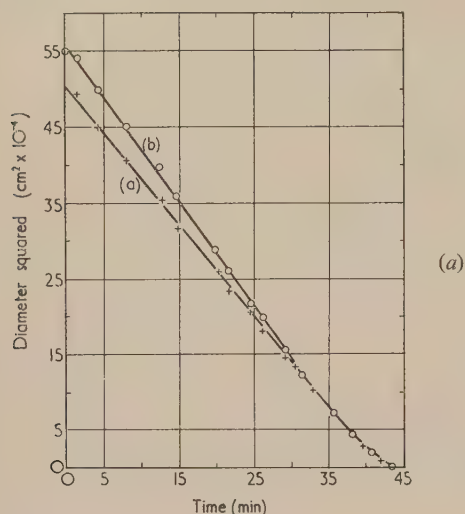


Fig. 3. (a) Plot of square of the bubble diameter against time (bubble decreasing in undersaturated water). (b). Plot of contact angle against bubble diameter

Theories of the lower diffusion coefficient associated with very small bubbles

Possible theories for interpreting the slow diffusion rate for air into or out of very small bubbles are:

- the effect of solid boundaries and saturated layers of dissolved gas around the bubble;
- a layer of charged particles on the bubble wall;
- dipole moments of the molecules on the bubble wall;

(d) the presence of an organic skin material surrounding the bubble.

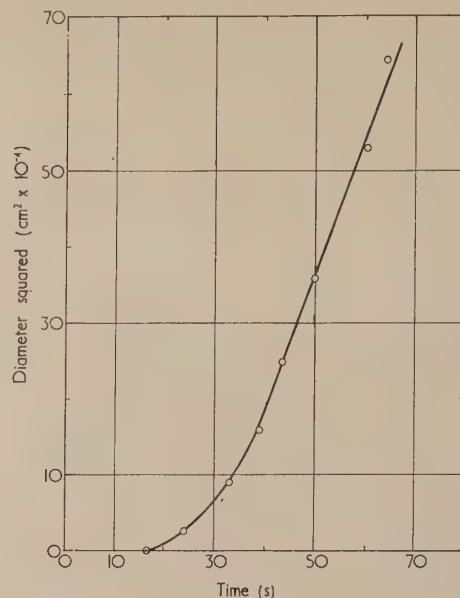


Fig. 4. Plot of square of the bubble diameter against time (bubble growing in supersaturated water)

The first three theories are unlikely to have much significance owing to the following factors—

(i) The change of the rate of diffusion of gas into or out of the bubble occurs at a given diameter that is *independent* of the initial bubble volume. Fig. 5 shows the change of D^2 with t for six bubbles of different initial volumes in undersaturated water. The diffusion coefficient of air out of these bubbles is seen to be reduced when the diameter of each bubble is 0.1 mm.

(ii) There is very little change in the diffusion rate out of small bubbles in water that has recently been well degassed.

(iii) Experiment shows that the addition of the wetting

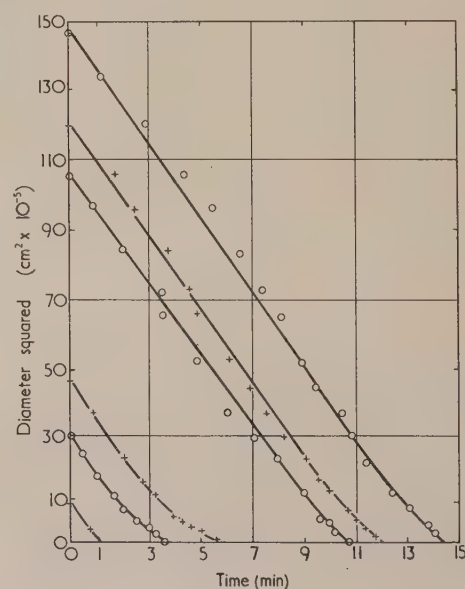


Fig. 5. Plot of square of bubble diameter against time for six bubbles of different initial volumes

agent Lissapol N to the water eliminates the reduction in the diffusion rate of gas associated with small bubbles.

The three results outlined above indicate that the most likely of the possible explanations is (d), that an organic skin of impurity surrounds the bubble.

The organic skin

Figs. 3(a) and 5 show that the diffusion rate of gas out of bubbles in undersaturated water is reduced to approximately 10% of the normal rate, when the bubble disappears into solution. After the bubble has disappeared, it has been found that a deposit of impurity occurs underneath the Perspex plate (Fig. 6) and this deposit is known not to be present before the bubble was formed. From observations with a low-powered microscope, it has been calculated that the volume of the deposit is between 10^{-7} and 10^{-8} cm³. A large number of similar bubbles has been studied and it has generally been found that the volume of the deposit was approximately constant. It was discovered, however, that a long exposure of the water to a vacuum was sufficient to reduce the volume of the impurity considerably. Then, a careful study of the change of size of very small bubbles indicated that the reduction in diffusion rate was not so pronounced. A few hours after the time of degassing, the deposit of impurity appeared to be of normal size.

Unsuccessful attempts were made to purify the water in order to eliminate the impurity. It was indicated by calculation that organic impurity in the water had to be less than 0.00001% of the total volume in order to prevent the deposit occurring. This degree of purity is not possible using the equipment designed for the experiments performed.

The diffusion coefficient of the organic skin

In order to find out how a skin of organic material surrounding a bubble causes the gas transport rate to be small for very small bubbles, it is necessary to know what material the skin consists of and its effective diffusion coefficient.

The method of finding the diffusion coefficient. It is assumed that the organic skin completely surrounds the water boundary of the bubble and it is of uniform thickness.

The growth of a bubble of radius R in supersaturated water is given by the equation (Epstein and Plesset):

$$\frac{dR}{dt} = \frac{k(c_i - c_s)}{\rho'} \left\{ \frac{1}{R} + \frac{1}{(\pi k t)^{1/2}} \right\} \quad (10)$$

If the supersaturation ratio is large, and if the water is initially at one atmosphere hydrostatic pressure, then:

$$\frac{dR}{dt} = 0.02k \left(\frac{c_i}{c_s} \right) \frac{1}{R} \quad (11)$$

Equation (11) is derived neglecting the effect of surface tension, but if the bubble is very small this has to be taken into account. Now c_i/c_s is $0.02/0.02p$, where p atmosphere is the initial gas pressure in the bubble. If the bubble is very small, the main contribution to the pressure is due to surface

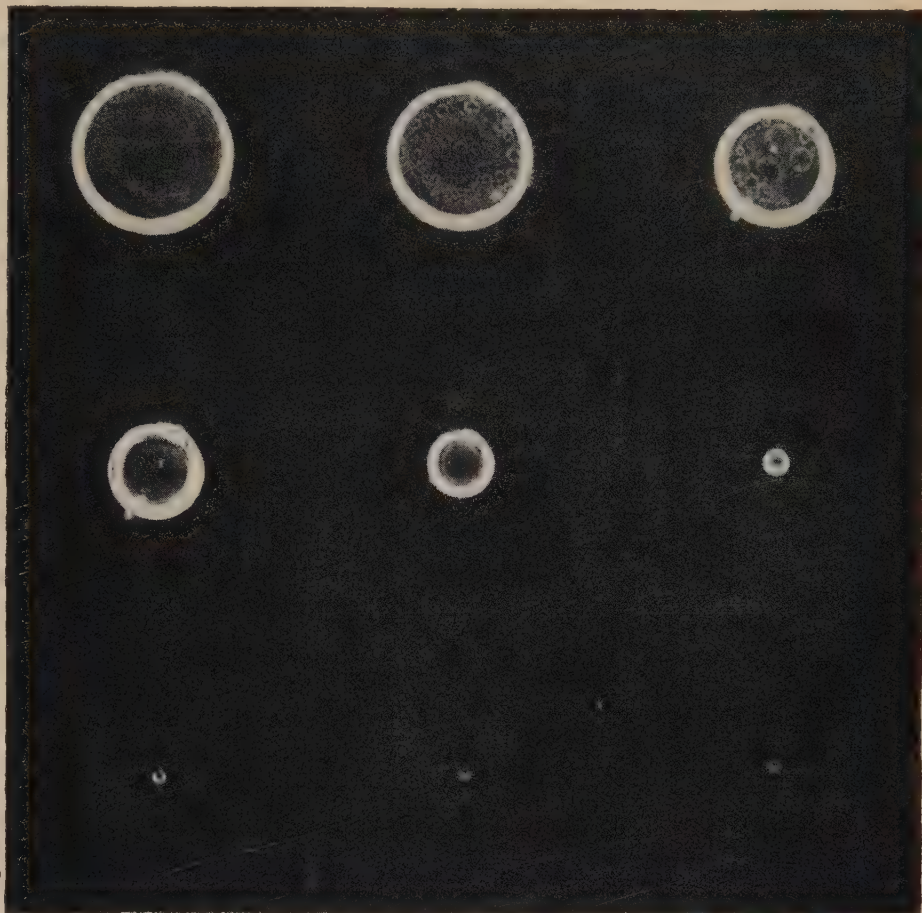


Fig. 6. Photographs taken every five minutes of an air bubble diminishing in size in undersaturated water until an impurity deposit is left

tension, as this will be much greater than the hydrostatic pressure outside the bubble; then

$$p = (2S/R)10^{-6} \quad (12)$$

where S is the surface tension coefficient associated with the skin. Applying equation (12), c_i/c_s will be $10^6 R/2S$.

Equation (11) therefore becomes:

$$dR/dt = 10^4 k/S \quad (13)$$

Considering the growth of a very small bubble with a skin of organic material of surface tension or tensile strength S' and diffusion coefficient k' , the change of radius will be given by the equation:

$$R - R_0 = 10^4 k' t / S' \quad (14)$$

where R_0 is the initial radius.

Experiment. The radius of a typical bubble growing in supersaturated water is plotted as a function of time (Fig. 7)

to a maximum radius of 0.2 mm. The gradient of this graph is $8 \times 10^{-4} \text{ cm s}^{-1}$. It is necessary to apply corrections for contact angle and the Perspex boundary, so that the gradient should be $1.28 \times 10^{-3} \text{ cm s}^{-1}$.

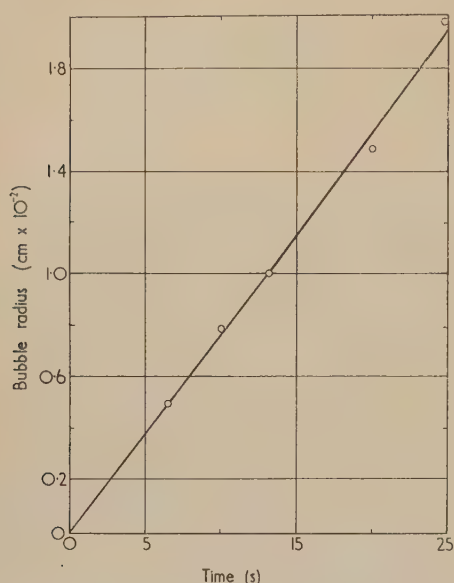


Fig. 7. Plot of bubble radius against time (bubble growing in supersaturated water)

The value of k' is found to be $2.6 \times 10^{-6} \text{ cm}^2 \text{ s}^{-1}$ on applying equation (14). This value of the diffusion coefficient of the organic skin is about one-eighth of the diffusion coefficient of air through pure water.

The tensile strength of the organic skin of impurity

The maximum diameters of bubbles growing on the side of a vertical Perspex wall has been measured as a function of water depth (Fig. 8). It is seen that the maximum diameter varies from 2 to 3.5 mm when the bubble breaks away from the Perspex and rises to the surface. If R' is the maximum

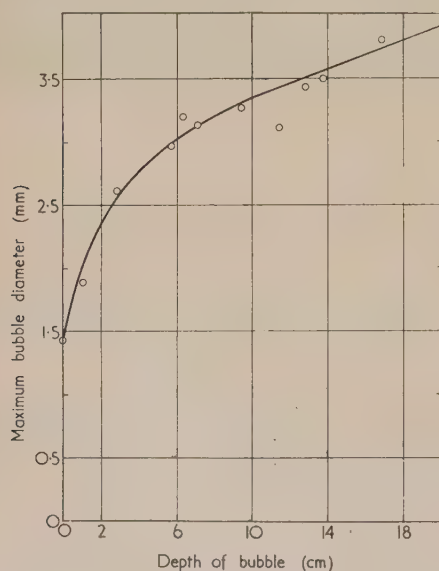


Fig. 8. Plot of maximum bubble diameter against its depth in supersaturated water

radius of the gas bubble, then the tensile strength S' of the skin is given by:

$$S' = \rho(R')^2 \left\{ \frac{2 + \cos \theta (2 + \sin^2 \theta)}{6 \sin \theta} \right\} \quad (15)$$

Observations indicated that the contact angle θ between Perspex and water was approximately 50° at the instant when the bubble broke away from the Perspex wall.

The maximum value of S' is calculated to be 32 dyn cm^{-1} at the largest water depth of 17 cm, with a minimum value of 8 dyn cm^{-1} at the surface.

Fox and Herzfeld⁽⁵⁾ calculated that the tensile strength of a fatty acid skin would be 50 dyn cm^{-1} , and that of a protein skin would be 5 dyn cm^{-1} . The present experimental results suggest that the organic skin consists partly of fatty acid and partly of protein materials, the ratio of which is dependent on the depth of the bubble in water.

Conclusion

The experimental evidence discussed in this paper suggests that many of the bubbles found in water are surrounded by skins of impurity. This skin has a maximum volume of 10^{-7} cm^3 , and has a diffusion coefficient of $2.6 \times 10^{-6} \text{ cm}^2 \text{ s}^{-1}$. The tensile strength of the skin varies with depth in the water and is between 8 and 32 dyn cm^{-1} .

Acknowledgement

The author wishes to thank Mr. J. Yarwood and Dr. L. E. Lawley for advice and supervision of the work.

References

- (1) EPSTEIN, P. S., and PLESSET, M. S. *J. Chem. Phys.*, **18**, p. 1505 (1950).
- (2) INTERNATIONAL CRITICAL TABLES. **5**, p. 62; **3**, p. 254 (New York: McGraw-Hill Book Co. Inc., 1932) (and also Ref. 1).
- (3) LIEBERMANN, L. *J. Appl. Phys.*, **28**, p. 205 (1957).
- (4) INTERNATIONAL CRITICAL TABLES. **5**, p. 62 (New York: McGraw-Hill Book Co. Inc., 1932).
- (5) FOX, F. E., and HERZFELD, K. F. *J. Acoust. Soc. Amer.*, **26**, p. 984 (1954).

Appendix

For a bubble in water with contact angle θ attached to a vertical Perspex wall, the volume is

$$\frac{\pi(R')^3}{3} \{2 + \cos \theta (2 + \sin^2 \theta)\} \quad (16)$$

The upthrust force is therefore

$$\frac{\pi \rho (R')^3}{3} \{2 + \cos \theta (2 + \sin^2 \theta)\} \quad (17)$$

and this is balanced by the tensile strength of the skin S' acting at the bubble-Perspex boundary. The length of this boundary is

$$2\pi R' \sin \theta \quad (18)$$

The force due to the skin will be

$$2\pi R' \sin \theta \cdot S' \quad (19)$$

Therefore

$$\frac{\pi \rho R'^3}{3} \{2 + \cos \theta (2 + \sin^2 \theta)\} = 2\pi R' \sin \theta \cdot S'$$

$$\text{Therefore } S' = \rho R'^2 \left\{ \frac{2 + \cos \theta (2 + \sin^2 \theta)}{6 \sin \theta} \right\} \quad (20)$$

Variation with particle size of the effective X-ray absorption coefficient of heterogeneous slabs

by G. B. MITRA, Ph.D., and A. J. C. WILSON, Ph.D., A.I.M., F.Inst.P., University College, Cardiff

Paper received 28 July, 1959]

Abstract

The effective absorption coefficient for transmission of X-rays through heterogeneous slabs differs from the weighted-mean absorption coefficient because of random fluctuations in the number of particles of each type of material along different parallel paths. The value of μ_{eff} is calculated for several models; for each it is less than μ , the difference becoming large for large particles.

1. Introduction

MANY authors⁽¹⁻⁶⁾ have given treatments of the effect of heterogeneity of specimen on the intensity of the X-rays diffracted. As Schäfer⁽⁴⁾ has pointed out, in a random distribution of the components of the mixture throughout the sample, the number of particles of one absorption coefficient encountered by the X-rays will differ in different parts of the specimen, even though the path length traversed is the same. By a random fluctuation it may happen that all particles traversed on one route are of one kind, or all of a different kind, or they may be of any intermediate mixture. It is difficult to treat this problem both generally and rigorously, and in the following paper some results are derived for special cases. In each the effective value of the absorption coefficient is found to be less than the absorption coefficient to be expected from the weighted mean of those of the substances making up the mixture. It is fairly easy to see on physical grounds why this should be so; a region of low absorption coefficient lets through more X-rays than are stopped by a similar region of high absorption coefficient. Most of the ideas developed here are implicit in Schäfer's paper, but his interest was in the ratio of the intensities diffracted by the components of a binary mixture, and the only explicit overlap is that he derives equation (8) for the particular case of $\mu_2 = 0$.

The easiest case to treat is simple transmission through a slab made of cubes of material, each of side a , packed so as to exclude air spaces. This can be treated both when there are two types of cube, of absorption coefficient μ_1 and μ_2 , present in proportions p_1 and p_2 ($p_2 = 1 - p_1$), or in the more general case where there are q different types of absorption coefficients $\mu_1, \mu_2, \dots, \mu_q$, in proportions p_i such that $p_1 + p_2 + \dots + p_q = 1$.

2. Mixture of two substances, binomial distribution

An X-ray beam traversing a heterogeneous slab of material of thickness T , composed of two materials of linear absorption coefficients μ_1 and μ_2 , is reduced in intensity by the factor

$$A = \exp(-\mu_1 x_1 - \mu_2 x_2) \quad (1)$$

where x_1 is the thickness encountered of the first material, and x_2 is the thickness of the second material. Clearly $x_1 +$

$x_2 = T$. On the average x_1 and x_2 will be in the ratio of the volumes of the two materials, but for any particular ray there may be a departure from this average because of statistical variations in the numbers of particles of the two kinds encountered. Take the particles to be cubes of uniform size a , packed without air spaces, so that $T = na$, where n is the number of layers. The value of x_1 may be any one of $0, a, 2a, \dots, na$, the mean value being $p_1 T = p_1 na$. With a random packing, x_1 will have a binomial distribution about this mean, the probability of a value of $x_1 = ka$ being

$$P(ka) = \frac{n! p_1^k (1 - p_1)^{n-k}}{k!(n-k)!} \quad (2)$$

The value for A , for a ray encountering k cubes of material absorption coefficient μ_1 and $(n - k)$ of absorption coefficient μ_2 , is

$$A_k = \exp(-\mu_1 ka) \times \exp\{-\mu_2 a(n - k)\} \quad (3)$$

$$\langle A \rangle = \sum_{k=0}^n A_k P(ka) \quad (4)$$

$$= \sum_{k=0}^n \frac{n! \{p_1 \exp(-\mu_1 a)\}^k \{(1 - p_1) \exp(-\mu_2 a)\}^{n-k}}{k!(n-k)!} \quad (5)$$

which is just the binomial expansion of

$$\langle A \rangle = \{p_1 \exp(-\mu_1 a) + (1 - p_1) \exp(-\mu_2 a)\}^n \quad (6)$$

With the effective absorption coefficient μ_{eff} defined so that

$$\langle A \rangle = \exp(-\mu_{\text{eff}} T) \quad (7)$$

comparison of equations (6) and (7) shows that

$$\mu_{\text{eff}} = -a^{-1} \log_e \{p_1 \exp(-\mu_1 a) + (1 - p_1) \exp(-\mu_2 a)\} \quad (8)$$

If $\mu_1 = \mu_2$, then μ_{eff} reduces to μ_1 , as it should, and if $\mu_1 a$ and $\mu_2 a$ are both small compared with unity, μ_{eff} reduces to the expected value

$$\langle \mu \rangle = p_1 \mu_1 + (1 - p_1) \mu_2 \quad (9)$$

Note that μ_{eff} does not depend on T (or n); the same value will therefore be valid for any specimen shape including, subject to a remark in Section 6 below, slabs or cylinders in reflexion.

If μ_2 is of the order of 0 and $\mu_1 a$ is of the order of unity, which would be some approximation to a fairly coarse powder with air gaps, then

$$\frac{\mu_{\text{eff}}}{\langle \mu \rangle} = - \frac{\log_e \{1 - p_1 + p_1 \exp(-\mu_1 a)\}}{p_1 \mu_1 a} \quad (10)$$

For $p_1 = \frac{1}{2}$ this ratio takes the values 0.98, 0.93, 0.76 for $\mu_1 a = 0.1, 0.3, 1.0$, so that the effect amounts to several per cent. (For heavy-aggregate cements and plasters $\mu_1 a$ may be very large.)

3. Mixture of q substances, multinomial distribution

The conclusions of the preceding section can readily be generalized to the case of q components, in proportions p_1, p_2, \dots, p_q , where

$$\sum_{j=1}^q p_j = 1 \quad (11)$$

It is convenient to assume that the numbering has been done so that $\mu_1 \geq \mu_2 \geq \dots \geq \mu_q$. For a ray that traverses n_1 cubes of type 1, n_2 of type 2, \dots , n_q of type q , the intensity transmitted is proportional to

$$A = \exp \left(- \sum_j n_j \mu_j a \right) \quad (12)$$

$$\text{where} \quad \sum_j n_j = n \quad (13)$$

The mean value of A for all rays will be

$$\langle A \rangle = \sum_{\text{all } n_j} P(n_1, \dots, n_q) \exp \left(- \sum_j n_j \mu_j a \right) \quad (14)$$

where, for a random arrangement of cubes, the P 's are given by the multinomial distribution

$$P(n_1, \dots, n_q) = \frac{n! p_1^{n_1} p_2^{n_2} \dots p_q^{n_q}}{n_1! n_2! \dots n_q!} \quad (15)$$

The value of $\langle A \rangle$ from equation (14) is easily seen to be

$$\langle A \rangle = \{ p_1 \exp(-\mu_1 a) + p_2 \exp(-\mu_2 a) + \dots + p_q \exp(-\mu_q a) \}^n \quad (16)$$

so that

$$\mu_{\text{eff}} = -\frac{1}{a} \log_e \{ p_1 \exp(-\mu_1 a) + p_2 \exp(-\mu_2 a) + \dots + p_q \exp(-\mu_q a) \} \quad (17)$$

For $q = 2$ this reduces to equation (10).

4. Gaussian approximations to binomial and multinomial distributions

For large values of n the binomial distribution (2) tends to the normal or Gaussian distribution

$$P(k)dk = \{2\pi np(1-p)\}^{-1/2} \exp \{-(k-np)^2/2np(1-p)\} dk \quad (18)$$

where $P(k)dk$ is the probability of a path of length between ka and $a(k+dk)$ in the material of absorption coefficient μ_1 . This gives finite probabilities for paths of length less than 0 or greater than T , but for large values of n these probabilities are small enough to be neglected, and the range of k can be taken to be from $-\infty$ to $+\infty$.

The value of A (equation 1) may be written

$$\begin{aligned} A &= \exp(-\mu_1 x_1 - \mu_2 x_2) \\ &= \exp\{-\mu_1 ka - \mu_2(n-k)a\} \\ &= \exp[-\{p\mu_1 + (1-p)\mu_2\}na - (\mu_1 - \mu_2)(k-np)a] \end{aligned} \quad (19)$$

$$= \exp\{-\langle \mu \rangle T - (\mu_1 - \mu_2)(k-np)a\} \quad (20)$$

thus making the variable the departure of k from its mean value np . This has the useful incidental result of bringing the mean value $\langle \mu \rangle$ of μ (equation 9) explicitly into the constant factor. Combining equations (18) and (20) gives

$$\begin{aligned} \langle A \rangle &= \exp(-\langle \mu \rangle T) \times \\ &\times \{2\pi np(1-p)\}^{-1/2} \int_{-\infty}^{\infty} \exp\{-(k-np)^2/2np(1-p) - \\ &\quad - (\mu_1 - \mu_2)a(k-np)\} dk \\ &= \exp\{-\langle \mu \rangle T + \frac{1}{2}(\mu_1 - \mu_2)^2 p(1-p)na^2\} \\ &= \exp[-\{\langle \mu \rangle - \frac{1}{2}(\mu_1 - \mu_2)^2 p(1-p)a\}T] \end{aligned} \quad (21)$$

The effective absorption coefficient is thus

$$\mu_{\text{eff}} = \langle \mu \rangle - \frac{1}{2}(\mu_1 - \mu_2)^2 p(1-p)a \quad (22)$$

somewhat less than the mean value. The difference vanishes in the trivial cases $\mu_1 = \mu_2$ or $p = 0$ or $p = 1$, and tends to zero with the particle size a .

A similar, somewhat tedious, calculation for the multinomial distribution leads to

$$\mu_{\text{eff}} = \langle \mu \rangle - \frac{1}{4}a \sum_{i \neq j} (\mu_i - \mu_j)^2 p_i p_j \quad (23)$$

for a mixture of q substances. Equation (17) may be reduced to this form by expanding the exponentials and logarithms as far as terms in a^2 .

5. General Gaussian approximations

The procedure in Section 4 suggests a general approximate line of approach, which will be developed first for a mixture of two materials. The average thickness of the first material encountered will be $x_1 = p_1 T$, and of the second material $x_2 = p_2 T = (1-p_1)T$. However, x_1 and x_2 will vary from these mean values, for one or more of the following reasons:

- statistical fluctuations in the proportions of particles of the two kinds encountered;
- variations in thickness of different parts of the individual particle, and
- the distribution of particle sizes.

The probability that the distance traversed in the first medium is between x_1 and $x_1 + dx_1$ may be represented by $P(x_1)dx_1$, where $P(x_1)$ has the properties

$$\int_0^T P(x_1)dx_1 = 1 \quad (24)$$

and

$$\langle x_1 \rangle = \int_0^T x_1 P(x_1)dx_1 = p_1 T \quad (25)$$

For any particular value of x_1 the transmission coefficient is

$$\begin{aligned} A &= \exp(-\mu_1 x_1) \times \exp(-\mu_2 x_2) \\ &= \exp(-\langle \mu \rangle T) \times \exp\{-\delta(x_1 - \langle x_1 \rangle)\} \end{aligned} \quad (26)$$

where

$$\langle \mu \rangle = p_1 \mu_1 + p_2 \mu_2 \quad (27)$$

and

$$\delta = (\mu_1 - \mu_2) \geq 0 \quad (28)$$

Averaging over all possible values of x_1 gives

$$\langle A \rangle = \exp(-\langle \mu \rangle T) \int_0^T \exp\{-\delta(x_1 - \langle x_1 \rangle)\} P(x_1)dx_1 \quad (29)$$

The exponential within the integral may be developed in a power series, giving

$$\begin{aligned} \langle A \rangle &= \exp(-\langle \mu \rangle T) (1 - 0 + \frac{1}{2!} M_2 \delta^2 - \frac{1}{3!} M_3 \delta^3 + \\ &\quad + \frac{1}{4!} M_4 \delta^4 - \dots) \end{aligned} \quad (30)$$

where the M 's are the moments of x_1 about its mean value $p_1 T$. For values of δ which are not too large one can write

$$\mu_{\text{eff}} = -T^{-1} \log_e \langle A \rangle \simeq \langle \mu \rangle - \frac{1}{2} M_2 \delta^2 / T \quad (31)$$

which is less than $\langle \mu \rangle$, in agreement with the statement made in Section 1. Equation (31) would be exact for $P(x_1)$ a Gaussian distribution sufficiently narrow that the limits in equation (29) can be regarded as $-\infty$ and $+\infty$ with respect

to $\langle x_1 \rangle$. Equation (30) leads to the same qualitative conclusion for:

- (a) δ small, whatever the form of $P(x_1)$;
- (b) $P(x_1)$ symmetrical about $\langle x_1 \rangle$, so that odd moments vanish;
- (c) $P(x_1)$ having negative odd moments.

[It would be nice to be able to draw the same qualitative conclusion for any values of $P(x_1)$, but so far a proof has not been devised, if indeed the conclusion is true.]

Now return to the general case of q components. The transmission coefficient for any particular set of path lengths x_i is

$$A = \exp \left(- \sum_i^q \mu_i x_i \right) \quad (32)$$

subject to

$$\sum_i^q x_i = T \quad (33)$$

$$\text{With } \xi_i = x_i - \langle x_i \rangle \quad (34)$$

this may be written

$$A = \exp \left(- \sum_i^q \mu_i \langle x_i \rangle - \sum_i^q \mu_i \xi_i \right) \quad (35)$$

$$= \exp (-\langle \mu \rangle T) \exp \left(- \sum_i^q \mu_i \xi_i \right) \quad (36)$$

$$\text{Clearly } \sum_i^q \xi_i = 0 \quad (37)$$

$$\text{so that } \xi_j = - \sum_{k \neq j}^q \xi_k \quad (38)$$

where ξ_i is the deviation from its mean value of any path length that it may be convenient to separate. Expanding the second exponential in equation (36) gives

$$A = \exp (-\langle \mu \rangle T) \left(1 - \sum_i^q \mu_i \xi_i + \sum_{i,j}^q \mu_i \mu_j \xi_i \xi_j - \dots \right) \quad (39)$$

On averaging, the second term in brackets vanishes, since $\langle \xi_i \rangle$ is zero for all values of i . The third term may be expressed in various forms; the obvious one is

$$\frac{1}{2} \sum_{i,j}^q \mu_i \mu_j M_{ij} \quad (40)$$

where M_{ij} is the second moment $\langle \xi_i \xi_j \rangle$. Then

$$\mu_{eff} \simeq \langle \mu \rangle - \frac{1}{2T} \sum_{i,j}^q \mu_i \mu_j M_{ij} \quad (41)$$

This does not much resemble either equation (23) or equation (31), but by a little manipulation and the use of equation (38) it may be put in the form

$$\mu_{eff} \simeq \langle \mu \rangle + \frac{1}{4T} \sum_{i \neq j}^q (\mu_i - \mu_j)^2 M_{ij} \quad (42)$$

Because of the relation (38) some of the values of M_{ij} are negative; in fact

$$M_{ij} = \langle \xi_i \xi_j \rangle = - \langle \xi_i \sum_{k \neq j}^q \xi_k \rangle = - \sum_{k \neq j}^q M_{ik}, \quad \sum_k M_{ik} = 0 \quad (43)$$

Without postulating details of the distribution function, it is not possible in general to get rid of the cross moments M_{ij} , but for $q = 2$ and $q = 3$ the relations (43) are just sufficient to express M_{ij} in terms of M_{ii} . For $q = 2$, equation (42) becomes

$$\mu_{eff} \simeq \langle \mu \rangle - \frac{1}{2} (\mu_1 - \mu_2)^2 M_{11} / T \quad (44)$$

which is equation (31) in slightly more elaborate notation. For $q = 3$, equations (43) can be solved for the cross moments;

$$M_{ij} = -\frac{1}{2} (M_{ii} + M_{jj} - M_{kk}) \quad (45)$$

and after a little reduction equation (42) becomes

$$\mu_{eff} \simeq \langle \mu \rangle - (2T)^{-1} \{ (\mu_1 - \mu_2)(\mu_1 - \mu_3)M_{11} + (\mu_2 - \mu_1)(\mu_2 - \mu_3)M_{22} + (\mu_3 - \mu_1)(\mu_3 - \mu_2)M_{33} \} \quad (46)$$

One might be tempted to estimate the order of magnitude of M_{ii} on general grounds. Since it is the variance of x_i , it will be the sum of the variances of the three fluctuations set out at the beginning of Section 5. For reason (i) one might take the multinomial variance $p_i(1-p_i)a_iT$, where a_i is now a mean particle size for particles of type i . The variance in the thickness of individual particles (ii) will be proportional to a_i^2 , with a proportionality factor probably less than unity. The distribution of particle sizes (iii) of particles of type i will probably have a variance again proportional to a_i^2 , but the proportionality factor may be considerably greater than unity. Adding all these together gives

$$M_{ii} = p_i(1-p_i)(a_iT + K_ia_i^2) \quad (47)$$

where K_i is of the order of magnitude of unity. Equation (46) then becomes

$$\mu_{eff} \simeq \langle \mu \rangle - \frac{1}{2} \sum_i^q p_i(1-p_i)\delta_i^2 a_i - \frac{1}{2T} \sum_i^q p_i(1-p_i)K_i\delta_i^2 a_i^2 \quad (48)$$

$$\text{where } \delta_i^2 = (\mu_i - \mu_j)(\mu_i - \mu_k) \quad (49)$$

The second correction term is smaller than the first by a ratio of the order of magnitude of a/T , and hence is negligible except for very thin specimens.

6. Diffraction by a heterogeneous specimen

The arguments developed so far have applied, strictly, only to direct transmission. It may be asked whether, in reflexion, the intensity ratios of the diffraction maxima for different types of particle will be distorted by the statistical fluctuations, a region of high concentration of low-absorbing material i giving a contribution to the i maxima too great to be compensated for by the weak production of i maxima from a region of high concentration of a high-absorbing material j . The authors have not been able to make any quantitative estimate of this effect; if it exists it appears to be an order of magnitude smaller.

Schäfer has shown that, if absorption within an individual particle is appreciable, the ratio of the intensities diffracted by the components of a binary mixture is altered in the ratio of the absorption factors of individual particles of the two kinds, but he does not treat the further effect, if any, of statistical fluctuations.

Acknowledgements

G. B. Mitra thanks the authorities of UNESCO for the grant of a fellowship; this work was done while he was on leave from the Indian Institute of Technology, Kharagpur, India.

References

- (1) ALEXANDER, L. E. *J. Appl. Phys.*, **21**, p. 126 (1950); **25**, p. 155 (1954).
- (2) ALEXANDER, L. E., and KLUG, H. P. *Analyt. Chem.*, **20**, p. 886 (1948).
- (3) BRINDLEY, G. W. *Phil. Mag.*, **36**, p. 347 (1945).
- (4) SCHÄFER, K. *Z. Phys.*, **86**, p. 738 (1933).
- (5) TAYLOR, A. *Phil. Mag.*, **35**, p. 215 (1944).
- (6) WILCHINSKY, Z. W. *Acta Cryst.*, **4**, p. 1 (1951).

Rotational hysteresis loss in grain-oriented silicon-iron

by W. F. ARCHENHOLD, B.Sc., H. F. SANDHAM, Ph.D., and J. E. THOMPSON, Ph.D.,
The English Electric Company Limited, Stafford

[Paper received 13 July, 1959]

Abstract

An improved torque magnetometer has been used to measure accurately the rotational hysteresis loss in grain-oriented silicon-iron for various percentage orientations and thicknesses. The experimental results are discussed in terms of multi-domain concepts and of the Stoner-Wohlfarth single-domain particle, of which the rotational hysteresis behaviour has been evaluated. The possible relevance of this theory and its extensions to the experimental results are considered.

Introduction

WHEN a disk of an anisotropic ferromagnetic material is rotated in a magnetic field, the torque acting on the disk depends on the orientation of the disk and field. The resulting graph of torque and orientation is known as a torque curve. On rotating the disk in one direction through 360° and then in the reverse direction, the two curves are not coincident. The difference between the two represents an energy loss which is known as the rotational hysteresis loss. The magnitude of this loss depends on the degree of magnetic saturation of the specimen. Brailsford^(1,2) has previously studied a number of magnetic sheet steels.

In recent years, there has been a considerable increase in the use of grain-oriented silicon-iron of various thicknesses, and no satisfactory theory has been developed to account for rotational hysteresis loss in these materials. Rotational hysteresis has been studied by means of an improved torque magnetometer employing a stabilizing device⁽³⁾ and measurement of the torque in terms of an electric current, which increases the accuracy of the measurement of the torque curve and, consequently, that of the loss. Further accuracy in loss measurement has been obtained by using a number of disks suitably offset in orientation, which eliminates to a large extent all the angular components of the anisotropy torque.

Torque curves

In a body-centred cubic crystal of iron the crystallographic direction representing minimum stored energy is the [100]. If the magnetization vector is turned out of the equilibrium position by application of a field at some angle to this direction, there arises a torque which varies with the angle between the intensity vector and easy direction of magnetization. The anisotropy energy can for the saturated condition be expressed in terms of the direction cosines of the angles to the crystallographic axes by:

$$E = K_0 + K_1(S_1^2S_2^2 + S_2^2S_3^2 + S_3^2S_1^2) + K_2S_1^2S_2^2S_3^2 \quad (1)$$

where K_0 , K_1 and K_2 are anisotropy constants and S_1 , S_2 , S_3 are the direction cosines of the intensity of magnetization relative to the principal axis of the cubic crystal.

The torque can be expressed independently of the degree of magnetic saturation as follows

$$L = A \sin(2\alpha + \delta_1) + B \sin(4\alpha + \delta_2) + C \sin(6\alpha + \delta_3) + L_H \quad (2)$$

where A , B and C , δ_1 , δ_2 and δ_3 are constants for a given specimen and degree of preferred orientation. The parameter L_H is the torque resulting from rotational hysteresis, and for rotation in an opposite sense the sign becomes reversed. Consequently, the difference in torque curves for rotation in a clockwise and an anti-clockwise direction becomes $2L_H$.

Elimination of the anisotropy terms

If β is the angular displacement of n disks placed successively one on top of each other then, for symmetry, $n = 2\pi/\beta$. For any given angular component to be cancelled:

$$\sin m\alpha + \sin m(\alpha + \beta) + \dots + \sin m\{\alpha + (n-1)\beta\} = 0 \quad (3)$$

The summation of this series is:

$$\sin \left\{ m\alpha + \frac{m}{2}(n-1)\beta \right\} \sin m\frac{\beta}{2} \cdot \operatorname{cosec} m\frac{\beta}{2} = 0 \quad (4)$$

or:

$$\sin \left\{ m\alpha + \frac{m}{2}(n-1) \cdot \frac{2\pi}{n} \right\} \sin m\pi \cdot \operatorname{cosec} \frac{\pi m}{n} = 0,$$

and a relationship is required between m and n so that this equation disappears independently of α . Provided $\operatorname{cosec} 2m\pi/n$ is not zero, the presence of the factor $\sin m\pi$ ensures that the above vanishes when $m = 2, 4, 6, \dots (2n-2)$, and as a general rule n disks will eliminate all terms up to and including $(2n-2)\alpha$.

The rotational hysteresis loss was measured with the 2α , 4α and 6α components eliminated in the torque curve. In practice, the torque curve had some slight angular dependence, which was attributed to slight errors in setting the individual disks into a compound disk, and to small variations in the degree of saturation at the corner of the specimens.

Degree of preferred crystal orientation in the samples

The restoring torque on a single disk of the (110) under saturated conditions is given by:

$$L = K_1 \left(\frac{2 \sin 2\alpha + 3 \sin 4\alpha}{8} \right) + K_2 \left(\frac{\sin 2\alpha + 4 \sin 4\alpha - 3 \sin 6\alpha}{64} \right) \quad (5)$$

where α is the angle between the saturating field and the [100].

To confirm that the limiting curve had been obtained, the

torque was plotted against the reciprocal of the field for various field strengths. The difference between the intercept torque corresponding to an infinite field and the maximum value found here was small. A "least-squares" fit of equation (5) to the experimental curves was made, and it was found that the preferred orientation could be adequately described by a single orientation, $[100] \parallel$ rolling direction, $(110) \parallel$ rolling plane, plus material randomly aligned. In this way an effective value of K_1 was obtained and the percentage orientation was then K_{1e}/K_1 , where K_{1e} is the effective value of K_1 for the material, and K_1 is the corresponding value for a single crystal of silicon iron, 2.87×10^5 erg/ml. The following results were obtained:

0.013 in. : 87%; 0.005 in. : 62%; 0.002 in. : 52%.

Alternating power loss was measured in the well-known Epstein Square.

Experimental results

Rotational hysteresis loss is plotted against various values of $(B - H)/(B - H)_s$ for various thicknesses of grain-oriented silicon-iron ($3\frac{1}{2}\%$) in Fig. 1. The quantity B is the

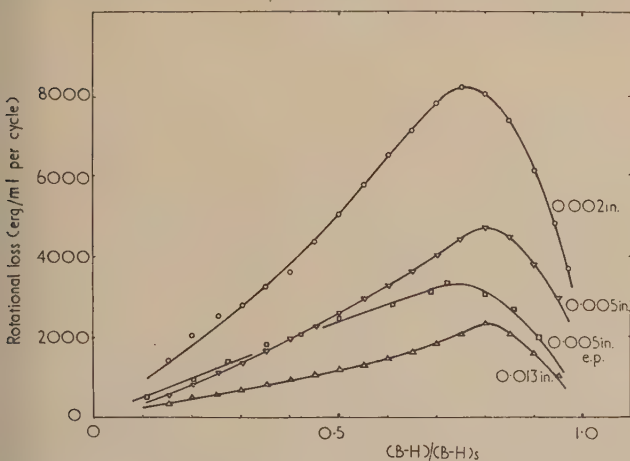


Fig. 1. Rotational loss as a function of the degree of magnetic saturation for four silicon-iron samples

The 0.005 in. e.p. specimen was electropolished from 0.013 in.

magnetic induction, H the effective field in the specimen, and the suffix s represents the saturation value. Values of B and H were obtained by winding a search coil directly on to the specimen and measuring the changes in flux on a ballistic galvanometer for reversals of the electromagnetic field. Corrections for air flux and demagnetizing field were applied.

To differentiate between the possibilities that the variation could be caused either by thickness or by orientation, the 0.013 in. material was electro-polished to 0.005 in., and this curve is also shown on Fig. 1. The electro-polished sample curve differs somewhat in shape from the remaining 0.005 in. curve, which indicates that the thickness, probably through the surface layer, influences rotational hysteresis loss.

The ratio of rotational loss to total alternating loss is shown as a function of $(B - H)/(B - H)_s$ in Fig. 2 for the various samples.

It is instructive to present the results in a different manner. Jacobs and Luborsky⁽⁵⁾ in their investigation into rotational hysteresis loss (W_R) of uniaxial single-domain particles and interacting particle chains plotted graphs of $Loss$ against H and W_R/I_S against $1/H$, where I_S is the intensity of magnetization. Fig. 3 gives the relationship W_R/I_S against $1/H$ for the

various thicknesses of the silicon-iron which shows similarity in shape but large differences in magnitude. The curve for the electro-polished sample is different in form from the other three curves and confirms that, apart from the difference that arises from orientation, a thickness effect is also present, this being possibly a surface phenomenon.

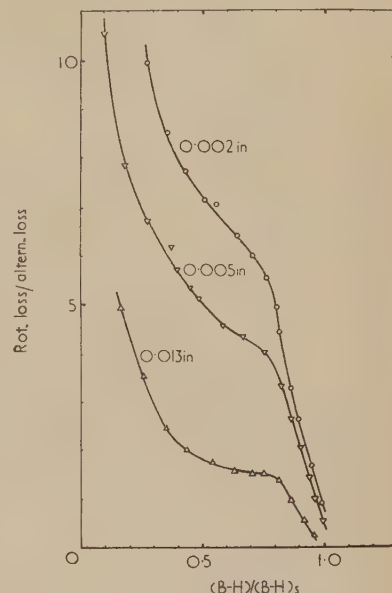


Fig. 2. Ratio of the rotational loss to hysteresis loss for the three thicknesses of silicon-iron strip

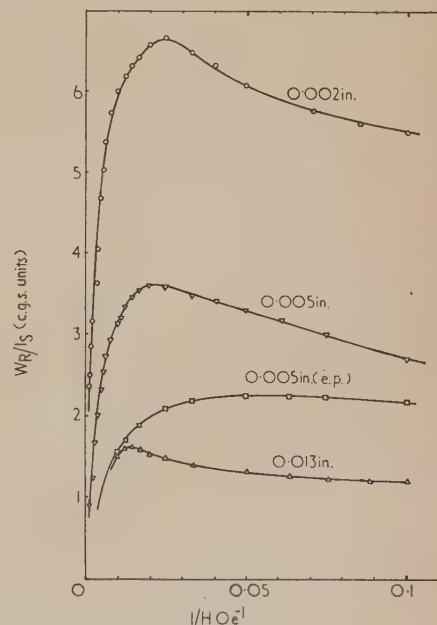


Fig. 3. Graph of W_R/I_S and $1/H$ for the various samples

Discussion of the experimental results

The concept of magnetization changes by domain-wall movements is well known, and the experiments on picture-frame crystals have shown how the d.c. $B-H$ loop is related to 180 deg. wall movements. In rotational hysteresis, the loss associated with such movements will give a loss per cycle equivalent to this d.c. $B-H$ loss. As can be observed from Fig. 2, the ratio of rotational loss to alternating loss is in general between 1 : 1 and 10 : 1. For the material used here,

the ratio of alternating to hysteresis loss is about 3 : 1 and, thus, there occurs during rotation, a large additional loss that requires explanation. Other domain-wall motions in multi-domain regions might be sufficient to account for this loss. It is known⁽⁶⁾ that complex domain-wall formations arise around inhomogeneities in the material, and the rotational behaviour of these may be relevant in any complete explanation of the experimental results.

Another possibility is that a series of holes or non-magnetic inclusions could be responsible for the rotational hysteresis loss. Yamashita and Tatsumoto⁽⁷⁾ have explained a particular magnetic anisotropy that is found in silicon-iron between two equivalent [100] in a (100), in terms of a line of holes that is present in the material. While such a system has a variation of energy with angle, no rotational hysteresis loss is possible.

However, small regions that are magnetically different from the bulk of the material could act as a single-domain particle and the possibility of rotational hysteresis in silicon-iron from this cause will be considered.

The basic Stoner-Wohlfarth⁽⁸⁾ model is of a particle sufficiently small that it acts as a single domain with an angular dependence of the energy on the direction of the applied field caused either by strain, by crystal anisotropy or by shape anisotropy. The variable part of the energy η is written:

$$\eta = -\frac{1}{4} \cos 2\psi - h \cos \phi \quad (6)$$

where h equals $HI_s/2K$ for crystalline anisotropy for example, K is the first anisotropy constant, and H is the effective field acting on the particle. The angle between the intensity and field vectors is denoted by ϕ , and ψ is the angle between the direction of easy magnetization and the intensity vector.

For rotational hysteresis, the H vector is taken as a constant and is rotated from an initial position aligned with the intensity vector, when there occurs a discrete energy jump for certain values of the field. This has been derived here explicitly and is given by the relationship:

$$-\Delta\eta = \frac{h^2 + 2}{3} \left(\frac{h^2 + 2}{3} \right)^{\frac{1}{2}} - \frac{7 - h^2}{6} \left(\frac{4h^2 - 1}{3} \right)^{\frac{1}{2}} \quad (7)$$

The value of h must lie within the range 0.5–1.0, the energy change being a maximum at $h = 0.5$ and zero at $h = 1.0$. The experimental results have been plotted in Fig. 4 assuming a crystal anisotropy effect, (that is $h = HI_s/2K$) and the curve

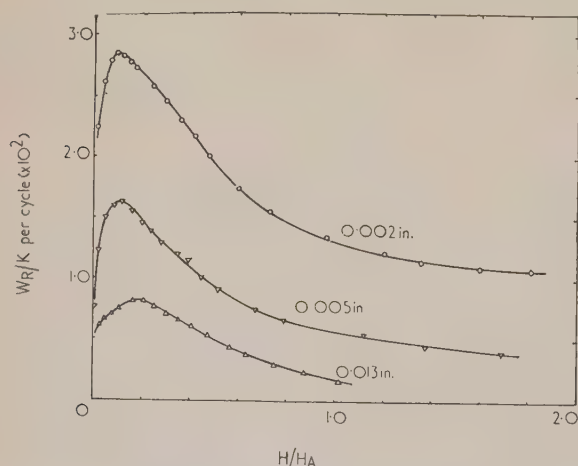


Fig. 4. Graph of W_R/K and H/H_A

W_R is the rotational hysteresis loss, K the first anisotropy constant for silicon-iron and H_A is defined as $2K/I_s$.

for equation (7) is shown in Fig. 5. The ordinate plotted is $(\Delta\eta)/K$ and for comparison to be made between Figs. 4 and 5, the numerical value from equation (7) has to be multiplied by 4, one factor 2 arising from two jumps per 360°, and a second factor 2 arising because the original energy expression was divided by $2K$ to give the equivalent h expression.

This model holds for single particles in isolation and it is probably an over-simplification for the type of material examined. Jacobs and Bean,⁽⁴⁾ Jacobs and Luborsky,⁽⁵⁾ and Wohlfarth⁽⁹⁾ have considered various idealized arrangements in which some particle interaction is allowed. The characteristic curve given by Jacobs and Luborsky⁽⁵⁾ for a chain of spherical particles with crystal anisotropy, spherical randomization of direction, and also anti-parallel rotation of the magnetization vectors is added to Fig. 5.

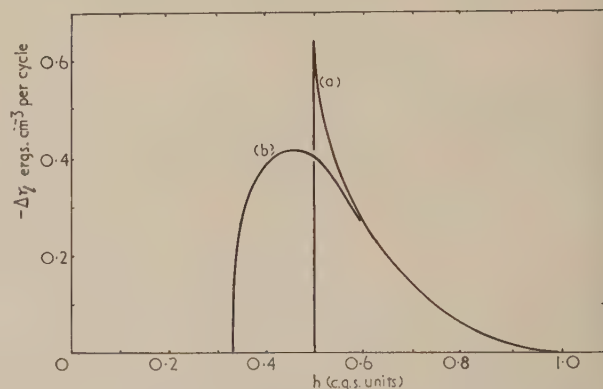


Fig. 5. Rotational Energy loss for (a) Stoner-Wohlfarth single-domain particle, (b) Jacobs and Luborsky with spherical randomness and the "fanning mechanism" of rotation

The observed magnitude of the rotational hysteresis, and perhaps its variation with field, could be explained by these models if one-hundredth of the volume of 0.002 in. thick material consisted of effectively single-domain particles with crystal anisotropy in the predominant role. By comparison of Figs. 4 and 5 it can be seen that the peak value of W_R/K occurs at a smaller value of H/H_A (where $H_A = 2K/I_s$), if the value of the external field is used for H , together with the first anisotropy constant; and there is no sharp cut-off below a certain value of H/H_A . When the particles are surrounded by a homogeneous medium of high permeability, the peak value given by the theory is unaltered, but it occurs at a lower value of external field. In soft ferromagnetic materials, because of the presence of the multi-domain particles (which are relatively large compared with the single-domain particles postulated), the effective field applied to the particle is difficult to assess. These effective fields will vary considerably from particle to particle, causing a wide spread in the critical values of h in terms of the external field.

A more rigorous treatment of the interaction of single-domain particles which might arise from strain, shape, or crystal anisotropy together or independently can lead to a better agreement with experimental values. The sites of such domains might be found to be at grain boundaries, dislocation rings, or in mosaic structures, and an examination of these materials by Bitter-pattern techniques under rotating magnetic fields should be of value in further work.

Acknowledgements

Thanks are expressed to Mr. V. A. Hughes for his encouragement and interest in this study, and to Mr. J. K. Brown,

Director of Research, for his interest and permission to publish this paper.

References

- (1) BRAILS福德, F. *I.E.E.*, **83**, p. 566 (1939a).
- (2) BRAILS福德, F. *I.E.E.*, **84**, p. 399 (1939b).
- (3) ARCHENHOLD, W. F., BROWN, A. C., and THOMPSON, J. E. Accepted for *J. Sci. Instrum.*
- (4) JACOBS, I. S., and BEAN, C. P. *Phys. Rev.*, **100**, p. 1060. (1955).

- (5) JACOBS, I. S., and LUBORSKY, F. E. *J. Appl. Phys.*, **28**, p. 467 (1957).
- (6) WILLIAMS, H. J., and SHOCKLEY, W. *Phys. Rev.*, **75**, p. 178 (1949).
- (7) YAMASHITA, T., and TATSUMOTO, E. *J. Phys. Soc. (Japan)*, **12**, p. 975 (1957).
- (8) STONER, E. C. and WOHLFARTH, E. P. *Phil. Trans. Roy. Soc.*, **240 A**, p. 599 (1948).
- (9) WOHLFARTH, E. P. *Proc. Roy. Soc.*, **232**, p. 208 (1955).

Measurement of tinplate thickness using fluorescent X-rays excited by a radioactive source

by J. F. CAMERON, B.Sc., and J. R. RHODES, B.A., Physics Group, Isotope Division, A.E.R.E., Harwell.

[Paper received 6 July, 1959]

Abstract

Using tritium bremsstrahlung as an X-ray source and a thin-windowed scintillation counter as a detector, a method of measuring the thickness of tinplated steel over the range 0.1–5.5 microns (1.00 lb per basis box) has been developed. The technique depends on absorption of the iron fluorescent X-radiation by the tin layer. An accuracy of 1% can be obtained with 95% confidence in a counting time of 30 seconds.

Introduction

THE measurement of the thickness of the tin coating on a sheet of iron is an extremely difficult problem because a typical tin coating may only be 15 μ in. (0.25 lb per basis box) thick, while the iron is about 0.010 in. thick and may only be constant to perhaps 0.001 in. Thus mechanical, electrical, magnetic, X-ray or beta-gauge total-thickness methods are ruled out. The methods most generally employed for determining the thickness of the coating are either chemical or electrochemical. In these methods the coating is removed from a known area and the amount of tin is determined either by the time taken to strip the tin electrochemically, by volumetric or gravimetric analysis or by loss of weight. These methods give an accuracy of about 1%, but they are laborious, destructive and time consuming and cannot be used to give a continuous indication of the tinplate as it is produced. Some modern electrolytic tinning lines operate at 2000 ft/min and a rapid, continuous and direct indication of the tin thickness is required which is independent of indirect factors such as line speed, plating current, solution temperature, etc., and requires only infrequent laboratory checks. It was to meet this demand for a non-destructive, non-contact, continuous measurement that X-ray fluoroscopy⁽¹⁻⁵⁾ was used.

Principles of X-ray fluoroscopy

The basic principles of the type of X-ray fluoroscopy used for tinplate thickness measurements are illustrated in Fig. 1. An X-ray beam incident on the tin-coated steel excites

secondary or fluorescent radiation in the steel base. The intensity of the emergent fluorescent beam depends on the thickness of the tin coating: both the incident exciting radiation and the emergent fluorescent radiation are partially absorbed in the tin layer so that the intensity decreases as the coating thickness increases. The intensity is measured

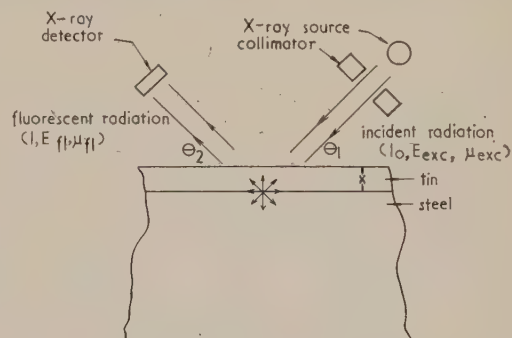


Fig. 1. Schematic diagram of X-ray fluorescence method of determining thickness of tinplate

with either a Geiger, scintillation or proportional counter and an empirical calibration curve relating detector counting rate to coating thickness is obtained using a set of tinplate samples of accurately known thickness. The energy of the X-radiation is chosen such that it excites predominantly the iron fluorescent radiation and very little tin. An X-ray tube voltage of about 25 kV peak is commonly used and, with the distribution of X-ray energies so obtained, iron *K* radiation (6.4 keV) is excited but the energy is insufficient to excite tin *K* radiation (25 keV). Some tin *L* radiation (3–4 keV) is excited, but it has such low energy that it is almost completely absorbed in the air and in the detector window.

For a coating of thickness t and density ρ , the intensity I of the radiation emerging from the surface is related to the thickness by an equation of the form:

$$I = kI_0 \exp \left\{ -\rho t \left(\frac{\mu_{exc}}{\sin \theta_1} + \frac{\mu_{f1}}{\sin \theta_2} \right) \right\} \quad (1)$$

where μ_{exc} , μ_{f1} are the tin mass-absorption coefficients for the exciting and the fluorescent radiations, θ_1 and θ_2 are the angles which the incident and emergent beams make with the surface, and k is a constant which measures the conversion of the incident to characteristic radiation energy. This equation is only an approximation to the practical case, where the exciting radiation has a heterogeneous distribution of energies and the incident and detected beams cover fairly wide solid angles, but it does indicate the sensitivity of the method.

With this method, cutting, marking or defacing the tinplate is eliminated and a measurement of the total coating weight is obtained, which includes the amount combined as iron-tin alloy. The method is not affected by normal variations in the thickness of the steel base or by thin tin oxide films and is independent of grain size and variations in composition. This method is used on some tinning lines to provide a rapid indication of deviations from the desired thickness.

Radioactive sources of electromagnetic radiation and X-ray detectors

Radioactive sources of X-rays are stable, compact, independent of power supplies and cheap in comparison with X-ray tubes and they are finding increasing uses in fluorescent X-ray spectrography and plating thickness measurements.⁽⁶⁻⁸⁾ The source most suitable for tinplate thickness measurement by the method outlined above is the electromagnetic radiation (bremsstrahlung) emitted when the beta particles (maximum energy, 18 keV) from tritium (half-life, 12.2 years) are absorbed. A suitable source of tritium bremsstrahlung is available in the form of tritium "targets"^(9,10) containing several curies of tritium in a thin layer of titanium or zirconium hydride secured to a thicker metallic backing. The sources used in this investigation were "thick" targets consisting of titanium and zirconium foils 0.001 cm thick melted on to tungsten disks 1.2 cm diameter, 0.5 mm thick containing 4.8 and 2.4 c of tritium gas respectively. The bremsstrahlung emitted from the zirconium source has a heterogeneous energy distribution with a maximum energy near 12 keV and a broad peak about 6.5 keV, when measured after filtering in 2 cm of air and in the 0.5 mm thick beryllium window of a proportional counter.⁽¹⁰⁾ The electromagnetic radiation emitted from a titanium target has a prominent TiK (4.5 keV) characteristic X-ray peak superimposed on a similar bremsstrahlung background. The zirconium target is to be preferred to the titanium target for tinplate thickness measurement primarily because the higher-energy bremsstrahlung obtained per curie of tritium is about twice that of a titanium target and also because the TiK radiation excites appreciable tin L radiation which considerably complicates the measurements.

The conversion efficiency for the zirconium target is such that 3.3×10^6 bremsstrahlung photons/s are emitted from the surface of a source containing 2.4 c of tritium, and it is estimated that the flux of radiation with energy greater than the K absorption edge of iron (7.1 keV) from this source is about 5×10^5 photons/sc. This is many orders of magnitude less than that obtained from an X-ray tube, but is nevertheless sufficient for many measurements. Because of the relatively small number of photons available it is essential to have the source and detector close to the specimen being measured.

Two detectors were used in this investigation, a proportional counter and a scintillation counter. The proportional counter (type PX130, by 20th Century Electronics) had a 24 mm diameter beryllium window, 0.5 mm thick, and was

filled to a pressure of 77 cm of mercury with a 70 : 7 xenon-methane mixture. The scintillation counter used a crystal of NaI(Tl), 25 mm diameter and 1.2 mm thick with a 0.5 mm thick beryllium window and a photomultiplier (type 9524, by E.M.I. Electronics Ltd.) with a 25 mm diameter photocathode. Auxiliary electronic apparatus consisted of an amplifier, high-voltage supply and either a scaler or a rate-meter.

Preliminary measurements of the spectra of radiation from the source and excited in the tinplate were obtained using the proportional counter in conjunction with a single-channel pulse-height analyser.

Experimental results

The geometrical arrangement of source and detector can be seen from the photograph shown in Fig. 2. The source is contained in a small brass holder with walls and base 0.5 mm thick, and the holder is located in the centre of the propor-

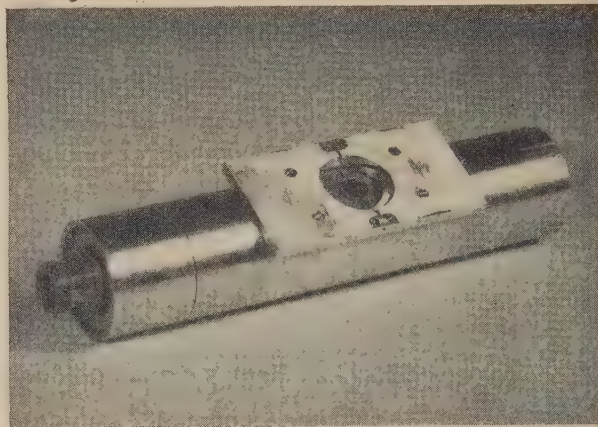


Fig. 2. Proportional-counter apparatus

tional-counter window by two short lengths of beryllium copper wire. Samples are placed on the platform (4 in. \times 2 in.), the underside of which is machined to the radius of curvature of the counter. With this arrangement, the series of energy spectra shown in Fig. 3(a) and 3(b) were obtained. When using a titanium source, both iron K and tin L radiation is excited and it can be seen that an increase in the thickness of the tin layer augments the intensity of the tin L_{α} radiation and absorbs some of the iron fluorescent radiation. The small peak seen on the curve for steel at about 4.5 keV is caused by scattered titanium X-rays. The zirconium source excites predominantly the iron fluorescent radiation. If a detector were used which counted all the radiation impinging on it, then with the titanium source, the change in counting rate with change in tin thickness would be small because the decrease in the intensity of the iron characteristic radiation with increasing thickness of tin is counteracted by an increase in the intensity of the tin L radiation. The contribution from the tin L radiation can be greatly reduced either by filtering it out with a 0.001 in. aluminium foil placed over the counter window or by biasing out this low energy component. The first method has been used successfully, although it has the disadvantage that it also reduces the intensity of the iron K radiation, but the second method is very difficult to apply to an industrial process because then the counting rate depends critically on the gain of the system. With the zirconium source these complications do not arise.

An empirical calibration curve shown in Fig. 4 was obtained using areas of tinplate samples adjacent to sections which

and been removed for electrolytic measurements of the coating thickness. A theoretical curve using the values: $\theta_1 = \theta_2 \doteq 60^\circ$; $\rho t = 0.72 \text{ mg/cm}^2$ per micron; $\mu_{\text{ex}} = 160 \text{ cm}^2/\text{g}$; $\mu_{f1} = 470 \text{ cm}^2/\text{g}$ in equation (1) and

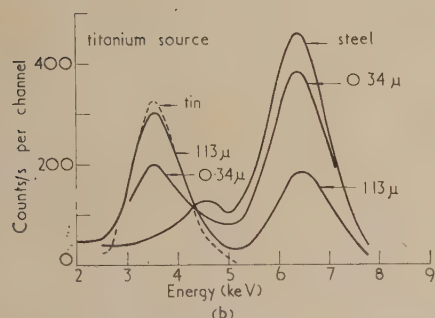
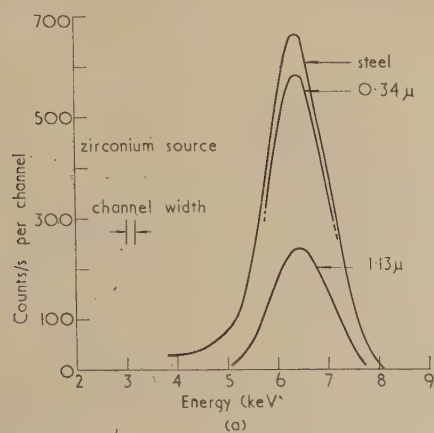


Fig. 3. Fluorescence spectra excited by (a) zirconium source and (b) titanium source

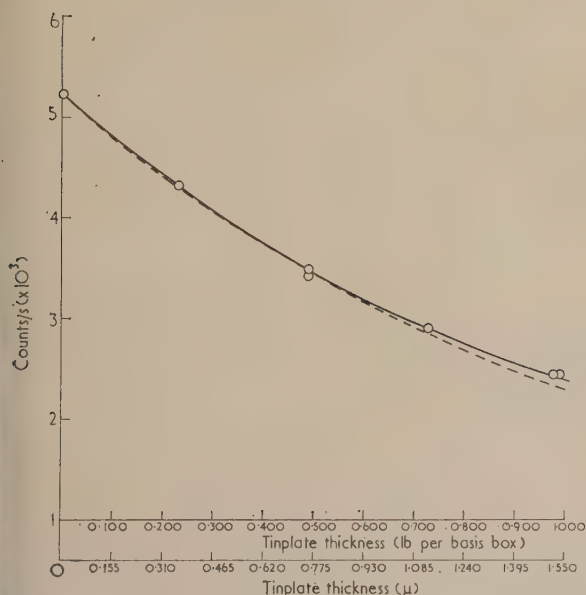


Fig. 4. Calibration curve of count rate plotted against tinplate thickness

normalized at zero tin thickness is shown by the dotted line. It is seen to be in reasonable agreement with the empirical curve considering the assumptions made, particularly with regard to μ_{ex} , which was obtained by summation over the

energy spectrum of the exciting radiation.⁽¹⁰⁾ The equation for the dotted curve is:

$$I = 5.2 \times 10^3 \exp(-0.53 t) \quad (\text{counts per second})$$

where t is in microns.

From the empirical calibration curve it can be seen that at a thickness of 0.775μ ($0.5 \text{ lb per basis box}$), a 1% variation in thickness corresponds to a 0.4% change in counting rate, which can be measured with 95% confidence in 70 s with the counting rates actually obtained.

Choice of detector

The pulse-height distribution obtained in the scintillation counter is only just resolved from the thermionic noise in the multiplier even in a tube selected for low noise, so there are only short plateau regions in the curves relating counting rate to tube voltage and discriminator bias, and the counting rate depends critically on the gain of the system. With the proportional counter, on the other hand, the pulse heights are well above any noise and a very flat plateau region can be obtained. The extent and slopes of the plateaux obtained with the scintillation and proportional counters on a sample of 0.76μ are given in the table.

Extent and slopes of plateau regions

	Counting rate versus e.h.t.		Counting rate versus bias	
	Plateau length (V)	Slope (%/V)	Plateau length (V)	Slope (%/V)
Scintillation counter	100 (1100–1200)	0.03	6 (10–16)	0.4
Proportional counter	At least 300 (2100–2400)	0.001	30 (10–40)	0.04

The components of the scintillation counter have an almost indefinite life, but the gas filling of the proportional counter is gradually broken down and has to be replaced. On the other hand, the gain of the scintillation counter is affected by small changes in temperature,⁽¹¹⁾ while that of the proportional counter is not. It was found with the scintillation counter, that a temperature change of 2.5°C over a period of hours produced a change in counting rate of 0.43% which, on a thickness of 0.76μ corresponds to a change in thickness of 1%. Because of the delay of an hour or so which occurs before a change of external temperature affects the crystal or the photomultiplier, short-term fluctuations in temperature will have a smaller effect. The temperature of the mains water supply is generally sufficiently constant to keep the errors in thickness from this cause to less than 1%.

With the proportional counter at room temperature and the scintillation counter cooled by mains water flowing through a cooling jacket, the reproducibility over a period of several days was within the statistical limits on counting, which corresponded to an error of less than 1% in thickness. Because of the limited time for inspection on commercial electrolytic tinning lines, very high counting rates are essential in order to reduce the relative statistical fluctuations in the counting rate. The counting rate obtained with the scintillation counter is approximately twice that of the proportional counter and the crystal area could readily be increased, which would make it possible to use several sources; but this is difficult in the case of the proportional counter.

In extending this instrument to a tinning line, the main difficulty is the dependence of counting rate on distance of the sample. It was found that the counting rate from a

sample as it is moved away from the surface of the detector increases to a broad maximum and then falls off, as one would expect from purely geometrical considerations. If the detector is positioned at the centre of the broad maximum then, provided the position of the strip is located to within ± 0.010 in. (which is quite feasible), the variation in counting rate is less than 0.2%.

The decrease in the source activity because of radioactive decay and loss of tritium gas amounts to less than 0.5% per month.

Variations in absorption caused by changes in air density can generally be neglected with the geometry used. For example, when the detector is 0.5 cm from the sample, a 10% change in air density will change the counting rate by about 0.2%, which corresponds to an error in thickness of about 0.5%. With the greater distances employed in some X-ray fluorescence measurements, this could be an important consideration. Instability in the apparatus is less important if the technique of intermittent automatic standardization is used.

A prototype instrument using a scintillation counter detector has now been installed in a tin-plate works and, if the initial trial period is satisfactory, it may be applied to continuous measurement on the tin-plating line.

Precautions necessary with tritium-bremsstrahlung sources

The hazard associated with the use of these sources, in terms of external radiation dose and inhalation of molecular tritium lost from the source, is practically negligible. Although about 10^6 photons are emitted per second, because of their low energy, they are rapidly attenuated in a few inches of air. Thus the radiation dose to the operators, with normal usage is negligible, and no shielding is required.

There is a slight loss of tritium gas from the sources amounting to about $50 \mu\text{c}$ in 24 h for a 1 c source.^(12, 13) There is, at present, no official maximum permissible level for molecular tritium, but from several figures which have been proposed⁽¹⁴⁾ a conservative estimate is of the order of one thousand times greater than the maximum permissible concentration of tritiated water in air. The recommended maximum permissible level of HTO for occupational workers is $10 \mu\text{c}/\text{m}^3$, and this is reduced by a factor of ten for non-occupational workers.⁽¹⁵⁾ Even if the apparatus were contained in a fairly small room of 50 m^3 capacity, the air would only need to be changed a few times every twenty-four hours to keep the concentration at one-thousandth of the tolerable level. Thus, in a normal, well-ventilated room the concentration should never approach a hazardous level.

Acknowledgements

The authors are grateful for the supply of standard and special sources from Dr. E. J. Wilson of the Gas Handling Group, Isotope Division, Harwell; and for technical assistance from P. F. Berry and B. J. Puckett of the Physics Group,

Isotope Division, Harwell. They are particularly glad to acknowledge the advice, encouragement and supply of calibration tinplate samples from Mr. J. Nelsey of the Steel Company of Wales.

References

- (1) LIEBHAFSKY, H. A., and ZEMANY, P. D. *Anal. Chem.*, **28**, p. 455 (1956).
- (2) WEBSTER, R. R. *Iron and Steel Engr.*, **32**, p. 65 (1955).
- (3) BEHR, F. A. *Nondestructive Testing*, p. 33 (July 1953).
- (4) BEEGHLY, H. F. *J. Electrochem. Soc.*, **97**, p. 52 (1950).
- (5) SHAKESPEARE, A. G., and WILSON, J. H. *Brit. Iron and Steel Assn*, MW/C/15 (1956).
- (6) COOK, G. B., MELLISH, C. E., and PAYNE, J. A. *Proc. Int. Conf. on Peaceful Uses of Atomic Energy*, **19**, p. 127 (United Nations, 1958).
- (7) MELLISH, C. E., and PAYNE, J. A. To be published (1959).
- (8) LEVEQUE, P., HOURS, R., MARTINELLI, P., MAY, S., SANDIER, J., BRILLANT, J. *Proc. Int. Conf. on Peaceful Uses of Atomic Energy*, **19**, p. 35 (United Nations, 1958).
- (9) *Radioactive Materials and Stable Isotopes*, A.E.R.E., Harwell, Catalogue No. 4 (1957).
- (10) CAMERON, J. F., RHODES, J. R., and BERRY, P. F. A.E.R.E., R. 3086 (1959).
- (11) KINARD, K. E. *Nucleonics*, **15**, p. 92 (1957).
- (12) CAMERON, J. F. A.E.R.E., I/M.29 (1953).
- (13) FRY, R. M., and GIBSON, J. A. B. Private communication.
- (14) FRY, R. M. A.E.R.E., HP/M.137 (1958).
- (15) *Recommendations of the International Commission on Radiological Protection*, Supplement No. 6, p. 48 (London: British Institute of Radiology, 1955).

Journal of Scientific Instruments

Contents of the January issue

- SPECIAL ARTICLE
- Parametric amplification. By K. W. H. Stevens.
- PAPERS
- Design and performance of a rapid-scanning X-ray diffractometer. By A. Skerchly.
- Two thermocouples suitable for measurement of temperatures up to 2800°C . By D. A. Davies.
- Design of laboratory furnaces. By P. L. Start and M. W. Thring.
- Apparatus for the measurement of the mechanical properties of fibres. By F. R. Morgan.
- Recording weight meter. By D. J. Steele.
- An electronic fluxmeter. By R. R. Birss and J. P. Fry.
- Densitometer wedge for measurements at low optical densities. By N. R. Silvester.
- LABORATORY AND WORKSHOP NOTES
- High-temperature burner for working silica. By J. Conaboy.
- Double-acting reversible message register. By C. J. Sumner.
- Slow-feed dispenser for abrasive suspensions. By J. Lobb.
- Device for straining and fracturing thin foil specimens inside an electron microscope. By P. J. E. Forsyth and R. N. Wilson.
- Improved form of spring-clip for holding down a work-piece. By P. W. Harrison.
- Photoelectric refractometer. By C. W. Latey.
- Simple technique for recording variations of a few centimetres in galvanometer reading. By R. G. Ackland.
- NOTES AND NEWS
- New instruments, materials and tools

THIS JOURNAL is produced monthly by The Institute of Physics, in London. It deals with all branches of applied physics (including theory and technique). All rights reserved. Responsibility for the statements contained herein attaches only to the writers.

EDITORIAL MATTER. Communications concerning editorial matter should be addressed to the Editor, The Institute of Physics, 47 Belgrave Square, London, S.W.1. (Telephone: Belgravia 6111.) Prospective authors are invited to prepare their scripts in accordance with the *Notes for Authors*. (Price 3s. 6d. including postage.)

REPRODUCTION. The Institute of Physics is a signatory to The Royal Society's Fair Copying Declaration. Details may be obtained upon application from The Royal Society, London, W.1.

ADVERTISEMENTS. Communications concerning advertisements should be addressed to the agents, Messrs. George Jackson (Fleet St.) Ltd., Cliffords Inn, Fleet Street, London, E.C.4. (Telephone: Holborn 3611-2.)

CLAIMS FOR MISSING JOURNALS. Claims from regular subscribers to this *Journal* for missing numbers will only be considered if received within 60 days of the date of mailing plus normal outward time of transit and time for lodging the claim. Losses attributable to failure to notify a change of address or to similar omissions will not be considered.

SUBSCRIPTION RATES. A new volume commences each January. The charge is £6 per volume (\$17 U.S.A.), including index (post paid), payable in advance. Single parts, so far as available, may be purchased at 12s. 6d. each (\$1.75 U.S.A.), post paid, cash with order. Orders should be sent to The Institute of Physics, 47 Belgrave Square, London, S.W.1, or to any bookseller.

Recent studies of noise problems

by G. G. PARFITT, Ph.D., A.R.C.S., D.I.C., Imperial College of Science and Technology, London, S.W.7

Abstract

Some fairly recent work on various aspects of acoustic noise was reviewed at a half-day symposium held in London in March 1959 by the Acoustics Group of The Physical Society. One group of papers discussed studies of the parameters of noise which were important in determining the subjective loudness, the possible damaging effects on human hearing, the influence on working efficiency and the annoyance caused in residential and working communities. Of the more purely technical papers, one considered some of the difficulties in making measurements of noise from aircraft to the relatively high degree of accuracy often required, while the other described results of measurements and analysis of the noise from automotive diesel engines.

PROMPTED by the great and growing importance nowadays of noise as a factor in industrial and urban life, the Acoustics Group of The Physical Society held a symposium on 24 March, 1959, to review some of the more recent progress in research on the scientific and allied problems involved. The large audience which attended the meeting, held at Imperial College, London, bore witness to the current importance of the subject.

The first four papers read dealt in various ways with the question of the influence of noise on people, i.e. how noise could be measured in a subjectively meaningful way, and what its effects on the hearing organs, on work and on recreation might be.

Mr. N. FLEMING and Mr. D. W. ROBINSON (Acoustics Section, National Physical Laboratory), first examined the problem of "The measurement of noise in relation to the effect on the listener". They pointed out that in most noise problems we were concerned ultimately with the effects on human beings, so that, in the long run, measurements of noise must be interpreted in terms of the subjective attributes of noise. Subjective characteristics could only be measured by subjective experiments, i.e. by taking the opinions of listeners. It was, however, desirable to be able to relate the subjective effects to the physical characteristics of noise so far as was possible. Of various subjective properties, such as loudness, annoyance, disturbance, etc., the first was likely to be least affected by the situation or occupation of the listener and so probably most directly related to objective parameters. There were a great many of these, but among them the overall sound pressure level and the frequency distribution were obviously two of the most important. However, the presence of pure-tone components, and the general inconstancy of the noise, whether short-term, as in the pulses from a pneumatic hammer, or longer-term, as from road or rail traffic passing by, were other important factors not necessarily or readily included in a measured spectrum. Ratio of peak to r.m.s. of an impulsive waveform, or the fraction of time for which an intermittent noise exceeded specified levels, might be convenient additional

parameters. The nature of the field, whether progressive or diffuse, and of the listening situation, whether binaural or not, were also relevant.

For assessing *annoyance*, so-called "community reaction" curves had been put forward by Stevens, Rosenblith and Bolt in the United States.⁽¹⁾ These provided a method of assessing the annoyance value from octave-band pressure measurements (see Mr. PURKIS's discussion below). An alternative quantity which had proved of value, especially for outdoor sounds, was simply the "A" scale reading of the standard sound level meter.^(2,3)

Loudness or loudness level could be measured unambiguously on the sone or phon scales by subjective measurements in the laboratory, using a group of 30 or more listeners, but the practical need was a reliable means of computing loudness from physical data. The various "equivalent tone" procedures for this were based on the principle of replacing the actual spectrum by a set of equivalent pure tones and then summing the loudnesses of these.

Quietsch⁽⁴⁾ in Germany and Stevens⁽⁵⁾ in the United States had modified the mode of addition to try to take account of the phenomenon of masking. Zwicker⁽⁶⁾ had recently approached the problem in more detail from the point of view of the Békésy place theory of hearing. The principle here was that sounds of a given frequency excited predominantly one characteristic region of the basilar membrane in the ear, the position of the region moving along the membrane as frequency increased. Accordingly, Zwicker split the spectrum of a sound up into a set of 24 bands and calculated their individual contributions to loudness by a method based on his experimental observations. A somewhat complex graphical summation process was then carried out which was aimed at reproducing the masking caused by the fact that the excitation of the basilar membrane tended to spread over into the region corresponding to adjacent higher frequencies. The method was promising as being more closely related to the known facts about hearing than earlier ones, but it remained to be seen how successful it would prove in practice.

Much work was being and still remained to be done in the field of loudness measurement, especially for the difficult cases of discontinuous or impulsive sounds. The field was one of great scientific interest to physicists, physiologists and psychologists, and at the same time of considerable commercial importance, for since noise was coming to be one of the controlling factors in aircraft development, very important decisions might hinge on quite small differences in loudness.

In the discussion Dr. A. J. KING drew attention to the potential importance of reverberation as influencing a listener's estimate of loudness of sound heard in a confined space. Mr. ROBINSON confirmed that measurements on the relative loudness of diffuse and plane progressive sound fields were now in progress at the N.P.L. Although fairly substantial differences in loudness were observed for single plane waves incident in various directions, the difference

between the diffuse field and the particular case of frontally incident plane waves did not appear to be large.

Prof. W. BURNS (Charing Cross Hospital Medical School) then took up the question of damage to hearing due to intense noise. He said that while established facts in this field were still rather scanty, three main types of auditory effect could conveniently be distinguished: these were temporary hearing loss, acoustic trauma, and occupational hearing loss. Taking these in order, temporary hearing loss or temporary threshold shift as it was sometimes called, occurred alone or in combination with permanent hearing loss; it occurred chiefly in the first few hours of an exposure period, such as a working day in noise, and diminished gradually after the cessation of the noise, to disappear perhaps after minutes, hours or days, the length of the recovery period depending on the severity of the exposure. By its nature, it was the only type of noise-induced hearing loss open to laboratory investigation on human subjects. In experimental temporary hearing loss, it had been found that, for stimulation by a pure tone at the higher levels, the temporary hearing loss occurred maximally at frequencies some half an octave above the frequency of the responsible tone. Bands of noise produced the same upward displacement. The second category of effect, acoustic trauma, was the permanent hearing loss following very short exposure to extremely intense noise, including explosive noise such as gunfire. The loss in this case is particularly in the 4000 c/s region. Last came occupational hearing loss, the cumulative deterioration of hearing due to daily exposure, for example, to industrial noise in the course of work. This tended to manifest itself first in the 4000 c/s region and to spread towards lower frequencies, becoming more serious for the sufferer as it invaded the frequency range important for speech perception. The important parameters were (1) the intensity of the noise; (2) its frequency: very low frequencies were probably rather less damaging, while there was no evidence that ultrasonic frequencies at present levels were a serious problem; (3) its duration: work was in progress to study the relative importance of intensity, duration and distribution of exposure with respect to time in determining the effective exposure; (4) its periodicity: little was yet known of the effects of impulsive noise as from a riveting hammer, compared with the effects of steady noise.

Professor BURNS pointed out that individuals varied widely in their susceptibility to noise, but considered it was not yet established that undue sensitivity to temporary hearing loss was an indication of a similar tendency for long-term cumulative damage. He commended the work of the American Standards Association which led to the Z24-X2 report in 1954,⁽⁷⁾ still our main source of data in this field, but pointed out that the presbycusis corrections used were now open to criticism. He concluded by referring to the criteria for permissible noise exposure for the protection of hearing given by Rosenblith and his co-workers,⁽⁸⁾ Burns and Littler⁽⁹⁾ and the American Academy of Ophthalmology and Otolaryngology.⁽¹⁰⁾ The latter recommended that if an industrial noise in the 300 to 600, or 600 to 1200 c/s bands exceeded 85 dB S.P.L., then a hearing conservation programme was called for.

Answering a query from Mr. E. R. WIGAN regarding the histological evidence of hearing damage, Professor BURNS said that it was very difficult to obtain on human beings, since changes occurring after death obscured the effects sought for. There was, however, evidence of damage to the hair cells in animal ears. The concussive blows which caused acoustic trauma gave similar effects. The magnitude of the

cochlear microphone potential was a convenient measure of the state of an ear in this respect.

The next speaker was Dr. D. E. BROADBENT (M.R.C. Applied Psychology Unit, Cambridge) who discussed the effects of noise on working efficiency. This was a subject, he had found, on which the strongest and most divergent views were held by the public, and one in which it required extreme care to obtain reliable and significant results. For example, most straightforward observations of the effect of noise-reduction measures in factories were incapable of giving reliable information if only because any feeling of goodwill towards the management for their efforts to improve working conditions was superimposed on the true effect of the noise. Laboratory tests of the effect of continuous, meaningless noise under controlled conditions, while often giving negative results, had, however, shown a significant deterioration of performance in noise in certain cases. The results could be interpreted by supposing that the noise tended to cause occasional momentary interruptions in a worker's ability to take in sensory information, rather as a blink interrupted vision temporarily. This did not normally affect the worker's total output, for the periods concerned were short and largely compensated for by extra effort subsequently. However, where the pace of work or action was dictated by factors outside the worker's control, or involved an element of unpredictability, and where momentary lapses of attention could lead to failures of reaction or mistakes, loud noise was likely to have significant effects.

Recent work in America had provided confirmation of these views. For example, the reaction time of soldiers to a faint light appearing in the field of view of a gun sight was significantly increased in the presence of loud noise. Any type of watch-keeping task was in fact subject to influence in this way. Again, a task involving a considerable effort of short term memory, such as carrying out mental arithmetic, was influenced by noise.

As regards level, about 90 dB total sound pressure level appeared to be the lowest at which effects were observable. Measurements of the frequency of errors in an experiment on response to light signals arriving in rapid succession for half an hour, and using high-frequency (> 2000 c/s) and low-frequency (< 2000 c/s) noise of equal loudness, showed the high-frequency noise to have the greater influence. The effects of interrupted noise had been studied recently. Short bursts of noise produced a drop in efficiency for perhaps a half-minute afterwards, with a compensating rise thereafter. However, subjects had been found to be less affected by interrupted (1 s on—1 s off) noise at 75 dB level than by steady noise.

Certain other puzzling effects had been observed recently. For instance, it had been found with subjects doing mental arithmetic that after they had been subjected to noise on one day, their performance was adversely affected also on the following day when working in quiet.

Dr. BROADBENT summed up by saying that in general noise did not affect rates of working, i.e. total output, but could increase the numbers of accidents, errors or rejects which occurred. He was able to report the results of a controlled factory experiment which had just become available, and in which the scrapage rate had been found lower in one department with reduced noise level, though there was also an increase in total output due to the "goodwill" effect mentioned earlier.

As always, the topic provoked a lively discussion. Answering Professor BURNS, Dr. BROADBENT agreed in general that if the levels of noise were such as to avoid the risk of hearing

damage, then efficiency should also be unaffected. Sudden startling noises were probably an exception, however. Asked about the effect of noise on intellectual work, he considered that it was possible for this to be unaffected if the noise level was not above some 90 dB, at least, if the noise was continuous and not unfamiliar. The effects at the lower levels were very variable and personal. It is possible to resist all effects of noise for a limited period, say half an hour, and some people were able to concentrate better in moderate noise than in quiet. It appeared in general that some degree of outside stimulation was a desirable thing; efficiency declined if people were cut off from all stimulus for too long.

Another aspect of noise tolerance was taken up by Mr. H. J. PURKIS (Building Research Station), who discussed the "Acceptable noise levels in communities". This was a very wide problem because of the many types of noise source, operating for varying amounts of time, at different times of day or night, and affecting people of widely differing temperaments occupied in different ways. It was impracticable in fact to attempt to define a criterion for every given noise and situation, but useful work had been done in a number of important cases.

The general approach must be to try to express, for example, average public reaction to disturbance, or interference with some appropriate activity such as speech or telephone use in offices, on a suitable scale, and to establish a relation between this and a scale of objective noise measurement.

The best method of sampling community opinion was through a careful statistical survey by competent and disinterested staff. More often, and less satisfactorily, it was someone concerned with the measurement, production or effect of the noise who asked the questions. In extreme cases complaints would serve to establish the top part of the scale. Frequently, however, only inspired guesswork was available to establish the levels for complaint and for negligible annoyance.

Two published criteria obtained by the survey method are those of Beranek for noise in offices⁽¹¹⁾ and of the Building Research Station for sound insulation in houses and flats.⁽¹²⁾ Beranek asked office staff to answer a written questionnaire dealing with the level of noise present in their offices, using a rating scale ranging from "very quiet" to "intolerably noisy". This was compared with direct measurements of the noise spectra, which were analysed to give the loudness level and the speech interference level, i.e. the average sound pressure level in the three octave bands from 600 to 4800 c/s. The results provided a criterion curve from which the average reaction to conditions in offices with known or predictable noise levels could be estimated and the interference with speech or telephone use assessed. For example, a speech interference level of 40 dB or a loudness level of 62 phons may be considered the maximum permissible in an executive office. For general secretarial offices some 15 units more may be tolerated. The Building Research Station carried out parallel tests in offices at London Airport and found generally similar results for the higher noise levels, about 80 phons proving to be the boundary between "noisy but acceptable", and "noisy and not acceptable".

The Building Research Station's grading system for sound insulation in flats and houses was based on a careful survey of conditions in some 1500 flats in three groups with differing sound insulation in their floors, namely 50 dB (high) 45 dB (medium) and 40 dB (low). It was found that in the high group, noise came only sixth on the list of complaints, while in the others it headed the list. In the high group, of those wanting better insulation, only 40% would consider paying

extra rent to cover it, while 75 to 80% in the other groups would consider doing so. It was noticeable, however, that the proportion of tenants claiming to be disturbed by noise in the low group was no greater than that in the high group. This reflects the fact that most of the tenants in the low group had previously lived in much worse conditions and were not prepared to complain about their present situation.

The average airborne insulation curves for the flats in the high and medium groups, with some modification at the higher frequencies where the insulation is more than adequate, have been adopted as limits for two defined grades of insulation. By comparison of the insulation of a given construction with these grades, the probable satisfaction or otherwise of tenants can be predicted with some confidence.

A criterion based on complaints was that of Stevens, Rosenblith and Bolt⁽¹⁾ for noise in residential communities in the U.S. Here, a ranking figure for the noise was obtained by comparison of the measured octave-band spectrum with a set of standard curves, the highest curve cut giving the rank. This was adjusted for a number of factors such as past history of exposure, special characteristics of the noise, the duration of the exposure, the time of day or night, etc., and the final corrected figure was applied to a criterion scale to determine the expected public response. The scale ranged from "no annoyance" to "vigorous legal action". The Building Research Station was at present attempting a similar study in connexion with noise complaints received by local authorities in Hertfordshire.

In discussion Mr. PURKIS agreed with Mr. FLEMING in that while the Stevens-Rosenblith-Bolt criterion might be expected to give satisfactory predictions of reaction in this country for noises at night, the tolerance of daytime noise here was probably greater than the curves suggested. Mr. EWING emphasized the importance of the level of the ambient background noise in determining the reaction to one particular noise, and he and Mr. E. R. WIGAN suggested that it was the extent by which the noise exceeded the background rather than its absolute level which was likely to be decisive in general. The criterion at present makes only a rather broad allowance for background conditions. Mr. ROBINSON pointed out that on general psychological grounds one would not expect a unique relation between noise level and annoyance, since judgments are made in different psychological "dimensions" in different personal circumstances. Mr. D. M. A. MERCER, like Mr. H. R. HUMPHREYS, had found general agreement with the ranking curves and stressed the importance of the pooling of experience in this country. Mr. PURKIS agreed to provide a clearing house for this purpose, and asked members to submit details of their experiences to him.

On the more technical side of the meeting, Mr. D. M. A. MERCER (Southampton University), discussed some of the "Measurement problems in aircraft noise". He was concerned primarily to point out the importance of some factors often neglected in practical work. For example, in ground measurements of engine noise in the open, the total noise power output was influenced by the presence of the ground and of any other reflecting surfaces. The magnitude of the ground effect depended on the nature of the source, and Ingard⁽¹³⁾ had shown that it could vary over a 12 dB range, with variations in source height for a quadrupole source. Again, the effects of interference between the direct sound and the ground reflection could produce effects on the level measured at a distance which were not always satisfactorily allowed for by summing over a range of frequencies even as large as an octave. Further, it was normally supposed that

symmetry of the radiation around a jet engine made it unnecessary to measure the noise at points above the engine. In one case, however, where this was done, differences with angle around the jet axis up to 10 dB were observed. (Symmetry could be checked if it was possible to mount the engine with its axis vertical during tests.)

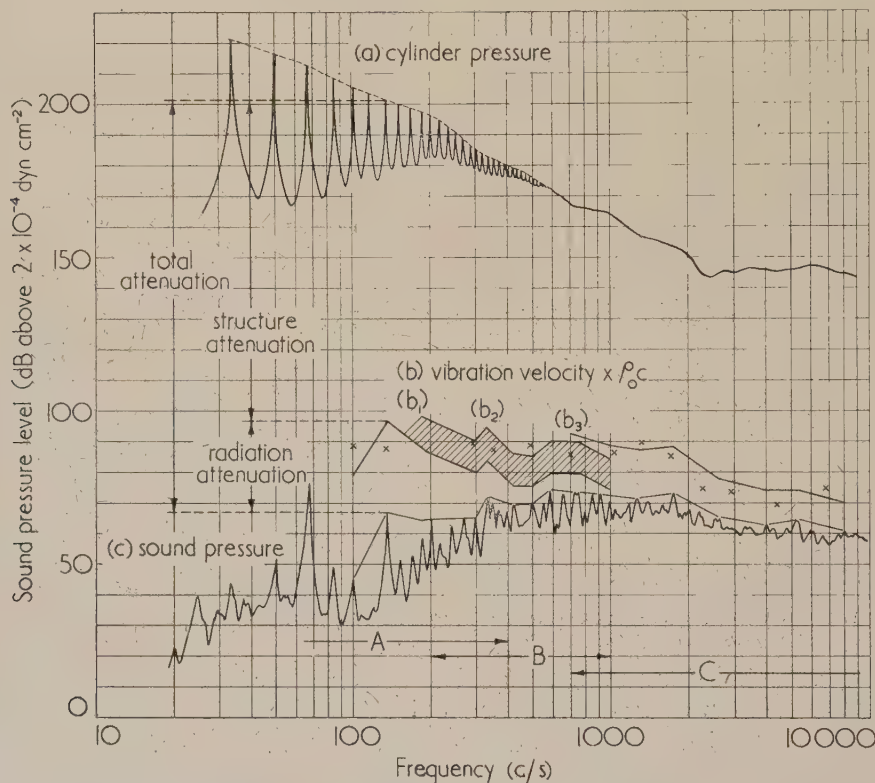
All these phenomena could be particularly important where "before and after" measurements of the relatively small effects of adding a silencer were concerned. In such tests it was essential that the height of the jet efflux and of the microphone above the ground should be the same before and after fitting the silencer, and also that the nature of the ground surface should not vary.

Engine-noise measurements were usually made on the circumference of a circle surrounding the engine, of a radius

found at lower frequencies. Again the turbulent jet might project into the absorbent splitters in the outlet duct, and the noise radiation influenced as a result.

In test running it was important that the engine condition should be kept constant. It was, nevertheless, difficult to maintain stability for more than a few minutes and especially from day to day. Where only the engine speed and not the thrust was known and kept constant, the operating conditions of the engine would vary with the ambient temperature, and this factor alone could produce differences of several decibels in noise output in differing climatic conditions. All these phenomena made it extremely difficult in general to compare noise levels with an accuracy to better than one or two decibels.

Mr. MERCER ended his talk with a brief discussion of the



Cylinder pressure, narrow band noise and vibration spectra for engine D

large enough for "far-field" conditions to be established, i.e. at least α^2/λ , where λ is the wavelength concerned and α is a typical dimension of the source. Since, however, the effective position of the source was not at the jet orifice, but in a region some way downstream in the jet, it was this latter position which should properly form the centre of the measuring circle. The position was, however, rather uncertain and dependent on frequency; it was usually necessary to make the radius quite large to make errors in the position negligible.⁽¹⁴⁾ About 200 ft was about as large as could be used if atmospheric attenuation was not to become significant.

In test cells the problems were different, but could still be serious. The limitations of space meant that measurements often had to be made in a region where neither the direct nor the reverberant sound was wholly predominant. If the microphone was close to the walls, pressure doubling would be

uses of correlation measurement in the field of aircraft noise. One typical case was to determine the relative contribution of one of several engines to the noise heard at, say, a point in the cabin. By determining the extent of the cross-correlation between the noise waveform recorded at the point in question and that recorded from a microphone placed close to the suspected engine, the contribution of that engine could be found. Correlation might be found for more than one value of delay-time, corresponding to the arrival of noise by multiple paths, e.g. air- and structure-borne noise. Provided that the noise was truly random and the apparatus in no way overloaded, the method was effective in detecting even very small contributions to the total noise. Difficulties could arise in the case of propeller engines, since the correlation principle broke down for pure tones. However, if the engine speeds could be made to differ slightly, even by one part in a thousand, measurements were still practicable, provided

stability could be maintained over a measuring period of perhaps half a minute.

Coming down to earth, a study of noise from automotive Diesel engines was then reported by Dr. A. E. W. AUSTEN and Dr. T. PRIEDE. They had found that when noise from air intakes and exhausts had been substantially eliminated by provision of suitable silencers, the spectra of residual noise from a number of typical engines were remarkably similar, and that all showed a broad peak in the range 800 to 2000 c/s, representing the objectionable hard knock characteristics of the Diesel. A petrol engine had its strongest peaks in the 400 to 600 c/s region. The total intensity (omitting low-frequency components due to the air-intake) in the range 150 to 9600 c/s was proportional to the cube of the engine speed and the power $4/3$ of the swept volume, but varied very little with the load. The latter effect corresponded to the small change in maximum cylinder pressure with load in the Diesel engine. In the petrol engine, cylinder pressure and noise decreased considerably with reduction of load, but the noise at full load was comparable with Diesel noise.

In general the noise arose from many sources in the engine, and treatment of certain of the more prominent secondary sources on a particular engine, including air-intake, valve and timing covers, and injection equipment, gave a reduction of estimated loudness of about 50%. When contributions from such sources were excluded, the remaining noise, radiated from the surfaces of the engine structure, was due to the direct effect of pressure variations in the cylinders. That this was the case was suggested by the fact that over a range of speed, load, etc., the difference in decibels between the cylinder pressure and the external sound pressure ("total attenuation" of the figure) was roughly constant at a given frequency. This difference represented the effective attenuation through the engine structure and air path, and fell at about 16 dB per octave as frequency increased from 100 to 1000 c/s and thereafter more slowly and irregularly. Order of magnitude calculation of the vibration amplitude of engine (particularly crankcase) surfaces set into bending vibrations by the vertical force due to cylinder pressure gave reasonable agreement with measured values ("structure attenuation" of the figure). With assumptions as to the size of the radiating surface these vibration amplitudes were also found to be in good agreement with calculations of the values necessary to produce the observed sound intensity; this is the "radiation attenuation" of the figure.

The mechanisms tentatively suggested for the radiation in the frequency ranges indicated in the figure were as follows:—

A, bodily vibration of whole engine, as displacement, caused by reaction of forces due to vibration of engine-fly-wheel-crankshaft system;

B, rotational vibrations about both horizontal and vertical axes of whole engine caused by reactions of forces due to resonant crankshaft bending vibrations and torsional oscillations, and

C, vibration of resonating sections of engine surfaces, generally crankcase, resulting from transmission of force due to cylinder pressure, both directly, and via crankshaft vibrations.

References

- (1) STEVENS, K. N., ROSENBLITH, W. A., and BOLT, R. H. *Noise Control*, **1**, p. 63 (1955).
- (2) YOUNG, R. W. *J. Acoust. Soc. Amer.*, **30**, p. 363 (1958).
- (3) RONGE, H. E. *Särtryck ur Ingeniörsvetenskapsakademien*, **8**, p. 354 (1955).
- (4) QUIETZSCH, G. V. *Akustische Beihefte*, **1**, p. 49 (1955).
- (5) STEVENS, S. S. *J. Acoust. Soc. Amer.*, **28**, p. 807 (1956).
- (6) ZWICKER, K. E. *Akustische Beihefte*, **1**, p. 237 (1958).
- (7) AMERICAN STANDARDS ASSOCIATION, 1954, REPORT Z24-X2: *The Relations of Hearing Loss to Noise Exposure* (New York: American Standards Association, 1954).
- (8) ROSENBLITH, W. A., STEVENS, K. N., and Staff of Bolt, Beranek and Newman Inc. *Handbook of Acoustic Noise Control* (Washington: Office of Technical Services, 1953).
- (9) BURNS, W., and LITTLER, T. S. *Modern Trends in Occupational Health* (London: Butterworth and Co. (Publishers) Ltd., in the press).
- (10) *Guide for Conservation of Hearing in Noise* (Los Angeles: American Academy of Ophthalmology and Otolaryngology, 1957).
- (11) BERANEK, L. L. *J. Acoust. Soc. Amer.*, **28**, p. 833 (1956).
- (12) National Building Studies Research Paper No. 27 (London: H.M. Stationery Office, 1958).
- (13) INGARD, U., and LAMB, G. L. *J. Acoust. Soc. Amer.*, **29**, p. 743 (1957).
- (14) DOELLING, N., MERCER, D. M. A., and Staff of Bolt, Beranek and Newman Inc., WADC Technical Report 54-401 (Washington: Office of Technical Services, July 1956).

High resistivity nickel-iron alloys with rectangular hysteresis loops

by A. HART, B.Sc., Ph.D.,* G.P.O. Engineering Department, Research Station, Dollis Hill, London, N.W.2

[Paper received 27 July, 1959]

Abstract

Because of its rectangular hysteresis loop, magnetically annealed 65/35 nickel-iron alloy is suitable for many applications. The alloy has a low resistivity, however, and eddy-current effects limit the performance of many devices made from the alloy. An alloy with similar magnetic characteristics and a higher resistivity is very desirable.

A method of magnetic annealing is described which allows magnetic properties, practically identical to those of 65/35 alloy, to be induced in alloys containing up to 3% molybdenum, and nickel and iron in the ratio 65/35. The resistivity of the 3% molybdenum alloy is $53 \mu\Omega \text{ cm}$, compared with $19 \mu\Omega \text{ cm}$, for the binary 65/35 alloy. The new annealing method takes rather longer than that previously used, but is no more difficult to carry out; it can be used on alloys which cannot be successfully treated by a "normal" magnetic anneal. Compared with available 50/50 grain-oriented alloy, the 3% molybdenum alloy has a lower coercivity and a higher resistivity, but its saturation flux density is some 20% less.

Introduction

AFTER a heat treatment in a magnetic field, an alloy containing 65% nickel and 35% iron exhibits a parallelogram-shaped hysteresis loop. The coercivity H_c is about 0.01 oersted and the remanence ratios B_r/B_m , after saturating in a field of 10 oersteds, are in the range 0.90–0.95. Because of these properties this alloy is suitable for numerous uses, e.g. in magnetic amplifiers, mechanical rectifiers, pulse generators, static delay lines, and matrix-type stores. In many of these applications, it would be advantageous to use an alloy of higher resistivity (the value of ρ for 65/35 is only $19 \times 10^{-6} \Omega \text{ cm}$), and an alloy containing 1% molybdenum has proved useful.^(1, 2)

Experimental method

Powder-metallurgy methods were used to produce alloys containing nickel and iron in the ratio 65/35 and additions of $1\frac{1}{2}$, 2, 3 and 4 wt % of molybdenum. Test specimens were punched from material 50μ thick, in the form of rings with 1 in. outer diameter and $\frac{1}{16}$ in. inner diameter. All specimens were annealed for fifteen hours at 1050°C in pure dry hydrogen. For the magnetic anneal the specimens were contained in a ceramic former on which primary and secondary coils were wound. The ceramic former was in close contact

with a thermocouple, and was inserted in a furnace suitable for annealing at temperatures up to 800°C . Measurements of B_r/B_m and H_c could be made, at temperature, using the normal ballistic method. The maximum field applied to the specimens was 10 oersteds.

For a given alloy, the Curie temperature (T_c) was first determined. The furnace temperature was then controlled at a value about 100°C below T_c , and the saturating field of 10 oersteds was applied to the specimen. At intervals, the B_r/B_m ratio and the coercivity of the specimen were measured. When these properties reached their equilibrium values the furnace was switched off, and the specimen allowed to cool to room temperature with the saturating field still applied. The room temperature values of B_r/B_m and H_c , which were usually different from their high-temperature values, were recorded. The (arbitrary) criterion of a successful anneal was that the room temperature remanence ratio should be greater than 0.90. The above procedure was repeated at several temperatures, in order to define the temperature range over which this criterion could be satisfied.

Results

Table 1 summarizes the results. Values of T_c and B_m at 10 oersteds, are rather approximate. As a rough guide, each 1% (by weight) of molybdenum reduces B_m by 4%, T_c by 20°C , and increases the resistivity ρ by $11 \times 10^{-6} \Omega \text{ cm}$. The figures in the table (column A) show the usual inverse relationship between temperature and time of anneal for

TABLE 1. Properties of magnetically-annealed alloys at thicknesses of 50μ

M_o (wt %)	T_c ($^\circ \text{C}$)	B_m (G)	ρ ($\mu\Omega \text{ cm}$)	A ($^\circ \text{C/h}$)	B ($^\circ \text{C/h}$)	B_r/B_m	H_c
0	593	13 900	19				
1	570	13 400	31				
1.5	557	13 100	37	508/3	450/12	0.94	0.01
2.0	553	12 900	43	488/6	450/12	0.96	0.05*
3.0	525	12 300	52	450/12	430/36	0.93	0.06*
4.0	512	12 000	64		430/40	0.85	0.05

B_m and B_r/B_m were both measured in a field of 10 oersteds. The magnetic annealing field was also 10 oersteds.

Column A: maximum temperature of anneal ($^\circ \text{C}$), and annealing time (h) required to give $B_r/B_m \geq 0.9$. The minimum temperature of anneal was the same for all alloys, 405°C , annealing time 44 h.

Column B: optimum treatment, giving B_r/B_m and H_c values shown in last two columns.

* These alloys did not have the best preliminary annealing treatment. Given the same treatment as the 1.5 and 4% alloys, these coercivities would be halved.

* Now with U.K.A.E.A. (I.G.) Windscale Works, Sellafield, Cumberland.

establishing equilibrium. As the temperature of anneal rises, the equilibrium B_r/B_m ratio at temperature falls, and so does the final room temperature ratio. This factor sets the upper limit on the temperature of anneal. The low-temperature limit is set by the long time required to reach equilibrium at temperatures below 400° C. It appears that the 4% molybdenum alloy could only attain a remanence of 0.90 by annealing at a temperature below 400° C, and this proves impracticable.

Earlier experiments have shown that similar remanence ratios can be induced in specimens with thicknesses in the range 200–15 μ . In going from 50 to 15 μ , however, the coercivity increases by a factor of about three, and this may make the use of thin specimens undesirable.⁽²⁾

The coercivities of the specimens at the temperature of anneal were about 0.01 oersted. "Annealing fields" of 10 and 1 oersteds were equally efficient in producing high remanence ratios. Reducing the field to 0.4 oersted, however, gave lower ratios.

Discussion

(i) The results reported give qualitative support to the theory of magnetic annealing proposed by Taniguchi.^(3,4) According to this theory the annealing process depends on atomic ordering, giving rise to a uniaxial anisotropy superposed on the "natural" anisotropy of the alloy. For a given alloy, the magnitude of the induced anisotropy depends on the quantity (σ_T^2/T) , where σ_T is the saturation magnetization at the annealing temperature T (° K). The effect of the magnetic anneal on the hysteresis loop of the alloy will be more marked the greater the ratio of induced/natural anisotropy. This ratio will be larger the lower the temperature of magnetic anneal, providing that this temperature is not so low that ordering cannot take place in the time available. In the case of the range of alloys studied here, the addition

in the presence of a field. For these alloys, because of their high Curie temperatures, sufficient ordering to produce a high anisotropy is attained during the time they are above 400° C. In the case of the 1.5% molybdenum alloy, the constant temperature magnetic anneal gave a higher remanence than the "normal" magnetic anneal.

It is interesting to note that the above theory predicts that any face-centred-cubic solid solution, as well as body-centred-cubic solid solutions with negative anisotropy, will be susceptible to magnetic annealing. There is thus the possibility of modifying the hysteresis loops of many alloys by a low-temperature heat treatment in a magnetic field.

(ii) Magnetically-annealed 65/35 alloy competes with grain-oriented 50/50 nickel-iron alloy in many applications. Owing to its uniaxial anisotropy, 65/35 alloy can only be employed wound into clockspring cores, whereas 50/50 alloy can also be used in the form of stamped laminations. Comparison of the two alloys is complicated, since a wide variation in remanence ratio and coercivity can be produced in either alloy, depending on its heat treatment during fabrication. The coercivity is also dependent on the thickness of the material, increasing in general with decrease in thickness in the range 5–100 μ . In testing the alloys, the maximum field used must be known, since B_r/B_m decreases with increase in field until saturation is reached.

Table 2 shows data obtained under known test conditions, with materials which were all approximately 50 μ thick. They may be taken as characteristic of the best alloys at present available. Since cores of the 3% molybdenum alloy have not been made, Table 2 first shows comparison between ring specimens of straight 65/35 alloy and rings of the 3% alloy. Cores of straight 65/35 alloy are then compared with cores of 50/50 alloy, both alloys being made by powder-metallurgy methods. Results for commercially made cores of 65/35 and 50/50 alloys are added. It is to be noted that the resistivities of these alloys are higher than the corre-

TABLE 2. Comparison of 50/50 and 65/35 type alloys

Test specimen	Specific gravity (g/cm ³)	($\mu\Omega$ cm)	T_c (° C)	B_m (G)	H_c (oersted)	B_r/B_m	H_m (oersted)
PM ₁	8.4	19	590	13 700	0.01–0.02	0.94–0.97	10
PM ₂	8.45	53	525	12 300	0.06*	0.93	10
PM ₃	8.4	19	590	13 700	0.015–0.03	0.94–0.98	10
PM ₄	8.25	32	500	15 300	0.1–0.15	0.95–0.97	7
C ₁	8.4	26	550	13 300	0.06	0.91	4.4
C ₂	8.25	45	500	15 400	0.12	0.94–0.97	7

PM₁: rings of powder-metallurgy 65/35 alloy

PM₂: rings of powder-metallurgy 65/35 alloy + 3% molybdenum

PM₃: cores of powder-metallurgy 65/35 alloy

PM₄: cores of powder-metallurgy 50/50 alloy

C₁: cores of commercially made 65/35 alloy

C₂: cores of commercially made 50/50 alloy

H_m is the field used during measurement of B_r/B_m .

* Modified preliminary annealing treatment, used for later materials, would halve the recorded value of H_c .

of molybdenum depresses the Curie temperature and reduces the saturation magnetization. To attain the same induced anisotropy, alloys with increased percentages of molybdenum must be annealed at lower temperatures. Hence, although the remanence ratio B_r/B_m has only an indirect connexion with the induced anisotropy, the results shown in Table 1 afford confirmation for the theory.

It is to be noted that alloys with up to 1½% by weight of molybdenum respond to a "normal" magnetic anneal, i.e. they achieve a high remanence ratio after cooling through the temperature range 600–400° C at a rate less than 150° C/h,

responding powder-metallurgy alloys. This may well be due to the introduction of small amounts of manganese.

Conclusions

A modified method of magnetic annealing, involving a longer time of anneal at a temperature lower than that "normally" used, successfully produces rectangular loops in alloys having a nickel/iron ratio of 65/35 with additions of up to 3% by weight of molybdenum. From the point of view of the B_r/B_m ratio and coercivity, these alloys are

practically identical with a straight 65/35 alloy; at the same time their resistivities lie in the range 31–53 $\mu\Omega$ cm, compared with 19 $\mu\Omega$ cm for the 65/35 alloy. The only disadvantage from the application standpoint is that each 1% addition of molybdenum reduces B_m by 4% and lowers the Curie point by about 20° C.

The 65/35 alloy could be used in many applications where eddy currents significantly affect the performance; in these cases substitution of a molybdenum bearing alloy will result in an improved performance. The new annealing procedure is simple enough to allow its use whenever a rectangular loop alloy of the 65/35 type is needed.

Compared with 50/50 alloy, the 3% molybdenum alloy is superior in that its coercivity is three or four times smaller, and its resistivity is appreciably larger. Its sole disadvantage is that the maximum induction attainable is some 20% less than that for the 50/50 alloy.

Acknowledgements

Acknowledgement is made to the Engineer-in-Chief of the Post Office and to the Controller of H.M. Stationery Office for permission to publish this paper.

The author is indebted to Mr. B. G. Parkin for a considerable number of preparatory experimental measurements.

References

- (1) *Post Office Engineering Department Research Report* 13438 (1953).
- (2) *Post Office Engineering Department Research Report* 13779, Pt. 1 (1955).
- (3) TANIGUCHI, S., and YAMAMOTO, M. *Sci. Rep. Res. Insts. Tôhoku Univ.*, A6, p. 330 (1954).
- (4) TANIGUCHI, S. *Sci. Rep. Res. Insts, Tôhoku Univ.*, A7, p. 269 (1955).

Viscosity and thermal conductivity of liquid boron trifluoride

by A. N. SPENCER, B.Sc., and M. C. J. TODD, B.Sc., A.Inst.P.,* United Kingdom Atomic Energy Authority, Research and Development Branch, Capenhurst, near Chester.

[Paper first received 3 April, and in final form 23 July, 1959]

Abstract

The normal liquid range of boron trifluoride is -100 to -127°C . Conventional methods have been adapted to measure viscosity and thermal conductivity throughout this range of temperature, and experimental results are presented.

Introduction

IN designing a plant for separating the boron-10 isotope from the natural mixture it was necessary to know the viscosity and thermal conductivity of liquid boron trifluoride. As no previous determinations have been described, these physical properties were measured. The measurements extend over the whole temperature range of the liquid, -100 to -127°C , and were made by conventional methods adapted for low-temperature work.

The boron trifluoride, supplied by Imperial Smelting Corporation, Ltd., was of 99.8% purity.

Viscosity

Method. An Ostwald type viscometer, shown in Fig. 1, was used. It was filled with liquid boron trifluoride by cooling the condenser with liquid nitrogen so that boron trifluoride gas condensed when admitted to the apparatus. The main body of the liquid then acted as a constant-temperature bath for the capillary tube. Heat leakage was kept low by a surrounding, unsilvered, vacuum jacket, the outer wall of which was itself kept cold by cold nitrogen gas boiling from liquid nitrogen in the bottom of a second, larger,

Dewar flask. Liquid was made to flow through the viscometer by raising the pressure of gas in the tubing leading to the bulbs

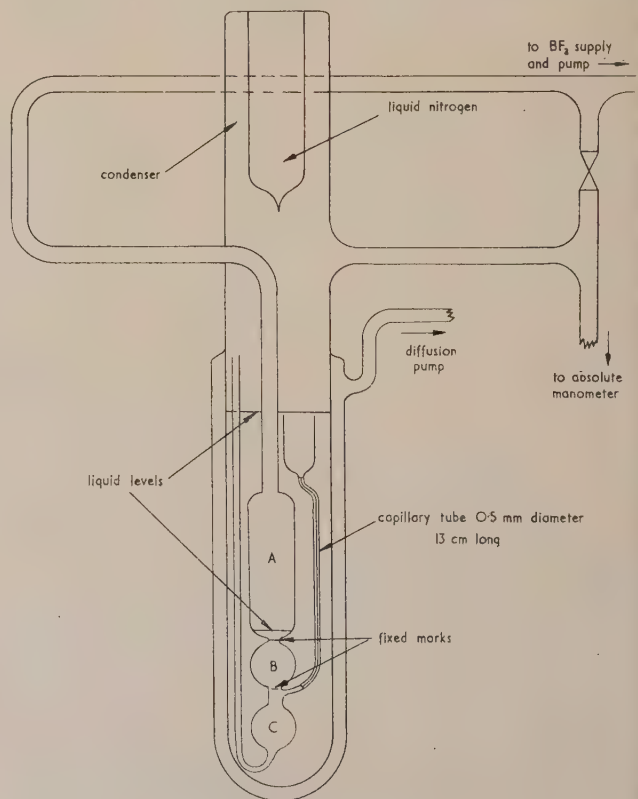


Fig. 1. The viscometer

* Now at Atomic Weapons Research Establishment Aldermaston, Berks.

so that liquid was expelled up the wide-bore tube. On re-equalizing the pressures, liquid flowed back into the bulbs through the capillary tube. The lower bulb *C* collected the liquid flowing back from the wide-bore tube, while the upper bulb *A* served only to reduce the volume of liquid required to fill the apparatus.

The standard liquid level to which the viscometer was filled was arranged to be 1 mm above the top of the capillary funnel, when the measuring bulb *B* was completely filled to the upper mark. A measurement was made by taking the time for the liquid to rise from the lower to the upper fixed mark. The vapour pressure above the liquid, measured on a mercury manometer, gave an indirect measure of temperature from published vapour-pressure data.^(1, 2, 3)

Liquid nitrogen was retained in the condenser until the liquid had cooled by refluxing to near the freezing point. At the lowest temperature, gas was admitted to restore the liquid level to the standard condition. Measurements were then made with the temperature increasing very slowly. Because of the decrease in density with increasing temperature, and the addition of more gas each time the liquid was blown back from the measuring bulb, the liquid level rose above the standard level as the temperature rose. Corrections were made by reducing the recorded times in proportion to the estimated excess head. On reaching the boiling point this correction was checked by allowing the excess liquid to boil off until the standard level was once more regained.

Results and discussion. The viscometer was calibrated with liquids of known viscosity⁽⁴⁾ before and after the measurements on boron trifluoride; these liquids were chosen because of their low water content, and were of Analar quality. From

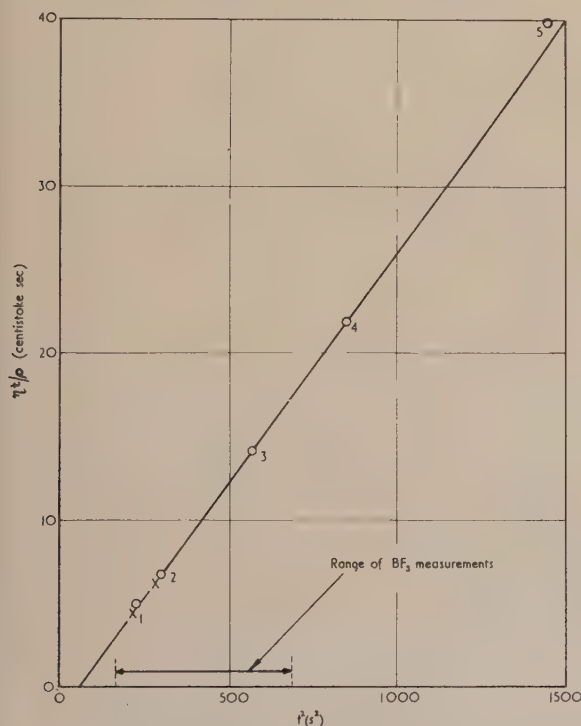


Fig. 2. Calibration of viscometer

× = calibration before boron trifluoride measurements.
○ = calibration after boron trifluoride measurements.

- (1) = ether.
- (2) = chloroform.
- (3) = carbon tetrachloride.
- (4) = benzene.
- (5) = water.

the calibration values shown in Fig. 2 the equation of the viscometer was determined to be:

$$\eta/\rho = 0.0275t - 1.6/t \text{ centistokes,}$$

where η is the viscosity in centipoises, ρ is the density in g/cm^3 , and t is the observed time in seconds. The first term represents the normal Poiseuille equation and the second is a correction term for the entry and exit losses.

The viscometer was constructed from Pyrex chemical glassware, of which the temperature coefficient of expansion, as measured by Buffington and Latimer,⁽⁵⁾ is 3.7×10^{-6} at 34°C decreasing to 1.7×10^{-6} at -152°C . Over the temperature range used it was therefore assumed that the constants of the viscometer varied by less than 0.1%, and no correction was made.

In preliminary measurements on boron trifluoride it was found that a thin solid film of boric acid was left at the bottom of the viscometer on evaporating the liquid, and that this went into solution on refilling the viscometer. Measurements were made after a considerable amount of this impurity had been allowed to accumulate. Compared with the results in Fig. 3, this impure liquid had a kinematic viscosity 14% higher. Before the final measurements were made, therefore, the apparatus was carefully cleaned.

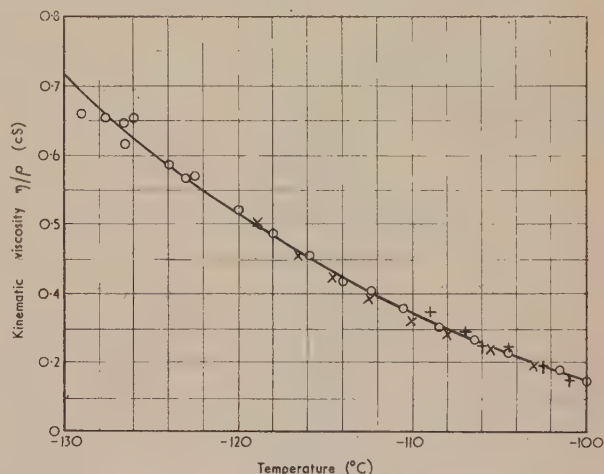


Fig. 3. Viscosity of liquid boron trifluoride

The values of kinematic viscosity of liquid boron trifluoride given in Fig. 3 are the results of three runs starting at different temperatures. It is considered that the amount of boric acid present at the end of these three runs would not have a measurable effect on the viscosity; the agreement between the runs indicates that there was no progressive contamination of the liquid.

The entry and exit loss is 9% of the Poiseuille term at the lower end of the temperature range, while at the higher end this fraction increases to 43%. These values are high for a precise measurement of viscosity, but were unavoidable in that the viscosity was predicted before the experiment to be not less than 0.5 cS. A capillary tube of less than 0.2 mm diameter would have been required to reduce the entry and exit losses to less than 1% of the Poiseuille term, but shortage of time did not allow the apparatus to be reconstructed. The accuracy of the measurements therefore depended on the accuracy of comparison with the calibrating liquids. Most, but not the whole, of the range could be covered by liquids which were readily available. For viscosities greater than 0.34 cS, the lowest viscosity of the calibrating liquids, it is

estimated that the accuracy of the viscosity measurements is $\pm 5\%$. For viscosities less than 0.34 cS, less reliance can be placed on the measured viscosities because of uncertainties in the validity of the viscometer equation. This becomes particularly important, as the Reynolds number for flow through the viscometer varies approximately inversely with the square of the viscosity. At the lowest measured viscosity of 0.28 cS, it is estimated that the entry and exit loss could be 30% greater than that indicated by the standard viscometer equation. It is therefore possible that the quoted viscosity at 100°C is too high and might be as low as 0.24 cS.

Thermal Conductivity

The conductivity cell constructed was of the coaxial cylinder type with radial heat flow, and closely resembled a cell used by Baxter, Vodden and Davies⁽⁶⁾ for liquids at ambient temperature and above. It consisted of two copper tubes mounted coaxially by means of Tufnol end-pieces, as shown in Fig. 4. The tubes and end-pieces were accurately machined

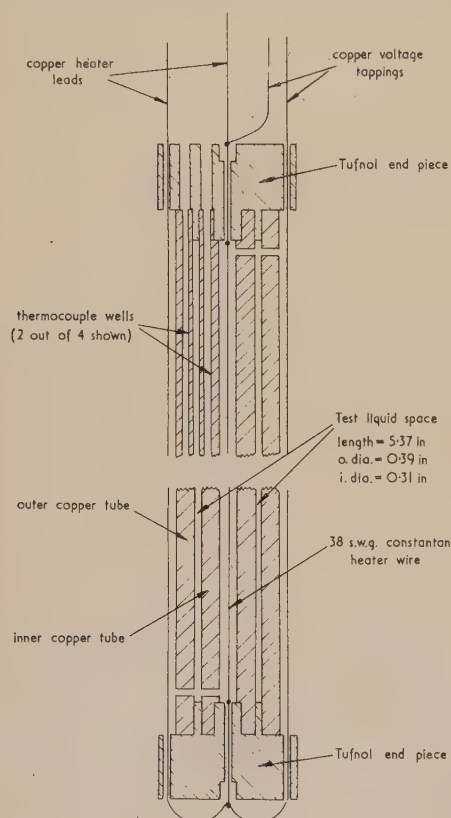


Fig. 4. Details of thermal conductivity cell

to ensure a high degree of uniformity of the thin annulus between the tubes. The tube walls had fine longitudinal holes housing 32 s.w.g. copper-constantan thermocouples. One pair was used differentially to measure the temperature difference across the liquid in the annulus, and the other two junctions, one in each tube, to measure the mean temperature. A heater wire located inside the inner tube was made of bare 38 s.w.g. constantan stretched taut along the axis, and had a resistance of $4.3\ \Omega$. It extended only over the length of the annulus, being soldered at each end to 38 s.w.g. copper leads. These leads passed through holes in the Tufnol end-pieces and were cemented into them. Just outside the end-

pieces, copper wires were soldered on to these current leads and served as tappings for measuring the voltage across the heater. The measured voltage was slightly in excess of the heater voltage, but the resulting inaccuracy in the measured conductivities (about 0.5%) was small compared with other inaccuracies and was neglected. Fine radial holes through the two tubes allowed the liquid easy access into the annulus and into the inside of the inner tube.

To enable the cell to be used at low temperatures it was contained in a double-walled glass vessel, shown in Fig. 5.

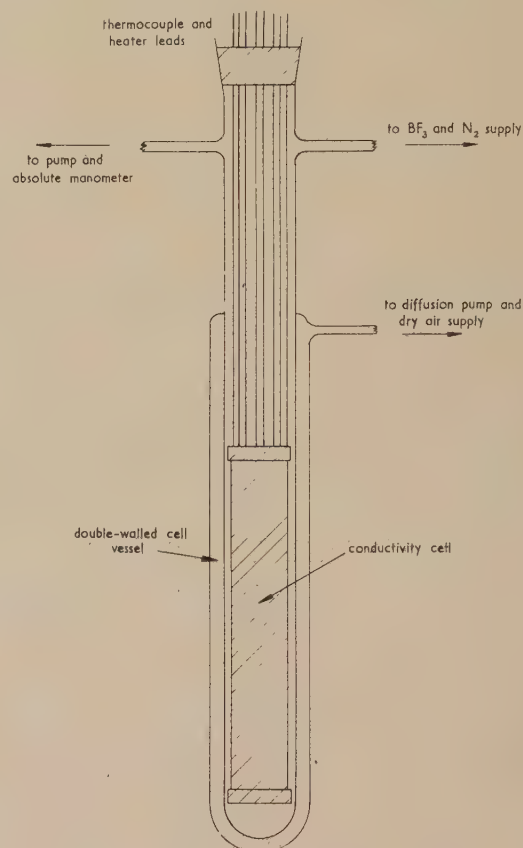


Fig. 5. The thermal conductivity apparatus

Both surfaces of the jacket between the two walls were silvered. The vessel was surrounded by liquid nitrogen in a large Dewar flask, and the various thermocouple and heater wires were taken out through a vacuum-tight seal. To condense boron trifluoride into the apparatus, the liquid-nitrogen level was raised above the double-walled jacket and boron trifluoride gas was fed into the cell. When the cell was completely immersed in liquid boron trifluoride, the liquid-nitrogen level was lowered to below the top of the jacket. The temperature could be controlled in the liquid range by maintaining a low enough pressure of dry air in the jacket for the heat supplied by the cell heater to balance the cooling effect of the liquid nitrogen bath; by varying the current and pressure it was possible to obtain steady temperatures over the whole range. Throughout the measurements dry, oxygen-free nitrogen was used to maintain a pressure of approximately atmospheric above the liquid boron trifluoride, which kept it from boiling.

The heater current was supplied by an accumulator; it was measured with a sub-standard ammeter, and the voltage drop across the heater was measured with a Unipivot volt-

meter. A potentiometer reading to 0.001 mV was used to measure the thermal e.m.f. of the differential thermocouple, which had been checked for absence of zero error before installation. The two absolute thermocouples were calibrated to measure the mean temperature to about 1° C. The measurements on boron trifluoride were made with heater currents from 0.40 to 0.94 A (corresponding with powers of 0.7–3.8 W and thermal e.m.f.'s of about 0.02–0.12 mV). Five samples were used in the course of the measurements; that is, five separate batches of boron trifluoride were condensed into the cell, but all were obtained from the same cylinder.

Results and discussion. It can be shown that, because of the high conductivity of copper, the temperature differential measured between the two tube walls can be taken as giving the temperature difference between the liquid surfaces. For the particular cell dimensions used, the usual equation for conduction through an annulus gives the conductivity as

$$k = \frac{W}{\Delta E} \cdot \frac{dE}{dT} \cdot 64.0 \times 10^{-5} \text{ cal cm}^{-1} \text{ s}^{-1} \text{ deg}^{-1} \text{ C},$$

where W is the heater power in watts, ΔE the thermal e.m.f. of the differential thermocouple in millivolts, and dE/dT the thermoelectric power at the mean temperature in mV/deg C.

Measurements on air, organic liquids and hydrogen

Fluid	Conductivity ($\text{cal cm}^{-1} \text{ s}^{-1} \text{ deg C}^{-1} \times 10^{-5}$)	Temperature (° C)	Source (reference)
Air	6.8	56	(9)
	Uncorr. 11.0	56	Authors
	6.5	39	(9)
	Uncorr. 10.7	39	Authors
Carbon tetra- chloride	24.8	20	(10)
	25.2	30	(6)
	24.5	39.5	(6)
	24.6	20	(11)
	23.8	40	(11)
	25.6	20	(12)
	24.9	40	(12)
	25.0	23	Authors
	25.1	33	Authors
Liquid paraffin	23.4	40	Authors
	29.9	25	(13)
	30.6	32.5	(6)
	30.2	25	(12)
Ethyl ether	29.7	20–30	Authors
	32.9	30	(14)
	31.1	20	(10)
	30.7	20	(11)
Hydrogen	31.2	25	Authors
	14.6	–182	(9)
	14.7	–182	Authors
	15.5	–176	(9)
	15.5	–176	Authors
	16.5	–169	(9)
	16.8	–169	Authors
	17.7	–161	(9)
	18.0	–161	Authors
	21.4	–137	(9)
	21.2	–137	Authors
	44.9	+40.5	(9)
	46.9	+40.5	Authors

Published tables⁽⁷⁾ were used for finding the mean temperature from the thermocouple readings, and the thermoelectric power.

It is assumed that convection is suppressed. This is true if the product of the Grashof and Prandtl numbers is less than 1000⁽⁸⁾; here, for boron trifluoride, where the maximum temperature difference employed was 4.3° C, this product did not exceed 4.6.

Some end losses will occur, and if it is assumed that they are proportional to the temperature difference, then W in the above equation must be replaced by $(W - B \Delta T)$, with the result that the true conductivity is the measured conductivity less a constant.

This end-loss correction was found by comparing the conductivity measured with the cell for air against the known value. Using air gives a large percentage correction which is easily observed, but gives some inaccuracy in the correction because a small fraction of the transfer is by radiation. The resulting inaccuracy in measured conductivities, however, is well within the overall accuracy of the method. As a check, measurements were also made, before and after measurements on boron trifluoride, on some organic liquids previously measured by other workers, namely liquid paraffin, carbon tetrachloride and ethyl ether. Finally, as a check at low temperatures, the apparatus was used to measure hydrogen at low temperatures; this was chosen because data on suitable liquids were not available and hydrogen, unlike most gases, has a high conductivity comparable with that of liquids. The results of these measurements are shown in the table. The end correction determined is $4.2 \times 10^{-5} \text{ cal cm}^{-1} \text{ s}^{-1} \text{ deg}^{-1} \text{ C}$; in the case of boron trifluoride this represents a correction of 8.5%.

Results for boron trifluoride are shown graphically in Fig. 6. There is a fairly large scatter, but no systematic

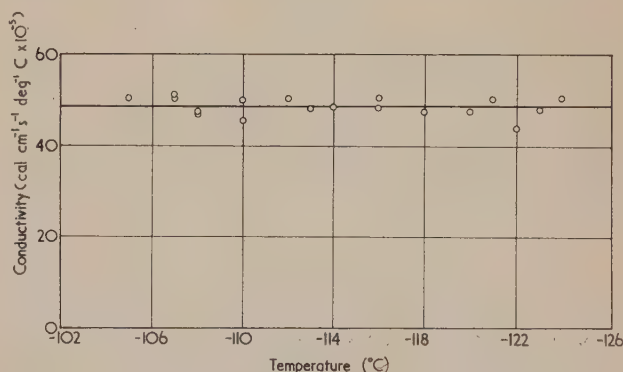


Fig. 6. The conductivity of boron trifluoride

dependence on the temperature difference employed (which confirms the absence of convection) or on the sample, which suggests that boric acid was not formed sufficiently to affect the results appreciably. The temperature range covered is small, and any temperature-dependence of the conductivity is small enough to be masked by the scatter. This is not surprising because most liquids vary only slightly in conductivity with temperature.

The conductivity can be taken as constant within the accuracy of the experiment. The mean of all the results is $48.6 \times 10^{-5} \text{ cal cm}^{-1} \text{ s}^{-1} \text{ deg}^{-1} \text{ C}$; the r.m.s. deviation about this value is $1.9 \times 10^{-5} \text{ cal cm}^{-1} \text{ s}^{-1} \text{ deg}^{-1} \text{ C}$. This scatter largely arises because the temperature was not absolutely steady while readings were taken. The satisfactory results obtained with the check substances indicate that any

systematic errors are small, and it is estimated that the value obtained is accurate to $\pm 5\%$.

Acknowledgements

This paper is published by permission of Sir William Cook, Managing Director, and Dr. H. Kronberger, Director of Research and Development, of the United Kingdom Atomic Energy Authority (Development and Engineering Group).

References

- (1) FARADAY, M. *Phil. Trans.*, **135**, p. 155 (1845).
- (2) LEBOUCHER, L., FISCHER, W., and BILTZ, W. *Z. Anorg. Chem.*, **207**, p. 61 (1932).
- (3) POHLAND, E., and HARLOS, W. *Z. Anorg. Chem.*, **207**, p. 242 (1932).
- (4) KAYE, G. W. C., and LABY, T. H. *Tables of Physical and Chemical Constants*, 11th ed. (London: Longmans, Green and Co., 1956).

- (5) BUFFINGTON, R. M., and LATIMER, W. M. *J. Amer. Chem. Soc.*, **48**, p. 2305 (1926).
- (6) BAXTER, S., VODDEN, H. A., and DAVIES, S. *J. Appl. Chem.*, **3**, p. 977 (1953).
- (7) SHENKER, H., and others. *Circ. Nat. Bur. Stand.*, No. 561 (1955).
- (8) FISHENDEN, M., and SAUNDERS, O. A. *An Introduction to Heat Transfer* (London: Oxford University Press, 1950).
- (9) HILSENATH, J., and others. *Circ. Nat. Bur. Stand.*, No. 564 (1955).
- (10) RIEDEL, L. *Chem.-Ingen.-Tech.*, **23**, p. 321 (1951).
- (11) MASON, H. L. *Trans Amer. Soc. Mech. Engrs*, **76**, p. 817 (1954).
- (12) CHALLONER, A. R., and POWELL, R. W. *Proc. Roy. Soc. A*, **238**, p. 90 (1956).
- (13) KAYE, G. W. C., and HIGGINS, W. F. *Proc. Roy. Soc. A*, **117**, p. 459 (1928).
- (14) BRIDGMAN, P. W. *Proc. Amer. Acad. Arts Sci.*, **59**, p. 141 (1923).

Absolute intensity measurements of the carbon and aluminium X-ray K-lines with a proportional counter

by R. M. DOLBY, B.S., Cavendish Laboratory, Cambridge

[Paper first received 25 May, and in final form 7 August, 1959]

Abstract

The efficiencies (quanta per electron per unit solid angle) of thick target carbon and aluminium X-ray K-line production, as a function of accelerating voltage, have been measured and plotted in the region below 10 kV. The construction and performance of the proportional counter with which the measurements were made is also described.

Introduction

A SMALL gas-flow proportional counter has been designed for detection of the characteristic radiations from light elements in connection with X-ray emission microanalysis.⁽¹⁻³⁾ The counter has first been employed in quantitative determinations of the aluminium (8.34 Å) and carbon (44 Å) K-emission efficiencies and their dependence on accelerating voltage.

Apparatus

A single lens (Fig. 1) focuses the exciting electron beam into a spot diameter 1 mm or less, the beam entering the specimen normally. X-rays may be collected by the counter within a solid angle as large as 0.71 steradian, but for the intensity experiments an angle of 0.47 steradian was used, i.e. a cone of semi-angle 22°, with axis inclined at 33° to the specimen surface in the backward direction (thick target conditions). The window, $\frac{3}{8}$ in. diameter Melinex, 6 μ thick, is coated with a 200 Å evaporated layer of aluminium on the inner surface. The counter itself is fabricated from brass, the cathode length being 1.9 in., with an inside diameter of

0.52 in. The cathode operates at negative h.t., and the anode wire, 0.0025 in. molybdenum-tungsten, is nominally at earth potential. This arrangement, together with an earthed guarding outer shield, eliminates leakage pulse problems. Argon plus 2.5% carbon dioxide flows at atmospheric pressure through the counter. The whole assembly, although situated

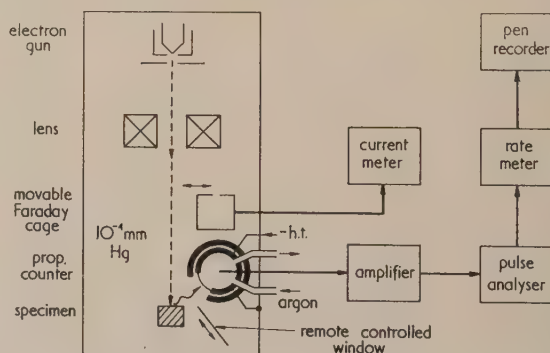


Fig. 1. Block diagram of apparatus used for absolute intensity measurements of carbon and aluminium X-ray K-lines

inside the specimen chamber, is moderately vacuum tight, and the apparatus can be operated with little difficulty at a pressure of 10^{-4} mm of mercury.

The overall counter efficiency is limited chiefly by the window transmission characteristics. For 6 μ thickness, the calculated transmission of Melinex (based on μ/ρ values from

Henke, White and Lundberg⁽⁴⁾) is 0.3% at 60 Å, rising to 7% at 44 Å, then dropping to "zero" at the carbon absorption edge. For the nitrogen and oxygen K-wavelengths (31.6 Å and 23.7 Å) the transmission is also "zero", but useful transmissions are reached for sodium, magnesium, and aluminium, the aluminium K_{α} transmission (8.34 Å) being 47%.

The transmission of the counter window at the carbon K and aluminium K wavelengths has been measured using a remote-controlled window, identical with that in the counter, which can be placed in the X-ray path between the specimen and counter. With a pulse-height analyser centred on the appropriate pulse-height distribution peaks, the measured transmissions were: carbon $K_{\alpha,\beta}$, 0.10 ± 0.005 , using accelerating voltages $V_0 = 1, 3$, and 10 kV; aluminium $K_{\alpha,\beta}$, 0.54 ± 0.03 , using $V_0 = 3$ kV. Once the X-rays have entered the counter, the efficiency of detection is 93% for aluminium K_{α} and 100% for carbon K_{α} , 50% of the absorption in the latter case occurring in the first 100 microns.

The production of 10 V pulses from carbon K quanta, using $0.4 \mu\text{s}$ differentiating and integrating time constants and an electronic gain of 400 000, required a calculated gas gain of 2500, which was obtained with a 1740 V counter potential. Under these conditions each voltage pulse (step) from the counter was about $100 \mu\text{V}$ (across 40 pF).

Fig. 2 shows typical pulse-height distributions obtained with the beam voltage and incident current held constant

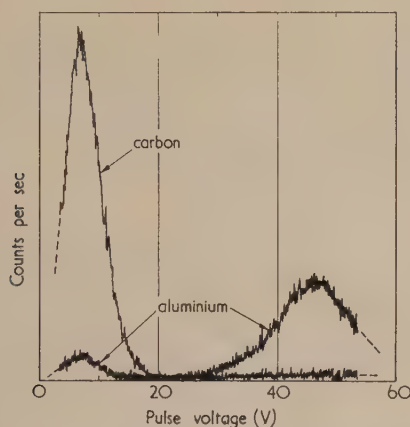


Fig. 2. Carbon K and aluminium K pulse height distributions. $V_0 = 3$ kV; same incident current for both specimens

for both the carbon and aluminium specimens, the curves being scanned automatically by a pulse-height analyser and pen recorder. The low energy peak on the aluminium curve is thought to be due to continuous radiation lying in the window transmission band, carbon K window fluorescence, and carbonaceous contamination of the aluminium specimen.

Representing averaged values from several pen recorder pulse-height distributions (characteristic plus continuous), the observed standard deviations were: carbon $K_{\alpha,\beta}$, 45%; aluminium $K_{\alpha,\beta}$, 17%. No special attempt towards obtaining higher energy resolution has been made.

Intensity measurements

The K efficiency data of Fig. 3 were obtained by measuring the incident current with a Faraday cage and vibrating-reed electrometer, and then observing the resulting counting rate in the K pulse height distribution. The settings or measurements of geometry, current, and count rate were repeated

three to six times for each point on the graph, using the same solid angle but widely differing currents (and count rates). Almost all the measurements were made in the ranges from 10^{-11} to 10^{-9} A and 1000–10 000 pulses per second. Typically, at 1 kV a carbon K count rate of 10 000 pulses/s was obtained with a current of about 2×10^{-9} A. For aluminium at 5 kV, 10 000 pulses/s were obtained with about 10^{-10} A.

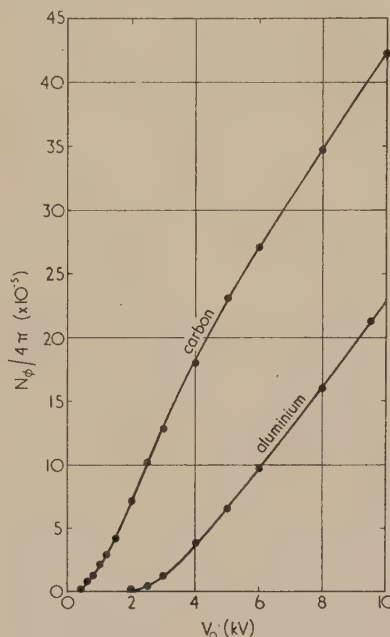


Fig. 3. Thick target $K_{\alpha,\beta}$ efficiency, $N_{\phi}/4\pi$, quanta per electron per unit solid angle, as a function of accelerating voltage V_0

Corrections and errors

Several correction factors were applied to the observed intensities. For carbon: continuous radiation, unrecorded quanta in the low energy tail of the pulse height distribution (see Fig. 2), ratemeter dead-time, window transmission, and specimen surface condition. For aluminium: continuous radiation, ratemeter dead-time, window transmission, and proportional counter quantum efficiency.

The continuous radiation correction for carbon was accomplished by measuring the continuous spectrum in the region of 1.5 keV, excited at $V_0 = 4$ kV and 8 kV. From these data the continuous quantum intensity per energy interval and the resulting pulse height distribution in the region of the carbon line were computed for each accelerating voltage, the results being subtracted from the observed total pulse-height distribution. Because of the monochromatizing effect of the counter window, the continuous corrections were only about 0.7% for $V_0 = 10$ kV and 1% for $V_0 = 1$ kV.

The continuous measurements on aluminium were made at 4 keV, with $V_0 = 9$ and 8 kV, and at 3 keV, with $V_0 = 4$ kV. A procedure similar to that with carbon indicated a continuous correction of about 10% for $V_0 = 9.5$ kV and 25% for $V_0 = 3$ kV.

The specimens themselves were pure carbon and aluminium well within the accuracy limits of the experiment. Slices of evaporator rods were used in the carbon intensity tests. They could not be highly polished because of their porous structure, about one third of the surface being covered by

pits several microns deep, with irregularities over the rest of the surface of about 1μ . An extremely rough (filed) specimen showed 93% output compared with a polished specimen.

In a later experiment a Premier Type I diamond with a highly polished surface was used as the target, its output being compared with that of the carbon specimen used in the K intensity determinations. The diamond was coated with about 150 \AA of aluminium as a precaution against undesirable surface charging effects, the carbon specimen also being coated (for this experiment only) to insure equal intensity comparison conditions. The diamond exhibited 43% greater K output than the carbon specimen, with intensity comparisons being made at $V_0 = 8$ and 2.5 kV . The lower voltage readings were difficult, however, owing to the effect of the aluminium film on the absorption of electrons and the production of aluminium K quanta. The factor of 43%, presumed to be due only to the smoothness of the diamond surface, is in agreement with optical microscope comparisons of the roughnesses of the two surfaces. The carbon K efficiencies of Fig. 3 include the surface condition correction.

No surface condition correction was made for the aluminium specimen, but there were few irregularities greater than a micron or two in extent. In view of aluminium's relatively low self-absorption of its own radiation (a thickness of 8μ transmits 50%), it seems unlikely that the surface condition error would be more than a few per cent.

No corrections were made for spurious effects due to back-scattered electrons. However, carbon K emission (of the Melinex window) due to backscattered electrons does not seem to be a problem, since:

- (a) the carbon specimen has a low backscattering coefficient;
- (b) only a small proportion of backscattered electrons have energies sufficiently high for carbon K excitation;
- (c) 1740 eV is subtracted from backscattered electron energy owing to the negative proportional counter potential appearing on the electrically conducting window.

Therefore, since there is no possibility for carbon K window emission below $V_0 \approx 2\text{ kV}$, and since the effect is reduced by the above factors for higher voltages, errors due to emission caused by backscattered electrons can be neglected.

In connection with backscattered electrons, it is clear from the curves of Lane and Zaffarano⁽⁵⁾ that it is not possible for electrons arising from a 10 kV primary beam to penetrate the 6μ Melinex window and enter the proportional counter. The pulse height distributions also showed no evidence for such an effect.

No correction was made for the window fluorescence contribution to the observed carbon K intensity, but a calculation shows that this effect should be substantially less than 1% for the voltage range under consideration.

Because of the combined effects of electron range and self-absorption of X-rays in a target, the measured intensity at a given voltage is dependent on the specimen-counter angle, especially for small angles and high voltages. The carbon curve above 3 kV should therefore be regarded with reserve, its shape probably being, in some degree, a specific result of the specimen-counter configuration previously described.

Systematic errors in the measuring and analysis process have been estimated. If it can be assumed that errors from the eleven sources which were taken into account will have random signs, then the standard deviation of the efficiency

values may be taken as about 10% for both the carbon and aluminium curves.

Comparisons with theory

The intensities in Fig. 3 have been plotted against V_0 instead of the usual quantity V_0/V_k (in which V_k is the appropriate K excitation voltage), this presentation clearly showing that for practical purposes carbon has a higher quantum efficiency than aluminium. If the intensities were plotted against V_0/V_k the carbon efficiency would appear to be lower, in accordance with the usual interpretation of carbon's lower fluorescence yield.⁽⁶⁾

The only theoretical treatments of characteristic X-ray emission with which these results may be compared on an absolute basis are those of Worthington and Tomlin⁽⁷⁾ and Archard.⁽⁸⁾ For aluminium the experimentally obtained efficiency at 5 kV , for example, is about twice as great as that predicted by Archard, but only one-fourth as great as the theoretical value of Worthington and Tomlin. For carbon the experimental efficiency at 2 kV is about seven times that predicted by Archard. All the carbon values are considerably higher than had been supposed, the observed intensities indicating, for example, that a total of about $8 \times 10^8\text{ K quanta/sec}/\mu\text{A}$ emerge from a thick carbon target using an accelerating voltage of 1 kV .

Worthington and Tomlin also give theoretical efficiencies for copper. It is interesting to note that the value for copper at 20 kV is the same as the experimental value for aluminium at only 5.7 kV and for carbon at only 2.3 kV . The observed high X-ray intensities of the lighter elements at low voltages are hence very encouraging for the extension of X-ray emission microanalysis into this region.

Acknowledgements

The author is indebted to Dr. V. E. Cosslett, under whom the investigations have been made, for helpful advice and suggestions, and to the Marshall Aid Commemorative Commission for financial assistance.

References

- (1) MULVEY, T., and CAMPBELL, A. J. *Brit. J. Appl. Phys.*, **9**, p. 406 (1958).
- (2) COSSLETT, V. E., and DUNCUMB, P. *Nature (London)*, **177**, p. 1172 (1956).
- (3) DOLBY, R. M. *Proc. Phys. Soc. (London)*, **73**, p. 81 (1959).
- (4) HENKE, B. L., WHITE, R., and LUNDBERG, B. *J. Appl. Phys.*, **28**, p. 98 (1957).
- (5) LANE, R. O., and ZAFFARANO, D. J. *Phys. Rev.*, **94**, p. 960 (1954).
- (6) COMPTON, A. H., and ALLISON, S. K. *X-rays in Theory and Experiment*, 2nd ed., p. 477 et seq. (New York: D. Van Nostrand, 1935).
- (7) WORTHINGTON, C. R., and TOMLIN, S. G. *Proc. Phys. Soc. A*, **69**, p. 401 (1956).
- (8) ARCHARD, G. D. *Proceedings of the Second Symposium on X-ray Microscopy and X-ray Microanalysis* (Amsterdam: Elsevier; in the press).

Investigation into one of the assumptions of the Hertz theory of contact

by C. STOREY, Constructors John Brown Limited, Research and Development Station, Leatherhead, Surrey

[Paper received 30 July, 1959]

Abstract

One of the limitations of Hertz's solution⁽¹⁾ of the contact problem is the assumption that, in the neighbourhood of contact, the surfaces of the bodies and, hence, the distance between their corresponding points can be represented by second degree equations. Subsequent theoretical work, mainly by I. Ya. Shtaerman,⁽²⁾ has provided a more general solution free from this limitation. It is the purpose of the present work to examine the effect of the inclusion of terms of higher degree than the second in the expression for the distance between the two bodies. Attention is confined to spheres and cylinders.

Introduction

IN the well-known theory of elastic contact proposed by Hertz⁽¹⁾ in his work of 1886, one of the assumptions made is that the distance $d(x, y)$ between points of the two bodies, measured normally to the common tangent plane before external pressure is applied, can be approximated by a quadratic form. This assumption is untenable in certain cases, as, for example, when the second derivatives of $d(x, y)$ vanish or are discontinuous at the origin.

The rather restrictive limitations imposed by the Hertzian theory were relaxed by the Russian mathematician I. Ya. Shtaerman⁽²⁾ in a series of papers written about 1940. In one of these papers, a solution of the contact problem in its most general form is given and the Hertz solution is deduced as a special case. For solids of revolution and cylinders (the plane problem) the rather complex fundamental integral equation of the general solution becomes considerably simplified and Shtaerman examines in detail this simplified equation for various different types of distance function. He also gives a method for solving the equation for a general distance function provided the fact that the pressure distribution is bounded at the limits of the contact surface is taken into account.

The purpose of the present work is to adapt some of these results to show, in the case of spheres and cylinders, how the neglect of terms of higher order than the second in the expansion of $d(x, y)$ affects the contact dimensions and the pressure distribution.

Theory

On making the same assumption as Hertz, with the exception of allowing a general distance function, Shtaerman's integral equations are found to give:

$$(\theta_1 + \theta_2) \int_0^{2\pi} \int_0^a p(r') \left(\frac{1}{r'} - \frac{1}{\sqrt{r'^2 - 2rr' \cos \phi + r^2}} \right) r' dr' d\phi = d(r) \quad (r \leq a) \quad (1)$$

$$2\pi \int_0^a p(r') r' dr' = P \quad (2)$$

in the case of bodies with axial symmetry, and:

$$2(\theta_1 + \theta_2) \int_a^b p(x') \log \left| \frac{x - x'}{x'} \right| dx' = d(x) \quad (-a \leq x \leq b) \quad (3)$$

$$\int_{-a}^b p(x') dx' = P \quad (4)$$

in the case of plane contact.

In these equations, a is the radius of contact in the first case and $(a \neq b)$ the contact width in the second, P is the total pressure between the bodies, p is the pressure distribution in the contact area, and $\theta = (1 - \sigma^2)/E$, where σ and E are Poisson's ratio and Young's modulus respectively.

It is now supposed that the bodies consist of a sphere of radius R_1 , resting in a similar sphere of radius R_2 . The first two terms in the series expansion of $d(r)$ are found to be

$$d(r) = \frac{1}{2} \left(\frac{1}{R_1} - \frac{1}{R_2} \right) + \frac{1}{8} \left(\frac{1}{R_1^3} - \frac{1}{R_2^3} \right) r^2 \quad (5)$$

If the solutions of equations (1) and (2) are denoted by $p_1(r')$ and a_1 when the first term only of equation (5) is taken into account, and by $p_2(r')$ and a_2 when both terms are taken into account, it can be verified by direct substitution that:

$$p_1(r') = \frac{2a_1}{\pi^2(\theta_1 + \theta_2)} \left(\frac{1}{R_1} - \frac{1}{R_2} \right) \left(1 - \frac{r'^2}{a_1^2} \right)^{1/2} \quad (6)$$

$$p_2(r') = \frac{2a_2}{\pi^2(\theta_1 + \theta_2)} \left(\frac{1}{R_1} - \frac{1}{R_2} \right) \left(1 - \frac{r'^2}{a_2^2} \right)^{1/2} \left\{ 1 + \frac{2a_2^2}{9} \left(\frac{1}{R_1^2} + \frac{1}{R_1 R_2} + \frac{1}{R_2^2} \right) \left(1 + \frac{2r'^2}{a_2^2} \right) \right\} \quad (7)$$

By substitution into equation (4), the radii of the contact circles in the two cases are given by:

$$\frac{4}{3} a_1^3 \left(\frac{1}{R_1} - \frac{1}{R_2} \right) = P\pi(\theta_1 + \theta_2) \quad (8)$$

$$\frac{8a_2^5}{15} \left(\frac{1}{R_1^3} - \frac{1}{R_2^3} \right) + \frac{4a_2^3}{3} \left(\frac{1}{R_1} - \frac{1}{R_2} \right) = P\pi(\theta_1 + \theta_2) \quad (9)$$

From equations (6) and (7), the maximum values of the pressure distribution are seen to be:

$$p_{1max} = \frac{2a_1}{\pi^2(\theta_1 + \theta_2)} \left(\frac{1}{R_1} - \frac{1}{R_2} \right) \quad (10)$$

$$p_{2max} = \frac{2a_2}{\pi^2(\theta_1 + \theta_2)} \left(\frac{1}{R_1} - \frac{1}{R_2} \right) \left\{ 1 + \frac{2a_2^2}{9} \left(\frac{1}{R_1^2} + \frac{1}{R_1 R_2} + \frac{1}{R_2^2} \right) \right\} \quad (11)$$

If now R_2 is written kR_1 where $\infty \geq k > 1$, and equations (8) and (9) are combined, then:

$$\frac{2(k^2 + k + 1)}{8k^2} \left(\frac{a_2}{R_1}\right)^5 + \left(\frac{a_2}{R_1}\right)^3 = \left(\frac{a_1}{R_1}\right)^3 \quad (12)$$

and in a similar manner by combination of equations (10) and (11):

$$\frac{p_{2\max}}{p_{1\max}} = \frac{a_2/R_1}{a_1/R_1} \left\{ 1 + \frac{2(k^2 + k + 1)}{9k^2} \left(\frac{a_2}{R_1}\right)^2 \right\} \quad (13)$$

Without details, the corresponding results for one cylinder inside another are:

$$\frac{3(k^2 + k + 1)}{8k^2} \left(\frac{a_2}{R_1}\right)^4 + \left(\frac{a_2}{R_1}\right)^2 = \left(\frac{a_1}{R_1}\right)^2 \quad (14)$$

and:

$$\frac{p_{2\max}}{p_{1\max}} = \frac{a_2/R_1}{a_1/R_1} \left\{ 1 + \frac{(k^2 + k + 1)}{4k^2} \left(\frac{a_2}{R_1}\right)^2 \right\} \quad (15)$$

Numerical results

Calculations have been carried out for values of a_1/R_1 from 0.2 by 0.2 to 1.0 and for two values of k , 1.05 and infinity. Table 1 shows the results for spheres and Table 2 the results for cylinders.

From an examination of these tables it is seen that the effect increases as a_1/R_1 increases, and as k decreases, that is, when the dimensions of the contact area are comparable with the radii of the bodies, and when the bodies have equal and opposite curvature. Finally, in order to see if the effect is appreciable in practice, a few typical values of a_1/R_1 are calculated. For example, in order to give an a_1/R_1 of 0.2, a one-inch sphere would need a value of P equal to 2.59×10^3 lb for $k = 1.05$, and 5.43×10^4 lb for $k = \infty$; or for a cylinder of 30 inches diameter, P would have to be 1.51×10^7 lb for $k = \infty$.

At the other end of the scale, the tip of a gramophone stylus with a radius of 0.001 in. say, would need a P of 2.6×10^{-3} lb for $k = 1.05$ and 5.4×10^{-2} lb for $k = \infty$

to give a_1/R_1 equal to 0.2. Thus it is seen that the effects discussed are unlikely to be appreciable in practical cases.

Table 1. Spheres

		a_1/R_1				
		0.2	0.4	0.6	0.8	1.0
a_2/R_1	$\left\{ \begin{array}{l} (k = \infty) \\ (k = 1.05) \end{array} \right.$	0.199	0.396	0.575	0.746	0.908
		0.197	0.381	0.546	0.681	0.825
$p_{2\max}/p_{1\max}$	$\left\{ \begin{array}{l} (k = \infty) \\ (k = 1.05) \end{array} \right.$	1.004	1.025	1.029	1.048	1.074
		1.009	1.040	1.082	1.102	1.182

Table 2. Cylinders

		a_1/R_1				
		0.2	0.4	0.6	0.8	1.0
a_2/R_1	$\left\{ \begin{array}{l} (k = \infty) \\ (k = 1.05) \end{array} \right.$	0.199	0.389	0.567	0.730	0.880
		0.196	0.373	0.527	0.660	0.779
$p_{2\max}/p_{1\max}$	$\left\{ \begin{array}{l} (k = \infty) \\ (k = 1.05) \end{array} \right.$	1.009	1.010	1.021	1.035	1.051
		1.009	1.025	1.052	1.082	1.116

Acknowledgements

Part of this work was carried out when the author was with British Railways Research Department, Derby, and thanks are due to the Director of Research, Mr. T. M. Herbert, for permission to publish this part.

The paper was concluded at the Research and Development Station of Constructors John Brown Limited, Leatherhead, and the Directors' permission to publish the remainder of the work is acknowledged.

References

- (1) HERTZ, H. *Misc. Papers* (Translated by Jones and Schott), p. 146 (London: Macmillan, 1896).
- (2) SHTAERMAN, I. YA. *Comptes Rendus De L'Académie des Sciences de L'U.R.S.S.*, XXV, No. 5 (1939); XXIX, No. 3 (1940); XXXI, No. 8 (1941); XXXVIII, No. 7 (1943).

Revised edition of Notes for authors

The Institute of Physics has recently published a 36-page revised edition of its booklet intended to assist less-experienced authors and to serve as a reference booklet for all those who wish to contribute to the Institute's publications. Under its new title *Notes for authors*, it gives hints on the preparation of scripts and diagrams, on the layout of mathematics, the correction of proofs and so on. In addition to a bibliography of reference books and works on technical writing, the pamphlet also contains lists of the spellings, symbols and abbreviations used by the Institute. These conform with British Standard 1991: Part I: 1954: *Letter symbols, signs and abbreviations, Part I, General* which authors of mathematical papers are also advised to consult.

Authors preparing contributions for submission to this *Journal* are invited to make use of the guidance available in the booklet, copies of which may be obtained from The Institute of Physics, price 3s. 6d. (including postage).

What is ferromagnetic resonance?

by R. A. WALDRON, M.A., A.Inst.P., Marconi's Wireless Telegraph Co. Ltd.,
Research Department, Great Baddow, Essex

[Paper first received 6 August, and in final form 8 October, 1959]

Abstract

It is pointed out that two distinct resonance effects take place in ferrite samples at microwave frequencies, ferromagnetic resonance and an effect due to the shape of the specimen. The latter effect is called Kittel resonance in this paper. It is commonly supposed that the two effects are the same, but it is shown that this is not the case. In ferromagnetic resonance, the diagonal and off-diagonal elements of the permeability tensor (μ and α respectively) exhibit anomalous dispersion, and microwave fields are excluded from the specimen. In Kittel resonance, nothing spectacular is happening to μ and α , but the fields in the specimen become very large, giving rise to a large loss; it is this effect that is observed in resonant cavity experiments. The behaviour of cavities and wave-guides containing ferrites is discussed in the light of these facts, and a new interpretation is arrived at of certain effects in wave-guides when $|\mu| < |\alpha|$.

1. Introduction

IT was shown by Polder⁽¹⁾ that when a ferrite is subjected to a (d.c.) polarizing field in the z -direction sufficiently strong to cause saturation, the induction b in the ferrite is related to the magnetic field h in the ferrite at microwave frequencies by

$$b = \mu_0 \begin{vmatrix} \mu & -j\alpha & 0 \\ j\alpha & \mu & 0 \\ 0 & 0 & 1 \end{vmatrix} h \quad (1)$$

Polder also showed that if M_s is the saturation magnetization in the z direction, and h_z the polarizing field in the specimen, the elements of the permeability tensor are

$$\mu = 1 + \frac{h_z M_s}{\mu_0(h_z^2 - H_r^2)}; \quad \alpha = \frac{H_r M_s}{\mu_0(h_z^2 - H_r^2)} \quad (2)$$

M_s is the quantity that many authors call $4\pi M_s$; it is convenient to adopt this notation, which avoids continual repetition of the factor 4π . It is assumed that H (d.c. or microwave) is the magnetic field in a region of free space with no ferrite present, and that on introducing ferrite the field in the ferrite due to H is h . In this paper, the d.c. magnetic field will be taken to be in the z direction, and the microwave magnetic field will always lie in the xy plane, except in Section 5, when a z component of microwave field may also be present. H_r is ω/γ , ω being the working frequency and γ the reciprocal of the gyromagnetic ratio. H_r is the value of H_z for which the frequency shift of a cavity is very large when the cavity contains a spherical sample;

for samples of this shape, it is the quantity which Kittel calls H_{eff} (that is, the effective value of H).

It is convenient to normalize h_z and M_s ; we write

$$p = \gamma M_s / \mu_0 \omega; \quad \sigma = \gamma h_z / \omega = h_z / H_r \quad (3)$$

Equations (2) can then be written:

$$\mu = 1 + \frac{p\sigma}{\sigma^2 - 1} = 1 + \sigma\alpha; \quad \alpha = \frac{p}{\sigma^2 - 1} \quad (4)$$

Rowen and von Aulock⁽²⁾ have related the induction b inside a ferrite sample to the microwave field H which exists in the absence of the sample by the external permeability tensor:

$$b = \mu_0 \begin{vmatrix} \eta & -j\kappa & 0 \\ j\kappa & \eta & 0 \\ 0 & 0 & 1 \end{vmatrix} H \quad (5)$$

Kittel^(3,4) gave, effectively, η as a function of H_z and M_s for various sample shapes.

It is apparent from equation (4) that when $\sigma = 1$, that is $h_z = H_r$, μ and α both become infinite. (This is in the lossless case, of course; in practice, their real parts become very large and change sign suddenly, while their imaginary parts go through maxima.) We shall define the condition $\sigma = 1$ as ferromagnetic resonance. It is also the case that, for some value of σ , depending on the shape of the specimen, η and κ become infinite; this condition will be called Kittel resonance. The two phenomena are quite different in nature, but confusion exists in the minds of some scientists working with ferrites in resonant cavities as to what they are observing when the absorption curve goes through a maximum (that is, the "Q" of the cavity goes through a minimum). One object of the present paper is to clarify this point. It is, in fact, in the Kittel condition that the absorption peak is observed; nothing spectacular happens at ferromagnetic resonance, as far as observations of the "Q" and the frequency of the cavity are concerned. This will be shown below as a consequence of certain mathematical results; Hogan⁽⁵⁾ has arrived at the same conclusions by different reasoning.

Several writers^(6,7) on the theory of wave-guides containing ferrites have confined themselves to the lossless case; for this reason they have avoided the region of ferromagnetic resonance ($\sigma = 1$) but have paid considerable attention to the neighbourhood of $\mu = 0$. It will be seen below that in fact the loss at ferromagnetic resonance is small, while the condition $\mu = 0$, in the case of a rod of circular cross-section, approximates to the Kittel resonance condition, where the losses are heavy. The author himself must also admit to having fallen into the trap.⁽⁸⁾

2. Some basic results

It will be necessary to refer to some basic results in the course of the discussion, and it is convenient to summarize them separately here. Polder's equations will be taken as approximations to the real parts of μ and α , and it is to be understood that the imaginary parts of μ and α become large when $\sigma = 1$.

2.1 *Frequency shifts of cavities containing ferrites.* Berk and Lengyel⁽⁹⁾ and the present author⁽¹⁰⁾ have shown that the frequency shift of a resonant cavity, on introducing a small ferrite sphere into a region of uniform magnetic field in the xy plane, is

$$\frac{\delta\omega}{\omega} \propto \frac{(\mu' - 1 \pm \alpha')V_1}{(\mu' + 2 \pm \alpha')V_0}, \quad (6)$$

where μ' and α' are the real parts of μ and α , and V_1 , V_0 are the volumes of sample and cavity respectively. The positive or negative signs are to be chosen according to the sense of circular polarization of the microwave field at the position of the ferrite. An analogous equation was first derived by Berk and Lengyel for the case of a rod of circular cross-section, with the polarizing field parallel to its axis. If the rod is taken to be the same length as the cavity, the volumes of cavity and specimen are in the same ratio as their cross-sectional areas, S_0 and S_1 , and the result may be written

$$\frac{\delta\omega}{\omega} \propto \frac{(\mu' - 1 \pm \alpha')S_1}{(\mu' + 1 \pm \alpha')S_0} \quad (7)$$

Again, the positive or negative signs are to be taken, depending on the sense of circular polarization. For a disk polarized normally to its plane, the formula^(11, 12) for the frequency shift is

$$\frac{\delta\omega}{\omega} \propto (\mu' - 1 \pm \alpha') \frac{V_1}{V_0}. \quad (8)$$

The absorption in the specimen is observed as a degrading of the "Q" of the empty cavity, Q_0 , to a value Q_1 for the cavity when the specimen is present. Writing $\mu = (\mu' - j\mu'')$, $\alpha = (\alpha' - j\alpha'')$, we have for a spherical sample,⁽¹⁰⁾

$$\frac{1}{Q_1} - \frac{1}{Q_0} \propto \frac{-6(\mu'' \pm \alpha'')}{(\mu' + 2 \pm \alpha')^2} \frac{V_1}{V_0}. \quad (9)$$

Similarly, for the rod sample,

$$\frac{1}{Q_1} - \frac{1}{Q_0} \propto \frac{-4(\mu'' \pm \alpha'')}{(\mu' + 1 \pm \alpha')^2} \frac{S_1}{S_0}. \quad (10)$$

For the disk sample,

$$\frac{1}{Q_1} - \frac{1}{Q_0} \propto -2(\mu'' \pm \alpha'') \frac{V_1}{V_0}. \quad (11)$$

In expressions (9), (10), and (11), the proportionality constants are the same as in expressions (6), (7), and (8), respectively. All these expressions depend on the assumption that $\mu'' \ll \mu'$ and $\alpha'' \ll \alpha'$, which will usually be the case, even close to ferromagnetic resonance.

2.2 *Magnetic fields in specimens.* As pointed out in Section 1, the microwave fields are considered to lie in the xy plane, so that in the following results the z components of field are all zero. For the x and y magnetic field components in a spherical specimen, we have^(9, 10)

$$\left. \begin{aligned} h_x &= 3 \left\{ \frac{(\mu + 2)H_x + j\alpha H_y}{(\mu + 2)^2 - \alpha^2} \right\} \\ h_y &= 3 \left\{ \frac{-j\alpha H_x + (\mu + 2)H_y}{(\mu + 2)^2 - \alpha^2} \right\} \end{aligned} \right\} \quad (12)$$

The fields in the rod-shaped specimen are^(9, 12, 13)

$$\left. \begin{aligned} h_x &= 2 \left\{ \frac{(\mu + 1)H_x + j\alpha H_y}{(\mu + 1)^2 - \alpha^2} \right\} \\ h_y &= 2 \left\{ \frac{-j\alpha H_x + (\mu + 1)H_y}{(\mu + 1)^2 - \alpha^2} \right\} \end{aligned} \right\} \quad (13)$$

For a disk-shaped specimen we have^(11, 13)

$$h_x = H_x, \quad h_y = H_y. \quad (14)$$

3. Ferromagnetic resonance

We have defined f.r. by the condition $\sigma = 1$, when, according to equations (4), μ and α become infinite. Let us now consider what happens in the ferrite in this condition, if a finite internal microwave field is maintained. Classically, the unpaired electrons that exist in the ferrite may be regarded as small magnetic dipoles; in the absence of a microwave field they line up, parallel to the d.c. polarizing field. If in some way the electrons are now disturbed from their equilibrium orientation, they will start to precess about this direction, like miniature gyroscopes. If the disturbance is due to a circularly polarized microwave magnetic field, not near the resonance frequency, the electrons precess with small amplitude, so that the axis of an electron describes a cone of small angle, the axis of the cone being defined by the polarizing field. Under these conditions, it is the microwave field that causes the precession. Because the precessional motion of the electrons is small, losses are small.

If the frequency of the microwave field is now made nearly equal to the value γh_z , h_z being the polarizing field internal to the specimen, the angle of the cone opens up and approaches 90 deg., provided that the microwave field is circularly polarized in the correct sense. The electron may now be thought of as polarized by the microwave field, being caused to precess by the couple due to h_z , instead of by the microwave field as in the non-resonant case; since the axis of the electron is now perpendicular to h_z and parallel to the microwave field, the couple due to the latter is zero, while that due to h_z is a maximum. It is this couple that fixes the resonance frequency, γh_z . This is a true resonance effect; large-amplitude precessional oscillations of the electrons are caused by a small microwave field, the largeness of the amplitude occurring because the field is at the correct frequency.

To understand what is meant by a microwave field "circularly polarized in the correct sense", it is helpful to think of a gyroscope with an applied couple. There is a tendency to precess, which will be maintained if, as the gyroscope moves, the axis of the couple also moves in the same way, so that relative to axes defined by the gyroscope the couple remains fixed. If the axis of the couple moves in the opposite direction to the gyroscope, the precession is not maintained. Thus gyromagnetic resonance occurs for a microwave field circularly polarized in one sense only; which is the right sense will depend on the orientation of the polarizing field.

When the electrons are displaced by the microwave field from their equilibrium orientation in the z direction, a microwave component of induction, \mathbf{b} , is created in the xy plane. This is related to the microwave field \mathbf{h} by equation (1). At ferromagnetic resonance, the axes of the electrons lie in the xy plane, so that \mathbf{b} is large. Thus ferromagnetic resonance, which is a peculiarity in the behaviour of electrons, manifests itself on the macroscopic scale by large values of μ and α .

Also, since the electrons are precessing with large angles, the opportunity for collisions (whatever may be meant by a "collision") is high, so that high losses are obtained; the imaginary parts of μ and α are therefore large.

It is important at this point to realize that high losses are obtained only if the field in the specimen remains finite; actually, the requirement of infinite μ and α is satisfied not by infinite b but by zero h , so that in fact the losses do not become high. Let us consider equations (12) and (13). For high values of μ and α , these reduce to

$$\left. \begin{aligned} h_x &= n \left\{ \frac{H_x + jH_y}{p + 2n} \right\} \\ h_y &= n \left\{ \frac{-jH_x + H_y}{p + 2n} \right\} \end{aligned} \right\} \quad (15)$$

where μ and α have been replaced by the values given in equations (4), and the limit taken as $\sigma \rightarrow 1$; n is 3 for the sphere, 2 for the rod. Now, for a circularly polarized applied microwave field, $H_y = \pm jH_x$, and for the "right" sense of circular polarization, the positive sign is to be taken. Thus, the right-hand sides of equations (15) vanish, so that in the resonance condition there is no microwave magnetic field in the ferrite, and notwithstanding the peak values of μ'' and α'' the losses remain small.

4. Kittel resonance

When the polarizing field is varied in a cavity experiment on a ferrite sample, it is found that for a particular value, with the right sense of circular polarization of the microwave field in the cavity, there is a very large frequency shift and a large drop in the "Q" of the cavity. From equations (6), (7), (9) and (10), these phenomena are seen to occur when the condition is satisfied that

$$\mu' + n \pm \alpha' = 0 \quad (16)$$

where n is 2 for a spherical sample and 1 for a cylindrical rod. It is clear from equations (12) and (13) that this is also the condition that the field in the specimen becomes very large, although the external field remains finite. Thus the heavy absorption, observed as a minimum value of "Q", is due not to anything spectacular in the values of μ'' and α'' , but to the fact that the microwave magnetic fields become highly concentrated in the specimen. This is not a true resonance effect. The heavy absorption is due to the increased probability and violence of "collisions" as the electrons precess with large angle, but this large angle of precession is caused by the large amplitude of the field. Since it follows from Kittel's theory^(3,4) that the effect occurs at values of polarizing field for which equation (16) holds, it seems appropriate to call it "Kittel resonance", bearing in mind that the resonance is now a shape effect.

For very large or very small polarizing fields (by small is not meant so small as to cause the ferrite to be unsaturated), only a small fraction of the microwave energy in the cavity is in the ferrite. This fraction is comparable in magnitude to $\epsilon V_1/V_0$, ϵ being the dielectric constant of the ferrite. At Kittel resonance, a very much larger fraction of the microwave energy is stored in the ferrite. At ferromagnetic resonance, a vanishingly small fraction of the microwave energy is stored in the ferrite—small, that is, compared with $\epsilon V_1/V_0$.

It is pertinent here to compare ferromagnetic and paramagnetic substances. In a paramagnetic substance, it is

legitimate to take the value of the field in the specimen to be equal to the field outside. This is true even at paramagnetic resonance, since even here μ and α do not depart greatly from their non-resonant values (1 for μ , and something small for α). Kittel made the same assumption for ferromagnetic substances. Thus, in effect, he treated external susceptibility instead of actual (intrinsic) susceptibility. The mistake was repeated by early workers on cavity measurements of ferrite properties, and pointed out by Rowen and von Aulock⁽²⁾ and the present author.⁽¹⁴⁾ For paramagnetic substances, evidently, there is no great difference between Kittel resonance and paramagnetic resonance, but for ferromagnetic substances the distinction is important.

Disk samples differ from other shapes in that the microwave field in the sample is the same as the external field, in the ideal case of a disk of finite thickness and infinite area, or finite area and infinitesimal thickness. (The ideal is never realized in practice, so that the theory of disks in cavities is not very accurate. The equality of internal and external fields is obtained at the cost of considerable distortion of the fields.) Thus for an ideal disk Kittel resonance and ferromagnetic resonance are the same thing, because the external permeability and permeability are identical, and both become infinite together.

5. Wave-guides containing ferrites

Several writers^(6,7,8) on the subject of wave-guides containing ferrites have set out with the intention of treating only the lossless case, and have for this reason avoided the condition of ferromagnetic resonance ($\sigma = 1$). It is clear from the foregoing discussion that the assumption that $\sigma = 1$ is the condition of heavy losses requires further examination, and it is also pertinent to examine the Kittel resonance condition. There are three cases that find practical application—the guide of circular cross-section, containing a co-axial rod of ferrite of circular cross-section, or a tube of ferrite of outer radius equal to that of the guide, and the guide of rectangular cross-section, containing a rod of rectangular cross-section, asymmetrically placed. In the first two cases, the d.c. polarizing field is applied axially, in the third transversely.

At the centre of an empty cylindrical waveguide, the magnetic field in the H_{pq} and E_{pq} modes ($p \neq 0$) is transverse and uniform. In the H_{0q} modes it is longitudinal, while in the E_{0q} modes it is zero. If a thin ferrite rod is placed at the centre of the guide, the magnetic field in the E_{0q} mode, being zero at the position of the ferrite, is unaffected; in the H_{0q} mode it is very little affected since in the z direction the permeability of the ferrite is equal to that of free space. The interesting cases are those for which $p \neq 0$; the situation is similar to that in a cavity with a cylindrical rod, and in the same way the microwave magnetic field in the ferrite is zero at ferromagnetic resonance ($\sigma = 1$). Thus there is no large loss, and a treatment of this situation which ignores losses is quite valid. In practice, the ferrite rods used are not very thin, so that the exclusion of the magnetic field from the ferrite will not be perfect; however, as long as the field in the ferrite is much smaller than the external field, the conclusions drawn from a lossless treatment should be valid. This picture may be expected to break down when the ferrite radius exceeds a certain value; for the filled guide, propagation does take place, but the microwave magnetic field must all be confined in the ferrite. It will now not become zero or infinite; the Kittel condition will not arise, while a heavy loss should be observed at ferromagnetic resonance. It is

reasonable to suppose that as the radius of the rod increases from zero to the guide radius the value of σ at which the heavy loss occurs will increase steadily from the Kittel value to unity. Thus for rods of the radii used in practice—about a quarter or a third of the guide radius—the heavy loss is likely to occur for a value of σ somewhat above the Kittel value.

When the ferrite is in the form of a tube of outer radius equal to that of the guide, the transverse component of magnetic field is parallel to the surface of the tube, and the situation is somewhat analogous to that of a disk polarized in one direction parallel to its plane, with a microwave field in some arbitrary direction in this plane, so that it may be expected that the heavy losses will occur at ferromagnetic resonance, which in this case coincides with Kittel resonance.

Returning to the case of the rod, and again considering it to be of small radius so that it can be regarded as immersed in a uniform field, let us now examine Kittel resonance more deeply. If we substitute for μ' and α' in equation (17), using Polder's equations (4), we find for the Kittel resonance condition

$$\sigma = 1 - (p/2) \quad (17)$$

Substituting this into equations (4) we find that for Kittel resonance

$$\mu = 1 - \left\{ \frac{1 - (p/2)}{1 - (p/4)} \right\}; \quad \alpha = \frac{-1}{1 - (p/4)}. \quad (18)$$

For values of p ranging from 0 to 1 (the values likely to be found in practice) the value of μ for Kittel resonance ranges from 0 to $\frac{1}{2}$; values of μ , α and σ at Kittel resonance are given for various values of p in Table 1. We also note that the value of σ at $\mu = 0$ is given by equation (4) to be

$$\sigma = \frac{1}{2}(p^2 + 4)^{1/2} - p. \quad (19)$$

Solutions of equation (19) are given in Table 2. It is evident from the values of σ in Tables 1 and 2 that the condition

Table 1. Values of μ , α , σ , for given p , in the Kittel resonance condition

p	σ	α	μ
0	1	-1	0
0.25	0.875	-1.067	0.067
0.5	0.75	-1.14	0.14
0.75	0.625	-1.23	0.23
1	0.5	-1.33	0.33

Table 2. Values of σ , for given p , at which $\mu = 0$

p	σ
0	1
0.25	0.883
0.5	0.781
0.75	0.693
1	0.618

$\mu = 0$ approximates to Kittel resonance. Further, the value of σ for $\mu = 0$ is rather higher than for the Kittel condition, and it has been seen that, for a rod of finite size, the absorption maximum is likely to occur for values of σ rather above the Kittel value. The theoretical conclusions drawn by the present author⁽⁸⁾ and others^(6, 7) for zero values of μ , on the assumption that losses are negligible, evidently need to be accepted with caution.

Duncan and Swern⁽¹⁵⁾ have investigated experimentally the behaviour of cylindrical wave-guides containing concentric

ferrite rods for large values of polarizing field. In Fig. 4 of their paper, in which guide wavelength is plotted against polarizing field, a resonance effect is apparent for a value of σ rather greater than the Kittel value. Unfortunately, they do not show values of polarizing field quite as high as the ferromagnetic resonance value, but it seems likely, on extrapolation of their curves, that nothing remarkable happens there. Their results therefore are in accordance with the theoretical deductions made in the present paper. Duncan and Swern themselves attributed the anomalous behaviour to exclusion of the magnetic field from the ferrite in the condition $|\mu| = |\alpha|$, that is, $(\mu + \alpha) = 0$. This, they argue, should cause the ferrite to behave to a certain extent like a perfect conductor. However, in the case of a perfect conductor, the electric field is excluded because ϵ is infinite; analogously, in a ferrite, it is when μ and α become infinite that magnetic fields are excluded, as we might have expected intuitively, and have seen to be the case in Section 3. It is clear from equations (12) that there is no question of the magnetic fields in the specimen vanishing when $|\mu| = |\alpha|$. Values of σ for the condition $|\mu| = |\alpha|$ are given in Table 3; these are seen to lie well below the Kittel values, whereas the present theory requires, and Duncan's and Swern's results demonstrate, a resonance effect for a value of σ somewhat above the Kittel value.

Table 3. Values of σ , for given p , for the condition $|\mu| = |\alpha|$

p	σ
0	1
0.25	0.75
0.5	0.5
0.75	0.25
1	0

Some experimental work has also been carried out by Seidel⁽¹⁶⁾ on rectangular wave-guides of small cross-section, filled with ferrite. He observes two effects. The first is a minimum of power propagated for $\mu \sim 0$, which is predicted by theory given in the same paper and also in reference (7). It is difficult to examine this effect analytically because of the non-uniformity of fields in a rectangular specimen, and the variation of the ferrite properties with position in the specimen because of the non-uniformity of the polarizing field. It seems not unlikely, however, that the effect is a distorted Kittel effect. The second effect is that there is no propagation when $\sigma = 1$, which Seidel calls susceptibility resonance and we call ferromagnetic resonance. This he attributes to heavy losses in the ferrite; it may, however, be due to the impossibility of a magnetic field's existing inside a ferrite at ferromagnetic resonance. It is difficult to say, on the evidence available, which is the correct view.

Acknowledgement

The author wishes to express his gratitude to the Engineer-in-Chief of Marconi's Wireless Telegraph Co. Ltd. for permission to publish this paper.

References

- (1) POLDER D. *Phil. Mag.*, **40**, p. 99 (1949).
- (2) ROWEN, J. H., and VON AULOCK, W. *Phys. Rev.*, **96**, p. 1151 (1954).
- (3) KITTEL, C. *Phys. Rev.*, **71**, p. 270 (1947).

- (4) KITTEL, C. *Phys. Rev.*, **73**, p. 155 (1948).
 (5) HOGAN, C. L. *Proc. I.R.E.*, **44**, p. 1345 (1956).
 (6) SUHL, H., and WALKER, L. R. *Bell. Syst. Tech. J.*, **33**, pp. 579, 939, 1133 (1954).
 (7) SEIDEL, H. *Bell. Syst. Tech. J.*, **36**, p. 409 (1957).
 (8) WALDRON, R. A. *J. Brit. I.R.E.*, **18**, pp. 597, 677, 733 (1958).
 (9) BERK, A. D., and LENGUEL, B. A. *Proc. I.R.E.*, **43**, p. 1587 (1955).
 (10) WALDRON, R. A. *Theory of the Measurement of the Elements of the Permeability Tensor of a Ferrite by means of a Resonant Cavity*. Convention on Ferrites, Paper No. 2225 R, London: The Institution of Electrical Engineers, October–November 1956.
 (11) VON AULOCK, W., and ROWEN, J. H. *Bell Syst. Tech. J.*, **36**, p. 427 (1957).
 (12) WALDRON, R. A. *Brit. J. Appl. Phys.*, **9**, p. 439 (1958).
 (13) WALDRON, R. A. *Brit. J. Appl. Phys.*, **10**, p. 20 (1959).
 (14) WALDRON, R. A. *Brit. J. Appl. Phys.*, **7**, p. 114 (1956).
 (15) DUNCAN, B. J., and SWERN, L. *Proc. I.R.E.*, **45**, p. 647 (1957).
 (16) SEIDEL, H. *Proc. I.R.E.*, **44**, p. 1410 (1956).

Evaporation and diffusion rate measurements on cathodes of sintered nickel containing alkaline-earth oxides

by J. F. RICHARDSON, B.A., Ph.D., Grad.Inst.P.,* and Prof. F. A. VICK, O.B.E., Ph.D., A.M.I.E.E., F.Inst.P.,†
 Physics Department, University College, Keele, Staffordshire

[Paper first received 18 June, and in final form 28 August, 1959]

Abstract

The evaporation rate of barium from a sintered nickel cathode and the diffusion rate of barium through it have been measured using ^{140}Ba and tracer techniques. Confirmation of the evaporation rates thus determined have been obtained by comparison with measurements made by a method due to Becker.

The activation energy of evaporation is 2.2 to 2.5 eV. Two diffusion processes operate, one predominant in the range 875 to 1020°C and one below 875°C. The activation energies are 2.5 and 0.5 eV respectively. The mechanism of diffusion at the higher temperatures appears to be Knudsen flow following evaporation from the inner surfaces, and that for the lower temperatures probably by surface diffusion.

Introduction

THE evaporation rates of the alkaline earth metals and their oxides from oxide-coated and dispenser cathodes with a tungsten base have been measured by several workers.⁽¹⁻¹⁵⁾ Such measurements are important, since the loss of alkaline earth material by evaporation is the main factor which governs the useful life of a cathode. The diffusion rate of barium through a cathode has been measured only for the oxide-coated cathode, by Bever,⁽¹⁶⁾ who found that two diffusion processes were operative. In the work to be reported concurrent measurements were made of the evaporation rate and the diffusion rate of barium for a cathode by the use of a radioactive tracer. The isotope used was ^{140}Ba which has a half-life of 12.8 days.

* Now at the Research Laboratory, Metropolitan-Vickers Electrical Co. Ltd., Trafford Park, Manchester, 17.

† Now at the Atomic Energy Research Establishment, Harwell, Didcot, Berks.

The rate of evaporation may be represented by an equation of the type

$$m = A \exp(-B/T) \quad (1)$$

where A is a constant which depends slightly on temperature and B is a constant which is equal to ϕ_E/k , where k is the Boltzmann constant and ϕ_E is the activation energy for evaporation, in electron volts. A plot of $\log m$ against $1/T$ then yields a slope from which ϕ_E may be calculated.

The activation energy for diffusion, ϕ_D , is determined by application of a solution of Fick's second law to diffusion in a semi-infinite cylinder. The concentration C at a point x from the source of diffusing material is given by⁽¹⁷⁾

$$C = \frac{M}{(\pi Dt)^{1/2}} \exp\left(-\frac{x^2}{4Dt}\right) \quad (2)$$

where M is the total amount of substance diffusing, t is the time for which it has been diffusing and D is the diffusion coefficient. The observed temperature dependence of the measured diffusion coefficient is found to follow the form

$$D = D_0 \exp(-\phi_D/RT) \quad (3)$$

where D_0 may be independent of temperature. By plotting $\log C$ versus x^2 , D can be found from the slope of the graph; then if $\log D$ is plotted against $1/T$ the slope gives ϕ_D .

Experimental procedure

The form of the tube used for the evaporation-diffusion measurements is shown in Fig. 1. The anode A consisted of a 2 cm diameter O-nickel disk which could be rotated in a horizontal plane to one side of the tube, by means of an external magnet acting on a glass-encased iron slug B , to expose to the cathode C an identical disk D which served as collector. The anode-cathode and the anode-collector separations were each about 1 mm. This arrangement

enabled thermionic emission measurements to be made on the valve during activation. All metal components were treated in a hydrogen furnace before use and the glassware was cleaned by washing successively in carbon tetrachloride, distilled water, nitric acid and several times in distilled water before oven-drying.

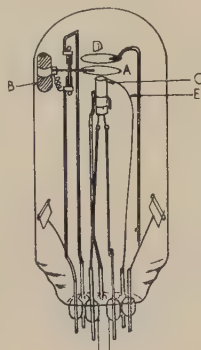


Fig. 1. The experimental tube

A cathode was produced by pressing 4–5 μ diameter nickel powder containing 0.1% silicon into one end of a 0.5 cm diameter O-nickel tube to give a plug about 3 mm thick. On to the back of this plug was pressed 0.25 g. of the "labelled" carbonate which consisted of a known amount of ^{140}Ba present in a given mass of normal barium carbonate. A piece of thin O-nickel sheet was pressed on to the back of the carbonate to protect the heater, which was inserted into the remaining cavity. On to the upper rim of the cathode tube, a 0.1 mm diameter tungsten wire *E* was welded to form the hot junction of a tungsten-nickel thermocouple. The assembly, as all those described in this paper, was mounted on a seven-pin, type FK10, C9 glass pinch (by Siemens Edison-Swan Ltd.), two barium getters were attached and the whole was sealed into a C9 glass envelope.

The valve was sealed on to the pumping system using foot-operated bellows for glass-blowing, since the presence of ^{140}Ba excluded any mouth-operated processes because of its high toxicity if ingested. The tube was baked out at 420°C for four hours. To break down the carbonate the cathode was gradually heated to 950°C, the pressure being maintained below 10^{-4} mm of mercury. The breakdown occupied twenty-four hours. Activation consisted of running the cathode at 950°C for another twenty-four hours with 250 V applied between cathode and anode, after which the emission was constant at a few milliamperes. The valve was rebaked and the metal parts were eddy-current heated. The getters were outgassed and fired and the valve was sealed off from the system.

The cathode was held at a fixed temperature for twenty-five hours, no emission being drawn, with the collector exposed to the cathode for short, timed intervals, thus reducing the re-evaporation of any collected material due to the collector becoming too hot. The heater was switched off, the valve was opened and the collector was carefully removed. Counts were made upon it using a type GM4 Geiger-Muller tube with a scaler and associated electronic equipment. The percentage of the total evaporant from the cathode which had been collected was determined from the cathode and collector dimensions and their separation, using the expression derived by Blachman,⁽¹⁸⁾ making it possible to determine the absolute value of the evaporation rate. The result gave one point on a plot of log (evaporation rate) versus $1/T$. Several such points gave a plot from the slope of which the activation energy of evaporation ϕ_E was found.

The cathode was removed from its cylinder, and all adhering material cleaned off the base, before the sides of the cathode were skimmed to remove any material which had diffused along the surface between the cathode and the cylinder. A lathe was used to remove the surface layers of the cathode in steps of about 0.01 mm. The cathode thickness after each operation was measured. Counts were made on each sample of cathode removed to determine the amount of barium present in each. A profile of the barium distribution was obtained by plotting log (counting rate) versus x^2 , where x was the distance from the base of the cathode to the centre of the section. The initial slope of this graph gave the value of the diffusion coefficient D for that particular cathode temperature. By obtaining several such coefficients and plotting log D versus $1/T$, the activation energy of diffusion ϕ_D was obtained from the slope. Each valve of this type constructed yielded one point on each of the ϕ_E and ϕ_D graphs.

To help to interpret the results obtained from the measurement of diffusion rates they were repeated with the cathode in argon at about 400 mm of mercury. The mean free path of argon at this pressure is 0.2 μ , which is much smaller than the expected average pore diameter in the cathode. The valves were made as before, except that the collector was omitted and the anode was fixed 1 mm above the cathode surface. Two tubes were processed at a time as shown in Fig. 2. The litre flask of argon was at a pressure of 1 atm.

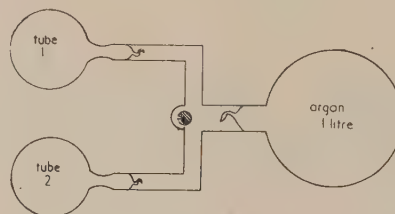


Fig. 2. Arrangement for filling pair of tubes with argon

The two seals in the side-arms of the tubes were broken to pump out the region between the valves and the argon seal. The system was baked and the metal components were eddy-current heated. The cathodes were processed as before, the system rebaked, the metal parts again eddy-current heated, the getters out-gassed and fired and the two tubes sealed off from the pumping system. The seal to the argon flask was broken, releasing gas into both tubes. Each tube was sealed and drawn off from the argon system at the constriction. The cathodes were treated as before and the diffusion curves were drawn to determine ϕ_D in argon.

For comparison with the results obtained with the ^{140}Ba , tubes were built to measure the evaporation rate by the Becker method.⁽¹⁾ The cathode was constructed as before except that Analar barium carbonate was used in place of the "labelled" carbonate. The form of the tubes necessary for such measurements is described in the literature. Evaporated material is collected on a tungsten wire from which the emission is measured until it has passed through a maximum. This maximum corresponds to total, or almost total, monolayer coverage of the wire. Knowing the time to attain this, and assuming Brodie and Jenkins⁽¹⁰⁾ value for the mass per unit area of monolayer, the evaporation rate could be calculated. With one tube it was possible to perform a whole range of measurements at different temperatures to obtain a value of ϕ_E .

One tube built for Becker-type measurements had two rectangular O-nickel plates, 4.5 \times 3.0 cm positioned 4 cm apart, one on each side of the cathode-wire system. After a

normal evaporation run the experiment was repeated with a voltage applied between the two deflector plates. This procedure was repeated for several temperatures to see if the evaporation rate was affected by an electrostatic field.

The surface diffusion rate of ^{140}Ba over nickel was measured as follows. The cathode nickel powder was pressed by means of a punch and die into the form of a bar. This was sintered in a tubular furnace in an atmosphere of hydrogen at 1100°C for an hour. Bars of about 12% porosity were selected to correspond to the cathode matrices. The bars were machined to $0.6\text{ cm wide} \times 0.3\text{ cm deep} \times 3.0\text{ cm long}$. A small step was cut in one end of the bar on which the active material was placed. The edge of this step was clearly defined and all distance measurements were made from it. A retaining strip of O-nickel was welded around the edge of the step to prevent any active material from spilling.

The bar was inserted centrally into a ceramic tube around which was a coil of Nichrome strip. All diffusion took place with the valve on the pumping system. After baking the valve, the coil was heated by passage of a current. The maximum bar temperature that could be obtained with this arrangement was 650°C . The bar was heated at constant temperature for forty-eight hours. The pressure in the system was always below 10^{-6} mm of mercury during the diffusion run. Some of the Nichrome evaporated in this time on to the inside of the glass envelope, but the ceramic tube shielded the bar from this evaporant.

After removal of the bar from the tube the step was machined off and the surfaces on the sides and bottom of the bar were skimmed before sectioning across the upper surface. The depth of each section was 0.5 mm . Counts were made on each section and the diffusion coefficient found as before. From the results obtained from several bars at different temperatures the activation energy of surface diffusion ϕ_S was obtained from the $\log D$ versus $1/T$ graph.

Results

Measurements of the evaporation rate of barium from the cathodes using ^{140}Ba were made in the temperature range 650 to 1020°C . The evaporation rate increased from 8.0×10^{-10} to $9.2 \times 10^{-7}\text{ g.cm}^{-2}\text{ s}^{-1}$ over this range. The results are plotted in Fig. 3 and fit a straight line from which $\phi_E = 2.19\text{ eV}$. The points between 800 and 900°C show the greatest divergence from the line.

The results from the Becker tubes were plotted as \log (atom layers s^{-1}) versus $1/T$ as shown in Fig. 4. From the

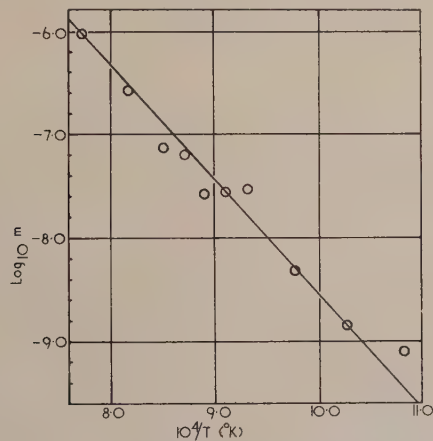


Fig. 3. Variation of evaporation rate of barium with temperature using ^{140}Ba

first tube the slope of the graph gave a value of ϕ_E of 2.48 eV . This was 0.3 eV higher than the value from the isotope measurements. The second tube gave results which yielded a value of ϕ_E of 2.53 eV . This was in good agreement with the result from the previous tube. The discrepancy between

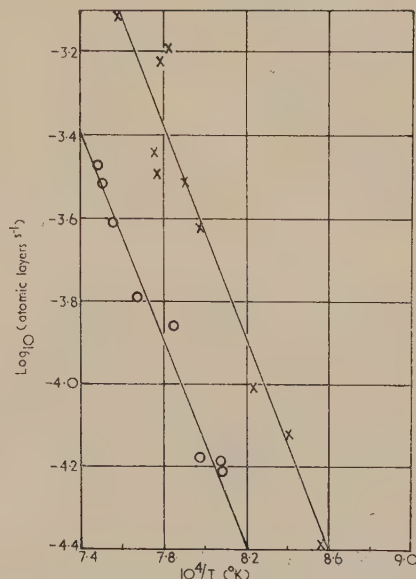


Fig. 4. Variation of evaporation rates of barium from Becker tube experiments

○ = tube 1. × = tube 2.

the results from the two methods is not large, and could be due to loss of collected material occurring by re-evaporation in the case of the tracer measurements. In the Becker method, the wire collects only a small fraction of the total quantity of barium evaporated from the cathode. Since this fraction is determined mainly by geometry, it is constant and the slope of Fig. 4 can be used directly to give ϕ_E . When account is taken of the geometrical factor, reasonable agreement between Figs. 3 and 4 for the evaporation rates is found. Typical results from the measurement of the evaporation rate, with and without an applied transverse electrostatic field, are given in Table 1. No significant difference was observed between the two cases, indicating that the evaporant from the cathode is not appreciably ionized.

Table 1. Evaporation rates with and without applied electrostatic field

Temperature ($^\circ\text{C}$)	Time for monolayer coverage with field applied (min)	Time for monolayer coverage without field applied (min)
1000	243	241
1000	232	229
1012	193	202
1012	207	198

The diffusion rate of barium was measured through fifteen cathodes in vacuum. A typical example of the diffusion profile obtained is shown in Fig. 5. It was apparent from the profiles that the activating material had diffused through the cathode and that a concentration had built up at the cathode surface. This was a confirmation of previous indications that some form of barium over the surface of the cathode, was responsible for the efficiency of this type of emitter. It also showed that the diffusion rate of barium through the

matrix was greater than the evaporation rate from a normal activated cathode.

An analysis of the diffusion profile was based on two assumptions. Some barium diffused into the cathode matrix during the breakdown of the carbonate, so that at the instant

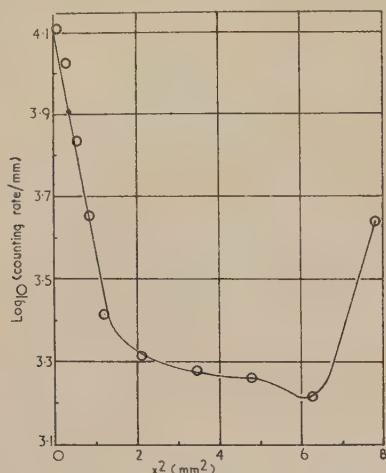


Fig. 5. Diffusion profile within the cathode at 975° C

from which the diffusion was timed the active material was not all confined below the base of the cathode. However, provided that each cathode was treated identically before the start of the timed diffusion, then the initial conditions for the measured period should be approximately the same in each cathode. From the profile a value of D was obtained, the logarithm of which was plotted against $1/T$ to give a slope from which ϕ_D was found. Since no absolute value of D is required to find ϕ_D , it was assumed that the difference in the initial slopes of the profiles was proportional to the difference of the diffusion coefficients.

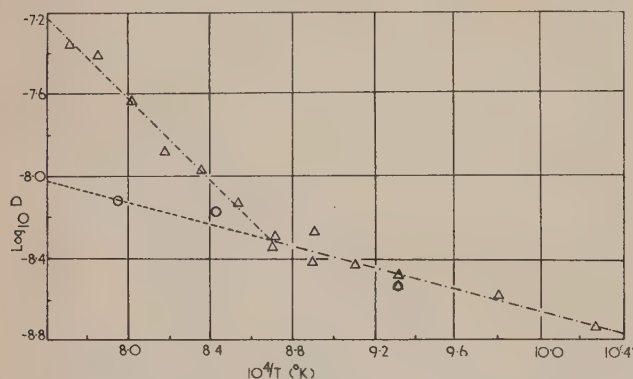


Fig. 6. Variation of diffusion coefficient with temperature

Δ = normal cathodes in vacuum.
 \circ = cathodes in an atmosphere of argon.

The second assumption arose from the build-up in concentration of barium at the cathode surface. This increase would give rise to some diffusion back to regions of lower concentration nearer to the centre of the matrix, thus tending to make the profile more shallow. It was assumed that this back diffusion had a negligible effect upon the initial slope of the diffusion profile.

The temperature range covered was from 700 to 1020° C and the diffusion coefficients changed from 1×10^{-9} to $5 \times 10^{-8} \text{ cm}^2 \text{ s}^{-1}$ over this range. The plot made to determine ϕ_D is shown in Fig. 6. This fitted two straight

lines intersecting at a temperature of about 875° C. The slope of the line over the lower temperature portion gave $\phi_D = 0.53 \text{ eV}$, and that over the higher temperature range gave a value of 1.99 eV . When the latter was corrected for the lower slope the value obtained for ϕ_D was 2.50 eV .

These results indicate that two diffusion processes must operate between 700 and 1000° C, one predominating below 875° C and the other above that temperature. Four cathodes of different porosities were made and run at 900° C to compare diffusion rates with porosity. The results from these and the previous cathode at this temperature are given in Table 2. These show that increase in porosity gives an increase in diffusion rate in the higher temperature region.

TABLE 2. Comparison of diffusion rate with porosity for five cathodes run at 900° C

Porosity (%)	$D(\text{cm}^2 \text{ s}^{-1}) (\times 10^{-9})$
10.6	5.3
12.1	7.3
12.8	9.8
17.2	13
29.7	17

Results were obtained from three cathodes heated in an atmosphere of argon. The $\log D$ versus $1/T$ plot is shown in Fig. 6. If the lower temperature slope of the diffusion plot with the cathode in vacuum is extrapolated to higher temperatures, then the values obtained with the cathodes in argon lie very close to this line. This implies that the diffusion process predominating at the higher temperatures has been reduced to a negligible factor by the inclusion of the inert gas in the tube.

Surface diffusion measurements were made on three bars over the limited temperature range. The profiles obtained were not straight lines, probably because a large depth of surface on the atomic scale had to be taken, and so some internal diffusion was also measured. The value of ϕ_S obtained was 0.89 eV . This is very approximate since it is based only upon three points on the graph.

Discussion

The value of ϕ_E for the material evaporated from the cathode is between 2.2 and 2.5 eV , most probably closer to the latter value. This is very similar to the activation energy of the higher temperature diffusion process. The exact nature of the evaporant was not determined, but it did contain barium, and from previously reported work⁽¹⁹⁾ it would seem that both barium and barium oxide are present in the evaporant.

The experiments indicated that the evaporant was not ionized. This is in agreement with the results of Rittner and others,⁽¹⁵⁾ who found that the evaporant from an impregnated cathode was not ionized. The period over which the cathodes were investigated did not exceed one hundred hours of life, so no conclusions can be drawn about the relationship between evaporation rate and cathode life. The evaporation over this initial period of life was constant at a given temperature. Since the cathodes used for these measurements were similar in construction to the L-cathode,⁽²⁰⁾ it is interesting that this result agrees with similar measurements on L-cathodes.⁽¹¹⁾ The normal M-cathode⁽²¹⁾ is more similar in construction to the impregnated cathode, and it has been found with the latter that the evaporation rate is given by a $t^{-1/2}$ law.⁽¹⁵⁾ It seems probable, therefore, that the evaporation rate from an M-cathode would obey a similar relationship.

The evaporation rate from the cathodes is quite high. By assuming a complete monolayer of barium atoms and the pores to be open, there will be of the order of 10^{14} barium atoms on the cathode surface. This is about 3×10^{-8} g of barium. At 1000°C the evaporation rate was 7×10^{-7} g cm $^{-2}$ s $^{-1}$, so 1.4×10^{-7} g are lost from the cathode per second. On the average this needs a new monolayer formed every 0.2 s. Assuming that the surface has the same porosity as the cathode as a whole, and using $\phi_S = 0.89$ eV as found by experiment, surface diffusion could not provide sufficient barium at this rate to cover the surface. A large percentage of the evaporant must come directly from the pore ends, without ever being sorbed on the surface. Whether this barium serves any useful purpose in the operation of the cathode depends upon whether the pore ends contribute to the emission. If it does not, then reduction of this evaporation would lead to a more economical cathode. At the higher temperatures, the rate of evaporation of nickel might well become significant.

Two diffusion processes were found to operate in the temperature range 700 to 1020°C . The one predominating up to 875°C has $\phi_D = 0.53$ eV; ϕ_S was found to be about 0.89 eV. It is suggested that this low temperature process is diffusion along the pore walls. If this is so, then increasing the porosity of the cathode would increase the wall area, and so the diffusion rate at any temperature below 875°C should increase with porosity.

The process operating above 875°C has an activation energy of 2.5 eV. The introduction of argon into the valves at 400 mm of mercury suppresses this process. It is proposed that the higher temperature mechanism is the Knudsen flow of barium, either free or as the oxide, or both, through the cathode pores. The vapour pressure of barium at 900°C is 1 mm of mercury, and that of barium oxide is 3×10^{-8} mm of mercury. Since argon at 400 mm of mercury can penetrate pores of diameter greater than 0.2μ readily, it would suppress Knudsen flow. The results also indicate that the majority of pores are greater than 0.2μ in diameter.

In an M-cathode there is no concentration gradient to start with, but diffusion takes place under a temperature gradient. The diffusion rate at any temperature is greater than the evaporation rate, so a build-up in the concentration of barium in some form is obtained near the surface, as confirmed by the diffusion profiles. If the two proposed processes in fact obtain, the barium and barium oxide must accumulate in the pores, blocking them up to a large extent but not affecting the evaporation rate if the temperature of the material remains constant. This would produce emission from the pore ends which would behave, presumably, as small oxide-coated cathodes, as suggested by Brodie and Jenkins.⁽²²⁾ If the high temperature diffusion is predominantly by Knudsen flow, then an increase in porosity should increase the diffusion rate. This is what was found in the four cathodes studied at 900°C . In BN cathodes the porosity is very low due to the high pressure used in forming them, and it seems likely that surface diffusion will predominate.

The conclusions arrived at are that barium and barium oxide move towards the cathode surface by two mechanisms; one, which predominates below 875°C , is by diffusion along the pore walls, and the other, which predominates above 875°C , is by Knudsen flow through the pores following evaporation from the pore walls. It is significant that the activation energy for diffusion above 875°C , ϕ_D , is very close to the activation energy for evaporation, ϕ_E , so it would appear that at the high temperatures it is evaporation

into the pores that needs the activation energy. On arrival at the cathode surface a high percentage of the Knudsen flow material is lost by evaporation. The nickel surface of the cathode is covered, although not completely, by adsorbed barium. Oxygen is probably present on the nickel surface below the barium. The surface material is continuously evaporating and being replaced from the interior. During the activation of the cathode the pore ends became blocked to some extent with barium and barium oxide. The pore ends may then contribute to the emission. The activation energies are as follows: (a) of evaporation, 2.2 – 2.5 eV; (b) of surface diffusion, 0.89 eV; (c) of the low temperature bulk diffusion process, 0.5 eV; and (d) of the higher temperature diffusion process, 2.5 eV.

Acknowledgements

The authors express their thanks to their colleagues and the technical staff of the Department for much help and advice; also to Siemens Edison-Swan Ltd., and Metropolitan-Vickers Electrical Co. Ltd. for the gift of materials. One of the authors (J. F. R.) wishes to thank Sir Willis Jackson, Director of Research and Education, Metropolitan-Vickers Electrical Co. Ltd., for permission to publish and for the opportunity of taking part in this work.

References

- (1) BECKER, J. A. *Phys. Rev.*, **34**, p. 1323 (1929).
- (2) PELCHOWITCH, I. *Philips Res. Rep.*, **9**, p. 42 (1954).
- (3) JENKINS, R. O., and NEWTON, R. H. C. *Nature (London)*, **163**, p. 572 (1949).
- (4) PLUMLEE, R. H., and SMITH, L. P. *J. Appl. Phys.*, **21**, p. 811 (1950).
- (5) ALDRICH, L. T. *J. Appl. Phys.*, **22**, p. 1168 (1951).
- (6) LEVERTON, W. F., and SHEPHERD, W. G. *J. Appl. Phys.*, **23**, p. 787 (1952).
- (7) PETERSON, R. W. *Bull. Amer. Phys. Soc.*, **27**, p. 9 (November 28, 1952).
- (8) AFFLECK, J. H., and HOLROYD, L. V. *Bull. Amer. Phys. Soc.*, **27**, p. 8 (November 28, 1952).
- (9) WOOTEN, L. A., RUCHLE, A. E., and MOORE, G. E. *J. Appl. Phys.*, **26**, p. 44 (1955).
- (10) BRODIE, I., and JENKINS, R. O. *J. Electronics*, **2**, p. 33 (1956).
- (11) RITTNER, E. S., AHLERT, R. H., and RUTLEDGE, W. C. *J. Appl. Phys.*, **28**, p. 156 (1957).
- (12) DU PRE, E. K., and RITTNER, E. S. *Phys. Rev.*, **82**, p. 573 (1951).
- (13) SCHAEFER, D. L., and WHITE, J. E. *J. Appl. Phys.*, **23**, p. 669 (1952).
- (14) BRODIE, I., and JENKINS, R. O. *J. Electronics*, **2**, p. 457 (1957).
- (15) RITTNER, E. S., RUTLEDGE, W. C., and AHLERT, R. H. *J. Appl. Phys.*, **28**, p. 1468 (1957).
- (16) BEVER, R. S. *J. Appl. Phys.*, **24**, p. 1008 (1953).
- (17) CRANK, J. *The Mathematics of Diffusion* (Oxford University Press, 1956).
- (18) BURTT, B. P. *Nucleonics*, **5**, p. 28 (August 1949).
- (19) RUTLEDGE, W. C., and RITTNER, E. S. *J. Appl. Phys.*, **28**, p. 167 (1957).
- (20) LEMMENS, H. J., JENSEN, M. J., and LOOSJES, R. *Philips Tech. Rev.*, **11**, p. 341 (1950).
- (21) RICHARDSON, J. F. *Brit. J. Appl. Phys.*, **8**, p. 361 (1957).
- (22) BRODIE, I., and JENKINS, R. O. *Brit. J. Appl. Phys.*, **8**, p. 27 (1957).

Relaxation times in lead film, superconductive, storage elements

by R. F. BROOM, B.Sc., and O. SIMPSON, M.A., Ph.D., Services Electronics Research Laboratory, Baldock, Herts.

[Paper received 27 July, 1959]

Abstract

An important factor in the performance of any thin film, superconductive, switching device is the speed with which superconductivity is restored after the film is driven into the normal conducting state. An experiment is described which measures the critical current of a lead film Crowe cell during the first microsecond after switching. The minimum writing time of such storage cells should be equal to the time required for the critical current to recover to one half of its initial value. Good correlation is found between the recovery times and the writing times for Crowe cells deposited on various substrates. Cells deposited on mica or sapphire recovered in 50 μ s, while those on glass required approximately three times as long. Measurements were also made of the critical current as a function of temperature, and these are used to derive cooling curves during the recovery phase. The cooling curves are not related to the thermal conductivities of the substrates in any simple way, probably because the rate of cooling is determined primarily by the thermal resistance between film and substrate.

1. Introduction

THE growing requirement for increased speed in components for fast electronic computers has stimulated research on superconductive switching, and a number of devices, both of the active switching and the passive memory storage types, have recently been described in the literature. The invention by Buck⁽¹⁾ of the cryotron was the first example of the use of the superconducting transition in a practical electronic device. The original cryotron switch consisted of a niobium solenoid wound round a thin tantalum wire. This type of construction is restricted to comparatively low switching speed, and interest is now chiefly centred on thin film devices.

The operation of any superconducting device involves the transition of some part of the structure from the superconducting to the normal state, and *vice versa*. The speed of operation depends upon the rate of propagation of the superconducting phase transition, and this in turn depends in a complicated way on the geometry of the structure and the amplitude and rate of rise of the driving pulses. Two other time factors are, however, equally important; these are the L/R time constant and the thermal relaxation time following the almost instantaneous rise in temperature, when current flows in metal which has been driven into the normal state. Thin film construction tends to increase the normal resistance and the rate of propagation of the superconducting transition, but the very high current densities, which may reach values in excess of 10^7 A/cm², can cause transient temperature rises of several degrees, even when a film is in contact with liquid helium.

A great deal of work on the phenomenological properties of thin film superconductors will be needed before it is possible to predict the optimum design for any superconductive component. The object of the work described in this paper was to investigate one aspect of the problem, namely the relaxation of a thin strip of superconductor after it has been driven into the normal state by a current pulse. In order to apply the results to a case of practical importance, the thin films used were made in the form of Crowe⁽²⁾ cells; it was thus possible to correlate the relaxation time directly with the switching speed of this kind of storage element. The conclusions are, however, relevant to any superconductive device employing thin films.

2. Experimental method

The Crowe cell, or trapped-flux storage device, consists of a thin film of a superconductor deposited on a flat substrate. In the present work lead was used as the superconductor and films were made by evaporation on to glass, mica or sapphire substrates. The film thickness was 600 Å and a single element consisted of a circular hole 2 mm in diameter bridged by a strip, called the cross-bar, of 0.1 mm width, Fig. 1. A drive wire located parallel to the cross-bar, and

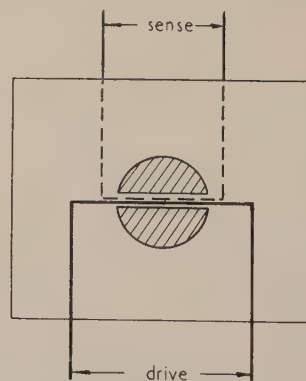


Fig. 1. Crowe cells used in the experiments. Lead film 600 Å thick, D-shaped holes 2 mm diameter, cross-bar 0.1 mm width. The drive and sense wires are detachable

inductively coupled to it, can be used to induce a circulating current in the film, which flows through the cross-bar and returns round the outside of the hole. Under certain conditions a rectangular driving pulse can induce a permanent supercurrent in the film, and, since the sense of circulation is determined by the sense of the driving pulse, one bit of information is thereby stored. This can subsequently be recovered by interrogation.

The mode of operation of the device has been discussed by Rhoderick.⁽³⁾ In order to store, the following conditions

must be fulfilled. (i) The current induced by the leading edge of the driving pulse must exceed the critical current I_c required to drive the cross-bar from the superconducting into the normal state; (ii) the duration of the driving pulse must be long enough for the cross-bar to relax into the superconducting state; (iii) the falling edge of the driving pulse must not induce a current sufficient to drive the cross-bar normal a second time. The minimum pulse length for which these conditions are satisfied determines the maximum speed of the storage element.

The energy of the magnetic field of the supercurrent is dissipated by Joule heating in the cross-bar when it is driven normal, and consequently the temperature of the cross-bar rises. Since the critical current is a decreasing function of temperature, becoming zero at the transition temperature T_c , the condition (iii) requires the driving pulse to be long enough for thermal recovery to occur. Rhoderick's analysis shows that the writing time (minimum pulse length for storage), is determined by the time required for the critical current to recover to one half of its value at the beginning of the cycle.

The critical current of the cross-bar, measured as a function of time, can be obtained as follows. The lead film is scored as shown in Fig. 2, so that the secondary current loop is no

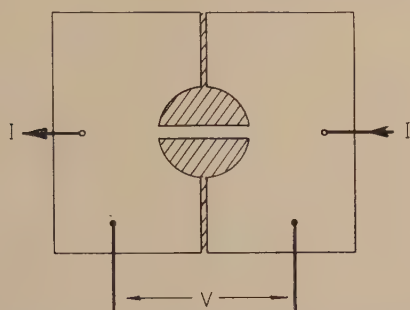


Fig. 2. Crowe cells with drive and sense wires detached, and lead film scored for measurement of I - V characteristic of the cross-bar

longer continuous. The drive wire is removed and electrodes are attached to measure the current-voltage characteristics of the cross-bar. Very short current pulses are fed through the cross-bar with the wave-form shown in Fig. 3, at a repetition rate of about 1 kc/s, the voltage being displayed

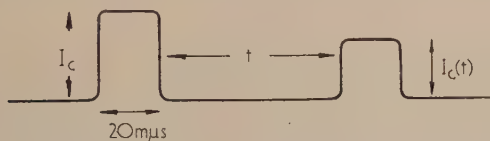


Fig. 3. Wave-form used for measurement of the I - V characteristic of the cross-bar. The repetition rate was 1 Kc/s

on an oscilloscope. So long as the cross-bar remains superconducting there can be no voltage drop across it. The first pulse is adjusted to an amplitude just sufficient to give a signal on the oscilloscope, i.e. the critical current of the cross-bar in equilibrium with the helium bath at 4.2° K. The critical current defined in this way depends on the pulse length of the driving current,⁽⁴⁾ in these experiments the pulse length was always 20 μ s. The second pulse, delayed by an interval t , is also adjusted to the minimum amplitude $I_c(t)$ required to give a signal. Amplitude $I_c(t)$ is thus the critical current appropriate to the state of the cross-bar at an elapsed

time t after the initial pulse. Fig. 4 shows the measured critical currents of three similar lead films of 600 Å thickness deposited on glass, mica and sapphire respectively, at times up to 1 μ s after being driven normal by a 20 μ s current pulse.

If the lead films were perfectly uniform, and at any given current density were either wholly superconducting or wholly normal, then the measurements of $I_c(t)$ shown in Fig. 4

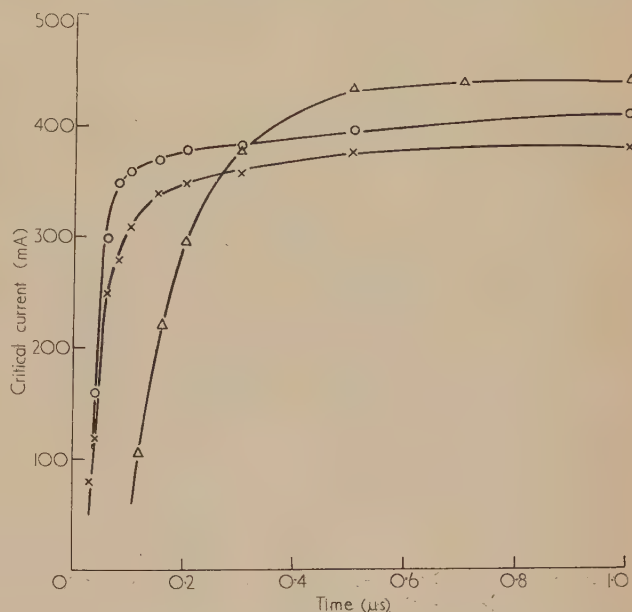


Fig. 4. Recovery of critical current of cross-bar following 20 μ s initial pulse

Δ = lead film on glass substrate.
× = mica substrate.
○ = sapphire substrate.

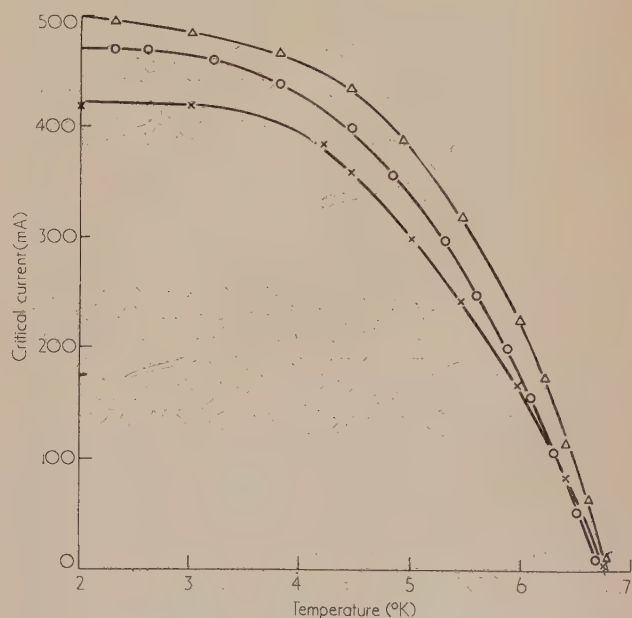


Fig. 5. Critical current of lead film cross-bar as a function of temperature

Δ = glass substrate.
× = mica substrate.
○ = sapphire substrate.

could be used to determine the temperature of the cross-bar as a function of time. Fig. 5 shows the critical currents $I_c(T)$ of the same lead films measured in a separate experiment as functions of the bath temperature from 2 to 7° K. There is a spread of about 20% between the different substrates, which is reasonable for such thin films, and each has a critical temperature of about 6.8° K which is 0.3° K below the critical temperature of bulk lead. Using the curves of Fig. 5 to calibrate the previous results, the cooling curves shown in Fig. 6 are obtained.

3. Discussion

Considering first the results shown in Fig. 4, the films deposited on mica and sapphire substrates both exhibit a very rapid recovery of about 80% of the equilibrium critical current in less than 0.1 μ s, followed by a slower recovery of the final 20%. The film on the glass substrate shows a rather different behaviour because, although recovery of the full critical current takes about 1 μ s, which is comparable with the other substrates, the initial increase is very much slower than either. The times required to recover 50% of the equilibrium critical currents can be read off the curves of Fig. 4. These values of $t(\frac{1}{2})$ are tabulated in the table,

Correlation of switching times with superconductive recovery times for lead films on various substrates

	glass	mica	sapphire
$t(\frac{1}{2})$ (m μ s)	162	50	45
$t(\text{write})$ (m μ s)	200–500	50–150	70–100
L/R observed	10–20 m μ s in normal operation		
$K(4.2^\circ \text{K})$ (W/cm $^\circ$ K)	10^{-3}	unknown	~ 1

together with the measured values of the minimum writing times $t(\text{write})$ of the same and similar films used as Crowe cells in a normal storing cycle. The writing time, though well defined for any one cell, was found to have rather a wide spread from one cell to another, and consequently a range of values representative of all the experimental cells made on each of the substrates has been given. The correlation between $t(\text{write})$ and $t(\frac{1}{2})$ is fairly good, and confirms Rhoderick's predictions which are based on the assumption that the current in the Crowe cell, when it is driven normal, decays almost to zero before the cross-bar returns to the superconducting state. This is equivalent to requiring the L/R time constant of the cells to be much less than $t(\frac{1}{2})$. Direct observation of the decay of the signal in the sense wire gives average values of 10 to 20 m μ s for L/R .

The cooling curves in Fig. 6 will give a faithful representation of the temperature of the lead film only if the transition between the normal and superconducting phases occurs instantaneously throughout the strip. Recent work by Broom and Rhoderick⁽⁴⁾ shows that in lead films the current-induced transition into the normal state is initiated at one or more weak points, and the consequent non-uniformity of Joule heating results in temperature gradients in the film. Since the experiment described in Section 2 measures the hottest part of the film, it is possible that the exact shape of the cooling curves in Fig. 6, and particularly the apparent existence of two decay components in the case of the mica and sapphire substrates, is the result of initial non-uniformity of temperature.

It is not possible to correlate the thermal decay rates with the properties of the various substrates, because little is known about thermal conductivities at liquid helium temperatures. Qualitatively sapphire is a very much better thermal conductor than glass, and mica is probably a good conductor also, although the effect of its anisotropy is

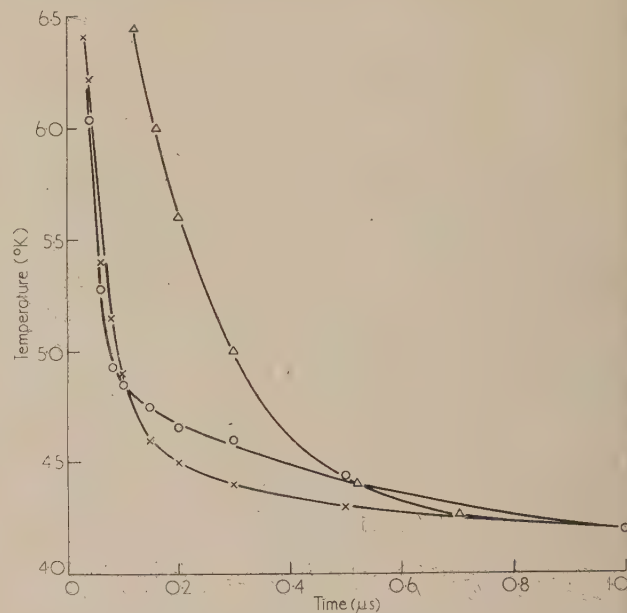


Fig. 6. Cooling curves of lead film cross-bars on various substrates

Δ = glass substrate.
 \times = mica substrate.
 \circ = sapphire substrate.

unknown; this is in general agreement with the results in the table. The rates of cooling are not, however, necessarily determined by the thermal conductivity of the substrate, because at 4° K the phonon mean free path is long compared with the thickness of both film and substrate. The thermal resistance at the interface between film and substrate is likely to be the controlling factor, in which case the optimum transfer of heat will occur when there is perfect acoustic matching between film and substrate.⁽⁵⁾

Acknowledgements

We are grateful to Dr. E. H. Rhoderick for many helpful discussions. Acknowledgement is made to the Admiralty for permission to publish this account.

References

- (1) BUCK, D. A. *Proc. Inst. Radio Engrs*, **44**, p. 482 (1956).
- (2) CROWE, J. W. *I.B.M. J. Res. Develop.*, **1**, p. 295 (1957).
- (3) RHODERICK, E. H. *Brit. J. Appl. Phys.*, **10**, p. 193 (1959).
- (4) BROOM, R. F., and RHODERICK, E. H. *Phys. Rev.* To be published.
- (5) LITTLE, W. A. *Canad. J. Phys.*, **37**, p. 334 (1959).

Microcracks, and the static and dynamic elastic constants of annealed and heavily cold-worked metals

by J. R. BRISTOW, B.Sc., Ph.D., F.Inst.P., A.M.I.Mech.E., Department of Applied Physics, Welsh College of Advanced Technology, Cardiff

[Paper first received 14 August, and in final form 6 October, 1959]

Abstract

The existence of sub-microscopic cracks in heavily cold-worked metals has been suggested in explanation of the very large discrepancies in dislocation densities estimated from changes in density and electrical resistivity, and release of stored energy on annealing such materials.

It is shown that microcracks will produce changes in the elastic constants of a material comparable with—but somewhat larger than—the change in electrical resistivity, rather than with change in density.

Measurements have been made, both statically and dynamically, of Young's modulus, the shear modulus and Poisson's ratio for annealed and heavily cold-worked aluminium, copper and nickel. No changes in moduli were found that could be ascribed to the presence of microcracks.

An unexpected result is a very large and consistent difference between the bulk moduli, and Poisson's ratio, determined statically and dynamically—a difference very much greater than can be accounted for by the usual thermodynamic relationship between isothermal and adiabatic moduli.

1. Introduction

IT has been suggested (Mott⁽¹⁾) that the fracture of ductile metals is preceded by the formation of sub-microscopic cracks as the result of the "pile-up" of dislocations produced by the intense plastic deformation which occurs before failure. Stroh⁽²⁾ developing this idea has shown that, theoretically, piled-up groups of dislocations can produce stable cracks, and further he (Stroh⁽³⁾) has shown that such microcracks can provide a possible explanation of the widely varying values for dislocation densities deduced from measurements of the changes in physical properties of heavily cold-worked metals on annealing.

For example, Clarebrough, Hargreaves and West⁽⁴⁾ have made a detailed study of the release of stored energy and the changes in density and electrical resistivity during the annealing of copper and nickel specimens previously heavily cold-worked to various degrees, and from their results, dislocation densities commonly deduced (see Boas⁽⁵⁾ and Stroh⁽³⁾) are of the order of 10^{11} , 10^{12} and 10^{13} lines per square centimetre from energy release, and density and electrical resistivity changes, respectively.

If Stroh's explanation of these discrepancies is correct then, since the amount of stored energy, and changes in density and resistivity are all three roughly linear against the strain to which the specimens were subjected, such cracks should be present in deformed materials even if still far from fracture.

It is shown below that if sub-microscopic cracks are indeed

present, in the form of either ribbon-shaped or penny-shaped cracks, then the apparent elastic constants of the materials are changed by amounts comparable with—but somewhat greater than—the changes in electrical resistivity.

Measurement of the effect of heavy cold-working on elastic constants should therefore be a good test of the presence (or absence) of such microcracks, particularly as the effect should be quite large in the case of the bulk moduli, as much as (see later) 10 to 20%. Hence, a series of determinations have been made of Young's modulus, the shear modulus and Poisson's ratio (thus allowing the bulk modulus to be calculated) for annealed and heavily cold-worked bars in aluminium, copper and nickel.

An alternative explanation of the results obtained by Clarebrough, Hargreaves and West⁽⁴⁾ is given by Seeger⁽⁶⁾ using a larger figure than Stroh, or Boas, for the volume of a dislocation line and assigning the increase in resistivity largely to stacking faults—although as Stroh⁽⁷⁾ remarks "he finds it necessary to attribute a rather large electrical resistance to a stacking fault".

2. Theory

If a length l of ribbon-shaped crack, having a mean cross-sectional area A_D , is introduced into unit volume of material the fractional change in density $\Delta D/D$ will be $A_D \cdot l$. Similarly, the fractional increase in electrical resistivity $\Delta \rho/\rho$ may be written as $A_R \cdot l$ and the fractional decrease in a macroscopic elastic constant $\Delta C/C$ as $A_C \cdot l$; where A_R and A_C are the *effective* cross-sectional areas for change of resistivity and elastic constant respectively.

Clearly, since current flow will be disturbed, and stresses will be relaxed, in a volume of material large compared with the physical size of a crack, we may expect A_R and A_C to have somewhat similar values and to be large compared with A_D . Indeed, A_R is immediately obtained from Stroh's⁽³⁾ calculations. For $\Delta \rho/\rho$ he obtains $\pi c^2 N/12$ where c is the width of the crack and N the number of cracks crossing unit area. If our l is identical with Stroh's N then $A_R = \pi c^2/12$. (That $N \equiv l$ is shown formally later.)

If a long straight crack is introduced into an isotropic material the change in strain energy W per unit length of crack will be a quadratic function of the values which the stress components p_{ij} had before the crack was introduced; and, contrary to what the well-known stress relaxation argument may suggest, this change will give an increase in total strain energy provided the external load remains constant (see Eshelby⁽⁸⁾).

Let the crack join the points $x_1 = \pm c/2$, $x_2 = 0$ and extend indefinitely along the x_3 axis. Then W will have the same form as the expression for the elastic energy density in

an orthotropic medium. But, clearly, the crack is undisturbed by simple tension or shear in its own plane, hence terms in p_{11} , p_{33} and p_{13} will be absent. Thus W has the form $Ap_{22}^2 + Bp_{23}^2 + Cp_{12}^2$.

Now, W is known for the three special cases where p_{22} , p_{23} or p_{12} is the only non-vanishing stress component—these cases are discussed by Griffith,⁽⁹⁾ Eshelby⁽⁸⁾ and Starr⁽¹⁰⁾ respectively—and hence the expression for the energy change per unit length is immediately obtained as

$$W = \frac{1}{8}\pi c^2\mu^{-1}[(1 - \sigma)(p_{22}^2 + p_{12}^2) + p_{23}^2] \quad (1)$$

where μ is the shear modulus and σ Poisson's ratio.

If we have a body containing a very large number of randomly orientated cracks subject to a simple tension T in the direction n_i then we insert the stress $p_{ij} = Tn_in_j$ in (1) and average over all possible directions of the crack and all orientations of its plane. We may equally well leave the crack fixed and average over all directions of the tension, then, since the average values are $\langle n_i^2 \rangle = 1/5$ and $\langle n_i^2 \cdot n_j^2 \rangle = \langle n_j^2 \cdot n_i^2 \rangle = 1/15$, we obtain for the average energy change per unit length of crack

$$\langle W \rangle = \frac{1}{8}\pi c^2\mu^{-1} \frac{(5 - 4\sigma)}{15} T^2 \quad (2)$$

Now for a length of crack per unit volume of ρ the energy density is $(\frac{1}{2} \cdot T^2/E + \langle W \rangle \rho)$ instead of $\frac{1}{2} \cdot T^2/E$ (where E is Young's modulus). The apparent Young's modulus E' is thus given by

$$1/E' = 1/E + 2\langle W \rangle \rho / T^2$$

Substituting for $\langle W \rangle$ from equation (2), replacing μ by $E/2(1 + \sigma)$ and assuming E and E' are only slightly different, we obtain

$$\Delta E/E = \frac{1}{12}\pi c^2\rho^2 \frac{(5 - 4\sigma)(1 + \sigma)}{5} \quad (3)$$

If we average over all directions n_i of the pure shear $p_{ij} = S(n_in_j - \frac{1}{3}\delta_{ij})$ and again compare energy densities we find

$$\Delta\mu/\mu = \frac{1}{12}\pi c^2\rho \frac{(10 - 7\sigma)}{5} \quad (4)$$

For hydrostatic pressure no averaging is necessary and we have immediately for the change in bulk modulus

$$\Delta K/K = \frac{1}{12}\pi c^2\rho^2 \frac{(1 - \sigma^2)}{(1 - 2\sigma)} \quad (5)$$

Consider now the change in resistivity produced by the presence of microcracks. The extra rate of electrical energy dissipation w due to unit length of crack must depend on the current i_i in the same way as the energy dissipation in an orthotropic medium, i.e. $w = \alpha i_1^2 + \beta i_2^2 + \gamma i_3^2$. Stroh⁽³⁾ shows that $\alpha = \gamma = 0$ and $\beta = \pi c^2\rho i^2/4$ where ρ is the resistivity of the material. The average increase in energy dissipation $\langle w \rangle$ for all relative orientations of crack and current is then $\pi c^2\rho i^2/12$, and the apparent resistivity ρ' of a unit cube containing a total length of crack l is given by $\rho' i^2 = \rho i^2 + \langle w \rangle l$. Hence, if ρ and ρ' differ only slightly

$$\Delta\rho/\rho = \frac{1}{12}\pi c^2 l \quad (6)$$

which is the same as that given by Stroh if $N \equiv l$.

Comparing equations (3), (4) and (5) with (6) and putting $\sigma = 1/3$ we obtain

$$-\Delta\rho/\rho = \frac{1}{1.95} \frac{\Delta E}{E} = \frac{1}{1.53} \frac{\Delta\mu}{\mu} = \frac{1}{5.33} \frac{\Delta K}{K} \quad (7)$$

If the cracks are penny-shaped, instead of ribbon-shaped,

the expression for the change in elastic energy will have cylindrical symmetry and as before be independent of p_{11} , p_{33} and p_{13} and thus has the form $Ap_{22}^2 + B(p_{12}^2 + p_{23}^2)$. The cases discussed by Sack⁽¹¹⁾ and Segedin⁽¹²⁾ fix A and B , and, proceeding as before, we obtain

$$\left. \begin{aligned} \Delta E/E &= \frac{16(1 - \sigma^2)(10 - 3\sigma)}{45(2 - \sigma)} a^3 n \\ \Delta\mu/\mu &= \frac{32}{45} (1 - \sigma)(5 - \sigma) a^3 n \\ \Delta K/K &= \frac{16(1 - \sigma^2)}{9(1 - 2\sigma)} a^3 n \end{aligned} \right\} \quad (8)$$

if there are n randomly orientated penny-shaped cracks per unit volume each of radius a .

The increase in electrical energy dissipation due to a penny-shaped crack may be found by considering the two problems: (1) a cavity is introduced into a uniform electric current flow i in a medium of resistivity ρ producing a change in the rate of energy dissipation ω , and (2) a solid of density δ moves with velocity v through a perfect fluid, the total kinetic energy of solid and fluid being t . Then it can be shown that $\omega = 2t$ if $\delta = \rho$, $v = i$ and the body and the cavity have the same form and orientation. Known results (Lamb⁽¹³⁾) for a moving disk then gives

$$\Delta\rho/\rho = \frac{8}{9} a^3 n \quad (9)$$

Comparing equations (8) with (9) we obtain

$$-\Delta\rho/\rho = \frac{1}{1.92} \frac{\Delta E}{E} = \frac{1}{1.50} \frac{\Delta\mu}{\mu} = \frac{1}{5.33} \frac{\Delta K}{K} \quad (10)$$

a result virtually the same as that for ribbon-shaped cracks given in equation (7).

In obtaining these relationships no account has been taken of the interaction between cracks, but, since the disturbance about a crack falls off in much the same way in both the elastic and electric problems, we may hope that the relationships (7) and (10) will not be greatly affected.

Stroh's cracks are wedged open at one end and so the relationships should be valid for compressive as well as tensile stresses. Strictly the crack length should alter with stress through movement of the unwedged end, but this effect should be small for stresses much less than those under which the cracks originally formed.

Using for $\Delta\rho/\rho$ the value used by Stroh for heavily deformed nickel, namely $\Delta\rho/\rho = 3.8 \times 10^{-2}$ we might expect $\Delta E/E \approx 0.08$ and $\Delta K/K \approx 0.2$.

3. Experimental

All the specimens examined were cylindrical bars of about one inch diameter and between ten and twelve inches in length. Six bars of each material were used, three heavily work hardened and three in a well annealed state. The hardening of the copper and nickel bars was obtained by drawing to about a 60% reduction on area, and of the aluminium by deformation in torsion. Details of composition, hardness and electrical resistivity are given in Table 1. (The resistivity was obtained from the fall of potential due to a heavy current flowing along the bars.)

The static determinations of Young's modulus and Poisson's ratio were made in a hydraulic testing machine, longitudinal extension and lateral contraction being measured with the aid of electrical wire resistance strain gauges. The technique of using wire resistance strain gauges has been

widely described and need not be discussed here; it suffices to say that all the usual precautions necessary to obtain accurate measurements were taken, and that multiple gauges were used not only to compensate for non-axial loading, etc., but also to help even-out the slight variations in gauge strain-sensitivity that of necessity occur. The shear modulus was obtained with the aid of a simple optical lever system to indicate the angle of twist under torque.

Table 1. Details of materials

Material	Composition	Hardness (V.H.N.)	Resistivity $\mu\Omega \text{ cm}$ (20°C)
Aluminium, soft	99.8% Al to spec. E.I.A.	17	2.84
Aluminium, hard		46	2.95
Copper, soft	99.85% Cu to B.S.S. 1037	48	1.69
Copper, hard		114	1.76
Nickel, soft	99.4% Ni (0.25% Mn; 0.15% Fe)	87	8.97
Nickel, hard		215	9.16

The dynamic elastic constants were obtained from the resonant frequencies for the longitudinal and torsional modes of vibration of the bars, and Poisson's ratio from the dispersion of extensional waves in cylindrical bars using the Pochhammer-Rayleigh-Chree equation (see, for example, Kolsky⁽¹⁴⁾). The bars were maintained in oscillation, and resonance detected, by an electro-mechanical transducer and a microphone, and also piezoelectrically.

In all cases the maximum strain the bars were subjected to under static conditions was about 2.4×10^{-4} . The soft aluminium and copper bars deformed plastically immediately on application of the smallest load and were therefore slightly deformed in tension to give elastic behaviour up to the strain mentioned above. This plastic strain amounted to somewhat less than a quarter per cent and gave an increase in hardness of one or two points. (The hardnesses given in Table 1 are for this slightly hardened condition.)

The dynamic measurements were made on the same specimens as the static, and the soft bars were therefore in the slightly hardened condition just referred to. The strain suffered by the bars dynamically was very small compared with that under static loading, being in fact about 10^{-8} .

All the measurements were made at room temperature which was always within $\pm 1.0^\circ \text{C}$ of 18.0°C .

4. Results

The values of Young's modulus (E), the shear modulus (μ), and Poisson's ratio (σ), determined experimentally are summarized in Table 2, together with values for the bulk modulus (K) calculated from E and σ , μ and σ , and E and μ , symbolized by $K_{E\sigma}$, $K_{\mu\sigma}$ and $K_{E\mu}$ respectively, and also Poisson's ratio calculated from E and μ , indicated by $\sigma_{E\mu}$.

The static values are the means of values from three bars each carrying eight strain gauges. Graphs of strain against load gave straight lines passing through the origin except for the soft nickel bars. The strain in the soft nickel bars was very slightly larger for increments of load at the beginning of loading (up to about 2.4×10^{-5} strain) than subsequently—perhaps due to the bars being of a magnetostrictive material—and the moduli were taken from the slope of the linear part of the curves.

The accuracy of the values given (based on the standard error of the mean) is conservatively estimated as $\pm 0.5\%$ for Young's modulus and $\pm 1.0\%$ for the shear modulus and Poisson's ratio for the aluminium and copper bars, and for

Table 2. Measured static and dynamic elastic constants (Moduli in units of $10^{11} \text{ dyn cm}^{-2}$)

	Static		Dynamic	
	Soft	Hard	Soft	Hard
Aluminium				
E (meas.)	6.58	6.92	6.9	7.08
μ (meas.)	2.62	2.46	2.67	2.65
σ (meas.)	0.350	0.327	0.364	0.366
$\sigma_{E\mu}$ (calc. from above values)	0.256	0.407	0.292	0.333
$K_{E\sigma}$ (calc. from above values)	7.31	6.67	8.45	8.8
$K_{\mu\sigma}$ (calc. from above values)	7.86	6.2	8.93	9.02
$K_{E\mu}$ (calc. from above values)	4.49	12.3	5.53	7.08
Copper				
E (meas.)	10.7	11.26	12.78	11.60
μ (meas.)	4.75	4.90	4.73	4.70
σ (meas.)	0.355	0.348	0.374	0.395
$\sigma_{E\mu}$ (calc. from above values)	0.126	0.149	0.351	0.234
$K_{E\sigma}$ (calc. from above values)	12.3	12.3	16.9	14.8
$K_{\mu\sigma}$ (calc. from above values)	14.8	14.4	17.2	22.1
$K_{E\mu}$ (calc. from above values)	4.77	5.35	15.1	7.27
Nickel				
E (meas.)	19.75	21.70	20.05	23.5
μ (meas.)	7.95	8.17	7.55	7.72
σ (meas.)	0.303	0.283	0.357	0.349
$\sigma_{E\mu}$ (calc. from above values)	0.301	0.329	0.328	0.562
$K_{E\sigma}$ (calc. from above values)	16.7	16.7	23.4	25.9
$K_{\mu\sigma}$ (calc. from above values)	16.7	16.1	23.9	22.4
$K_{E\mu}$ (calc. from above values)	16.5	21.1	19.4	—

the nickel bars $\pm 0.25\%$ for Young's modulus and the shear modulus and $\pm 0.5\%$ for Poisson's ratio.

Since frequency and linear dimensions can readily be measured to a high order of accuracy, the dynamic values are certainly accurate to $\pm 0.1\%$, or better.

5. Discussion

Perhaps the most obvious feature of the results in Table 2 is the large difference between the static and dynamic values but this will be left for the moment and considered later.

Taking the static and dynamic values as separate and independent sets of results, it will be noticed that although $K_{E\sigma}$ and $K_{\mu\sigma}$ are always similar they usually differ from $K_{E\mu}$ very considerably, and also that Poisson's ratio calculated from E and μ ($\sigma_{E\mu}$) is usually very different from the value obtained by direct measurement (σ), indicating a certain degree of anisotropy. However, the specimens used are such that it is possible to correct for anisotropy by the method of Pursey and Cox⁽¹⁵⁾; values of the isotropic elastic constants so obtained are given in Table 3.

Table 3. *Isotropic static and dynamic elastic constants (Moduli in units of 10^{11} dyn cm $^{-2}$)*

	Static		Dynamic		Bridgman, ⁽¹⁶⁾
	Soft	Hard	Soft	Hard	
<i>Aluminium</i>					
E	6.83	6.68	7.10	7.17	
μ	2.55	2.52	2.62	2.63	
σ	0.339	0.326	0.356	0.363	
K	6.4	6.6	8.3	8.7	7.45
<i>Copper</i>					
E	11.68	12.17	12.89	12.27	
μ	4.43	4.61	4.70	4.50	
σ	0.316	0.320	0.371	0.363	
K	10.6	11.3	14.7	14.95	13.9
<i>Nickel</i>					
E	19.75	21.27	20.24	22.00	
μ	7.95	8.29	7.48	8.16	
σ	0.302	0.282	0.354	0.349	
K	16.6	16.3	23.6	24.3	18.9

Considering the static and dynamic isotropic values in Table 3 separately there is no consistent decrease in the elastic constants on cold-working; indeed, in most cases the values for the hardened material is greater than for the soft. Particularly noticeable is the similarity between the values for the bulk modulus, when from the electrical resistivities, according to equations (7) and (10), the values for the hardened materials would be expected to be about 10% less for nickel and 20% for aluminium and copper.

It is concluded, therefore, that the hypothesis that on cold-working dislocation pile-up to form microcracks in metals, is not correct. Likewise the results would not support any suggestion that any other imperfections which would behave like microcracks—such as planar groups of vacancies—are produced by cold-working.

Concerning Seeger's views on the cause of resistivity increase on cold-working, if it is supposed that all the stored energy is in the dislocations edging stacking fault areas, then using equations (6) and (9), assuming the faults are opaque to electrons, and are large compared with the wavelength of the conduction electrons, we may determine the width c , or the diameter a , of the fault areas, and the total area. We find that $c \approx a \approx 10^{-6}$, and that faults occur every few hundred atomic layers. (Even if the reflexion coefficients of the fault area is a lot less than one, these values are, of course, not greatly affected.) Smallman and Westmacott⁽¹⁷⁾ have deduced from X-ray diffraction results that stacking faults can occur every 300 (111) atomic planes in copper and every 150 in nickel.

Now correction for anisotropy by the method of Pursey and Cox leads to values for Young's modulus and the shear modulus from which Poisson's ratio and the bulk modulus are then obtained. Hence, since both Poisson's ratio and the bulk modulus are very sensitive to the exact values of Young's modulus and the shear modulus, the differences between the bulk moduli for the soft and hardened materials may not be significant. Nevertheless in every case the bulk modulus for the hardened material is noticeably greater than for the soft ($K_{\text{hard}} > K_{\text{soft}}$), save for one exception, namely for the static measurements on nickel. An increase in bulk modulus could be caused by the production of interstitials, but according to the theoretical estimates of Dienes⁽¹⁸⁾ and Nabarro⁽¹⁹⁾ something like a half per cent of interstitials would be required to explain the values found. However, since the values for the

bulk moduli for the soft and hardened conditions are so nearly the same (still considering the static and dynamic results separately), it is reasonable to suppose that the changes in Young's modulus and the shear modulus are real.

The remaining point to be considered is the difference between the static and dynamic values, and here the most striking results are perhaps that consistently the dynamic Poisson's ratio is greater than the static ($\sigma_{\text{dynamic}} > \sigma_{\text{static}}$), and that consistently the dynamic bulk modulus is much greater than the static ($K_{\text{dynamic}} > K_{\text{static}}$), with Bridgman's⁽¹⁶⁾ values of the bulk modulus, determined directly, falling roughly mid-way between our static and dynamic values. The usual thermodynamic relationship between the isothermal and adiabatic moduli is obviously quite inadequate to explain the differences as exhibited in either Tables 2 or 3, and if the work of Hughes and Kelley⁽²⁰⁾ and Lazarus⁽²¹⁾, on the effect of pressure and unidirectional stress on elastic constants is any guide, it seems unlikely that deviations from a strictly linear relationship between stress and strain will provide an explanation. Hence there seems little doubt that the same physical constants are not determined by the static and dynamic methods, contrary to usually accepted views. Indeed, it is interesting to note that, judging from the values of Poisson's ratio measured (σ) and calculated from Young's modulus and the shear modulus (σ_{E}) in Table 2, the anisotropy of the bars is different statically and dynamically and in one case, that of hardened aluminium, the "sense" of the anisotropy is different statically and dynamically. Values of the bulk modulus, calculated from values of Young's modulus and the shear modulus given by other authors, are found to be generally low (compared with Bridgman's) for measurements made early in the century (and likely to be by static methods), and high for more modern determinations made by dynamic methods. Markham⁽²²⁾ has given static and dynamic values—the latter by an ultrasonic pulse technique—for Young's modulus and Poisson's ratio for ten different steels, and the values of the bulk modulus and Poisson's ratio calculated from these are given in Table 4. The dynamic values of the bulk modulus are consistently greater than the static, by 10% or more, and the dynamic Poisson's ratios are always greater than the static, except for the last steel in the table, where it seems likely that the table is in error. Markham's results, then, show the same differences between static and dynamic values for steel as ours for aluminium, copper and nickel.

Table 4. *Static and dynamic values of σ and K calculated from values of E and μ for various steels given by Markham⁽²²⁾*

Steel	σ		K	
	Static	Dynamic	Static ($\times 10^{11}$ dyn cm $^{-2}$)	Dynamic
0.4% C	0.271	0.287	21.8	24.0
0.4% C	0.275	0.286	22.3	24.0
0.9% C	0.285	0.292	22.7	24.3
3.0% Ni (30–35 tons)	0.270	0.289	21.2	23.6
3½% Ni (45–50 tons)	0.280	0.290	22.1	23.6
CrVa	0.252	0.287	20.4	24.2
3% NiCr	0.272	0.290	21.2	23.5
3½% NiCr	0.257	0.290	19.8	22.7
NiCrMo (75–80 tons)	0.259	0.290	20.2	23.6
NiCr (95–105 tons)	0.327(?)	0.290	29.2(?)	23.5

That any type of defect, or a relaxation phenomenon, is responsible for this difference appears unlikely; perhaps the explanation lies along the lines of the views of Laval⁽²³⁾ and

Raman and his collaborators^(24, 25) who maintain that the conventional theory of elasticity requires modification.

Acknowledgements

The author is much indebted to Dr. J. D. Eshelby without whose help this work could not have been undertaken, and also to The Aluminium Development Association, The Mond Nickel Co. Ltd., and Thomas Bolton and Sons, Ltd., who provided the aluminium, nickel and copper bars.

References

- (1) MOTT, N. F. *Proc. Roy. Soc. A*, **220**, p. 1 (1953).
- (2) STROH, A. N. *Proc. Roy. Soc. A*, **218**, p. 391 (1953); **223**, p. 404 (1954); **232**, p. 548 (1955).
- (3) STROH, A. N. *Phil. Mag.* (8), **2**, p. 1 (1957).
- (4) CLAREBROUGH, L. M., HARGREAVES, M. E., and WEST, G. W. *Proc. Roy. Soc. A*, **232**, p. 252 (1955); *Phil. Mag.* (8), **1**, p. 528 (1956).
- (5) BOAS, W. *Dislocations and Mechanical Properties of Crystals* (Lake Placid Conference Report), Table I, p. 340 (New York: John Wiley and Sons, Inc., 1956).
- (6) SEEGER, A. *Dislocations and Mechanical Properties of Crystals* (Lake Placid Conference Report), p. 347 (New York: John Wiley and Sons, Inc., 1956); *Canad. J. Phys.*, **34**, p. 1219 (1956).
- (7) STROH, A. N. *Advances in Phys.*, **6**, p. 459 (1957).
- (8) ESHELBY, J. D. *Proc. Roy. Soc. A*, **241**, p. 376 (1957).
- (9) GRIFFITH, A. *Proc. Intern. Congr. App. Mech. (Delft)*, p. 55 (1924).
- (10) STARR, A. T. *Proc. Camb. Phil. Soc.*, **24**, p. 489 (1928).
- (11) SACK, R. W. *Proc. Phys. Soc. (London)*, **58**, p. 729 (1946).
- (12) SEGEDIN, C. M. *Proc. Camb. Phil. Soc.*, **47**, p. 396 (1951).
- (13) LAMB, H. *Hydrodynamics*, p. 132 (London: Cambridge University Press, 1916).
- (14) KOLSKY, H. *Stress Waves in Solids*, p. 59 (London: Oxford University Press, 1953).
- (15) PURSEY, H., and COX, H. L. *Phil. Mag.* (7), **45**, p. 295 (1954).
- (16) BRIDGMAN, P. W. *The Physics of High Pressures*, 2nd ed. (London: G. Bell and Sons, Ltd., 1949).
- (17) SMALLMAN, R. E., and WESTMACOTT, K. *Phil. Mag.* (8), **2**, p. 669 (1957).
- (18) DIENES, G. J. *Phys. Rev.*, **87**, pp. 228, 666 (1952).
- (19) NABARRO, F. R. N. *Phys. Rev.*, **87**, p. 665 (1952).
- (20) HUGHES, D. S., and KELLEY, J. L. *Phys. Rev.*, **92**, p. 1145 (1954).
- (21) LAZARUS, D. *Phys. Rev.*, **76**, p. 545 (1949).
- (22) MARKHAM, M. P. *Brit. J. Appl. Phys.*, Supplement No. 6, *Physics of Non-Destructive Testing*, p. S 56 (1957).
- (23) LAVAL, J. *C.R. Acad. Sci. (Paris)*, **232**, p. 1847 (1951); **238**, p. 1773 (1954); *J. Phys. Radium*, **18**, pp. 289, 369 (1957); **19**, p. 509 (1958).
- (24) RAMAN, SIR C. V., and KRISHNAMURTI, D. *Proc. Ind. Acad. Sci.*, **42**, p. 111 (1955).
- (25) RAMAN, SIR C. V., and VISWANATHAN, K. S. *Proc. Ind. Acad. Sci.*, **42**, pp. 1, 51 (1955).

Theory of the parallel plate viscometer

by A. N. GENT, B.Sc., Ph.D., A.Inst.P., The British Rubber Producers' Research Association, Welwyn Garden City, Herts

[Paper first received 7 September, and in final form, 20 October, 1959]

Abstract

The theoretical treatment for the rate of approach of two parallel circular plates separated by a viscous liquid is subject to the limiting condition that the separation of the plates must be small compared to the test-piece radius. The theory is extended to apply to test-pieces of any thickness and the modified treatment is shown to be in accord with experimental measurements on a sample of coal-tar pitch.

Introduction

THE parallel plate viscometer takes two forms: (a) when the sample fills the space between the plates and exudes from between them when the compressive load is applied; and (b) when the radius of the plates is larger than that of the sample throughout the test. The Wallace plastimeter⁽¹⁾ is representative of method (a), in which the effective radius of the test-piece is constant and given by the radius of the plates, and the Williams plastimeter⁽²⁾ of method (b), where the effective volume of the test-piece is constant.

A theoretical solution has been obtained⁽³⁻⁶⁾ for the rate

of approach of two parallel circular plates separated by an incompressible Newtonian viscous liquid, and may be employed in both cases in order to determine viscosities in the range 10^4 to 10^9 poises.⁽⁶⁾ However, the theory is subject to the limiting condition that the separation of the plates h must be small compared to the test-piece radius R ; it has been suggested⁽⁶⁾ that h must be less than $R/10$ for the theoretical relations to apply. This has several disadvantages. Firstly, for very viscous materials, relatively large forces must be applied. Secondly, when the test-piece thickness is sufficiently small, it is difficult to determine accurately although, because it appears in the theoretical relations in the form h^2 and h^4 , considerable accuracy is desirable. Thirdly, any departure from the boundary conditions assumed to hold at the plates is clearly more serious for relatively thin test-pieces.

The theoretical treatment is extended below to apply to test-pieces of any thickness. Only method (b) is considered, because this appears to be experimentally more convenient.⁽⁶⁾ In a later section, experimental measurements on a sample of coal-tar pitch are described and compared with the predictions of the theoretical treatment.

Theoretical treatment

An approximate theoretical relation has recently been obtained^(7, 8) for the stiffness of a circular disk of an incompressible elastic material subjected to axial compression between two parallel rigid plates to which it adheres. The deformation is assumed to comprise two parts: (1) a simple compression given by the approach of one rigid plate towards the other; and (2) the subsequent displacements that are necessary to restore points in the planes of the rigid plates to their original positions in these planes. The corresponding forces F_1 and F_2 which must be applied to the plates to maintain the two displacement systems are then calculated, their sum giving the total compressive force.

The second component of force F_2 is only calculable by means of the simplifying assumption that horizontal planes remain plane during the deformation, as seems probable when the cylinder radius is much greater than the height. However, when the radius is comparable to or smaller than the height, the force F_2 is relatively small, and, hence, when the assumption seems improbable, its consequences are relatively unimportant. The relation obtained should therefore be applicable to a wide range of thicknesses, as is found experimentally.^(7, 8)

On substituting the viscosity η for the rigidity modulus and the rate of approach dh/dt of the plates for the elastic displacement of one plate with respect to the other, the corresponding forces in the viscous case may be obtained immediately as

$$F_1 = -\frac{3\eta V \frac{dh}{dt}}{h^2},$$

and:

$$F_2 = -\frac{3\eta V^2 \frac{dh}{dt}}{2\pi h^5},$$

where h is the separation of the plates at time t and V is the volume of the test-piece. On integrating between the limits $t = t$ and $t = 0$, the plate separation h at a time t may be obtained as a function of the applied force $F (= F_1 + F_2)$ in the form:

$$\frac{Ft}{3\eta V} = \left(\frac{1}{h} - \frac{1}{h_0}\right) + \frac{V}{8\pi} \left(\frac{1}{h^4} - \frac{1}{h_0^4}\right) \quad (1)$$

where h_0 is the plate separation at $t = 0$. The second term on the right-hand side of equation (1) corresponds to the solution given by Dienes and Klemm,⁽⁶⁾ stated to be valid when the test-piece radius R is greater than $10h_0$. When R is equal to $10h_0$, the first term on the right-hand side is at most only 2% of the second term and hence may be considered negligibly small, in agreement with their observations.

Experimental results

A sample of coal-tar pitch was prepared in the form of a solid cylinder 1.3 cm in height and 0.33 cm in radius, and placed between two horizontal flat steel plates so that its axis was normal to the plane of the plates. Measurements were made by means of a dial gauge of the plate separation, that is, the height of the test-piece, at various times after the application of a load of 5 kg to the upper plate. The measured plate separation h is plotted in Fig. 1 against the time t for which the load had acted.

The condition necessary for the restricted theory to apply, that the radius of the sample is greater than $10h$, does not

obtain for a sample of the volume used until the height is less than 0.115 cm. It was found on plotting h^{-4} against t that although a linear relationship existed for small values of h as the restricted theory predicts, serious departures from linearity were evident for values of h greater than about 0.15 cm, that is, for the majority of the measurements.

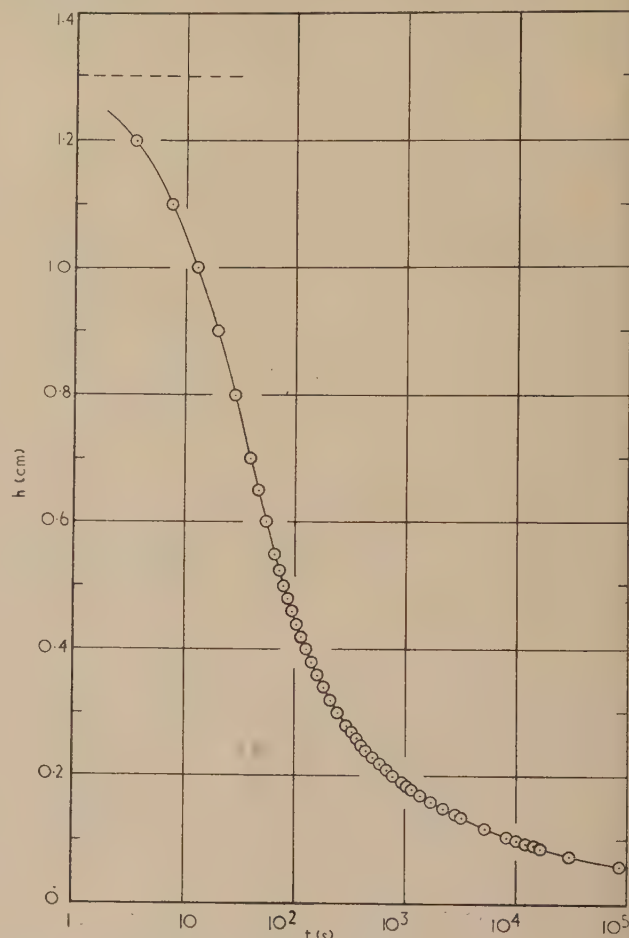


Fig. 1. Plate separation h after a time t under a constant load of 5 kg

Values of the expression on the right-hand side of equation (1), denoted $\phi(h)$, were then calculated and plotted against the time t for which the load had been applied, using logarithmic scales. The resulting relationship is shown in Fig. 2. It is seen to be substantially linear over the entire range of measurement with a slope of unity, indicating proportionality between $\phi(h)$ and t , as equation (1) predicts. From the intercept and the measured test-piece volume, namely 0.451 cm³, the viscosity of the coal-tar pitch used was calculated to be 1.96×10^8 poises.

Measurements were made of the viscosity of the same material by a Couette method.⁽⁹⁾ The observed rotation of the inner cylinder of the viscometer is plotted in Fig. 3 against the time of action of the constant torque applied to it. The resulting relationship is seen to be accurately linear, and, on releasing the inner cylinder, no measurable recovery was observed. The material seems, therefore, to be satisfactorily Newtonian. From the slope of the linear relation of Fig. 3 and the dimensions of the instrument the viscosity was calculated to be 1.92×10^8 poises.

The excellent agreement with the value obtained using the

parallel-plate viscometer is probably fortuitous to some extent. The experiments were carried out at $20^{\circ}\text{C} \pm 0.25^{\circ}\text{C}$, while the viscosity was found to depend markedly on temperature, being reduced by 15% for a 1°C rise. A discrepancy

test-piece thickness upon the time of action of the compressive force over a wide range of thickness.

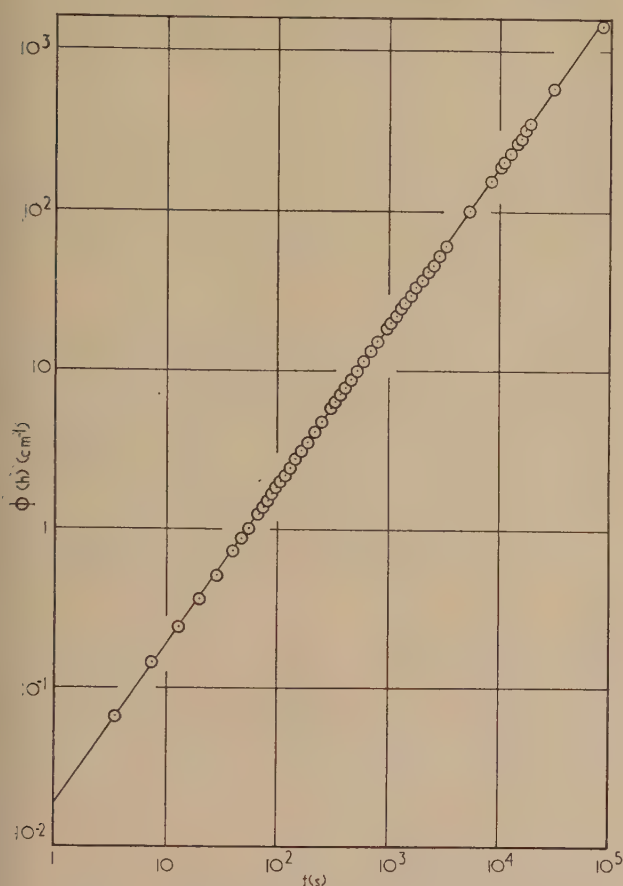


Fig. 2. Experimental relation between $\phi(h)$ and t

of up to 8% (corresponding to a temperature variation of up to 0.5°C) would therefore have been acceptable.

It is concluded that the modified theory of the parallel-plate viscometer successfully describes the dependence of

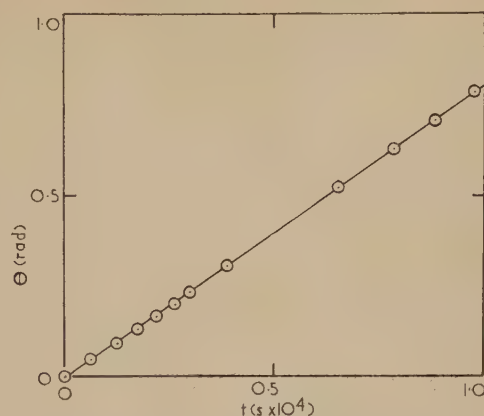


Fig. 3. Rotation θ of the inner cylinder of the viscometer after a time t under a constant torque

Acknowledgements

This work arises out of a programme of research undertaken by the Board of the British Rubber Producers' Research Association. The author acknowledges helpful discussions with Mr. N. E. Waters, and assistance with the experimental measurements by Mr. D. J. Hill, of these laboratories.

References

- (1) SCOTT, J. R. *I.R.I. Trans*, **29**, p. 175 (1953).
- (2) WILLIAMS, I. *Industr. Engng Chem. (Industr.)*, **16**, p. 362 (1924).
- (3) STEFAN, M. J. *Akad. Wiss. Wien Math.-Naturwiss. Kl. Abt. IIa*, **69**, p. 713 (1874).
- (4) HEALEY, A. *I.R.I. Trans*, **1**, p. 334 (1926).
- (5) SCOTT, J. R. *I.R.I. Trans*, **7**, p. 169 (1931).
- (6) DIENES, G. J., and KLEMM, H. F. *J. Appl. Phys.*, **17**, p. 458 (1946).
- (7) GENT, A. N. *Rubb. Chem. Technol.*, **31**, p. 395 (1958).
- (8) GENT, A. N., and LINDLEY, P. B. *Proc. Instn Mech. Engrs (London)*, **173**, p. 111 (1959).
- (9) LEE A. R., and WARREN, J. B. *J. Sci. Instrum.*, **17**, p. 63 (1940).

CORRESPONDENCE

Interaction between two equal-sized equal-settling spheres moving through a viscous liquid

In a paper by Eveson, Hall and Ward, published on p. 43 in the January 1959 issue of this *Journal*, it has been stated that, in experiments involving two identical spheres falling in mutual proximity through a viscous fluid,

- (a) no rotation of the spheres took place,
- (b) the relative positions of the spheres was maintained,

when the Reynolds number of an individual sphere, based on diameter and terminal velocity, was less than 10^{-2} . The second of these conclusions has recently been supported by the theory of Kynch* based on Stokes' approximations.

* KYNCH, G. J. *J. of Fluid Mechanics*, **5**, Pt. 2, p. 193, 1959.

These observations are not consistent with the general conclusions drawn from experiments, covering a range of Reynolds numbers from 10 to 10^{-3} , which we have been carrying out using solid spheres in castor oil at 23°C . The oil was contained in a Perspex tank, of 20 cm square cross-section and 90 cm deep. Observations were carried out over the middle 40 cm of the spheres' 90 cm fall. They showed that:

- (i) a rotational motion was developed in all cases, and was such that each sphere rotated about its horizontal diameter perpendicular to the line of centres, the left-hand sphere rotating clockwise and the right-hand sphere anti-clockwise;
- (ii) the relative positions of the two spheres changed with time in the sense that the trailing sphere tended to

overtake the leading sphere; the two spheres ultimately stabilizing in the same horizontal plane. This effect increases with Reynolds number, but it is not, however, readily apparent over short distances of travel when the Reynolds number is of the order of 10^{-3} .

We feel these results can be justified by simple reasoning. In the Stokes' flow round a single sphere the fluid is subjected to a velocity shear and so, when a second sphere is introduced into the fluid, the first-order approximation (which ignores the more complex interactions which arise) indicates that the spheres should rotate in the sense we have observed.

The Stokes' solution, as Kynch found, leaves the relative positions unchanged. This, however, ignores inertia terms in the equation of motion. Oseen's well-known attempt to account for inertia produces a certain amount of asymmetry in the flow around a single sphere about the horizontal plane through its centre. Applying this small modification to our "first-order" solution for the motion of two spheres, it is seen that inertia results in a tendency for the spheres to align themselves in the same horizontal plane qualitatively as observed.

Chemical Defence Experimental
Establishment,
Porton Down,
Salisbury, Wilts.

H. W. MATTHEWS
F. B. SMITH

[13 July, 1959]

During the course of an investigation, which is an extension of the work described in the previous paper, we have

noted that two equal interacting spheres rotate in the manner described by Matthews and Smith. The rate of rotation is small. For instance, two 0.345 cm diameter Perspex spheres settling through castor oil at 20° C, with their line of centres horizontal and with a distance of about 1.2 diameters between sphere centres, rotated with an angular velocity of about 0.1 rad/s. At such low rates of rotation the Coriolis force is negligible compared with the gravitational force acting on the sphere, and the rate of rotation decreases with increase in the distance between the sphere centres.

Provided the two spheres were identical, we have never observed the phenomenon described in item (ii) by Matthews and Smith. Allowing for the low Reynolds numbers obtaining in most of our experiments, and for the fact that the motion of the interacting spheres was followed over a relatively short distance (about 20 cm), we believe that a significant change in the relative positions of the two interacting spheres should have been detectable in our experiments if, in fact, the spheres were moving with different velocities. It would be interesting to have details of the spheres and of the experimental technique, particularly for sphere release, used by Matthews and Smith. Also it would be interesting to know if, in their experiments, the trailing sphere caught up with the leading sphere for all initial positions of the two spheres relative to each other, including the case where two spheres are falling one directly above the other.

Department of Mining,
University of Birmingham

G. F. EVESON
[31 August, 1959]

Journal of Scientific Instruments

Contents of the February issue

PAPERS

- X-ray diffraction by single crystals at low temperatures: a cryostat for use with liquid hydrogen. By J. H. Robertson.
- Simple device for use with platform weighbridges in the accurate determination of burning rates. By J. E. Roughton.
- An electroluminescent digital indicator with a silicon carbide coding matrix. By D. H. Mash.
- Some techniques for recording and measuring time-resolved spectra. A. H. Gabriel.
- An electromicrobalance for weighing fibres. By F. R. Morgan.
- Portable airglow photometer. By B. J. O'BRIEN, and G. De La Harpe.
- Direct method for determining the velocity of nuclear particles. By B. F. Hampton.
- Recording calorimeter for the measurement of heats of wetting, mixing, or solution. By F. A. P. Maggs and P. H. Schwabe.
- Twin-head goniometer for the study of diffusely reflected X-rays. W. A. Wooster and G. A. Wooster.

LABORATORY AND WORKSHOP NOTES

- Simple method of mounting and stretching thin gauze, sheet or foil. By P. A. Einstein.
- Simple refrigerant level controller for cold traps. C. W. Nutt and A. J. Biddlestone.
- Crystal oscillation mechanism for use with automatic X-ray diffractometers. U. W. Arndt, T. H. Faulkner and D. C. Phillips.
- Simple method of temperature control. By H. A. Vodden.
- Valve and adapter for the grease-free connexion of glass sample tubes to a mass spectrometer inlet system. By J. R. Richards.
- Diffuse-light integrator. By N. W. Wooten.
- Bubble method for magnetic susceptibility of liquids. By A. O. Mathai.

NOTES AND NEWS

New instruments, materials and tools

THIS JOURNAL is produced monthly by The Institute of Physics, in London. It deals with all branches of applied physics (including theory and technique). All rights reserved. Responsibility for the statements contained herein attaches only to the writers.

EDITORIAL MATTER. Communications concerning editorial matter should be addressed to the Editor, The Institute of Physics, 47 Belgrave Square, London, S.W.1. (Telephone: Belgravia 6111.) Prospective authors are invited to prepare their scripts in accordance with the *Notes for Authors*. (Price 3s. 6d. including postage.)

REPRODUCTION. The Institute of Physics is a signatory to The Royal Society's Fair Copying Declaration. Details may be obtained upon application from The Royal Society, London, W.1.

ADVERTISEMENTS. Communications concerning advertisements should be addressed to the agents, Messrs. George Jackson (Fleet St.) Ltd., Cliffords Inn, Fleet Street, London, E.C.4. (Telephone: Holborn 3611-2.)

CLAIMS FOR MISSING JOURNALS. Claims from regular subscribers to this *Journal* for missing numbers will only be considered if received within 60 days of the date of mailing plus normal outward time of transit and time for lodging the claim. Losses attributable to failure to notify a change of address or to similar omissions will not be considered.

SUBSCRIPTION RATES. A new volume commences each January. The charge is £6 per volume (\$17 U.S.A.), including index (post paid), payable in advance. Single parts, so far as available, may be purchased at 12s. 6d. each (\$1.75 U.S.A.), post paid, cash with order. Orders should be sent to The Institute of Physics, 47 Belgrave Square, London, S.W.1, or to any bookseller.

Summarized proceedings of a conference on X-ray analysis Leeds, April 1959

The 1959 Spring Conference of the X-Ray Analysis Group of The Institute of Physics was held in the University of Leeds on 17 and 18 April, 1959. The conference was devoted to clay minerals and biological fibres and the proceedings are summarized in this Report.

PROF. G. W. BRINDLEY of the Department of Ceramic Technology, The Pennsylvania State University, and Prof. W. T. ASTBURY of the Department of Bio-molecular Structure, University of Leeds, were invited to survey the present situation and possible future developments in their respective fields.

Clay minerals

Prof. BRINDLEY first gave a brief survey of the typical silicate layer structures found in clays. The types of layer found in each clay were described, and it was shown how the polymorphism which is common in these minerals is caused by the variety of sequences in which the layers may be stacked together. Detailed structure determinations of many clays have still to be carried out, and may be done either by X-ray examination of analogous macrocrystalline materials, or by

lying clay mineral structure are understood, and that it is unlikely that any radically new structure will be found. Detailed structure analysis of dickite by Newnham and Brindley⁽¹⁾ has shown how the distortions and rotations of the silicon-oxygen tetrahedra are responsible for the previously unexplained cell parameters of some minerals such as kaolinite. This work has also found application in work on micas, in which Bradley has taken the departure from ideal geometry as a basis for a study of cell parameters, and Radoslovich has suggested an explanation for the relative frequency of occurrence of the various polymorphs of mica. More refined structure analysis has also been carried out on chlorites, in which the work of Brindley, Oughton and Robinson has been extended by Steinfink to a detailed study of particular polymorphs.

In discussing possible future developments, Prof. Brindley stressed the potentialities of electron diffraction in clay mineral work, where X-ray examination of single crystals is often impossible. It would eventually be accepted that an examination of a clay mineral requires X-ray powder photography of randomly orientated crystallites, similar work on specimens with a high degree of orientation, electron micrography and electron diffraction by single crystals. Examples of electron micrography and electron diffraction patterns of

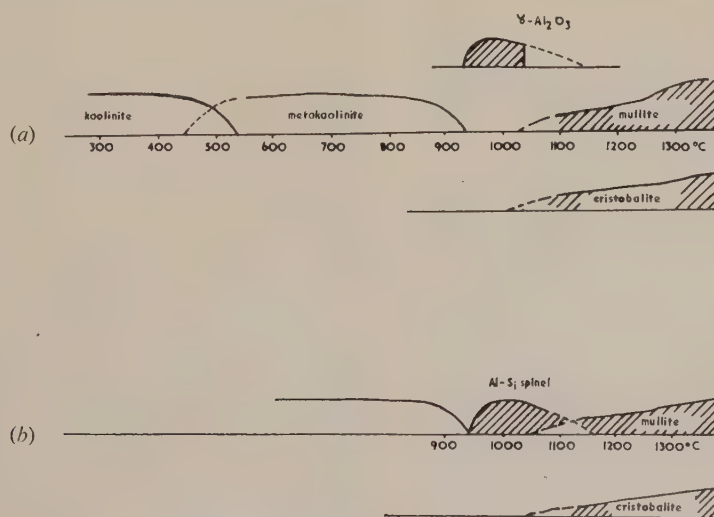


Fig. 1. Kaolinite-Mullite transformation series
(a) Old version; (b) new version.

electron diffraction studies of clays themselves, when the experimental technique of the latter method has been improved sufficiently to make quantitative work possible. Other problems still not fully understood are interstratification in clay minerals and the thermal reactions occurring in clays and minerals generally.

In a review of the present state of knowledge of each class of clay mineral, it was pointed out that the principles under-

sepiolite and scarbroite were shown, to illustrate the ease with which information can be obtained in the early stages of an examination by this method.

In conclusion, Prof. Brindley described how ideas on the thermal transformations of kaolinite have been revised in the light of recent single-crystal work.⁽²⁾ The principal difference between the old and new versions (Fig. 1) lies in the transformation at 925°C. A cubic phase with an aluminium-

silicon spinel-type structure is formed, the [111] direction of the spinel structure being perpendicular to the cleavage plane of the kaolinite. With this orientation, the hexagonal oxygen layers of the kaolinite fall naturally into position in the spinel structure with very little rearrangement taking place.

During the discussion which followed, Mr. H. P. ROOKSBY (General Electric Co. Ltd., Wembley) suggested that it would be wise to regard these transition phases as ordered aggregates rather than as true single crystals. Dr. J. W. JEFFERY (Birkbeck College, London) said that the movement of silicon through an oxygen framework from one tetrahedral position to another should now, perhaps, be expected in high-temperature transformations, since this had been found in studies of the thermal transformations of the calcium silicates.

Dr. D. M. C. MACEWAN (Queen's College, Dundee) described a project of extending the series of curves calculated by Brown and MacEwan so as to provide an atlas of inter-stratification effects. The Fourier transform method was chosen, and gave results which agreed well with those obtained by the Hendricks-Teller method.

The diffraction given by a mixed layer structure may be represented by

$$I(r^*) = \Theta(\theta) |F(r^*)|^2 \Phi(r^*)$$

where Θ is the usual angular factor, $F(r^*)$ the structure factor of the layer, and Φ a function representing the effect of the mixing. This assumes a single value of F , but if F is variable one cannot separate Φ from $|F|^2$. Cases involving a single value of F , and where it is useful to consider Φ separately, are, however, numerous enough to make the results widely applicable.

Calculations for a Gaussian distribution of particle size are giving better results than earlier ones made for a definite number of layers per particle. A series of probability coefficients (σ_n) was calculated for each type of mixture (e.g. 0.4/0.6 random). Once these have been calculated, they will do for any pair of spacings, and only the appropriate spacing values have to be inserted in order to obtain the final table for calculation. Where F is variable, graphs of the function $F_1 F_2^* + F_2 F_1^*$ must also be made.

The calculations were made for a series of spacing ratios very close to actual observable spacings, and also with Φ having a finite repeat distance S . The function being then symmetrical about $\frac{1}{2}S$, it need only be represented up to this value to calculate diffraction effects up to any value of r^* .

It has been noted that a small change in the spacing ratio may modify the intensities of the maxima drastically, though not their positions. This observation may be of value for the quantitative determination of mixed layer minerals.

Mr. H. P. ROOKSBY then described some examples of pseudomorphic transformations in the iron oxide and aluminium oxide systems, and indicated a few new points of interest concerning the crystallography of the anhydrous oxides.

Electron micrographs show that goethite crystals change to haematite without change of shape. During the change, the hexagonal close-packed oxygen framework of goethite suffers little disturbance. The X-ray photographs show that small sub-units of haematite are first formed, reflexions corresponding to these sub-units being sharp. As the temperature is raised, ordering of the iron atoms throughout larger units of the oxygen framework takes place, and the definition of the rest of the reflexions improves.

The transformation of lepidocrocite to γ -ferric oxide was discussed as an example of a change involving cubic close-

packing of oxygen atoms. The X-ray diffraction patterns of γ -ferric oxide show superlattice lines, and several types of superlattice have been found. The various super-structures may be caused by the ordering of the vacant sites present in the structure.

The orientation relationship between γ -ferric oxide and lepidocrocite is very similar to that between the aluminium oxyhydroxide boehmite and its transformation product δ -alumina. But in this latter case a complication arises due to what appears at first sight to be a tetragonal deformation of the spinel structure. Further information has recently been gained from examination of a specimen of flame-sprayed alumina which was found to be in the γ -form. By heating at 1100°C for an hour, this could be converted entirely to the δ -form. From this, complete powder diffraction data have been compiled for the δ -structure, and it now appears probable that, whilst the departure from the cubic spinel arrangement may be basically tetragonal, a superstructure exists of which one axis is a multiple of the spinel dimension. It is possible that there is an analogy between this δ -structure and tetragonal γ -ferric oxide.

During the discussion, Dr. H. SAALFELD suggested that the differences between the δ -structure and a cubic spinel may be similar to those which exist between θ - Al_2O_3 and β - Ga_2O_3 . Prof. BRINDLEY said that recent work by Dr. M. Nakahira and himself had shown that when boehmite, $\text{AlO}(\text{OH})$, prepared from gibbsite, was carefully dehydrated, a long spacing ranging from about 30 to 90 Å was obtained, which became larger as the dehydration proceeded towards completion. No evidence was obtained for a specific structure corresponding to the composition $\text{Al}_2\text{O}_3 \cdot \frac{1}{2} \text{H}_2\text{O}$ or HAl_2O_5 (hydrogen spinel), though water contents of this order yielded a long spacing within the range observed. Higher order reflexions were not obtained, and it is considered that the residual OH groups are statistically ordered with an average lattice spacing in the range 30–90 Å.

Prof. J. J. FRIPIAT (University of Louvain, Belgium) gave an account of a study of the surface chemistry of the aluminosilicates, the problems investigated being the atomic structure of the surface, its electrical charge and the nature of the functional groups located on the surface.

A series of aluminosilicate gels was prepared with increasing alumina content and the charge on the particles of each gel was measured. The charge was found to pass through a maximum value, and this corresponded to a similar maximum in the measured values of cation exchange capacity (c.e.c.). In an examination of kaolinite, the c.e.c. appeared to be dependent on the number of aluminium ions in tetrahedral co-ordination located on the edges of the crystallites.

The chief difficulty in investigating the nature of the groups on the surface of aluminosilicates is that these groups are mainly OH ions which are difficult to distinguish from adsorbed water molecules. Estimates of the surface density of OH ions were made using infra-red absorption and conductimetric methods. Absolute methods of measuring surface density of OH ions were developed which involved replacement of the OH by OD ions.

Dr. G. BROWN (Rothamsted Experimental Station, Harpenden), in a paper by himself and Dr. I. STEPHEN, described an investigation of iddingsite which was carried out in order to find the reason for its optical homogeneity and to obtain information on the naturally-occurring alteration process from olivine to iddingsite.

Oscillation and Weissenberg photographs revealed the presence of three constituents of the crystals examined. Sharp reflexions were obtained from the unchanged olivine

in the crystals, and the remaining reflexions, given by the transformation products, were shown to be those of goethite in three orientations and a layer silicate.

Both olivine and goethite contain hexagonal close-packed sheets of oxygen atoms, and to form goethite from olivine in the three orientations found in these crystals, only slight adjustments of the oxygen framework are required. The cation rearrangements could easily take place by ionic diffusion.

The structure of the layer silicate is highly disordered. The hexagonal layers are stacked parallel and equidistant, but random shifts of the layers occur in directions parallel to the layers. From such lattice parameter measurements as could be made on this mineral, the layer silicate appeared to be probably of the vermiculite or smectite group, though a detailed examination was not made. The formation of a layer silicate from olivine does involve some disruption of the oxygen framework of the olivine.

This investigation has shown that the unusual feature of iddingsite, its optical homogeneity, is caused by the regular orientation of the small crystals of both components throughout a single grain. The parallel alinement arises from the nature of the alteration, the products of which inherit, goethite completely and the layer silicate partly, the oxygen framework of the original olivine.

In the discussion, it was reported that Dr. P. GAY and Mr. R. J. LEMAITRE (University of Cambridge) have reached similar conclusions to those of Brown and Stephen, and have shown also that the alteration of the olivine to the layer silicate may probably proceed by way of the formation of chain structures.

Dr. W. E. WORRALL (University of Leeds), in a paper by himself and Prof. A. L. ROBERTS, gave the results of a study of some German clays. Their cation exchange capacity (c.e.c.) was found to be related to the disorder present in the structure and the degree of ionic substitution. Similar relations had already been found in British clays, and comparisons between the British and German clays were made.

In an earlier investigation by Dr. Worrall, samples of several British fireclays were separated into different-sized fractions by centrifugal sedimentation. Each fraction was analysed both chemically and by X-ray diffraction, and its c.e.c. determined. Three important features of the results were noticed. Firstly, as the particle size decreased, the chemical composition approached that of pure kaolinite. Secondly, there was a deficiency of aluminium, caused by substitution of iron and magnesium. Thirdly, the c.e.c. of the finer fractions was independent of particle size. It seems likely that the high c.e.c. can be accounted for by the substitution, and is certainly not caused simply by the small particle size.

A similar examination of the German clays was carried out in order to find whether fireclay minerals existed with degrees of substitution different from those of the British clays. The results confirmed that the German clays did contain such minerals, and that the c.e.c. was roughly proportional to the degree of substitution, although where Fe^{3+} replaces Al^{3+} , disorder may result without affecting the c.e.c.

Prof. J. J. FRIPIAT, in discussion, stated that his work led to conclusions opposed to those of Dr. Worrall, in that the c.e.c. of pure kaolin was found to be dependent upon particle size. It has also been shown that the c.e.c. can be increased, not only by ionic substitution, but by the adsorption of silica on the edges of the kaolinite crystals, forming a zeolite-type material.

Dr. F. VAUGHAN (British Ceramics Research Association, Penkhull, Stoke-on-Trent) described work on the dehydration products of kaolinite. The paper began with a review of previous work on the thermal dehydration and structural transformations of kaolinite. In particular, the interpretations to be placed on the endothermic dehydration process at 580°C and the exothermic reactions at 980 and 1200°C were discussed. Evidence was provided for the existence of amorphous silica when kaolinite is heated to 1150°C , and the exothermic reaction is probably due to the conversion of about 7–8% of this to cristobalite.

Experiments have been carried out on the adsorption of moisture by the high-temperature products of china clays, fireclays and ball clays, using a differential thermobalance. Samples heated to 1000°C gained continuously in weight on cooling to room temperature, some gain being observed even at 900°C . The increase was greatest in the specimens containing the finest particles.

The adsorption of water caused the specimens to expand. Test pieces were heated to high temperatures, cooled to room temperature in a vacuum, and the increase in size measured when the test piece was removed from the vacuum and allowed to adsorb water. The magnitude of the expansion was less in those specimens which had been heated to the highest temperatures, since the internal surface area is reduced at high temperatures, owing to the aggregation of the crystals.

Experiments showed that the expansion is probably due to the adsorption of water by amorphous silica, since adsorption by crystalline phases does not cause expansion, and very little glass is developed in the heated china clays as they contain little potash mica. The expansion which is caused by the adsorption of water may be made the basis of a method of following the development of non-crystalline reaction products in heated kaolinitic clays.

Mr. H. P. ROOKSBY asked, during the discussion, whether γ -alumina had been found to undergo moisture expansion, since it was present in the samples examined, and might have contributed to the expansion. In reply, Dr. Vaughan said that it was not known whether amorphous alumina would expand under the conditions described. In any case, it seemed likely that γ -alumina would have been well crystallized at 1150°C . Some expansion at lower temperatures, however, could be caused by amorphous alumina.

Dr. W. J. DUFFIN (University of Hull), in a paper by himself and Dr. J. GOODYEAR, gave an account of the first X-ray investigation of the structure of scarbroite, a mineral originally described by Vernon in 1829.

Scarbroite is found only in a small cove, just south of South Bay, Scarborough. It is a white, compact material, of which natural specimens can be obtained which give no impurity lines in X-ray powder photographs. Electron micrographs show that the crystallites average about 10^{-4} cm across. The empirical formula for the mineral appears to be $\text{Al}_2(\text{CO}_3)_3 \cdot \text{Al}(\text{OH})_3 \cdot 12 \cdot 9 \cdot 15 \cdot 6 \text{H}_2\text{O}$.

Two phases, referred to as hydros-carbroite and scarbroite, are shown to exist in the freshly obtained material. The former changes irreversibly to the latter, more stable, form when the mineral is exposed to the air for some weeks.

Heating at 40°C causes hydros-carbroite to change in a few hours. Weight loss measurements show that, after heating at 100°C , the composition is probably $\text{Al}_2(\text{CO}_3)_3 \cdot \text{Al}(\text{OH})_3 \cdot 12 \cdot 9$. At 130°C the scarbroite changes to a further modification, meta-scarbroite, with a completely different X-ray powder pattern. No measurable lines remain above 230°C . The structural changes above 100°C are accompanied by loss of water and carbon dioxide.

Electron diffraction photographs of scarbroite show the structure to be pseudo-hexagonal, but a similar examination of the other forms has not been carried out. The X-ray patterns have been tentatively indexed in terms of the following orthorhombic unit cells:

Hydroscarbroite	$a_0 = 19.54 \text{ \AA}$	$b_0 = 31.01 \text{ \AA}$	$c_0 = 17.99 \text{ \AA}$
Scarbroite	$a_0 = 19.53 \text{ \AA}$	$b_0 = 30.15 \text{ \AA}$	$c_0 = 17.33 \text{ \AA}$
Meta-scarbroite (at 140°C)	$a_0 = 15.58 \text{ \AA}$	$b_0 = 26.84 \text{ \AA}$	$c_0 = 12.84 \text{ \AA}$

Biological fibres

The second section of the Conference dealing with biological fibres attracted a number of interesting contributions and stimulated renewed controversy about some long-standing problems.

Prof. ASTBURY, in opening the proceedings, commented on the widespread developments of fibre science and indicated the necessity for pursuing investigations by using simultaneously a number of collateral techniques. Of the three structures which dominated this section of the meeting, namely cellulose, silk and keratin, he noted that cellulose was perhaps the most completely characterized, although there was room for further refinement of the details of the system. Keratin structure still remains one of the major problems and is as yet incompletely solved.

The first paper of the group entitled "The internal and surface structure of cellulose microfibrils" by Prof. R. D. PRESTON (University of Leeds) was then read by Mr. D. S. BELFORD (Hickson's Timber Co. Ltd., Castleford). Evidence was presented that two distinct types of cellulosic materials were found naturally. The majority of sources of cellulose yield fibre X-ray diffraction patterns, and are rarely amenable to observation by electron diffraction analysis. However, with the algae, *Valonia*, *Cladophora* and *Chaetomorpha*, all of which are highly crystalline, well orientated, sharp electron diffraction patterns may be obtained. Further, the first and second of these algae show differences in chemical reactivity and both hydrolyse to give glucose only. Thus it is considered that the distinctive term "eucellulose" might be applied to them. The electron diffraction diagrams obtained are held to be incompatible with the dimensions of the Meyer and Misch unit cell, and the X-ray diagrams show evidence of preferential uniplanar orientation with the (101) planes parallel to the cell wall surface.

Differences in the intensity ratios of the 101, 10 $\bar{1}$ and 002 reflexions, as compared with normal cellulose, are readily observable. In some of the diagrams the 002 reflexion is weak or perhaps even absent, whereas usually it is well pronounced. Some of these differences may simply be due to the fact that normal cellulose is composed of sets of oriented structures effectively arranged at random about a central rotation axis.

Experiments on the uptake of metal on the surface of some wood celluloses has shown that a preferential organization results which leads to electron diffraction patterns being obtainable. These show the presence of two systems, designated type I and type II, with two-dimensional lattices, the parameters of which are given below.

Type I	$p = 6.15 \text{ \AA}$	$q = 7.05 \text{ \AA}$	$\theta = 90^\circ$
Type II	$p = 7.32 \text{ \AA}$	$q = 5.68 \text{ \AA}$	$\theta = 87-90^\circ$

The patterns appear to be derived from a monolayer of (in this case) copper atoms absorbed on the surface and have

no apparent correlation with the normal three-dimensional cellulose lattice.

In reply to a question by Dr. J. MANN (British Rayon Research Association, Manchester) on the justification for using the term "eucellulose" when the simpler term "cellulose" appeared sufficient, Mr. D. S. Belford replied that he thought that both the physical and chemical differences appeared to be sufficiently marked to uphold the distinction at present, but that further investigation would be advantageous.

The next paper, "Ordered molecular arrangements in cellulose I and cellulose II", was a joint communication from the laboratories of the British Rayon Research Association. It was read by Dr. D. W. JONES. The contribution dealt with a preliminary crystallographic structure investigation, guided mainly by X-ray and electron diffraction and infra-red spectroscopy techniques, of cellulose I and cellulose II. Cellulose I has been found⁽³⁾ to be capable of classification into two groups by means of infra-red spectra. These groups are designated type A (*Valonia* and bacterial cellulose) and type B (ramie and other native celluloses) corresponding broadly to Preston's classification on other evidence.

The basic structural ideas adopted were those of Meyer and Misch,⁽⁴⁾ but the further attempt has been made to try to solve the problem of the precise nature of hydrogen bonding in the structure. To do this the structure factors from a wholly crystalline model have been calculated and compared with those observed. A major aid in establishing possible configurations within the broad Meyer and Misch framework has been provided by the earlier infra-red work reported by Marrinan and Mann.⁽³⁾ This work had shown that in cellulose I there were two intramolecular hydrogen bonds roughly parallel to the chain direction, whereas in cellulose II there were, in addition, three nearly perpendicular bonds.

For cellulose I agreement between the observed and predicted intensities was not good, but the most promising structure appeared to be a system involving internal hydrogen bonds down each chain, together with interchain hydrogen bonding in the (002) plane. For cellulose II, a possible solution involved three interchain hydrogen bonds connecting the centre chain (reversed) and corner chains into the (10 $\bar{1}$) plane.

In conclusion, it was emphasized that the study related only to the most highly organized regions of the cellulose and that better agreements may be obtained when the degree of order was taken into consideration.

This paper stimulated much comment and Mr. H. J. WOODS (University of Leeds) asked whether the authors were definitely in favour of hydrogen bonding in the (002) plane of cellulose I. Had they considered the possibility (suggested by Frey-Wyssling⁽⁵⁾) of bonding in the (101) and (10 $\bar{1}$) planes? Dr. Jones replied that such structures had been considered but that they involved unsatisfactory bond lengths and angles, and to this Mr. Woods concurred.

A further item of interest was the presentation of a photograph taken by Dr. JEFFREY of fibres from connective tissue. These gave cellulose-like patterns but may possibly have been due to some other polysaccharide.

"The structure of silk fibroins" was the title of the next paper presented by Dr. J. O. WARWICKER (British Cotton Industry Research Association, Manchester) in which the X-ray diffraction examination of over fifty fibres produced by silk spinning organisms belonging to the orders *Lepidoptera* and *Araneae* was reported. This work has revealed that the classification of silk fibroins by means of

their X-ray diagrams does not rigidly follow the biological classification. However, in all the fibroins examined, the fibre repeat distance was found to be $6.95 \pm 0.5 \text{ \AA}$, and many diffraction diagrams had common spacings. The evidence was found to be compatible with the anti-parallel pleated sheet structure proposed for *Bombyx mori* and *Antheraea pernyi* by Pauling and others.^(6,7) Such sheets pack into orthorhombic unit cells, two dimensions of which (b and c) are fixed whilst the third distance (a) corresponds to the inter-sheet separation.

Satisfactory indexing may usually be obtained by assuming that the main equatorial reflexions can be indexed as 200 and 120. However, in the case of *Lasiocampa quercus* this is not so, and the indexing of these reflexions must be assumed to be 210 and 120. The results may be summarized in the following table.

Dimensions of unit cells of silk fibroins (\AA)

Representative fibroin	a	b	c (fibre axis)
<i>Bombyx mori</i>	9.3	9.44	6.95 ± 0.05
<i>Anaphe moloneyi</i>	10.0	9.44	6.95 ± 0.05
<i>Antheraea mylitta</i>	10.6	9.44	6.95 ± 0.05
<i>Caligula japonica</i>	10.6	9.44	6.95 ± 0.05
<i>Lasiocampa quercus</i>	15.0	9.44	6.95 ± 0.05
<i>Nephila senegalensis</i>	15.7	9.44	6.95 ± 0.05

It may be seen that two of the X-ray diagrams have identical unit cells. However, as the relative intensities of the reflexions differ, it is concluded that the residue sequences in the chains are probably different also. The occurrence of such large interchain spacings is also important in that it may allow bulky residues to be accommodated under conditions of high order.

Dr. K. D. PARKER and Dr. K. M. RUDALL (University of Leeds) then reported on "Silk fibres with folded protein chains". The X-ray diffraction pattern obtained from the lacewing fly *Chrysopa* is of singular significance, since it appears to be derived from a system of chains (with the hydroxyamino acid serine, dominating) that lie transverse to the main fibre axis, unlike those in normal silk.⁽⁸⁾ Its well-ordered structure is evident with sharp, clear diffraction "spots", and the transformation to the parallel β -form may be accomplished by extending the fibres up to about six times their original length. The *Chrysopa* lattice configuration is believed to be related to the cross- β configuration obtained after supercontraction of animal hair fibres, and if the diffraction pattern can be unambiguously interpreted it will be a great advance in the knowledge of these structures. Such work is proceeding.

Dr. N. PEACOCK (University of Leeds) further extended interest in the cross- β configuration by describing some of his recent experiments⁽⁹⁾ on supercontraction in wool keratin fibres.

The supercontracted form may be produced when the fibres are boiled in 5% sodium bisulphite solution or treated in urea-reducer solutions at $40\text{--}50^\circ\text{C}$, and subsequently stretched. The urea-reducer treatment is the more effective, and there are two types of result depending upon the pH of the treatment.

(1) At pH 6.4-8 the supercontraction is 30%, and on stretching the fibres the X-ray pattern shows cross- β and some oriented β -keratin.

(2) At pH ≤ 6 the supercontraction is 40% and, on

stretching the fibres, the X-ray pattern shows both cross- β and parallel- β which orientate simultaneously, but no α . When fibres treated as in (1) are further treated in boiling water, they supercontract a further 10%, and on stretching show a similar X-ray pattern to those of type (2).

The sector photograph (Fig. 2) comparing the principal reflexions in cross- β and parallel- β shows the former to be of

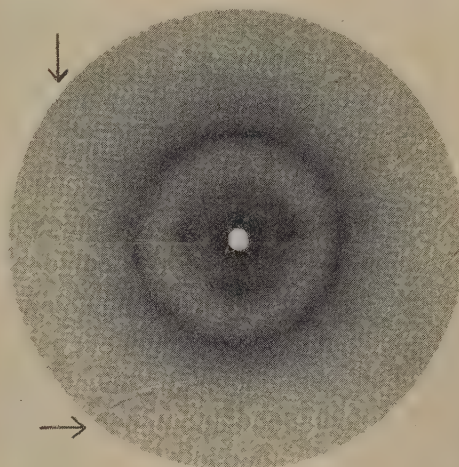


Fig. 2. Sector X-ray diffraction photographs of Lincoln wool keratin showing the difference in spacing between the (200) plane of parallel- β and the axial spacing of cross- β . The fibre axis direction is indicated by an arrow

slightly greater spacing (4.71 \AA) than the latter (4.65 \AA). The 4.71 \AA reflexion is always sharp radially; it improves in orientation on stretching, but there is no sign of any conversion to parallel- β up to the breaking point, which is variable since the fibres are very weak. Thus the polypeptide chains appear to lie generally along the length of the fibres but with transverse folds, as postulated by Rudall, maintained by stronger bonding than in other proteins.

Supercontraction accompanied by the appearance of the β form is a typical example of denaturation, and the above results indicate that two types of denaturation may occur in keratin, producing two distinct crystallographic forms, and both forms are disoriented in the supercontracted fibres. Further, it would appear that the cross- β form is not the complete answer to the problem of supercontraction, which is the result of effects in both the observable crystalline regions and the more obscure poorly-ordered regions.

In further discussion it was pointed out that there may be lattices other than the postulated transverse silk configuration which are compatible with the *Chrysopa* diagram.

Then followed a joint paper by Prof. W. C. PRICE, Dr. G. R. WILKINSON and Dr. E. M. BRADBURY (King's College, London) on "Structural studies of biological fibres by means of polarized infra-red radiation". A brief review of the type of information which could be extracted from such investigations was given first.

Dichroic studies often enabled bond directions, particularly those of NH and OH bonds, to be determined, and the degree of hydration could be derived from quantitative measurements on the relevant absorption bands. Further, both deuteration and denaturation kinetics could be investigated by observing the magnitudes and contours of particular

absorption bands. As an example of the power of such techniques, the illustration shown in Fig. 3 may be cited. This shows part of the spectrum of collagen and the effect of partial deuteration on the dichroism of the intramolecularly bonded NH groups. The result obtained is in good agreement⁽¹⁰⁾ with the postulated structure which involves lateral hydrogen bonding of the NH groups.

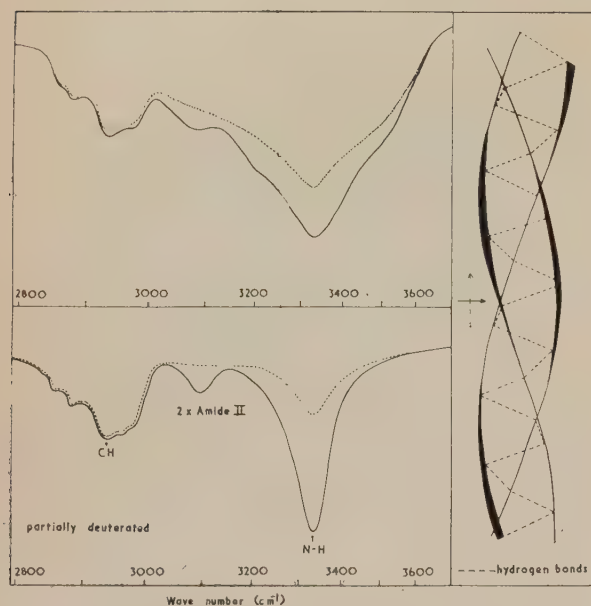


Fig. 3. The effect of partial deuteration on the infra-red dichroism of the N-H stretching mode in collagen

— = electric vector perpendicular to fibre axis
 = electric vector parallel to fibre axis

Mr. H. W. EMERTON (Albert E. Reed and Co. Ltd., Maidstone) then read a paper on "The structure of softwood fibres and its significance in papermaking". He began by defining paper as a mat of naturally occurring cellulose fibres deposited from a dilute aqueous suspension. Physically the process of making paper was characterized by the gradual replacement of cellulose-water hydrogen bonds by direct intercellulose hydrogen bonds. The processes and structures were illustrated by some beautiful optical and electron micrographs.

In order to facilitate adequate cross-linking of the sheets, the fibres must first be flexed in water in regions of great turbulence. During this process, which is known as beating, the water acts as a plasticizer and is imbibed into the fibres. Finally it was demonstrated that the "yielding up" of the water involved the development of marked torsional stresses, which under certain conditions could leave the paper in a state of strain, thus contributing to its ultimate failure. As an illustration of this a tracheid with its central region fixed to a microscope slide (Fig. 4) was found to successively twist and straighten, depending on whether it was dry or wet. It was also noted that this effect was not peculiar to the particular tracheid under consideration, but had been observed by other workers.

The final paper, "Some problems in the equatorial scattering of keratin", was delivered by Mr. H. J. WOODS (University of Leeds). He first noted the renewed interest in recent years in the equatorial small-angle scatter of keratin, because of the success of the electron microscope in revealing micro-

fibrillar texture in mature fibres heavily stained with osmium. Since heavy metal (Hg, PG, OS, Ag) staining is an effective way of modifying the small-angle equatorial scatter, a fruitful field of co-operation between the two techniques is opened up. In a quantitative assessment of the X-ray scattering, the absorption effects become very important on account of the relatively high uptake of metal; specimen sizes have to be drastically reduced and exposures which are optimal for the



Fig. 4. Behaviour of a tracheid (a) on drying and (b) on wetting

(enhanced) small-angle scatter are too short to show the large-angle reflexions. Whether the latter are affected by the incorporation of metal is of importance to the chemist seeking specific reactions. Results of experiments, in which corrections for specimen size and absorption were applied, show that the intensity of the 9.8 \AA equatorial reflexion of keratin is, in fact, reduced by a factor of three or more in fibres heavily stained with mercury acetate. In such fibres, a very intense background is observed at deviations of $2\theta < 5^\circ$; and photometer traces at angles inclined to the

equator indicate that most of this is in the form of an unoriented halo about the central beam. There are also, however, indications of an "equatorial streak" superposed on the general halo and underlying the small-angle maxima.

units so nearly close-packed as those in keratin, the calculated intensities become negative at certain values of 2θ when simplified radial distribution functions are used.

In subsequent discussion Dr. G. E. PRINGLE (University of Leeds) felt that there were grounds for altering the relative weights of the two terms in the Debye formula when applied to this particular system. However, on further reflexion the difficulties were ascribed to some internal contradiction arising from the arbitrary choice of trial radial density functions. Dr. J. SIKORSKI (University of Leeds) confirmed that electron micrographs of transverse sections of keratin fibres revealed microfibrillar packing data which appeared to be in general agreement with the X-ray diffraction results. He also expressed disappointment about the failure of certain metallic complexes to reveal microfibrillar structure and drew attention to the apparently dissimilar distributions of microfibrils in the *ortho*- and *para*-cortex which should not be overlooked in a refined analysis.

During the meeting a small but impressive international exhibition of apparatus, and a collection of books arranged by the Brotherton Library illustrating the development of crystallography, were on view. An evening discourse on "The new survey of English dialects" by Prof. H. ORTON (University of Leeds) attracted many, and altogether this Spring Conference was a memorable one.

A. SKERTCHLY
R. STEADMAN

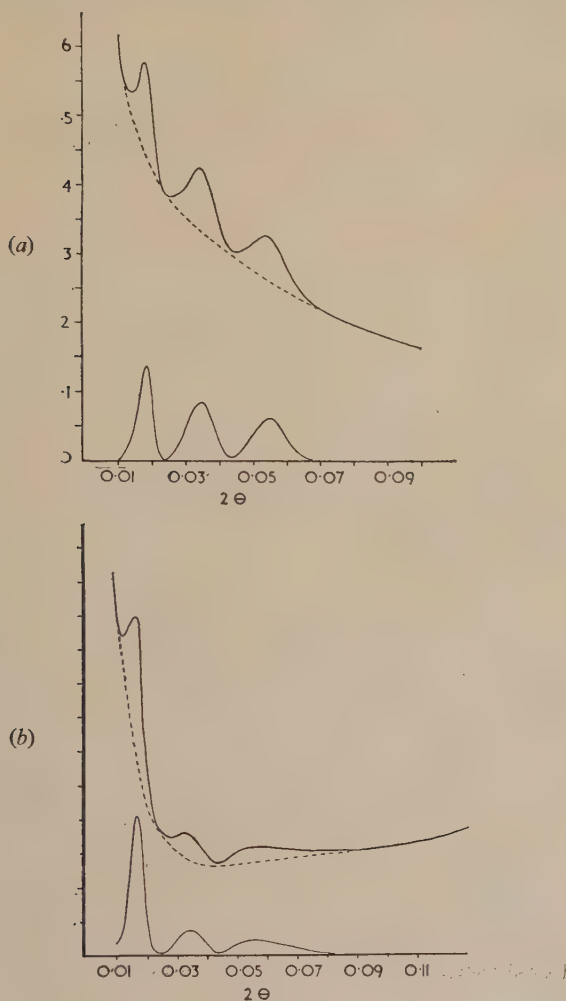


Fig. 5. Equatorial intensity distribution of untreated and treated keratin fibres

(a) Mohair reduced with $\text{Hg}(\text{OAc})_2$
(b) Human hair (untreated)

Assuming a background of this kind, the analysis of the equatorial intensity curve for untreated and treated fibres is as shown in Fig. 5. It will be seen that the "reflexions" at 40 and 27 Å are enhanced more than that at 90 Å. Attempts to explain these results, in terms of a model of randomly distributed microfibrils of uniform diameter, have failed to yield acceptable results because, for systems of scattering

References

- (1) NEWNHAM, R. E., and BRINDLEY, G. W. *Acta Cryst.*, **9**, p. 759 (1956); *Acta Cryst.*, **10**, p. 88 (1957).
- (2) BRINDLEY, G. W., and NAKAHIRA, M. *J. Amer. Ceram. Soc.*, **42**, p. 311 (1959).
- (3) MARRINAN, H. J., and MANN, J. *J. Polymer Sci.*, **21**, p. 301 (1956).
- (4) MEYER, K. H., and MISCH, L. *Helv. Chim. Acta*, **20**, p. 232 (1937).
- (5) FREY-WYSSLING, A. *Biochim. Biophys. Acta*, **18**, p. 166 (1955).
- (6) MARSH, R. E., COREY, R. B., and PAULING, L. *Biochim. Biophys. Acta*, **16**, p. 1 (1955).
- (7) MARSH, R. E., COREY, R. B., and PAULING, L. *Acta Cryst.*, **8**, p. 710 (1955).
- (8) PARKER, K. D., and RUDALL, K. M. *Nature (London)*, **179**, p. 905 (1957).
- (9) PEACOCK, N. *Biochim. Biophys. Acta*, **32**, p. 220 (1959).
- (10) BRADBURY, E. M., BURGE, R. E., RANDALL, J. T., and WILKINSON, G. R. *Disc. Faraday Soc.*, **25**, p. 173 (1958).

Influence of instrumental aberrations on the Schultz technique for the measurement of pole figures

by B. GALE, Ph.D., and D. GRIFFITHS,* National Physical Laboratory, Teddington, Middlesex

[Paper first received 2 July, and in final form 28 October, 1959]

Abstract

An experimental and theoretical investigation of the Schulz reflexion technique for measuring pole figures has shown that it is capable of giving accurate results provided the integrated intensities are measured. A detailed discussion is given of the influence of the aberrations of the optical system on the diffraction-line shapes from which it is concluded that the integrated intensities are unaffected by tilting the specimen and that, for large tilts, the vertical height of the beam is limited only by its overlap of the specimen or by lack of resolution of neighbouring diffraction lines.

THIS paper describes an approximate treatment of the effects of incident-beam and detector-slit dimensions, specimen tilt and diffraction-line width on the determination of the pole figures of sheet materials using the Schulz technique.⁽¹⁾ In this method the two degrees of freedom required to span the pole figure are a rotation about the normal to the sheet surface and a rotation of this normal in the plane bisecting the incident and diffracted X-ray beams.

In his original paper, Schulz claimed that by suitably limiting the height of the incident and diffracted beams it was possible to vary the angle of tilt χ of the specimen normal with respect to the horizontal plane in the range $|\chi| \leq 80$ deg. without appreciably altering the recorded diffracted intensity. This, of course, is not surprising since, in the limiting case when the beam height is zero, the corresponding range would be $|\chi| \leq 90$ deg. However, Chernock and Beck⁽²⁾ have published results which show a decrease in the recorded intensity for $|\chi| > 40$ deg. arising from an appreciable defocusing effect. To obviate this, a correction factor was determined from a calibration experiment in which the diffracted intensity from a specimen with random orientation was measured under the same experimental conditions. At large χ values, this correction factor was very large and the accuracy of measurement correspondingly decreased. To avoid this, a number of specimens could be cut at various orientations with respect to the sheet surface, but the specimen preparation then becomes more involved, requiring the use of special jigs with a consequent loss in the ease and rapidity of preparation.^(3,4) Since a recent investigation required the accurate determination of the central region of the (0002) pole figure of titanium, it was decided to examine the technique in more detail.

The measurements made during this work were performed on a diffractometer (type X.R.D.3, by General Electric),

which had been modified to incorporate a quartz crystal monochromator. The monochromator was mounted on a table which could be rotated, with fine control, about a vertical axis. It was enclosed in a shielding box fitted with adjustable inlet and outlet apertures which was mounted on a carriage and could be moved along an arm pivoted about an axis passing through the X-ray source. The whole monochromator assembly, together with the X-ray tube, could be aligned relative to the diffractometer table by a rotation about a vertical axis at the 180 deg. position on the Brentano focusing circle. The specimen was mounted on a goniometer which permitted rotations about the vertical diffractometer axis, the normal to the specimen surface and a horizontal axis in this surface. The accuracy of construction was such that the horizontal axis was not displaced by more than about 10^{-4} in. for the whole range of χ . The X-ray beam was principally determined by two apertures. One was the outlet aperture of the monochromator shielding box, which was used to define the height of the focused image of the X-ray source. The other was set about 4 cm in front of the specimen and was about 18 cm away from the first. This defined the horizontal divergence of the beam and the vertical height of the specimen irradiated; the latter, which was critical, was adjusted by micrometer screws.

In discussing this problem, a simplified model of the optical system is used and a rectangular co-ordinate system was chosen such that OZ is the vertical rotation axis of the diffractometer and OX passes through the centroid of the effective X-ray source (Fig. 1). In the experimental arrangement used here this is the focus of the monochromator and it is considered to be rectangular, of width E_1 and height E_2 and to lie in the plane $X + R = 0$. The incident beam passes through a rectangular aperture of width E_4 and height E_5 , the centroid of which also lies on OX . To simplify the subsequent treatment, it is assumed that this aperture is

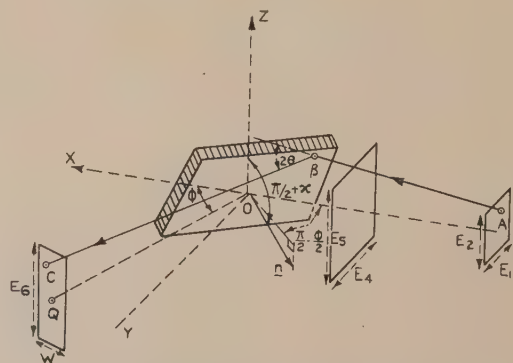


Fig. 1. Simplified model of optical system

* Now at Nelson Research Laboratories of the English Electric Co. Ltd., Stafford.

sufficiently close to the specimen to permit umbra-penumbra effects to be ignored. The specimen is a flat plate, the front face of which passes through "O" and whose unit normal vector \mathbf{n} has polar co-ordinates $\frac{1}{2}\pi + \frac{1}{2}\phi$, $\frac{1}{2}\pi + \chi$. The detector aperture of height E_6 and width W lies in a plane tangential to the cylinder with axis OZ and radius R , its centroid Q having cylindrical co-ordinates $(R, \phi, 0)$. Accurate alinement of the apertures so that their centres and the horizontal goniometer axis all lie in the same plane was achieved using a vernier height gauge and was checked by comparing the intensities, recorded by a narrow detector slit set on the diffraction-line peak, for equal positive and negative values of χ . It is estimated that, by using this method, the deviations from coplanarity were not greater than about 0.005 cm.

The radiation emitted from a source element at A having co-ordinates $R(-1, \epsilon_1, \epsilon_2)$ is proportional to $R^2 d\epsilon_1 d\epsilon_2$. It is assumed that the variation with emission direction and source element can be ignored, so that the intensity incident at a point B within the specimen is given by:

$$I = \frac{I_0 R^2}{(AB)^2} \exp(-\mu l) d\epsilon_1 d\epsilon_2$$

where I_0 is a constant, μ is the linear absorption coefficient and l is the path length of the incident beam in the specimen. The direction of a diffracted ray can be defined by the polar angle with respect to AB , which is equal to twice the Bragg angle θ , and an azimuth angle ψ . If S_0 and S_1 are unit vectors parallel to the incident and diffracted rays, ψ can be defined as the angle between the planes $(S_1 S_0)$ and (OZ, S_0) . The intensity diffracted per unit volume as a function of θ and ψ for a randomly oriented set of mosaic crystals is given⁽⁵⁾ by:

$$I_D(\theta, \psi) = I_B N^2 \lambda^3 \left(\frac{e^2}{mc^2} \right)^2 \frac{q}{4\pi} \operatorname{cosec} \theta |F|^2 P(\theta) f(\theta)$$

where N is the number of crystal cells per unit volume; λ , e , m and c are respectively the incident wavelength, the electronic charge and mass and the velocity of light; q is the multiplying factor; F is the structure factor; $P(\theta)$ is the polarization factor and $f(\theta)$ is a normalized function which represents the shape of the diffraction line produced by the lattice distortion and the spectral distribution. The diffracted beam is attenuated by a factor $\exp(-\mu l')$, where l' is the diffracted path length in the specimen, and the intensity at a point C , having cylindrical co-ordinates $(R, \xi, R\epsilon_6)$ produced by the source element at A and the scattering element at B with Cartesian co-ordinates $R(\epsilon_3, \epsilon_4, \epsilon_5)$ is given by:

$$\Delta I(\xi, \epsilon_6, \chi) = \frac{K}{(AB)^2} \operatorname{cosec} \theta P(\theta) f(\theta) \exp\{-\mu(l + l')\} \left| \frac{D(\theta, \psi)}{D(\epsilon_6 \xi)} \right| d\epsilon_1 d\epsilon_2 d\epsilon_3 d\epsilon_4 d\epsilon_5,$$

where K is a constant equal to $\frac{1}{4} N^2 \lambda^3 \left(\frac{e^2}{mc^2} \right)^2 q |F|^2 R^5$, F being assumed to vary sufficiently slowly over the range of θ for which $f(\theta)$ is appreciable. The intensity $I(\xi, \epsilon_6, \chi)$ produced by the whole source and the whole of the irradiated part of the specimen is then given by the five-fold integral over the range of $\epsilon_1 \dots \epsilon_5$, where θ , ψ , l and l' are evaluated in terms of ξ , ϵ_6 and these variables. The quantities $\epsilon_1 \dots \epsilon_6$ measure the deviations of the incident and diffracted rays relative to the case when the emitting area, the scattering volumes and the detecting aperture all have zero extension. The ϵ_1 products are thus here referred to as aberrations by analogy

with normal optical usage. These quantities are all less than 2×10^{-2} so that functions of them can be represented to a high degree of accuracy by second-order power series. The measured intensity $I_w(\phi, \chi)$, when the detector slit has an angular width W and its centroid is at the point with cylindrical co-ordinates $(R, \phi, 0)$, is given by:

$$I_w(\phi, \chi) = \frac{1}{W} \int_{\phi-W/2}^{\phi+W/2} \int_{-E_6/2R}^{E_6/2R} I(\xi, \epsilon_6, \chi) d\xi d\epsilon_6$$

which becomes:

$$I_w(\phi, \chi) = \frac{1}{W} \int_{\phi-W/2}^{\phi+W/2} I_0(\xi, \chi) d\xi, \quad (1)$$

and the integrated intensity of a diffraction line will be given, as a function of the tilt χ , by:

$$J(\chi) = \int_{\phi_1}^{\phi_2} I_0(\phi, \chi) d\phi,$$

where the limits of integration are taken to be sufficiently large to include all appreciable intensity without overlap on to neighbouring lines, and can be experimentally determined by adding the intensities recorded at a succession of ϕ values differing by $\Delta\phi = W$. The integrated intensity is also given by:

$$RK \int_1 \dots \int_6 |AB|^{-2} \operatorname{cosec} \theta P(\theta) f(\theta) \exp\{-\mu(l + l')\} d\epsilon_1 \dots d\epsilon_6 \frac{\partial \psi d\theta}{\partial \epsilon_6},$$

where $\frac{\partial \psi}{\partial \epsilon_6}$ is obtained from the relation:

$$\cos \psi \sin 2\theta |S_0 \cdot OZ| = (S_1 \cdot OZ) - \cos 2\theta (S_0 \cdot OZ).$$

It will now be shown that, whereas $J(\chi)$ is insensitive to the aberrations ϵ_i and the tilt χ , $I_0(\phi, \chi)$ is sensitive to both ϵ_5 and χ and can, in most cases, be calculated by a simple convolution treatment. Before proceeding to the detailed calculation, and in order to facilitate the evaluation of the absorption effect, it is convenient to replace the variables ϵ_i by a new set ϵ'_i defined by the relations:

$$\begin{aligned} \epsilon_1 &= \epsilon'_1, \quad \epsilon_2 = \epsilon'_2, \quad \epsilon_6 = \epsilon'_6 \\ \begin{pmatrix} \epsilon_3 \\ \epsilon_4 \\ \epsilon_5 \end{pmatrix} &= \begin{pmatrix} \cos \chi \sin \phi/2 & \cos \phi/2 & -\sin \chi \sin \phi/2 \\ -\cos \chi \cos \phi/2 & \sin \phi/2 & \sin \chi \cos \phi/2 \\ \sin \chi & 0 & \cos \chi \end{pmatrix} \begin{pmatrix} \epsilon'_3 \\ \epsilon'_4 \\ \epsilon'_5 \end{pmatrix} \end{aligned}$$

where ϕ is a function of $\epsilon'_1 \dots \epsilon'_6$ determined by the Bragg equation:

$$S_1 \cdot S_0 = \cos 2\theta$$

which, to the second order, can be shown to be given by:

$$\begin{aligned} S_1 \cdot S_0 &= 2\theta - \epsilon'_1 - 2 \cos \theta (\cos \chi \epsilon'_3 - \sin \chi \epsilon'_5) + \\ &+ \cos \theta \epsilon'_1 \epsilon'_4 - \frac{1}{2} \cot 2\theta \epsilon'^2_2 + (\sin \chi \epsilon'_3 + \cos \chi \epsilon'_5) \cot \theta \epsilon'_2 \\ &- \operatorname{cosec} 2\theta \epsilon'_2 \epsilon'_6 - \cot \theta \sin^2 \chi \epsilon'^2_3 - \sin 2\chi \cot \theta \epsilon'_3 \epsilon'_5 + \\ &+ \sin \chi \cot \theta \epsilon'_3 \epsilon'_6 - \sin 2\theta \epsilon'^2_4 \\ &- \cos^2 \chi \cot \theta \epsilon'^2_5 + \cot \theta \cos \chi \epsilon'_5 \epsilon'_6 - \frac{1}{2} \cot 2\theta \epsilon'^2_6 \end{aligned}$$

The depth of the scattering point B below the specimen surface is now given by $R\epsilon'_3$ and the experimental absorption term becomes:

$$\exp\{\mu R \epsilon'_3 [(S_0 \cdot \mathbf{n})^{-1} - (S_1 \cdot \mathbf{n})^{-1}]\},$$

and the limits of integration will be:

$$|\epsilon'_1| \leq \frac{E_1}{2R}, \quad |\epsilon'_2| \leq \frac{E_2}{2R}, \quad 0 \leq \epsilon'_3 \leq \infty,$$

$$|\epsilon'_4| \leq \frac{E_4}{2R} \operatorname{cosec} \phi/2, \quad |\epsilon'_5| \leq \frac{E_5}{2R} \sec \chi, \quad |\epsilon'_6| \leq \frac{E_6}{2R},$$

$$\theta(\epsilon'_1 \dots \epsilon'_6, \phi_1) \leq \theta \leq \theta(\epsilon'_1 \dots \epsilon'_6, \phi_2)$$

and those for ϵ'_3 and ϵ'_4 require a little discussion. The integration with respect to ϵ'_4 is most conveniently performed by expanding $\operatorname{cosec} \phi/2$ as a second-order power series in ϵ'_2 and solving the limit inequalities in terms of ϵ'_4 . Thus:

$$|\epsilon'_4| \leq \frac{E_4}{2R} \operatorname{cosec} \theta (1 + A + \{\epsilon_4'^2 - \frac{1}{2} \operatorname{cosec} \theta \epsilon'_1 \epsilon'_4\} \cos^2 \theta)$$

where A is a power series in $\epsilon'_1 \epsilon'_2 \epsilon'_3 \epsilon'_5$ and ϵ'_6 of order greater than one. Now if the upper root, which is given approximately by $(2R \sec \theta \tan \theta)/E_4$, is greater than $2L/R$, where L is the length of the specimen, then the integration range is given by:

$$|\epsilon'_4| \leq \frac{E_4}{2R} (1 + A) \operatorname{cosec} \theta.$$

The condition of this relation is normally obeyed, for if typical values for L , E_4 and R of 2, 0.3 and 15 cm respectively are inserted, it is only necessary for θ to be greater than about 15 minutes. Now to the zeroth order in ϵ'_i $(S_0 \cdot n)^{-1} - (S_1 \cdot n)^{-1}$ is given by $-2 \sec \chi \operatorname{cosec} \theta$, so that when the integration with respect to ϵ'_4 is performed, the ϵ'_3 integral will be of the form:

$$\int_0^\infty G(\epsilon'_3) \exp[-\alpha \epsilon'_3 \{1 + H(\epsilon'_3)\}] d\epsilon'_3,$$

where $\alpha = 2\mu R \sec \chi \operatorname{cosec} \theta$, $G(\epsilon'_3) = \sum_{n=0}^\infty g_n \epsilon_3'^n$ and $H(\epsilon'_3) = \sum_{n=0}^\infty h_n \epsilon_3'^n$; the coefficients g_n and h_n being functions of θ and ϵ'_j ($j \neq 3, 4$). Expanding $\exp\{-\alpha \epsilon'_3 H(\epsilon'_3)\}$ as a power series in ϵ'_3 and integrating term by term, the integral is given by:

$$\frac{g_0}{\alpha} \left\{ (1+h)^{-1} + \frac{1}{\alpha^2} g_1 (1+h_0)^{-2} - 2g_0 h_1 (1+h)^{-3} \right\} + \dots$$

In general, this series is asymptotic, but since μR is approximately 10000, all terms except the first may be neglected. Further simplifications arise in considering the integrations with respect to ϵ'_1 , ϵ'_2 , ϵ'_5 and ϵ'_6 , for, if the variation of the normalized "integrated intensity", represented by the ratio $J(\chi)/J(0)$, is required to the second order of the aperture dimensions, it is only necessary to calculate the integrands to the same order. It is then evident from the form of the integration limits that integrand terms of the form ϵ'_i and $\epsilon'_i \epsilon'_j$, for $i \neq j$ and $i, j = 1, 2, 4, 5$ and 6, will not contribute to $J(\chi)$ and they need not therefore be considered in evaluating either $|AB|^{-2}$, $\partial \psi / \partial \epsilon'_6$, or $(1+h_0)^{-1}$. It is also considered that the variations of the polarization and other trigonometric factors, like that of $|F|$, are sufficiently small over the range for which $f(\theta)$ is appreciable that their values can be taken to be those appropriate to $\bar{\theta}$, the centroid of $f(\theta)$. With all these considerations in mind $J(\chi)/J(0)$ can, after some manipulation, be shown to be given by:

$$\frac{J(\chi)}{J(0)} = 1 + \frac{1}{12} \left(\frac{3}{2} \cos^2 \bar{\theta} + \cos^2 2\bar{\theta} - \cot^2 \bar{\theta} \right) \left(\frac{E_5}{R} \right)_2 \tan^2 \chi,$$

The maximum defocusing effect evidently occurs at small values of $\bar{\theta}$ and for $\bar{\theta}$ approximately equal to 10 deg. and E_5/R

approximately equal to 2×10^{-2} , the effect is approximately $10^{-3} \tan^2 \chi$. Thus in most practical cases, the intensity diminution is less than 1% except when the tilt is so large that the incident beam overlaps the specimen. Some experimental results showing the variation of integrated intensity with tilt are shown in the table and it is evident that the predicted constancy is confirmed. Defocusing is not, therefore, a prime disadvantage from this point of view but as will now be shown it can lead to other difficulties.

Measured values of $J(\chi)/J(0)$ for two values of E_5 (estimated experimental error was about $\pm 0.01\%$)

$\frac{E_5}{R} \chi$ (in.)	0	10	20	30	40	50	60
0.047	1.00	1.00 ₅	0.98 ₅	1.01	1.02 ₅	0.99	1.01
0.096	1.00	1.01	0.99	1.02 ₅	1.02	0.99	1.01

In order to calculate $I_0(\phi)$ it is convenient to proceed as follows. Consider the beam defined by the slit element ϵ'_5 , $\epsilon'_5 + d\epsilon'_5$, for which the centroid of the corresponding diffracted intensity $\Delta I_0(\phi, \epsilon'_5)$ will be given by:

$$\bar{\phi} = \frac{\int_{\phi_1}^{\phi_2} \phi \Delta I_0(\phi, \epsilon'_5) d\phi}{\int_{\phi_1}^{\phi_2} \Delta I_0(\phi, \epsilon'_5) d\phi}.$$

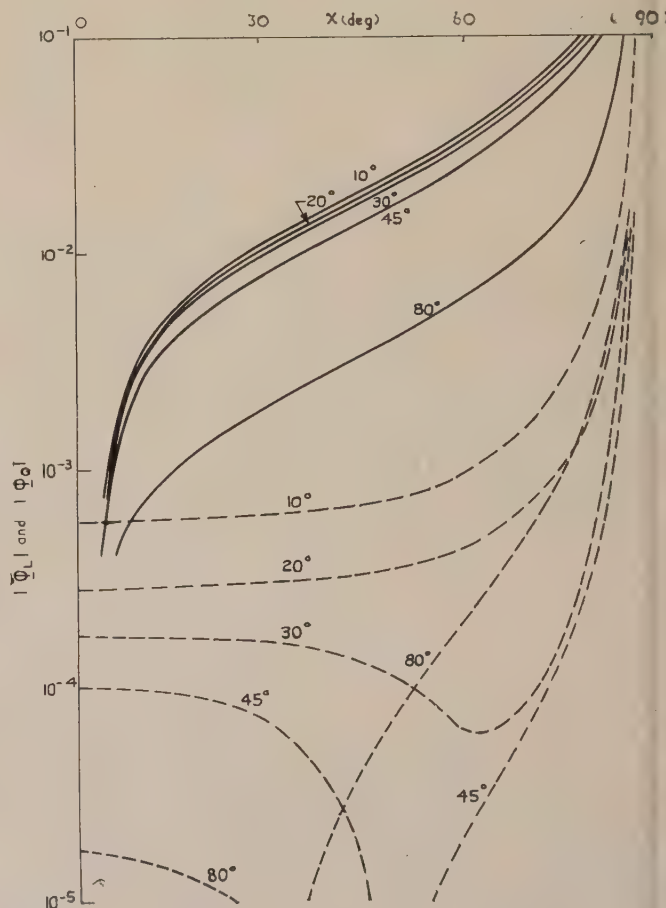


Fig. 2. Variation of the linear $\bar{\phi}_L$ (full line) and quadratic $\bar{\phi}_Q$ (dotted line) terms in the equation (2) for the displacement of the diffraction line profile $\Delta I_0(\phi, \epsilon'_5)$ for $\bar{\theta} = 10, 20, 30, 45$ and 80 deg.

Then if, as before, the trigonometric functions are assumed to vary sufficiently slowly, $\bar{\phi}$ will, to the second order, be given by:

$$\begin{aligned} \bar{\phi} = & 2\bar{\theta} + 2 \cos \bar{\theta} \sin \chi \epsilon'_s - \\ & - \frac{1}{24R^2} \cot 2\bar{\theta} (E_2^2 + E_6^2) - \frac{1}{6} \cot \bar{\theta} \left\{ \frac{(E_4)^2}{R} \right\} + \\ & + \{2(\sin 2\bar{\theta} - \cos^2 \bar{\theta}) \cot \bar{\theta} \sin^2 \chi - \cot \bar{\theta} \cos^2 \chi\} \epsilon_s'^2. \end{aligned} \quad (2)$$

The only terms depending on the tilt are those involving ϵ'_s and the variations of the linear $|\bar{\phi}_L|$ and quadratic $|\bar{\phi}_Q|$ terms with χ for various $\bar{\theta}$ values and for a typical extreme value for $\epsilon'_s \sec \chi$ of 10^{-2} are shown in Fig. 2. It is evident that for $10 \text{ deg.} \leq \theta \leq 80 \text{ deg.}$, the centroid shift, $\bar{\phi}_L + \bar{\phi}_Q$, is less than about 2 minutes at $\chi = 0$ and that for $10 \text{ deg.} \leq \chi \leq 75 \text{ deg.}$, $\bar{\phi}_L$ is at least six times greater than $\bar{\phi}_Q$, and in most cases the ratio is of the order 100. The width $W(\epsilon'_s)$ of $\Delta I_0(\phi \epsilon'_s)$ can be defined by the square root of its variance, except for certain special distributions which will not be considered here. Thus:

$$W^2(\epsilon'_s) = \frac{\int \phi^2 \Delta I_0(\epsilon'_s \phi) d\phi}{\int \Delta I_0(\epsilon'_s \phi) d\phi} - \bar{\phi}^2,$$

which, with the previous assumption about the trigonometric functions, can be shown to be given by:

$$\begin{aligned} W^2(\epsilon'_s) = & W_f^2 + \frac{1}{12} \left(\frac{E_1}{R} \right)^2 + \\ & + \frac{1}{720R^4} (E_2^4 + 5E_2^2 E_6^2 + E_6^4) \cot^2 2\bar{\theta} + \\ & + \frac{1}{45} \left(\frac{E_4}{R} \right)^4 \cot^2 \bar{\theta} + \frac{1}{12R^2} \cot^2 \bar{\theta} \cos^2 \chi \epsilon_s'^2 (E_2^2 + E_6^2) + \\ & + 4(\sin 2\bar{\theta} - \cos^2 \bar{\theta} \cot \bar{\theta})^2 \sin^4 \chi \epsilon_s'^4 \end{aligned} \quad (3)$$

Thus $W^2(\epsilon'_s)$ can be considered as the sum of contributions from the scattering function W_f^2 , the ray divergences W_D^2 , given by the second, third and fourth terms, and the specimen tilt W_χ^2 given by the last two terms. The variations of W_χ and $(W_D^2 + W_f^2)^{1/2}$ are shown in Fig. 3 for the two cases $W_f = 0$ and $W_f = e \tan \bar{\theta}$, where e is approximately 6×10^{-3} and is the average lattice strain of a typical cold-worked material. It is evident that W is the dominant term, being greater than about $5(W_D^2 + W_f^2)^{1/2}$ in the range $0 \leq \chi \leq 60 \text{ deg.}$ for $\bar{\theta} = 30 \text{ deg.}$, and in the range $0 \leq \chi \leq 40 \text{ deg.}$ for $\bar{\theta} = 20 \text{ deg.}$ On the basis of these numerical estimations of the influence of the various parameters on the centroid and line width of $\Delta I_0(\epsilon'_s \phi)$ it is possible to use a very much simplified treatment of the diffraction-line profile. Let the shape of $\Delta I_0(\epsilon'_s \phi)$ be independent of ϵ'_s and let its centroid be given by $\bar{\phi} = 2\bar{\theta} + \bar{\phi}_L$. This assumption will only be a

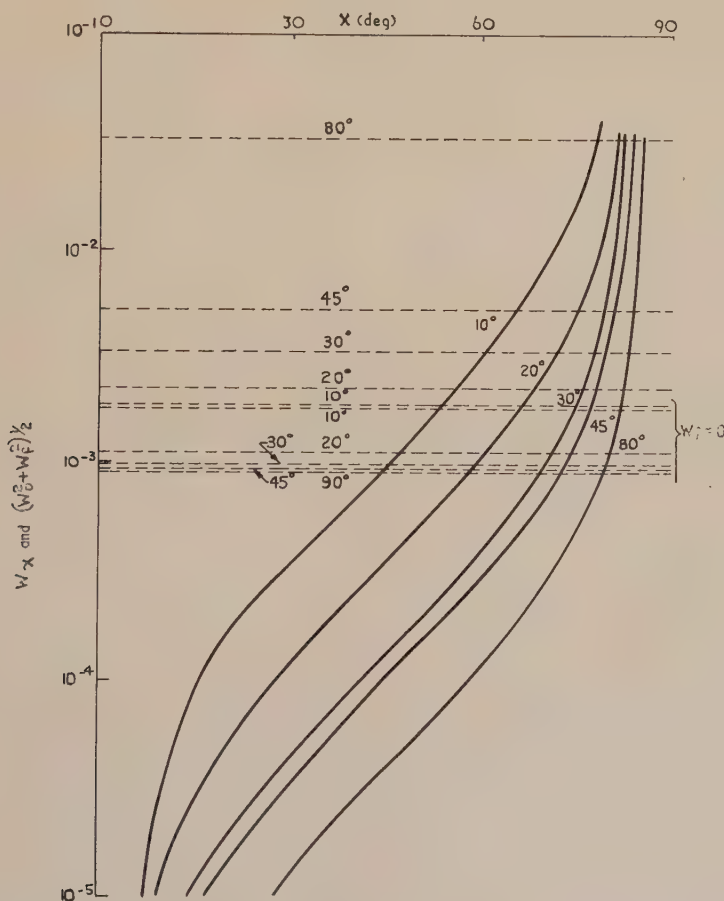


Fig. 3. Variation of the terms W_χ (full line) and $(w_D^2 + w_f^2)^{1/2}$ (dotted line) in equation (3) for the width of $\Delta I_0(\phi, \phi_s')$ for $\bar{\theta} = 10, 20, 30, 45$ and 80 deg.

good approximation for the $\bar{\theta}$ and χ values deduced in the discussion of the behaviour of the line width, since the shift of the centroid near $\chi = 0$ is negligible. However, the variation in $\Delta I_0(\phi)$ as χ increases will only modify the extremities of the $I_0(\phi\chi)$ distribution; for, as will be shown, the width of $I(\phi\chi)$ is approximately equal to $2\phi_L$ and this is at least ten times greater than the width of $\Delta I_0(\phi)$ in the range $0 \leq \chi \leq 60$ deg. The range of dominance of ϕ_L and $(W_B^2 + W_F^2)^{1/2}$ will increase rapidly for smaller values of ϵ_5 so that the extremities of $I_0(\phi)$ are again most sensitively affected.

The diffracted intensity $I_0(\phi)$ will now be given by:

$$I_0(\phi\chi) = \frac{1}{2a} \int_{-a}^a \Delta I_0(\phi - \phi_L) d\phi_L$$

where

$$a = \cos \theta \tan \chi \frac{E_5}{R},$$

from which $I_w(\phi\chi)$ can be calculated using equation (1). To facilitate the investigation of the effect of tilt, the calibration function $C_w(\phi\chi)$, defined by the ratio $I_w(\phi, \chi)/I_0(\phi, 0)$, was calculated and measured. $\Delta I_0(\phi)$ in this approximation is given by $I_0(\phi, 0)$ and it was found experimentally that it could be closely represented by a Gaussian function of the form:

$$\Delta I_0(\phi) = \frac{1}{\tau\sqrt{2\pi}} \exp \left\{ - \left(\frac{\phi - 2\bar{\theta}}{\tau\sqrt{2}} \right)^2 \right\},$$

where τ is related to the integral width ω is defined by:

$$\omega = \frac{\int_{-\infty}^{+\infty} \Delta I_0(\phi) d\phi}{\Delta I_0(\phi)_{\max}} = \tau\sqrt{2\pi}$$

Using the Gaussian function, $I_0(\phi\chi)$ will be given by:

$$I_0(\phi\chi) = \frac{1}{4a} \left\{ \operatorname{erf} \left(\frac{\phi + a - 2\bar{\theta}}{\tau\sqrt{2}} \right) - \operatorname{erf} \left(\frac{\phi - a - 2\bar{\theta}}{\tau\sqrt{2}} \right) \right\}$$

where:

$$\operatorname{erf} z = \frac{2}{\sqrt{\pi}} \int_0^z e^{-y^2} dy = 1 - \operatorname{erf}(-z);$$

and $I_w(\phi z)$ is given by:

$$I_w(\phi z) = \frac{1}{4Wa} \int_{-W/2}^{W/2} \left\{ \operatorname{erf} \left(\frac{a - \phi'}{\tau\sqrt{2}} \right) + \operatorname{erf} \left(\frac{a + \phi'}{\tau\sqrt{2}} \right) \right\} d\phi'$$

or

$$I_w(\phi z) = \frac{\tau}{2Wa} \left\{ \alpha_1 \operatorname{erf} \alpha_1 - \alpha_2 \operatorname{erf} \alpha_2 + \frac{1}{\sqrt{\pi}} (e^{-\alpha_1^2} - e^{-\alpha_2^2}) \right\}$$

where:

$$\left(\frac{\alpha_1}{\alpha_2} \right) = \frac{1}{\tau\sqrt{2}} \left(a \pm \frac{W}{2} \right).$$

Thus:

$$I_w(\phi 0) = \frac{2}{W} \operatorname{erf} \left(\frac{W}{2\sqrt{2}\tau} \right),$$

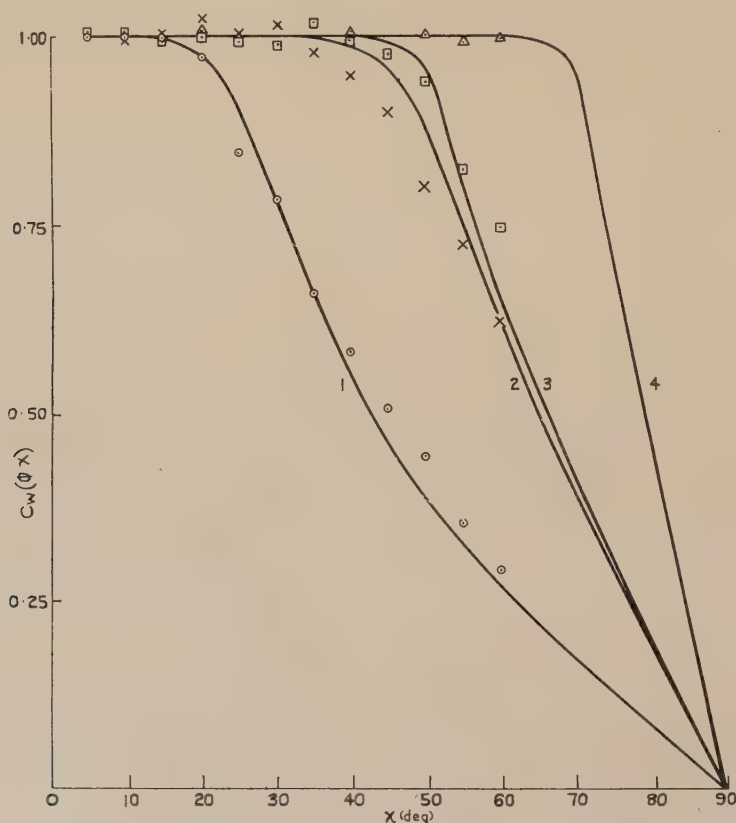


Fig. 4. Variation of the calculated and measured calibration function $C_w(\phi, \chi)$ for two values of E_5 and two values of W

Calculated curve	Measured points		
1	○	$E_5 = 0.047$ in.	$W = 0.4$ deg.
2	×	$E_5 = 0.020$ in.	$W = 0.4$ deg.
3	□	$E_5 = 0.047$ in.	$W = 1.0$ deg.
4	△	$E_5 = 0.020$ in.	$W = 1.0$ deg.

and the calibration function is given by:

$$C_W(\phi\chi) = \frac{\tau\sqrt{2}}{2\alpha \operatorname{erf}\left(\frac{W}{2\tau\sqrt{2}}\right)} \left\{ \alpha_1 \operatorname{erf} \alpha_1 - \alpha_2 \operatorname{erf} \alpha_2 + \frac{1}{\sqrt{\pi}} (e^{-\alpha_1^2} - e^{-\alpha_2^2}) \right\}$$

Values of $C_W(\phi\chi)$ were measured for the (111) line of an annealed Ni powder compact and are shown, in comparison with the appropriate calculated curves, in Fig. 4.

In view of the good agreement between the experimental and theoretical values of $C_W(\phi\chi)$, it is evident that the observed variation is due to the defocusing of the diffracted beam produced by the specimen tilt. Chernock and Beck⁽²⁾ came to the same conclusion but found a more rapid variation which could be caused by inaccurate alinement of the aperture system. The agreement would be expected, from previous considerations, to be even better for a cold-worked specimen

which unfortunately could not be accurately measured for large χ values because of their low intensities. In particular it is evident that to resolve two diffraction lines separated by $\Delta\theta \simeq 0.9$ deg. at $\theta \simeq 20$ deg. and $\chi \simeq 60$ deg. it is necessary to reduce the incident beam height to about 0.09 cm. This would be the case for the (0002) and (10 $\bar{1}$ 1) lines of titanium and this considerably limited the speed and accuracy of measurements made on some (0002) pole figures.

To reduce the time required in measuring the integrated intensities an alternative procedure has been suggested.^(4,6) By correcting the intensity measured by a narrow slit placed at the peak of the diffraction line, using a previously determined calibration curve, it is possible to measure the intensities of lines which are not completely resolved and also continuously record them as a function of the azimuthal angle about the normal to the specimen surface. However, as used in References 4 and 6, this method is open to objection. The calibration material was annealed, whereas the pole

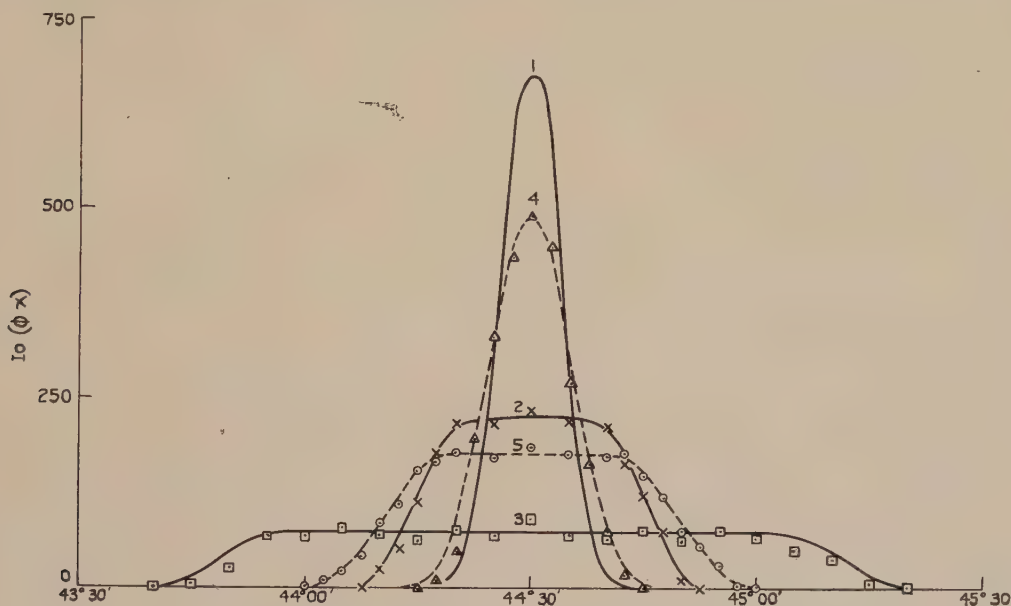


Fig. 5. Diffraction-line profiles $I_0(\phi, \chi)$ for three values of χ and two values of E_s

- | | | |
|---|-------------|---|
| 1. Least squares Gaussian approximation to measured curve | $\chi = 0$ | |
| 2. Calculated curve | Full line | Measured point \times $E_s = 0.047$ in. $\chi = 30$ deg. |
| 3. Calculated curve | Full line | Measured point \square $E_s = 0.047$ in. $\chi = 60$ deg. |
| 4. Calculated curve | Dotted line | Measured point \triangle $E_s = 0.020$ in. $\chi = 30$ deg. |
| 5. Calculated curve | Dotted line | Measured point \circ $E_s = 0.020$ in. $\chi = 60$ deg. |
- 4 and 5 are normalized to the same area as 1, 2, 3.

so that, even in the most unfavourable case, the test is satisfactory. From the theoretical treatment it is now possible to determine the optimum conditions for determining a particular pole figure using this technique. For accuracy and speed of measurement it is necessary to irradiate as large an area as possible and to have a grain size as small as possible. For materials with cubic symmetry where the diffraction lines are widely separated, the permissible height of the incident beam is limited solely by the vertical divergence which, as has been shown, can be large without producing any appreciable variation in the integrated intensity $J(\chi)$. For materials with a lower symmetry, the height of the incident beam may be primarily determined by the separation of the diffraction lines. The diffraction line profiles $I_0(\phi, \chi)$ of the Ni (111) diffraction line are shown in Fig. 5, for $E_s = 0.05$ and 0.12 cm and $\chi = 0, 30$ and 60 deg. These calculated curves are in fair agreement with the experimental points

figure intensity determinations were made on heavily cold-worked materials. The variations of $C_W(\phi\chi)$ for diffraction lines having typical integral widths of 0.11 and 0.33 deg. at $\chi = 0$ for annealed and cold-worked materials respectively were calculated for a beam height of 0.05 cm and a detector slit width of 0.2 deg. and are shown in Fig. 6. There is evidently a large difference between the two curves and if the calibration technique had been used in these circumstances, an error of about 50% would have been incurred at $\chi \simeq 50$ deg. Thus it would appear necessary to prepare a calibration specimen of randomly oriented grains or particles having the same degree of cold work as the specimen to be examined. This procedure, if possible, would increase the work enormously.

The main conclusion of this work is that the Schulz technique can be used without calibration curves provided that the integrated intensity of the diffraction line is measured

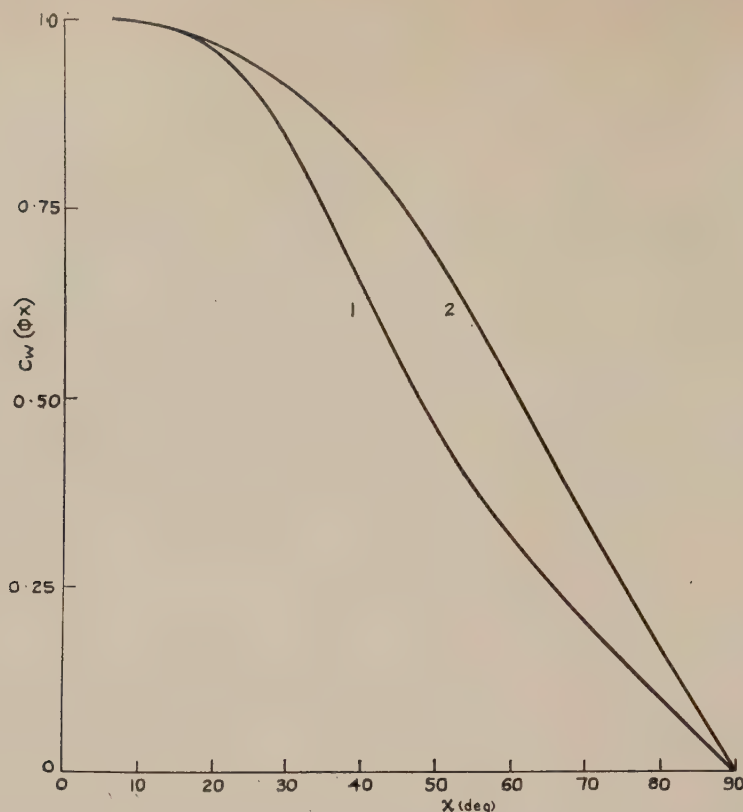


Fig. 6. Variation of the calibration function $C_w(\phi)$ for two values of the integral width ω of $I_0(\phi)$

Curve 1. $\omega = 0.11$ deg. } $E_5 = 0.020$ in. $W = 0.2$ deg.
 Curve 2. $\omega = 0.33$ deg.

and provided that the vertical height of the incident beam is limited either by its overlap of the specimen at large tilts or by overlap of neighbouring defocused diffraction lines.

Acknowledgement

This work was carried out as part of the General Research Programme of the National Physical Laboratory and is published by permission of the Director of the Laboratory.

References

- (1) SCHULZ, L. G. *J. Appl. Phys. (America)*, **20**, p. 1030 (1949).
- (2) CHERNOCK, W. P., and BECK, P. A. *J. Appl. Phys. (America)*, **23**, p. 341 (1952).
- (3) CHERNOCK, W. P., MUELLER, M. H., FISH, H. R., and BECK, P. A. *Rev. Sci. Instrum.*, **24**, p. 925 (1953).
- (4) MUELLER, M. H., and KNOTT, H. W. *Rev. Sci. Instrum.*, **25**, p. 1115 (1954).
- (5) JAMES, R. W. *The Optical Principles of the Diffraction of X-rays* (London: G. Bell and Sons Ltd., 1948).
- (6) FULLER, M. L., and VAUX, G. *J. Metals*, **5**, p. 1038 (1953).

Fourier series associated with duty cycles

by C. G. MAYO, M.A., B.Sc., M.I.E.E., and J. W. HEAD, M.A., F.Inst.P., B.B.C. Research Department, Tadworth, Surrey

(Paper first received 28 October, and in final form 16 November, 1959)

Abstract

An arbitrary function $F(\theta)$ of period 2π may be divided (by "time multiplex") into n parts $H_k F(\theta)$ [$k = 0, 1, \dots, (n-1)$] each of which is only different from zero for $1/n$ th of the cycle [when $2k\pi/n < \theta < (2k+2)\pi/n$] and is then equal to $F(\theta)$. The Fourier series for $F(\theta)$ (in its exponential form) may also be divided (by "frequency multiplex") into n sub-series $F_u(\theta)$ ($u = 0, 1, \dots, n-1$) each of which contains only every n th term of the series for $F(\theta)$, that is to say, terms involving $\exp(sn + u)i\theta$ where s is an integer. A relation is established between the time-multiplex subdivisions $H_k F(\theta)$ and the frequency-multiplex subdivisions $F_u(\theta)$ and special cases are considered, namely (a) all the $H_k F(\theta)$ zero except one, (b) $F(\theta)$ constant for $1/n$ th of the cycle and otherwise zero, when the behaviour of the series obtained can be checked by contour-integration methods of series summation. In case (a) all the $F_u(\theta)$ are equal while $F(\theta)$ is different from zero, and mutually cancel otherwise.

Introduction

IF an electrical circuit contains a switch which is closed for $1/n$ th of each cycle only, the current through the switch will have the essential property of being arbitrary for $1/n$ th of the cycle and zero for the remainder. Only the case when n is integral will be considered. This current, like other periodic waveforms, can be expressed as a Fourier series. The original objective was to determine the essential peculiarities of such Fourier series, but this has led to a more general consideration of the Fourier series of an arbitrary periodic function, and the way in which the behaviour of the function in various parts of the period affects the Fourier series.

The main result obtained involves what may appropriately be termed the time-multiplex and frequency-multiplex subdivisions of an arbitrary periodic function. Let a period (which is taken as being from 0 to 2π) be divided into n equal sections of which the $(k+1)$ th is from $2k\pi/n$ to $(2k+2)\pi/n$. Then the time-multiplex subdivision $H_k F(\theta)$ [equal to $F(\theta)$ in the $(k+1)$ th section and zero otherwise, and defined precisely below] is regarded as an entity requiring special attention, independently of its behaviour in other sections.

$H_k F(\theta)$ is defined [equation (8) below] in terms of Heaviside's "unit-step". $H_k F(\theta)$ is thus essentially a discontinuous function, and isolated discontinuities are easily handled by means of Fourier series. It is to Heaviside that is owed this possibility of explicitly formulating a function having isolated discontinuities so that these make no essential difference to the manner of deriving the coefficients for a Fourier series.

If a function $f(x)$ is integrated between finite limits, for the purpose of this article the value of $f(x)$ outside those

limits is irrelevant. This ought to imply that $f(x)$ is then zero—in other words, the insertion of finite limits indicates that a function is integrated which changes discontinuously to zero at those limits. Unfortunately this discontinuous nature of the integrand associated with the use of finite limits has been implied and not stated, and has therefore not been fully appreciated, and until recently there has been no convenient mathematical notation for indicating such a discontinuity. Heaviside, however, clearly perceived this, and corrected the deficiency of notation at the same time, by using:

$$I(x) = \int_{-\infty}^{\infty} f(x)[H(x-a) - H(x-b)]dx$$

to denote what is normally called the integral from a to b of $f(x)$ with respect to x ; $H(\xi)$ is Heaviside's unit step, zero for negative ξ and unity for positive ξ . In $I(x)$, the discontinuous nature of the integrand at $x=a$ and $x=b$ is explicitly stated. Heaviside's use of this notation did much to clarify phenomena involving isolated discontinuities and led to the relative success of his operational calculus.

It is also assumed here that $F(\theta)$ has a Fourier series the coefficients of which are determined in the usual way, but this series will be expressed exponentially with $C_r \exp(ir\theta)$ as a typical term, where r is an integer between $-\infty$ and $+\infty$. The complex coefficients C_{-r} and C_r will be conjugate since $F(\theta)$ is real, and can be paired to give a real series of sine and cosine terms, but in fact it is not advantageous to do this. The exponential form of the series simplifies the analysis and leads to a clearer understanding.

For frequency-multiplex subdivision of $F(\theta)$, only $1/n$ th of the exponential terms of the Fourier series is taken, so that a typical term of the subdivision $F_u(\theta)$ is

$$C_{sn+u} \exp[i(sn+u)\theta]$$

where s is any integer from $-\infty$ to $+\infty$ and u a fixed integer from 0 to $(n-1)$ inclusive.

The basic relationship obtained in this article is a linear one between the time-multiplex subdivisions of $F(\theta)$ at "corresponding" points (separated by an angular distance which is an integral multiple of $2\pi/n$) and the frequency-multiplex subdivisions of $F(\theta)$. The coefficients in this relationship are powers of the n th roots of unity.

To obtain this basic relationship, certain well-known properties are used of the complex number $\exp(2i\pi/n)$ (which is abbreviated to x throughout). These properties have been outlined in the following section to make this article self-contained. Not only x but any power of x is an n th root of unity. Power-station engineers accustomed to three-phase work use "sequences" which are in effect linear combinations of the currents in the three phases, the coefficients of which involve the cube roots of unity (that is, $n=3$). In particular, a certain system of linear simultaneous equations (or the equivalent matrix equation) has a simple explicit solution.

The frequency-multiplex subdivisions $F_u(\theta)$ which enter into the basic relation obtained below are individually complex quantities—infinite series containing complex terms which cannot be arranged in conjugate pairs unless u is either zero or $\frac{1}{2}n$ (n even). For other values of u , $F_u(\theta)$ and $F_{n-u}(\theta)$ are conjugate quantities which must be paired in order to obtain physically significant results, just as a polynomial can be factorized into complex linear factors or real quadratic factors obtained by combining the complex linear factors in conjugate pairs. During the analysis, however, it is easier to work with the individual $F_u(\theta)$ just as it is often easier to work with the individual complex factor of a polynomial.

The special case when $F(\theta)$ is constant (where different from zero) is also discussed. This throws light on the summation of certain infinite series which are not easy to sum by classical methods.

The n th roots of unity

If

$$\xi^n = 1, \quad (n \neq 1), \quad (1)$$

then ξ must be x^r where x is $\exp(2i\pi/n)$ and r is any integer from 0 to $(n-1)$ inclusive. The positions of these roots for $n=5$ and $n=6$ on the Argand diagram are given in Figs. 1(a) and 1(b) respectively. Fig. 1(a) is typical of the general arrangement when n is odd and Fig. 1(b) of that when n is even. The roots are always on the circumference of a circle of unit radius and the angular distance between

zero for any root of equation (1) other than unity. This fact will be used frequently, and is referred to briefly as “the sum of n consecutive powers of an n th root of unity (other than unity) is zero”.

In general, it is easier to do all calculation with the n th roots of unity as individual complex quantities, and only combine them in conjugate pairs when a final result is reached. When these n th roots are dealt with individually, there is no essential difference between the cases when n is odd and when n is even. Now consider the symmetrical set of linear simultaneous equations:

$$\sum_{r=0}^{n-1} x^{rk} Y_r = A_k, \quad (k = 0, 1 \dots n-1), \quad (3)$$

where x means $\exp(2i\pi/n)$ as before. In equation (3) the quantities A_k are regarded as given and the quantities Y_r ($r = 0, 1 \dots n-1$) are “unknowns”. If equation (3) is multiplied by x^{-rk} and summed with respect to k , then:

$$nY_r = \sum_{k=0}^{n-1} x^{-rk} A_k, \quad (4)$$

because the coefficient of Y_r is clearly n while the coefficient of Y_s is the sum of n different powers of an n th root of unity (which can be regarded as consecutive if suitable multiples of n are subtracted from or added to the indices). This can conveniently be expressed in matrix notation. The n equations (3) are replaced by the single matrix equation:

$$[x^{rk}] [Y] = [A], \quad (5)$$

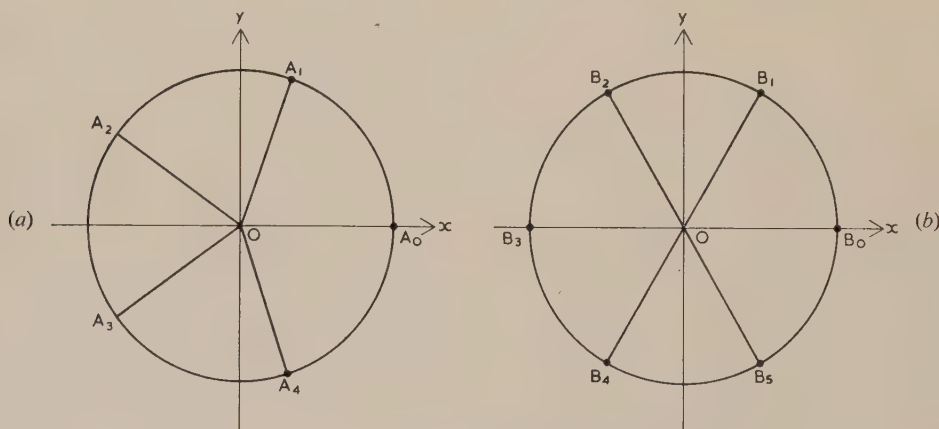


Fig. 1. The n th roots of unity on the Argand diagram

(a) $n = 5$ (angular distance between A_0A_1 , A_1A_2 , etc., is 72 deg.)

(b) $n = 6$ (angular distance between B_0B_1 , B_1B_2 , etc., is 60 deg.)

consecutive roots is $2\pi/n$ radians. The sum of all the roots (including unity) is zero. This may be immediately obvious. If not, consider equal masses placed at the points $A_0A_1 \dots A_4$ of Fig. 1(a) or $B_0B_1 \dots B_5$ of Fig. 1(b); the centre of mass of the arrangement will be at the centre. Alternatively, equation (1) has no term in ξ^{n-1} and, therefore, the sum of the roots of this equation is zero.

Further, Figs 1(a) and 1(b) are both symmetrical about the real axis. That is to say, the various roots can be taken together in conjugate pairs, like A_1 and A_4 or B_2 and B_4 . A_0 is always an “odd” root, but it is a real root. Likewise, when n is even, $B_{n/2}$ is also an “odd” real root. Since:

$$\xi^n - 1 = (\xi - 1)(\xi^{n-1} + \xi^{n-2} + \dots + \xi^2 + \xi + 1), \quad (2)$$

the second factor on the right-hand side of equation (2) is

where $[Y]$ is the column matrix with elements $Y_0, Y_1 \dots Y_{n-1}$ and $[A]$ is the column matrix with elements $A_0, A_1 \dots A_{n-1}$ while $[x^{rk}]$ is a square matrix with n rows and n columns, r and k ranging from 0 to $n-1$ inclusive. Since the sum of n different powers of an n th root of unity is zero, then:

$$[x^{rk}] [x^{-rk}] = n[I], \quad (6)$$

where $[I]$ is the unit matrix of order n . It follows that:

$$[Y] = \frac{1}{n} [x^{-rk}] [A], \quad (7)$$

so that given the quantities A_k [equation (3) or (5)] the quantities Y_r [equation (4) or (7)] can be deduced and vice versa

Time-multiplex and frequency-multiplex splitting

The basic relation. Suppose that $F(\theta)$ is periodic with period 2π , so that $F(\theta) = F(\theta) + 2\nu\pi$ where ν is any integer. Let the period during which θ increases from 0 to 2π be divided into n equal sections and consider the function $H_k F(\theta)$ derived from $F(\theta)$ by the formula:

$$H_k F(\theta) = \left[H\left(\theta - \frac{2k\pi}{n}\right) - H\left\{\theta - \frac{(2k+2)\pi}{n}\right\} \right] F(\theta) \quad (8)$$

for $k = 0, 1 \dots n-1$, where $H(\xi)$ denotes Heaviside's unit function. Since $H(\xi)$ is zero when ξ is negative and unity when ξ is positive, $H_k F(\theta)$ in equation (8) will be zero except when θ is between $2k\pi/n$ and $(2k+2)\pi/n$; for these values of θ , $H_k F(\theta)$ is $F(\theta)$. Thus $H_k F(\theta)$ specifies the behaviour of $F(\theta)$ in the $(k+1)$ th section of the period

$$[2k\pi/n < \theta < (2k+2)\pi/n]$$

without reference to its behaviour in any other section. Then*:

$$F(\theta) = \sum_{k=0}^{n-1} H_k F(\theta). \quad (9)$$

Equation (8) thus splits $F(\theta)$ into n parts, and this process will be referred to as "time-multiplex splitting".

Now let $F(\theta)$ be expressed as a Fourier series:†

$$F(\theta) = \sum_{r=-\infty}^{\infty} C_r \exp(ir\theta), \quad (10)$$

$$\text{where } C_r = \frac{1}{2\pi} \int_0^{2\pi} F(\phi) \exp(-ir\phi) d\phi. \quad (11)$$

If $F(\theta)$ is real, the coefficients C_{-r} and C_r will be conjugate, and they can be taken together to give the more usual sine and cosine form of the series. The n functions $F_u(\theta)$ are defined by the formula:

$$F_u(\theta) = \sum_{s=-\infty}^{\infty} C_{sn+u} \exp\{i(sn+u)\theta\}, \quad (u = 0, 1 \dots n-1), \quad (12)$$

so that each $F_u(\theta)$ contains $1/n$ th of the terms of the Fourier series of equation (10), but in general $F_u(\theta)$ does not contain pairs of conjugate complex terms [the exceptional cases being when $u = 0$ or $\frac{1}{2}n$ (n even)].

At this stage the functions $F_u(\theta)$ defined by equation (12) have been arbitrarily introduced, and it is not obvious that they have an important significance. These will be called the n "frequency-multiplex" subdivisions of $F(\theta)$. It is perhaps worth passing notice that $F_0(\theta)$ is periodic with period $2\pi/n$ and repeats itself in every section. It is this fact that suggests that the other quantities $F_u(\theta)$ may be in some way significant.

Equation (12) specifies $F_u(\theta)$ for all values of θ . It is, however, of interest to consider separately the behaviour of $F_u(\theta)$ in each of the n sections already specified in connexion

* More generally, we can start with n periodic functions $F_0(\theta), F_1(\theta) \dots F_{n-1}(\theta)$ each with period 2π and such that the $(k+1)$ th of these, $F_k(\theta)$, is only different from zero for $2k\pi/n < \theta < (2k+2)\pi/n$. In this case, $F(\theta)$ can be defined by means of equation (9) but there may be no ordinary analytic expression for $F(\theta)$.

† $H_k F(\theta)$ could also be expressed similarly as a Fourier series, and the sum of all the Fourier series so obtained, with respect to k , would be the series specified by equation (10). There is, however, no advantage in doing this; it is easier to specialize $F(\theta)$ if necessary.

with the time-multiplex splitting of $F(\theta)$, and to express any section of $F_u(\theta)$ in "intrinsic co-ordinates", that is to say, in terms of a variable which is zero at the beginning of the section and increases to $2\pi/n$ at the end of it. Therefore, if $\theta = \theta_m + 2m\pi/n$ ($0 < \theta_m < 2\pi/n$) in section $(m+1)$ and, if this section is denoted by F_{um} , then:

$$F_{um} = F_u(\theta_m + 2m\pi/n). \quad (13)$$

If a factor $\exp(iu\theta)$ is taken out of the right-hand side of equation (12), the remaining factor is unaltered if θ is increased by any integral multiple of $2\pi/n$, so that:

$$F_{um} = \exp\left(\frac{2im\pi u}{n}\right) F_{u0} = x^{imu} F_{u0}. \quad (14)$$

If these equations are summed with respect to u for fixed m , the left-hand side becomes simply

$$F(\theta_m + 2m\pi/n) \quad (0 < \theta_m < 2\pi/n),$$

which is denoted by ${}_m F$, and which means the $(m+1)$ th section of $F(\theta)$ expressed in terms of its intrinsic co-ordinate θ_m , so that:

$${}_m F = \sum_{u=0}^{n-1} x^{imu} F_{u0}. \quad (15)$$

If now m is allowed to take all values from 0 to $(n-1)$ inclusive, equation (15) becomes a set of n simultaneous equations of the form discussed above [equation (3)] where the quantities F_{u0} can be regarded as the unknowns and the quantities ${}_m F$ are given. The solution of equations (15) [analogous to equation (4)] is:

$$F_{u0} = \frac{1}{n} \sum_{m=0}^{n-1} x^{-imu} {}_m F. \quad (16)$$

This is the basic relationship, specifying all the quantities F_{u0} at any point θ_0 in the first section ($0 < \theta_0 < 2\pi/n$) in terms of the quantities ${}_m F$, that is to say, the values of $F(\theta)$ at the points which "correspond" to θ_0 in the other sections because they are separated from θ_0 by integral multiples of $2\pi/n$. Equation (16) is thus essentially a relationship between the frequency-multiplex subdivisions of $F(\theta)$ in the first section on the one hand, and the time-multiplex subdivisions of $F(\theta)$ (at points which "correspond" in the various sections) on the other. The fact that it is F_{u0} —first-section values—that are specified by equation (16) does not really involve any loss of generality, since $F(\theta)$ is unrestricted and the θ -origin may be taken where it is convenient. If $F_u(\phi)$ is considered where ϕ is outside the first section, it is only necessary to find the "corresponding" point in the first section, which is separated from ϕ by an integral multiple of $2\pi/n$, and to apply equation (14). Thus equation (16) in fact specifies all the $F_u(\theta)$ for all values of θ .

Now let the special case be considered in which $F(\theta)$ is replaced by $H_0 F(\theta)$, that is to say, is only different from zero in the first section. Then the right-hand side of equation (16) reduces to a single term when $m = 0$ and so, for all u ,

$$F_{u0} = \frac{1}{n} F, \quad (17)$$

where F_{u0} is now a frequency-multiplex subdivision of $H_0 F(\theta)$ obtained in a manner analogous to equation (12). Thus in this special case, when a function $H_0 F(\theta)$ is dealt with which is only different from zero in the first section ($0 < \theta_0 < 2\pi/n$), then the remarkable result occurs that the frequency-multiplex subdivisions F_{u0} are all real and equal in the first section, but

become out of step and mutually cancel in any other section [by virtue of equation (14)].

Although mathematically equation (16) and the important special case, equation (17), are quite clear, the physical significance of the complex quantities F_u and F_{u0} (which in general do not contain pairs of conjugate terms) is not obvious. However,

$$F_u(\theta) \text{ and } F_{n-u}(\theta) \quad (18)$$

are always conjugate expressions, so that the basic relationship can be expressed in terms of real and physically significant quantities [both in the general case, equation (16), and in the special case, equation (17)] by suitable pairing. Equation (16), however, appears to express this basic relation in its simplest possible form.

Special case of constant current in the duty cycle

Now consider a further specialization in which $F(\theta)$ is constant (and equal to unity) for $1/n$ th of the cycle and zero for the remainder. If $F(\theta)$ is taken to be non-zero for $0 < \theta < 2\pi/n$, the equation corresponding to equation (17) becomes:

$$F_u = \frac{1}{n}, \quad (0 < \theta < 2\pi/n). \quad (19)$$

Now, in this case:

$$F_u = \sum_{s=-\infty}^{\infty} \frac{\sin \{(sn+u)\pi/n\}}{(sn+u)\pi} \exp \{i(sn+u)(\theta - \pi/n)\}, \quad (20a)$$

or

$$F_u = \frac{1}{n} \sin \frac{u\pi}{n} \sum_{s=-\infty}^{\infty} \frac{n}{\pi} (-1)^s \frac{\exp \{i(sn+u)(\theta - \pi/n)\}}{sn+u}. \quad (20b)$$

The correctness of equation (20b) can be checked by applying contour-integration theory to the function $\phi(z)$ of the complex variable z defined by:

$$\phi(z) = \frac{\exp \{iz(\theta - \pi/n)\}}{z \sin \{(z-u)\pi/n\}}, \quad (21)$$

which is shown to be closely related to the right-hand side of equation (20b) as follows:

$\phi(z)$ has a pole at $z=0$ with residue $-1/\sin(u\pi/n)$ and poles at $z=(sn+u)$ for any integral s with residue $[n(-1)^s \exp \{i(sn+u)(\theta - \pi/n)\}]/\pi(sn+u)$. If θ is between 0 and $2\pi/n$, the integral of $\phi(z)$ round the "great circle" is zero, and therefore the sum of the residues of $\phi(z)$ is zero. This gives:

$$\frac{n}{\pi} \sum_{s=-\infty}^{\infty} \frac{(-1)^s}{sn+u} \exp \{i(sn+u)(\theta - \pi/n)\} = \frac{1}{\sin(u\pi/n)}. \quad (22)$$

Substitution from equation (22) into equation (20b) confirms that F_u is constant and equal to $1/n$ for all n when $0 < \theta < 2\pi/n$.

If θ is put equal to π/n in equation (22), then:

$$\sum_{s=-\infty}^{\infty} \frac{(-1)^s}{sn+u} = \frac{\pi}{n \sin(u\pi/n)}, \quad (23)$$

and series having terms with alternate signs, the denominators of which form an arithmetic progression, can be summed explicitly and easily.

If equation (14) is now applied, it can be seen that F_u changes discontinuously when θ crosses the boundary values 0 or $2\pi/n$, and similarly changes discontinuously when θ passes through any other value $2r\pi/n$ for integral r , so that,

although equation (22) applies only for $0 < \theta < 2\pi/n$, in fact independent confirmation has been obtained that all the F_u are as predicted in all sections. It is clear that equation (16), and the important special case, equation (17), can be used as a very powerful means of determining the sums of series which would be difficult to obtain otherwise.

Rough diagrams of the frequency-multiplex divisions of both current and voltage are given in Fig. 2 for the case

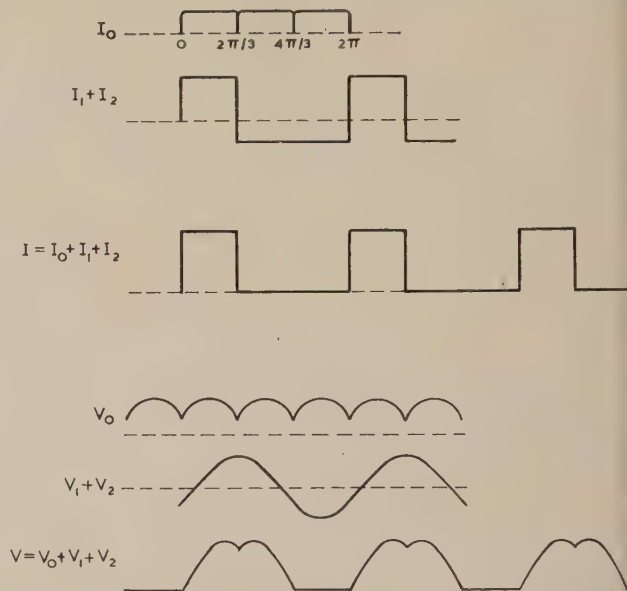


Fig. 2. Rough diagrams of voltage and current waveforms when $n=3$ and the total current is constant in the duty cycle (0 to $2\pi/3$) and zero otherwise

when the duty cycle is $2\pi/3$ (that is, $n=3$) and the current is constant during the duty cycle and zero otherwise. Thus, I_0 corresponds to F_0 in the notation of equation (19); as I_1 (corresponding to F_1) and I_2 (corresponding to F_2) are complex conjugate quantities, only $(I_1 + I_2)$ can be represented conveniently. The corresponding voltages V_0 , V_1 and V_2 have been calculated on the assumption that the switch is ideal, that is to say, has zero impedance in the duty cycle and infinite impedance otherwise.

Conclusions

Let the arbitrary function $F(\theta)$ of period 2π be partitioned into n "time-multiplex" parts $H_k F(\theta)$ each of which differs from zero only for $1/n$ th of the cycle

$$\{2k\pi/n < \theta < (2k+2)\pi/n\}.$$

Suppose also that $F(\theta)$ is divided into n complex parts F_u by "frequency-multiplex" subdivision. Then relationships have been established between the $H_k F(\theta)$ and the F_u in the general case. In the special case when $F(\theta)$ is only different from zero for $1/n$ th of the cycle, this relation simplifies: all the F_u are equal and real, having the common value $\{F(\theta)\}/n$ when $F(\theta)$ is different from zero. For the remainder of the cycle, the F_u mutually cancel although no individual F_u is, in general, zero.

Acknowledgements

The authors wish to express their thanks to the Director of Engineering of the B.B.C. for permission to publish this paper.

Contents

	PAGE		PAGE
<i>Special report</i>		<i>Miscellaneous</i>	
The teaching of mathematics to physicists.	108	Annual reports on the progress of chemistry. Vol. LV	114
		The physical chemistry of steel making	114
		Progress in metal physics 7	114
		Progress in vacuum science and technology	114
		Recent research in molecular beams: A collection of papers dedicated to Otto Stern on the occasion of his 70th birthday	114
<i>Acoustics</i>			
Absorption and dispersion of ultrasonic waves	108		
<i>Heat, thermometry and low temperature physics</i>		<i>Nuclear and cosmic ray physics, apparatus, techniques and data</i>	
A supplement to "Helium"	108	Bibliography of the stable isotopes of oxygen (^{17}O and ^{18}O)	114
Experimental techniques in low-temperature physics	108	Directory of nuclear reactors. Vol. 1. Power reactors	115
Handbuch der Kältetechnik. Band 7: Sorptions-Kälte- maschinen	109	Encyclopaedia of physics. Vol. XXXVIII/2. Neutrons and related gamma ray problems	115
Instationäre Wärmespannungen	109	Nuclear reactor shielding (Nuclear Engineering Monographs, No. 4)	115
Progress in cryogenics. Vol. 1	109	Nuclear reactor control and instrumentation. (Nuclear Engineering Monographs, No. 5)	115
		Steam cycles for nuclear power plant (Nuclear Engineering Monographs, No. 6)	116
<i>Magnetic, electrical and electronic devices and properties</i>		Plasma physics and the problem of controlled thermonuclear reactions. Vol. 3	116
A new method in the theory of superconductivity	110	Principles of radiation dosimetry	116
Circuit theory of linear noisy networks	110	Proceedings of the international conference on nuclear physics: Low energy nuclear interactions and nuclear structure, Paris, 1958	116
Proceedings of the fourth national conference on tube techniques	110	Radioisotopes for industry	116
Solid state magnetic and dielectric devices	110		
<i>Mathematical theories, techniques, computers and control systems, and mechanics</i>		<i>Reference books</i>	
Applications of finite groups	111	Adhesives guide	117
Control system components	111	Handbook of chemical microscopy. Vol. 1	117
Course of theoretical physics. Vol. 7. Theory of elasticity	112	Methods of experimental physics. Vol. 1. Classical methods	117
Dynamische vorgänge in linearen Systemen der Nachrich- ten-und Regelungstechnik	112	Quantum chemistry integrals and tables	117
Grundlagen der Selbsttätigen Regelung. Band II: Einige Probleme aus der Theorie der nichtlinearen Regelungs- systeme	112	Technische Kunstgriffe bei physikalischen Untersuchungen	118
Proceedings of the third national congress of applied mechanics	112		
Sampling inspection tables. Single and double sampling	113	<i>Solid state physics and crystallography</i>	
Theorie der stabilität einer bewegung	113	Dendritic crystallization	118
		Vector space and its application in crystal-structure investigation	118

New books section

Special Report

The teaching of mathematics to physicists. 2nd ed. (London: The Institute of Physics, 1959.) Pp. 26. Price (non-members of the Institute) 2s. 6d.

The Institute of Physics has recently published a revised edition of the report originally published under the above title in 1944. Since that time it has twice been reprinted and the present version has been considerably revised—in some respects fundamentally—in the light of experience since the war and of what is believed to be the need for the future.

The report has been prepared by a committee appointed by the Board of The Institute of Physics. The text headings are: Elementary mathematics; Mathematics for physicists; Rigour and generality; The literature of physics and mathematics; Pure and applied mathematics; Staff; Courses; Examinations. Appendix I. A suggested syllabus in mathematics for students reading for honours degrees in physics; Appendix II. Questions set in the Graduateship examination of The Institute of Physics.

The report is obtainable from The Institute of Physics, 47, Belgrave Square, London, S.W.1, and is available free of charge to members of the Institute.

Acoustics

Absorption and dispersion of ultrasonic waves. By K. F. HERZFELD and T. A. LITVITZ. (New York: Academic Press Inc.; London: Academic Books Ltd., 1959.) Pp. xviii + 535. Price £5 3s. 6d.

This book is Volume 7 of the Monographs on Pure and Applied Physics published by the Academic Press and edited by Professor Massey. It is devoted entirely to a detailed account of the absorption and dispersion of ultrasonic waves in gases and liquids treated from the point of view of molecular structure. There is not, at the moment, any other book which covers the same fields in such a comprehensive manner, and this book should therefore prove a valuable addition to the literature of ultrasonics.

The book is divided into three sections. The first describes the general theories of relaxation in fluids, with detailed mathematical developments of such topics as the Stokes-Navier equations of hydrodynamics, the absorption and dispersion of sound waves, and relaxation times and degrees of freedom. The absorption of high intensity sound waves is treated briefly at the end of this section, where occurs the only discussion of cavitation.

Section B of the book deals with gases. After a chapter giving the results of applying the various theoretical treatments mentioned in the first section to pure gases and gas mixtures, there is a chapter of twelve pages describing experimental methods. As may be gathered from the number of pages involved, detailed descriptions of experimental techniques are not given. In spite of this, there is much useful information for the experimentalist, as brief reviews are given of the methods used by various workers, with references and comments about the advantages and accuracy of the techniques. Similar remarks apply to the short chapter of eight pages dealing with experimental techniques for liquids, which is in the next section of the book.

Section C deals with ultrasonic absorption in liquids, and starts with a general review of the development of the topic, followed by a theoretical treatment of relaxation,

viscosity and related subjects. There is a chapter on Kneser liquids, and finally a very comprehensive account of the molecular behaviour of associated liquids and liquids of high viscosity.

The authors state that they intend their book to be a treatise giving the connexions between ultrasonic data, chemical reaction rates, and the theories of the gas, liquid and glassy states of matter. As such, the book succeeds or fails mainly according to its comprehensiveness. The very detailed treatment of the various theories, and particularly the correlations between theory and experiment, together with the copious references and tables of data ensure that the writers have made a success of their project. It is unfortunate that the important topics of absorption in solids and high polymer solutions had to be omitted in order to keep the size of the book reasonable. It is a pity that a similar consideration could not have been applied to the price.

The book should prove valuable, not only to research workers in the field of ultrasonics, but also to those interested in the general field of molecular phenomena.

N. H. LANGTON

Heat, thermometry and low temperature physics

A supplement to "Helium". By E. M. LIFSHITS and E. L. ANDRONIKASHVILI. (New York: Consultants Bureau, Inc., London: Chapman and Hall Ltd., 1959.) Pp. v + 167. Price 60s.

When Keesom's classic *Helium* was translated into Russian in 1949, two chapters were added. The volume under review is a translation of this additional material—a theoretical chapter by Lifshits and an experimental one by Andronikashvili.

Lifshits' chapter is an admirable account of the theory of liquid helium developed by Landau and his school. The explanation of the basis of the theory and the interpretation of its conclusions are stressed, while the mathematical development is sketched fairly lightly. Quite apart from the value of its contents, this chapter deserves to be widely studied as an example of clarity in exposition.

Andronikashvili's chapter covers experimental work on liquid helium from 1939 to 1948. Prominence is given to the work of Kapitza but other work is included. The description of experiments and the interpretation of results is fairly detailed, making it of interest to the specialist rather than the general reader. For the specialist, however, the delay of a decade in translation makes this chapter largely of historical interest.

The wisdom of producing an expensive translation of a ten-year-old work of limited appeal could be questioned, but all who are interested in this field will want access to a copy. There is a number of minor errors, presumably of translation, but they do not materially detract from the value of the book.

R. W. HILL

Experimental techniques in low-temperature physics. By GUY KENDALL WHITE. (London: Oxford University Press, 1959.) Pp. viii + 328. Price 45s.

The increased commercial production of equipment for low temperature investigations, both gas liquefiers and ancillary apparatus, together with the necessity of extending investigations to the lowest possible temperatures, has led to a rapid

growth in the number of laboratories where facilities for such work are available. Formerly, when low temperature work was largely concentrated in a few specialist laboratories, it was possible to instruct investigators in the necessary techniques at these centres; but this is no longer possible and many workers have had to find their knowledge the hard way by searching journals for hints and making their own mistakes. Such simple operations as, for example, the transfer of liquid helium from one vessel to another, present their own special problems. As the author says in the preface, "Often these problems are not very difficult, but nevertheless the technical information and published experience which may help to solve them are spread over a wide range of years and journals".

This book by Dr. White sets out to instruct in the more usual low temperature techniques and it will ease the path of the newcomer to the field in providing much information in an easily accessible form and giving plenty of references to the literature where more details may be found. There are two main sections to the book dealing with general topics and the research cryostat respectively; a final shorter section discusses physical data of interest and use to the cryogenist. The treatment is essentially practical in approach and gives an account of how to do things with sufficient mathematics, where necessary, to justify accepted design procedures. As is to be expected in a book of this kind, some sections are more informative than others, but the author has had a difficult task in compressing so much information into a book of reasonable size and price. The book is the first of its kind in being wholly given over to the techniques of low temperature work, and it will meet a long-felt need. Research students just starting such work and those people wishing to extend investigations over a wider temperature range will find this publication timely and of great help; it can be thoroughly recommended to them. The established worker in the field will also find much of value in this book. F. E. HOARE

Handbuch der Kältetechnik. Band 7: Sorptions-Kältemaschinen. By W. NIEBERGALL. (Berlin: Springer-Verlag, 1959.) Pp. xviii + 540. Price DM. 76.80.

The twelve volumes of the *Handbuch der Kältetechnik*, edited by Prof. R. Plank, represent an extremely ambitious project, requiring for its success a series of highly qualified authors who are prepared to devote a great deal of their time to writing. In most cases the problem has been solved by the co-operation of several authors but the present volume of about 300 000 words is entirely written by Prof. Niebergall, one of Plank's pupils. In it he has dealt comprehensively with all aspects of refrigeration machines based on adsorption and absorption processes. The first section of the book deals with the theoretical considerations involved in these processes and in their application for the production of cold. The author begins with the thermodynamics of two-component systems and then discusses on this basis the efficiency and applicability of the various types of cooling devices. This is followed by a full survey of the combinations of substances which can be used in machines of this type and here a great number of valuable data are made available. Numerical examples, illustrating the problems treated in these theoretical chapters, help greatly to clarify the discussion.

The following two sections of the book are devoted to a more detailed description and discussion of small and large cooling installations. They deal with an assessment of the construction and design features of actual plant of which

drawings, half-tone illustrations and performance diagrams are given.

The book is clearly addressed to the specialist in the field who will welcome the compilation of all the relevant data and discussion in one volume. It may also find its use as a reference book to which refrigeration engineers in general can turn for information on all aspects of sorption machines.

K. MENDELSSOHN

Instationäre Wärmespannungen. By H. PARKUS. (Wien: Springer-Verlag, 1959.) Pp. v + 165. Price DM. 18.50.

The author explains that this is a continuation and conclusion to an earlier book, written by him in collaboration with E. Melan, on thermal stresses due to a constant temperature field.

After an introduction, mainly on the dynamics of the problem, he takes up problems in order of increasing complexity, beginning with the instantaneous source in an infinite medium. He then proceeds to dipoles and to semi-infinite and spherical media; a number of problems for the cylinder conclude this section. Next, the author treats periodic temperature changes.

In all the above, the problems are treated as quasi-static, accelerations being neglected. In Chapter V the author takes up in some detail a few cases where dynamical effects are important. The book concludes with two chapters, the one on thermal stresses in viscoelastic materials and the other on the same problem for substances showing plasticity.

The treatment is clear throughout, and likely to make more appeal to the applied mathematician than to the engineer, but the latter may well be grateful for some of the results and the detailed curves illustrating them. J. H. AWBERY

Progress in cryogenics. Vol. 1. Edited by K. MENDELSSOHN. (London: Heywood and Co. Ltd., 1959.) Pp. viii + 259. Price 63s.

This book is the first volume of a new "progress" series in which it is the intention to deal with the technology associated with low temperature work. The increasing use of low temperatures, not only to elucidate the fundamental properties of matter, but also to make use of these properties in the regions where they have practical importance and application has led to rapid development and this makes it difficult, if not impossible, for one person to keep abreast of all the literature being published. Similar rapid developments in other fields make "progress" series particularly welcome. The newcomer is provided with an authoritative survey of the work already done and references which enable the details to be sought in the original publications where necessary, whilst the established worker will appreciate the critical appraisal of work in his field and the chance to read of techniques developed in other branches which may be applicable to his own.

The present volume contains seven articles dealing with superconducting circuits, thermoelectric cooling, powder insulation, low temperature distillation, mechanical properties of metals, frozen free radicals, calorimetry, specific heat determination by the temperature wave method and ultrasonic attenuation in metals. There is a nice balance between those topics where the main interest is technical, in the sense that the ideas and techniques may have importance for applications in the development of new devices, and those where the techniques described may lead to a greater understanding of the properties of matter. It would be invidious to single out

particular articles for detailed criticism but it can be stated that those dealing with topics in which the reviewer is particularly interested have been read with considerable profit. The others have been most welcome in providing readable reviews of subjects about which one is for ever intending to do some reading but is put off by the necessity of going to the originals. The editor has set himself and the contributors a difficult task in trying to separate the methods and the results of low temperature investigations. The distinction is not clear-cut and the overlap is necessarily greater in some fields than in others. This is apparent in these articles but in no way detracts from their usefulness since they all provide details of experimental methods which are unlikely to be found elsewhere than in the original publications.

The production of the book in clean type and with good diagrams makes it easy to read. The publication of further volumes in the series will be awaited with interest.

F. E. HOARE

Magnetic, electrical and electronic devices and properties

A new method in the theory of superconductivity. By N. N. BOGOLIUBOV, V. V. TOLMACHEV and D. V. SHIRKOV. (New York: Consultants Bureau, Inc.; London: Chapman and Hall Ltd., 1959.) Pp. iii + 121. Price 50s.

This book represents a translation of the authors' important original contribution to the theory of superconductivity. As such it is, of course, written in the style of an original paper, and requires fairly advanced knowledge of modern methods in theoretical physics. The particular method used here has since been applied to other questions involving interacting fermions (e.g. to large atomic nuclei). The book will, therefore, be of interest to theoretical physicists working on many body problems.

H. FRÖHLICH

Circuit theory of linear noisy networks. By H. A. HAUS and R. B. ADLER. (New York: John Wiley and Sons, Inc., and The Massachusetts Institute of Technology; London: Chapman and Hall Ltd., 1959.) Pp. xii + 79. Price 36s.

The book is highly mathematical, and as a result difficult for a physicist to assess. It has the great merit, however, of having been written with the application to actual physical situations clearly and explicitly stated throughout.

It is the second of two Monographs already published by The Massachusetts Institute of Technology in which published and other researches are brought together in a way which could not be done by publication in journals. At the same time, it is not a text-book covering a wide field. The treatment is therefore concentrated and contains conclusions justified by fully developed and orderly theory.

There is room for more publication of this sort, whereby the spate of publication in journals might be reduced by publishing only summaries of papers which support or amplify the effect of prior publications. If this could be done without suppressing discussion, the average amount of interest and information contained in papers published in full would be increased.

The subsequent publication of Monographs of this kind, covering a large programme of research, would enable the results to be presented in a better form, and be more quickly assimilated by a wider range of specialists than is at present possible.

The topic dealt with in this book is the spot noise factor F , with particular reference to optimizing the performance

of cascaded amplifiers $F_1, F_2 \dots$ etc., having power gains $G_1, G_2 \dots$ etc. The first step is the production of a new noise figure called the "Noise Measure" M , given by $(F - 1)/(1 - 1/G)$. The procedure consists of considering amplifiers in a very general way, to produce a comprehensive definition of the "Noise Measure", from which the optimization required can be carried out.

Conclusions are set out mainly for the cases in which the internal impedance of the amplifier is positive. However, the authors view the application to amplifiers having negative impedance as being of the greater future importance in view of the growing use of masers.

C. S. BULL

Proceedings of the fourth national conference on tube techniques. (New York: New York University Press, 1959.) Pp. 270. Price \$7.50.

This volume contains forty-six papers and abstracts of papers which were read at the 4th National Conference on (Thermionic) Tube Techniques. Sponsored by the Working Group on Tube Techniques, the Advisory Group on Electron Tubes, and the Office of the Director of Defense and Engineering, the conference was held in September, 1958.

Solid state magnetic and dielectric devices. Edited by H. W. KATZ. (New York: John Wiley and Sons Inc.; London: Chapman and Hall, Ltd., 1959.) Pp. xxi + 542. Price 108s.

The purpose of the book is to present a complete account of the theory and applications of solid state devices apart from those which utilize semiconductor properties. Thus the various applications of the newer magnetic and dielectric materials (particularly ferrites and ferroelectrics) are brought together in one volume. These materials exhibit a variety of physical properties which make them potentially useful in a wide range of devices and components. Although the authors "have tried to unify the diverse aspects of the broad field of magnetic and dielectric devices", it is hardly surprising that such topics as electromechanical filters, microwave ferrites and the applications of square loop materials still seem to be distinct and unrelated.

The first two chapters give an outline of the theoretical background of the dielectric and magnetic properties of materials, the reader being assumed to have a general background in field theory. The third chapter describes electrostrictive and magnetostrictive properties and derives the equivalent circuits of various simple geometries, and the fourth discusses non-linear behaviour. These four chapters give the theoretical background from which the descriptions of particular applications are developed.

The chapter entitled "Electromechanical applications" gives a detailed description of the properties of ceramic transformers and filters and their equivalent circuits. No mention is made, however, of vibration exciters (e.g. ultrasonic generators and drills) or vibration detectors (e.g. hydrophones and accelerometers). Subsequent chapters describe applications of ferrites (including antenna rods, inductors, transformers and microwave devices), magnetic and dielectric amplifiers, digital techniques employing square loop materials, magnetic recording, and finally magnetic and dielectric measurements. The five appendices deal respectively with reciprocity, tensor dielectric constant of a plasma, magnetoresistance, parametric devices, and properties of available materials.

There are over 400 references, a list being given at the end of each chapter. The book is also provided with an index and the preface includes a useful outline of the scope of each of the chapters and appendices. There are ten authors and four contributors, all of whom "have had extensive experience in some phase of solid state devices over the last five years", but no indication is given of the authorship of each chapter. The standard of presentation is high, the material being clearly and concisely written.

It is difficult in a book of such extensive coverage to single out inaccuracies but two omissions were noticed. Firstly, although the m.k.s. units of ϵ_0 (permittivity of free space) are given (p. 2), the numerical value of μ_0 (permeability of free space) is given without units (p. 17). Secondly, a ferroelectric substance is defined (p. 72) as a substance that "has an electric dipole moment and is said to be spontaneously polarized". The other necessary condition, that the dipole moment can be reversed by an applied electric field, is omitted.

The claim that the book will be especially useful to readers interested in new computer components, new materials for filters, and delay lines certainly appears justified. The book is thus complementary to the several books on solid state devices based on semiconductor properties.

R. C. KELL

Mathematical theories, techniques, computers and control systems, and mechanics

Applications of finite groups. By J. S. LOMONT. (New York: Academic Press Inc.; London: Academic Books, 1959.) Pp. xi + 346. Price 86s.

It is very difficult to decide what kind of reader the author of this book had in mind when he wrote it. It is therefore important to tell the intending purchaser exactly what he is buying. To quote from the preface the objects of the book are: "(1) To provide a mathematical background (primarily representation theory) in finite groups which is adequate both for reading this book and for reading the physics literature, and (2) to provide a variety of instructive and interesting examples of applications of finite groups to problems of physics. It is assumed that the reader has been exposed to matrix theory and general group theory. Also a knowledge of quantum mechanics is presupposed."

The first chapter, dealing with matrices, consists of a list of definitions and theorems without proof. Considerable familiarity with the subject is assumed, and it may be legitimate in a review chapter of this kind to collect together results which are needed for reading the rest of the book. The second chapter, on groups, is similar—definitions, theorems, examples but no proofs. In the third chapter, on representations, an outline of a proof is occasionally given but again it consists in the main of statements of theorems and illustrative examples. Chapter IV is a substantial one on applications including molecular vibrations, symmetric waveguide junctions, crystallographic point groups and space groups, wave functions in crystals, non-relativistic wave functions and stationary perturbation theory. This is a useful chapter containing much that is of interest to physicists. Chapter V is also useful, in that it contains much material, mainly on "little groups" which has not been collected together before. There are further chapters on space group representations and energy bands, on symmetric groups, and on applications to atomic structure.

Long lists of books are given in the bibliographies at the

ends of the chapters (but not, curiously enough, Chapter V). There is also a long list of references at the end. These bibliographies are of doubtful value. They include almost every book that has been written on the subject and are in no way tied to the text. It would be much more useful if specific references (to proofs of theorems for example) were given in the body of the book, and if a small number of well-chosen works were quoted at the ends of the chapters. A source of minor irritation is that English titles are given to papers in other languages, and which have not been translated. It would be better to give the original titles in these cases.

This is certainly not a book for the beginner. It is a compendium of results for the expert who knows his way about and who likes to have results collected together in this way.

M. R. HOPKINS

Control system components. By J. E. GIBSON and F. B. TUTEUR. (New York: McGraw-Hill Book Co. Inc.; London: McGraw-Hill Publishing Co. Ltd., 1958.) Pp. ix + 493. Price 93s.

This is a useful book which covers most of the components a control engineer is likely to need in designing a control system. It covers sensing elements for position control systems but there is very little on other types of measuring instrument. Since the range of instruments used "on line" in process control applications is now rapidly increasing, it would be unreasonable to expect any wide coverage, but it is a pity that there is no mention of the instruments used for measuring temperature, pressure, level and flow which, of necessity, form part of most process control loops. Otherwise, the book is very comprehensive and is a useful combination of theoretical and descriptive material. The coverage of electrical components required for position control systems is very complete and, in general, well set out. The treatment of electrical networks is particularly well done, since the difficult subject of network synthesis is taken just far enough but no further, as is necessary for the synthesis of compensating networks of the type required in control systems. The chapters on d.c. and power amplifiers cover all the types likely to be used, including simple transistor circuits, relay amplifiers and, in the chapter on d.c. machines, rotary amplifiers. The methods of drift compensation of d.c. amplifiers are adequately covered, but the authors apparently believe it is possible to construct d.c. amplifiers with zero drift (p. 63) and do not appreciate that the most serious cause of drift is not heater voltage variation but small unpredictable changes of the cathode work function, which result in small changes of grid/cathode potential difference. Since this is indistinguishable from the input grid/cathode voltage, it can only be deducted and compensated by a chopper device. This is a very serious omission, which should be put right if there is a second edition.

Written by electrical engineers, it is not surprising that it has an electrical bias but mechanical, hydraulic and pneumatic components are not neglected, this section taking up rather more than a third of the whole book. All the more usual types of components are covered, in a way that makes clear both their method of operation and their characteristics when used in a control system. The coverage of the book would have been more complete and the balance improved if something has been said about four-bar linkages and link mechanisms in general, since, in conjunction with mechanical and pneumatic components, these can still be used in place of electric networks in process controllers.

It does not set out to be a text-book on the design of any of the components described and space would not allow of this. Taken as a whole, it should be extremely useful to the control engineer as a guide to what components are available and how they can best be used. Most important, it should encourage the design of systems combining the most suitable components, whether they be electric or mechanical, which is very much to be desired.

J. F. COALES

Course of theoretical physics. Vol. 7. Theory of elasticity.

By L. D. LANDAU and E. M. LIFSHITZ. Translated from the Russian by J. B. SYKES and W. H. REID. (London: Pergamon Press Ltd., 1959.) Pp. viii + 134. Price 40s.

Despite the importance of the subject, the number of books on the classical theory of elasticity which are both reliable and readable is not large. For this reason the appearance of the present translation, which satisfies both these requirements, is exceptionally welcome. With the refinement of mathematical development to which it has been subjected, the classical theory has come to appear almost as a branch of pure mathematics, divorced from the physics of real materials. Landau and Lifshitz, with their continual reference to the observational basis of the subject, never lose sight of this essential connexion. With the increasing importance of constructional materials having complex elastic properties, this reference back to fundamentals, with clear indications of the points at which approximations (representing limitations on the behaviour of real materials) are introduced, is very necessary.

The text is divided into four sections: I, Fundamental equations, II, The equilibrium of rods and plates, III, Elastic waves and IV, Thermal conduction and viscosity in solids. The use of tensor notation, coupled with a lucid style, enables a very considerable range to be covered in a relatively small number of pages, and with admirable balance.

I shall be surprised if this book does not come to be regarded as a masterpiece.

L. R. G. TRELOAR

Dynamische Vorgänge in linearen Systemen der Nachrichten- und Regelungstechnik. By H. KAUFMANN. (München: R. Oldenbourg, 1959.) Pp. 211. Price DM. 26.50.

There are two basic mathematical problems arising in the technique of telecommunication and control by the use of linear, mechanical or electrical transmitting systems, namely the analytical problem of how a given system will respond to an arbitrary input, and the synthetic problem of constructing a system in such a way that it will respond in a desired way to a given input. Both these problems are of very great practical importance. The dynamical phenomena occurring in transmitting systems can be described in terms of measurement in two apparently different ways, namely by either recording the output as a function of time for given input signals or by measuring the response of the system to sinusoidal inputs as a function of frequency. In actual fact both methods of descriptions are completely equivalent, the time- and frequency-representations being connected to each other by Fourier and Laplace transformations.

In the first part of the book under review the author gives a very clear, concise and, at the same time, rigorous presentation of the mathematical theory of this dualism, with many examples, including the criteria for the stability of the transmitting systems. The second part is devoted to approximation methods for the analysis and synthesis of networks, the

use of characteristic parameters for such networks and the theory of so-called "sampled data systems" with particular reference to the use of digital computers. An appendix contains some useful tables.

The author's German style is excellent, and English readers with a fairly elementary knowledge of the language should have no great difficulty in following the arguments. The book can be warmly recommended to all workers in the field.

R. FÜRTH

Grundlagen der Selbsttätigen Regelung. Band II: Einige Probleme aus der Theorie der nichtlinearen Regelungssysteme. By W. W. SOLODOVNIKOW. (München: R. Oldenbourg, 1959.) Pp. viii + 449. Price DM. 52.

This is a German translation of the second volume of what is probably the leading Russian work in the automatic control field, and as such it is of immediate interest. The volume, as its title indicates, deals with various relatively unconnected aspects of non-linear systems, but in the absence of any general non-linear theory this is to be expected. The treatment is not global, the general emphasis being on oscillations and transients in non-linear systems. The selected topics are presumably those in which the Russian background is widest.

The book is divided into four sections, of which the two first deal with phase-plane methods, and linear approximation techniques. The practising control engineer already familiar with non-linear concepts may consider some of the early chapters (dealing with classification of discontinuity types and examples thereof) somewhat long-winded; but the material in these sections is probably more comprehensive than has appeared in any single Western work. The approximation methods described and compared are the so-called "small parameter" method derived from Poincaré and the first-harmonic methods, including the describing-function technique.

The third section is exclusively concerned with relay servomechanisms, which are considered in useful detail, whilst the final section deals with graphical analysis of non-linear and variable-parameter systems for which integro-differential equations can be formulated. This section is based largely on original Russian work.

The extensive bibliography contains Russian references predominantly; these are given in both Cyrillic and anglicized form. Diagrams are well presented, and are repeated where desirable. This book is probably the best opportunity yet presented to the control engineer of familiarizing himself with Russian work and concepts in this field, whilst its exhaustive treatment, supported by numerous application examples, make it useful in its own right to the non-linear systems specialist.

D. ALLENDEN

Proceedings of the third national congress of applied mechanics. (New York: The American Society of Mechanical Engineers on behalf of the congress; London: Pergamon Press, 1958.) Pp. xxvi + 864. Price £7.

Whilst there is a convincing argument for informality in the presentation of a paper at a congress, and also perhaps in the presentation of reprints, the published proceedings should have as much scrutiny given to each paper as if those papers were individually submitted to the journal of a learned society. In this case the editorial panel do not seem to have used their powers which should be theirs.

New Physical Monographs

MASERS

Gordon Troup has written what is probably the first book to be published on this new subject: the devices employed in obtaining Microwave Amplification and Oscillation by Stimulated Emission of Radiation. The author has kept the text fully abreast of major recent developments. **13s 6d**

APPLICATIONS OF THERMOELECTRICITY

H. J. Goldsmid provides the first short introductory book by a specialist working in this field. There is a rapidly growing interest in research on thermoelectric materials, and this elementary account will be useful to those entering the field for the first time as well as to students whose main interests lie elsewhere. **10s 6d**

PHOTONS AND ELECTRONS

K. H. Spring. This is the second edition, revised and with some new material. **10s 6d**

THE MANY BODY PROBLEM

The subject for the annual University of Grenoble Summer School, 1958, was the 'many body problem'. Papers were read by scientists from Great Britain, the U.S.A., U.S.S.R., Holland, Denmark and France. These are reprinted in this 700-page book and should be of great interest to theoretical physicists and nuclear scientists. **100s**

METHUEN

36 Essex Street . London W C 2

New Books

ELECTRON PHYSICS

The Physics of the Free Electron

By **Dr. O. KLEMPERER**, *Imperial College of Science and Technology, University of London.*

Though designed as a text for undergraduate students, some sections have been included which would suit a graduate course. The author has added material, carefully selected from his experience in industrial research, which provides the fundamental equipment required in electronic engineering and serves the needs of other disciplines which have a practical bias.

Fundamental for the whole subject of electron physics is the study of the properties of the free electron, and this is the subject of the present book. Following a short historical note, Part 1 contains a brief survey of methods for the production of electron rays; a detailed discussion of the main problems of electron motion, of electron optics, of the flow of electrons in dense space charges and of the statistical fluctuations in low intensity beams. It contains too, a short description of experimental methods for the detection of free electrons. Part 2 deals with the fundamental properties of the free electron, namely, with its charge, mass, wave-length, spin, and magnetic moment, and it includes a description of their study by quantitative methods.

Price 32s. 6d.

Introduction to PRACTICAL INFRA-RED SPECTROSCOPY

By **Dr. A. D. CROSS**, *Imperial College of Science and Technology, University of London.*

Few organic chemists engaged in molecular structural research or analytical control can now avoid calling upon infra-red absorption measurements for guidance at one time or another. Whether they have to make the measurements themselves or receive spectral charts of their compounds recorded by technicians, it is vital that they should have sufficient understanding of what is involved if they are to assess the results and make the correct interpretation.

Over the past few years Dr. Cross has introduced many newcomers to the general operating procedures and sampling techniques of infra-red absorption spectroscopy. His book outlines concisely all the essentials of the theory, measurements and applications with a well-chosen set of standard reference data set out in a readily usable form. It will prove of real use to the student and others seeking a thoroughly up-to-date introduction to the subject.

Price 17s. 6d.

TANTALUM & NIOBIUM

By **Dr. G. L. MILLER**, *Director of Research, Murex Ltd.*

This new volume in the *Metallurgy of the Rarer Metals Series* contains all the available chemical and metallurgical information on Tantalum and Niobium. It includes all the published work from the time of von Bolton and earlier as well as the results of the latest investigations from laboratories all over the world.

The chemical processing of the metals is described very fully from the decomposition of the ores to the separation and purification of the metals; from the Marignac process to modern liquid-liquid techniques. The critical description of metal production covers all known processes, including those used industrially; those which have possibilities and those of academic interest only. The description of the consolidation of the metals is given in detail from the earliest work on sintering up to the latest arc-melting and electron bombardment techniques. The reactions of the metals with chemicals, gases and liquid metals are described as well as their physical and mechanical properties. The production of their alloys and more important compounds are also described.

Price 120s.

Descriptive literature available, post free, from

**BUTTERWORTHS
SCIENTIFIC PUBLICATIONS**

4 & 5 Bell Yard, London WC2

New HEYWOOD Scientific Books

Progress Series

PROGRESS IN SEMICONDUCTORS

Volume 4.

This fourth volume of an international series designed for physicists, electronic engineers and designers, contains eight critical reviews by leading scientists on special aspects of the semiconductor field.

For the first time contributions are included from the Soviet Union, Holland, Japan and Germany.

General Editor: Alan F. Gibson, B.Sc., Ph.D., Royal Radar Establishment, Malvern.

American Editor: Professor R. E. Burgess, Vancouver, B.C.

European Editor: Dr. F. A. Kröger, Salfords.

291 pages

63s.

Copies of Volume 3 containing 7 papers, price 55s., are still available.

PROGRESS IN NON-DESTRUCTIVE TESTING

Volume 2.

This is the second volume of a new series of international reports, which will appear annually, on progress in scientific work which forms the basis of non-destructive testing. In its widest sense, non-destructive testing means any type of non-destructive measurement carried out on solids, liquids and gases for examining aspects of their physical, chemical or biological condition.

The *Progress in Non-Destructive Testing* series will cover the six principal methods of flaw detection—visual examination, penetrant testing, magnetic testing, radiography, eddy-current testing and ultrasonic testing. Each subject will not necessarily be covered every year, but it is

hoped to include at least one annual review each year on the medical aspects of the subject.

Edited by E. G. Stanford, M.Sc., Ph.D., A.M.I.E.E., F.Inst.P. and J. H. Fearon, B.Sc., A.M.I.E.E.

250 pages

55s.

Copies of Volume 1, price 60s., are still available.

PROGRESS IN CRYOGENICS

Volume 1.

This series of volumes, edited by a Vice-President of the Physical Society, will cover the production, maintenance and measurement of low temperatures and their practical application to the techniques used in basic research.

Editor: K. Mendelssohn, D.Phil. (Berlin), M.A. (Oxon.), F.Inst.P., F.R.S.

259 pages

63s.

Volume 2 in preparation.

PROGRESS IN DIELECTRICS

Volume 2.

This is the second volume in a new annual international series covering the whole range of the newer dielectric materials. The series will endeavour to co-ordinate current knowledge of dielectric phenomena, materials and techniques and to review recent progress.

Edited by: J. B. Birks, B.A., Ph.D., D.Sc., F.Inst.P., A.M.I.E.E., of Manchester University, and J. H. Schulman, Ph.D., of the U.S. Naval Research Laboratory.

225 pages

55s.

These volumes may be obtained from all booksellers, or in case of difficulty order from the publishers:

HEYWOOD & COMPANY LIMITED

DRURY HOUSE, RUSSELL STREET, LONDON, W.C.2.

A comprehensive catalogue of all Heywood books will be supplied on application to the Publicity Department at the above address

Recent

McGraw-Hill

Books

APPLEGATE: Cathodic Protection

One of the first comprehensive treatments of the topic, this book presents the principles of underground and underwater corrosion of metals, describing the foremost methods of protection and exemplifying theory by practical illustrations. The many wide applications of the subject make this book invaluable in almost all engineering fields.

70s

KOTEL'NIKOV: The Theory of Optimum Noise Immunity

translated by R. A. Silverman

This distinguished work by a Russian engineer presents an analysis of the effect of noise on reception in an arbitrary communication system and defines the ideal performance. Interpretation of the subject is simplified by extensive use of geometric models. Although Kotel'nikov is no longer alone in this research work, a great deal of information is made available here for the first time.

58s

LION: Instrumentation in Scientific Research

Research workers and students of all branches of engineering will find in this book a complete, illustrated collection of the existing methods and systems used as input transducers in electrical instrumentation. The subject is treated as a logical science, and therefore physics rather than the technical means of each method is stressed.

74s

WELLARD: Resistance and Resistors

A thorough treatment of one of the most frequently used components, this book covers basic aspects of resistance and describes each kind of resistor, the materials used in its manufacture, and the characteristics associated with each type. Comprehensive tables are given which include most manufacturers' data on any type, so the full technical scope of what is available can easily be determined.

66s

McGraw-Hill Publishing Company Limited

McGraw-Hill House London EC4

*Just
published!*

From steel making to space flight-

**Liquefied Gases and Low-Temperature
Techniques are Everywhere Today
in Science and Industry!**

LOW-TEMPERATURE TECHNIQUES

F. DIN, A.R.C.S., B.Sc., Ph.D.
AND
A. H. COCKETT, B.Sc., F.Inst.P.

A NEWNES PRACTICAL SCIENCE BOOK

LOW-TEMPERATURE TECHNIQUES

F. DIN,
A.R.C.S., B.Sc., Ph.D.
and
A. H. COCKETT,
B.Sc., F.Inst.P.

This account of the uses of liquefied gases and low-temperature techniques in science and industry serves to demonstrate their wide diversity, ranging from domestic refrigerators to steel making and space flight. The refrigeration industry is about one hundred years old and the air-separation industry is about half this age, whilst the exciting new industrial developments with liquid hydrogen and helium have all taken place within the last decade. The rate of expansion and development in the industry is very great, and it is certain that more and more scientists and technologists, to say nothing of the ordinary people, will become increasingly aware that low temperatures are more than something they have to endure in the winter!

CONTENTS INCLUDE:

Geographical and Historical. Producing and Measuring Low Temperatures. Properties of Materials at Low Temperatures. Gas Separation. Refrigeration, Storage, Transport and Uses of Liquefied Gases. Index. With Photographic Illustrations and many Line Diagrams Throughout.

40s.
net

*From all booksellers
... or in case of difficulty
at 41s. by post direct
from George Newnes
Limited, Tower House,
Southampton Street,
London, W.C.2*

The emphasis on the practical side of the subject ensures that this book will be of great value to students, laboratory workers and technologists in all scientific and industrial fields.

A NEWNES PRACTICAL SCIENCE BOOK

A selection of titles from our 1960 Spring list

ENCYCLOPAEDIC DICTIONARY OF PHYSICS

Editor-in-Chief: J. THEWLIS

This will consist of eight volumes, covering more than 15,000 terms in pure and applied physics. The eighth volume will be a seven-language glossary of physical terms.

Set of 8 volumes: £75 net (\$225.00)

Pre-publication price: £50 net (\$150.00)

PROGRESS IN BIOPHYSICS AND PHYSICAL CHEMISTRY

Volume 10

Edited by J. A. V. BUTLER and B. KATZ

Tenth in a series designed to cover the ground between the physical and biological sciences.

In preparation

ELECTRODYNAMICS OF CONTINUOUS MEDIA

Course of Theoretical Physics. Volume 8

by L. D. LANDAU and E. M. LIFSHITZ

Deals with the theory of electromagnetic fields in matter and with the theory of the macroscopic electric and magnetic properties of matter.

Approx. 90s. net

THERMAL REACTOR THEORY

Second Edition (First English)

by A. D. GALANIN

This book, translated from the Russian, gives a comprehensive account of the theory of thermal nuclear reactors.

Approx. £4 net (\$15.00)

BOUNDARY LAYER AND FLOW CONTROL— PRINCIPLES AND APPLICATIONS

Edited by G. V. LACHMANN

Thirty-four authors of international repute encompass the entire field of boundary layer control.

Approx. £5 5s. net (\$16.00)

Please write for fully descriptive leaflets

PHYSICAL OCEANOGRAPHY

Volumes 1 and 2

by ALBERT DEFANT

A text-book on the fundamentals of this geographical-geophysical science. Deals with the general geography of the oceans, the physics and chemistry of sea-water, and dynamics of the world's oceans.

In preparation

HYDRODYNAMICS OF OCEANS AND ATMOSPHERES

by CARL ECKART

A systematic introduction to the hydrodynamics of the earth's atmosphere and oceans, under the action of gravitational and Coriolis forces.

In preparation

DYNAMICS OF CLIMATE

Edited by RICHARD L. PFEFFER

Proceedings of a conference on the application of numerical integration techniques to the problem of the general circulation.

35s. net (\$6.50)

ANTARCTIC METEOROLOGY

Edited by L. J. DWYER

Proceedings of the 1959 symposium sponsored by the Australian Bureau of Meteorology under the auspices of the Australian Academy of Science and the C.S.A.G.I.

In preparation

ANNALS OF THE INTERNATIONAL GEOPHYSICAL YEAR

This series is the central record of the International Geophysical Year, giving readers full information on this vast project. The latest in the Series are:

Volume X. Report of the Fifth meeting of the Special Committee.

Volume XI. First results of I.G.Y. Rocket and Satellite Research.

£6 net (\$17.00) per volume



PERGAMON PRESS

OXFORD LONDON NEW YORK PARIS

Headington Hill Hall, Oxford

122 East 55th Street, New York 22, N.Y.

4 & 5 Fitzroy Square, London W.1

24 Rue des Écoles, Paris V^e

I found the presentation of the papers such as to make their study unnecessarily laborious, and even in the general lectures, sufficient care does not seem to have been taken, for example, in stating the assumptions and their justification, so that one feels that essential parts of an argument are evaded.

It may be because of this that, for example, many of the papers presented have ignored the coupling between thermal and dynamic strain. Interesting problems in the stress world which have, or will soon celebrate their centenary, such as mean value theorems, and a quantitative expression of St. Venant's principle are given an airing in such a way that their value is diminished. Mean value theorems can give the location of maximum stresses, St. Venant's principle is very powerful in simplifying theoretical and experimental treatments. Rigorous analysis on either of these topics could have had real practical value.

There is a growing tendency towards the indiscriminate use of proper names to describe results, procedures, and assumptions that could be better shown in two or three lines of writing and algebra. Where the matter has been properly published a reference number then completes the picture. Phrases such as Euler-Bernouilli hypotheses, Ritz averaging, Hertzian impact, Poisson-Kirchoff treatment, the Kane-Mindlin equation (to describe the body stress equations in cylindrical polar co-ordinates), in my view, prevent a clear statement of the problem being considered.

One could list the deficiencies of presentation that will irritate the careful reader, such as the 45% "error" in dynamic strain which was "expected", the undefined symbols, the unspecified rotating axes, the wrong signs in Newton's second law, and frequent obscurity in many of the papers.

I am unable to recommend this volume, and hope that stricter refereeing of the papers presented at the next congress will be insisted upon before publication.

C. SNELL

Sampling inspection tables. Single and double sampling.

2nd ed. By H. F. DODGE and H. G. ROMIG. (New York: John Wiley and Sons, Inc.; London: Chapman and Hall Ltd., 1959.) Pp. xi + 224. Price 64s.

As stated in the introduction, engineers of the Western Electric Co., were pioneers in the application of statistical methods to the inspection of manufactured products and a newly formed department of the Bell Telephone Laboratories sponsored developments.

Single sampling tables were published in October 1929 in Vol. VIII, No. 4 of the *Bell System Technical Journal*. Double sampling tables became available in Great Britain during the Second World War and are now generally well known. (*Bell System Technical Journal*, XX, No. 1, January 1941.) That a second edition of these tables, considerably amplified by a large number of illustrations of operating characteristic curves, is published in 1959 is a criticism of the slowness with which another and economically important application of statistical methods has developed in industry.

This criticism is justified by the instructions given in Chapter 3 on the action to be taken in setting up a double sampling scheme. For example, the composition of the lot submitted to test "should have characteristics which are the result of a common system of causes". The explanation of this phrase which is there given demands knowledge which can be readily secured from the examination of much smaller samples than those associated with these Inspection Tables.

Procedures are well known and are widely practised in many industries by which these small samples are selected for

test (usually measurement) at intervals from the production line, the results being plotted on charts, the introduction of which was due to the activities of the group of men in the Bell Telephone Laboratories. (*Bell System Technical Journal*, VI, p. 593.)

When these procedures are closely integrated with production, their purpose being to assist in maintenance of the plant, final inspection is sometimes unnecessary. If such final inspection is deemed desirable and the procedures adopted which are described so admirably in the book now reviewed, the inspection department has information available on which it can determine whether or not the composition of the lot fulfils the condition outlined in chapter 3.

This publication reflects the high standard of all the work that derives from the Bell Telephone Laboratories. The production of the book is above criticism and the addition of the operating characteristic curves for a large number of sampling plans will assist those who still have to purchase components of which little is known either of their quality or of the conditions under which they were manufactured.

Careful reading of the description of the conditions which should govern the use of sampling tables will avoid the disappointment which arises when these conditions are not satisfied.

B. P. DUDGING

Theorie der stabilität einer bewegung. By J. G. MALKIN. (Munich: R. Oldenbourg, 1959.) Pp. xiii + 402. Price DM. 47.

The theory of stability of motion dates back to investigations by Lagrange upon the stability of a system in equilibrium. Subsequent authors concerned themselves with stability problems of a special nature, including the fundamental considerations of Poincaré. The treatment of stability in full generality was undertaken by Liapounoff in 1892 and since that time has been well developed both in Russia and in the West.

This particular volume, a German translation by Prof. W. Hahn and Dr. R. Reissig from the original Russian work by J. Malkin, attempts to set forth the theory as introduced by Liapounoff and developed by his successors. As a result, the translators have made available to those handicapped by a knowledge of Western languages only, a remarkably lucid and succinct translation of an impressive quantity of hitherto inaccessible Russian work.

Starting from fundamental definitions of stability and instability, the author defines the problem, introduces two modes of attack (the first and second method of Liapounoff) and then considers in detail a wide variety of problems connected with systems dynamically defined by differential equations—linear or non-linear with constant or periodic coefficients. He divides all motions into two categories, stationary and non-stationary, and solves the stability problem for each type in turn, using the powerful second method of Liapounoff.

The nature of the subject is perforce abstract and mathematical, but at each step in the theoretical development the theory is amply illustrated by mechanical examples so that the applied mathematician, theoretical physicist, or systems engineer should find this book understandable.

It is regrettable that developments by Western authors have been for the most part overlooked by the author but these omissions are consistent with the goal of presenting the theory as developed by Liapounoff and his school.

M. N. MOORE

Miscellaneous

Annual reports on the progress of chemistry. Vol. LV. (London: The Chemical Society, 1958.) Pp. xv + 527. Price 40s.

The 30 Reports in this volume are grouped into the following sections: General and physical chemistry; Inorganic chemistry; Organic chemistry; Biological chemistry; Analytical chemistry; Crystallography. The volume includes a subject and author index.

The physical chemistry of steel making. Edited by J. F. ELLIOTT. (New York: John Wiley and Sons, Inc., and The Technology Press of the Massachusetts Institute of Technology; London: Chapman and Hall, Ltd., 1958.) Pp. xiii + 257. Price 120s.

The title of this book may be a little misleading; it is by no means a text-book but a report of the proceedings of a conference held in America in 1956. The forty-odd papers range from the highly academic to the practical and come from authors in several European countries and Japan as well as from American sources.

To select individual papers for comment is invidious; of the theoretical papers, however, mention should be made of one on the activity of carbon by Rist and Chipman and two excellent papers by Richardson on oxide slags and activities in silicate melts. On the more practical side, Darken's paper on the reactions in the open hearth furnace and a German paper on deoxidation with silicon call for special commendation. There is a noteworthy contribution by Kalling on physical chemistry as applied to developments in process metallurgy and a very useful section with five papers on solidification of castings and ingots. A general discussion on research planning rounds off the whole.

As is general with Proceedings, such a volume should be on the reference shelves of larger libraries; the general reader would be better advised to note its existence and borrow it when he specifically wishes to consult it.

K. C. BARRACLOUGH

Progress in metal physics 7. Edited by B. CHALMERS and R. KING. (London: Pergamon Press Ltd., 1959.) Pp. viii + 408. Price £5 5s.

This volume contains five review articles, all of which are informative and well written. J. N. Hobstetter describes recent work on "Equilibrium, diffusion and imperfections in semiconductors", and points out how this may assist workers studying metals. L. Kaufman and M. Cohen write authoritatively on "Thermodynamics and kinetics of martensitic transformations", and A. L. Titchener and M. B. Bever give a very clear assessment of our present knowledge of "The stored energy of cold work". Both of these surveys are useful to the non-specialist, as is also H. M. Rosenberg's description of "The properties of metals at low temperatures". This deals with both transport phenomena and mechanical properties, emphasizing recent interest in these fields. Finally, R. I. Jaffee contributes a review of "The physical metallurgy of titanium alloys" which will be welcomed by many research workers. Nevertheless, any attempt to cover all aspects of the properties of a particular metal results in some loss of coherency, and one feels that this is scientifically less pleasing than are surveys of particular topics.

Each year, more papers are published, and there are probably

fewer readers of each paper. Our knowledge of work in fields related to those in which we have a direct interest now depends largely on the collections of review articles which have been a prominent feature of post-war scientific publishing. *Progress in metal physics* was among the first of these in its subject, and remains the most generally useful.

J. W. CHRISTIAN

Progress in vacuum science and technology. Edited by A. S. D. BARRETT. (London: Pergamon Press Ltd., 1959.) Pp. 160. Price 70s.

The papers that are gathered together in this volume cover many aspects of present-day vacuum practice. Each paper provides a detailed review of a particular aspect of the work. The subjects covered are: education in vacuum practice at colleges in the United Kingdom, some problems in the valve industry, vacuum metallurgy in the United States of America, vacuum fumigation, vacuum drying and finally molecular distillation. Each section is presented by an author of known eminence in the particular field. The overall result is a well-written and well-presented volume which serves to show the growing importance of vacuum science in modern industry.

J. H. LECK

Recent research in molecular beams: A collection of papers dedicated to Otto Stern on the occasion of his 70th birthday. Edited by I. ESTERMANN. (New York: Academic Press, Inc.; London: Academic Books Ltd., 1959.) Pp. 190. Price 52s.

In his preface, the editor stresses the theme of the book thus: "The most appropriate way of paying tribute to a scientist on such an occasion is to present a series of scientific papers which have been inspired by his work and have carried it beyond the limits of his own efforts." Accordingly, many of the ten chapters could equally well have been submitted to research periodicals and indeed one paper previously has been so published. The first paper—and regrettably the shortest—describes the early development of this field of research at Hamburg under Stern, and other papers describe current research programmes at institutes in the U.S.A.

Though parts will not appeal to the non-specialist, research workers in other fields will find much to interest them. The paper entitled "Molecular scattering at the solid surface" reveals intriguing results in a subject which acquires a new significance with the advent of space-flight. G. A. JONES

Nuclear and cosmic ray physics, apparatus, techniques and data

Bibliography of the stable isotopes of oxygen (^{17}O and ^{18}O). Compiled and Edited by D. SAMUEL and F. STECKEL. (London: Pergamon Press, 1959.) Pp. viii + 224. Price 50s.

This book lists all papers published on the stable isotopes of oxygen up to the end of 1957. Reference is made to over 700 papers dealing with the separation and use of these isotopes (mostly, of course, of ^{18}O). The bibliography consists of two parts; first an author index in which each entry gives the author(s), title, reference and chemical

abstracts reference, but no comments; and then a subject index with cross-reference to the author index. Work on nuclear reactions has not been included unless other data of interest are reported.

The bibliography seems to be remarkably complete. The book will be of value to those who are interested in the separation of ^{17}O and ^{18}O , and more particularly, perhaps, to those who are interested in the use of these isotopes as tracers. It brought to the notice of the writer three or four papers in his own field of interest, which were previously unknown to him.

The book is well produced and it is easy to find what one is looking for.

T. F. JOHNS

Directory of nuclear reactors. Vol. I. Power reactors.

(Vienna: The International Atomic Energy Agency, 1959.) Pp. 214. Price 21s.

The purpose of this directory is to make available important details of various power reactor projects. Information is presented in such a way as to provide easy reference. The basic criterium for the selection of reactor projects for inclusion was that the reactors should be in regular operation, and producing useful electric power, by the end of 1962. Reactors with an electric power output of under 2 MW are not included.

The first page contains general information, reactor physics data and information on the core. The second and third pages provide sketches of the fuel element assembly and of the horizontal and vertical sections of the reactor. On the fourth page information is grouped under the following headings: fuel element, core heat transfer, control, reactor vessel and overall dimensions, and fluid flow. The fifth page shows a simplified flow diagram and the sixth page provides information on reflector and shielding, containment and turbo-generator; when available, information is given on cost estimates and operating staff. The description of each reactor ends with general remarks and bibliographical data.

The drawings and diagrams published are not intended to cover the construction and design aspects in great detail, but are provided to convey a general idea of the layout and disposition of various components of the reactor and its associated equipment.

This directory is bound in such a way that the pages may be easily extracted and placed in a loose-leaf binder. In the present arrangement reactors are grouped according to the coolant used in them (e.g. gas-cooled reactors, liquid-metal cooled reactors, etc.).

Encyclopaedia of physics. Vol. XXXVIII/2. Neutrons and related gamma ray problems. Edited by S. FLÜGGE. (Berlin: Springer-Verlag, 1959.) Pp. 868. Price DM.178.

This volume of the encyclopaedia contains two sections, entitled respectively "The production and slowing down of neutrons", written by Prof. E. Amaldi, and "Penetration and diffusion of X-rays" by Drs. O. Fanu, L. V. Spencer and M. J. Berger. Both deal with one of the aspects of the degradation of radiation in matter, and although their application lies in different fields, there is much similarity between the mathematical methods employed.

The section by Prof. Amaldi occupies 659 out of the 817 pages of text in this book, and is certainly one of the most exhaustive reviews of the subject yet written. A detailed introduction starts with a brief historical survey of the dis-

covery of the neutron and its properties and then proceeds to outline the physical problems involved in predicting the behaviour of a neutron from source to capture. Following this are sections dealing with neutron sources, with slowing down processes and finally with the diffusion of thermal neutrons. Necessarily, such a thorough treatment deals principally with well-established aspects of the subject—and indeed it is here that its real value as a reference book lies—and with this in mind it is very gratifying to see that little of relevance prior to 1958 has been missed. The reader will, however, do well to remember that interest in neutron thermalization by bound atoms has been recently increasing and this book may not remain complete in this field for very long.

Not unnaturally it is possible to pick out some errors of detail. Some of these are trivial, such as the misquotation of the electron energy available from the Harwell linac and some more serious, as for example the implication on p. 170 that the theoretical γ -n yields obtained by Mrs. Biram have been quantitatively confirmed by experiment. (In fact experimental yields lie well below theory.) The almost complete omission of any mention of the nuclear reactor as a source seems strange until it is realized that this is the subject of another volume in the encyclopaedia, which again emphasises that this book must not be considered on its own, but as one volume of a much larger work.

The second section, written by several co-authors all from the National Bureau of Standards, Washington, deals principally from a theoretical standpoint with the propagation of X-rays through matter. The treatment appears every bit as exhaustive as the previous section, and it should prove invaluable to all who work with X-rays. However it does appear a pity now that linacs up to 30 MeV are becoming common as X-rays sources that only very rarely are figures quoted for energies above 5 MeV.

An important feature of any work of reference is the efficiency of its index, and here there is little to complain about. As a volume in an encyclopaedia intended mainly for reference this book will be invaluable and should save much time searching through more specialized text-books. It is indeed a pity that its price will place it out of reach of many students.

M. J. POOLE

Nuclear reactor shielding. (Nuclear Engineering Monographs, No. 4.) By J. R. HARRISON. (London: Temple Press, 1958.) Pp. viii + 68. Price 10s. 6d.

Although in the past few years several advanced text-books on the theory and practice of shielding have been published, no elementary introduction has been available until the publication of this Nuclear Engineering Monograph. Being both well written and clearly presented, it can be thoroughly recommended as a text mainly directed at the increasing number of scientists and engineers who require an appreciation of the basic problems of shielding together with an indication of their solutions.

M. D. CLARK

Nuclear reactor control and instrumentation. (Nuclear Engineering Monographs, No. 5.) By J. H. BOWEN and E. F. O. MASTERS. (London: Temple Press Ltd., 1959.) Pp. x + 78. Price 12s. 6d.

This is an introduction to the control of gas-cooled graphite-moderated reactors. The basic physics of neutron kinetics, the effects of temperature changes on the operation of reactors

and the theory of control rods are adequately covered, although, in spite of the title, too little space is devoted to instrumentation. Several worked-out examples are provided and this should be of great help to the student who will find the book a valuable supplement to standard text-books.

N. SOLNTSEFF

Steam cycles for nuclear power plant. (Nuclear Engineering Monographs, No. 6.) By W. R. WOOTON. (London: Temple Press, 1958.) Pp. vii + 66. Price 10s. 6d.

This publication manages to compress into sixty-four pages a summary of the methods used in steam cycle calculations for nuclear power systems. Gas cooled—graphite moderated and water cooled—water moderated systems are covered. The effects of changes in the variables are given in graphical form and the descriptive text together with worked examples shows how the curves are obtained; clear indications of the factors limiting performance are given and the book gives a sound introduction to the subject.

R. W. NICHOLS

Plasma physics and the problem of controlled thermonuclear reactions. Vol. 3. Edited by M. A. LEONTOVICH and J. TURKEVICH. Translated from the Russian by J. B. SYKES. (London: Pergamon Press Ltd., 1959.) Pp. 422. Price £8.

This is the third volume of a collection of Russian papers of various dates on thermonuclear reactions and allied subjects. They confirm that Russian scientists have been working on most of the ideas on this subject familiar to us in the West.

Theoretical papers outnumber the experimental in this volume and perhaps also have the edge in quality. A notable one is an early paper by Budker on the theory of containment by "magnetic mirrors" which comes first in the volume. The Russians have, as is well known, pressed this line of attack to the extent of making the gigantic mirror machine Ogra now being tested. American experiments on this method were one of the most notable features of the outstanding U.S. exhibit at the Geneva conference, August 1958. The ability to move plasma about and to compress it adiabatically which the mirror method confers, makes it extremely attractive and gives it an aesthetic appeal exceeding that of most of the others. However, the losses through the mirrors are very considerable and it remains to be seen if it will come out any better in the end than more obvious methods such as those which have been used in ZETA and are to be developed in the new ICSE (Intermediate Current Stabilized Experiment).

Other papers deal with ring discharges and even forms of the arrangement known in U.S. as Picket Fence, which ought to have good stability but at the expense of containment.

The translation on the whole seems good, though there are places where one suspects that the meaning would have been clearer in the original to Russian readers. The printing has been done by some method not involving "justifying" the edges but that is no disadvantage in a book of this kind.

G. P. THOMSON

Principles of radiation dosimetry. By G. N. WHYTE. (New York: John Wiley and Sons Inc.; London: Chapman and Hall Ltd., 1959.) Pp. vii + 124. Price 56s.

Radiation dose, a concept first developed in the medical application of X- and γ -rays, has become increasingly valuable in other fields during the last 15 years. Professor

Whyte gives a good account of the physical principles used in establishing systems of units and measurement for assessing the physical, chemical and biological effects of ionizing radiations, charged particles and neutrons. He writes clearly and tersely, at a level suitable for honours or post-graduate students in physics.

J. M. A. LENIHAN

Proceedings of the international conference on nuclear physics: Low energy nuclear interactions and nuclear structure, Paris, 1958. Presented by Mme. P. GUGENBERGER. (London: Crosby Lockwood and Son, Ltd., 1959.) Pp. xxiv + 950. Price £7.

The subject of this international conference on nuclear physics, held under the auspices of U.N.E.S.C.O. and I.U.P.A.P., was "Low energy nuclear interactions and nuclear structure", and it took place in Paris in July 1958. The conference languages were French and English. This volume contains an "In Memoriam" to Prof. F. Joliot together with his opening speech to the conference given only a few weeks before his death.

The volume is divided into two parts. The first part contains a summary of the papers given in the different sessions by rapporteurs, and the discussion on these summaries. They are entitled: Diffusion élastique; Dimensions et forces nucléaires; Interaction directe; Ions lourds; Réactions photonucléaires; Modèle à particules indépendantes et rapports avec le modèle collectif; Modèle collectif; Structure de la matière nucléaire; Interactions faibles. Théorie et données expérimentales récentes, and include conclusions by L. Rosenfeld.

The second part contains fifty-six papers grouped into the following sections: Réactions nucléaires, Forces nucléaires; Réactions photonucléaires; Modèles nucléaires; Structure de la matière Nucléaire; Interactions faibles; Dimensions nucléaires, Divers.

Radioisotopes for industry. By R. S. ROCHLIN and W. W. SCHULTZ. (New York: Reinhold Publishing Corporation; London: Chapman and Hall Ltd., 1959.) Pp. ix + 190. Price 38s.

Of all the new materials afforded to us by modern technology surely none are more versatile or more promising of future benefits than radioactive isotopes. They are already widely used in industry, but their potential uses are legion and as yet hardly touched upon. Further progress is not restricted by supply, which is generally ample; but by the difficulty of making industrialists sufficiently aware of the prospects. To this end, reviews of isotope uses such as this one, serve a useful purpose.

This book is directed to plant managers and engineers, having no prior knowledge of radioactivity or nuclear science. Accordingly the treatment is frankly superficial, but it is nevertheless excellent for its purpose. The authors are with the General Electric Company of America, and they clearly have first-hand knowledge of industrial nucleonics. Their examples are well chosen and varied—though perhaps a little weak on the chemical side—and their writing reflects the enterprise and enthusiasm with which American industry has adopted these new aids to productivity.

Most industrialists and engineers will benefit from scanning these pages, and it will be a dullard indeed who gleans no new ideas from them. There is a quite useful bibliography for further reading.

W. P. GROVE

Reference books

Adhesives guide. By J. HURD. (Chislehurst: British Scientific Instrument Research Association, 1959.) Pp. viii + 138. Price 20s.

Mrs. Hurd has given a great deal of thought to the compilation of this reference book. Although written as a comprehensive answer to inquiries received by The British Scientific Instrument Research Association from its member firms, the book is issued as an open publication for all to buy. And there is no doubt that a great many people will buy it, because it supplies a need no other book does.

Adhesives guide makes it clear that it does not pretend to be a treatise on adhesion; instead, it gives "tabulated data on 400 individual adhesives made by about 100 firms". It starts with a useful Introduction which includes a number of do's and don'ts (but not in those words), a page on testing adhesives, and a few words on such things as surface preparation. Considering the number of patents on the subject, perhaps something might have been said about creating a wettable surface on polyethylene to make it adhesionable with a wider range of adhesives.

The contents proper begin with a section on selecting the right adhesives for the job. The part dealing with wood adhesives shows that note has been taken of the doctrines of the Forest Products Research Laboratory.

Another section is called "Encyclopaedia of basic types of adhesive"; and at the back of the book is a bibliography showing from where most of this information was obtained.

Section 3 is called "Classification of manufacturers by basic types of adhesive made". Only one or two omissions were noticed.

Sections 4 and 5 contain an alphabetical list of manufacturers and an alphabetical list of adhesives by their trade names. When read in conjunction with the earlier chapters, the user is supplied with all the general information he needs, except the more specific advice that only the adhesives manufacturer can give.

Finally there is an appendix which includes the formulations of a dozen or so different types of adhesives, some quite modern and some time-honoured.

Collecting all the information and presenting it in such an easy-to-get-at manner is a praiseworthy effort, and *Adhesives guide* will thoroughly deserve the blessings its readers will bestow on it.

C. A. A. RAYNER

Handbook of chemical microscopy. Vol. 1. 3rd ed. By EMILE MONNIN CHAMOT and CLYDE WALTER MASON. (New York: John Wiley and Sons Inc.; London: Chapman and Hall Ltd., 1958.) Pp. xii + 502. Price 112s.

A third edition of "Chamot and Mason" speaks for itself. It is assured of a welcome by that circle of specialists who have learnt to rely upon former issues as their stock-in-trade and working companions. The reason for this is that authors have always managed to blend useful information (applicable at bench level) with enough theory to make sure that the basic elements are secure in the reader's mind. Of the present book, nine of the sixteen chapters deal largely with problems of instrumentation, and the rest with methods of determining various physical constants, e.g. birefringence, indices of refraction, particle-size and so forth.

It is true, as the authors say, that microscopists have more than their fair share of serendipity (the reviewer would refer inquirers to Horace Walpole for details), but this is partly because microscopy is an observational science, with great rewards for visual accuracy. Nearly every page is provided

with copious references; these are not fanciful entries to suggest erudition, but all much to the point.

There is an exceptionally good description of phase-contrast microscopy; the early "feelers" of Bratuschek (1892) after this method had to wait for the masterly analysis of Zernike (1935) before much progress was made. Now it has become routine. The essential thing to realize is that axial illumination involves lowering the resolution, and therefore light coming from a condenser fitted with an annulus is necessary.

These are but examples of modern developments which are clearly presented, and their limitations appreciated.

F. I. G. RAWLINS

Methods of experimental physics. Vol. 1. **Classical methods.**

Edited by I. ESTERMANN. (New York: Academic Press, Inc.; London: Academic Books Ltd., 1959.) Pp. xii + 596. Price 91s. 6d.

This is the first volume of a series of six in which it is the aim, according to the foreword, to give a "... concise presentation of the most important methods used in experimental physics ... written so as to be of value to all research workers who use physical methods. Finally the volumes should be organized in such a way that they will provide essential tools for graduate students in physics."

These aims suggest that it is hoped the complete work will become a standard reference for experimental techniques at the post-graduate and research level. Whilst recognizing that a judgement based on one volume only is perhaps not valid, it is considered unlikely that the aims will be realized. In many cases the topics are treated at a level below that of British undergraduate courses, and in others with the absence of that degree of detail which is necessary in making a realistic assessment of different experimental methods. Other sections appear remarkably incomplete although these deficiencies may be rectified in the further volumes. The editor has clearly kept a very light rein on the contributors and although this has advantages in some cases of collaborated effort it is more likely to lead to a greater disparity of standard and of approach than can easily be tolerated in a book intended to form part of a coherent work of reference.

Naturally there is much useful information in the volume but generally it is as readily available elsewhere and in a form more useful to the experimenter. The editor and his colleagues have undertaken a work of considerable magnitude and difficulty and it is to be regretted that the outcome is less satisfactory than could be wished for.

F. E. HOARE

Quantum chemistry integrals and tables. By J. MILLER, J. M. GERHAUSER and F. A. MATSEN. (Austin: University of Texas Press, 1959.) Pp. 1125. Price \$15.00.

Practically no numerical calculations of the electron energies and distribution in a molecule are possible without the need to evaluate integrals. These may be exchange integrals, arising out of the indistinguishability of all the electrons in the molecule, or they may be Coulomb integrals measuring the repulsion which any one electron exerts on any other. Similar integrals occur in atoms, but they are simple, for the very obvious reason that in an atom there is only one nucleus, but in a molecule there are at least two and may be many; as a result the integrand will usually involve distances from more than one origin.

The evaluation of these molecular integrals is exceedingly difficult. It is probable—as was stated at a recent international

conference of molecular quantum mechanicians—that our continuing inability to find adequate simple techniques for evaluating these integrals has held up progress in this field for 10–15 years! Every help in the task is therefore welcome. The present book serves a notable purpose toward this end. It gives an excellent list of formulae both for one-electron and two-electron integrals. It then goes on to provide over 1000 pages of numerical values. The values themselves are mostly values of intermediate functions (known as A_n , B_n , G_n and W_n functions) from which, on using the appropriate formula from the first part of the book, any two-centre integral can be computed.

The amount of work in this volume is prodigious. All the items were computed on an electronic computer, and the final product has been reproduced photographically to eliminate errors in type-setting. Most of the entries are given to twelve significant figures.

There is no other set of published tables of this kind to match this volume. It is cheap, even at fifteen dollars, and owes much to support from the Humble Oil Company and other outside sources. Until every university and research institute has its own computer, with the necessary programmes, this collection will be indispensable. C. A. COULSON

Technische Kunstgriffe bei physikalischen Untersuchungen.

By E. v. ANGERER. Edited by H. EBERT. (Braunschweig: Friedr. Vieweg and Sohn, 1959.) Pp. vii + 464. Price DM. 24.80.

Although the preface to this book states that it is the 12th edition of a compilation which has been in existence for 35 years it is the first time I have seen a copy. I am most impressed. It is one of the few books on laboratory arts and techniques which is both a detailed reference book and yet has also an air of readability about it. The first section deals with materials—their properties and how to prepare them, how to use and treat them and how to manipulate them. The value to a laboratory worker lies in the ready availability, close together, of detailed descriptions of the mechanical, electrical, optical and other physical properties of metals and non metals (including plastics, glasses, some liquids and gases). The second describes a series of processes and the third section a number of techniques and instrumentation. Working in a laboratory is covered in the fourth section.

Perhaps the most striking feature of the book is the extensive list of references. No words are wasted on detailed description when the most satisfactory way of getting the information is from the original literature; a very important point in this is that commercial suppliers are quoted when any specific instrument or product is mentioned; the list of manufacturers included is world-wide—about a sixth are non-German firms.

While I could criticize the book on omissions this would be unfair—a book such as this cannot be complete; what it does omit is in the field of a specialist and not the sudden need of some more general worker. It has, however, one serious drawback—it is in German. This, regrettably, reduces its value enormously for the average English scientist. A similar book in English would certainly be an asset in all physical laboratories. H. O. PULS

Solid state physics and crystallography

Dendritic crystallization. By D. D. SARTOVKIN. Translated from the Russian by J. E. S. BRADLEY. (New York: Consultants Bureau Inc.; London: Chapman and Hall Ltd., 1959.) Pp. 126. Price \$6.00.

This brief monograph is concerned with an attempt to explain the origin of dendritic crystallization in terms of included impurities. It is a curious work. Beginning with some observations made by the Russian metallurgist Chernov in 1868 on dendrites in steels, the book seems largely devoted to contributions from Russian scientists. The bibliography itself is peculiarly arranged. In alphabetical order are 103 references to Russian scientists, then following this, in alphabetical order are a mere further 23 references to scientists of other nationalities. Considering that impurities are considered to be the cause of dendrites there are notable omissions. For instance, Buckley's comprehensive book on the influence of impurity on form growth is not even mentioned. The important subject of "whiskers" is neglected, and theories on dislocations are treated in a very summary fashion.

The only really novel contribution is the employment of a stereoscopic microscope, but even then only quite low magnifications are anywhere exploited in the whole monograph.

Nevertheless this is a useful translation in that it makes available in English a summary of the work of a very important Russian school of experimental crystallographers, and this is a great boon to those like your reviewer who know no Russian. S. TOLANSKY

Vector space and its application in crystal-structure investigation. By M. J. BUEGER. (New York: John Wiley and Sons Inc.; London: Chapman and Hall Ltd., 1959.) Pp. xiv + 347. Price 96s.

This is a valuable and original book, and as its title suggests it has a very wide field of application to crystal structure analysis. In many aspects of crystal work a considerable facility with geometry is desirable and the author is perhaps the best modern writer for the clear and elegant development of the geometrical basis. The book provides a valuable review of the theory and interpretation of the Patterson function, and especially of the author's own work in this subject. The chapters on vector sets and on image-seeking functions are particularly important and suggestive.

In a pioneer attempt such as this there is plenty of scope for some differences of opinion. The reviewer wonders whether the introduction of the concept of "implication diagram" is really necessary, when the diagram is really nothing more than a guess at the actual structure. Also the rather long discussion of the relative value of product, minimum and sum function seems a little pedantic. All these functions will work in practice, even when quite crudely applied, and to the reviewer the sum function still seems the most natural one to use.

These are, however, very minor criticisms of a most interesting and stimulating volume, which is extremely well produced and illustrated, and will no doubt already be in the possession of all serious workers in the field of X-ray analysis. C. A. BEEVERS

Inter-observer checks on standards of performance in evaluating thermal precipitator slides

by J. W. J. FAY, Ph.D., D.I.C., J. R. ASHEFORD, M.A., Ph.D., and P. H. SMITH, A.R.C.S., B.Sc.,
National Coal Board, Scientific Department, London

[Paper first received 16 June, and in final form 18 August, 1959]

Abstract

The problems associated with a monitoring procedure for maintaining satisfactory levels of counting thermal precipitator slides by members of a widely scattered team are discussed, with particular reference to the Pneumoconiosis Field Research of the National Coal Board. Experience within the research, since it started in 1953, is described and details are given of a new procedure based on a hierarchy, topped by a small number of "Master Counters", the mean of whose counting levels is taken as the standard of reference of the whole team.

The results obtained are summarized and it is concluded that the method gives an adequate measure of control. Some improvements to be applied in future checks are mentioned.

Introduction

THE estimation of dust concentrations in the respirable size range, using the thermal precipitator,⁽¹⁾ involves the counting on a microscope, with the aid of a calibrated graticule, of the number of particles within a certain size range occurring in a sample region of the dust strip deposited on a microscope cover slip. The problem of achieving and maintaining uniform standards of evaluation by a number of operators is by no means a new one, and check procedures and the results obtained from their use have been described.⁽²⁾

In the National Coal Board's Pneumoconiosis Field Research,⁽³⁾ one branch of the investigation is directed towards the estimation of the dust exposures of the men working at selected collieries, and the 1–5 μ count on the standard thermal precipitator slide is the routine basis for calculating the dust concentrations in terms of particles per cubic centimetre of air. Upwards of fifty operators are involved at twenty-five different collieries, and in order to ensure that their independent estimates of dust levels are free from substantial bias, and are therefore comparable with each other, an appreciable proportion of the available counting effort has to be expended in regular checks. In devising a procedure for maintaining these standards, it is important to strike a balance between minimal interference with the routine collection of results and the satisfactory monitoring of the performances (i.e. the counting levels) of the investigators producing the results. This paper describes the development of a system of monitoring which has been applied successfully within the research.

The achievement and assessment of uniform levels of performance within a team

The first step towards uniformity of performance amongst a team of observers is to train them to achieve satisfactory

initial standards. This has been done by means of training courses, where the participants, after preliminary instruction, evaluate typical routine slides, both jointly and separately, the instruction and examination being continued until the performance of the team as a whole is satisfactorily consistent. This is a fairly easy result to achieve, but the bigger problem remains to maintain these standards when the individual members of the team are scattered in comparative isolation at their various bases throughout the coalfields.

With a relatively small number of operators the evaluation of the same test slides by all participants according to a "Latin Square" design provides the best type of check procedure, since it allows the effect of deterioration of the specimen (if any) to be eliminated. (A "Latin Square" design is one in which the number of slides, or batches of slides, is equal to the number of participants, each of whom counts one batch first, one second and so on. Any systematic effect due to circulation is then eliminated in the comparison over the period.) However, the time taken to circulate the slides is so long that with more than a few participants the results are obtained too late to be of value for applying any necessary corrective measures to adjust current performance. With up to about twenty operators it is, however, possible to employ a curtailed circulation plan, based on "Youden Squares". (In the "Youden Square" design employed each participant evaluated one slide, or batch of slides, in common with each of the other participants. The Youden Square retains many of the advantages of the Latin Square, but reduces the number of slides to be evaluated by any one observer. In particular, it allows each man's bias to be estimated with equal precision.) This procedure was used in the early days (1953–1955) of the research, when the number of participants was only sixteen.

In order to obtain a realistic measure of performance, the slides used for test purposes in both courses and checks were typical ones selected from those obtained in the routine sampling programme. No attempt was made to choose slides which would be "easy" to evaluate. Although the investigators involved were all shown to be counting within $\pm 26\%$ of their mean in the 1–5 μ size range, and thirteen of the sixteen were within $\pm 11\%$,⁽⁴⁾ significant differences were revealed and a further series of training courses was held at the end of 1955.

Before these courses took place, the field sampling team had been expanded to a total of fifty-five men, thirty-nine technicians (Junior Investigators) having been added to the sixteen scientists (Senior Investigators) who comprised the original team. The new men had been trained locally by their seniors, and their standards of performance were assessed by means of an independent check.⁽⁵⁾ This showed that in the 1–5 μ range the individual counting levels for the whole team lay between 0.78 and 1.44 compared with the

mean achieved by the Senior Investigators, all but three counting within $\pm 27\%$ of the mean, and all but ten within $\pm 15\%$. Again these levels were not considered satisfactory, although the relative inexperience of the new men was recognized, and a further series of training courses for them was held.

Development of new monitoring procedures

With the need to monitor the counting levels of fifty-five people, and to take rapid corrective action in the event of serious departure from the mean level by any one or more of them, it was evident that the orthodox procedures were inadequate, and that something much more flexible and rapid of evaluation was required.

The sixteen Senior Investigators were divided on a regional basis into four groups of four, and from each group one experienced man with a good standard of performance was selected as the "Master Counter" for that region. These four Master Counters constituted the National Check, and the mean of their counting levels was adopted as the standard of reference for the entire team, all other levels of performance being referred to that mean. Each Master Counter, together with the three other Senior Investigators in his own region, formed one of the four Regional Checks, and each Senior Investigator, in association with the Junior Investigators under his jurisdiction (numbering from one to five), constituted the sixteen Local Checks.

The 1955 training courses, and the subsequent inter-investigator counting checks, were designed and carried out on this basis. In this way the counting level of every investigator could be related, through the appropriate Local, Regional and National Checks, to the mean level of the four Master Counters, and thus a means of comparison was available throughout the team.

The question arose as to what proportion of the investigators' effort should be devoted to check counting, and a balance had to be struck between time consumed and usefulness of the results obtained. In the event it was decided to circulate a batch of four check slides every month amongst the Master Counters, using a Latin Square design over a four-month period. Similarly, a batch of four slides was circulated every month in each Regional Check, again according to a Latin Square design. In the Local Checks only two slides were circulated each month, to avoid too much time being spent on check counting by the Senior Investigators. As it was, the need arose to make 190 slide evaluations each month for check purposes, this representing about 15% of the time available for all counting work by the team, and rather less than 10% of the total time available for all purposes.

The results each month were analysed to produce a "league table" of counting levels, embracing all members of the team. The circulation of this table to all Senior Investigators kept them fully informed of the level of both themselves and their Junior Investigators. This procedure has two main drawbacks. One is that the number of check slides counted by any one man (especially a Junior Investigator) in any one month may be too small to provide a significant result, because of the residual error in the counting process, due, for example, to the fact that different observers do not evaluate identical sample areas of the dust deposit on the slide.⁽⁶⁾ However, it was usually possible to assess a man's standard with confidence on the basis of the counts from two or three successive months, and the use of this "cumulative bias" figure enabled any necessary corrective action (e.g. special training courses) to be taken in adequate time. Another disadvantage of the system is that a temporary deviation or random fluctuation on the part of, say, a Master Counter gives rise to an apparent temporary change of standards, in that particular month, on the part of the other Senior Investigators in his region, and through them of their Junior Investigators. However, both these disadvantages are short-term effects and are removed by considering cumulative (or average) biases over a period. They were, however, carefully taken into account before any corrective action was recommended in individual cases during the course of the check.

Results obtained by the new system

The individual biases revealed month-by-month by the Master Counters are summarized in Table 1, and those for the other Senior Investigators in Table 2. For the reasons already given an individual result for any one month is subject to considerable random fluctuation and performances are better judged in terms of the average bias of each investigator, as shown in the last column of each table. Over the period of sixteen months constituting the check, the four Master Counters all maintained average levels within $\pm 1\%$ of their mean, and their individual monthly biases are randomly distributed about the mean, with no tendency on the part of any one man to count high or low. Similar results were obtained by the other Senior Investigators, except that the range of biases is wider, the average values varying between 0.95 and 1.10. No Senior Investigator counted persistently at a different level from the mean of the Master Counters, some of the individual biases for each man being above and some below that mean.

The turnover of junior staff is high and a summary comparable to Tables 1 and 2 cannot conveniently be made. However, the corresponding individual monthly performances

Table 1. *Individual biases revealed in the 1-5 μ range, Master Counters*

Counter	Circulation	Referred to mean of Master Counters															
		1st	2nd	3rd	4th	5th	6th	7th	8th	9th	10th	11th	12th	13th	14th	15th	Overall
M.1		1.01	1.04	1.07	1.08	0.91	0.88	0.98	0.96	1.01	0.93	0.93	1.22	1.09	1.04	0.90	1.00
M.2		1.00	0.98	0.99	0.94	1.07	1.04	1.05	0.97	0.99	1.00	1.01	0.85	0.88	0.97	1.23	0.99
M.3		0.96	1.00	0.93	0.99	0.91	0.96	1.08	1.03	1.01	1.03	1.07	0.95	1.06	1.04	0.97	1.00
M.4		1.03	0.99	1.01	0.99	1.12	1.13	0.92	1.04	0.99	1.05	1.00	1.02	0.98	0.95	0.93	1.01

Table 2. *Individual biases revealed in the 1-5 μ range, other Senior Investigators*

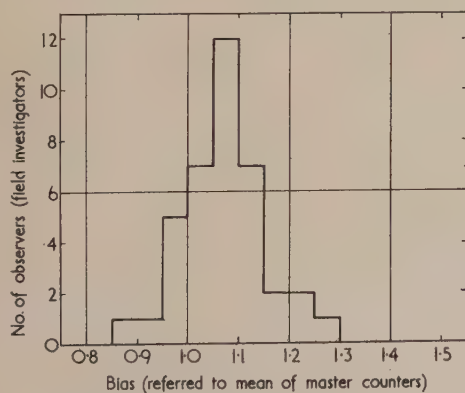
Circulation Counter	Referred to mean of Master Counters															
	1st	2nd	3rd	4th	5th	6th	7th	8th	9th	10th	11th	12th	13th	14th	15th	16th
S. 1	0.96	0.90	0.91	0.88	1.04	0.98	0.76	0.88	0.92	1.17	1.04	1.19	1.00	0.80	0.97	1.22
S. 2	1.05	1.00	1.08	1.00	0.95	1.05	0.89	0.90	1.01	0.92	0.84	1.29	1.20	1.02	0.90	1.02
S. 3	1.07	1.04	0.92	0.94	0.84	0.98	1.14	0.93	0.96	1.18	1.23	1.02	1.06	1.06	0.99	1.04
S. 4	1.03	0.93	1.03	0.99	0.92	1.06	1.46	1.15	1.00	1.05						(1.06)
S. 5	0.93	0.92	1.03	0.98	0.86	1.08	1.01	1.08	1.10	1.19	1.37	1.65	1.12	1.19	0.91	1.07
S. 6	1.03	0.92	0.91	0.82	0.96	0.84	0.85	1.14	0.85	1.06	0.97	1.11	1.06	0.81	1.00	1.09
S. 7	1.15	1.04	0.96	0.92	1.13	1.18	0.92	1.06	1.07	1.16	1.11	1.25	1.17	0.90	0.97	1.24
S. 8	0.98	1.23	1.02	1.11	1.03	1.09	1.00	1.22	0.94	1.17	0.89	1.51	1.39	1.18	1.01	0.97
S. 9	1.11	0.88	0.91	0.99	1.10	0.81	1.02	0.84	0.99	0.83	1.05	0.94	1.04	1.06	1.33	0.98
S.10	0.86	0.76	0.73	0.91	0.95	0.90	1.04	0.99	1.09	1.16	1.05	1.01	0.92	0.92	1.01	1.02
S.11	0.92	0.83	0.90	1.00	1.19	0.89	1.02	0.79	1.01	0.91	0.99	0.92	1.10	0.97	1.23	0.91
S.12	1.16	0.71	0.95	1.09	1.36	0.73	0.99	1.04	1.19	1.06	1.35	1.15	0.94	1.02	1.21	0.90

Table 3. *Individual biases revealed in the 1-5 μ range, all Investigators*

Circulation	Referred to mean of Master Counters															
	1st	2nd	3rd	4th	5th	6th	7th	8th	9th	10th	11th	12th	13th	14th	15th	16th
No. of investigators operational	49	47	46	46	45	49	50	53	55	54	53	50	49	50	52	50
No. within $\pm 10\%$ of mean of Master Counters	29	22	31	29	20	18	23	23	34	25	23	16	23	29	28	30
No. within $\pm 20\%$ of mean of Master Counters	43	32	36	42	34	30	39	39	47	40	37	32	41	42	41	42
Highest bias	1.38	1.35	1.38	1.35	1.56	1.51	1.47	1.39	1.72	1.40	1.59	2.74	1.39	1.47	1.52	1.60
Lowest bias	0.74	0.62	0.68	0.71	0.66	0.68	0.72	0.74	0.77	0.80	0.83	0.80	0.73	0.78	0.79	0.78

of the team as a whole, including the Junior Investigators, are summarized in Table 3, and the histogram in the figure shows the distribution of the average biases of those Junior Investigators who participated in at least six circulations of test slides. It is evident that the team as a whole has adopted standards similar to that of the mean of the Master Counters.

course of the check, and the two with the highest biases left after relatively few months. The tendency shown in the figure for the biases to be slightly high is interesting in view of the tendency discussed in the next section for the check counts to be slightly higher than the corresponding routine counts on the test slides.

Distribution of counting biases (1-5 μ)

Not unexpectedly, the range of biases is wider among the Junior Investigators than among the Seniors, but only three out of about forty investigators involved counted consistently above the mean of the Master Counters (average biases 1.09, 1.24 and 1.43), and none below. All three exceptions were with the team for less than a year during the

Standard of performance in the checks compared with that in routine counting

The investigators know when they are carrying out the check counts and it is important to determine whether their "check" counting levels differ from those applied on the routine counts. A comparison has therefore been made between the counts returned on the original routine evaluation of each of the slides used in the check, and the counts returned on the same slide in the check. In general the slides originating from any given counter were not evaluated by the same counter during the check, and the "check" count corresponding to each slide was obtained by "correcting" the counts returned during the check to the mean of the Master Counters. This was done by applying a factor corresponding to the inverse of the reference counter's bias relative to the mean of the Master Counters for that particular month. The results are summarized in Table 4. Although the majority of the routine counts have been confirmed by those from the check counts, there is a slight tendency for the latter to be higher. It must, however, be noted that no attempt has been made to apply a correction for individual

biases to the routine counts, and this could well account for the small differences found.

Variation of standards with time

The reference standard represented by the mean counting level of the four Master Counters is such an important factor that it is essential to investigate its consistency with time. If it were subject to any considerable change over the period of the research, errors would be introduced when comparing results obtained at different stages of the dust measurements. During the course of the check about 200 slides were therefore circulated on more than one occasion, with a minimum interval of three months between. The corrected mean traverse counts obtained on the two occasions are shown at Table 5, and a summary of the consistency of the counting levels revealed is given at Table 6. No marked trend is apparent, and the results confirm that the mean of the Master Counters provided a stable standard of reference throughout the check.

Deterioration of standards in the absence of a regular system of checking

The expenditure on counting checks of something like 10% of the total effort available for environmental studies is a considerable demand on the resources, and in order to investigate whether any relaxation was permissible an experiment was conducted at the end of the check described above. An interval of six months was allowed to elapse without any

Table 4. Comparison of routine and check counts

Routine evaluation (particles per traverse in the 1 - 5 size range)																		No. of slides												
320 - 339																	1	1												
300 - 319																														
280 - 299																														1
260 - 279																														
240 - 259																														
220 - 239																														
200 - 219																														
180 - 199																														
160 - 179																														
140 - 159																														
120 - 139																														
100 - 119																														
80 - 99																														
60 - 79																														
40 - 59																														
20 - 39																														
0 - 19																														
0 - 19																														
20 - 39																														
40 - 59																														
60 - 79																														
80 - 99																														
100 - 119																														
120 - 139																														
140 - 159																														
160 - 179																														
180 - 199																														
200 - 219																														
220 - 239																														
240 - 259																														
260 - 279																														
280 - 299																														
300 - 319																														
320 - 339																														
340 - 359																														
360 - 379																														
380 - 399																														

(particles per traverse in the 1-5 size range
"corrected" to the mean of the Master Counters.)

Table 5. Comparison of counts made in different circulations, 1-5 μ size range

No. of slides

1st. corrected mean traverse count

320-329																																																																																																																																																																																																																																																																																																																																																																																																																																																																																																																																																																																																																																																																																																																																																																																																																																																																																																																																																																																																																																																																																																																																																																																																																																																																																																																																																																																																																																																																								
---------	--	--	--	--	--	--	--	--	--	--	--	--	--	--	--	--	--	--	--	--	--	--	--	--	--	--	--	--	--	--	--	--	--	--	--	--	--	--	--	--	--	--	--	--	--	--	--	--	--	--	--	--	--	--	--	--	--	--	--	--	--	--	--	--	--	--	--	--	--	--	--	--	--	--	--	--	--	--	--	--	--	--	--	--	--	--	--	--	--	--	--	--	--	--	--	--	--	--	--	--	--	--	--	--	--	--	--	--	--	--	--	--	--	--	--	--	--	--	--	--	--	--	--	--	--	--	--	--	--	--	--	--	--	--	--	--	--	--	--	--	--	--	--	--	--	--	--	--	--	--	--	--	--	--	--	--	--	--	--	--	--	--	--	--	--	--	--	--	--	--	--	--	--	--	--	--	--	--	--	--	--	--	--	--	--	--	--	--	--	--	--	--	--	--	--	--	--	--	--	--	--	--	--	--	--	--	--	--	--	--	--	--	--	--	--	--	--	--	--	--	--	--	--	--	--	--	--	--	--	--	--	--	--	--	--	--	--	--	--	--	--	--	--	--	--	--	--	--	--	--	--	--	--	--	--	--	--	--	--	--	--	--	--	--	--	--	--	--	--	--	--	--	--	--	--	--	--	--	--	--	--	--	--	--	--	--	--	--	--	--	--	--	--	--	--	--	--	--	--	--	--	--	--	--	--	--	--	--	--	--	--	--	--	--	--	--	--	--	--	--	--	--	--	--	--	--	--	--	--	--	--	--	--	--	--	--	--	--	--	--	--	--	--	--	--	--	--	--	--	--	--	--	--	--	--	--	--	--	--	--	--	--	--	--	--	--	--	--	--	--	--	--	--	--	--	--	--	--	--	--	--	--	--	--	--	--	--	--	--	--	--	--	--	--	--	--	--	--	--	--	--	--	--	--	--	--	--	--	--	--	--	--	--	--	--	--	--	--	--	--	--	--	--	--	--	--	--	--	--	--	--	--	--	--	--	--	--	--	--	--	--	--	--	--	--	--	--	--	--	--	--	--	--	--	--	--	--	--	--	--	--	--	--	--	--	--	--	--	--	--	--	--	--	--	--	--	--	--	--	--	--	--	--	--	--	--	--	--	--	--	--	--	--	--	--	--	--	--	--	--	--	--	--	--	--	--	--	--	--	--	--	--	--	--	--	--	--	--	--	--	--	--	--	--	--	--	--	--	--	--	--	--	--	--	--	--	--	--	--	--	--	--	--	--	--	--	--	--	--	--	--	--	--	--	--	--	--	--	--	--	--	--	--	--	--	--	--	--	--	--	--	--	--	--	--	--	--	--	--	--	--	--	--	--	--	--	--	--	--	--	--	--	--	--	--	--	--	--	--	--	--	--	--	--	--	--	--	--	--	--	--	--	--	--	--	--	--	--	--	--	--	--	--	--	--	--	--	--	--	--	--	--	--	--	--	--	--	--	--	--	--	--	--	--	--	--	--	--	--	--	--	--	--	--	--	--	--	--	--	--	--	--	--	--	--	--	--	--	--	--	--	--	--	--	--	--	--	--	--	--	--	--	--	--	--	--	--	--	--	--	--	--	--	--	--	--	--	--	--	--	--	--	--	--	--	--	--	--	--	--	--	--	--	--	--	--	--	--	--	--	--	--	--	--	--	--	--	--	--	--	--	--	--	--	--	--	--	--	--	--	--	--	--	--	--	--	--	--	--	--	--	--	--	--	--	--	--	--	--	--	--	--	--	--	--	--	--	--	--	--	--	--	--	--	--	--	--	--	--	--	--	--	--	--	--	--	--	--	--	--	--	--	--	--	--	--	--	--	--	--	--	--	--	--	--	--	--	--	--	--	--	--	--	--	--	--	--	--	--	--	--	--	--	--	--	--	--	--	--	--	--	--	--	--	--	--	--	--	--	--	--	--	--	--	--	--	--	--	--	--	--	--	--	--	--	--	--	--	--	--	--	--	--	--	--	--	--	--	--	--	--	--	--	--	--	--	--	--	--	--	--	--	--	--	--	--	--	--	--	--	--	--	--	--	--	--	--	--	--	--	--	--	--	--	--	--	--	--	--	--	--	--	--	--	--	--	--	--	--	--	--	--	--	--	--	--	--	--	--	--	--	--	--	--	--	--	--	--	--	--	--	--	--	--	--	--	--	--	--	--	--	--	--	--	--	--	--	--	--	--	--	--	--	--	--	--	--	--	--	--	--	--	--	--	--	--	--	--	--	--	--	--	--	--	--	--	--	--	--	--	--	--	--	--	--	--	--	--	--	--	--	--	--	--	--	--	--	--	--	--	--	--	--	--	--	--	--	--	--	--	--	--	--	--	--	--	--	--	--	--	--	--	--	--	--	--	--	--	--	--	--	--	--	--	--	--	--	--	--	--	--	--	--	--	--	--	--	--	--	--	--	--	--	--	--	--	--	--	--	--	--	--	--	--	--	--	--	--	--	--	--	--	--	--	--	--	--	--	--	--	--	--	--	--	--	--	--	--	--	--	--	--	--	--	--	--	--	--	--	--	--	--	--	--	--	--	--	--	--	--	--	--	--	--	--	--	--	--	--	--	--	--	--	--	--	--	--	--	--	--	--	--	--	--	--	--	--	--	--	--	--	--	--	--	--	--	--	--	--	--	--	--	--	--	--	--	--	--	--	--	--	--	--	--	--	--	--	--	--	--	--	--	--	--	--	--	--	--	--	--	--	--	--	--	--	--	--	--	--	--	--	--	--	--	--	--	--	--	--	--	--	--	--	--	--	--	--	--	--	--	--	--	--	--	--	--	--	--	--	--	--	--	--	--	--	--	--	--	--	--	--	--	--	--	--	--	--	--	--	--	--	--	--	--	--	--	--	--	--	--	--	--	--	--	--	--	--	--	--	--	--	--	--	--	--	--	--	--	--	--	--	--	--	--	--	--	--	--	--	--	--	--	--	--	--	--	--	--	--	--	--	--	--	--	--	--	--	--	--	--	--	--	--	--	--	--	--	--	--	--	--	--	--	--	--	--	--	--	--	--	--	--	--	--	--	--	--	--	--	--	--	--	--	--	--	--	--	--	--	--	--	--	--	--	--	--	--	--	--	--	--	--	--	--	--	--	--	--	--	--	--	--	--	--	--	--	--	--	--	--	--	--	--	--	--	--	--	--	--	--	--	--	--	--	--	--	--	--	--	--	--	--	--	--	--	--	--	--	--	--	--	--	--	--	--	--

Table 6. *Stability of performance*

No. of slides circulated twice	No. of slides for which the recount was 20% or more higher than the original	No. of slides for which the recount was within $\pm 20\%$ of the original	No. of slides for which the recount was 20% or more lower than the original
198	14	155	29

checks, and at the end of that period sixteen slides, all of which had previously been evaluated in the check, were re-circulated in the National and Regional Groups. The results showed two interesting features.

In the first place the inter-observer variation increased. For example, whereas the range of the biases among the fourteen Senior Investigators (two had left in the interval and their replacements were not operational) was 0.95–1.10 at the end of the regular check, it had increased to 0.81–1.22 by the time of the final re-evaluation.

Secondly, the mean of the Master Counters had apparently risen by 8% during the six months without checks. This particular feature may be explained by the fact that one of the four Master Counters had ceased regular counting when transferred to another post before the final re-check, and his lack of regular practice probably had a considerable effect upon his counting level. If his results are excluded, the apparent change in mean level of the Master Counters is reduced to 5%, which is within the limits to be expected by chance, in view of the relatively small numbers of slides involved in the re-count.

The effect of the circulation of the monthly "league table"

Although the summaries covering all men were circulated every month, the Senior Investigators were instructed not to take any conscious action about their counting levels unless advised to do so on the basis of the analysis of the results. Nevertheless, one might imagine that the tables might encourage an unconscious effort by an observer to "correct" his performance, and the correlation between each Senior Investigator's counting bias for one circulation with that for another circulation has been examined. Since at the time of counting the n th batch of slides the investigator was aware of his counting level up to and including the $(n-2)$ th circulation, it might be expected that the bias of the n th circulation would be "corrected" (i.e. nearer the mean of the Master Counters) compared with the $(n-2)$ th. This may be examined by comparing the biases reported in Tables 1 and 2. These show, and statistical analysis confirms, that there is no evidence of any systematic corrective effect of this type.

Other factors which might affect performance

By careful design of the check (e.g. by basing the circulations of slides within each group for each phase of the check on a Latin Square) it has been possible to monitor several other factors which might affect the results. Some of these factors had already been examined in earlier checks,⁽⁴⁾ but the present trials afforded an opportunity for further investigation.

For example, the present experiment confirmed that, using the standard paper-ring mounting procedure for preparing the slides, no appreciable deterioration in the course of circulation by post occurred, even after as many as six journeys. This is an important and useful conclusion, as it means that test slides may safely be re-circulated at intervals to monitor the stability of counting levels.

The trial was also designed to investigate whether the investigators could spend a whole day on slide evaluation without any appreciable changes in their counting level or variability, and no evidence was found of such an observer fatigue.

Conclusions

Experience in counting checks in the Pneumoconiosis Field Research has shown that reasonable consistency in the evaluation of thermal precipitator slides can be achieved and maintained, even with a large number of observers located at different places. The concept of a small number of Master Counters, whose mean level is used as a standard of reference for the whole team, has proved highly successful, and, indeed, its use has been extended to other sections of the National Coal Board's Scientific Department.

The Master Counters must, of course, be experienced and reliable performers, and it is highly desirable that they be regularly engaged on slide evaluation, and not brought in occasionally in the way of consultants. Even if these requirements are met, their counting levels should be monitored frequently.

For monitoring the standards of performance of a large team, the pyramidal hierarchy based on Master Counters and Regional Groups can be made to work satisfactorily, and sufficiently rapid results can be obtained to enable any necessary corrective action to be taken in sufficient time for it to be effective. Again, regular checks are required, with the rapid publication of the results. The performance tends to deteriorate in their absence.

Experience in the check described in this paper has pinpointed two weaknesses of the procedure adopted, and these are being put right in the check which is now in progress within the Pneumoconiosis Field Research team. In the first place, the somewhat haphazard re-circulation of slides for monitoring the stability of the counting levels has now been replaced by a more systematic programme for the frequent re-circulation of test slides. This will give a better check on any trends with time. Secondly, a change has been made in the procedure for monitoring the performance of the Junior Investigators. These men are responsible for a large proportion of the routine evaluation of slides in the course of the research, and the system of Local Checks has been modified. Instead of circulating test slides for the purpose, the new procedure requires the Senior Investigator responsible to re-count two routine slides each week from among those initially collected and evaluated by each Junior Investigator in his team. The check slides are chosen randomly and without the prior knowledge of the Junior Investigator concerned, thus providing a direct check on the counting levels applied by the Junior Investigators for their routine slides. The performance of the Senior Investigators will continue to be monitored by a procedure similar to that described in this paper, but the frequency of checking has been reduced to once every two months, and the Master Counters are now counting a smaller proportion of slides compared with the other Senior Investigators.

Acknowledgements

This work represents part of the Pneumoconiosis Field Research of the National Coal Board and the results are published by permission of the Board.

References

- (1) GREEN, H. L., and WATSON, H. H. *Medical Research Council Special Report Series No. 199* (1935).

- (2) HOLDSWORTH, J. F., PRICE, F. HENLEY, and TOMLINSON R. C. *Brit. J. Appl. Phys., Suppl. 3*, Paper E.1, p. S.96 (1954).
 (3) FAY, J. W. J. *Nature (London)*, **180**, p. 309 (1957).
 (4) ASHFORD, J. R. *N.C.B. Report SC. 320/CC/2* (Confidential) (1955).
 (5) SMITH, P. H. *N.C.B. Report SC. 321/CC/3* (Confidential) (1955).
 (6) ASHFORD, J. R. *Brit. J. Appl. Phys.*, **11**, p. 13 (1960).

Anode surface effects in diodes containing oxide-coated cathodes

by B. J. HOPKINS, B.A., Ph.D., A.Inst.P., The Physical Laboratories, The University, Southampton

[Paper first received 7 September, and in final form 16 November, 1959]

Abstract

Two types of experimental tube have been built to study the behaviour of thin films deposited on the anode by evaporation during the breakdown and activation of calcium and barium oxide coated cathodes. First, with diodes of cylindrical symmetry, a contact-potential-difference method has been used to follow the changes in anode work function during activation of the cathode at several anode potentials. Emission-poisoning effects have been related to changes in the anode work function and it appears that there are two separate contaminating films on the anode surface: a very tightly held electropositive layer and a loosely bound electronegative layer. The emission decay process by the decomposition of compounds on the anode does not explain the results adequately. The second tube contained a movable glass electrode upon which a gold film could be deposited by evaporation. The results from these tubes confirmed those from the cylindrical diodes and also the validity of the contact-potential-difference method.

Several emission-slumping effects that take place at characteristic anode potentials have been reported. Headrick and Lederer⁽¹⁰⁾ first observed that cathode poisoning occurred when the voltage between their anode and cathode exceeded about 7 V. Metson⁽²⁾ has since been able to distinguish three independent poisoning potentials corresponding to electron energies of 5.56, 9.4 and 15.9 eV. From the work of Jacobs⁽¹⁾ and more recently Wright,⁽⁶⁾ Metson attributes these to the decomposition of oxides, chlorides and sulphates on the surface of the anode. In a later publication⁽⁷⁾ Metson claims that it is possible to relate such voltage-dependent poisoning effects to the nature of the organic binder. The existence of these contaminating anode films has been accepted for many years although very little is certain regarding their exact nature or mode of formation.

It is well known that the high-vacuum thermionic diode is capable of converting heat to electrical power. Recently the possibility of obtaining a high efficiency with a transducer of this kind has been investigated both experimentally⁽¹¹⁾ and theoretically.⁽¹²⁾ Of the three requirements that such a diode must fulfil to provide a technologically significant amount of power,⁽¹²⁾ one is that the work function of the anode shall be low. Thus, should it be possible in the future to overcome the technical difficulties of making such a transducer, then the control of the anode work function would become of prime importance.

In view of the lack of information about the anode, a programme of research has been started, the preliminary results of which are reported in this paper.

Initially the investigations were conducted in diodes of cylindrical symmetry fitted with nickel anodes. The results obtained with these tubes were then confirmed by the use of a tube design which had electrodes with planar symmetry. In the latter, emission could be drawn to either a nickel anode or a clean gold film deposited on a glass substrate.

Apparatus and techniques

Diodes with cylindrical symmetry similar to those used for this work have been described in a previous paper.⁽¹³⁾ The cathodes were essentially "O" nickel sleeves fitted with

Introduction

THE behaviour of thermionic devices containing oxide-coated cathodes has been the subject of much research during the last fifty years. The bulk of the work, however, has been concerned with the oxide cathode and there has been relatively little specifically designed to study the anode. That the condition of the latter is important when considering the properties of the diode has become increasingly apparent in recent years. Thus, it is now well established that cathode material deposited on the anode during breakdown and activation can, under the influence of electron bombardment, decompose and return to the cathode to affect its emission properties.⁽¹⁻⁷⁾ In 1930 Thompson⁽⁸⁾ observed that the pulsed emission from an oxide cathode was very much greater than the d.c. emission at the same cathode temperature. This has since been confirmed by others⁽⁹⁾ and is frequently explained in terms of anode contaminants, although Nergaard⁽⁹⁾ has given an alternative explanation in terms of his "mobile donor hypothesis".

internal thermocouples and sprayed with a carbonate suspension (containing a nitro-cellulose binder) to a thickness of about 100 μ .

The tube design with planar symmetry comprised a fixed assembly which held the cathode and a movable arm which carried the anodes. This arm could be rotated magnetically from outside the tube. The oxide cathode was prepared on an "O" nickel base (stamped into a cylindrical button 1.9 cm in diameter) by spraying the latter with a carbonate suspension. The large buttons were indirectly heated by means of a ceramic-insulated tungsten wire 0.51 mm in diameter. The temperature of the cathode was measured using a tungsten-nickel thermocouple welded inside the cathode button. The usual nickel anode was a button of the same shape as the cathode mounted on the movable arm so as to be above and parallel to the cathode in one fixed position of the arm. To the opposite side of the movable arm, the hard-glass electrode was sealed (see Fig. 1). Electrical contact with the evaporated

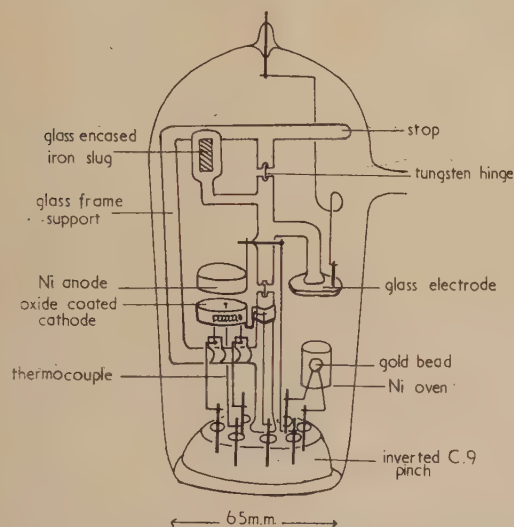


Fig. 1. The experimental tube having electrodes with planar symmetry

gold film was established *via* a tungsten rod sealed through the electrode. The surface of the electrode, together with the exposed section of the tungsten rod, was ground flat and then flame polished. When required, the gold film was deposited on the glass electrode by evaporation in high vacuum of a pure gold bead (originally prepared in hydrogen). This was fitted in such a position that the glass electrode could be covered with gold while the nickel anode was over the cathode. The deposition of gold on other parts of the tube was prevented by a cylindrical nickel screen surrounding the bead. The whole assembly was mounted on a glass frame sealed to an inverted C.9 pinch as on Fig. 1.

The completed tubes were evacuated using a conventional high-vacuum train. Baking took place at 450° C for periods between 6 and 24 hours. The metal parts, including the anode, were outgassed either by eddy currents or by direct heating. The cathode temperature was always raised slowly, usually over a period of 24 hours, in order to convert the carbonate into oxide. (When this procedure was not followed, the oxide tended to flake away from the base. This was especially true of the large button cathodes.) The tubes were usually sealed from the system at a pressure of less than 10^{-6} mm of mercury, and a getter was fired just before sealing.

Experimental results

The work function of the anode surface was followed by observing the contact potential difference between it and the oxide-coated cathode. The slope of a Richardson line was taken as the work function of the latter. The data for both measurements was obtained from emission characteristics. Similar methods have previously been reported in the literature.^(1, 14, 15) As a means of measuring the absolute work function of the anode, this method is open to objection. In the later tubes with planar symmetry, it has been possible to compare the results using this method with those from a true contact p.d. method.

Low cathode temperatures (less than 750° K) were used throughout the emission measurements. In this way, cathode evaporation was reduced to a minimum except during activation when the cathode temperature was raised to 1200° K. Both barium oxide and calcium oxide cathodes have been used; tubes 1 to 6 all had coatings of the latter. Calcium oxide has two advantages over barium oxide when investigating the anode. Firstly, activation states are much more stable, since calcium oxide is very slow to activate,⁽¹³⁾ and secondly, even in the highest states of activation, the emission is sufficiently low to ensure that the collector temperature does not rise. Purely thermal effects at the anode can then be eliminated. The tubes with planar symmetry were used only in the fully activated state, and all had barium oxide cathodes.

Results from the tubes with cylindrical symmetry

Tubes 1 and 2. It has been observed in the present work and elsewhere^(16, 17) that activation of the cathode with a high anode potential (between 10 and 100 V) leads to a low contact p.d. (— to +1 V). Tube 1 was typical; the slope of the Richardson line was 1.73 eV and the contact p.d. —0.2 V. The apparent anode work function was therefore 1.5 eV.

With an anode potential as low as 4 V, the contact p.d. rises during activation and the anode work function approaches 5 eV. After the activation of tube 2 with 4 V continuously applied to the anode, the contact p.d. was 3.22 V. The Richardson slope was 2.08 eV so that the work function of the anode was 5.3 eV. When a high potential was applied to this tube in an attempt to increase the activity of the cathode still further, the emission was poisoned and the anode work function fell. Only after prolonged treatment of the cathode at a high temperature (1200° K) with the anode maintained at 100 V could the original activation of the cathode be regained and finally surpassed. When this was achieved, the anode again had a work function between 1 and 2 eV.

Tube 3. This tube was activated in three separate stages with a constant potential of 6 V applied. In this manner, it was found possible to keep the anode work function constant within 0.5 eV. This is shown in Table 1.

Table 1. Activation of tube 3

	Unactivated state	Activation states			
		1	2	3	
c.p.d.	1.1	2.1	2.0	2.0	V
ϕ (Rich.)	2.20	6 V 1.92	6 V 1.56	6 V 1.50	eV
ϕ (anode)	3.3	4.0	3.6	3.5	eV

Tube 4. Two voltages (4 and 8 V—see discussion of the results) were applied in turn to the anode during the activation

Table 2. *Activation of tube 4*

		Activation states										
	Unactivated state	1		2		3		4		5		
c.p.d.	0.3	2.3		0.7		1.6		1.1		1.0		V
ϕ (Rich.)	2.44	4 V	2.26	8 V	2.30	4 V	2.06	8 V	1.90	8 V	1.73	eV
ϕ (anode)	2.7	→	4.6	→	3.0	→	3.7	→	3.0	→	2.7	eV

of tube 4 through five states of activity. The measurements made in each state are summarized in Table 2. The Richardson lines also showed that states 2 and 4 were de-activated states.

Tube 5. The effect of heating the anode was investigated in this tube part-way through the activation process. Initial activation to state 1 caused the changes shown in Table 3.

Table 3. *Activation of tube 5*

	Unactivated state		state 1	
c.p.d.	0.7		1.7	V
ϕ (Richardson)	2.03	6 V	1.52	eV
ϕ (anode)	2.7	\longrightarrow	3.2	eV

In state 1, the anode was heated to about 1000° K. This had two effects. Firstly, the cathode emission was poisoned (the Richardson work function increased to 1.78 eV) and

secondly the contact p.d. fell to 0.36 eV. These changes correspond to a fall in the anode work function from 3.2 eV to 2.1 eV during the time its temperature was raised. The original high state of activation could be recovered by activating with 8 V applied to the anode.

Tube 6. With the final cylindrical diode, activation was followed through two states with only 4 V applied to the anode. In state 2, when further activation was not possible without increasing the anode potential, the latter was raised to 8 V and measurements made in three more states.

Results from the tubes with planar symmetry

Three such tubes were constructed and all the cathodes were fully activated with 50 V applied to the anode. At a fixed cathode temperature, emission was drawn first to the contaminated nickel anode and then to a pure gold film freshly deposited on the glass electrode. The emission characteristics obtained in this manner for the first two

Table 4. *Activation of tube 6*

		Activation states										
	Unactivated state	1		2		3		4		5		
c.p.d.	0.9	2.4		3.2		2.3		1.4		0.2		V
ϕ (Rich.)	2.12	4 V	1.76	4 V	2.08	8 V	2.18	8 V	1.85	8 V	1.88	eV
ϕ (anode)	3.0	→	4.2	→	5.3	→	4.5	→	3.2	→	2.1	eV

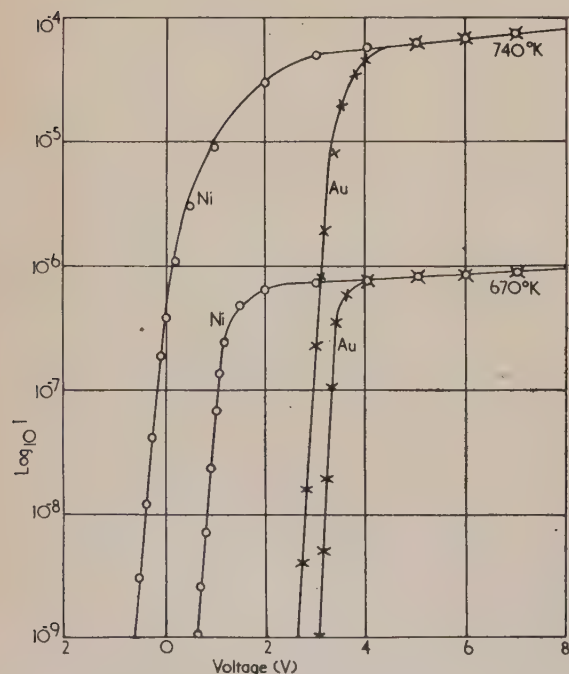


Fig. 2. Emission characteristics for tubes 7 and 8 taken first to the contaminated nickel anode and then to a clean gold film

tubes are shown in Fig. 2. The results from the three tubes are summarized in Table 5.

Table 5. *Activation of tubes with planar symmetry*

	ϕ (Richardson) (eV)	c.p.d. (oxide to Ni) (V)	c.p.d. (oxide to Au) (V)
Tube 7	1.54	0.55	3.50
Tube 8	1.74	1.25	3.45
Tube 9	1.70	0.95	3.40

The change in the contact p.d. when a clean gold film is substituted for the contaminated nickel has also been used to determine the work function of the anode surface by a method independent of the Richardson-line technique but assuming the work function of the gold surface. All of the work functions are then measured by a contact p.d. method and small temperature differences involved can be neglected. The results of this procedure are shown in Table 6, the anode work functions marked ϕ_A (c.p.d.) are those measured from the contact p.d. shift assuming the value of 4.7 eV for

Table 6. *Comparison of work functions*

	ϕ_A (by Richardson) (eV)	ϕ_A (by c.p.d.) (eV)
Tube 7	2.09	1.75
Tube 8	2.99	2.50
Tube 9	2.69	2.25

the work function of gold.⁽¹⁹⁾ The other figure is that calculated from the Richardson work function.

Discussion of results

The measurements with the first two tubes demonstrate that the anode is contaminated by at least two distinct materials. Tube 1 shows that, under normal high-voltage operation of the diode, the anode becomes contaminated with electropositive material which reduces its work function to about 2 eV. Tube 2 shows how the anode work function increases when the activating potential on the anode is reduced. This increase in the anode work function, together with the cathode poisoning that takes place when the anode potential of a "low-voltage-activated tube" is increased, can only be explained by the formation of an electronegative layer over the electropositive contaminated anode. An explanation in terms of the evaporation of a single compound (such as barium oxide or calcium oxide) on to the anode, and its subsequent decomposition under electron bombardment cannot be applied to these results unless it can be shown that the work function of that compound can be as high as 5 eV. The work of Moore and Allison,⁽¹⁵⁾ however, indicates that a work function in the region of 1 eV is more probable.

Experiments with tubes 1 and 2 indicate certain "critical" anode potentials. Below about 5 V, the anode work function increased during activation. When the anode potential was increased to about 7 V, the cathode was poisoned and the anode work function began to fall. These potentials are uncorrected for contact p.d.

In tube 3, a compromise anode potential was chosen and the tube activated continuously with 6 V applied to the anode. For the three activation states of the cathode, this potential corresponded to an electron energy of 4 eV (the contact p.d. remained at about 2 V). From the relative constancy of the anode work function it is thought that an equilibrium was established between the deposition of the electronegative contaminant on the anode and its removal by the electron bombardment. This electron energy of about 4 eV therefore appears to be the critical energy at which the electronegative material is liberated from the anode.

Taking into account this result, the two potentials which were applied alternately to the anode during the activation of tubes 4 and 6 were 4 and 8 V, corresponding roughly to 3 and 6 eV of electron energy. The anode work function of tube 4 increased from 2.7 eV in the unactivated state to 4.6 eV in state 2 after a period with 4 V applied to the anode. Increasing this potential to 8 V caused poisoning of the cathode emission and a fall in the anode work function as the electronegative element was removed. Activation to state 3, again with 4 V applied to the anode, further raised the anode work function to 3.7 eV. Reactivation with 8 V again caused poisoning and a fall in the anode work function. After the final activation, the anode work function had fallen to its value in the unactivated state, that is, 2.7 eV. This tube shows that, throughout activation, electronegative material is being liberated from the cathode and that the quantity (as judged by the work-function differences) diminishes with increasing activation. Plumlee⁽¹⁸⁾ has made a similar observation using a mass spectrometer technique to follow oxygen evolution from the cathode. Heating the anode in tube 5 had an effect similar to raising the anode potential; the cathode was poisoned and the anode work function reduced. The electropositive element, however, remained on the anode surface at this temperature.

Tube 6 demonstrates the rise in the anode work function during low-voltage activation until a value of 5.3 eV is attained at highest activity. In this state, the application of 8 V caused a steady fall to 2.1 eV.

The results from the final three tubes 7, 8 and 9 confirm that the low contact p.d. is caused by electropositive contamination of the anode since the use of a clean, deposited good surface caused a large change in the contact p.d.

The literature concerning the evaporation from oxide-coated cathodes indicates that for both barium oxide⁽²⁰⁾ and calcium oxide⁽²¹⁾ the principal material reaching the anode surface is the free metal. Wooton, Ruehle and Moore,⁽²⁰⁾ in an attempt to explain the adhesion of barium metal to their hot anode, have suggested that oxides of magnesium and nickel are formed at the anode by carbon-dioxide oxidation during breakdown, and that the barium is tenaciously held by these oxides. Such a mechanism, if correct, would explain why it has not been possible in the present work to remove the electropositive layer from the anode surface either by heating or by electron bombardment. It might also explain the high threshold energy (300 V) observed by Jacobs⁽²²⁾ for the transfer of barium from the anode to the cathode by bombarding electrons. Alternatively, the alkali metal may diffuse into the nickel, forming a reservoir from which the surface can be replenished. Such a process is known to take place in platinum when it is used as the core material of the cathode.

The electronegative element present on the anode surface after low-voltage activation (and which is easily removed either by heating or by electron bombardment) is most likely to be oxygen. Numerous workers have shown that this is eliminated from an oxide cathode during activation.⁽¹⁸⁾

The results given in Table 6 make it possible to check the validity of the work-function technique used for following the anode surface. This table shows that the anode work function using the Richardson line differs from a true contact p.d. method by about 15%. For the purpose of the arguments described above, this is sufficiently accurate, especially as the method tends always to over-estimate the anode work function. The reason may lie in the use of the Richardson-line technique, or it could be explained in terms of a voltage drop across the oxide, since this would affect the measured value of the contact p.d. used in determining $\phi_A(\text{Rich.})$. If the latter is the case, then it is evident that the energies of the electrons reaching the anode must be reduced by 15%.

Conclusions

The behaviour of the anode during activation at several anode potentials may be summarized thus:

During breakdown or the early stages of activation, alkali-earth metal evaporates from the cathode and by some unknown process is bound firmly to the surface of the anode, reducing its work function to less than 2 eV. During the activation process, oxygen is liberated from the cathode, the quantity decreasing with increasing activation. This is adsorbed on the anode surface, probably loosely on top of the electropositive layer. At electron energies of less than 4 eV, this oxygen remains on the anode, a fact which is reflected in an increase in anode work function as activation proceeds. When the anode potential exceeds 6 V, the energy acquired by the bombarding electrons is sufficient to dislodge the oxygen. Should there be an accumulation of oxygen on the anode—caused by low-voltage activation or, possibly, by flashing the cathode—then this can return to the cathode and poison the emission. This, of course, is accompanied by a

fall in the anode work function as the electropositive contaminant is exposed.

Acknowledgements

The author wishes to acknowledge the advice of Prof. F. A. Vick (now at the Atomic Energy Research Establishment, Harwell), in whose laboratories at Keele the work was started. Thanks are also due to Prof. A. M. Taylor for facilities to continue the work at Southampton.

References

- (1) JACOBS, H. *J. Appl. Phys.*, **17**, p. 596 (1946).
- (2) METSON, G. H. *Proc. Phys. Soc. (London)*, **62B**, p. 589 (1949).
- (3) WRIGHT, D. A. *Proc. Phys. Soc. (London)*, **62B**, p. 398 (1949).
- (4) FEASTER, G. R. *J. Appl. Phys.*, **20**, p. 415 (1949).
- (5) AMAKASU, K., and IMAI, T. *J. Appl. Phys.*, **24**, p. 107 (1952).
- (6) WRIGHT, D. A. *Brit. J. Appl. Phys.*, **5**, p. 108 (1954).
- (7) METSON, G. H. *Advances in Electronics and Electron Physics*, Vol. 8 (New York: Academic Press Inc., 1956).
- (8) THOMPSON, B. J. *Phys. Rev.*, **36**, p. 1415 (1930).
- (9) NERGAARD, L. S. *R.C.A. Rev.*, **13**, p. 464 (1952).
- (10) HEADRICK, L. B., and LEDERER, E. A. *Phys. Rev.*, **50**, p. 1094 (1936).
- (11) HATSOPoulos, G. M., and KAYE, J. *J. Appl. Phys.*, **29**, p. 1124 (1958).
- (12) NOTTINGHAM, W. B. *J. Appl. Phys.*, **30**, p. 413 (1959).
- (13) HOPKINS, B. J., and VICK, F. A. *Brit. J. Appl. Phys.*, **9**, p. 257 (1958).
- (14) HUNG, C. S. *J. Appl. Phys.*, **21**, p. 37 (1950).
- (15) MOORE, G. E., and ALLISON, H. W. *Phys. Rev.*, **77**, p. 246 (1950).
- (16) FAN, H. Y. *J. Appl. Phys.*, **14**, p. 552 (1943).
- (17) SHEPHERD, A. A. *Brit. J. Appl. Phys.*, **4**, p. 70 (1953).
- (18) PLUMLEE, R. H. *R.C.A. Rev.*, **17**, p. 190 (1956).
- (19) RIVIERE, J. C. *Proc. Phys. Soc. (London)*, **70B**, p. 676 (1957).
- (20) WOOTON, L. A., RUEHLE, A. E., and MOORE, G. E. *J. Appl. Phys.*, **26**, p. 44 (1955).
- (21) PELCHOWITCH, I. *Phil. Res. Reps.*, **9**, p. 42 (1954).
- (22) JACOB, L. *Proc. Phys. Soc. (London)*, **70B**, p. 235 (1957).

Purification of organic materials by zone refining

by J. H. BEYNON, B.Sc., F.Inst.P., and R. A. SAUNDERS, B.Sc., Grad.Inst.P., Imperial Chemical Industries Limited, Dyestuffs Division, Blackley, Manchester

[Paper received 16th October, 1959]

Abstract

Three zone refiners are described which between them are suitable for dealing with materials having melting points in the range -10 to $+300^{\circ}\text{C}$ in quantities of from 0.5 to 9000 g. Some of the more interesting results are discussed in detail, and a list of compounds which have proved amenable to this method of purification is given.

A NEED has arisen in the mass-spectrometry programme of this laboratory for the preparation of very pure organic materials in order that reference spectra can be produced. If this can be done, it makes the task of identification of impurities in new samples much easier because impurity peaks can readily be found by a comparison with the reference spectrum. In addition, it is sometimes very helpful in the identification of trace impurities if the impurity concentration can be increased significantly. Zone refining is a technique which sometimes provides the means to achieve both these requirements and has, therefore, been used for many materials with melting points in the range -10 to 300°C . Materials melting at temperatures above 300°C are often unstable because of the prolonged exposure to heat that is required in this method.

Because of differences in thermal conductivity, surface tension, viscosity, specific volume change on melting, latent

heat of fusion, speed of crystal formation and tendency of the liquid to supercool, and so on, between metals and organic chemicals, the apparatus used for refining them will differ in several respects. Organic compounds generally contract on solidification, the change of volume being often as great as 25% (as with anthracene) and occasionally even more (as with phthalic anhydride). It is necessary, then, to start melting at a free surface. In addition, it has been shown that, when organic compounds are refined in a horizontal tube, liquid from the molten zone can run back along the solid, thus reducing the efficiency of the process.⁽¹⁾

Description of apparatus

One of the refiners is shown in Fig. 1 and is similar to that used by Herington, Handley and Cook⁽¹⁾ except that a positive drive for the heaters is provided by a rotating-screw mechanism, and six tubes can be accommodated simultaneously. Only one of the six heaters is shown in position in order to avoid confusion. The design of the heater is shown in Fig. 2, and has the advantage that the heating is by radiation and is confined to a short length of sample. If a heated metal cylinder is used to melt the sample, the heat spreads to a greater extent. The former heater is, therefore, more efficient for melting a "slice" of the sample and is always

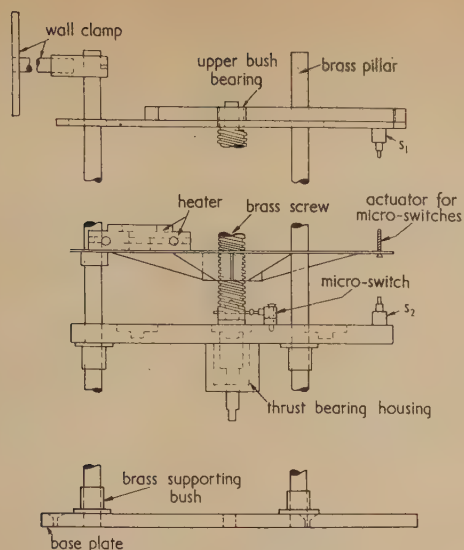


Fig. 1. Large-scale refiner

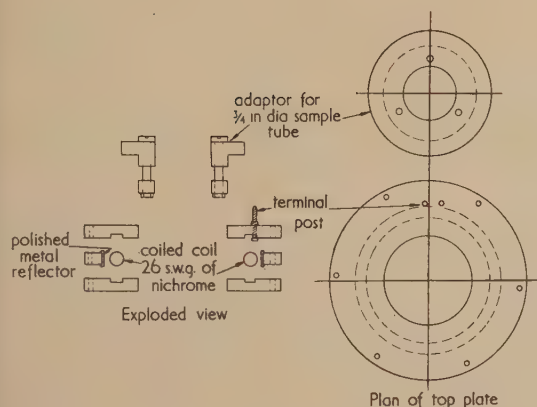


Fig. 2. Heater (material: Sindanyo)

used for the largest sample tubes (1–1½ in. diameter). For tubes of less than 1 in. diameter, melting through the sample presents little difficulty, and it is then more convenient to use a heated metal tube. Aluminium adaptors have been made to fit inside the tubular heaters in order to accommodate tubes of ¼ and ½ in. diameter.

A velodyne motor is used to turn the central brass screw of the refiner, through a 500 : 1 gear-box. The motor-control circuit is shown in Fig. 3. Under normal running conditions, the direction of rotation is such as to drive the heaters slowly downwards. When the heaters reach the bottom of their travel, they actuate the microswitch S_2 . This operates the relay and causes the motor to reverse. The heaters are then driven upwards at a fast rate until they actuate the upper microswitch S_1 . This unlocks the relay, and the heaters are driven downwards again on the next zone-melting operation. A great improvement in running the motor at a steady speed was achieved by driving the control circuit from a stabilized mains supply. This stabilized supply is also necessary for the heaters to keep the molten zone length constant. If the zone increases in size to any great extent, the tube breaks. In some cases it has been found necessary to reduce the heat supply as the zone passes down the sample, particularly when sample tubes of larger diameter are used. This arises because the refining process takes impurities down the tube, which results in a lowering of the melting point of the mixture in the lower sections of the tube. Thus, less heat is required to maintain a zone of constant length on progressing down the sample. In other words, if the heat supplied is constant, more material is melted and this may cause a sufficient expansion to crack the tube. This reduction of heating is achieved by operating several micro-switches successively on the downward travel of the heaters, which switch resistors in series with the heating coils. It has also been found necessary to shield the apparatus from draughts so that the rate of cooling above the zone is steady.

This refiner can be used to purify materials in tubes of $\frac{1}{4}$ to $1\frac{1}{2}$ in. diameter and can handle six tubes simultaneously. The $1\frac{1}{2}$ in. diameter tubes can hold about $1\frac{1}{2}$ kg and so, with six tubes, up to 9 kg can be purified at one time. It has been found that these tubes are about the largest that can be used

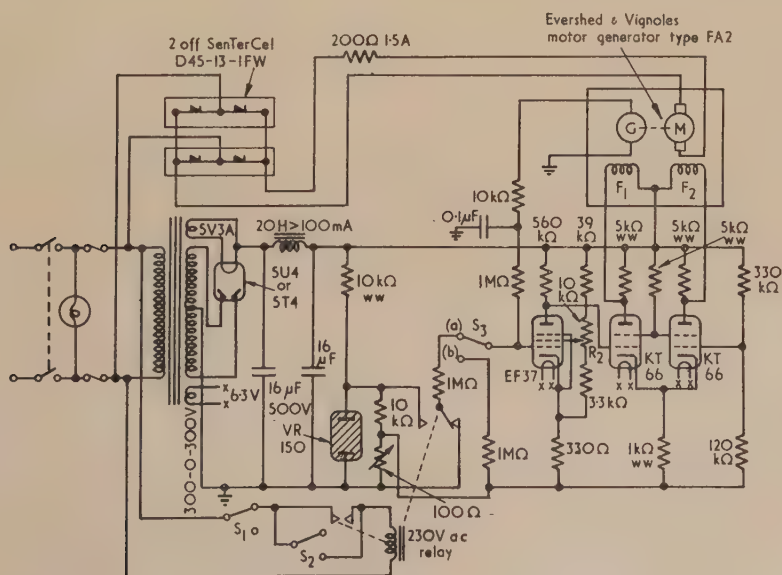


Fig. 3. Velodyne circuit

for organic materials without employing some method of stirring the molten zone.

Another, and very simple, apparatus shown in Fig. 4 has been used for refining small quantities of material down to about 0.5 g. Tubes of 2–5 mm diameter are suspended by a cotton thread and drawn through a heater consisting of a single loop of 26 s.w.g. nichrome wire. This heater is supplied from a 12 V transformer, and the current is regulated by a series rheostat.

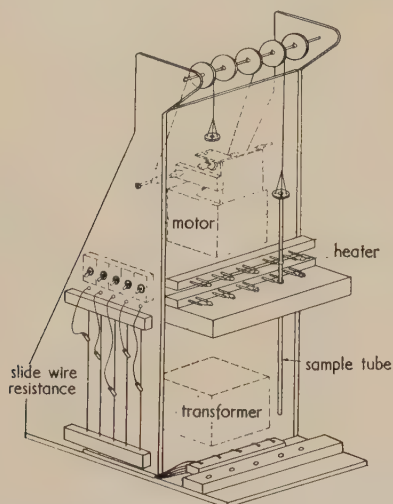


Fig. 4. Small-scale refiner

The apparatus used to refine materials with melting points below 50° C is shown in Fig. 5. A similar method has been described by Süe, Pauly and Nouaille⁽²⁾ who used a horizontal sample tube. A freezing mixture is made up in the inner of two concentric aluminium cylinders, the intervening space between the cylinders being filled with a polyurethane foam which provides good thermal insulation. A number of bars which pierce this insulating material connect a series of aluminium blocks to the inner cylinder. Holes drilled through the centre of the blocks hold a glass tube through which the sample tube is able to slide. It is necessary to separate the



Fig. 5. Low-temperature refiner

sample tube from the aluminium blocks in this way because a thick layer of ice forms round each block and causes the outer glass tube to adhere firmly to them. Heaters are wound round the glass in each space between the blocks so that alternate molten and frozen zones are produced in the sample.

The zones are caused to move with respect to the sample by means of the slow anti-clockwise rotation of the cam *A*. The sample tube is, therefore, raised through the vertical height *d*, which is the distance between the heaters, and then falls back suddenly to its starting position. In this way each molten zone is made to travel along the sample. In this apparatus, a clock-motor, making one rotation in two hours, is used to drive the cam. The sample tube is then raised and lowered once every two hours. A great merit of this process is that, once it has been set in operation, it needs no further attention until it is necessary to remove the purified material.

Discussion of results

Benzoic acid. 1½ kg of A.R. benzoic acid has been refined in a 1½ in. diameter tube. Melting point measurements on the starting material showed it to be about 99.3% pure, while measurements on the upper part of the sample after seven passes of the molten zone showed that it was 99.97 ± 0.03% pure. The sample was markedly more crystalline at the top end of the sample than at the centre. In fact, the sample at the upper end began to grow as a single crystal after a few passes; the single crystal, however, cracked under strain on cooling. It has been observed that, as a general rule, the purer the compound, the larger the crystal size.

1-, 4-, 5-trichloroanthraquinone. After thirty passes, this dyestuff intermediate underwent a marked change of colour. A greenish zone appeared in the top three or four inches, due to the presence of 1-, 4-, 5-, 8-tetrachloroanthraquinone. The material in the next six or seven inches became bright yellow, while the remainder of the tube was darkly coloured. When the material from this tube was powdered, it all appeared yellow, but on looking at the tube after the refining process it was easy to detect the regions containing the impurities. The colour of the molten zone gives an even more sensitive test of the presence of impurities and the progress of purification can often be followed by visual inspection of the molten zone or by measurements of its absorption spectrum.

4-chloro-2-nitroaniline. It was possible, in this case, to detect four trace impurities after just two passes of the molten zone. Further refining would have risked the possibility of concentrating explosive poly-nitro impurities. The impurities detected were (C₆H₃)NH₂Cl₂, (C₆H₃)NO₂Cl₂, (C₆H₄)NH₂Cl and (C₆H₂)NH₂NO₂Cl₂.

2-nitro, 4-methylaniline. The trace impurities (C₆H₄)NO₂CH₃ and (C₆H₂)(CH₃)₃NH₂ were detected after two passages. Further refining was not carried out for the same reasons as the previous sample.

Skatole (3-methylindole). This compound is of interest because the objectionable smell with which it is associated completely disappeared on zone refining.

Crude naphthalene. Although, as a general rule, zone refining is most effective when the starting material is already fairly pure, it has been found possible to purify crude naphthalene. The melting point of the top layer of sample was raised to 80.2° C after nine passes from an original figure of 73.5° C for the crude material.

It was possible, as a result of the above refining process, to identify a large number of impurities by mass spectro-

metric examination. Because of the complexity of the spectra obtained, an attempt was made first to fractionate the impurities into as many component parts as possible, and, at the same time, to remove as much of the residual naphthalene as possible. In this way the following impurities were identified: chrysene or isomer, anthracene or phenanthrene, phenyl toluene or diphenyl methane, fluorene, dimethyl naphthalene, acenaphthene, acenaphthalene, anethole or tetrahydro α -naphthol, methyl-naphthalene, thionaphthene, tetrahydronaphthalene, dihydronaphthalene, cumene or a trimethyl benzene, indan, indene.

In the course of the above refining, it was of considerable advantage in speeding the process to use a much longer molten-zone length than usual (up to about 6 in. in the case of a tube 30 in. long) for the first two or three passes. The zone length was then reduced by steps until it was of normal length (about 1-1½ in.). The longer zone length is able to carry a large quantity of impurity without producing saturation of the zone.

Anthracene. An impurity which has proved to be difficult to remove from anthracene is carbazole. This may be seen from Table 1, which shows the results obtained after 18 and 32 passages of the molten zone.

Table 1. *Reduction of impurities in anthracene*

Impurity	Carbazole (%)	Hexahydro-anthracene (%)	Methyl-anthracene (%)
Initial concentration	0.80	0.64	0.19
Concentration after 18 passes	0.38	0.05	<0.005
Concentration after 32 passes	0.11	<0.005	<0.005

Even material as difficult to remove by crystallization from the melt as carbazole can be eliminated by the application of a sufficient number of passes of the molten zone, and the number required lies in the range that can be attained in practice. In order to obtain a greater reduction in the concentration of the carbazole, the refining process was carried out progressively, starting with six tubes and removing the partially purified material from each and placing this in new tubes which were then further refined. This was carried out successively until all the pure material was concentrated in one tube. In this way, it was possible to reduce the carbazole content to less than 1 part in 20000 in a sample of 15 g in a total time of 45 days.

A similar procedure has also been followed to increase the concentration of trace impurities in other compounds. For this, the material in the lower portions of the sample tube is used, provided, of course, the impurity is one that has lowered the melting point of the substance and has thus travelled down the tube. Enhancements of the order of 10^4 have been achieved in suitable cases.

1-amino-2-methylanthraquinone. The impurities were identified as diamino-methylanthraquinone and aminodimethyl-anthraquinone. The concentrations at various points in the tube after the material had received thirty-three passes are given in Table 2.

3-methoxybenzanthrone. The most abundant impurity in this substance—chloromethoxybenzanthrone—has a partition coefficient greater than unity. Although it was possible to move this impurity, the rate of movement was very slow,⁽³⁾ as can be seen from the figures quoted in Table 3. For such an impurity it was of great help, in speeding the

Table 2. *Concentration of impurities in 1-amino-2-methyl-anthraquinone along tube*

Impurity	Diaminomethyl-anthraquinone (%)	Aminodimethyl-anthraquinone (%)
Initial concentration	0.31	0.31
Top layer	0.20	0.05
3 in. from top	0.20	0.05
6 in. from top	0.20	0.07
9 in. from top	0.25	0.14

refining process, to use a much longer molten zone-length than usual (about 4 or 5 in.), as was the case when refining a very impure material. The impurity, which is able to move one zone-length up the column on each pass, is thus enabled to move much farther, and this procedure was very useful in the initial stages. The zone was gradually returned to a normal length of about 1 in. as the number of passes increased. The material formed a column 24 in. high and received forty-eight passes of the molten zone.

Table 3. *Concentration of impurities in 3-methoxybenzanthrone along the tube*

Impurity	Chloromethoxy-benzanthrone (%)	Dimethoxy-benzanthrone (%)	Chloro-benzanthrone (%)
Initial concentration	2.0	0.12	0.66
Top of column	3.4	0.04	0.12
8 in. from top	2.1	0.06	0.19
16 in. from top	1.07	0.11	0.78
Bottom of column	0.70	0.17	0.78

Almost every compound which has been examined so far, and found to be stable at its melting point, has responded to purification by this method. Care must be exercised in deciding that a compound is unstable. Benzanthrone, for example, which is stable at its melting point, darkened when the zone first passed along it; but this darkening was caused by thermal decomposition of an impurity in the benzanthrone.

Some of the compounds successfully purified, in addition to those mentioned above, are: acetamide, diphenyl acetic acid, phenoxy acetic acid, aldrin, aniline, 2-methyl, 4-nitro aniline, antipyrine, N, N-dimethyl-p-nitrosoaniline, methylene aniline, p-nitroaniline, p-anisidine, anthranilic acid, anthraquinone, 1-amino-2-cyanoanthraquinone, 1-chloro-2-methylanthraquinone, 1-, 5-dihydroxyanthraquinone, 1-, 8-dihydroxyanthraquinone, 1-hydroxyanthraquinone, 1-methylaminoanthraquinone, azobenzene, 1:2 benzanthrone, benzamide, benzene, dibenzyl, cetyl alcohol, 2-methyl, 4-chlorophenol, 2-, 5-dimethyl phenol, 2-cyanocyclopentylidenimine, fluorenone, 2-, 3-dimethylindole, 1-, 3-, 5-, 7-tetramethylindole, 1-, 2-, 3-, 5-, 7-pentamethylindole, maleic anhydride, dichloromaleic anhydride, phenanthrene, 2- α -methyl-cyclohexyl-4-methylphenol, p-tert-butylphenol, pyrazolone, 1-p-tolyl-3-methyl-5-pyrazolone, pyrene, resorcinol, succinic acid, sulphur, dimethyl terephthalate, urea, δ -cyanovaleramide.

References

- (1) HERINGTON, E. F. G., HANDLEY, R., and COOK, A. J. *Chem. and Ind.*, p. 292 (1956).
- (2) SÜE, P., PAULY, J., and NOUAILLE, A. *Bull. Soc. Chim. France*, 5, p. 593 (1958).
- (3) PFANN, W. G. *Zone Melting*, p. 112 (New York: John Wiley, 1958).

Stroboscopic radiography with a linear accelerator

by B. J. VINCENT, B.Sc., Grad.Inst.P., Ministry of Supply, Armament Research and Development Establishment, Fort Halstead

[Paper first received 12 August, and in final form 18 September, 1959]

Abstract

High-definition stroboscopic radiographs of an internal combustion engine have been obtained. Efficient use of the large accelerator output has enabled fine-grain film and a large film-focus distance to be used. The radiographs have been used to check the performance of the engine valves under running conditions. Comparison is made with stroboscopic radiography using a betatron. Methods of synchronization and some possible uses of stroboscopic radiography are briefly discussed.

Introduction

ELECTRON linear accelerators are essentially devices producing beams of electrons with energies in the megavolt range. The acceleration occurs in a linear path and over short distances. This renders beam extraction easier and allows the use of a poorer vacuum than is the case in cyclic accelerators such as the betatron. Earlier types of linear accelerator used a resonant-cavity method in which electrons were accelerated by large potentials built up in a cavity resonating at the frequency of an applied radio-frequency wave.⁽¹⁾ Insulation problems arise in this method, and the modern practice is to use a travelling wave technique.⁽²⁾ In this method, radio-frequency energy, usually of 10 cm wavelength, is passed into a specially shaped waveguide. The waveguide is circular in section and has a number of annular constrictions, or irises, distributed along its length. The function of these is to control the velocity of the wave in the guide. The wave has a component of electric field in its direction of motion and this is employed to accelerate electrons injected into the guide at the same point as the high-frequency power. Initially, the electron velocity is designed to be equal to the velocity of the wave at the point of injection. Thereafter, the wave velocity is held equal to the increasing velocity of the electrons by the spacing of the irises, so that both electrons and wave keep in step. Thus, neglecting attenuation of the wave, the electrons experience a constant unidirectional force and the highest potential required in the whole system is the initial electron potential. In the A.R.D.E. accelerator, the electrons are injected with an energy of 50 keV and, although their final energy is 5 MeV, 50 keV is the highest potential difference employed. Insulation problems are thus minimized.

Electrons of this energy may be put to various uses, but in order to produce a high-energy X-ray beam they must strike a suitable target usually made of gold or tungsten. Earlier machines of this type were built primarily for therapeutic medical work, but it was soon realized that the large outputs of high-energy radiation should have many uses in industrial radiography, particularly for the examination of heavy steel sections ranging in thickness from four to

fifteen inches. The A.R.D.E. accelerator was designed for industrial work of this nature and has proved to be of great value in this field. It is, however, possible to exploit some of the characteristics of the machine for use in other fields. One of these is stroboscopic radiography.

In order to obtain adequate radio-frequency power and amplitude levels, it is necessary to resort to pulsed operation with a high-power magnetron. Consequently, the X-ray output is also pulsed, the pulse duration being about $1.8 \mu\text{s}$. Pulses are normally generated by an internal trigger unit which is locked to mains frequency and which produces four fixed repetition frequencies of 100, 200, 400 and 500 pulses per second. The machine may, however, equally well be operated from an external trigger system provided that the repetition frequency is in the range 20 to 500 pulses per second. This permits the stroboscopic radiography of recurrently moving objects if the object is made to provide a suitable triggering signal each time it reaches a fixed point in its cycle. This signal triggers the accelerator output so that a film placed behind the object only receives radiation during a few microseconds after the triggering position has been reached. A latent image is thus built up on the film by the superposition of a large number of small rapid exposures.

In order to obtain a practical evaluation of the possibilities of stroboscopic radiography, a Villiers single-cylinder petrol engine was chosen as a test object since it possesses a number of components of varying shape, size and material which execute a variety of types of motion.

Experimental details

(a) *Initiating system.* A 9-inch diameter tufnol disk was attached to a pulley on the engine flywheel in such a manner that it could be set at eight angular positions relative to the crankshaft. A small brass contact, set into the edge of the disk, was earthed through the engine case and made contact with a leaf spring pressing on the edge of the disk. The required synchronizing trigger pulse was generated by the earthing of the leaf spring through the brass contact. The system is shown diagrammatically in Figs. (1) and (2). The engine was run at 1800 rev/min so that the accelerator was, in consequence, run at the same rate (30 pulses per second). Under these conditions, the output of radiation was 30 r/min at one metre.

(b) *Radiographic technique.* Preliminary experiments were carried out with the engine stationary. Calculation shows that with a 6-metre film-focus distance, the geometric lack of sharpness corresponding to the 2 mm focal spot and the depth of the engine, 25 cm, was 0.088 mm. This is much smaller than the inherent lack of sharpness of X-ray film with 5 MeV radiation (about 0.45 mm) and can in conse-

quence be neglected. An exposure of 400 r at one metre using a 0.005 in. front lead screen and 0.02 in. back screen was found to give radiographs of adequate density.

By the use of a sandwich of three films and choice of a suitable development time for each,⁽³⁾ it was found possible to obtain radiographs of high, low and medium contrast. Low-contrast radiographs, showing as many engine features as possible, were obtained using Crystalex film (by Kodak) and developing for three minutes. High-contrast films, which emphasized such details as the contact breaker gap, were obtained using Industrial F film (by Ilford) and developing for seven and a half minutes. Industrial B film

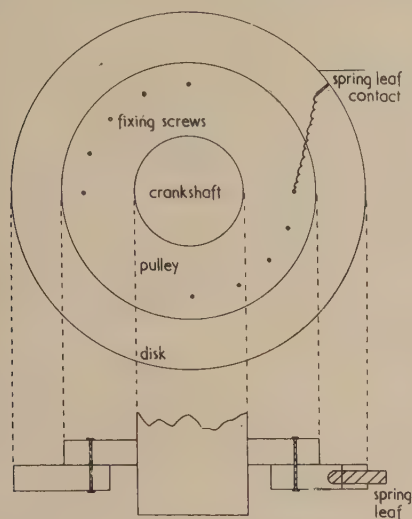


Fig. 1. Mechanical synchronizing system

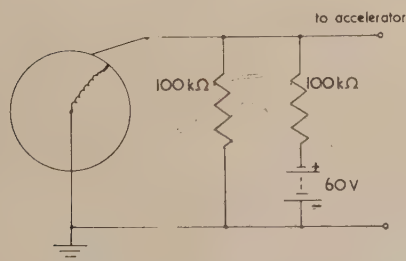


Fig. 2. Electrical synchronizing system

(by Ilford) was used to obtain good positive prints giving an overall picture of the engine. This film was developed for two minutes.

(c) *Image blur resulting from motion.* The duration of the X-ray pulse is about $2 \mu\text{s}$ and the fastest moving part of the engine, the outer edge of the flywheel, should therefore have a movement blur of about 0.03 mm. This, again, is much less than the inherent lack of sharpness of the film and is, therefore, negligible.

The detection of faulty mechanisms and asynchronous vibration of components by increased blurring of the image is therefore, in this case, determined by the inherent film lack of sharpness and the limit of detectability of the eye. The latter is usually taken to be about 0.1 mm, so that, if a commonly accepted lack of sharpness summation law:

$$U_{\text{total}}^2 = \sum U_i^2,$$

is assumed, the minimum additional detectable blur becomes

approximately $0.45\sqrt{U_s}$, where U_s is the lack of sharpness in the stationary state.

If U_s is made equal to the film's lack of sharpness (that is, 0.45 mm) an additional lack of sharpness resulting from motion of 0.3 mm would be required before further image blurring from this cause became noticeable. Thus, given good synchronization, the engine could have been driven about ten times faster before motion blurring became apparent.

(d) *Engine details.* The engine worked on the four-stroke principle in which two revolutions of the crankshaft are required to complete an individual engine cycle; one revolution is concerned with expelling burnt gases and recharging the cylinder with air and petrol vapour and the next revolution with compression and ignition of the fuel to produce power. Valves permitting the flow of fuel and exhaust gases are therefore required to function only on every other revolution of the crankshaft and this is achieved by operating the valves by means of cams attached to a shaft rotating at half the crankshaft speed. The present radiographs were taken using one radiation pulse per revolution and consequently the two parts of the engine cycle are not distinguished. However, since between two radiation pulses (that is, one crankshaft revolution), the valve camshaft has only rotated 180 deg., it is possible to see a valve cam in two diametrically opposite positions.

Practical results

Stroboscopic radiographs of the engine taken in eight different positions, one of which is shown in Fig. 3, made it possible to check the performance of the engine valves under running conditions. This was done by measuring the valve lift on the radiographs with a microscope and comparing it with measurements made with a micrometer on the stationary engine. The results are shown in Fig. 4.

The valves are normally held against their seatings by a spring, and will only rise when forced to do so by the cam pushing up the valve tappets and valve. The valve-spring system has associated with it a natural time period depending on the strength of the spring and mass of the valve. If the period becomes long compared with the period of the engine cycle because of deterioration of the spring, the valve will tend to lag in returning to its seating and will "float".

Fig. 4 indicates that the valves were functioning reasonably correctly during the exposures. Each of the experimental dynamic points is the mean of at least six measurements, the four upper points showing a spread of about $\pm 1\%$ and the four lower points about $\pm 3\%$. Two of the points on the inlet-valve curve lie below the static curve. This is unlikely to be correct and is attributed to the film's lack of sharpness which renders the precise demarkation of the valve image difficult. This error might be reduced by increasing the contrast of the valve image and by careful matching of the various radiographs with respect to density. Greater precision of demarkation and reproducibility should then result. Comparison of static and dynamic radiographs rather than physical measurements in the static condition might also lead to a more accurate assessment, since the various factors influencing the measurements would then apply to both conditions. The results would be more strictly comparable and, with care, should have an accuracy of $\pm 1\%$.

In addition to the valves, it was also possible to distinguish many other components of the engine. The piston, which is

of aluminium alloy, can be distinguished clearly in spite of its low density, and the piston rings threading the top of the piston are also easily visible. Other features to be seen are the camshaft and timing gears, valve cams, tappets and springs and the ignition-contact-breaker gap. Some detail in the small- and big-end bearings is present on the original radiographs and careful alinement on these would show up fine clearances, particularly if the bearing was long



Fig. 3. Radiograph of moving engine

in the direction of radiation. (The accelerator can record a 0.001 in. gap, 0.5 in. deep.)

The accelerator functioned quite satisfactorily during the exposures, the close agreement between the theoretical exposure time (13.3 min) and a timed exposure (14 min) indicating that the great majority of engine revolutions produced a successful triggering pulse. The exposure time in minutes may be calculated from the equation:

$$t = D/f,$$

where D is the exposure dose in roentgens measured at one metre, and f is the stroboscopic frequency in pulses per second. This equation assumes that the normal output of 16.7 mr per pulse is obtained.

General observations

One of the most useful features of the stroboscopic technique is that mechanisms can be studied under exactly the same conditions as they will meet in actual use. The method is applicable to any repetitively acting mechanism from which synchronizing signals may be obtained, under any working conditions of loading and wear, since little or no

power is drawn from the system under examination. Causes of failure and malfunctioning of working systems can be seen in action, where previously their existence could only be inferred.

The penetrating radiation emitted from the accelerator permits the examination of large machines, and the latitude of the radiographs permits about a two-inch change in section to be accommodated in steel. In principle, stereoscopic radiographs are obtainable and such a technique might be valuable in the examination of specimens of unknown internal structure.

The radiograph in Fig. 3 shows that, in addition to the study of the valve action described previously, clear images of the piston rings are also obtained, so that a study of the dynamic behaviour of these might be undertaken.

Another field of application is in the study of turbine blades at high rotational speeds, although it is possible that, for this application, the pulse duration of the present machine might have to be reduced. Vibration testing is yet another field that has great promise. Many small components which have transparent envelopes are already subjected to visual stroboscopic vibration testing and some work has been carried out with lightly cased, opaque objects using low-voltage X-rays. The linear accelerator opens the possibility of widening the field to include larger and more heavily cased components.

A series of stroboscopic radiographs can be assembled and reproduced on ciné film to produce a film demonstrating the

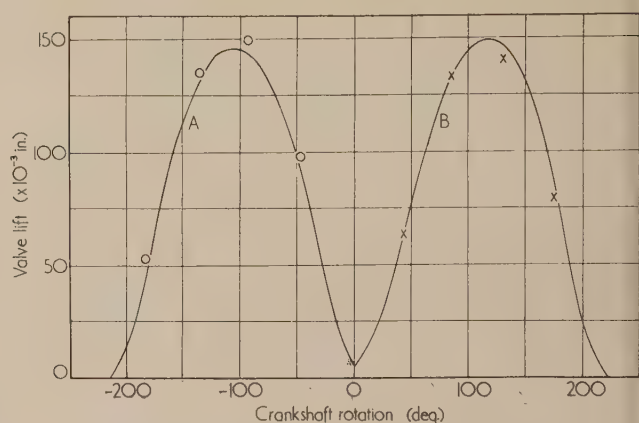


Fig. 4. Dynamic behaviour of engine valves

- A Exhaust valve—static condition.
- Exhaust valve—dynamic condition.
- B Inlet valve—static condition.
- × Inlet valve—dynamic condition.

action of the mechanism and revealing possible faults. Such a film has been made from the radiographs of the petrol engine. This, although it demonstrates no particular faults in the engine, demonstrates the motions of various parts and emphasizes small movements such as those of the valve springs. For a complete study of the engine motion, more exposures per revolution are desirable.

Comparison with a 15 MeV betatron

Mitchell and Pulk⁽⁴⁾ have used a 15 MeV betatron for stroboscopic radiography, synchronization being obtained by taking two signals from the test object. These signals

operated a "gate" which ensured that electron injection into the betatron occurred only in the $440\ \mu\text{s}$ interval between the signals. The actual radiation flash was obtained simultaneously with the second signal providing that electron injection had in fact occurred. The magnitude and quality of the radiation depended on the time of injection relative to the signals. Since the stroboscopic frequency and the operating frequency of the betatron are, in general, unrelated, the majority of occasions suitable for electron injection are wasted because they occur outside the interval defined by the two signals. This, together with the variable output of the radiation pulse, lowers the efficiency of the betatron when used stroboscopically.

This is the most important difference between stroboscopic work with the linear accelerator and the betatron. The accelerator output is high under stroboscopic conditions, both because it is higher normally than the betatron and because it can be 100% efficient. This means that shorter exposures and better films may be used. In addition, lower stroboscopic frequencies are possible while keeping reasonable exposure times, and larger film-focus distances can be employed. The advantage in the latter arises not so much from small geometrical lack of sharpness, which is relatively unimportant compared with the film's lack of sharpness, but from a larger field and smaller geometrical distortion. A further disadvantage of the betatron is the long duration of the radiation pulse ($10\text{--}15\ \mu\text{s}$) compared with that of the accelerator ($2\ \mu\text{s}$). This long duration limits the maximum linear velocity observable without blurring. However, the fine focal spot associated with betatrons might render projection techniques possible, thus facilitating the measurement of small displacements in a mechanism. It is doubtful whether such a technique would be profitable with the linear accelerator.

Production of the synchronizing pulse

The mechanical pick-up employed on the Villiers engine is quite satisfactory at the frequency employed. However, it is possible that other methods may have advantages under different circumstances. Mitchell and Pulk⁽⁴⁾ used a magnetic pick-up, and this had the advantage that no physical contact was made with the moving apparatus. It should also be possible to use a capacitive method. In cases where there are no external moving parts, there appear to be two possible solutions. The first is to pick up acoustic vibrations and to convert these into electrical pulses with a microphone. The second is to place a Geiger counter, screened so as to accept only a narrow pencil of radiation, behind the film and to adjust the accelerator triggering rate manually until a steady signal is obtained from the counter. A stationary radiograph

would provide information concerning a suitable position for the counter.

The present range of trigger frequency can be extended simply, if required. This can be achieved by accepting, say, only every other trigger pulse from the test object, or by multiplying a low trigger frequency and inhibiting actual radiation from all but the actual trigger pulse, using an electron beam deflexion technique. If it is assumed that synchronization is possible, the only limiting factors are blurring due to the finite length of the radiation pulse at high frequencies and excessive time of exposure at low frequencies. It has been suggested that at very low stroboscopic frequencies it would be possible to produce a number of radiation pulses in place of each single pulse. This method would be valuable when the linear velocity of components is low enough to make blurring due to motion insignificant during a time of at least 2 ms, since this time represents the minimum time possible between radiation pulses.

Conclusions

It is concluded that the linear accelerator is a suitable machine for producing stroboscopic radiographs and that no modification either to the accelerator or to the standard radiographic technique is required. The accelerator operates in a satisfactory manner and will accept fairly low trigger repetition frequencies. Comparison of theoretical and experimental exposure times confirms that the machine can be made as efficient during stroboscopic radiography as during normal working. A simple mechanical device is suitable for synchronization at stroboscopic rates up to at least 1800 rev/min, and probably higher still. Finally, the quality of the radiographs produced is suitable for making measurements of fairly small displacements and affords a method of checking the efficiency of machinery in operation.

Acknowledgement

Crown copyright reserved. Reproduced with the permission of the Controller, H.M.S.O.

References

- (1) MILLS, B. Y. *Instn. Elec. Engrs. Proc.*, Pt. 3, **97**, p. 425 (1950).
- (2) MILLER, C. W. *Engineering*, **180**, p. 374 (1955).
- (3) DURANT, R. L. *Brit. J. Appl. Phys.*, **2**, p. 42 (1951).
- (4) MITCHELL, C., and PULK, R. A. *Non-destructive Testing*, **14**, No. 5, p. 24 (1956).

Notes and comments

Index of Crystallographic Supplies

In September 1956 the first edition was published of the *Index of Manufacturers of Apparatus and Materials Used in Crystallography*. The second edition has recently been published under the title *Index of Crystallographic Supplies*. A limited number of copies of this publication are available free of charge to *bona fide* crystallographers who are resident in the United Kingdom, and who have not already received a copy. Applications will be dealt with in strict order of receipt and should be made to The Institute of Physics, 47, Belgrave Square, London, S.W.1, as soon as possible.

Creep Information Centre

A Creep Information Centre is being established at the National Engineering Laboratory of the Department of Scientific and Industrial Research, East Kilbride, Glasgow. This centre is intended to fill the need for an information centre for data on all strength properties of high-temperature steels, and it is intended that it shall eventually become the national centre for information on the strength of high-temperature materials.

The centre is now ready to accept relative data particularly on creep properties, for which the industrial demand is greatest.

The Royal Society's Fair Copying Declaration

The Institute, in common with more than 70 other scientific and learned societies, has subscribed to the Royal Society's Declaration on 'Fair Copying' which reads as follows:—

We will regard it as fair dealing for the purpose of private study or research when a non-profit-making organization, such as a library, archives office, museum or information service, owning or handling scientific or technical periodicals published by us makes and delivers a single reproduction of a part of an issue thereof to a person or his agent representing in writing that he desires such reproduction in lieu of a loan or manual transcription and that he requires it solely for the purpose of private study, research criticism or review, and that he undertakes not to sell or reproduce for publication the copy supplied, provided:

1. The recipient of the copy is given notice that he is liable for infringement of copyright by misuse of the copy, and that it is illegal to use the copy for any further reproduction.
2. The organization making and furnishing the copy does so without profit to itself.
3. Proper acknowledgement is given to the publication from which the copy is made.

4. Not more than one copy of any one excerpt shall be furnished to any one person.

The exemption from liability of the library, archives office, museum or information service herein provided shall extend to every officer, agent or employee of such organization in the making and delivery of such reproduction when acting within the scope of his authority of employment. This exemption for the organization itself carries with it responsibility to see that employees caution those receiving copies against the misuse of material reproduced.

We reserve the right to take action against any person or organization copying or misusing for any purpose whatever the whole or part of a work published by us without abiding by the conditions laid down herein unless the person or organization has our special permission in respect of the item to be copied.

We reserve the right to withdraw this declaration.

Instrument Abstracts

Instrument Abstracts is a monthly journal devoted to abstracts of the world's technical literature relating to scientific and industrial instruments. It is prepared by the British Scientific Instrument Research Association and is now printed and published by Messrs. Taylor and Francis Ltd., of London.

Instrument Abstracts is to cover a wider field than it has done previously and in more detail. The subscription price is £4 p.a. (\$12.00), including postage.

Journal of Scientific Instruments

Contents of the March issue

PAPERS

- Simple dosage meter for high-intensity thermal radiation. By P. H. Thomas and P. G. Smith.
 Design of a single electrode capacitor for use with moisture meters and similar apparatus. By D. F. Leach and J. M. M. Neilson.
 Method of measuring the angular deflexion in a dynamometer. By M. Axson and J. M. Magarshack.
 Apparatus for investigating total hemispherical emissivity. By J. H. Cairns.
 Oscillator measuring equipment for vibrating-wire gauges. By W. H. Ward and J. E. Cheney.
 Extensometer for semi-rigid materials. C. D. Kinloch and N. E. Waters.
 Design criterion for correction of parallax at the best focus for definition. By G. W. Hamstead.
 Direct measurement of $\int i^2 \cdot dt$ by a method based on the Hall effect. By S. C. Ryder-Smith, A. E. Guile and A. E. Barrington.
 Simple ultramicro-pipette for electron microscopy. R. Hardy, J. R. Majer, and S. Travers.

LABORATORY AND WORKSHOP NOTES

- Simple photoelectric demodulator. By A. Kolin and R. T. Kado.
 Gas-quenching apparatus for high-speed thermal analysis. By R. D. Garwood, J. R. Moon, and B. F. Thrush.

NOTES AND NEWS

New instruments, materials and tools New books Notes and comments

THIS JOURNAL is produced monthly by The Institute of Physics, in London. It deals with all branches of applied physics (including theory and technique). All rights reserved. Responsibility for the statements contained herein attaches only to the writers.

EDITORIAL MATTER. Communications concerning editorial matter should be addressed to the Editor, The Institute of Physics, 47 Belgrave Square, London, S.W.1. (Telephone: Belgravia 6111.) Prospective authors are invited to prepare their scripts in accordance with the *Notes for Authors*. (Price 3s. 6d. including postage.)

REPRODUCTION. The Institute of Physics is a signatory to The Royal Society's Fair Copying Declaration. Details may be obtained upon application from The Royal Society, London, W.1.

ADVERTISEMENTS. Communications concerning advertisements should be addressed to the agents, Messrs. George Jackson (Fleet St.) Ltd., Cliffords Inn, Fleet Street, London, E.C.4. (Telephone: Holborn 3611-2.)

CLAIMS FOR MISSING JOURNALS. Claims from regular subscribers to this *Journal* for missing numbers will only be considered if received within 60 days of the date of mailing plus normal outward time of transit and time for lodging the claim. Losses attributable to failure to notify a change of address or to similar omissions will not be considered.

SUBSCRIPTION RATES. A new volume commences each January. The charge is £6 per volume (\$17 U.S.A.), including index (post paid), payable in advance. Single parts, so far as available, may be purchased at 12s. 6d. each (\$1.75 U.S.A.), post paid, cash with order. Orders should be sent to The Institute of Physics, 47 Belgrave Square, London, S.W.1, or to any bookseller.

Summarized proceedings of a conference on solid state physics—Melbourne, August 1959

The Australian Branch of The Institute of Physics held a conference on solid state physics in Melbourne from 7-21 August, 1959. This conference was the first of its kind to be held in Australia and attracted an attendance of about one hundred and thirty. In all, 46 papers, ranging over a wide field, were presented and these are summarized; they include papers on superconductivity, transport properties, surface properties, optics, theoretical physics, magnetism, plastic deformation and crystal imperfections.

AFTER the opening of the Conference by Dr. F. W. G. WHITE [Chairman, Commonwealth Scientific and Industrial Research Organization (C.S.I.R.O.), Melbourne], Professor C. S. BARRETT (Institute for the Study of Metals, University of Chicago, presented the first paper which described an X-ray study of bismuth at low temperatures.* The bismuth lattice may be considered as two interpenetrating face-centred rhombohedral sub-lattices, one sub-lattice being displaced from the mid-point positions of the other by a small distance, b , along a $[111]$ direction. If d is the spacing of (111) planes, the parameter b/d is 0.40437 ± 0.00008 at 4.2°K , 0.40403 ± 0.00008 at 78°K , and 0.4041 ± 0.0005 at $296 \pm 2^\circ \text{K}$. The small, but significant, decrease in parameter on raising the temperature from 4.2 to 78°K conflicts with the theory of the structure propounded by E. I. Blount and M. H. Cohen. However, Cohen has suggested that the conflict can be resolved if the thermal expansion which occurs in this temperature range lessens the resistance of the structure to the displacement from cubicity.

Superconductivity

In the first of a group of papers on superconductivity, Dr. J. C. FISHER (General Electric Research Laboratories, Schenectady) spoke on alternative superconducting ground states.* He compared (a) the trial ground state composed of a linear combination of normal state configurations in which individual electron states of opposite momentum and equal spin projection ($k \uparrow, -k \uparrow$) and ($k \downarrow, -k \downarrow$) are both either occupied or unoccupied, with (b) the trial ground state with ($k \uparrow, -k \downarrow$) pairing proposed by Bardeen, Cooper and Schrieffer.⁽¹⁾ The two states lead to identical thermodynamics when an average matrix element $-V = \langle V'_{kk'} \rangle_{av}$ is treated as a disposable parameter, but they have different one-electron matrix elements between corresponding states. Spin paramagnetism is predicted for state (a) but not for state (b). Both states must be regarded as possibilities until more details of the electron-phonon interaction in superconductors are known. In reply to discussion, Dr. Fisher

pointed out that a mixture of the two states would be thermodynamically unfavourable.

Dr. P. G. HARPER (Division of Electrotechnology, C.S.I.R.O., Sydney) described his work on the displaced lattice state and its connexion with superconductivity. If the electron-phonon interaction in a metal is considered without regard for anharmonic terms, two solutions for the lattice displacements are found.⁽²⁾ The first consists of vibrations about the usual lattice sites, the electron-phonon interaction simply renormalizing the phonon frequencies. The second solution involves a static displacement of the ions, described by a linear superposition of sinusoidal displacements. This solution leads to a lattice state having an energy gap large enough to prevent electron-phonon scattering processes and a specific heat different from that associated with the first solution. A reasonable suggestion is that the first solution describes the normal state and the second the superconducting state. Such a suggestion should be verifiable by experiment since the static displacements have a mean-square value of about mk_0/ρ where m is the electronic mass, k_0 is the Fermi wave number, and ρ is the density. This should produce a measureable increase in the background scattering of X-rays or neutrons.

Dr. M. J. BUCKINGHAM (Physics Department, University of Sydney) discussed the nature of the thermodynamic transitions in superconductors and liquid helium. Both these "superfluid" states of matter exhibit singular rotational and magnetic behaviour and long-range correlations exist in each of them. However, high resolution calorimetric measurements indicate that the nature of the thermodynamic transition is quite different in the two cases. In superconductors, there is a discontinuity in the specific heat and no anticipation, on the high temperature side, of the approach of a transition. In helium, the specific heat both above and below the transition tends to infinity continuously.

Transport properties

Dr. F. J. BLATT (Department of Physics, Michigan State University) read the first paper of a series on transport properties. This described work carried out with Dr. H. G. SATZ on the theory of the electrical resistivity of thin films. For thin indium wires at low temperatures, Olsen⁽³⁾ has shown that both the residual and the temperature-dependent parts of the resistivity increase as the diameter of the wire is reduced. He suggested that small-angle phonon scattering may take electrons to the surface where they suffer diffuse scattering and cause the observed effects. An extremely crude analysis shows that such a mechanism can account, at least to some extent, for the dependence of the resistivity of a wire on size and temperature. On the other hand, electron-electron scattering may also contribute to the resistivity of a wire by bringing carriers to the surface. Analysis shows that this also leads to a dependence on size and temperature of the

* Papers marked in this way will be published in a special issue of the *Australian Journal of Physics*, 1960.

observed type, but the dependence on size is small and could account for, at most, only a small part of the observed effect.

Dr. P. G. KLEMENS (Division of Physics, C.S.I.R.O., Sydney) discussed the band structure of monovalent metals and their alloys.* The consequences of the Bloch theory of the conduction properties of metals can be evaluated only for a metal having a single conduction band with a spherical Fermi surface. Although monovalent metals provide the closest approach to such an ideal metal, even here the Fermi surface is significantly aspherical. Some information about the true shape of the Fermi surface in monovalent metals and their alloys can be obtained from the deviations between experimental results and theoretical predictions, provided Umklapp processes and phonon-drag effects are taken fully into account. Further experimental data on the conduction properties of alloys is urgently needed.

Mr. W. R. G. KEMP (Division of Physics, C.S.I.R.O., Sydney), in a paper with Dr. P. G. KLEMENS, showed how measurements of the lattice thermal conductivity of alloys at liquid-helium temperatures can provide information about electron-phonon interactions and about the density of dislocations.* Measurements on a series of dilute alloys of copper, silver, and gold show that, in the pure metals, the conduction electrons must interact with the transverse elastic waves nearly as strongly as with the longitudinal waves. Furthermore, the variation of conductivity with the composition of the alloys implies that, even in the annealed state, the alloys contain 10^{10} to 10^{11} dislocation lines/cm². A comparison of the densities estimated in this way with those estimated from measurements of stored energy suggests that the thermal conductivity theory overestimates dislocation densities by a factor of 3 to 6. In discussion, Dr. J. J. GILMAN (General Electric Research Laboratories, Schenectady) pointed out that by etching he measures a dislocation density in copper of only 10^5 – 10^6 lines/cm².

Dr. H. M. ROSENBERG (Clarendon Laboratory, Oxford) described work done with Miss J. N. LOMER (University of Reading) on the detection of dislocations in copper-zinc alloys by measurements of the heat conductivity at low temperatures.⁽⁴⁾ Comparison of these results with counts made by transmission electron microscopy suggests that the theory of Klemens⁽⁵⁾ overestimates dislocation densities by a factor of about six. In discussion, Dr. Gilman pointed out that application of the theory to lithium fluoride increases this discrepancy to a factor of about 70.

Dr. F. J. BLATT (Department of Physics, Michigan State University), in a paper with Drs. M. GARBER, R. H. KROPSCHOT, and B. R. SCOTT, discussed the resistivity and thermoelectric power of copper, silver, and alloys of these metals containing one atomic per cent of germanium, indium, tin, or antimony.* The residual resistivity has been measured on all specimens after severe plastic deformation and after subsequent annealing. As expected, the pure metals show a decrease in resistivity on annealing but all the alloys show an increase in residual resistivity. The behaviour of the alloys can be explained if it is assumed that, during the deformation, the large number of vacancies generated permits the impurity atoms to align themselves along dislocation lines and so reduce their total effect on the resistivity. The thermoelectric powers of the alloys have been measured between 8 and 350° K and the results analysed using the Mott-Friedel relation.⁽⁶⁾ Good agreement with theory is obtained only if the absolute thermoelectric power of the pure metals is assumed to consist of a free-electron contribution together with a phonon-drag contribution. This phonon-drag contribution is of the

correct magnitude and shows the expected dependence on temperature and impurity content.

Dr. G. K. WHITE (Division of Physics, C.S.I.R.O., Sydney) concluded this section of the conference by discussing how thermal conductivity measurements on alloys can give information about the interactions of phonons with each other and with point defects.* By a suitable choice of impurity, the electronic heat conductivity of a pure metal can be suppressed and its lattice conductivity measured. This has been done for copper, silver, and gold by using alloys containing 0.1 atomic per cent of iron, arsenic, germanium, or tin. Comparison of these values with those expected theoretically leads to a value for the Grüneisen constant of the metal. For these metals, the value so deduced is 30–40% greater than that calculated from the expansion coefficient, specific heat, and compressibility. When higher concentrations of gold, zinc, platinum, or chromium are introduced, the interaction of the impurity atoms with the lattice waves can be measured. The results show that the scattering is due, not only to the mass difference between an impurity atom and a solvent atom, but also to such effects as the strain around the impurity.

Surface properties and related topics

Professor R. GOMER (Institute for the Study of Metals, University of Chicago) discussed field emission through dielectric layers.* Field emission experiments have shown that the adsorption of inert gases on tungsten occurs by multilayer physical adsorption. Details of the emission through such layers can be explained by assuming that the inert gas atoms represent short-range but deep potential holes within the field-emission barrier. The effect can be treated quantitatively by two approximate methods. The first yields scattering lengths while the second gives dimensions for the potential wells. The two approximations give consistent results and reasonable values for the effective nuclear charge of neon, argon, krypton, or xenon.

Dr. G. J. OGLIVIE (Division of Tribophysics, C.S.I.R.O., Melbourne) described some effects on metal surfaces caused by bombardment with inert gas ions of energies between 10 eV and 4 keV.* Most of the work has been carried out on single crystals of silver or Cu₃Au bombarded with argon ions though comparable results have been obtained after bombardment with helium or xenon. Three principal effects have been observed, viz. (i) a thin surface layer is disoriented by the bombardment, (ii) in Cu₃Au the surface layer is depleted in copper and a sharp boundary exists between the surface layer and the matrix below, and (iii) some atoms from the surface are forced into the bulk of the crystal. By studying the atoms ejected from the surface, it has been found that, at least for silver, these are ejected preferentially in $\langle 110 \rangle$ directions, i.e. parallel to the most closely-packed directions in the crystal. The present theories of sputtering⁽⁷⁾ are inadequate to explain all these effects.

Dr. N. H. FLETCHER (Division of Radiophysics, C.S.I.R.O., Sydney) discussed the nucleation and growth of ice crystals on crystalline substrates.* When various surface imperfections are considered as nucleation sites for ice crystals the points of emergence of dislocations are not found to be preferred sites since the embryo crystal has a high strain energy. However, steps and re-entrant corners do encourage nucleation. Embryos initially grow by two-dimensional nucleation, but ultimately a dislocation mechanism for growth becomes important. Professor Gomer suggested that micro-cracks 50–100 Å across might serve as nucleation sites since they appear to do so in the growth of whiskers. Dr. Fletcher

greed that this could be so sometimes, but not in general
nce, for silver iodide aerosols, particles as small as
00–400 Å in diameter are efficient nuclei for ice crystals.

Dr. A. K. HEAD (Division of Tribophysics, C.S.I.R.O.,
Melbourne) discussed the equilibrium arrangements of dislo-
cations interacting with boundaries and surface films.* He
presented numerical results for two cases. The first concerns
an infinite solid having different shear moduli on either side
of a plane boundary and containing a group of dislocations
in a slip plane in the side with lower modulus. When a stress
is applied forcing the group towards the boundary, the
equilibrium positions of the dislocations can be determined
and the distance of the leading dislocation from the boundary
is found to be roughly proportional to $n^{-1/2}$, where n is the
number of dislocations in the group. The second case con-
cerns a thin film on the plane face of a semi-infinite solid
where the film has a shear modulus greater than that of the
bulk. Here, the stress necessary to force the leading dislo-
cation into the film has been calculated for values of elastic
moduli corresponding to a film of rhodium on silver and to a
film of oxide on aluminium. Dr. Head closed by pointing
out that while, in general, analytic solutions are not available
for calculating the positions of dislocations in a given arrange-
ment, computers can now be used for cases where the physical
constants are known. These calculations should be carried
out frequently in order to test theories that may be attractive
qualitatively.

Mr. C. CANDLER (School of Mines, Adelaide) produced
arguments to show that the photographic process is a
diatomic reaction.* If sensitive areas exist in unexposed
crystals, the number of grains developed after exposure
should follow a Poisson law. However, the grain counts of
Sheppard *et al.*, Slade *et al.*, and Toy⁽⁸⁾ do not fit such a law,
but instead are consistent with the theory that a development
centre is formed by a diatomic reaction triggered by P trapped
electrons. The value of P is in general non-integral but no
adequate explanation for this can be given.

Optics and related topics

One day of the conference was devoted to papers dealing
with optical and related properties. The first paper, by Mr.
T. J. SEED (Department of Physics, University of Canterbury,
N.Z.), described the construction and testing of a phosphor-
photomultiplier soft X-ray spectrograph. This instrument
has been designed to measure the intensity of soft X-ray
spectral lines, the measurement of these being difficult by
the usual photographic methods. The electron beam to the
anode is modulated to produce a pulsed X-ray beam which,
after diffraction by a grating, impinges on a phosphor. The
scintillations of the phosphor operate a photomultiplier
whose output is amplified and fed to a coherent detector.
As the phosphor-photomultiplier traverses a Rowland circle,
the output of the detector is printed on a chart recorder.
Work is still in progress to improve the intensity of the signal.

Dr. S. E. WILLIAMS (Department of Physics, University of
Western Australia) discussed the soft X-ray spectra obtained
from lithium, magnesium, aluminium, and their alloys. Soft
X-ray band emission spectra in the region 40–1000 Å have
been observed from solid targets of lithium–magnesium alloys.
The variation of the spectra with time indicates that the
incident electron beam causes lithium to migrate to the
surface. Although this migration prevents accurate measure-
ments of band shape, the second Brillouin zone appears to
be depopulated as the amount of lithium in the alloy is
increased, the zone being emptied by about 40% lithium.

Spectra from targets of aluminium and magnesium coated
with thin films of lithium have also been measured. The
Mg L_{23} band shows a complete depopulation of the second
Brillouin zone while the Al L_{23} band does not; this suggests
that an alloy is formed in the first case but not in the second.
Thin films of lithium on beryllium and of silver, sodium, or
potassium on magnesium have no effect on the band spectra
from the underlying metal. In answer to discussion, Dr.
Williams stated that voltages up to 6 kV have been used,
but no significant effect of voltage has been found.

Mr. N. K. JONES (Weapons Research Establishment, South
Australia) discussed the infrared absorption in cadmium oxide.
He presented the results of a series of measurements of the
reflectivity and transmission of thin (0.1 μ) layers of cadmium
oxide, correlated with data on the Hall coefficient and
electrical conductivity.

Mr. W. A. RUNCIMAN and Mr. B. G. WYBOURNE (Depart-
ment of Physics, University of Canterbury, N.Z.) described
calculations on the solid-state spectra of rare-earth ions.
Mr. Runciman outlined the general problem of interpreting
the spectra of trivalent rare-earth ions in crystal fields. The
methods due to Racah are being used in the calculation of
the Coulomb, spin-orbit, and crystal field interactions.
Intermediate coupling calculations, using perturbation theory,
have resulted in good agreement with experiment for gado-
linium, configuration f^7 . Calculations are still in progress
on the spin-orbit matrices for the f^4 configuration, the
matrix elements being applicable, with a change of sign, to
holmium, configuration f^{10} . Mr. Wybourne then described
a term analysis of the experimentally-known energy levels
of the rare-earth ions Pr^{3+} , Tm^{3+} , Nd^{3+} , and Er^{3+} . A
least-squares method is used to obtain the best fit between
the experimental and theoretical energy levels in terms of the
Slater integral ratios and the spin-orbit coupling constant.
The possibility of orbit-orbit interactions has also been
investigated successfully.

Dr. G. S. BOGLE (Division of Physics, C.S.I.R.O., Sydney)
described some experiments on a paramagnetic resonance
spectrum involving interacting spin-pairs. Mr. H. F.
SYMMONS and he have studied a chromium–aluminium salt
(5% of $\text{C}(\text{NH}_2)_3 \cdot \text{Cr}(\text{SO}_4)_2 \cdot 6\text{H}_2\text{O}$ + 95% of $\text{C}(\text{NH}_2)_3 \cdot \text{Al}(\text{SO}_4)_2 \cdot 6\text{H}_2\text{O}$) which contains a sufficient concentration
of paramagnetic ions to produce lines in the spectrum due
to the interactions of close pairs of such ions. Although the
paramagnetic ions are separated by diamagnetic ions, exchange
interaction appears to operate significantly. It is therefore
probable that measurements of this kind will prove a
powerful tool for investigating exchange interactions in solids.

Mr. D. H. GOODE (Department of Physics, University of
Canterbury, N.Z.) discussed the aggregation of F-centres in
the alkali halides. The aggregation of F-centres in sodium
chloride, potassium chloride, potassium bromide, and
potassium iodide, under the action of F light at room tem-
perature, has been studied by measuring the absorption
spectra at liquid-air temperatures. In all cases, the M, R,
and N bands are produced, but in potassium iodide a new
phenomenon occurs. The F band is completely bleached
and a broad band appears in its place, this band having a
half-width independent of temperature up to 300° K and
having an area equal to the area under the original F band.
This phenomenon also occurs in potassium chloride on
exposure to light from a carbon arc.

Dr. J. J. O'DWYER (Department of Applied Physics,
University of New South Wales) discussed the dielectric
breakdown of alkali halides at high temperatures.* Three
types of breakdown can be distinguished, *viz.* intrinsic,

thermal, and avalanche. The apparent inconsistencies between existing experimental data on the breakdown of the alkali halides at high temperatures can be reduced if the breakdown is assumed to be thermal in nature rather than intrinsic. On the assumption that the electrical conductivity is principally ionic, the thermal breakdown strength is calculable without involving disposable parameters. Such a calculation correctly predicts the magnitude of the breakdown strength and its dependence on temperature.

Dr. J. S. DRYDEN (Division of Electrotechnology, C.S.I.R.O., Sydney), in a paper with Mr. J. S. COOK, discussed the intensity of dielectric absorption in alkali halides as a function of the concentration of divalent cation impurities.* Studies have been made on sodium chloride containing calcium and on potassium chloride containing strontium. The intensity of the absorption provides a measure of the proportion of cation impurities which have associated with vacancies to form dipoles. In equilibrium at room temperature, a high proportion of the impurities are associated with vacancies in aggregates more complex than dipoles.

Mr. C. BILLINGTON (Division of Chemical Physics, C.S.I.R.O., Melbourne) described a method of measuring the decay of phosphorescence, in which the resolution is an order of magnitude better than that of previous methods. It operates most usefully where the decay processes have lifetimes between 10 μ s and 50 ms. The results show that, in general, phosphorescence is due to several different processes operating concurrently and that these processes do not have counterparts in the emission spectra. The resolution of the method is sufficient to distinguish between up to six or so processes and to determine the rate constants of each.

Dr. L. E. LYONS (Department of Physical Chemistry, University of Sydney), in a paper with Mr. J. W. WHITE, described the luminescence from 4 to 298° K of anthracene and solutions of tetracene in anthracene. The luminescence spectra vary markedly with temperature. Changes in the intensity of certain anthracene bands occur over the same range of temperature as changes in the efficiency of energy transfer from anthracene to tetracene.

Theoretical physics

One session, devoted to aspects of theoretical physics, was opened by Dr. R. O. DAVIES (Queen Mary College, University of London) with a discussion of a generalization of Grüneisen's theory of solids.⁽⁹⁾ This is based on a model involving 3N distinct harmonic oscillators. The average values of the derivatives, with respect to volume, of the frequency spectrum are assumed constant and the theory yields approximate values of all the thermodynamic properties. For the solid rare gases, the appropriate averages can be estimated in two ways, the results being comparable and in reasonable agreement with experiment. The method cannot be successfully extended to metals since the complexity of the binding forces makes theoretical estimates of the Grüneisen constants impossible while experimental estimates depend sensitively on the assumed potential energy function.

Dr. G. C. FLETCHER (Department of Applied Mathematics, University of Sydney) described some of his recent work on the thermal expansion of solids. Numerical work on an electronic computer has provided a more accurate treatment of the equation of state of a crystalline solid than has been available previously. However the results are still not in good agreement with experimental values.

Dr. R. E. B. MAKINSON (Physics Department, University of Sydney), with Mr. A. P. ROBERTS, described some calculations relevant to a zone theory of liquids.* A one-dimensional model is considered in which an electron moves in an energy field which is nearly periodic over short distances but has no long-range order. The number of states of the electron per unit energy range has been calculated numerically for a number of chains of identical delta-function potential wells, the number of wells usually being 2000. The distance between adjacent wells had a cut-off parabolic distribution about the mean value. Provided the r.m.s. deviation of the distribution is small enough, a definite energy gap appears in the spectrum. The gap disappears when the wells are displaced half a lattice length, on the average, from ordered positions after a few hundred lattice lengths. Smoothing out the short-range disorder increases the width of the gap, but a variation in the long-range order has little effect. In reply to discussion, Dr. Makinson warned against carrying over any of the quantitative results to a real three-dimensional liquid though he felt that the general ideas were applicable.

Magnetism

Dr. W. M. LOMER (Atomic Energy Research Establishment, Harwell) discussed the susceptibility of chromium-based alloys of transition elements.* Chromium is believed to be antiferromagnetic below room temperature; therefore the effect of an antiferromagnetic matrix on the properties of dilute solutions of atoms having well-defined magnetic moments has been calculated. The anomalies in the susceptibility-temperature relations for binary and ternary alloys of chromium with iron, cobalt, and vanadium can be rationalized by considering a model that involves small spin-orientation forces arising from the ferromagnetism. Alloying with vanadium appears to reduce the spin moment on the chromium atoms but to introduce no localized spins itself. The temperature-independent contribution of cobalt in solution is interpreted in terms of local spins locked by the antiferromagnetism of the matrix. The interpretation implies that significant anomalies exist in the specific heats of many of these alloys below about 100° K. Accurate measurements to test this would be interesting.

Dr. R. J. WEISS (Watertown Arsenal, Massachusetts), in a paper with Drs. L. CORLISS and J. HASTINGS (Brookhaven National Laboratory), described some neutron diffraction work on chromium, which indicates the presence of antiferromagnetic anti-phase domains. Several single crystals of chromium from various sources all show a fine structure in the magnetic superlattice lines (100, 111, and 211), the structure being dependent on crystal orientation. The splitting of the peaks correlates roughly with an anti-phase periodicity of about 20 lattice spacings but the details are not understood. For all single crystals the Néel temperature is about 35° C but, when the specimens are powdered, the Néel temperature rises to about 300° C, i.e. to values comparable with that found previously by Shull on a powdered specimen. No explanation for this variation in Néel temperature can be given at present.

Plastic deformation and crystal imperfections

Several sessions of the conference were devoted to various aspects of deformation and defects in crystals. The first session was opened by Professor B. E. WARREN (Massachusetts Institute of Technology) with a description of

an X-ray method for measuring twin faulting in face-centred cubic metals.⁽¹⁰⁾ In these metals, deformation faulting produces peak shifts, but twin faulting produces an asymmetry in the powder pattern reflexions and the amount of asymmetry is a direct measure of the twin-faulting probability, β . The asymmetry is determined most simply by treating the overlapping peaks 111 and 200 together. For 70/30 brass filed under liquid nitrogen, a value of $\beta = 0.07$ has been found. In reply to discussion, Professor Warren stated that for body-centred cubic metals, deformation faults produce no peak shifts and twin faults produce an asymmetry that is probably too small to measure.

Mr. N. A. MCKINNON (Aeronautical Research Laboratories, Melbourne) discussed slip and work-hardening at small strains in crystals of aluminium and its alloys. An intensive study, by optical and X-ray methods, of the surfaces of deformed single crystals of aluminium has shown that secondary slip systems are active during the first stage ("easy glide") of work-hardening. The rate of hardening and the extent of this stage are determined by this secondary slip. In single crystals of aluminium-silver alloys, evidence of secondary slip has been found almost from the beginning of the easy-glide region. This has been done by studying the distribution of precipitate in the interior of crystals which have been aged after tensile deformation in the freshly-quenched condition. In general, far more slip is visible in the interior of a crystal than on the surface.

Mr. F. P. BULLEN (Aeronautical Research Laboratories, Melbourne), in a paper with Dr. N. LOUAT, presented a theory of brittle fracture in single crystals of zinc. The cleavage fracture of a hexagonal close-packed structure has been considered in terms of various linear arrays of dislocations on the assumption that the dislocations do not move during propagation of the crack. The energy required to propagate fracture imposes severe restrictions on the type and size of array, but a satisfactory array has been found which predicts fracture stresses for zinc having the observed size and dependence on orientation.

Dr. J. B. LEAN (Broken Hill Pty. Co. Ltd., Central Research Laboratories, Newcastle, Australia) discussed a low-temperature yield instability in iron. When specimens of a 0.07% carbon steel were tested in tension at liquid-air temperatures, a serration appeared in the yield-extension zone of the load-elongation curve, the associated plastic deformation occurring in a limited region of the specimen. The magnitude of the serration depended on the difference between the upper and lower yield points and on the rigidity of the testing machines. This phenomenon can be considered by noting that, during the fall in stress from the upper to the lower yield point, some of the elastic energy stored in the specimen and testing machine is used to deform plastically a limited region of the specimen at a comparatively high rate. There will thus be a rapid rise in temperature of this region leading to the observed instability.

Dr. N. LOUAT (Aeronautical Research Laboratories, Melbourne) discussed the evidence for the existence of an appreciable Peierls-Nabarro force in iron and steel.* The lower yield strength σ of iron and steel can be expressed as $\sigma = \sigma_0 + k l^{-1/2}$ where l is the mean grain diameter and σ_0, k are independent of l . The frictional stress σ_0 can then be separated into a temperature-independent part attributable to solute hardening and a temperature-dependent part τ . It has been suggested that τ arises from the existence of an appreciable Peierls-Nabarro force, but the variation of τ with temperature is incompatible with the classical description of the Peierls-Nabarro force. The most plausible explanation

for τ seems to be that it arises from a stress-induced narrowing of dislocations in a pile-up.

Dr. Z. S. BASINSKI (National Research Council, Ottawa) described the discontinuous adiabatic deformation of metals at very low temperatures.* Most metals show a serrated stress-strain curve for deformation at very low temperatures. Work on aluminium alloys deformed at 4.2° K has shown that the drops in load are associated with local rises in temperature of up to 55° K. Thus the serrations can be attributed to a lowering of the yield stress due to the rise in temperature rather than to an inherent mechanical instability in the lattice. In reply to discussion, Dr. Basinski said that the alloys used showed no evidence of twinning. Dr. T. H. BLEWITT (Oak Ridge National Laboratory) commented that he had deformed lead at liquid-helium temperature, but had found that it remained in the superconducting state, i.e. its temperature could not have exceeded 7.2° K.

Dr. Basinski then presented two papers on the effect of temperature and strain rate on the deformation of metals.* The first paper dealt with work at low temperature on polycrystalline specimens of iron deformed through the Lüders deformation and then cycled up and down in temperature and in strain rate. The results are consistent with the model of dislocations locked by a force of the Peierls-Nabarro type. The Cottrell-Stokes relation⁽¹¹⁾ does not appear to be obeyed. The second paper considered the deformation of magnesium single crystals. Again, the reversible changes of yield stress have been measured for changes in temperature and strain rate. For temperatures below 46° K, the Cottrell-Stokes relation appears to be obeyed, but it breaks down at higher temperatures. The general mechanism of hardening in magnesium is very similar to that occurring in face-centred cubic metals and long-range interactions between dislocations seem relatively unimportant. In discussion, Dr. M. E. HARGREAVES (Division of Tribophysics, C.S.I.R.O., Melbourne) pointed out that the rates of hardening in zinc are much smaller than those in copper, e.g. the rate of hardening in the linear-hardening stage for zinc is less than the rate of hardening in the easy glide stage for copper. Furthermore, the temperature dependence of the rate of hardening in the easy-glide stage is not observed in face-centred cubic metals.

Dr. M. E. HARGREAVES, in a paper with Dr. L. M. CLAREBROUGH (Division of Tribophysics, C.S.I.R.O., Melbourne), showed that the principal features of the orientation-dependence of work-hardening in crystals of face-centred cubic metals can be explained in terms of the likelihood of formation of Lomer-Cottrell sessile dislocations in two directions on the primary slip-plane.* This has been deduced from the known variation of resolved shear-stress with orientation, for the possible secondary slip systems, and from metallographic observations of slip and deformation bands.

Dr. T. H. BLEWITT (Oak Ridge National Laboratory) discussed the radiation hardening of copper. The yield stress of copper can be greatly increased by irradiation with fast neutrons and this hardening can be removed by annealing up to 700° K. In general, the yield stress can be given by an expression of the form $\sigma = f(\phi^{1/3})g(T^{1/2})$, where ϕ is the neutron dose and T the temperature, over reasonably wide ranges of ϕ and T ; in this equation, f and g are linear functions. This result suggests that both source hardening and lattice-friction hardening are operative, although the latter might be expected to give a dependence on dose rather of the form $f(\phi^{1/2})$. In answer to discussion, Dr. Blewitt pointed out that irradiation produces no metallographic changes in an undeformed specimen. Further, the hardness

recovers by about 20% at room temperature and completely by 300 or 400° C, without any signs of recrystallization.

Dr. H. M. ROSENBERG (Clarendon Laboratory, Oxford) in a paper with Dr. D. HULL (Atomic Energy Research Establishment, Harwell) described some experiments on alkali metals at low temperatures.⁽¹²⁾ Tensile tests and measurements of electrical resistivity have been carried out on sodium, lithium, and potassium at temperatures down to 4.2° K. Since sodium and lithium both transform to hexagonal close-packed or face-centred cubic structures at low temperatures, their behaviour is strongly influenced by the presence of stacking faults. No such complication appears to occur in potassium.

Dr. T. H. BLEWITT discussed some of the effects of neutron irradiation on metals at low temperatures.* Copper has been irradiated at 18° K and the energy and change in electrical resistivity associated with the annealing process occurring at about 35° K have been measured. If, as is usual, this process is assumed to be a recombination of interstitial-vacancy pairs with an energy release on recombination of 3–5 eV, the results indicate 2–4 atoms displaced per neutron hit and a resistivity change of 7–12 $\mu\Omega$ cm/atomic per cent of pairs. These results are in contrast with the theoretical estimates of 120 displacements per hit and 1–2 $\mu\Omega$ cm/atomic per cent of pairs. In gold, after a similar irradiation, no annealing process has been found near 35° K. In another series of experiments, copper, silver, gold, and aluminium have all been irradiated at 3.8° K. In gold, no sharply-defined annealing process occurs at any annealing temperature between 4 and 40° K. The kinetics of the annealing processes in copper and aluminium have been studied in detail and, in both metals, annealing has started by 7° K. The activation energy has been measured for temperatures between 10 and 40° K but, for both metals, it varies markedly with temperature and suggests impossibly small values for the number of jumps associated with the annealing. It seems obvious that the use of a simple rate equation with a unique activation energy is inadequate.

Dr. L. M. CLAREBROUGH (Division of Tribophysics, C.S.I.R.O., Melbourne), in a paper with Dr. M. E. HARGREAVES and Mr. M. H. LORETTO, described work on lattice defects and order-disorder in α brass. Measurements of energy, resistivity, and density have shown that a Cu_3Zn superlattice exists with a critical temperature at about 245° C. Since both disorder and vacancies can be produced by either quenching or deformation, the effects due to both are confused and measurements of the release of stored energy have provided the clearest way of separating the two effects and studying their individual properties.

Professor B. E. WARREN (Massachusetts Institute of Technology) discussed the intensity of X-rays scattered at small angles by double Bragg reflection in a cold-worked metal.* If a polycrystalline specimen is deformed so that each grain splits into a number of subgrains, there will be a resultant scattering of X-rays at small angles due to successive Bragg reflexions in different subgrains. Provided the grains were initially oriented at random, the small-angle intensity is a function only of the initial grain size G and a subgrain correlation function $p(\phi)$ which gives the distribution in orientation of the subgrains of a given grain. Under favourable conditions, both G and $p(\phi)$ can be determined from the angular variation of the small-angle scattering. This is of great use since the usual high-angle measurements give no information about $p(\phi)$.

Dr. M. S. PATERSON (Department of Geophysics, Australian National University, Canberra) described his work

on strain recovery after deformation at high pressures. Specimens of calcite have been placed under a hydrostatic pressure of 8000 atmospheres, compressed uniaxially by about 20%, the uniaxial load removed, and then the hydrostatic pressure reduced. No appreciable elastic after-effect occurs while the hydrostatic pressure is maintained but a progressive strain recovery occurs as the pressure is reduced. This recovery amounts to about 15% of the original plastic strain in both coarse-grained and fine-grained polycrystalline calcite, but is rather less in single crystals. Two processes appear to be involved. The first, common to all specimens, occurs progressively during the whole range of pressure reduction and seems to be accompanied by very little change in density. Thus it seems to involve plastic shear strains, even though the external stresses are purely hydrostatic. The second, occurring only in the aggregates and only at pressures below 2000 atmospheres, appears to be a parting of the grain boundaries.

The final paper, on dislocation mobilities and plastic flow in crystals, was given by Dr. J. J. GILMAN (General Electric Research Laboratories, Schenectady).* Experimental work on the velocity of dislocations in crystals of lithium fluoride and silicon-iron (3% silicon) shows that the stress necessary to move a dislocation with a given velocity is directly proportional to the yield stress of the crystal, i.e. these crystals exhibit a plastic resistance to the motion of dislocations. Furthermore, for a large group of face-centred cubic metals the yield stress is proportional to Young's modulus which suggests that a plastic resistance determines the yield stress in these metals as well. Similar correlations exist for crystals of body-centred cubic metals and for some other lattice types. It therefore seems reasonable to assume that in most crystals the yield stress is determined primarily by the plastic resistance to dislocation motion rather than by the stress needed to operate sources of dislocations or to force dislocations through a forest of other dislocations.

Division of Tribophysics, C.S.I.R.O., J. F. NICHOLAS
University of Melbourne,
Australia.

References

- (1) BARDEEN, J., COOPER, L. N., and SCHRIEFFER, J. R. *Phys. Rev.*, **108**, p. 1175 (1957).
- (2) HARPER, P. G. *Proc. Phys. Soc. (London) B*, **70**, p. 390 (1957).
- (3) OLSEN, J. L. *Helv. Phys. Acta*, **31**, p. 713 (1958).
- (4) LOMER, J. N., and ROSENBERG, H. M. *Phil. Mag.*, **4**, p. 467 (1959).
- (5) KLEMENS, P. G. *Proc. Phys. Soc. (London) A*, **68**, p. 111 (1955).
- (6) FRIEDEL, J. *Adv. Phys.*, **3**, p. 446 (1954).
- (7) WEHNER, G. K. *Phys. Rev.*, **102**, p. 690 (1956); HENSCHKE, E. B. *Phys. Rev.*, **106**, p. 738 (1957); *J. Appl. Phys.*, **28**, p. 411 (1957).
- (8) SHEPPARD, S. E., TRIVELLI, A. P. H., and LOVELAND, R. P. *J. Franklin Inst.*, **200**, p. 51 (1925); SLADE, R. E., and HIGSON, G. I. *Proc. Roy. Soc. A*, **98**, p. 154 (1921). TOY, F. C. *Proc. Roy. Soc. A*, **100**, p. 11 (1921); *Phil. Mag.*, **44**, p. 352 (1922).
- (9) DAVIES, R. O., and PARKE, S. *Phil. Mag.*, **4**, p. 34 (1959).
- (10) WARREN, B. E. *Prog. Met. Phys.*, **8**, p. 147 (1959).
- (11) COTTRELL, A. H., and STOKES, R. J. *Proc. Roy. Soc. A*, **233**, p. 17 (1955).
- (12) HULL, D., and ROSENBERG, H. M. *Phil. Mag.*, **4**, p. 303 (1959).

Very high energy ultrasonics*

by E. A. NEPPIRAS, B.Sc., A.R.C.S., Mullard Research Laboratories, Salfords, Surrey

Abstract

The field of high power ultrasonics covers the power region where irreversible changes can be produced in the medium. In Table 1 are listed the more important effects and uses of high energy ultrasonics. The field is very large; useful applications now touch almost every industry. In the final column of the table approximate figures are quoted for the order of the ultrasonic intensity required in the various applications. In gases and liquids the intensities obtainable are severely limited. In liquids this limit is fixed by cavitation which sets in at a rather low level. Cavitation can be avoided by pressurization, and then very high energies can be transmitted. But this is inconvenient and seldom used in practice. The field of very high energy ultrasonics is therefore practically confined to solids, as indicated in the table.

Choice of transducer

AN important fact to bear in mind in selecting transducers for very high power work is that the choice is not limited by considerations of power handling capacity or saturation of the transducer material. The reason is that it is never feasible to use the transducer alone

focusing device. Limiting intensities are then fixed by the mechanical strength of the material of the concentrator and not by any characteristic of the transducer. Transducers can therefore always be driven at low intensities, and therefore economically, since the material will be operated in linear region of its electromechanical characteristic.

So far, almost all ultrasonics work in the very high energy field has been confined to rather low frequencies, only just above the audible limit, 18 to 40 kc/s. This choice is chiefly dictated by considerations of elastic loss in the system: at high frequency and high strain, the losses, particularly in coupling members and concentrators, would become inconveniently high.

Low frequency types of piezomagnetic and piezoelectric transducers are invariably used in this work. Piezomagnetic vibrators for high power work are illustrated in Fig. 1. Transducers may be operated in four useful modes of vibration—extensional, radial, torsional and flexural. The "window" type of construction is the most useful for extensional mode operation. Transducers are either of laminated metal or ferrite, wound generally with a single coil carrying both direct polarizing and alternating drive currents, the drive frequency being adjusted to the longitudinal resonance of the transducer. This resonant frequency is given by

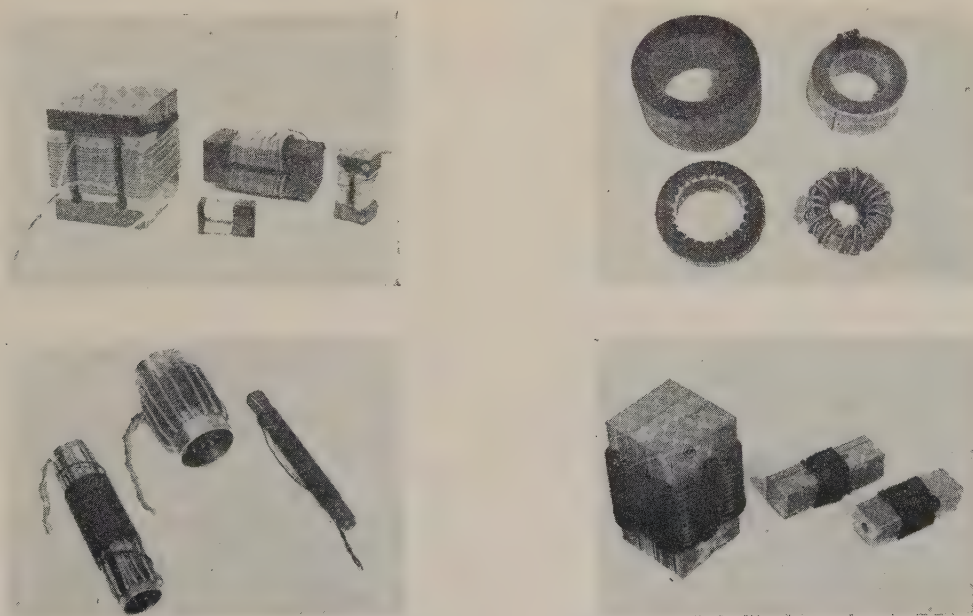


Fig. 1. Piezomagnetic transducer types

to generate the high intensities required. It is always necessary to couple to the load through some form of external

$C_e/2l$, where C_e is the phase velocity of extensional elastic waves in the material and l is the "effective length" of the transducer. This effective length is somewhat greater than the actual length, due to the effect of the window slot.

Radial transducers are either laminated metal rings or

* Based on a lecture given to the Acoustics Group of the Physical Society on 14 May, 1959.

Table 1. *Effects and applications of high energy ultrasonics*

<i>Continuous phase medium</i>	<i>Effects and applications</i>	<i>Optimum frequencies (kc/s)</i>	<i>Approx. acoustic intensity (W cm⁻²)</i>
GAS	Separation of gas mixtures Production of aerosols—spraying Coagulation of aerosols	10–100 1–25	Any
	Shaking—mixing—flow promotion Thermal effects—therapy Precipitation of hydrosols	500–2000	0.5–1.5
LIQUID	CAVITATION		
	Degassing Tensile strengths of liquids Sonoluminescence—sonochemiluminescence Hot-spot chemistry Fundamental oxidation reactions	0–40 500–2000	Any 1–5 1–5
	<i>Disruptive</i> Erosion studies Descaling Tinning Cell disruption Bactericidal Sterilization Pasteurization Depolymerization	<i>Dispersive</i> Emulsification Dispersing solids Cleaning fabrics Degreasing Cleaning solids Electrolytic dispersion Grain refinement of metals	<i>Acceleration of rate processes</i> Chemical reactions Maturing Surface reactions Diffusion Tanning—dyeing Extraction Accelerated solution Emulsion polymerization
		5–40	1–5
	Shaking—mixing—flow promotion Investigating non-linear effects Destructive testing—fatigue—adhesive bonds—wear Cold welding Machining—drilling—tapping—polishing	0–50 Any 20–25	Any 10 ² –10 ⁶ 10 ² –10 ⁴

ferrite tubes, wound with a single toroidal coil carrying polarization and drive currents. The drive frequency in this case is adjusted to the radial resonance of the ring, given by $C_e/2\pi r$ where r is the mean radius. These transducers are very valuable in medium power applications but have also recently been used in very high power work.

Torsional transducers are tubes of metal or ferrite, wound with two coils, longitudinal and toroidal, carrying respectively polarization and drive currents. The resultant field produces a drive force tending to twist the tube, thereby coupling strongly into a torsional mode of vibration, the fundamental frequency given by $C_s/2l$, where C_s is the phase velocity of shear waves in the material and l the length of the tube.

Flexing vibrators are essentially two extensional mode transducers coupled mechanically at the ends. The two halves are driven in opposite phases so that one-half extends while the other contracts, coupling therefore strongly into flexure. The fundamental frequency of flexure is approximately

$$9\pi KC_e/8l^2$$

where l is the effective length of the transducer and K the radius of gyration of a cross-section about a centre-line perpendicular to the plane of bending. The transducer types shown in Fig. 1 are all used in very high power work. Although only piezomagnetic transducers are shown, analogous types of piezoelectric ceramic transducers are available and may be used alternatively.

In Table 2 are listed approximate data for the six most useful transducer materials for high energy work, four piezo-

magnetic and two piezoelectric. Of these, the ferrite and lead zirconate titanate are comparatively new materials, not yet widely used in ultrasonic work. The new 7A2 ferrite combines very high efficiency with low cost, and is potentially much the most valuable of the materials listed.⁽¹⁾ But since it has only recently become available, most high power work to date and all that to be described in this paper, uses metallic types of transducer.

Table 2. *Properties of piezomagnetic and piezoelectric transducer materials*

<i>Material</i>	<i>Electro-mechanical coupling coefficient Extensional mode</i>	<i>Curie temp. (°C)</i>	<i>Potential efficiency for typical window transducers (%)</i>	<i>Approx. relative cost on volume basis</i>
Nickel (pure annealed)	0.310	365	60	10
45-Permalloy (45% nickel iron)	0.17	440	65	7
Alfer (13% Al; 87% Fe)	0.27	500	70	5
7A2 Ferrite (Ni, Cu, Co ferrite)	0.24	530	98	3
Barium titanate (90% Ba, 4% Pb 6% Ca titanate)	0.48	115	65	4
PZT 5 (Lead zirconate titanate)	0.70	400	72	12

Velocity transformer design

Transducers must be driven at low economical levels and high intensities obtained by velocity transformation external to the transducers. Velocity transformers are of fundamental importance in very high power work. Basically, they are simply tapered metal stubs. Any tapering will provide an increase in the particle motion but the transformation ratio and the resonant dimensions will depend largely on the exact form of the taper.

the solutions of the wave equation, the following relation may be deduced: $v_m = (S_m/\rho c)$ (Shape Factor), or, since the maximum value of S_m is the fatigue strength, F , the maximum velocity obtainable from a given transformer is $(F/\rho c)$ (Shape Factor).

This is the product of two parameters: $(F/\rho c)$, which is simply a material constant; and the Shape Factor, which depends only on the geometry of the taper used. In designing a transformer for maximum possible end velocity we should

Table 3. Solutions of the wave equation for velocity transformers with simple tapers

Taper	Velocity distribution	Velocity transformation ratio
Conical $d = d_0(1 - \alpha x)$	$v = \frac{v_0}{(1 - \alpha x)} \left(\cos kx - \frac{\alpha}{k} \sin kx \right)$	$R = (d_0/d_l) \left\{ \cos kl - \frac{(d_0/d_l - 1)}{d_0 kl/d_l} \sin kl \right\}$
Exponential $d = d_0 e^{-\beta x}$	$v = v_0 e^{\beta x} \left(\cos k_1 x - \frac{\beta}{k_1} \sin k_1 x \right)$	$R = d_0/d_l$
Catenoidal $d = d_0 \cosh \gamma(l - x)$	$v = \frac{v_0 \cosh \gamma l}{\cosh \gamma(l - x)} \left(\cos k_2 x - \frac{\gamma}{k_2} \tanh \gamma l \cdot \sin k_2 x \right)$	$R = d_0/d_l \cos k_2 l$
Double quarter-wave		
Cylinder $d = d_0 (0 < x < l/2)$	$v = v_0 \cos kx (0 < x < l/2)$	$R = (d_0/d_l)^2$
$d = d_l (l/2 < x < l)$	$v = (d_0/d_l)^2 \cdot v_0 \cos kx (l/2 < x < l)$	
$d = \text{diameter}$	$k = 2\pi/\lambda$	$\lambda = \text{wavelength of extensional waves}$
$d_0 = \text{input diameter}$	$k_1 = (k^2 - \beta^2)^{1/2}$	
$d_l = \text{output diameter}$	$k_2 = (k^2 - \gamma^2)^{1/2}$	

In designing resonant velocity transformers, the well-known equation for velocity distribution in a horn is used:

$$\frac{\partial^2 v}{\partial x^2} + \frac{\partial v}{\partial x} \cdot \frac{\partial}{\partial x} [\log_e A(x)] = \frac{1}{c^2} \frac{\partial^2 v}{\partial t^2} = -\frac{\omega^2}{c^2} \cdot v$$

for sinusoidal vibrations. Here, ω is the angular frequency, c the velocity of extensional or shear waves in the material and the function $A(x)$ defines the taper profile. By substituting appropriate simple functions for A and solving for resonant boundary conditions, the resonant dimensions, velocity distribution and velocity transformation ratio are obtained.^(2, 3) Table 3 gives the solutions for four simple types of taper: conical, exponential, catenoidal and double quarter-wave cylindrical.

These solutions are for extensional mode operation. The stress distribution is obtained by differentiating the velocity distribution with respect to x , and is not included in the table. Fig. 2 shows these solutions graphically for transformers of the same resonant frequency and the same end diameters in all cases. The double quarter-wave cylinder gives by far the greatest transformation. Since it is also a very simple shape, easily and cheaply produced, it is often used.

Unfortunately, transformation is not the only consideration, especially where high intensities are required. Obviously the maximum end-face velocity is finally limited by the dynamic strength of the material of the transformer. Thus, in designing for maximum possible output velocity the important consideration is the relation between maximum velocity and maximum stress in the material. The graphs of Fig. 2 show that the smoothly tapered types are superior to the double cylinder in this respect.

The above discussion refers to transformers for extensional mode operation. Design principles are similar for the other useful modes—torsional and flexural—if the appropriate transmission constants are used.

If the peak velocity (v_m) and stress (S_m) are calculated from

aim at maximum values for both these parameters. Values of the parameter $(F/\rho c)$ are shown in Table 4 for a number of alloys recently used for constructing mechanical transformers. Titanium alloy 318 is by far the best available for this purpose.

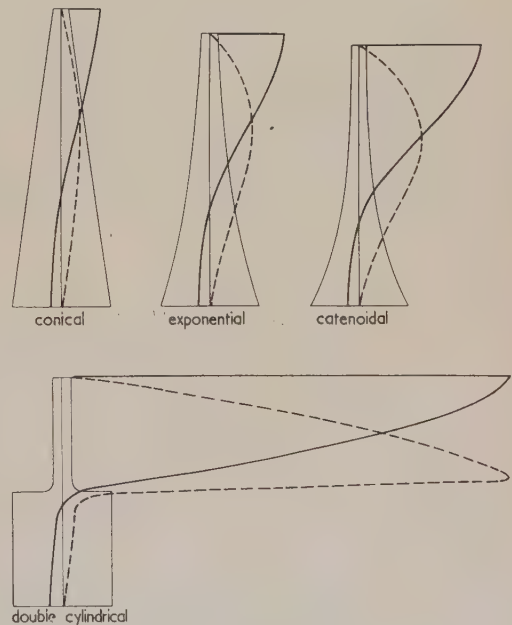


Fig. 2. Distribution of velocity and stress in resonant velocity transformers (end diameter ratio 6/1)

$$\frac{\partial^2 v}{\partial x^2} + \frac{\partial v}{\partial x} \cdot \frac{\partial}{\partial x} (\log_e A) = \frac{1}{c^2} \frac{\partial^2 v}{\partial t^2} = -\frac{\omega^2 v}{c^2} \text{ for sinusoidal vibrations, } \rightarrow v = v(x) \text{ and } S = S(x)$$

— velocity - - - stress

Table 4. *Maximum velocities obtainable from transducer materials*

Material	Density, ρ (g/cm ³)	Velocity of sound, C (cm/s) $\times 10^5$	Fatigue stress, F (dyn/cm ²) $\times 10^9$	Mechanical Q at approx. $F/2$	Maximum particle velocity in untapered rod $v = F/\rho c$ (cm/s)	Maximum possible particle velocity (cm/s)
Naval brass (BS 251)	8.45	3.23	1.5	3 000	550	1726
Aluminium bronze (Hidurax)	8.5	4.07	1.85	17 000	535	1680
K-Monel	8.9	4.3	1.78	5 300	465	1460
Duralumin (DTD 363)	2.79	5.13	1.90	> 50 000	1320	4150
Hiduminium (RR 77)	2.9	5.12	1.94	> 100 000	1306	4105
Tool steel (KE 672)	7.9	5.24	5.5	1 400	1320	4150
Titanium (ICI 318 A)	4.51	4.9	7.2	24 000	3258	10240

v_{max} and S_{max} are obtained from the solution of the wave equation:

then $v_{max} = \frac{S_{max}}{\rho c}$ (shape factor) and maximum possible $v = \left(\frac{F}{\rho c}\right)$ (shape factor)

Obviously, also, an optimum shape exists which will give maximum value of the Shape Factor. It is not difficult to see that this optimum taper must satisfy the condition of constant stress in the whole volume of the material of the transformer. Substituting the condition $(\partial v/\partial x) = \text{constant}$ in the wave equation, the optimum shape is found to be a Gaussian-type curve. In practice, it is necessary to design only for the final $\lambda/4$ section of the transformer. But the shape must be adjusted at the free end to conform with the boundary condition requiring zero stress here, and the choice of boundary function will determine the resonant length and ratio of end diameters and will therefore also affect the value of the Shape Factor. There are, however, practical limits to both end diameters which must be such as to avoid unwanted mode conversion. Taking this into account, the last column of Table 4 gives approximate values for the maximum velocities obtainable using the optimum taper with the material listed. Using the optimum taper in the best available material, a peak velocity of 10 240 cm/s is achieved. This appears to be the maximum oscillatory velocity obtainable at present with these solid vibrators. It corresponds, for

example, to a displacement amplitude of about 2 mm peak-to-peak at 20 kc/s, a value which has almost been reached in practical systems. Such large amplitude vibrators are likely to have important applications in projected work in the very high energy field.

Any number of half wavelength low-loss sections may be added to these vibrators without sacrificing much in efficiency. It is sometimes convenient to use very long resonant lines to transmit ultrasonics at high power to remote places. It is even feasible to curve the axis, provided the curvature is not too great.

Drive generators

The usual method of energizing piezomagnetic transducers is to use a variable frequency oscillator-amplifier to supply the h.f. drive current to the transducer. D.C. for polarization is taken through the same coil and separated from the drive by using choke-capacitance coupling, as shown in Fig. 3(a).

In some applications of high energy ultrasonics the acoustic load reactance may change appreciably during the test or treatment. This will be reflected in a change in the resonant

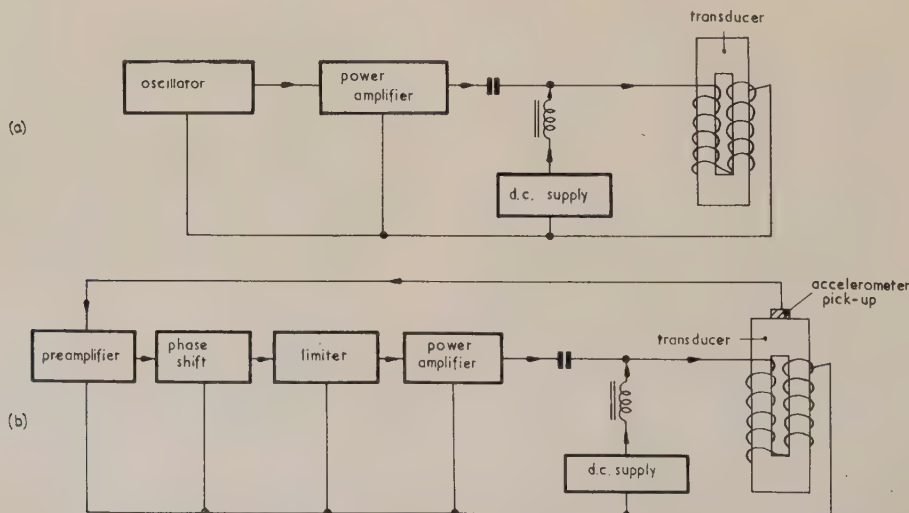


Fig. 3. Electronic drive systems for piezomagnetic transducers: (a) tuned manually; (b) self-excited

frequency of the vibrator. To avoid periodic tuning adjustment the use of a self-oscillatory system is therefore indicated. In the system shown in Fig. 3(b) a small accelerometer pick-up fixed to the free transducer face gives a voltage proportional to the oscillatory amplitude. This signal is returned to the drive amplifier through pre-amplifier, phasing and limiter circuits and used to maintain the system on resonance. The transducer forms part of a self-oscillatory loop and tuning is eliminated.⁽⁴⁾

These high energy ultrasonic vibrators are finding new applications in research and industry. These are discussed briefly below.

Destructive testing

It will be obvious that large amplitude transformers can be used to couple into any resonant solid load stresses capable of fatiguing the material. At the same time, the drive vibrator will operate at a low, safe stress. This provides a useful and simple research tool for rapid fatigue analysis and for investigating non-linear effects in solids at high strain.

For fatigue work, any piece of material approximately resonant in the required mode will serve as the specimen. In practice, it is often convenient to provide some stress amplification in the specimen, with the advantage that it can then be driven at a lower velocity than would otherwise be needed. In fact, special large amplitude transformers are rarely needed and simple double cylindrical types will often suffice. Sketches of typical resonant specimens which have been developed for metal fatigue studies under axial load are included in Fig. 4. The tapering produces an increase

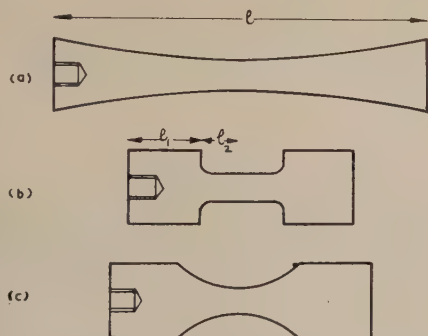


Fig. 4. Typical resonant specimens for fatigue studies

$$(a) l = (2c'/\omega) \tan^{-1} (\omega/\beta c'); \quad \beta l = \log_e R; \\ c' = c(1 - \beta^2 c^2/\omega^2)^{-1/2}$$

$$(b) R = \cot \pi l_1/l \cdot \cot \pi l_2/l; \quad l = \pi c/\omega; \quad (c) \text{ tuned empirically}$$

in stress over the central region, where the fatigue break will occur. In practice there are definite limits to the amount of tapering which can be tolerated. We must obviously retain a useful volume for test; also, as the section is reduced, a danger exists of coupling into unwanted modes of vibration, for example, from axial load (extensional) to flexure.

Figs. 5 and 6 illustrate the simplest possible type of vibrator for carrying out metal fatigue tests in axial push-pull. It consists of three half-wavelength sections: transducer, velocity transformer and specimen. A flange turned in the nodal plane of the coupling transformer serves as support for the vibrator. Included in Fig. 6 are plots of velocity and strain down the system. The strain reaches a high peak at the centre of the specimen, where the fatigue break will occur. A small barium titanate accelerometer fixed to the transducer face is used to provide self-maintenance. The voltage output from the accelerometer is also recorded on a

calibrated valve voltmeter and used to indicate the strain in the specimen.

In carrying out fatigue measurements the specimen is driven at a convenient strain level and the number of cycles to fracture recorded. This is repeated with a number of specimens over a suitable strain range. In this way the necessary data is collected for plotting out the strain-endurance characteristic for the material. Typical plots for two alloys

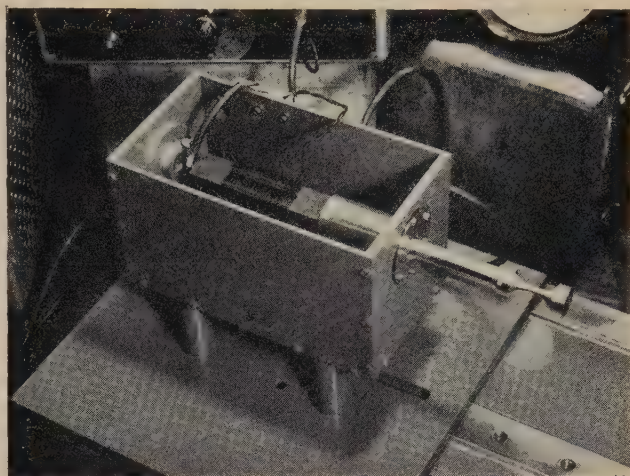


Fig. 5. Ultrasonic fatigue test vibrator for free-free tension-compression tests

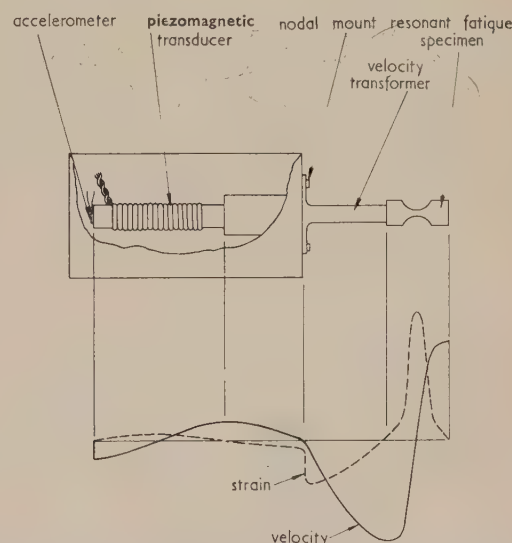


Fig. 6. Distribution of velocity and stress in vibrator for axial load fatigue tests

taken on this machine are reproduced in Fig. 7. Endurance limits measured at high frequency are found to be always a little higher than corresponding low frequency figures. A theoretical explanation for this discrepancy has been proposed, based on dislocation theory, but there is little quantitative agreement with actual measurements. Sufficient data for a complete S-N plot can be obtained well within one day; 10^8 reversals take only about an hour and a half at 18 kc/s.

The above discussion refers to axial load tests. For testing in bending and torsion the appropriate transducers and transformers operated in flexural and torsional modes are, of course, used.

Apart from metal fatigue, this ultrasonic equipment has been found useful for several other types of accelerated strength tests.⁽⁴⁾ For testing adhesive bonds, quarter-wavelength sections of the two materials are cemented together with the required adhesive. This composite structure

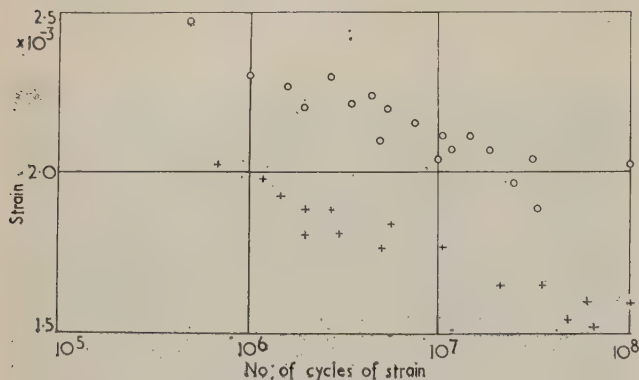


Fig. 7. Strain-N plots for alloys measured at 18 kc/s

+ specimens of brass BS 251
o light alloy DTD 423

is then used as the resonant fatigue specimen [Fig. 8(a)]. Some stress amplification may be obtained if desired by turning down the centre section of the specimen as indicated in Fig. 8(b). For testing adhesion to material in the form of thin sheet, a convenient technique is to sandwich the sheet between two quarter-wave sections of the other material. In this way, two bonds are tested together [Fig. 8(c)]. For testing adhesion of thin films, the film may be bonded to the end of a half-wavelength section of the base material [Fig. 8(d) and (e)]. The film is shaken as a lumped mass and the stress at the bond is the product of the mass of the film and peak acceleration in the stub.

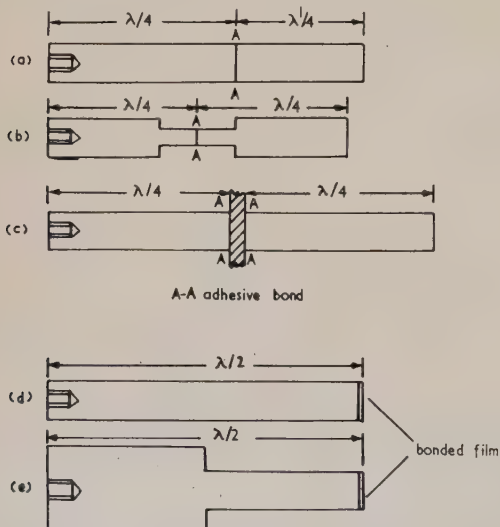


Fig. 8. Typical resonant specimens for adhesive bond tests

These vibrators are useful research tools. But apart from research, destructive testing by ultrasonics may well become a valuable industrial technique. Apart from obvious advantages of speed and silent operation, the equipment is simple and inexpensive to produce. But the fact that the endurance

limit is a function of the operating frequency is a disadvantage, indicating need for calibration in a practical tester. At the higher frequencies, elastic losses in the specimen are higher and it becomes necessary to provide external cooling, either liquid or forced air. An alternative technique is to design the specimen to give good conduction cooling away from the highly stressed region.

Since these vibrators are highly resonant devices, they would seem, at first sight, to be restricted to single-frequency operation. This is not so, and the sketch of Fig. 9 shows how a range of frequencies can be covered using a common transducer and transformer with interchangeable screw-on

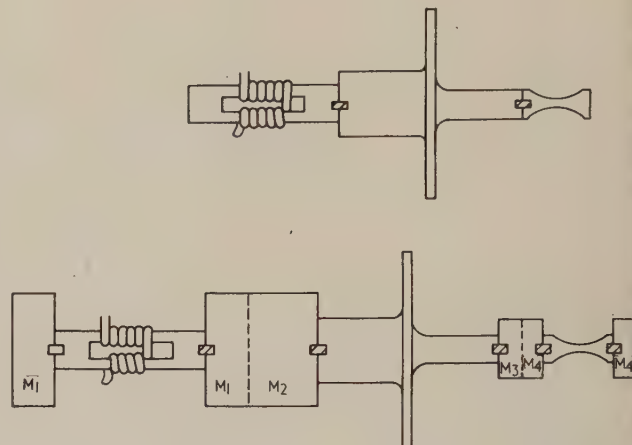


Fig. 9. Vibrator assembly for fatigue testing at variable frequency

M_1 , $(M_2 + M_3)$, $(M_3 + M_4)$ and M_4 are screw-on lossless masses; $\omega^2 MC = 1$ for every resonant section, where M and C are the equivalent mass and compliance of the section

masses. The addition of lossless masses reduces the resonant frequency of the system without affecting the efficiency. A sufficient number of these interchangeable masses allows operation at a large number of spot frequencies covering a wide total range. Research which is now urgently required is the investigation of fatigue and non-linear behaviour in solids at frequencies from a few kilocycles per second upwards. The vibrator of Fig. 9 may be used for this purpose. Results of this research could assist considerably in an understanding of the basic mechanism of fatigue in metals.

Non-linear effects

The simple basic vibrators described above may be used in applications other than destructive testing. For example, the equipment has been adapted to measure internal friction at high strain in metals.^(4, 5) Specimen results are given in Fig. 10 which shows internal friction (Q^{-1}) as a function of strain for three alloys of interest. The values of Q were deduced from calorimetric measurements of power dissipation.

It is sometimes possible to distinguish three distinct regions of loss. A linear, or nearly linear region is followed by a region in which the loss increases with strain, sometimes in regular manner. This is a reversible strain region. The strain can be cycled downwards from any point, even into the linear region, and the starting point recovered in each cycle. In the final, plastic range the loss increases very rapidly with strain, ending with fatigue. This is the irreversible part of the characteristic. The existence of these three distinct

loss regions can be explained, qualitatively at least, in terms of modern dislocation theory.

Not only the internal friction, but also the elastic modulus, is a function of the strain. In other words, both parts of the complex modulus are strain dependent at high strain. For a resonant vibrator the change in the real part of the modulus can be related to the change in resonant frequency, which is easily measured with great accuracy. Below the plastic region the modulus decreases in a regular manner with increase in

includes plots of the distribution of oscillatory motion and stress in the weld rod. It has been established that it is desirable to produce as large a motion as possible at the weld junction. Velocity transformers developing the maximum possible motion may therefore be used with advantage.

It will be obvious that this method of welding will only work well for the more ductile materials—materials with a large plastic range. Although referred to as cold welding, it is not strictly so. Elastic losses are always very high in the

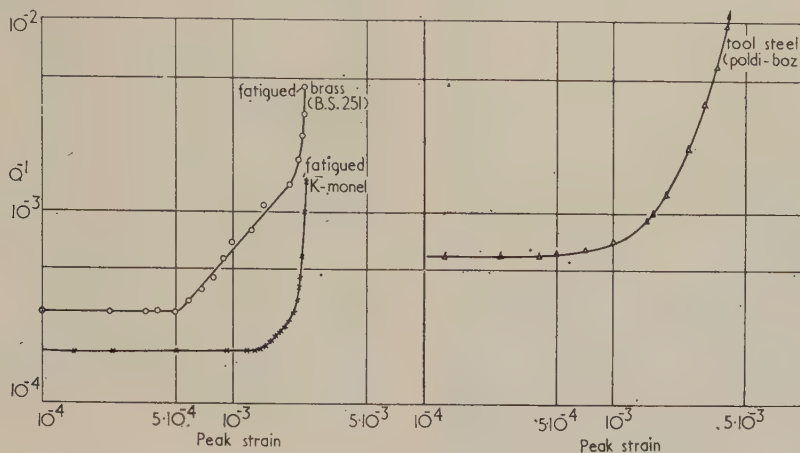


Fig. 10. Internal friction, Q^{-1} , in various alloys measured at 20 kc/s

strain. Dislocation theory can be used to predict quantitatively with considerable accuracy the change occurring in this region. In the plastic range, the change becomes very rapid and quantitatively unpredictable.

Ultrasonic cold welding

Two important industrial applications have emerged from work on high energy ultrasonics in solids—cold welding and machining. For such applications, where a rugged type of construction is essential, metallic piezomagnetic transducers have been used, and will probably continue to be used, in preference to ceramic transducers.

If two metals are strained in the plastic region and forced together under pressure a weld can often be produced. A complicating factor is the oxide skin which is always present on metal surfaces; this will prevent uniform alloying. The oxide can generally be broken up if, in addition to the stress, some relative motion can be produced between the surfaces. This is the principle of ultrasonic welding. The aim is to produce both tangential motion and stress at the weld junction. If this can be done, good welds can often be obtained.^(6, 7)

The sketch of Fig. 11 shows the essentials of one type of vibrator used for experimental cold welding. An extensional mode transducer-transformer system drives a cross-piece into flexure. A window-type piezomagnetic transducer is used, with a smoothly tapered large-amplitude transformer. The top end of the flexing rod is clamped rigidly and the pieces to be joined are placed on an anvil which is forced up into contact with the free end of the flexor. The dimensions of the flexing rod are adjusted so that when vibrated at the drive resonance, the weld junction will be intermediate between a displacement antinode and a stress antinode. Both motion and stress will be developed at the weld, as required. Fig. 11

plastic region and the temperature rise may be quite appreciable. The trick in this application is to arrange conditions to achieve plasticity, but to avoid actual fatigue. But fatigue of the weld is a real danger and often occurs in practice. Since relative movement must be produced between the work-pieces, the mass and thickness of the piece in contact with the weld rod is important, and the technique is

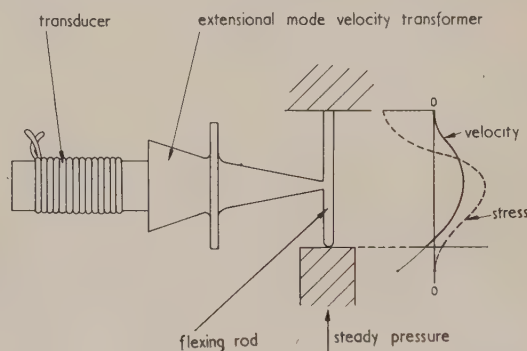


Fig. 11. Typical vibrator for ultrasonic cold welding

strictly limited to jobs in which one component is comparatively thin. There is no restriction on the size or mass of the other component. The method has been used for spot welds and seam welds in aluminium, light alloys, copper and brass. Practical advantages of the technique are very little distortion of the materials and the ability to join dissimilar metals, particularly in thin sheet.

Ultrasonic machining

An application of the ultrasonic destructive test equipment not previously mentioned is for accelerated tests of wear in

solids produced by hammer blows or frictional forces.⁽⁸⁾ Although not a very important application in itself, experiments on these lines are important in that they first suggested the industrial application of ultrasonic machining.^(2, 9, 10) This is really only an accelerated wear technique, in which the conditions are arranged to produce the maximum possible rates of removal of material.

Simple experiments show that wear produced by direct hammer blows can only occur by plastic flow and no material is actually removed. Wear involving removal of material requires shear stresses. These can be obtained by applying the stresses tangentially or, more conveniently, by using a

the other hand, the abrasive tends to become absorbed and very little material is removed. The technique is therefore chiefly valuable for very brittle substances like glass, ceramics, precious stones and sintered materials. The great practical advantage of the method is that since the normal motion of the tool is longitudinal, holes of any shape can be cut. The tool impresses its image into the work. In very brittle substances machining rates of several centimetres per minute can be achieved.

Fig. 12 shows typical vibrators used in practical machining tools. They all use metallic piezomagnetic transducers. The three extensional mode vibrators are simple $2\lambda/2$ systems rated at 2000, 60 and 20 W input respectively. They are useful for drilling, slicing, trepanning, blanking and grinding operations. The flexing vibrator uses a double window type transducer with double cylindrical transformer, the small end of which consists of a piece of threaded rod. The large amplitude lateral vibrations in the rod can be used, with an abrasive cutting medium, to tap threads in brittle materials. The ring-type vibrator is, in effect, an ultrasonic threading die. The transducer is driven in the radial mode. Wedge-type velocity transformers are used to generate intense radial motion at the centre which carries a thread, as in a conventional die. Threads can be produced on rods of very hard brittle materials when the die is vibrated in the presence of an abrasive paste.

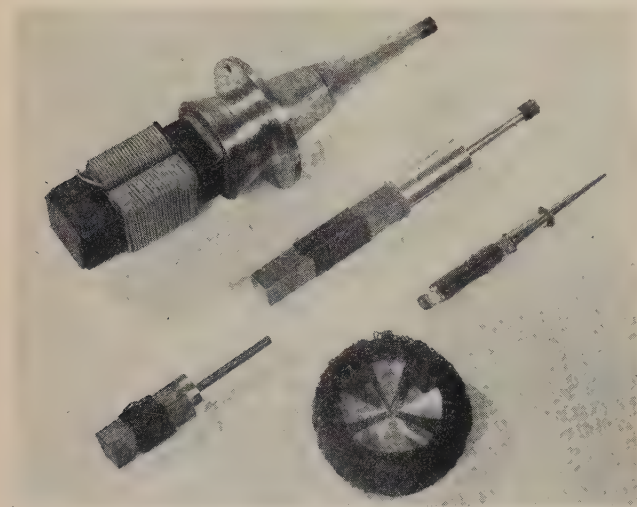


Fig. 12. Typical vibrators for ultrasonic machining

hammer tool with an abrasive powder. The abrasive spreads the stresses in all directions in the surface of the work-piece and the shear component is effective in removing material. This is the principle of ultrasonic machining. The abrasive is dispersed in a low viscosity liquid, for example, water. This helps to achieve a good acoustic bond and also acts as coolant for the tool and work-piece. Measurements show that cutting rates increase very rapidly with the particle motion of the tool. This is therefore another application of large amplitude coupling transformers. Cutting rates are also very dependent on the steady pressure imposed between the tool and the work. But the most important requirement of all is that the work material must be brittle. In brittle substances, stresses generated in the surface cannot spread by plastic flow and chipping occurs. In ductile materials, on

References

- (1) VAN DER BURGT, C. M. *Matronics*, No. 15 (September 1958).
- (2) NEPPIRAS, E. A. *Proceedings of the Conference on Technology of Engineering Manufacture*, p. 417 (London: Institution of Mechanical Engineers, 1958).
- (3) MERKULOV, G. *Soviet Physics—Acoustics*, **3**, p. 246 (1957).
- (4) NEPPIRAS, E. A. *Proc. Amer. Soc. for Test. Mater.* (In the press) (1959).
- (5) MASON, W. P. *J. Acoust. Soc. Amer.*, **28**, p. 1207 (1956).
- (6) JONES, J. B. *Metal Prog.*, **73** (4), p. 68 (April 1958).
- (7) COLLINS, F. R., DOWD, J. D., and BRENNKE, M. W. *Welding Journal*, **38**, p. 969 (1959).
- (8) MASON, W. P., and WICK, R. F. *J. Acoust. Soc. Amer.*, **25**, p. 209 (1951).
- (9) NEPPIRAS, E. A. *J. Sci. Instrum.*, **30**, p. 72 (1953).
- (10) NEPPIRAS, E. A., and FOSKETT, R. *Philips Tech. Rev.*, **18**, pp. 325–334 and 368–379 (1956–57).

Spectral emission of radiation by glass

by J. R. BEATTIE, B.Sc., A.Inst.P., and E. COEN, Dr.Phys., Pilkington Bros. Ltd., St. Helens, Lancashire.

[Paper received 26 June, 1959]

Abstract

The spectral radiation emitted normally from the surface of a thin sheet of glass having a specified temperature distribution throughout its thickness is calculated for the wavelength range 1.0 to 6.0 μ . From the results obtained, the design of a radiation pyrometer capable of measuring both the surface and inside temperatures of the glass is described. The pyrometer consists of two radiation detectors, one with a filter to measure only the radiation arising from, and hence the temperature of, the surface of the glass, the other with a filter to measure the radiation arising from the interior of the glass and which therefore has a response dependent on the temperature distribution within the glass.

Introduction

THE measurement of the temperature of flat glass is of great importance in the annealing and toughening processes. The temperature may be measured either by placing a thermocouple in contact with the surface, or by using a radiation pyrometer set at a distance from the surface. Unless great care is exercised in the location and use of contact thermocouples, large temperature errors will result. These are due either to poor contact between the thermocouple and the surface, or to the conduction of heat along the thermocouple leads and supports causing a fall in temperature at the point of contact. To overcome the difficulties associated with contact thermocouples one of the usual methods of radiation pyrometry may be used.⁽¹⁻³⁾ These methods are, however, restricted to opaque objects where the energy received arises entirely from the surface.

Any attempt to apply these methods to the measurement of the temperature of a partially transparent material, such as glass, will be complicated by the fact that the energy received will arise not only from the surface but also from the interior of the glass, which may be at a different temperature to that of the surface. Thus it is necessary, if a radiation pyrometer is to be used, that a knowledge of the emission of radiation by glass should be obtained.

McMahon,⁽⁴⁾ in his study of the spectral emissivity of partially transparent materials having a constant temperature throughout their thickness, introduced the concept of the spectral volume emissive power, which he defined as the spectral radiation emitted at a given temperature by unit volume into unit solid angle of space. He derived an equation analogous to Kirchhoff's law which normally applies to opaque materials only and which, in its simplest form, may be written as

$$J_{\lambda T} = \epsilon_{\lambda T}(1 - R_{\lambda T}) \quad (1)$$

where $J_{\lambda T}$ is the emissive power of the material at absolute temperature T and wavelength λ , $R_{\lambda T}$ the reflectivity of the

material for the same temperature and wavelength and $\epsilon_{\lambda T}$ the spectral emissive power of a black body. Although McMahon's final results are correct, his treatment fails to show the dependence of the spectral volume emissive power within the material on its refractive index.⁽⁵⁾ Gardon,⁽⁶⁾ who uses McMahon's concept of the spectral volume emissive power, has treated the emissivity of transparent materials as a three-dimensional problem, and at the same time has introduced the refractive index into his calculations.

The work herein described differs from McMahon's and Gardon's in that the spectral emission of radiation from the glass is derived for specified temperature gradients within the glass. From these results, the radiation pyrometer described below, suitable for measuring both the surface and internal temperatures of the glass, has been developed.

The spectral emissive power

The spectral emissive power for radiation emitted normally to the surface, rather than the hemispherical emissive power, is here considered because it is the radiation which is, in general, received by a radiation pyrometer.

It is shown in the Appendix that the spectral emissive power of flat glass, having either a uniform temperature, a linear temperature or a parabolic temperature distribution throughout its thickness, is given by

$$E_{\lambda} = (1 - R_{\lambda}) \frac{\alpha_{\lambda} c_1}{\pi \lambda^5} \int_0^d \exp\left(-\frac{c_2}{\lambda T}\right) \exp(-\alpha_{\lambda} x) dx + R_{\lambda} \exp(-\alpha_{\lambda} d) (1 - R_{\lambda}) \frac{\alpha_{\lambda} c_1}{\pi \lambda^5} \int_0^d \exp\left(-\frac{c_2}{\lambda T}\right) \times \exp(-\alpha_{\lambda} x) dx \quad (2)$$

where $T = T_0$ for $0 \leq x \leq d$; constant temperature throughout the glass

$T = T_0 + ax$ for $0 \leq x \leq d/2$
 $T = T_m - a(x - d/2)$ for $d/2 \leq x \leq d$ } linear temperature distribution

$T = T_0 + ax^2 + bx$ for $0 \leq x \leq d$; parabolic temperature distribution

T_0 = surface temperature of the glass ($^{\circ}\text{K}$)

T_m = maximum temperature along centre line of the glass ($^{\circ}\text{K}$)

α_{λ} = absorption coefficient of the glass at wavelength λ (cm^{-1})

R_{λ} = reflexion coefficient of the surface at wavelength λ
 d = thickness of the glass (cm)

The first term in equation (2) is the direct radiation arriving at the front surface of the glass and entering the atmosphere. The second term is the radiation reflected from the rear

surface of the glass, arriving back at the front surface, and entering the atmosphere.

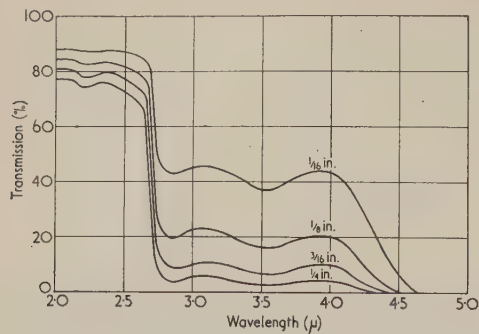


Fig. 1. Spectral transmission of polished plate glass (various thicknesses)

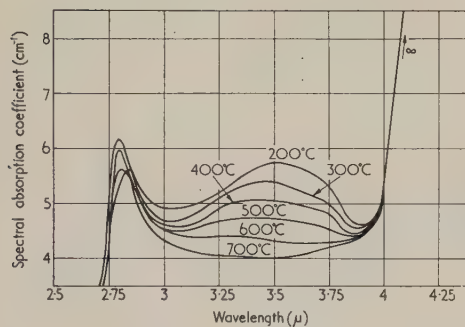


Fig. 2. Spectral absorption coefficient of plate glass

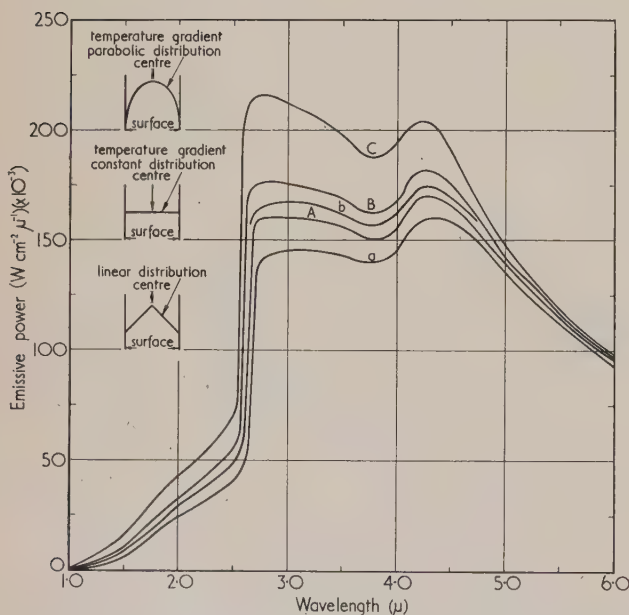


Fig. 3. Spectral energy emitted perpendicularly from the surface of plate glass 0.3 cm thick, having a given temperature gradient

Curve *a*: constant temperature throughout thickness, 600° C. Curves *A*, *B*, *C*: parabolic distribution of temperature. Surface temperature, 600° C. Maximum temperature: curve *A*, 625° C; curve *B*, 650° C; curve *C*, 700° C. Curve *b*: linear distribution of temperature: surface, 600° C; maximum, 650° C

For a typical soda lime silica glass composition, the glass is opaque at wavelengths greater than 5.0 μ (Fig. 1). Thus α_λ is infinite (Fig. 2) and hence $\exp(-\alpha_\lambda d)$ is zero. In the wavelength range 2.75 to 4.5 μ, R_λ has a value of approximately 0.04, and $\exp(-\alpha_\lambda d)$ has values of 0.3 and 0.09 for 3 and 6 mm thicknesses of glass respectively. Hence the maximum value of $R_\lambda \exp(-\alpha_\lambda d)$ is 0.012, and therefore all internal reflexions of radiation, other than the first reflexion at the rear surface of the glass and which involve higher orders of $R_\lambda \exp(-\alpha_\lambda d)$ can be neglected.

The solution of equation (2) is complicated by the fact that, within the wavelength region 2.75 to 4.5 μ, α_λ depends not only on the wavelength of the radiation but also on the temperature of the glass (Fig. 2). To simplify the com-

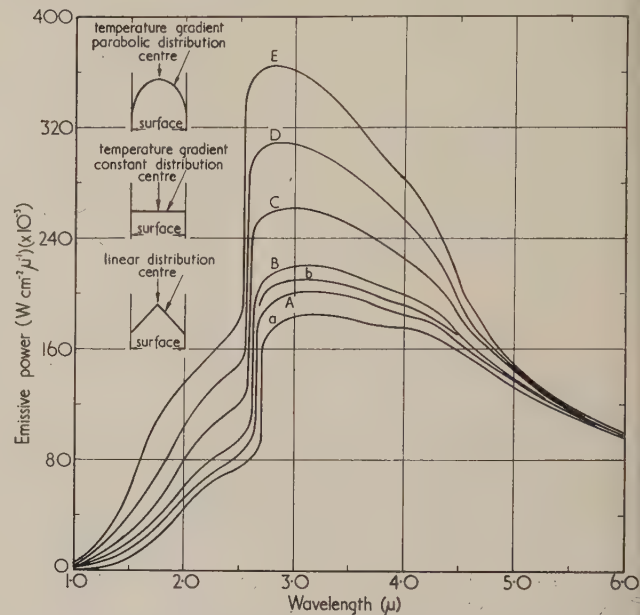


Fig. 4. Spectral energy emitted perpendicularly from the surface of plate glass 0.6 cm thick, having a given temperature gradient

Curve *a*: constant temperature throughout thickness, 600° C. Curves *A*, *B*, *C*, *D*, *E*: parabolic distribution of temperature. Surface temperature, 600° C. Maximum temperature: curve *A*, 625° C; curve *B*, 650° C; curve *C*, 700° C; curve *D*, 750° C; curve *E*, 800° C. Curve *b*, linear distribution of temperature. Surface, 600° C; maximum, 650° C

putations, values for α_λ obtained for glass having a constant temperature of 300 and 600° C throughout its thickness are used when considering glass surface temperatures, within the range 200 to 400° C and 500 to 1000° C respectively.

The spectral emissive powers calculated from equation (2) for 3 and 6 mm thick flat glass, having a surface temperature of 600° C, are shown in Figs. 3 and 4 respectively. The resultant spectral emissivity curves are given in Fig. 5. These curves are obtained from the ratio of the spectral emissive power of the glass, for each thickness and temperature gradient, to the corresponding spectral emissive power of a black body, having the same temperature as the surface of the glass.

Application of the results

From Figs. 3 and 4 it is seen that the total emissive power, which is given by the areas under the curves, is dependent on the thickness and the temperature of the glass and on

any temperature variations existing within the glass. Also, owing to the fact that as the temperature of a black body increases (Fig. 6), progressively greater fractions of radiant energy are emitted at shorter wavelength regions where the

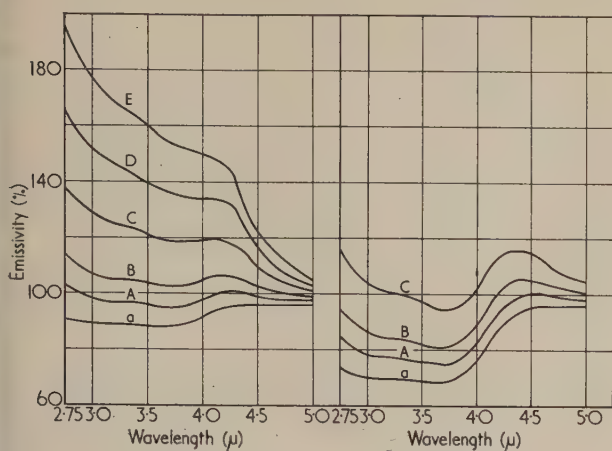


Fig. 5. Equivalent spectral emissivity relative to black body, temperature 600°C

Left: plate glass, thickness 0.6 cm

Curve *a*: constant temperature throughout thickness, 600°C. Curves *A*, *B*, *C*, *D*, *E*: parabolic distribution of temperature. Surface temperature, 600°C. Maximum temperature: curve *A*, 625°C; curve *B*, 650°C; curve *C*, 700°C; curve *D*, 750°C; curve *E*, 800°C

Right: plate glass, thickness 0.3 cm

Curve *a*: constant temperature throughout thickness, 600°C. Curves *A*, *B*, *C*: parabolic distribution of temperature. Surface temperature, 600°C. Maximum temperature: curve *A*, 625°C; curve *B*, 650°C; curve *C*, 700°C

spectral emissivity of the glass is low, it follows that the total emissivity decreases with increase in temperature. Since the total radiation emitted by the glass is dependent on all these factors, it is clear that any application of a total radiation pyrometer to the measurement of the temperature would be highly unsatisfactory.

(a) *Surface temperature measurement.* Figs. 3 and 4 show that at wavelengths greater than 5.0 μ, the spectral emissivity

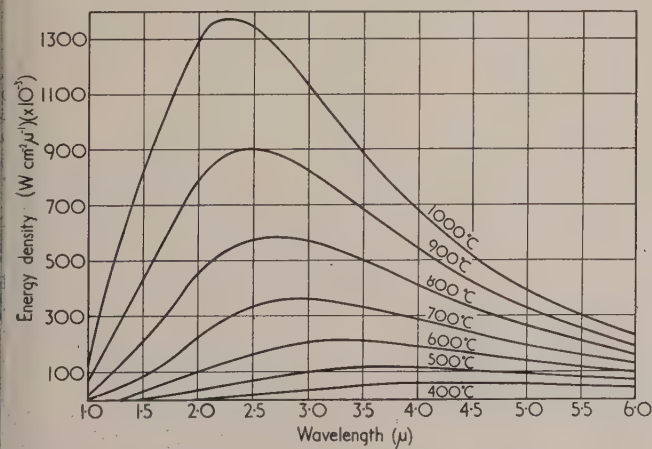


Fig. 6. Black body radiation emitted perpendicularly according to Wien's law $E = \frac{1}{\pi} \frac{c_1}{\lambda^5} \exp\left(\frac{-c_2}{\lambda T}\right)$

of glass is independent of thickness and temperature gradients within the glass. Since at wavelengths beyond 5.0 μ (Fig. 1) the glass is opaque to radiation, a pyrometer sensitive only to these wavelengths will have a response which is dependent only on the energy emitted from the surface, and hence on the surface temperature. The design of such a pyrometer developed in this laboratory has been described in detail.⁽⁷⁾

Unfortunately, the filter used to isolate the required wavelength region exhibited some transmission at wavelengths less than 5.0 μ, in which region the transmission of the glass is not zero, and hence the response of the pyrometer was not completely independent of the thickness of the glass. However, new filters capable of selective transmission in the required wavelength range are now available. One such filter is manufactured by Eastman Kodak Ltd., and transmits from 5 to 15 μ.

(b) *Measurement of the temperature gradient within sheet glass.* Referring again to Figs. 3, 4 and 5, it is seen that, within the wavelength region 2.75 to 4.5 μ, the radiation emitted normally from the surface of the glass is dependent on the temperature within the glass and on the thickness of the glass. By using a monochromator, therefore, to derive the curve showing the spectral normal emission of radiation from the glass, and also knowing the surface temperature and thickness of the glass, the form of the temperature gradient within the glass can be determined.

During the manufacturing process it is not possible in many instances, especially where temperature conditions are changing rapidly as in the toughening process, to measure the complete curve of the spectral emission of radiation from the glass for a given set of conditions, and hence some other method is required. During the forced cooling of the surface of glass in the toughening process it can be assumed that the temperature distribution within the glass is parabolic. In the annealing process the temperature distribution will probably lie between that of a linear and parabolic temperature distribution (Figs. 3 and 4). A measure of the temperature difference between the central plane and the surface of the glass can therefore be obtained from a knowledge of the thickness and surface temperature of the glass, and the total radiation emitted by the glass in the wavelength region 2.75 to 4.5 μ.

Construction of the pyrometer

In order to measure the total radiation emitted normally from the surface of the glass in the wavelength region 2.75 to 4.5 μ, it is necessary to obtain a filter which exhibits a selective transmission within this region. Such a filter is obtained by combining a lead sulphide filter with fused silica, 2 mm thick. The transmission curve of this combined filter is shown in Fig. 7.

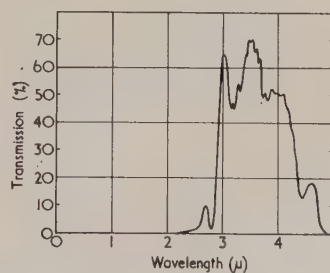


Fig. 7. Spectral transmission of lead sulphide-fused silica filter

The pyrometer (Fig. 8) consists of a glass surface-temperature pyrometer, which is sensitive only to wavelengths greater than 5.0μ (and hence has a response which is independent of the thickness of the glass and the temperature gradients within the glass) mounted integrally with another pyrometer, which is sensitive only to radiation within the wavelength limits determined by the lead sulphide-fused silica filter. Schwarz type FT17 thermopiles fitted with

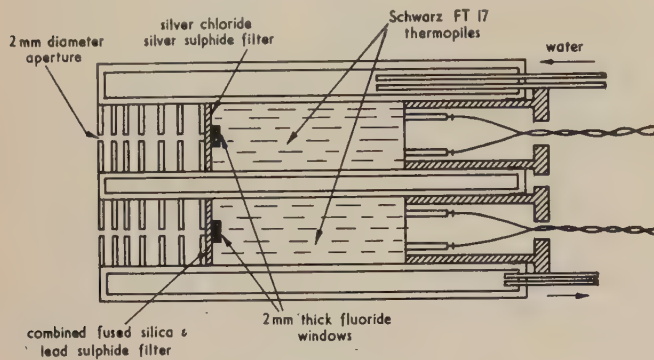


Fig. 8. Construction of composite pyrometer

fluorite windows (manufactured by Hilger and Watts Ltd.) are used as the detectors of radiant energy. The thermopiles have a sensitivity of $17 \mu\text{V}/\mu\text{W}$ and a response time of 0.4 s to 90% of full-scale deflexion. The two pyrometers are contained in a water-cooled housing in order to eliminate any errors which would be introduced should there be excessive variations in the ambient temperature.

Calibration of the pyrometer

The composite pyrometer is sighted on to the exit aperture of a black-body furnace, and the output of each thermopile is measured as the temperature of the furnace is increased in steps of approximately 30°C from 200 to 1000°C . Since the emissivity of the glass within the wavelength range of each filter differs from that of a black body, the black-body calibration curve for each thermopile must be multiplied by a correction factor (equivalent emissivity) which is given by the ratio of the energy emitted by the glass, at each temperature, relative to that emitted by a black body at the same temperature and transmitted by each filter on to its corresponding thermopile.

The glass surface temperature thermopile has a lower wavelength cut-off of 5.0μ and an upper wavelength cut-off of 13μ , determined by the silver chloride-silver sulphide filter and fluoride window (Fig. 9) of the thermopile respectively. Within this wavelength region the spectral absorption coefficient of the glass is infinite; that is, the transmission is zero, and hence the spectral emissivity of the glass (Fig. 10) is determined by its spectral reflectivity. Thus, if E_λ is the spectral emissivity of the glass, $\epsilon_{\lambda T}$ the spectral hemispherical emissive power of a black-body temperature $T(^{\circ}\text{K})$ and ϕ_λ the spectral transmission of the filter at the same wavelength, it follows that:

- (i) the radiant energy emitted normally from the surface of the glass at wavelength λ and passing through the filter on to the thermopile is $(\epsilon_{\lambda T} E_\lambda \phi_\lambda / \pi)$; and
- (ii) the radiation emitted normally from a black body at the same wavelength and temperature and passing through the filter is $(\epsilon_{\lambda T} \phi_\lambda / \pi)$.

By calculating (i) and (ii) at wavelength intervals throughout the transmission range of the filter, two curves may be drawn showing, respectively (curve *A*), the energy transmitted by the filter from the glass at $T^{\circ}\text{K}$, and (curve *B*) the energy

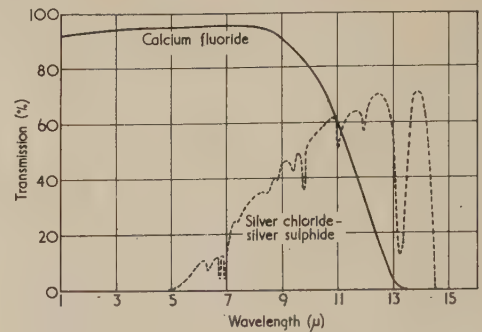


Fig. 9. Spectral transmission of silver chloride-silver sulphide filter and 2 mm thick sample calcium fluoride

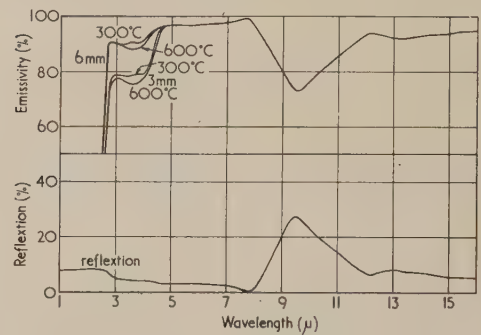


Fig. 10. Spectral reflexion and spectral emissivity of 6 mm polished plate glass

from a black body at the same temperature. The total energy transmitted by the filter from the glass and the black body is given by the area under curves *A* and *B* respectively. The ratio of the area under curve *A* to that under curve *B* gives the correction factor (equivalent emissivity) by which the response of the thermopile to the energy emitted from the black body must be multiplied, in order to obtain the response to the energy emitted normally from the surface of glass at the same temperature. The equivalent emissivity of the glass obtained in this way, at various temperatures, is shown in Fig. 11.

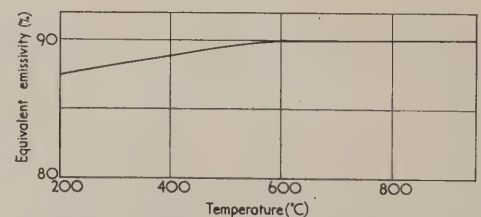


Fig. 11. Equivalent emissivity of plate glass in conjunction with silver chloride silver sulphide-calcium fluoride filter

To obtain the correction factor for the thermopile employing the lead sulphide-fused silica filter, let:

$\epsilon_{\lambda T}$ = spectral hemispherical emissive power at wavelength λ of a black-body temperature $T^{\circ}\text{K}$.

$E_{\lambda d}$ = spectral emissive power at wavelength λ of glass

thickness d cm having a surface temperature T° K and a parabolic temperature gradient giving a centre temperature T_M° K.

τ_λ = spectral transmission of the lead sulphide-fused silica filter at wavelength λ ,

then:

- (iii) the energy of wavelength λ emitted by the black-body temperature T° K and transmitted by the filter equals $\epsilon_{\lambda T} \tau_\lambda / \pi$;
- (iv) the energy emitted by the glass thickness d cm surface temperature T° K and centre temperature T_M° K equals $(\epsilon_{\lambda T} \tau_\lambda E_{\lambda d}'' / \pi)$. The equivalent spectral emissivity of the glass within the transmission range of the filter is then calculated in exactly the same way as for the surface temperature pyrometer.

The equivalent emissivities of flat glass 6 and 3 mm thick, having surface temperatures within the range 300 to 1000°C and parabolic temperature distributions within the glass giving centre line temperatures of 25, 50, 100 and 150°C greater than that of the surface, are shown in Figs. 12 and 13.

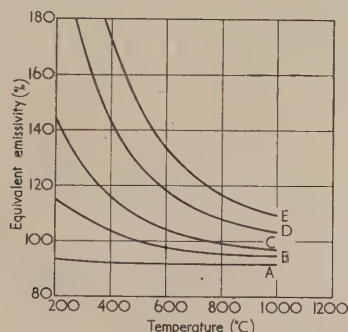


Fig. 12. Equivalent emissivity of 6 mm plate glass in conjunction with lead sulphide-fused silica filters

Curve A, constant temperature; curve B, parabolic temperature gradient, 25°C centre temperature; curve C, parabolic temperature gradient, 50°C centre temperature; curve D, parabolic temperature gradient, 100°C centre temperature; curve E, parabolic temperature gradient, 150°C centre temperature

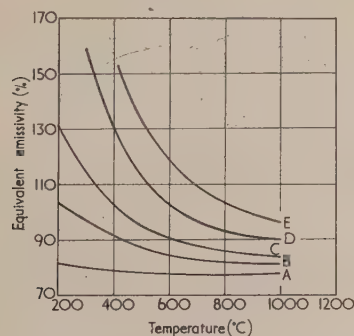


Fig. 13. Equivalent emissivity of 3 mm plate glass in conjunction with lead sulphide-fused silica filters

Curve A, constant temperature; curve B, parabolic temperature gradient, 25°C centre temperature; curve C, parabolic temperature gradient, 50°C centre temperature; curve D, parabolic temperature gradient, 100°C centre temperature; curve E, parabolic temperature gradient, 150°C centre temperature

The black body and corrected calibration curves of the two thermopiles for 6 mm thick flat glass are shown in Fig. 14.

To measure the surface and centre temperatures of the glass, the pyrometer is sighted on the surface of the glass and each thermopile connected to a separate recording potentiometer having a full-scale response time of one second. The output of the surface temperature thermopile is then read from the corresponding recorder (say 600°C) and, having measured the thickness of the glass (say 6 mm), the temperature at the centre of the glass is obtained from Fig. 14 by locating the measured surface temperature on the X-axis, and reading off on the Y-axis the centre line temperature (650°C) corresponding to the output (1.45 mV) recorded by the temperature difference thermopile.

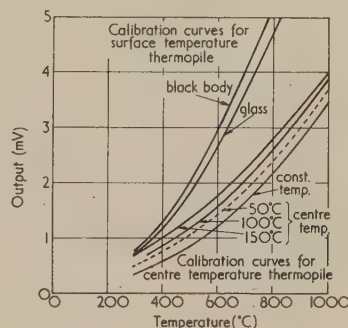


Fig. 14. Calibration curves of composite pyrometer

The calibration may be checked by sighting the pyrometer on a sheet of glass as it is rapidly withdrawn from a furnace, the glass having been allowed to remain in the furnace long enough for it to attain a constant temperature throughout its thickness. If the calibration is correct then both thermopiles will record the same temperature.

Dependence of the calibration on α_λ

In deriving the spectral emissive power for the glass, a different value of α_λ is used for flat glass having surface temperatures within the range 200 to 400°C, compared with that used in the case of flat glass having surface temperatures within the range 500 to 1000°C. Whilst the values of α_λ chosen are correct for surface temperatures of 300 and 600°C respectively and for a constant temperature throughout the glass, they are certainly not correct for glass having other surface temperatures and temperature distributions within

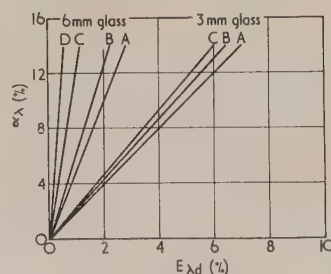


Fig. 15. Dependence of $E_{\lambda d}'''$ for 3 and 6 mm thick glass on α_λ . Curve A, constant temperature; curve B, 25°C parabolic temperature gradient; curve C, 100°C parabolic temperature gradient; curve D, 150°C parabolic temperature gradient

the glass. However, since α_λ does not change by more than 5% from the chosen values (Fig. 2) within each temperature range, it is seen from Fig. 15 that the maximum error in $E'_{\lambda d}$, and hence in the calibration of the temperature difference thermopile for the glass chosen, is less than 0.5% for 6 mm thick glass and less than 2% for 3 mm thick glass. For glass having a constant temperature throughout its thickness, a change in α_λ of 5% produces a change in $E'_{\lambda d}$ of 1%.

Therefore, unless the change in α_λ is taken into account, in the calibration, an error of measurement of not greater than 0.5% in the centre temperature can be expected for 6 mm thick glass and of not greater than 2% for 3 mm thick glass.

Applications

One application of the pyrometer is in the study of the temperature difference set-up between the surface and the central regions of the glass during the forced cooling of the surface in the toughening process. These temperature differences have been calculated by Gardon⁽⁸⁾ in his theoretical treatment of the temperature distributions in glass plates undergoing heat treatment.

Another application is the study of the temperature of flat glass, both during the formation of the ribbon and the subsequent annealing process.

Acknowledgements

The authors wish to thank Mr. W. J. R. Merren, Group Director of Research, Messrs. Pilkington Bros. Ltd. for permission to publish the paper, Mr. F. J. Grove who supplied the information on the spectral absorption and reflexion of the glass, Mr. K. Harrison who programmed the computer and Mr. K. J. B. Wolfe, Head of the Triplex Fundamental Research Laboratories, who supplied the necessary facilities for checking the calibration of the pyrometer and its application to the measurement of the temperature of glass during the toughening process.

References

- (1) PARKER, R. C., and MARSHALL, P. R. *Proc. Instn Mech. Engrs*, **158**, p. 209 (1948).
- (2) DRURY, M. D., PERRY, K. P., and LAND, T. *J. Iron Steel Inst.*, **169**, p. 245 (1951).
- (3) HARRISON, T. R. and WANAMAKER, W. H. *Temperature: Its Measurement and Control* (New York: Rheinhold Publishing Corporation, 1941).
- (4) MCMAHON, H. O. *J. Opt. Soc. Amer.*, **40**, pp. 376-80 (1950).
- (5) DRUDE, P. *Lehrbuch, Der Optik*, p. 494 (Leipzig: S. Hirzel, 1912).
- (6) GARDON, R. *J. Amer. Ceram. Soc.*, **39**, pp. 278-87 (1956).
- (7) BEATTIE, J. R. *Trans Soc. Glass Tech.*, **38**, pp. 457-69 (1954).
- (8) GARDON, R. *J. Amer. Ceram. Soc.*, **41**, pp. 200-209 (1958).

Appendix

Calculation of the spectral normal emissive power of flat glass

Consider a layer of glass thickness dx , distance x cm below the surface (Fig. 16). Let the temperature distribution

through the glass from O to d be a function of x such that, if $T_0^\circ\text{K}$ and $T_M^\circ\text{K}$ are the temperatures of the surface and centre of the glass respectively, and $T^\circ\text{K}$ the temperature at any other point within the glass, then:

- for $0 \leq x \leq d$ $T = T_0$; constant temperature distribution
- for $0 \leq x \leq d/2$ $T = T_0 + ax$; linear temperature distribution
for $d/2 \leq x \leq d$ $T = T_M - a(x - d/2)$
- for $0 \leq x \leq d$ $T = T_0 + ax^2 + bx$; parabolic temperature distribution.

Let α_λ be the spectral absorption coefficient of the glass characteristic of wavelength λ and n the refractive index of the material. Then the spectral volume emissive power $j_{\lambda T}$, that is the energy emitted at a given temperature by unit volume of the material into unit solid angle, is given by

$$j_{\lambda T} = (\alpha_\lambda n^2 / \pi) \epsilon_{\lambda T} \quad (3)$$

where $\epsilon_{\lambda T} = \frac{c_1 \exp(-c_2/\lambda T)}{\lambda^5}$ and is the hemispherical

emissive power of a black body, temperature $T^\circ\text{K}$. The energy emitted normally to its surface by the element of material thickness dx , therefore, is $j_{\lambda T} dx$.

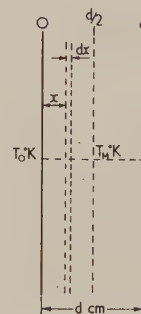


Fig. 16. Section through flat glass

Hence the energy arriving at the front surface of the glass

$$I_{\lambda T} = j_{\lambda T} \exp(-\alpha_\lambda x) dx \quad (4)$$

where $\exp(-\alpha_\lambda x)$ equals the spectral transmission of the glass from O to x cm. The energy emitted from the surface of the glass into the atmosphere, therefore, is

$$I_{\lambda T}(1 - R_\lambda)/n^2 \quad (5)$$

where R_λ equals the spectral reflexion of the glass at the surface. Therefore, the energy from the total thickness O to d cm arriving at the surface and emitted into the atmosphere is given by

$$\int_0^d \frac{I_{\lambda T}}{n^2} (1 - R_\lambda) dx \quad (6)$$

Similarly, the energy arriving at the rear surface of the glass and reflected back to the front surface of the glass and entering the atmosphere is given by

$$R_\lambda \exp(-\alpha_\lambda d) \int_0^d \frac{I_{\lambda T}}{n^2} (1 - R_\lambda) dx \quad (7)$$

Therefore the total energy emitted normal to the surface of the glass is

$$\begin{aligned}
 E_{\lambda d} &= \int_0^d \frac{I_{\lambda T}}{n^2} (1 - R_{\lambda}) dx + R_{\lambda} \exp(-\alpha_{\lambda} d) \int_0^d \frac{I_{\lambda T}}{n^2} (1 - R_{\lambda}) dx \\
 &= (1 - R_{\lambda}) \{1 + R_{\lambda} \exp(-\alpha_{\lambda} d)\} \int_0^d I_{\lambda T} dx \\
 &= (1 - R_{\lambda}) \{1 + R_{\lambda} \exp(-\alpha_{\lambda} d)\} \frac{\alpha_{\lambda} c_1}{\pi \lambda^5} \times \\
 &\quad \times \int_0^d \exp\left(\frac{-c_2}{\lambda T}\right) \exp(-\alpha_{\lambda} x) dx \quad (8)
 \end{aligned}$$

The spectral normal emissive powers for the three temperature distributions considered, therefore, are given by:

(a) *Constant temperature.* Substituting $T = T_0$ in equation (8)

$$\begin{aligned}
 E'_{\lambda d} &= (1 - R_{\lambda}) \{1 + R_{\lambda} \exp(-\alpha_{\lambda} d)\} \frac{\alpha_{\lambda} c_1}{\pi \lambda^5} \times \\
 &\quad \times \int_0^d \exp\left(\frac{-c_2}{\lambda T_0}\right) \exp(-\alpha_{\lambda} x) dx \\
 &= (1 - R_{\lambda}) \{1 + R_{\lambda} \exp(-\alpha_{\lambda} d)\} \frac{\epsilon_{\lambda T_0}}{\pi} \{1 - \exp(-\alpha_{\lambda} d)\} \quad (9)
 \end{aligned}$$

(b) *Linear temperature gradient.* Substituting $T = T_0 + ax$ for $0 \leq x \leq d/2$ and $T = T_M - a(x - d/2)$ for $d/2 \leq x \leq d$ in equation (8)

$$\begin{aligned}
 E''_{\lambda d} &= (1 - R_{\lambda}) \{1 + R_{\lambda} \exp(-\alpha_{\lambda} d)\} \frac{\alpha_{\lambda} c_1}{\pi \lambda^5} \times \\
 &\quad \times \left\{ \int_0^{d/2} \exp\left\{-\frac{c_2}{\lambda(T_0 + ax)}\right\} \exp(-\alpha_{\lambda} x) dx + \right. \\
 &\quad \left. + \exp\left(\frac{-\alpha_{\lambda} d}{2}\right) \int_{d/2}^d \exp\left[-\frac{c_2}{\lambda\left(T_M - a\left(x - \frac{d}{2}\right)\right)}\right] \right. \\
 &\quad \left. \exp\left\{-\alpha_{\lambda}\left(x - \frac{d}{2}\right)\right\} dx \right\} \\
 &= (1 - R_{\lambda}) \{1 + R_{\lambda} \exp(-\alpha_{\lambda} d)\} \frac{\alpha_{\lambda} c_1}{\pi \lambda^5} \times \\
 &\quad \times \left\{ \int_0^{d/2} \exp\left[-\frac{c_2}{\lambda T_0} \left(1 + \frac{ax}{T_0}\right)\right] \exp(-\alpha_{\lambda} x) dx + \right. \\
 &\quad \left. + \exp\left(\frac{-\alpha_{\lambda} d}{2}\right) \int_{d/2}^d \exp\left[-\frac{c_2}{\lambda T_M} \left(1 - \frac{a(x - d/2)}{T_M}\right)\right] \right. \\
 &\quad \left. \exp\left\{-\alpha_{\lambda}\left(x - \frac{d}{2}\right)\right\} dx \right\}
 \end{aligned}$$

$$\begin{aligned}
 &= (1 - R_{\lambda}) \{1 + R_{\lambda} \exp(-\alpha_{\lambda} d)\} \frac{\alpha_{\lambda} c_1}{\pi \lambda^5} \times \\
 &\quad \times \left\{ \int_0^{d/2} \exp\left\{\frac{-c_2}{\lambda T_0} \left(1 - \frac{ax}{T_0}\right)\right\} \exp(-\alpha_{\lambda} x) dx + \right. \\
 &\quad \left. + \exp\left(\frac{-\alpha_{\lambda} d}{2}\right) \int_{d/2}^d \exp\left[\frac{-c_2}{\lambda T_M} \left(1 + a \frac{(x - d/2)}{T_M}\right)\right] \right. \\
 &\quad \left. \exp\left\{-\alpha_{\lambda}\left(x - \frac{d}{2}\right)\right\} dx \right\} \\
 &= (1 - R_{\lambda}) \{1 + R_{\lambda} \exp(-\alpha_{\lambda} d)\} \frac{\alpha_{\lambda} c_1}{\pi \lambda^5} \times \\
 &\quad \times \left[\exp\left(\frac{-c_2}{\lambda T_0}\right) \int_0^{d/2} \exp\left\{x \left(\frac{ac_2}{\lambda T_0^2} - \alpha_{\lambda}\right)\right\} dx + \right. \\
 &\quad \left. + \exp\left(\frac{-c_2}{\lambda T_M}\right) \exp\left(\frac{ac_2 d}{2\lambda T_M}\right) \times \right. \\
 &\quad \left. \times \int_{d/2}^d \exp\left\{-x \left(\frac{ac_2}{\lambda T_M^2} + \alpha_{\lambda}\right)\right\} dx \right] \\
 &= (1 - R_{\lambda}) \{1 + R_{\lambda} \exp(-\alpha_{\lambda} d)\} \frac{\alpha_{\lambda} c_1}{\pi \lambda^5} \times \\
 &\quad \times \left\{ \frac{\exp(-c_2/\lambda T_0)}{(ac_2/\lambda T_0^2) - \alpha_{\lambda}} \left\{ \exp\left(\frac{ac_2}{2\lambda T_0^2} - \alpha_{\lambda}\right) - 1 \right\} + \right. \\
 &\quad \left. + \frac{\exp(-c_2/\lambda T_M) \exp(ac_2 d/2\lambda T_M^2)}{-(ac_2/\lambda T_M^2) + \alpha_{\lambda}} \times \right. \\
 &\quad \left. \times \left[\exp\left\{-d \left(\frac{ac_2}{\lambda T_M^2} + \alpha_{\lambda}\right)\right\} - \right. \right. \\
 &\quad \left. \left. - \exp\left\{-\frac{d}{2} \left(\frac{ac_2}{\lambda T_M^2} + \alpha_{\lambda}\right)\right\} \right] \right\} \\
 &= \frac{(1 - R_{\lambda}) \{1 + R_{\lambda} \exp(-\alpha_{\lambda} d)\}}{\pi} \times \\
 &\quad \times \left[\frac{\lambda T_0}{1 - (ac_2/\alpha_{\lambda} \lambda T_0^2)} \left\{ 1 - \exp\left(\frac{dac_2}{2\lambda T_0^2}\right) \exp(-\alpha_{\lambda} d/2) \right\} + \right. \\
 &\quad \left. + \frac{\epsilon_{\lambda TM} \exp(-\alpha_{\lambda} d/2)}{1 + (ac_2/\alpha_{\lambda} \lambda T_M^2)} \right. \\
 &\quad \left. \left\{ 1 - \exp\left(\frac{-dac_2}{2\lambda T_M^2}\right) \exp(-\alpha_{\lambda} d/2) \right\} \right] \quad (10)
 \end{aligned}$$

(c) *Parabolic temperature gradient.* Substituting $T = T_0 + ax^2 + bx$ in equation (8)

$$\begin{aligned}
 E'''_{\lambda d} &= (1 - R_{\lambda}) \{1 + R_{\lambda} \exp(-\alpha_{\lambda} d)\} \frac{\alpha_{\lambda} c_1}{\pi \lambda^5} \times \\
 &\quad \times \int_0^d \exp\{-c_2/\lambda(T_0 + ax^2 + bx)\} \exp(-\alpha_{\lambda} x) dx \quad (11)
 \end{aligned}$$

This equation has been solved numerically on the Ferranti Pegasus Computer.

Reflexion electron microscopy using diffracted electrons

by J. S. HALLIDAY, Ph.D., A.Inst.P., and R. C. NEWMAN, Ph.D., A.R.C.S., Research Laboratory, Associated Electrical Industries, Aldermaston Court, Aldermaston, Berkshire

[Paper first received 24 September, and in final form 14 December, 1959]

Abstract

Crystalline surfaces have been examined in the reflexion electron microscope with the angles of illumination and viewing adjusted so that diffracted electrons contributed to the images. In this way, the size and distribution of the diffracting regions have been determined. A resolution of 80 Å has been obtained, which is at least four times better than that obtained in normal reflexion micrographs.

Introduction

THE surfaces of solids and of thin coatings, deposits and growths on such surfaces are often examined by electron diffraction, using the reflexion technique. Analysis of the patterns gives (i) the crystallographic structure, and hence in many cases the chemical composition, of the surfaces;^(1, 2) (ii) the size of the diffracting regions, provided that they are smaller than 200 Å; and (iii) in the case of single-crystal substrates, the relative orientations of the surface deposits. However, the distribution of these deposits and the proportion of the surface which contributes to the diffraction patterns cannot be derived, and deductions about the general surface topography can only be made on relatively few occasions.

The general surface topography may be studied in several ways, one of which is by reflexion electron microscopy. In this instance, the specimen surface is illuminated by an electron beam, the glancing angle θ_1 being small as in electron-diffraction experiments, and the electrons that are scattered through any chosen angle β (defined by the tilt of the electron gun and the position of the aperture in the objective lens of the microscope) are used to form an image of the surface. In general, β is arbitrary and usually greater than 4 deg., and hence inelastically scattered electrons which have lost an appreciable amount of energy are focused to form the image. The resolution is consequently limited by chromatic aberrations in the objective lens and the smallest resolvable object distance δ is given by

$$\delta = C_c \alpha (\Delta V/V) \quad (1)$$

where C_c is the chromatic-aberration constant of the objective lens, α is the semi-angular aperture of that lens and $(\Delta V/V)$ is the fractional energy spread of the scattered electrons. Under optimum conditions, δ is about 400 Å when β is less than 6 deg.⁽³⁾

In principle, it would seem that the distribution of the crystalline components on a surface and the proportion of a surface which contributes towards a diffraction pattern could be obtained from a study of specimens in the reflexion electron microscope, if the angle β were set equal to the angles of deviation of electrons diffracted by the surface components. This possibility was first suggested by Haine

and Hirst⁽³⁾ who observed bright spots in some images and attributed them to electrons diffracted through the objective aperture by suitably oriented crystallites. Subsequently, it has been realized that the energy spread of such diffracted electrons should be much smaller than that of inelastically scattered electrons, and hence the resolution of images formed under these circumstances should be limited by spherical rather than chromatic aberration, as in transmission-electron microscopy.

The present experiments were therefore made in order to assess the potentialities of reflexion electron microscopy using diffraction conditions. The specimens examined were etched single crystals of germanium and metallic-iron deposits on single crystals of silicon; these specimens were selected because they produced high-contrast reflexion diffraction patterns.

Experimental

The initial experiments were made with an electron microscope, type EM3, by Metropolitan-Vickers,⁽⁴⁾ modified for reflexion working.⁽³⁾ The illuminating system was tilted mechanically and the amount of tilt β measured with a dial gauge. The absolute and relative errors in β were 0.05 and 0.02 deg. respectively.

The specimens should be illuminated with a parallel beam of electrons for optimum diffraction conditions. In order to approximate to these conditions in a reproducible manner, the condenser-lens current was switched off during the experiments. The semi-angle of the incident cone of electrons was then 0.138 deg. (computed from instrumental dimensions, see Table 1) and the minor axis of the elliptical area of specimen illuminated was 1100 μ .

In this microscope, the objective aperture can be raised almost up to the plane of the specimen, and experiments were carried out with the aperture in this upper position and in its normal position. The aperture could not be raised sufficiently to permit the electron diffraction pattern to be observed in the microscope.

Table 1. Some dimensions of the EM3 electron microscope

Distance from:

Gun filament to condenser aperture	11.4 cm
Condenser aperture to specimen	11.4 cm
Specimen to objective aperture in its lower position	1.27 cm
Specimen to photographic plate	61 cm
Second projector lens to photographic plate	30.5 cm
Objective aperture diameter	50 μ
Condenser aperture diameter	550 μ

Some high-resolution micrographs were obtained using a prototype of the Metropolitan-Vickers EM6 electron

microscope.⁽⁵⁾ In this instrument the illuminating beam is tilted electromagnetically⁽⁶⁾ and the following method was devised for setting up the microscope to obtain diffraction micrographs. The instrument was alined for transmission working, and a diffraction pattern obtained from a thin film put in at the same level as a reflexion specimen. The objective aperture was then inserted, so that the unscattered central beam of electrons was transmitted, and the electron beam gradually tilted until part of each diffraction ring passed through the aperture. The energizing current through the deflector coils was thus correlated with the d -spacings.

The specimen holder was the prototype of that fitted to the EM6 electron microscope and the following independent movements of the specimen were possible:

- (1) in and out of the beam;
- (2) translation across the beam;
- (3) azimuth;
- (4) tilt with respect to the axis of the imaging section of the microscope.

This tilt θ_2 could be set anywhere in the range 0 to 14 deg. and relative changes of one minute of arc could be made. For a given value β of the gun tilt, movement (4) obviously alters θ_2 , and the glancing angle θ_1 of the illuminating electron beam simultaneously.

Specimen preparation

The surfaces of the single-crystal germanium specimens were cut to within 1 deg. of the (100) lattice plane. The specimens were then ground on 600-grade carborundum paper and afterwards etched lightly in CP4,* to remove the worked surface layer. They were then given a WAg etch†⁽⁷⁾ which produces small-scale facets on the surface (some silver is deposited, but this is easily removed). The size of the facets could be varied by adjusting the period of etching, which was usually between five and ten seconds.

The silicon specimens were cut to the (111) lattice plane and etched in a mixture of 50% hydrofluoric acid and 50% nitric acid, followed by a short etch in a boiling 10% solution of potassium hydroxide. It was found that iron, a specific trace impurity in the potassium hydroxide, was deposited during the second etching.⁽⁸⁾

Results

Examination of specimens by electron diffraction. The specimens were first examined in a diffraction camera to ensure that clean surfaces had been produced by the etching treatments. A typical pattern from a germanium crystal, examined along the [011] azimuth, is shown in Fig. 1. The Kikuchi line pattern indicates the high perfection of the crystal. The fine spikes which extend from each spot presumably result from refraction of electrons at well-developed facets.

It is worth noting that "forbidden" reflexions for the diamond lattice, where $(h + k + l)$ is equal to $(4n - 2)$ with n an integer, appear as the result of dynamical scattering when reflexions for which h , k and l are all odd are also present (see also Lang⁽⁹⁾); "forbidden" reflexions were not observed at the [001] azimuth. In the experiments to be

* The recipe for CP4 is as follows: 25 ml. nitric acid, 15 ml. hydrofluoric acid, 15 ml. acetic acid, 0.2 ml. bromine.

† The recipe for the Westinghouse silver etch is as follows: 20 ml. hydrofluoric acid, 10 ml. nitric acid and 20 ml. of a 5% silver nitrate solution in water.

described, the specimen was set at a random azimuth, where the number of intense reflexions was very small and the "forbidden" reflexions were very weak. The diffraction pattern obtained from the etched silicon crystals showed a spot pattern from the silicon and a high-contrast ring pattern from the randomly oriented iron.⁽⁸⁾

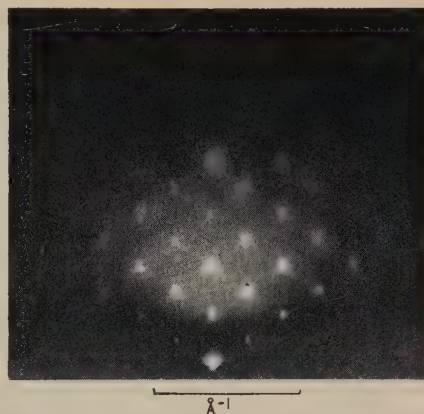


Fig. 1. Reflexion electron diffraction pattern of etched (100) germanium single-crystal surface, [011] azimuth

Experiments in the EM3 with germanium crystals. The specimen tilt θ_2 was first adjusted until the specimen face was

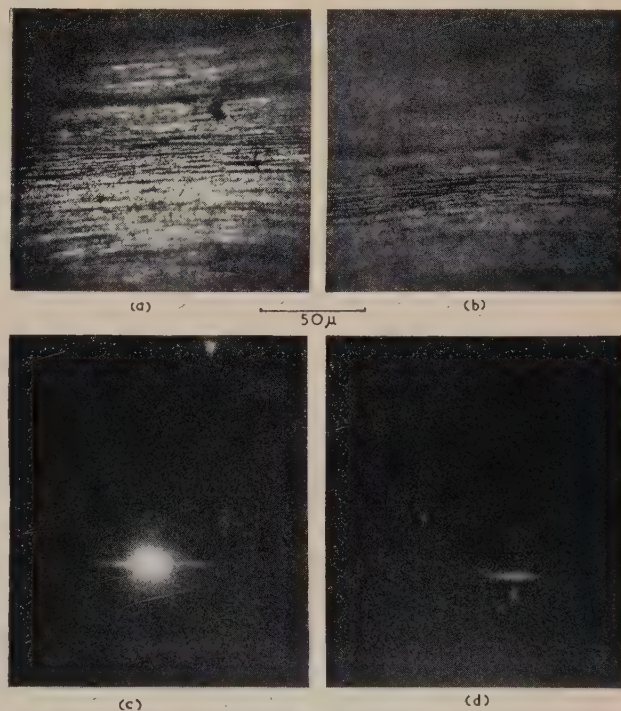


Fig. 2. Reflexion electron micrographs and electron diffraction patterns obtained with etched germanium single crystal

Electron micrographs

- (a) β and θ_2 set to observe electrons diffracted through 2θ (400),
- (b) same area as in (a) but with θ_2 reduced

Diffraction patterns

- (c) and (d) correspond to micrographs (a) and (b) respectively

parallel to the electron optical axis ($\theta_2 = 0$) and the gun tilt β was made equal to $2\theta(400)$, where $\theta(400)$ was the calculated Bragg angle for the germanium (400) reflexion (the operating voltage was assumed to be 50 kV). θ_2 was then gradually increased until a bright circular region appeared in the image. The intensity of this region was made as high as possible by successive fine adjustments of β and θ_2 . The excess brightness may be judged by comparison of Figs. 2(a) and 2(b), of the same area of the specimen. For Fig. 2(a), β and θ_2 were set for maximum brightness and for Fig. 2(b), θ_2 was slightly below the optimum setting. The corresponding diffraction patterns are shown in Figs. 2(c) and 2(d). Subsequently, β was doubled and trebled and θ_2 increased until bright regions were again observed. The values of β obtained under conditions for optimum brightness are shown in Table 2, together with calculated values of $2\theta(400)$, $2\theta(800)$ and $2\theta(1200)$. The results show conclusively that the bright regions are due to diffraction effects and indicate that the accelerating potential was between 47.5 and 50 kV.

On many occasions θ_2 was not exactly equal to $\beta/2$. The reason is that the measurements of θ_2 were made with respect to the crystal surface and not to the (100) planes. However, when a bright region corresponding to the (400) reflexion had been obtained and the conditions reset for the (800) reflexion, the increase in θ_2 was half the increase in β .

Table 2. Theoretical and experimental gun tilts β expected for diffraction conditions (given in degrees)

	kV	$\lambda \text{ \AA}$	$\beta(400)$	$\beta(800)$	$\beta(1200)$
Theoretical	47.5	0.0548	2.22	4.45	6.67
($a_0 \text{ Ge} = 5.646 \text{ \AA}$)	50.0	0.0534	2.17	4.33	6.50
Experimental	—	—	2.20 ± 0.10	4.43 ± 0.10	6.50 ± 0.08

The diameter of the bright region in Fig. 2(a) is about 100μ , which is considerably smaller than the illuminated area of specimen. The position of the bright region in the image was not affected by lateral displacement of the gun assembly but followed any translational movement of the objective aperture. It is concluded, therefore, that the

diffracted electrons to emerge at all angles between $(\theta - \Delta\theta)$ and $(\theta + \Delta\theta)$, where $\Delta\theta = \lambda/2e$ and e is the depth of penetration normal to the diffracting planes. This effect is illustrated in Fig. 3. This explanation was confirmed by raising the aperture to its upper position, when the diameter of the bright zone gradually diminished to about 60μ . The value of $\Delta\theta$ was computed from the dimensions of the apparatus and the diameter of the bright zone with the aperture in the lower position and, with λ equal to 0.055 \AA , e was found to be 14 \AA .

Subsequently, the range of specimen tilt values $\theta_2 \pm \Delta\theta_2$ for which the bright region remained visible in the area of surface under observation was determined, β being kept at the optimum value. Average results, obtained at different parts of the same specimen, are summarized in Table 3.

Table 3. Experimental values of tolerance in specimen tilt $\Delta\theta_2$ (given in degrees)

$\Delta\theta_2(400)$	$\Delta\theta_2(800)$	$\Delta\theta_2(1200)$
$\pm(0.40 \pm 0.10)$	$\pm(0.21 \pm 0.04)$	± 0.08 (one result)

The finite tolerance in the value of θ_2 is due to the limited extent e' of the individual diffractive asperities in the direction of the electron beam. $\Delta\theta_2$ then equals d/e' , where d is the interplanar spacing corresponding to the value β (see Fig. 4).

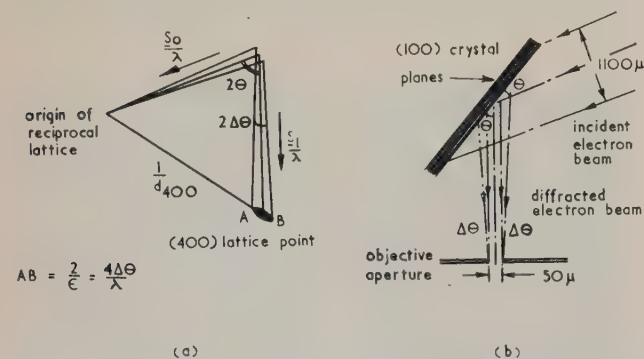


Fig. 3. Schematic representation of effect of limited electron penetration normal to specimen surface e on angular tolerance of the diffracted electrons $\Delta\theta$, and hence on size of bright zone

(a) reciprocal space
(b) real space

The relationship between $\Delta\theta_2$ and d is confirmed by the results shown in Table 3. Substantially similar values of $\Delta\theta_2$ were obtained when the specimen azimuth was changed by 90 deg. When very small viewing angles were encountered

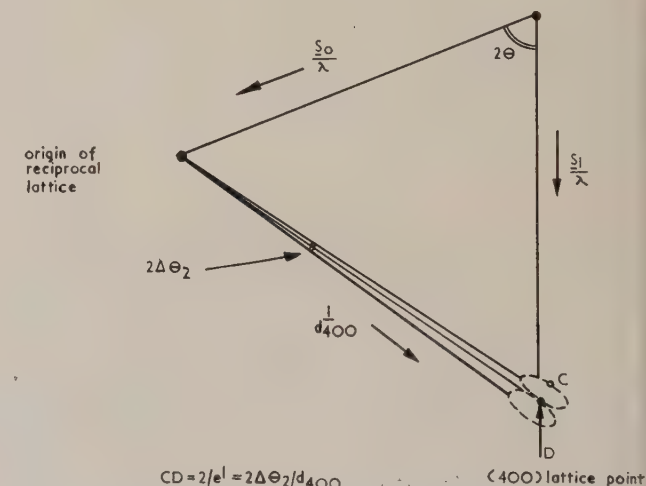


Fig. 4. Schematic reciprocal space diagram showing effect of limited extent of diffracting asperities e' on the range of angles of specimen tilt for which diffraction effects are observed

(because of non-parallelism of the crystal surface and crystal planes) the intensity of the inelastically scattered electrons which passed through the aperture rapidly increased as described by Haine and Hirst,⁽³⁾ and thus it was not always possible to obtain reliable estimates of $\Delta\theta_2$.

In one region of a particular specimen the value of $\Delta\theta_2$ for the (400) reflexion was $\pm(0.22 \pm 0.02)$ degrees, which gives a value for e' of (370 ± 34) Å. The same area of the specimen was then examined at a higher magnification, so that the individual diffracting areas in the bright region were resolved. Direct measurements of the micrographs showed that the mean diameter of these areas was (403 ± 46) Å, which is in reasonable agreement with the estimated value above.

Experiments in the EM6. The single crystals used in these experiments were etched for a short period only to produce the smallest possible diffracting asperities. These specimens were examined at an instrumental magnification of 10000 times.

When diffraction conditions were obtained, it was observed that the diffracting asperities rapidly became dim, because of the growth of contamination on the specimen surface. The following procedure was adopted to minimize this effect. The instrument and specimen were adjusted until some diffracting asperities were in focus and the specimen was then translated across the beam to expose a clean area of surface which was immediately photographed.

Fig. 5 shows many focused diffracting areas about 100 Å across on an etched germanium surface. In the original negative, two spots are distinctly resolved at A (Fig. 5),

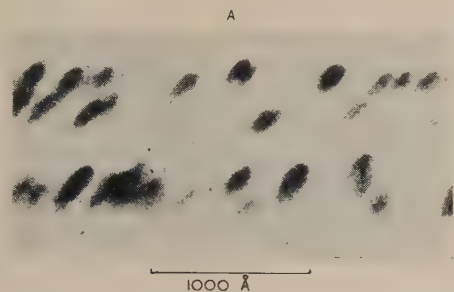


Fig. 5. High-magnification reflexion micrograph showing small individual diffracting asperities on etched germanium surface. β and θ_2 set for (400) diffraction effects (reversed print)

within a distance of about 160 Å, and therefore it follows that the resolution is at least as good as 80 Å. When the iron deposits on single crystal silicon specimens were examined, the iron was found to be in the form of discrete particles about 2000 Å across and distributed at random over the surface.

Discussion

The results show that the asperities on solid surfaces which contribute to reflexion electron-diffraction patterns can be revealed by examining the surfaces in a reflexion electron microscope, when the angles are adjusted to satisfy the Bragg condition. This effect was first observed by Haine and Hirst⁽³⁾ who used polycrystalline specimens whereas the present experiments have been mainly concerned with single crystals. The technique is more valuable for the latter type of specimen since all diffracting regions can be observed simultaneously. With polycrystalline samples only those crystallites which diffract electrons in a plane normal to the specimen surface can be observed, unless means are provided for tilting the specimen about an axis which is parallel to the incident electron beam.

It has been shown that the approximate size of the diffracting asperities can be measured, even when the magnification is so low that the individual asperities cannot be resolved. Under these conditions the average size is estimated from the range of gun and specimen tilts for which diffraction still occurs for a given crystal reflexion. These small angular tolerances are interpreted in terms of the finite extent of the reciprocal lattice points and it has been shown that such estimates agree with direct measurements taken from high magnification micrographs. An advantage of high-magnification micrographs is that the size of large diffracting crystallites, greater than 200 Å, say, can be measured, as in the instance of the iron deposits on silicon. This is not normally possible from electron diffraction patterns since such large crystallites cause negligible broadening of the diffracted beams. It was not possible, however, to determine the detailed shape of small individual diffracting asperities, which had been indicated by fine structure in the electron diffraction patterns.

A resolution of 80 Å has been obtained, which is about four times better than that observed in normal reflexion electron micrographs, but is not as good as that obtained with transmission conditions. One reason for the lack of a better resolution is that much plural scattering occurs in reflexion experiments and thus many electrons which emerge at the Bragg angle will have lost energy as a result of inelastic collisions. Therefore, the resolution is still likely to be limited by chromatic aberration, although to a lesser degree than in normal reflexion microscopy.

The detection of very small diffracting regions would be exceedingly difficult even if a higher resolution could be obtained, because of their inherently low contrast; the number of electrons diffracted by such a region is small, being proportional to its volume. Furthermore, these electrons would be dispersed over a significantly larger angular range than that accepted by the objective aperture. Because of the latter effect, cleavage faces of single crystals could only be examined if high-order reflexions were used, and if the crystal were set at an azimuth well away from a principal crystallographic direction.

A technical difficulty encountered was the formation of carbon contamination on the specimen surfaces.^(10, 11) This caused a lowering of contrast and possibly led to a diminished resolution, although these effects were minimized by photographing areas which had not previously been examined. In principle, contamination can be eliminated if, (a) the specimen is surrounded by a cold trap,⁽¹⁰⁾ (b) heated to about 200° C,⁽¹⁰⁾ (c) bombarded with ions,⁽¹²⁾ or (d) exposed to a local region of higher oxygen pressure.⁽¹³⁾

Acknowledgements

The authors wish to thank Mr. G. Rickards for his assistance in the operation of the EM6 electron microscope. Thanks are also due to Dr. T. E. Allibone, Director of the Research Laboratory, Associated Electrical Industries, for permission to publish this paper.

References

- (1) THOMSON, G. P., and COCHRANE, W. *Theory and Practice of Electron Diffraction* (London: Macmillan, 1939).
- (2) PINSKER, Z. G. *Electron Diffraction* (London: Butterworths, 1953).
- (3) HAINE, M. E., and HIRST, W. *Brit. J. Appl. Phys.*, **4**, p. 239 (1953).

- (4) HAINE, M. E., PAGE, R. S., and GARFITT, R. G. *J. Appl. Phys.*, **21**, p. 173 (1950).
- (5) HAINE, M. E., and PAGE, R. S. *Proc. 1st Regional Conference on Electron Microscopy in Europe (Stockholm)*, p. 32 (1956).
- (6) HAINE, M. E., AGAR, A. W., and MULVEY, T. *J. Sci. Instrum.*, **45**, p. 357 (1958).
- (7) WYNNE, R. H., and GOLDBERG, C. *J. Metals*, **5**, p. 436 (1953).
- (8) HOLMES, P. J., and NEWMAN, R. C. *Proc. Inst. Elect. Engrs*, **106 B**, Suppl. 15, p. 287 (1959).
- (9) LANG, A. R. *Acta Cryst.*, **10**, p. 252 (1957).
- (10) ENNOS, A. E. *Brit. J. Appl. Phys.*, **4**, p. 101 (1953).
- (11) ENNOS, A. E. *Brit. J. Appl. Phys.*, **5**, p. 27 (1954).
- (12) FERT, CH. *C.R. Acad. Sci. (Paris)*, **238**, p. 333 (1954).
- (13) HEIDE, H. G. *Proc. 4th International Conference on Electron Microscopy (Berlin)*, Paper No. 11.09 (1958).

X-ray microbeam study of deformation bands in aluminium

by D. LEWIS, Ph.D., M.Sc., A.Inst.P., A.I.M., Crystallography Department, Battersea College of Technology, London

[Paper first received 2 June, and in final form 10 August, 1959]

Abstract

An experiment has been devised to measure the relative contribution of plastic bending and mosaic structure to asterism formation. Adjacent X-ray microbeam photographs were taken across a broad deformation band in a crystal of aluminium and the total curvature (estimated from the asterisms) compared with that from a normal X-ray beam covering the same distance. It was shown that the asterism must be mostly due to fragmentation. Orientation determinations show that the raised portion of the band consists mainly of portions of the crystal that have not rotated in accordance with the theory of Taylor and Elam.⁽¹⁾

Introduction

WHEN a piece of metal containing large grains is cold-worked, the grains usually become crossed with bands called deformation bands (not to be confused with slip bands, which are finer). The bands may be a millimetre or more in width and are apparently produced in all cubic metals. According to Honeycombe,⁽²⁾ they may be observed in aluminium single crystals extended in tension after elongation by as little as 1%. Barrett⁽³⁾ considers that they consist of lamellar regions within which differing orientations have arisen as a result of slip.

The development of deformation bands is an important cause of asterisms in X-ray photographs. This was conclusively shown by Gay and Honeycombe⁽⁴⁾ using an X-ray microbeam technique, when asterisms were obtained only when the microbeam struck a band. However, the exact mechanism governing the relationship between the bands and the asterisms has never been clearly established. A theory of local curvature was put forward by Burgers⁽⁵⁾ [Fig. 1(a)], and this has been developed by other workers (for example, Goldschmidt,⁽⁶⁾ but Barrett⁽³⁾ has shown that microscopic variations in orientation will produce asterisms [Fig. 1(b)].

It is usually assumed in modern work that the major cause of asterism is plastic bending across the deformation band,⁽⁷⁾ although the existence of smaller misorientations has been shown by Honeycombe,⁽⁸⁾ Gay, Hirsch and Kelly⁽⁹⁾ and others.

In this work, it was decided to investigate the relative proportion of the two effects in causing the asterism by an experiment using both normal-size X-ray beams and micro-

beams. These microbeams were produced and located by the method described previously by Lewis⁽¹⁰⁾ in which the beams are produced by a fine-focus X-ray tube in combination with a pin-hole in platinum foil, and located by a microscopical method using a fluorescent single crystal and a long-working distance microscope objective.

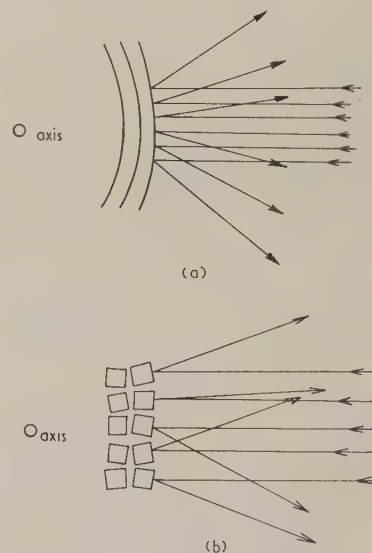


Fig. 1. Production of asterism (a) by lattice curvature, and (b) by mosaic structure

The idea behind the experiment is that if the asterism is caused by lattice curvature alone, as in Fig. 1(a), then in a succession of adjacent back-reflexion microbeam pictures the total angular curvature of the lattice will be equal to that obtained by adding the angular curvatures of each adjacent region. This should be equal to that obtained by straddling the area covered by the adjacent microbeam photographs with one normal-size X-ray beam.

On the other hand, if the asterism is caused by fragmentation of the lattice into a mosaic structure, as in Fig. 1(b), then the sum of the apparent curvatures from the adjacent microbeam photographs will be far greater than that obtained from the normal-size X-ray beam straddling the region.

The length of the asterism may be used as a measure of the range of misorientation in the region, although there are

considerable limitations that may prevent a streak developing to its full extent—for example, the spectrum of the primary X-ray ends sharply at the short-wavelength limit, and of the long-wavelength end, the intensity may be very low. Intensity variations in the streak may be due to the absorption edge characteristics of the silver and bromine in the emulsion as well as to the distribution of diffracting material over the range of orientation. The absorption edge characteristics of the diffracting material also play a part in the intensity distribution.

Subject to these limitations (provided that the photographs are taken under the same conditions of voltage, exposure time, development, etc.) the length of the asterism may be taken as a measure of the range of misorientation of the material. The fact that a smaller asterism is associated with a smaller-diameter X-ray beam has already been observed by Calnan,⁽¹¹⁾ although with far larger beams than those used in this work.

Experimental

To obtain a suitable specimen for this experiment, some tensile specimens for the Hounsfield tensometer were carefully turned from spectroscopically pure aluminium rod. These specimens were electrolytically polished to remove the cold-worked layers and then annealed at 600° C for 12 hours to relieve the strain. They were then strained by 3% and annealed again at 600° C for 12 hours. Previous experiments had shown that this produced a grain size of approximately 1 cm. The specimens were then electrolytically polished again, deformed in tension by approximately 10% and then examined visually for deformation bands. Those specimens showing well-developed parallel bands were examined by normal-size X-ray beams and, in each case, large asterisms were obtained, thus confirming the observations of previous workers concerning the association of the two effects.

One specimen showing very broad deformation bands and giving large asterisms was examined using microbeams. More than twenty Laue pictures were taken to cover the region considered, and the angular deviation of each asterism streak was estimated by enlarging the photograph and using a standard Greninger chart.

The specimens were then mounted in a cold-setting plastic and carefully sectioned in the region examined. The specimens were then polished by the standard procedure, finishing with 1 μ diamond dust. The height of the deformation band above the valleys was then measured.

Results

The normal-size X-ray beam used at a specimen-to-film distance of 3 cm had a diameter at the specimen of 1.5 mm and gave an asterism streak of 14 deg. (Fig. 4). The X-ray microbeams had a diameter of 90 μ at the specimen using a specimen-to-film distance of 5 mm. The angular ranges of misorientation in the "microasterisms" (a name suggested by Prof. J. D. Bernal) are given in Fig. 2.

It may be seen at once that the range of misorientation of some of the microasterisms is comparable with the normal-size beam asterism and one has a value of as much as 10 deg. The total value of the angular misorientation obtained by adding together individual deviations is 65 deg. and the area covered is less than that of the normal-size beam giving a range of only 14 deg. The microasterism of 10 deg. alone is nearly equal to the normal-size beam asterism and yet only covers an area with a diameter of 6% of the other.

From the fact that many of the microasterisms were obtained from regions of the deformation band showing no

apparent curvature it may be assumed that plastic bending is not an essential requirement for the development of asterisms. The range of curvature of the band measured directly was approximately 16 deg., in reasonable agreement with that measured using the normal-size X-ray beam measurement of 14 deg.

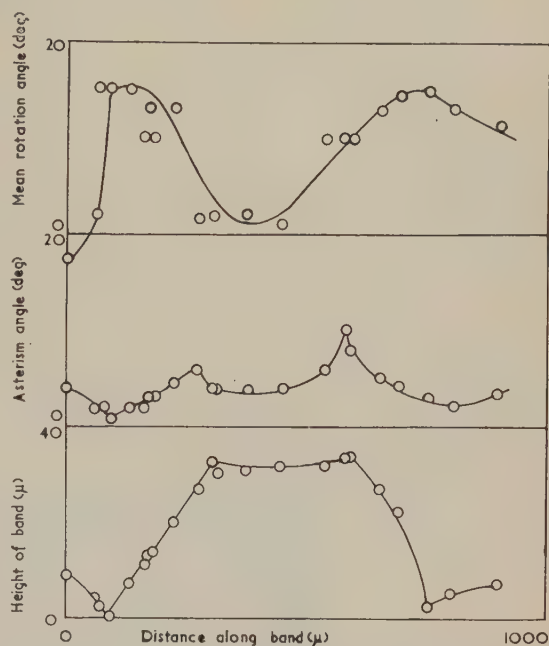


Fig. 2. Graphs showing lattice rotation angle and asterism angle plotted against height of deformation band

It has thus been shown that the main cause of asterism is the development of a mosaic structure with a misorientation about one axis. This misorientation is associated with the macroscopic bending of the crystal in the deformation band and has a total range of angular misorientation equal to this bending.

Orientation studies

The orientation of the crystal after deformation was determined from the normal-size beam photograph in Fig. 4. This is shown in Fig. 3 where *A* and *B* represent the range of the asterism referred to the tensile axis.

It is well known that a face-centred cubic crystal will tend to slip in the [111] plane along the [110] direction in this

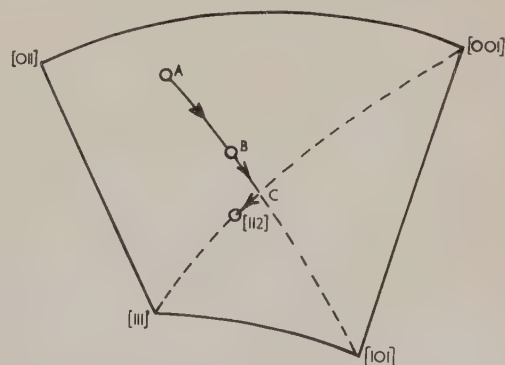


Fig. 3. Stereogram showing motion of crystal with respect to the tension axis
A → *C*, single slip
C → [112], double slip
AB, Laue asterism

plane, this being the direction of closest atomic packing in these crystals. This has been shown by Carpenter and Elam⁽¹⁾ to mean that in any given orientation of a crystal with respect to the tensile axis, the axis will move along the Great Circle joining the axis with the [101] pole on the stereographic projection. The particular [101] pole selected will be that lying across the nearest Great Circle joining the [111] and [100] poles.

On reaching this Great Circle, the crystal will then be symmetrical in position with respect to another [101] pole, when double slip will occur. This will continue until fracture, with a slight further rotation of the crystal towards the [112] pole along the [111]-[001] Great Circle.

It was evident on plotting the stereograms of the tensile axis on the standard cube projection that the points *A* and *B* were exactly on the Great Circle joining *A* to the [101] pole as also were the intermediate parts of the asterisms. It may therefore be reasonable to assume that the asterism on the normal-beam photograph joining *A* to *B* along the Great Circle delineates the motion of the crystal during the elongation. Thus some parts of the crystal still have the original orientation *A* and some parts have moved the maximum change in orientation, that is, to *B*.

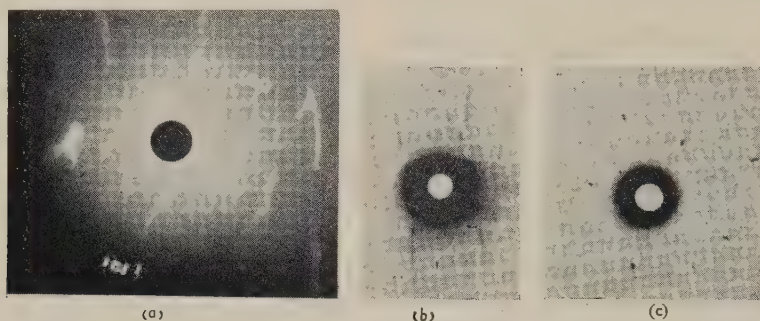


Fig. 4. (a) Macrobeam photograph from band; (b) and (c) microbeam photographs from band

Microbeam orientation studies

The orientations of the microbeam Laue photographs were each plotted in a similar way. The orientations determined from these microbeam photographs all lay on or very near the line *AB*, although some of the photographs in the middle of the deformation band gave small asterisms at an angle to the line *AB* indicating that the motion of portions of the band was not uniform. A graph of the mean angle of motion of the portion of the crystal from the point *A* along the line *AB* against the profile of the band is shown in Fig. 2.

From Fig. 2, it may be seen that the central portion of the deformation band has moved little from the original portion of the crystal. This is also the portion of the band raised above the general level of the surface. Where the band shows a marked change in orientation of the profile a change in the orientation of the lattice also occurs correspondingly. If this figure is compared with the Cahn⁽¹²⁾ theory of the formation of bands it will be seen that the concept of the bands consisting of slabs of material of different orientations is, in general, borne out. Entrapped within the deformation band, parts of the crystal are still in approximately the original orientation, although, in many cases, the photographs indicate that fragmentation has occurred into two or more crystallites, some showing asterisms. Away from the immediate region of the band the crystal has rotated to the new orientation. Changes in orientation have also occurred across the cusps.

As the raised portion of the band shows the greatest microasterisms, this indicates that the slab of material that has not been able to rotate has suffered considerable fragmentation, whereas the portion of the crystal that has rotated to the new orientation has suffered much less fragmentation. The crystals at this stage will therefore have a banded structure consisting of alternate layers of material having a mosaic structure showing strongly preferred orientation, and other material with relatively little deformation.

Dislocation densities

One theoretical aspect of the work that has been carried out concerns the calculation of dislocation densities. With the values of asterism obtained in this work, and assuming that the cause of the asterism is the development of a mosaic structure, values of dislocation densities of the order of 10^{10} per cm^2 are obtained. If it is assumed that the asterism is due to simple curvature alone, values of 10^8 per cm^2 are obtained. The higher values of dislocation density can be presumed, as this work indicates that mosaic structure is the main cause of the asterism. This aspect will be discussed in a later paper.

Acknowledgements

Thanks are due to Prof. J. D. Bernal of Birkbeck College and L. W. Derry of Battersea College of Technology for helpful discussions.

References

- (1) TAYLOR, G. I., and ELAM, C. F. *Proc. Roy. Soc. A*, **108**, p. 28 (1925).
- (2) HONEYCOMBE, R. W. K. *Proc. Phys. Soc. (London)*, **63A**, p. 673 (1950).
- (3) BARRETT, C. S. *Trans. A.I.M.E.*, **135**, p. 296 (1939).
- (4) GAY, P., and HONEYCOMBE, R. W. K. *Proc. Phys. Soc. (London)*, **64A**, p. 844 (1951).
- (5) BURGERS, J. M. *Proc. Phys. Soc. (London)*, **52**, p. 23 (1940).
- (6) GOLDSCHMIDT, H. J. *Acta Cryst.*, **5**, p. 256 (1952).
- (7) HIRSCH, P. B. *Progress in Metal Physics*, Vol. 6, p. 297 (1956).
- (8) HONEYCOMBE, R. W. K. *J. Inst. Metals*, **80**, p. 49 (1951-1952).
- (9) GAY, P., HIRSCH, P. B., and KELLY, A. *Acta Cryst.*, **7**, p. 41 (1954).
- (10) LEWIS, D. *J. Sci. Instrum.*, **32**, p. 467 (1955).
- (11) CALNAN, E. A. *Acta Cryst.*, **5**, p. 557 (1952).
- (12) CAHN, R. W. *J. Inst. Metals*, **79**, p. 129 (1951).

Simple rotary dynamic testing machine

by A. N. GENT, Ph.D., A.Inst.P., A.I.R.I., The British Rubber Producers' Research Association, Welwyn Garden City, Herts

[Paper first received 24 September, and in final form, 29 October, 1959]

Abstract

A test machine is described for determining the dynamic shear properties of rubber-like materials. It imposes a simple shear deformation, the direction of which is continuously rotated. The observations are easily made, and enable the dynamic shear modulus and damping factor to be determined rapidly; moreover, a relatively wide frequency range seems feasible. The instrument therefore appears suitable for general application. Measurements on a soft butyl rubber vulcanizate are described and compared with observations of free torsional oscillations. Good agreement is obtained.

The test-piece is subjected to a rotating shear of constant amplitude, and hence the elastically-stored energy is held constant. The observed energy dissipation therefore confirms a hypothesis of Greenwood and Tabor,⁽¹⁾ that dissipation may occur under such conditions, and indicates the limitations of the "hysteresis" concept that the dissipated energy is a constant fraction of the elastically-stored energy.

Introduction

KIMBALL AND LOVELL⁽²⁾ measured energy dissipation during cyclic deformation, using a test-piece in the form of a cantilever rotated about its axis. The method has recently been applied by Maxwell^(3,4) to the study of the visco-elastic behaviour of polymethyl methacrylate ("Perspex"), because it enables the dynamic mechanical properties to be evaluated very simply for a wide range of deformation frequencies. It has two disadvantages, however. Firstly, the test-piece is not uniformly deformed; in fact, the largest strains are imposed in the neighbourhood of the clamped or bonded faces and, hence, are particularly susceptible to inadequate fastening arrangements. The non-uniformity of strain is also undesirable when examining materials which show a non-linear dependence of their visco-elastic reactions on the strain amplitude. Secondly, the examination of soft materials (for example, vulcanized rubbers) is not easily accomplished, because the test specimen consists of a long thin rod which may be unable to support its own weight statically, and will whirl or whip at relatively low frequencies of rotation. A test machine has therefore been devised, and is described below, which imposes a homogeneous deformation on a rotating test-piece of a soft material, and permits the ready evaluation of the dynamic shear properties.

It is customary to describe the behaviour of visco-elastic materials under linear simple harmonic deformations by a complex shear modulus having real (n') and imaginary (n'') components. The experimental measurements described in a later section for a test-piece of vulcanized butyl rubber are expressed in terms of the real component n' and the damping

factor d , or ratio n''/n' . The latter quantity is alternatively described as the tangent of the angle δ of mechanical loss.

Experimental arrangement

The apparatus is shown diagrammatically in Fig. 1. The test-piece consists of a pair of rubber cylinders R bonded on their plane faces to metal end-pieces. The rubber cylinders are disposed on a common axis, with the inner metal end-pieces fastened rigidly together to form the composite test-piece. The outer metal end-pieces are secured in double ball races so that the test-piece may rotate freely about its axis, the rotation being imposed by a belt drive from a variable-speed motor. The central end-pieces are surrounded by a

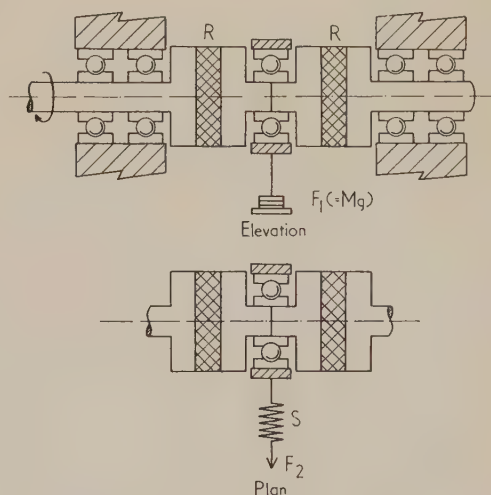


Fig. 1. Experimental arrangement

ball race to the outer casing of which weights are applied, thus producing a vertical movement at right-angles to the axis of rotation. The two rubber cylinders are thus subjected to a simple shear deformation, the direction of which is continuously rotated.

The central ball-race assembly moves spontaneously out of alignment, by a horizontal displacement perpendicular to the axis of rotation. This displacement is caused by energy dissipation in the rubber cylinders. By means of a calibrated helical spring S the magnitude of the horizontal force F_2 necessary to restore the central assembly to its original position in the horizontal plane may be determined. This constitutes one of the experimentally-observed quantities; the other is the magnitude of the vertical deflexion ϵ of the central assembly under the imposed vertical force F_1 .

Determination of n' and d

The rotating shear displacement to which the rubber cylinders are subjected may be resolved into two linear, mutually perpendicular, simple harmonic motions:

$$x = \varepsilon \sin pt$$

$$y = \varepsilon \sin(pt + \frac{1}{2}\pi)$$

where p is the rotation velocity. The corresponding sinusoidally-varying forces are readily calculated. They are found to constitute a rotating force which leads the rotating displacement ε by an angle δ (equal to $\tan^{-1}d$), and is of magnitude $A(n'^2 + n'^2)^{1/2}\varepsilon$, where A is the geometrical constant for the test-piece. (A is given by $2\pi r^2/h$ for two cylinders of radius r and thickness h .)

The force component F_1 in phase with the displacement is, therefore:

$$F_1 = An'\varepsilon$$

and the component F_2 , perpendicular to it, is given by:

$$F_2 = dF_1$$

The dynamic shear properties n' and d are therefore simple functions of the experimentally-observed quantities.

Experimental results

In Fig. 2, measured values of the horizontal force F_2 necessary to restore the central assembly to its initial position horizontally are plotted against the corresponding values of the imposed vertical force F_1 for two rates of rotation, for

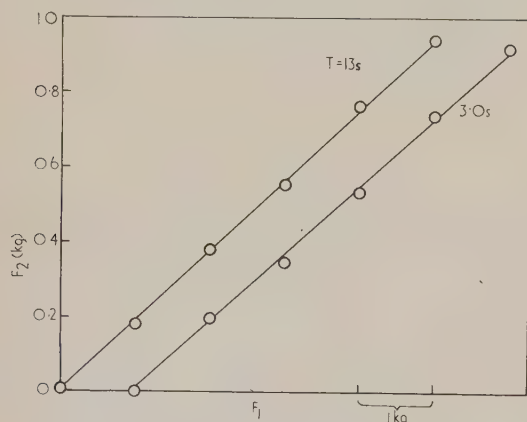


Fig. 2. Experimental relations between F_2 and F_1 at two periods of revolution, 1.3 and 3.0 s

test-pieces of a butyl rubber vulcanizate. The rubber cylinders were 1.27 cm in radius and 0.635 cm thick. The mix-formulation and vulcanization conditions are described in the Appendix. The periods of revolution were 1.3 and 3.0 s.

Linear relations are seen to apply, within the experimental error, and from the slopes, values of the damping factor d of 0.186 and 0.179 respectively are obtained. Linear relations were also obtained between the vertical deflexion ε and the applied vertical load F_1 . From the slopes, values of the shear modulus n' were calculated at a number of different periods of revolution. The values obtained, corrected for the small bending contribution (about 3%) with test-pieces of the present dimensions,⁽⁵⁾ are given in the table.

Dynamic shear properties from (a) rotary machine and (b) free torsional oscillations

Period, T (s)	a		b	
	n' (kg/cm ²)	d	n' (kg/cm ²)	d
0.55	3.65	—	—	—
1.30	—	0.186	3.43	0.184
1.72	3.26	—	3.38	0.174
3.00	—	0.179	—	—
3.40	3.14	—	3.52	0.170

Measurements were also made of the decay of torsional oscillations in the same test-pieces. A large inertia beam was attached to one metal end-piece at right-angles to the axis of the test-piece and set swinging, the other metal end-piece being rigidly clamped. The oscillations were observed by means of a lamp and scale, and were found to decay logarithmically, as is shown in Fig. 3, where a representative

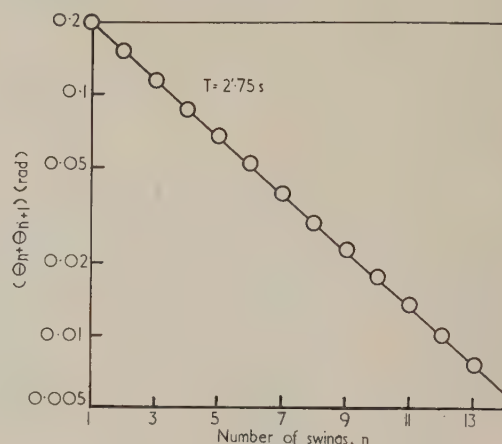


Fig. 3. Decay of torsional oscillations

plot of the double amplitude of swing against the number of swings is portrayed. Values of the damping factor d were calculated from the slope of similar linear relations for a number of values of the period of oscillation, varied by suitably adjusting the inertia of the swinging beam. The values obtained are given in the table, together with the corresponding values of the shear modulus n' , calculated from the measured period of vibration, the moment of inertia and the test-piece dimensions.

The free-vibration measurements are seen to be in good agreement with the rotary-machine observations, over the restricted range of frequencies practicable with the former system. The values obtained for d are closely similar to those obtained by means of the rotary machine, at corresponding periods of revolution. The values of n' are similar to, but slightly larger than, the corresponding rotary-machine determinations. This may be due to inaccuracy in determining the test-piece dimensions—particularly the radius, which enters the calculation of torsional stiffness to the fourth power—or to slight yielding of the ball-race grips, which would contribute to the observed deflexions with the rotary machine.

Discussion

It has been commonly assumed that the energy dissipated in one deformation cycle is a constant, or substantially constant, fraction of the maximum energy stored in the material during the deformation. This conception leads to anomalies when the deformation cycle does not contain the

origin, that is, when a *deformed* rubber is subjected to a deformation cycle about its deformed state.⁽⁶⁾ Greenwood and Tabor,⁽¹⁾ in considering energy dissipation during complex deformation cycles, have suggested that energy may be dissipated even when the elastically-stored energy is held constant.

The rotary machine described imposes a simple shear of constant amount, but the direction of which is continuously rotated. The elastically stored energy is, of course, unchanged on rotation. The existence of the force F_2 , and the energy dissipation it reflects, therefore constitutes an effective substantiation of Greenwood and Tabor's hypothesis.

Other deformation cycles can be envisaged which have a maximum stored energy equal to the (constant) value in the present one. The amount of energy dissipated per cycle may well differ, however. For example, in a simple shear oscillation, the energy dissipated per cycle is $\pi An''\epsilon^2$, whereas a rotating shear of the same amount gives rise to an out-of-phase force F_2 (equal to $An''\epsilon$) acting over a distance $2\pi\epsilon$ per cycle, and hence an energy dissipation per cycle of $2\pi An''\epsilon^2$ —twice the former amount. The concept of a constant fractional energy loss is, therefore, untenable.

No attempt has been made to determine the range of conditions which may be employed with the rotary machine. It seems clear, however, that the absence of reciprocating members and substantial moving parts should permit a relatively large frequency range to be examined. The inherent simplicity of operation and the ease with which the shear

properties can be derived should also make the method suitable for general application.

Acknowledgements

The author is indebted to Mr. D. J. Hill for experimental assistance. This work arises out of a programme of research undertaken by the Board of the British Rubber Producers' Research Association.

Appendix

Preparation of the test-pieces

The mix employed had the following composition in parts by weight: butyl rubber (Polysar Butyl 400) 100, zinc oxide 5, stearic acid 1, tetramethyl thiuram disulphide 4. Vulcanization was effected by heating for 50 min at 140°C.

References

- (1) GREENWOOD, J. A., and TABOR, D. *Proc. Phys. Soc. (London)*, **71**, p. 989 (1958).
- (2) KIMBALL, A. L., and LOVELL, D. E. *Phys. Rev.*, **30**, p. 948 (1927).
- (3) MAXWELL, B. *J. Polym. Sci.*, **17**, p. 151 (1955).
- (4) MAXWELL, B. *J. Polym. Sci.*, **20**, p. 551 (1956).
- (5) RIVLIN, R. S., and SAUNDERS, D. W. *I.R.I. Trans.*, **24**, p. 296 (1949).
- (6) DAVIES, D. M. *Nature (London)*, **170**, p. 937 (1952).

CORRESPONDENCE

Annealing silicon monoxide films on aluminium mirrors

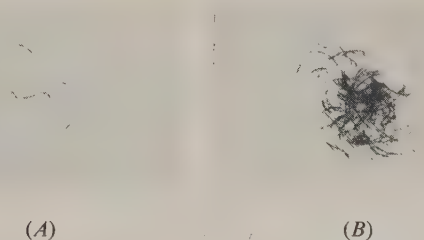
Silica coatings produced by thermal evaporation of silicon monoxide in a vacuum are often used for protecting aluminium front surface mirrors, and we have recently undertaken a short study of their properties. A number of silicon monoxide-protected mirrors were prepared and it was observed that when the metal and silicon monoxide layers were scratched by a steel pin they were removed as a fine dust which sprang from the mirror surface in the path of the stylus. Further examination showed that a load on the steel point necessary to remove the silicon monoxide film always resulted in removal of the aluminium and particles of the glass. This indicated that the silicon monoxide films were not soft or poorly adherent to the aluminium underlayer but were in a highly stressed and brittle state. When the surface of the coating was cut by scratching the surface forces became unbalanced, thereby releasing the stresses within the film. Heat treatment of evaporated metal films removes stresses and defects in their structure produced during condensation and it was believed that heat treatment of silicon monoxide films might have a similar effect.

A number of evaporated coatings were annealed to test the foregoing hypothesis. The aluminium and silicon monoxide films were evaporated in a vacuum chamber exhausted by a 50 litres/s oil diffusion pump. The evaporation system consisted of two offset vapour sources evaporating upwards on to a rotating work-holder. The technique used for evaporating the silicon monoxide was that described by Hass.⁽¹⁾ The glass used in the tests was soda-lime green plate $\frac{1}{8}$ in. thick. A constant current was passed through the molybdenum boat used for evaporating the silicon monoxide

films, so that the deposition rate was 100 Å/min and a quarter-wavelength film was deposited in ten minutes.

The wear resistance of the films was tested by mounting the test specimen on a support which rotated through one revolution for every three strokes of the abrading head, so that the rubber followed a number of flat spirals on the film.⁽²⁾ The abrader was made of a hard rubber loaded with 302 grade emery. The brittle silicon monoxide films were not uniformly worn away by the abrasive particles, as for example occurs with magnesium fluoride films, but were scratched right through, leaving behind spiral furrows. The protective films were therefore graded according to whether they had been scratched through by the abrader or merely surface marred.

Heating the silicon monoxide film either during or after deposition produced durable top layers providing the glass attained a temperature of 200°C. The images of the



Scratch patterns produced on silicon monoxide-protected aluminium mirrors by abrasion with a rubber loaded with grade 302 emery. Weight on abrading head 112 lb/in.² and specimens abraded for 100 strokes. Sample A, heat-treated at 200°C. Sample B, heat-treated at 180°C

abrasion scratch patterns formed on silicon monoxide-protected mirrors, after baking at 180 and 200° C, are shown in the figure. The picture was made by exposing photographic paper with the abraded mirrors resting on its surface. These results show that 180° C is insufficient for annealing purposes. At 200° C or above the baking period made negligible difference to the hardness of the film, but there was evidence that films heated at 180° C improved in hardness with baking time. When thick films of 4500 Å thickness were deposited over a period of 45 min the coatings were still under stress because the glass temperature did not rise to the annealing value. To find whether the rate of cooling after annealing had any effect on the brittleness of a silicon monoxide coating, a film was deposited on to a cold substrate which was then halved and baked at 300° C. One half of the specimen was allowed to cool slowly in the oven whilst the other was cooled quickly on a water-cooled plate. When tested for wear resistance both specimen halves were of the same high durability.

The wear resistance of the annealed silicon monoxide films was improved by burnishing them with a soft cloth which probably compressed the film into a more compact state and lubricated its surface with organic materials from the polisher. An unannealed film still remained brittle after burnishing and could be easily scratched.

It is not possible to deposit the aluminium on to a hot substrate as this produces mirrors with a brownish tinted reflexion, because grain growth and oxidation of the condensing metal film is promoted at high substrate temperatures. Also, it was found in these tests that heating the aluminium after deposition, but before evaporation of the silicon monoxide, produced quarter-wavelength silicon monoxide films with a diffuse reflectance. It is known that heating a metal film will usually cause grain growth in the deposit and it is believed that the silicon monoxide grows on the enlarged grains to form an even more irregular structure. Thus in the centre of the rotary work-holder, where the angle of vapour incidence was consistently high, the silicon monoxide films were always diffusely reflecting. Holland⁽³⁾ has shown how condensation on an irregular surface at high incidence angles produces an even rougher deposit because the film growth is limited to surface prominences. Normally, when aluminium and silicon monoxide films are deposited, the glass is pre-heated by the glow discharge used for cleaning and further heated by radiation from the vapour sources, which can be considerable if the silicon monoxide is volatilized slowly to aid its oxidation. However, it is best to anneal the silicon monoxide film after its deposition and avoid undue temperature rise during coating.

The foregoing investigation has shown that silicon monoxide films deposited on to cold substrates possess internal stresses which produce brittle layers. Such films

resemble in properties the strained layer which is formed on toughened glass by rapidly chilling the surface. Brittle silicon monoxide films may be annealed by heating to 200° C or above and it is preferable to do this after deposition to avoid grain growth in the silica or metal film. Other work in our Laboratory has shown that thick silicon monoxide films (approximately 1 μ) may peel from the support due to internal stresses, but stable films can be prepared by annealing.

Acknowledgements are made to Mr. A. S. D. Barrett, Technical Director of Edwards High Vacuum Ltd., for permission to publish this note.

Research Laboratories,
Edwards High Vacuum Ltd.,
Crawley,
Sussex.

L. HOLLAND
T. PUTNER
R. BALL
[30 October, 1959]

References

- (1) HASS, G. *J. Opt. Soc. Amer.*, **39** pp. 532-540 (1949).
- (2) HOLLAND, L., and VAN DAM, E. W. *J. Opt. Soc. Amer.*, **46**, pp. 773-777 (1956).
- (3) HOLLAND, L. *The vacuum deposition of thin films* (London: Chapman and Hall Ltd., 1956).

Journal of Scientific Instruments

Contents of the April issue

PAPERS

- Accurate direct-reading hydrostatic balance. By A. T. J. Hayward.
Apparatus for the measurement of Young's modulus, between -200 and 700° C by transverse vibration in vacuum. By H. J. Stokes.
Automatic decantation for routine sub-sieve sizing. By F. Horsfall and A. Jowett.
Wax-atomizer for producing spherical dust particles. By G. K. Greenough.
Position transducer using a divided circle and coded scale. By I. R. Young.
Radiometer for field use. By J. H. McGuire and H. Wraight.
New method of sample interchange in a solid-source mass spectrometer. By B. R. F. Kendall.
Low-angle Geiger diffractometer for use with monochromatic radiation. By P. W. Teare.
Improved eye-piece graticule for measuring X-ray powder diffraction patterns. By W. G. Perdok and G. Boom.
Tunable galvanometer amplifier. By R. M. Huey and B. J. Lancaster.
Measurement of cyclic strain. By T. M. Dowell and J. A. Mackinnon.
The determination of the profiles of water waves. By J. A. Sandover and C. Taylor.
Instrument for recording the resistance during the deposition of a thin film. By J. A. Bennett and T. P. Flanagan.
Improved smoke density recorder. By R. Lambie.

LABORATORY AND WORKSHOP NOTES

- Electronic leak detector. By D. J. Dowling.
Filament winding machine. By D. Barker.
Determination of the density of glass fibres. By B. D. Coates.
Protection of diffusion pumps against inadequate cooling. By B. C. Cox.
An electromechanical low frequency oscillator. By E. W. Dickson.

NOTES AND NEWS

New instruments, materials and tools. New books

THIS JOURNAL is produced monthly by The Institute of Physics, in London. It deals with all branches of applied physics (including theory and technique). All rights reserved. Responsibility for the statements contained herein attaches only to the writers.

EDITORIAL MATTER. Communications concerning editorial matter should be addressed to the Editor, The Institute of Physics, 47 Belgrave Square, London, S.W.1. (Telephone: Belgravia 6111.) Prospective authors are invited to prepare their scripts in accordance with the *Notes for Authors*. (Price 3s. 6d. including postage.)

REPRODUCTION. The Institute of Physics is a signatory to The Royal Society's Fair Copying Declaration. Details may be obtained upon application from The Royal Society, London, W.1.

ADVERTISEMENTS. Communications concerning advertisements should be addressed to the agents, Messrs. George Jackson (Fleet St.) Ltd., Cliffords Inn, Fleet Street, London, E.C.4. (Telephone: Holborn 3611-2.)

CLAIMS FOR MISSING JOURNALS. Claims from regular subscribers to this *Journal* for missing numbers will only be considered if received within 60 days of the date of mailing plus normal outward time of transit and time for lodging the claim. Losses attributable to failure to notify a change of address or to similar omissions will not be considered.

SUBSCRIPTION RATES. A new volume commences each January. The charge is £6 per volume (\$17 U.S.A.), including index (post paid), payable in advance. Single parts, so far as available, may be purchased at 12s. 6d. each (\$1.75 U.S.A.), post paid, cash with order. Orders should be sent to The Institute of Physics, 47 Belgrave Square, London, S.W.1, or to any bookseller.

Electron probe methods of X-ray microanalysis*

by P. DUNCUMB, M.A., Ph.D., A.Inst.P.,† Cavendish Laboratory, Cambridge

Abstract

The use of an electron probe to produce a point source of X-rays permits chemical analysis, by X-ray absorption or fluorescence spectroscopy, of regions down to 1 to 10 μ in diameter. For the study of surfaces, the emission method, in which the probe excites the specimen itself, is more suitable; this gives a resolving power of about 1 μ and a detection sensitivity of 10^{-14} g. By means of a scanning technique, an image of the surface can be formed with a selected emission line, so that the distribution of a particular element is presented visually. The three methods are described with typical applications and are shown to be in many respects complementary.

Introduction

THE discovery by Moseley in 1913 of the simple laws governing X-ray spectra led to the development of X-ray spectroscopy for chemical analysis. The early work, summarized by von Hevesy in 1932,⁽¹⁾ covered on a macro scale the three main methods which are of interest today. These are: (1) *absorption spectroscopy*, in which the amount of a particular element in a thin section of material can be determined from its X-ray absorption at known wavelengths; (2) *fluorescence spectroscopy*, in which the characteristic radiation of elements present in a specimen is excited by an X-ray beam; and (3) *emission spectroscopy*, in which the specimen is directly excited by a beam of electrons. Since that time the fluorescence method has received the most attention, since a standard X-ray tube can be used with the specimen in air and the method is essentially non-destructive. However, recent developments of electron-optical techniques for producing a finely focused beam of electrons, or electron probe, have reawakened interest in the other two methods, and both absorption and emission spectroscopy can now be applied to regions in the specimen down to 1 μ in diameter. In addition, the development of suitable counters for X-ray detection has made it possible to measure accurately the low intensities which are available. The original work of Castaing^(2,3) on the emission method of microanalysis has opened a new field of research, and several instruments are now becoming commercially available for this purpose. The development of all three methods of microanalysis has been reported at two Symposia, one held in Cambridge in 1956⁽⁴⁾ and the other in Stockholm in 1959.⁽⁵⁾

Formation of the electron probe—the X-ray projection microscope

The principle of focusing an electron beam to produce a point source of X-rays was originally proposed by von

Ardenne⁽⁶⁾ and the first instrument for projection micro-radiography was built by Cosslett and Nixon in 1951.⁽⁷⁾ Two magnetic lenses (Fig. 1) form a demagnified image of a thermionic electron source on a metal foil target, which also acts as the vacuum wall; the electrons are accelerated through a potential commonly between 5 and 20 kV. A point source of X-rays normally about 1 μ in diameter is thus produced, and is used to project an image of the specimen, which is

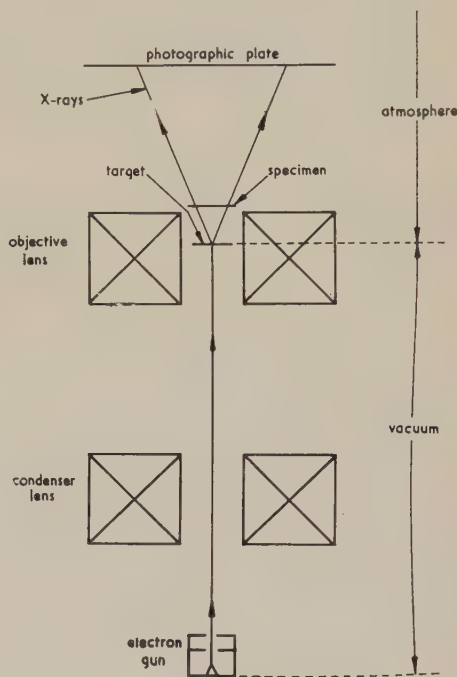


Fig. 1. The X-ray projection microscope (Cosslett and Nixon)

placed close to the source in air, on to a photographic plate or fluorescent screen. The high specific intensity of the X-ray source, which may be in the region of 100 kW/mm², coupled with the short distance between specimen and source makes the instrument also suitable for microdiffraction.⁽⁸⁾

The resolving power of the instrument is approximately equal to the X-ray source diameter, and is limited by three main factors. These are the geometrical diameter of the electron probe, spherical aberration in the objective lens and enlargement of the source due to penetration of the electrons in the target. In principle, these can be reduced to any desired level by adjustment of the demagnification, lens aperture and accelerating voltage respectively, but only at the expense of X-ray intensity. The optimum combination must therefore be found to give the smallest X-ray source for a given intensity, sufficient to expose the recording emulsion in reasonable time; in practice a resolution of 1 μ can

* Based on a lecture given to the Non-Destructive Testing Group of The Institute of Physics—14 March, 1958.

† Now at Tube Investments Research Laboratories, Hinxton Hall, Cambridge.

normally be obtained with an exposure of a few minutes. Features in the design which make this possible are an electron gun of high efficiency and an objective lens of short focal length and hence low spherical aberration.

Results demonstrating a resolution of $1\ \mu$ with biological specimens have been shown by Cosslett and Nixon,⁽⁹⁾ using an accelerating voltage of 10 kV and a target of $1\ \mu$ tungsten foil. Metallurgical and other applications, with the accelerating voltage increased to 20 kV, have also been described,⁽⁸⁾ together with examples of the use of a stereographic technique. Subsequently a resolution of $0.1\ \mu$ was shown to be possible⁽¹⁰⁾ by employing a thin gold leaf target only $0.1\ \mu$ thick. With a voltage of 7 to 10 kV, electrons penetrate a foil of this thickness so that the lateral spread is reduced. At this resolution, Fresnel diffraction at edges in the specimen is sometimes visible, and astigmatism of the pole-piece of the objective lens due to imperfect machining begins to be troublesome. These factors must therefore be taken into account if the resolution is to be further improved, though sufficient intensity would be maintained only with increased gun brightness and reduced spherical aberration. Practical methods of making these improvements in a probe-forming system are discussed by Mulvey.⁽¹¹⁾

Absorption microanalysis

The first attempts to obtain quantitative information from X-rays transmitted through a small region of a thin specimen were made by Engström,⁽¹²⁾ using contact microradiography. In this method, the specimen in the form of a thin section is held in close contact with a fine-grained photographic emulsion of the Lippmann type. It is then exposed to X-rays of the required wavelength from a normal X-ray tube. The density in the developed image may be determined over areas of a few microns square, from which, after calibration, the transmitted X-ray intensity may be obtained.

The analysis of one specific element is carried out by measuring the transmission at two different wavelengths chosen to be on opposite sides of a characteristic absorption edge of the element to be determined (Fig. 2). If the wavelengths selected lie close to the edge, the ratio of the measured transmissions is determined almost entirely by the mass per unit area of the element present and is only slightly affected by the presence of other elements in the matrix. Knowing the

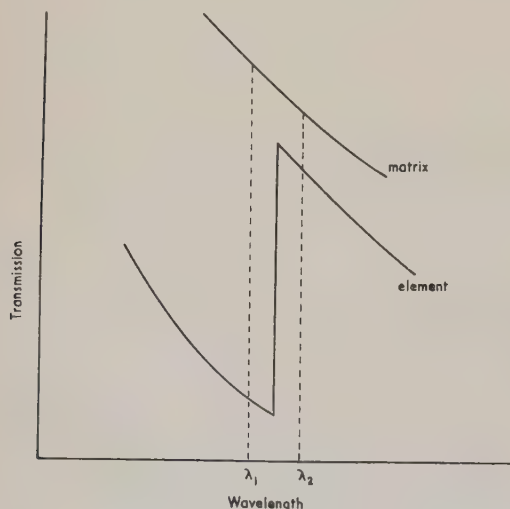


Fig. 2. The two-wavelength principle of absorption analysis for a specific element

density and thickness of the section, the weight concentration can thus be found.

Although the contact method has the advantage that information from over a wide area in the specimen is recorded simultaneously, the resolution is limited in practice by the accuracy required, since the number of silver grains in any given area is subject to statistical fluctuation. In any case, the resolution can be no better than that of the light optical system which is used to examine or microphotometer the emulsion. A further difficulty is that systematic error may arise from crystalline diffraction in the specimen, or from X-ray fluorescence; these effects have not been fully evaluated.

Long^(13, 14, 15, 16) has shown that many of these difficulties are avoided by use of a point focus X-ray tube. With the specimen close to the target to give a high primary magnification, the intensity measurement can be made directly with a counter system in the plane of the enlarged image, thus avoiding the photographic process altogether [Fig. 3(a)]. If,

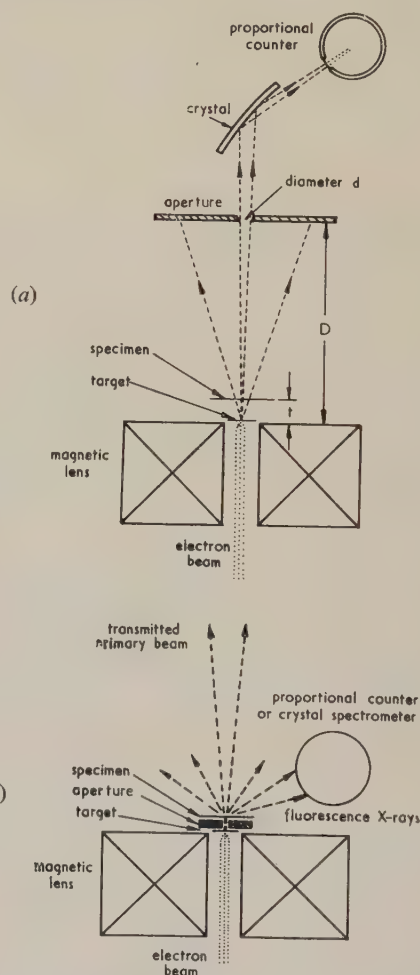


Fig. 3. X-ray projection microscope used as a point source for microanalysis by (a) absorption, (b) fluorescence (Long)

for example, the specimen is placed $100\ \mu(t)$ from the target, an aperture $1\ \text{mm}(d)$ in diameter at a distance of $10\ \text{cm}(D)$ from the specimen can be used to select the radiation which has passed through an area $1\ \mu$ in diameter. A crystal spectrometer above the aperture is then used to measure the intensity of the appropriate wavelengths in the transmitted beam. To eliminate the effect of drift in X-ray output from the point

focus tube over long counting periods, the analysing crystal is switched alternately between the two wavelengths to be measured, and the counts routed to appropriate scalars.

The total counting time required at each wavelength is dependent on the statistical accuracy required, and under favourable conditions the intensity transmitted through a $1\ \mu$ area on the specimen can be determined with 1% accuracy in a period of the order of a minute. For specimens absorbing a large fraction of the primary beam, the counting time is correspondingly increased. Errors other than statistical have also been evaluated by Long^(14, 15) and the method has been checked by measurements of calcium in gypsum crystals of known thickness. An overall accuracy of $\pm 2\%$ is obtained for amounts ranging from 0.1 to 2 mg/cm². The method has also been used in a detailed study of calcium in the cementum of monkey teeth⁽¹⁷⁾ and in some naturally occurring minerals.⁽¹⁸⁾ More recently Nilsson,⁽¹⁹⁾ also using a point focus tube, has studied the mineral phase in healing bone fractures.

Fluorescence microanalysis

In addition to its use for absorption work, the point focus X-ray tube may also be used for microanalysis by X-ray fluorescence.^(13, 14) A small aperture is placed immediately above the target [Fig. 3(b)] so that fluorescence is excited only in a selected region of the specimen. This must be as close as possible to the X-ray source in order to exploit the high specific loading of the target, and, with a thin specimen, it is thus convenient to collect the fluorescence radiation after transmission through it. A large fraction of the total fluorescence can be collected with a proportional counter, which gives adequate wavelength resolution for many problems. However, if elements closer than about 3 in atomic number are present, it is necessary to use a crystal spectrometer, which also reduces the background of scattered radiation to below the natural contribution from cosmic and gamma ray activity. Since continuous radiation is almost entirely absent, the spectrum obtained resembles the typical emission spectrum described later in Fig. 4, but with relatively

less background between the peaks. Small peaks, resulting from elements in low concentration, are thus detectable, though the counting time required is long if the peak height is comparable with the natural background of a few counts per minute. Rapid identification of the major elements is, however, possible.

Long⁽¹⁴⁾ has estimated the concentration sensitivity for calcium in a light matrix, such as biological material, and finds that under optimum working conditions, about 0.01% should be detectable over a volume in the specimen of $(10\ \mu)^3$. This is for a current of $20\ \mu\text{A}$ at 25 kV incident on a $2\ \mu$ spot in a copper target; the maximum current is limited in this case by melting of the target. The sensitivity is improved to 0.003% for the detection of iron under similar conditions, and estimates made by Zeitz and Baez⁽²⁰⁾ after allowing for different working conditions, are in broad agreement.

To confirm this estimate, Long has measured the calcium fluorescence from known specimens of gypsum and calcite and has obtained close agreement with theory for specimen thicknesses ranging from 10 to 120 μ . The chief practical difficulty has been the production of a suitable aperture, small enough to restrict the illuminated area at the specimen and yet thick enough to prevent radiation from the target from reaching the spectrometer. So far the smallest aperture which has been used is 50 μ in diameter, but it appears practicable to reduce this to 10 μ —the value taken in the calculation. The method may thus have considerable value in the estimation of trace elements in light matrices, such as biological material, and a resolution in the region of 10 μ is possible.

Emission microanalysis

The best approach for the study of surfaces is offered by the emission method, in which the electron probe is focused on a selected point of the specimen itself. The characteristic X-ray emission then gives both qualitative and quantitative information about elements present in the volume irradiated by the electrons. Disadvantages of the emission method in comparison with absorption or fluorescence analysis are that the specimen must be placed in the vacuum and that material of low thermal conductivity is liable to damage at normal intensity of bombardment (0.1 to 1 μA at 25 kV). Nevertheless it has been successfully applied to mineralogical and biological specimens as well as to metals to give chemical information which can be obtained in no other way. In combination with a technique of scanning the electron probe over the specimen, to be described later, it gives a rapid means of obtaining both the concentration of a given element at a selected point, and also its distribution over the surface.

A typical emission spectrum plotted with a lithium fluoride spectrometer is shown in Fig. 4. This was excited from a volume of about $1\ \mu^3$ in a steel of given composition, and illustrates how constituents may be identified from the Bragg angle or wavelength of the characteristic peaks, and the amounts measured from the peak heights. The amount of copper was 0.17% and although the $\text{CuK}\alpha$ peak is not visible in (a) it can be readily detected in (b) by using a high probe current (1 μA) and plotting the spectrum slowly ($\frac{1}{4}$ /min) to reduce background fluctuations. The minimum detectable concentration in this case may thus be estimated at about 0.05%.

The relation between resolution and X-ray intensity has been discussed by Wittry⁽²¹⁾ and, with particular reference to the scanning microanalyser, by Duncumb⁽²²⁾; the considerations are similar to those already noted for the X-ray

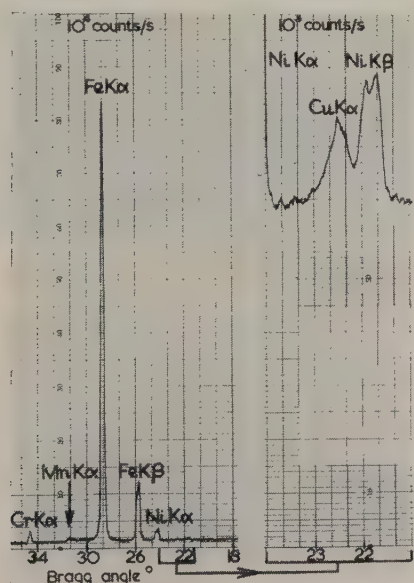


Fig. 4. X-ray emission spectrum from steel of given composition (Cr, 1.3%; Mn, 0.49%; Ni, 4.16%; Cu, 0.17%; Fe, 93.2%): (a) complete spectrum; (b) part of spectrum at greater sensitivity to show $\text{CuK}\alpha$ peak (Duncumb)

projection microscope. In general, sufficient intensity for analysis with a crystal spectrometer can be obtained with a resolution in the neighbourhood of 1μ . A simple air spectrometer is adequate for analysis of elements heavier than about calcium ($Z = 20$, $\text{CaK}\alpha = 3.4\text{ \AA}$), but with a vacuum spectrometer the range can be extended to include magnesium ($Z = 12$, $\text{MgK}\alpha = 9.9\text{ \AA}$) or even sodium. No crystals with high enough reflectivity are at present available to extend the range much beyond this, but Dolby⁽²³⁾ has shown that a proportional counter may be used to detect carbon radiation ($Z = 6$, $\text{CK}\alpha = 44\text{ \AA}$) with useful wavelength resolution. If necessary the wavelength resolution may be effectively improved by special techniques of pulse analysis.^(24, 25) An alternative possibility is to use a diffraction grating with detection by film or electron multiplier.⁽²⁶⁾

At the present early stage in the development of emission microanalysis much of the interest centres on instrument design. The essential requirements for such an apparatus are (i) an efficient electron-optical system to form the electron probe, (ii) some means of positioning it at a known point on the specimen surface, and (iii) one or more spectrometers to analyse the emitted radiation, preferably collected at a high angle to the surface in the backward direction to minimize absorption effects within the specimen. These are at once seen to conflict, since, to minimize spherical aberration of the final lens, the focal length should be as short as possible, necessitating the specimen to be close to or inside the lens. The polepiece thus tends to obscure the high angle radiation, and, if it is required to position and observe the specimen during analysis, an optical microscope must be built into the electron lens. The relative weights put on these features have therefore caused existing designs to differ widely, depending on what the equipment is required to do. In mineralogical work, for example, the need to be able to examine rough surfaces with a high emergent angle overrules the desirability of a short focal-length lens. The high probe current which this would permit cannot in any case be used, owing to the low thermal conductivity of most minerals. On the other hand, to detect trace elements present in a polished metal specimen, the high probe current required may swing the balance the other way. It thus seems unlikely at present that one design will satisfy all applications.

Castaing's original instrument⁽³⁾ employed a conventional electron gun and two electrostatic lenses to focus the probe clear of the second lens. The specimen was viewed and

positioned through an optical microscope outside the lens by means of an inclined mirror between the lens and specimen. By tilting the specimen slightly, it was possible to collect X-rays at an angle of 16° to the surface and to analyse them with a curved quartz crystal and Geiger counter. In a later instrument⁽²⁷⁾ now made commercially, Castaing has changed to a magnetic lens system, which permits a reflecting light objective to be built coaxially into the final lens, as shown in Fig. 5. This gives an improved optical image, having a resolution of about 0.7μ and in addition considerably reduces spherical aberration. Two high precision spectrometers are incorporated, both in vacuum, one using quartz for elements heavier than chlorine ($Z = 17$) and the other using mica for elements down to magnesium ($Z = 12$). A view of the complete instrument with the right-hand spectrometer open to air is shown in Fig. 6.

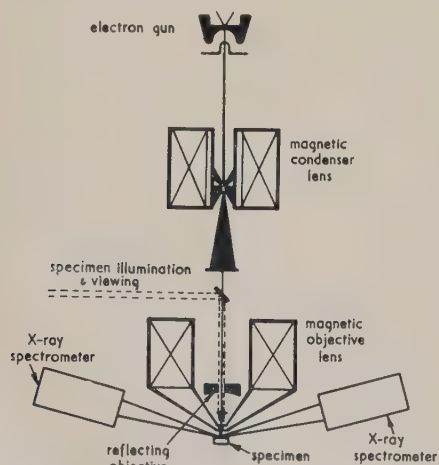


Fig. 5. Principle of static probe microanalyser (Castaing)

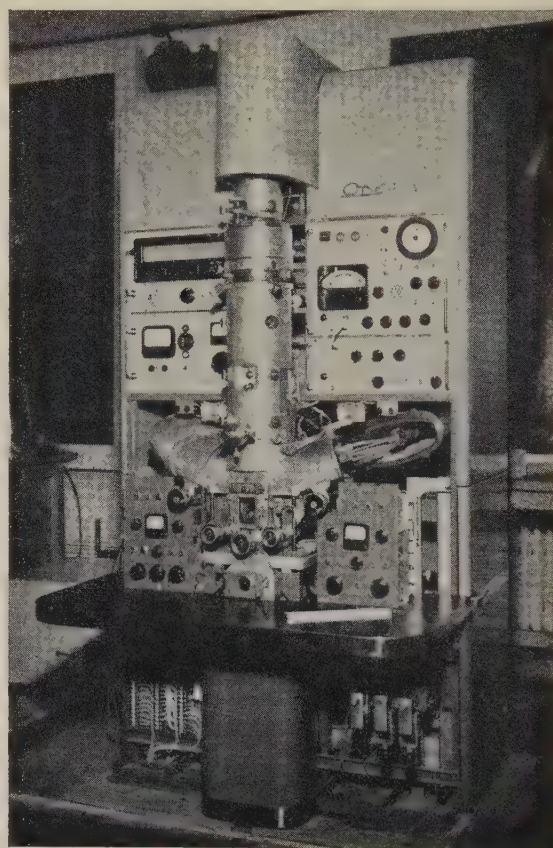


Fig. 6. Static probe microanalyser (Castaing)

The difficulty of combining the light-optical and electron-optical systems has been avoided by Mulvey,^(11, 26) though it is in this case not possible to view and analyse the specimen simultaneously. The electron gun (Fig. 7) is at the base of the column, and the probe is focused on a tilted specimen just above the second magnetic lens. X-rays are collected horizontally and analysed by a focusing spectrometer which can be evacuated. The specimen is mounted on a drum, which also carries reference samples, and can be rotated through 180° for examination under an optical microscope at the top of the apparatus. The accuracy of the bearings and movements is such that the point of impact of the probe falls within 1μ of the cross wires of the optical microscope, under which the specimen is first positioned by rotation and

axial movement of the drum. Following the analysis, the point of impact can be confirmed by observation of the carbon contamination spot which results when the probe is stationary on the specimen for some minutes. This machine is also available commercially.

Independently of Castaing, an instrument was developed in the Soviet Union by Borovskii,^(28, 29, 30) using an electron microscope double condenser lens to give a $2\ \mu$ probe. A quartz crystal in transmission is used for the analysis of elements in the ranges $Z = 26$ –42 and 72–92. This instrument is now manufactured as the RSASH-2, and a later model, the RSASH-3, is available to extend the range to magnesium ($Z = 12$).

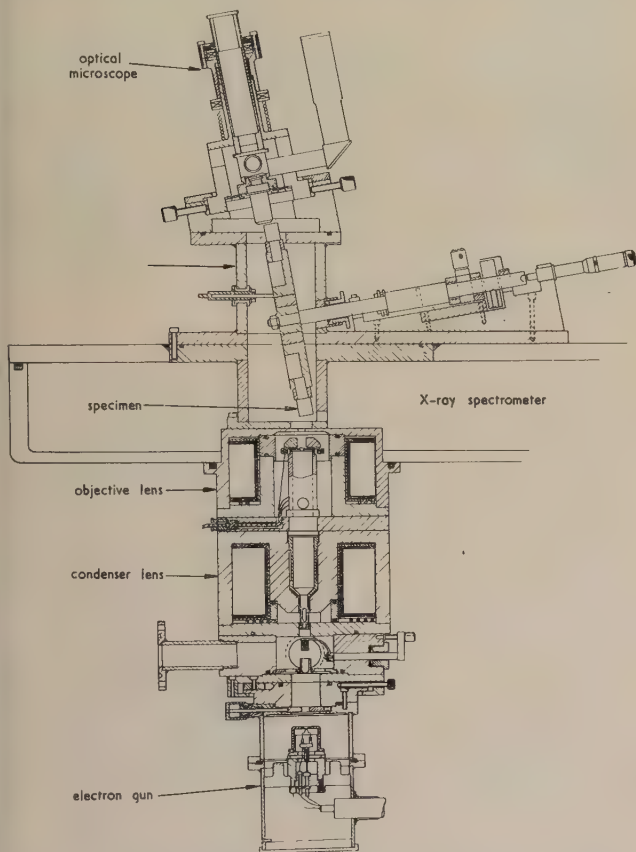


Fig. 7. Microanalyser for static and scanning emission microanalysis (Mulvey)

Birks and Brooks⁽³¹⁾ have converted an RCA-EMT electron microscope for microanalysis, using a light-optical system similar to that in Castaing's first instrument. Three spectrometers are used to analyse different elements simultaneously; in this way the variations of each element along a line in the specimen can be accurately correlated and the effect of drift in probe current minimized.

Another variation in the design of static probe instruments is shown by Wittry,⁽³²⁾ who obtains a short focal length by positioning the specimen in the polepiece gap, which is sufficiently large to accommodate the X-ray port and light objective plus inclined mirror for positioning. Buschman and Norton⁽³³⁾ have built an instrument using electrostatic lenses; the tilted specimen is observed optically by its reflexion in the polished upper surface of the final lens. The resolution claimed for both these instruments is about $5\ \mu$.

The interpretation of experimental results has been fully

discussed by Castaing and Descamps.⁽³⁴⁾ To a first approximation, the concentration of an element is proportional to the intensity of its characteristic line emission. Calibration may be effected by comparison with a pure sample of each element, and a relative accuracy of 1% is possible in the determination of high concentrations, with a minimum detectable concentration, in favourable cases, of less than 0.1%.

Departure from linearity between characteristic intensity and concentration sometimes occurs, due to absorption of the X-ray beam within the specimen or to fluorescence radiation excited in the matrix surrounding the region of analysis. For example, in the unfavourable case of a 60% Fe, 40% Cr alloy, where $\text{FeK}\alpha$ radiation is strongly absorbed by the chromium causing fluorescence, the apparent composition would be 47% Fe, 44% Cr. This is for an accelerating voltage of 25 kV and an emergent angle of 20° ; the absorption effect is reduced by an increase in emergent angle and a decrease in accelerating voltage. Further error occurs when elements of widely differing atomic number are present, and in cases where the corrections are not easily calculable it is often preferable to calibrate with a sample of known composition close to that of the specimen rather than with pure elements.

Uses to which the various forms of static probe microanalyser have been put are too numerous to be listed fully. By far the greater number of published applications have come from the French school using the Castaing instrument. Castaing, Philibert and Crussard^(35, 36) have illustrated the use of the technique by studying manganese segregation in steel, selective oxidation during scaling, sulphide and carbide phases in steel, and diffusion couples of Fe-Cu and U-Zr. Castaing and Descamps⁽³⁷⁾ have concentrated on the analysis of light alloys of elements down to Mg, identifying, for example, the Mg_2Si phase in an alloy of Al-Mg-Si. The most recent work comes from Philibert and Bizouard,⁽³⁸⁾ who carried out systematic studies of further segregation, oxidation and diffusion couple problems. In particular, in samples undergoing "Thomas" conversion they have succeeded in tracing the variation of phosphorus across the surface down to concentrations of 0.1%; the detection of a light element in such low concentration as this requires very careful design of the crystal spectrometer. The mineral constituents of oolite and other ores^(35, 36, 38) have also been investigated by the French workers, together with samples of sediment and cosmic dust from the sea bed.⁽³⁷⁾ For non-conducting specimens it is necessary to evaporate a thin metallic film on the surface to prevent charging.

Other metallurgical studies have been reported in the United States by Birks and Brooks;⁽³¹⁾ a study of the structure of meteorites has been carried out by Austin and others.^(39, 40) Wittry has used his machine for the analysis of Fe-Cr alloy⁽³²⁾ and later for study of semiconductor alloys.⁽⁴¹⁾ In this country, Mulvey has described the use of his instrument to identify lead inclusions in a layer of enamel, and to demonstrate the diffusion of tungsten in iron during spark hardening.⁽²⁶⁾ Later his machine was converted for scanning microanalysis; the original technique was developed at Cambridge and is now described.

The X-ray scanning microanalyser

Considerable advantages result from being able to scan the electron probe over the specimen in a raster pattern. The principle is illustrated in Fig. 8, which shows a block diagram of the original instrument developed by Cosslett and

Duncumb,⁽⁴²⁻⁴⁵⁾ The electron probe is scanned over the specimen surface in synchronism with the spot on a cathode-ray tube screen, which is brightness-modulated by the signal from a spectrometer detecting characteristic emission of a selected element. In this way, an image of the specimen surface showing the distribution of the element is obtained,

the specimen—was removed by incorporating a lens of the pinhole type⁽⁴⁸⁾ with the focus outside the polepiece.

A sectional diagram of the column of this instrument is shown in Fig. 9. Two lenses are used to focus the probe on to the specimen immediately beneath the second lens, in the upper bore of which deflexion coils are mounted to scan the

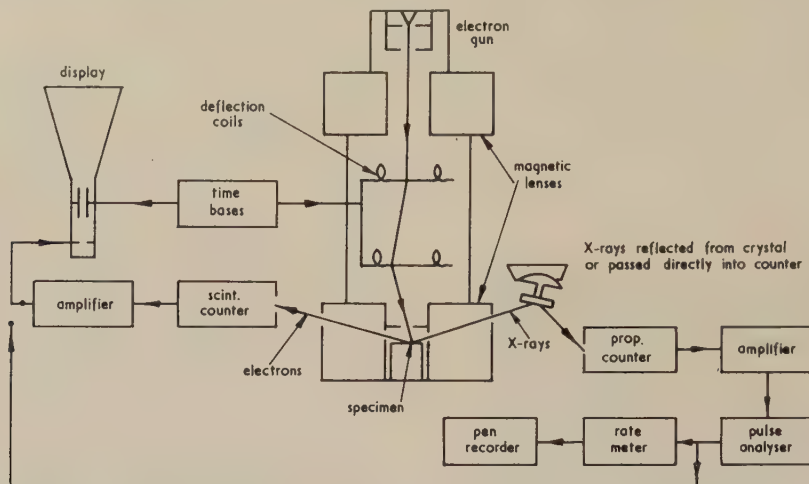


Fig. 8. Principle of X-ray scanning microanalyser (Cosslett and Duncumb)

and after stopping the scan, the electron probe can be accurately positioned from the image afterglow (about 20 s) for quantitative analysis. The same limitations apply to resolution and range of atomic number as in the static probe microanalyser.

It is also advantageous to form an image in terms of the electrons back-scattered from the surface in a manner similar to the electron scanning microscope of Smith and Oatley,⁽⁴⁶⁾ and a scintillation counter is used to collect electrons of high energy. This shows the surface topography with contrast similar to the optical image obtained in oblique illumination, and gives qualitative information about the variation of atomic number over the surface—a useful feature, for example, in the study of such problems as dense impurities in beryllium.

With two methods of image formation, it is thus unnecessary to rely on an accurately aligned optical microscope for focusing and probe positioning; improvement of the resolution much beyond $1\ \mu$ would in any case make the optical method inadequate. In addition, errors which can occur due to distortion of the lens field by a ferromagnetic specimen are eliminated.

In the first instrument, as Fig. 8 indicates, the specimen was accommodated in the bore of the polepiece and X-rays or scattered electrons collected through the polepiece gap. For reasons described previously this was to keep the spherical aberration of the lens low, and permitted a current of several microamps to be delivered into a $1\ \mu$ probe. It was found, however, that for most applications, a probe current of $0.1\ \mu\text{A}$ was sufficient, giving a characteristic count rate for pure elements in the neighbourhood of iron of about $10^4/\text{s}$. Although this was not sufficient to give an image completely free of statistical noise, it was possible by photographing the image for several minutes to reduce the noise to a low level. Thus, in a second instrument constructed by Duncumb and Melford at Tube Investments Research Laboratories,⁽⁴⁷⁾ the major disadvantage of this arrangement—the restricted size and the difficulty of interchange of

probe over the specimen surface. The maximum area of scan is about $0.5 \times 0.5\ \text{mm}$, limited by off-axis lens aberrations. Emitted X-rays and scattered electrons are collected at 20° to the specimen surface through ports in the lens

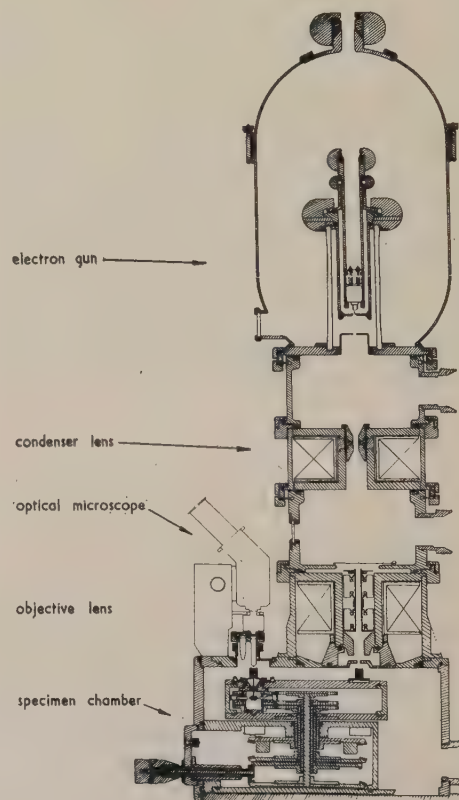


Fig. 9. Electron-optical system of X-ray scanning microanalyser (Duncumb and Melford)

casing in a plane perpendicular to that of the diagram. The specimen is mounted on a horizontal table, and may be traversed or rotated about the optical axis or moved from under the electron beam to an optical microscope or airlock. Several other positions on the table accommodate standard

cobalt and nickel as in the sound metal. Grain boundary enrichment of chromium is just visible in the sound metal in some cases balanced by cobalt deficiency. It is evident that qualitative information of this sort can be amassed considerably more rapidly than in a point-by-point analysis using a static probe instrument. The next step in a detailed investigation would be quantitative analysis of certain features revealed by this study.

Other applications have included the study of copper, nickel and tin segregation in mild steel,^(50,51) exsolution intergrowths in natural minerals,⁽⁵²⁾ crystallization in a copper-bismuth alloy⁽⁴⁹⁾ and the identification of carbide particles down to 0.3μ in size in an extraction replica.⁽²²⁾

Recent interest has been devoted to improving resolution by use of an accelerating voltage reduced to about 6 kV instead of the normal 20 to 30 kV.⁽⁵³⁾ A thin-window proportional counter is used to detect the low intensity long wavelength X-rays and a resolution of about 0.3μ has been observed in the particular case of an aluminium-tin alloy. However, the method cannot be universally applied at present owing to the poor wavelength resolution of the counter and to absorption of soft radiation in the counter window. Such conditions thus lay great stress on the need for improving proportional counters and techniques of pulse height analysis—factors discussed by Mulvey and Campbell⁽⁵⁴⁾ and by Dolby.^(23, 24, 25)

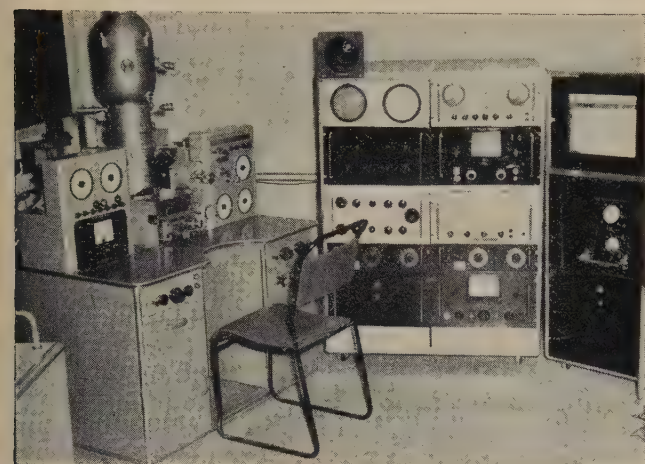


Fig. 10. X-ray scanning microanalyser (Duncumb and Melford)

samples. A complete view of the instrument is given in Fig. 10, showing the column and control desk on the left, the scanning and counting racks in the middle and pen recorder on the right. This instrument is also manufactured commercially.

As with the static probe instrument, wide variations in design are possible. Long⁽¹⁴⁾ has described a scanning microanalyser intended for mineralogical work in which the probe is focused 1.8 cm outside the lens to give space for a rock section mounted on a standard glass slide. This is held at 45° to the electron-optical axis so that X-rays can be collected at a high angle to the surface, which may be observed during analysis either in transmitted or reflected light. Optical fluorescence at the point of impact is often visible and gives additional qualitative information. Electrostatic scanning plates are located between lens and specimen. Also using electrostatic deflexion, Mulvey⁽⁴⁹⁾ has added a simple scanning system to his static probe instrument, the plates in this case being located in the polepiece gap.

The type of information that can be obtained with the X-ray scanning microanalyser is illustrated in Fig. 11. The specimen is a section cut normal to the surface, of a piece of high temperature alloy exhibiting corrosion. The electron image [Fig. 11(a)] shows a region of corrosion extending inward from the left. Inclusions in the sound metal are also visible, but as the specimen was not etched grain boundaries are not apparent. Fig. 11(b) was obtained by use of proportional counter and pulse analyser to select a band of wavelengths including $\text{SK}\alpha$ (5.37 Å) and $\text{MoL}\alpha$ (5.41 Å) radiations; the crystal spectrometer identified these with the smaller and larger inclusions respectively, but gave insufficient intensity for image formation. Figs. 11(c-f) were obtained using the spectrometer to select $\text{TiK}\alpha$, $\text{CrK}\alpha$, $\text{CoK}\alpha$ and $\text{NiK}\alpha$ radiations, and the main conclusions are as follows. Molybdenum occurs mainly together with titanium in the metal, but it appears to be absent from the scale. Sulphur is present at the interface particularly at grain boundaries. The scale itself is enriched in chromium and is surrounded by material deficient in chromium but containing

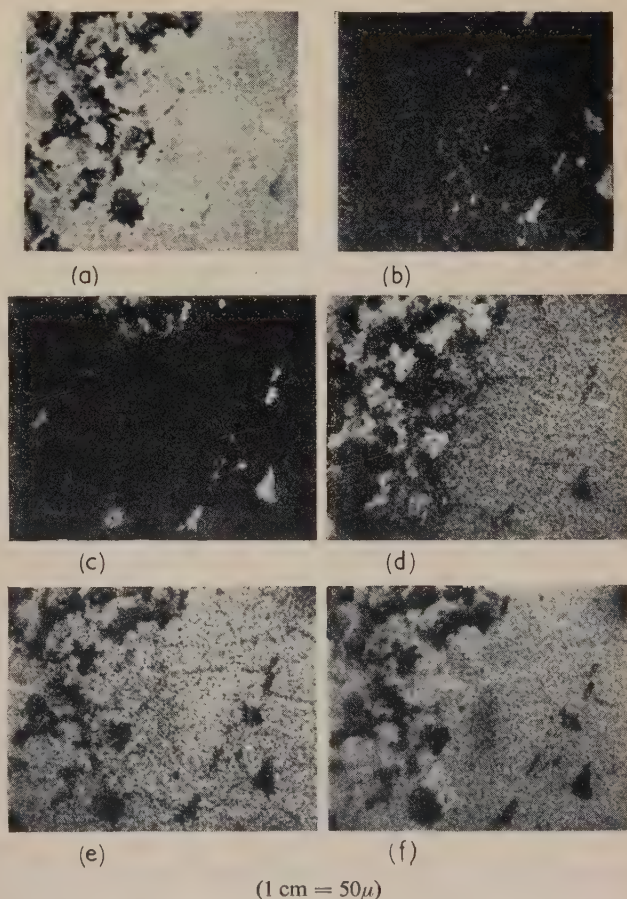


Fig. 11. Scanning electron and X-ray micrographs of high temperature alloy showing corrosion (Duncumb, by permission of Shell Research Laboratories)

(a) electron; (b) $\text{SK} + \text{MoL}$; (c) $\text{TiK}\alpha$; (d) $\text{CrK}\alpha$; (e) $\text{CoK}\alpha$; (f) $\text{NiK}\alpha$

Conclusions

The three methods of X-ray microanalysis which have been described—absorption, fluorescence and emission—are essentially complementary. The absorption method is suited to the accurate determination of a known element distributed throughout the thickness of a section of biological or mineral material, whereas, by the fluorescence method, unknown elements in such specimens can be rapidly identified with poorer resolution but high concentration sensitivity. The emission method can be used only for the study of surfaces, but gives a resolution of 1μ and permits rapid qualitative and quantitative analysis. By means of the scanning technique, the distribution of a particular element over the surface can be obtained as a visible image on a cathode-ray tube, and the electron probe positioned on a particular feature with an accuracy of better than its own diameter. Apparatus, at least for emission analysis, is becoming available, and it is likely that the use and extension of these electron probe methods of microanalysis will add materially to knowledge of the microstructure of many classes of material.

References

- (1) HEVESY, G. VON. *Chemical Analysis by X-rays and its Applications* (New York: McGraw-Hill Book Co. Inc., 1932).
- (2) CASTAING, R., and GUINIER, A. Proceedings of Conference on Electron Microscopy, Delft, 1949 (Delft: Martinus Nijhoff).
- (3) CASTAING, R. Thesis, Paris University, O.N.E.R.A. publ. no. 55 (1951).
- (4) Procs. of Symposium on X-ray Microscopy and Micro-radiography, Cambridge 1956 (New York: Academic Press Inc., 1957).
- (5) Procs. of Symposium on X-ray Microscopy and Micro-analysis, Stockholm 1959 (Amsterdam: Elsevier Publishing Co.).
- (6) ARDENNE, M. VON. *Naturwissenschaften*, **27**, p. 485 (1939).
- (7) COSSLETT, V. E., and NIXON, W. C. *Nature (London)*, **168**, p. 24 (1951).
- (8) NIXON, W. C. Procs. of Conference on Electron Microscopy, p. 307, London 1954 (London: Royal Microscopical Society).
- (9) COSSLETT, V. E., and NIXON, W. C. *J. Appl. Phys.*, **24**, p. 616 (1953).
- (10) NIXON, W. C. *Proc. Roy. Soc. A*, **232**, p. 475 (1955).
- (11) MULVEY, T. *J. Sci. Instrum.*, **36**, p. 350 (1959).
- (12) ENGSTRÖM, A. *Acta Radiol., Suppl.*, **63** (1946).
- (13) LONG, J. V. P., and COSSLETT, V. E. Ref. (4), p. 435.
- (14) LONG, J. V. P. Thesis, Cambridge University (1958).
- (15) LONG, J. V. P. *J. Sci. Instrum.*, **35**, p. 323 (1958).
- (16) LONG, J. V. P. Ref. (5), paper 17.
- (17) RÖCKERT, H. *Acta Odontologica Scandinavica*, **16**, Suppl. 25 (1958).
- (18) LONG, J. V. P., and MCCONNELL, J. D. C. *Min. Mag.*, **32**, p. 117 (1959).
- (19) NILSSON, U. *Acta Orthopaedica Scandinavica*, Suppl. 37 (1959).
- (20) ZEITZ, L., and BAEZ, A. V. Ref. (4), p. 417.
- (21) WITTRY, D. B. *J. Appl. Phys.*, **29**, p. 1543 (1958).
- (22) DUNCUMB, P. *Brit. J. Appl. Phys.*, **10**, p. 420 (1959).
- (23) DOLBY, R. M. *Brit. J. Appl. Phys.*, **11**, p. 64 (1960).
- (24) DOLBY, R. M. *Proc. Phys. Soc. (London)*, **73**, p. 81 (1959).
- (25) DOLBY, R. M., and COSSLETT, V. E. Ref. (5), paper 51.
- (26) MULVEY, T. *Mem. Sci. Rev. Met.*, **56**, p. 163 (1959).
- (27) CASTAING, R. *Laboratoires*, **17**, p. 7 (1956).
- (28) BOROVSKII, I. B. *Problemy Metallurgii, Moscow*, p. 135 (1953).
- (29) BOROVSKII, I. B., and IL'IN, N. P. *Zavodskaya Laboratoriya*, **10**, p. 1234 (1957).
- (30) BOROVSKII, I. B. Ref. (5), paper 49.
- (31) BIRKS, L. S., and BROOKS, E. J. *Rev. Sci. Instrum.*, **28**, p. 709 (1957).
- (32) WITTRY, D. B. Thesis, California Institute of Technology (1957).
- (33) BUSCHMANN, E. C., and NORTON, J. F. General Electric Co. Laboratory Report 57GL201 (1957).
- (34) CASTAING, R., and DESCAMPS, J. *J. Phys. Radium*, **16**, p. 304 (1955).
- (35) CASTAING, R., PHILIBERT, J., and CRUSSARD, C. *J. Metals*, **9**, p. 389 (1957).
- (36) PHILIBERT, J., and CRUSSARD, C. *J. Iron Steel Inst.*, **183**, p. 42 (1956).
- (37) CASTAING, R., and DESCAMPS, J. *La Recherche Aeronautique*, **63**, p. 41 (1958).
- (38) PHILIBERT, J., and BIZOUARD, H. *Mem. Sci. Rev. Met.*, **56**, p. 187 (1959).
- (39) MARINGER, R. E., RICHARD, N. A., and AUSTIN, A. E. *Trans. Met. Soc. AIME*, **215**, p. 56 (1959).
- (40) AUSTIN, A. E., RICHARD, N. A., and SCHWARTZ, C. M. Ref. (5), paper 58.
- (41) WITTRY, D. B., AXELROD, J. M., and MCCALDIN, J. O. Procs. A.I.M.E. Conference on Semiconductors, Boston, 1959.
- (42) COSSLETT, V. E., and DUNCUMB, P. *Nature (London)*, **177**, p. 1172 (1956).
- (43) DUNCUMB, P., and COSSLETT, V. E. Ref. (4), p. 374.
- (44) DUNCUMB, P. Ref. (4), p. 617.
- (45) DUNCUMB, P. Thesis, Cambridge University (1957).
- (46) SMITH, K. C. A., and OATLEY, C. W. *Brit. J. Appl. Phys.*, **6**, p. 391 (1955).
- (47) DUNCUMB, P., and MELFORD, D. A. Ref. (5), paper 52.
- (48) LIEBMANN, G. *Proc. Phys. Soc. (London)*, **B68**, p. 682 (1955).
- (49) BERNARD, A., BRYSON-HAYNES, D., and MULVEY, T. *J. Sci. Instrum.*, **36**, p. 438 (1959).
- (50) MELFORD, D. A., and DUNCUMB, P. *Metallurgia, Manchr.*, **57**, p. 159 (1958).
- (51) MELFORD, D. A. Ref. (5), paper 59.
- (52) AGRELL, S. O., and LONG, J. V. P. Ref. (5), paper 57.
- (53) DUNCUMB, P. Ref. (5), paper 53.
- (54) MULVEY, T., and CAMPBELL, A. J. *Brit. J. Appl. Phys.*, **9**, p. 406 (1958).

Location of p - n and l - h junctions in semiconductors

by P. A. ILES, M.Sc., A.Inst.P.,* and P. J. COPPEN, B.Sc., A.Inst.P.,†

Electronics Laboratory, Defence Research Telecommunications Establishment, Ottawa, Canada

Abstract

This article summarizes the properties of p - n and l - h junctions and the methods which have used these properties to locate them. Critical comments are made and criteria are given which must be considered when choosing a method, and some methods are recommended for the elements germanium and silicon. Lastly, an idea is given of the range of useful understanding of semiconductors which has resulted from use of these methods.

1. Introduction

INTENSIVE study of semiconductors has taken place in the last fifteen years. In device work and basic studies, p - n and l - h junctions have claimed much of this attention. With increasing control over crystal perfection and the distribution of active impurities, semiconductor properties can be altered over very small distances, and attempts have been made to attain comparable precision in ascertaining the location of junctions. To this end, most of the differences in material properties around a junction have been exploited. In this article, an attempt is made to include sufficient information to allow the best choice of a location method in a specific case. It is hoped that those not directly concerned with this topic will gain some idea of the principles involved and of the usefulness of the methods described.

2. Junctions: definitions and properties

A p - n junction can be taken as the plane over which the net impurity concentration changes sign, provided that this change is sufficiently abrupt to give a region of space charge, and assuming that the net impurity concentration is equal to the mobile carrier concentration. This definition does not include a class of p - n junction to be discussed later in this section, but is sufficiently general for the purposes of this article.

A p - n junction can rectify. For a forward bias, the current increases approximately exponentially with applied voltage, and there occurs the phenomenon of minority carrier injection; that is, holes are injected into the n -side from the p -side and electrons are injected into the p -side from the n -side. This can lead to modulation of the conductivity of the p - and n -regions since, to preserve charge neutrality, electrons and holes enter the appropriate regions at the external contacts. The reverse current can be considered to be approximately constant with voltage, up to a maximum voltage, since it consists of the extraction of minority carriers from both regions of the semiconductor close to the junction. In practical junctions, this current may not saturate, but it will be much smaller than the forward current. p - n junction properties are discussed fully elsewhere,^(1,2) but the above account is sufficient for this paper.

An l - h (or low-high impurity concentration) junction^(3,4) is the boundary between two semiconductor regions of different conductivity, but the same conductivity type. This

junction cannot rectify, and majority carrier flow is not impeded; the junction does, in fact, impede the flow of minority carriers to an extent which depends on the ratio of the high to the low impurity concentration.

Resistivity striations are alternations of high and low resistivity produced by certain crystal growth conditions; these alternations can take place within distances of 0.005 in. or less along the crystal growth axis. The impurity ratio is rarely large enough to show the above l - h junction properties fully. However, these striations can be regarded as a limiting case of l - h junctions, and their location is of great practical interest because of their frequent occurrence.

A technologically important junction is the p - i - n , in which a layer of intrinsic semiconductor separates the p - and n -regions. Since the intrinsic layer is often actually p - or n -type of very high resistivity, the p - i - n junction can be considered as a p - n junction in series with an l - h junction.

It is possible to modify the carrier concentration just below the surface of a semiconductor crystal by charges trapped in energy states at the semiconductor surface. This modification can lead to a surface layer of conductivity type different from that of the bulk material. A p - n junction is then formed just below the surface of the semiconductor. There has been no change of impurity concentration, so this p - n junction is not included in the definition above. This junction is of very great importance in the consideration of rectifying metal-semiconductor contacts. Its properties depend critically on the surface conditions, and thus it seems unlikely that this junction could be located by any method presented here, since these generally require some surface preparation, which modifies the junction. Similar remarks apply to l - h surface junctions formed by charges trapped in surface states. These also will not be considered here.

The differences in the material either side of the junction may be enlisted to aid in location. It is convenient to divide these material properties into two groups, primary and derived, the latter depending on the former. The primary properties may include the concentration of majority carriers n , their sign, and their mobility μ . The principal indication of a p - n junction is the change in majority carrier sign, and for an l - h junction, the change in n . These changes are usually detected through changes in some derived properties, although it is possible to measure n by radioactive or infrared techniques which will be mentioned later. The derived properties include the conductivity σ , the Hall coefficient R , the thermoelectric power θ , and possibly the electrochemical electrode potential. We have, for extrinsic samples,

$$\sigma = |e|n\mu \quad (1)$$

$$R \propto [n(\pm e)]^{-1} \quad (2)$$

$$\theta \propto \log n/(\pm e) \quad (3)$$

In principle, the change in magnitude of σ , R , or θ can be used to detect l - h junctions, and the change in sign of R or θ , to detect p - n junctions. However, to use R is not practical owing to the great difficulty of either moving two probes (one either side of the specimen) along the specimen while retaining very accurate alignment of the probes, or obtaining a very fine, localized magnetic field. The electrode

* Now at Hoffman Electronics Corporation, El Monte, California, U.S.A.

† Now at Texas Instruments Incorporated, Dallas, Texas, U.S.A.

potential is thought to be a function of carrier density and perhaps sign, and in practice, l - h and p - n junctions can be located by the reaction of the specimen with electrolytes.

p - n and l - h junctions may be located by the direct use of their properties. The rectification property of p - n junctions can be used to give preferential electrolytic etching. The difference in conductivity at l - h junctions can lead to the same result. The charge equilibrium at a p - n or l - h junction can be disturbed by photons raising trapped electrons into the conduction band, raising valence electrons into traps, or producing hole-electron pairs. Any of these disturbances will produce a photovoltage across the junction which can be used to locate it.

3. Summary of published methods

Earlier authors⁽⁵⁻⁷⁾ have collected and described some of the different ways of finding junctions. It is convenient to divide the known methods into three groups, *probe*, *visual*, and *other* methods. In the first group of methods, the semiconductor is explored with a fine probe, or set of probes. Several electrical properties of the semiconductor are used to show when the probes are near to, or when they cross, a junction. In the second group, the physical or chemical differences at the junction region are exploited to leave a visible record of the junction position. This has been called delineation of the junction. The third group consists of methods which involve equipment not usually available where junction location is required.

Probe methods

Four-probe method.⁽⁸⁻¹⁰⁾ Four collinear probes are placed on the semiconductor and can be moved relative to it. Current is passed through the outer probes, and the voltage developed across the inner pair is measured (Fig. 1). If the

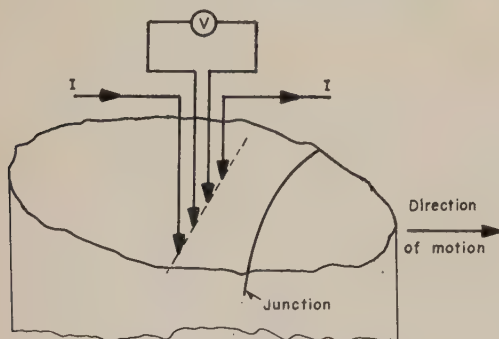


Fig. 1. The four-probe method

probes are equally spaced and away from a boundary, the resistivity (ρ) is given by $\rho = 2\pi l(V/I)$ where l is the probe spacing (assumed equal here), V is the voltage, and I is the current. If the probes straddle the junction the accuracy is poor, and in addition a p - n junction may impede majority current flow through the current probes. Better accuracy is obtained if the probes are aligned as nearly parallel as possible to the suspected junction plane, and then moved perpendicular to it. If there is no resistivity difference between the p - and n -regions, this method will not succeed for p - n junctions. Even for different resistivities the uncertainty in junction position will be approximately three times the probe spacing each side of the junction, because near the junction the boundary conditions implicit in the above formula are violated. The method is usable for l - h junctions, although here again the same boundary limitation makes close-spaced

l - h junctions difficult to locate. Provided the boundary conditions are not violated this method can be used on semiconductors of any shape.

Two-probe method.^(10,11) Here the current probes of the four-probe method are replaced by large area electrical contacts to a semiconductor bar of uniform cross-section. A voltage is measured between two probes of fixed spacing, in line with the current direction, as they are moved relative to the semiconductor (Fig. 2). For a p - n junction, the voltage is applied in the reverse direction, and the cutting of the bar and the electrode placing are arranged to pass current across the junction. Then, if the probes are moved along the bar, a sudden peak in voltage is shown as the probes straddle the junction (Fig. 3). As the probes cross an l - h junction, the sudden change of conductivity causes a change of voltage between them (Fig. 4).

Single-probe method.^(6,12-14) This resembles the two-probe method, except that one of the two voltage probes is fixed and the other moves along the bar. It is best to place the fixed probe away from the end contact to avoid difficulties from possible carrier fluctuations there. Once again the current direction is arranged to lie across the l - h or p - n junction. The varying potential difference between the two probes is measured as the spacing changes. l - h junctions

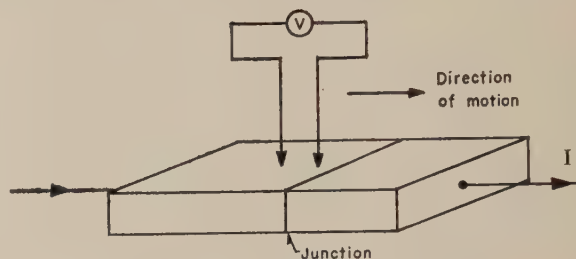


Fig. 2. The two-probe method

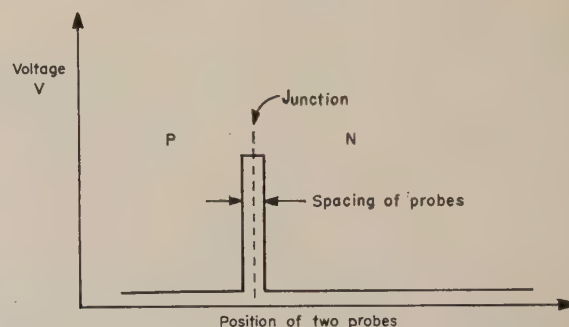


Fig. 3. Voltage between probes for a reverse-biased p - n junction. If the resistivity varies in the p - or n -regions, the lines will not be horizontal as shown

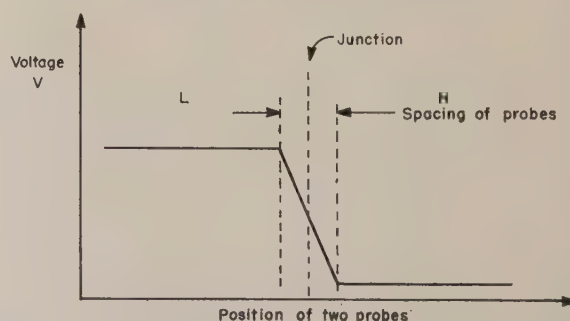


Fig. 4. Voltage between probes for an l - h junction. If the resistivity is not constant in the l - or h -regions, the lines will not be horizontal as shown

are shown by the point at which the curve relating potential and distance shows a discontinuity (Fig. 5). For a p - n junction, the polarity is arranged to bias the junction in the reverse direction. The junction is then shown as a change in voltage as the moving probe crosses it (Fig. 6). The accuracy

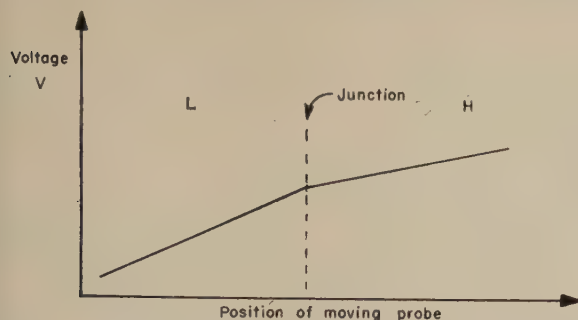


Fig. 5. Voltage observed when a single probe moves across an l - h junction

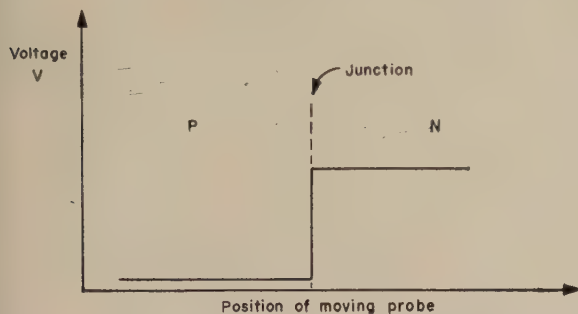


Fig. 6. Voltage for single probe crossing a reverse-biased p - n junction. If resistivities are not constant, lines will not be horizontal

is higher than for the two previous methods since a single probe alone is moved and the practical problems are thereby simplified. If p - n junction location is required and quantitative resistivity values are not wanted, this method does not require a specimen of uniform cross-section. This is because the reverse biased junction passes very little current and nearly all of the applied voltage appears across the junction itself, which is consequently easily detected.

This method has been applied to locate fine resistivity striations in crystals. One of the most accurate experiments was that of Hogarth and Baynham⁽¹⁴⁾ where the l - h junction at the edge of a highly dislocated region in germanium was detected with a resolution of 0.4μ . In measurements on this fine scale, the cross-sectional area need not be constant, provided it changes very little over the distance probed.

Thermoelectric probe method.^(12, 15, 16) Two probes, one hotter than the other, are placed on the semiconductor, and since the sign of the thermoelectric power differs for the two semiconductor types, the hotter probe becomes positive on the n -type region, and negative on the p -type region. p - n junctions may be found in this way, and the method does not require the p - n junction to be left rectifying after any necessary surface treatment.

The magnitude of the voltage is greater as the conductivity rises so that, in principle, l - h junctions can be located. However, unless the change in conductivity across the junction is great, it may be difficult to control the temperature rise closely enough at the hot probe to indicate magnitudes in conductivity.

Photovoltaic methods. The photovoltage at a junction may be used in two ways:—

(a) *Photo-probe method.*⁽⁶⁾ While the junction is illuminated, two probes are placed on the semiconductor, and when they straddle the junction, a voltage is observed. For best accuracy one probe is fixed and the other moved over small distances.

(b) *Light beam method.*⁽¹⁷⁻²⁰⁾ If the semiconductor around the junction is in the dark, or only weakly illuminated, and a fine spot or line of light is moved along the sample, a voltage will be observed across leads attached to the semiconductor when the edge of the light spot is within one minority carrier diffusion length of the junction (Fig. 7). The junction itself

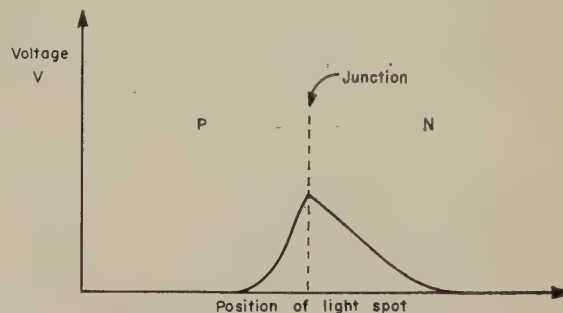


Fig. 7. Voltage observed as light spot crosses a p - n junction. The lifetimes in the two regions are assumed unequal

is shown by the position of the light spot when the voltage is at a maximum. This maximum is sharp if the surface conditions around the junction do not lead to stray inversion layers.

Note: for (a) or (b) the light intensity or the sensitivity of the voltage measurement should generally be greater for l - h than for p - n junctions.

Rectification direction method.^(6, 21) Good electrical contacts are made to both regions of the semiconductor and a probe moved along the sample. If an alternating voltage is connected between the contact and the probe, and the current-voltage characteristic displayed on a cathode-ray oscilloscope, the shape of the characteristic shows the direction of rectification, and therefore whether the sample under the probe is p - or n -type. This method does not require the p - n junction to be left rectifying after surface treatment, although usually the semiconductor must be etched for this method. Unless there is a very large conductivity change involved, this method fails for l - h junctions.

Visual methods

Preferential etching rate. The rate of attack of a semiconductor by either chemical or electrolytic etches depends on the magnitude and type of the conductivity. Hence l - h and p - n junctions may be revealed.

(a) *Chemical etch.*⁽²²⁻²⁴⁾ Most of the commonly used etching solutions, such as mixtures of hydrofluoric acid and either nitric acid or hydrogen peroxide, show sufficient preference in attack to locate junctions. This method is sensitive enough to display resistivity striations in germanium with a resistivity ratio of 1.5. Fig. 8 shows p - n junctions revealed by this method.

(b) *Electrolytic etch.*⁽²⁴⁻²⁹⁾ This can be done in several ways.

Firstly, the semiconductor sample is placed in the solution and biased positively with respect to an inert cathode. For a p - n junction, the etching current passes only through the p -semiconductor, leading to a greater etching rate for the p -type than for the n -type material. Jackson⁽²⁵⁾ used this method for germanium, and pointed out that the method

does not require the junction to have good electrical properties. However, the voltage had to be kept below the breakdown voltage of the rectifying barrier at the n -germanium-electrolyte interface. Multiple junctions could also be shown. This method should be applicable to l - h junctions since the h -region should etch more than the l -region.

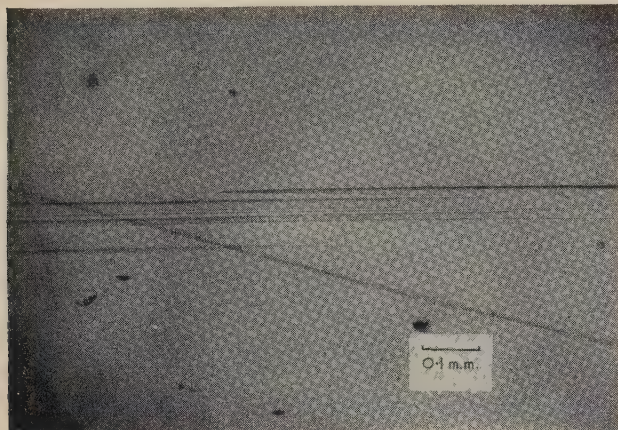


Fig. 8. Delineation of regions of n -type silicon in a p -type crystal by chemical etching. Comparison with Fig. 9 will indicate which are the n -regions. The etch used was a mixture of five volumes of concentrated nitric acid, three volumes of 48% hydrofluoric acid, and three volumes of glacial acetic acid. The crystal was sectioned along the growth axis; the n -regions are thin sheets extending across the crystal perpendicular to the growth axis.

Secondly, if a p - n junction is reverse biased, and no subsidiary electrode is used, the n - is etched more than the p -semiconductor.^(26, 27) A series of p - n junctions can be revealed by use of alternating current.

Thirdly, if a junction is passing current and a small subsidiary cathode is moved through the electrolyte near the semiconductor after the p - n junctions have been revealed as above, l - h junctions are exposed since the h -regions carry more current, and etch more, than the l -regions. Pankove⁽²⁷⁾ successfully used a thin layer of electrolyte on germanium.

Preferential surface finish. Under some conditions chemical or electrical etching leaves the semiconductor surface with a different surface texture. This difference in texture may be in smoothness, or in the amount or intensity of pitting. In the first of the electrolytic etch methods mentioned above, the n -region surface finish is unaltered during the etching; in the second, for a single p - n junction or for the n - p - n structure with a.c. applied, the texture of the p -surface is unaltered while the n -region has an etched finish. In addition, if the breakdown voltage at the n -semiconductor-electrolyte interface is exceeded, localized breakdown occurs, and pitting may follow.⁽³⁰⁻³²⁾ Besides the difference between p - and n -regions, lower resistivity n -regions, which have lower breakdown voltage than higher resistivity n -regions, may suffer greater pitting in a given etching procedure. Thus l - h junctions in n -semiconductor may be revealed. The pitting is greater if external sources of holes, such as light, heat, or injecting contacts are not present.

Preferential stain.^(27, 33-36) Some etch solutions will stain one conductivity type of a semiconductor. Pankove⁽²⁷⁾ found that several of the solutions used for electrolytic etching stained p -germanium dark relative to n -germanium, when the etching was done at high temperature (greater than 80° C). Fuller⁽³⁴⁾ found for silicon that very slowly etching

solutions (0.5% concentrated nitric acid in hydrofluoric acid) stained p -silicon black. Other methods for silicon include stronger mixtures of nitric acid in hydrofluoric acid⁽³⁵⁾ and the use of 48% hydrofluoric acid with strong illumination of the specimen.⁽³⁶⁾ Fuller also mentions that the darkness of the staining of the p -silicon increases as the resistivity falls. Thus l - h junctions may be displayed in p -silicon.⁽³⁷⁾

Preferential plate. It is sometimes possible to deposit metal preferentially on some parts of a semiconductor when it is immersed in metal salt solutions. If no additional electrodes or applied potentials are used, the process is called chemiplating. Electroplating is also used.

(a) **Chemiplate.**^(36, 38-40) This has been applied very successfully to silicon and less so to germanium. The differences in deposition arise presumably from the differences in electrode potential of the semiconductor regions either side of the junction. The deposition takes place from salt solutions containing metal ions and ingredients which control the surface reactions. For silicon, solvents for silicon dioxide such as hydrofluoric acid or hot alkalis are used as controlling agents. Silverman and Benn⁽³⁸⁾ deposited gold on silicon and germanium from hot cyanide solutions containing potassium hydroxide. Whoriskey⁽³⁶⁾ illuminated a p - n junction in a dilute copper salt solution containing hydrofluoric acid, and deposited copper on n -silicon. Iles and Coppin⁽³⁹⁾ used silver fluoride in two ways. For dilute solutions, illumination was necessary and deposition occurred on n -silicon. For stronger solutions (although still far from saturated), the deposition took place in the dark on the lower conductivity silicon regardless of conductivity type. For l - h junctions formed (for example) by boron diffusion into p -silicon, silver fluoride solution deposited silver preferentially on the lower conductivity region. Turner⁽⁴⁰⁾ reported preferential deposition of several metals (silver, copper, antimony, gold, and platinum) on silicon. His work confirmed that there is a strong dependence on surface finish as well as on conductivity and conductivity type. The mechanism of deposition may be altered by illumination of the sample, but the reaction may be made more reproducible. Fig. 9 shows the delineation of p - n junctions by chemiplating, the sample being the same as in Fig. 8.

(b) **Electroplate.** This has been applied in two ways.

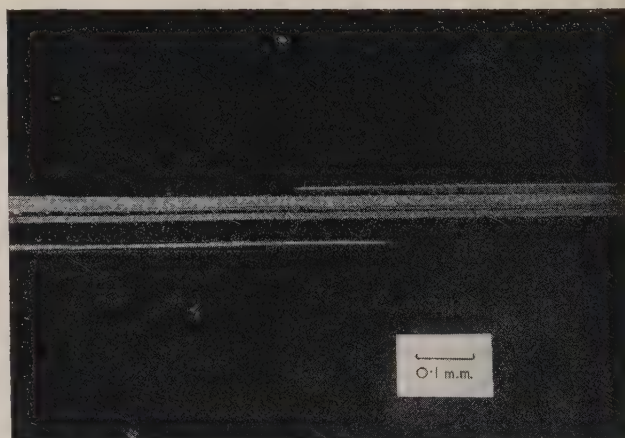


Fig. 9. Delineation of n -regions in a p -type silicon crystal by chemiplating. A dilute silver nitrate solution, containing a little hydrofluoric acid, was used. The specimen, which is the crystal shown in Fig. 8, was illuminated with a strong light during immersion in the solution. Silver has been deposited on the n -regions; these appear bright in the photograph. The p - n junctions are represented by the edges of the silver deposit

Firstly,⁽⁴¹⁾ for l - h junctions or striations in an n -semiconductor, the semiconductor is made negative with respect to a metal anode in the metal salt solution. The voltage is pulsed to avoid depletion of the electrolyte. In this case the metal plates more heavily on the h -regions where most current flows. In principle the method may also be used for p -semiconductors but, in order to get sufficient plating, the voltage may have to exceed the breakdown voltage at the semiconductor-electrolyte interface. Here, too, the h -regions should plate more.

Secondly,^(6, 42) for p - n junctions, a reverse bias is applied and an electrode is biased negative with respect to the n -region and positive with respect to the p -region. Metal ions are deposited on the p -semiconductor. Pulsing of the current, for example by manual interruption, aids definition.

Accumulation of dielectric powder.⁽⁴³⁾ Particles of a solid of high dielectric constant, such as barium titanate, are suspended in an insulating liquid placed over the junction. For a well-etched, reverse-biased p - n junction, sufficient electric field can be built up to heap the solid particles at the region of the highest field, which occurs at the junction. When the liquid is dried and the field removed the powder is left in position. Amick and Goldstein⁽⁴⁴⁾ have used electroscopic powders successfully for delineation.

Reduction of dye. Law and Meigs⁽⁴⁵⁾ have described a method of delineation. A dye, such as methylene blue, is applied to a reverse biased junction. The dye on the p -region is thereby reduced to a colourless form. If the unreduced dye on the n -region is removed, the colourless dye left can be oxidized in air to show the p -region.

Other methods

Autoradiograph.^(46, 47) If one impurity introduced into the semiconductor is a radioactive isotope, subsequent detection by a Geiger counter or by photographic film will show where the isotope has collected. This method has been used very successfully in detecting impurity variations during crystal growth. The same method has been used widely in diffusion studies.

Scanning electron microscope.⁽⁴⁸⁾ If a fine electron beam is scanned across the semiconductor, the slight difference in potential, between p - and n -regions and the surroundings, causes a change in the pattern of secondary electrons leaving the semiconductor. This produces a brightness variation on a fluorescent screen. The small diameter of the beam (a few hundred Ångstrom units) should allow good information on potential changes around the junction.

Infra-red beam.⁽⁴⁹⁾ The absorption of infra-red radiation transmitted by a semiconductor rises if the number of free charge carriers increases. By using a fine beam, the carrier density around several junction varieties, with and without applied voltage, has been explored.

Particle beam. A beam of charged particles falling near a junction can produce a voltage.^(50, 51) This effect should locate junctions, but no such uses of it have been published.

Use of visible light from p - n junctions.^(52, 53) If sufficient reverse bias is applied to a well-etched p - n junction, it may be possible to see the radiation emitted from near the junction when the fast-moving charge carriers recombine. This has been observed for grown and shallow diffused junctions.

4. Criteria

Most of the location methods discussed imply that the existence of a junction or junctions is known and, in some cases, even the approximate position. For junctions under

metal contacts, visual inspection will suffice; in cases where the approximate position is not known, a quick check over a specimen with the four-probe or thermoelectric probe is advisable to locate approximately any l - h or p - n junctions which may be present.

The principal criteria to be considered in choosing a method of finding a junction are:

- (1) whether there is a need for delineation in addition to location;
 - (2) the general form of the specimen containing the junction and the amount and type of surface preparation of the specimen.
 - (3) the particular semiconductor material involved; and
 - (4) the accuracy required.
- There are other subsidiary criteria, which are:
- (5) the need for electrical contacts;
 - (6) the possible contamination of the specimen;
 - (7) the necessity for mounting or potting if the specimen is small; and
 - (8) the possible use of dangerous chemicals.

The location methods reviewed in Section 3 will be discussed in the light of the above criteria.

(1) The first criterion will indicate from which group a location method is to be chosen. Usually, the probing methods locate only by reference to the position of the system moving the probes relative to the semiconductor. It is, however, possible to obtain effective delineation with the probe methods by making reference marks on the semiconductor. Bond and Smits⁽⁶⁾ have made powerful use of scratches in strips of Aquadag to delineate p - n junctions. The visual methods can delineate the junction position over large areas of the semiconductor.

(2) If the junction lies in the body of the specimen, suitable cutting can leave the junction intersecting some of the outer surfaces. Any of the probe and visual methods can then be applied at once, subject only to their specific requirements of shaping and surface preparation. On some surfaces the possible presence of inversion layers must be borne in mind; these layers are less likely if the surface is not etched. If the junction lies close to one surface of the specimen and the depth is too small to allow vertical sectioning, a cylindrical depression or a bevel may be ground on the surface of the specimen which is close to the junction so that the junction plane intersects the bevelled surface. The position of this line of intersection relative to the edge of the bevel on the surface is a measure of the depth of the junction; a linear magnification of about sixty is achieved for a bevel making an angle of 1° with the surface. Alternatively, the surface close to the junction may be successively ground off parallel to the junction plane. If the semiconductor is checked between stages of grinding, the junction can be located with an accuracy limited by that of the grinding (to within $1\ \mu$).⁽⁵⁴⁾

A ground or sandblasted surface is best for the first four probe methods. This surface helps to ensure non-rectifying probe contacts and to prevent the probes slipping. The light-beam and rectification direction methods demand an etched surface, the former because generally no impairment of the junction's rectifying properties can be tolerated, and the latter because the probe-semiconductor contact must rectify. For a semiconductor with a fairly wide forbidden energy gap such as silicon, the photo-probe can be used with a ground surface. Etched surfaces are not to be desired since masking of the specimen is required to prevent dissolution over all of it. Stream etching⁽²⁸⁾ with weak solutions may remove the need for masking. With two exceptions, the

visual methods do not require any particular surface finish; firstly, a ground surface is perhaps best for the preferential etch rate method, since the initiation of the etching is then likely to be more even over the surface of the specimen; secondly, some of the chemi-plating methods work best with mechanically prepared surfaces since etched surfaces may lead to reversal of the effects.

(3) In principle the probe methods should be applicable to all semiconductors. Apart from electroplating and electrolytic etching, the visual methods may not apply to all semiconductors; if they do, considerable work may be required to find the optimum conditions and solutions. However, this additional work may be well justified in practice for accuracy and subsequent convenience.

(4) The four-probe method can be discounted at once on the grounds of accuracy. Taking a probe spacing of 0.005 in. as the lowest practical limit before splaying gives variable results, the accuracy is as poor as ± 0.015 in. The two-probe method can also be discounted because, although its accuracy can approach that of the single-probe method, the latter is preferable when convenience is considered. Unreliability reduces the accuracy for the rectification direction method, and also for the thermoelectric probe if the latter is used on semiconductor of low impurity content. The most generally accurate probe methods are the single-probe and photovoltaic methods. The single- and photo-probe methods are accurate probably to less than one micron, depending on a fine micromanipulator movement.⁽¹⁴⁾ The ultimate limitation is that of plastic deformation, which occurs even under low pressures if the point is too sharp. For the light beam method, a light spot as small as one micron is possible⁽⁵⁵⁾ (smaller if shorter wavelengths are used), but the optical equipment needed is an added complication. If location by means of the thermoelectric probe is done in high ambient illumination, a photovoltage may be superimposed on the thermoelectric voltage. Since these two voltages are in opposition, although a p - n junction is still located, confusion may arise as to which region is p - or n -type.

Inaccuracy may arise with samples of semiconductors of small forbidden energy gap; these may be almost intrinsic at room temperature. Consequently, such samples may have to be cooled to allow location. The accuracy of the above methods may be retained if they are still effective at the temperatures involved. A method may have to be selected from the viewpoint of its easy adaptation to the changed conditions. If the ratio of the electron to hole mobility is very different from unity, then an error will occur in any method which depends on the conductivity. For example, the mobility ratio of indium antimonide is of the order of 80 : 1, necessitating care.

The visual methods, etching, staining, and plating, are capable of accuracies of the same order as the best of the probe methods, namely to about a micron (Figs. 8 and 9). The highest accuracy with staining and plating is obtained with a surface of fine structure, so a polished surface is best. The surface may be chemically polished or mechanically polished; the latter is preferable for convenience, but the former is useful for a large sample where the surface containing the junction is not flat. Previous remarks regarding chemi-plating and etched surfaces should be borne in mind.

The finding of the depth of a junction or junctions very close to a surface of a slice of semiconductor is of great technological importance owing to the extensive use of such structures in devices. Such junction depths may be only a few microns or less. As mentioned above, the use of a low angle bevel is customary, when the depth may be found

from the bevel angle and the position of the junction on the bevelled surface. However, a direct depth measurement by interferometry⁽⁶⁾ is possible, the only requirements being that the bevelled and top surfaces be specular, and the transition into the bevel be specular or very abrupt. The bevelled surface must be microscopically flat to ensure interference fringes which are sufficiently straight to permit accurate measurement. With delineation methods then, the junction depth can be found in terms of the wavelength of the light used. It is typically possible to measure depths to $\pm \frac{1}{2}$ of an interference fringe, i.e. for the sodium D-line, to $\pm 0.15 \mu$. An example of delineation with interference

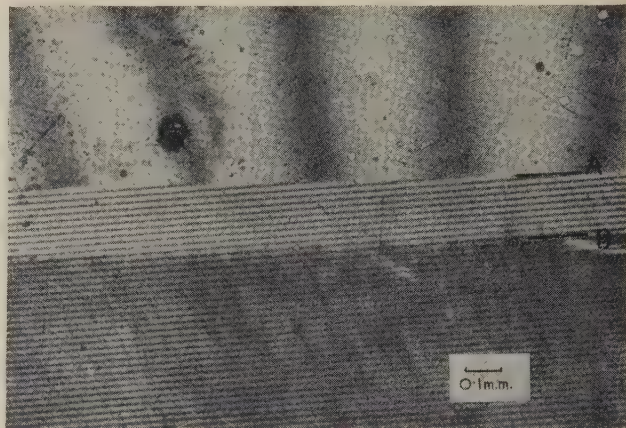


Fig. 10. Delineation of a p - n junction formed by diffusion of boron into n -silicon. The original top surface extends to A . A 1° bevel has been formed below A . Silver was deposited, as in Fig. 9, on the n -silicon (below B). Interference fringes are superimposed. The mirror was arranged to be nearly parallel to the top surface, giving broad fringes, and the closer fringes form in the air wedge above the bevelled surface. The junction depth is measured by counting the number of narrow fringes between the top of the bevel, and the edge of the silver

fringes superimposed is given in Fig. 10. Generally, preferential plating is preferred to staining or etching because of the greater contrast given by the metal layer at the junction under the vertical illumination used in the interferometer. However, Goldey⁽⁵⁶⁾ has published excellent photographs showing the combination of interference fringes and Fuller's stain on silicon. If possible, it is preferable to deposit metal below the junction so that the interference fringes can be counted above it.

(5) Several methods require non-rectifying contacts to be made to the sample. In the case of the single probe, these contacts must be ohmic, and stable, and must not appreciably disturb the carrier concentration in the sample. These contacts may be difficult to make on wide band-gap semiconductors. For the electrolytic and electroplating methods a relatively crude contact is probably good enough.

(6) Contamination of the specimen may be a problem in device manufacture or even in fundamental work when subsequent processing is required. This contamination may arise from trace impurities in the etches or cleaning solutions, or from metal left after plating. Care is needed to use solutions as pure as possible and to remove any metal plating thoroughly. The most troublesome impurities are the fast diffusing ones which may reduce the carrier lifetime.

(7) The disadvantage of special potting or mounting is that if it is done well, it may be difficult to reclaim the sample for subsequent processing. However, most small samples

will require mounting on a jig for bevel grinding and polishing or to grind a flat for probing, etc.

(8) Most of the visual methods do use unpleasant chemicals, but are not considered impractical.

The dielectric powder method demands a junction capable of withstanding a high reverse voltage. Fowler and Levesque⁽²²⁾ have used this method very successfully for germanium, and Fuller and Ditzenger⁽⁵⁷⁾ have delineated complex p - n junctions over a large sample.

An important consideration for the probing methods is that some lend themselves readily to an automatic scanning system. Bell Telephone Laboratories have made a machine⁽⁵⁸⁾ which senses when a wire, used as a potential probe, is on the base region of a grown transistor, and then welds the wire to the base.

Etching, staining, and electroplating leave permanent records. With care, chemiplated layers are stable, although because they are usually thin they are susceptible to deterioration. Adhesion of these layers is poor on polished surfaces (very poor if these are etched), but fair on ground surfaces, and also better for some metals than others. These considerations must be borne in mind if a permanent record is required.

5. Recommendations

As a consequence of the above discussion, it is possible to choose location methods giving maximum convenience for the accuracy required.

By far the most convenient are the preferential stain and preferential plate (provided they are suitable for p - n or I - h junctions in the semiconductor to be tested) since no contacts or masking are required, and surface preparation is not difficult. If these methods do not work for a particular semiconductor, then the best visual methods are probably the electrolytic or chemical etch-rate ones.

The thermoelectric probe method is convenient for p - n junctions, but the photo-probe is more reliable. For the utmost reliability for p - n and I - h junctions, the single-probe method is the best. This method also probably constitutes the best check on the accuracy of the visual methods; this is occasionally necessary because of the uncertainty regarding the mechanism of their operation.

It is clearly not possible to recommend the best methods for all semiconductors. Some suggestions are made about the methods thought by the authors to be best for the two most studied semiconductors.

Germanium

(a) p - n junctions. The photo-probe is the best probe method. The best visual method is electroplating, in view of the ease with which contacts can be applied to germanium. A solution of copper ammonium hydroxide is convenient, the copper depositing on the p -germanium.⁽⁴²⁾ Also, chemical etching, using CP_4 ,⁽⁵⁹⁾ or other hydrofluoric and nitric acid mixtures, or hydrofluoric acid and hydrogen peroxide mixtures, is useful. The dielectric powder method must be included if only because of the fine results it has yielded.

(b) I - h junctions. The single- or photo-probe methods are preferable. Electroplating, or chemical etching with hydrofluoric and nitric acid mixtures, are the best visual methods.

Silicon

(a) p - n junctions. The photo-probe is the best probe method. The best visual methods are the preferential stain using hydrofluoric acid in a strong light, and chemiplating.

In the latter case, solutions, diluted to slow the displacement processes occurring in the dark, deposit metal on ground or mechanically polished n -silicon when the junction is illuminated.

(b) I - h Junctions. The single-probe method is preferable. In addition if the conductivity differences are great, staining by hydrofluoric acid plus light may be successful for p -silicon. Also some of the chemiplating methods are valuable, especially silver fluoride solutions, either comparatively strong, or dilute with additional light.

6. Applications of location methods

In the above sections the emphasis has been on the exploitation of the differences existing at junctions in order to show their position. Here some brief examples are given of useful additions to semiconductor knowledge resulting from practical application of the methods. These examples may be of interest to those not directly concerned with location.

Conditions existing during crystal growth have been elucidated. p - n or I - h junctions formed during growth by impurity addition,⁽⁶⁰⁾ evaporation of impurity from a melt in vacuum,⁽⁶¹⁾ or deliberate or unavoidable alteration of the crystal growth parameters, have shown the shape of the liquid-solid interface.⁽³⁷⁾ Variations of impurity concentration in the melt have been shown by electroplating,⁽⁴¹⁾ preferential etching,⁽²²⁾ or probing⁽⁴¹⁾ the crystal. Silicon grown from a stirred melt in a silica crucible contains oxygen,⁽⁶²⁾ and here junction delineation has shown the extent of donor formation when oxygen atoms precipitate in p -silicon during heat treatment near 450° C, and has enabled calculation of the diffusion constant of oxygen in silicon.⁽⁶³⁾

Examination of sectioned alloy junctions can reveal details of the alloy process.⁽⁶⁴⁻⁶⁷⁾ These details include the shape of the alloy front, preferential dissolution by the alloying metal of different crystallographic planes, impurity segregation on refreezing, and the effect of dislocations⁽⁶⁸⁾ or the surface condition of the crystal⁽⁶⁹⁾ on the wetting of that surface by the alloying metal.

Electrical forming can convert a point contact on a semiconductor into a junction by a combination of alloying, diffusion, and thermal shock.^(70, 71) Fine probing and electroplating⁽⁷²⁾ have been used to explore these formed regions.

Many essential features of the diffusion of impurities have been learned from junction depth measurements. Surface concentrations resulting from different ways of applying impurities to the semiconductor, and diffusion constants for impurities have been measured.^(15, 33) The lack of uniformity of a delineated diffused junction has been traced to stray impurities, dust particles, scratches or other surface damage.⁽⁷³⁾ Also observable have been the extent of surface diffusion, the amount of diffusion along heavily dislocated planes,⁽⁷⁴⁾ and the effectiveness of layers which mask against some impurities.⁽⁷⁵⁾

The drastic reduction of minority carrier lifetime in germanium has shown by diffusion to be caused by stray copper atoms. Junction location has helped to show the extension to semiconductors of many phenomena such as the mass action interaction of impurities, and ion-pairing, previously found mainly in liquids.⁽⁷⁶⁾

Lastly, the inversion layer channel formed by some ambient surface conditions near the junction has been shown responsible for the changing performance of a device.⁽⁷⁷⁾

In all these cases practical demonstration has led to greater correlation between theory and practice.

References

- (1) SHOCKLEY, W. *Bell Syst. Tech. J.*, **28**, p. 435 (1949).
- (2) DUNLAP, W. C. *An Introduction to Semiconductors*, pp. 145-77 (New York: John Wiley and Sons Inc., 1957).
- (3) ARTHUR, J. B., GIBSON, A. F., and GUNN, J. B. *Proc. Phys. Soc. (London) B*, **69**, p. 697 (1956).
- (4) GUNN, J. B. *J. Electronics and Control*, **4**, p. 17 (1958).
- (5) SMITH, K. D. *Transistor Technology*, **1**, pp. 286-93 (New York: D. Van Nostrand Co. Inc., 1958).
- (6) BOND, W. L. and SMITS, F. M. *Bell Syst. Tech. J.*, **35**, p. 1209 (1957).
- (7) BOND, W. L. *Bell Lab. Record*, **35**, p. 1 (1957).
- (8) VALDES, L. B. *Proc. Inst. Radio Engrs*, **42**, p. 420 (1954).
- (9) UHLIR, A. *Bell Syst. Tech. J.*, **34**, p. 105 (1955).
- (10) BRADLEY, W. *Transistor Technology*, **1**, p. 149 (New York: D. Van Nostrand Co. Inc., 1958).
- (11) OROSHNIK, J. *Sylvania Technol.*, **10**, p. 17 (1957).
- (12) SMITH, K. D. *Transistor Technology*, **1**, p. 293 (New York: D. Van Nostrand Co. Inc., 1958).
- (13) PEARSON, G. L., READ, W. T., and SHOCKLEY, W. *Phys. Rev.*, **85**, p. 1055 (1952).
- (14) HOGARTH, C. A., and BAYNHAM, A. C. *Proc. Phys. Soc. (London)*, **71**, p. 647 (1958).
- (15) DUNLAP, W. C. *Phys. Rev.*, **94**, p. 1531 (1954).
- (16) BELIVEAU, M. *Electronics*, **31**, p. 106 (1958).
- (17) PIETENPOL, W. J. U.S. Patent 2,790,952 (30 April, 1957).
- (18) GOUCHER, F. S., PEARSON, G. L., SPARKS, M., TEAL, G. K., and SHOCKLEY, W. *Phys. Rev.*, **81**, p. 637 (1951).
- (19) SHIVE, J. N. *Proc. Inst. Radio Engrs*, **40**, p. 1410 (1952).
- (20) OROSHNIK, J., and MANY, A. *J. Electrochem. Soc.*, **106**, p. 360 (1959).
- (21) DUNLAP, W. C. *An Introduction to Semiconductors*, p. 195 (New York: John Wiley and Sons Inc., 1957).
- (22) FOWLER, A., and LEVESQUE, P. *J. Appl. Phys.*, **26**, p. 641 (1955).
- (23) ROLFE, J. *Brit. J. Appl. Phys.*, **7**, p. 109 (1956).
- (24) WANG, P. *Sylvania Technol.*, **11**, p. 50 (1958).
- (25) JACKSON, R. W. *J. Appl. Phys.*, **27**, p. 309 (1956).
- (26) BILLIG, E., and DOWD, J. J. *Nature (London)*, **172**, p. 115 (1953).
- (27) PANKOVE, J. I. *R.C.A. Rev.*, **16**, p. 398 (1955).
- (28) SULLIVAN, M. V., and EIGLER, J. H. *J. Electrochem. Soc.*, **103**, p. 132 (1956).
- (29) LESK, I. A., and GONZALES, R. E. *J. Electrochem. Soc.*, **105**, p. 469 (1958).
- (30) UHLIR, A. *Bell Syst. Tech. J.*, **35**, p. 333 (1956).
- (31) ELLIS, W. C. *Phys. Rev.*, **100**, p. 1140 (1955).
- (32) TURNER, D. R. *J. Electrochem. Soc.*, **105**, p. 402 (1958).
- (33) FULLER, C. S., and DITZENBERGER, J. A. *J. Appl. Phys.*, **27**, p. 544 (1956).
- (34) FULLER, C. S. U.S. Patent 2,700,740 (3 April, 1956).
- (35) BILLIG, E., and GASSON, D. B. *J. Appl. Phys.*, **28**, p. 1242 (1957).
- (36) WHORISKEY, P. J. *J. Appl. Phys.*, **29**, p. 867 (1958).
- (37) TANENBAUM, M., VALDES, L. B., BUEHLER, E., and HANNAY, N. B. *J. Appl. Phys.*, **26**, p. 686 (1955).
- (38) SILVERMAN, S. J., and BENN, D. R. *J. Electrochem. Soc.*, **105**, p. 170 (1958).
- (39) ILES, P. A., and COPPEN, P. J. *J. Appl. Phys.*, **29**, p. 1514 (1958).
- (40) TURNER, D. R. *J. Electrochem. Soc.*, **106**, p. 701 (1959).
- (41) CAMP, P. R. *J. Appl. Phys.*, **25**, p. 459 (1954).
- (42) MUELLER, C. W., and DITRICK, N. H. *R.C.A. Rev.*, **17**, p. 46 (1956).
- (43) PEARSON, G. L. U.S. Patent 2,669,692 (16 February, 1954).
- (44) AMICK, J. A., and GOLDSTEIN, B. *J. Appl. Phys.*, **30**, p. 1471 (1959).
- (45) LAW, J. T., and MEIGS, P. S. U.S. Patent 2,837,471 (3 June, 1958).
- (46) SLICHTER, W. P., and BURTON, J. A. *Transistor Technology*, **1**, pp. 113-19 (New York: D. Van Nostrand Co. Inc., 1958).
- (47) FULLER, C. S., STRUTHERS, J. D., DITZENBERGER, J. A., and WOLFSTIRN, K. B. *Phys. Rev.*, **93**, p. 1182 (1954).
- (48) OATLEY, C. W., and EVERHART, T. E. *J. Electronics*, **2**, p. 568 (1957).
- (49) HARRICK, N. J. *J. Appl. Phys.*, **29**, p. 764 (1958).
- (50) EHRENBERG, W., LANG, CHI-SAI, and WEST, R. *Proc. Phys. Soc. (London) A*, **64**, p. 424 (1951).
- (51) RAPPAPORT, P., LOFERSKI, J. J., and LINDER, E. G. *R.C.A. Rev.*, **17**, p. 100 (1956).
- (52) NEWMAN, R. *Phys. Rev.*, **100**, p. 700 (1955).
- (53) CHYNOWETH, A. G., and MCKAY, K. G. *Phys. Rev.*, **102**, p. 369 (1956).
- (54) LETAW, H., SLIFKIN, L. M., and PORTNOY, W. M. *Rev. Sci. Instrum.*, **25**, p. 865 (1954).
- (55) DUTTON, D. *Photoconductivity Conference*, p. 593 (New York: John Wiley and Sons Inc., 1956).
- (56) GOLDEY, J. M. *Bell Lab. Record*, **37**, p. 224 (1959).
- (57) FULLER, C. S., and DITZENBERGER, J. A. *J. Appl. Phys.*, **28**, p. 40 (1957).
- (58) *Bell Lab. Record*, **33**, p. 108 (1955).
- (59) HAYNES, J. R., and SHOCKLEY, W. *Phys. Rev.*, **81**, p. 838 (1951).
- (60) TEAL, G. K., SPARKS, M., and BUEHLER, E. *Phys. Rev.*, **81**, p. 637 (1951).
- (61) BRADSHAW, S. E., and MLAVSKY, A. I. *J. Electronics*, **2**, p. 134 (1956).
- (62) KAISER, W., and KECK, P. H. *J. Appl. Phys.*, **28**, p. 882 (1957).
- (63) LOGAN, R. A., and PETERS, A. J. *J. Appl. Phys.*, **28**, p. 819 (1957).
- (64) HANSON, J. S. *I.B.M. J. Res. Developm.*, **1**, p. 279 (1957).
- (65) PETERSON, J. W., MCGLASSEN, J., and HITTINGER, W. C. *J. Metals*, **9**, p. 823 (1957).
- (66) MUELLER, C. W. *R.C.A. Rev.*, **18**, p. 205 (1957).
- (67) BURCHAM, N. P., MILLER, L. E., ROBILLARD, T. R., VANDERWAL, N. C., and WESTBERG, R. W. *Transistor Technology*, **3**, p. 175 (New York: D. Van Nostrand Co. Inc., 1958).
- (68) PANKOVE, J. I. *J. Appl. Phys.*, **28**, p. 1054 (1957).
- (69) ROSE, A. S. *R.C.A. Rev.*, **19**, p. 423 (1958).
- (70) VALDES, L. B. *Proc. Inst. Radio Engrs*, **40**, p. 445 (1952).
- (71) SIM, A. C. *J. Electronics and Control*, **3**, p. 139 (1957).
- (72) MILLER, L. E., and FORSTER, J. H. *Bell Syst. Tech. J.*, **35**, p. 767 (1956).
- (73) KEYWELL, F. *J. Appl. Phys.*, **29**, p. 871 (1958).
- (74) KARSTENSEN, F. *J. Electronics and Control*, **3**, p. 305 (1957).
- (75) FROSCH, C. J., and DERICK, L. *J. Electrochem. Soc.*, **104**, p. 547 (1957).
- (76) REISS, H., FULLER, C. S., and MORIN, F. J. *Bell Syst. Tech. J.*, **35**, p. 535 (1956).
- (77) LEVESQUE, P. *J. Appl. Phys.*, **27**, p. 1104 (1956).

Accuracy of selected-area microdiffraction in the electron microscope

by A. W. AGAR, B.Sc., F.Inst.P., A.M.I.E.E., Aeon Laboratories, Egham, Surrey

[Paper first received 14 December, 1959, and in final form 22 January, 1960]

Abstract

Because of the spherical aberration at the objective lens, the area of an object defined by the selector aperture for microdiffraction experiments does not exactly correspond to the actual parts of the specimen contributing to the pattern. Further errors may arise through incorrect lens settings. The magnitude of the possible errors and the electron-optical explanation are discussed. The theoretical results are in reasonable agreement with the experimentally observed errors. It is concluded that especial care is required in studies of thin metal foils where misorientations between grains are being measured.

Introduction

THE facility for obtaining a microdiffraction pattern from a selected area of an object viewed in an electron microscope is in increasing use. Particularly important applications are for the identification of precipitates extracted in replicas from a specimen surface and for work on orientation determination and measurement of the misorientations at sub-boundaries in thin foils.

The essence of the method (Fig. 1) is that a diffraction pattern from an object is formed at the back focal plane of the objective lens when the illumination on to the object is parallel. This pattern is projected by the intermediate lens on to the object plane of the projector lens, which magnifies it sufficiently for measurements of the pattern to be made with reasonable accuracy. By application of geometrical optics, and if it is assumed that the objective lens is perfect, it can be shown that a selector aperture in the image plane

of the object lens defines a much smaller area in the plane of the object (the diameter is M^{-1} times diameter of aperture, where M equals the magnification of the objective lens), and any diffraction pattern observed must originate from such an area.

In order to attain the state illustrated in Fig. 1, it is important to set up the correct electron-optical conditions by careful adherence to the operating procedure, which consists of the following four stages:

- (1) Adjustment of the intermediate-lens strength until the selector aperture is in focus. This ensures that the object plane of the intermediate lens is coincident with the plane of the aperture.
- (2) Adjustment of the objective lens strength to bring the object into focus. This ensures that the image of the object is in the same plane as the selector aperture.
- (3) Weakening of the intermediate-lens strength until its object plane coincides with the back focal plane of the objective lens. This position is judged by making the central spot of the pattern as small and round as possible.
- (4) Defocusing of the condenser lens to obtain near-parallel illumination of the object.

A typical result of the technique, applied to a crystal of molybdenum disulphide, is shown in Fig. 2. This crystal

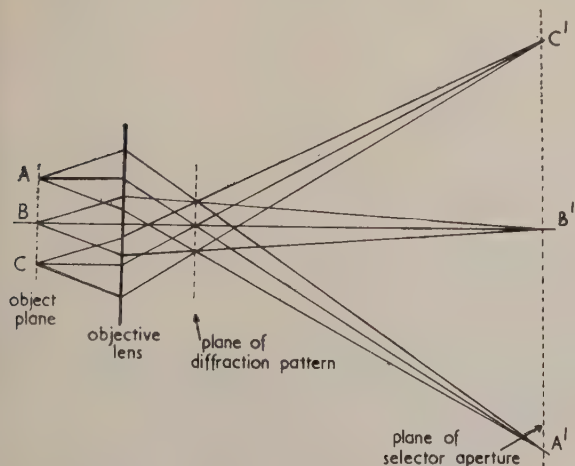


Fig. 1. Formation of a diffraction pattern and image of object

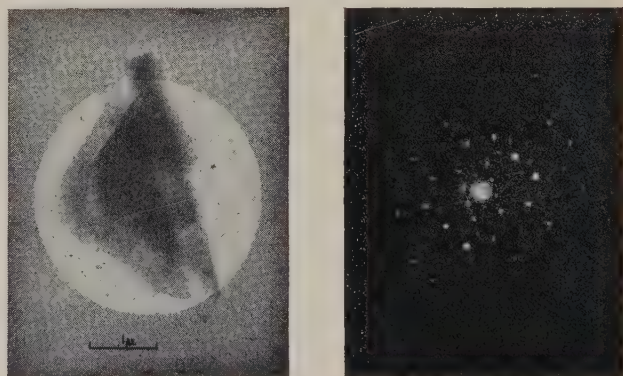


Fig. 2. Molybdenum disulphide crystal and diffraction pattern

Light region represents "selected area"

was used as a test object in the experiments to be described since it gave rise to many orders of diffraction and its boundaries were clearly defined.

When the imperfections of real lenses are taken into account, it is no longer certain that the area of the object from which

diffracted beams originate to form the image is the same as that defined by the selector aperture, even if the lens settings are made with accuracy. Although microscope designers have made this clear, the extent of the probable errors were not precisely stated, and a series of experiments were therefore designed to define such errors as well as possible.

Error arising from spherical aberration at the objective lens

To test this aberration, a crystal was placed at different distances from the edge of the virtual selector aperture in the object plane, and each resulting diffraction pattern was recorded. Care was taken to follow the operating procedure defined above, and the exposures of the patterns were standardized at $1\frac{1}{4}$ min for a constant amount of defocusing of the condenser lens. It was found that several orders of diffraction could be obtained from a crystal completely outside the area defined by the selector aperture (Fig. 3). The diameter of the selected area was $3.3\ \mu$.

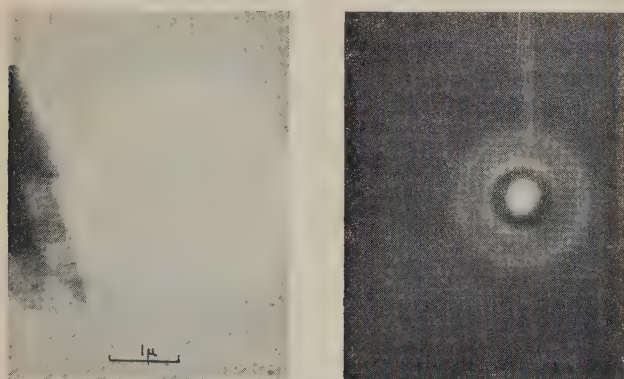


Fig. 3. Crystal just outside "selected area" and resultant diffraction pattern

The diffraction orders visible for different minimum distances of an edge of the crystal from the virtual aperture in the object plane are detailed in Table 1. When the partial diffraction pattern observed appears in the same quadrant of the image as the image of the crystal from which it is derived, it has been termed an erect pattern. It may sometimes appear in the opposite quadrant and is then labelled "inverted". As would be expected, the outer orders of diffraction, which enter the lens at a wide aperture angle, are refracted the more strongly because of spherical aberration, and appear in the final image. It is seen that a crystal whose nearest point to the virtual aperture is nearly $0.5\ \mu$ away, can give rise to a ninth-order diffraction image.

Fig. 4 is a ray diagram illustrating how the higher-order diffraction spots are affected by a lens with spherical aberration. ABC is a typical paraxial ray from an object point A

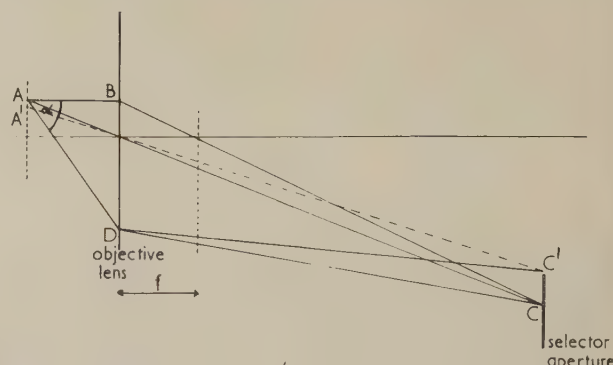


Fig. 4. Shift of high-order diffraction caused by spherical aberration

to an image point C in the plane of the selector aperture. It will be observed that A lies outside the area defined by the virtual selector aperture in the object plane. The diffracted ray AD would be refracted along the path DC by a perfect lens but, in a lens with spherical aberration, will take the path DC' . The object point conjugate with C' for a perfect lens is A' . Then, by definition, AA' equals the radius r_s of the confusion disk caused by spherical aberration for the aperture angle α . The displacement of the ray in the plane of the selector aperture is Mr_s where M is the magnification of the objective lens. AA' thus contains points not included in the selected area from which rays diffracted through angles less than α may form an image in the diffraction pattern because of spherical aberration.

Table 2. Calculated radius of aberration disk for different diffraction orders

Diffraction order	Angle	r_s (μ)
1	$51'$	0.0027
2	$1^\circ-42'$	0.0214
3	$2^\circ-33'$	0.0725
4	$3^\circ-24'$	0.17
5	$4^\circ-15'$	0.335
6	$5^\circ-06'$	0.58
7	$5^\circ-57'$	0.92
8	$6^\circ-48'$	1.37
9	$7^\circ-39'$	1.96
10	$8^\circ-30'$	2.68

r_s = radius of aberration disk for plane of disk of minimum confusion,

$$r_s = \frac{1}{8} C_s \alpha^3,$$

$$C_s = 0.33\text{ cm},$$

Crystal MoS_2 , giving diffraction orders at multiples of $51'$ in $(a, 0, 0)$ direction.

Table 2 shows the radius of the confusion disk for different deflexion angles calculated for the plane of the circle of least confusion. The values refer* to a lens with spherical-aberration constant C_s equal to 0.33 cm .

* RUSKA, E., and WOLFF, O. *Zeits. fur Wiss. Mik und Mik. Tech.*, 62, p. 466 (1956).

Table 1. Diffraction orders visible for different distances of object behind selector aperture image

Minimum distance of crystal from selector aperture edge (on plate) (mm)	Effective distance in object plane (μ)	Diffraction orders visible
0.1	0.011	8-12 erect
		1-5 inverted
0.5	0.055	7-10 erect
		1-3 inverted
0.5	0.055	7-12 erect
		1-5 inverted
0.7	0.077	6-10 erect
3.2	0.34	7-10 erect
3.5	0.37	7-10 erect
4.7	0.5	9 only

Diameter of selected area = $3.3\ \mu$.

The radius of the confusion disk for a given order of diffraction (Table 2) can be compared with the observed results of Table 1. For very small distances of the crystal edge behind the virtual aperture, the possible experimental errors are of the same order as the measurements (see later section), and correlation is difficult. At greater separations, however, there is some discrepancy between observed and calculated results. This is partly to be expected, because a finite area of the crystal must be diffracting before the intensity in the diffraction spots becomes great enough to be detected.

Errors arising from incorrect operation

(a) *Objective lens setting.* A common error in operation is a failure to focus the image of the object accurately into the plane of the selector aperture. A crystal just outside the virtual selector aperture was photographed at a series of settings of objective lens current, the remainder of the operating procedure being followed correctly. The results are summarized in Table 3A, from which it is seen that a large error in setting the objective-lens current could result in even first-order diffraction from a crystal not within the defining area. The Siemens Elmiskop I possesses accurately calibrated steps of current for the lenses, and the medium-fine controller of the objective lens results in a current change

of $260\mu\text{A}$ for each step position. The focusing current for the objective lens was 429 mA at the diffraction position. Thus each step corresponded to a change in focal length of 2.9μ (f is 2.4 mm). The position determined as the best focus position for correct operation is denoted by F , and the number of steps over- or under-focused are shown in Table 3A.

The effect of moving from far under focus to far over focus is seen to be the inversion of the diffraction pattern (Table 3B and Fig. 5). In certain intermediate settings, the inner orders

Table 3. Variation of diffraction pattern with objective lens focus

Objective focus	Change in focal length (μ)	Diffraction orders visible
<i>A: Object 0.05μ from edge of virtual selector aperture</i>		
$F - 3$	$+8.7$	1-6 inverted 9-12 erect
F (best visual focus)	0	1-4 inverted 7-10 erect
$F + 1$	-2.9	1-3 inverted 8-12 erect
$F + 3$	-8.7	(very faint) 7-11 erect
$F + 5$	-14.5	3-11 erect
$F + 8$	-23.2	1-10 erect
<i>B: Object 0.5μ from edge of virtual selector aperture</i>		
F	0	9 only (v. faint)
$F + 18$	-52.2	1-8 erect
$F - 18$	$+52.2$	1-9 inverted
<i>C: Object 0.05μ from edge of virtual selector aperture</i>		
$F' + 3$	-8.7	4-11 erect
F' (set for no spots visible)	0	7-10 erect
$F' - 1$	$+2.9$	1-3 inverted (v. faint) 7-10 erect
$F' - 3$	$+8.7$	1-3 inverted 7-10 erect
$F' - 8$	$+23.2$	1-6 inverted 7-9 erect (faint)
$F' - 20$	$+58$	1-10 inverted

Increments of objective lens current refer to the number of steps of the medium control on Siemens Elmiskop I; 1 step represents a change of $260\mu\text{A}$ in a current of about 430 mA (0.6% change).

Focal length = 2.4 mm .

F' is believed to approximate to Gaussian focus.

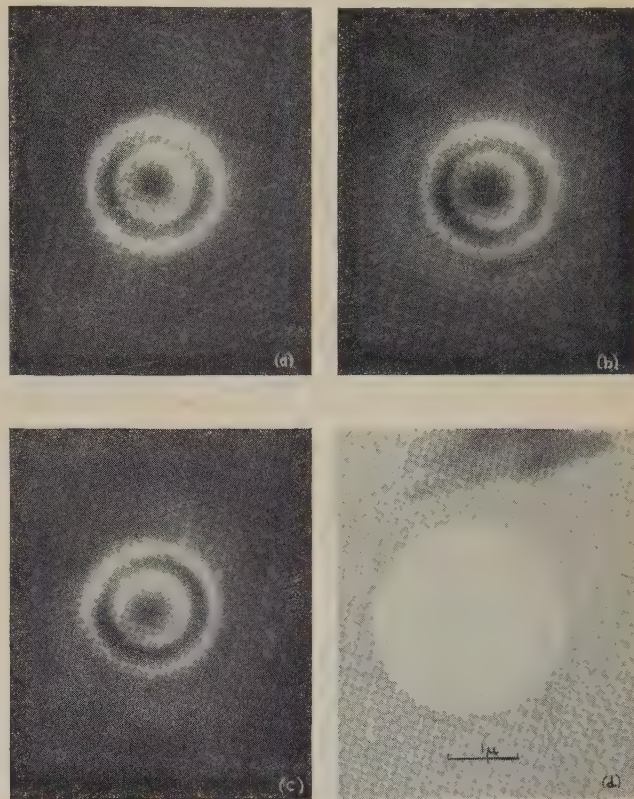


Fig. 5. (a) Diffraction pattern for objective lens 52.2μ underfocused; (b) diffraction pattern at correct objective lens setting; (c) diffraction pattern for objective lens 52.2μ over-focused; (d) crystal and "selected area"

of diffraction are on one side of the central spot, and the outer orders on the other. It was noticed that inner diffraction orders appeared at the point chosen as the best focus for the object, but that these disappeared when the lens was over-focused by about three steps of the medium controller. A further experiment was then tried of setting the objective current in the normal way, obtaining the diffraction pattern, and then altering the objective-lens strength until the diffraction pattern disappeared (as far as could be judged on the screen—some spots were later found on the plate). This point was denoted as F' , and observations were made at further different settings of the objective lens strength (Table 3C). These results confirm the observations first made (Table 3A).

These observations can now be considered in the light of the optics of the system. It is necessary to consider an object point A which forms an image through a perfect lens (Fig. 6), which could just be screened by the virtual selector aperture when the objective lens strength was such that the selector aperture lay in the conjugate plane to the object. If the objective lens strength is increased, the electrons diffracted

towards the lens axis (that is, AC) are now refracted through the selector aperture. If the objective lens strength is decreased, the reverse effect occurs, and rays such as AD can appear in the image. This explains the inversion of the diffraction pattern with change in objective lens strength. It will be noted that for an overfocused lens, the pattern will appear on the same side of the axis as the object; it will be inverted with respect to the object when the lens is under-focused.

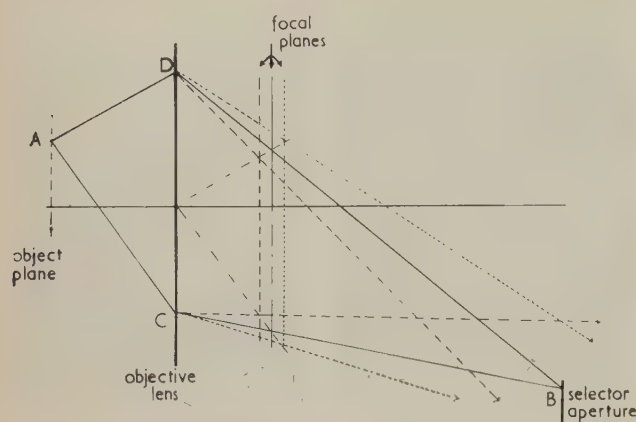


Fig. 6. Effect of objective-lens strength on diffraction pattern

— lens focused.
 lens under-focused.
 --- lens over-focused.

The effect of a lens with spherical aberration may now be introduced. Since each diffracted ray passes through only a narrow zone of the objective lens, the spherical aberration, and hence the effective focal length of the lens, will vary with the angle of diffraction. The effect is shown in Fig. 7, where the construction illustrates that the diffraction pattern is formed on a paraboloidal image surface, with its centre at the Gaussian focal plane of the lens.

When the objective lens is "correctly" focused, it is in fact over-focused for the higher diffraction orders which are therefore visible as an erect image. Over-focusing of the lens will enable more of the lower orders of diffraction to pass through the selector aperture as an erect pattern, until eventually the first-order diffraction is imaged. When the objective lens strength is decreased, an inverted image of

the pattern is to be expected. However, the shortening of the effective focal length for the higher orders of diffraction (by spherical aberration) will at first counteract the under-focusing. Consequently, the inverted image of the lower orders of diffraction will appear first, and they may be seen at the same time as the erect higher orders. With increased under-focusing of the lens, the erect pattern will disappear and the inverted pattern will grow. This theory satisfactorily accounts for the effects observed in the experiments on the phenomenon. It suggests an additional caution in the examination of material contained within the selected area, since it is clearly possible that part of a diffraction pattern

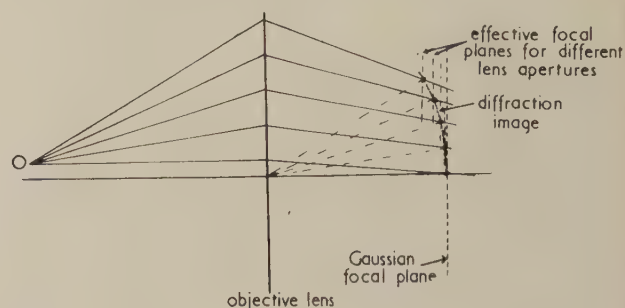


Fig. 7. Formation of curved diffraction image caused by spherical aberration

from a selected region may be lost at the selector aperture if the focusing of the objective lens is not carefully carried out.

It will be recalled that, with the objective lens accurately focused, a few lower order spots appeared in the diffraction image (inverted). These disappeared when the focal length of the objective lens was decreased by about 8.7μ . This can be explained qualitatively by assuming that the best focus is judged as being at the focal distance of the circle of least confusion, whereas the diffraction pattern is centred on the Gaussian focus. To explain the observed change in objective-lens current, however, it would be necessary to assume that the objective lens was accepting a beam of semi-angle about 2.5×10^{-2} radians, which seems much too high. The effective change in focal length of the objective lens was calculated for the different diffraction orders, and this has been tabulated in Table 4. These figures can be compared with the observed change in the focal length of the objective lens which was found to be required to invert

Table 4. Comparison of calculated and observed values for changes in objective-lens zonal foci related to diffraction orders imaged

Diffraction order	Angle	Calculated distance of zonal focus from paraxial focus (μ)	Limiting diffraction order observed (inverted pattern)	Distance of zonal focus from Gaussian focus (μ)
1	51'	0.74		
2	1°-42'	2.9		
3	2°-33'	6.6	3	2.9
			3	5.8
			3	8.7
4	3°-24'	11.8	4	11.6
5	4°-15'	18.5		
6	5°-6'	26.6	6	17.2
			6	23.2
7	5°-57'	36.4		
8	6°-48'	47.5		
9	7°-39'	60	9	52
10	8°-30'	74	10	58

different diffraction orders. It has been assumed that Gaussian focus lies at the focus point F' which has been equated to $F-3$ from Table 3A for some of the results. The agreement is good enough to sustain the general validity of the theory.

(b) *Intermediate Lens Setting.* The general criterion for the setting of the intermediate lens strength to form an image of the back focal plane of the objective lens is to make the central spot of the diffraction pattern as small and round

of the intermediate lens was found to be required between these two settings.

A series of photographs was made at slightly different settings of intermediate lens strength to see what effects could be observed. Although many spots appeared quite unaltered, there were clear changes in the appearance of some of the spots (Fig. 8). While an electron optical explanation of the effects is not attempted here, it seems worth mentioning that the detailed appearance of a spot can be modified by the setting of the intermediate lens strength.

Operational errors

The operational procedure for obtaining the diffraction pattern was examined to determine the possible setting accuracy for the process. The intermediate lens could be focused on to the selector aperture with an accuracy of one step on the medium current controller (1 step equals $380 \mu\text{A}$). The setting could be judged most easily with the objective aperture removed. The setting of the objective lens was attempted with a metal foil as object, since it is with metal foils that the effects of errors in operation are likely to be most serious. It was found to be difficult to set the objective-lens strength more accurately than ± 1 medium step, and quite easy to suffer an error of 3 steps of the controller unless considerable care was taken. The setting of the intermediate lens to form the image of the diffraction pattern could be done with considerable precision, and no difficulties ought to occur from this source.

Conclusions

The apparent area selected in the microdiffraction technique may be materially different from that actually contributing to the diffraction pattern obtained. In general, the effects will not be serious in orientation determination, but may be important in identification of different phases, and in the analysis of sub-boundaries in thin foils. For example, in using selected area diffraction to analyse mis-orientation boundaries, one must ensure that a second boundary does not lie close to the area selected, or some diffraction spots in the higher orders may suffer a splitting because of the second mis-orientation. The effect will be particularly large in the higher orders, which are the ones naturally used in measuring spot splitting. As an example of an error caused by spherical aberration, spot splitting in a seventh order diffraction could arise from a boundary at least $\frac{1}{2} \mu$ away from the area apparently selected. The distance would quickly be increased by errors in lens-current settings. With consideration for the effect of errors which might be incurred if care was not taken, it might be possible for a first-order reflexion to be recorded from a part of the object 1000 \AA away from the edge of the virtual selector aperture.

It remains only to add that these measurements were made on an instrument with low spherical aberration. Microscopes of older design will probably show considerably larger errors.

Acknowledgements

The author would like to acknowledge the discussions with Mr. R. Phillips of this laboratory, and Mr. T. Mulvey of the A.E.I. Research Laboratory, Aldermaston, which brought this problem to his attention, and to thank Mr. Phillips for critical discussions during the progress of the work.



(a)



(b)



(c)

Fig. 8. Part of diffraction pattern of molybdenum disulphide; (a) with intermediate-lens strength 1.37% weaker than (b); (b) with intermediate lens correctly set (55 mA) for imaging diffraction pattern; (c) with intermediate-lens strength 1.37% stronger than (b)

as possible. The spot is formed of unscattered electrons (or inelastically scattered electrons) from the whole beam illuminating the object. Consequently, there is a tendency to focus the intermediate lens in the plane of the disk of minimum confusion for the objective lens. If one of the first-order diffraction spots is observed instead, a slightly different setting of the intermediate lens may be necessary, as such spots must be close to the Gaussian focal plane. In practice, a change of 1 step of the medium control ($380 \mu\text{A}$)

Vibration phenomena in detonation waves in hydrogen-oxygen mixtures

by D. H. EDWARDS, Ph.D., and T. G. JONES, Ph.D., Department of Physics, University College of Wales, Aberystwyth

[Paper received 27 April, 1959]

Abstract

A photographic investigation is described, using a Schlieren system and rotating-drum camera, of detonation waves in hydrogen-oxygen mixtures propagating in a 1.6 cm diameter tube of circular section. It is found that mixtures near the limits of detonability exhibit the phenomenon of spin in which the motion is of long wavelength and the frequency is in agreement with values predicted by existing theories. In stronger detonating mixtures a high-frequency spin of short wavelength is present which shows the same characteristics on a streak photograph as a normal long wavelength spin; measured values of frequency and wavelength agree reasonably well with those calculated. In a range of mixtures of intermediate composition both types of vibration are present. Longitudinal pressure waves, the recurrence frequency of which is twice that of the fundamental mode transverse vibration, are also observed behind the detonation front in all mixtures; the existence of these waves is confirmed by pressure recordings and a possible explanation of their origin is discussed.

Introduction

WHILST the idealizations embodied in the hydrodynamic theory of detonation appear entirely satisfactory for plane waves propagating in readily detonable gas mixtures, detonation waves in mixtures near the limits of detonability show considerable deviations from the ideal wave. One phenomenon, exhibited by such "weak" waves travelling in straight tubes, in which the motion is no longer one-dimensional, is that commonly termed "spin" which was first observed by Campbell and Woodhead⁽¹⁾ in carbon-monoxide-oxygen mixtures. Extensive photographic studies of this phenomenon have subsequently been made by numerous investigators,^(2, 3, 4) and it has been established that it is present in all mixtures near the detonation limits⁽⁵⁾ and frequently during the build-up of a normal detonation wave.⁽⁶⁾ Various hypotheses were proposed by Campbell and Finch,⁽²⁾ Jost,⁽⁷⁾ Becker⁽⁸⁾ and Doering⁽⁹⁾ to explain how spinning waves arise and to account for their properties in terms of the characteristics observed on streak luminous photographs. In each of these theories, however, serious difficulties arise and they are incapable of giving a satisfactory and consistent explanation of all the observed facts. By considering a mechanism whereby the natural frequencies of the burnt gases in the tube can be excited and maintained, Manson,⁽¹⁰⁾ Fay⁽¹¹⁾ and Toennies and Wagner⁽¹²⁾ have developed essentially the same theories which predict spin frequencies in close agreement with those observed. Furthermore, the detailed physical picture given by Fay appears to

be the most satisfactory description yet given of the principal characteristics of the whole phenomenon.

Since the publication of the above theories, Greifer and others⁽¹³⁾ have observed retrograde striations of very high recurrence frequencies on their streak Schlieren photographs, undetected by previous investigators owing to the inadequate resolution obtainable with their apparatus, both in spinning carbon-monoxide-oxygen mixtures and in non-spinning hydrogen-oxygen mixtures. These authors suggest that the high frequency striae could arise from some mechanism of discontinuous propagation which may indeed be a general property of the stable detonation state.

In the present investigation, streak Schlieren photographs have been obtained for detonation waves in a range of compositions of hydrogen-oxygen mixtures, and an interpretation of the results is attempted in terms of the concepts proposed by Fay.

Theory

In his theory of spinning detonation Fay considers the general case of three-dimensional vibrations in the burnt gases which are assumed to be at a uniform average temperature and pressure. Although the amplitude of the pressure vibrations occurring in spinning waves can be considerable (e.g. about 7 atm in $8\text{H}_2 + \text{O}_2$), it is assumed that linear sound theory provides a reasonable approximation for the purposes of calculation of the frequencies of vibration. An appropriate solution of the wave equation for a cylindrical pipe is found which describes a wave, the crest of which rotates at a uniform angular velocity about the tube axis. These vibratory pressure waves give rise to heating and cooling effects which cause the combustion to proceed irregularly; the resulting non-uniform heat release provides the energy source which maintains the pressure vibration. When the boundary conditions at the tube wall, which is assumed to be perfectly rigid, and the detonation front are satisfied, an expression is obtained for the vibrational frequency ν at the detonation front

$$\nu = \frac{c_1 k_n}{2\pi r_0} \left(\frac{Z - 1}{Z + 1} \right)^{1/2} \quad (1)$$

where r_0 is the tube radius, c_1 , the sound velocity in the burnt gases and k_n is the first zero of the first derivative of the Bessel function J_n ; the nodal number is taken to be unity as it is assumed that nodes only occur at the walls of the tube: Z is a dimensionless quality termed the specific acoustic impedance and represents the ratio of the characteristic impedance for the particular mode of vibration in question to ρc_1 , where ρ is the density of the burnt gases. The charac-

teristic impedance is evaluated at the detonation front and is defined as the ratio of the vibrational wave pressure to vibrational velocity in the direction of propagation of the detonation wave. It is easily shown that Z can be expressed in the form

$$Z = -\{(k_n l / 2\pi r_0)^2 + 1\}^{1/2} \quad (2)$$

where l is the wavelength in the direction of the tube axis. When $Z = -\infty$ the vibrational motion is purely transverse and equation (1) becomes

$$v_n = c_1 k_n / 2\pi r_0 \quad (3)$$

The condition that Z should be large is seen from equation (2) to obtain when $l \gg r_0$. From an analysis of the spin photographs of Bone, Frazer and Wheeler,⁽⁴⁾ Fay finds that $l \approx 60r_0$ which gives a value of $Z \approx -20$. Since the value of v_n is little affected by considering Z to be infinite rather than -20 , equation (3) is sufficiently accurate in predicting the spin frequency and it is concluded that the experimental evidence indicates that the motion is almost entirely transverse in spinning carbon-monoxide-oxygen mixtures. A possibility which has to be considered is that the finiteness of the experimentally determined value of Z could arise from the idealization of perfectly rigid tube walls. Observations made of the wall vibrations, however, by means of a condenser microphone set to measure radial motion of the wall, show that the highest frequency excited in the present tube during the passage of a detonation wave is of the order of 10 kc/s. This frequency is sufficiently removed from spin frequencies so as not to affect the value of Z .

Experimental details

Observations are made on detonation waves propagated in a brass explosion tube 1.6 cm internal diameter and 3.2 mm thick wall which has a smooth internal surface. The tube consists of three sections, each having flanges at both ends which are fitted with rubber O-rings; the flanges enable the three sections to be bolted together to form a continuous air-tight tube. The first section, termed the driving section, is 1 m long and is followed by the main experimental section of approximately 4 m in length; the length of the third section, used for optical observations, is 22 cm. Both ends of the tube can be closed by flat plates bolted to the flanges. For filling purposes the driving and main sections can be isolated from each other by clamping a thin film of cellophane between their adjoining flanges. The optical section is constructed from a solid block of brass into which are set, along the direction of the tube axis, plate glass windows 6 mm thick and 15 cm long in the manner shown in Fig. 1.

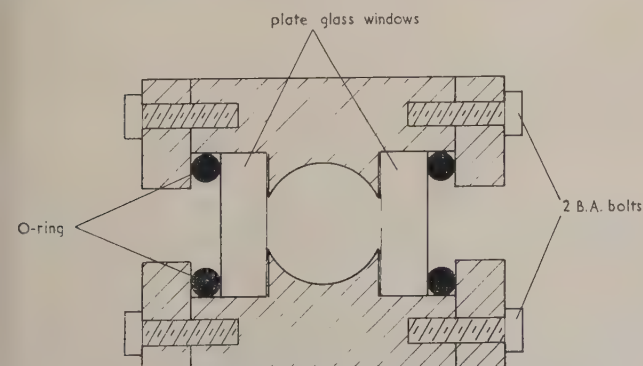


Fig. 1. Section through the optical working section

Before admitting the gas mixtures the whole tube is initially evacuated to a pressure of 0.1 mm of mercury. The driving section is then filled with an equivolume mixture of acetylene and oxygen while, at the same time, the hydrogen-oxygen mixture under test is admitted into the main section; the initial pressure of both mixtures is atmospheric. The test mixtures are prepared in large pre-mixing cylinders, the partial pressure of the constituent gases having been accurately measured by a mercury manometer. All the gases used are obtained from commercial high-pressure cylinders. Detonation is initiated in the driving mixture by electrically firing a copper acetylide matchhead. A powerful plane detonation wave is thus generated which ruptures the cellophane diaphragm and initiates detonation in the test mixture.

The Schlieren optical system is a twin-lens parallel beam type in which the two Schlieren lenses are $f/6.3$, 36 in. focal length telephoto lenses. The field of view of the system is limited by a slit, 10 cm long and 1.6 mm wide, placed near one of the windows of the optical section; the image of this slit as it is swept across the film gives the traces referred to as streak photographs. With an image reduction ratio of 4.5 : 1 the width of the slit image on the film is 0.36 mm and the effective writing speed of the drum camera is of the order of 0.7 mm/ μ s. The speed of rotation of the camera drum is determined at the instant of firing from a measurement of the frequency of pulses from a photocell, which is arranged to detect the reflexions of a beam of light from the faces of a stainless steel mirror mounted on the drum axis. A suitable line source of high intensity is provided by a capillary mercury arc lamp of the type described by Edwards and Owen⁽¹⁴⁾; this arc can be operated continuously for alignment purposes and flashed by a capacitor discharge. The lamp is triggered at a suitable interval before the arrival of the detonation wave in the field of view by a voltage pulse from an ionization probe (see Knight and Duff)⁽¹⁵⁾ set in the wall of the tube at a short distance from the working section. In order to record density gradients both normal and perpendicular to the wave-front, a knife-edge mounting is available which can be orientated either perpendicular or parallel to the tube axis.

Results

Detonation waves in a number of hydrogen-oxygen mixtures in the composition range $8H_2 + O_2$ to $H_2 + 3O_2$ have been studied by the method of streak Schlieren photography. According to the generally accepted interpretation of the spin phenomenon, outlined above, the pressure crests and troughs which form at the detonation front extend backwards into the burnt gas and are orientated parallel to the tube axis. Such pressure waves give rise to density gradients perpendicular to the direction of flow. It would therefore be expected that a Schlieren knife-edge, orientated parallel to the tube axis, would be the most favourable for the observation of the characteristic horizontal bands appearing on streak photographs of spinning waves. On the other hand, a knife-edge placed perpendicular to the tube axis is best suited for the recording of the backward moving detonation waves and particle paths. Both methods have been employed with all the mixtures in the present study.

Photographs obtained with a horizontal knife-edge for the two mixtures at both ends of the composition range, $8H_2 + O_2$, and $H_2 + 3O_2$, show pronounced horizontal bands which persist for the total duration of the photograph which is of the order of 1 ms. A typical photograph obtained with $H_2 + 3O_2$ is shown in Fig. 2(a). Vertical knife-edge

photographs obtained for these two mixtures show the particle paths and retrograde striations together with the characteristic undulation of the wave-front; the result obtained for $H_2 + 3O_2$ is given in Fig. 2(b). Mixtures in the composition range $4H_2 + O_2$ to $H_2 + 2O_2$ give photographs of an entirely different character to those obtained with the above mixtures. Thus, when a horizontal knife-edge is used, the relatively broad and strong horizontal bands are absent, but there now appears another set of horizontal bands of very much higher frequency which originate at the detonation

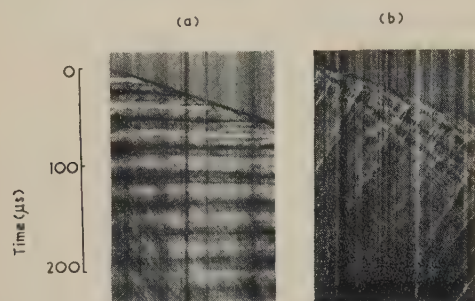


Fig. 2. Streak Schlieren photographs of the detonation wave in the mixture $H_2 + 3O_2$ using (a) a horizontal knife-edge and (b) a vertical knife-edge. Length of window is 10 cm

front and extend for a distance of roughly 2 cm behind it. Similarly, with the vertical knife-edge photographs, the pronounced particle paths and detonation waves are replaced by high-frequency backward-moving striae which again persist for only a comparatively short distance behind the front, although for a somewhat greater distance than the horizontal striae. The recurrence frequencies of these striae are given in Table 1; the values quoted for the high frequencies are to be regarded as approximate only, owing to the limitations of the resolution obtainable with the apparatus.

Table 1. Observed frequencies of retrograde and horizontal striations in various hydrogen-oxygen mixtures in a 1.6 cm diameter tube

Mixture	Frequency of retrograde striations (kc/s)	Frequency of horizontal striations (kc/s)	Fundamental mode spin frequency (calculated) (kc/s)
$8H_2 + O_2$	—*	75.6	80.7
$6H_2 + O_2$	935.0	210, 71.2	76.2
$4H_2 + O_2$	1420	373	71.7
$2H_2 + O_2$	2540	—*	59.4
$H_2 + O_2$	1665	511	48.6
$H_2 + 2O_2$	757	350	40.7
$H_2 + 3O_2$	103	34.9	37.1

* Striations are present but are too faint to be measured

A further series of experiments was carried out to examine the nature of the transition from the waves which are characterized by the strong low-frequency bands to those which exhibit the high-frequency effects. Three mixtures were taken with compositions lying between $H_2 + 3O_2$ and $H_2 + 2O_2$ and the photographs obtained with a horizontal knife-edge are shown in Fig. 3 (a, b, c). It is clear from these that both the low- and high-frequency bands are present and, as the hydrogen-concentration is increased from $H_2 + 3O_2$, the low-frequency bands become progressively weaker and have almost disappeared in $4H_2 + 9O_2$. The same effect is observed on the photograph obtained for

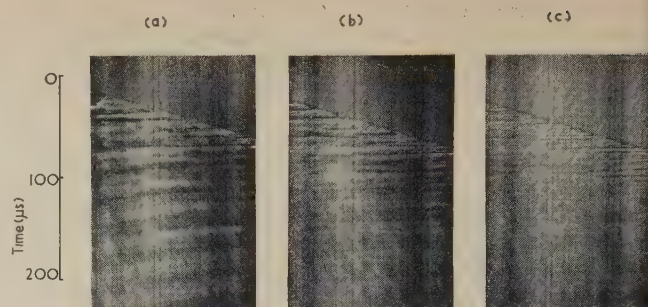


Fig. 3. Streak Schlieren photographs of the detonation wave, obtained with a horizontal knife-edge, for the mixtures (a) $4H_2 + 11O_2$, (b) $4H_2 + 10O_2$ and (c) $4H_2 + 9O_2$.

$6H_2 + O_2$ which also shows both sets of horizontal bands; the values of their recurrence frequency is given in Table 2.

A particularly interesting feature of the photographs obtained with a vertical knife-edge is the appearance of weak bands behind the detonation front and lying almost parallel to it. These were first noticed on photographs for mixtures near the stoichiometric composition, but closer examination

Table 2. Mixtures exhibiting both long and short wavelength vibrations

Mixture	Frequency of short wavelength horizontal striations (kc/s)	Frequency of long wavelength horizontal striations (kc/s)	Calculated spin frequency v_n (kc/s)
$6H_2 + O_2$	210	71.2	76.2 ($n = 1$)
$4H_2 + 10O_2$	242	119.7	113.3 ($n = 4$)
$4H_2 + 11O_2$	132	37.9	37.1 ($n = 1$)

revealed their presence for all mixtures although they were difficult to detect in some cases being masked by other strong effects present. These bands must correspond to forward-moving weak compression waves where the velocity is just greater than that of the detonation front. Since these bands are not sufficiently distinct to show clearly on a reproduction of the original photographs they are shown in the sketch of Fig. 4; the mixture is $H_2 + O_2$ and the diagram includes the

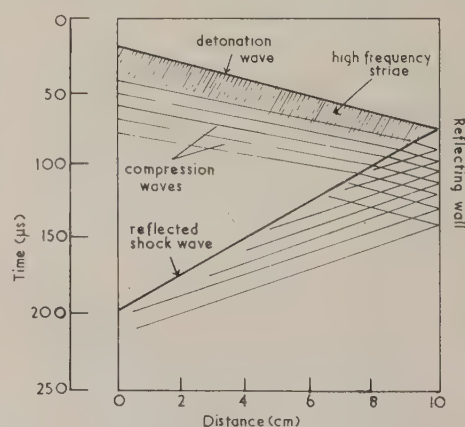


Fig. 4. Sketch of Schlieren photograph using a vertical knife-edge for the detonation wave in $H_2 + O_2$ and the shock wave arising from its reflexion at a rigid wall

shock wave arising from the normal reflexion of the detonation front at a rigid stop placed in the tube. The curious thing is that the recurrence frequency of these bands is approximately twice the calculated fundamental mode spin

frequency for each mixture. As far as the authors are aware no previous investigator appears to have commented on these waves; any doubts of their existence, however, were dispelled when further evidence was obtained from pressure measurements. An example of a reflexion pressure record for a detonation wave in $\text{H}_2 + \text{O}_2$ is shown in Fig. 5, which was obtained by a piezoelectric pressure bar gauge of the type described by Edwards.⁽¹⁶⁾ The frequency of the regular

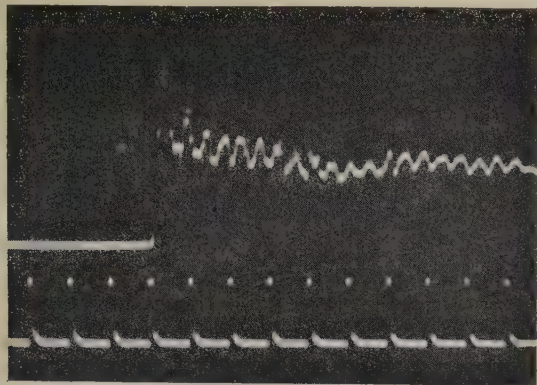


Fig. 5. Pressure record obtained when a detonation wave in $\text{H}_2 + \text{O}_2$ is reflected at a rigid wall
Timing marks: $20 \mu\text{s}$

pressure oscillations following the detonation wave is 93.3 kc/s which again is about twice the calculated fundamental mode spin frequency, 48.6 kc/s , for this mixture. Indeed, this was found to be true for the reflexion pressure records of all mixtures, spinning and non-spinning alike. On the other hand, the static pressure records for mixtures in the range $6\text{H}_2 + \text{O}_2$ to $\text{H}_2 + 2\text{O}_2$ show no signs of regular oscillation, whereas the strongly spinning mixtures $3\text{H}_2 + \text{O}_2$ and $\text{H}_2 + 3\text{O}_2$, as would be expected, give records with large amplitude pressure oscillations, the frequencies of which agree with those of the horizontal bands in the Schlieren photographs.

Discussion

There can be no doubt that the two mixtures $8\text{H}_2 + \text{O}_2$ and $\text{H}_2 + 3\text{O}_2$ spin in the fundamental tangential mode in the manner predicted by Fay's theory. It is true that the observed frequencies in Table 1 are somewhat lower than the calculated values, but the discrepancy can probably be attributed to the fact that the sound velocity in the burnt gases is lower than the ideal value assumed owing to cooling of the gases. The period of the motion is greater than the duration of the photographs which is of the order of 0.90 ms ; this is in agreement with the photographic evidence of Duff and Knight⁽¹⁷⁾ who observed a duration of the order of 1 ms in carbon-monoxide-oxygen mixtures. Evidence obtained from static pressure records in the present tube indicates that the duration is at least of the order of 1.8 ms . A time of 1 ms in $\text{H}_2 + 3\text{O}_2$, for example, would correspond to a wavelength l of roughly 100 cm ; consequently Fay's assumption that $l \approx 60r_0$ is valid for these mixtures.

The high-frequency striations observed in the stronger mixtures confirm the results of Greifer and others who detected retrograde striations, when using a vertical knife-edge, with a recurrence frequency of the order of 1 Mc/s in a mixture of approximate composition $3\text{H}_2 + \text{O}_2$ confined in a tube of section $1 \times \frac{3}{4} \text{ in.}$ The agreement with the present results, allowing for the difference in tube geometry, is reasonably

good. These authors suggest that the striations may be miniature retonation waves arising from some mechanism of discontinuous propagation of the detonation. They do not, however, report observing horizontal striations which, according to the theory, constitute an essential criterion of a spinning detonation; consequently these waves are described as non-spinning. The results obtained in the present investigation with a horizontal knife-edge show the presence of density gradients which must correspond to a tangential mode of vibration of the gas.

The question arises whether the high-frequency phenomenon can be interpreted on the mechanical theory. Clearly the condition $l \gg r_0$ is not satisfied in this case and if the measured value of l of the order of 2 cm for $\text{H}_2 + \text{O}_2$ is substituted in equation (2) ($c_1 = 1300 \text{ m/s}$ and $n = 1$) the value obtained for the impedance Z is -1.26 . A possible explanation for the low value of Z is found if it is assumed that the plane longitudinal waves following the detonation front are responsible for exciting this vibration. In a normally spinning wave the energy source of the vibration is of the same frequency as the natural frequency of the transverse motion ν_n , and $Z = -\infty$. If, however, the frequency of the exciting disturbance is 2ν , which is the observed value for the compression waves, then Z becomes -1.15 for the fundamental mode which, considering the uncertainties in the determination of l , is in reasonable agreement with the experimentally estimated value of -1.26 obtained above for $\text{H}_2 + \text{O}_2$. From equations (1) and (2) the observed frequency ν can be related to the wavelength l and frequency of transverse motion ν_n by

$$\nu = (c_1/l) + \{(c_1^2/l^2) + \nu_n^2\}^{1/2} \quad (4)$$

When l is small $(a/l)^2 \gg \nu_n^2$ so that the observed frequency $\nu \approx 2c_1/l$. For example in the case of $4\text{H}_2 + \text{O}_2$ where $\nu_{\text{obs}} = 373 \text{ kc/s}$ and $c_1 = 1942 \text{ m/s}$, the value obtained for l from the above expression is 1 cm compared with an observed value of the order of 2 cm . Hence in this instance, as in all the other mixtures, the calculated wavelength, although not in close agreement with that observed, is of the right order of magnitude; this difference is attributed primarily to a lack of precision in defining the wavelength on the photographs. For this reason an attempt to describe the precise mode of the transverse oscillation on the basis of the measurements of l and ν is not possible.

Table 2 gives the observed frequencies for the three mixtures which exhibit both the long wavelength and high-frequency spin. In the mixtures $6\text{H}_2 + \text{O}_2$ and $4\text{H}_2 + 11\text{O}_2$ the lower frequencies of 71.2 and 37.9 kc/s evidently correspond to the fundamental mode transverse vibration where the theoretical values are 76.2 and 38.0 kc/s respectively. For the mixture $4\text{H}_2 + 10\text{O}_2$ the value of the lower frequency is 119.7 kc/s which corresponds to a fourth mode vibration for which the calculated value is 113.3 kc/s . High harmonic spins of up to the fifth mode have been observed by Bone, Frazer and Wheeler in carbon-monoxide-oxygen mixtures to which small quantities of $2\text{H}_2 + \text{O}_2$ had been added. Beyond the composition $2\text{CO} + \text{O}_2 + \frac{1}{2}(2\text{H}_2 + \text{O}_2)$ they report that further additions of $2\text{H}_2 + \text{O}_2$ caused the spin to disappear completely. This fact is equally true of the hydrogen-oxygen mixtures, for in the mixture $4\text{H}_2 + 9\text{O}_2$ the long wavelength spin has almost disappeared and in $\text{H}_2 + 2\text{O}_2$ is completely absent. The fact which has now been established is that the high-frequency vibration is a property common to the detonation waves in all mixtures propagated in small diameter tubes.

Measured values of the wave velocities in this tube, given

in Table 3, are significantly lower than the theoretical values, the deviations increasing the further the mixture composition is removed from the stoichiometric. The lowering of the wave velocities in small diameter tubes has been studied by Berets and others,⁽¹⁸⁾ who argue that the dependence of velocity on tube diameter arises from energy losses to the tube wall. These losses may be caused by cooling or frictional effects at the tube wall which result in a rarefaction wave being propagated into the gas from the wall, which in turn would cause a lowering of the temperature and hence of the rate of chemical reaction. Pressure measurements made in this

Table 3. *Detonation wave velocities in 1.6 cm diameter tube*

Mixture	Velocity (observed) (m/s)	Velocity (theoretical) (m/s)	Standard deviation (%)	Deviation from theory (%)
8H ₂ + O ₂	3542	3802	0.5	-6.8
6H ₂ + O ₂	3550	3750	0.4	-5.3
4H ₂ + O ₂	3268	3425	0.3	-4.6
2H ₂ + O ₂	2769	2853	1.0	-3.0
H ₂ + O ₂	2315	2333	0.2	-0.8
H ₂ + 2O ₂	1901	1941	0.2	-2.1
H ₂ + 3O ₂	1683	1759	0.2	-4.3

Laboratory confirm this hypothesis and, in particular, the energy losses to the wall in the 1.6 cm diameter tube are so great that an ideal wave cannot be propagated in any hydrogen-oxygen mixture. In fact, all the waves studied in this tube are sub-ideal in the sense defined by Brinkley and Richardson⁽¹⁹⁾; in such waves the chemical reaction is incomplete at the Chapman-Jouguet plane and continues in the rarefaction wave. In a one-dimensional wave a part of this energy released in the rarefaction wave is delivered upstream as positive pressure pulses. The compression waves obtained in the Schlieren photographs could, therefore, arise in this manner. If this interpretation is accepted then it appears that the high-frequency vibrations observed in detonation waves in this tube are directly attributable to the strong energy losses to the tube wall. Wall cooling or friction effects has been tentatively suggested by Fay as being responsible for spin in certain mixtures not too close to the detonation limits and which would, in the absence of wall effects, support a plane ideal wave.

From the data of Bone, Frazer and Wheeler on spinning carbon-monoxide-oxygen detonations, the ratio of the number of retonation waves to horizontal striations is 1.8. Fay proposes that these retonation waves are probably a standing wave of the second mode with a theoretical ratio of 1.65. In the present experiments the ratio of the number of retrograde to horizontal striations varies between the limits of approximately 2.2 for H₂ + 2O₂ to 3.8 for 4H₂ + O₂; these would therefore correspond to standing waves of the third and sixth modes with theoretical ratios of 2.28 and 4.05 respectively.

Conclusions

From the above considerations the following conclusions may be advanced concerning spinning in hydrogen-oxygen mixtures.

(1) Normal or "helical" spin appears in mixtures near the detonation limits owing to the inherently low rate of the chemical reaction, and consequently the shock-heating process is insufficient to maintain a plane detonation wave.

(2) In small diameter tubes, high-frequency spin is present in mixtures which, when confined in larger diameter tubes, are capable of supporting a stable detonation wave. This vibration, which has the same appearance as normal spin on a streak photograph, except that it is of much shorter wavelength, is maintained by longitudinal pressure waves generated in the rarefaction wave.

(3) Evidence from velocity and pressure measurement indicates that all detonation waves in the 1.6 cm tube are sub-ideal due to energy losses to the tube wall and the chemical reaction is incomplete at the Chapman-Jouguet plane. Pressure pulses thus arise from combustion taking place in the rear of the detonation wave. The recurrence frequency of these pressure pulses in all the hydrogen-oxygen mixtures is about twice the calculated fundamental mode frequency of tangential vibration.

(4) The transition from normal to high-frequency spin with variation of mixture composition is a gradual process; in a range of dilute mixtures the two phenomena are found to be present together.

Acknowledgement

The authors wish to thank Dr. J. C. Breeze for the pressure records and Prof. T. V. Davies for several helpful discussions.

References

- (1) CAMPBELL, C., and WOODHEAD, D. W. *J. Chem. Soc.* **129**, p. 3010 (1926); **130**, p. 1572 (1927).
- (2) CAMPBELL, C., and FINCH, A. C. *J. Chem. Soc.*, **131**, p. 2094 (1928).
- (3) BONE, W. A., and FRASER, R. P. *Phil. Trans. A*, **228**, p. 197 (1929); **230**, p. 371 (1932).
- (4) BONE, W. A., and FRASER, R. P., and WHEELER, W. H. *Phil. Trans. A*, **235**, p. 29 (1936).
- (5) LAFFITE, P. *Science of Petroleum*, Vol. IV, p. 299 (Oxford University Press, 1938).
- (6) MOORADIAN, A. J., and GORDON, W. E. *J. Chem. Phys.* **19**, p. 1166 (1951).
- (7) JOST, W. *Explosions and Combustion Processes in Gases* (New York: McGraw-Hill Co., 1946).
- (8) BECKER, R. *Z. Elektrochem.*, **42**, p. 457 (1936).
- (9) DOERING, W. *Ann. Phys. (Leipzig)*, **43**, p. 421 (1943).
- (10) MANSON, N. *Propagation des Détonations et des Déflagrations dans les Mélanges Gazeux* (Paris: L'Office National d'études et de Recherches Aéronautiques, 1947).
- (11) FAY, J. A. *J. Chem. Phys.*, **20**, p. 942 (1952).
- (12) TOENNIES, J. P., and WAGNER, H. G. *Z. Elektrochem.* **59**, p. 7 (1955).
- (13) GREIFER, B., COOPER, J. C., GIBSON, F. C., and MASOM, C. M. *Amer. J. Appl. Phys.*, **28**, p. 289 (1957).
- (14) EDWARDS, D. H., and OWEN, J. D. *J. Sci. Instrum.*, **34**, p. 160 (1957).
- (15) KNIGHT, H. T., and DUFF, R. E. *Rev. Sci. Instrum.*, **26**, p. 257 (1955).
- (16) EDWARDS, D. H. *J. Sci. Instrum.*, **35**, p. 346 (1958).
- (17) DUFF, R. E., and KNIGHT, H. T. *J. Chem. Phys.*, **20**, p. 1493 (1952).
- (18) BERETS, D. J., GREENE, E. F., and KISTIAKOWSKY, G. H. *J. Amer. Chem. Soc.*, **72**, p. 1080 (1950).
- (19) BRINKLEY, S. R., and RICHARDSON, J. M. *IVth Symposium (International) on Combustion*, p. 450 (Baltimore: Williams and Wilkins, 1953).

High alloy steels for use as a thermal conductivity standard

by R. W. POWELL, D.Sc., Ph.D., F.Inst.P., and R. P. TYE, National Physical Laboratory, Teddington, Middlesex

[Paper first received 20 November, and in final form 24 December, 1959]

Abstract

An absolute longitudinal steady state heat flow method is described for the determination of the thermal conductivity of a bar of Macloy G steel over the range 0 to 180° C. The results of this method are in good agreement with those of a comparative method against Armco iron that is used for the range 300 to 800° C and values are quoted for the full range which are believed to be accurate to about ±2%. Comparison is made with some previous determinations on a sample of Era ATV steel.

These steels are suggested as suitable for use as standard materials for comparative thermal conductivity determinations on metals of low conductivity.

For materials of differing conductivity some compensation can be obtained by adjustment of the diameters of the rods. However, there is an obvious need for having suitable standard materials covering a range of thermal conductivities. Metals other than Armco iron have been used from time to time, for instance a 0.8% carbon steel and a stainless steel for determinations on molten metals,⁽¹⁴⁾ a nickel-chromium alloy for mica conductivity⁽¹⁵⁾ and Era ATV forged steel for determinations on refractory discs.⁽¹⁶⁾

The present paper describes work that has been undertaken to establish a high alloy steel as such a thermal conductivity standard. The steel chosen was, Firth Vickers "Macloy G steel" having the following typical percentage composition

C	Si	Mn	S	P	Cr	Ni	Fe	(by difference)
0.49	1.9	0.58	0.016	0.012	16.75	36.5	43.752	

Introduction

CONSIDERABLE use has been made of the comparative longitudinal heat-flow method for thermal conductivity determinations on metals. In a version of the method frequently adopted by the writers⁽¹⁻¹¹⁾ a composite rod consisting of a test and standard rod securely joined together has been mounted within a guard tube, heated electrically by a heater wound on the free end of the standard rod and water-cooled at the free end of the test rod. This method ensures that the heat flowing in the test rod when equilibrium is reached can be derived in terms of two quite different sets of measurements the heat given up and absorbed by a water-flow calorimeter fitted to its lower end and the temperature established in the rod of known thermal conductivity.

The thermal conductivity of some large bars of Armco iron was carefully determined from room temperature to 800° C^(12, 13) and rods machined from this supply have been commonly used for the comparative measurements. In order to facilitate the matching of the temperature gradients in the composite rod and guard tube it is an advantage for the gradients established in the two rods to be of the same order.

Preliminary tests

The sample of steel was supplied in the form of a bar measuring approximately 3.75 in. in diameter and 45 in. in length. The bar was stated to have been heated to 1050° C and cooled in air.

In order to check the uniformity of the bar and its stability after various treatments a number of electrical resistivity determinations were made by the normal method involving comparison of the potential differences across a specified section of the bar with that established across a standard resistor when carrying the same current.

These measurements were first made on various sections along the length of the bar, and on rods of 0.76 cm diameter and 9.45 cm length and of 0.61 cm diameter and 7.35 cm length which had been machined from a disk cut from one end of the original bar. All measurements made at room temperature agreed to within 1%.

The larger of the two test rods was then mounted in an

Table. Thermal conductivity, electrical resistivity and Lorenz function of Macloy G steel and Era ATV steel

Temperature (° C)	Macloy G steel			Era A.T.V. steel		
	Thermal conductivity (J cm/cm ² s deg C)	Electrical resistivity (μΩ cm ² /cm)	Lorenz function (J Ω/s deg C °K)	Thermal conductivity (J cm/cm ² s deg C)	Electrical resistivity (μΩ cm ² /cm)	Lorenz function (J Ω/s deg C °K)
-252.8	—	98.0	—	—	—	—
-183	—	99.6	—	—	—	—
0	0.103	105.6	3.98 × 10 ⁻⁸	0.109	98.0	3.91 × 10 ⁻⁸
100	0.122	108.8	3.56	0.126	102.7	3.47
200	0.141	112.2	3.35	0.138	106.9	3.12
300	0.160	115.4	3.22	0.155	111.0	3.00
400	0.178	118.4	3.13	0.168	114.2	2.85
500	0.194	120.9	3.03	0.184	117.3	2.79
600	0.207	123.0	2.92	0.197	120.1	2.71
700	0.221	125.0	2.84	0.213	122.2	2.67
800	(0.235)	126.3	(2.77)	(0.226)	(123.6)	(2.60)

evacuated tube and electrical resistivity measurements made during heating to 920° C and on subsequent cooling.

The smaller test rod was used for similar measurements to the low temperatures produced by immersion in liquid oxygen and in liquid hydrogen.

After each of the above treatments the electrical resistivity at room temperature agreed with the original value to well within 1%, which indicated that the selected steel would be suitable for use as a thermal conductivity standard.

The electrical resistivity values obtained in the course of these tests are included in the third column of the table.

Thermal conductivity measurements

From earlier work on high alloy steels it was to be anticipated that the thermal conductivity to be measured would be about 0.1 Jcm/cm²s deg C at room temperature, and would increase with increase in temperature. Whilst the longitudinal heat flow method can be used for materials having thermal conductivities of this order, the low value makes it difficult to achieve the customary 1 to 2% accuracy, particularly near room temperature.

In view of this the decision was reached to make an absolute determination from about 30° C up to as high a temperature as possible, on a bar of large diameter and, for extension to higher temperatures, to resort to the normal comparative method using bars of Macloy G steel and Armco iron of 1 in. diameter. The initial work with the large-diameter bar would provide an independent means of measurement for the low-temperature end of the curve and its agreement or otherwise with the Armco-iron comparison method could be judged from the relative position of the line obtained from the higher temperature experiments.

Absolute method

For the purpose of this determination, a 16 in. length of the 3½ in. diameter bar of Macloy G steel was machined to have a cavity 3½ in. in diameter and ¼ in. deep at one end and a cavity 3¼ in. in diameter and ⅛ in. deep at the other end. The rod was mounted vertically with the larger cavity uppermost and this was closed by screwing a lid of the same metal over the cavity. Within this cavity was a heater constructed of 28 s.w.g. nichrome close-coiled wire, three spiralled units, being welded in parallel and the whole unit packed into the cavity and insulated by means of sheets of mica and alumina powder. Potential leads were attached close to where the heater leads emerged through holes in the lid which were lined with ceramic insulators. A cooling unit, composed of several turns of copper tubing was soldered into the lower cavity.

To assist in the measurement of the specimen temperature in the vicinity of the heated and cooled ends, axial slots were machined for about 3 in. from each end and on two perpendicular diameters. These were of a size and depth just suitable for lengths of hypodermic stainless-steel tubing, of approximately 1.0 mm internal and 1.25 mm external diameter to be hammered tightly into position with their surfaces flush with the external surface of the rods. These tubes projected well beyond the ends of the rods, as shown in Fig. 1 and served to take an exploring thermocouple of 40 s.w.g. nickel-chromium constantan wires, insulated with fine twin-bore silica tubing.

Three sets of four similar thermocouples were welded on to the mid-section of the specimen at 120° intervals around it and at spacings of about 6 cm, giving working sections of 18 cm approximately.

The specimen was concentric within a steel guard tube 12 in. in diameter and 21 in. long which carried three sets of similar thermocouples welded to its inner surface in closely corresponding positions. The base of the guard tube was cooled by water flowing in a few turns of copper tubing, and two heaters insulated by mica, were wound on the tube to cover areas of from 2.5 to 12.3 cm and 23.5 to 31.2 cm from the top. A larger unheated tube surrounded the assembly, and the specimen and the outer tubes rested on a magnesia asbestos base supported by a steel base plate, having a central hole about 7 in. in diameter.

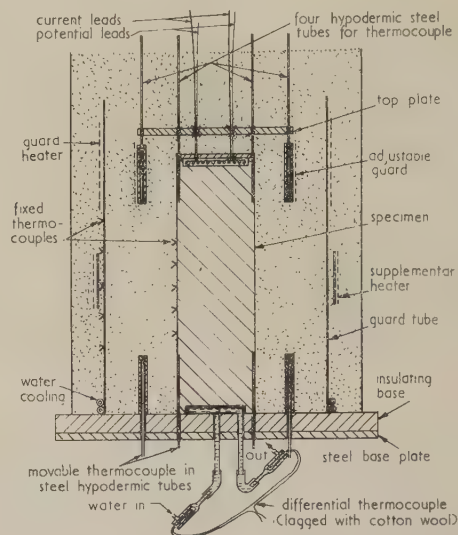


Fig. 1. Absolute thermal conductivity apparatus (diagrammatic drawing not to scale)

The interspaces between the specimen and guard tube and between the guard and outer tubes were packed with dry insulating powder. As this was done the various intermediate metal guards shown in Fig. 1 were inserted. These were of mild steel and carried heaters and further fine steel tubes for the introduction of thermocouples.

A calibrated, multijunction differential thermocouple was connected in the inflowing and outflowing water cooling tubes at the base of the specimen and was thermally insulated with cotton wool. The water was supplied from a constant-level tank.

In conducting an experiment a gradient in temperature was established from the top of the specimen and the various heaters adjusted so that corresponding levels of the specimen and guard tube were at closely matched temperatures, the temperatures of the plate above the specimen and the upper guard collar were adjusted to be close to that of the top of the specimen. When equilibrium had been attained for these conditions, observations were made of the various fixed thermocouples and a moveable thermocouple was used to make temperature explorations within the various tubes provided in the specimen and guards. The electrical energy supplied to the specimen heater was also observed as well as the reading of the differential thermocouple and the rate of flow of the cooling water from the base of the specimen.

To evaluate these results, the observed temperatures of the specimen and guard tube, as measured by both fixed and moveable thermocouples, were plotted against position, as measured from a fixed reference point. Good agreement was obtained for the sets of thermocouples located in different

planes. These conformed closely to a linear temperature gradient and the mean gradient as calculated from the upper and lower groups of specimen thermocouples was mainly used. Two estimates could then be made of the energy flowing in the specimen mid-way between these groups, one based on H_e the electrical energy supplied, and the other on H_w the heat absorbed by the water-flow calorimeter. Allowance was made for the following corrections. In the case of H_e (i) heat interchange between the top of the specimen and the top guard plate, (ii) heat interchange between the specimen and the guard collar, (iii) heat interchange between the specimen and the guard tube over the length from the base of the collar to the centre of the working section, (iv) heat loss along the tubes for the exploring thermocouple. In the case of H_w (i) heat transfer to the differential couples from the surroundings, (ii) heat transfer from the magnesia-asbestos base, (iii) heat transfer between the lower guard collar and the specimen (iv) heat transfer between the specimen and the guard tube over the length from the centre of the working section to the top of the lower guard collar. These corrections were usually small and their total seldom exceeded 2% of the energy flowing in the specimen. From 16 sets of observations made in this first run the mean corrected value of H_e was 2.8% less than the mean corrected value of H_w .

The most likely explanation for this difference appeared to be the transference of some unmeasured heat from the heater leads to the specimen. In this first assembly the heater leads, which were each composed of 8 strands of the same wire as the heater, emerged near the centre of the top of the specimen and passed up at the outside of the upper guard plate. Thus some 20 cm of this wire could have been in close proximity to the top of the specimen, and, being embedded in insulating powder, its temperature would have exceeded that of its surroundings.

In a later assembly these heater leads passed straight up through holes in the guard plate and the bead insulators on the leads made good contact with both the wire and the plate. A further change made had been to weld on 18 s.w.g. copper current leads which had thermocouples attached directly to the leads near the levels at which they emerged from the specimen and passed through the guard plate. The heat flow in this length of lead could then be calculated and applied as a further correction to H_e . Another change made in this assembly had been to replace one of the sets of thermocouples

in the specimen and guard tube by platinum and platinum-10% rhodium thermocouples. As a result of these changes, the mean of fifteen sets of observations gave the corrected value of H_w 1.3% above that of H_e , a definite improvement, but still not exact agreement. The difference was considered likely to result from heat flowing through the insulating powder in parallel with the specimen and guard, which could have an influence on the heat flow in the specimen.

From this later set of experiments it was deduced that the contribution from the heater leads in the first series was likely to have amounted to about 1.5% and an additional correction of 1.5% was added to H_e for this series. The thermal conductivity was then derived from the equation

$$K = \frac{(H_e + H_w) \text{ corrected}}{2AdT/dl}$$

where the numerator is the mean of the two energy measurements, after correction, A is the cross-sectional area of the specimen and dT/dl the mean temperature gradient in the working section of the specimen.

It should be observed that the values of dT/dl for the various sets of thermocouples all agreed to within 1% and as the independent energy measurements only differed on the average by $\frac{3}{4}$ % from the mean value, the thermal conductivity is believed to be accurate to within 1 to 2%.

Fig. 2 contains the derived values for the thermal conductivity plotted against the mean temperature for the two sets of experiments using this method. The variation with temperature appears to be linear, and all points are within 3.5% of the straight line $K = 0.103 + 0.000189T$ drawn in the figure, which has been obtained by the method of least squares.

Comparative method for higher temperatures

Attempts were made to extend the measurements to higher temperatures using the absolute method described above, but without applying any basal water cooling. These, however, did not prove satisfactory mainly because of fluctuations in the ambient temperature and the decision was reached to employ the comparative method normally used.⁽¹¹⁾ A rod of Macloy G steel, 1 in. in diameter and 9 in. in length, was joined to a similar rod of Armco iron and the thermal conductivity of the steel derived from assumed values for the iron.⁽¹²⁾

Four platinum-platinum (90%) rhodium (10%) thermocouples had been attached to the steel bar at spacings of about 4 cm, and three to the Armco iron. Thermal conductivity values based on different pairs of the specimen thermocouples were derived and these are shown in Fig. 3. The experimental points are seen to cover temperatures ranging from about 300 to 820°C and the values corresponding to the various thermocouple combinations are seen to be in good agreement up to 700°C. Above this temperature a tendency towards higher thermal conductivity values is apparent, but the deviation from the normal line is thought to result from contamination of the top thermocouple. That this was so was confirmed when similar departures (shown dotted in Fig. 3) were obtained for repeat measurements at two lower temperatures. Room temperature electrical resistivity measurements made on the rod at the conclusion of the test agreed to within 1% with the initial values and indicated that no change in the material had occurred. The smooth curve drawn through the experimental points in Fig. 3 has accordingly been continued above 700°C without change of curvature. The line derived for the range 0 to 200°C is also included in Fig. 3 and it will be seen that the thermal conductivity values obtained at

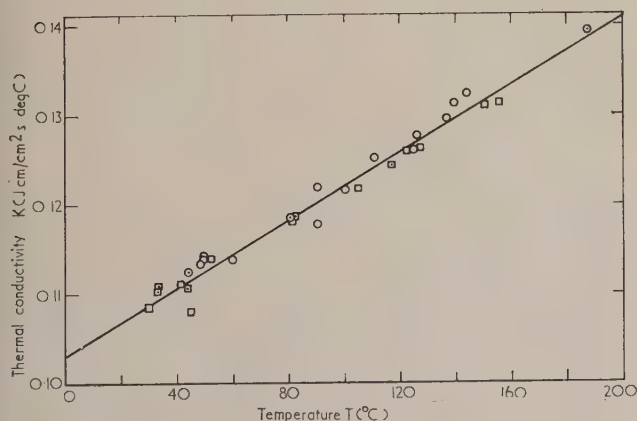


Fig. 2. Thermal conductivity of Macloy G steel, absolute method

○, first assembly; □ second assembly
 $k = 0.103 + 1.89 \times 10^{-4} T$

about 300° C by means of the comparative method agree to within 2% with values indicated by this line. Indeed, the curve (shown as a thin line) through the present points joins the continuation of this line at about 300° C.

Good agreement is clearly apparent between the results of the absolute and comparative methods in the region of 200 to 300° C. In the course of the comparative measurements to 800° C the Armco iron did not exceed a mean temperature of about 500° C, and it should be remarked that this temperature is well within the range over which the values of various workers for the thermal conductivity of Armco iron agree to within a few per cent.^(5, 17, 18)

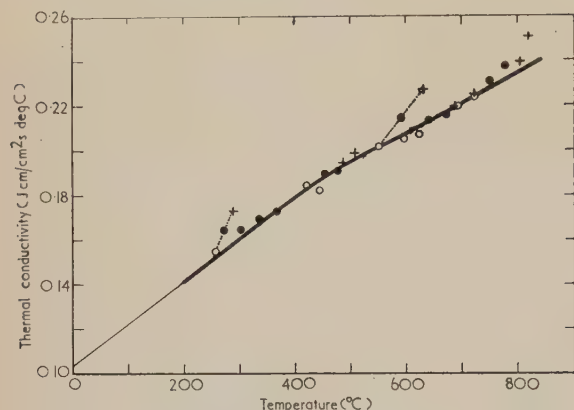


Fig. 3. Thermal conductivity of Macloy G steel

+, based on thermocouples 1 and 2;
●, based on thermocouples 1 and 4;
○, based on thermocouples 3 and 4;
..... line connecting repeat values on cooling,
—— absolute method.

Thermal conductivity values read from the curve of Fig. 3 at 100° C intervals are included in the table. These are the values which it is proposed should be used when Macloy G steel is employed as a thermal conductivity standard. Up to at least 700° C these values are considered accurate to within 2%.

Discussion of results

Prior to the present work, Era ATV forged steel (supplied by Hadfield's Ltd.) of composition, wt %, 0.46 C, 26.86 Ni, 15.2 Cr, 1.18 Mn, 1.3 Si, 2.77 W, 0.014 S, 0.018 P, and bal Fe, had been the steel of lowest iron content for which thermal conductivity measurements had been made by one of the present writers.⁽¹⁾ Recently a further sample of Era ATV steel has been measured and the results are in excellent agreement with the values obtained in 1936. This steel is also suitable for use as a thermal conductivity standard and the table contains values of the thermal conductivity, electrical resistivity and Lorenz function of both steels. The thermal conductivities of the two steels agree to within about 6%, but whereas Macloy G has a 5% lower thermal conductivity at 0° C, its thermal conductivity is greater by about a corresponding amount over the range 400 to 600° C. At 0° C the two Lorenz functions are in close agreement and indicate appreciable components of lattice conductivity, 38.4% and 37.3% for Macloy G and Era ATV, respectively. It would seem that the more highly alloyed steel retains a

rather higher lattice component at higher temperatures, and at 700° C the respective lattice components are 13.7% and 8.2% of the thermal conductivities.

The electrical resistivity of any sample to be used as a standard should be measured at room temperature, and the thermal conductivity adjusted for any difference. The required changes are likely to be small and will decrease with increase in temperature.

Acknowledgements

The work described above has been carried out as part of the research programme of the National Physical Laboratory, and this paper is published by permission of the Director of the Laboratory.

The authors desire to acknowledge the assistance rendered by Mr. G. A. Bainbridge and Mr. J. E. W. Jones who assisted with the experimental work at different periods during the investigation.

References

- (1) POWELL, R. W. *Proc. Phys. Soc. (London)*, **48**, p. 381 (1936).
- (2) GROOTENHUIS, P., POWELL, R. W., and TYE, R. P. *Proc. Phys. Soc. (London) B*, **65**, p. 509 (1952).
- (3) POWELL, R. W. *Phil. Mag.*, **44**, p. 645 (1953).
- (4) POWELL, R. W. *Trans. Brit. Ceramic Soc.*, **53**, p. 389 (1954).
- (5) POWELL, R. W. *Research*, **7**, p. 492 (1954).
- (6) POWELL, R. W. *J. Iron Steel Inst.*, **184**, p. 6 (1956).
- (7) POWELL, R. W., and TYE, R. P. *J. Iron Steel Inst.*, **184**, p. 10 (1956).
- (8) POWELL, R. W., and TYE, R. P. *J. Iron Steel Inst.*, **184**, p. 286 (1956).
- (9) POWELL, R. W. *J. Inst. Metals*, **85**, p. 553 (1957).
- (10) POWELL, R. W., and TYE, R. P. *J. Inst. Metals*, **85**, p. 185 (1957).
- (11) POWELL, R. W., and TYE, R. P. *The Thermal and Electrical Conductivities of Some Nickel Chromium (Nimonic) Alloys* (*The Engineer*, to be published).
- (12) POWELL, R. W. *Proc. Phys. Soc. (London)*, **46**, p. 659 (1934).
- (13) POWELL, R. W. *Proc. Phys. Soc. (London)*, **51**, p. 407 (1939).
- (14) POWELL, R. W., and TYE, R. P. *Proceedings of the Joint Conference on Thermodynamic and Transport Properties of Fluids*, p. 182 (London: Institution of Mechanical Engineers, 1958).
- (15) POWELL, R. W., and GRIFFITHS, E. *Proc. Roy. Soc. A*, **163**, p. 189 (1937).
- (16) GRIFFITHS, E., and CHALLONER, A. R. *Trans. Brit. Ceramic Soc.*, **40**, p. 40 (1941).
- (17) LUCKS, C. F., and DEEM, H. W. *ASTM Special Technical Publication No. 227* (1958).
- (18) HEDGE, J. C., and FIELDHOUSE, I. B. *Armour Research Foundation of Illinois Inst. of Tech. Project No. G.022.D.3. Report dated 20 September, 1956.*

Correction of errors in electron stereomicroscopy

by O. C. WELLS, M.A., Ph.D., Engineering Laboratory, University of Cambridge.*

Paper first received 9th November 1959, and in final form 8 January, 1960]

Abstract

A method is described for analysing electron stereomicrographs. Three position co-ordinates are computed for each object point from the four co-ordinate measurements (two from each micrograph) that are available for each point from the stereo pair. The method allows for the correction of tilt error and perspective error, and for the estimation of the magnitude of the errors that remain. An example of the application of the method is described.

Introduction

ELECTRON stereomicroscopy consists of calculating the three-dimensional form of an object from a pair of electron micrographs obtained by viewing the object from different directions. Of importance are the mathematical methods that are available for the calculation of the object dimensions from the information that can be measured from the micrographs. In an analysis published by Garrod and Nankivell⁽¹⁾ it was shown that a number of possible sources of error exist, among which is *tilt error*, or the error resulting from a difference in magnification between the two micrographs of the stereo pair, produced when the optical axis of the electron microscope and the axis about which the specimen is tilted do not accurately intersect. Other errors exist because of distortion of the field of view or because of inaccuracies in the measurements made from the micrographs. In this paper, a method is worked out for eliminating tilt error and perspective error and then for estimating the magnitude of the errors that remain. The basis of the method is that only *three* position co-ordinates for each image point need to be calculated, and, in general, *four* co-ordinate measurements (two from each micrograph) are available for each point. This problem arose in the course of a study of metallographic fracture specimens in the scanning electron microscope,^(2, 3) but it is believed that the same method could be applied to studies in the transmission or reflexion electron microscopes as well.

Elimination of tilt error

In Fig. 1 images of object points defined in the co-ordinate system $OXYZ$ are formed by the two lenses L_1 and L_2 in the planes $O_1X_1Z_1$ and $O_2X_2Z_2$ to give a pair of stereomicrographs. The angle O_1OO_2 between the two lines of sight is 2θ . It is supposed that a point $B(x, y, z)$ in the object space forms the image $B_1(x_1, z_1)$ in the $O_1X_1Z_1$ plane and $B_2(x_2, z_2)$ in the $O_2X_2Z_2$ plane. The four lengths x_1, z_1, x_2 and z_2 will be measured from the two micrographs and from these four quantities, the three unknowns x, y and z are to be calculated.

The error known as *tilt error* arises when the electron

optical axis does not intersect the axis about which the specimen is rotated, so that there is a difference in the distances between the lenses L_1 and L_2 and the specimen. In Fig. 1, it is assumed that the distances O_1L_1 and O_2L_2 remain fixed (and equal to L) between the taking of the two micrographs. Then, OL_1 equals O_1L_1/M_1 and OL_2 equals O_2L_2/M_2 , where M_1 and M_2 are magnifications of the two micrographs for points close to O . The lenses L_1 and L_2 correspond to the objective lens in the microscope during the taking of the two micrographs, while the distance L is a function of the column length and of the strengths of the second and final electron lenses. Variations in the strength of the objective lens will have no effect upon the value of L . Elimination of the tilt error is possible if an accurate estimate of M_1/M_2 can be obtained.

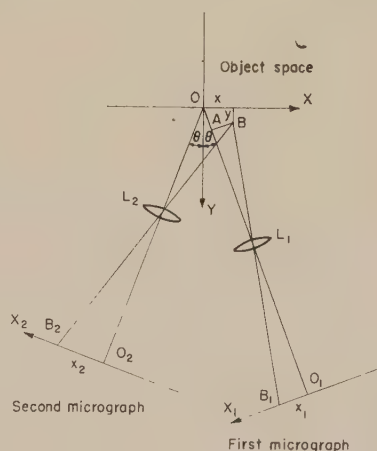


Fig. 1. Proposed co-ordinate systems. In each case, the Z -axis is at right-angles to the paper

In Fig. 1, the four relationships such as

$$\frac{O_1B_1}{O_1L_1} = \frac{AB}{AL_1},$$

where A is the foot of the perpendicular from B on to OL_1 lead to the equations:

$$\left. \begin{aligned} x(x_1 \sin \theta + L \cos \theta) + y(x_1 \cos \theta - L \sin \theta) - \frac{x_1 L}{M_1} &= 0, \\ x(-x_1 \sin \theta + L \cos \theta) + y(x_2 \cos \theta + L \sin \theta) - \frac{x_2 L}{M_2} &= 0, \\ xz_1 \sin \theta + yz_1 \cos \theta + zL - \frac{z_1 L}{M_1} &= 0, \\ -xz_2 \sin \theta + yz_2 \cos \theta + zL - \frac{z_2 L}{M_2} &= 0, \end{aligned} \right\} \quad (1)$$

* Now at Research Laboratories, Westinghouse Electric Corporation, Pittsburgh 35, Pa., U.S.A.

which may be regarded as simultaneous equations in the four unknowns M_1x , M_1y , M_1z and M_1/M_2 . Elimination of M_1x , M_1y and M_1z from these equations leads, without approximation, to the result:

$$\frac{M_1}{M_2} = \frac{z_1 - (z_2x_1/L) \operatorname{cosec} 2\theta + (z_1x_2/L) \cot 2\theta}{z_2 - (z_2x_1/L) \cot 2\theta + (z_1x_2/L) \operatorname{cosec} 2\theta} \quad (2)$$

from which M_1/M_2 may be estimated with an accuracy of about one per cent. This is done by plotting numerator against denominator, using values of x_1 , z_1 , x_2 and z_2 tabulated for a number of points in the object and by measuring the gradient of the best-fitting straight line.

At this stage, it is necessary to distinguish between the effects of tilt error and the effects of perspective error in the equations. *Perspective error* arises from the fact that the foreground of a foreshortened micrograph is reproduced at a higher magnification than is the background, and is responsible for the correction terms in the numerator and denominator of equation (2). If the equations (1) are rewritten, ignoring the effects of perspective error (that is, by assuming that the two images are magnified orthogonal projections of the object) then they can be reduced to the more familiar form:

$$\left. \begin{aligned} x \cos \theta - y \sin \theta - \frac{x_1}{M_1} &= 0, \\ x \cos \theta + y \sin \theta - \frac{x_2}{M_2} &= 0, \\ z - \frac{z_1}{M_1} &= 0, \\ z - \frac{z_2}{M_2} &= 0, \end{aligned} \right\} \quad (3)$$

from which

$$\left. \begin{aligned} x &= \frac{1}{2 \cos \theta} \left(\frac{x_1}{M_1} + \frac{x_2}{M_2} \right) = X, \text{ say,} \\ y &= \frac{1}{2 \sin \theta} \left(\frac{x_2}{M_2} - \frac{x_1}{M_1} \right) = Y, \\ z &= \frac{z_1}{M_1} = Z, \\ z &= \frac{z_2}{M_2} = Z', \end{aligned} \right\} \quad (4)$$

where X , Y , Z and Z' are trial values for x , y and z sufficiently accurate for the elimination of tilt error. (For the moment, it is convenient to retain Z and Z' as different quantities.)

Elimination of perspective error

The solutions given in equations (4) are sufficiently accurate to eliminate tilt error, if the correct values for M_1 and M_2 are used. To eliminate perspective error as well, a further set of correction terms is required. To obtain these it is assumed that:

$$\left. \begin{aligned} x &= X + h \\ y &= Y + k \\ z &= Z + l \\ z' &= Z' + m \end{aligned} \right\} \quad (5)$$

where h , k , l and m are the required correction terms. If these values are substituted back into the equation (1), then:

$$\left. \begin{aligned} h &= \frac{-(x_1 - x_2)X \tan \theta}{2L} - \frac{(x_1 + x_2)Y}{2L}, \\ k &= \frac{(x_1 + x_2)X}{2L} + \frac{(x_1 - x_2)Y \cot \theta}{2L}, \\ l &= \frac{-z_1(X \sin \theta - Y \cos \theta)}{L}, \\ m &= \frac{z_2(X \sin \theta - Y \cos \theta)}{L}, \end{aligned} \right\} \quad (6)$$

from which it can be seen that the magnitude of perspective error will be, in the majority of cases, quite small. In a practical case, the image size might be 5×5 cm, the magnification, 5000 diameters and the working distance, 0.3 cm. The field of view examined will then be $10 \times 10 \mu$. L will be equal 0.3×5000 , or 1500 cm, and therefore:

$$\left| \frac{x_1}{L} \right| < \frac{2.5}{1500},$$

which equals 1.7×10^{-3} . The correction terms in this case will be of the order of 0.2% of the side length of the micrographs.

Estimation of the errors that remain

The magnitude of the errors that remain after all corrections have been applied may be estimated geometrically by measuring the distances that the experimental points lie from the best-fitting straight line drawn through a plot of the numerator and denominator values in equation (2) for a selection of image points, or they may be estimated analytically by determining the differences between the Z and Z' values in equations (4) and (5).

A plot obtained in practice between z_1 and z_2 is shown in Fig. 2, from which it was determined that M_1 exceeded M_2 by a factor of 1.04 ± 0.01 , and that the probable error in the co-ordinate measurements was of the order of 1% of the

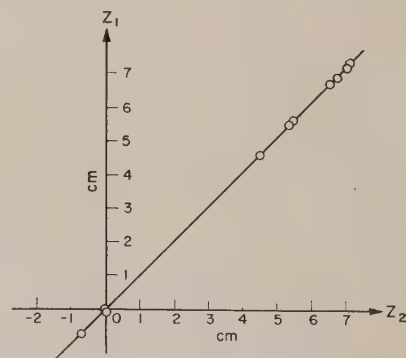


Fig. 2. Plot of z_1 against z_2 to determine M_1/M_2

side length of the micrographs. These measurements were obtained during a study of fracture surfaces using the scanning electron microscope.^(2,3) With this instrument, a wide choice is possible in the angle of observation of the object, and the mathematics was made simple by the use of lines of sight for the two micrographs accurately perpendicular to each other, and by the use of a co-ordinate system based directly on the lines of sight and not, as in Fig. 1, on the bisectors of the angles between them. The probable errors in the co-ordinate values of the object points having

been estimated, then the probable errors in such quantities as are to be calculated from them may be estimated.

Location of the Z-axis in the micrographs

One of the difficulties that arises in practice is to locate the Z-axis with sufficient accuracy in the two micrographs. This axis is parallel to the line about which the specimen is rotated in the specimen holder and, in practice, probably the simplest method of locating it is to measure the direction of the shift in the image when the traverse control is operated in the direction of that axis. The Z-axis may also be located geometrically or analytically by a study of the micrographs themselves, as discussed in the Appendix.

Conclusion

The method of calculating three-dimensional co-ordinates for each object point is well suited to the analysis of rough specimens such as fractured metal surfaces in which it is not always possible to locate a flat reference plane. Angles between planes, heights of points above planes, lengths of line elements, and so on, may be calculated from the tabulated co-ordinate values without difficulty. The method given above for calculating M_1/M_2 and for determining the probable error in the co-ordinate measurements enables an estimate to be made of the probable error in the final calculated quantities. Points that have been misidentified can be detected and eliminated if their Z-co-ordinates are sufficiently different. Correction terms may also be applied for distortions in the field of view of the microscope.⁽³⁾ Although the method is tedious if only a single pair of micrographs is to be analysed, for an extensive analysis of a large number of pairs of micrographs it would be the method to use, for almost all of the operations could be carried out using a computer.

References

- (1) GARROD, R. I., and NANKIVELL, J. F. *Brit. J. Appl. Phys.*, **9**, p. 214 (1958).
- (2) TIPPER, S. F., DAGG, D. I., and WELLS, O. C. *J. Iron and Steel Institute*, **193**, p. 133 (1959).
- (3) WELLS, O. C. Ph.D. Dissertation (University of Cambridge, 1957).

Appendix

Location of the Z-axis

In addition to the method described above, the Z-axis may be located geometrically or analytically from the positions $(x_a y_a)$, $(x_b y_b)$, $(x_c y_c)$ and $(0, 0)$ in the first micrograph and $(x'_a y'_a)$, $(x'_b y'_b)$, $(x'_c y'_c)$ and $(0, 0)$ in the second micrograph (measured relative to arbitrary axes drawn on the two micrographs) of four non-coplanar object points A, B, C, O which in the object space are given by the co-ordinates $(X_a Y_a Z_a)$,

$(X_b Y_b Z_b)$, $(X_c Y_c Z_c)$ and $(0, 0, 0)$. If the Z-axis in the first micrograph makes an angle ϕ with the X-axis, then $\tan \phi$ is given by the equation:

$$\tan \phi = - \frac{\begin{vmatrix} x_a & x_b & x_c \\ x'_a & x'_b & x'_c \\ y_a & y_b & y_c \end{vmatrix}}{\begin{vmatrix} y_a & y_b & y_c \\ x_a & x_b & x_c \\ y'_a & y'_b & y'_c \end{vmatrix}} \quad (7)$$

The derivation of this equation is as follows. In Fig. 3, the tetrahedron $ABCO$ is viewed from the direction QO to give the first micrograph and from the direction PO to give

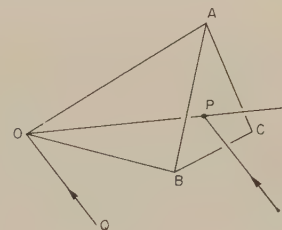


Fig. 3. Location of the Z-axis

the second micrograph. The point P is assumed to lie in the plane ABC . If the line OP in the object space projects into the line O_1P_1 in the first micrograph, then the required direction of the Z-axis in the first micrograph will be at right-angles to the direction of O_1P_1 . If it is assumed that the object points $ABCOP$ are projected orthogonally into the points A_1, B_1, C_1, O_1, P_1 in the first micrograph and into the points A_2, B_2, C_2, O_2, P_2 in the second micrograph, then for some scalar values of λ and μ :

$$\left. \begin{aligned} \overline{AP} &= \lambda \overline{AB} + \mu \overline{AC}, \\ \overline{A_1P_1} &= \lambda \overline{A_1B_1} + \mu \overline{A_1C_1}, \\ \overline{A_2P_2} &= \lambda \overline{A_2B_2} + \mu \overline{A_2C_2}, \end{aligned} \right\} \quad (8)$$

from which, by the elimination of λ and μ , the co-ordinates of P_1 in the first micrograph may be obtained. Equation (7) then follows directly because, if the direction O_1P_1 makes an angle ϕ with the vertical direction in the micrograph, then $\tan \phi$ will be $-(y_p/x_p)$, where x_p and y_p are the co-ordinates of the point P as projected into the first micrograph.

To obtain an accurate location of the Z-axis by this method, a plot should be prepared of the numerator of equation (7) against the denominator for a selection of tetrahedra $ABCO$, selected so that in each case the tetrahedron departs as far as possible from planar form. It will be noticed that M_1 and M_2 cancel out from the numerator and denominator in equation (7). Having determined the direction of the Z-axis by this method, the ratio of M_1 to M_2 may be determined by plotting the numerator against the denominator of equation (2) as before.

Contact electrification and polarization of nylon threads

by R. G. C. ARRIDGE, M.A., B.Sc., A.Inst.P., Research Dept., British Nylon Spinners Limited, Pontypool, Mon.

[Paper first received on 5 August, and in final form 17 December, 1959]

Abstract

A study has been made at different relative humidities of the way in which electric charges on nylon threads decay. For relative humidities of less than about 35%, the charges remain localized and decay in magnitude at very nearly an exponential rate. For relative humidities greater than 35% the charges spread out along the thread and the decay of peak charge with time can be approximately represented by a $t^{-1/2}$ law rather than by an exponential one.

If a diffusion equation of the type $\rho = At^{-1/2} \exp(-x^2/4Dt)$ is applied to the latter results, values of the diffusion constant D are obtained which are independent, within the accuracy of the experiment, of (i) the sign of charge and (ii) whether it was a contact charge or a polarization charge. D varies exponentially with relative humidity.

Apparatus

IN order to study the spreading of charge along a nylon thread, the apparatus shown in Fig. 1 was used. The nylon thread was held between insulating clamps (made from solid nylon) on a trolley free to move back and forth

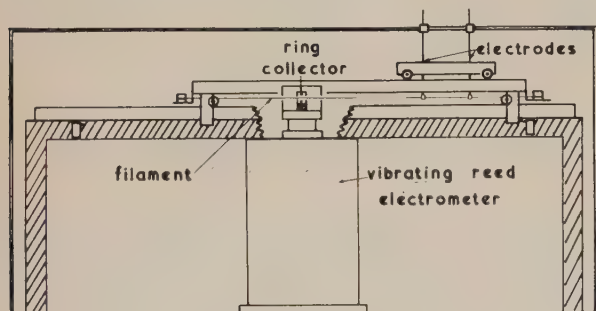


Fig. 1. Apparatus

along a miniature railway line in such a way as to allow the thread to pass through a Faraday cylinder or a ring collector (Fig. 2) attached to a vibrating-reed electrometer. The movement of the trolley was geared to, and driven by, a Brown recorder so that charge distributions along the thread could be recorded. An electrode system, consisting of short cylinders of brass surrounding the thread, could be moved along the thread on a secondary trolley running on top of the first. The whole apparatus was enclosed in a cabinet made of aluminium sheet. This served as an electrostatic shield and also allowed various atmospheres to be used. The relative humidity in the cabinet was measured by a humidity sensitive element accurate to about 5% r.h.

Experimental

An undrawn nylon monofil, 114 μ in diameter, was used. It had been spun without the finish normally used for anti-

static purposes. Electrostatic charges could be placed on this yarn at any desired point by contact with a metal rod, the type of metal determining the sign of the charge. Charges could also be induced on the yarn by means of the electrode system and the rate of build-up and decay of these charges studied.

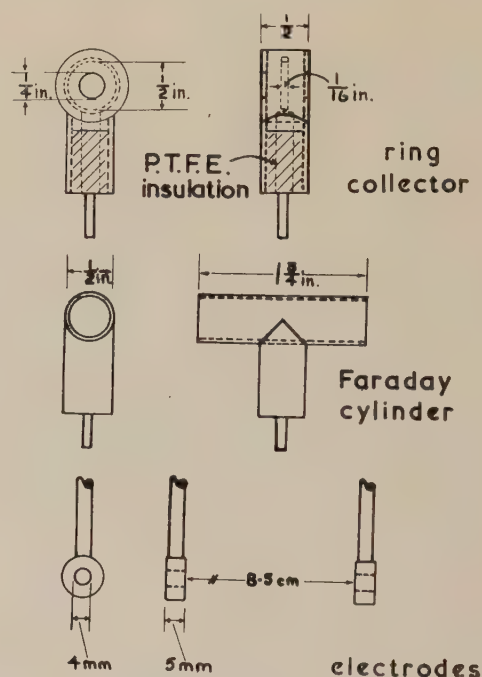


Fig. 2. Charge collectors and electrodes

Decay of point charges. Figs. 3 and 4 show the decay of point charges on linear and logarithmic time scales respectively. A straight line on the first represents exponential decay, on the second a decay of the type t^{-n} . Relative humidities of 0, 30, 42, 50 and 65% and charges of both signs were used. From the shape of the graphs it appears that the initial decay is approximately exponential for 0 and 30% r.h., but that for 42% r.h. and greater the initial decay rate is nearer the t^{-n} form. This change of initial decay rate coincides with the onset of charge spreading, as will be shown below. For 0 and 30% r.h., negligible spreading of charge occurred while, for 42% r.h. and above, the spreading followed a diffusion equation quite well. For diffusion of a point concentration in one dimension, a law of the form of equation (1) holds:

$$\rho = \frac{A}{2(\pi Dt)^{1/2}} \exp\left(\frac{-x^2}{4Dt}\right). \quad (1)$$

Clearly, for $x = 0$ (that is, the peak value), this equation gives a decay law of the form $t^{-1/2}$ while, for the width of the curve at time t , it is useful to find the value x^2/t for $\rho = \frac{1}{2}$

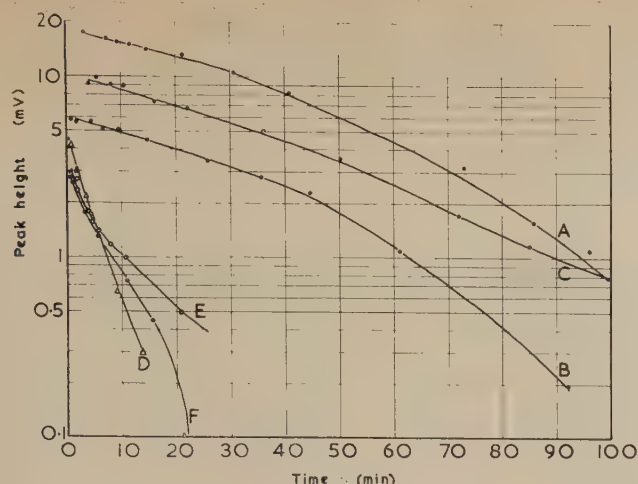
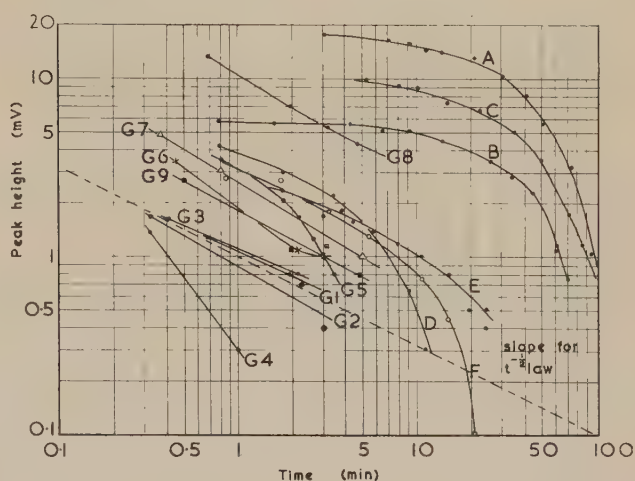


Fig. 3. Decay of point charges: linear time scale

- A = charge decay negative, r.h. = 0%
 B = charge decay positive, r.h. = 0%
 C = charge decay negative, r.h. = 30%
 D(Δ) = charge decay negative, r.h. = 50%
 E(\circ) = charge decay positive, r.h. = 42%
 F = charge decay negative, r.h. = 42%

Fig. 4. Decay of point charges: logarithmic time scale

- A = charge decay negative, r.h. = 0%
 B = charge decay positive, r.h. = 0%
 C = charge decay negative, r.h. = 30%
 D = charge decay negative, r.h. = 50%
 E = charge decay positive, r.h. = 42%
 F = charge decay negative, r.h. = 42%
 G = charge decay positive, r.h. = 65%



and $\frac{1}{3}$ peak value. The diffusion constant D for the half peak values is then given by:

$$D = \frac{1}{4 \log 2} \overline{(x^2/t)},$$

and for the one third peak values:

$$D = \frac{1}{4 \log 3} \overline{(x^2/t)}.$$

These mean values are given in Table 1, together with standard deviations. (Relative humidities of 0 and 30% are omitted since, even after 100 minutes, the half-peak width had only increased by, at the most, 50%.)

Build-up and decay of polarization charges. By applying known potentials to the cylindrical electrodes (which were not in contact with the thread), charge could be drawn along the thread leaving a depleted region on either side and a concentration under the electrode. The rate at which this

Diffusion constants for different types of charge and their dependence on relative humidity

Exp. No.	Type	r.h. (%)	$(x^2/t)_{1/2}$		No. of obs.	$(x^2/t)_{1/3}$		No. of obs.	$D(\text{cm}^2/\text{s})$	
			Mean	S.D.		Mean	S.D.		from $(x^2/t)_{1/2}$	from $(x^2/t)_{1/3}$
D	charge decay -	50	0.64	0.08	7	0.97	0.10	6	0.0039	0.0037
E	charge decay +	42	0.47	0.09	6	0.62	0.05	5	0.0028	0.0023
F	charge decay -	42	0.30	0.03	6	0.45	0.04	5	0.0018	0.0017
G(1-9)	charge decay +	65	7.0	0.15	13	11.05	1.0	12	0.042	0.042
H	polar. - 120 V	38	0.05	0.006	5	0.08	0.011	5	0.00033	0.00029
I	polar. - 120 V	46	0.53	0.12	5	0.82	0.20	5	0.0032	0.0031
J	polar. + 120 V	50	0.49	0.09	6	0.75	0.11	6	0.0029	0.0028
K	polar. + 120 V	50	0.33	0.04	6	0.50	0.05	6	0.0020	0.0019
L	polar. + 120 V	65	9.9	0.53	4				0.059	
M	polar. - 120 V	65	28.1	6.5	4				0.17	

		r.h.			
A	Charge decay -	0	0.30	0.42	Half peak width in cms. of yarn at beginning and end of experiment.
B	Charge decay +	0	0.36	0.42	
C	Charge decay -	30%	0.70	1.00	

concentration built up and decayed was also found to follow a diffusion equation. Fig. 5 shows the decay of polarization charges for r.h. 38, 46, 50 and 65% and the rate of build-up

(b) The measurement of charge by the ring collector is inaccurate for two reasons: its potential is proportional to charge and to position, thus a thread line carrying a charge

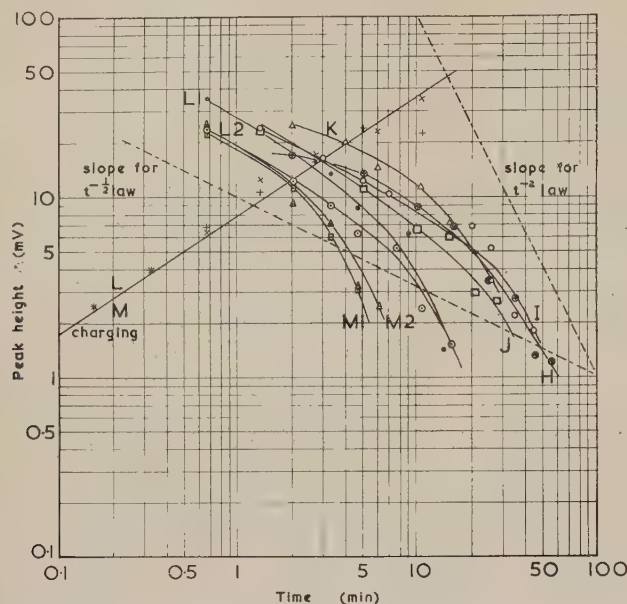


Fig. 5. Decay of polarization charges, logarithmic time scale

- H (⊕) = polarization - 120 V, r.h. = 38%
- I (○) = polarization - 120 V, r.h. = 46%
- J (□) = polarization + 120 V, r.h. = 50%
- K (△) = polarization + 120 V, r.h. = 50%
- L₁ (●) = polarization + 120 V, r.h. = 65%
- L₂ (○) = polarization + 120 V, r.h. = 65%
- M₁ (□) = polarization - 120 V, r.h. = 65%
- M₂ (△) = polarization - 120 V, r.h. = 65%

for 65% r.h. The law is approximately $t^{-1/2}$. Values of x^2/t for $\frac{1}{2}$ and $\frac{1}{3}$ peak height are shown in Table 1 for comparison with values obtained from charge decay.

Fig. 6 shows the variation of the mean diffusion constant D with relative humidity. The relation is approximately exponential. The vertical lines shown give, for each point, the limits of twice the standard deviation of a single value.

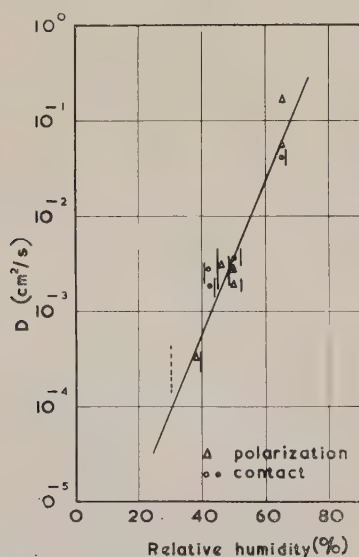


Fig. 6. Dependence of diffusion constant on humidity

Discussion

Experimental factors limiting the accuracy of the interpretation.

(a) The charge concentrations are not strictly at one point, particularly for the induced charges and hence application of the diffusion equation, equation (1), is not fully justified.

requires accurate centring and a limited aperture. These conditions were only approximately satisfied.

(c) The time taken for a traverse of the thread line through the measuring ring collector was, for high humidity, an appreciable fraction of the time taken for diffusion. A correction for this effect would be necessary for full accuracy.

Use of diffusion equation. The equation for the density of free charge carriers in one dimension is:

$$\frac{\partial \rho}{\partial t} = D \frac{\partial^2 \rho}{\partial x^2} + \mu \frac{\partial (E\rho)}{\partial x}, \quad (2)$$

where D is the diffusion constant, μ the mobility and E is given by the equation:

$$E(x) = \int \frac{\rho dx' dy' dz' (x - x')}{|r|^3}, \quad (3)$$

where ρ is the charge density, and:

$$r^2 = (x - x')^2 + (y - y')^2 + (z - z')^2.$$

If ρ is assumed to be a function of x' only, then the integrations over y' and z' can be completed, giving:

$$E = 2\pi \int \rho(x')(x - x') dx' \left[\frac{1}{|x - x'|} - \frac{1}{\{(x - x')^2 + a^2\}^{1/2}} \right], \quad (4)$$

where a is the radius of the thread. Consideration of orders of magnitude shows that only points in the immediate neighbourhood of x need be considered, and expansion of $\rho(x')$ in a Taylor series in the region $(x - \beta, x + \beta)$ shows that contributions to E arise only from terms with an odd derivative, provided that points on either side of x are taken in pairs. Thus E is a function of $\partial \rho / \partial x$, $\partial^3 \rho / \partial x^3$, and higher derivatives. If E is written as $\partial \rho / \partial x f(\beta)$, the higher orders being neglected, then equation (2) becomes:

$$\frac{\partial \rho}{\partial t} = D \frac{\partial^2 \rho}{\partial x^2} + \mu f(\beta) \left(\frac{\partial \rho}{\partial x} \right)^2 + \mu f(\beta) \rho \frac{\partial^2 \rho}{\partial x^2}. \quad (5)$$

The conduction terms may thus contribute to diffusion in regions of high charge density, but only over a short range. Use of the diffusion equation alone neglects the conduction term in the above equation, but considerably simplifies its practical application to the present problem since exact solutions of equation (2) have not been found, although several solutions of the static problem (that is, $\partial\rho/\partial t = 0$) have been published, for example, J. R. MacDonald.⁽¹⁾ With the rather insensitive experimental apparatus described, it is indeed doubtful whether differences between the diffusion equation (1) and equation (2) could be detected. A study of the static space charge distributions will be made for comparison with the theoretical distributions given by MacDonald.⁽¹⁾

Nature of the charge decay process. A change in the type of decay appears to occur at about 35% r.h. Below this level, the initial decay is approximately exponential whereas, above it, it follows the diffusion equation fairly well. The steep fall away from the $t^{-1/2}$ slope at large value of time may be partially accounted for by assuming that exponential decay to the atmosphere occurs in addition to diffusion along the thread. That is, the appropriate equation is:

$$\frac{\partial\rho}{\partial t} = D\frac{\partial^2\rho}{\partial x^2} - c\rho.$$

The substitution $\rho = \rho' \exp(-ct)$ reduces this to the ordinary diffusion equation and the decay of the peak height with time is:

$$\rho = At^{-1/2} \exp(-ct),$$

and the second term predominates at high values of t , causing a fall away from linearity on the logarithmic scale, similar to that found. The apparent absence of spreading at low humidity may be explained by postulating that, at low humidity, there is a saturation current in which the charges are too few to be detected. It is as if the charge were being "piped" along the thread from the local concentration

whereas, at higher humidities, the flow is free, being unconstrained by saturation. The diffusion constant changes rapidly with relative humidity, the relation being approximately exponential as shown by Fig. 6, and this lends credence to the view that the conduction process in nylon is ionic. With the Einstein relation between diffusion constant and mobility, that is:

$$\mu = \frac{eD}{kt},$$

then it would be expected that the conductivity of nylon, being proportional to the mobility, should also increase exponentially with relative humidity. This is, in fact, found by Hearle.⁽²⁾ The similarity of the decay behaviour for both contact charges and polarization charges suggests that the *same carriers are involved in both* and that they are, therefore, both ionic. However, further experiments must be made to decide unequivocally what the carriers are and what their signs are if there is more than one type.

A study of the build-up and decay of charges on nylon film was reported by V. E. Shashoua in a recent paper,⁽³⁾ but in this work, only peak charge was measured and the potentials were very much greater (1000–10000 V). The r.m.s. decay reported was exponential with respect to time and the half-life of charge decay was found to follow an exponential-type law with respect to relative humidity.

Acknowledgement

Thanks are due to British Nylon Spinners Ltd., for permission to publish this work.

References

- (1) MACDONALD, J. R. *J. Chem. Phys.*, **30**, p. 806 (1959).
- (2) HEARLE, J. W. S. *J. Text. Inst.*, **44**, p. T117 (1953).
- (3) SHASHOUA, V. E. *J. Polymer Sci.*, **33**, p. 65 (1958).

Resistance-temperature relationship of platinum at low temperatures and its influence on precision thermometry

by G. C. LOWENTHAL, B.A., M.Sc., A.Inst.P.,* and A. F. A. HARPER, M.Sc., F.Inst.P., Commonwealth Scientific and Industrial Research Organization, Division of Physics, Sydney, Australia

[Paper received 11 November, 1959]

Abstract

An analysis of the results of measurements of the resistance of platinum as a function of its temperature and purity indicates that known weaknesses in the Callender-Van Dusen equation can be explained by the presence of a point of inflexion in the resistance-temperature curve near 86° K, only a few degrees below the present lower limit of the International Temperature Scale (I.T.S.). A satisfactory interpolation formula for temperature measurement below 90° K can be obtained if account is taken of the fact that dR/dT for platinum is the greater the purer the metal only above about 26° K, while the reverse is true below that temperature. This suggests the use of the normal boiling point of neon (27·07° K) as an intermediate fixed point. If this point should prove adequately reproducible, it should prove practicable to

extend the I.T.S. by means of the simple so-called Cragoe function from 90 to 27° K, preferably with a break in the range at the triple point of oxygen (54·36° K).

Introduction

FOR the range 0 to -190°C , the International Temperature Scale of 1927† makes use of the formula:

$$R_t = R_0(1 + At + Bt^2 + C(t - 100)t^3), \quad (1)$$

connecting the resistance R_t with the corresponding temperature t ($^\circ\text{C}$) of a platinum resistance thermometer, the four calibration constants R_0 , A , B and C being determined

† The first International Temperature Scale (I.T.S.) was set up in 1927⁽⁶⁾ and is generally referred to as I.T.S. 1927. In 1948 an amended version was decided upon.⁽⁷⁾ This scale (I.T.S. 1948) is still current but has been further amended in 1954.⁽⁸⁾

* Now at the University of New South Wales, Sydney.

by calibrations at the ice point and near the normal boiling points of water, sulphur and oxygen. Equation (1) was suggested by Van Dusen⁽¹⁾ who had shown it to fit the results of published gas thermometric calibrations of platinum resistors^(2, 3) and also some previously unpublished results obtained in 1918 at the National Bureau of Standards, U.S.A. Van Dusen suggested this equation because of its relative simplicity and similarity with the well-established Callendar equation:

$$R_t = R_0(1 + At + Bt^2), \quad (2)$$

used originally between 0 and 660° C (I.T.S. 1927) and now between 0 and 630° C (I.T.S. 1948).

However, Keesom⁽⁴⁾ pointed out that equation (1) did not produce a temperature scale agreeing with the Thermodynamic Temperature Scale (T.T.S.) to better than 0.04 deg. C while the accuracy of gas thermometry at Leiden was better than ± 0.02 deg. C (but see Henning⁽⁵⁾).

In 1932, Heuse and Otto⁽⁹⁾ measured the differences between the two scales at several temperatures between 0 and -130°C using two thermometers with α values of 0.003 9146 and 0.003 9158, where $\alpha = (R_{100} - R_0)/100R_0$ and serves as an indicator for the purity of the platinum. (I.T.S. 1927 stipulated that α must be greater than 0.003 90 while I.T.S. 1948 requires α to exceed 0.003 910.) Results obtained by Heuse and Otto are reproduced in Table 1. The figures in this table represent averages for both thermometers over several readings taken at or very near each of the indicated temperatures. They show that especially near -80°C , the difference (T.T.S. - I.T.S.) is rather large.

Table 1. Differences between International and Thermodynamic Temperature Scales (after Heuse and Otto⁽⁹⁾)

t (°C)	(T.T.S.)-(I.T.S.) (°C)
-42	0.040
-45	0.026
-73	0.032
-78	0.039
-80	0.051
-108	0.028
-129	0.015

Table 2. Differences between International and Thermodynamic Temperature Scales (after Keesom and Dammers⁽¹⁰⁾)

t (°C)	$\{(T.T.S.)-(I.T.S.)\}_{av}$ (°C)	t (°C)	$\{(T.T.S.)-(I.T.S.)\}_{av}$ (°C)
0	0	-100	0.021
-10	0.005	-110	0.010
-20	0.010	-120	-0.002
-30	0.016	-130	-0.015
-40	0.022	-140	-0.020
-50	0.026	-150	-0.015
-60	0.032	-160	-0.010
-70	0.037	-170	-0.005
-80	0.042	-180	-0.002
-90	0.038	-183	0

In 1935 Keesom and Dammers⁽¹⁰⁾ (see also Keesom⁽¹¹⁾) intercompared the I.T.S. and T.T.S. down to -183°C using five thermometers, four of which had α values between 0.003 912 and 0.003 915 while a fifth had an α of 0.003 907. The averages of the results for the four purer thermometers are reproduced in Table 2. Maximum deviations from these averages were 0.005 deg. C. Again (T.T.S. - I.T.S.) rises to a maximum near -80°C but then decreases sharply; it becomes negative near -120°C and remains so for the rest of the range.

Allowing for the claimed accuracy of the gas thermometric measurements, the results in Tables 1 and 2 disagree significantly only near -130°C . Nevertheless, because it was held to be doubtful that the relatively irregular errors found by Keesom and Dammers could be reasonably explained other than as errors in the gas thermometry,⁽¹²⁾ no action was taken to allow for these differences. Unfortunately, no further intercomparisons of the I.T.S. and T.T.S. in this range have been published which could help to resolve this question.

The position is clearer at lower temperatures where it became evident beyond doubt that between -183 and -190°C differences between the I.T.S. and T.T.S. steadily increased, reaching several hundredths of a degree at -190°C (I.T.S. 1948, Part IV). This point was remedied in the 1948 revision of the I.T.S. by simply ending the scale at -182.97°C .

Resistance-temperature characteristics for the range 0 to -190°C

Above 0°C , the resistance-temperature relationship of platinum is approximately linear, in agreement with theory.⁽¹³⁾ This near-linearity is implicit in the usual formulation of equation (2):

$$t = \theta + \delta \left(\frac{t}{100} \right) \left(\frac{t - 100}{100} \right),$$

where

$$\theta = 100(R - R_0)/(R_{100} - R_0) \quad \text{and} \quad 1.482 \leq \delta < 1.498.$$

The quadratic "correction term" never amounts to more than a few per cent of the θ term. This relatively simple relationship ceases to hold, however, as t approaches the Debye temperature of platinum (about -45°C). It was to account for this more complicated behaviour that Van Dusen⁽¹⁾ introduced the additional term in t^3 and t^4 . This single addition, however, is clearly inadequate.

An inspection of measurements extending below -183°C ⁽¹⁴⁻¹⁶⁾ shows that d^2R/dt^2 of platinum changes sign at about -185°C , the exact temperature of the change depending on the purity of the platinum. Below this temperature $|dR/dt|$ actually decreases while equation (1) predicts a continuing increase. It is the discrepancy between $(dR/dt)_{I.T.S.}$ and $(dR/dt)_{T.T.S.}$ which caused I.T.S. 1927 to rise increasingly above the T.T.S. below -183°C . Moreover, this same discrepancy explains the fact noted by Los and Morrison⁽¹⁷⁾ that an extension of platinum resistance thermometry below -183°C leads to a discontinuity in dR/dt at this temperature.

Since $|dR/dt|_{I.T.S.}$ is definitely greater than $|dR/dt|_{T.T.S.}$ below -183°C , it would seem likely that even for some part of the range above -183°C $|dR/dt|_{I.T.S.}$ would still exceed $|dR/dt|_{T.T.S.}$ so that in this region the I.T.S. might well be above the T.T.S. This was, in fact, what Keesom and Dammers found (see Table 2). With increasing temperature, however, $|dR/dt|_{I.T.S.}$ must become smaller than $|dR/dt|_{T.T.S.}$ for otherwise equation (1) would also have failed altogether in this range. Here the corrections listed in Tables 1 and 2 indicate that $|dR/dt|_{I.T.S.}$ values remain smaller than the corresponding T.T.S. values for a considerable part of the range above about -140°C , with the result that between about 0 and -100°C , the I.T.S. lies below the T.T.S.

It would appear then that the failure of equation (1) below -183°C , the difference between $(dR/dt)_{I.T.S.}$ and $(dR/dt)_{T.T.S.}$ at -183°C and the results of Keesom and Dammers⁽¹⁰⁾ can all be explained readily in terms of known characteristics of

the resistance-temperature relationship of platinum above -190°C .

Resistance-temperature characteristics for the range below 90°K

Low-temperature platinum resistance thermometry (below 90°K) received a strong stimulus with the establishment by the National Bureau of Standards⁽¹⁵⁾ of a so-called Provisional Temperature Scale (P.T.S.). The P.T.S. comprised a selected platinum resistance thermometer (L6) which had been calibrated between 95°K and 10°K at degree intervals against a gas thermometer, other thermometers being calibrated by comparison with it. This procedure was adopted because no satisfactory interpolation formulae could be found for this range. Reviewing results obtained with some 50 thermometers calibrated on the P.T.S.,⁽¹²⁾ Cragoe pointed out that, for nearly all of them, the ratio

$$\frac{W_T - W_1}{W_2 - W_1} = Y_T \text{ (say),} \quad (3)$$

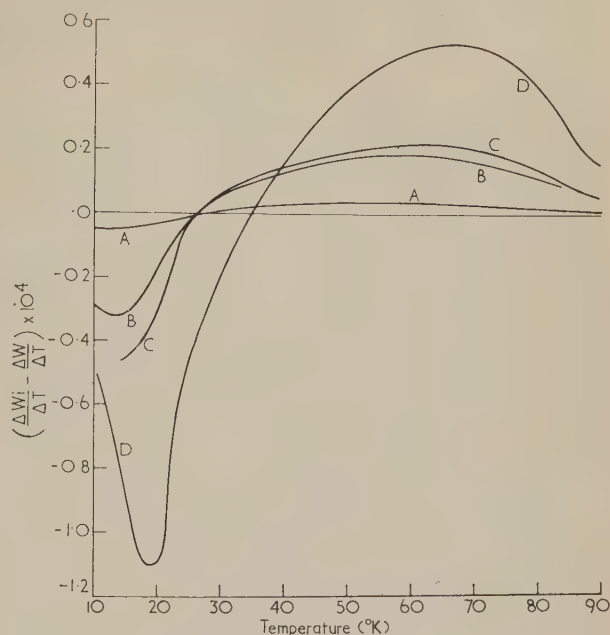
is, at least to a first approximation, a function of temperature only. Here for each thermometer, $W_T = R_T/R_{273}$ and W_1, W_2 are corresponding ratios at two selected calibration temperatures. The function Y_T (known as the Cragoe function) is readily derived from the P.T.S. (see, for example, Los and Morrison⁽¹⁷⁾). It was hoped at the time that equation (3) could serve for the realization of a practical temperature scale in close agreement with the thermodynamic scale down to about 20°K .⁽¹⁹⁾ Such a scale would be independent of the P.T.S.

However, agreement between Y_T values obtained with different thermometers was really satisfactory only in the range 90 – 50°K with W_1 and W_2 determined respectively at the triple point and normal boiling point of oxygen ($54\cdot36^{\circ}\text{K}$ and $90\cdot19^{\circ}\text{K}$ respectively^(18, 20)). Results were far less satisfactory for the range 90 – 20°K with W_1 determined at the normal boiling point of equilibrium hydrogen ($20\cdot27^{\circ}\text{K}$). Restriction of consideration to the range 54 to 20°K ($W_1 = 20\cdot27^{\circ}\text{K}$, $W_2 = 54\cdot36^{\circ}\text{K}$) produced no significant improvement. Even thermometers of the highest purity gave Y_T values which, near 30°K , differed by the equivalent of nearly $0\cdot01$ deg. $\text{K}^{(17)}$; the differences were much greater for less favourable cases.⁽¹⁸⁾

The failure of expression (3) for the interval 90 to 20°K or even 54 to 20°K can be shown to result largely from the characteristics of the W_T, T relationship of platinum in this range. This is illustrated in the figure where the difference is shown between smoothed curves of $\Delta W/\Delta T$ plotted against T for each of four thermometers varying in impurity content over a wide range and the curve of $\Delta W/\Delta T$ against T of an ideally pure resistor ($\Delta W_i/\Delta T$). The results show that for thermometers made from platinum pure enough to satisfy present I.T.S. requirements ($\alpha > 0\cdot003\,910$), dW/dT is the greater the purer the platinum above about 26°K but is the smaller the purer the platinum below that temperature.

It follows at once that expression (3) can hold only for a range lying entirely above 26°K . This is so because equation (3) demands that any two calibrated thermometers having resistance ratios W_T and W'_T respectively must have $(dW/dT)_T$ proportional to $(dW'/dT)_T$. It can be seen from the figure that this condition cannot in general be satisfied for a range which passes through 26°K . It could hold only in those special cases where thermometers are almost identical in their respective impurity contents, so that both their α -values and their residual resistances near 4°K are sub-

stantially equal. If α -values differ by as little as 1 part in 2000, expression (3) will, for accurate thermometry, require a correction term.^(17, 21)



Effect of purity on $\Delta W/\Delta T$

Values are plotted differentially, relative to $\Delta W_i/\Delta T$, for ideally pure platinum

Curve A: Chambre Centrale des Mesures, Ch6,⁽¹⁶⁾

$\alpha \approx 0\cdot003\,926$

Curve B: Hoge and Brickwedde, L6,⁽¹⁵⁾ $\alpha \approx 0\cdot003\,917$

Curve C: Henning and Otto, PTR204,⁽¹⁴⁾ $\alpha \approx 0\cdot003\,91$

Curve D: Onnes and Tuyn, 1915-23,⁽²⁷⁾ $\alpha < 0\cdot003\,9$

If, on the other hand, W_1 in expression (3) is determined at the normal boiling point of neon ($27\cdot07^{\circ}\text{K}$), which happens to be just above the critical temperature of 26°K , Y_T values within the equivalent of a few millidegrees can be expected for thermometers having $\alpha > 0\cdot003\,920$ (or possibly even $\alpha > 0\cdot003\,910$) and satisfying a further purity criterion in respect of the relative resistances at the oxygen and neon boiling points.⁽²⁰⁾ Provided then that the neon boiling point should prove adequately reproducible—it was last measured in 1936⁽²²⁾—expression (3) should prove suitable for the extension of the I.T.S. down to 27°K .

The extension to 27°K could probably be effected without the need for an intermediate calibration point. Nevertheless, a break in the range at $54\cdot36^{\circ}\text{K}$ could offer three important advantages: it is likely to improve overall reproducibility; the extension from 90°K to 54°K could be made on the basis of published data; and temperatures down to 54°K can be reached with comparatively simple equipment. To realize the triple point of oxygen, cooling can be obtained by pumping over solid nitrogen⁽²³⁾; the pure oxygen, the coolant and the thermometer could be contained in a cell of the type used by Michels *et al.*⁽²⁴⁾ for the realization of the triple point of argon. Temperatures near and below the boiling point of neon, on the other hand, can only be attained in laboratories equipped with the much more complex facilities for the use of liquid helium or liquid hydrogen; specially designed thermometer bulbs^(25, 26) are also required.

Conclusion

It has been shown that the lowest section of the I.T.S. (0 to -183°C) cannot be expected to yield a satisfactory agree-

ment with the thermodynamic scale because of the characteristics of the resistance-temperature relationship of platinum in this range. The most serious consequence of this is that the I.T.S. now fails to join smoothly to the T.T.S. at -183°C .⁽¹⁷⁾ This fault will have to be remedied before the I.T.S. can be extended to lower temperatures.

Concerning the manner of extending the I.T.S., it is suggested that this be carried out in the first instance to the temperature of the triple point of oxygen ($54\cdot36^{\circ}\text{K}$). Ample experimental proof is available⁽¹⁷⁻²⁰⁾ to indicate that this could be done in terms of a selected set of values of the simple Cragoe function, expression (3), although this will have to be supplemented by a suitable criterion for the purity of the platinum. Such an extension would be further facilitated by the fact that a temperature of 54°K can be reached without specialized low-temperature equipment. A further extension to about 27°K could be effected in terms of selected values of the simple Cragoe function in conjunction with a suitable purity criterion by the use of the boiling point of neon as an additional calibration point, provided it proves to be sufficiently reproducible. However, no extension of this procedure to a range which includes 26°K can be expected to give a reliable scale because of the change in the properties of near-pure platinum which occurs near this temperature. Platinum resistance thermometry can, of course, be employed usefully below 26°K , the lower limit being near 10°K where dR/dT of platinum becomes inconveniently small. A method of setting up a practical temperature scale from 27°K to near the triple point of equilibrium hydrogen ($13\cdot81^{\circ}\text{K}$) using in part a suggestion made by the National Bureau of Standards, U.S.A., has been outlined elsewhere.⁽²⁰⁾

References

- (1) VAN DUSEN, M. S. *J. Am. Chem. Soc.*, **47**, p. 326 (1925).
- (2) HENNING, F. *Ann. d. Physik.* (4), **40**, p. 635 (1913).
- (3) HENNING, F., and HEUSE, W. *Z. f. Physik.*, **23**, p. 95 (1924).
- (4) KEESOM, W. H. *Physica*, **9**, p. 385 (1929).
- (5) HENNING, F. *Z. ges. Kalte-Ind.*, **37**, p. 169 (1930).
- (6) *Trav. Bur. Int. Poids Mes.*, **18** (1930).
- (7) *P.V. Com. Int. Poids Mes.*, **21**, p. T19 (1948); also STIMSON, H. F. *Nat. Bur. Stand. J. Research*, **42**, p. 209 (1949).
- (8) *P.V. Com. Int. Poids Mes.*, **24**, p. T20 (1954).
- (9) HEUSE, W., and OTTO, J. *Ann. d. Physik.* (5), **14**, p. 181 (1932).
- (10) KEESOM, W. H., and DAMMERS, B. G. *Physica*, **2**, p. 1080 (1935).
- (11) KEESOM, W. H. *P.V. Com. Int. Poids Mes.*, **19**, p. T105 (1939).
- (12) MUELLER, E. F. *Temperature. Its measurement and control in science and industry*, **1**, p. 162 (New York: Reinhold Publishing Corp., 1941).
- (13) MOTT, N. F., and JONES, H. *The theory of the properties of metals and alloys*, p. 244 (Oxford: Clarendon Press, 1936).
- (14) HENNING, F., and OTTO, J. *Z. ges. Kalte-Ind.*, **39**, p. 86 (1932).
- (15) HOGE, J. H., and BRICKWEDDE, F. G. *Nat. Bur. Stand. J. Research*, **22**, p. 351, RP 1188 (1939).
- (16) Memorandum, Chambre Centrale des Mesures et Instruments de Mesure (U.R.S.S.), *P.V. Com. Int. Poids Mes.*, **24**, p. T141 (1954).
- (17) LOS, J. M., and MORRISON, J. A. *Canad. J. Phys.*, **29**, p. 142 (1951).
- (18) STULL, D. R. *Chem. Eng. News*, **27**, p. 2772 (1949).
- (19) Memorandum, National Bureau of Standards, *P.V. Com. Int. Poids Mes.*, **21**, p. T84 (1948).
- (20) LOWENTHAL, G. C., KEMP, W. R. G., and HARPER, A. F. A. *Bull. Inst. Intern. Froid, Annexe* 1958, **1**, p. 107 (1958).
- (21) BARBER, C. R. *P.V. Com. Int. Poids Mes.*, **26**, p. T52 (1958).
- (22) HENNING, F., and OTTO, J. *Physik Z.*, **37**, p. 639 (1936).
- (23) KEESOM, W. H., and LISMAN, J. H. C. *Commun. Leiden* No. 239a (1935).
- (24) MICHELS, A., WASSENAAR, T., SLUYTERS, TH., and DEGRAAF, W. *Physica*, **23**, p. 89 (1957).
- (25) SOUTHARD, J. G., and MILNER, R. T. *J. Am. Chem. Soc.*, **55**, p. 4384 (1933).
- (26) BARBER, C. R. *J. Sci. Instrum.*, **32**, p. 416 (1955).
- (27) ONNES, H. K., and TUYN, W. *Commun. Leiden, Suppl.* **58**, No. 180 (1926); also *International Critical Tables*, **6**, p. 130 (New York: McGraw-Hill, 1929).

Journal of Scientific Instruments

Contents of the May issue

- SPECIAL ARTICLE
The Physical Society's Exhibition—London, 1960. By T. B. Rymer.
- PAPERS
Yarn-speed meter—a low-torque instrument for measuring the linear speed of low-inertia systems. By D. L. Munden and T. K. Morley.
Production and tensile testing of strain-free metal specimens. By G. Greetham and A. J. Martin.
Primary standard barometer of range 0 to 1200 mb. By K. W. T. Elliott, D. C. Wilson, F. C. P. Mason and P. H. Biggs.
Heat transport anemometer of high stability. By A. J. Dyer.
Vacuum sublimation apparatus for preparation of thin sources of α -active materials. By N. Jackson.
Vacuum furnace for high temperature X-ray diffractometry. By J. N. Van Nieuwerkerk.
Apparatus for the zone refining of copper. By E. D. Tolmie.
- LABORATORY AND WORKSHOP NOTES
New method of cold hearth melting. By W. H. Shepherd.
Automatically operated balanced filters for counter diffractometer. By H. A. McKinstry and M. A. Short.
Gratings for measuring separation of equidistant parallel straight lines. By R. M. Dawson.
Design of a small rolling mill for use at low temperatures. By E. D. Tolmie and A. C. Roberts.
Two-way oil-filled dash pot. By A. W. Williams and L. Riddiford.
Grips for tensile tests on very extensible tapes. By A. G. Day.
- CORRESPONDENCE
Effect of ambient airspeed on efficiency of thermal-precipitator. From J. R. Hodgkinson, A. Critchlow and N. Stanley.
Comments on the A.S.T.M. Powder Data File—5. From J. W. Hughes, Isabel Lewis and A. J. C. Wilson.
- NOTES AND NEWS
Notes and comments

THIS JOURNAL is produced monthly by The Institute of Physics, in London. It deals with all branches of applied physics (including theory and technique). All rights reserved. Responsibility for the statements contained herein attaches only to the writers.

EDITORIAL MATTER. Communications concerning editorial matter should be addressed to the Editor, The Institute of Physics, 47 Belgrave Square, London, S.W.1. (Telephone: Belgravia 6111.) Prospective authors are invited to prepare their scripts in accordance with the *Notes for Authors*. (Price 3s. 6d. including postage.)

REPRODUCTION. The Institute of Physics is a signatory to The Royal Society's Fair Copying Declaration. Details may be obtained upon application from The Royal Society, London, W.1.

ADVERTISEMENTS. Communications concerning advertisements should be addressed to the agents, Messrs. George Jackson (Fleet St.) Ltd., Cliffords Inn, Fleet Street, London, E.C.4. (Telephone: Holborn 3611-2.)

CLAIMS FOR MISSING JOURNALS. Claims from regular subscribers to this *Journal* for missing numbers will only be considered if received within 60 days of the date of mailing plus normal outward time of transit and time for lodging the claim. Losses attributable to failure to notify a change of address or to similar omissions will not be considered.

SUBSCRIPTION RATES. A new volume commences each January. The charge is £6 per volume (\$17 U.S.A.), including index (post paid), payable in advance. Single parts, so far as available, may be purchased at 12s. 6d. each (\$1.75 U.S.A.), post paid, cash with order. Orders should be sent to The Institute of Physics, 47 Belgrave Square, London, S.W.1, or to any bookseller.

Principles of thermoelectric devices

by H. J. GOLDSMID, B.Sc., Ph.D., Research Laboratories of The General Electric Company Limited, Wembley, England

Abstract

In recent years, the use of semiconductor thermojunctions has improved the efficiency of generation by means of the Seebeck effect and has made thermoelectric refrigeration a practical possibility. By using semiconducting compounds of high mean atomic weight, Seebeck coefficients of about $200 \mu\text{V}/^\circ\text{C}$ have been obtained without the ratio of electrical to thermal conductivity departing too far from the value given by the Wiedemann-Franz law for metals. The most favourable semiconductors have been improved still further by alloying with isomorphous materials. Devices employing the thermoelectric effects are discussed.

Introduction

IT is only in recent years that the production of reasonably efficient thermoelectric devices has become possible although the principal thermoelectric effects were known early in the nineteenth century. Seebeck observed thermoelectric voltages in 1821 and Peltier found the reversible thermal effects which bear his name in 1834, though both these workers did not at first realize the true meaning of their discoveries.

For a very long time, thermocouples have been used for measuring temperature, and thermopiles are equally well established for detection of heat radiation. Both these devices are applications of the Seebeck effect and, although they are inefficient from a thermodynamic point of view, sensitive ancillary apparatus has made their use possible. However, the use of the Peltier effect for thermoelectric refrigeration was impossible with the thermocouples which were available up to a short time ago, since, even with a low efficiency, reasonable temperature differences between the junctions could not be established.

Theoretical studies of thermoelectric generation⁽¹⁾ and refrigeration⁽²⁾ were first made by Altenkirch. It is obvious that, besides large thermoelectric coefficients, a high electrical conductivity is required to minimize the Joule heating losses in the thermoelements. Also, a low thermal conductivity is needed to prevent excessive heat transfer from the hot to the cold junctions. Altenkirch expressed these qualitative considerations in the form of a simple figure of merit involving the Seebeck coefficients and the ratios of the electrical to the thermal conductivity in the materials forming a junction.

For a long time, no thermocouples with a reasonable figure of merit were available. However, in the past few years there has been rapid progress in the field of semiconductors and it is this fact which has led to important advances in thermoelectric materials. A maximum lowering of temperature by means of the Peltier effect of 26°C was reported in 1954⁽³⁾ and by 1958 this figure had been raised

to 80°C .⁽⁴⁾ Thus, thermoelectric cooling devices are at last a practical proposition. The improved thermoelectric materials may also be used for thermoelectric generation with moderate hot-junction temperatures. However, comparable generator materials for use at high temperatures are not yet available.

Coefficient of performance for refrigeration

It has always been customary to assume the validity of the Kelvin relations in the theory of thermoelectric cooling. Whereas it is the Peltier coefficient π which enters directly into the expressions for the thermoelectric cooling, it is the Seebeck coefficient* α which is much more easily measured. These two parameters are related by Kelvin's first law:

$$\pi = \alpha T. \quad (1)$$

Lord Kelvin's proof of equation (1), which was based on the principles of reversible thermodynamics, cannot be applied strictly to a real thermocouple. However, the use of irreversible thermodynamics⁽⁵⁾ has also led to the Kelvin relations. Experimentally, equation (1) has been verified for a number of thermocouple materials and its validity will be accepted here. It must be pointed out, however, that it has been reported to break down for germanium. For this semiconductor, Shtenbek and Baranskii⁽⁶⁾ observed that the Peltier coefficient π is significantly less than the product αT .

It is not proposed to consider the theory of thermoelectric applications in detail. Instead, expressions for the coefficient of performance of a thermoelectric refrigerator and the efficiency of a generator will merely be quoted. For their derivation, reference should be made to the works of Altenkirch,^(1, 2) Gehlhoff and others,⁽⁷⁾ Ioffe⁽⁸⁾ or Harman.⁽⁹⁾

The coefficient of performance ϕ of a refrigerator is defined as the ratio of the rate of removal of heat from the source to the rate of expenditure of energy. For Peltier cooling, using a given pair of thermoelectric materials, the coefficient of performance is a function of the relative dimensions of the thermocouple branches and of the current passing through them. When optimum values of these quantities are taken, it is found that:

$$\phi = \frac{T}{\Delta T} \cdot \frac{(1 + ZT)^{1/2} - 1}{(1 + ZT)^{1/2} + 1} - \frac{1}{2}, \quad (2)$$

* The ratio of the voltage developed by a thermocouple to the temperature difference between its junctions has, in the past, usually been referred to as the thermoelectric power or the thermal e.m.f. coefficient. In accordance with the recommendations of a task group of the A.I.E.E./I.R.E., it is proposed to adopt the term "Seebeck coefficient" here.

where T is the mean temperature, ΔT is the temperature difference between the junctions and:

$$Z = \frac{(\alpha_p - \alpha_n)^2}{\{(\kappa_p/\sigma_p)^{1/2} + (\kappa_n/\sigma_n)^{1/2}\}^2} \quad (3)$$

κ and σ are the thermal and electrical conductivities respectively and the subscripts p and n refer to the positive and negative branches of the couple; $(\alpha_p - \alpha_n)$ is the differential Seebeck coefficient. Since, for given hot and cold junction temperatures, the coefficient of performance ϕ depends only on Z , the latter quantity is a figure of merit.

If ZT is very much greater than unity, the thermoelectric refrigerator becomes an ideal thermodynamic machine with:

$$\phi_{ideal} = \frac{T}{\Delta T} - \frac{1}{2}$$

It should be noted, however, that only recently have thermocouples with ZT even approaching unity become available. Fig. 1 shows how the coefficient of performance depends on the temperature difference for values of Z between 10^{-3} and $4 \times 10^{-3}/^\circ\text{K}$.

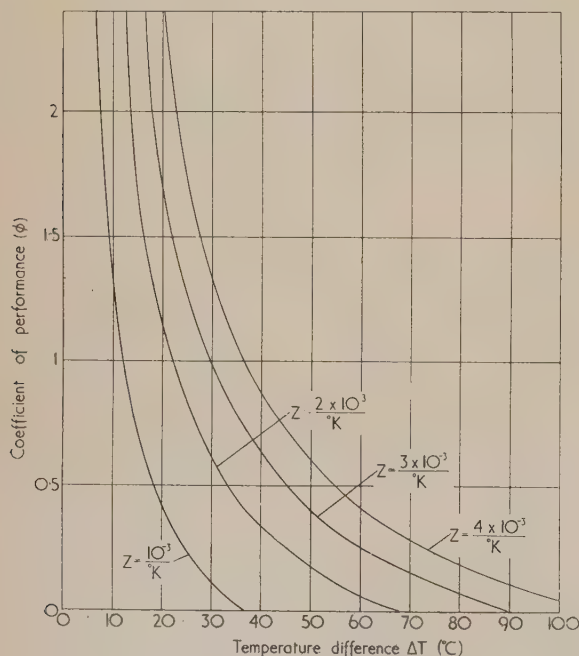


Fig. 1. Coefficient of performance plotted against temperature difference for a mean temperature of 290°K

In the search for new thermoelectric materials, it is not particularly convenient to use the figure of merit Z as defined by equation (3). Instead it is usual to employ a figure of merit z for a single thermoelement which is defined by:

$$z = \frac{\alpha^2 \sigma}{\kappa} \quad (3a)$$

α being the absolute Seebeck coefficient. The best thermocouples usually consist of branches with comparable values of z ; Z is then approximately equal to the mean of z_n and z_p .

The temperature, for which the parameters appearing in z should be specified, is not immediately obvious. The Joule heating and thermal-conduction processes involve the whole

of a thermoelement, so it is clear that mean values of the conductivities σ and κ are required. On the other hand, since the Peltier effect occurs only at the junctions, it might be thought that the value of α at the temperature of the heat source should be used. This conclusion is found to be false if the Thomson effect is taken into account.⁽⁸⁾

The Thomson heating in a thermoelement is $I \int_H^C \gamma dT$, where γ is the Thomson coefficient and I is the electric current. Of this heating, half will appear at each junction. According to the second Kelvin relation,

$$\frac{d\alpha}{dT} = \frac{\gamma}{T}$$

Thus the Thomson heat appearing at the cold junction is $\frac{1}{2} I \int_H^C T d\alpha$. Now this quantity is much smaller than the Peltier cooling $IT_C \alpha_C$ so, as a reasonable approximation, it may be stated that:

$$\frac{1}{2} I \int_H^C T d\alpha \simeq IT_C \int_H^C d\alpha = \frac{1}{2} IT_C (\alpha_C - \alpha_H)$$

It may be noted that α_H is generally greater than α_C so the Thomson effect usually results in additional cooling. The overall thermoelectric cooling is $IT_C \{\alpha_C + (\alpha_H - \alpha_C)/2\}$. Thus, inclusion of the Thomson effect does not alter the form of equation (2) for the coefficient of performance ϕ , provided that the figure of merit is expressed in terms of the mean Seebeck coefficient rather than the value at the cold-junction temperature.

Efficiency for generation

The efficiency ψ of a generator is the ratio of the power delivered to the load to the rate at which heat is supplied from the source. It is quite easy to calculate the value of ψ for a thermocouple the properties of which are independent of temperature.⁽⁸⁾ For maximum efficiency, it is not sufficient that the dimensions of the arms should be matched; it is also necessary that the resistance R_L of the load should be related to the resistance R of the generator by:

$$\frac{R_L}{R} = r = (1 + ZT)^{1/2} \quad (4)$$

The efficiency is then:

$$\psi = \frac{\Delta T}{\frac{\Delta T}{2} + \frac{(r+1)}{(r-1)} T} \quad (5)$$

For high efficiency, a large temperature difference is desirable. However, when this difference is large, one can seldom assume that the thermocouple properties are even approximately constant. In this case, it may be desirable to cover the complete range of temperature in two or more stages⁽⁹⁾ using the most appropriate materials for each stage. In fact, the maximum theoretical efficiency is approached as the number of stages tends towards infinity. Then:

$$\psi_\infty = 1 - \exp \left\{ - \int_C^H \frac{(r-1)dT}{(r+1)T} \right\} \quad (6)$$

There are reasons for thinking that the choice of the optimum thermoelectric materials for use over each part of the temperature range might lead to a more or less constant value of ZT . If ZT is assumed to be temperature independent, equation (6) reduces to:

$$\psi_{\infty} = 1 - \left(\frac{T_C}{T_H} \right)^{(r-1)/(r+1)} \quad (7)$$

Fig. 2 shows how the efficiency varies with hot-junction temperature according to equation (7), the cold-junction temperature being 300° K.

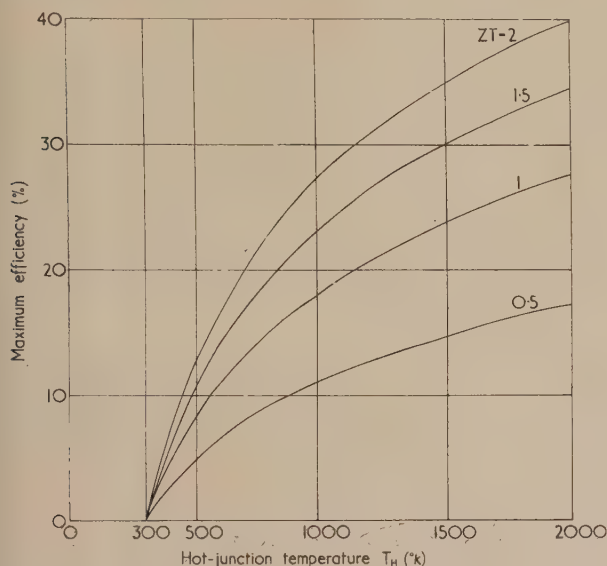


Fig. 2. Maximum efficiency of a thermoelectric generator with ZT constant and the cold junctions at 300° K

Incidentally, the performance of a thermoelectric refrigerator is also improved by using a multiple-stage arrangement,⁽²⁾ particularly if the temperature difference is large.

Thermoelectric properties of semiconductors

The ratio of the electrical to thermal conductivity is approximately the same for all metals at a given temperature. Thus, in the best metallic thermoelements, the Seebeck coefficient should be as large as possible. However, even in such materials as bismuth, antimony and their alloys, it is less than 100 $\mu\text{V}/^\circ\text{C}$. Only by using semiconductors can one obtain higher Seebeck coefficients, and, in fact, with some semiconductors values of more than 1 mV/ $^\circ\text{C}$ may be reached.

It is not immediately obvious that semiconductors are superior to metals. In most semiconductors, the number of charge carriers is so small that the lattice component of the thermal conductivity is much larger than the electronic component. Thus, the ratio of the electrical to thermal conductivity falls well below its value for a metal. In spite of this fact, recent experience has shown that the best semiconductors are better for thermoelectric applications than the best metals.

The relevant properties of a semiconductor may be expressed in terms of a single variable, the most convenient

being the reduced Fermi potential η . For an extrinsic semiconductor⁽¹⁰⁾:

$$\alpha = \pm \frac{k}{e} \left(\frac{5}{2} + \lambda - \eta \right), \quad (8)$$

if classical statistics may be employed. The positive sign applies for a p -type conductor and the negative sign for an n -type conductor. It is assumed that the relaxation time τ for the charge carriers may be expressed as:

$$\tau \propto E^\lambda, \quad (9)$$

where E is their energy. The electrical conductivity is:

$$\sigma = ne\mu, \quad (10)$$

where μ is the carrier mobility and n , the carrier concentration, is given by:

$$n = 2 \left(\frac{2\pi m^* kT}{h^2} \right)^{3/2} \exp(-\eta), \quad (11)$$

m^* being the effective mass of a carrier.

The total thermal conductivity is given by:

$$\kappa = \kappa_l + \kappa_e, \quad (12)$$

κ_l being the lattice component and κ_e the electronic component. Again, assuming classical statistics to be applicable:

$$\kappa_e = \left(\frac{5}{2} + \lambda \right) \left(\frac{k}{e} \right)^2 \sigma T. \quad (13)$$

The figure of merit z may now be expressed in terms of the reduced Fermi potential but before it is done, the effects of intrinsic conduction and of phonon-drag should be mentioned.

In a mixed semiconductor, the Seebeck coefficient is a weighted average of the contributions from the electrons and holes separately. These contributions are of opposite sign, so that the product $\alpha^2\sigma$ is reduced below its value for extrinsic material. It should also be noted that the electronic thermal conductivity tends to rise in the mixed and intrinsic ranges of conduction since the charge carriers then transport not only their kinetic energy but also their ionization energy.⁽¹¹⁾ It is concluded that, from all points of view, mixed semiconductors should be avoided in thermoelectric applications. An exception to this rule is to be found in the case of semiconductors like InSb with a high ratio of electron-to-hole mobility. Even if such materials become intrinsic, the holes provide almost negligible contributions to the Seebeck coefficient and electrical conductivity and, moreover, there is no appreciable transfer of ionization energy by bipolar thermo-diffusion. Thus, in this case, there is no objection to mixed or intrinsic conduction.

For some semiconductors, for example, germanium and silicon, particularly below room temperature, it is found that equation (8) for the Seebeck coefficient is inadequate. This is because, when there is a temperature gradient, a current of phonons tends to transfer momentum to the charge carriers and, thus, to establish an additional thermoelectric voltage. However, this, the phonon-drag effect, is only appreciable in semiconductors with a high ratio of lattice thermal conductivity to carrier mobility and even then only at low carrier concentrations. These are precisely the materials which are unfavourable if a high figure of merit z is required, as will be shown later, so it is not necessary to consider the phonon-drag effect any further.

Optimum Fermi potential

From equations (8) to (13), z may be expressed as:

$$z = \frac{\left(\frac{5}{2} + \lambda - \eta\right)^2}{\left(2 \frac{k^2}{e} FG \exp \eta\right)^{-1} + \left(\frac{5}{2} + \lambda\right) T}, \quad (14)$$

where:

$$F = \frac{\mu}{\kappa_l} \left(\frac{m^*}{m}\right)^{3/2} \quad (15)$$

and:

$$G = \left(\frac{2\pi mkT}{h^2}\right)^{3/2} \quad (16)$$

The position of the Fermi level depends on the carrier concentration and may be adjusted by the introduction or removal of donor or acceptor impurities. The optimum Fermi potential is found by setting $dz/d\eta$ equal to zero. Then:

$$\eta + 4\left(\frac{5}{2} + \lambda\right) \frac{k^2}{e} FGT \exp \eta = \frac{1}{2} + \lambda. \quad (17)$$

In most semiconductors, even for high carrier concentrations, the lattice component of the thermal conductivity is much greater than the electronic component. In this case, η should be equal to $(\frac{1}{2} + \lambda)$: for the usual forms of scattering, λ is greater than or equal to $-\frac{1}{2}$, so η is greater than or

statistics may be obtained from the opposite assumption of complete degeneracy. It may then be shown that the Seebeck coefficient varies inversely with η . The concentration of charge carriers is proportional to $\eta^{3/2}$ and their mobility* to η^λ . Thus the product $\alpha^2\sigma$ is proportional to $\eta^{(2\lambda-1/2)}$. If λ is less than $\frac{1}{2}$, $\alpha^2\sigma$ falls as η increases. Thus, in this case, as predicted from classical statistics, $\alpha^2\sigma$ should have a maximum value in the range of partial degeneracy. On the other hand, if λ is greater than $\frac{1}{2}$, $\alpha^2\sigma$ rises with η in the degenerate range and the classical prediction of a maximum is clearly false. It should be noted that, even in this case, the figure of merit z should have a maximum in the range of partial degeneracy since the thermal conductivity κ is also a function of η .

In general, the calculation of the figure of merit using classical statistics leads to an under-estimation of its value. However, for the particular case of lattice scattering with λ equal to $-\frac{1}{2}$, there is very little difference between the values of either the maximum of the product $\alpha^2\sigma$ or of the optimum Fermi potential predicted from classical or from Fermi-Dirac statistics, as shown in Fig. 3. It is estimated that, whatever the form of scattering, the optimum Seebeck coefficient should be determined by experiment in view of the probability of complicating features (for example, impurity band effects) in the conduction processes at the correspondingly high carrier concentrations.

In spite of its basis on classical statistics, equation (14) does show correctly that the major factor which determines the optimum figure of merit z for a given semiconductor is the quantity F . The value of the scattering parameter λ should also be of some importance.

Semiconductor compounds

Of the semiconductor parameters involved in the factor F , that which shows the most systematic variation from one material to another is the lattice thermal conductivity κ_l . For a series of elements in one group of the periodic table, such as those of group IV, germanium, silicon and diamond, the thermal conductivity decreases as the atomic weight increases. In a series of compounds such as the alkali halides or the III-V intermetallics, there is a similar trend⁽¹³⁾ as shown in Fig. 4. For ionic compounds it seems that the ratios of the atomic weights of the constituent atoms are important; the greater the atomic weight ratio, the smaller the thermal conductivity.

From these observations it is predicted that a high atomic weight (or mean atomic weight for compounds) is favourable since there is no similar decrease of carrier mobility with atomic weight. It is, however, difficult to predict the best series of semiconductors since, for a series having a range of high carrier mobilities (corresponding to covalent bonding), the thermal conductivities are also high. Conversely, ionic compounds with their low thermal conductivities also have low mobilities. It is possible that the most favourable materials have bonding which is intermediate between covalent and ionic. There is nothing to suggest that compounds are necessarily superior to elements, but so far, possibly because the choice is wider, compound semiconductors have proved to be the more useful.

Further consideration is complicated by the interdependence of mobility and effective mass. If the charge

* It is assumed that the relaxation time is a function of the energy of the carriers but not directly of their concentration.

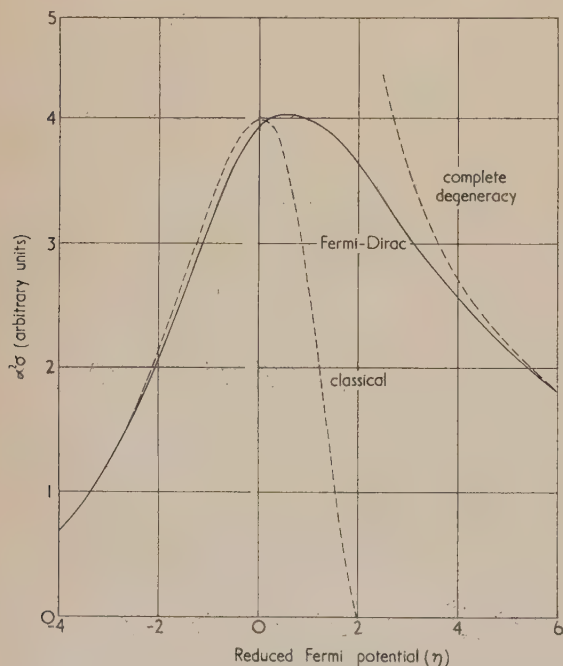


Fig. 3. The product $\alpha^2\sigma$ plotted against the reduced Fermi potential for λ equal to $-\frac{1}{2}$

equal to 0 at the optimum carrier concentration. Even for the best of present-day thermoelectric materials, for which the second term on the left-hand side of equation (17) is not negligible, the optimum value of η would not appear to be less than -0.6 . It is, therefore, clear that classical statistics should not be employed.⁽¹²⁾

Some idea of the errors arising from the use of classical

carriers are scattered by ionized impurities, the scattering law (with λ equal to $3/2$) has a favourable effect in the expression for the Seebeck coefficient, but, in practice, it has not been found that the overall effect of impurity scattering is beneficial.⁽⁸⁾ In fact, impurity scattering in the semiconductors used for thermoelectric applications is seldom observed. This is because the dielectric constant in such materials is

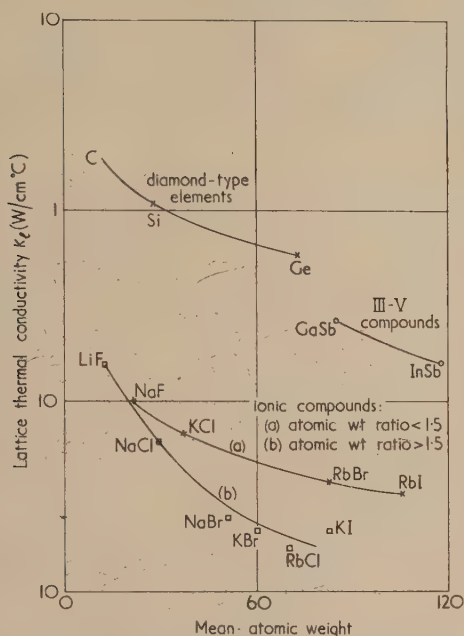


Fig. 4. Lattice thermal conductivity against mean atomic weight (after A. V. Ioffe and A. F. Ioffe)

high and this tends to localize the field of an ionized impurity. It is, therefore, justifiable to confine attention to lattice scattering. It will also be supposed that covalent binding is predominant and that optical-mode scattering is absent.

In the general case of a many-valley semiconductor with non-spherical energy surfaces⁽¹⁴⁾:

$$\mu \propto Nm_i^{-1}m^{*(-3/2)}$$

where N is the number of valleys and m_i is the inertial mass, which must be distinguished from m^* the density-of-states mass which occurs in equation (11). In this case:

$$F \propto \frac{N}{m_i}$$

Thus it appears that a semiconductor with a low-inertial effective mass and as many valleys as possible is desirable, though it is always possible that multiplicity of the valleys could lead to inter-valley scattering.

Of the many semiconductors which have been studied, the two which have been found most useful for thermoelectric applications are PbTe and Bi₂Te₃. Both, of course, satisfy the criterion of high mean atomic weight and consequently the lattice thermal conductivity is low for both. For PbTe, it is about 2×10^{-2} W/cm°C while for Bi₂Te₃ it is about 1.5×10^{-2} W/cm°C. The density-of-states effective mass for electrons in PbTe is about $0.4m$; magnetoresistance measurements by Scanlon⁽¹⁵⁾ suggest that it is a four- or eight-valley semiconductor. The figure of merit of an

n -type sample mentioned by Ioffe⁽⁸⁾ was $0.9 \times 10^{-3}/^\circ\text{K}$; with a more favourable Seebeck coefficient a value of say $1.5 \times 10^{-3}/^\circ\text{K}$ might be obtained. p -type PbTe has a somewhat lower maximum figure of merit.

The determination of the effective masses of electrons and holes in Bi₂Te₃ is rather difficult on account of its anisotropy. Bi₂Te₃ has a layer structure and the conductivities in the cleavage planes and perpendicular to them are quite different. In fact, the figure of merit is appreciably lower if current is passed in the perpendicular direction. The Hall effect is dependent on the direction of the magnetic field. Most workers seem to have used a magnetic field perpendicular to the cleavage planes and have found that both the electron and hole effective masses exceed the free electron mass. The corresponding electron mobility is only about $300\text{ cm}^2/\text{V s}$. However, recent galvanomagnetic measurements⁽¹⁶⁾ show that a six-valley model is applicable to n -type Bi₂Te₃ and that the application of such a model yields a density-of-states effective mass for an electron of about $0.45m$. The mobility then exceeds $1000\text{ cm}^2/\text{V s}$. A three-valley model is thought to apply for p -type Bi₂Te₃⁽¹⁷⁾; the density-of-states mass of a hole is again only about half the free electron mass. The inertial effective masses for both electrons and holes are, of course, less than the density-of-states masses. Thus Bi₂Te₃ satisfies the ideal condition of a many-valley semiconductor with a low inertial mass and a high mean atomic weight.

The thermoelectric properties of Bi₂Te₃⁽¹⁸⁾ are shown in Fig. 5. In the region of mixed conduction (between A and B),

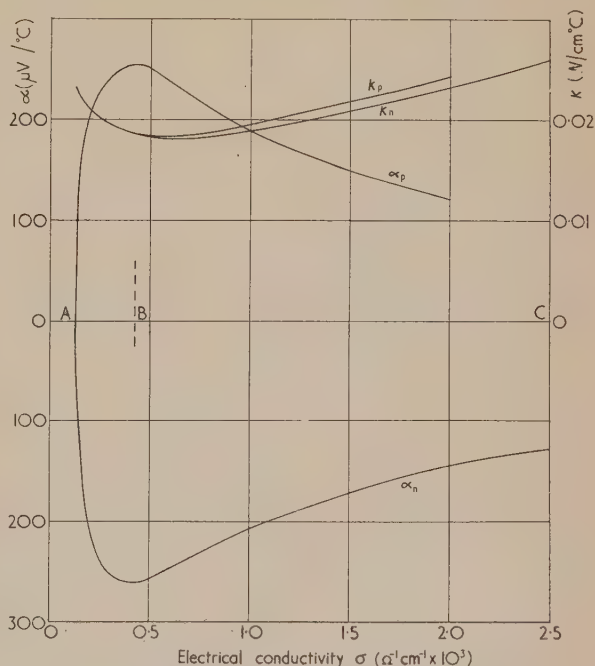


Fig. 5. Thermoelectric properties of Bi₂Te₃ at room temperature

the unfavourable relationship between the Seebeck coefficient α and the electrical conductivity σ may be seen, together with the rise of thermal conductivity associated with the transport of ionization energy. Material for thermocouples should obviously be selected from the extrinsic region (B to C). Maximum values for z_p and z_n of 1.8 and $2.3 \times 10^{-3}/^\circ\text{K}$ respectively occur for an electrical conductivity of about $1000/\Omega\text{ cm}$. The figure of merit for a thermocouple between

p-type and *n*-type Bi_2Te_3 is $2.0 \times 10^{-3}/^\circ\text{K}$ and the maximum Peltier cooling, at a mean temperature of 17°C , is 65°C .

At the present time, Bi_2Te_3 is also the best compound for use in thermoelectric generation provided that the hot-junction temperature is not excessive. At temperatures much higher than 200°C , it is very difficult to prevent the onset of intrinsic conduction even by heavy doping; irreversible chemical effects may also become apparent. To obtain high efficiency of generation, it is desirable that materials which are capable of withstanding high temperatures should be available. Thus, the thermoelectric properties of a number of refractory materials (for example, oxides and silicides of the transition metals⁽¹⁹⁾) are being studied. However, at the moment, no such compound has a sufficiently high figure of merit to be really useful.

Semiconductor alloys

Ioffe and his colleagues⁽²⁰⁾ have shown how the figure of merit may be improved further. The ratio of mobility to thermal conductivity for a semiconductor may be raised by the addition of an isomorphous material to form a solid solution. In such a solid solution there is very little disturbance of the long-range periodicity of the lattice, but the short-range order is considerably disturbed. Now the wavelengths associated with electrons or holes in semiconductors are several tens of interatomic distances, so that scattering of charge carriers results from upsetting the long-range order of the lattice. On the other hand, the heat-conduction phonons have wavelengths of only a few interatomic distances so they are effectively scattered by the disturbances in the short-range order which result from the formation of a solid solution. In this way, the lattice thermal conductivity is considerably reduced.

As might be expected, the effect of alloying on the thermal conductivity is greatest for those semiconductors which have a long mean free path for phonons. Thus, in pure germanium, the phonon free-path length is about thirty-five interatomic distances and is reduced to three interatomic distances in a 50% Si-Ge alloy. The corresponding thermal conductivities are 0.6 and $0.05 \text{ W/cm}^\circ\text{C}$. In the semiconducting compounds used for thermoelectric applications, the phonon free paths are only two or three interatomic distances even before alloying. Thus, the corresponding solid solutions show only a relatively small change in the lattice thermal conductivity. In the PbTe-PbSe system, the thermal conductivity falls by a factor of two⁽²¹⁾; in the $\text{Bi}_2\text{Te}_3\text{-Sb}_2\text{Te}_3$ system the thermal conductivity is reduced to about two-thirds of the value for Bi_2Te_3 itself. The changes of thermal resistivity with composition in the systems which have been mentioned are shown in Fig. 6; x is the atomic concentration of the minority constituent.

A lower limit to the lattice thermal conductivity of an alloy is reached when the phonon free-path length falls to the order of the interatomic spacing. The question arises whether or not the criterion of high atomic weight still applies under these conditions. The basic equation for the thermal conductivity is:

$$\kappa_l = \frac{1}{3} cvl, \quad (18)$$

where c is the thermal capacity per unit volume, v is the velocity of sound and l is the phonon free-path length. From Dulong and Petit's law, c is proportional to ρ/A where ρ is the density and A the atomic weight. Also, the

velocity of sound may be related to the Debye temperature θ ; v is proportional to $\theta(A/\rho)^{1/3}$. Finally, the interatomic spacing is proportional to $(A/\rho)^{1/3}$. Thus, in the present case:

$$(\kappa_l)_{\min} \propto \left(\frac{\rho}{A}\right)^{1/3} \theta. \quad (19)$$

The ratio ρ/A tends to fall rather slowly with A but since the thermal conductivity is only proportional to its cube root the variation is relatively unimportant. Thus, the value of κ_l corresponding to the minimum phonon free path is primarily dependent on the Debye temperature and the criterion of a high mean atomic weight for thermoelectric applications still holds.

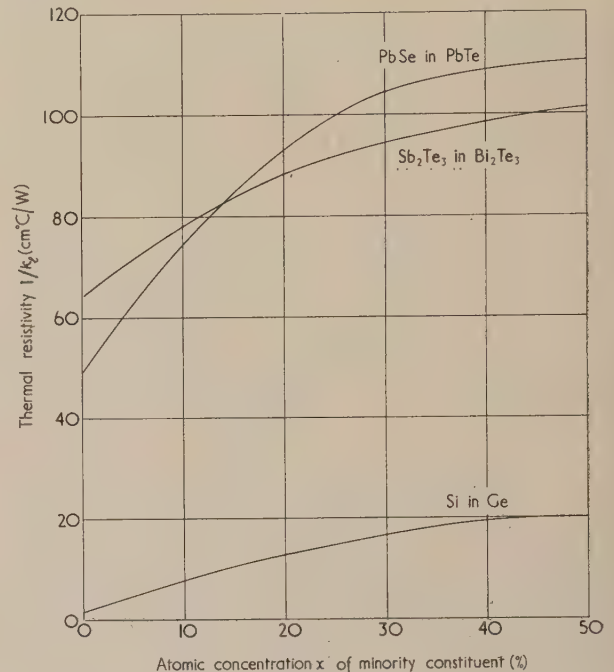


Fig. 6. Thermal resistivity of semiconductor alloys

The use of semiconductor alloys has led to significant improvements in the figure of merit. Ioffe⁽⁸⁾ has reported that the ratio of mobility to thermal conductivity in a PbTe-PbSe alloy is one-and-a-half times the value for PbTe . Similar improvements are found in the $\text{Bi}_2\text{Te}_3\text{-Sb}_2\text{Te}_3\text{-Bi}_2\text{Se}_3$ system⁽⁴⁾; the maximum figure of merit for a thermocouple has now been raised to about $3 \times 10^{-3}/^\circ\text{K}$, which corresponds to a maximum Peltier cooling of some 90°C at a mean temperature of 17°C .

So far, very little work on the use of alloys as generator materials has been reported. However, Bowers and others⁽²²⁾ have found that the addition of InP to InAs increases its figure of merit appreciably in the temperature range $450\text{--}800^\circ\text{C}$. A value of z_n exceeding $0.7 \times 10^{-3}/^\circ\text{K}$ at about 700°C was observed.

Recently Airapetyants and others⁽²³⁾ have reported some experiments which suggest that the effects of alloying are rather more complicated than had been thought at first. They found that the addition of Sb_2Te_3 to Bi_2Te_3 resulted in a reduction of the electron mobility but the hole mobility did not fall. On the other hand, on the addition of Bi_2S_3 to Bi_2Te_3 the hole mobility was found to decrease much more rapidly than the electron mobility. The changes in the

ratio of electron to hole mobility are shown in Fig. 7. Airapetyants and his colleagues explained their results by associating the motion of electrons with the electropositive (that is, Bi) sub-lattice and the motion of holes with the electronegative (that is, Te) sub-lattice. Any disturbance in one of the sub-lattices results in appreciable scattering of the appropriate carriers.

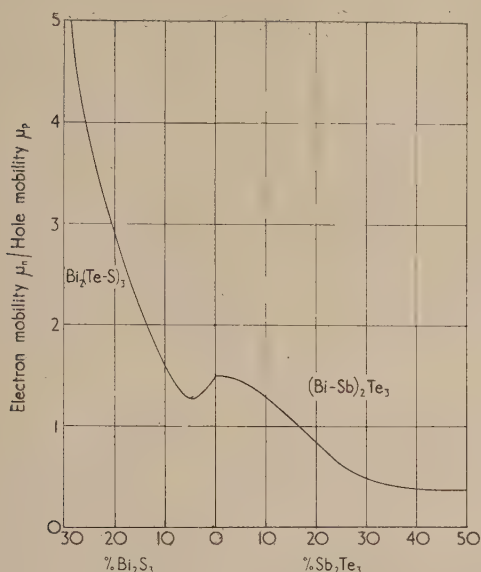


Fig. 7. Ratio of electron to hole mobility in alloys of Bi_2Te_3

Similar results were found for solid solutions of PbTe . The ratio of electron to hole mobility rises on the addition of PbSe and falls on the addition of SnTe .

These experiments suggest that n -type thermoelements should be prepared from alloys in which there is substitution in the electronegative sub-lattice while p -type thermoelements should consist of alloys in which the electropositive element is replaced. The situation may be more complicated if there are changes in the effective masses on alloying, but the Soviet workers claim that the best thermocouples use a Bi_2Te_3 - Sb_2Te_3 alloy as the positive material and a Bi_2Te_3 - Bi_2Se_3 alloy as the negative material.⁽²⁴⁾

It is perhaps useful at this point to consider the manner in which z rises with the factor F of equation (15). For poor thermoelectric materials, the electronic component of the thermal conductivity is negligible and z is directly proportional to F . However, for good materials, at the optimum Seebeck coefficient, the electronic component is an appreciable fraction of the total thermal conductivity. Thus, in this case, z rises more slowly with F . For example, in the best of the present-day alloys, F approaches 4×10^4 practical e.m.u. at 300°K . If this figure could be raised by a factor of ten (though it is difficult to imagine how such an increase would be obtained), the corresponding value of z would be $14 \times 10^{-3}^\circ \text{K}$ at an optimum Seebeck coefficient of about $350 \mu\text{V}/^\circ \text{C}$. The ten-fold increase in F would result in no more than a four-fold improvement in z .

Construction and performance of thermoelectric refrigerators

So far, only the physics of thermoelectric cooling has been considered, but because it has been seen that reasonable temperature differences may be obtained, attention will be

turned to the practical problems of applying the new thermoelectric materials. In the design of a thermoelectric device it must be remembered that the temperature difference in the expression for the coefficient of performance is always higher than that between the source and sink, although the aim should be to make the two temperature differences as close as possible. This and other problems which arise in applying the Peltier cooling effect may be understood with reference to the thermoelectric refrigerator shown in Fig. 8. It is not proposed to discuss the construction of a thermoelectric generator. The principles involved are the same as for a thermoelectric refrigerator but there is the added complication of providing good electrical and thermal contacts at elevated temperatures.

The cooling unit in Fig. 8 consists of an array of thermoelements with their ends joined by metal (for example,

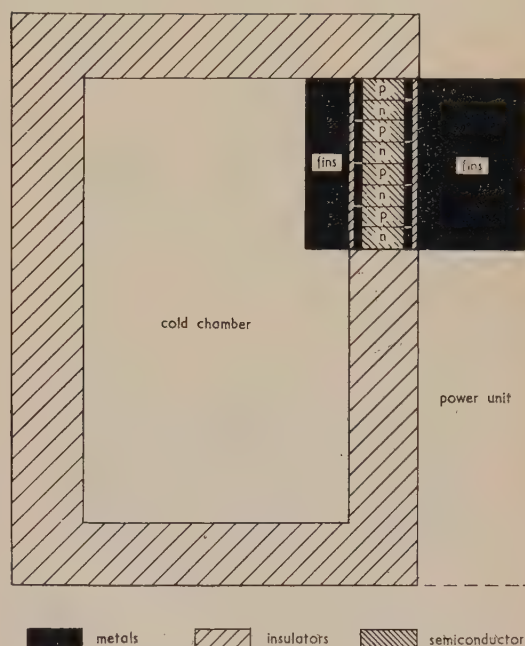


Fig. 8. Construction of a thermoelectric refrigerator

copper) bridges. The bridges form the cold and hot junctions and it is necessary to provide good heat transfer between them and the fins which project into the refrigerated chamber and the ambient air. At the same time, the fins must be electrically insulated from the thermocouples. Ioffe⁽⁸⁾ has reported that negligible thermal resistances may be attained if the metal surfaces are ground flat and clamped together after coating with a varnish loaded with aluminium powder; thin sheets of mica are interposed for electrical insulation. In deciding on the fin areas, it is necessary to balance the increased cost of large fins against the poor heat transfer associated with small fins.

A fairly elaborate power unit is required if the refrigerator is to be operated from an a.c. mains supply. It must include a transformer (as otherwise the number of thermocouples is excessive), and a full-wave rectifier and a choke to provide smooth direct current. The regulation of the temperature of the cold chamber is an additional problem. If the current through the cooling unit is switched off, heat is still transferred by conduction through the thermoelements, so a simple on-off control is inefficient. It is preferable to adjust

the current to a steady value which is appropriate to the load and the temperature difference.

To estimate the coefficient of performance, it is supposed that a temperature difference of, say, 25°C must be maintained between the cold chamber and the surroundings. The temperature differences between the junctions and the fin roots should not amount to more than one or two degrees, and the fin temperatures should lie within 5°C of those of the surroundings. It is, therefore, necessary to maintain a temperature difference of some 40°C between the thermocouple junctions. Reference to Fig. 1 shows that with the latest thermoelectric materials the coefficient of performance should be about 0.7.

An interesting possibility is a combination of thermoelectric generator and refrigerator. By the choice of an appropriate temperature for the heat source, the voltage generated by a single couple can be matched to that required for the operation of a second couple acting as a refrigerator. Such a device is illustrated in Fig. 9. Its advantages are its

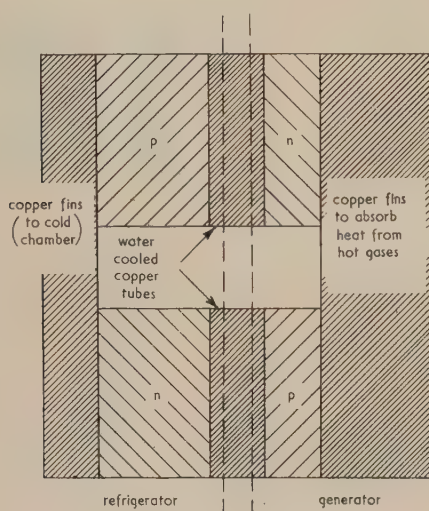


Fig. 9. Thermoelectric generator-refrigerator

capacity for working directly from a heat source and its extreme simplicity, since it enables one to dispense with the hundreds of thermocouples required for a normal thermoelectric refrigerator. Its disadvantage is a very low overall coefficient of performance; this is the product of the coefficient of performance of the refrigerating couple and the efficiency of the generating couple, the latter probably being less than 10%.

Small-scale thermoelectric devices

Thermoelectric cooling is ideal when the amount of heat to be transferred is small. Many small-scale applications are to be found in scientific and technical equipment. Ioffe⁽⁸⁾ has described thermoelectric thermostats and thermoelectrically cooled microtomes; two other cooling devices will be considered here.

The cooling of the mirror of a dew-point hygrometer by the Peltier effect is particularly attractive since only a single thermocouple is needed. A simple system for continuously recording the dew-point is shown in Fig. 10. The metallic bridge of the couple takes the form of a polished mirror; its reflectivity changes when water condenses upon it. The change of reflectivity is detected by means of a cadmium-

sulphide photoconductive cell. After amplification, the signal from the photocell is used to operate a relay which reverses the direction of the current through the couple. The mirror is thus alternately heated and cooled as dew is formed and evaporates, and the temperature oscillates over a short range about the dew-point.

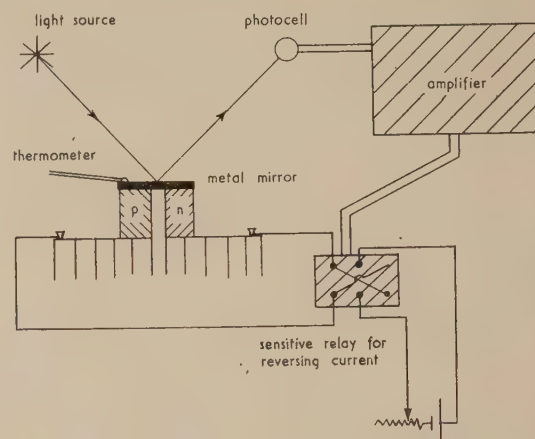


Fig. 10. Thermoelectrically cooled dew-point hygrometer

Another useful device is the thermoelectrically cooled vacuum baffle described by Kolenko⁽²⁴⁾ and illustrated in Fig. 11. The metallic bridges between the thermoelements take the form of baffle plates shaped as shown in the diagram. There are fourteen of these plates which overlap one another,

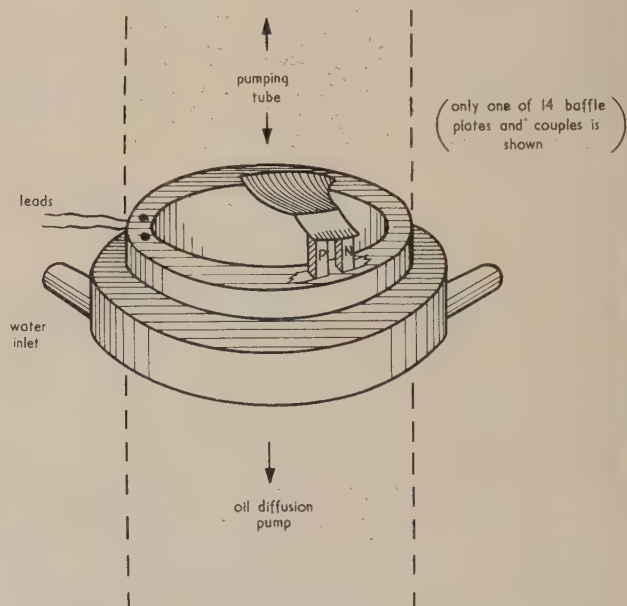


Fig. 11. Thermoelectrically cooled vacuum baffle (after Kolenko)

so that an oil molecule travelling up the pumping tube must undergo several collisions with them. The hot junctions are in thermal contact with a water-cooled ring. The use of such a baffle enables one to dispense with a liquid-air trap.

An example of the use of thermoelectric generation at moderate temperatures is to be found in the thermopile for

detecting infra-red radiation. This instrument consists of a few thermoelements with one set of junctions connected to a heat sink. The remaining junctions are formed from thin metal-foil receivers. The receivers are blackened so as to absorb the incoming radiation, while the enclosure is evacuated to minimize the loss of absorbed heat. There is, of course, loss of heat by re-radiation and for maximum sensitivity this loss should be equal to the heat conducted down the elements. Clearly, the highest sensitivity is obtained when the generation efficiency is a maximum. It is also essential for the thermopile to have a very small response time since it is preferable to chop the incident radiation at a few cycles per second and amplify the output from the thermopile. Schwarz⁽²⁵⁾ used conical thermoelements to reduce the thermal inertia of his thermopiles.

The solar generator constructed by Telkes⁽²⁶⁾ was really no more than an enlarged radiation thermopile. For this, the heat losses were minimized by double-glazing the face of the unit which was directed towards the sun.

Conclusions

The advances in thermoelectric materials during the past few years now allow thermoelectric refrigerators to be used in small-scale applications instead of machines of either the compression or absorption type. In this field, the coefficient of performance is often a secondary consideration. The thermoelectric refrigerator has the advantages of silence, no moving parts and the absence of gases, but the factor which will determine whether or not it becomes more widely used is an economic one.

There are also several uses to which present-day thermoelectric generators could be put. However, the really attractive large-scale applications require much greater efficiencies than are attainable at the moment. To make such thermoelectric generators practicable, it will be necessary to raise the figure of merit in the room-temperature region and, also, to provide comparable material which is stable at high temperatures.

References

- (1) ALTENKIRCH, E. *Phys. Z.*, **10**, p. 560 (1909).
- (2) ALTENKIRCH, E. *Phys. Z.*, **12**, p. 920 (1911).
- (3) GOLDSMID, H. J., and DOUGLAS, R. W. *Brit. J. Appl. Phys.*, **5**, p. 386 (1954).
- (4) WRIGHT, D. A. *Nature*, **181**, p. 834 (1958).
- (5) CALLEN, H. B. *Phys. Rev.*, **73**, p. 1349 (1948).

- (6) SHTENBEK, M., and BARANSKIĬ, P. I. *Zh. Tekh. Fiz.*, **27**, p. 233 (1957).
- (7) GEHLHOFF, P. O., JUSTI, E., and KOHLER, M. *Abh. Braunsch. Wiss. Gesell*, **2**, p. 149 (1950).
- (8) IOFFE, A. F. *Semiconductor Thermoelements and Thermoelectric Cooling*. (Translated from the Russian—London: Infosearch, 1957.)
- (9) HARMAN, T. C. *J. Appl. Phys.*, **29**, p. 1471 (1958).
- (10) WILSON, A. H. *The Theory of Metals*, 2nd edn. (Cambridge University Press, 1953).
- (11) PRICE, P. J. *Phil. Mag.*, **46**, p. 1252 (1955).
- (12) STAVITSKAYA, T. S., and STIL'BANS, L. S. *Zh. Tekh. Fiz.*, **28**, p. 484 (1958).
- (13) IOFFE, A. V., and IOFFE, A. F. *Dokl. Akad. Nauk., S.S.S.R.*, **97**, p. 821 (1954).
- (14) HERRING, C. *Bell. Syst. Tech. J.*, **34**, p. 1342 (1956).
- (15) SCANLON, W. W. *J. Phys. Chem. Solids*, **8**, p. 423 (1959).
- (16) DRABBLE, J. R., GROVES, R. D., and WOLFE, R. *Proc. Phys. Soc.*, **71**, p. 430 (1958).
- (17) AUSTIN, I. G. *Proc. Phys. Soc.* (Awaiting publication.)
- (18) GOLDSMID, H. J., SHEARD, A. R., and WRIGHT, D. A. *Brit. J. Appl. Phys.*, **9**, p. 365 (1958).
- (19) NIKITIN, E. N. *Zh. Tekh. Fiz.*, **28**, pp. 23 and 26 (1958).
- (20) IOFFE, A. F., AIRAPETYANTS, S. V., IOFFE, A. V., KOLOMOETS, N. V., and STIL'BANS, L. S. *Dokl. Akad. Nauk., S.S.S.R.*, **106**, p. 1981 (1956).
- (21) IOFFE, A. V., and IOFFE, A. F. *Izv. Akad. Nauk., S.S.S.R.*, **20**, p. 65 (1956).
- (22) BOWERS, R., BAUERLE, J. E., and CORNISH, A. J. *J. Appl. Phys.*, **30**, p. 1050 (1959).
- (23) AIRAPETYANTS, S. V., EFIMOVA, B. A., STAVITSKAYA, T. S., STIL'BANS, L. S., and SYSOEVA, L. M. *Zh. Tekh. Fiz.*, **27**, p. 2167 (1957).
- (24) GORDYAKOVA, G. N., KOKOSH, G. V., and SINANI, S. S. *Zh. Tekh. Fiz.*, **28**, p. 3 (1958).
- (24) KOLENKO, E. A. *Vestnik. Akad. Nauk., S.S.S.R.*, **27**, p. 50 (1957).
- (25) SCHWARZ, E. *Research*, **5**, p. 407 (1952).
- (26) TELKES, M. *J. Appl. Phys.*, **25**, p. 765 (1954).

Choice of frequency for eddy-current tube testing*

by F. R. BAREHAM, B.Sc., A.Inst.P., The British Non-Ferrous Metals Research Association, London, N.W.1

[Paper first received 4 December 1959, and in final form 22 January 1960]

Abstract

Eddy-current testing can be used to detect faults in metal tubes by passing the tube through a pair of short solenoidal coils which are energized by an alternating current. The decrease in density of the induced eddy-currents from the outer surface is determined by the frequency of the energizing current and by the electrical properties and dimensions of the tube. Since the eddy-currents flow in a circumferential direction, their distribution is not, as often assumed in the past, the same as when current flows in the direction of the axis. The distribution of eddy-currents flowing circumferentially is given in general terms for non-magnetic tubes and the results can be used in conjunction with a nomogram to determine suitable frequencies for many practical applications.

Introduction

EDDY-CURRENT testing may be used to detect faults, such as cracks, in long metal tubes by passing the tube through a pair of short solenoidal coils. The coils, which form part of a balanced circuit, are energized by an alternating current so that eddy-currents flow in a circumferential direction round the tube wall. The circuit containing the coils is balanced using a uniform tube which is free from faults. An unbalanced condition arises when a fault appears inside one of the coils and the resulting out-of-balance voltage can be used to trigger automatic rejecting mechanisms.

When alternating currents flow in conductors, the current density is not generally uniform and, in the present case, is greater towards the outer surfaces of the tube. Faults can only be detected when adequate current density exists in the region of the fault and, in practical applications of eddy-current testing, a knowledge of current distributions is of fundamental importance. In the past, it has been widely assumed that the distribution of eddy-currents flowing in a circumferential direction is the same as for currents flowing in an axial direction along a conductor. For axial current flow it has been shown⁽¹⁾ that, at low frequencies, the current density is uniform across the section of a circular conductor while, at high frequencies, the current flows predominantly in the outer skin. The so-called "skin-depth" equation⁽²⁾ resulting from the consideration of axial current flow has been used to find suitable frequencies for eddy-current tube testing. This treatment is incorrect because the boundary conditions applicable to axial current flow do not apply to circumferential current flow. In the latter case simple electromagnetic theory shows that, at low frequencies, the current

density in circular conductors decreases linearly from the outer surface and is zero at the centre. A further objection to the use of the "skin-depth" equation, even for longitudinal currents, is that it only applies when the radius of the conductor is several times the "skin-depth".

Hochschild,⁽³⁾ realizing the limitations of "skin-depth" considerations, has calculated the distribution of eddy-currents induced by infinitely long solenoidal coils in solid circular bars, and his results show, at low frequencies, a linear decrease in current density from the outer surface. He has also extended his theory to the more general case of three concentric cylinders which could be applied to an air-cored tube. One of the boundary conditions used was continuity of the tangential component of current flow, which is not generally true since it implies that the current density at the inner wall of a hollow tube is zero.

In this paper, a simplification of the practical problem is made by calculating the distribution of eddy-currents induced by an infinitely long solenoidal coil in an infinitely long non-magnetic tube.

Distribution of eddy-currents in circular metal tubes

General field equations. Maxwell's equations defining the electric and magnetic fields in any electrical medium (neglecting displacement currents) are:

$$\text{curl } \vec{E} = \frac{-d\vec{B}}{dt}; \quad (1)$$

$$\text{curl } \vec{H} = \vec{i}; \quad (2)$$

and Ohm's law is:

$$\vec{i} = \sigma \vec{E}, \quad (3)$$

where \vec{E} is the vector electric field, \vec{H} the vector magnetic field, \vec{B} the vector magnetic induction, \vec{i} the vector current density, σ the electrical conductivity of the medium and t represents time. Also:

$$\vec{B} = \mu \vec{H} \quad (4)$$

where μ is the magnetic permeability of the medium which, in the present case of non-magnetic tubes, is the same both inside the tube wall and in the surrounding air.

When an infinitely long circular metal tube is mounted inside an infinitely long solenoid, the axis being common, the magnetic field acts only in a direction parallel to the common axis and is a function only of the radius r while the electric field acts only in a circumferential direction and is also a function of radius only. Thus from the definition of the curl of a vector:

$$\text{curl } \vec{E} = \frac{1}{r} \cdot \frac{d(r\vec{E})}{dr} \quad (5)$$

* Based on Research Reports Nos. 1203 and 1253 issued to members of The British Non-Ferrous Metals Research Association in July 1958 and September 1959, respectively.

and: $\text{curl } \bar{H} = \frac{-d\bar{H}}{dr}$ (6)

Equations (2), (3) and (6) give:

$$\frac{-d\bar{H}}{dr} = \sigma \bar{E}, \quad (7)$$

while equations (1), (4) and (5) give:

$$\frac{1}{r} \cdot \frac{d(r\bar{E})}{dr} = -\mu \frac{d\bar{H}}{dt} \quad (8)$$

Equations (7) and (8) give:

$$-\frac{1}{r} \cdot \frac{d}{dr} \left(\frac{r}{\sigma} \cdot \frac{d\bar{H}}{dr} \right) = -\mu \frac{d\bar{H}}{dt},$$

that is: $\frac{d^2\bar{H}}{dr^2} + \frac{1}{r} \cdot \frac{d\bar{H}}{dr} = \sigma\mu \frac{d\bar{H}}{dt}$ (9)

If \bar{H} varies sinusoidally with time then:

$$\frac{d\bar{H}}{dt} = j\omega\bar{H}, \quad (10)$$

where ω is the angular velocity of \bar{H} , and equation (9) may be written as:

$$\frac{d^2\bar{H}}{dr^2} + \frac{1}{r} \cdot \frac{d\bar{H}}{dr} - jk^2\bar{H} = 0, \quad (11)$$

where k^2 equals $\omega\sigma\mu$. Also, equations (2) and (6) give:

$$\bar{i} = \frac{-d\bar{H}}{dr} \quad (12)$$

The solution of equation (11) is⁽⁴⁾:

$$\bar{H} = cI_0(kr\sqrt{j}) + dK_0(kr\sqrt{j}), \quad (13)$$

where $I_0(kr\sqrt{j})$ and $K_0(kr\sqrt{j})$ are modified Bessel functions of zero order and c and d are constants determined by the boundary conditions.

Particular solution for hollow metal tubes. The boundary conditions which must be met in this problem are:

- (i) continuity of the normal components of \bar{B} and \bar{i} ;
- (ii) continuity of the tangential components of \bar{H} and \bar{E} .

The first condition is automatically satisfied since the normal components of \bar{B} and \bar{i} are zero at all points within the solenoid. From equations (2), (3), (4) and (6), the electric field can be defined at any point in the tube wall by:

$$\bar{E} = -\frac{1}{\sigma} \cdot \frac{d\bar{H}}{dr},$$

that is, by:

$$\bar{E} = -\frac{1}{\sigma} \cdot \frac{d}{dr} \{cI_0(kr\sqrt{j}) + dK_0(kr\sqrt{j})\},$$

or:

$$\bar{E} = -\frac{k\sqrt{j}}{\sigma} \{cI_1(kr\sqrt{j}) - dK_1(kr\sqrt{j})\}. \quad (14)$$

An expression for the electric field inside the central air core can be obtained from equations (1), (5) and (10):

$$\frac{1}{r} \cdot \frac{d}{dr} (r\bar{E}) = -j\omega\mu\bar{H},$$

which on integration gives:

$$\bar{E} = -\frac{j\omega\mu r\bar{H}}{2} + \frac{e}{r},$$

where the constant e must be zero since \bar{E} must be finite for all values of r . That is:

$$\bar{E} = -\frac{j\omega\mu r\bar{H}}{2}. \quad (15)$$

At the inner surface of the tube ($r = a$), where the magnetic field is \bar{H}_0 the tangential component of \bar{E} must be continuous and equating the expressions for \bar{E} in equations (14) and (15) give:

$$\frac{(ka\sqrt{j})}{2}\bar{H}_0 = cI_1(ka\sqrt{j}) - dK_1(ka\sqrt{j}). \quad (16)$$

Also, since the tangential component of \bar{H} must be continuous at both surfaces of the tube, we may write at the inner surface:

$$\bar{H}_0 = cI_0(ka\sqrt{j}) + dK_0(ka\sqrt{j}), \quad (17)$$

while, at the outer surface of the tube ($r = b$), where the magnetic field is \bar{H}_s and can be readily calculated:

$$\bar{H}_s = cI_0(kb\sqrt{j}) + dK_0(kb\sqrt{j}). \quad (18)$$

Writing $\alpha = ka\sqrt{j}$, $\beta = kb\sqrt{j}$ and $\gamma = kr\sqrt{j}$,

equations (16), (17) and (18) become:

$$\frac{1}{2}\alpha\bar{H}_0 = cI_0(\alpha) - dK_0(\alpha); \quad (19)$$

$$\bar{H}_0 = cI_0(\alpha) + dK_0(\alpha); \quad (20)$$

$$\bar{H}_s = cI_0(\beta) + dK_0(\beta). \quad (21)$$

Equations (19), (20) and (21) give:

$$c = \frac{\bar{H}_s G}{GI_0(\beta) + FK_0(\beta)}; \quad (22)$$

$$d = \frac{\bar{H}_s F}{GI_0(\beta) + FK_0(\beta)}; \quad (23)$$

where $F = I_1(\alpha) - \frac{1}{2}\alpha I_0(\alpha), \quad (24)$

and $G = K_1(\alpha) + \frac{1}{2}\alpha K_0(\alpha). \quad (25)$

Thus the magnetic field at any point in the tube wall becomes:

$$\bar{H} = \bar{H}_s \left\{ \frac{GI_0(\gamma) + FK_0(\gamma)}{GI_0(\beta) + FK_0(\beta)} \right\}, \quad (26)$$

while the magnetic field at any point in the central air core is:

$$\bar{H}_0 = \bar{H}_s \left\{ \frac{GI_0(\alpha) + FK_0(\alpha)}{GI_0(\beta) + FK_0(\beta)} \right\}, \quad (27)$$

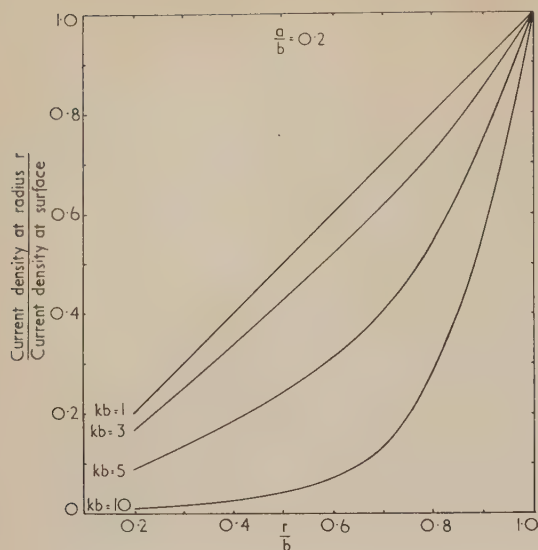
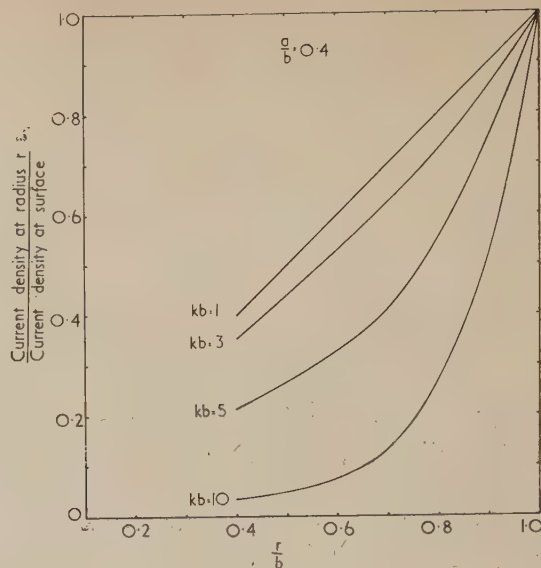
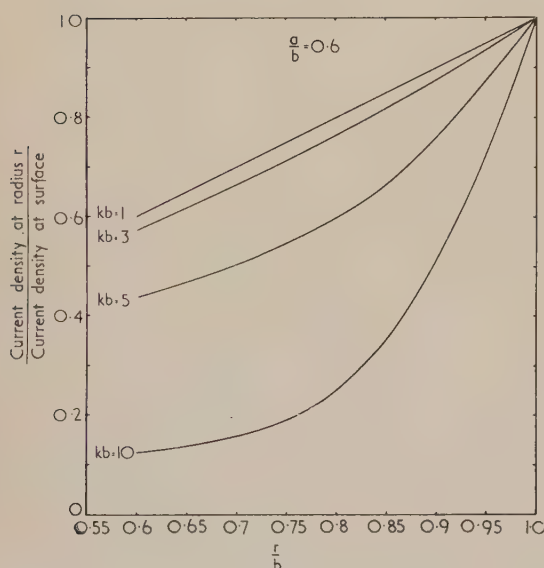
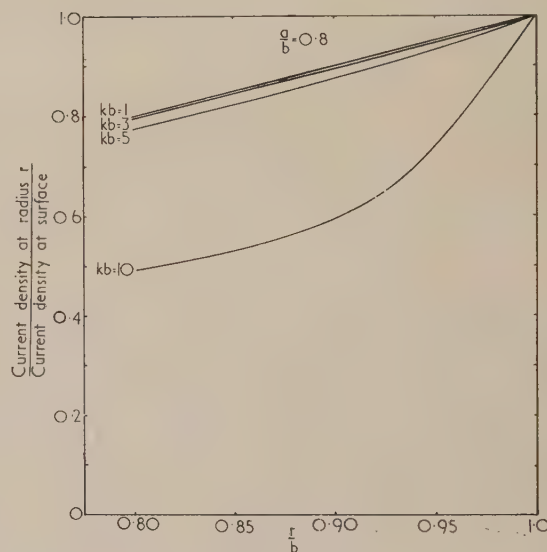
which is constant throughout the air core. The current density at any point in the tube wall is given by equations (12) and (26) and is:

$$\bar{i} = -\bar{H}_s \cdot k \cdot \left\{ \frac{GI_1(\gamma) - FK_1(\gamma)}{GI_0(\beta) + FK_0(\beta)} \right\} \cdot \sqrt{j}.$$

If the current density at the outer surface is \bar{i}_s , then:

$$\frac{\bar{i}}{\bar{i}_s} = \frac{GI_1(\gamma) - FK_1(\gamma)}{GI_1(\beta) - FK_1(\beta)}. \quad (28)$$

Numerical computation. The expansion of equation (28) is extremely cumbersome, and it was more convenient to compute the real and imaginary parts of the separate terms using standard transformations⁽⁵⁾ and grouping the results for various ratios b/a of outside to inside diameter of the tube, each group being subdivided to indicate several values of the


 Fig. 1. $a/b = 0.2$

 Fig. 2. $a/b = 0.4$

 Fig. 3. $a/b = 0.6$

 Fig. 4. $a/b = 0.8$

 Figs. 1-4. Variation of ratio of current density at radius r to current density at surface with ratio r/b

frequency-dependent term kb . The modulus and argument of the final computation give, in general terms, the amplitude and phase of eddy-currents at any point in the wall of a non-magnetic tube. The results are shown graphically in Figs. 1-8.

Choice of frequency

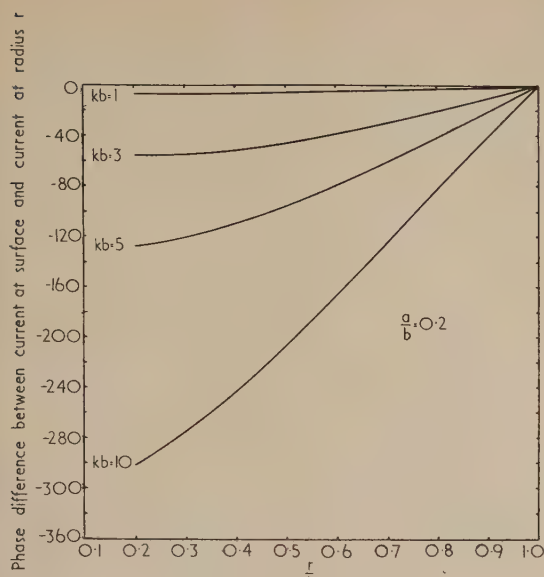
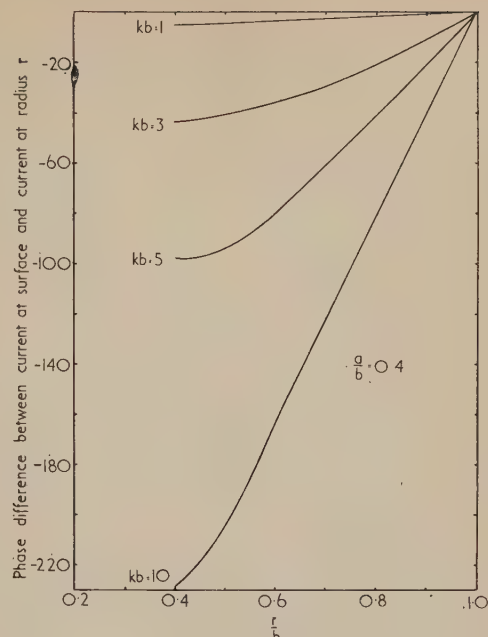
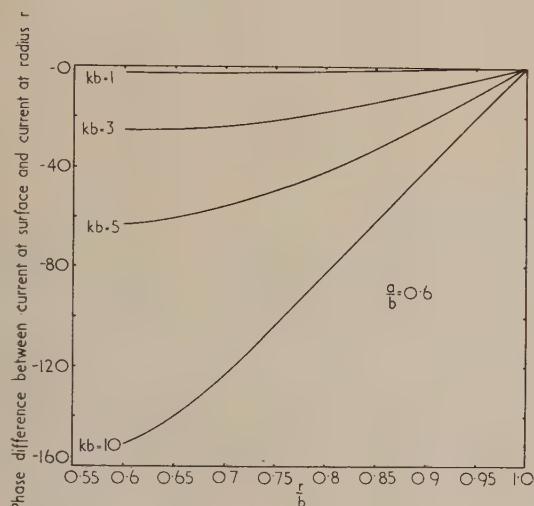
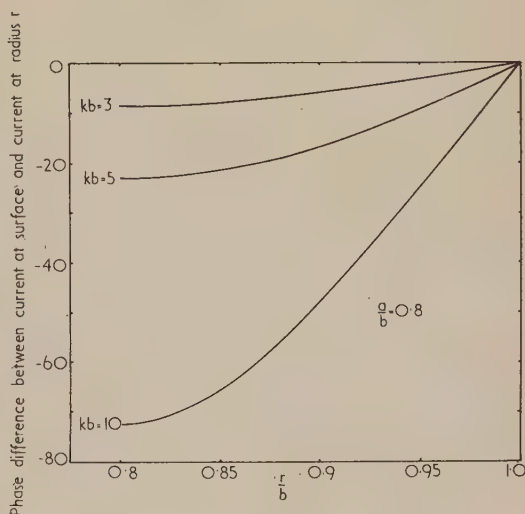
The frequency suitable for any given application may be estimated by referring to the current-distribution curves having the nearest value of a/b (that is the ratio of inside to outside diameter). If the whole of the tube wall is to be inspected, a low value of kb is required, whereas a higher value can be used for inspecting the outer surface. The curves show that considerable latitude can be allowed in choosing a value of kb and it is desirable to use the highest value, as this gives a high frequency and, consequently, the most efficient electrical coupling between the coil and the tube.

When kb has been chosen, the frequency f (in c/s) can be determined from the relationship:

$$f = \frac{(kb)^2}{2\pi\sigma\mu b^2} \text{ c.p.s.} \quad (29)$$

where $2b$ is the outside diameter of tube (m), σ the conductivity of tube ($\text{mho } m^{-1}$) and, as before, μ equals $4\pi \times 10^{-7}$ (h.m^{-1}).

Alternatively, the nomogram of Fig. 9 may be used by noting the intersection of a straight edge placed between the appropriate values of kb and the outside diameter of the tube, with the R line. The frequency may then be read off by placing the straight edge across the same value of R and the conductivity of the tube. The guide lines on the nomogram show that a tube 1 in. o.d. and 20% I.A.C.S. may be tested using a value of kb of 5 with a frequency of approximately 2 kc/s. If necessary, the range of the nomogram can

Fig. 5. $a/b = 0.2$ Fig. 6. $a/b = 0.4$ Fig. 7. $a/b = 0.6$ Fig. 8. $a/b = 0.8$

Figs. 5-8. Variation in phase difference in current at surface and current at radius r with ratio r/b

be extended, bearing in mind the relation between f , σ and b defined in equation (29). In plotting the nomogram the value of resistivity corresponding to 100% I.A.C.S. was taken as 1.724×10^{-6} ohm cm at 20°C .

Application to short coils

To estimate the errors arising when the theory for infinitely long solenoidal coils is applied to short coils it is necessary to consider the axial components (H_z) of the magnetic field at any point $P(Z, r)$ close to a single turn of wire (Fig. 10). For any constant value of r , H_z is maximum at $Z = 0$ and decreases to a negligible value at $Z = \pm 2q$. The distribution of eddy-currents in the Z -direction follows a similar pattern, and the ratio i/i_s is still defined by equation (28), if mutual induction effects along the length of the tube can be

neglected. This is a reasonable assumption, particularly for tubes of low conductivity, since the energizing field at the surface is much stronger than the opposing field set up by the eddy-currents.

Fig. 11 is an estimate, obtained by arithmetical integration, of how H_z varies in the r -direction across the plane of the coil ($Z = 0$). To obtain efficient coupling, the tube and coil must be in close proximity but, allowing for the dimensions of the coil former, it is unusual for b/q to exceed 0.8. For thin-wall tubes (such that $b/q = a/b = 0.8$) the magnetic field across the tube wall is sufficiently uniform to justify use of equation (28). When tubes with thicker walls are tested with short coils, the fall in current density across the tube wall will be greater than indicated by long-coil theory. Even then, the change in magnetic field is unlikely to change the calculated current by more than about 30%.

Discussion

The choice of frequency is widest when testing thin-walled tubes. For a $\frac{1}{2}$ in. o.d. \times 18 s.w.g. tube, a/b is approxi-

change in the current distribution. "Skin-depth" considerations would show a difference in current density at the inner wall of 5:1 over this frequency range; and it is in the important case of testing thin-walled tubes that the results presented here differ so markedly from previous theories. It is found in practice that the choice of frequency is not as critical as "skin-depth" considerations suggest and the results given here are a quantitative expression of this view. In practice, the frequency range might be restricted if the lower values of kb give frequencies too low for efficient

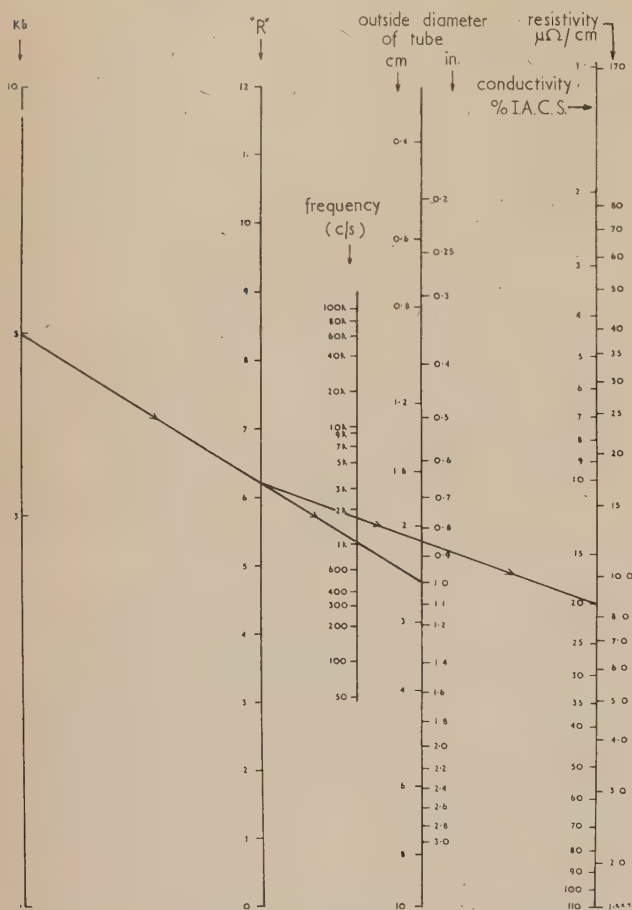


Fig. 9. Nomogram for determining frequency in eddy-current tube testing (based on infinitely long solenoid coils)

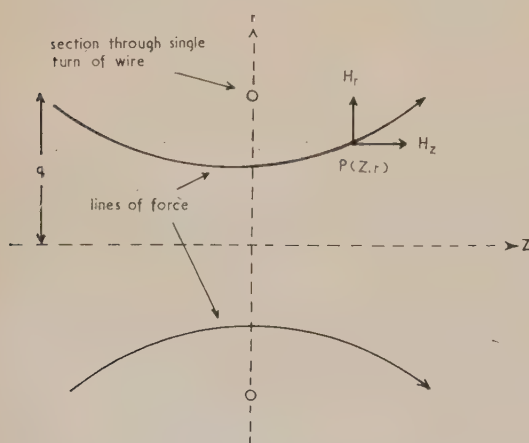


Fig. 10. Field due to single turn of wire

mately 0.8 and the relevant current distribution curve (Fig. 4) shows that values of kb between 1 and 5 may be used for inspecting throughout the tube wall. This permits frequencies in the ratio 25:1 to be used without any significant

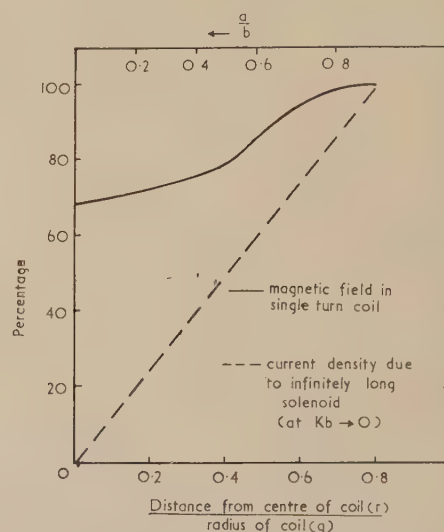


Fig. 11. Magnetic field in single turn of wire (—) and current density (at $kb \rightarrow 0$) due to infinitely long solenoid (---)

electrical coupling between the coil and the tube, and might be further restricted if phase-sensitive detection was used. However, considerable latitude in the choice of frequency would probably remain. The results also suggest that a very wide range of tubes could be tested using a few spot frequencies (for example, 10^2 , 10^3 , 10^4 and 10^5 c/s), and imply that quite simple apparatus could be used for a wide variety of practical problems. Although the results given here have been obtained by considering infinitely long solenoids, they have given satisfactory results in a number of tube-testing problems and should be useful as a guide in other cases.

Acknowledgements

Thanks are due to Dr. J. Topping of the Brunel College of Technology for valuable discussions and to the Director and Council of The British Non-Ferrous Metals Research Association for permission to publish this paper.

References

- (1), (4), (5). McLACHLAN, N. W. *Bessel Functions for Engineers*, pp. 156, 137, 140 respectively (Oxford: Clarendon Press, 1955).
- (2) KING, R. W. P., et al. *Transmission Lines, Antennas and Waveguides*, p. 12 (New York: McGraw-Hill Book Co., 1945).
- (3) HOCHSCHILD, R. *Mathematical Foundations of Non-Destructive Testing by Eddy-Current Methods*, U.S.A.E.C. Report No. NYO-3576, 1953.

Charge localization on the surfaces of oxide-coated cathodes

by B. J. HOPKINS, B.A., Ph.D., A.Inst.P.,* and Professor F. A. VICK, O.B.E., Ph.D., A.M.I.E.E., F.Inst.P.,†
Physics Department, University College of North Staffordshire, Keele, Staffs.

[Paper first received 18 June, and in final form 24 August, 1959]

Abstract

Anomalous results obtained while using the Kelvin method of determining contact potential differences between oxide-coated cathodes and an evaporated gold film reference surface in an atmosphere of hydrogen have been investigated. Very high contact potential differences have been associated with a separation of charge from ionized gas on the passage of a discharge current. This charge, either positive ions or electrons, remains on the surface of the oxide cathode for periods (sometimes as long as several days) dependent on the conductivity of the oxide coating. This in turn depends upon the nature of the oxide material, its state of activation and its temperature. Experiments are also described on the behaviour of probe cathodes in hydrogen.

1. Introduction

THE measurements described arose from a programme of research designed to study the processes that govern electron emission from oxide-coated cathodes in the presence of hydrogen and also under gas discharge conditions. A further aim was to use the oxide cathode as a surface of known but variable work function so as to demonstrate in a quantitative manner a relation thought to exist between the minimum sparking potential and the work function of a cathode in hydrogen. Both of these investigations required the changes in cathode work function to be followed closely in the presence of a gas. The Kelvin method of measuring contact potential differences was adopted, using a vibrating gold reference surface of which the work function was assumed known.⁽¹⁾ Early in the work anomalous results were obtained involving apparent contact potential differences of tens of volts. This paper is concerned with experiments designed to investigate the cause of these very high values.

2. Apparatus and techniques

2.1 The vacuum system. Two vacuum systems were used, one to provide hydrogen in a good state of purity and the other to remove air, carbon dioxide, etc., from the experimental tube. Hydrogen was initially produced in a voltameter by the electrolysis of a solution of barium hydroxide in distilled water. The gas was allowed to stand over phosphorus pentoxide for several hours and then a previously outgassed palladium osmosis tube was heated allowing the hydrogen to pass into an evacuated reservoir. The experimental tube was isolated from this gas supply by a second palladium osmosis tube.

* Now at the University of Southampton.

† Now at Atomic Energy Research Establishment, Harwell, Didcot, Berks.

The experimental tube and the rest of the associated apparatus could be evacuated to a pressure of lower than 10^{-6} mm of mercury by means of a conventional pumping train. After sealing from the pumps the necessary high vacuum was attained by using the techniques described by Alpert.⁽²⁾ An inverted ionization gauge exactly similar to those described by Bayard and Alpert⁽³⁾ was sealed to the system close to each new experimental tube. In the absence of any leaks a final pressure lower than 10^{-10} mm of mercury was obtained. As a further precaution a molybdenum getter was also fitted close to the experimental tube. When the low pressure had been attained, the required amount of hydrogen (usually several millimetres of mercury) was admitted by heating the second palladium osmosis tube. The pressure of hydrogen in the experimental tube was taken to be the same as that in the reservoir, in which the pressure was measured on a three-metre manometer filled with Apiezon B oil. Direct contact between the tube and the oil in the manometer was prevented by the second palladium osmosis tube. Between the hydrogen and the high vacuum system was an arrangement of breakers and constrictions which allowed the tube to be evacuated several times. This arrangement was very useful for studying the same cathode in several states of activation.

2.2 The experimental tube. Fig. 1 is a photograph of a typical tube. The hard glass assembly was mounted on a seven-lead C9 glass pinch (by Siemens Ediswan Ltd.). The fixed glass frame *A* acted as a support for a movable section *B* which could be rotated about its axis by the action of an external magnet on a piece of soft iron enclosed in glass, *C*. The nickel anode *D* and vibrating electrode *E* were mounted on the movable section and the oxide cathode *F* on the fixed frame.

The cathode consisted of an "O" nickel button 1.9 cm in diameter to which a tungsten thermocouple lead *G* was attached. After hydrogen furnacing at 1000°C the cathode was sprayed with alkaline earth carbonate (either calcium or barium carbonate, both supplied by the General Electric Co. Ltd.) to the required thickness. The button was indirectly heated by a coil of tungsten wire *H* insulated from it.

The rotating arm had two fixed positions, one of which is shown in Fig. 1. The other is with anode *D* over the oxide cathode. The glass arm *I* prevented the movable assembly from rotating through 360°.

The method of preparing the glass reference electrode has already been described.⁽¹⁾ In the present work a slightly larger size was used to accommodate the larger cathodes. Vibration of this electrode was achieved by means of two crossed tungsten strips, *J*. Following Davies and Fitch,⁽¹⁾ the reference surface was a film of high purity gold evaporated under very good vacuum conditions. The gold evaporating bead was prepared on a tungsten wire *K* in hydrogen and

was welded to the pinch in such a way that when the nickel anode was over the cathode gold could be evaporated on to the surface of the glass electrode. To prevent shorting out the leads on the pinch after the evaporation of the gold, the bead was surrounded by the nickel shield, *L*.

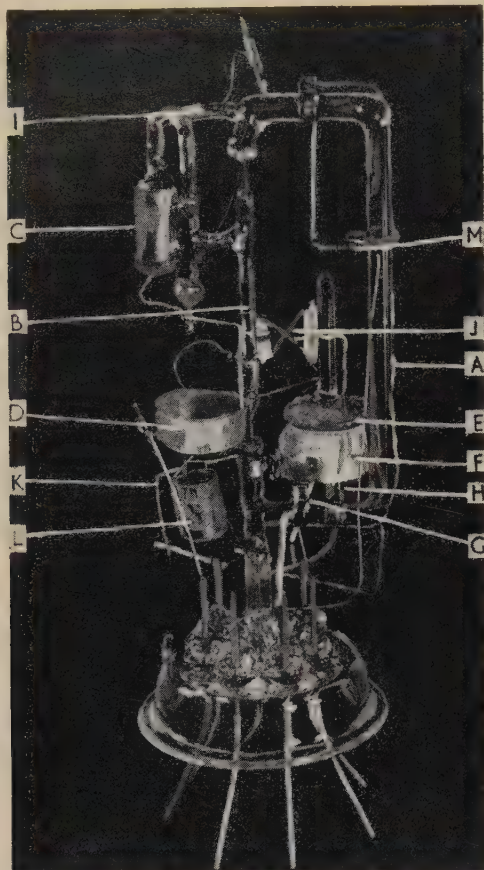


Fig. 1. The experimental tube

The envelope of the tube was coated internally with a film of colloidal graphite which could be earthed from the outside *via* a tungsten seal and spring contact. Such a screen was found to be necessary, otherwise consistent results were not obtained with the Kelvin technique. Finally the envelope was drop-sealed to the pinch and the completed tube sealed to the system. The tubes were processed in the standard manner except that the carbonates were broken down to oxide over a period of about 24 h. In this way it was possible to avoid the flaking of the oxide that occurs if the cathode is heated too quickly. The tube, ionization gauge, getter and breakers, etc., were baked for 48 h at 420° C before and after the breakdown of the carbonates. The usual outgassing cycles were then commenced. Almost all of the metallic parts could be heated either directly or by means of eddy-currents to a bright red heat. At seal-off the pressure was about $5 \cdot 10^{-7}$ mm of mercury. After firing the getter and operating the ion pump for about six hours the pressure usually fell below 10^{-10} mm of mercury.

2.3 Measurements. The cathode temperature was measured by means of the nickel-tungsten thermocouple welded to the inside of the cathode button. A calibration has been published by Fan.⁽⁴⁾

The electrical breakdown of the anode-cathode gap in

hydrogen could be brought about by a potential drawn from an r.f. power pack stable to 1 part in 1000 over the voltage range 0 to 1000 V. A limiting resistance of 1 MΩ in series with the gap prevented excessive current flowing after breakdown.

The capacitance between the cathode and the vibrating electrode in these tubes is about 1 μμF. Since the contact potential difference between them is also quite small, the charge flowing through an external resistance is very small. A suitable value for this resistance was found to be $10^9 \Omega$ and it was made the input resistance for the first electrometer stage of an amplifier. The output from the amplifier, which was of the conventional low frequency type, was fed directly on to the Y-plates of a Cossor double-beam oscilloscope with a suitable time base. The maximum voltage sensitivity of the oscilloscope was 15 mV. The overall voltage gain was better than 10000. The vibration of the gold electrode was adjusted to about 20 c/s since at this frequency the amplitude of the signal was large and interference from the a.c. supply was not excessive. In spite of this frequency difference, however, great care had to be taken with the screening of components. Earthed metal boxes and screened coaxial cable were used for this purpose. The backing-off potential was drawn from batteries *via* a 1000 Ω linear potentiometer.

3. Experimental

The Kelvin method was originally chosen to follow the changes in work function of an oxide cathode in the presence of hydrogen in order to relate work function and minimum sparking potential measurements. A report of this side of the investigations has appeared elsewhere.⁽⁵⁾ During the early stages of this investigation, however, very high values of the contact potential difference (c.p.d.) between the oxide and the gold reference surface were recorded, occasionally as high as 90 V, though more usually about 15 V. Closer investigation revealed that these anomalous p.d.'s occurred only in tubes that had been subject to the passage of a low pressure gas discharge. Tubes in which no discharge measurements had been made always showed the normal c.p.d. of about 2 or 3 V dependent on the nature and activity of the cathode. The remainder of this section is devoted to a description of experiments designed to study the anomalous c.p.d.'s.

3.1 The anomalous c.p.d. was not stable but gradually decayed over a period of time until the normal value was

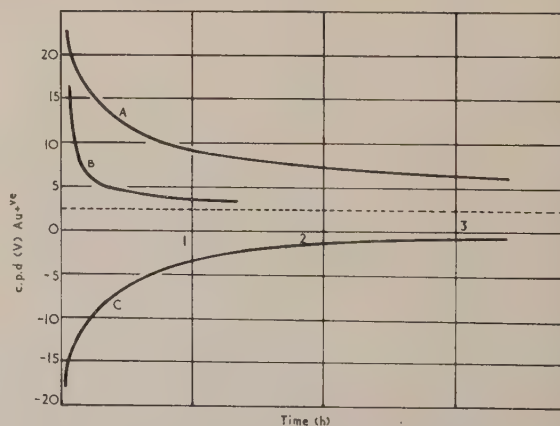


Fig. 2. Decay of abnormal c.p.d. (Tube VE VII, BaO)
A, after normal discharge; B, cathode warm; C, after reverse discharge

reached. The appearance of the decay curve is shown in Fig. 2 (curve *A*). Because of the time lag involved in changing over the electrodes the c.p.d. could not be measured until some 60 s after the passage of the discharge. Very often the decay to the normal c.p.d. took several days, though this time appeared to be dependent on the nature and activity of the oxide.

3.2 The passage of a reverse discharge using the oxide as the anode and the nickel button as the cathode again caused a large c.p.d. to appear but this time of opposite polarity. The decay curve for this case is also shown in Fig. 2 (curve *C*).

3.3 The effect of heating (to about 700° K) a cathode with an anomalous c.p.d. was to restore normal conditions within a few seconds. At lower temperatures a decay curve could be plotted. A typical curve is also shown in Fig. 2 (curve *B*).

3.4 Evacuation of the tube immediately after a discharge appeared to have no effect on the decay curve.

At this stage two tubes were designed specifically to study the anomalous c.p.d.'s. They incorporated a tungsten filament several centimetres above the cathode (*M* in Fig. 1) which could be used to evaporate electrons on to the cathode either under the influence of the field produced by the anomalous c.p.d., or by the application of an external field.

3.5 With the first tube containing such a filament a test was made before hydrogen was admitted. This involved heating the filament until electron emission took place and then applying a 50 V accelerating potential between the cathode and the filament such that electrons were driven to the cathode surface. After cooling the filament the gold reference electrode was moved into position and a negative c.p.d. of 25 V was measured between the gold and the oxide surface. This decayed in exactly the same way as the anomalous c.p.d. with hydrogen present.

3.6 Continuing with the same tube, hydrogen was admitted and a normal discharge passed between the cathode and the nickel anode. After moving the gold electrode into position the c.p.d. was followed as a function of time for 100 min. At point *A* (Fig. 3) on the decay curve electrons

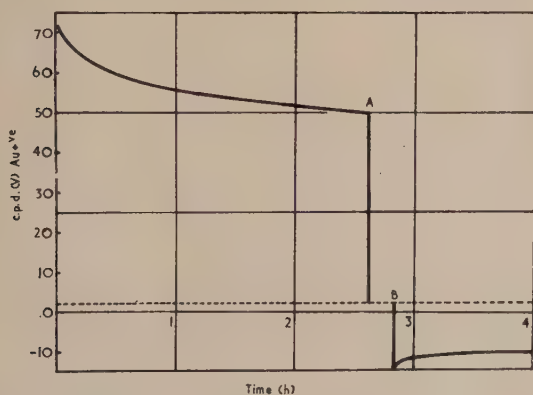


Fig. 3. Effect of electrons from outside the cathode on the abnormal c.p.d.

A, electrons evaporated on to cathode from heated filament; *B*, cathode 50 V positive with respect to anode, and electrons drawn from the filament. (Tube VE IX, CaO.)

were evaporated from the filament on to the cathode with no applied field (the reference electrode was moved slightly to one side so that the filament could "see" the cathode). About $4 \cdot 10^{-8}$ C of charge passed during the process, and subsequently the c.p.d. had returned to its normal value of about 2 V (*B* in Fig. 3). At point *B* the oxide was made 50 V

positive with respect to the filament and electrons drawn to the cathode. A negative c.p.d. was now observed when the gold electrode was returned into position over the cathode. This had a maximum value of 15 V and followed the usual decay curve.

3.7 The final experiments devised to study these anomalous c.p.d.'s involved following the decay curves with the cathode at known elevated temperatures. This was done at a number of temperatures with two activation states of a calcium oxide cathode. With the oxide unactivated the curves shown in Fig. 4 were obtained at four temperatures. After activation

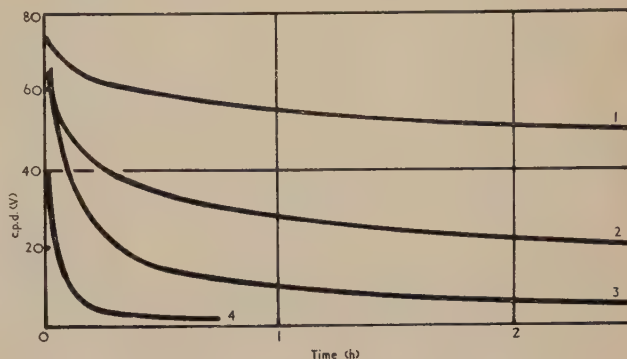


Fig. 4. Decay curves for tube VE IX, CaO, unactivated, at elevated temperatures

Curve (1), 293° K; (2), 310° K; (3), 340° K; (4), 395° K

six similar curves were obtained between the temperatures of 300 and 480° K. The significance of these curves will be discussed below.

4. Discussion of the results

It is evident that such anomalously high c.p.d.'s could not be due to the normal work function difference between a gold reference surface and an oxide cathode. The following working hypothesis was therefore proposed and subsequently tested in the experiments described.

Since the high c.p.d.'s occurred only after the passage of a discharge it seems most likely that they were caused by the separation of charged particles from the ionized gas on to some insulating surface connected to one of the electrodes. The establishment of positive charge on the surface of an insulator has been described previously by Malter⁽⁶⁾ for thin films of aluminium oxide that had been subject to electron bombardment. In Malter's experiments (which gave null results for calcium oxide) the positive charge was caused by the high secondary emission coefficient of the surface. In our case the voltage used was below that necessary for the secondary emission coefficient to exceed one. In these tubes there are two possible surfaces with a sufficiently high insulation: (i) certain parts of the glass supports that could not be coated with Aquadag and (ii) the oxide cathode surface. The indications with previous calcium and barium oxide cathodes have been that the bulk oxide would have a high resistance at room temperature.^(7, 8) If the cathode surface is of a similar composition to the cathode bulk then it would be possible for charge to remain on the surface for long times.

A consideration of the tube design and of the effect of warming the cathode on the decay of the c.p.d. allows the glass to be eliminated as the insulating charged surface

responsible for the anomalous c.p.d.'s. The only glass surfaces that could collect sufficient charge during a discharge to affect the c.p.d. appreciably are the sides of the supporting frame around the cathode and the upper surface of the reference electrode. Since during processing the glass near to the cathode invariably becomes covered with a film of evaporated material from the cathode it is unlikely that its insulation will be very high. Further, on warming the cathode the conductivity of the oxide increases and the c.p.d. rapidly falls to its predischARGE value. The Pyrex glass near to the cathode is hardly warmed during this process (the reference electrode can be moved to the other side of the tube) which seems to confirm that the anomalous c.p.d.'s are caused by the cathode and not by charge on adjacent glass components.

The overall process is probably as follows: When the cathode is operated at a negative potential in the discharge, positive hydrogen ions are driven to the cathode surface. Because the resistance of the oxide is high at room temperature, these ions are neutralized only very slowly by the electron current either through the bulk or over the surface of the oxide.

With this explanation in mind the observations made above can be explained. The reverse discharge, for example, covers the cathode surface with electrons, and, therefore, produces an anomalously high negative c.p.d. This decays slightly more rapidly than the usual decay with positive ions on the oxide surface and this is thought to be a consequence of rectification in the oxide. Calculations of the resistances involved in the passage of current in both directions through the oxide have been made (see below) from the decay curves. The results indicate that the resistance to the passage of electrons from the metal to the oxide is about six times greater than the resistance to flow in the opposite direction. Although rectification effects have been observed in this laboratory with both calcium and barium cathodes using probe tubes,^(7,8) the magnitude has never been as large as these calculations suggest. One of the reasons for this was probably that much larger potential gradients are involved than in the conductivity measurements with probe tubes (a factor of about 100). As a check hydrogen was admitted to a probe diode⁽⁷⁾ with an activated BaO cathode and the conduction current plotted as a function of probe potential (positive and negative) from 0 to 100 V. At the highest voltages the slopes of the two curves indicated that the resistance to electron flow from the metal to the semiconductor was four times greater than in the opposite direction, a fairly good confirmation of the resistances calculated from the decay curves.

The experiments using the auxiliary filament can readily be explained in terms of the hypothesis above. Experiment 3.5 shows that the presence of the gas is unimportant except as a means of putting charge on to the oxide surface. Electrons could be evaporated on to the cathode *in vacuo* and the charge decayed in the same manner as in the presence of hydrogen. It may be concluded, therefore, that the gas does not play any appreciable part in the neutralization of the charge on the cathode.

In the presence of the hydrogen it was observed that the positive ions on the oxide surface could be neutralized by charge drawn from the hot filament. Under the influence of an accelerating potential the electrons could be driven to the oxide so that they first neutralized the positive ions and then built up a negative anomalous c.p.d.

The final experiment in which the decay was plotted at several temperatures and in two activation states of a calcium oxide cathode was an attempt to obtain two conductivity

lines as a function of reciprocal temperature. Since the arrangement behaves as a capacitor with series leakage resistor, it is possible to apply the usual equation (assuming that the resistance, R , is ohmic over the range of values of V):

$$V = V_0 e^{-t/RC}$$

where the symbols have their usual meaning. Hence the product RC can be calculated from the slope of a logarithmic plot. On plotting the decay curves of Fig. 4 in the form $\log \text{c.p.d.}$ against time, linear regions (shown in Fig. 5) were

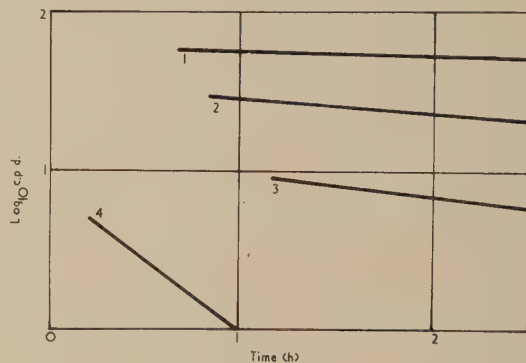


Fig. 5. Regions of the curves of Fig. 4 for which the relation $V = V_0 \exp(-t/RC)$ applies

obtained. The slopes of these lines gave values of the product RC as a function of the temperature. Assuming C to be a constant for any given tube it is possible to make plots of $\log 1/RC$ against $1/T$ which should be linear over the region in which R is ohmic. The slopes of such lines should correspond with the activation energies of the particular oxide used (calcium oxide in this instance). This procedure was carried out with one cathode in two activation states and the lines of Fig. 6 obtained. It will be observed that activation had the

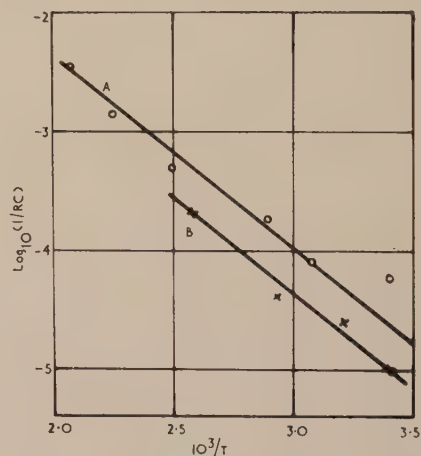


Fig. 6. Calculated conductivity curves for tube VE IX (CaO) A, activated; B, unactivated

usual effect of moving the whole curve upwards so that for any fixed temperature the conductivity was greater. The slopes of the lines gave an activation energy for the conductivity process of 0.35 eV. This is in poor agreement with previous independent results⁽⁷⁾ which indicate an activation

energy of 0.81 eV. Once again this result was checked by reference to a probe tube containing hydrogen introduced *via* a palladium osmosis tube. The linearity of the vacuum conductivity line of the probe tube was replaced after hydrogen had been admitted by a curve. Over the same temperature range covered by the decay curves (480° K to room temperature) a line could be drawn through the probe tube conductivity curve which had a slope of between 0.3 and 0.4 eV. Thus, although the measured slope of the conductivity curves calculated from the decay curves does not agree with that to be expected with a CaO cathode *in vacuo*, the observed slope is confirmed by probe tube measurements in hydrogen.

A partial explanation for the large alteration in apparent activation energy in the presence of hydrogen is thought to be the cooling effect of the gas on the outside layers of the oxide. Such cooling would cause a very large temperature gradient between the cathode base, where the temperature was measured, and the surface of the oxide. The gradient will vary with the temperature of the base and therefore cause curvature in the plots of $1/T$ against the logarithm of the conductivity. This conclusion could again be checked by the use of a probe tube since the increase in the thermal gradient across the oxide in the presence of hydrogen over that *in vacuo* should be obvious from the current-voltage characteristic. Normally these do not pass through the origin due to the thermoelectric e.m.f. caused by the temperature gradient between the cathode and the probe. The cooling effect of the hydrogen on the outer layers of the oxide should result in a much larger thermoelectric e.m.f. *In vacuo* at a temperature of 625° K the probe was 20 mV positive with respect to the cathode. After admitting hydrogen (with the cathode base at approximately the same temperature) the probe was found to be 140 mV positive with respect to the cathode. It may therefore be concluded that the difference between the mean temperature of the oxide and that of the base metal is much greater in the presence of hydrogen, a result in confirmation with the calculated conductivity curves.

In view of the previous discussion, disagreement is to be expected at elevated temperatures between the conductivity calculated from the decay curves and the vacuum conductivity measured by means of a probe tube. At room temperature, however, these two independent measurements should be in agreement. The difficulty about attempting to compare these two conductivities is that the thicknesses of the oxide coatings involved were not measured, thus it is only possible to compare resistances. The vacuum resistance was obtained for a calcium oxide cathode by extrapolating a conductivity curve from previous work to room temperature {Fig. 7 of Ref. (7)}. This indicated a cathode resistance of approximately $10^{15} \Omega$. The resistance of the cathode in hydrogen was obtained from the appropriate value of RC at room temperature using a calculated value of C ($1 \mu\mu\text{F}$). The result so obtained was $4 \cdot 10^{15} \Omega$. Such good agreement is thought to be fortuitous in view of the approximations involved, but even so it confirms the concept that the main charge decay mechanism is by conduction through the oxide.

It will be observed from Fig. 5 that the whole of the decay curves do not obey the relation $V = V_0 \exp(-t/RC)$. For a short period after the passage of the discharge the decay is much faster than exponential. The explanation for this is not yet known, though it is thought that this region of rapid decay may be caused by the non-ohmic nature of the oxide at high field strengths. Alternatively some process other than normal conduction through the oxide may be operative for a short period after the discharge.

5. Conclusions

The phenomenon of charge localization on the surface of an oxide cathode is established in the work described above. Both positive hydrogen ions and electrons have been found to remain on the oxide surface for long periods dependent on the conductivity of the oxide (which in turn depends on the nature of the oxide, its activity and temperature). Over a period of time, which can be as long as several days for cold unactivated calcium oxide cathodes, the charge on the oxide is gradually neutralized either by an electron current over the oxide surface or through the bulk oxide.

A study of the decay of the anomalous contact potential difference with time suggested a method for determining the resistance of the oxide at low temperatures. When applied to activated and unactivated states of the same cathode, plots were obtained which had an unusually low apparent activation energy for the conduction process. This is thought to be caused by the cooling effect of the hydrogen on the outer layers of the oxide and means that the resistance of the oxide can be measured from the decay curves only at room temperature.

The bearing of the experiments and their interpretation in certain ideas concerning low temperature conductivity by means of barium layers⁽⁹⁾ and barium ions⁽¹⁰⁾ is not yet clear since little is known about the condition of the oxide cathode surface in the presence of gas. It seems likely, however, that further experiments along these lines should provide valuable information about the surface of the oxide and especially about the nature of the conductivity process at low temperatures.

6. Acknowledgements

One of us (B. J. H.) makes acknowledgements to Metropolitan Vickers Electrical Co. Ltd. for a scholarship which enabled him to take part in the work, and we thank the same company for the gift of materials and apparatus. Thanks are also due to the General Electric Co. Ltd. and to the Siemens-Edison-Swan Co. Ltd. for the gift of materials, apparatus or equipment, and also to Dr. A. A. Shepherd of Ferranti Ltd. for the gift of the cathode buttons.

We also wish to thank Mr. C. H. B. Mee and other colleagues for helpful discussion of some aspects of the work, Mr. F. Rowerth and Mr. H. Birchall of the College technical staff for assistance in the preparation of the paper, and the referee for a helpful comment.

References

- (1) DAVIES, D. E., and FITCH, R. K. *Brit. J. Appl. Phys.*, **11**, p. 502 (1959).
- (2) ALPERT, D. *J. Appl. Phys.*, **24**, p. 860 (1953).
- (3) BAYARD, R. T., and ALPERT, D. *Rev. Sci. Inst.*, **21**, p. 571 (1950).
- (4) FAN, H. Y. *J. Appl. Phys.*, **14**, p. 552 (1943).
- (5) DAVIES, D. E., and HOPKINS, B. J. *Brit. J. Appl. Phys.*, **11**, p. 498 (1959).
- (6) MALTER, L. *Phys. Rev.*, **50**, p. 48 (1936).
- (7) HOPKINS, B. J., and VICK, F. A. *Brit. J. Appl. Phys.*, **9**, p. 257 (1958).
- (8) HOPKINS, B. J. M.Sc. Thesis, Birmingham University (1957).
- (9) WRIGHT, D. A. *Brit. J. Appl. Phys.*, **1**, p. 150 (1950).
- (10) HIGGINSON, G. S. *Brit. J. Appl. Phys.*, **9**, p. 106 (1958).

New technique for measurement of low dissolved-air content of water

by D. M. J. P. MANLEY, Ph.D., B.Sc., A.Inst.P.,* Mathematics and Physics Department, The Polytechnic, Regent Street, London

[Paper first received 13 October, 1959, and in final form 13 January, 1960]

Abstract

A method is described to measure the dissolved-air content of water enclosed in a vessel. This method uses an air bubble and is very suitable for the measurement of the air content of undersaturated samples. Tests have been made of typical specimens and the limitations of the technique are discussed.

A METHOD has been developed to measure the dissolved-content of water when the saturated gas pressure is below about 100 mm of mercury. Other methods⁽¹⁻³⁾ developed for the measurement of this quantity decrease in accuracy for low dissolved-gas content.

The water under test is contained in a Perspex cell (Fig. 1) of 70 ml. volume with an extensible brass bellows. The

bubble will slowly decrease in volume. When the bubble diameter is only a few eye-piece divisions, the pressure in the water is lowered, causing the bubble to expand. A few preliminary expansions of the bubble are made to arrive at the specific volume above which the bubble grows slowly. This growth is caused by the diffusion of gas from solution in the water into the bubble and indicates that the partial pressure of gas in the bubble is lower than the saturated gas pressure in the surrounding water.

After a period of time, the bubble expansion ceases and it can then be concluded that the partial pressure of gas (P_1 atm) inside the bubble is approximately equal to the saturated gas pressure (P_s atm) of the surrounding water. The dissolved gas content of the water will be $S_0 P_s$ (ml./ml. at 1 atm) where S_0 is the solubility of the gas in the water. The gas pressure (P_1 atm) in the bubble is calculated by first measuring the diameter d_1 of the bubble in the expanded state, and then immediately applying a pressure of one atmosphere to the water. The reduced diameter d_2 of the bubble is then measured within a few seconds and assuming Boyle's law and that the bubble is spherical, the pressure P_1 is given by:

$$P_1 = \frac{(d_2)^3}{(d_1)^3} \text{ (atm).}$$

It can be shown from surface-tension theory that gas bubbles less than 2 mm diameter are approximately spherical.

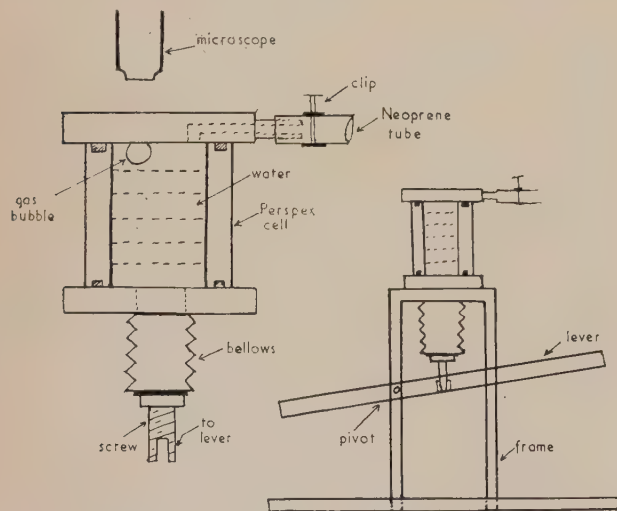


Fig. 1. (a) Perspex cell for measuring the gas content of a liquid. (b) View of general apparatus

water pressure can be varied by applying pressure or tension to these bellows. The cell is filled through a neoprene tube, and a clip is used to seal the cell for experiments. An air bubble is formed under the top Perspex plate of the cell by extending the bellows. A low-powered microscope with a calibrated eye-piece scale is used to measure the bubble diameter. The bubble is first reduced in volume by applying, by means of the bellows, a pressure of one atmosphere in the water. For a liquid which is undersaturated with gas, the

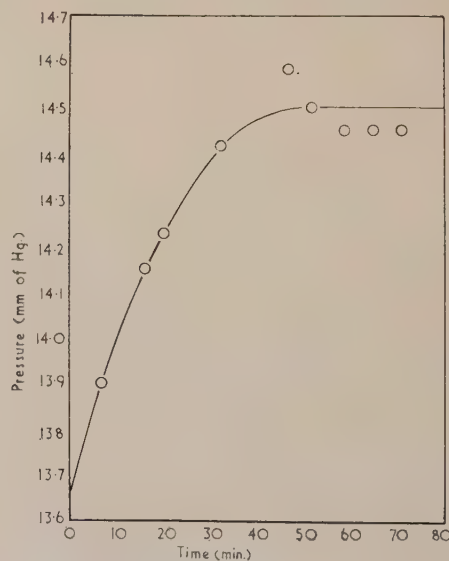


Fig. 2. The variation of the gas pressure in an expanded bubble in a liquid with time

* Now with the British Broadcasting Corporation Research Dept., Nightingale Square, London, S.W.12.

Fig. 2 shows the variation of the gas pressure of a typical expanded bubble with time, calculated from several measurements of d_1 and d_2 . It is seen that the saturated gas pressure is about 14.5 mm of mercury; that is, when the bubble ceases to grow. This result gives a calculated result for the dissolved gas content of the water as 3.8×10^{-4} ml./ml. at 1 atm.

Tests on many samples of undersaturated water have shown that this technique used for the measurement of the dissolved gas content gave consistent results when the saturated gas pressure was between a few and about 100 mm of mercury. The limit of operation of this technique for very low dissolved-gas contents occurs when the expanded bubble has to be so large for gas to diffuse from solution that it cannot be measured in the field of view of the microscope. When the saturated gas pressure is above 100 mm of mercury, it has

been found that the accuracy of results calculated for dissolved content is limited by the accuracy of the measurement of bubble diameters and, for higher dissolved-gas content, the final value for d_1 when there is diffusion equilibrium may only be approximately observed after a considerable length of time.

References

- (1) WINKLER, L. W. *Die Löslichkeit des Sauerstoffs in Wasser. Deut. chem. Ges. Ber.*, **22**, pp. 1764–1774 (1889).
- (2) PETERS, J. P., and VAN SLYKE, D. D. *Quantitative clinical chemistry, Vol. II, Methods*, pp. 106 and 229 (Baltimore: William and Wilkins, 1932).
- (3) WILLIAMS, E. E. *M.E.R.L. Fluids Report No. 15* (1953).

Determination of orientation of bismuth single crystals using back-reflexion technique

by H. D. MALLON, B.Sc., A.R.T.C., A.I.M., and C. G. WILSON, M.Sc., A.Inst.P.,
Royal Military College of Science, Shrivenham, Swindon, Wilts

[Paper first received 25 November, 1959, and in final form 25 January, 1960]

Abstract

The ambiguity in interpretation of orientation from back-reflexion photographs of bismuth single crystals is resolved by taking photographs about the trigonal axis or the normal to the (111) plane. The trigonal axis which is also the optic axis is uniquely determined by using polarized light.

As has already been noted,⁽¹⁾ the determination of orientation of a bismuth single crystal is very difficult using the standard back-reflexion method of Greninger,⁽²⁾ because of the almost cubic symmetry associated with the unit cell. Bismuth belongs to the rhombohedral system and although its smallest unit cell has the parameters $a = 4.74$ kX, $\alpha = 57^\circ 14'$, it is usually represented as a face-centred rhombohedron with $a = 6.57$ kX, and $\alpha = 87^\circ 34'$. Since the axial angle on this representation is almost 90° , the quasi-cubic nature of the crystal lattice is immediately apparent. Because of the near cubic symmetry of bismuth the two back-reflexion Laue photographs taken first with the trigonal axis ([111] direction) and then with the normal to the ($\bar{1}\bar{1}\bar{1}$) plane parallel to the X-ray beam, are almost identical. It is true that small angular differences exist between any two pairs of corresponding spots in the different orientations but, because of the limited accuracy

available in using the back-reflexion technique, it is impossible to distinguish between the alternative orientations.

This paper is concerned with the determination of the orientation of bismuth crystals prepared by growth from a capillary tube. The specimens, about 1 cm^2 in cross-section, were mounted in cold-setting acrylic resin and electro-polished. Back-reflexion X-ray photographs were taken with the crystal face normal to the beam using a copper target with a film-to-crystal distance of 3 cm. A stereogram was constructed from this film using a transparent Greninger chart and a 30 cm Wulff net. To determine the crystal orientation it is necessary to identify at least two spots on the film uniquely. Within the ambiguity mentioned earlier, it is not difficult to identify important junctions on the stereogram by making use of the symmetry associated with such points and the known inter-zonal angles tabulated by Vickers.⁽³⁾

It has been found that the unique identification of the Laue spots is made possible by first identifying, by its three-fold symmetry, the position of the (111) pole—or the ($\bar{1}\bar{1}\bar{1}$) pole which gives a similar array of spots—on the film. The crystal is then re-orientated so that the normal to the (111) or ($\bar{1}\bar{1}\bar{1}$) plane is made parallel to the X-ray beam. A new photograph is taken which will display the true trigonal symmetry of the crystal if the (111) pole is at the centre and the quasi-trigonal symmetry in the alternative ($\bar{1}\bar{1}\bar{1}$) setting.

It is not necessary to adjust the orientation so that either pole is exactly at the centre of the film since the symmetry of the orientation is sufficiently revealed when the required pole is within one degree of the centre. Photographs of two crystals showing the alternative symmetrical orientations obtained by this means are shown in the figure. It is not possible, without extreme care, to decide which pole, that is, (111) or $\bar{1}\bar{1}\bar{1}$, lies at the centre of each film.

To distinguish the two cases, a technique using polarized light has been developed. It is well known that the optic

intensities of the corresponding spots are markedly different. Very similar standard photographs have been taken at X-ray operating voltages between 20 and 40 kV using the copper target. It is evident from photographs taken with and without a nickel filter in the incident X-ray beam that the differences in spot intensities is caused by the characteristic copper K α radiation reinforcing the reflexions from different planes in the two cases. Thus, the (111) and $\bar{1}\bar{1}\bar{1}$ projections and the zones containing other important poles are easily distinguished and the ambiguous orientation determined from the photograph taken with the X-ray beam normal to the crystal is resolved.

Experimental difficulties may occur if either pole lies near the periphery of the film because of the large re-orientation required on the goniometer arc. The quality of the photograph deteriorates for very oblique orientations of the crystal face relative to the X-ray beam. In such cases, it may be advisable to cut the crystal and polish the new surface so as to bring the pole within a small angular displacement from the beam.

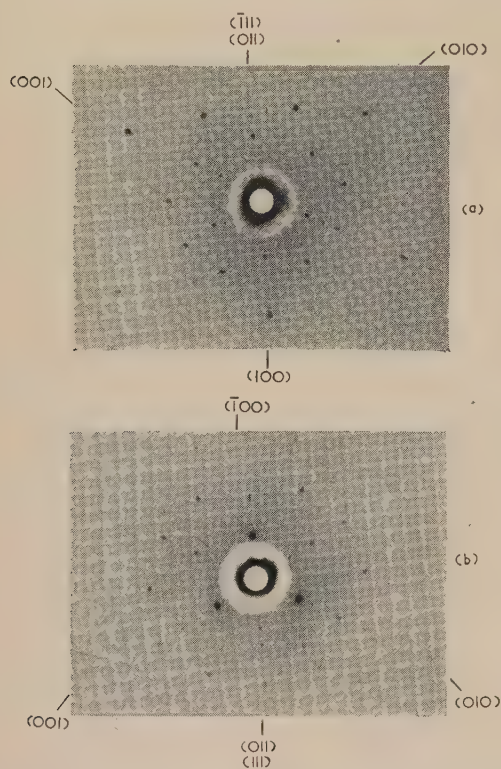
It may be noted that, for the determination of orientation within the accuracy of the method, it is only necessary to take care with the first setting of the crystal, that is, when the X-ray beam is normal to the face, since the subsequent photograph with (111) or $\bar{1}\bar{1}\bar{1}$ at the centre of the film is merely used for identification by comparison with the standard photographs shown in the figure. Alternatively, if the identifying photograph with the (111) or $\bar{1}\bar{1}\bar{1}$ pole at the centre of the film is taken with care the stereogram of this film can be drawn using the Greninger chart and, by comparison with the appropriate standard photograph in the figure, the (011) pole can be identified. The orientation for this setting is thus determined. The orientation of the first setting is then obtained by noting the changes in goniometer readings and re-orientating the stereogram accordingly. This latter method is speedy but suffers slight inaccuracy because of the reduction in film quality with orientation from the normal.

Acknowledgements

The authors wish to thank Lt. I. G. Runciman, B.Met., for making the single crystals used, and Mr. F. J. Spooner, B.Sc., for his assistance in taking X-ray photographs. This paper is published by permission of the Dean of the Royal Military College of Science.

References

- (1) HURLE, D. T. J., and WEINTROUB, S. *Brit. J. Appl. Phys.*, **10**, p. 336 (1959).
- (2) BARRETT, C. S. *Structure of Metals*, 2nd ed., p. 188 (London: McGraw-Hill Pub. Co. Ltd., 1952).
- (3) VICKERS, W. *J. Metals*, **9**, p. 287 (1957).



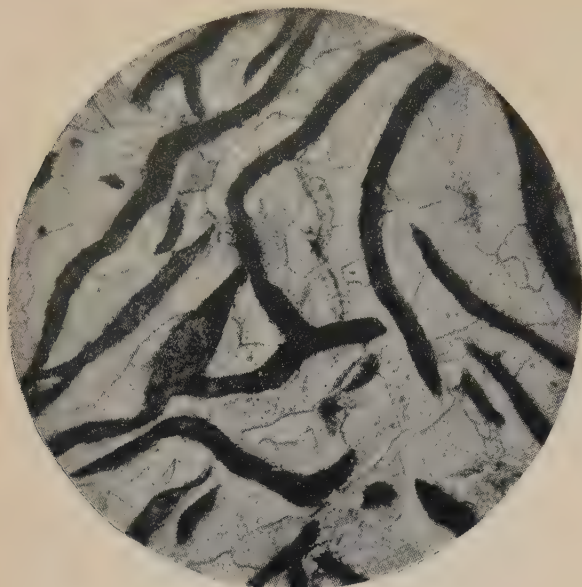
Photograph of two crystals: (a) normal to (111) plane parallel to X-ray beam, (b) normal to $\bar{1}\bar{1}\bar{1}$ plane parallel to X-ray beam

axis of bismuth is parallel to the [111] direction of the crystal so that plane-polarized light reflected from a polished bismuth crystal cut normal to this direction gives extinction in all positions when viewed through crossed polars. With this technique, the back-reflexion photograph of the crystal in this orientation is obtained. This is indicated in the figure, photograph (a). From this figure, the distinction between the two orientations is obvious. The angular relations between the main zones represented by the lines of spots radiating from the centres of the two films are nearly the same but the

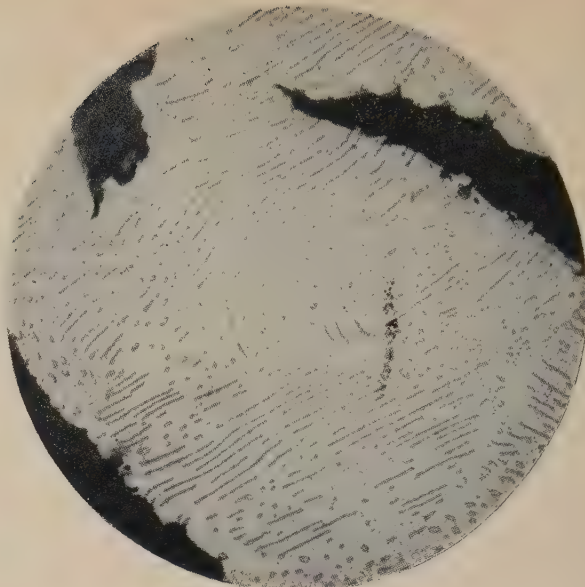
Contents

	PAGE		PAGE
<i>Chemistry, biophysics, and properties of materials</i>		<i>Miscellaneous (continued)</i>	
Advances in mass spectrometry	232	Radio stations: installation, design and practice	237
Exploding wires	232	The Robertson guide to world screw thread standards	237
Fracture	232	Rocket propulsion	237
Metallurgy of the rarer metals. No. 6: Tantalum and niobium	232	Scientific Russian	237
Méthodes générales d'essai et de contrôle en laboratoire. Vol. 1. Mesures géométriques et mécaniques	233	Studies in crystal physics	237
Non-homogeneity in elasticity and plasticity	233		
Physical methods of investigating textiles	233	<i>Nuclear and cosmic-ray physics, apparatus, techniques and data</i>	
Plansee proceedings 1958: High melting metals	233	Atlas of γ -ray spectra from radiative capture of thermal neutrons	238
Proceedings of the first national biophysics conference	233	International conference on high-energy accelerators and instrumentation—CERN 1959	238
Radiation biology	234	The theory of elementary particles	238
Vacuum metallurgy	234		
		<i>Photography, microscopy and optics</i>	
<i>Heat, thermometry and low and high temperature physics</i>		Der Raman-Effekt	239
Physicochemical measurements at high temperatures	234	Elektronenmikroskopische Untersuchungs-und Präparationsmethoden	239
Problems of low temperatures physics and thermodynamics	235	Photomicrography	239
Property measurements at high temperatures	235		
		<i>Theoretical physics, mathematical techniques, computers and control systems</i>	
<i>Magnetic, electrical and electronic devices and properties</i>		Grundlagen der selbsttätigen Regelung	240
Advances in electronics and electron physics. Vol. X	235	Introduction to the theory of quantized fields	240
The magnetodynamics of conducting fluids	236	Manual of mathematical physics	240
Masers. Microwave amplification and oscillation by stimulated emission	236	Proceedings of the fifth annual computer application symposium	241
Proceedings on an international symposium on the theory of switching. Parts I and II	236	Statistical methods in radio wave propagation	241
		The theory of storage	241
<i>Miscellaneous</i>		Vibration engineering	241
Classification and indexing in science	236		
Mechanical design of laboratory apparatus	236		

New books section



(a)



(b)

Photomicrographs of (a) Ferritic cast iron $\times 225$ and (b) Spheroidized cast iron $\times 1500$. These illustrations, which have been slightly reduced from the originals, appear in the 2nd ed. of *Photomicrography* by Dr. Roy M. Allen, published by D. Van Nostrand Co. Ltd., and reviewed on p. 239.

Chemistry, biophysics, and properties of materials

Advances in mass spectrometry. Edited by J. D. WALDRON. (Oxford: Pergamon Press Ltd., 1959.) Pp. xiii + 704. Price £6.

This volume contains the proceedings of a joint conference organized by the Hydrocarbon Research Group of The Institute of Petroleum and A.S.T.M. Committee E.14 and held at the University of London in September, 1958. The papers by recognized international specialists are intended to give up-to-date information on research, development and applications in this field.

In addition the book contains a very extensive bibliography prepared by the research group of Metropolitan-Vickers Electrical Co. Ltd., covering the period 1938 to 1957, and containing some 2000 references.

Exploding wires. Edited by W. G. CHACE, and H. K. MOORE. (New York: Plenum Press, Inc.; London: Chapman and Hall, Ltd., 1959.) Pp. ii + 373. Price 76s.

This book is based on the conference on the "Exploding Wire Phenomenon", held at the Air Force Cambridge Research Centre in Boston, Massachusetts, in April, 1959. The volume not only records the proceedings of the conference, but is claimed by the publishers to fill a gap in the literature on the subject. The work is particularly intended for workers in high-speed photography, shock wave and thermonuclear and fluid physics research.

Fracture. Edited by B. L. AVERBACH, D. K. FELBECK, G. T. HAHN and D. A. THOMAS. (Massachusetts: The Technology Press of Massachusetts Institute of Technology; New York: John Wiley and Sons, Inc., London: Chapman and Hall, Ltd., 1959.) Pp. xvii + 646. Price £7.

This book is concerned with atomic changes of structure

when materials fracture. It is based on the proceedings of a conference at which a number of research workers in the field participated. Current theories and experiments are critically considered for the cleavage, ductile, fatigue, and high temperature mechanisms of fracture for metals, ceramics, and polymers. One of the most valuable features of the book is in the delineation of future research needs.

The conference was sponsored by the National Science Foundation Office of Naval Research, Air Force Office of Scientific Research, Ship Structure Committee. It was organized and directed by the Conference on Fracture of the National Academy of Sciences-National Research Council.

Metallurgy of the rarer metals. No. 6: Tantalum and niobium.

By G. L. MILLER. (London: Butterworths Scientific Publications, 1959.) Pp. xxii + 767. Price £6.

Volume 6 in the series is a welcome addition. As usual, the book embraces all aspects, from occurrence ores, extraction, purification and fabrication of the two metals through the physical, mechanical and chemical properties to analytical and metallographic methods of examination and binary alloy systems.

Chapter 2 contains a full description of the uses of the two metals, particularly electronic components utilizing tantalum. It is a pity that the nuclear energy developments in niobium, which served to bring the metal into prominence, occupy only two pages. An error occurs in the description of the Dounreay fast reactor fuel element, attributing the mechanism of failure under rapid temperature rise to the lower melting point of vanadium, whereas it should be the lower melting point of vanadium-uranium alloy (formed either by diffusion or penetration of liquid uranium) as against the resistance of niobium to liquid uranium penetration below about 1300°C .

The use of arc melting and the electron beam method in preparation of very pure metal is of interest to physicists. There is some duplication of results in chapters 8 and 9, e.g.

Table 85 is merely the lower lines of Table 84, and Table 99 includes one line of Table 98. Insufficient stress is laid on the effect of impurities on physical and mechanical properties. Although the author mentions this at the beginning of relevant chapters, and is careful to quote impurity levels in all work carried out by his own company, he does not, in the reviewers' opinion, emphasize sufficiently the dangers inherent in many published results which make no mention of purity.

For those requiring an encyclopaedia of published work on tantalum and niobium, this book can definitely be recommended. It deserves to be on the library shelves of all progressive users of metallic materials. C. R. TOTTLE

Méthodes générales d'essai et de contrôle en laboratoire. Vol. 1. Mesures géométriques et mécaniques. By R. L'HERMITE. (Paris: Editions Eyrolles, 1959.) Pp. xii + 739. Price 9700 frs.

This is the first volume of a series on material testing with special reference to materials used mainly by civil engineers. The present volume is devoted mainly to a general broad description of methods and approaches dealing with measurements over wide ranges of lengths, areas, volumes and densities, shape and size distribution of granules, porosity and specific surface, time, velocity, weights, forces and strains, strength, hardness and wear, internal friction and fatigue.

Supporting chapters deal with the role of expert witnesses, the theory of experiment and statistical methods. The second volume is planned to deal with essentially physical and chemical methods in general, whereas further volumes will be devoted to particular materials and products—and the investigation of failures.

The book is intended to explain to experts in other fields just what material test stations are doing and how and why it is done. The approach and standard is comparable with that of a good guide-lecturer showing intelligent and technically trained visitors round a research establishment during an "open day". Each chapter is concluded with a short bibliography for those who want to know a little more.

The book is generously illustrated with excellent diagrams and many half-tone engravings, and the quality of paper and printing are such that even the structure of fracture surfaces can be studied with profit. The binding, however, is rather poor.

The writing is clear and fluid and the *Concise Oxford French Dictionary* was found to be adequate for the more specialized vocabulary. The book therefore could serve well as a means for reading oneself into the specialized French of this branch of technology as well as a lucid introduction to the tools of an important branch of applied physics.

O. KANTOROWICZ

Non-homogeneity in elasticity and plasticity. Edited by W. OLSZAK. (Oxford: Pergamon Press Ltd., 1959.) Pp. xxiii + 528. Price £5.

This book contains 52 theoretical and experimental papers prepared by specialists, for the symposium held in Warsaw in September, 1958, organized by the International Union of Theoretical and Applied Mechanics in co-operation with the Polish Academy of Sciences.

Two survey papers summarize the actual status of investigations; while solutions to beam, plate, shell, plane and three-dimensional problems are covered together with experimental observations. Applications to physical metallurgy in both

the elastic and the plastic range are also discussed. In two longer papers, Professor W. Olszak and Dr. W. Urbanowski summarize their extensive work on plastic non-homogeneity, and Dr. M. A. Biot reviews his current and past work on stability problems of non-homogeneous viscoelastic media.

Physical methods of investigating textiles. Edited by R. MEREDITH and J. W. S. HEARLE. (New York: Interscience Publishers, Inc.; London: Interscience Publishers Ltd., 1959.) Pp. ix + 411. Price 88s.

A striking aspect of the work of our leading Colleges of Technology is the importance they attach to special courses of lectures of a graduate or post-graduate standard, given by experts in various branches of knowledge or modern techniques, all linked together with a common purpose.

The value of such lectures is well illustrated in this book, which records a series of lectures given in Manchester in the winter of 1956–57. The subject, of course, is vast, and so the emphasis throughout is on newer techniques rather than many traditional ones adequately dealt with elsewhere. This greatly enhances the value of the book.

Fourteen chapters cover a wide range of techniques and yarn and fabric properties, and include X-ray techniques, infra-red spectroscopy, mechanical properties of fibres, yarns, and fabrics, transmission of heat, moisture and air, and electrical properties. A final substantial chapter on the application of nuclear physics to textile problems shows the tremendous impact physics has made in the textile field in recent years. Comprehensive lists of references are given at the end of each chapter.

The names of the Editors are sufficient guarantee of the quality and standing of this book, and no physicist seriously interested in textiles should be without it, or without easy access to it. F. C. TOY

Plansee proceedings 1958: High melting metals. Edited by F. BENESOVSKY. (Oxford: Pergamon Press and Metallwerk Plansee AG. Reutte/Tyrol, 1959.) Pp. xii + 465. Price 83s. 6d.

The papers collected in these proceedings, presented at the third Plansee Seminar held in Reutte, Tyrol, in June, 1958, have been classified in six parts. The first part deals with theoretical questions, such as the mechanism of sintering and the structure of high-melting metals; the second part with tungsten and tungsten alloys; the third part with molybdenum and molybdenum alloys; tantalum, niobium as well as rarer metals and their alloys are dealt with in parts four and five while the final part combines the papers on metal-metal oxide materials.

Proceedings of the first national biophysics conference. Edited by H. QUATLER and H. J. MOROWITZ. (New Haven: Yale University Press; London: Oxford University Press, 1959.) Pp. xxvii + 756. Price £6.

This volume is a partial record of the First National (U.S.A.) Conference on Biophysics, held in Columbus, Ohio, in March, 1957. It contains papers submitted by invitation of the program committee or editors, papers submitted by the authors and selected by the editors, and all abstracts which were submitted for presentation at the conference. The rule of not rejecting any abstract for any reason was adhered to,

though sometimes with difficulty; as a result this book represents a composite view of the frontiers of biophysics as seen by more than 200 investigators.

Radiation biology. Edited by J. H. MARTIN. (London: Butterworths Scientific Publications, 1959.) Pp. xi + 304. Price 63s.

The Australian Radiation Society's second conference, held in Melbourne, in 1958, was concerned with the interaction of ionizing radiation in living cells. The published Proceedings contains 29 papers which provide sources of new data not only for research workers interested in the purely scientific objectives of the conference, but for those concerned generally with the human implication of radiation biology.

Vacuum metallurgy. Edited by R. F. BUNSHAH. (New York: Reinhold Publishing Corporation; London: Chapman and Hall, Ltd., 1958.) Pp. xviii + 472. Price 100s.

Melting, sintering and distilling metals in vacuo were methods first used in the preparation of reactive metals, but in the last twenty years these techniques, which form the basis of vacuum metallurgy, have been greatly extended and also applied in the conventional metal industries. Apart from studying the properties of vacuum produced metals workers concerned with their large scale production have had to investigate a number of diverse topics which can be broadly grouped as follows:— (1) Degassing and thermo-chemical reactions occurring in systems based on solid or liquid metal/refractory support/residual gas atmosphere; (2) High temperature heating techniques such as those based on radiation; electrical induction; electrical arcs and more recently electron bombardment techniques, (3) Vacuum systems with special attention to the rapid pumping of reactive gases at high mass throughputs. Intense work in these fields has resulted in the industrial use of vacuum metallurgy for preparing titanium, degassing steel, etc. and the most recent development of electron beam welding.

In June 1957 a course of 27 lectures on Vacuum Metallurgy was given at New York University by an international group of experts and these lectures have been collected together in the book reviewed here. The subject matter of the book can be roughly divided as outlined in the previous paragraph and with such a bewildering range of disciplines it is hardly possible to give a balanced review.

The section on vacuum equipment is of interest because it shows how the needs of vacuum metallurgy have stimulated the development of new types of pumps, e.g. mechanical and vapour booster pumps, which are not even alluded to in high vacuum text books written say ten years ago. In the light of this it is a pity that the contributor of this section has not made the most of his opportunity. Thus attention has been given mainly to American and German pumping equipment and advanced plant independently developed in this country has been somewhat neglected. Thus the maximum backing pressure of an oil ejector pump is given as about 1 mm Hg, whereas with a whole range of British pumps the maximum backing pressure is 3 mm Hg. Also, the discussion on the possible use of ultra-high vacuum for preparing highly degassed metals over emphasizes the possible use of getter-ion pumping, and does not discuss the more conventional diffusion pump system which when suitably trapped is capable of continuously pumping at very low pressures with much

greater gas throughputs. Another and more serious weakness is the failure to give practical data on the working pressure one can hope to achieve when pumping typical loads with different pumping systems. Knowledge of the pumping speed of a particular system is inadequate if one does not know the gas evolution rate which is likely to be encountered. The discussion on vacuum gauges presents little which could not be obtained from a standard vacuum text. One would like to have seen discussion of methods of analysing the vacuum atmosphere and measuring partial pressures since for research a knowledge of the nature and concentration of the gases present is more important than an indication of their total pressure.

Much useful data is given on practical methods of heating and designing crucibles. Also it is interesting to read of the novel methods developed for degassing steel and welcome to see that Russian scientists have contributed articles on their experiences in this field.

Certain aspects of vacuum evaporation have quite correctly been considered here as branches of vacuum metallurgy, e.g. the continuous evaporation of metals on to plastic foils. However, refractory reactions and vapour source design are not deeply discussed and the standard of reporting in this section hardly justifies its inclusion.

As is often the case with collected papers there is a certain amount of repetition and it is a pity that the Editor could not have resisted the tendency of some of his contributors to turn their papers into general reviews rather than keep to the subject in hand.

Many of the papers have appeared in one form or another in the various symposia which have been held over the last five years but this is the first time an effort has been made to group them within one cover and the book should be of great value to the student of this growing technology

L. HOLLAND

Heat, thermometry and low and high temperature physics

Physicochemical measurements at high temperatures. Edited by J. O'M. BOCKRIS, J. L. WHITE and J. D. MACKENZIE. (London: Butterworths Scientific Publications, 1959.) Pp. viii + 394. Price 75s.

The book under review originated with a research team originally working at the Imperial College of Science and Technology, but some American contributors were subsequently co-opted. It was intended "to present material which contained the essence of what present and future chemists need at the beginning of and during experimental investigations in this field". The temperature range involved covers the region between 500 and 2500° C.

The book falls into two parts: the first is of a general nature and covers methods of measuring, attaining and controlling high temperatures. The performance of refractory materials under these conditions is discussed. The second half deals with more specialized applications such as the study of phase equilibria in silicate systems, the study of chemical equilibrium in extraction metallurgy and the measurement of heat evolution, liquid densities, surface tension and vapour pressures. There are also chapters on the electrochemistry and the transmission of light and sound in high temperature systems. An account of viscosity and diffusivity measurements under these difficult conditions is included.

The specialist chapters provide first-hand accounts of

extensive researches in various laboratories of international repute. They form an exceptionally useful guide to literature and should be indispensable to anybody applying these techniques for the first time.

The earlier, more general, chapters are a little disappointing. The chapter on temperature measurement has been allowed to become a mere catalogue. Little attempt is made to assess the merits of the different methods. Graphite-clay thermocouples are listed without any note of warning! The disappearing filament pyrometer receives scant attention. The tables of optical data neglect to detail the relationship between the emissivity of a material and the allowable size of aperture which ensures the "black body" behaviour of a cavity. Although most experiments in this field rely on furnace windows, no mention of the transmission coefficients (for light of 6500 Å) could be found for quartz, Pyrex, Perspex or water.

The chapter on the stability of refractory materials presents a vast amount of thermodynamic data. (Appendix 5 also includes a particularly useful list of references from which additional information can be obtained.) The method of presentation, however, seems clumsy, and the reviewer feels that an opportunity has been lost in not displaying the information in graphical fashion as was first suggested by Ellingham (c.f. J.S.C.I., 127, 1944 and 69, 59, 1950).

The book concludes with seven appendices which include practical hints on testing refractories and the preparation of molybdenum and tungsten apparatus. Expansion coefficients, melting points and vapour pressures are listed: (in the last instance a graphical approach as in *Rev. Sci. Instrum.*, 19, p. 921 1948 would have been more useful.)

The book can be recommended to the physical chemist about to undertake measurements at high temperatures. It should give him the benefit of experience acquired in the foremost laboratories in the U.K. and the U.S.A.

H. W. DAVIDSON

Problems of low temperature physics and thermodynamics. (Oxford: Pergamon Press Ltd., for the International Institute of Refrigeration, 1959.) Pp. 341. Price 70s.

This volume contains the proceedings of the meeting held at the University of Delft, Holland, of Commission 1 of the International Institute of Refrigeration.

Forty-eight papers were presented at the meeting, and the general subjects chosen were: cryogenic apparatus; thermometry; the disturbed crystal lattice; transport phenomena in liquids and gases.

Bibliographical references and the discussion that followed each paper are included.

Property measurements at high temperatures. By W. D. KINGERY. (New York: John Wiley and Sons, Inc.; London: Chapman and Hall Ltd., 1959.) Pp. xii + 416. Price £6 12s.

The book is devoted to a review of methods of measurement and of the properties of materials at temperatures above 1400° C. The author is a refractories expert, and therefore tends to look at the subject particularly from the point of view of the refractory oxides. However, he defends the preparation of an encyclopaedic book by one author on the grounds that it gives a continuous treatment throughout and there is no doubt that there is much to be said for this point of view. On the other hand, there is a tendency for him to review

branches of the subject in which he is not an expert by quoting from the literature or from hearsay and giving results without adequate proof or information that he has convinced himself that they are correct. Some are obviously quoted from his own unpublished experiments and here one would like to see more detail of the experiments.

It should, however, be emphasized that a book on this subject is extremely timely as the whole field of combustion technology is ranging into temperatures higher than those achieved with the combustion of rich fuels with cold air. Industrial furnaces are now being built to give temperatures up to 2000° C by combustion of rich fuels with preheated air and with oxygen, and with special fuels and oxygen, temperatures up to 3000° C are frequently obtained in industrial processes such as the oxygen blowing of steel. It is true that work on ZETA and similar attempts to produce nuclear fusion have shifted the interests of many physicists to temperatures of the orders of millions of degrees Kelvin, but nevertheless the intermediate range above ordinary combustion temperatures and up to arc temperatures are of extreme interest and will have many practical applications in the future. The use of a solar furnace in France for nitrogen fixation reactions at 3000° C is an application which has recently appeared in the newspapers. A large solar furnace is also being built in America for experiments in this range of temperatures. The present book discusses, the compressed arc on which a paper has recently been written for the Institute of Physics, and the use of imaging of high temperature sources into a hollow furnace, both from the sun where a theoretical maximum furnace temperature of about 5000° K can be reached and from the high intensity carbon arc which gives an anode temperature of about 7000° K and can be focused with a pair of mirrors.

The book is designed for postgraduates and research workers, but is perhaps a little elementary on certain aspects for them and does not contain as many references as they would like. Nevertheless it is the first complete survey of the field and anyone working in this field cannot afford to do without it. The fourteen chapters cover all the properties of solids, liquids and gases at these temperatures on which any significant measurements have been obtained.

M. W. THRING

Magnetic, electrical and electronic devices and properties

Advances in electronics and electron physics. Vol. X. Edited by L. MARTON. (New York: Academic Press Inc.; London: Academic Books Ltd., 1958.) Pp. x + 320. Price 80s.

This is the tenth volume of a well-known series containing specialized review articles. The book contains six contributions:— 1. Non-uniform d.c. electron flow in magnetically focused cylindrical beams, by W. G. Dow; 2. Defects in diamond-type semiconductor crystals, by E. Billig and E. J. Holmes; 3. Micro-wave optics, by J. Brown; 4. Developments in computer logical organization, by W. L. Lawless; 5. On some aspects of tube reliability, by E. G. Rowe; 6. Recent developments in the cathode ray oscilloscope, by J. E. Day.

According to the editorial, these books are published with the specialist research worker in mind, but it is difficult for a reviewer to judge them on this basis. In any case, if such an expensive book is to succeed, each article cannot be addressed

exclusively to fellow specialists. It ought to be possible for any reader anxious to learn something of advances in a subject only broadly related to his own to turn to it for information.

Needless to say this double criterion is difficult to satisfy and one suspects that some authors did not try. The first somewhat mathematical article on electron optics and the fourth non-mathematical article on computers are presumably addressed to specialists. This reviewer found the latter one in particular almost unreadable. Against that the author of the interesting article 6 on oscilloscope developments must have had the non-specialist reader particularly in mind.

The section on crystal defects is largely concerned with dislocations and many of these are well illustrated by photographs. Diffraction and interferometry figure prominently in article 3 on microwaves, which is written from the standpoint of optics. It is a pity that the subject of coherence, which is so important in optics, is dismissed in one line. The section on tube reliability is concerned with valve manufacture and contains some interesting and surprising statistical information.

Even if articles 1 and 4 are not easy reading, there must be few physicists who would not learn a good deal from the book. It is very well produced and contains the usual large number of references. But it is expensive, and this reviewer feels that the selection of subject matter is perhaps not quite as successful as in some earlier volumes.

L. MANDEL

The magnetodynamics of conducting fluids. Edited by D. BERSHADER. (Stanford, California: Stanford University Press; London: Oxford University Press, 1959.) Pp. viii + 145. Price 36s.

Seven analyses covering the underlying behaviour of conducting fluids in magnetic fields are contained in this third volume to originate from the Lockheed-sponsored symposium on magnetohydrodynamics.

Electromagnetic theory and fluid mechanics are combined from the continuum point of view in order to discuss the physical concepts and obtain results relating to the influence of magnetic fields on wave propagation, shock tube flows, subsonic and supersonic nozzle flows, subsonic and viscous boundary layers. Though the studies are largely analytical, to them have been added some experimental results dealing with magneto-hydrodynamic lift and with shock wave behaviour. Particular attention is paid to new features which have no counterpart in ordinary fluid mechanics.

Masers. Microwave amplification and oscillation by stimulated emission. Edited by G. TROUP. (London: Methuen and Co. Ltd., 1959.) Pp. x + 168. Price 13s. 6d.

A discussion of the stimulated emission process is followed, in this volume, by a brief outline of methods used to obtain the conditions necessary for amplification. The effects of various physical processes upon amplifier efficiency, and upon the effective frequency response of a molecular transition used to amplify, are described. The book goes on to give derivations of the gain, bandwidth, and noise factor of the travelling-wave line type of stimulated emission amplifier, and of the resonant cavity type of amplifier.

A review of the experimental work on "masers" is given, together with a bibliography.

Proceedings on an international symposium on the theory of switching. Parts I and II. (Cambridge, Massachusetts: Harvard University Press; London: Oxford University Press, 1959.) Pp. xi + 305. Price £6 per set.

These Proceedings consist of 39 papers which were presented at Harvard University in April, 1957, in sessions dealing with abstract models, contact networks, magnetic and transistor logic, switching systems, and new switches. The authors of eleven of the papers came from institutions abroad.

Miscellaneous

Classification and indexing in science. By B. C. VICKERY. (London: Butterworths Scientific Publications; New York: Academic Press Inc., 1958.) Pp. xvii + 184. Price 25s.

In physics, as in other sciences, the evergrowing volume of publication in the form of books, reports and journal articles presents serious problems both to the research worker and to the documentalists. The former is becoming increasingly dependent on the latter to organize the published literature in such a way that desired information can be retrieved as speedily and efficiently as possible. Traditional classification schemes are being found inadequate to codify the complex relations between specific subjects represented in the typical scientific document of today.

The author of this work enjoys an international reputation as an authority on the theory of classification, and is here concerned to display the modern techniques for the subject analysis of scientific literature. In the first chapter he demonstrates the need for classification as the basis of information retrieval, and in particular the need for faceted classification to match the faceted pattern of scientific topics. The next two chapters deal in detail with the construction of classification schedules and the question of notation for the classified catalogue—these chapters are highly specialized and mainly of interest to the practising classificationist. Chapter 4 surveys the potentialities of machines for storing and retrieving information, and the final chapter demonstrates the way in which an alphabetical subject index, based on the faceted scheme of classification, should be constructed. Appendices (which occupy a third of the book) include a survey of the historical aspects of the classification of science, examples of faceted classifications, and a discussion of the notion of categories. A second revised and enlarged edition of this work has already appeared only a year after first publication.

Although much of the book is primarily of interest to librarians and documentalists, physicists should gain from it an increased understanding of the way in which modern scientific knowledge may be organized. The work should have practical value, too, in teaching the more efficient arrangement of personal information files and the more efficient use of scientific libraries.

G. M. PATERSON

Mechanical design of laboratory apparatus. Edited by H. J. J. BRADDICK. (New York: Reinhold Publishing Corporation; London: Chapman and Hall, Ltd., published on behalf of The Institute of Physics, 1960.) Pp. 47. Price 6s.

This monograph has been written in order to help young scientific workers to design and assemble laboratory apparatus. Although some of the ordinary elements of

VITREOSIL

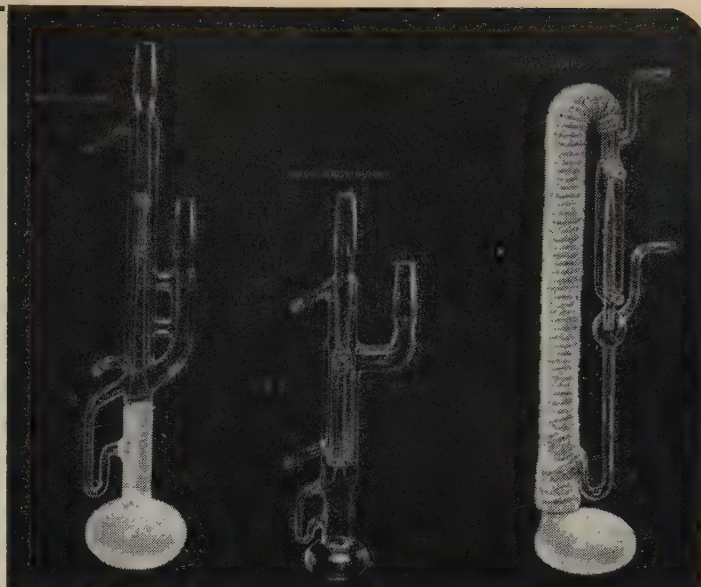
MERCURY VAPOUR PUMPS

FOR HIGH VACUUM

A highly efficient, yet inexpensive, high vacuum system can readily be assembled by using either a Vitreosil single-stage, or two-stage, pump together with a Vitreosil fore-pump.

We also manufacture an extensive range of Vitreosil Industrial Ware.

Leaflet L14 may be obtained on request



THE THERMAL SYNDICATE LTD.

P.O. BOX NO. 6, WALLSEND, NORTHUMBERLAND

Telephone: Wallsend 62-3242/3

LONDON OFFICE: 9 BERKELEY STREET, W.1. Tel.: Hyde Park 1711/2



QUANTUM MECHANICS

R.M. Sillitto F.Inst.P.

This book is an attempt to present quantum mechanics in a modern way, building up the formalism from a set of postulates which emerge naturally from a consideration of a few well-established results of experimental optics and atomic and electron physics

224 pp.

Demy 8vo

35s. net

EDINBURGH

University Press

AGENTS: NELSON

A.E.R.E. HARWELL

WANTAGE RESEARCH LABORATORY PHYSICISTS

with a **FIRST** or **GOOD SECOND CLASS HONOURS DEGREE**, are invited to join a team in the **TECHNOLOGICAL IRRADIATION GROUP** engaged in **RESEARCH** and **DEVELOPMENT** on **GAMMA RADIATION PROCESSING**.

The work involves chiefly the:

- ESTABLISHMENT OF DESIGN PRINCIPLES AND DATA FOR THE USE OF LARGE SCALE SOURCES OF RADIATION IN PLANTS OF DIVERSE APPLICATION.
- PRECISE MEASUREMENT OF A WIDE RANGE OF DOSE RATES BOTH IN EXPERIMENTAL AND ROUTINE INDUSTRIAL APPLICATIONS.

SALARY: £690-£1,500 p.a.

A minimum salary of £870 will be paid for those with 3 years' **POST GRADUATE TRAINING**.

Housing and superannuation schemes.

Please send **POST CARD** for details to the Group Recruitment Officer (1562/166), U.K.A.E.A., Atomic Energy Research Establishment, **HARWELL**, Didcot, Berks.

Recent

McGraw-Hill

Books

CARROLL: Industrial Instrument Servicing Handbook

For quick, easy reference, here are all the engineering data for modern industrial process measuring and control instruments. Over fifty types are explained in detail; for each one the handbook provides principles of operation, servicing, maintenance, and complete calibrating instructions.

£6 4s

LINDSAY: Mechanical Radiation

One of the *International Series in Pure and Applied Physics*, this new treatment of a subject of growing importance provides an introduction to wave motion, using mechanical radiation as the principal basis of discussion. The subject is presented in integrated form by bringing together a unified treatment of the most significant radiation aspects of acoustics. All important recent advances are covered, making the book as up-to-date as possible.

77s 6d

D'AZZO & HOUPIS: Control Systems Analysis and Synthesis

The unified approach and logical presentation of topics make this an ideal text for introductory courses in automatic feedback controls, at undergraduate and advanced technical college level. The authors present the fundamentals clearly and explicitly, in easily understandable sequence.

£5 4s 6d

MIDDLETON: An Introduction to Statistical Communication Theory

Written by one of the pioneers in the field, this book is a unified approach to the basic theory and advanced applications of random signals in communications. While the particular treatment deals mainly with electrical and electronic systems, the general methods described apply in other areas of communication. Also one of the *International Series in Pure and Applied Physics*, the book is the first new systematic approach to random noise theory.

£9 14s

McGraw-Hill Publishing Company Limited

McGraw-Hill House London EC4

NEW HEYWOOD BOOKS

FROM YOUR BOOKSELLER
OR THE PUBLISHERS

HEYWOOD & COMPANY LIMITED

Drury House, Russell Street
London, W.C.2.

MICROBIAL FLORA OF THE MOUTH

K. A. Bisset, B.Sc., Ph.D., D.Sc., and G. H. G. Davis, B.Sc., Ph.D.

This unique volume deals fully with the many groups of oral bacteria that are not comprehensively described elsewhere, and its purpose is to study the whole subject from the systematic viewpoint.

91 pages

22s. 6d.

PROGRESS IN INDUSTRIAL MICROBIOLOGY, VOL. II

Edited by D. J. D. Hockenfull, M.A., Ph.D., M.I.Biol.

This is an annual series for botanists, bacteriologists, biochemists, chemical engineers and mathematicians.

194 pages

45s.

PROGRESS IN NON-DESTRUCTIVE TESTING, VOL. II

Edited by E. G. Stanford, M.Sc., Ph.D., A.M.I.E.E., A. Inst. P. and J. H. Fearon, B.Sc., A.M.I.E.E.

An international series covering the six principal methods of flaw detection—visual examination, penetrant testing, magnetic testing, radiography, eddy-current testing and ultrasonic testing. Each subject will not necessarily be covered every year.

250 pages

55s.

PROGRESS IN CRYOGENICS, Volume II

Editor: K. Mendelssohn, D.Phil.(Berlin), M.A.(Oxon), F.Inst.P., F.R.S.

Edited by a vice-President of the Physical Society, this series of volumes covers the production, maintenance and measurement of low temperatures and their practical application to the techniques used in basic research.

280 pages

63s.

Chapman & Hall

Selected Books from our List

PHYSICS For Students of Science and Engineering

by

R. RESNICK & D. HALLIDAY

Professors of Physics at Rensselaer Polytechnic Institute and University of Pittsburgh, respectively)

A JOHN WILEY BOOK

This work aims to cater for a revision of the traditional course in general physics which the authors claim is called for by the current intimate connection between engineering practice and scientific research. The book reflects the new opinion of the role of physics in engineering education. The 'nuts and bolts' have been removed, but the fundamentals of classical physics have been stressed. The work is in two volumes, the first dealing with mechanics, wave motion, and heat, and the second with electro-magnetism, optics, and quantum physics. *48s. per volume*

MAGNESIUM AND ITS ALLOYS

by

C. SHELDON ROBERTS

(Fairchild Semiconductor Corporation)

A JOHN WILEY BOOK

This concise and thorough presentation of the latest theory and practice concerning this important and interesting metal will be of great value to physicists, chemists, and others interested in solid materials. The extraction, refining, and casting of the metal as well as its chemical and physical properties are considered in detail. *72s.*



INSTITUTE OF PHYSICS BOOKS

Ready this month:

A PHYSICS ANTHOLOGY

Edited by **NORMAN CLARKE**

A compilation of articles of wide interest contributed to the Institute of Physics' *Bulletin* over the past few years, now made available in volume form to a wider public. *35s.*

Just Published:

MECHANICAL DESIGN OF LABORATORY APPARATUS

By **H. J. J. BRADDICK**

The latest addition to the Series of Monographs for Students. *6s.*

Again available:

X-RAY DIFFRACTION By Polycrystalline Materials

General Editors:

**H. S. PEISER; H. P. ROOKSBY;
A. J. C. WILSON**

This comprehensive account of the special, and practically important, methods of investigating crystals in powdered or polycrystalline condition has now been reprinted with certain revisions to the text. *75s.*

37 Essex Street, London, W.C.2.

New Books

PROGRESS IN AUTOMATION

Edited by Dr. **ANDREW D. BOOTH**, *University of London.*

This first volume of the Series is devoted to eleven papers from leading British experts in the field of mechanical automation. Their writings form a record of the considerable achievements made in Great Britain on devices for industrial control.

Following a brief historical introduction to the subject, the contributors present a thorough examination of some of the fundamental techniques and treat in detail a number of automatic systems. The book includes a chapter on the implications of automatic inspection, a matter which is of considerable importance in a number of industrial fields at the present time.

Price 45s.

IONIZATION PHENOMENA IN GASES

By Dr. **GORDON FRANCIS**, *formerly of the Clarendon Laboratory, Oxford, and now at U.K. Atomic Energy Research Establishment, Harwell.*

This book is intended to be complementary to the several textbooks on ionized gases published in recent years. For this reason Dr. Francis has avoided repeating accounts of the more well-known discharges—the arc, spark and glow, for example—and has treated instead those branches of the subject which are closely linked with other branches of physics, and which cannot be studied except by intensive searching through the literature. Thus in atmospheric phenomena one finds links with astrophysics, high-frequency discharges and radio wave propagation; and in high-current discharges with nuclear physics and electrodynamics. A brief chapter on fundamental processes is included to provide a general background for the reader who is not very familiar with the subject.

The book is written mainly for those finishing their degrees at University, or about to begin research, in the hope that they may see a broader picture than is often revealed by specialized and sharply divided curricula. The author lays stress on the physical principles of the behaviour of ionized media, sometimes at the expense of mathematical rigour, and includes up-to-date discoveries and ideas, where these have some notable physical importance. Selected parts of current thermonuclear research have been included and here again, an understanding of physical principles has been the aim.

Price 60s.

HYPERSONIC FLOW

Edited by Professor **A. R. COLLAR** and Dr. **J. TINKLER.**

The study of hypersonic flow is a relatively new field of enquiry, greatly stimulated by the remarkable achievements in rocket propulsion of the past few years. This book offers something to all those interested in the subject of hypersonics, whether they are already actively engaged in it, or whether they wish to extend their knowledge of subsonic and supersonic aerodynamics to include the special characteristics of flow at very high speeds. There is also much material concerning the properties of gases at high temperatures which will be of interest to physicists.

The volume is a record of the 1959 Colston Symposium held at Bristol. The scope of the papers presented comprises surveys and details of experimental facilities, techniques for stimulating hypersonic flight conditions in the laboratory, experimental results, investigation of the properties of gases at elevated temperatures, theoretical solutions of particular flow problems including unsteady flow, and applied research in the form of studies of configuration, propulsion, and kinetic heating of vehicles designed for hypersonic flight.

Price 70s.

Descriptive literature available, post free, from

BUTTERWORTHS SCIENTIFIC PUBLICATIONS

4 & 5 Bell Yard, London WC2

INTRODUCING A MOST IMPORTANT AND AUTHORITATIVE NEW ENCYCLOPEDIA

THE INTERNATIONAL ENCYCLOPEDIA OF PHYSICAL CHEMISTRY AND CHEMICAL PHYSICS

Editors-in-Chief

E. A. GUGGENHEIM, Reading

J. E. MAYER, California, La Jolla

F. C. TOMPKINS, Imperial College, London

Chairman of the Editorial Advisory Group:

I. R. MAXWELL, Publisher at Pergamon Press

The *International Encyclopedia of Physical Chemistry and Chemical Physics* is to be an authoritative and comprehensive presentation of the domain of knowledge which lies between and overlaps chemistry and physics. Each volume—between 50 and 100 volumes are now planned—will be written primarily for the physical chemist and chemical physicist but many volumes will be of value to other scientists: to chemists and physicists generally and also to biochemists and biophysicists. Experimental details of an essentially practical nature are not emphasized in the Encyclopedia, but a thorough background of the theoretical aspect of techniques is included so that these may be understood and applied to the fullest extent.

The Editors-in-Chief have arranged the subjects to be included in the Encyclopedia in twenty-two topics. These groups were chosen to establish continuity and coherence within the Encyclopedia so that the relationship of each volume to the others is manifest. Each volume is restricted to about 200 pages as each has a large measure of independence and may be purchased separately without reference to other books in the series.

The Encyclopedia is international in character and will be produced to the highest professional and editorial standards. It is written in English as this is the language understood, if not spoken, by the greatest number of scientists.

When complete the Encyclopedia will be a compendium and synthesis of physical chemistry and chemical physics as these subjects stand at mid-century. It will be a landmark in scientific publishing and will be used for many years by scientists, university teachers and students.

Members of the Honorary Editorial Advisory Board

J. N. Agar, Cambridge
R. M. Barrer, London
C. E. H. Bawn, Liverpool
N. S. Bayliss, Western Australia
R. P. Bell, Oxford
C. J. F. Böttcher, Leiden
F. P. Bowden, Cambridge
G. M. Burnett, Aberdeen
J. A. V. Butler, London
C. A. Coulson, Oxford
J. S. Courtney-Pratt, Cambridge
D. P. Craig, London
F. S. Dainton, Leeds
C. W. Davies, London
B. V. Derjaguin, Moscow
M. J. S. Dewar, Chicago
G. Duyckaerts, Liège
D. D. Eley, Nottingham
H. Eyring, Utah
P. J. Flory, Mellon Institute
R. M. Fuoss, Yale
P. A. Giguère, Laval

W. Groth, Bonn
J. Guéron, Paris
C. Kemball, Queen's, Belfast
J. A. A. Ketelaar, Amsterdam
G. B. Kistiakowsky, Harvard
H. C. Longuet-Higgins, Cambridge
R. C. Lord, Massachusetts Institute of Technology
M. Magat, Paris
R. Mecke, Freiburg
Sir Harry Melville, D.S.I.R., London
S. Mizushima, Tokyo
J. A. Morrison, N.R.C., Ottawa
R. S. Mulliken, Chicago
R. G. W. Norrish, Cambridge
R. S. Nyholm, London
J. T. G. Overbeek, Utrecht
K. S. Pitzer, California, (Berkeley)
John R. Platt, Chicago
George Porter, Sheffield
I. Prigogine, Brussels (Free University)
R. E. Richards, Oxford

Sir Eric Rideal, London
J. Monteath Robertson, Glasgow
E. G. Rochow, Harvard
G. Scatchard, Massachusetts Institute of Technology
Glenn T. Seaborg, California (Berkeley)
N. Sheppard, Cambridge
R. Smoluchowski, Carnegie Institute of Technology
H. Stammreich, Sao Paulo
E. W. R. Steacie, N.R.C., Ottawa
Sir Hugh Taylor, Princeton
H. G. Thode, McMaster
H. W. Thompson, Oxford
D. Turnbull, G. E., Schenectady
A. R. J. P. Ubbelohde, London
H. C. Urey, California (La Jolla)
E. J. W. Verwey, Phillips, Eindhoven
B. Vodar, Laboratoire de Bellevue, France
M. Kent Wilson, Tufts
W. F. K. Wynne-Jones, King's College, Newcastle-upon-Tyne



PERGAMON PRESS

OXFORD

Headington Hill Hall, Oxford

4 & 5

AL CHEMISTRY AND CHEMICAL PHYSICS

Nearly 100 volumes will be published (with the assistance of a distinguished board of responsible editors), grouped in the following topics . . .

1 MATHEMATICAL TECHNIQUES

Editor: H. Jones

2 CLASSICAL AND QUANTUM MECHANICS

Editor: Per-Olof Löwdin

3 ELECTRONIC STRUCTURE OF ATOMS

Editor: Clyde Hutchison, Jr.

4 MOLECULAR BINDING

Editor being appointed

5 MOLECULAR PROPERTIES

(a) Electronic
(b) Non-Electronic
Editors being appointed

6 KINETIC THEORY OF GASES

Editor: E. A. Guggenheim

7 CLASSICAL THERMODYNAMICS

Editor: D. H. Everett

8 STATISTICAL MECHANICS

Editor: J. E. Mayer

9 TRANSPORT PHENOMENA

Editor: J. E. Mayer

10 THE FLUID STATE

Editor: J. S. Rowlinson

11 THE IDEAL CRYSTALLINE STATE

Editor: M. Blackman

12 IMPERFECTIONS IN SOLIDS

Editor: A. B. Lidiard

13 MIXTURES, SOLUTIONS, CHEMICAL AND PHASE EQUILIBRIA

Editor: M. L. McGlashan

14 PROPERTIES OF INTERFACES

Editor: D. H. Everett

15 EQUILIBRIUM PROPERTIES OF ELECTROLYTE SOLUTIONS

Editor: R. A. Robinson

16 TRANSPORT PROPERTIES OF ELECTROLYTES

Editor: R. H. Stokes

17 MACROMOLECULES

Editor: C. E. H. Bawn

18 DIELECTRIC AND MAGNETIC PROPERTIES

Editor: Willard Stout

19 GAS KINETICS

Editor: A. F. Trotman-Dickenson

20 SOLUTION KINETICS

Editor: R. M. Noyes

21 SOLID AND SURFACE KINETICS

Editor: F. C. Tompkins

22 RADIATION CHEMISTRY

Editor: Robert Livingston

Topic 6 KINETIC THEORY OF GASES

Editor: E. A. Guggenheim

Just published

Volume I

ELEMENTS OF THE KINETIC THEORY OF GASES

by E. A. Guggenheim, M.A., Sc.D., F.R.S.

This volume describes in an elementary way the most important features of the kinetic theory of gases, and as such will prove most useful to physical chemists and chemical physicists who would not normally have a standard of mathematics necessary for the more advanced treatments.

The author is known for his researches and several books on thermodynamics and related matters, but this is his first book on non-equilibrium properties.

17s. 6d. (\$3.00)

Write now for full details of this outstanding series

LONDON

NEW YORK

NATIONAL PHYSICAL LABORATORY, (D.S.I.R.), Teddington, Middlesex, requires Scientific/Senior Scientific Officers: **Standards Division**. Two Physicists or Electrical Engineers (Ref. A42/9A) for work on atomic frequency standards and accurate determination of atomic constants including the gyromagnetic ratio of proton and ratio of charge to mass of elementary particles. Research experience in experimental atomic physics desirable. **Applied Physics Division**, for work on radio-carbon dating. Experience in physical chemistry, radio-chemistry or low level counting an advantage. (Ref. F365/0A). **Quals.**:—1st or 2nd Class Hons. degree or equiv. (Minimum 3 years post-graduate experience for S.S.O.). **Salary ranges**:—(Men) S.O. £655–£1,150. S.S.O. £1,233–£1,460. Forms from Ministry of Labour, Technical and Scientific Register (K), 26 King Street, London, S.W.1, quoting appropriate reference.

UNITED NATIONS

The INTERNATIONAL ATOMIC ENERGY AGENCY seeks highly qualified experts for Technical Assistance appointments overseas as below:

Radiobiology: Argentina, 1 year.

Health Physics: Persia, 6 months.

Medical applications of radioisotopes; Argentina, 1 year.

Agricultural applications of radioisotopes; Vietnam, 1 year.

Other posts may be notified later.

Salaries range between £260 and £298 (approx.) per month, plus generous allowances. All emoluments tax-free. For job descriptions and application forms write **URGENTLY** to Ministry of Labour, 26–28 King St., London, S.W.1, quoting E9/AEA/7 and stating post(s) applied for.

THE INSTITUTE OF PHYSICS

has recently published

a revised edition

of

Notes for Authors

THIS booklet is intended to assist less-experienced authors and to serve as a reference booklet for all those who wish to contribute to the Institute's publications. It gives hints on the preparation of scripts and diagrams, on the layout of mathematics, the correction of proofs and so on. In addition to a bibliography of reference books and works on technical writing, the pamphlet also contains lists of the spellings, symbols and abbreviations used by the Institute.

AUTHORS preparing contributions for submission to the *British Journal of Applied Physics*, the *Journal of Scientific Instruments*, or other Institute publications, are invited to make use of the guidance available in the booklet.

Copies are obtainable from

THE INSTITUTE OF PHYSICS

47 BELGRAVE SQUARE

LONDON, S.W.1

PRICE 3s. 6d.

out this month

Methods of solving complicated problems to derive the fullest advantage from modern computers

Numerical methods for high speed computers

G. N. Lance, M.Sc., Ph.D., M.I.A.S., AFR. A.E. S.

Collects those methods of solving complicated problems which have been fully developed by research mathematicians to make the fullest possible use of all types of modern automatic high speed computing machines. This book will prove invaluable to programmers, mathematicians, engineers, physicists, chemists and scientists generally who are interested in the application of electronic computers to the solution of their own particular problems.

42s. net by post 42s. 11d. 176 pp.

from leading booksellers

Published for DATA PROCESSING by

Iliffe & Sons Ltd., Dorset House, Stamford Street, London, S.E.1.

Scientific Papers, II

SIR GEOFFREY TAYLOR

The second volume of the *Scientific Papers*, edited by DR G. K. BATCHELOR, is the first of three to be devoted to work mainly on the mechanics of fluids. It contains papers on meteorology, oceanography and turbulent flow.

75s. net

Radar Meteorology

LOUIS J. BATTAN

A complete guide to the use of radar for studying and forecasting weather, by the Professor of Meteorology at the University of Arizona. 77 text-figures; 15 tables.

UNIVERSITY OF CHICAGO PRESS 45s. net

CAMBRIDGE
UNIVERSITY PRESS



R. OLDENBOURG VERLAG

Regelungstechnik und Nachrichtenverarbeitung

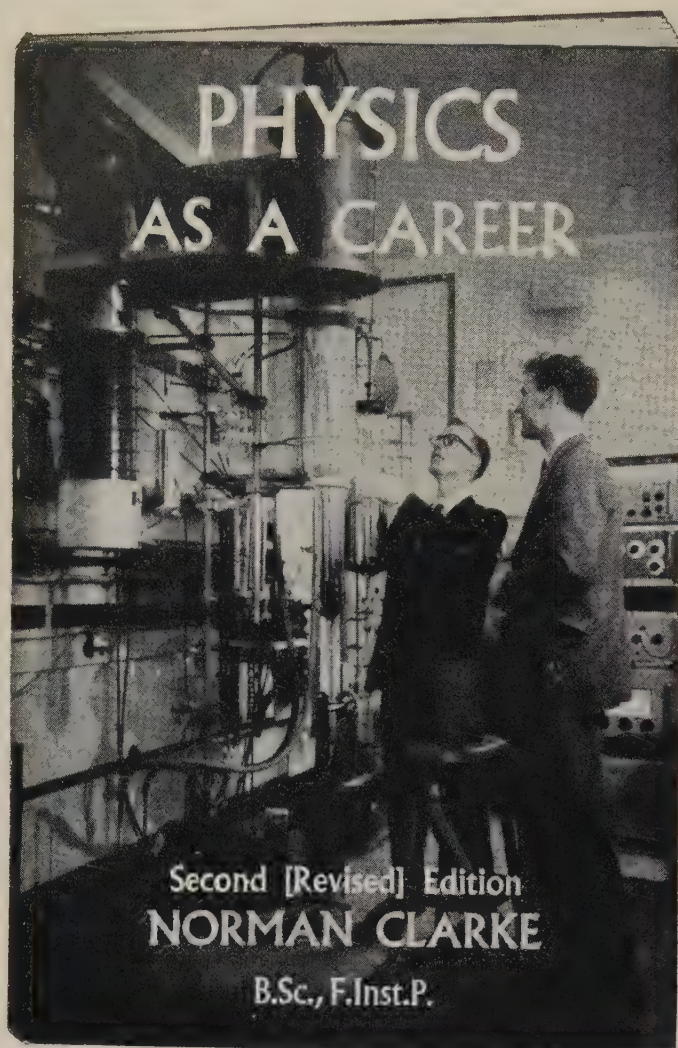
Die Anfänge der Regelungstechnik liegen noch nicht lange zurück. Das erste Oldenbourg-Buch aus diesem Gebiet—zugleich eine der ersten deutschen Arbeiten zur Regelungstechnik überhaupt—erschien 1930, das zweite 1944.

Seitdem ist das neue Literaturgebiet bei Oldenbourg systematisch bearbeitet worden. Neben den Arbeiten deutscher Fachleute erschienen Übersetzungen aus dem Russischen, Amerikanischen und Französischen. 1953 wurde die Zeitschrift "Regelungstechnik" begründet; als Ergänzung für den Betriebsingenieur folgte 1959 die Zeitschrift "Regelungstechnische Praxis". Auch die Veröffentlichung der Ergebnisse deutscher und internationaler Fachtagungen wurde dem Verlag R. Oldenbourg anvertraut.

Aus dieser intensiven Beschäftigung mit der Literatur über selbsttätige Regelungen und aus langjähriger Erfahrung mit Veröffentlichungen zur Fernmeldetechnik ergab sich für den Verlag bald die Notwendigkeit, auch dem neuen Gebiet der Nachrichtenverarbeitung in Technik, Wissenschaft, Wirtschaft und Verwaltung besondere Aufmerksamkeit zu widmen. Seit 1959 erscheint daher die Zeitschrift "Elektronische Rechanlagen". Ausserdem konnte bereits eine Anzahl entsprechender Werke veröffentlicht oder angekündigt werden.

Ein zwölfseitiges Verzeichnis "Regelungstechnik und Nachrichtenverarbeitung" steht zur Verfügung.

Write to: **R. Oldenbourg Rosenheimer Str. 145,
München 8 Germany**



Published for The Institute of Physics by

CHAPMAN & HALL LTD.
37 Essex Street, London, W.C.2

Retail price 8s. 6d.

Price to Members of the Institute, 6s. 6d. including postage.

Obtainable through any bookseller; Members of The Institute of Physics should obtain their copies from the Institute and remittances should accompany orders.

SOME PRESS COMMENTS:

"This admirable little book . . . does more than indicate the nature and prospects of the great variety of posts open to qualified physicists . . . it contains much sound advice relating to the training of a physicist and to his subsequent professional activities."

Times Educational Supplement.

"The book should prove excellent for students whilst every schoolmaster, who has at any time to advise a pupil, should have one."

Machinery Lloyd.

"Well-written and authoritative little book . . . a most useful survey of physics as a career . . . every grammar and public school with a science side will need it."

The School Librarian.

". . . a clear, concise and well written account of the fields of work open to those who intend to enter the profession of physics and the remuneration to be expected."

*Journal of the
Royal Institute of Chemistry.*

"invaluable." *Education.*

"contains a great deal of practical information and advice . . . other professional bodies would do well to commission surveys of a similar kind."

Glasgow Herald.

"well written and well illustrated. . . . There should be a copy in every school library in Britain."

Boys' Own Paper.

machine design are frequently used in the physical laboratory, they do not usually appear in the education of the physicist and may involve a technical vocabulary unfamiliar to him. Some space, therefore, is devoted to such matters as the influence of design on the ease of construction, and the use and interconnection of sub-assemblies.

The "Monographs for Students" series is intended for general reading for students in courses for Higher National Certificate in Applied Physics. It will also be found useful in the first two years of a degree course.

Radio stations: installation, design and practice. By G. A. CHAPPEL. (Oxford: Pergamon Press Ltd., 1959.) Pp. viii + 248. Price 50s.

This book helps to fill what has hitherto been a gap in the literature of radio engineering—the installation of equipment. Broadly speaking, it deals with all apparatus other than actual transmitters and receivers, and although the author uses the word "design" in the title, it is only in a limited sense, with respect to ancillary though often essential apparatus.

There are chapters on Station sites; Buildings; Masts and towers; Transmission lines; Aerial systems; Transmission line switching systems; Earth systems; Station wiring, control wiring and power supply; Control units; Equipment racks; and Message distribution systems. All these things are of real importance to the engineer on a station site, but in many cases are omitted from text books.

The book is written from a very practical point of view, and the author is to be congratulated on producing a work that will be useful to many engineers who are responsible for the day-to-day running of stations. Much of the information can provide guidance as to procedure under conditions of emergency, or modification. There will, of course, inevitably be some divergence between the author's statements and the views of particular firms regarding their equipment, but this does not detract from the book.

It might have been pointed out in a few places, that such matters as the rigging of large aerial systems, or the planning of complex control units, are really the work of specialists, but this omission does not spoil a very useful book.

J. H. JUPE

The Robertson guide to world screw thread standards. (Bedford: W. H. A. Robertson and Co. Ltd., 1959.) Pp. 41. Price 10s.

The primary object of this guide is to aid those who are interested in the production or supply of screw threads to national standards with which they are not familiar. Over 2000 Standards are listed from the 33 countries which have published their own National Standards for screw threads. In addition, 108 screw thread forms are illustrated together with self-tapping screws.

Rocket propulsion. By M. BARRÈRE, A. JAUMOTTE, B. F. DE VEUBEKE and J. VANDENKERKHOVE. (London: D. Van Nostrand Co. Ltd., 1959.) Pp. xxxi + 829. Price £6 15s. 0d.

This is a greatly enlarged version of a book published in France and Belgium in 1956. The great increase in the unclassified literature since that time has been integrated into the text by a complete rewriting, and by sharing the work among four authors the book has been published with only a short time-lag. The literature is covered down to the autumn of 1958,

and moreover has actually been digested and incorporated into a systematic body of knowledge.

The book can be used by mathematicians, physicists and engineers as a survey of the whole field of rocket engines and fuels, liquid and solid, or as an introduction to some particular problem. The mathematics is kept simple, and is used freely for exposition of principles and to draw semiquantitative conclusions. References are given to more detailed papers, and their results are often given as graphs.

The book could also form a design manual for engineers. Worked examples are given in the text, and there are many useful tables of propellant and nozzle properties. Permanent principles emerge as clearly as present-day methods.

M. Barrère has contributed the chapters on general relations, the calculation of combustion products and their thermodynamic properties, test stands and physical measurements, and, as regards liquid propellants, the chapters on motor design, combustion instabilities, and the main properties of various propellants. M. Vandenberghe has written three chapters on solid propellant properties, the internal ballistics of the engine, design methods for choosing the best motor for a given application, and (with M. Jaumotte) a chapter on nozzle theory. M. de Veubeke has written two chapters on the trajectories of long-range rockets and satellite launchers, and on methods for optimizing vehicle performance. This is the part which is likely to be most quickly outdated.

This is an excellent book for the purposes mentioned above. Its price may seem high, but it is, in fact, the cheapest way to get all this information.

J. CORNER

Scientific Russian. By G. CONDOYANNIS. (New York: John Wiley and Sons, Inc.; London: Chapman and Hall Ltd., 1959.) Pp. xii + 225. Price 28s.

This is a most useful little book. For this reason, it is worth while to raise a number of points which might be improved for future editions.

As there is no vocabulary, all but the simplest "practice passages" might be omitted, since the student might as well work through a short paper in a scientific journal with his dictionary. In the space so saved, it would be advantageous to include a list of standardized transliterations of the Russian characters now almost universally accepted in Britain and U.S.A. Though phonetically inferior to those suitable for teaching, their use makes it possible for any Russian word or name to be correctly re-converted into Cyrillic characters. A small but important improvement would be, in the "teaching" transliterations, to conform to the common practice of using an apostrophe for the "soft mark" rather than a comma, which can be misleading. Also Cyrillic italics are sufficiently different to require their inclusion as a separate column in the table of letters: the novice will not recognize all of them.

It remains to be seen whether the tenuous binding will be sufficiently durable. Perhaps it is hoped that, by the time the book falls to pieces, the student will no longer need it! A number of misprints in the Russian also require attention.

G. W. SCOTT BLAIR

Studies in crystal physics. By M. A. JASWON. (London: Butterworths Scientific Publications Ltd., 1959.) Pp. 42. Price 10s. 6d.

This booklet contains 5 papers on crystal physics reprinted from *Research* (11, 1958). Each paper touches upon a different topic but all are concerned with physical effects related primarily to the crystal structure rather than to the

specific kind of atom involved. The fifth paper provides the thermodynamic background. The titles of the papers are as follows: Some properties of crystal lattices; Imperfections in nearly perfect crystals; X-ray diffraction by imperfect crystals; The martensite phase change in metals; The thermodynamic behaviour of solids.

Nuclear and cosmic-ray physics, apparatus, techniques and data

Atlas of γ -ray spectra from radiative capture of thermal neutrons. By L. V. GROSHEV, A. M. DEMIDOV, V. N. LUTSENKO and V. I. PELEKHOV. (Translated from the Russian by J. B. SYKES. (Oxford: Pergamon Press Ltd., 1959.) Pp. 198. Price £7.

The spectra of γ -rays from the capture of thermal neutrons are so complex that this compilation of experimental data on the subject will be a very useful reference book. Detailed spectra are given for capture by 60 elements. In most cases the spectra are those obtained by the authors using a magnetic Compton spectrometer, but where these are not available the results of other experiments are used. All the experimental work on each element is summarized in tables of γ -ray energies and intensities which reveal a satisfactory pattern of agreement between the results from various laboratories. Energy level diagrams are used to indicate the relation between the thermal capture results and other nuclear data measurements. Also included is a table of cross sections, binding energies, nuclear spins, etc., which are needed to interpret the γ -ray spectra with an extensive list of references.

The use of photographic reproduction gives a quality which is, in general, better than in the Russian original although the occasional distortions which the latter contains are thus included. The atlas has been produced with commendable speed but with an unfortunate sacrifice in terms of price.

J. R. BIRD

International conference on high-energy accelerators and instrumentation—CERN 1959. Edited by L. KOWARSKI. (Geneva: CERN European Organization for Nuclear Research, 1959. Pp. xvii + 721. Price Sw.Fr.50.

This volume contains the proceedings of a conference held in Geneva in September 1959 and sponsored by The International Union of Pure and Applied Physics (IUPAP).

The conference was divided into 11 sessions, the titles of which were as follows: Session 1—The need for new particle accelerators; Session 2A—Advances in high-energy particle accelerators; Session 2B—Advances in high-energy particle accelerators; Session 3—Fundamental limitations in accelerators; Session 3A—Status reports on high-energy accelerators; Session 4—Production, transport and separation of particles from high-energy machines; Session 5A—Large hydrogen bubble chambers; Session 5A—(parallel)—Radio electronics for accelerators; Session 5B—Propane and other heavy liquid chambers; Session 6—Picture evaluation for track chambers; Session 7—Counters and other high-energy particle detectors.

The theory of elementary particles. By J. HAMILTON (Oxford: Clarendon Press; London: Oxford University Press, 1959.) Pp. ix + 482. Price 75s.

There are at present sixteen elementary particles in physics. Of these, fourteen are expected to have anti-particles different

from themselves and nine of these have so far been identified experimentally. This total of thirty has remained unchanged for several years, so that physicists have been able to concentrate their efforts on an explanation of the properties of these particles. The similar problem with regard to the chemical elements was solved through the discovery of the proton and the electron and their role in atomic structure. It should be realised that the mere fact that we can see certain regularities and relationships between the elementary particles implies that we refuse to treat them as elementary, but rather look for something more elementary—or perhaps more fundamental—behind and beyond them. Present indications are that this something is not an even more elementary particle, but is to be found among the invariance and symmetry properties of the space-time continuum and of abstruse mathematical spaces such as isotopic space and perhaps others. The search for mathematical spaces is replacing the search for elementary particles.

But as yet we know far too little of these particles that we call elementary, to pursue this programme to its successful conclusion, and, at any rate, for the calculations of detailed properties such as transition probabilities and lifetimes we require more than a knowledge of symmetry properties. There is, therefore, another side to the investigation of elementary particles, based on the quantization of fields of which these particles are quanta. Work along these lines dates back some thirty years, but it is only in the last fifteen that powerful new methods have been devised to overcome some of the mathematical difficulties. Many others remain.

This book is a most thorough and competent guide through all the trials and dangers of both these branches of theoretical elementary particle physics. It is clearly the author's expectation that the reader—I almost said "the pilgrim"—is fore-armed with the necessary mathematical and physical armoury without which the task could not be accomplished, but in return he fully explains how the weapons should be used. This is not, therefore, a book for the experimental man who wants to know what the theoreticians are up to, but for the theoretician who wants to practice in the field. As such the book is excellent and will become quite indispensable.

The work opens with a masterly condensation of the classical background material and then proceeds to the quantization of boson and fermion fields. Perturbation theory is treated by means of the S-matrix, and the more recent developments, which do not depend on perturbation theory and are associated largely with the names of Chew and Low, follow, together with a treatment of dispersion relations. Selection rules are mentioned throughout, but are treated fully, together with the invariance properties connected with parity, time reversal and charge conjugation, in a separate chapter. The book ends with chapters on polarized beams and on the foundations of field quantization through the action principle. There is a most useful appendix on Green's functions and a table of elementary particles which is not yet out of date.

The author never forgets that the purpose of physical theory is to give an account of experimental facts and it is refreshing to find graphs of experimental scattering cross-sections sandwiched between lengthy formulae. (Symptomatic of this approach are the last two chapters, one of which deals with the mathematics that has been developed for the analysis of certain experiments, while the other merely adds beauty to an otherwise satisfactory theoretical edifice.) Some of the more difficult concepts are illuminated by means of classical analogies which students new to the subject will find most helpful. Thus, for instance, field quantization is preceded by an account of the vibrating membrane and dispersion

relations are introduced through their application to the optical refractive index.

This is an important book, because it brings the reader up to date in an important field of physics in which techniques are changing constantly and rapidly. It is a difficult and lengthy book, but so is the subject it treats. It is in fact so long, that it is easy to lose the main trend of the argument in the mass of detail. And yet it is not long enough, for the author has found it necessary to bring in a large number of asides in the shape of brief footnotes (at a rate of approximately two per page!) which often do no more than point to a difficulty, leaving the reader to find his own solution.

The beautiful mathematical type setting of the Oxford University Press is a great aid to ease of reading. But is it not time the Press abandoned its archaic system of referencing, with its *ibid.*, *op. cit.* and footnote symbols? There are ten of these on p. 335!

L. R. B. ELTON

Photography, microscopy and optics

Der Raman-Effekt. By F. MATOSI. (Braunschweig: Friedr. Vieweg und Sohn; 1959.) Pp. 84. Price DM 10.80.

This little book is the second edition of the seventh number to appear in the series "Verfahrens und Messkunde der Naturwissenschaft". The latest references quoted are dated 1958. The author has worked extensively in the infra-red as well as in this field. It is an excellent summary of the theory, practice, and applications of the Effect.

A. C. MENZIES

Elektronenmikroskopische Untersuchungs- und Präparationsmethoden. By L. REIMER. (Berlin: Springer Verlag, 1959.) Pp. viii + 300. Price DM 58.

Electron microscopy, more than most other specialized techniques, involves a wide range of preparative and operational methods. One of the first activities of the Electron Microscopy Group of The Institute of Physics was to arrange for the compilation of a handbook of the methods as then known, under the editorship of Dr. D. G. Drummond. It was published in 1950 by the Royal Microscopical Society, under the title of *The Practice of Electron Microscopy*, and was at once recognized as the standard authority. Despite the rapid advances made since then, in both specimen techniques and in the design and operation of the microscope, no other work has appeared of the same nature. The need for an up-to-date treatment has now been met by a German author, in a text of rather more than twice the length of "Drummond". It gives more attention than the latter to the fundamental processes of imaging with electron lenses and the interaction of electrons with matter—scattering, energy loss, diffraction, interference. The first half of the book is devoted to these topics and to operational techniques, including determination of magnification and resolution, correcting astigmatism, dark field and stereo-microscopy, and micro-diffraction. The second half describes the various methods of preparing and mounting the specimen, including modern methods of thin section cutting. On the whole, more space is devoted to biological than to inorganic and metallurgical procedures, the impact of the new techniques for preparing very thin metal foils probably being too recent for inclusion; only two pages are devoted to this topic. Otherwise, the author has included most of the significant work published up

to the end of 1958, and some from early 1959. Each of the 22 chapters ends with a short selection of references for further reading, and at the end of the text there is a fairly comprehensive list of suppliers of materials and apparatus. The text is clearly written, well produced and illustrated with 135 line diagrams. There is also a half-tone supplement of 20 plates, comprising some 50 separate illustrations of typical electron micrographs. These will be a great help to those new to the subject, as standards of what is attainable by modern methods.

Altogether, the author has succeeded in his aim of providing a comprehensive survey of the subject in a text of convenient length. Inevitably there is some unevenness of treatment where so wide a range of topics has to be covered; the alternative of collecting a group of experts to write each on his own subject, as Drummond did, would in these days require a volume of twice the length for authoritative coverage. Such a massive "Handbuch" may still come, but in the meantime the present work will prove invaluable to old hands and newcomers alike.

V. E. COSSLETT

Photomicrography. 2nd ed. By R. M. ALLEN. (New York: D. van Nostrand Co. Inc.; London: D. van Nostrand Co. Ltd., 1958.) Pp. xiii + 441. Price 67s. 6d.

There are few good books, in spite of numerous attempts, on the use of the microscope and still fewer on the special art of photographing through it. Dr. Allen's book, in its original edition, has long been recognized as one of the best and now, brought up to date after an interval of 17 years, it must rank as the most complete treatment available. One of its principal merits is the operational approach of the author, who has clearly had first-hand experience of a wide variety of types of modern equipment. The basic principles of the optical microscope are set out in the first chapter, and those of phase and interference microscopy in a later one, but most of the text is concerned with the description of microscopes and the way to get the best results with them. There is also an interesting and unusual chapter on home-made equipment, which will be of special help to small laboratories and to the amateurs of microscopy, who are still legion. The author interprets his title in the proper sense of photography through the microscope, but includes also a chapter on microphotography, in view of the growing interest in recording information in ultra-small format. There is in addition a short chapter on the electron microscope which, however, hardly does justice either to the instrument or to its applications. Here, as also in one or two other sections such as that on ultra-violet microscopy, the reader would welcome a list of references for further reading.

In all the techniques of optical microscopy there is a remarkably full treatment, illustrated with many line diagrams, photographs of apparatus and micrographs, which show what to avoid as well as what to aim at. There is also a compilation of practical techniques and formulas for dark-room work covering all relevant aspects of photography. Not least, the book ends with a selection of 54 photomicrographs, at magnifications ranging from $4\times$ to $4500\times$ (see p. 232). Many of these are works of art in their own right, as well as illustrating different practical problems of microscopy; full exposure details are given with each. Only a lifetime spent in the subject, and a deep affection for it, could have produced such a comprehensive account. The book can be recommended to all involved in the practice of microscopy, and particularly to that great majority who have had to pick

up the subject as they went along, in the absence of a reliable handbook. Here is what we have been looking for, and the author is to be congratulated on meeting this long-felt need.

V. E. COSSLETT

Theoretical physics, mathematical techniques, computers and control systems

Grundlagen der selbsttätigen Regelung. Band 1. By W. W. SOLODOVNIKOV. (München: R. Oldenbourg Verlag, 1959.) Pp. xvi + 727. Price DM 65.

This is Volume 1 of a German translation of the book *Foundations of automatic regulation* published under the editorship of Prof. Solodovnikov in Russian in 1954. It is a large book (over 1100 pages in the Russian edition) giving a systematic presentation of the whole of automatic regulation theory. It has two parts: Part 1 is on linear systems and Part 2 on nonlinear systems. Volume 1 of the German translation corresponds to Part 1 and is subtitled *General foundations of the theory of linear automatic regulation systems*. Its principal sections are entitled:— (i) Generalities, differential equations, transfer and impulse response functions of regulation systems; (ii) Stability analysis of systems of automatic regulation; (iii) Analysis of quality and synthesis of correcting elements of systems of automatic regulation. Foundations of the theory of impulse regulation; (iv) Some problems of analysis and synthesis of regulation systems with random inputs.

The book has been written collectively by 19 specialists who are leaders in the Soviet school of automatic control. As a result, each part of the book is written by a person who is extremely well qualified on that subject.

The aim of the book, as gathered from the preface is to give an account of the basic methods of the theory of automatic regulation and at the same time to present the subject as a whole, clarifying its present status. This itself is of interest. However, the book also provides the theoretical basis of two further volumes which will deal with contemporary practice in automatic regulation.

At each stage, the essentials of the theory are presented in an exceptionally clear and balanced way without unnecessary details. Well-known ideas are given new interest by their precise formulation.

In the reviewer's opinion, this is a most important book, especially as it is, to his knowledge, the first general book on the Soviet approach to regulation theory available to the person who cannot read Russian. The Soviet work has only recently begun to attract notice in this country and this book is one indication of the high level it has achieved. The book could easily be made the basis of an advanced course in regulation theory.

J. F. BARRETT

Introduction to the theory of quantized fields. By N. N. BOGOLIUBOV and D. V. SHIRKOV. Translated from the Russian by G. M. VOLKOFF. (New York: Interscience Publishers, Inc.; London: Interscience Publishers Ltd., 1959.) Pp. xvi + 720. Price £6 8s. 0d.

This book will undoubtedly establish itself as one of the most important text books of the quantum theory of fields. This theory is probably the most advanced part of present day theoretical physics, advanced not only in its subject matter—the description of the most elementary constituents of matter—but also in the mathematical techniques it employs.

In the classical period, problems of physics have repeatedly stimulated the development of entirely new fields of mathematics, but in the present century physical theory has, on the whole, received more than it has given to mathematics. For instance, general relativity was built on the already existing foundations of Riemannian geometry and quantum mechanics on the theory of linear operators which, unknown to most theoretical physicists, already existed in quite an advanced stage of mathematical development. In very recent times however, the position has again been reversed, as this book, very clearly demonstrates.

The quantum theory of fields as first developed gave rise to notorious mathematical inconsistencies; at the same time it was a theory of such complexity that it appeared difficult to disentangle real inconsistency from bad approximation. In the years since the war, however, great strides forward were made which clarified the basic structure of the theory and crystallized out the main mathematical problems. This process was accompanied by spectacular successes in physical prediction, at least within the limited field of quantum electrodynamics. One feature of the new techniques was the free use of "improper functions" (of which Dirac's δ -function is the simplest example, already familiar in quantum mechanics). To-day a sound mathematical theory of these functions (distributions) is well established, thanks to the work of L. Schwartz and S. L. Sobolev. The treatment of field theory under review takes full cognizance of the newly acquired understanding of these functions and, without being any more particular about details of mathematical rigour than one expects from an applied mathematical text, it presents the subject in a manner in which the effect of using improper functions is continually clearly demonstrated. The result is a novel presentation of the whole theory of "renormalization" which is probably more satisfactory than any previous text.

Whereas renormalization theory may by now be called a well-understood branch of field theory, there have been important new developments in other directions during the very last few years, to which the first author of this book has himself made most significant contributions. These new ideas (functional integration, the renormalization group, dispersion relations) are described here in the same spirit as the foregoing with much attention to the essential mathematical problems but without any pedantic pursuance of rigour. These later chapters will not only be a stimulus to research workers in field theory, but one hopes also to mathematicians, for the problems described—in a way, one feels, mathematicians will appreciate—could certainly suggest new developments in relatively little explored fields of mathematics.

The Russian original of this book was completed by the authors as late as February 1957 and it is greatly to the credit of Dr. Volkoff and Interscience Publishers to have made and issued a translation so soon. In the circumstances one may forgive the rather large number of small misprints in the text.

N. KEMMER

Manual of mathematical physics. By P. I. RICHARDS. (Oxford: Pergamon Press Ltd., 1959.) Pp. xi + 486. Price £5 10s.

"The goal of this book is to condense established theoretical physics, its applications and its mathematical equipment into a single reference volume of reasonable size". It is, perhaps, debatable what is the scope of the subject theoretical physics, and since Mr. Richards covers more in the way of mathemati-

cal equipment than one might at first expect, the first function of the reviewer should be to outline this scope. Mr. Richards divides his book into two parts entitled Physics and Mathematics respectively. In Part I his chapter headings are Mechanics, Thermodynamics, Electromagnetic Theory, Relativity, Quantum Mechanics and Statistical Physics, whilst in Part II they are Algebra, Differentiation and Integration, Infinite Series, Vector Analysis, Determinants and Matrices, Functions of a Complex Variable, Integral Transforms, Ordinary Differential Equations, Partial Differential Equations, Integral Equations, Variational Problems and Linear Programming, Spaces, Eigenvalue Problems and Perturbation Theory, Probability and Game Theory, Tensor analysis and Group Theory.

The scope is in my opinion unnecessarily ambitious. No one is going to tackle any branch of theoretical physics seriously unless he has a large portion of Part II, the more elementary aspects, in his grasp. In short my preference would have been for a Part I enhanced at the expense of Part II. One serious omission is the dearth of references to standard texts.

The style is so condensed throughout that I doubt if it is possible to learn about any subject in it *ab initio* but for providing a quick reminder of something one may have forgotten or imperfectly remembered there is nothing like it to my knowledge. Whether there is a demand for such a book is a different question; I myself have strong reservations but it would certainly have an advantage for anyone teaching theoretical physics on a desert island and limited to a library of one volume.

L. HOWARTH

Proceedings of the fifth annual computer application symposium. (Chicago: Armour Research Foundation of Illinois Institute of Technology, 1959.) Pp. x + 153. Price \$3.00.

The seven papers presented on the first day of this symposium, held in October, 1958, concerned the business and management applications of computers and the seven on the second day concerned engineering and scientific applications. These papers and the panel discussions on them are reproduced in this volume.

Statistical methods in radio wave propagation. Edited by W. C. HOFFMAN. (Oxford: Pergamon Press Ltd., 1960.) Pp. xiii + 334. Price 90s.

This volume contains the papers read at a symposium held in June, 1958 at the University of California.

The papers are classified mainly into two broad categories: (i) those dealing primarily with statistical theory and methodology and (ii) those papers which emphasize radio propagation phenomena having a joint statistical and physical structure. A third category of practical importance has been added and this is entitled "Instrumentation." A summary of the panel discussion on outstanding problems is contained in the preface, and a bibliography is included.

The theory of storage. By P. A. P. MORAN. (London: Methuen and Co. Ltd., 1959.) Pp. 111. Price 13s. 6d.

This is the first book to appear in the new Methuen series of

monographs on applied probability and statistics. A concise account is given of recent work, by the author and others, on a class of problem in which the input or output of a storage system is a random process and the corresponding output or input is determined by a rule. This problem arises in numerous practical situations such as the storage of water in a reservoir, in the first case, or the storage of stock in a warehouse, in the second case. The essential feature of the situation is the existence of a random element, so that it is necessary to use the theory of probability in the study of the behaviour of the system. An introductory chapter presents the essential mathematical background of probability theory. This is followed by three chapters on the mathematical formulation and methods of solution of simple examples of storage problems. Consideration is given to finite and infinite systems and to discrete and continuous variables. It is demonstrated that there is an analogy between the problems of reservoirs and of queues and that both are related, in a complementary manner, to warehouse problems. The author emphasises the complexity of the analytical methods required to solve even the simplest type of practical problem. In the study of most real situations, one would use numerical methods and a digital computer. The fifth chapter deals with a powerful numerical method, known as Monte Carlo, which is based on sampling techniques. The final chapter is concerned with an extension of the original problem, where the rule of output or input is no longer given but is chosen to optimize the system. This type of problem, which is of great current interest in many practical fields, is at present largely unsolved. Progress here appears to depend greatly on the use of large digital computers.

This new Methuen series of monographs fulfils a definite need and there is no reason why it should not achieve the same success as the well-established series on physical subjects. However, the book under review is not easy to read, due mainly to the large amount of mathematical symbols which interrupts the continuity of the text. If these monographs are intended for a wide audience, from Honours students to technical management, it would be desirable for the mathematics to be separated more clearly from the main text.

A. FONDA

Vibration engineering. By W. KER WILSON. (London: Charles Griffin and Co. Ltd., 1959.) Pp. xii + 292. Price 90s.

Dr. Ker Wilson, who is Chief Research Engineer of de Havilland Engine Co., describes his book as a practical treatise on the balancing of engines, mechanical vibration and vibration isolation; it should prove of great interest to anyone concerned with these practical problems of engine design.

The first quarter of the book deals with the fundamentals of torsional vibration and engine balancing in an entirely straight-forward and conventional way. The remaining three-quarters of the book are devoted to the fundamentals of vibration isolation and contains chapters on frequency calculations, mounting arrangements and systems, forced and resonant vibrations, critical speeds, foundation vibrations and the influence of elastic foundations. The book contains many worked numerical examples.

E. K. FRANKL

Measurement of surface stress in austenitic steel

by J. C. MOORE, B.Sc., Grad.Inst.P., Fairey Aviation Ltd., Hayes, Middlesex

[Paper first received 2 February, and in final form 19 February, 1960]

Abstract

A method is described to evaluate macro-surface stresses in an austenitic steel. A multi-exposure, X-ray back-reflexion technique is employed, and surface-stress values obtained by this method are compared with theoretical values.

Introduction

THE evaluation of surface stress by a two-exposure, X-ray back-reflexion technique, has been previously described,^(1,2) and recently Hawkes⁽³⁾ developed a multi-exposure technique, with graphical solution, and applied it to the stress analysis of aluminium alloys and martensitic high tensile steels. This paper now describes how the multi-exposure technique can be applied to determine surface stresses in an austenitic steel.

Multi-exposure X-ray back-reflexion technique

The surface stress component acting in direction ϕ with respect to some fixed direction in the surface is given by the equation⁽²⁾:

$$\sigma_{\phi} = \frac{d_{\psi} - d_{\perp}}{d_{\perp}} \cdot \frac{E}{(1 + \nu)} \cdot \frac{1}{\sin^2 \psi} \quad (1)$$

where σ_{ϕ} is the surface stress component in direction ϕ ; d_{ψ} is the interplanar spacing of (hkl) planes inclined ψ to the surface normal and measured in direction ϕ ; d_{\perp} is the interplanar spacing of (hkl) planes parallel to surface and measured in direction ϕ ; E is the Young's modulus; and ν is the Poisson's ratio.

When an incident X-ray beam is diffracted by a specimen, the diffracted beam is inclined 2θ to the incident beam, where θ is the Bragg angle. This angle is related to the wavelength of the X-rays and to the interplanar spacing of the diffracting planes of the specimen by the Bragg equation:

$$n\lambda = 2d \sin \theta$$

where n is 1, 2, 3, . . . ; λ is the wavelength of X-ray beam; and d is the interplanar spacing of diffracting planes. Hence:

$$\frac{d_{\psi} - d_{\perp}}{d_{\perp}} = \frac{\sin \theta_{\perp} - \sin \theta_{\psi}}{\sin \theta_{\psi}}$$

Equation (1) may therefore be expressed as:

$$\sigma_{\phi} = \frac{\sin \theta_{\perp} - \sin \theta_{\psi}}{\sin \theta_{\psi}} \cdot \frac{E}{(1 + \nu) \sin^2 \psi}$$

or:

$$\operatorname{cosec} \theta_{\psi} = \frac{\sigma_{\phi}(1 + \nu) \sin^2 \psi}{E \sin \theta_{\perp}} + \frac{1}{\sin \theta_{\perp}}$$

That is, $\operatorname{cosec} \theta_{\psi}$ is a linear function of $\sin^2 \psi$.

Thus, if back-reflexion photographs are taken with the specimen surface direction ϕ at various inclinations to the incident beam, a number of values of $\operatorname{cosec} \theta_{\psi}$ and the corresponding values of $\sin^2 \psi$ are obtainable. A $\operatorname{cosec} \theta_{\psi}/\sin^2 \psi$ graph may then be constructed and from the resulting straight line the value of the surface stress component σ_{ϕ} can be evaluated. To obtain accurate values of $\operatorname{cosec} \theta_{\psi}$ and $\sin^2 \psi$ from a back-reflexion film, it is necessary to calibrate the specimen-to-film distance. This is achieved by covering the metallic surface under examination with a very thin coating of a pure powder. This furnishes on the film its own back-reflexion lines, which are then used for calibration and also as fiduciary marks from which to measure unsymmetrical line-shift encountered during oblique exposures.

There are, therefore, three main conditions to be satisfied before the above technique can be applied to a particular material:

(i) A radiation must be used which will be diffracted by the material, in a position of high Bragg angle, and the intensity of the diffracted beam must be sufficient to produce a measurable line on the back-reflexion film.

(ii) A calibrating powder must be used which will also furnish a diffracted beam of sufficient intensity in the required position. The calibrating powder must be of high purity and obtainable with a strain-free lattice.

(iii) It is necessary to verify that the theory assuming crystallographic isotropy can be applied to a material not necessarily isotropic.

If the above conditions can be satisfied, then the technique may be used as a non-destructive method of surface stress evaluation.

Application to austenitic steel

The multi-exposure, X-ray back-reflexion technique has been successfully applied to austenitic steel using manganese $K\alpha$ radiation and pure, strain-free nickel powder for calibration. It was found that manganese $K\alpha$ radiation furnished suitable high-angle diffractions from the $\{3, 1, 1\}$ planes of both the austenitic and nickel face-centred cubic structures. Diffraction occurred from the $\{3, 1, 1\}$ austenitic planes at a Bragg angle of approximately 76 deg. and from the $\{3, 1, 1\}$ nickel planes, at a Bragg angle of 81 deg. 33 min. Verification, to show if the theory assuming isotropy could be applied to an anisotropic austenitic steel, was obtained by measuring the stress on both faces of austenitic steel strips constrained in circular arcs, and these values were compared with theoretical values derived from elementary bending formulae.

Procedure

The material investigated was an austenitic stainless steel type F.S.M.I., by Firth Vickers (17 : 4 : 6 :: chromium :

nickel: manganese: + nitrogen) in the cold-rolled and tempered condition (80 t/in.² tensile strength). Two specimens *A* and *B* (8.0 × 0.75 in.) were cut from a 20 s.w.g. (0.036 in. thick) sheet in the transverse rolling direction. To remove high residual surface stresses, the specimens were electropolished on both sides until they were 0.030 in. thick. They were then constrained to various circular arcs, and the surface stresses induced by bending were calculated using elementary bending theory and also measured by the multi-exposure, X-ray back-reflexion technique. Initial surface-stress values were obtained for the straight strips, and during bending the elastic limit was never exceeded.

Finely divided nickel powder, obtained in a strain-free condition by the carbonyl process, was used to calibrate the specimen-to-film distance. It was applied to the specimen surface in the form of a thin paste, made by mixing the powder with pure Vaseline.

Manganese radiation was obtained by inserting into a Raymax X-ray crystallographic unit a copper anode electroplated with 0.002 in. of manganese. The unit was operated at 40 kV with a tube current of 5 mA. Unfiltered radiation was used.

For each stress determination, six back-reflexion photographs were obtained from the specimen, two with the incident beam normal to the surface of the specimen, two with the incident beam inclined at 30 deg. to the surface normal (one either side of the normal) and two at 45 deg. incidence (also, one either side of the normal). The back-reflexion films used were rectangular in shape, and the radiation was collimated with a vertical slit perpendicular to the length of the film. The specimen was continuously oscillated $\pm 1\frac{1}{2}$ deg. through its mean position in order to bring more {3, 1, 1} crystal planes into a diffracting position.

With reference to Fig. 1, it is evident that two different values of $\sin^2 \psi$ and the corresponding values of $\operatorname{cosec} \theta_\psi$,

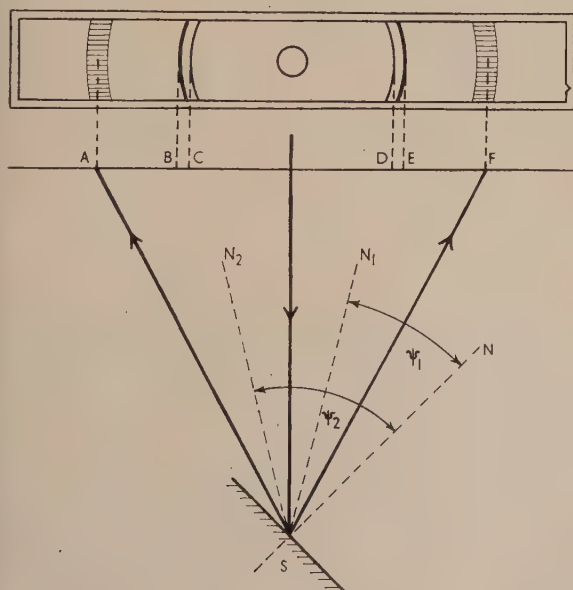


Fig. 1. The geometry of diffraction

are obtainable from each back-reflexion photograph. Therefore, precaution was taken to ensure that the film was not measured in a reversed position, relative to its exposure aspect—hence the fiducial mark to the right of the film.

Diffraction lines *A* and *F* are the unresolved $K\alpha_1$ and $K\alpha_2$

lines of the manganese radiation diffracted from the {3, 1, 1} crystal planes of the austenitic lattice. *B* and *E* are the $K\alpha_1$ lines diffracted from the {3, 1, 1} crystal planes of the nickel lattice and *C* and *D* are the corresponding $K\alpha_2$ components. SN_1 and SN_2 are the normals to the reflecting planes contributing to diffraction lines *A* and *F* respectively. The stress values, recorded in the table, were obtained by using the method of calculation outlined by Hawkes,⁽³⁾ the back-reflexion films being measured on a vernier scale by visual means.

Results

The results given in the table are in tons per square inch, and the normal sign convention has been employed, that is, positive for tensile stresses and negative for compressive stresses. The material constants used to evaluate these results were:

$$\text{Young's modulus} = 11.8 \times 10^3 \text{ t/in.}^2;$$

$$\text{Poisson's ratio} = 0.33.$$

Comparison of the theoretical and X-ray stress measurements made on austenitic steel strip

Theoretical surface stress (t/in. ²)	X-ray stress with correction due to initial stress (t/in. ²)	
	Specimen A	Specimen B
+37.7	+37.1	+40.1
+26.6	+25.9	+31.9
+16.5	+17.6	+15.7
+7.5	+7.1	+5.9
−7.5	−5.9	−9.2
−16.5	−17.3	−10.8
−26.6	−26.3	−29.5
−37.7	−30.6	−36.7

Initial surface stress on Specimen *A* = −5.8

Initial surface stress on Specimen *B* = −6.2

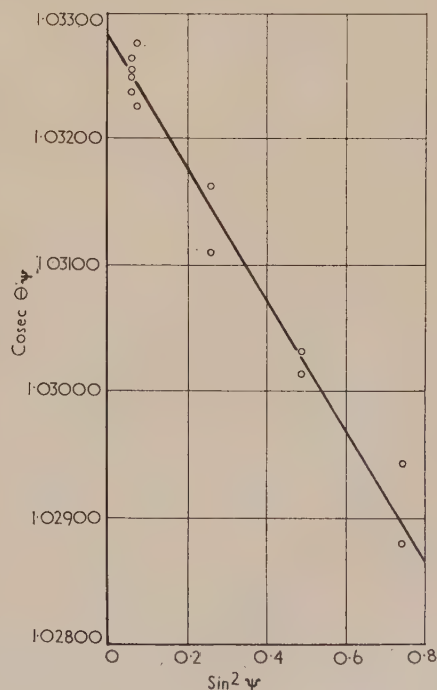


Fig. 2. Relationship of $\operatorname{cosec} \theta_\psi$ and $\sin^2 \psi$ corresponding to a compressive stress of 42.9 t/in.²

Discussion

The accuracy of results indicated by the table is better than might be expected considering that the unresolved manganese $K\alpha$ doublet was used and also that film measurements were made without recourse to a microphotometer. This is probably accounted for by the fact that an error of 0.02 cm in film measurement corresponds to an error in $\csc \theta_\psi$ of 0.000175, which can be tolerated as it is within the usual scatter of points found on the $\csc \theta_\psi / \sin^2 \psi$ graph. In addition, a probable further contribution to accuracy is that the final stress result is derived from measurement of line shift rather than actual line position. Nevertheless, a good microphotometer could be advantageously used for film measurement. Fig. 2 is the graph of $\csc \theta_\psi$ against $\sin^2 \psi$ from which the compressive stress value of 36.7 t/in.², recorded in the table, was derived. It is reproduced to indicate the typical scatter of points experienced.

The use of a powder for calibration of the specimen-to-film distance has been found to be far more convenient than any direct measurement. Although high-angle diffraction is not an extremely accurate method of measurement of specimen-to-film distance, the use of the calibrating powder has the distinct advantage that all films may be standardized and allowances made for film shrinkage.

Conclusions

Previous work⁽³⁾ has shown that theory assuming isotropic crystallographic behaviour can be applied to evaluate surface

stress in anisotropic material. This fact is now endorsed by the successful application of the isotropic theory to an austenitic steel reported herein. The results clearly indicate that the multi-exposure, X-ray back-reflexion technique can be used as a non-destructive method for the evaluation of macro-surface stresses in austenitic steel, provided that distinct X-ray diffraction from the specimen surface is not restricted by an oxide or protective film.

Acknowledgements

The author wishes to acknowledge the work of Messrs. G. Munday and G. Hawkes, who developed the technique as applied to aluminium alloys and martensitic steels. The author also wishes to thank Mr. W. E. Cooper, Head of Materials Laboratory, Fairey Aviation Limited, who initiated this investigation, and also the Directors of Fairey Aviation Ltd. for permission to publish this paper.

References

- (1) FROMMER, L., and LLOYD, E. H. *J. Inst. Metals*, **70**, p. 91 (1944).
- (2) BARRET, C. S. *Structure of Metals*, 2nd Edition, p. 316 (London: McGraw-Hill Publishing Co. Ltd., 1953).
- (3) HAWKES, G. A. *Brit. J. Appl. Phys.*, **8**, p. 229 (1957).

Analogy between the slow motion of a viscous fluid and the extension and flexure of plates: a geometric demonstration by means of moiré fringes

by T. H. RICHARDS, M.Sc., Department of Civil Engineering, University of Birmingham

[Paper first received 11 March, and in final form 17 December, 1959]

Abstract

That the problems of extension and flexure of plates and the slow two-dimensional motion of an incompressible viscous fluid are analogous is well known. In this paper, emphasis is placed on some of the geometrical properties of the stream function and Airy stress-function surfaces. Through these properties a method is described wherein visualization of flow and stress conditions is obtained by analogy, the flexure problem of plates being the vehicle for solution.

Introduction

ON reduction to mathematical terms, many physically independent phenomena are found to be expressible in identical forms. When such an identity exists, the physical systems are said to be analogous. This state of affairs recurs frequently in applied mechanics, and a number

of useful features results. For example, the more familiar, or physically simpler case may be employed as a calculating device for the less familiar, or again, a known solution to a particular problem provides a family of solutions to a whole system of analogous problems.

The analogies of interest in this work are those wherein the solution to a problem in the flexure of plates is applicable to a class of problems in the extension of plates and the slow motion in two dimensions of a viscous, incompressible fluid. The existence of these analogies is well known; Lord Rayleigh⁽¹⁾ seems to have been the first to notice the similarity between slow fluid motions and flexure, whilst Goodier⁽²⁾ discussed the correspondence between fluid motion and plane stress. The so-called "slab-slice" analogy was also contemplated at an early date; the first record of any application known to the present author being dated 1908.⁽³⁾ Comparatively recently, interest seems to have been taken once more in the slab-slice analogy, as, for example,

in the papers by Southwell⁽⁴⁾ or Mindlin.⁽⁵⁾ In spite of this early knowledge, there does not seem to have been very much use made of these analogies in experimental work.

In two-dimensional hydrodynamics and elasticity, theoretical discussions are facilitated by the introduction of the stream function and the Airy stress function respectively. These functions of two variables define surfaces, certain geometrical properties of which are a measure of quantities of interest in the particular physical problem at hand. For example, the component slopes of the stream-function surface are proportional to component velocities, whilst the curvatures of the Airy surface give the component stresses.

The stream and Airy functions define mathematical surfaces, whereas a flexed plate presents a real physical surface, which may be studied quantitatively. These facts formed the basis of the present investigation, wherein the flexed plate was employed as an analogue device for simulating the other two associated problems.

The geometry of the flexed plate—the slab—was examined by means of a novel experimental technique developed by Ligtenberg.⁽⁶⁾ This optical method gave moiré fringe photographs, from which slopes of the plate were obtained directly. Since, in these problems, a double differentiation of the appropriate basic function is involved, this is an important advantage: first derivatives are measured directly so that only one differentiation operation is necessary, with consequent improvement of accuracy. The function itself may be found by graphical or numerical integration, which are comparatively accurate operations.

The purpose of the present paper, then, is to describe a practical application of the analogies to a geometric method of visualizing two-dimensional stress and flow conditions, the flexure problem being the vehicle for solution.*

Notation

- A = boundary loading function or boundary velocity function; area
 a = distance between model and screen in moiré apparatus
 B = boundary loading function or boundary velocity function
 b = width of plate
 D = flexural rigidity of a slab, $D = Eh^3/12(1 - \nu^2)$
 d = distance between lines on screen of Moiré apparatus
 E = Young's modulus
 h = slab thickness; ordinate of integral curve
 l = direction cosine; distance of pole from origin
 M = with subscripts x, y, xy , bending and twisting moments
 m = direction cosine; scale on a graph
 N = fringe order on moiré fringe photograph
 n = scale on a graph; distance along the normal to a curve
 Q = with subscripts, transverse shear force per unit length of arc
 S = distance on fringe order plot
 s = distance along an arc
 \bar{U}, U, u = velocity components in the x -direction

- \bar{V}, V, v = velocity components in the y -direction
 w = deflexion of the middle surface of a slab
 \bar{X}, \bar{Y} = surface forces
 x, y, z = co-ordinates
 α = angle between normal to a curve and the x -direction; constant of integration
 β, γ = constants of integration
 δ = differential settlement
 λ = constant of proportionality
 θ = angle of inclination of a graph
 ν = Poisson's ratio
 σ = normal stress
 τ = shear stress
 ϕ = function; slope of a flexed plate
 χ = Airy stress function
 ψ = stream function
 ω = vorticity
 Ω = angular velocity
 ∇^2 = Laplace operator
 ∇^4 = biharmonic operator

Mathematical background

In this section, the theories relating to fluid motion, flexure and extension of plates are summarized and discussed independently. The similarities will be indicated and synthesized subsequently in the analogy statement.

Flexure of thin plates. In the approximate theory of flexure, the middle surface of the plate is considered bent but not stretched. Then the bending and twisting moments are related to the deflexion function $w(x, y)$ by⁽⁷⁾:

$$\left. \begin{aligned} M_x &= -D \left(\frac{\partial^2 w}{\partial x^2} + \nu \frac{\partial^2 w}{\partial y^2} \right), \\ M_y &= -D \left(\frac{\partial^2 w}{\partial y^2} + \nu \frac{\partial^2 w}{\partial x^2} \right), \\ M_{xy} &= D(1 - \nu) \frac{\partial^2 w}{\partial x \partial y}. \end{aligned} \right\} \quad (1)$$

From the conditions of equilibrium (Fig. 1) and equations (1), the transverse shear forces are:

$$Q_x = -D \frac{\partial(\nabla^2 w)}{\partial x}, \quad Q_y = -D \frac{\partial(\nabla^2 w)}{\partial y}. \quad (2)$$

From these relations, the partial differential equation describing the deflexion surface is obtained as:

$$\nabla^4 w = \frac{q}{D}, \quad (3)$$

where $q(x, y)$ is the transverse loading function.

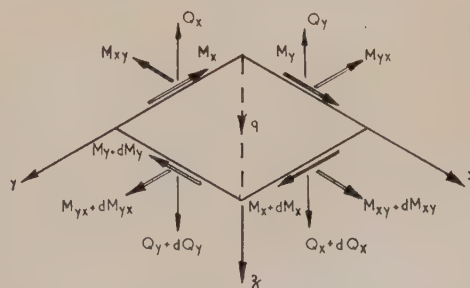


Fig. 1. Loading system for element of flexed plate

* Since the preparation of this paper, the author's attention has been drawn to a recent letter by Southwell.⁽¹¹⁾ In that letter, a problem in the flexure of plates was used to resolve a paradox in fluid motion, the value of reasoning by analogy being demonstrated very convincingly.

The boundary conditions imposed upon the solutions to equation (3) may be classified in the manner used by Southwell⁽⁴⁾:

- Case A, where edge displacements are specified;
Case B, where edge tractions are specified.

For present purposes, Case A only is of interest. Then the boundary-value problem may be stated

$$\nabla^4 w = \frac{q}{D} \text{ over the region,}$$

$$w \text{ and } \frac{\partial w}{\partial n} \left(\text{or } \frac{\partial w}{\partial x} \text{ and } \frac{\partial w}{\partial y} \right) \text{ specified on the boundary.}$$

In the particular case where there is no transverse load,

$$\nabla^4 w = 0 \text{ over the region.}$$

The foregoing equations show that if the geometry of the deflexion surface is known, the stress analysis of the slab is complete: components of curvature and twists are proportional to moments, whilst the rates of change of the average curvature give shear forces.

Extension of thin plates. When the middle surface is stretched by edge forces but not bent, the solution of the two-dimensional problem is facilitated by introducing the Airy stress function $\chi(x, y)$.⁽⁸⁾ The function is introduced in such a way that the equations of equilibrium are satisfied identically, and it must be chosen so that the compatibility conditions are also fulfilled. When body forces are negligible, these conditions are satisfied if

$$\nabla^4 \chi = 0, \quad (4)$$

and, by definition, the stresses are related to χ by

$$\sigma_x = \frac{\partial^2 \chi}{\partial y^2}, \quad \sigma_y = \frac{\partial^2 \chi}{\partial x^2}, \quad \tau_{xy} = -\frac{\partial^2 \chi}{\partial x \partial y}. \quad (5)$$

The boundary conditions may again be classified as Case A or Case B; here only Case B, where edge tractions are specified, is of interest. Then, as shown in Appendix 1, the boundary conditions in terms of χ are:

$$\left. \begin{aligned} \chi &= \int (Bl - Am) ds + \alpha x + \beta y + \gamma \\ \frac{\partial \chi}{\partial n} &= Al + Bm + \alpha l + \beta m. \end{aligned} \right\} \quad (6)$$

The statement of the boundary value problem for Case B of the extensional problem is therefore:

$$\nabla^4 \chi = 0 \text{ over the region,}$$

$$\chi \text{ and } \frac{\partial \chi}{\partial n} \left(\text{or } \frac{\partial \chi}{\partial x}, \frac{\partial \chi}{\partial y} \right) \text{ specified on the boundary.}$$

The function $\chi(x, y)$ defines a surface or stress hill constructed over the region of the plate and, provided the slopes are small, certain geometrical properties are important. From equations (5), it can be seen that the curvature in a given direction gives the direct stress component at right-angles, whilst the twist gives the shearing stress. Further properties of the surface are considered in Appendix 1.

Slow steady motion of viscous, incompressible fluid. The general differential equations describing fluid motion are the Navier-Stokes equations.⁽⁹⁾ Under circumstances where

flow is two-dimensional, steady and incompressible, and viscous forces predominate, these equations reduce to

$$\left. \begin{aligned} -\frac{\partial p}{\partial x} + \mu \nabla^2 u &= 0, \\ -\frac{\partial p}{\partial y} + \mu \nabla^2 v &= 0. \end{aligned} \right\} \quad (7)$$

The equation of continuity⁽⁹⁾ permits the introduction of a stream function $\psi(x, y)$ such that the velocity components u and v in the x - and y -directions are:

$$u = \frac{\partial \psi}{\partial y}, \quad v = -\frac{\partial \psi}{\partial x}. \quad (8)$$

Then elimination of p from equations (7) gives:

$$\nabla^4 \psi = 0 \quad (9)$$

which is the equation describing the flow.

Again, two classes of boundary conditions may be specified:

Case A, where, at rigid boundaries, there must be no slip

Case B, where, at a free surface, or surface of contact of two dissimilar fluids, there must be equilibrium of surface forces.

If the boundaries are long compared with their distance apart, Case A only is of real interest in describing the motion at regions far away from the ends. Then, as shown in Appendix 2, the boundary conditions in terms of ψ are

$$\left. \begin{aligned} \psi &= \int (Bl - Am) + \gamma, \\ \frac{\partial \psi}{\partial n} &= Al + Bm, \end{aligned} \right\} \quad (10)$$

and the complete statement of the boundary value problem is

$$\nabla^4 \psi = 0 \text{ over the region,}$$

$$\psi \text{ and } \frac{\partial \psi}{\partial n} \left(\text{or } \frac{\partial \psi}{\partial x}, \frac{\partial \psi}{\partial y} \right) \text{ specified on the boundary.}$$

The function $\psi(x, y)$ defines a surface or stream function hill constructed over the region, this surface having some interesting geometrical properties. The slope in a given direction is proportional to the velocity component at right angles. Streamlines, defined by $\psi = \text{constant}$, are contours of the surface. Further properties are considered in Appendix 2.

The analogies. From the preceding paragraphs it is seen that the boundary-value problems for each case are identical and are of the form

$$\nabla^4 \phi = 0 \text{ over the region,}$$

$$\phi \text{ and } \frac{\partial \phi}{\partial n} \left(\text{or } \frac{\partial \phi}{\partial x} \text{ and } \frac{\partial \phi}{\partial y} \right) \text{ specified on the boundary,}$$

where ϕ is some function to be determined.

The analogy is thus complete and it would appear that a solution to any given problem is also a solution to an analogous though physically different one. However, when contemplating a hydrodynamic analogue to a given flexural or extensional problem, it is important to verify whether or not the required analogue is in fact physically realizable as a steady configuration. This point is further discussed in Appendix 3.

The interpretation of ϕ as a surface has been emphasized. For the extension and fluid flow problems, the surface is a purely mathematical concept, whereas the deflexion surface of a flexed plate is real. It therefore seems eminently desirable that the flexed plate be regarded as a vehicle for the study of all three problems, since deflexions, slopes and curvatures can easily be obtained from measurements.

In Table 1 are listed some analogous quantities. The measurements were made by means of Ligtenberg's method.

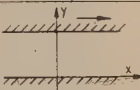


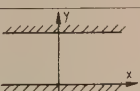

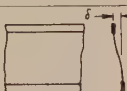
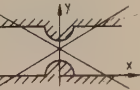


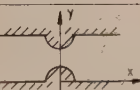
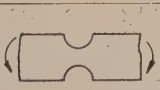
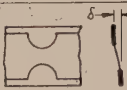
Table 1. Analogous quantities

Flexure problem: w surface	Extension problem: χ surface	Fluid-flow problem: ψ surface
elevation	measure of moment	measure of flow rate
slope	measure of force	measure of velocity
curvature	measure of stress	measure of skin friction (when curvature is normal to boundary)
mean curvature	measure of sum of principal stresses	measure of vorticity

Study of special cases. For the purposes of the investigation, the cases listed in Table 2 were examined. In all of them, two boundaries are very long compared with their distance apart. A theoretical analysis is presented in Appendix 3.

It has been pointed out that there must be steady flow in the hydrodynamic problem. In case (3) of Table 2, the geometry is changing as time goes on, so that the flow is not steady. This is therefore an example for which the threefold analogue breaks down.

Table 2. Cases for examination

	Hydrodynamic problem	Extensional problem	Flexural analogue
1	 flow induced by relative motion of boundaries	 plain plate in pure tension	 cylindrical bending
2	 flow under pressure	 plain plate in pure bending	 cylindrical differential settlement
3	 flow induced by relative motion of boundaries	 notched plate in pure tension	 cylindrical bending
4	 flow under pressure	 notched plate in pure bending	 cylindrical differential settlement

Moiré method

In the method developed by Ligtenberg, the slopes of loaded-model slabs are obtained directly from optical interference patterns. Moiré fringes result from the superposition of two sets of lines and the method used in their formation is a novel one.

A polished model (Fig. 2) acts as a first surface mirror. The highly illuminated screen S has ruled on it a set of

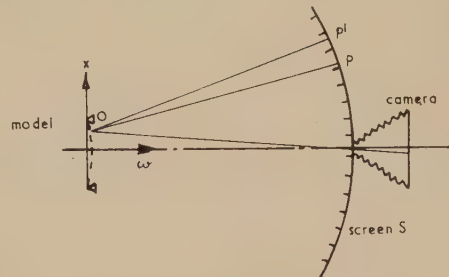


Fig. 2. Schematic arrangement of moiré apparatus

parallel lines, equally spaced at a distance d apart, so that, provided the model is unflexed, the camera records the undistorted image of these lines. When the slab is loaded, a distorted image of the lines is obtained, and a superposition of the two images by a double exposure of the photographic plate results in the formation of moiré fringes. The screen has a particular shape determined by Ligtenberg so that the fringes are contours of constant slope. In fact, the screen is a segment of a cylinder having the ruled lines as generators.

It is seen from Fig. 2 that, with an unloaded model, an image of point P will be obtained in the camera. After loading, the image of P' will coincide with that of P . Ligtenberg showed that a moiré fringe is obtained whenever

$$PP' = Nd, \quad (11)$$

where N is a whole number called the "fringe order."

For the usual flexure theory to hold, the model deflexions must be small so that:

$$PP' = a \angle POP',$$

where a is the distance from model to screen. Therefore:

$$\phi = N \frac{d}{2a}. \quad (12)$$

The fringes give the slope in the direction normal to the ruled lines, so that the measurement of gradients in several directions involves the rotation of the screen relative to the model. For example, if the x -direction on the model is normal to the lines, then:

$$\frac{\partial w}{\partial x} = \frac{N_x d}{2a}. \quad (13)$$

From the fringe photographs, a curve of N versus distance may be easily obtained, and the true slopes found using equation (13). The second derivatives and the deflexion are then found by differentiation and integration. A method of analyzing moiré fringes is given in Appendix 4.

Models and photographic details

All the models were made of $\frac{1}{8}$ in. thick black perspex sheet. The rigid clamps required along the two main boundaries (see Appendix 3) were of heavy-gauge steel plates bolted on either side of the perspex to form a sandwich, the inner edges of these clamps being formed to the required contour.

For models 1 and 3, it was necessary to apply a pure bending moment. This was achieved by mounting the edge clamps on knife edges and applying equal loads at the ends of the arms shown in Fig. 3. The relative displacements δ

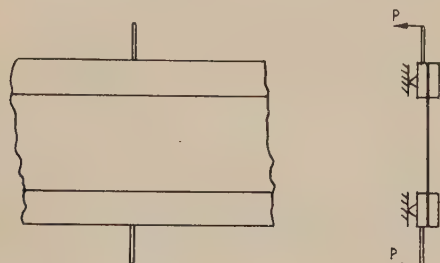


Fig. 3. Method of applying pure bending to slabs 1 and 3

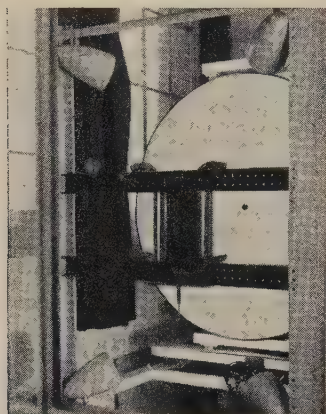


Fig. 4. Model mounted in moiré apparatus

of models 2 and 4 were obtained by packing pieces and G-clamps.

A model loaded in the moiré apparatus is shown in the photograph of Fig. 4, wherein will be noticed the necessity for the slab to be mounted vertically. Models 2 and 4 were held in position by means of the G-clamps, whereas it was necessary to support the weight of models 1 and 3 on two ball bearings. These were bearing on the ends of the boundary plates and resting on a small platform fixed to the frame of the apparatus.

The screen was illuminated by four photoflood lamps, experience showing that uniform lighting was of utmost importance. With Kodak Kodalith plates, good negatives were obtained when each of the two exposures lasted three minutes using a 13.5 cm f4.5 camera lens stopped down to f/36.

For the complete analysis of models 1 and 2, it was necessary to determine the flexural rigidity D of the slab material. For this method a square plate loaded at its four corners was used in the manner described by Ligtenberg.⁽⁶⁾

Results and discussion

Typical fringe photographs are shown in Figs. 5 to 9, the caption appropriate to each figure being sufficient description. From these photographs it will be seen that the distortion of the fringes at the ends is very localized, the assumption

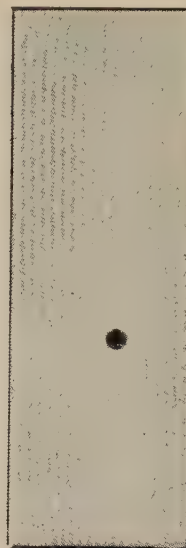


Fig. 5. Fringe photograph for Case 1:

Contours of constant $\frac{\partial w}{\partial y}$



Fig. 6. Fringe photograph for Case 1:

Contours of constant $\frac{\partial w}{\partial x}$

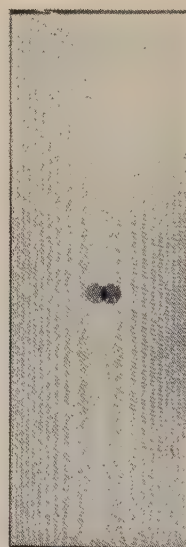


Fig. 7. Fringe photograph for Case 2:

Contours of constant $\frac{\partial w}{\partial y}$

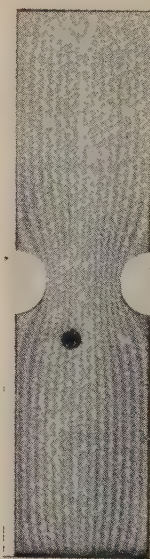


Fig. 8. Fringe photograph for Case 3:

Contours of constant $\frac{\partial w}{\partial y}$

that the conditions on these boundaries need not be satisfied exactly in these cases thus being justified.

The plain models sustaining cylindrical bending and uniform differential settlement were analyzed fully and the results presented in graphical form in Figs. 10 and 11, the full lines representing the theoretical values and the circles

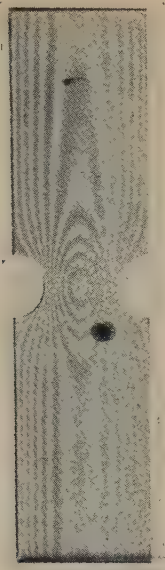


Fig. 9. Fringe photograph for Case 4:
Contours of constant $\partial w/\partial y$

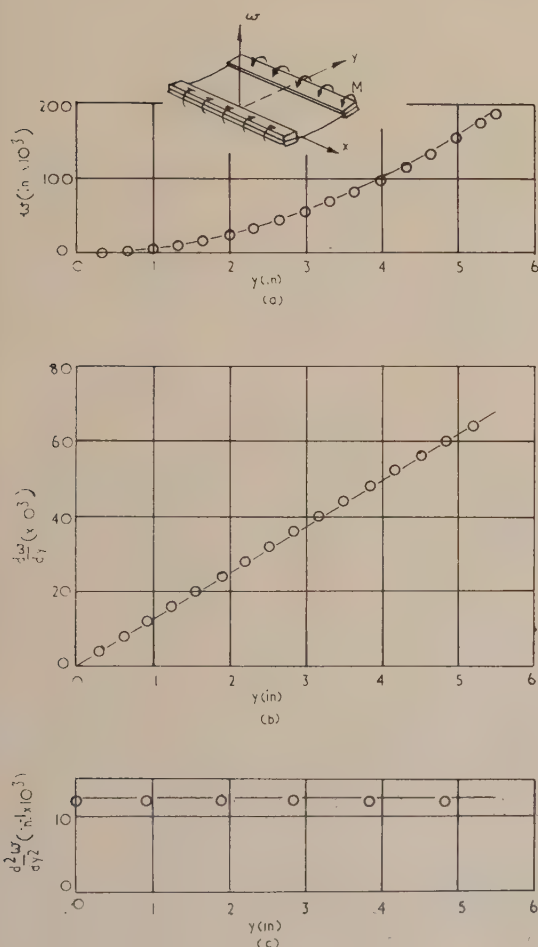


Fig. 10. Plots of deflection, slope and curvature for Case 1
 $M = \frac{1}{8}$ lb in./in.; $y_{max} = 5.5$ in.
○, experiment; —, theory.

the experimental results. In all cases agreement between experiment and theory is seen to be good.

The figures show the quantities of interest in the stress analysis of slabs, but as mentioned elsewhere in this report, they also represent—to within a constant of proportionality—analogue quantities. Thus from Fig. 10(a) the maximum ordinate is proportional to the total rate of flow, and Fig. 10(b) represents the linear velocity profile in the flow

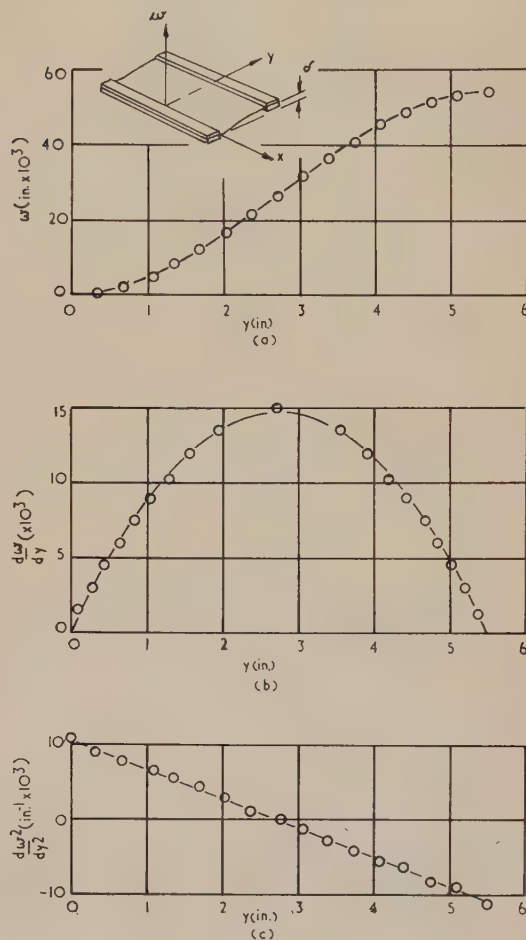


Fig. 11. Plots of deflection, slope and curvature for Case 2

$\delta = 0.054$ in.; $y_{max} = 5.5$ in.
○, experiment; —, theory.

postulated in Maxwell's definition of viscosity. Also from Fig. 10(b), the maximum ordinate represents the force transmitted by the section in the plane-stress analogue, whilst Fig. 10(c) demonstrates the uniform stress distribution of this problem.

In Fig. 11(a), the maximum ordinate again represents total flow rate. Fig. 11(b) shows the parabolic velocity profile for viscous flow through a channel, and it may be deduced from the fact that the curve returns to zero that, in the plane-stress problem, no resultant force is transmitted. Fig. 11(c) can be interpreted as the familiar linear-stress distribution in a beam sustaining a pure bending moment.

The streamline pattern for one example of Case 4, Table 2, is shown in Fig. 12. Cases 3 and 4 were studied with interest centred on the analogous plane-stress problem. Stress concentration factors were accordingly obtained for bars

having semi-circular notches and sustaining simple tension and pure bending. Table 3 compares the values found with those by Timoshenko.⁽¹⁰⁾

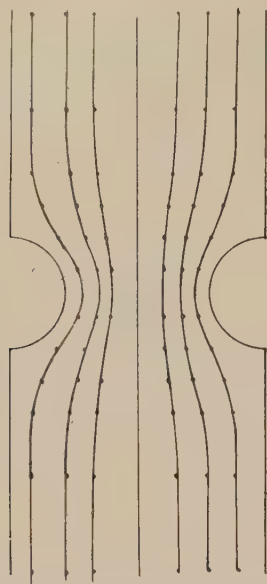
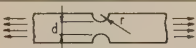



Fig. 12. Selected streamlines constructed from integral of fringe pattern

Table 3. Comparison of values

r/d				
	Analogy	Timoshenko	Analogy	Timoshenko
0.2	2.08	2.02	1.52	1.57
0.31	1.77	1.80	1.30	1.42
0.4	1.68	1.65	1.38	1.34

Stress-concentration factors are ratios of curvatures and are therefore independent of the constant of proportionality relating the flexural and extensional problems. The tabulated values may also be interpreted as "moment-concentration factors" for the flexure problem. Except for one case, agreement is quite good. Two sources of error are inherent in the method itself. Firstly, small local variations in the model thickness occur; flexural rigidity involves thickness raised to the power three so that quite noticeable local changes in curvature can occur if non-uniform plates are used for the models. Secondly, and more noticeably, rigid clamping at the boundaries is extremely difficult to achieve. Consequently, curvatures at the boundaries tend to be reduced, especially where contours are irregular, leading to low values for the stress-concentration factors.

Conclusions

Emphasis on the properties of the surfaces defined by stream functions and Airy stress functions have been found helpful to an understanding of the nature of problems in fluid motion and elasticity. The application of the moiré method to the study of the flexure of plates has proved to be a useful means of demonstrating these problems by analogy. One model flexed in two ways provided a solution

for five or six physically independent problems according as the required hydrodynamic analogue was not or was physically realizable as a steady configuration. The latter point has demonstrated that the class of problems for which the three-fold analogy holds is much smaller than it would appear at first sight.

Acknowledgement

The author would like to thank Prof. S. C. Redshaw of the University of Birmingham for providing facilities for the execution of this work, and for his encouragement whilst the investigation was in progress.

References

- (1) RAYLEIGH, LORD. *Philosophical Magazine*, **35** (Series 5), p. 354 (1893).
- (2) GOODIER, J. N. *Philosophical Magazine*, **17** (Series 7), p. 554 (1934).
- (3) HETENYI, M. *Handbook of experimental stress analysis* (New York: John Wiley and Son, 1950).
- (4) SOUTHWELL, R. V. *Quarterly Journal of Mechanics and Applied Mathematics*, **III** (Part 3), p. 257 (1950).
- (5) MINDLIN, R. D. *Quarterly of Applied Mathematics*, **IV**, 3, p. 279 (1946).
- (6) LIGTENBERG, F. K. *Proceedings of the Society for Experimental Stress Analysis*, **XII**, 2, p. 83 (1955).
- (7) TIMOSHENKO, S. *Theory of plates and shells*, 1st edition (New York: McGraw-Hill, 1940).
- (8) TIMOSHENKO, S., and GOODIER, J. N. *Theory of elasticity*, 2nd edition (New York: McGraw-Hill, 1951).
- (9) LAMB, H. *Hydrodynamics*, 4th edition (London: Cambridge University Press, 1916).
- (10) TIMOSHENKO, S. *Strength of materials*, **2**, 3rd edition (New York: D. Van Nostrand, 1957).
- (11) SOUTHWELL, R. V. *Nature, Letter to the Editor*, **181**, 4618, p. 1257 (1958).

Additional references

- FOX, L., and SOUTHWELL, R. V. *Philosophical Transactions of the Royal Society, series A*, **239**, p. 419 (1940-1946).
 WESTERGAARD, H. M. *Transactions A.S.M.E.*, **56**, 3, p. 141 (1934).

Appendix 1

Boundary conditions for plane stress and properties of the χ surface

Boundary conditions—Case B. The conditions of equilibrium at a boundary in terms of stresses are⁽⁸⁾:

$$\left. \begin{aligned} \bar{X} &= l\sigma_x + m\tau_{xy}, \\ \bar{Y} &= m\sigma_y + l\tau_{xy}. \end{aligned} \right\} \quad (13A)$$

Substitution for σ_x , σ_y and τ_{xy} in terms of χ gives:

$$\left. \begin{aligned} \bar{X} &= \frac{\partial}{\partial s} \left(\frac{\partial \chi}{\partial y} \right), \\ \bar{Y} &= - \frac{\partial}{\partial s} \left(\frac{\partial \chi}{\partial x} \right). \end{aligned} \right\} \quad (14)$$

On integration:

$$\left. \begin{aligned} \frac{\partial \chi}{\partial x} &= -\int \bar{Y} ds + \alpha = -A + \alpha \\ \frac{\partial \chi}{\partial y} &= \int \bar{X} ds + \beta = B + \beta, \end{aligned} \right\} \quad (15)$$

where A and B are boundary loading functions, using Mindlin's notation.⁽⁵⁾ If it is noted that, for any function $f(x, y)$:

$$\left. \begin{aligned} \frac{\partial f}{\partial s} &= \frac{\partial f}{\partial x} \frac{\partial x}{\partial s} + \frac{\partial f}{\partial y} \frac{\partial y}{\partial s}, \\ \frac{\partial f}{\partial n} &= \frac{\partial f}{\partial x} \frac{\partial x}{\partial n} + \frac{\partial f}{\partial y} \frac{\partial y}{\partial n}, \end{aligned} \right\} \quad (16)$$

and that in Fig. 13:

$$\left. \begin{aligned} \frac{\partial x}{\partial n} &= \frac{\partial y}{\partial s} = \cos \alpha = l, \\ -\frac{\partial x}{\partial s} &= \frac{\partial y}{\partial n} = \sin \alpha = m, \end{aligned} \right\} \quad (17)$$

then, equations (15) give:

$$\chi = \int (Bl - Am) ds + \alpha x + \beta y + \gamma, \quad (18)$$

$$\frac{\partial \chi}{\partial n} = Al + Bm + \alpha l + \beta m. \quad (19)$$

In practice, it will usually be more convenient to use equations (15) and (18). Hence the boundary conditions in Case B of the extensional problem are:

χ and $\frac{\partial \chi}{\partial n}$ (or $\frac{\partial \chi}{\partial x}$ and $\frac{\partial \chi}{\partial y}$) specified on the boundary.

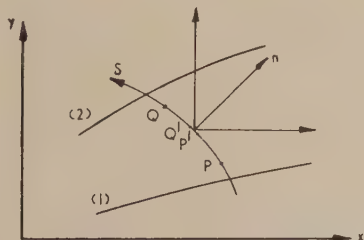


Fig. 13. Portion of plane stress or fluid-flow field between boundaries 1 and 2

Properties of the χ -surface. If the slopes of the χ -surface are small, then the components of curvature are proportional to second derivatives. Therefore, according to equations (5), the curvatures of the surface give direct stresses, and twists give shearing stresses.

If any section C (Fig. 13) joining two points P and Q , is considered, then, for an element of arc $P'Q'$ whose normal has direction cosines l and m , considerations of equilibrium give the horizontal and vertical components of force on the element as:

$$\bar{X} = \frac{\partial}{\partial s} \left(\frac{\partial \chi}{\partial y} \right) ds \quad \text{and} \quad \bar{Y} = -\frac{\partial}{\partial s} \left(\frac{\partial \chi}{\partial x} \right) ds. \quad (20)$$

Integration then gives the components of the resultant force across the section PQ :

$$\left. \begin{aligned} \bar{X} &= \int_P^Q \bar{X} ds = \left(\frac{\partial \chi}{\partial y} \right)_Q - \left(\frac{\partial \chi}{\partial y} \right)_P \\ \bar{Y} &= \int_P^Q \bar{Y} ds = \left(\frac{\partial \chi}{\partial x} \right)_P - \left(\frac{\partial \chi}{\partial x} \right)_Q \end{aligned} \right\} \quad (21)$$

Equations (21) state that the change in component slopes of the surface between two points represents the components of the resultant force transmitted over the section. In particular, if P and Q lie on boundaries 1 and 2 free from stress, equations (15) state that $\partial \chi / \partial x$ and $\partial \chi / \partial y$ have constant values along the boundaries. It follows, therefore, that the resultant force across any section joining stress-free boundaries is constant—as would be expected from equilibrium conditions.

\bar{X} and \bar{Y} will have moments about the origin, and if clockwise moments are taken as positive, then:

$$\mathbf{M} = \int_P^Q \bar{X} y ds - \int_P^Q \bar{Y} x ds,$$

that is:

$$\mathbf{M} = \left[y \frac{\partial \chi}{\partial y} + x \frac{\partial \chi}{\partial x} \right]_P^Q - (\chi_Q - \chi_P) \quad (22)$$

If P and Q lie on stress-free boundaries 1 and 2 respectively then, without loss of generality, it may be assumed that:

$$\chi_1 = \frac{\partial \chi}{\partial x}_1 = \frac{\partial \chi}{\partial y}_1 = 0.$$

Thus:

$$\mathbf{M}_{1,2} = \left[y \frac{\partial \chi}{\partial y} + x \frac{\partial \chi}{\partial x} \right]_2 - \chi_2. \quad (23)$$

If, in particular, the slopes of the surface were arranged to be zero along boundary 2, then its elevation relative to boundary 1 would give the value of the pure bending moment transmitted over the section, equations (21) showing that the resultant force is zero. It is readily seen that for a bar transmitting a pure bending moment this relative elevation of the stress-free boundaries will be constant along their length.

Appendix 2

Boundary conditions for two-dimensional, slow, viscous flow, and properties of the ψ surface

Boundary conditions—Case A. If the rigid boundary has a velocity of translation with components \bar{U} and \bar{V} in the x - and y -directions and an angular velocity Ω (positive anti-clockwise) then:

$$\left. \begin{aligned} u &= \frac{\partial \psi}{\partial y} = \bar{U} - \Omega y, \\ -v &= \frac{\partial \psi}{\partial x} = -\bar{V} - \Omega x. \end{aligned} \right\} \quad (24)$$

Then, from relations (16) and (17) of Appendix 1:

$$\left. \begin{aligned} \psi &= \int (Bl - Am) ds + \gamma, \\ \frac{\partial \psi}{\partial n} &= Al + Bm, \end{aligned} \right\} \quad (25)$$

where $A = -(\bar{V} + \Omega y)$ and $B = (\bar{U} - \Omega x)$ are boundary

velocity functions. The boundary conditions for Case A of the fluid flow are then:

$$\psi \text{ and } \frac{\partial \psi}{\partial n} \text{ specified on the boundary.}$$

Properties of the ψ surface. From the definition of ψ , the slope of the surface in a given direction is proportional to the velocity at right-angles. For the flow across any section PQ (Fig. 13), the flow rate $d\psi$ across an element $P'Q'$ of length ds is, by definition:

$$d\psi = (u \cos \alpha + v \sin \alpha) ds = \frac{\partial \psi}{\partial s} ds.$$

Integration from P to Q gives:

$$\text{Flow rate across } PQ = \psi_Q - \psi_P. \quad (26)$$

That is, the flow rate is proportional to the relative elevation of the ψ -surface and is independent of the section joining P and Q .

For two-dimensional flow, the vorticity vector reduces to the one component normal to the plane. As a function of the cartesian velocity components:

$$2\omega = \frac{\partial v}{\partial x} - \frac{\partial u}{\partial y}, \quad (27)$$

and, expressed in terms of the stream function:

$$2\omega = -\nabla^2 \psi. \quad (28)$$

The mean curvature of the surface is therefore seen to be a measure of the vorticity. A further interesting property is obtained as follows. From equations (7):

$$-\frac{\partial p}{\partial x} \cdot \frac{\partial y}{\partial s} = -\frac{\partial p}{\partial x} \cdot \frac{\partial x}{\partial n} = -\mu \nabla^2 \left(\frac{\partial \psi}{\partial y} \right) \cdot \frac{\partial y}{\partial s}, \quad (29)$$

$$-\frac{\partial p}{\partial y} \cdot \frac{\partial x}{\partial s} = \frac{\partial p}{\partial y} \cdot \frac{\partial y}{\partial n} = \mu \nabla^2 \left(\frac{\partial \psi}{\partial x} \right) \cdot \frac{\partial x}{\partial s}. \quad (30)$$

If equation (29) is subtracted from equation (30):

$$\frac{\partial p}{\partial n} = \mu \frac{\partial}{\partial s} (\nabla^2 \psi) \quad (31)$$

That is, the rate of change of mean curvature is a measure of the pressure gradient in a direction at right-angles. However, considerations of accuracy show that this property is of little value for present purposes.

Appendix 3

Analysis of special cases

The particular cases studied in this work are those in which two boundaries 1 and 2 are very long compared with the distance between them. Then the condition on boundaries 3 and 4, say, have negligible effect on the stress and velocity distributions in the region of interest. As a basis for this discussion, the fluid-flow problems will be considered specified, whence the corresponding flexural and extensional problems will be inferred by analogy. The hydrodynamic problems may be classed as (i) fluid motion induced by relative motion of the boundaries, and (ii) fluid motion under pressure between stationary boundaries.

(i) *Relative motion of boundaries.* From the equations (25) of Appendix 2, the conditions on boundary i are:

$$\left. \begin{aligned} \psi_i &= \int (B_i l - A_i m) ds + \gamma_i, \\ \frac{\partial \psi}{\partial n} \Big|_i &= A_i l + B_i m, \end{aligned} \right\} \quad (32)$$

where:

$$A_i = -(\bar{V}_i + \Omega_i x), \quad B_i = (\bar{U}_i - \Omega_i y).$$

If the boundaries are in relative motion, one of them, say 1, may be considered at rest. Then:

$$\bar{U}_1 = \bar{V}_1 = \Omega_1 = 0,$$

so that:

$$\psi_1 = \gamma_1 \quad \text{and} \quad \frac{\partial \psi}{\partial n} \Big|_1 = 0.$$

Now γ_1 is arbitrary, but since it is only changes in ψ which are significant, γ_1 may be taken to be zero. Hence:

$$\psi_1 = \frac{\partial \psi}{\partial n} \Big|_1 = \frac{\partial \psi}{\partial x} \Big|_1 = \frac{\partial \psi}{\partial y} \Big|_1 = 0 \quad (33)$$

In a discussion of the conditions on boundary 2, it is necessary to recall that the flow must be steady if ψ is to be a biharmonic function. Now since boundary 1 is at rest, it follows that the rigid boundary 2 may not have an irregularity because the geometry, and hence the nature of the flow, would change as time went on. Furthermore, the boundary must move tangential to itself. Thus, if boundary 2 has translation in the x -direction, it follows from equations (32), in which $l = 0$ and $m = 1$, that

$$\left. \begin{aligned} \psi_2 &= \gamma_2 \\ \frac{\partial \psi}{\partial y} \Big|_2 &= \bar{U}_2, \\ \frac{\partial \psi}{\partial x} \Big|_2 &= 0. \end{aligned} \right\} \quad (34)$$

The interpretation of the analogous flexure problem is simple. Equations (33) and (34) will be satisfied by sandwiching the edges of the slab between rigid plate clamps having the correct contours, slope and elevation. Boundary 1 presents no difficulty. At boundary 2, the slope is specified but, as yet, the identity of ψ_2 with w_2 , which is a measure of the total flow rate, is not established. The problem is thus reduced to finding the loading arrangement necessary to obtain the slope such that w_2 is correct.

For Case 1, Table 2, the boundaries are parallel and have no irregularities so that flow is the simple Couette type wherein the pressure gradient in the x -direction is zero. Then from equation (31), Appendix 2:

$$\frac{\partial p}{\partial x} = \mu \frac{\partial}{\partial y} (\nabla^2 \psi) = 0.$$

But, from the condition of parallel flow:

$$\frac{\partial^2 \psi}{\partial x^2} = -\frac{\partial v}{\partial x} = 0.$$

Therefore:

$$\frac{\partial^2 \psi}{\partial y^2} = \text{const.}$$

The analogous slab must therefore be flexed in such a way that the curvature in the y -direction is constant; this is

achieved by applying a pure couple about an axis parallel to the x -direction (see Table 2). Since the length of the slab is large compared with the width, cylindrical bending is assured, so that $\partial^2 w / \partial x^2$ automatically equals zero.

To obtain the analogous extensional-elastic problem, it is noticed that $\partial^2 w / \partial y^2 \equiv \partial^2 \chi / \partial y^2$ is constant, whilst $\partial^2 \chi / \partial x^2$ and $\partial^2 \chi / \partial x \partial y$ are zero (from the condition of cylindrical bending). That is, the slice sustains a uniaxial tension with σ_x constant, σ_y and τ_{xy} equal to zero. If the principle of Saint Venant is invoked, a meaning may thus be attributed to the lack of importance of the *exact* satisfaction of the conditions on boundaries 3 and 4.

For the case in which there is an irregularity in boundary 1, it is noticed that the disturbance created in the flow is of a local character. Then, at regions sufficiently removed from this irregularity, cylindrical bending is again required, so that the loading arrangement must be the same as described above.

Any rigid-body movement which it is deemed necessary to apply to the above surfaces to effect a correspondence does not alter the extensional analogue. Rigid-body movements represent linear functions and their inclusion in an Airy function does not affect the stresses. A similar argument holds for the flexure problem.

(ii) *Motion under pressure.* If:

$$\bar{U}_2 = \bar{V}_2 = \bar{\Omega}_2 = 0,$$

motion can only result from a pressure difference—boundary 1 has already been specified as being at rest. Then the boundary conditions are:

$$\begin{aligned} \psi_1 &= \frac{\partial \psi}{\partial x} \Big|_1 = \frac{\partial \psi}{\partial y} \Big|_1 = 0, \\ \frac{\partial \psi}{\partial x} \Big|_2 &= \frac{\partial \psi}{\partial y} \Big|_2 = 0, \\ \psi_2 &= \gamma_2, \end{aligned}$$

where γ_2 will be proportional to the flow rate between the boundaries and is a constant for all sections since the flow is incompressible. The flexure analogue again makes use of rigid clamps, the conditions:

$$\gamma_2 \equiv w_2 = \delta \quad \text{and} \quad \frac{\partial w}{\partial y} \Big|_2 = 0$$

being achieved, as depicted in Cases 2 and 4 in Table 2, by means of packing pieces. The analogue might be regarded as uniform differential settlement of the slab boundaries. From equation (21), Appendix I, the extensional analogue is seen to be a bar transmitting a pure bending moment. A meaning may now be attributed to the case of flexure when $\partial w / \partial y \Big|_2$ is obtained such that w_2 is not correct according to the earlier analysis. Such a case implies in the fluid-flow problem a superposition of flow caused by the relative motion of boundaries and the pressure difference. The extensional analogue represents a bar sustaining a combined bending moment and direct stress. That this superposition is permissible is seen from the fact that the equation $\nabla^4 \phi = 0$ is linear.

Analysis of the flexure problems of Cases 1 and 2 in Table 2. Cases 1 and 2 of Table 2 are amenable to a mathematical treatment, so that they present an opportunity for a comparison of experimental results with theory. The other cases are very difficult mathematically, but the extensional elastic problems have been studied by the photoelastic method, so that a comparison of results is again possible.

If a long slab sustaining a uniform bending moment M per unit length, as illustrated in Table 2 is considered, then at regions sufficiently removed from the short edges, the slab will be bent cylindrically; that is, w is independent of x . To describe the flexure problem under these circumstances, it is adequate to consider a strip parallel to the y -axis and of unit width.

If at $y = 0$, $w = dw/dy = 0$, it may easily be shown that:

$$w = \frac{1}{2} \cdot \frac{M}{D} \cdot y^2; \quad (35)$$

$$\frac{dw}{dy} = \frac{M}{D} \cdot y; \quad (36)$$

$$\frac{d^2 w}{dy^2} = \frac{M}{D}. \quad (37)$$

If the constants of proportionality are introduced, the analogous problems are readily seen. For example, equation (36) represents the linear-velocity profile of viscous motion of the type postulated in Maxwell's definition of viscosity, whilst equation (37) shows that the extensional problem is that of a plate sustaining a tensile stress:

$$\sigma_x = \lambda(M/D).$$

If a long slab of width b , sustaining a uniform differential settlement δ as depicted in Table 2 (where $\omega = dw/dy = 0$ at $y = 0$, $w = \delta$, $dw/dy = 0$ at $y = b$) is now considered, then:

$$w = \frac{\delta}{b^2} \cdot y^2 \left(1 - \frac{2y}{b}\right), \quad (38)$$

$$\frac{dw}{dy} = \frac{6\delta}{b^2} \cdot y \left(1 - \frac{y}{b}\right), \quad (39)$$

$$\frac{d^2 w}{dy^2} = \frac{6\delta}{b^2} \left(1 - \frac{2y}{b}\right). \quad (40)$$

Here, equation (39) represents, to within a constant of proportionality, the parabolic velocity profile of viscous flow under pressure in a parallel-sided channel and equation (40) gives the linear distribution of stress experienced by a uniform beam under pure bending.

Appendix 4

Analysis of moiré fringes

For present purposes, the deflexion, slopes and curvatures of the flexed plate are required. Moiré fringes are a measure of slope as shown in equation (13). Thus a full analysis requires numerical or graphical differentiation and integration. Graphical work was found to be more convenient in this work.

Differentiation. A curve is plotted of fringe order against distance, and the angle of inclination at selected points obtained by means of an optical differentiator. The tangent of this angle is then obtained from tables, so that:

$$\tan \theta_s = \frac{\partial \bar{N}}{\partial \bar{S}},$$

\bar{N} and \bar{S} being measured in inches. If the vertical and horizontal scales are n fringes/in. and m in. on model/in. respectively, then:

$$N = n\bar{N}, \quad S = m\bar{S}.$$

Therefore:

$$\frac{\partial \phi}{\partial s} - \frac{\partial^2 w}{\partial s^2} - \frac{1}{2} \frac{d}{a} \cdot \frac{n}{m} \cdot \tan \theta_s \quad (41)$$

where $\partial^2 w / \partial s^2$ is the curvature component in the direction s on the model. Differentiation is therefore a simple operation, although care has to be taken in plotting the ($\bar{N} \sim \bar{S}$) curve.

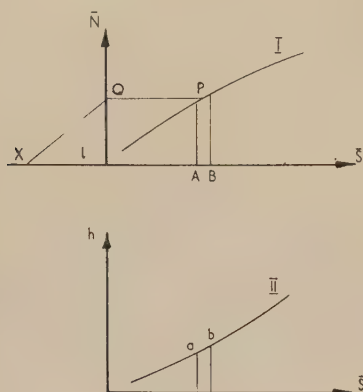


Fig. 14. Illustration of method of integration

Integration. The slope curve *I* (Fig. 14) is divided into segments, and the mid-ordinates such as *P* projected on to the \bar{N} -axis at *Q*. The line *XQ* is drawn from a pole *X* at a convenient distance *l* in. from 0, and *ab* is drawn on curve *II*, parallel to *XQ*. Then:

$$\Delta h = \frac{\Delta A}{l} \text{ in.}$$

Thus, in moving from *A* to *B*, the increment of ordinate of curve *II* gives the increment of area under curve *I*. If this process is repeated for all segments, the integral curve is obtained, and:

$$h = \frac{\int dA}{l}$$

With the same scales as for differentiation:

$$h = \frac{2a}{d} \int \frac{1}{mnl} \phi ds = \frac{2a}{d} \cdot \frac{w}{mnl}$$

Therefore:

$$w = mnl \frac{d}{2a} \cdot h, \quad (42)$$

where *w* is the deflexion of the model. If this process is carried out for several sections, contours of *w*, which represent streamlines in the hydrodynamic analogue, are obtained.

Determination of the elastic moduli of tin single crystals, and their variation with temperature*

by D. G. HOUSE, B.Sc., Grad.Inst.P.,† and E. V. VERNON, B.Sc., Ph.D., A.Inst.P.,‡ Physics Department, University of Southampton

[Paper first received 18 September, and in final form 15 December, 1959]

Abstract

An apparatus is described for the measurement of the frequencies of resonance of longitudinal and torsional vibrations of circular cylindrical rods at temperatures in the range -180 to $+195^\circ \text{C}$. The values obtained have been used to determine the elastic moduli of single crystals of tin over this range of temperature. The equations relating the elastic moduli to these frequencies of resonance for tetragonal crystal symmetry are given. The values of the elastic moduli at 15°C are given as $S_{11} = 41.6$, $S_{33} = 14.9$, $S_{44} = 45.6$, $S_{66} = 42.8$, $S_{12} = -31.2$ and $S_{13} = -4.8$ in units of $10^{-13} \text{ cm}^2 \text{ dyn}^{-1}$.

Introduction

WIDE differences occur in the data published for the elastic moduli (coefficients of compliance) of tin at room temperature. As Vernon⁽¹⁾ has recently described an apparatus for the determination of the elastic moduli of metal single crystals in the form of long circular

cylindrical rods, it was considered worth while to make a fresh measurement of the moduli of tin, and in addition to cover a wide range of temperature. The moduli were determined by exciting single-crystal rods into resonance by applied electrostatic forces, and measuring the frequency of resonance, resonance being detected by a frequency-modulation apparatus. The single-crystal rods, of known crystallographic orientation, were grown from the melt by the method of slow solidification. Each, in turn, was held at its middle with the rod axis vertical, and with the electrode close to, but not in contact with its upper end. Both the rod and electrode were inside an evacuated metal vessel which could be heated or cooled. The vessel was suspended in a large vacuum flask by a thin-walled stainless-steel tube of low thermal conductivity, and was thus well insulated thermally from the surroundings.

Both the longitudinal and torsional frequencies of resonance of a number of crystal rods of different orientations were measured over the temperature range -180 to $+195^\circ \text{C}$. The moduli at 15°C were found to be: $S_{11} = 41.6$; $S_{33} = 14.9$; $S_{44} = 45.6$; $S_{66} = 42.8$; $S_{12} = -31.2$ and $S_{13} = -4.8$ (in units of $10^{-13} \text{ cm}^2 \text{ dyn}^{-1}$).§

* The work described in this paper forms the substance of a thesis for the degree of Ph.D. of Southampton University awarded to D. G. House.

† Now at A.W.R.E., Aldermaston.

‡ Now in Electronics Department, University of Southampton.

§ This unit is used throughout this paper, and will not be mentioned further.

Expressions for the elastic moduli of crystal rods, and the equations relating them to the frequencies of resonance

The expression for the Young's modulus E of a crystal rod which is not constrained and in which the principal crystallographic axes make angles ψ_x , ψ_y and ψ_z with the rod axis, has been given for the general case by Love⁽²⁾ and Hearmon.⁽³⁾ For the metal tin, which has tetragonal symmetry, the effective elastic moduli are S_{11} , S_{33} , S_{12} , S_{13} , S_{44} and S_{66} , and the expression reduces to:

$$\frac{1}{E_F} = S'_{33} = (\gamma_1^4 + \gamma_2^4)S_{11} + \gamma_3^4 S_{33} + \gamma_1^2 \gamma_2^2 (2S_{12} + S_{66}) + \gamma_3^2 (\gamma_1^2 + \gamma_2^2) (2S_{13} + S_{66}), \quad (1)$$

where $\gamma_1 = \cos \psi_x$, $\gamma_2 = \cos \psi_y$ and $\gamma_3 = \cos \psi_z$. The fundamental frequency of resonance f of vibration of a long thin uniform rod of length l and of material of density ρ is given by:

$$f = \frac{1}{2l} \left(\frac{E}{\rho} \right)^{1/2} \quad (2)$$

where E is the appropriate Young's modulus. Coupling between the longitudinal stress and shear strain will in general modify the frequency of resonance. The appropriate Young's modulus E is then called the "pure" Young's modulus E_p , and is related to E_F , the "free" Young's modulus in accordance with Hearmon⁽⁴⁾ by:

$$E_p = E_F / (1 - \epsilon) \quad (3)$$

For tetragonal symmetry the general relationship for ϵ , given by Hearmon,⁽³⁾ becomes:

$$\begin{aligned} \frac{1}{2} S'_{33} S'_g \epsilon = & \{ \gamma_1^6 + \gamma_2^6 - (\gamma_1^4 + \gamma_2^4)^2 \} S_{11}^2 + (1 - \gamma_3^2) \gamma_3^6 S_{33}^2 - \\ & - 2 \gamma_3^4 (\gamma_1^4 + \gamma_2^4) S_{11} S_{33} + \\ & + \{ (\gamma_1^2 + \gamma_2^2 - 4 \gamma_1^2 \gamma_2^2) \gamma_1^2 \gamma_2^2 \} (S_{12} + \frac{1}{2} S_{66})^2 + \\ & + \{ \gamma_3^2 (1 - \gamma_3^2) (1 - 2 \gamma_3^2) \} (S_{13} + \frac{1}{2} S_{44})^2 + \\ & + \gamma_1^2 \gamma_2^2 \{ 1 - \gamma_3^2 - 2(\gamma_1^4 + \gamma_2^4) \} S_{11} (2S_{12} + S_{66}) - \\ & - 2 \gamma_1^2 \gamma_2^2 \gamma_3^4 S_{33} (2S_{12} + S_{66}) + \\ & + \gamma_3^2 (\gamma_1^4 + \gamma_2^4) (2\gamma_3^2 - 1) S_{11} (2S_{13} + S_{44}) - \\ & - \gamma_3^4 (1 - \gamma_3^2) (1 - 2\gamma_3^2) S_{33} (2S_{13} + S_{44}) + \\ & + \gamma_1^2 \gamma_2^2 \gamma_3^2 (2\gamma_3^2 - 1) (2S_{12} + S_{66}) (2S_{13} + S_{44}), \end{aligned} \quad (4)$$

where S'_g is the reciprocal of the rigidity modulus G_F of the rod.

In practice, the radius of the rod was appreciable and so a correction was made to the measured harmonic frequencies of resonance f_n to obtain f . Only the odd harmonics were used, since the rod was clamped at its centre. The frequency f is given by Vernon⁽¹⁾ as

$$f_n = f(1 - kn^2), \quad (5)$$

where n is the harmonic number, and k is a constant containing the Poisson's ratio of the rod.

The free rigidity modulus G_F of a crystal rod, in the case of tetragonal symmetry from Hearmon,⁽³⁾ is given by:

$$\begin{aligned} \frac{1}{G_F} = S'_g = & 2(1 - \gamma_3^2 - \gamma_1^4 - \gamma_2^4) S_{11} + \\ & + 2\gamma_3^2 (1 - \gamma_3^2) (S_{33} - 2S_{13}) - 4\gamma_1^2 \gamma_2^2 S_{12} + \\ & + \frac{1}{2} (1 - 3\gamma_3^2 + 4\gamma_3^4) S_{44} + \frac{1}{2} (1 - \gamma_3^2 - 4\gamma_1^2 \gamma_2^2) S_{66} \end{aligned} \quad (6)$$

The torsional frequency of resonance of a rod is:

$$\frac{1}{2l} \left(\frac{G_P}{\rho} \right)^{1/2}, \quad (7)$$

where G_P is the pure rigidity modulus which, as the specimens had a large length to diameter ratio (> 20), is related to the free rigidity modulus G_F by the equation (Brown⁽⁵⁾):

$$G_P = G_F / (1 - \epsilon) \quad (8)$$

where ϵ is the torsion-flexure coupling and has the same value as the longitudinal shear coupling coefficient.

Apparatus

A block diagram of the apparatus is shown in Fig. 1, and details of the electronic apparatus to excite and detect

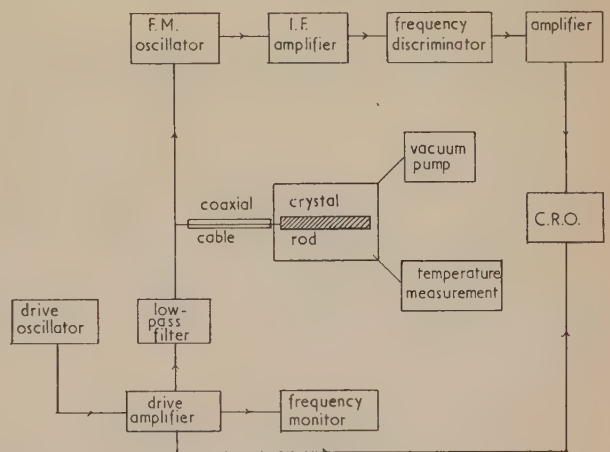


Fig. 1. Block diagram

resonance in the crystal rods are given by Vernon.⁽¹⁾ A stable oscillator of variable frequency was used to produce the electrostatic drive, and a "Cintel" frequency monitor to measure the frequencies of resonance.

In Fig. 2, the assembly for mounting the drive electrode

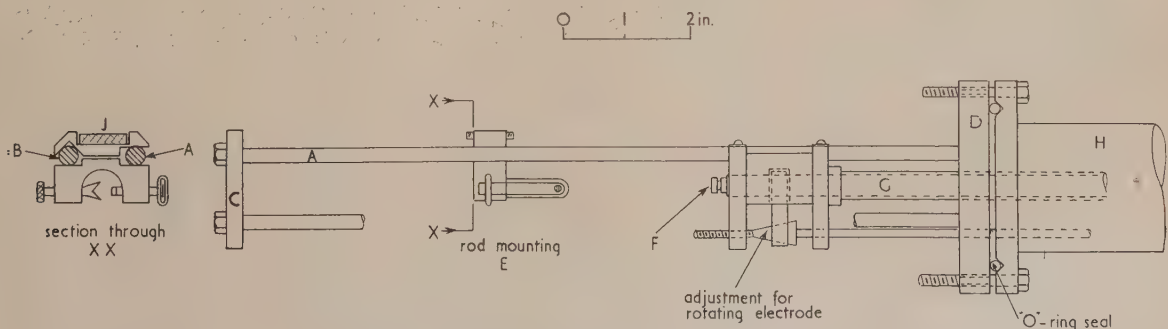


Fig. 2. Crystal-rod and electrode-drive assembly

and the crystal rod are shown diagrammatically. The assembly consisted of four vertical stainless-steel rods, 1 ft long and $\frac{1}{4}$ in. in diameter (of which two, *A* and *B*, are illustrated) held by the two brass flanges *C* and *D*. Two of these rods acted as guides for the crystal rod support *E* and the drive electrode *F*; in order to accommodate crystal rods of various lengths, *E* could be fixed at any desired height by the locking nut *J*. The crystal was held at its middle point in the support *E* by three co-planar knife edges. The electrode *F* was held against two rods, of which *A* is one, by strong springs so that it could slide smoothly along them. The electrode was connected to a fine-pitch screw at the top of the mounting by a thin-walled stainless-steel tube *G*, $\frac{7}{16}$ in. in diameter. By means of the screw, the position of the electrode was adjusted relative to the end of the crystal rod. Provision was made for rotating the electrode by a cone and screw.

The coaxial cable, which connected the electrode with the electronic apparatus, entered the tube through a vacuum seal at its upper end. The flange *D* was joined to a flange at the end of a 2 in. diameter, thin-walled stainless-steel tube *H* of low thermal conductivity, by screwed studding. An O-ring seal made of polytetrafluorethylene was used to make the joint vacuum tight, and also to reduce thermal conduction between the assembly and the steel tube. The polytetrafluorethylene was found to withstand, very satisfactorily, the temperature extremes to which the apparatus was subjected during the measurements.

One of two similar brass tubes was used to enclose the assembly up to the flange *D*, the method of fixing and vacuum sealing being the same as that used to join the flange *D* to the tube *H*. The first tube, for use above room temperature, had an electrical heater, capable of dissipating about 30 W, wound over its surface; the second for use at low temperatures had a helix of copper tubing soldered to its surface, through which liquid oxygen or nitrogen could be passed.

The pressure in the assembly could be reduced by pumping through a side arm attached to the upper end of the large stainless-steel tube, and the heat flow between the assembly and the surroundings was reduced by enclosing the assembly in a 3 in. diameter vacuum flask.

of the brass tube surrounding the specimen constant for up to 30 minutes. For the temperature range 20 to 200°C the brass tube carrying the electrical heater was fixed to the assembly. It was found that the temperature of the crystal rod could be kept within $\pm 1^\circ\text{C}$ for at least 20 minutes without recourse to a thermostat by adopting the following procedure. The apparatus was filled with dry air, and heated slowly to the required temperature. On reaching this temperature the current was reduced by about half and the assembly evacuated to a pressure of about 10^{-2} mm of mercury by a rotary vacuum pump.

A similar procedure was used for the low temperature range 20 to -180°C , the tube carrying the electrical heater being replaced by the tube with the helix of copper tubing. Cooling was effected by pumping liquid oxygen or nitrogen at a controlled rate through the helix. A given temperature could be maintained to within $\pm 1^\circ\text{C}$ for at least 20 minutes.

Measurements of the frequencies of resonance were made at intervals of approximately 10°C for both increasing and decreasing temperatures over the entire range of -180 to $+200^\circ\text{C}$. About 5 litres of liquid oxygen, or 8 litres of nitrogen were required for the low temperature range. Accurate measurement of the temperature of the crystal rods could not be obtained directly, as any attachment to the rod would have completely damped out the resonance. Therefore, a comparison rod was fixed close to the crystal rod and the temperature measured by copper constantan thermocouples fixed to each end of the rod. The thermocouples were calibrated at the boiling point of oxygen, the sublimation point of carbon dioxide, the ice point, the steam point, and the solidification point of tin. To obtain the temperature difference between the comparison rod and a crystal rod, the temperature of a typical tin crystal rod was measured by thermocouples placed at its ends, the temperature being varied as already described. The difference in temperature between the ends of the crystal rod was found to be 2.5°C at the extremes of the temperature range used. The temperature difference between corresponding positions in the crystal rod and comparison rod was found to be about 2°C at these extremes.

Production of the single-crystal rods

Thirteen single-crystal rods (designated *A-M* in Table 1) were grown from "Copper Pass S tin" of 99.997% purity by the method of slow solidification from the melt. Rods of

Temperature adjustment and measurement

To measure the elastic moduli of the crystal rods at various temperatures, it was necessary to maintain the temperature

Table 1. S'_{33} , S'_g , and ϵ for the crystals at room temperature

(1) Crystal	(2) Orientation (deg.)			(3) ϵ	(4) S'_{33} corrected for ϵ	(5) S'_{33} from computed moduli	(6) $(S'_{33 \text{ comp.}} - S'_{33})$ S'_{33} $\times 100$	(7) S'_g corrected for ϵ	(8) S'_g from computed moduli	(9) $(S'_g \text{ comp.} - S'_g)$ S'_g $\times 100$
	ψ_x	ψ_y	ψ_z							
<i>A</i>	90	90	0	0	14.9	14.9	0.0	45.6	45.6	0.0
<i>B</i>	72	86	18	0	15.7	15.7	0.0	51.9	49.0	5.8
<i>C</i>	62	89	28	0.001	17.5	17.5	0.0	51.2	52.0	1.6
<i>D</i>	74	44	51	0.004	20.5	21.2	3.5	56.9	63.5	10.0
<i>E</i>	30	89	60	0.004	30.1	30.8	2.3	48.7	52.2	7.6
<i>F</i>	37	64	66	0.013	20.8	21.1	1.5	68.1	75.7	10.0
<i>G</i>	41	50	83	0.002	15.6	16.2	4.0	106.0	101.8	4.2
<i>H</i>	29	62	83	0.011	23.4	23.5	0.4	68.0	79.3	16.6
<i>I</i>	69	21	84	0.012	29.6	30.1	1.6	54.6	65.6	16.6
<i>J</i>	37	53	87	0.003	17.9	17.9	0	84.1	91.0	8.2
<i>K</i>	67	23	90	0.009	26.1	28.3	4.4	62.0	70.7	11.4
<i>L</i>	31	59	90	0.007	19.6	20.4	4.0	80.4	84.1	4.6
<i>M</i>	0	90	90	0	41.6	41.6	0.0	44.2	44.2	0.0

Note: The moduli S'_{33} and S'_g are expressed in units of $10^{-13} \text{ cm}^2 \text{ dyn}^{-1}$

uniform circular cross-section were produced by the technique described by Vernon⁽⁶⁾ in which a pair of similar semi-circular precision-glass troughs were used as the crystal mould. The crystals *A* and *M* were grown from seed crystals. It was impossible to grow a single crystal, free from imperfections, with the *a*-axis along the rod by means of the conventional furnace which produces a solid-liquid interface in the rod normal to the rod axis. Any imperfection in the seed appeared to produce grain boundary motion, resulting in the growth of a crystal rod of different orientation from that expected. However, even with the use of perfect seed crystals gross lineage occurred in the final crystal rod. This is in accordance with the observations of Teghtsoonian and Chalmers^(7,8) on tin. Aust and Chalmers⁽⁹⁾ described how lineage was inhibited in the growth of aluminium crystals by the use of a tilted solid-liquid interface. This technique was found to be effective for tin, if a solid-liquid interface at an angle of about 70 deg. to the rod axis was used.

The orientations ψ_x, ψ_y, ψ_z of the crystals were measured to ± 1 deg. by an optical goniometer.

Results

(a) *At room temperature.* The values of $E(=E_p)$ and $G(=G_p)$ were calculated from the appropriate frequencies of resonance of the thirteen tin single crystals at 15°C, by means of equations (2) and (7) respectively, taking a value for the density ρ of tin as 7.29 gm cm⁻³. As ϵ is zero in the case of crystal *A*, S_{33} was obtained directly by the use of equations (1) and (3), and S_{44} by the use of equations (6) and (8). Similarly, as ϵ was also zero for crystal *M*, S_{11} and $\frac{1}{2}(S_{44} + S_{66})$, and consequently S_{66} itself, were calculated by the use of these equations. Two other crystals were then used to obtain approximate values of S_{12} and S_{13} , assuming ϵ to be small. Hence, as all the moduli were then known approximately, the correction factor ϵ could be computed to a sufficiently high order of accuracy. The values of S'_{33} and S'_g for all the crystals were then calculated; the results are given in Table 1, columns (4) and (7) respectively.

As a check on the internal accuracy of the method, and the validity of the coupling correction ϵ , a programme was drawn up for a "Pegasus" computer to select all the possible combinations of four equations utilizing the experimental results for longitudinal vibration of the crystals *B* to *M*. The solutions obtained by the computer gave 495 values for each of the moduli $S_{11}, S_{33}, (2S_{12} + S_{66}), (2S_{13} + S_{44})$, of which 130 sets of values were such that S_{11} and S_{33} lay within the limits $39.0 < S_{11} < 43$ and $12.0 < S_{33} < 17.0$ respectively. The other sets of values differed widely; this was due to the small, and therefore relatively inaccurate, magnitudes of the determinants involved in the solution of the equations. This showed that certain combinations of equations could not be used to yield reliable values of the moduli.

The average values for the moduli from the 130 sets are $S_{11} = 41.0$; $S_{33} = 15.0$; $(2S_{12} + S_{66}) = -19.5$ and $(2S_{13} + S_{44}) = 36.1$. The values for S_{33} and S_{11} agree within 1% with those obtained directly from the crystals *A* and *M* respectively. S'_{33} computed from the longitudinal equation (1) using the values of the moduli obtained from crystals *A* and *M* and the averaged values of $(2S_{12} + S_{66})$ and $(2S_{13} + S_{44})$, is shown in Table 1, column (5). In column (6), the difference between the corrected experimental value and the computed value is expressed as a percentage, and it will be seen that the average discrepancy is 2% and the greatest 4.4%. The following results can therefore be

accepted from the longitudinal measurements: $S_{11} = 41.6$; $S_{33} = 14.9$; $(2S_{12} + S_{66}) = -19.5$ and $(2S_{13} + S_{44}) = 36.1$. An accuracy of $\pm 1\%$ is claimed for S_{11} and S_{33} , and $\pm 2\%$ for $(2S_{12} + S_{66})$ and $(2S_{13} + S_{44})$.

From the values of S'_g for the crystals *A* and *M* it follows directly that: $S_{44} = 45.6$ and $\frac{1}{2}(S_{44} + S_{66}) = 44.2$, and hence $S_{66} = 42.8$. These values of S_{44} and S_{66} , in combination with the values of $(2S_{12} + S_{66})$ and $(2S_{13} + S_{44})$ from the longitudinal results, give $S_{12} = -31.2$, and $S_{13} = -4.8$, which when substituted in the relations for S'_g in equation (6) for the thirteen crystals give the values for S'_g in column (8) of Table 1. Agreement with the corrected experimental values in column (7) is not good. The use of the "Pegasus" computer on the torsional results did not give consistent results. The lack of agreement is probably due to torsion-flexure coupling not accounted for by the correction term ϵ , and double refraction of the torsional waves in the crystal (see Musgrave^(10,11)). These effects were not investigated further, as satisfactory results were given by the crystals *A* and *M*, where neither effect can occur.

It is possible to calculate a value for the effective Poisson's ratio [see Vernon,⁽¹⁾ equation (2)] from the measurements of the harmonic frequencies of longitudinal resonance in the crystals. For crystals of most orientations, the ratio is a complicated function of S_{12} and S_{13} but for crystals of the type *A*, with the *c*-axis along the rod, only S_{13} is involved. This method gives a value for S_{13} of 4.4, which compares favourably with 4.8 already quoted, as this latter figure is the difference between two large quantities.

(b) *Temperature variation of the moduli.* Determinations of S'_{33} and S'_g were made on the thirteen tin crystals at intervals of 10°C over the range -180 to $+195^\circ\text{C}$, and the values of the elastic moduli were computed using the data from crystals *A*, *E*, *K* and *M*. No correction was made for changes in length or density of the crystal rods, as these were negligible. The values obtained at intervals of 30°C are given in Table 2. The crystals *C*, *D* and *J* were used to

Table 2. Variation of the elastic moduli with temperature

Temp. (°C)	S_{11}	S_{33}	S_{44}	S_{66}	$-S_{12}$	$-S_{13}$
+195	105.6	18.5	58.7	50.5	91.0	8.5
165	83.8	17.7	55.8	49.2	71.1	7.7
135	68.5	17.0	53.0	47.6	56.2	6.9
105	58.3	16.5	50.5	45.9	46.5	6.1
75	51.2	15.9	48.5	44.7	39.9	5.6
45	46.0	15.4	46.9	43.7	35.0	5.1
15	41.6	14.9	45.6	42.8	31.2	4.8
-15	38.0	14.4	44.5	41.6	27.5	4.5
-45	34.9	14.0	43.3	40.9	25.0	4.2
-75	32.5	13.6	42.3	40.1	22.7	4.0
-105	30.5	13.3	41.3	39.5	20.8	3.8
-135	28.9	13.0	40.4	39.0	19.5	3.6
-165	27.3	12.6	39.6	38.4	18.3	3.4
-180	26.6	12.5	39.2	38.2	17.6	3.3

Table 3. Differences in the measured and calculated values of S'_{33} and S'_g at the temperature extremes

Crystal	Temperature = +195°C		Temperature = -180°C	
	% difference in meas. and calc. S'_{33}	% difference in meas. and calc. S'_g	% difference in meas. and calc. S'_{33}	% difference in meas. and calc. S'_g
<i>C</i>	3.3	23.5	3.5	6.6
<i>D</i>	1.6	20.0	2.0	9.1
<i>J</i>	3.5	16.1	1.3	7.0

check the consistency at the highest and lowest temperature (see Table 3).

Discussion of results

All the available data for the moduli of tin at room temperature is collected in Table 4. The authors' results differ somewhat from those of the other investigators except in the case of Bradfield.⁽¹²⁾ His measurements were made on two single crystals, one with the a -axis along the rod, and the other with the c -axis along the rod. These crystals were supplied by the present authors, and S_{11} and S_{33} were obtained in a similar way to that described here. S_{44} and S_{66} were obtained from torsional resonance of the rods, by means of a magnetostrictive oscillator and detector. S_{13} was computed from Poisson's ratio measurements on longitudinal vibrations. The orientations of these crystals have since been checked by X-ray diffraction photographs.

the deflexion was extremely small, the accuracy of the result ($46 \times 10^{-13} \text{ cm}^2 \text{ dyn}^{-1}$) is only $\pm 20\%$. However, the accuracy is sufficient to confirm the present results in preference to previous results. The results quoted also fulfil the conditions for crystal stability discussed by Alers and Neighbours.⁽¹⁸⁾

It is interesting to note that, if the results obtained by the various authors are expressed in terms of the elastic constants C_{11} , C_{33} , C_{44} , C_{66} , C_{12} and C_{13} , the scatter is considerably less than for the corresponding S values. The C values have been measured directly only in the case of Mason and Bömmel.⁽¹⁷⁾

Acknowledgements

Thanks are expressed to Mr. S. Weintraub of the Physics Department, Southampton University, for helpful discussions, and Professor A. M. Taylor for the facilities provided in the

Table 4. Published data on the elastic moduli of tin at room temperature

S_{11}	C_{11}	S_{33}	C_{33}	S_{44}	C_{44}	S_{66}	C_{66}	$-S_{12}$	C_{12}	$-S_{13}$	C_{13}	β	Temp.	Method	Authority
18.5	8.4†	11.8	9.7†	57.0	1.75†	135.0	0.74†	9.9	4.9†	2.5	2.8†	19.0	Room	Static	Bridgman ⁽¹⁴⁾
15.5	—	—	—	—	—	—	—	—	—	—	—	—	20° C	Comp. Osc.	Landauer ⁽¹⁵⁾
14.6	8.6†	8.5	13.3†	20.6	4.9†	19.0	5.3†	5.3	3.5†	2.07	3.0†	18.7	Room	X-ray	Prasad and Wooster ⁽¹⁶⁾
16.2	7.4	13.4	8.7	45.5	2.2	44.2	2.3	4.1	2.3	3.4	2.8	24.0	Room	Ultrasonics	Mason and Bömmel ⁽¹⁷⁾
41.6*	—	14.9	—	45.6	—	41.9*	—	—	—	4.3	—	—	Room	Resonance	Bradfield ⁽¹²⁾
41.6	7.6†	14.9	9.7†	45.6	2.2†	42.8	2.3†	31.2	6.2†	4.8	4.4†	16.5	15° C	Resonance	Present Authors

S -values in units $10^{-13} \text{ cm}^2 \text{ dyn}^{-1}$; C -values in units $10^{11} \text{ dyn cm}^{-2}$.

† Computed from S -values, see Zwicker.⁽¹⁹⁾

* N.P.L. state that there will be small corrections to be applied to these figures.

An additional check on the accuracy of the results for the elastic moduli is given by the bulk compressibility β , defined by $2(S_{11} + S_{12} + 2S_{13}) + S_{33}$. Bridgman⁽¹³⁾ has determined β directly, and obtained a value of 18.1. Table 4 shows the values obtained from the various workers' results, and it is seen that, in spite of the markedly different values given here, the value of β agrees well with the measured value. A value of β equal to 18.1 results if the value of S_{13} equal to -4.4 obtained from the Poisson's ratio determination on the crystal A is taken.

It should be noted that, whilst there is some doubt about the effect of the longitudinal-shear coupling and the torsion-flexure coupling, the four moduli S_{11} , S_{33} , S_{44} and S_{66} have been obtained from specimens in which this coupling cannot occur. It is therefore felt that quoting an accuracy of $\pm 1\%$ for the values of these moduli is justified. The moduli S_{12} and S_{13} were calculated from data obtained on crystals where some degree of coupling existed, and there is consequently more doubt concerning the accuracy. However, the results obtained with the "Pegasus" computer from the longitudinal resonance results indicate that an accuracy of $\pm 2\%$ for S_{12} and S_{13} is justified.

The large discrepancies between the value of S'_g corrected for ϵ and the value of S'_g from computed moduli seem to point to inadequate theory of the torsion-flexure coupling, but do not detract from the accuracy of S_{44} and S_{66} .

As the value obtained for S_{11} is widely different from previous values, an approximate value for the static modulus was found by a simple bending-beam experiment on a crystal with the a -axis along the rod. The deflexion of the beam was measured by an optical lever, but as

Department. The authors are pleased to acknowledge the valuable assistance of Mr. G. Bradfield of the Basic Physics Division, National Physical Laboratory, Teddington, both in the initial stages of the work and the corroboration of the results. The authors wish to thank the Director of the National Physical Laboratory for permission to publish the results obtained in the Laboratory.

The authors are also pleased to record that this work was assisted by a grant of funds by Imperial Chemical Industries Limited, Metals Division. One of the authors (D. G. H.) is grateful to Southampton University for a post-graduate maintenance grant.

References

- (1) VERNON, E. V. *J. Sci. Instrum.*, **35**, p. 28 (1958).
- (2) LOVE, A. E. H. *The Mathematical Theory of Elasticity* (England: Cambridge University Press, 1927).
- (3) HEARMON, R. F. S. *Rev. Mod. Phys.*, **18**, p. 409 (1946).
- (4) HEARMON, R. F. S. *Proc. Phys. Soc.*, **55**, p. 67 (1943).
- (5) BROWN, W. F. *Phys. Rev.*, **58**, p. 998 (1940).
- (6) VERNON, E. V. *J. Sci. Instrum.*, **36**, p. 198 (1959).
- (7) TEGHTSOONIAN, E., and CHALMERS, B. *Canad. J. Phys.*, **29**, p. 370 (1951).
- (8) TEGHTSOONIAN, E., and CHALMERS, B. *Canad. J. Phys.*, **30**, p. 388 (1952).
- (9) AUST, K. T., and CHALMERS, B. *Canad. J. Phys.*, **36**, p. 977 (1958).
- (10) MUSGRAVE, M. J. P. *Proc. Roy. Soc.*, **A226**, p. 339 (1954).

- (11) MUSGRAVE, M. J. P. *Acta Cryst.*, **10**, p. 316 (1957).
- (12) BRADFIELD, G. Private communication of results of measurements made at the National Physical Laboratory (1959).
- (13) BRIDGMAN, P. W. *Proc. Amer. Acad. Arts. Sci.*, **77**, p. 189 (1949).
- (14) BRIDGMAN, P. W. *Proc. Amer. Acad. Arts. Sci.*, **60**, p. 305 (1925).
- (15) LANDAUER, J. K. *Phys. Rev.*, **96**, p. 296 (1954).
- (16) PRASAD, S. C., and WOOSTER, W. A. *Acta Cryst.*, **8**, p. 682 (1955).
- (17) MASON, W. P., and BÖMMEL, H. E. *J. Acous. Soc. Amer.*, **28**, p. 930 (1956).
- (18) ALERS, G. A., and NEIGHBOURS, J. R. *J. Appl. Phys.*, **28**, p. 1514 (1957).
- (19) ZWICKER, B. *Helv. Phys. Acta.*, **19**, p. 523 (1946).

Measurement of atomic differential scattering cross-sections

by J. S. HALLIDAY, Ph.D., F.Inst.P., Research Laboratory, Associated Electrical Industries, Aldermaston, Berkshire

Paper received 22 October, 1959]

Abstract

The derivation of the atomic differential scattering cross-section $(d\sigma_T/d\omega)_0$ from the intensity distribution in the background of electron diffraction patterns is discussed, bearing in mind the possible effects of plural scattering. It is shown that the variation of $(d\sigma_T/d\omega)_0$ with specimen thickness reported by Haine and Agar⁽¹⁾ is not real but appeared because the decrease in the unscattered intensity was over-estimated. After correction, their values for $(d\sigma_T/d\omega)_0$ are in reasonable agreement with Lenz's⁽²⁾ theoretical values for angles between 10^{-3} and 2×10^{-2} radians, but the experimental rate of decrease of $(d\sigma_T/d\omega)_0$ with increasing angle is smaller than expected. The effect of plural scattering on the intensity distributions from thicker specimens is not as great as that predicted by Lenz.⁽²⁾

Introduction

HAINES and Agar⁽¹⁾ have described absolute-intensity measurements of electron diffraction patterns obtained from films of several elements, using the experimental prototype of the Metropolitan-Vickers E.M.6 electron microscope.⁽³⁾ In particular, the background intensities were measured for angles of deviation in the range 10^{-3} to 2×10^{-2} rad, which the authors call the scatter pattern, and most of the experiments were made with 50 kV electrons. Atomic differential-scattering cross-sections were deduced and compared with those predicted by Lenz,⁽²⁾ assuming that both elastic and inelastic electron scattering occur. Whilst the theory and experimental results were in reasonable agreement when exceedingly thin carbon films were used, an apparent variation of the cross-sections with film thickness was found. In addition, the cross-sections obtained with thin gold, aluminium and copper films were generally 30% smaller than those predicted theoretically.

In this paper, the method for deducing the experimental cross-sections from the intensity variations is reviewed and a better procedure formulated. The results published by Haine and Agar⁽¹⁾ are recomputed with the theoretical data and it is shown that some of the previous inconsistencies are resolved. In addition, the intensity variations are compared

with theoretical angular distributions which include the effects of plural electron scattering; these distributions and their derivation are described in the last part of Lenz's paper.⁽²⁾

Theory

It is assumed that the number of atoms per c.c. of film is N , which is given by ρ/NA , where ρ and A are the density and atomic weight of the specimen and N is Avogadro's number. The thickness of a monolayer t^* is obviously $N^{-1/3}$ cm and the number of atoms per cm² of such a layer is $N^{2/3}$. If σ_T is the total atomic scattering cross-sections, then the total scattering cross-section per cm² of a monatomic layer is $\sigma_T N^{2/3}$. This is equal to t^*/λ_T , since $\sigma_T N$ is the reciprocal of the electron mean free path λ_T .

If an electron beam intensity I_0 is incident on a monolayer, the intensity I which is unscattered after passing through the layer is given by $I_0(1 - t^*/\lambda_T)$. When there are m layers, the total film thickness t is given by mt^* and the corresponding value of I is $I_0(1 - t^*/\lambda_T)^{t/t^*}$. Thus the total fraction of electrons which are scattered after passing through a film is given by:

$$\frac{I_0 - I}{I_0} = 1 - \left(1 - \frac{t^*}{\lambda_T}\right)^{t/t^*}. \quad (1)$$

Now t^*/λ_T is small and therefore this exact relation may be replaced by:

$$\frac{I_0 - I}{I_0} = 1 - \exp\left(-\frac{t}{\lambda_T}\right), \quad (2)$$

even when $t \rightarrow t^*$ (see the points on curve 1, Fig. 1). When $t \ll \lambda_T$, a further approximation can be introduced, giving:

$$\frac{(I_0 - I)}{I_0} = \frac{t}{\lambda_T}. \quad (3)$$

This approximation was implicit in the analysis made by Haine and Agar. Comparison of the straight line 2, Fig. 1, given by equation (3), with curve 1 shows that this approximation leads to a 5% over-estimation of the scattered intensity with carbon films only 20 Å thick.

Some electrons will be plurally scattered on passing through a film, and the probability that an electron will be scattered n times is given by the Poisson distribution⁽⁴⁾:

$$W_n = \frac{\exp(-t/\lambda_T)}{n!} \left(\frac{t}{\lambda_T}\right)^n \quad (4)$$

From this it follows that the fraction of the electrons which are scattered is:

$$\frac{\sum_{n=1}^{\infty} W_n}{\sum_{n=0}^{\infty} W_n} = 1 - \exp\left(-\frac{t}{\lambda_T}\right),$$

in agreement with equation (2). The fractions of electrons that are singly and plurally scattered are obviously given, respectively, by:

$$\frac{W_1}{\sum_{n=0}^{\infty} W_n} \quad \text{and} \quad \frac{\sum_{n=2}^{\infty} W_n}{\sum_{n=0}^{\infty} W_n}.$$

These have been illustrated for carbon films by curves 3 and 4 in Fig. 1. It can be seen that plural scattering is significant even for a 20 Å carbon film and that, if t is greater than about $1.2\lambda_T$, plural scattering predominates.

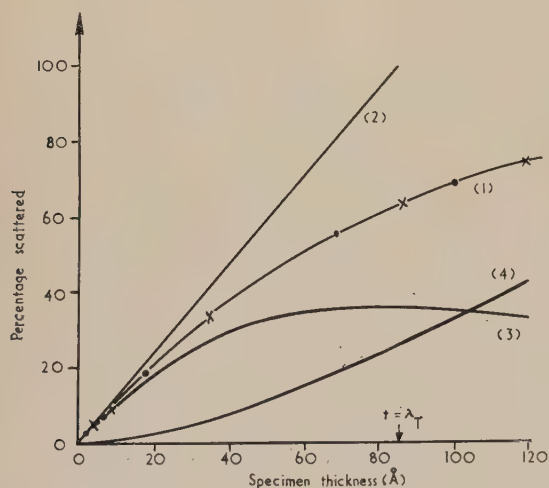


Fig. 1. Theoretical variation of percentage of electrons scattered with specimen thickness, assuming carbon films and operating voltage of 50 kV

- Curve 1: Total percentage of scattered electrons, points \times using equation (1) and points \bullet using equation (2).
- Curve 2: Total percentage of scattered electrons, using equation (3).
- Curve 3: Percentage of singly scattered electrons, using equation (4).
- Curve 4: Percentage of plurally scattered electrons, using equation (4).

In electron-scattering experiments, the photographic plate must accept all electrons scattered in the angular range defined by the apparatus. If diffraction effects are ignored, the angular distribution of these electrons will be the same as that from a single atom if single scattering only is significant. As the angular distribution of plurally scattered electrons will in general differ from that from a single atom, one would expect to detect changes in the angular distri-

bution of electrons with, for example, carbon films as thin as 20 Å. Therefore one may deduce from the experimental angular distributions themselves whether redistribution is significant or not, without appealing to any theory of the angular distribution of plurally scattered electrons.

If redistribution is negligible, the angular distribution will be that for a single atom, and the fraction of the scattered electrons will be given by equation (2). Then the intensity of electrons scattered into a unit solid angle for an angle of deviation θ and from a film of area S is:

$$J_\theta = \frac{S(d\sigma_T/d\omega)_\theta}{\sigma_T} \cdot I_0 \left\{ 1 - \exp\left(-\frac{t}{\lambda_T}\right) \right\},$$

where $(d\sigma_T/d\omega)_\theta$ is the corresponding atomic differential scattering cross-section ($I_\theta + I_\theta^1$ in the notation used by Haine and Agar⁽¹⁾). Thus:

$$\left(\frac{d\sigma_T}{d\omega}\right)_\theta = \frac{J_\theta}{SI_0} \cdot \frac{\sigma_T}{\{1 - \exp(-t/\lambda_T)\}}, \quad (5)$$

and, when $t \ll \lambda_T$:

$$\left(\frac{d\sigma_T}{d\omega}\right)_\theta = \frac{J_\theta}{SI_0} \cdot \frac{1}{Nt}. \quad (6)$$

If the angular redistribution is insignificant, then $(d\sigma_T/d\omega)_\theta$, considered as a function of θ , should be independent of thickness, and the values of $(d\sigma_T/d\omega)_\theta$ deduced from these experiments with the aid of equation (5) should represent true atomic differential cross-sections. If redistribution becomes significant for sufficiently thick films, this will become apparent in that the curves of $(d\sigma_T/d\omega)_\theta$ against θ will alter their shape as the thickness increases, and will no longer represent the atomic differential cross-section.

The experimental intensities may also be compared with theoretical distributions which take into account both the increasing amount of scatter and the angular redistribution caused by plural scattering. Such distributions have been calculated by Lenz⁽²⁾ for carbon, chromium and gold films. At present this comparison must be regarded as a second approach, because any discrepancy between the theoretical and experimental distributions may be due as much to errors in the theoretical differential scattering cross-sections as to inadequacies in the plural scattering theory.

Re-examination of results published by Haine and Agar

Differential scattering cross-sections. Haine and Agar⁽¹⁾ used an equation identical to equation (6) to derive their experimental differential scattering cross-sections, irrespective of the thickness of the specimens. These cross-sections have therefore been multiplied by the appropriate values of $t/\lambda_T \{1 - \exp(-t/\lambda_T)\}$ to obtain values of $(d\sigma_T/d\omega)_\theta$ which would have been given by equation (5).

The variations of $(d\sigma_T/d\omega)_\theta$ with θ deduced by Haine and Agar for carbon atoms have been reproduced in Fig. 2(a), using the more convenient logarithmic scales. The recalculated variations are given in Fig. 2(b). Comparison of these figures reveals that the reported dependence of $(d\sigma_T/d\omega)_\theta$ on film thickness resulted mainly from the oversimplified form of the equation that had been used to derive the values of $(d\sigma_T/d\omega)_\theta$. The unchanging form of the variation of $(d\sigma_T/d\omega)_\theta$ with θ for all thicknesses indicates that the angular redistribution caused by plural scattering was insignificant with these carbon films, even though a very high degree of plural scattering must have occurred in the

thicker specimens. From equation (4), it has been estimated that the fraction of the scattered electrons which were only singly scattered must have varied from about 0.8 to about 0.002 as the carbon film thickness increased from 30 to 740 Å.

There is still a small apparent variation of $(d\sigma_T/d\omega)_\theta$ with thickness in Fig. 2(b). This may be caused by errors in the

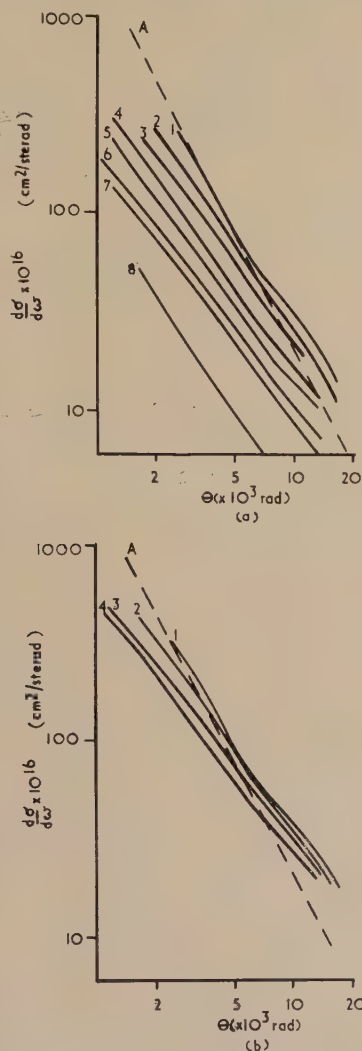


Fig. 2. Differential scattering cross-section for carbon

(a) According to Haine and Agar⁽¹⁾ (b) Corrected

- | | | |
|---------|----------|----------------------|
| 1. 30 Å | 5. 110 Å | 1. 30 Å |
| 2. 45 Å | 6. 190 Å | 2. 45 and 740 Å |
| 3. 55 Å | 7. 290 Å | 3. 55 and 290 Å |
| 4. 75 Å | 8. 740 Å | 4. 75, 110 and 190 Å |

A. According to Lenz's theory⁽²⁾

measurements of specimen thickness or by an error in the theoretical value of λ_T . Haine and Agar⁽¹⁾ have stated that Cosslett and Cosslett⁽⁵⁾ remeasured the thickness of some of the carbon films and were of the opinion that they were thicker than Haine and Agar had supposed. Whilst the reason for this discrepancy has not been satisfactorily resolved, if values suggested by Cosslett and Cosslett⁽⁵⁾ are used, the slight dependence of $(d\sigma_T/d\omega)_\theta$ on thickness is still apparent, but the values of $(d\sigma_T/d\omega)_\theta$ are smaller. Whatever the absolute thickness of the carbon films was, it is clear that

the slope of the experimental $(d\sigma_T/d\omega)_\theta$ curves is slightly less than that predicted by Lenz.⁽²⁾ If the form of the theoretical curve is in error over this limited angular range, then errors in σ_T , and therefore λ_T , may well be expected.

The recalculated experimental variations of $(d\sigma_T/d\omega)_\theta$ for silver, aluminium, gold and copper are shown in Figs. 3, 4, 5 and 6 respectively; the corresponding theoretical curves

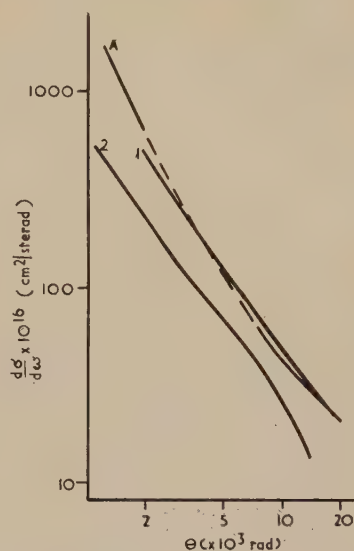


Fig. 3. Differential scattering cross-section for silver
1. 60 Å 2. 180 Å A. According to Lenz's theory⁽²⁾

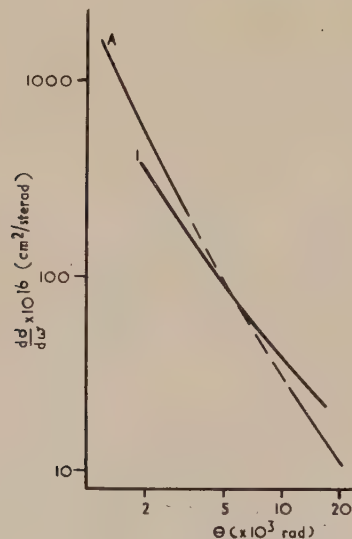


Fig. 4. Differential scattering cross-section for aluminium
1. 90 Å A. According to Lenz's theory⁽²⁾

were also recalculated for each element. Apart from the copper results, the extent of the correlation between theory and experiment is about the same as that obtained with carbon. With the thinnest films, the experimental cross-sections are approximately 50% low when θ is about 2×10^{-3} rad and approximately 50% high when θ is about 15×10^{-3} rad.

Comparison with Lenz's plural scattering theory. Lenz⁽²⁾ has calculated the proportion of the total number of incident

electrons deflected through angles between θ and $(\theta + d\theta)$ to be $f(\theta) \cdot \theta d\theta$, assuming that plural elastic and inelastic scattering occurs. The function $f(\theta)$ is obviously equal to $2\pi J_\theta / SI_0$ and therefore experimental values of $f(\theta)$ can be obtained by multiplying the values of $(d\sigma_T/d\omega)_\theta$ published by Haine and Agar⁽¹⁾ by $2\pi Nt$.

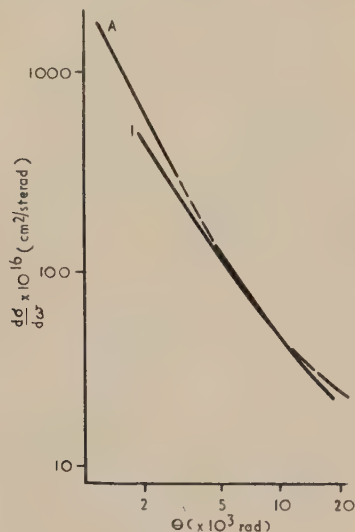


Fig. 5. Differential scattering cross-section for gold

1. 80 Å A. According to Lenz's theory⁽²⁾

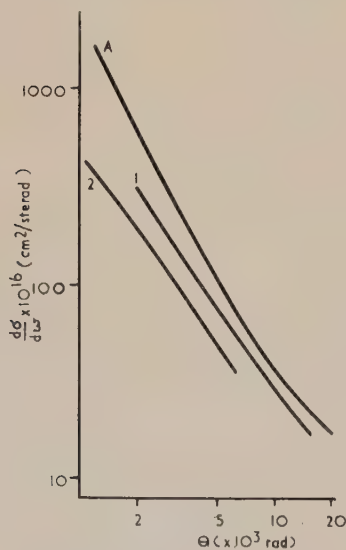


Fig. 6. Differential scattering cross-section for copper

1. 50 Å 2. 350 Å A. According to Lenz's theory⁽²⁾

The carbon $f(\theta)$ -curves are shown in Fig. 7. Whilst the experimental curves reveal no significant angular redistribution of the scattered electrons, as previously noted, an appreciable redistribution had been predicted by Lenz.⁽²⁾ At angles less than 10^{-2} rad, the theoretical $f(\theta)$ -values decrease for all specimen thickness greater than 225 Å, because of the spreading of more electrons into larger angles. Fig. 8 shows the corresponding experimental and theoretical $f(\theta)$ -curves for gold. Once again it is apparent that the predicted angular redistribution has not occurred.

Relative intensity variations, gold films. It is unfortunate that only one set of quantitative measurements with a gold film have been published by Haine and Agar.⁽¹⁾ However

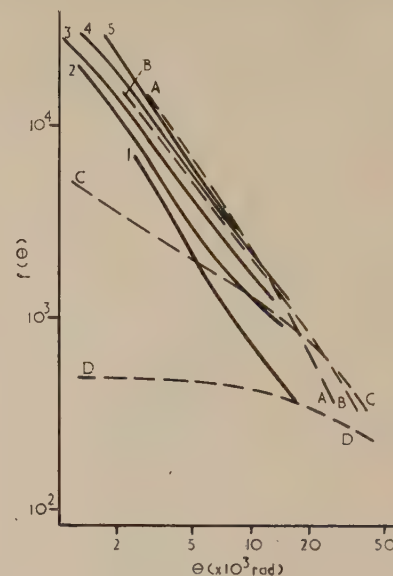


Fig. 7. Intensity variations for carbon films

Experimental ⁽¹⁾		Theoretical ⁽²⁾	
t	t/λ_T	t	t/λ_T
1. 30 Å	0.35	A	2.65
2. 110 Å	1.30	B	5.30
3. 190 Å	2.24	C	10.60
4. 290 Å	3.41	D	21.20
5. 740 Å	8.70		

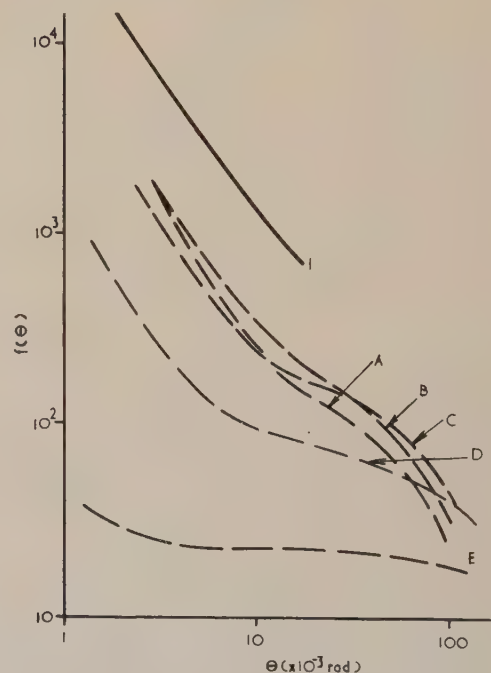


Fig. 8. Intensity variations from gold films

Experimental ⁽¹⁾		Theoretical ⁽²⁾	
t	t/λ_T	t	t/λ_T
1. 80 Å	2.20	A	0.71
		B	1.43
		C	2.86
		D	5.72
		E	11.44

some relative measurements of background-intensity variations obtained with gold specimens have been made by P. H. Borcherds and the author. The diffraction patterns were obtained in a high-voltage electron-diffraction camera operated at 117 kV and the results are shown in Fig. 9. The corresponding angles of deviation at 50 kV have been included along the abscissa so that these results may be compared with those in Fig. 8. With reference to the values of t/λ_T listed in the captions of these two figures, it can be seen that the form of the curves 1 in both figures should be closely similar, and this is so.

The interesting new information in Fig. 9 is that the relative intensities at the smaller angles decrease with

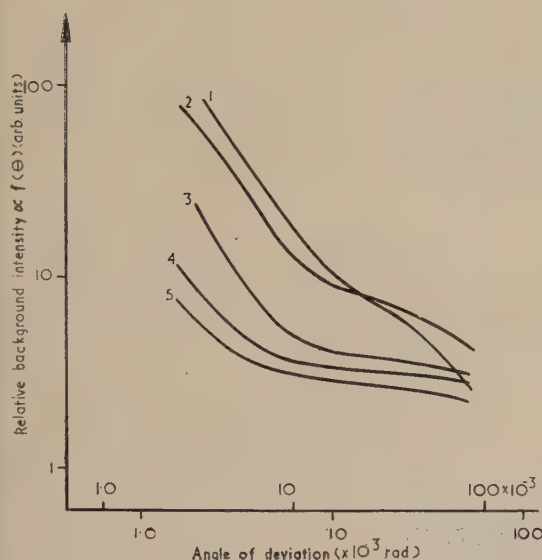


Fig. 9. Relative intensity variations from gold films

Intensity $\propto f(\theta)$.

Top abscissa scale for 50 kV.

Bottom abscissa scale for 117 kV.

t	t/λ_T
1. 150 Å	2.00
2. 250 Å	3.34
3. 580 Å	7.75
4. 690 Å	9.21
5. 833 Å	11.12

increasing thickness, as predicted by Lenz⁽²⁾ (see the broken curves in Fig. 8). Thus, within similar ranges of t/λ_T , the gold results tend to follow Lenz's⁽²⁾ theoretical curves more closely than the carbon ones (Fig. 7). However, with both the gold and carbon specimens, it is apparent that the intensities at small angles are greater than those predicted by the plural scattering theory. It should also be noted that with the gold specimens the experimental rate of decrease of $f(\theta)$ with increasing t/λ_T at a fixed small value of θ , is slower than that predicted and, as described elsewhere,⁽⁶⁾ the experimental rate of decrease of $f(\theta)$ with increasing θ is more rapid at small angles than that predicted. Similar discrepancies have been found with iron specimens (Halliday⁽⁶⁾).

Discussion

It is now clear that the experimental differential scattering cross-sections deduced by Haine and Agar⁽¹⁾ were incorrect

for all except the very thinnest specimens, because the effect of the progressive weakening of the unscattered electron intensity as the beam passed through the specimens was over-estimated. Now that allowance has been made for this, it appears that most of the experimental differential cross-sections are in reasonable agreement with Lenz's⁽²⁾ theoretical values over the range of angles of deviation 10^{-3} to 2×10^{-2} rad. However, all the results show that, within this range, the rate of decrease of $(d\sigma_T/d\omega)_\theta$ with increasing θ is slightly less than that predicted. It is concluded that the theory is probably inadequate for angles of deviation less than 10^{-3} rad and greater than 2×10^{-2} rad.

This conclusion is supported by the differences between the experimental intensity distributions and those proposed by Lenz⁽²⁾ for plural scattering conditions. At present a positive reason for these discrepancies cannot be given, but they would be explained if the values of $(d\sigma_T/d\omega)_\theta$ at angles much smaller than 10^{-3} rad were very much underestimated by Lenz's⁽²⁾ theory. The great majority of electrons scattered through angles less than 10^{-2} rad has suffered inelastic scattering acts and Lenz's equations for the theoretical inelastic differential-scattering cross-sections only include those acts which cause ionization of the atoms. It is very likely that many inelastic scattering acts do not involve such large energy losses and would probably not involve such large angles of deviation. If this error in the theoretical cross-sections does exist, then one would expect the angular redistribution caused by plural scattering within the range up to 10^{-2} rad to be less rapid than that proposed by Lenz.⁽²⁾ Furthermore, the redistribution would be even less rapid for atoms of small atomic number, for which the proportion of inelastic scattering is much greater, and, therefore, less for carbon than for gold. Another consequence of such an error in the theory would be that the theoretical contrast of images produced in the electron microscope would be much better than that obtained experimentally. This discrepancy has been found and the results of this investigation will be described later.

Acknowledgements

The author wishes to thank Mr. A. W. Agar, Dr. M. E. Haine and Mr. D. P. R. Petrie for many stimulating and helpful discussions during the preparation of this paper, and Dr. T. E. Allibone, F.R.S., Director of the Laboratory, for permission to publish it.

References

- (1) HAINE, M. E., and AGAR, A. W. *Brit. J. Appl. Phys.*, **10**, p. 341 (1959).
- (2) LENZ, F. *Z. Naturf.*, **9a**, p. 185 (1954).
- (3) HAINE, M. E., and PAGE, R. S. *Proc. 1st Regional Conference on Electron Microscopy in Europe, Stockholm*, p. 32 (1956).
- (4) ZEITLER, E., and BAHR, G. F. *Exp. Cell Res.*, **12**, p. 44 (1957).
- (5) COSSLETT, A., and COSSLETT, V. E. *Brit. J. Appl. Phys.*, **8**, p. 374 (1957).
- (6) HALLIDAY, J. S. *4th International Conference on Electron Microscopy, Berlin*, paper 26.06 (1958).

Notes and comments

Automatic control in Soviet industry

We have received a copy of a report, published under the above title, of a two-weeks visit to the Soviet Union of a team of six British engineers during May, 1959. The report contains a directory of the Institutes and persons visited with an indication of their field of work, the conclusions of the team, suggestion for further visits, and detailed accounts of work in progress in the Soviet Union.

Notes on discussions with Mr. S. N. Alexander, the leader of an American team which was met by the British team, are included together with a note by Professor A. Tustin on his visit to Poland.

Copies of the report (gratis) are obtainable from the Honorary Secretary, Group B, British Conference on Automation and Computation, c/o Institution of Electrical Engineers, Savoy Place, London, W.C.2.

Glass Technology; Physics and Chemistry of Glasses

From the beginning of this year The Society of Glass Technology's *Journal* has been divided. *Glass Technology* contains reports of applications of science in industry. *Physics and Chemistry of Glasses* has reports of original studies of physics and chemistry of glass both experimental and theoretical. It is to include such items as electrical properties, infra-red absorption relaxation processes, thermodynamics of the glassy state, viscosity and X-ray diffraction.

Both periodicals contain abstracts, letters and book reviews. They are well produced and we congratulate the Society's Editor Professor R. W. Douglas and the Assistant Editor Mr. R. Haresnape on the results of their efforts and wish them all success with this new venture of the Society.

Coke and chemistry, U.S.S.R.

The Russian technical journal *Koks i Khimiya* is now being translated into English and published monthly under the above title at an annual subscription rate of £5 5s. This journal is sponsored by the Department of Scientific and Industrial Research and is produced by the Coal Tar Research Association in collaboration with the British Coke Research Association.

Each issue consists of approximately 60 pages and the original tables and diagrams are reproduced in the English version. Current advances in Russian coking technology are described and should be of interest to technical staff concerned in the production of metallurgical and gas coke and the recovery and refining of the by-products of coal carbonization.

Further information, specimen copies and order forms may be obtained from the Intelligence Officer, The Coal Tar

Research Association, Oxford Road, Gomersal, Leeds, or from the Information Officer, The British Coke Research Association, Chesterfield, Derbyshire.

The Electronic Guide

This new directory is to be published annually to assist workers in electronics to locate articles in which they might be interested. The articles are listed by titles only and have appeared in nearly fifty periodicals published in the Western world. The guide is easy to follow and contains a bibliographic section which lists the names, addresses, and subscription prices of all the periodicals mentioned.

Further details may be obtained from References for Research Division, Electronic Guide Publishing Co., Burbank, California, U.S.A. The price is \$7.50 per volume.

Erratum.

In the paper entitled "Dielectric properties of water/alumina" by J. L. Wood, which appeared on page 404 of the September 1959 issue of this *Journal* it should be noted that, after equation (1) on p. 405 the value of the entropy of activation Δs should be $+14.7$ e.u./mole, instead of the value given.

Journal of Scientific Instruments

Contents of the June issue

PAPERS

- Compensated Wheatstone's bridge circuit for gas-chromatographic catharometry. By A. B. Littlewood.
- Transistor cup anemometer. By R. R. McGregor.
- Photoelectric comparator for Rayleigh fringe electrophoresis patterns. By C. C. Curtain.
- Rand soil-pressure cell for low pressures, high accuracy and long-term stability. By J. E. Jennings and J. B. Burland.
- R.F. admittance bridge for liquid-dielectric measurements. By R. G. Bennett.
- Equipment for the encapsulation of semiconductor devices. By R. D. Knight.
- Tilting and rotating specimen stage for electron microscopy and electron diffraction. By R. E. Burge and H. R. Munden.
- Use of a liquid scintillator counter for beta particles. By T. B. Ryves.
- Epoxy-resin joints for sealed-off, high-vacuum tubes. By J. F. Sayers.
- High frequency light modulation. By R. L. Williams.
- Beam method for the measurement of internal friction. By J. E. Thompson.
- Technique for replicating fibre surfaces by rolling. By J. Mølgaard.
- Laboratory magnetic elutriator for purification and isolation of ferrimagnetic mineral sands. By W. R. B. Martin.

LABORATORY AND WORKSHOP NOTES

- Automatic polishing technique for electro-thinning metals for transmission electron microscopy. By V. A. Phillips and J. A. Hugo.
- Two-valve electrometer circuit. By J. P. Keene.
- Welding copper pipe to stainless-steel flanges in a laboratory workshop. By J. Leece.
- Simple multi-position level. By C. J. Sumner.
- Report on a pump-operated air aspirator. By A. Nunlist and P. H. Kitto.
- Construction of a thermocouple for measuring surface temperatures. By L. Ongkiehiong and J. van Duijn.
- Simple agitating device for partition experiments. By L. Bishop, H. J. de Bruijn and R. B. Temple.

CORRESPONDENCE

- Influence of protective paper on X-ray diffraction photographs. From H. Ruck. M. Kouris and R. St. J. Manley.

NOTES AND NEWS Notes and comments

THIS JOURNAL is produced monthly by The Institute of Physics, in London. It deals with all branches of applied physics (including theory and technique). All rights reserved. Responsibility for the statements contained herein attaches only to the writers.

EDITORIAL MATTER. Communications concerning editorial matter should be addressed to the Editor, The Institute of Physics, 47 Belgrave Square, London, S.W.1. (Telephone: Belgravia 6111.) Prospective authors are invited to prepare their scripts in accordance with the *Notes for Authors*. (Price 3s. 6d. including postage.)

REPRODUCTION. The Institute of Physics is a signatory to The Royal Society's Fair Copying Declaration. Details may be obtained upon application from The Royal Society, London, W.1.

ADVERTISEMENTS. Communications concerning advertisements should be addressed to the agents, Messrs. George Jackson (Fleet St.) Ltd., Cliffords Inn, Fleet Street, London, E.C.4. (Telephone: Holborn 3611-2.)

CLAIMS FOR MISSING JOURNALS. Claims from regular subscribers to this *Journal* for missing numbers will only be considered if received within 60 days of the date of mailing plus normal outward time of transit and time for lodging the claim. Losses attributable to failure to notify a change of address or to similar omissions will not be considered.

SUBSCRIPTION RATES. A new volume commences each January. The charge is £6 per volume (\$17 U.S.A.), including index (post paid), payable in advance. Single parts, so far as available, may be purchased at 12s. 6d. each (\$1.75 U.S.A.), post paid, cash with order. Orders should be sent to The Institute of Physics, 47 Belgrave Square, London, S.W.1, or to any bookseller.

Design and performance of a compact surge generator

by E. THORNTON, B.Sc., Atomic Weapons Research Establishment, Aldermaston, Berkshire

[Paper first received 30 October, 1959, and in final form 24 February, 1960]

Abstract

A compact surge generator for investigation of a fast, linear, pinched discharge using only moderate energy storage is described. The technique of construction using an explosive switch to obtain low inductance, and the method of measuring current are discussed. The behaviour of the surge generator when short circuited is determined from the current waveform, and inductance and resistance values are deduced. The inductance and resistance of the switch are much less than those for the whole circuit, with a linear discharge in deuterium.

assuming a sheath current at the walls, of $10 \text{ m}\mu\text{H}$. For fast discharge operation, it would be desirable to have a short-circuit inductance less than this (that is, with the discharge tube replaced by a short circuit of negligible inductance). The surge generator described has an inductance of about $2 \text{ m}\mu\text{H}$, so that at least 75% of the total circuit inductance is in the discharge.

Introduction

THE surge generator is used primarily for electrical measurements on the fast, linear discharge, and is the $95 \mu\text{F}$, 10 kV version briefly described by Gabriel *et alia*. In the thermonuclear field, and using a linear, pinched discharge, the use of only a moderate energy storage (4500 J , maximum) requires rapid contraction of the plasma under the self-magnetic field, if high temperatures are to be attained and assuming that energy is quickly lost by the plasma. It is necessary to attain currents of the order of 200 kA in a few microseconds.

The main difficulty in the construction of a compact surge generator for this purpose is in reducing the circuit inductance to a sufficiently low value to obtain the required rise time, in particular in obtaining a low-inductance switch and low-inductance capacitors. The low inductance of the surge generator, obtained by using the explosive switch and by symmetrical construction, together with the absence of trigger and conventional spark-gap leads, results in a much lower level of electrical interference from both radiation and multiple earthing.

Basic principles of construction

The basic principle used to obtain low inductance is to bring the outgoing and return current leads as close together as possible at all parts of the circuit, and to make them as wide as possible, instead of using conventional wiring. The result is a compact construction consisting, in effect, of two concentric "shells" with a thin insulating layer in between, this type of construction extending to the capacitors themselves. In addition, reference to Fig. 2 shows the ease with which the explosive switch is adapted to this form of construction. The use of insulating sheet between the contacts of the switch enables them to be brought much closer together than in the conventional narrow current-channel spark-gap switch, with considerable reduction of inductance.

Surge generator

The discharge tube is of silica, 30 cm long, 12.5 cm outside diameter, with 0.5 cm walls. This has a minimum inductance,

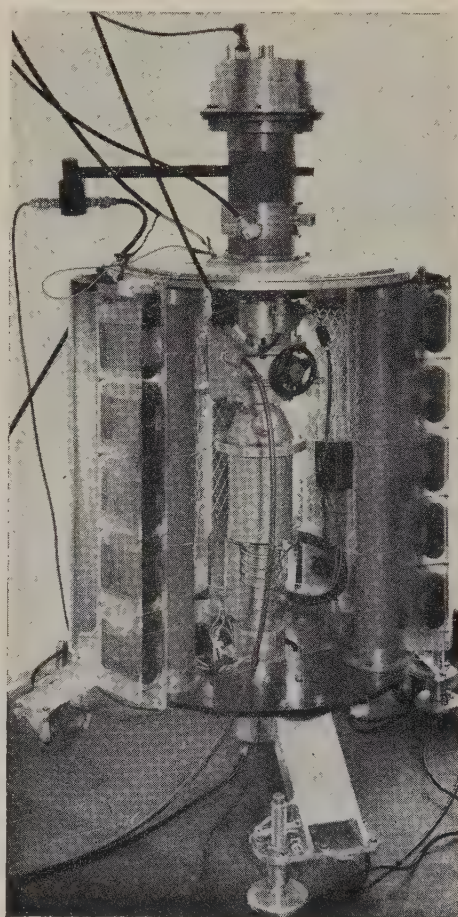


Fig. 1. Photograph of complete surge generator

The surge generator is of moderate energy storage ($95 \mu\text{F}$, 10 kV , 4.5 kJ , maximum; actually $82 \mu\text{F}$ were used in the experiment described) and the size of the main table of the apparatus is determined by the size of the capacitor units grouped round it. The capacitors are $1 \mu\text{F}$, 10 kV basic units with strip leads, developed by Howell.⁽¹⁾ These are grouped into 5 and $10 \mu\text{F}$ blocks which are disposed round the table. The gap in the blocks on one side is to allow access to the vacuum system; the otherwise symmetrical

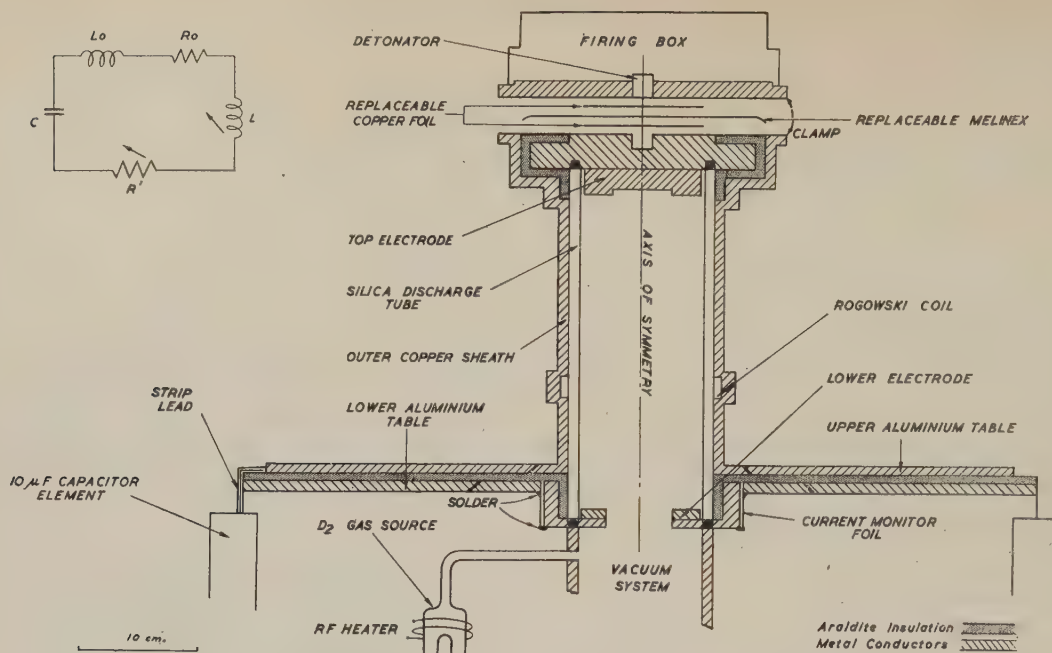


Fig. 2. Diagrammatic cross-section of the table, and the equivalent circuit

arrangement is to minimize inductance (Fig. 1). The explosive switch is also symmetrically mounted on top of the discharge tube (Fig. 2). Insulation between the conductors is of Araldite, which also acts as a mechanical support. The insulation thickness is normally 0.05 in., which is as thin as can be cast and accurately machined without electrical breakdown. The main table is of aluminium with insulation of 0.1 in. Araldite; as an alternative, much thinner melinex sheet has been used with a slight improvement in circuit inductance, but as the main interest is in the resin insulation and its possibilities for complete encapsulation of the components, it is not considered here. Fig. 2 is a diagrammatic cross-section of the apparatus to show the current-carrying parts and the positioning of capacitors, current monitor and explosive switch, and also the equivalent circuit used in analysis of the results.

Table of estimated inductance values

	(L in μH)
Main table	0.65
Capacitors	0.2
Centre section	0.45
(current monitor and discharge-chamber support)	
Switch assembly (excluding foils)	0.3
Switch (replaceable foils)	0.35
Total (short circuit)	1.95
Discharge tube	10.5
Total	12.45

In the equivalent circuit, L_0 and R_0 are the inductance and resistance of the surge generator external to the actual switch contacts and discharge tube, while L and R are the time-varying values of the switch and plasma. R_0 and R^1 are normally lumped together as R . The melinex and copper foils of the switch are replaced at each firing. The figure shows how they are clamped to achieve low inductance.

The table shows the estimated inductance of the various parts of the apparatus.

Current monitor

Current monitoring is achieved by means of a resistive shunt, the voltage across this being monitored on an oscilloscope. The design of high-current shunts has been reviewed by Silsbee⁽²⁾ and shunts for currents of these magnitudes used by Park⁽³⁾ and Durnford and Reynolds.⁽⁴⁾ The self-inductance of the shunt has been reduced by the method of construction and the time constant is less than 30 μs in the case of platinum shunts, which were used in the experiments described. Copper, platinum and, later, constantan (all of which are easily soldered) have been used in the shunts, and heating has been limited to 100°C so that the joints and insulation are not damaged.

The frequency response of a copper shunt is poor and both copper and platinum have a high temperature coefficient of resistance, resulting in a progressive increase in resistance during a discharge.

In the experiments described, platinum shunts were used, and allowance for the increase in resistance made in these results. In later experiments it is proposed to use constantan, with negligible temperature coefficient. Construction of a circular shunt is shown in Fig. 3. The resistive foil of platinum is 0.002 in. thick and the melinex 0.001 in. The d.c. resistance is $3 \times 10^{-4} \Omega$ and the estimated inductive reactances at 1 Mc/s is about $0.3 \times 10^{-4} \Omega$. The estimated accuracy of current measurement including the oscillography is 10%.

To minimize interference caused by multiple earthing in the presence of surge currents, the single earth of the circuit was defined by one of the current monitor leads and the explosive switch was fired while isolated.

Measurements

Measurements to be described are to show that the current shunt gives a fairly accurate measure of current with time, to check the estimated inductance values while short circuited,

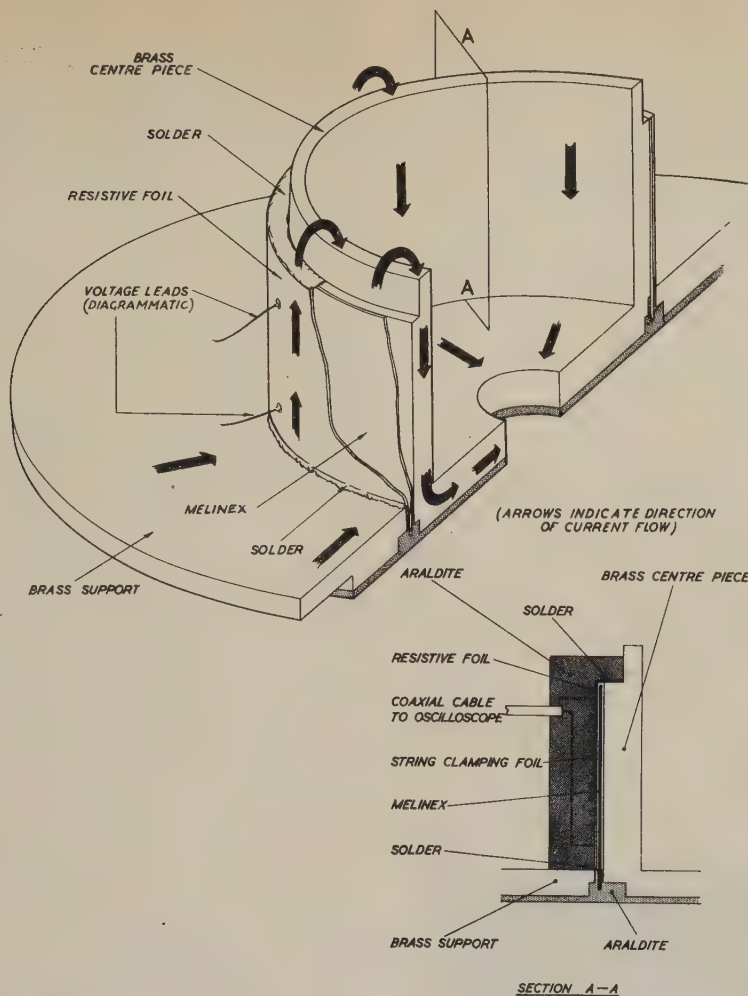


Fig. 3. Diagram illustrating construction, and the operation of current monitor

and to show that most of the total circuit inductance and resistance with the deuterium discharge are associated with the latter. Measurements are of a current oscillogram with the discharge tube short-circuited at 3.4 kV and one for a deuterium discharge at 10 kV.

Results

Fig. 4 shows a current oscillogram with the discharge tube short-circuited, and the particular arrangement used gave an estimated inductance of 1.5 mμH assuming a diameter of

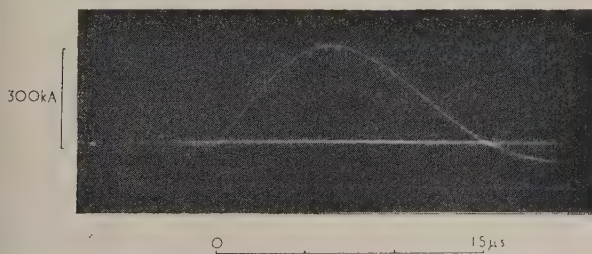


Fig. 4. Current waveform on short circuit (82 μF, 3.4 kV)

0.5 cm for the conducting shock wave from the explosive charge. The smaller value of inductance compared with that of the table results from the use of a main table with a value of L of 0.2 mμH instead of the Araldite-insulated one described.

Agreement to within 10% was obtained between the known capacitor charge and the area under the current oscillogram. This shows agreement between the dynamic and d.c. shunt resistances. The absence of a visible step on the front edge of the oscillogram indicates a negligible self inductance. This is further discussed in Appendix 1. An elementary analysis of the oscillogram, using the measured peak current together with, first by the time-to-peak current and secondly the time-to-first-zero current gave two values of inductance and resistance:

- (1) L (total) = 3.4 mμH, $R = 5.7 \times 10^{-3} \Omega$
- (2) L (total) = 2.4 mμH, $R = 4.7 \times 10^{-3} \Omega$

The initial inductance, estimated from the initial rate of change of current of 6×10^{11} A/s at 3.4 kV was 5.7 mμH.

The oscillogram is less than critically damped, and as interest is mainly in the rise-to-peak current (where the current is determined primarily by inductance), it is possible to determine the time variation of inductance by assuming a fixed value of R . With reference to the equivalent circuit of Fig. 2, and if a short-circuited discharge tube is assumed, then:

$$\frac{d}{dt}(L + L_0)I = \frac{1}{C}(Q_0 - \int_0^t I dt) - RI \quad (1)$$

Fig. 5 shows curves of $L + L_0$ plotted against time for a number of fixed values of R , obtained by progressive integration on the IBM704 computer. Up to 0.4 μs, the inductance values are relatively insensitive to resistance and at

later times should tend to about $2 \text{ m}\mu\text{H}$, as given by the average and calculated values. The inductance and resistance values are further discussed in Appendix 2.

Except during the first 0.1 or $0.2 \mu\text{s}$, which corresponds to the very early stages before the pinching of the discharge in deuterium (Fig. 6), the L and R values above are small compared with the averaged values for the deuterium discharge for which an oscillogram is shown in Fig. 6. The latter shows the characteristic pinches during the rise-to-peak current, and a simple analysis using the time-to-peak current and zero current as before gives L to equal $40 \text{ m}\mu\text{H}$ approximately and R to equal $20 \times 10^{-3} \Omega$.

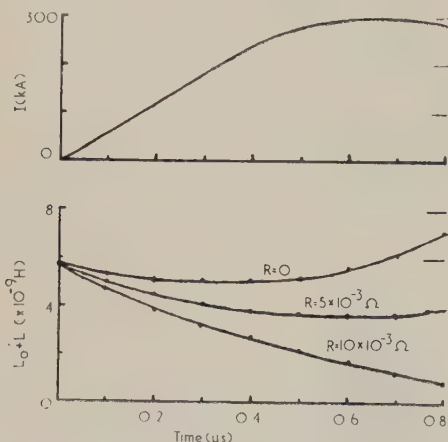


Fig. 5. Variation with time of current and inductance of surge generator on short circuit ($82 \mu\text{F}$, 3.4 kV)

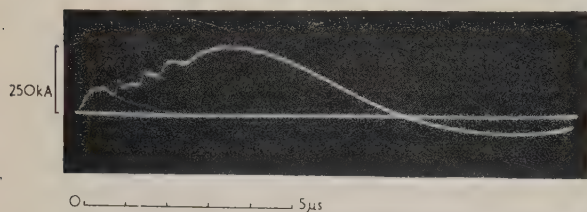


Fig. 6. Current waveform with deuterium discharge (105μ pressure, $95 \mu\text{F}$, 10 kV)

Application of the surge generator in the thermonuclear field

The compactness and portability of the surge generator make it a useful tool in the field of plasma physics when used in conjunction with diagnostic apparatus. In particular, a slightly modified version using a horizontally mounted discharge tube has been used by Gabriel⁽⁵⁾ for optical measurements.

Conclusion

The technique of construction with low inductance enables initial rates of rise of current of about $2 \times 10^{12} \text{ A/s}$ at 10 kV to be achieved. The rate of rise is limited by the initial switch inductance which is higher than expected from the dimensions of the end of the detonator and the shock wave associated with it, presumably because of the electrical breakdown occurring over a smaller area. The initial resistance also appears to be high. Both variables, however, fall rapidly in one- or two-tenths of a microsecond to about $2 \text{ m}\mu\text{H}$ and $5 \times 10^{-3} \Omega$ respectively.

The changing of the switch at each firing is a factor which reduces the speed of operation but, in practice, it is changed in about 2 min, comparable with the time taken to develop

records. As there is a large amount of analysis to perform on a single record, long series of firings are not common.

The current shunt gives reliable measurements of current in the tenth-microsecond region, and analysis of the current oscillogram gives values of inductance and resistance for the short-circuit arrangement much smaller than those for the apparatus with a linear discharge, so that the current waveform is determined primarily by the capacitance and voltage of the capacitor, and by the characteristics of the discharge.

Acknowledgements

The author would like to thank Mr. I. Maddock and Mr. R. J. Wilson for their interest and support and for helpful discussions; the Engineering Sections at A.W.R.E. involved in the design and manufacture of mechanical and electrical components, especially Mr. D. E. Lloyd, Mr. P. D. Gawn and Mr. F. R. Brown; and Mr. S. M. Moulton for much of the routine operation and computing involved.

References

- (1) GABRIEL, A. H., HOWELL, V. T. S., THORNTON, E., and WILSON, R. J. (in course of publication). *J. Sci. Instrum.*
- (2) SILSBEE, F. B. *Bureau of Standards, J. of Research*, **4**, p. 73 (1930).
- (3) PARK, J. H. *Bureau of Standards, J. of Research*, **39** (September 1947).
- (4) DURNFORD, J., and REYNOLDS, P. *Proc. I.E.E.*, Part IV, p. 101 (1954).
- (5) GABRIEL, A. H. *Proc. Fourth International Conf. on Ionisation Phenomena in Gases, Uppsala, 1959*.

Appendix 1

Frequency response of the shunt

The initial circuit inductance is $5.7 \text{ m}\mu\text{H}$ and this, together with the lack of a visible step on the current oscillogram indicates that the shunt time constant is less than $30 \mu\text{s}$. If the initial circuit resistance was extremely high, about 3 orders of magnitude greater than the mean value, the step would not show because of the stray capacitance of the recording equipment. However, this extreme resistance would alter the oscillogram considerably in the first $0.1 \mu\text{s}$.

Appendix 2

Inductance and resistance values

Two ways of obtaining the circuit inductance and resistances have been used, firstly from average values and secondly, on the assumption of a fixed resistance and an inductance/time curve. The first method does not give values in the initial stages of the discharge, the second gives the inductance in the initial stages. If it is remembered that the inductance tends to about $2 \text{ m}\mu\text{H}$ in the later part of the discharge, it will be seen from Fig. 5 that the resistance during this time appears to lie between 0 and $10^{-2} \Omega$. After peak current ($0.66 \mu\text{s}$), a value of about $5 \times 10^{-3} \Omega$ is in agreement with the average values. In the period before $0.2 \mu\text{s}$, the resistance could increase beyond $10^{-2} \Omega$ without radically modifying the inductance. Since the mean inductance to $0.66 \mu\text{s}$ is $3.4 \text{ m}\mu\text{H}$, while the initial inductance is $5.7 \text{ m}\mu\text{H}$, it seems likely that the initial resistance is in fact higher than $10^{-2} \Omega$, but falls in about $0.1 \mu\text{s}$ to less than this. If the resistance did behave in this way the inductance would fall more rapidly initially than in Fig. 6 and would level out at about $2 \text{ m}\mu\text{H}$ in $0.2 \mu\text{s}$.

Optical methods for the study of flames in turbulent pre-mixed gas streams

by M. D. FOX, B.Sc., Grad.Inst.P., and F. J. WEINBERG, D.Sc., Ph.D., D.I.C., A.Inst.P., Department of Chemical Engineering, Imperial College of Science and Technology, London

[Paper first received 29 January, and in final form 19 February, 1960]

Abstract

Three optical methods for the investigation of flame processes in turbulent gases are described. All are based on ray deflexion by the steep refractive-index gradient occasioned by large temperature and composition changes across the flame front. This is utilized in three different optical systems designed (1) to give a measure of the randomness of orientation of the fluctuating flame front in any locality; (2) to delineate the instantaneous flame-front surface; and (3) to map time-mean deflexion (and hence optical path) distributions. Their purpose and use is discussed and illustrated by examples of the records obtained.

Introduction

CHANGES in temperature and composition occasioned by combustion cause variations in refractive index. Optical methods (using extraneous light sources) which in some form display such variations, have proved a powerful tool in combustion research.^(1,2) They are characterized by their non-interference with the delicate flame processes, their absence of inertia and their ability to produce instantaneous records of transient phenomena with high-intensity, short-duration light sources. In all these respects, they are very different from methods employing material probes for similar studies. Much the same advantages are desirable in the study of the parameters of turbulence in flowing gases generally.

Methods such as schlieren and shadowgraphy by which visualization of some instantaneous flame surface (for example, the locus of points giving rise to maximum ray deflexion) can be achieved have previously been applied to turbulent flames (for example, reference 3). They have provided the most direct evidence on which existing, semi-quantitative concepts of turbulent flame propagation are based. The exact (and predictive) understanding of this phenomenon is, however, still in its somewhat superannuated infancy. In recent years, quantitative optical analysis of laminar flames, such as the use of temperature distributions obtained by the mapping of ray deflexions⁽⁴⁻⁷⁾ has contributed to rapid advances in that field. The work here presented forms part of an attempt to apply quantitative optical methods similarly to turbulent flames.

The basic difference between the régimes of turbulent and laminar flames is the introduction of fluctuations on both temporal and spatial scales. If turbulence is homogeneous, it will be seen that the averaging of effects on either scale leads to the same results. For a short optical path, any method is capable of producing two extreme forms of record:

The first, hereafter referred to as the "instantaneous" record, covers all exposure times short enough to "freeze" the phenomenon. For longer exposure times, the information conveyed by the record becomes a function of this time, until a time is reached beyond which further increases again lead to changes only in the local intensity of blackening rather than in its distribution. The second régime will be referred to as the "time exposure". The time interval in between these two states is a measure of the time scale of the turbulent fluctuations, but the complexity of this region considerably exceeds its usefulness. For a long optical path, that is, for a geometrical path such that the (distance) scale of turbulence is negligible in comparison, the above-mentioned averaging ensures that the two types of record are the same. Such considerations impose certain restrictions on available optical methods. Thus it will be seen that if, as is indeed inevitable, the fluctuations in optical path exceed half the wavelength used, no legible interferograms of time exposures are physically possible.

The purpose of the present work is to measure quantities relevant to current theories of turbulent flame propagation and conclusions concerning these aspects of combustion theory will be published elsewhere. Some of the optical methods, however, are likely to be of more general interest and applicability and, since their functions and potential uses are self-explanatory, will be presented here without any flame theory.

The three methods detailed below are all based on ray deflexions, but were designed to fulfil the following three distinct requirements of the problem: the first is to give a measure of the randomness of orientation of the flame front by means of a time-mean polar diagram of deflexions over any desired zone of the flame; the second is intended to delineate (instantaneously) the flame-front surface, producing a contour suitable for geometrical measurements; the third, intended to give information of time-mean distributions of gas properties, is to record quantitatively the distribution of deflexions in one direction over several selected regions of the field. More detailed motives are discussed under individual methods.

All flames used were burner-stabilized. Initial flow-velocity distributions were destroyed by means of a nozzle, terminating in either a circular or a rectangular slot section for the study of axially symmetrical and (approximately) two-dimensional flames respectively. In the latter case, wedge-shaped flames, the apices of which were stabilized on a wire bisecting the shorter sides of the rectangle, were used for some purposes. Turbulence was augmented or modified by various configurations of grids and other devices introducing velocity gradients into the approach flow. The reactants were pre-mixed propane and air.

Polar distribution of deflexions

In a laminar flame, the orientation of the flame front—that is, the local angle between the perpendicular to the flame surface and the flow-velocity vector—is constant in time and varies in distance only gradually (not at all in specially contrived flames). In turbulent flames, on the contrary, orientation fluctuates both in time and space. The extent of disorientation is, in fact, a measure of the effect of turbulence on the flame front, which was required for present purposes. It was desired to confine such measurement to any chosen region of the flame at a time, so that the effect of, for instance, a device inducing turbulence in the gas could be assessed in each part of the stream.

The distribution of ray deflexions in laminar pre-mixed flames has been measured experimentally⁽⁴⁻⁷⁾ and derived theoretically.⁽⁸⁻¹⁰⁾ The following features of the results are relevant here. The deflexions of rays initially parallel to the flame front start at zero on the cold side, rise to a maximum at quite a low temperature (approximately $1\frac{1}{2}$ times the initial absolute temperature) and fall to zero again towards the final maximum temperature, all deflexion being in the direction of the perpendicular to the flame-front surface towards the cold side. The effect of an oblique element of flame front may be resolved into two components; the refractive-index distribution along the ray producing no deflexion and that perpendicular to the ray, which may be treated as above. Moreover, the thickness of a laminar flame front in a near stoichiometric mixture is so small that effects of curvature become negligible for radii of curvature exceeding 1 mm. Thus, any radius vector of a polar-deflexion diagram is given by the vector sum over the ray path of deflexions caused by all those elements of flame front perpendicular to it whose cold (unburnt) sides lie in that direction. The diagram corresponding to a laminar two-dimensional flame whose cross-section is a straight-sided V subtending an angle α is therefore an inverted V of apex angle $(\pi - \alpha)$, if the transilluminating beam traverses the flame perpendicular to this section. The apex, which is the origin of the polar diagram, contains all undeflected light and, on a photograph, would be expected to spread somewhat. At the other extreme, a perfectly disordered system

corresponding to random turbulence of very high intensity would give rise to a perfectly circular diagram.

A parallel light beam traversing the test zone before being focused (in the absence of deflexions) to an image of the point source of the collimator is the simplest optical system with the desired properties—Fig. 1(a). A photographic plate placed at the focus of the second lens or mirror (focal length f) will record a polar diagram, each radius vector of which is the sum over the transilluminated region of $f\theta$ in the direction of θ , the deflexion. If illumination is not uniform, the summation must be weighted accordingly. The region over which deflexions are summed may be confined by an aperture of any desired shape or size. It must be borne in mind, however, that the diffraction pattern caused by the aperture will be featured on the polar diagram so that anything beyond simple slots or knife edges may cause difficulties in interpretation. The same applies to any aberrations of the system and comparison with a “blank” is always advisable.

Fig. 2 illustrates the use of the system in the present instance. The parallel beam was confined by a horizontal

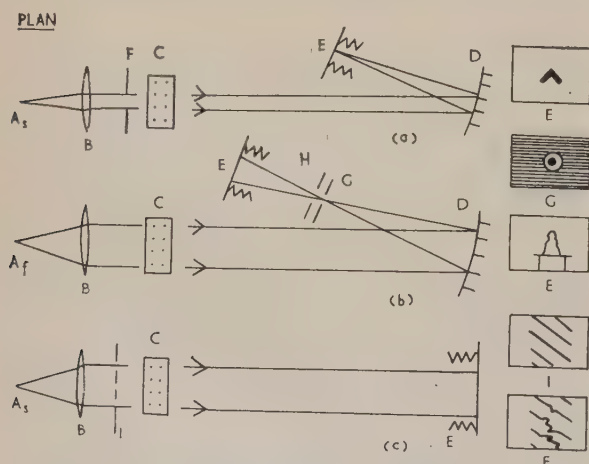


Fig. 1. Schematic diagram of optical systems

A , effective point source (pinhole; real source and condenser not shown), subscripts denote “steady” or “flash”; B , collimating lens; C , refractive-index field under investigation; D , schlieren mirror; E , photographic plate; F , movable slit; G , ring-shaped schlieren aperture; H , high-speed shutter; I , screen of inclined slits.



Fig. 2. Polar deflexion diagrams: wedge-shaped turbulent flame

slit of width 0.35 cm before traversing a wedge-shaped flame of length 3.0 cm, parallel to the stabilizing wire. It was refocused by a “schlieren” mirror of focal length 2.44 m on a photographic plate exposed for 10 s (that is, a “time exposure”). The polar diagrams, one above the other in Fig. 1, correspond to equivalent heights of the confining slit, the vertical-distance intervals being 0.5 cm. It will be seen that a complete transition from near-laminarity at the stabilizing wire to near-randomness at the upper end of the flame front occurs. The vertical line is the diffraction pattern due to the confining slit.

Instantaneous flame-front delineation

The flow velocity of the gas may be determined either as an average value (over the burner mouth) from the volumetric flow rate or locally, by recording the intermittent tracks of small gas-borne particles illuminated by an intense Tyndall beam which is stroboscopically interrupted at a known frequency. This is not sufficient, however, to determine the local velocity of propagation of the front, because the component of velocity perpendicular to the flame can be ascertained only if the orientation of the surface to the approach flow is known at every point. This obviously presents no serious difficulty in the case of laminar flames.

Perhaps the principal tenet of current concepts of turbulent flame propagation is that, within régimes of turbulence relevant here, the increased velocity of flame propagation is due to the increase in flame area. That is, all local-velocity components perpendicular everywhere to the instantaneous shape of the convoluted flame front are thought to be equal to the propagation velocity of the laminar flame. This is the background to the requirement of recording instantaneous flame shape.

A schlieren method based on the optical system used by Töpler⁽¹¹⁾ is suitable for visualization of such refractive index fields. The peculiarity of the present demand is that the normal increase in marking intensity with increase in deflexion is not only unnecessary but indeed undesirable. It is essential that the instantaneous contour of the *outermost* boundary separating burnt from unburnt gas be displayed. If this embodies locally peaks of very small dimensions, for instance, the consequent deflexion may be too small. An increase in sensitivity alone does not answer the need, because, even in an axially symmetrical flame, the resultant increased marking of larger convolutions nearer the axis might mask the true periphery in the plane perpendicular to the optic axis.

Accordingly, a schlieren "blind" was produced, consisting of a small, clear ring on an opaque background, which has the following properties. Undeflected light is arrested by the small central spot so that all zones of no deflexion appear dark. Small deflexions in any direction are marked by equal luminosity. Large deflexions in any direction again give rise to dark regions. Since the deflexion field is continuous, every zone of large deflexion is flanked by regions of small deflexion. Thus, parts of the flame front giving rise to large deflexions must appear as bright double lines—

Fig. 3(a). This, however, leads to no confusion because of the small width of flame zones.

The optical system is shown in Fig. 1(b). The light source used was a flash tube, Siemens type SF.14, fed from a bank of four capacitors each 2 μ F in value, connected in parallel and charged to between 4 and 5 kV. The flash was triggered by a spark gap energized by an induction coil on opening a synchronized camera shutter. The flash was focused on a pin hole. The exposure times were of the order of 10^{-5} s. The schlieren mirror mentioned above was used. Fig. 3(a) shows regions on the periphery of an axially symmetrical flame recorded by this method. To the eye, the flame presents the appearance shown in Fig. 3(b), which is a direct photograph of a one-second exposure.

Deflexion distribution measurement

In a geometrically simple laminar system, the distribution of ray deflexions is readily convertible^(5, 7) to refractive index (and hence temperature or composition) distribution. Knowledge of time-mean optical path distribution is an important requirement in the present investigation, for several reasons.

Parameters of turbulence are calculable^(12, 13) from diffusion rates of gas properties such as temperature or the concentration of one gas in another. The spread with height of an initially fine jet of hot or foreign gas in the turbulent carrier stream can, for instance, be used for this purpose. Deflexion mapping offers a method of achieving this without introducing material thermometers or sampling probes.

Apart from measurement of eddy diffusivity in the cold approach stream, deflexion mapping may be applied to the flame itself. Interpretation is facilitated if the time-mean flame surface is locally parallel to the traversing light beam. Thus, in the case of a fluctuating, corrugated flame front which is thin in comparison with the amplitude of the corrugations, time-mean distribution of deflexions perpendicular to the average flame position will yield the spatial distribution of hot products. For this purpose, the flame front may be regarded as a surface of discontinuity separating the cold reactants (subscript *r*) from the hot products (subscript *p*). The refractive indices, n_r and n_p , respectively, are readily calculable. The latter involves the final flame temperature deducible from thermochemical data. For very-high-temperature flames, the effects of molecular dissociation on refractive index may give rise to some error in n . Such errors, however, do not affect the result appreciably since at such temperatures the gas density in any case differs from vacuum by less than 14% of its N.T.P. value.

For a ray along x , the direction parallel to the average flame-front surface, the time-mean optical path D corresponding to a distance in the flame X is:

$$D = \int_0^X n dx = X \{n_r - f(n_r - n_p)\},$$

where f is the time-mean fraction of the path occupied by hot products. The time-mean ray deflection θ in terms of y —the co-ordinate perpendicular to the average flame-front surface—is therefore:

$$\theta \simeq \frac{dD}{dy} = -X(n_r - n_p) \frac{df}{dy}.$$

The equality is virtually exact for the magnitude of deflexions encountered; the negative sign signifies deflexion in the direction of y decreasing (that is, towards the cold boundary). Distribution of θ in y thus gives the distribution of f —the

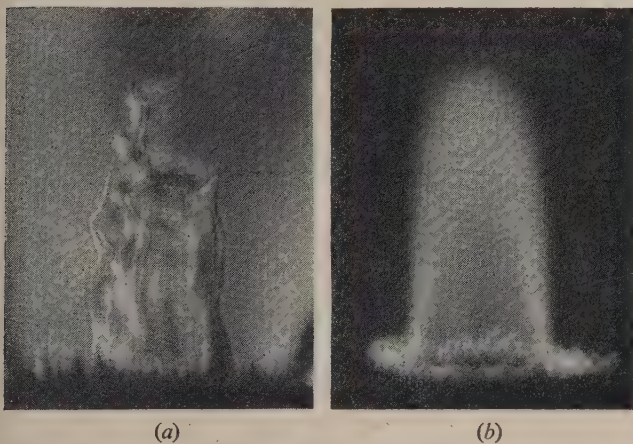


Fig. 3. Axially symmetrical flame:

- (a) Instantaneous contour;
- (b) As seen by eye.

probability of encountering burnt gas at any height. This varies from zero to unity in traversing the slab confined between the extremities of amplitude of the corrugations.

In previous work on flat laminar flames, distributions of ray deflexions were obtained by recording the distorted images of inclined slits through which was passed a beam of parallel light. Fig. 4 shows the record obtained when a

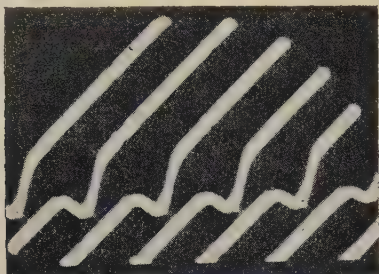


Fig. 4. Inclined slit record: Flat horizontal laminar flame

parallel beam is confined by a series of slits before passing through a flat (horizontal) laminar flame at 45 deg. to the slits and thereafter on to a photographic plate at some distance d beyond the flame. In this instance, no lens was used between flame and plate so that the linear deflexion in the photograph, resulting from the deflexion θ in the flame, is $d\theta$. The theory in the presence of a lens has been published previously.⁽⁷⁾ Records such as that shown in Fig. 4 have been the starting point of elaborate analyses^(5, 6, 7) of processes occurring within laminar flame fronts.

Fig. 5 shows the results of applying this optical system, Fig. 1(c), at an exposure of 1 min, to the spread of heat in a



Fig. 5. Inclined slit record: ("time" exposure). Gas above heated coil (turbulent flow)

turbulent stream. A small coil (diameter 1 mm, length 1 cm) of fine wire (diameter 0.2 mm) was suspended in the stream with its axis parallel to the direction of illumination and perpendicular to the mean flow direction. The coil was heated electrically to a temperature of about 500°C.; the time-mean distribution of refractive index downstream of the heat source is readily calculable from the record.

In Fig. 6, the deflexion field was due to a wedge-shaped turbulent flame, the long side of which was parallel to the optic axis. The length of the flame in the direction of the rays (3.0 cm) was considerably greater than the scale of turbulence, so that distance averaging precludes the measurement of localized instantaneous refractive-index distributions. Fig. 7 shows the record obtained at an exposure time of

about 10^{-5} s using a flash of the same duration as that used in Fig. 3(b) which, as has been seen, is brief enough to produce an "instantaneous exposure" as defined above.

From photographs such as that shown in Fig. 6 the time-mean distribution of the reactant-to-product ratio perpendicular to the average flame front plane is calculable.



Fig. 6. Inclined slit record: ("time" exposure). Wedge-shaped turbulent flame

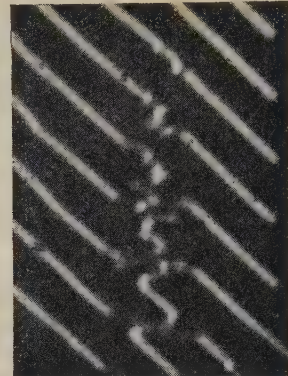


Fig. 7. Inclined slit record: ("instantaneous" exposure). Wedge-shaped turbulent flame

Conclusions

Ray deflexion techniques have been established which fulfil three distinct requirements in the study of turbulent flames and allied phenomena. Some information made available by their application, detailed above, is not obtainable by other methods without material interference with the systems studied.

Acknowledgements

It is a pleasure to thank Professor D. M. Newitt, F.R.S., and Dr. J. H. Burgoyne for their interest in and encouragement throughout the investigation of which this work forms part. One of us (M.D.F.) is indebted to the U.S. Air Force for financial support. This work is being carried out under Contract A.F.61 (514)—1013 of the U.S.A.F.

References

- (1) WEINBERG, F. J. *Sixth Symposium (International) on Combustion*, p. 765 (New York: Reinhold, 1956).
- (2) WEINBERG, F. J. *Geometric-optical techniques in combustion research*. Progress in Combustion Science and Technology Series (London: Pergamon, 1959).
- (3) WOHL, K., SHORE, L., VON ROSENBERG, H., and WEIL, C. W., *Fourth Symposium (International) on Combustion*, p. 620 (Baltimore: Williams and Wilkins, 1953).
- (4) DIXON-LEWIS, G., and WILSON, M. J. G., *Fourth Symposium (International) on Combustion*, p. 263 (Baltimore: Williams and Wilkins, 1953).
- (5) BURGOWNE, J. H., and WEINBERG, F. J. *Fourth Symposium (International) on Combustion*, p. 297 (Baltimore: Williams and Wilkins, 1953) and *Proc. Roy. Soc., A*, **224**, p. 286 (1954).
- (6) LEVY, A., and WEINBERG, F. J. *Seventh Symposium (International) on Combustion*, p. 296 (London: Butterworths, 1959).
- (7) LEVY, A., and WEINBERG, F. J. *Combustion and Flame*, **3**, p. 229 (1959).

- (8) WEINBERG, F. J. *Fuel*, **34**, S.84 (1955) and **35**, p. 161 (1956).
 (9) ZAREMBO, K. S., and ZEL'DOVICH, YA. B. *Zhur. Fiz. Khim. (U.S.S.R.)*, **22**, p. 427 (1948).
 (10) WEINBERG, F. J. *Proc. Roy. Soc., A*, **235**, p. 510 (1956), and **A.243**, p. 107 (1957).
 (11) TÖPLER, A. *Ann. Phys. u. Chem. (J. C. Poggendorff)*, **127**, p. 556 (1866); **128**, p. 126 (1866); **131**, pp. 33 and 180 (1867); **134**, p. 194 (1868).
 (12) WESTENBERG, A. A. *J. Chem. Phys.*, **22**, p. 814 (1954).
 (13) WESTENBERG, A. A., and RICE, J. L. *Combustion and Flame*, **3**, p. 459 (1959).

A study of large strains and the effect of different values of Poisson's ratio

by H. FESSLER, M.Sc., Ph.D., A.M.I.Mech.E., University of Nottingham, and
 B. H. LEWIN, B.Sc., Ph.D., A.M.I.Mech.E., Birmingham College of Advanced Technology

[Paper first received 12 November, 1959, and in final form 24 February, 1960]

Abstract

The frozen-stress photoelastic technique was used to study the stresses on the inner surfaces of T-junctions of pipes subjected to different internal pressures. The peak stresses were always proportional to the applied pressure.

The peak strains at a T-junction of hollow pipes under diametral compression were measured for identical shapes, made of materials of different Poisson's ratios. Within the limits of experimental accuracy, the peak strains were found to be independent of Poisson's ratio.

Introduction

THIS paper presents an experimental investigation of the two phenomena which may cause variations in stress distribution between frozen-stress photoelastic models and metal prototypes of the same shape. Even with the best materials available for frozen-stress analysis, it is frequently necessary to apply strains much greater than the elastic strains in metal prototypes for the model to show sufficiently large fringe orders. The value of Poisson's ratio for frozen-stress materials is 0.5 whereas it is approximately 0.3 for metals commonly used in highly stressed components.

No general mathematical method is known to the authors which can be used to convert the measured stresses obtained for one value of Poisson's ratio to the stresses in the same shape, under the same loading conditions, but made of a material of different Poisson's ratio. Therefore the effect of changes of Poisson's ratio may be *calculated* only for problems for which a general solution exists which is based on theory of elasticity. In these cases, it is possible to substitute different values of Poisson's ratio in the solution and this has been done.^(1,2) In all other cases, the effect can only be investigated experimentally.⁽³⁾ The effect of large elastic strains could only be *calculated* for problems for which a solution exists which is based on the theory of finite strains.

The problem studied in this paper is the intersection of hollow cylinders. In this, there are stress concentrations with large stress gradients. These are likely to produce severe local distortions which may be expected to accentuate the effects of large strains. The complexity of the shape makes it unlikely that a theoretical solution could be devised which would predict the stresses at the intersection accurately.

The large strain effect is studied in T-junctions of branched pipes subjected to internal pressure. These pipes were long enough for the junction to be unaffected by the end closures. In any one model, the ratios of bore to outside diameter of main pipe and branch were the same. The Poisson's ratio effect is studied with short T-pieces made of different materials and subjected to concentrated compressive forces at the centre of intersection.

Definitions

- b = inside diameter of branch
 d = inside diameter of main pipe
 p = internal pressure
 f = suffix for frozen-stress test
 x, y, z = cartesian co-ordinates
 A = cross-sectional area of point-loaded model in $y = 0$ plane
 B = outside diameter of branch
 D = outside diameter of main pipe
 E = Young's Modulus
 F = material fringe value
 N_a = fringe order in plane $y = 0$
 N_h = fringe order normal to plane $y = 0$
 P = force applied to point-loaded models
 σ_a = axial stress
 σ_h = hoop stress
 ϵ_{max} = greatest strain
 ϵ' = mean strain
 ν = Poisson's ratio

Crutch is the region near the intersection of the inner surfaces and near the plane $y = 0$.

Stress ratio equals (measured stress / hoop stress on inner surface of undisturbed pipe).

Large-strain effect

Seven models were tested to investigate the effect of large strains on the stress distribution on the inner surface of branched pipes subjected to internal pressure. The general shape of these models is shown by dotted lines in Fig. 1. The manufacture of these models has been described.⁽⁴⁾

The pressure fluid was a dense oil and the models were immersed in pitch to reduce the stresses caused by the weight of the model itself. The dimensions of these models are shown in Table 1. The outside diameter D of the main pipe was 3 in. for all models.

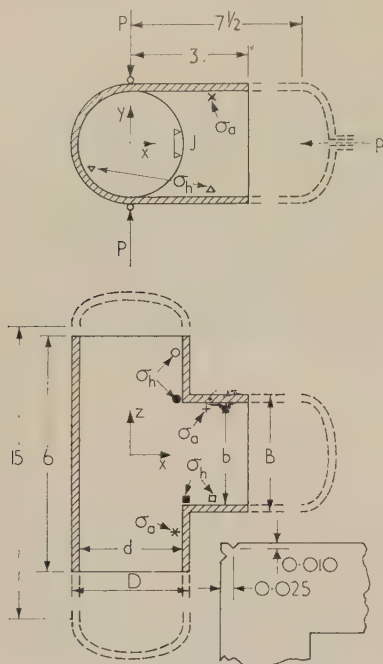


Fig. 1. Models and notation

Full lines show point loaded models; dotted lines show pressure loaded models
Inset shows magnified section of point-loaded models with small grooves for location of extensometer. Symbols refer to pressure-loaded models
Dimensions are in inches

Table 1. Dimensions of models

Model No.	$\frac{d}{D} = \frac{b}{B}$	$\frac{b}{d}$
1, 2, 3	0.333	1.0
4, 5	0.708	0.5
6, 7	0.750	1.0

Axial slices were cut from the models and the stresses marked with the symbols $+$, $*$, \times and ∇ in Fig. 1 were determined from these slices. To evaluate the hoop stresses in branched pipes may be compared with the stresses near a hole in a flat plate.⁽⁴⁾ The similarity of the curves for hoop stresses in branch \square and main pipe \circ and of axial stresses $+$ and $*$ illustrates that this concept is reasonable. The symbols \bullet and \blacksquare show the values of the hoop stresses \circ and \square

The models were calibrated by determining the applied pressure in fringes per inch from shear difference type numerical integrations⁽⁵⁾ in the undisturbed parts of the pipes. All results were expressed as stress ratios, defined as the measured stress divided by the hoop stress on the inner surface of the undisturbed pipe.

The results for Model 5 are shown in Fig. 2. The distance ratios $2x/d$ and $2z/b$ were chosen so that the stresses in branched pipes may be compared with the stresses near a hole in a flat plate.⁽⁴⁾ The similarity of the curves for hoop stresses in branch \square and main pipe \circ and of axial stresses $+$ and $*$ illustrates that this concept is reasonable. The symbols \bullet and \blacksquare show the values of the hoop stresses \circ and \square

plotted to an enlarged scale of distance ratio to assist in the extrapolation to the peak stresses at the intersection of the inner surfaces.

The arrows at the right-hand edge of Fig. 2 indicate the hoop- and axial-stress ratios calculated from Lamé's equations. All the stresses approximate to these values at infinity. The hoop stresses in the main pipe shown by the symbol ∇ in Fig. 1 were not recorded in Fig. 2. These stresses increased from a negative value at the intersection (determined by the internal pressure) to small tensile values.

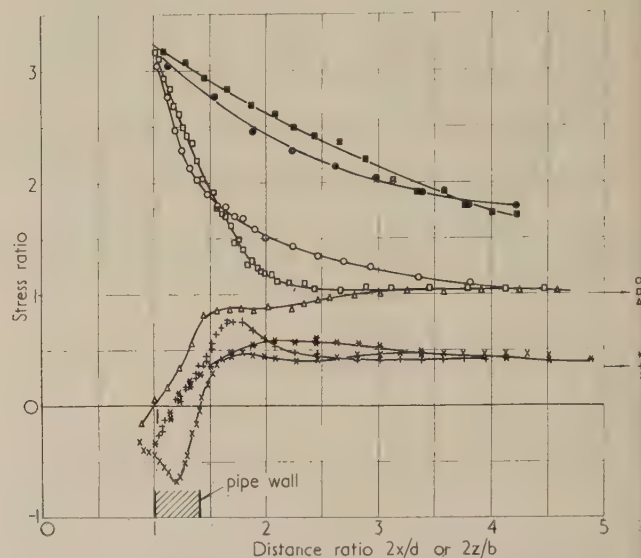


Fig. 2. Stresses on inner surface of Model 5 (symbols are defined in Fig. 1)

The results for Model 4 were not significantly different from those shown for Model 5. The results for the other five models exhibited the characteristics shown in Fig. 2, namely large hoop stresses at the crutch (see Definitions) which decrease fairly rapidly to the stresses in the undisturbed cylinder, and comparatively small axial stresses which also approximate to the stresses in the undisturbed cylinder.

Because the stress distributions were so similar, it was only important to compare the peak stresses in the different models. This was done in Fig. 3. The pairs of points show

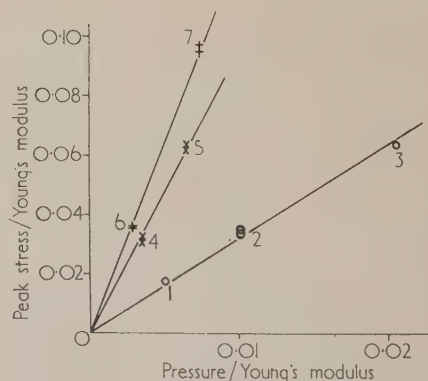


Fig. 3. Peak stresses in models tested under different internal pressures

the peak stresses in the opposite surfaces, one obtained from the extrapolation of hoop stresses in the main pipe, the other from extrapolation of hoop stresses in the branch.

The reference numbers of the models are shown near the experimental results. It may be concluded from Fig. 3 that the peak stresses are proportional to the applied pressure to an accuracy of $\pm 6\%$. Tests carried out on 36 models of branched pipes of varying proportions indicated that the peak stresses are subject to an experimental scatter of about $\pm 6\%$. Fig. 4 shows that the expansions of these models at the y -axis is proportional to the applied pressure. It may therefore be concluded that, in these perfectly elastic models, no evidence of a large strain effect was found with peak stresses up to 10% of Young's modulus.

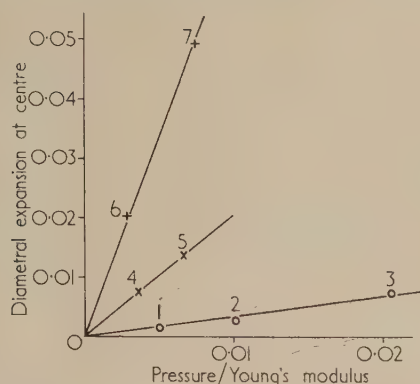


Fig. 4. Expansion of models tested under different internal pressures

Effect of Poisson's ratio

The effect of variation of Poisson's ratio on the peak stresses was studied by measurement of the peak strains because the intersection of pipes is a three-dimensional problem and all known photoelastic materials have a Poisson's ratio of $\frac{1}{2}$ under frozen-stress conditions. Other three-dimensional photoelastic techniques were rejected as too complex and too inaccurate.

Electrical-resistance strain gauges were not used because the large strain gradient which was known to exist near the peak stresses would have necessitated very large models if accurate results were required. A mechanical extensometer of the twisted strip type by S. E. Johanssen was used because this instrument is very sensitive and accurate.

As it is not practicable to subject a Johanssen extensometer to hydrostatic pressure, an alternative method of loading the models had to be devised. The peak stresses in branched pipes under internal pressure occur in the $y = 0$ plane (Fig. 1) and are tensile, in the y -direction. These conditions would also apply if the branched pipes on either side of the $y = 0$ plane were pulled apart by forces in the $+y$ and $-y$ directions. Because such a pull would be difficult to apply, it was decided to reverse the loading and to apply a compressive

force. A concentrated force P acting at the intersection of $x = 0$ and $z = 0$ was chosen because this was expected to produce high stress concentrations, and resulted in a well defined loading system which bore some similarity to loading by internal pressure.

The lengths of the pipes had to be shortened to the sizes shown by the full lines in Fig. 1 to allow the extensometer to be fitted on the inside of the pipes. To locate the extensometer accurately, the smallest practicable grooves were machined in the model as near to the intersection as possible. These grooves are shown on the large-scale inset in Fig. 1. The shape chosen for these tests was an equal-sized branch ($b = d$) with a fairly thin wall ($b/B = 0.875$). The wall thickness of the Araldite model varied between 0.187 and 0.189 in. because the portions of the outer surface which could not be turned on a lathe had to be filed to the correct profile.

For accurate measurement of elastic strains it was necessary to choose materials with high limits of proportionality (of stress to strain) compared with their Young's Moduli. A high-strength aluminium alloy was selected as a material with Poisson's ratio of about $\frac{1}{4}$. Araldite casting resin B satisfies the above requirement also and has a Poisson's ratio 0.4 when tested at room temperature and 0.5 under frozen-stress conditions.

The concentrated force P was applied by weights through $\frac{1}{8}$ in. diameter steel balls located on the y -axis (Fig. 1). Because frozen-stress tests of branched pipes under internal pressure had shown that the stress gradient in the y -direction on either side of the $y = 0$ plane was small, it was possible to use a 0.4015-in. gauge length in the extensometer (indicated as J in Fig. 1) in the four positions on either side of both crutches of each model. The gauge length of the extensometer was not altered and was measured before and after the tests and found unchanged. Loads were applied in at least eight increments and decrements and the gauge deflexions were exactly proportional to the load increments in every case. The variations in the slopes of these graphs (called J values in Table 2) were attributed to small errors in the geometry of the locating grooves. The calibration constant of the extensometer was checked with slip gauges.

When the J -value has been multiplied by the calibration constant and divided by the gauge length, the strain per unit load ϵ_{max}/P is obtained. To compare results for materials of different Young's moduli, these results were converted into strain concentration factors:

$$\frac{\epsilon_{max}}{\epsilon'} = \frac{\epsilon_{max}/P}{\epsilon'/P} = \frac{\epsilon_{max}/P}{1/AE},$$

where the mean strain ϵ' is defined as the strain at the crutch which would occur if the load P were distributed uniformly over A , the cross-sectional area of the model in the $y = 0$ plane (2.32 in.²).

Table 2. Strain-concentration factors

(1)	(2)	(3)	(4)	(5)
Material	Alum. alloy	Araldite casting resin β		
Shape	original	original	deformed	deformed
Test	J	J	frozen stress	J
Modulus, lb/in. ²	10.42×10^6	0.4603×10^6	2.11×10^3	0.4603×10^6
Poisson's ratio	$\frac{1}{4}$	0.4	0.5	0.4
J value divisions/lb	$0.0279 \pm 2.5\%$	$0.630 \pm 3\%$	—	$0.692 \pm 4.2\%$
Greatest ϵ' (%)	0.0039	0.0050	0.0418	0.0050
ϵ_{max}/ϵ'	33.7 ± 0.8	33.7 ± 1.0	35.8 ± 1.2	37.0 ± 1.5

These arbitrarily defined strain-concentration factors for the aluminium alloy model and for the Araldite model before and after stress-freezing, are recorded in Table 2 in columns 2, 3 and 5 with other relevant information. The Young's modulus of the aluminium alloy was determined from tensile specimens in the direction of and across the grain of the forgings. These values differed by $3\frac{1}{2}\%$ and the mean value was used for the calculation. The Young's modulus of Araldite at room temperature was determined from the deflexions of a beam subject to pure bending.

After the Araldite model had been subjected to an extensometer test (column 3 in Table 2) a frozen stress test was carried out. The values recorded in column 5 of Table 2 were obtained from tests performed at room temperature on the deformed frozen stress model before this model was sliced.

For the frozen stress test, a force P_f equal to 1.98 lb was applied, and the model was immersed in a dense oil to reduce the effect of the weight of the model itself. Subsequently it was found necessary to consider the influence of the effective weight of the upper half (y positive) of the model on the peak stresses. Consideration of the model as an arch suggested that the concentrated force P should be increased by 2.9% to allow for the (distributed) effective weight.

After a central slice (defined by the planes $y = \pm 0.025$ in.) had been cut out of the Araldite model, one of the remaining pieces was subjected to another frozen-stress cycle under the action of its own weight only. Fringe readings near the crutch confirmed that 3% should be added to P , and this was done.

Axial stresses were obtained from the central slice and are recorded in Fig. 5a. The hoop stresses, shown in Fig. 5b, were measured in sub-slices cut from the central slice. From these graphs, the hoop and axial stresses at the roots of the

notches were read as $N_h = 24.6 \pm 0.8$ and $N_a = 1.33$ fringes/in. respectively. The material-fringe value F and Young's modulus E_f under frozen-stress conditions were determined from a tensile strip cut from the model. The strain concentration factor is:

$$\frac{\varepsilon_{max}}{\varepsilon'} = \frac{F(N_h - \nu N_a)/E_f}{P_f/AE_f} = \frac{FA}{P_f}(N_h - \nu N_a)$$

This expression is independent of E_f but its value depends on Poisson's ratio ν , which was taken as 0.5 on the basis of other tests. The results are recorded in column 4 in Table 2.

The variations in $\varepsilon_{max}/\varepsilon'$ in columns 2, 3 and 5 are based on the variation in J values for the different gauge positions. The variation in column 4 is based on the difference in hoop stresses between the main pipe and branch shown in Fig. 5b. Variation resulting from other experimental factors is difficult to estimate.

Comparison of the J values in Table 2, columns 3 and 5 shows that the mean compression per pound was 10% greater after the frozen stress test than before. Because both series of tests were carried out on the same model with the

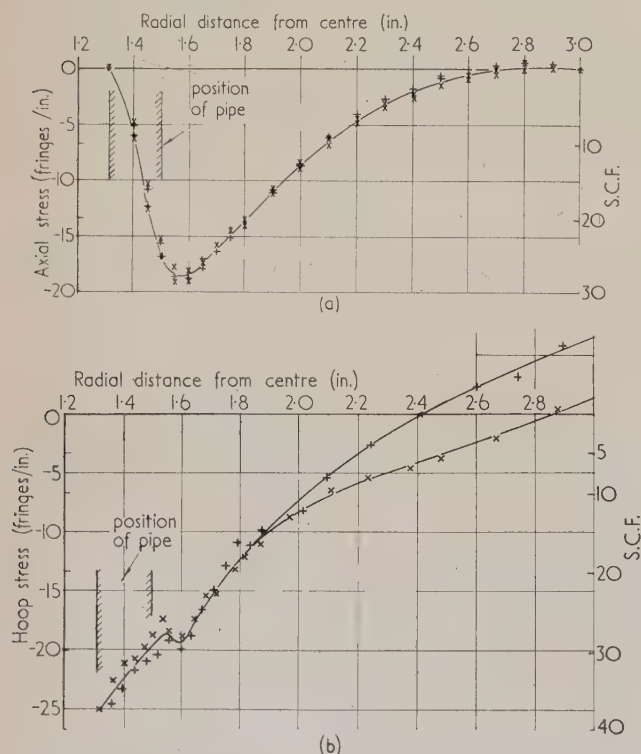


Fig. 5. Frozen stresses in point-loaded model on inner surface in plane $y = 0$ on x positive side; (a) axial, (b) hoop
 × refers to main pipe
 + refers to branch

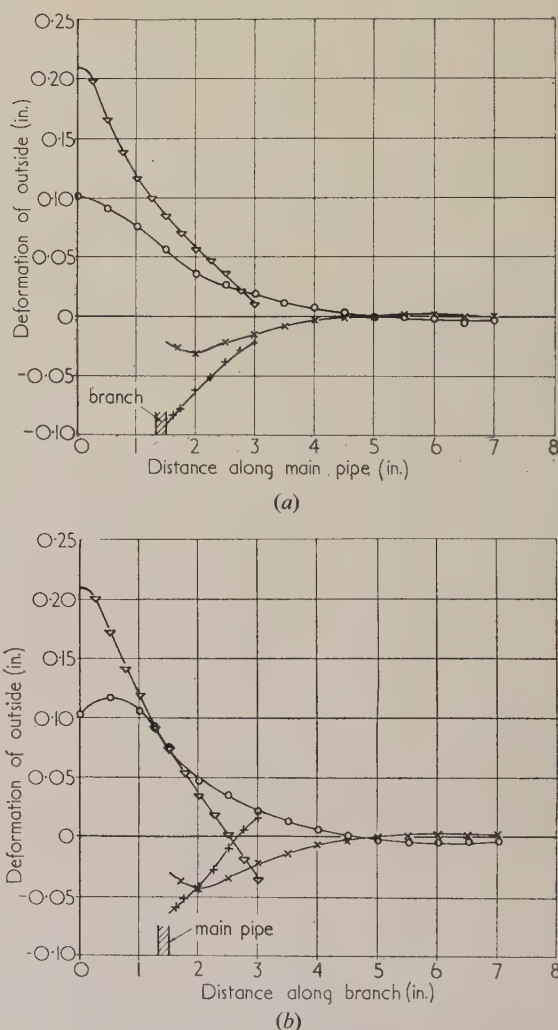


Fig. 6. Deformation of pressure-loaded model and reversed deformation of point-loaded model

- ▽ point loaded in line deformation
- + point loaded transverse deformation
- pressure loaded deformation in y -direction
- × pressure loaded deformation in x - or z -direction

same instrument in the same apparatus, this increase in strain concentration was attributed to the large distortion of the model during the stress-freezing cycle. This large distortion, produced by a mean strain about eight times greater than the greatest mean strain during room temperature loading may also be seen from Fig. 6.

If it is assumed that the difference in the strain-concentration factors $\epsilon_{\max}/\epsilon'$ in columns 3 and 5 is caused by this deformation, this difference may be subtracted from the strain-concentration factor obtained from the frozen-stress test when considering the effect of Poisson's ratio on the strain concentration in a branched pipe subject to moderate deformation. This gives the following:—

Poisson's ratio	0.25	0.4	0.5
Strain-concentration factor	33.7	33.7	32.5

The greatest difference is less than 4%. Because of the large number of experimental measurements required to obtain these results, it was concluded that, in this problem of severe local bending, the strain-concentration factor does not vary significantly with increasing values of Poisson's ratio. The same conclusion would have to be drawn from the values of strain concentration factors shown in columns 2-4 in Table 2; that is, ignoring the large distortion of the frozen-stress model.

Comparison of point- and pressure-loaded models

A pressure-loaded model of the same main pipe and branch diameters as the point-loaded models has been tested. The deformation of this model may be compared with the

frozen-stress deformation of the point loaded model. The diametral deformations of the outer surfaces of the two models are recorded in Fig. 6. The expansion of the pressure-loaded pipe remote from the junction has been subtracted to show the distortion near the junction better. To assist comparison, the deformation in the y -direction has been considered positive for both models, although \circ points represent an increase in diameter and ∇ represent a decrease.

It may be seen that there is some similarity between the deformations. Because quantitative comparisons of the deformations or stresses in these two models would have to be based on some arbitrary assumptions about the effect of the point loads, no such comparisons are presented.

Acknowledgements

The authors wish to thank Professor J. A. Pope who, as Head of the Department of Mechanical Engineering, provided all necessary facilities for this work.

References

- (1) FESSLER, H., and OLLERTON, E. *Brit. J. Appl. Phys.*, **8**, p. 387 (1957).
- (2) FESSLER, H., and ROSE, R. T. *Proc. I. Mech. E.*, **171**, p. 633 (1957).
- (3) CLUTTERBUCK, M. *Brit. J. Appl. Phys.*, **9**, p. 323 (1958).
- (4) FESSLER, H., and LEWIN, B. H. *Brit. J. Appl. Phys.*, **7**, p. 8 (1956) and **7**, p. 76 (1956).
- (5) FESSLER, H., and ROSE, R. T. *J. Mech. and Phys. of Solids*, **1**, p. 127 (1953).

Strength of irradiated drawn and undrawn nylon*

by C. C. HSIAO, Ph.D., Y. C. DAS, Ph.D., and A. HAYNES, B.S., University of Minnesota, Minneapolis, Minnesota

[Paper first received 28 December, 1959, and in final form 4 March, 1960]

Abstract

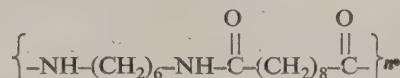
This investigation describes the effect of reactor irradiation on the strength properties of oriented and unoriented nylon filaments. It is found that both the ultimate strength and the elastic modulus of the undrawn sample decreases markedly to a minimum upon receiving a reactor radiation indexed by the thermal neutron component of 6×10^{17} nvt as compared with that of the drawn sample. However, at somewhat higher levels of irradiation the ultimate tensile strength and the modulus of elasticity of the undrawn nylon increases while that of the drawn nylon continues to decrease until they approach to nearly the same level. At still a higher dose of reactor irradiation the ultimate tensile strength of both drawn and undrawn samples drops sharply while the modulus of elasticity increases sharply.

A CONSIDERABLE amount of fundamental and applied research on radiation effects has been reported in the literature.⁽¹⁾ The major changes in such materials are essentially caused by ionization,⁽²⁾ electronic excitation and

atomic displacement, which eventually produce structural changes. For linear polymers, either scission or cross-linking of long chains usually occurs and, as a consequence, many physical properties and the mechanical behaviour are changed.⁽³⁾

It is also known that variations in physical and mechanical properties of linear solid polymers are intimately associated with the orientation of their molecular structure.⁽⁴⁻¹²⁾ However, in current available literature on the study of irradiated solid polymers, little or no attention has been given to this effect.⁽¹³⁻¹⁶⁾ The experiments described here were undertaken to determine the effect of reactor irradiation on some of the physical and mechanical properties of oriented and non-oriented nylon filaments.

The oriented nylon was "Tyne" 610 nylon filament having an average diameter of about 0.0147 in. which was drawn from the unoriented nylon wire of about 0.0295 in. in diameter. The structure of 610 nylon may be represented by n units of the following chemical components:



* Research supported in part by the U.S. Atomic Energy Commission.

Both types of sample were irradiated in sealed aluminium capsules for the same length of time in different regions in a graphite hole in the Material Testing Reactor with a total irradiation of 420 MWD and approximate accumulated perturbed thermal nvt values from 4.3×10^{17} to 1.3×10^{19} at a temperature of about 100°F . The thermal neutron-flux traverse was determined from measurements of $^{23}\frac{1}{2}\%$ cobalt-aluminium alloy-wire sections irradiated together with the samples. The mean accumulated perturbed thermal nvt values and the estimated fast neutron and gamma rays for individual sample capsules are given in the table. Since the thermal neutron doses were actually determined, their nvt values are used for this report as an index. It should not be taken that the thermal neutron irradiation alone is the prime contributor to the radiation effect. No attempt was made to calculate the equivalent energy absorbed for gamma rays, thermal and fast neutrons as precise calculations can become very complex and laborious.⁽²⁾

Table of irradiation doses for drawn and undrawn nylon*

Capsule No.	Accumulated perturbed thermal neutron dose (nvt)	Estimated accumulated fast neutron traverse ($\Sigma n \geq 1 \text{ MeV}$) (nvt)	Estimated intensity of gamma protons (+)
1	4.3×10^{17}	3.3×10^{14}	8.6×10^{10}
2	7.4×10^{17}	5.6×10^{14}	1.3×10^{11}
3	1.2×10^{18}	1.0×10^{15}	1.8×10^{11}
4	2.0×10^{18}	1.6×10^{15}	2.8×10^{11}
5	3.4×10^{18}	2.7×10^{15}	4.3×10^{11}
6	5.7×10^{18}	4.6×10^{15}	6.6×10^{11}
7	8.6×10^{18}	7.8×10^{15}	9.6×10^{11}
8	1.1×10^{19}	1.3×10^{16}	1.3×10^{12}
9	1.3×10^{19}	2.2×10^{16}	1.4×10^{12}

* The experiment was carried out in VG-20 hole of MTR for a total of 420 MWD at 40 MW. Data were supplied by the engineering office of the MTR, Idaho Falls, Idaho.

All of the irradiated samples were investigated at room temperature by simple tension with a constant, nominal strain rate of 0.2 per minute. To compare more closely the ultimate tensile strength for both types of samples, in Fig. 1 is plotted the variation of the ultimate tensile strength against the levels of irradiation. For the irradiated undrawn nylon, the ultimate tensile strength was observed to decrease appreciably as compared with that of the non-irradiated undrawn nylon. The destruction of the crystallinity of the sample was suspected to be the mechanism of the reduction of the mechanical strength, as has been reported earlier.^(13, 17) A minimum ultimate tensile strength of about 400 lb/in.² was

found to occur after an undrawn nylon sample was given an accumulated thermal neutron dose (nvt) of 6×10^{17} neutrons/cm². At a higher level of thermal neutron dose, the mechanism of molecular cross-linking was believed to be predominant, which in turn increased the ultimate tensile strength. At relatively high doses of irradiation (of the order of 10^{19} nvt), the nylon samples became extremely glassy. The fracture strength was, however, greatly reduced. Whether the high glassy state was a result of the saturation of cross-linking or of the oxidation of the sample, or both, was not determined.

As for the drawn nylon, the ultimate tensile strength was found to be inversely proportional to the logarithm of thermal neutron irradiation for thermal neutron doses of about 4×10^{18} nvt. However, from the given initial portion of the strength curve in Fig. 1, it appeared that the high degree of molecular orientation maintained the fracture strength a good deal higher than that of the undrawn sample.

In the unirradiated material, the stress/strain relationship consists of three stages—the initial, the orientation and the final stage—whereas in an irradiated material it seems that only one stage occurs. Now it is evident that the improved strength of the drawn nylon is the result of reaching the orientation stage before subjection to irradiation. But when the thermal neutron doses became larger and larger (greater than 2×10^{18} nvt), both the drawn and undrawn samples were found to have comparable ultimate tensile strength. Beyond the thermal neutron dose of 10^{19} nvt, like the undrawn nylon, the samples of drawn nylon also become extremely glassy and the fracture strength fell sharply. This is in agreement with the earlier findings that a rapid loss in strength occurred when nylon 66 was irradiated in air.⁽¹⁷⁾ An analysis, however, showed considerable increase in (—COOH) end groups, indicating that scission and branching had occurred.

This high glassy state can easily be observed from the graph of the variation of the modulus of elasticity, as shown in Fig. 2. The coincidence is that after a fairly high dose of neutron irradiation, the modulus of elasticity of both drawn and undrawn nylon samples returned to the initial value of the undrawn sample without any irradiation. Beyond a thermal neutron dose of 10^{19} nvt, the elastic modulus was found to increase sharply.

Within the range of thermal neutron irradiation investigated, the minimum elastic modulus for the undrawn nylon was found to occur like the lowest ultimate strength, after a sample had received an accumulated thermal neutron dose of 6×10^{17} nvt. This agrees in general with the results obtained by dynamic measurements.⁽¹⁸⁾

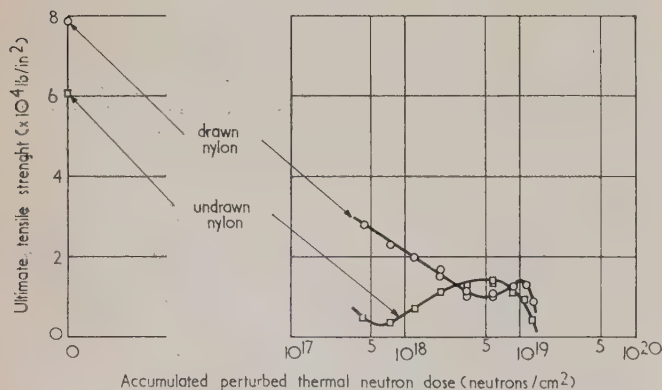


Fig. 1. Effect of reactor irradiation on strength of drawn and undrawn nylon

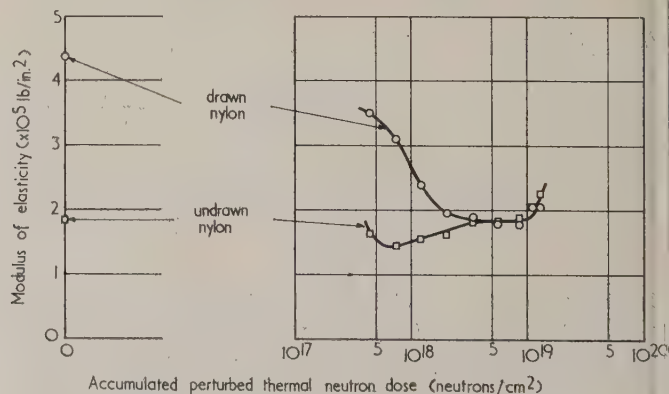


Fig. 2. Effect of reactor irradiation on elastic modulus of drawn and undrawn nylon

In summarizing the above findings, both the modulus of elasticity and the tensile strength of the oriented samples of nylon decrease as the levels of accumulated perturbed thermal nvt increases. The return of the magnitude of the modulus of elasticity to that of the unoriented nylon seems to indicate that the microscopic molecular units have lost their preferred orientation as the result of irradiation.

Acknowledgement

The authors are indebted to Professor J. A. Sauer for his very valuable and helpful discussions.

References

- (1) PECIAK, F. A., and SUN, K. H. *Nuclear Engineering and Science Congress* (sponsored by Engineering Joint Council), Preprint No. 243 (1955).
- (2) CALKINS, V. P. *Neuleonics*, **12**, p. 9 (1954).
- (3) DIENES, G. J. *J. Appl. Phys.*, **24**, p. 666 (1953).
- (4) KRATHY, O. *Kolloid Z.*, **70**, p. 14 (1935).
- (5) SYOTEN, OKA. *Kolloid Z.*, **86**, p. 242 (1939).

- (6) HERMANS, P. H. *Kolloid Z.*, **87**, pp. 138 and 306 (1939).
- (7) MÜLLER, F. H. *Kolloid Z.*, **95**, p. 138 (1941).
- (8) BAILEY, J. *India Rubber World*, **118**, p. 225 (1948).
- (9) ALFREY, T. (JR.). *Mechanical Behavior of High Polymers*, p. 500 (London: Interscience Publishers Ltd., 1948).
- (10) HSIAO, C. C., and SAUER, J. A. *J. Appl. Phys.*, **21**, p. 1071 (1950).
- (11) HSIAO, C. C. *J. Appl. Phys.*, **30**, p. 1492 (1959).
- (12) HSIAO, C. C., and SAUER, J. A. *J. Appl. Phys.*, **24**, p. 957 (1953).
- (13) SISMAN, O., and BOPP, C. D. *O.R.N.L.*—928, p. 27 (1951).
- (14) BOPP, C. D., and SISMAN, O. *O.R.N.L.*—1373, p. 1 (1953).
- (15) *O.N.R. Symposium Report, ACR-2* (1955).
- (16) SISMAN, O., and BOPP, C. D. *Summary Report, Second Pacific Area National Meeting of A.S.T.M.* (September 1956).
- (17) LITTLE, K. *Nature (London)*, **173**, p. 680 (1954).
- (18) SAUER, J. A. Private communication.

Variation of permanent-magnet properties with crystal orientation in columnar crystal alloys*

by M. McCAIG, Ph.D., F.Inst.P., and W. WRIGHT, B.Sc., F.I.M., Permanent Magnet Association, Central Research Laboratory, Sheffield

[Paper received 1 February, 1960]

Abstract

The crystal orientations of three casts of a columnar permanent-magnet alloy have been compared. The same alloy has also been cut and tested at various angles to the columnar axis. Coercivity and $(BH)_{max}$ fall off less rapidly with angle than is predicted by Stoner and Wohlfarth, but may agree better with more modern theories, some of which have not yet been worked out in a form suitable for comparison. It is concluded that variations in the properties of columnar permanent-magnet alloys are still not wholly accounted for, although spread of crystal orientation may be a contributory factor.

Introduction

ALCOMAX III is an anisotropic permanent-magnet alloy (by members of the Permanent Magnet Association) in which a preferred direction of magnetization is produced by cooling in a magnetic field. This process is more effective if the magnetic field coincides with a crystal [100] axis. Columax (by members of the Permanent Magnet Association) is a commercially available alloy with a columnar structure such that all the grains have one [100] axis nearly parallel to a given direction. Unfortunately, the properties of the commercially available magnets are invariably lower

than those of the best laboratory samples. Even in the laboratory, consistency of properties leaves much to be desired, and the variation in properties may be quite large, even in samples which superficially appear to have equally good crystal orientation.

The investigation reported here was an attempt to relate the variable magnetic properties to the deviation of the [100] axes of the columnar crystals from the assumed mean axis in which the field was applied during heat treatment.

Experimental method and results

Four casts of nominal composition 25% cobalt, 13.5% nickel, 8% aluminium, 3% copper, 0.8% niobium and balance iron were made. Their magnetic properties are shown in the table. Samples from casts A, B and C were submitted to an X-ray determination of crystal orientation. Seven to twelve crystals were examined on a side face of each sample and a similar number on an end face, using the modification due to Greninger⁽¹⁾ of the Laue back-reflexion technique. There was, of course, a certain difficulty in choosing the crystals for observation without introducing sampling errors. Parallel to the X-ray examination, columnar samples of casts B and D were successively ground so that magnetic tests could be made at increasing angles to the columnar (and field-treatment) direction.

The B_r , $(BH)_{max}$ and H_c values of these samples expressed as a percentage of the value for zero angle are plotted against

* This paper was presented to the Conference on "Some aspects of magnetism", organized by The Institute of Physics in Sheffield, 22-24 September, 1959.

Magnetic properties of samples used and X-ray data on the maximum and mean angles between the crystal and columnar axes

Cast	B_r (G)	$(BH)_{max}$ (M.G.O.)	H_c (Oe)	End face		Side face		Grand Mean (°)
				Max. (°)	Mean (°)	Max. (°)	Mean (°)	
A	14,300	8.8	775	14.5	6.0	5.0	3.4	4.8
B	13,550	8.1	786	6.0	4.1	9.0	4.8	4.5
C	13,800	7.3	720	16.0	10.0	12.0	7.2	9.2
D	14,150	7.8	735	—	—	—	—	—

the angle at which the test was made in Figs. 1, 2 and 3. Theoretical curves derived from the work of Stoner and Wohlfarth,⁽²⁾ for single-domain particles, and of Zijlstra⁽³⁾ for $(BH)_{max}$ only—are shown on the same figures.

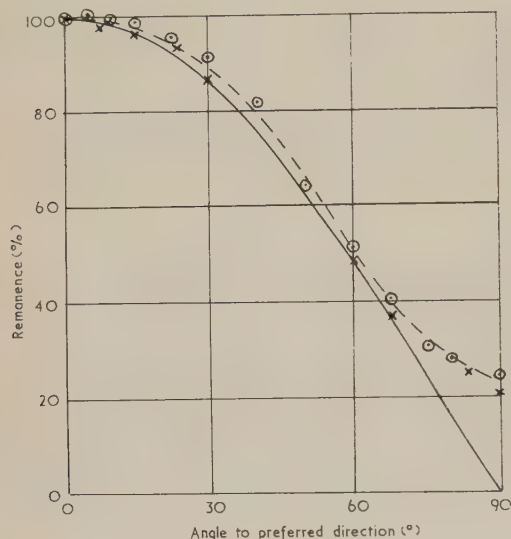


Fig. 1. Variation of remanence with angle to preferred direction

— Stoner and Wohlfarth
- - - Experimental, ○ sample B, × sample D

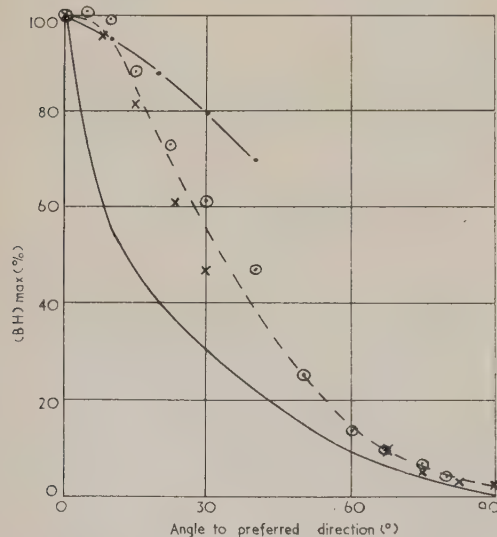


Fig. 2. Variation of $(BH)_{max}$ with angle to preferred direction

— Stoner and Wohlfarth
- - - Experimental, ○ sample B, × sample D
- . - Zijlstra

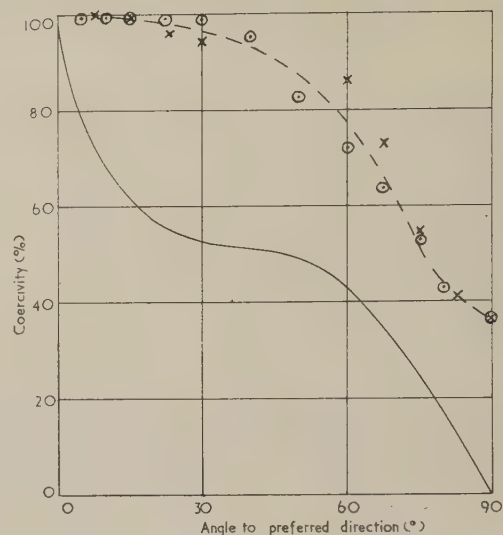


Fig. 3. Variation of coercivity with angle to preferred direction

— Stoner and Wohlfarth
- - - Experimental, ○ sample B, × sample D

Discussion

The sample with the worst magnetic results had the largest spread of angles between the crystal [100] axes and the test direction, but there was little difference in the mean spread of the other two samples, although the energy of one was 0.7 M.G.O. better than the other. It should, however, be noted that the X-ray data for the sample A happen to include one badly misoriented grain. If such sampling hazards are taken into account, there seems to be some correlation between the angular spread of the crystal axes and the magnetic properties, although the evidence is not quite conclusive.

The results of the angular-grinding experiments show good agreement between the two samples examined, the values being indicated by circles and crosses respectively on the graphs. The experimental curve for B_r agrees well with the theoretical curve of Stoner and Wohlfarth up to 60°, but the curves for $(BH)_{max}$ and H_c fall off much less steeply than the theoretical curves. The measured coercivity is practically constant up to 20°. The curve for $(BH)_{max}$ due to Zijlstra was obtained from an empirical power formula made to fit experimental measurements on a single crystal of Ticonal G (by Mullard) treated along the [100], [110] and [111] axes and is not strictly comparable with those obtained in the present experiment. Our curves were derived from samples treated in all cases parallel to [100] axes, and then tested at varying angles, so that the steeper fall off of $(BH)_{max}$ was not unexpected. The Zijlstra experiment should approximate more closely to results which would be obtained on a columnar

sample with a spread of crystal direction. On the other hand, the alloy used by Zijlstra probably showed a rather smaller difference between the columnar and random properties than those used in the present experiment. The Stoner and Wohlfarth curves had suggested that the small differences in crystal orientation found by X-rays could account for the large differences in magnetic properties. The grinding experiments described above, and Zijlstra's work make it likely that crystal misorientation can only be a contributory cause of inferior magnetic properties.

To understand the differences between experiment and Stoner and Wohlfarth's theory, it should be realized that the latter applies to coherent rotation in perfectly aligned, single-domain particles which do not interact. In the permanent-magnet alloy, the single-domain particles, if they were parallel to the crystal axes, would be distributed in a cone of semi-vertical angle of about 10 deg. There would certainly be interaction and probably incoherent rotation such as curling or buckling. Wohlfarth⁽⁴⁾ has reviewed work on these phenomena and has considered their effect on the angular variation of coercivity and remanence. Unfortunately, the theory has not been worked out for a model which corresponds very closely to the probable state of affairs in the present columnar alloys, but it is clear that a much less rapid change of coercivity with angle than that predicted by the

older theory is to be expected. With convenient hypotheses about interaction, particle orientation, and the nature of the rotation process (curling, buckling or coherent rotation), it is possible to find a theoretical model which will predict almost any single experimental result. To distinguish which is the best theoretical model, a large number of experimental measurements under varying conditions would be required. It is hoped that the present experiments may make some contribution to the solution of this wider problem.

Acknowledgements

The authors thank Messrs. A. Rogers of the English Steel Corporation and R. D. Pinkney of W. Jessop and Sons Ltd., who were responsible for the X-ray examination, and Mr. J. E. Gould for helpful discussion throughout the work.

References

- (1) GRENINGER, A. B. *Trans. A.I.M.E.*, **117**, p. 75 (1935); and **122**, p. 74 (1936).
- (2) STONER, E. C., and WOHLFARTH, E. P. *Phil. Trans. Roy. Soc. A*, **240**, p. 599 (1948).
- (3) ZIJLSTRA, H. *J. Appl. Phys.*, **27**, p. 1249 (1956).
- (4) WOHLFARTH, E. P. *Phil. Mag. Sup.*, **8**, No. 30, p. 87 (1959).

Power law for creep

by B. J. RIGBY, Commonwealth Scientific and Industrial Research Organization, Wool Research Laboratories, Ryde, New South Wales, Australia

[Paper received 25 January, 1960]

Abstract

A model is discussed which gives rise to the widely used power law for creep under constant load, namely, $dl/dt = \Omega t^{-n}$, where l is the strain, t the time, Ω a function dependent on temperature and load and n an exponent which may have any value between 0 and 1. In this model, the exponent n is interpreted as a function of the number of "flow units" which must be activated simultaneously before flow can take place.

A common intermediate value of n is $2/3$, which leads to the well-known Andrade creep law

$$l = \eta t^{1/3} \quad (4)$$

Naturally enough, many materials have a creep behaviour which is fitted by a combination of equations (2), (3) and (4), one form of the law usually predominating within a certain load and temperature range. The parameters Ω , β , γ and η are found to be functions of the temperature and applied load.

Despite the wide use of the power law (1), there appears to be no general theory underlying it, although particular cases have been derived, especially with reference to metals.⁽³⁾

Kennedy⁽¹⁾ discussed a model of the creep mechanism "in which the units of the structure each contribute a finite strain to the aggregate by changing over from one (stable) state to another". Kennedy showed experimentally that this model gives a creep behaviour of the correct general form, and concluded that this is the basic creep mechanism, true for all materials. Burte and Halsey⁽⁴⁾ developed a similar theory for polymeric materials in which a polymer molecule could elongate by changing its configuration from one stable state to another.

It will be shown that the power law (1) is implicit in a generalized development of the latter model, as first indicated by Peters.⁽⁵⁾ Burte and Halsey treated the extension of a fibrous material as a process in which a molecular unit of

Introduction

It has been observed by many authors^(1,2) that the creep under constant load of a wide variety of materials may be represented by a power law, of the form

$$dl/dt = \Omega t^{-n} \quad (1)$$

where l is the strain, t the time and n an exponent which may lie between 0 and 1. In practice it is found that certain values of n are usually preferred. For example, $n = 1$ leads to the logarithmic creep law

$$l = \beta \log t \quad t > 1 \quad (2)$$

This law has been found to apply to the creep of rubber, glass and various metals. A steady state creep strain results when $n = 0$, the other extreme value, i.e.

$$l = \gamma t \quad (3)$$

the material in a state A could pass over an energy barrier (ΔF) into a new configuration or state B , from which it could not be further elongated. The material in the state B was taken to be at higher energy level (by the amount ΔF^*) than that in state A , so that it would tend under thermal motion to return to state A . This type of model was developed primarily for reversible extension of fibrous materials such as wool, hair, etc. If the concentration of material in the B state is made proportional to the elongation of the molecular unit, then the rate of extension of the material may be written

$$db/dt = (1 - b)KD \exp(\alpha f) - bK \exp(-\alpha f) \quad (5)$$

where $b = l/l'_\infty$

l is elongation

l'_∞ is elongation when all the material is in the B state

t is time

f is force

$K = kT/h \{\exp(-\Delta F/RT)\}$

$D = \exp(-\Delta F^*/RT)$

k is Boltzmann constant

h is Planck's constant

T is absolute temperature

R is gas constant

The rate of elongation is taken to be affected by the force in the exponential manner, $\exp(\alpha f)$, which means that the free energy barrier is a linear function of the applied force. It is clear that for many materials the reverse reaction, represented by the term $bK \exp(-\alpha f)$, would be negligible, or even non-existent.

Before proceeding with the consequences of this model, we will discuss another type of flow which is included as a special case in equation (5), and which gives rise to the steady-state equation (3). This type of flow occurs when the molecular unit does not change its configuration, but glides past its neighbours, surmounting an energy barrier due to friction, cross-linkages, etc., in the process. This flow has been discussed extensively by Eyring and co-workers.⁽⁶⁾ In this case, since b now is zero, or at a constant value at all times, and since D will also now equal 1, equation (5), may be written

$$\left. \begin{aligned} \text{or} \quad dl/dt &= K \exp(\alpha f) \text{ for } b = 0 \\ dl/dt &\approx K \sinh \alpha f \text{ for } b = \text{constant} \end{aligned} \right\} \quad (6)$$

where dl/dt is now the overall rate of slip of "flow units" past each other.

The second equation is the familiar Eyring form. Both equations give rise to a creep law ($f = \text{constant}$) of the form (3).

Returning now to flow phenomena, in which the molecular unit does change its configuration, we see that equation (5) gives rise to a creep law, namely,

$$\frac{l}{l'_\infty} = \frac{1}{1 + D^{-1} \exp(-2\alpha f)} \{1 - \exp(-t/\tau)\} \quad (7)$$

an exponential creep law, in which the time constant τ is dependent on the applied load thus

$$\tau = K\{D \exp(\alpha f) + \exp(-\alpha f)\}.$$

It has been pointed out by Peters with reference to the mechanical behaviour of wool⁽⁵⁾ that under certain conditions a number of molecular units may have to be activated simultaneously before any elongation can take place; in this case the equation (5) has to be rewritten as

$$db/dt = (1 - b)^m A^m - b^m B^m \quad (8)$$

where m is the number of units acting simultaneously. For convenience A and B have been written to replace $KD \exp(\alpha f)$ and $K \exp(-\alpha f)$ respectively. This type of formulation is reasonable for materials which absorb liquids and swell easily, for then we might expect the number of units acting co-operatively (m) would decrease as the amount of penetrant increases, owing to the severing and weakening of bonds between units. For materials which do not absorb, however, m might still be reasonably expected to take on different values in different temperature ranges. Again, we might expect the value of m to decrease with an increase of temperature, and in the limit when the material has melted ($m = 0$), to flow according to a simple law such as (3).

For simplicity we will now assume that the reverse term $b^m B^m$ in equation (8) may be ignored. The condition for this approximation to hold is seen by examining equation (5); it is, $D \exp(2\alpha f) \gg 1$. With the flow units arranged in parallel the approximation is reasonable anyway, since any unit tending to return to its initial configuration would have the load concentrated upon it, making the return very unlikely. Under these circumstances equation (8) becomes

$$db/dt = A^m(1 - b)^m \quad (9)$$

Upon integration between the limits 0 and b we obtain

$$\{1/(1 - b)^{m-1}\} - 1 = A^m(m - 1)t \quad (10)$$

This is the general equation for creep in the Burte and Halsey (or Kennedy) type model. It is easily rearranged into a form similar to equation (1). This is

$$\frac{db}{dt} = A^m \{1 + A^m(m - 1)t\}^{m/(1-m)}, \quad (m \neq 1) \quad (11)$$

Equations (10) or (11) may be taken as the general power law for the creep of materials which flow according to the definition given earlier.

Equation (11) is more general than equation (1) and overcomes the objection implicit in equation (1) that the strain rate should become infinitely great as $t \rightarrow 0$. Further, as t becomes large, the equation becomes identical with equation (1), and $n = -m/(m - 1)$.

Both forms (10) and (11) are commonly used, although equation (11) is more general since it includes the logarithmic form (2). It can be seen that the exponent in equation (11) varies between 0 and 1, as is found for a wide variety of materials by Kennedy.⁽¹⁾

Some special cases of equations (10) and (11) will now be considered. The case $m = 1$ has already been given. It is the exponential law (7). When $m = 2$ we obtain the rectangular hyperbolic law

$$\frac{1}{l} = \frac{1}{A^2 t} + \frac{1}{l'_\infty} \quad (12)$$

This has been found by Feughelman to fit the behaviour of wool in water.⁽⁷⁾

A limiting case obtains as m becomes large and the exponent $m/(1 - m)$ in equation (11) approaches -1 . We may then write

$$db/dt = A^m(1 + mA^m t)^{-1}$$

which gives rise to the well-known logarithmic law

$$b = (1/m) \log(mA^m t + 1) \quad (13)$$

This type of creep has been found to apply to dry wool⁽⁸⁾ and is support for the present theory, since m would certainly be expected to increase as water is extracted from the fibre.

A form similar to Andrade's law [equation (4)] results when $m = 4$, although it should be noted that equation (4) describes an unlimited creep, whereas the present model gives rise to a limiting strain. Some simplification results when it is noted that, since $(1 - b)$ is always less than 1, $1 \ll \{1/(1 - b)^{m-1}\}$, when b approaches 1 and/or m becomes large. Using this approximation in the case when $m = 4$, gives rise to an Andrade form (i.e. on containing $t^{1/3}$), namely,

$$(1 - b) = (3A^4)^{1/3} t^{1/3} \quad (14)$$

It was stated earlier that the Andrade form is frequently observed, and it has just been seen that the exponent $\frac{1}{3}$ results from the theory when $m = 4$. However, there does not seem to be any particular reason why the value 4 should be preferred in actual materials. At the moment the only explanation which can be given is that the value $m = 4$ lies in a unique position. For if $m > 4$ the creep law rapidly takes on the logarithmic form, equation (13), while for $m < 3$ distinct forms result as shown by equations (6), (7) and (12). In other words, if $m > 4$ we would expect equation (13), while if $m < 3$ there is a good chance of obtaining equation (14).

Another possibility is that, for many substances, 4 turns out to be the mean value of the number of units acting co-operatively.

Substitution of

$$A = \frac{kT}{h} \exp \{ -(\Delta F + \Delta F^*)/RT \} \exp (\alpha f)$$

into the above equations allows of the calculation of the behaviour at various loads and temperatures, assuming that m is not a function of either variable, e.g. from equations (3) and (6) we find $\gamma = (kT/h) \exp (-\Delta F/RT) \exp (\alpha f)$, and such a dependence upon temperature and stress is observed.

Conclusions

In conclusion it should be noted that:

(1) the above discussion is applicable to non-reversible creep phenomena or to reversible phenomena in which the recovery mechanism is negligible under load, and for which a limiting strain is reached after a long time;

(2) in reality the value of m (the number of units which have to be simultaneously activated) would probably be distributed. However, the choice of a distribution function is rather arbitrary, and is not considered at this stage;

(3) the value of m is very likely a function of temperature and load, or at least the value of m is only fixed within certain temperature and load ranges, e.g. above and below transition temperatures. As stated earlier, m is also quite likely a function of the moisture content of such materials as wool, hair, wood, etc.

References

- (1) KENNEDY, A. J. *J. Mech. Phys. Solids*, **1**, p. 172 (1953).
- (2) COTTRELL, A. H. *J. Mech. Phys. Solids*, **1**, p. 53 (1952).
- (3) SULLY, A. H. *Progress in Metal Physics*, Vol. 6, p. 135 (1956).
- (4) BURTE, H., and HALSEY, G. *Text. Res. J.*, **17**, p. 465 (1947).
- (5) PETERS, L. *Proc. International Wool Conference*, Vol. D, p. 71 (1955).
- (6) EYRING, H., and HALSEY, G. *High Polymer Physics*. Edited by H. A. Robinson, p. 61 (New York: Chemical Publication Co., 1948).
- (7) FEUGHELMAN, M. *J. Text. Inst.*, **45**, p. T630 (1954).
- (8) RIGBY, B. J. *J. Text. Inst.*, **49**, p. T379 (1958).

Experimental and theoretical investigations on the oscillating cylinder viscometer for Newtonian liquids

By the late ALI ABDEL KERIM IBRAHIM, Ph.D., and ABDEL MONEM I KABIEL, Ph.D.,*
Physics Department, Faculty of Science, The University, Alexandria, Egypt

[Paper first received 13 July, 1956, revised 5 May, 1958, and in final form 21 March, 1960]

Abstract

A new and exact theory of the oscillating cylinder viscometer⁽¹⁻⁵⁾ is given for Newtonian liquids. The final solution is not a direct relation between the measured quantity ∂/ϕ_0 (∂ being the angular displacement of the suspended cylinder and ϕ_0 the displacement of oscillation inexorably imposed on the outer cylinder) and the desired quantity η (η is the coefficient of viscosity), since the Bessel function involves η . To render this direct and applicable to Newtonian liquids a dimensionless parameter is introduced into the final solution. The theoretical relation which is derived subject to the condition that η is proportional to n (n being the frequency) satisfies the experimental curve which is subject to the condition that η is constant, at only one point; hence from the co-

ordinates of this point and the dimensionless parameter chosen, the value of η can be determined. Experiments have been carried out on different concentrations of glycerol. The results obtained confirm the validity of theory and method.

The extension of this method to non-Newtonian liquids will be given later in another paper.

Theory

CONSIDER a cylindrical bob of diameter $2a$ and moment of inertia I about its major axis, suspended coaxially by a delicate torsion wire of torsion constant τ to a depth l in a cup of diameter $2b$ containing a liquid of density ρ and viscosity coefficient η .

The cup is caused to oscillate, about its vertical axis,

* Now at Institute of Physical Chemistry, Freiburg University, Freiburg i. Br., Germany.

through a very small fixed angular amplitude ϕ_0 (of the order of approximately 1°) so that the liquid is following the forced oscillations of the cup.

Since the motion is axially symmetric and in two dimensions, the velocity V of the liquid at any radial distance r is given by,

$$\frac{1}{\nu} \cdot \frac{\partial V}{\partial t} = \frac{\partial^2 V}{\partial r^2} + \frac{1}{r} \cdot \frac{\partial V}{\partial r} - \frac{V}{r^2} \quad (1)$$

where ν is the kinematic viscosity of the liquid.

The angular displacement of the liquid at any radial distance from the central vertical axis is given by

$$\theta = \phi e^{i\omega t} \quad (2)$$

where ϕ is a function of r only, and $\omega = 2\pi \times$ frequency of the outer cylinder.

Therefore, equation (1) may have the form

$$\frac{\partial^2 \phi}{\partial r^2} + \frac{3}{r} \cdot \frac{\partial \phi}{\partial r} + \frac{B^2}{i} \phi = 0 \quad (3)$$

$$\text{where } B = (2\pi\rho n/\eta)^{1/2} \quad (4)$$

n being the frequency of the outer cylinder.

The solution of equation (3) may be obtained in terms of the modified Bessel functions of complex argument. Thus

$$\phi = \frac{1}{r} [AI_1(i^{1/2}Br) + CK_1(i^{1/2}Br)] \quad (5)$$

where A and C are two arbitrary constants to be determined by the boundary conditions. Therefore, the angular displacement is given by

$$\theta = \frac{1}{r} [AI_1(i^{1/2}Br) + CK_1(i^{1/2}Br)] e^{i\omega t} \quad (6)$$

the angular velocity is given by

$$\dot{\theta} = \frac{i\omega}{r} [AI_1(i^{1/2}Br) + CK_1(i^{1/2}Br)] e^{i\omega t} \quad (7)$$

the rate of change of the relative motion of adjacent layers of the liquid is given by

$$\frac{d\dot{\theta}}{dr} = \frac{i^{3/2}\omega B}{r} [AI_2(i^{1/2}Br) - CK_2(i^{1/2}Br)] e^{i\omega t} \quad (8)$$

and the angular velocity gradient in the neighbourhood of the inner cylinder is given by

$$\left(\frac{d\dot{\theta}}{dr}\right)_{r=a} = \frac{i^{3/2}\omega B}{a} [AI_2(i^{1/2}Ba) - CK_2(i^{1/2}Ba)] e^{i\omega t} \quad (9)$$

The equation of motion of the inner cylinder. The suspended bob experiences:

(i) the shearing torque C' due to the liquid, given by

$$C' = 2\pi l a^3 \eta \frac{d}{dr} \bigg|_{r=a} \quad (10)$$

(ii) the torque C'' due to the suspension wire, given by

$$C'' = -\tau \vartheta \quad (11)$$

where ϑ is the angular displacement of the suspended cylinder.

Consequently, the equation of motion of the suspended cylinder is

$$I\ddot{\vartheta}|_{\vartheta=\vartheta} + \tau\vartheta = G\eta \frac{d\dot{\theta}}{dr} \bigg|_{r=a} \quad (12)$$

where G/l is an apparatus constant equal to $2\pi a^3$.

$$\text{Hence } \vartheta = \frac{G\eta}{\tau - I\omega^2} \frac{d\dot{\theta}}{dr} \bigg|_{r=a} \quad (13)$$

$$\text{and } \dot{\theta}|_{r=a} = \frac{G\eta}{\tau - I\omega^2} \cdot \frac{\omega^2 B i^{1/2}}{a} [CK_2(i^{1/2}Ba) - AI_2(i^{1/2}Ba)] e^{i\omega t} \quad (14)$$

where $\dot{\theta}|_{r=a}$ is the angular velocity of the liquid in the neighbourhood of the curved surface of the inner cylinder.

The boundary conditions. The arbitrary constants A and C are determined by the boundary conditions. The two conditions are:

$$\begin{aligned} \text{(i) when } r &= a & \dot{\theta} &= i\omega\vartheta \\ \text{(ii) when } r &= b & \dot{\theta} &= i\omega\phi_0 e^{i\omega t} \end{aligned}$$

where ϕ_0 is the amplitude of oscillation inexorably imposed on the outer cylinder.

$$\text{Therefore } C = \frac{\phi_0 b E}{EK_1(i^{1/2}Bb) - FI_1(i^{1/2}Bb)} \quad (15)$$

$$\text{and } A = \frac{-\phi_0 b F}{EK_1(i^{1/2}Bb) - FI_1(i^{1/2}Bb)} \quad (16)$$

$$\begin{aligned} \text{where } E &= \gamma I_1(i^{1/2}Ba) - i^{3/2}I_2(i^{1/2}Ba) \\ F &= \gamma K_1(i^{1/2}Ba) + i^{3/2}K_2(i^{1/2}Ba) \end{aligned}$$

$$\text{and } \gamma = \frac{\tau - I\omega^2}{G\eta\omega B}$$

$$\text{Therefore } \frac{\dot{\theta}}{\phi_0} = \frac{i\omega b e^{i\omega t}}{r} \cdot \frac{EK_1(i^{1/2}Br) - FI_1(i^{1/2}Br)}{EK_1(i^{1/2}Bb) - FI_1(i^{1/2}Bb)} \quad (17)$$

$$\text{and } \frac{1}{\phi_0} \cdot \frac{d\dot{\theta}}{dr} = \frac{i^{3/2}\omega B b}{r} \cdot \frac{EK_2(i^{1/2}Br) + FI_2(i^{1/2}Br)}{EK_1(i^{1/2}Bb) - FI_1(i^{1/2}Bb)} \quad (18)$$

It is often convenient to consider the modulus or the absolute value. From equation (17) we have

$$\left(\frac{\dot{\theta}}{\phi_0}\right)^2 = \frac{\omega^2 b^2}{r^2} \cdot \frac{L^2(r) + M^2(r)}{L^2(b) + M^2(b)} \quad (19)$$

where

$$\begin{aligned} L(r) &= -(Pkei_1Br + Qker_1Br + Rbei_1Br + Sber_1Br) \\ M(r) &= Pker_1Br - Qkei_1Br + Rber_1Br - Sbei_1Br \end{aligned} \quad (20)$$

$$P = ReE = \gamma bei_1Ba - 2^{-1/2}(ber_2Ba + bei_2Ba)^{-1/2}$$

$$Q = ImE = -\gamma ber_1Ba + 2^{-1/2}(ber_2Ba - bei_2Ba)^{-1/2}$$

$$R = ReF = -\gamma kei_1Ba + 2^{-1/2}(ker_2Ba + kei_2Ba)^{-1/2}$$

$$S = ImF = \gamma ker_1Ba - 2^{-1/2}(ker_2Ba - kei_2Ba)^{-1/2}$$

A similar result may be obtained for $L(b)$ and $M(b)$ by inserting $r = b$ in equation (20).

Equation (19) gives the angular velocity amplitude through the liquid at any distance from the curved surface of the inner cylinder. It is related to the linear velocity amplitude $|V|$ (which is actually measured in practice at some point using the hot wire anemometer)

$$|V/\phi_0| = r|\dot{\theta}/\phi_0| \quad (21)$$

$$\text{and } \left|\frac{\dot{\theta}}{\phi_0}\right|_{r=a}^2 = \frac{\omega^2 b^2}{a^2} \cdot \frac{L^2(a) + M^2(a)}{L^2(b) + M^2(b)} \quad (22)$$

By the aid of the well-known Wronskian relation for Bessel functions it may be shown that

$$L^2(a) + M^2(a) = 1/(B^2a^2) \quad (23)$$

$$\text{also } \left| \frac{d\theta}{dr} \right|_{r=a}^2 = \frac{\omega^2 \phi_0^2 b^2}{a^4} \cdot \frac{\gamma^2}{L^2(b) + M^2(b)} \quad (24)$$

$$\text{and } \left| \frac{dV}{dr} \right|_{r=a} = a \left| \frac{d\theta}{dr} \right|_{r=a} + |\dot{\theta}|_{r=a} \quad (25)$$

But, from equations (6) and (7), it follows that

$$|\dot{\theta}| = \omega|\theta| = \omega\phi|\phi| \quad (26)$$

Therefore, from equation (19), we have

$$\begin{aligned} \left| \frac{\theta}{\phi_0} \right|^2 &= \frac{1}{\omega^2} |\dot{\theta}|^2 / \phi_0^2 \\ &= \left(\frac{b}{r} \right)^2 \cdot \frac{L^2(r) + M^2(r)}{L^2(b) + M^2(b)} \end{aligned} \quad (27)$$

This gives the angular amplitude of oscillation in the liquid at any radial distance r such that $b \leq r \leq a$.

Also, if ψ is the ratio of the displacement of the inner cylinder to that of the outer cylinder, then

$$\begin{aligned} \psi^2 &= \left(\frac{b}{a} \right)^2 \cdot \frac{L^2(a) + M^2(a)}{L^2(b) + M^2(b)} \\ &= \frac{b^2}{B^2 a^4 [L^2(b) + M^2(b)]} \end{aligned} \quad (28)$$

Equation (28) represents the exact relationship between the measured quantity ψ and the desired quantity η . This relationship can also be obtained by comparing equations (13) and (24).

Viscosity determination

Although equation (28) represents the exact relationship between the measured quantity ψ and the desired quantity η , yet it is neither a direct nor a simple relation, since the Bessel function involves η .

To render equation (28) direct and applicable to Newtonian liquids we introduce a dimensionless parameter defined by

$$Ba = X \quad (29)$$

where a is the radius of the inner cylinder, B is defined by equation (4) and X may take any positive value.

Then, from equations (28) and (29) we obtain

$$\psi^2 = \frac{A_1 n^4}{B_1 + C_1 n^2 + D_1 n^4} \quad (30)$$

where A_1 , B_1 , C_1 , and D_1 are constants whose values depend on:

- (i) the density of the liquid,
- (ii) the constants of the apparatus used,
- (iii) the numerical value of X chosen.

Also from equations (4) and (29) we obtain

$$\eta = 2\pi a^2 (n_s / X^2) \quad (31)$$

where n_s is the value of the frequency which corresponds to the value of X chosen for a particular liquid and apparatus. The theoretical curve (for a particular apparatus) derived from equation (30) depends on the numerical value of X chosen, which corresponds to a certain value of n_s for a given liquid and a given apparatus.

It is found that the theoretical curve, which is derived subject to the condition that η is proportional to the frequency, coincides with the experimental curve (for the same liquid and apparatus), which is subject to the condition that η is constant, at three points.

- (i) at the point (0, 0),
- (ii) at the point (n_r , 1), i.e. the peak, where n_r is the resonant frequency,
- (iii) at the point (n_s , ψ_s), where ψ_s is the value of ψ corresponding to the frequency n_s .

Of these only the third point depends on the viscosity of the liquid or on the chosen value of X .

Hence, by substituting the chosen value of X and the corresponding value of n_s in equation (31) the value of η is determined.

The apparatus constants used in our calculations are as follows:

$$\begin{aligned} a &= 0.45 \text{ cm} & b &= 0.63 \text{ cm} \\ \tau &= 459.6 \text{ g cm}^2 \text{ s}^{-2} & G/I &= 0.57277 \text{ cm}^3 \end{aligned}$$

Also, the following two values of X have been chosen:

- (i) $Ba = X = 0.5$ so that $Bb = (Xb/a) = 0.7$

Substituting the values of Ba and Bb in equation (28) we obtain

$$\psi^2 = \frac{7.84}{7.8421 - 0.0155\gamma + 0.1175\gamma^2}$$

where

$$\gamma = \frac{459.6 - 4\pi^2 n^2 I}{20.267 \rho \ln^2}$$

$$\text{or } \psi^2 = \frac{3.2521 \rho^2 I^2 n^4}{[(3.2538 \rho^2 I^2 + 0.1834 I^2 + 0.01247 \rho I I) n^4 - (0.1451 \rho I + 4.2672 I) n^2 + 24.820]} \quad (32)$$

- (ii) $Ba = 1$ so that $Bb = 1.4$

$$\text{Here } \psi^2 = \frac{1.96}{1.9609 - 0.0309\gamma + 0.1175\gamma^2}$$

where

$$\gamma = \frac{459.6 - 4\pi^2 n^2 I}{10.183 \rho \ln^2}$$

$$\text{or } \psi^2 = \frac{2.0326 \rho^2 I^2 n^4}{[(2.0335 \rho^2 I^2 + 0.1834 I^2 + 0.01243 \rho I I) n^4 - (0.1446 \rho I + 4.2672 I) n^2 + 24.82]} \quad (33)$$

Equations (32) and (33) are particular cases of the general equation (30).

The apparatus

The apparatus mainly consists of three parts:

- (i) the oscillating cylinder viscometer,
- (ii) the electric motor,
- (iii) the frequency changer.

(i) *The oscillating cylinder viscometer.* This is composed of the inner cylinder which is solid and suspended by a fine torsion wire of known characteristics. The diameter of this cylinder is 9 mm. The length of the cylinder is 12.4 cm. At its upper end two mirrors are fixed, one for reflecting a beam of light for measuring the deflexion of the inner cylinder, and the other for balancing and thus keeping the cylinder in a vertical position. The length of the wire can be changed when desired. The outer cylinder has an inner diameter 12.6 mm and of length 14.8 cm. It oscillates about its axis in a simple harmonic motion being driven by the frequency changer in the following way.

An arm is connected from one end by a loose screw to a horizontal bar which moves forwards and backwards in a long horizontal grooved support. Gear teeth are formed in

this horizontal bar and thus act as a rack. This rack meshed with a small gear which is rigidly fixed to a vertical spindle which in turn is fixed to a cup. This cup is coupled to a part acting as a seat for the outer cylinder. The outer cylinder is seated in this part and is secured to it by three set screws. A mirror is fixed to the cup for measuring the deflexion of the outer cylinder. The cylinders were alined by adjusting an upper support which can move in different planes and holds the suspension wire by a chuck. It was thus possible to move the chuck, and consequently the suspended inner cylinder, in three planes.

(ii) *The electric motor.* The electric motor is a 1/6 B.H.P., single phase, a.c. motor 110 volts, turning at a constant speed of 1435 r.p.m. The motion is taken from the motor to the frequency changer through a horizontal V-belt.

(iii) *The frequency changer.* The frequency changer consists of four cone pulleys having the same length but with different diameters. The motion from the motor is taken to a cone *A*, then by a horizontal belt to a cone *B*. Cone *B* is connected to a cone *C* (which is below *B*) by means of a vertical belt running on two grooved pulleys which can be changed to give different speeds. Another horizontal belt transmits the motion from cone *C* to the fourth cone *D* (which is below *A*), which has, at the end of its spindle, a disk with a diametrical groove. Through this groove slides a piece of metal connected to the arm [refer to (i)]. When the cone *D* rotates, this arm is given simple harmonic motion whose amplitude depends on the position of the piece of metal in the groove. Cones *B* and *C* are suspended on a separate support pivoted at its bottom, and under the effect of two springs, these two cones are always kept away from cones *A* and *D*; thus maintaining the required initial tension in the horizontal belts and so eliminating any possibility of slip between the belts and cones. The speed of cone *D* can be measured by a tachometer and then checked by a stop-watch for low frequency. The horizontal belts can be moved to give the required frequency.

Results

Experiments have been carried out on different concentrations of glycerine. Figs. 1 and 2 represent the variation of ψ with n for the respective concentrations. The dotted line in each figure shows the dimensionless parameter curve, while the full line represents the experimental curve.

Tables 1 and 2 provide the final results which confirm the validity of theory and method.

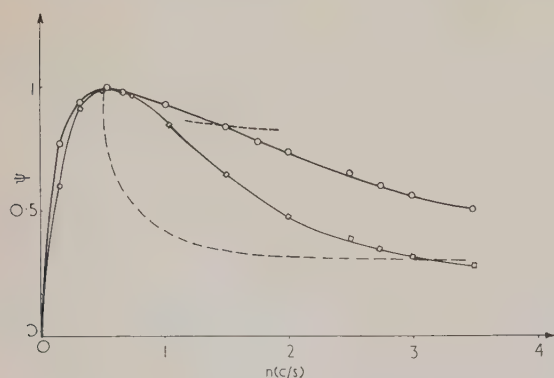


Fig. 1. Variation of ψ with n for different concentrations of glycerine

○, $\rho = 1.259$; □, $\rho = 1.245$

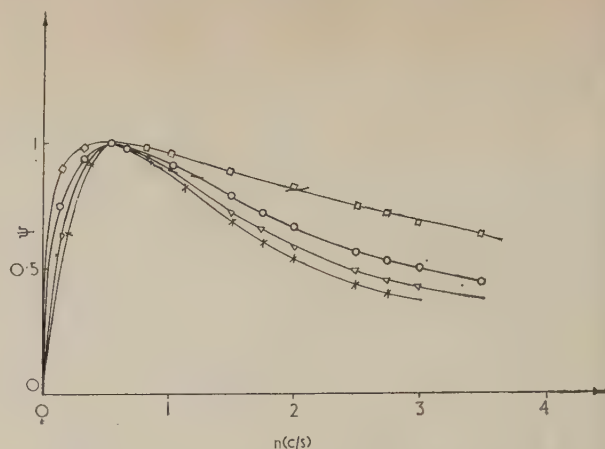


Fig. 2. Variation of ψ with n for different concentrations of glycerine

□, $\rho = 1.261$; ○, $\rho = 1.257$; △, $\rho = 1.254$; ×, $\rho = 1.251$

Table 1. Final results for the different concentrations of glycerine

Density of glycerine ρ (g cm ⁻³)	Temperature (°C)	l (cm)	X	n_s (s ⁻¹)	η (P)
1.257	23.8	10.6	0.5	1.2	7.58
1.259	23.6	10.6	0.5	1.44	9.22
1.254	24	10.6	0.5	1.0	6.38

$I = 39.48$ g cm².

l is the length of immersion of the inner cylinder in the liquid and I is the moment of inertia of the suspended cylinder.

Table 2. Final results for the different concentrations of glycerine

Density of glycerine ρ (g cm ⁻³)	Temperature (°C)	l (cm)	X	n_s (s ⁻¹)	η (P)
1.251	23.3	10.6	0.5	0.84	5.34
1.261	23.0	10.2	0.5	2.0	12.21
1.245	20.2	10.2	1	3.07	4.86

Conclusion

Our general results may be summed up as follows:

For low frequencies of the outer cylinder less than 25 c/min and liquids of viscosity just less than 5 P, the motion of the inner cylinder is not perfect simple harmonic motion and that is probably why the observed readings in this region are subject to experimental error and inconvenient.

As the frequency increases it appears that resonance occurs between the liquid and the inner cylinder at a certain frequency almost exactly equal to the frequency of free oscillation of the inner cylinder and the torsion wire (Figs. 1 and 2). Copper rings were used to vary the moment of inertia of the inner cylinder and, consequently, the resonant frequency of the instrument. The use of these rings enables measurements to be made over a wide range of viscosity.

In addition it appears from Tables 1 and 2 that the results obtained confirm the validity of the theory given and method discussed and indicate

- (i) the negligibility of the end effect, if $a/2l$ is very small; if not, the neglect of end effect will affect the results.
- (ii) the sensitivity of the apparatus for change of concentration of glycerine.

Acknowledgement

The authors are greatly indebted to this Journal's referees, particularly Mr. G. F. Miller and Dr. A. H. Cook for valuable comments and help.

References

- (1) OLDROYD, J. G. *Quart. J. Mech. Math.*, **4**, p. 271 (1951).
- (2) MARKOVITZ, H. *J. Appl. Phys.*, **23**, p. 1070 (1952).
- (3) IBRAHIM, A. A. K., and KABIEL, A. M. *J. Appl. Phys.*, **23**, p. 754 (1952).
- (4) IBRAHIM, A. A. K., and KABIEL, A. M. *Zamp. Fasc.*, **5**, p. 5 (1954).
- (5) IBRAHIM, A. A. K., and KABIEL, A. M. *Zamp. Fasc.*, **6**, p. 5 (1955).

Method of recording low-angle X-ray scattering when intensity scattered by specimen changes rapidly with time

by P. W. TEARE, B.Sc.,* Aluminium Laboratories Ltd., Banbury, Oxfordshire

[Paper first received 2 December, 1959, and in final form 3 March, 1960]

Abstract

A new technique is described for the collection of scattered X-ray intensity data at low angles. The technique is applicable to specimens producing scatter that is time variant. The use of the method is illustrated by an example taken from an age hardening aluminium-zinc alloy. Two methods of recording the intensity data are discussed and it is thought that an improvement in the facility of recording could be obtained by the use of proportional counting.

Introduction

INTENSITY measurements of X-ray scattering at low angles are normally made by sampling the scatter curve at selected points within the angle of scatter ϵ . The intensity of the scattering is usually low, and for reasonable statistical accuracy, counting periods of 2–5 min. for each point in the angle ϵ are common. Thus, about one hour is required to record the scatter curve for, say, fifteen sampling points.

In the application of low-angle scatter measurements to aluminium alloy systems undergoing age hardening, the period of time required to record the scattered intensities is frequently insignificant in comparison with the ageing time. That is, the hardening process is very slow. However, in certain cases, as in the aluminium-zinc alloys, ageing is extremely rapid.⁽¹⁾ An aluminium-13%-zinc-alloy aged at room temperature has, for example, undergone about 70% of the total hardness change within twenty minutes.

The normal method of recording low-angle scatter which, as mentioned above, may take an hour or more, is obviously inadequate to study the changes in the scatter curves associated with the rapid ageing occurring in the aluminium-zinc alloys. A new method of recording low-angle scatter has been developed which overcomes this difficulty and produces a complete set of isochronal scatter curves. As an illustration, the description of the recording procedure has been

related to the types of scatter curve associated with the aluminium-zinc alloys. It should, however, be emphasized that the method is applicable to all types of scattering curve.

Description of method

A polycrystalline sample of an aluminium-15%-zinc alloy, 0.0025 in. thick, was solution-treated for thirty minutes at 450° C, water quenched and transferred directly to the low-angle diffractometer.⁽²⁾ The time lapse between quenching and the start of intensity measurements was about 45 s. In this example, four such experiments were used to define a section of scatter curve between A and B (Fig. 1). In the first experiment, the counter was set on angle corresponding to point 1 in Fig. 1 and a 30 s count made. The counter

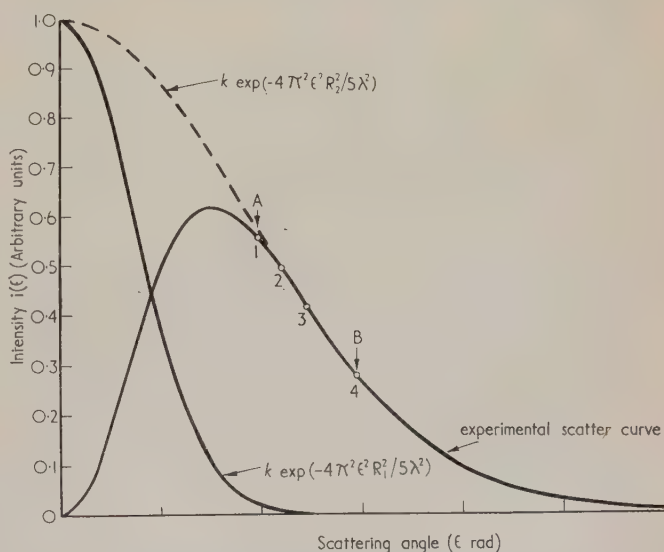


Fig. 1. A typical scatter curve obtained from an alloy of aluminium and 15%, by weight, zinc with its two exponential components

* Now at Central Electricity Research Laboratories, Leatherhead, Surrey.

was moved to angle 2, and after a time lapse of 30 s from the termination of the first count, a further 30 s count was made. Alternation between angles 1 and 2 in this manner was continued until there was little change in the intensity scattered with time. For an alloy in the condition described above, this took about 15 min. The whole experiment was repeated for the angles corresponding to points 2 and 3, 3 and 4, and finally 4 and 1. The order in which the angles are quoted is significant. With this order, the 30 s blank intervals in the curve of scattered intensity for angle 2 in the first experiment were filled during the second experiment and so on.

Fig. 2 shows a plot of the scattered intensities against time for each of the four angles. *AB* in Fig. 2 represents a section

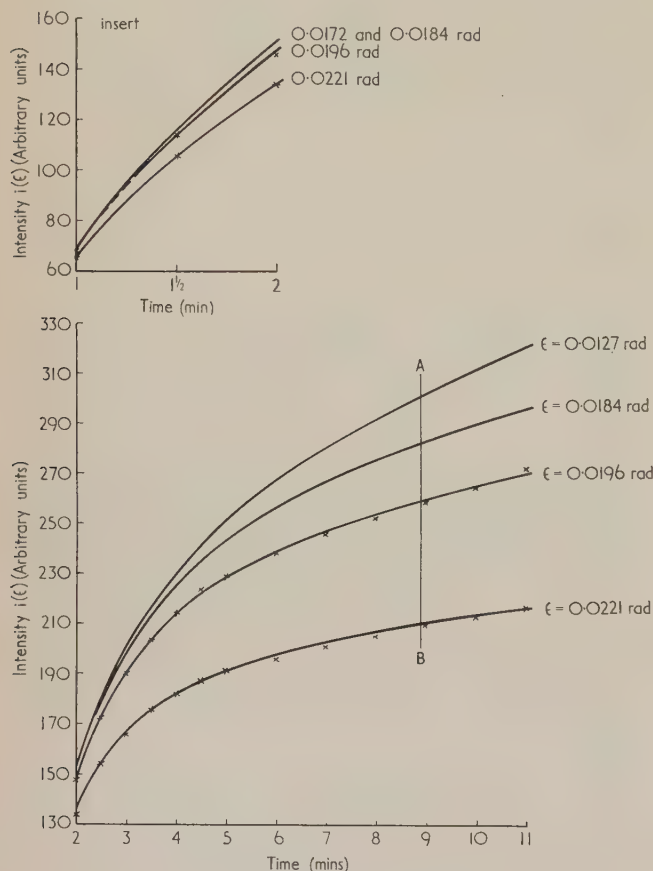


Fig. 2. Scattered intensity plotted against time for the four sampling points

of the scatter curve at a point t in time after quenching, with the proviso that the scattered intensities suffer from inaccuracies due to the change in count rate arising from the ageing process during the 30 s count period. In the example being considered, the change in scattered intensity with time was fairly gradual. If the change is rapid, the count period must be reduced from 30 s to a period which gives a reasonable determination of the scatter curve. Each of the sections *AB* may now be replotted into its corresponding section of the scatter curve as in Fig. 3.

Discussion

The method suffers from the obvious disadvantage that the count period is short. This may be overcome in two ways:

either by increasing the X-ray intensity or by repeating the whole cycle of measurements a sufficient number of times to give a reasonable mean count rate. The second method has been used. However, this is rather tedious, and consideration is being given to the applicability of proportional counting. This should permit larger scatter-slit apertures with a corresponding increase in X-ray output because of the greater area of the monochromating crystal under irradiation.

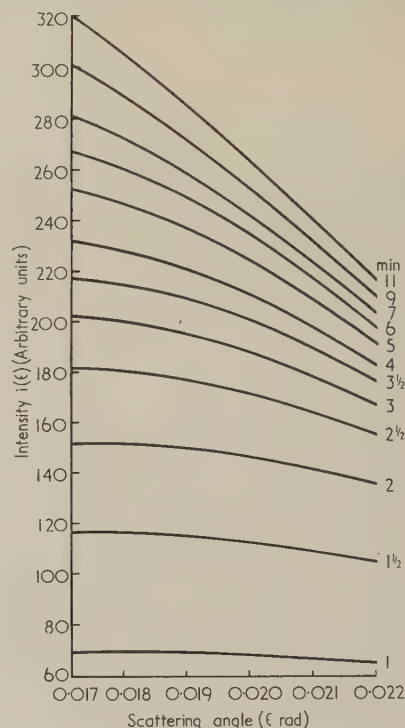


Fig. 3. Sections of the scatter curves *AB* plotted at selected time intervals

Whilst the method is of general applicability, it should not be used without some knowledge of the behaviour of the intensity of scattering over a period of time. For example, if the second method described above is used, it is advantageous to sample the scatter curve at as few points as is consistent with obtaining the information required. For the alloy already considered, the scatter curve shown in Fig. 1 may be represented by an equation in the form:

$$i(\varepsilon) = K \exp\left(-\frac{4\pi^2\varepsilon^2 R_1^2}{5\lambda^2}\right) - K \exp\left(-\frac{4\pi^2\varepsilon^2 R_2^2}{5\lambda^2}\right) \quad (1)$$

where, ε is the scattering angle in radians, i is the intensity scattered, R_1 is the radius of the cluster nucleus, R_2 is the radius of the nucleus plus its denuded zone, K is a factor depending on the composition of the cluster, and the number of clusters present in unit volume, and λ is the wavelength of the X-radiation.

In Fig. 1, the scatter curve has also been separated into the two exponential components of equation 1.

To obtain information about the change in both R_1 and R_2 with time, it is obviously necessary to select an angular range *AB* by a preliminary experiment containing scatter curves in which both the exponential components of equation (1) are contributory. For the aluminium-15% zinc alloy being studied this was quite simple. After the first

15 min. period of ageing in which the change of scattering was rapid, the subsequent changes were very much slower. In fact, there was little difference between the scatter curves obtained after ageing for one and four hours at room temperature. The scatter curve after ageing for four hours was thus used to define the angular range AB .

If the angular range required cannot be simply determined

by a preliminary experiment, it may be necessary to apply the method described to the whole angular range of the scattering.

References

- (1) PERRYMAN, E. C. W., and BLADE, J. C. *J. Inst. Metals*, **77**, p. 263 and Fig. 22, p. 283 (1950).
- (2) TEARE, P. W. *J. Sci. Instrum.*, **37**, p. 132 (1960).

Influence of temperature on the spectral composition of the zinc sulphide luminescence

by I. SOUDEK,* Research Institute for the Vacuum-Electrotechnics, Prague, Czechoslovakia

[Paper first received 15 April, 1958, and in final form 11 January, 1960]

Abstract

The temperature dependence of the spectral composition has been presented by a new method which shows better the relative changes of the form of the emission band. On the main emission band of some zinc and zinc-cadmium sulphides, between the liquid air temperature and the temperature break-point, certain effects have been observed; these are that (a) below 180° K the short wave side of the emission band of all phosphors grows faster than the long wave side with increasing temperature, (b) that in the neighbourhood of 220° K, the intensity of the whole band has a minimum for all copper-activated and copper-contaminated⁽⁴⁾ phosphors, and that (c), above 220° K, some phosphors behave inversely as (a). These effects can be explained by the existence of two temperature-dependent processes having inverse influence on the form of the emission band, one being similar to the hole-migration process and the other being in connexion with the thermal liberation of trapped electrons.

Introduction

DURING the last twenty years of the application of the band model on the luminescence of zinc sulphide, the conception of the emission band form has been thoroughly investigated; notwithstanding, there are still some points which need clarification. According to an opinion commonly held during the early days of the band model, the form of the emission band is due to the thermal broadening of a line which results from the radiative transition between the lower edge of the conduction band and the activator level. First observations of the temperature dependence of the spectral composition are noted by Schön,⁽¹⁾ who states that the width of the emission band does not tend to fall to zero at the absolute zero temperature, and from this fact he deduces that a broad energetic spectrum of activator levels is involved.⁽²⁾ Extensive research of the temperature dependence has been carried out by Klick⁽³⁾ who has measured spectral curves of phosphors at 4, 77 and 300° K. His results show, for the main emission bands of phosphors of the zinc sulphide type, that the form of the bands undergoes only small changes which are difficult to connect with any

theory. The temperature intervals in his measurements are large, and therefore his method does not show the exact form of this dependence. To examine the effect thoroughly, experiments have been arranged in which the spectral curves have been measured in smaller temperature intervals.

Experimental

Phosphors were put in a thick layer on the base of a metal cylinder placed in a Dewar flask, which was cooled with liquid air and electrically heated in steps of 20 to 30° C. After every temperature increase, the spectral composition of the luminescence was measured by means of a spectrophotometer composed of a glass prism monochromator and a photomultiplier. A mercury discharge tube with a Wood's filter bulb served as exciting source.

Measurements on four phosphors, which were used in previous researches,⁽⁴⁻⁷⁾ are described. For convenience, the designation of the samples by letters is the same as used in previous publications. Sample *L* is a copper-activated zinc-cadmium sulphide with 15 wt% cadmium sulphide. Other samples are activated by 100 p.p.m. of silver; samples *A* and *B* are mixed sulphides containing 51% cadmium sulphide, sample *D* is a pure zinc sulphide. Sample *B* contains 10 p.p.m. of nickel as killer and sample *A* is contaminated by copper in the concentration of the order of 1 p.p.m.; this contamination has been discussed in the earlier work.⁽⁴⁾

A considerable influence of the copper contamination could be detected as described in Ref. 4. Two, almost similar, emission spectra of phosphors *A* and *B*, belonging to the silver activator, have a different temperature dependence according to the copper content. Silver-activated phosphors, containing some cadmium sulphide, where the contamination by copper does not exceed a certain threshold value (probably of the order of 0.1 or 1 p.p.m.) show a deformation of the emission band which can best be interpreted as its shift to shorter wavelengths with increasing temperature. These results⁽⁵⁾ are in good agreement with observations on monocystals of cadmium sulphide⁽⁸⁾ and on the calcium wolframate.⁽⁹⁾ As has been pointed out in Ref. 5, apart from the shift, a broadening of the long-wave tail of the emission band takes place, but this is a less evident effect. On other phosphors, among them on a copper-activated zinc sulphide, an inverse shift has been reported.⁽¹⁰⁾ This has been con-

* Now at the Institute of Physics, Charles University, Prague.

firmed for temperatures near and greater than the room temperature.

At lower temperatures, the temperature dependence of the form of the emission band of copper-containing phosphors is not so simple. The results of measurements on the yellow-green emission band of the sample *L* are illustrated in Fig. 1. The intensity of luminescence in the band maximum decreases between 96 and 226° K by 32% and increases between 226 and 300° K again by 62%. Besides that, a slight shift of the band can be observed which, between 96 and 226° K, tends towards shorter wavelengths with increasing temperature, and at higher temperatures has the inverse direction. The position of the band maximum is preserved to a tolerance of a few millimicrons, and it is more the edges undergoing changes which cause the band shape deformations; these results are similar to those of Klick.⁽³⁾

The kind of presentation of the results which has been used in Fig. 1 is rather confusing, if a greater number of

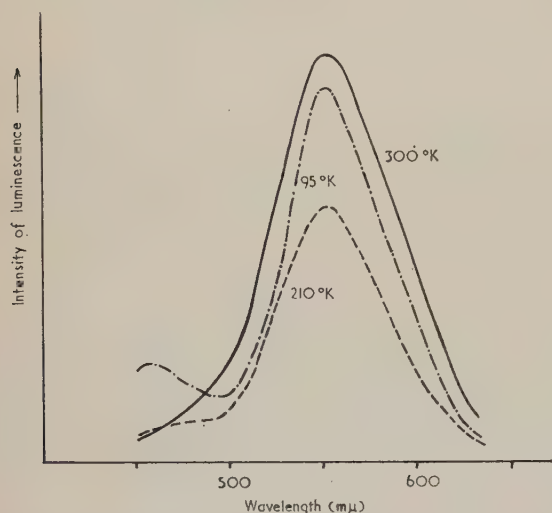


Fig. 1. Influence of temperature on the spectral composition of the luminescence of sample *L* in conventional demonstration

curves has to be presented in one figure. Therefore a more suitable system has been developed in which the logarithm of the intensity of luminescence for a limited number of selected wavelengths is plotted as a function of temperature. The curves are more simple and do not cross as frequently as those in the previous method. The logarithmic ordinate scale gives the same relative precision for all parts of the spectrum. A change of the intensity without a change of the form of the band manifests itself by a shift of all the curves by the same distance; the lines connecting them are therefore parallel. Any difference from the parallelism indicates a change of the form of the spectral curve. The results of the measurements which are shown in Fig. 1 are demonstrated by the new method in Fig. 2. The curve for 460 mμ shows the temperature dependence of the intensity of the short wave secondary band and is principally different from other curves. The dependences of the short wave side of the main band in this and in following figures are plotted with circles and full lines, the dependences of the long wave side are plotted with points and dashed lines.

From Fig. 2, neglecting the secondary band, it is seen that between 96 and 180° K the short wave side of the main band increases, whereas the long wave side (580 mμ) slightly decreases, and thus a shift to shorter wavelengths results. In the neighbourhood of 220° K a minimum of the intensity

of the whole emission band can be observed. At still higher temperatures, the long wave side of the curve (620 mμ) increases more steeply with increasing temperature than the short wave side (500 mμ), which means that the spectral curve is shifted to longer wavelengths. To a greater extent, thermal quenching does not take place below 500° K.

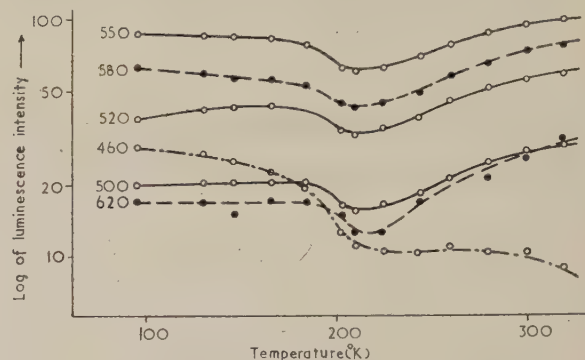


Fig. 2. Results of Fig. 1, replotted as described in text. Numbers near the curves indicate the wavelength in millimicrons

It is interesting to note that a similar effect can be observed on silver-activated phosphors which emit the typical band of silver, but show effects which are presumed to be derived from copper contamination; namely the thermal hysteresis of the luminescence intensity and the existence of a long wave secondary emission band, observable at elevated temperatures.⁽⁴⁾ Fig. 3 shows the result of measurements on the sample *A*. Again, between 110 and 180° K, one sees an increase of the intensity of the short wave side of the main emission band, and near 237° K a minimum of the intensity concerning the whole band. At higher temperatures, two effects act simultaneously, namely the recovery after the

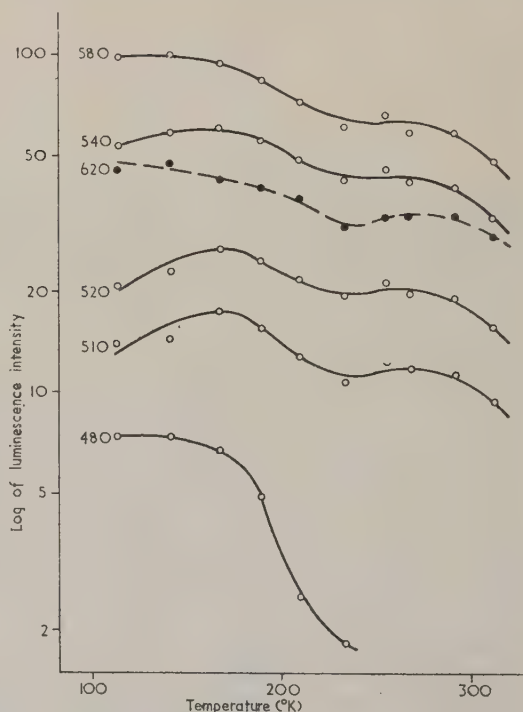


Fig. 3. The temperature dependence of the spectral composition of the luminescence of sample *A*

intensity minimum and the appearance of the temperature quenching, and therefore the long wave shift of the emission band is not too clear.

Fig. 4 shows the temperature dependence of the spectral composition of the luminescence of a silver-activated zinc

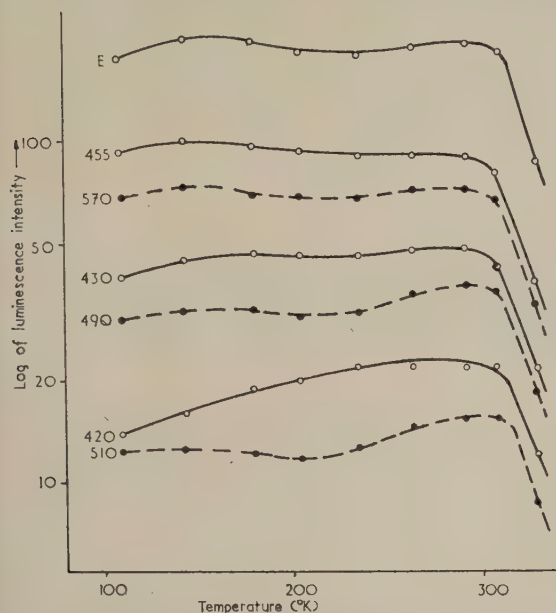


Fig. 4. The temperature dependence of the spectral composition of the luminescence of sample *D*. The curve *E* represents the temperature dependence of the integral of the spectral curve

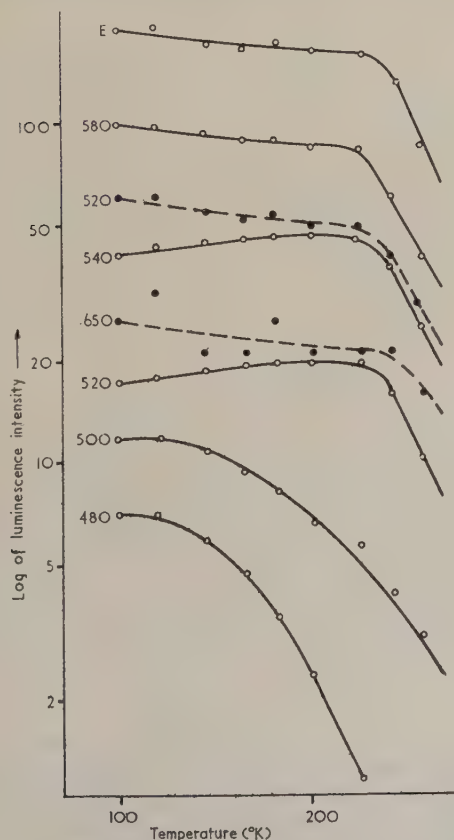


Fig. 5. The temperature dependence of the spectral composition of the luminescence of sample *B*

sulphide which does not show the specific properties associated with the contamination by copper (sample *D*). The low-temperature part of the curves indicates—in accordance with the measurements on all other phosphors—a shift of the emission band to shorter wavelengths with increasing temperature. The intensity minimum at 220° K is not observable on the short wave side of the emission band and is very small on the long wave side. Again at higher temperatures an evident shift of the band to longer wavelengths can be observed. Though small, the intensity minimum near 220° K manifest itself in the integral of the curve *E*.

In Fig. 5, the temperature dependence of the form of the emission band of the sample *B* is presented. In previous measurements this sample exhibited none of the effects ascribed to the copper contamination, and its emission band merely shifts to shorter wavelengths with increasing temperature throughout the temperature range between the liquid air and quenching temperatures, as described in Ref. 5.

Discussion

These results cannot be explained by temperature-dependent changes of the absorption coefficient and of the index of refraction of the base material, because these changes are too small and rather independent of the wavelength.⁽¹¹⁾ The deformation of the emission band must therefore be a property of the emission process itself. If one accepts the assumption that the width of the emission band corresponds to the form of the energy spectrum of the activator levels, the long wave shift of the emission band with increasing temperature may be explained by the migration of holes or a similar process; some evidence of the existence of such a process within a single emission band can be deduced from the intensity dependence of the emission spectrum.⁽⁶⁾ However, this process fails to explain the inverse shift; this shift is only temperature-dependent and not intensity-dependent, and therefore a new mechanism has to be found.

The experiments of different authors^(7, 12) suggest that the electron which accomplishes the radiative transition passes previously through a metastable state from which it must be liberated thermally. With increasing temperature the duration of this metastable state decreases. If the hole migrates meanwhile from lower to higher discrete levels with a temperature-independent speed, then the decrease of the duration of the metastable state increases the probability of recombination of the electron with a hole in a lower level, and therefore it can cause a shift of the spectral curve to shorter wavelengths. According to the properties of the lattice imperfections involved, either the hole migration or the trapping of electrons determines the temperature dependence of the form of the emission band. A change of their properties (e.g. a structural change in their neighbourhood) may cause a change of the prevailing influence. A change of this kind probably takes place in copper-containing phosphors near 220° K.

The unusual behaviour of the sample *D* can be explained by the influence of the copper contamination which is too weak to cause, for example, the intensity hysteresis, but is strong enough to manifest itself in the temperature dependence of the spectral curve. It is known that it is not possible to prepare a copper-free zinc sulphide and that a copper content of the order of 0.1 p.p.m. must always be taken into consideration. This tiny amount of copper may in some way be bound to the zinc sulphide; therefore, this unremovable remainder of copper would decrease with increasing cadmium sulphide content.

Acknowledgement

The author wishes to thank E. Haidingerová for technical assistance.

References

- (1) SCHÖN, M. *Verh. Dt. Phys. Ges.*, **23**, p. 76 (1942).
- (2) SCHÖN, M. *Ann. Phys. (Leipzig)*, **3**, p. 343 (1948).
- (3) KLICK, C. C. *J. Opt. Soc. Amer.*, **41**, p. 816 (1951).
- (4) SOUDEK, I. *Čzech. J. Phys.*, **8**, p. 66 (1958).
- (5) SOUDEK, I. *Čs. čas. fys.*, **9**, p. 246 (1959).
- (6) SOUDEK, I. *Czech. J. Phys.*, **8**, p. 336 (1958).
- (7) SOUDEK, I. *Czech. J. Phys.*, **9**, p. 590 (1959).
- (8) LUDWIG, W., and SEIWERT, R. *Z. Phys. Chem. (Leipzig)*, **207**, p. 250 (1957).
- (9) VLAM, C. C. *Brit. J. Appl. Phys.*, **5**, p. 443 (1954).
- (10) BRINKMAN, H., and VLAM, C. C. *Physica*, **14**, p. 650 (1949).
- (11) COOGAN, C. K. *Proc. Phys. Soc. (London) B*, **70**, p. 845 (1957).
- (12) WILLIAMS, F. E., and EYRING, H. *J. Chem. Phys.*, **15**, p. 289 (1947).

Thermal propagation of a normal region in a thin superconducting film and its application to a new type of bistable element

by R. F. BROOM, B.Sc., and E. H. RHODERICK, M.A., Ph.D., Services Electronics Research Laboratory, Baldock, Hertfordshire

[Paper first received 12 January, and in final form 13 February, 1960]

Abstract

The movement of the interphase boundary due to Joule heating in a partially superconducting film carrying a current is analysed. It is shown that there is a value of the current at which the boundary remains stationary; above this value the normal region grows, and below it, the normal region collapses. As the current approaches the critical current of the film, the speed of propagation becomes very large and of the right order to explain the authors' previous observations⁽¹⁾ on the rate of return of resistance to thin superconducting strips driven into the normal state by rectangular current pulses.

The current required to maintain the boundary stationary is much less than that necessary to generate a normal region initially. This enables a new type of bistable element to be constructed, consisting of a strip of superconducting film carrying a continuous current equal to that necessary to maintain the boundary stationary. A short pulse of current in the same sense as the standing current generates a normal region in the film which is subsequently held constant by the standing current, while a short pulse in the opposite sense cancels the standing current long enough for the film to become completely superconducting again. This device is extremely simple in construction and can be switched from one state to the other in 10 μ s.

growth increased, while just below the critical value the strip possessed a barely observable resistance (of order $10^{-3} \Omega$) which appeared without any delay greater than the resolution of the apparatus (about 15 μ s).

The following explanation of these phenomena was proposed. The very small resistance which appears without any observable delay is presumed to result from a flaw in the strip, which has a smaller critical current than the bulk of the film, being driven normal. Immediately the flaw is driven normal, Joule heat is produced and its temperature rises, approaching an equilibrium value asymptotically. If the simplifying assumptions are made that the dimension of the normal region parallel to the length of the strip is negligible, that the length of the strip is infinite and that the ordinary thermal conductivity equations hold, it may be shown that the rise in temperature of the flaw is:

$$\theta = \frac{I^2 R}{2w} (dK\alpha)^{-1/2} \operatorname{erf} \left(\frac{t\alpha}{pcd} \right)^{1/2},$$

where I is the current, R the resistance of the normal region (about $10^{-3} \Omega$), w , d , K , ρ and c the width, thickness, thermal conductivity, density and specific heat respectively of the film, t the time, and $\alpha w \theta$ the rate of loss of heat to the surroundings per unit length of the strip. The quantity pcd/α is the time constant with which the entire strip would cool if it were at a uniform temperature and there were no Joule heating. The above equation may therefore be written:

$$\theta = \theta_{\infty} \operatorname{erf} (t/\tau)^{1/2},$$

where

$$\theta_{\infty} = (I^2 R / 2w) (dK\alpha)^{-1/2}.$$

θ_{∞} is the equilibrium rise in temperature of the flaw and τ the cooling time constant. (Throughout this paper θ denotes the difference between the temperature of the film and that of the bath.) Experiments in this laboratory⁽²⁾ have shown that τ is markedly dependent on the substrate, so α must be

Introduction

IN a previous paper⁽¹⁾ the authors describe experiments in which strips of thin superconducting films were driven into the normal state by rectangular pulses of current. For current amplitudes just above a critical value, there was a delay of the order of a microsecond before any appreciable resistance returned to the film, and the resistance subsequently grew at a finite rate. As the current was increased above this critical value, the delay decreased and the rate of

predominantly limited by the rate of loss of heat from film to substrate and is presumably determined by the thermal resistance caused by the acoustic mismatch at the interface.⁽³⁾ In this paper times of about a microsecond or less will be considered, during which period there is insufficient energy available to cause significant heating of the substrate. The latter will therefore be regarded as an infinite heat sink.

The variation of the temperature of the normal region with time is shown in Fig. 1. Provided the equilibrium temperature θ_∞ exceeds the critical temperature θ_c of the surrounding

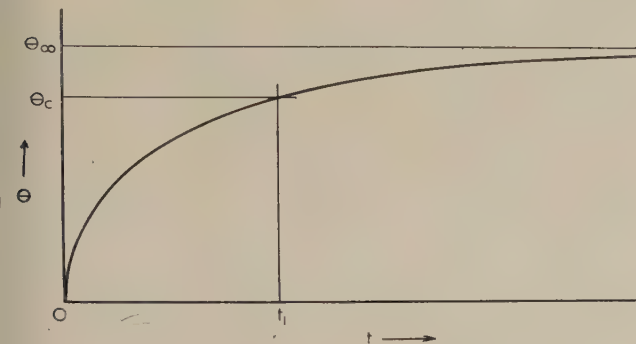


Fig. 1. Variation with time of the temperature of an infinitesimally small normal region in an infinite superconducting strip carrying a current

superconducting region, which is a function of the current I , the temperature of the flaw will reach θ_c at a time t_1 . When this happens, the adjacent superconducting material will be forced into the normal state, and the Joule heating will increase because of the added resistance. In our previous paper⁽¹⁾ it was postulated that this process is cumulative, and results in the propagation of the normal phase after a delay t_1 through a thermal spreading mechanism of the sort described by Bremer and Newhouse.⁽⁴⁾ The propagation rates observed by Bremer and Newhouse were smaller than those necessary to explain our results by a factor of 10^5 , and it was suggested in reference (1) that this might be because their films were much thicker and current densities much smaller than those used by us. The purpose of the present paper is to consider this process in more detail, to determine whether or not it leads to propagation rates of the right order of magnitude.

The thermal propagation process

If one considers a current passing through a superconducting strip, a fixed length of which is in the normal phase, then the variation of the temperature of the strip as a function of time and distance along the strip is well known.⁽⁵⁾ However, if the possibility is admitted that the normal region may grow as the adjacent superconducting material attains the critical temperature, the problem of the subsequent motion of the boundary is a formidable one which is probably insoluble without the use of a computer. A simpler problem is therefore considered here which can be easily solved using standard mathematical techniques, and which is sufficiently close to the real problem to provide some insight into the thermal propagation mechanism.

We consider the problem of an infinitely long strip carrying a current I , half of which is in the normal and half in the superconducting state, and inquire how the interphase boundary moves as a result of the Joule heating of the normal region. Suppose that the resistance of the strip in the normal phase is r per unit length and that the strip loses

heat to its surroundings (chiefly to the substrate) at a rate $\alpha w \theta$ per unit length, where w is the width of the strip, and assume that the strip is sufficiently thin for the temperature variation normal to the surface of the substrate to be negligible. At large distances from the interphase boundary in the normal region, the temperature approaches the value $\theta_1 = I^2 r / \alpha w$ at which the Joule heat just balances the loss of heat to the surroundings; at large distances from the boundary in the superconducting region, the temperature of the film approaches that of the substrate so that θ is zero. The temperature distribution at any instant of time therefore resembles that shown in Fig. 2, the interphase boundary occurring at x_1 , where θ equals θ_c .^{*} It is assumed that, as

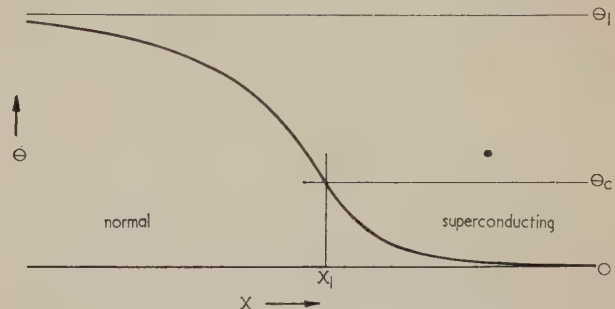


Fig. 2. Variation of temperature along the length of an infinite current-carrying strip, part of which is superconducting and part normal

the temperature distribution changes with time, the boundary moves so that it always occurs at the point where θ equals θ_c , and that there is no time lag in this process. (Preliminary experiments in this laboratory on tin films driven into the normal state by a pulsed magnetic field⁽⁶⁾ have shown that the restoration of resistance is complete in a time which is certainly not greater than $15 \mu\text{s}$ even for fields barely above the critical value, while radio-frequency experiments by Woodford and Feucht⁽⁷⁾ suggest that it may be as small as $1 \mu\text{s}$. It is reasonable to suppose that transitions taking place under the combined effects of current and temperature are equally fast, in which case they can be considered as instantaneous on the time scale of interest here.) It is also assumed that there is no thermal barrier at the interphase boundary, since the densities and velocities of sound in the two phases are almost identical, and that the difference between the thermal conductivities in the normal and superconducting phases,⁽⁸⁾ which is small near the critical temperature, may be neglected. The differential equations governing the temperature of the strip are, in the normal region ($x < x_1$):

$$\frac{\partial^2 \theta}{\partial x^2} - A \frac{\partial \theta}{\partial t} - B\theta + C = 0 \quad (1a)$$

and, in the superconducting region ($x > x_1$):

$$\frac{\partial^2 \theta}{\partial x^2} - A \frac{\partial \theta}{\partial t} - B\theta = 0. \quad (1b)$$

Here $A = cp/K$, $B = \alpha/dK$, $C = I^2 r / wdK$, and the remaining symbols are as defined previously. We now assume that there is a solution in which the interphase boundary moves with a constant velocity v and the temperature profile remains

* θ_c denotes the excess temperature above the bath temperature at which the strip becomes normal when carrying a current I , and is therefore a decreasing function of I which vanishes when I equals the critical current corresponding to the bath temperature.

constant relative to the boundary, so that the solution is of the form $\theta = \theta(x - vt)$, and seek the conditions that must be satisfied for such a solution to exist. It is convenient to choose the origin of co-ordinates so that $x_1 = vt$ and to introduce a new variable $\xi = (x - x_1) = (x - vt)$, so that $\theta = \theta(\xi)$.

The equations (1) now become,

$$\theta'' + Av\theta' - B\theta + C = 0, \quad (\xi < 0), \quad (2a)$$

and

$$\theta'' + Av\theta' - B\theta = 0, \quad (\xi > 0). \quad (2b)$$

The solutions which satisfy the requirements $\theta \rightarrow \theta_1$ as $\xi \rightarrow -\infty$, and $\theta \rightarrow 0$ as $\xi \rightarrow +\infty$, are:

$$\theta = D \exp(\sigma_1 \xi) + \theta_1, \quad (\xi < 0), \quad (3a)$$

and

$$\theta = E \exp(\sigma_2 \xi), \quad (\xi > 0), \quad (3b)$$

where:

$$\sigma_1 = -\frac{1}{2}\{Av - (A^2v^2 + 4B)^{1/2}\},$$

$$\sigma_2 = -\frac{1}{2}\{Av + (A^2v^2 + 4B)^{1/2}\},$$

and D and E are constants which are fixed by the conditions that, at the boundary between the two phases, θ equals θ_c and θ' is continuous. These require that:

$$D + \theta_1 = E = \theta_c$$

and

$$\sigma_1(\theta_c - \theta_1) = \sigma_2\theta_c.$$

The latter equation can be re-arranged to give:

$$Av\theta_1 = (\theta_1 - 2\theta_c)(A^2v^2 + 4B)^{1/2},$$

where the positive square root is taken. Since A and θ_1 are both positive, v is positive or negative according as θ_1 is greater or less than $2\theta_c$. This gives the novel result that the normal region may either grow or collapse depending on whether θ_1 is greater or less than $2\theta_c$: if θ_1 equals $2\theta_c$, the boundary remains stationary, as may easily be verified by showing that a time-independent solution of equations (1) is possible when $\theta_1 = 2\theta_c$. Finally, the following expression for v is obtained:

$$v = \frac{B^{1/2}}{A} (\theta_1 - 2\theta_c) \{\theta_c(\theta_1 - \theta_c)\}^{-1/2} - \frac{(\alpha K/d)^{1/2}}{cp} (\theta_1 - 2\theta_c) \{\theta_c(\theta_1 - \theta_c)\}^{-1/2}.$$

Since the problem is such that θ_1 is necessarily greater than θ_c , v is real.

To find the order of magnitude of v , consider the case of the lead strips used previously⁽¹⁾ by the authors. For these strips, d is about 500 Å, and if the bulk values for the thermal conductivity⁽⁸⁾ and specific heat⁽⁹⁾ appropriate to the normal phase near 4° K are assumed, then K is approximately 10 W deg.⁻¹ cm.⁻¹, and c is approximately 8×10^{-4} J deg.⁻¹ g.⁻¹. Experiments in this laboratory with lead films on mica substrates have yielded values of 1 to 10 W deg.⁻¹ cm.⁻² for α , and 3 W deg.⁻¹ cm.⁻² will be used as a representative value. The factor $(\alpha K/d)^{1/2}/cp$ now becomes ~ 0.3 cm/ μ s. The experiments of reference (1) were carried out with currents such that θ_c was less than 1° K, while θ_1 was of the order of 10° K, consequently $(\theta_1 - 2\theta_c)\{\theta_c(\theta_1 - \theta_c)\}^{-1/2} \simeq (\theta_1/\theta_c)^{1/2} \sim 3$ or more, and $v \sim 0.3(\theta_1/\theta_c)^{1/2} \sim 1$ cm/ μ s. As I approaches the "true" critical current corresponding to the bath temperature, by which is meant the critical current for a perfect film in the

absence of heating effects, θ_c approaches zero and v may become much larger.

In the experiments previously described by the authors,⁽¹⁾ the strips were 2 mm long, and propagation velocities of the order of 1 cm/ μ s are adequate to explain the results. This apparently excellent numerical agreement is somewhat fortuitous. In the first place, a value for K appropriate to bulk material has been used, whereas, in films of thickness of the order of 1000 Å, K will be limited by boundary scattering to a value perhaps as much as 50 times smaller than the bulk value. However, since v is proportional to $K^{1/2}$, this is not as serious as it seems at first. In the second place, the quantities K , c and α are not really constants but depend on temperature, and the first two have different values in the superconducting and normal phases. The use of average values for these quantities and the uncertainty in θ_c means that one cannot expect more than order-of-magnitude agreement. In principle, it is possible to make v as large as one wishes by making θ_c small enough, that is, by choosing I sufficiently near to the "true" critical current. In practice, since no film is perfect and θ_c would vary along the length of the strip, the theory would be no longer applicable when this stage is reached.

Experimental confirmation

In the introduction, the authors' previous experiments⁽¹⁾ were interpreted as being due to the production of Joule heat at a flaw, the temperature of which then increased until it was ultimately able to initiate the thermal spreading process. A necessary condition for this is that θ_∞ is greater than θ_c , that is, $(I^2 R/2w)(K\alpha d)^{-1/2} > \theta_c$. If an "apparent d.c. critical current" I_1 is defined by replacing the inequality sign by an equality, I_1 is the current at which the temperature of the flaw rises just sufficiently to make the spreading process begin after an infinite delay. If the spreading process is to be initiated in times of the order of microseconds or less, then currents appreciably greater than I_1 are necessary, as was shown in reference (1). Once the normal region has spread sufficiently for its behaviour to approach that of an infinitely long strip (this means that its length must be larger than $B^{-1/2}$, that is, of the order of 10^{-2} cm), the analysis of the preceding section will begin to apply, and the normal region will spread provided θ_1 is greater than $2\theta_c$, that is, $I^2 r/\alpha w$ is greater than $2\theta_c$. If I_2 is the threshold current for the latter process, then I_2 is appreciably less than I_1 for the strips used in reference (1), since I_1^2/I_2^2 is equal to $(r/R)(Kd/\alpha)^{1/2}$, which is of the order of 40. (This conclusion remains valid even if K has been overestimated by as much as a factor of 100.) It follows that, once the normal region has been started, it can be propagated by currents much smaller than that required to initiate it. The following experiments confirm that this is indeed the case.

With an experimental arrangement identical with that used in reference (1), provision was made for using current pulses of the form shown in Fig. 3(a), the amplitudes of the 0.1 μ s "ignition pulse" and 0.5 μ s "pedestal" being independently variable. With a lead strip 2 mm \times 0.125 mm \times 500 Å deposited on a mica substrate and having a full normal resistance (measured just above T_c) of 1.47 Ω , the amplitude of the ignition pulse was set at a value of 800 mA, which was sufficient to initiate the spreading process at a bath temperature of 4.2° K and to make it continue until the resistance of the strip was 0.3 Ω . With the pedestal set at 320 mA, the resistance remained constant at the values

0.3 Ω after the ignition pulse had finished, the variation of resistance with time being shown by the full line in Fig. 3(b). The amplitude of the pedestal required to maintain the resistance constant was not as critical as one might expect from the foregoing theory. Thus, for a current of 400 mA the resistance grew noticeably after the end of the ignition pulse, as shown by the broken line, while for a current of

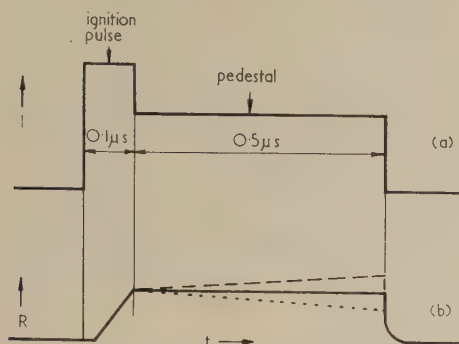


Fig. 3. Variation with time of (a) current, and (b) resistance for lead strip 2 mm \times 0.125 mm \times 500 Å at 4.2° K.

250 mA it decreased, as shown by the dotted line; over a range of $\pm 25\%$ the resistance remained substantially constant. The state of the film when the pedestal is set so as to maintain the resistance constant is one in which it is partly in the normal and partly in the superconducting state, the extent of the normal region depending on the amplitude and duration of the ignition pulse. When the ignition pulse was reduced below 760 mA, which was the minimum required to initiate the spreading process with a pulse length of 0.1 μ s, no resistance appeared at all. It is possible for the spreading process to start from more than one flaw, and there was evidence in some of the films studied in reference (1) that this was indeed happening; in this case, the rates of growth of the normal regions should be independent of each other provided their separation remains greater than about 10^{-2} cm.

The value of current for which the normal region remains constant in extent should enable a test to be made of the relation:

$$\theta_1 = I_2^2 r / \alpha w = 2\theta_c.$$

Unfortunately, α is known much less exactly than any of the other quantities, and the most sensible procedure is to use the relation to evaluate α . For the lead strip on a mica substrate described above, the critical temperature with a current of 320 mA flowing through it was 6.05° K, so that θ_c equalled 1.85° K at a bath temperature of 4.2° K. This gives $\alpha \simeq 16$ W deg. $^{-1}$ cm $^{-2}$, which is in reasonable agreement with the independent estimate of 1–10 W deg. $^{-1}$ cm $^{-2}$ quoted previously.

Application to a bistable element

In the previous section it was pointed out that the d.c. critical current I_1 is greater than the current I_2 with which the normal region can be held stationary. For the lead strip quoted above, I_1 is 550 mA and I_2 is 320 mA. It should therefore be possible to construct a bistable element consisting of a superconducting strip carrying a continuous current equal to I_2 . Application of an ignition pulse would initiate a normal region (or regions), which would spread to an extent determined by the amplitude and duration of the ignition pulse, and the normal region would subsequently be held stationary by the standing current I_2 . Application

of an "extinction" pulse equal to $-I_2$ and of duration comparable with the cooling time constant of the strip would reduce the total current to zero sufficiently long for the strip to become completely superconducting once more, and the strip would remain in this state after the extinction pulse had ended.

A bistable element of this sort has been constructed using the lead strip described above. A standing current of +300 mA was passed through the strip, and an ignition pulse of +700 mA and 20 μ s duration and an extinction pulse of -300 mA and 0.1 μ s duration were used. This strip operated as expected, a resistance of 1.1 Ω being generated by the ignition pulse and maintained by the standing current until it was destroyed by the extinction pulse.

There are two advantages to be gained by using tin rather than lead for such an element. Firstly, by working near the critical temperature the critical current may be reduced very considerably compared with that of a lead strip, which has the twofold advantage of reducing the amplitudes of the triggering pulses and of decreasing the power dissipation in the resistive state. Secondly, because of the smaller cooling time constant of tin, a much shorter extinction pulse may be used. A bistable element has been constructed from a tin strip deposited on a mica substrate, with dimensions the same as those of the lead strip mentioned above and a normal resistance of 6.6 Ω . This was operated at a temperature of 2.95° K, with a standing current of 11 mA and ignition and extinction pulses of +22 and -11 mA respectively. Both pulses could be as short as 10 μ s in duration. The d.c. critical current was 28 mA, and the resistance generated by the ignition pulse 0.9 Ω . The current and voltage waveforms for this strip are shown in Fig. 4, the repetition rate

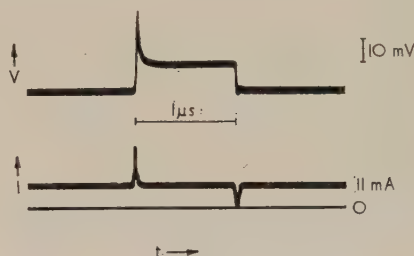


Fig. 4. Voltage and current oscillograms for tin strip 2 mm \times 0.125 mm \times 450 Å at 2.95° K.

The zero current baseline has been drawn to show the standing current. The ignition and extinction pulses are of 20 μ s duration.

being 2 kc/s. The baseline corresponding to zero current has been drawn to show the standing current. This figure illustrates a situation in which the strip was in the "on" (resistive) state for 1 μ s and in the "off" (completely superconducting) state for 500 μ s. The amount of Joule heat produced during the former interval was so small in relation to the heat capacity of the substrate that the latter remained essentially at the bath temperature. If the order of the ignition and extinction pulses was reversed, so that the strip was in the resistive state for 500 μ s and completely superconducting for 1 μ s, then the Joule heat became sufficient to raise the substrate above the bath temperature; the substrate remained at this new temperature during the "off" period because of its long thermal time constant, and the film cooled down to the substrate temperature rather than to the temperature of the helium. This reduced the value of θ_c and resulted in a larger resistance (1.8 Ω) being generated by the ignition pulse. This new value of resistance subsequently remained

constant because the correct value of the maintaining current is much less sensitive to θ_c .

This bistable element could conceivably find some application in computer design. Among its advantages are extreme simplicity of construction, high speed of operation, low drive current and non-destructive read-out in the form of a d.c. voltage. Its obvious disadvantage is that it consumes power (about 10^{-4} W) in the "on" state, which limits the number of such elements that could be used without excessive helium consumption to the order of 10^4 . Although in all the films which have been made so far the ignition process seems to involve one or more flaws, similar bistable operation could equally well be obtained with a perfect film, since the "true" critical current is greater than the "apparent d.c. critical current" I_1 . It is the prevailing fashion to concoct a name for any device embodying a new principle; the name "calotron" seems appropriate to the present one because of the important part played by heating in its mode of operation.

Conclusion

The most important result of this paper is that thermal propagation of the interphase boundary in thin superconducting films carrying a current may be a much faster process than has previously been realized. It appears to be the fastest known process in solids in which changes in lattice temperature play an essential role. Apart from its application to the design of new superconducting devices, it could well play an important part in the operation of existing ones. For example, in the planar cryotron⁽¹⁰⁾ the amount of resistance introduced into the gate by a current in the control strip just above the threshold value is usually of the order of $10^{-3} \Omega$ or less. If the gate strip carries a current close to its d.c. critical current, this small amount of resistance may be rapidly multiplied as a result of the thermal spreading process. In the Crowe cell⁽¹¹⁾ also, thermal propagation almost certainly makes an important

contribution to the growth of resistance in the crossbar, while the reverse process in which the normal region collapses may play a part in its subsequent recovery. Since thermal relaxation times may be as short as 10 μ s or less if an appropriate choice of film and substrate material is made, the use of a phenomenon in which heating plays an essential part is unobjectionable in many applications.

Acknowledgements

The authors are indebted to D. M. Eagles and D. J. Oliver for help with the heat-conduction problem, and to the Admiralty for permission to publish this paper.

References

- (1) BROOM, R. F., and RHODERICK, E. H. *Phys. Rev.*, **116**, p. 344 (1959).
- (2) BROOM, R. F., and SIMPSON, O. *Brit. J. Appl. Phys.*, **11**, p. 78 (1960).
- (3) LITTLE, W. A. *Canad. J. Phys.*, **37**, p. 334 (1959).
- (4) BREMER, J. W., and NEWHOUSE, V. L. *Phys. Rev. Lett.*, **1**, p. 282 (1958).
- (5) CARSLAW, H. S., and JAEGER, J. C. *Conduction of Heat in Solids*, 1st Ed., p. 136 (Oxford: University Press, 1947).
- (6) OLIVER, D. J. To be published.
- (7) WOODFORD, J. B., and FEUCHT, D. L. *Proc. Inst. Radio Engrs*, **46**, p. 1871 (1958).
- (8) MENDELSSOHN, K. *Progress in Low Temperature Physics*, **1**, p. 191 (Amsterdam: North Holland Pub. Co., 1955).
- (9) DOLECEK, R. L. *Annexe 1955-3, Supp. au Bulletin de L'Institut International du Froid*, p. 300 (1955).
- (10) YOUNG, D. R. *Progress in Cryogenics*, **1**, p. 29 (London: Heywood and Co. Ltd., 1959).
- (11) CROWE, J. W. *I.B.M. J.*, **1**, p. 295 (1957).

Etch pits and dislocations in cadmium sulphide crystals

by J. WOODS, B.Sc., Ph.D., A.Inst.P.,* Research Laboratories of The General Electric Company Limited, Wembley, England

[Paper received 2 March, 1960]

Abstract

A technique is described for producing dislocation etch pits on (0001), (000 $\bar{1}$) and {10 $\bar{1}$ 0} growth faces of cadmium sulphide crystals. Methods are also described whereby the dislocations are decorated by precipitation of either gallium or copper. The strongest proof that the etch pits are formed where dislocation lines cut the free surfaces is provided by (1) the characteristic etch pattern formed after indentation; (2) the densities of etch pits in intersecting low-angle grain boundaries; and (3) the coincidence of etch pits and decorated lines. Various other observations support the main evidence.

In conclusion, it is shown that the dislocation content can play an important part in determining some of the electrical properties of the crystals. In particular, copper

is rendered ineffective as an acceptor by precipitation, and dislocations introduced in cadmium sulphide/chlorine crystals by plastic bending lead to the formation of acceptors.

Introduction

UP to the present, attempts to explain the various aspects of the photoconductive and luminescent processes in cadmium sulphide have been based on the concept of the point defect. Little attention has been given to other types of crystal imperfection. Recently, a study of the growth and dissolution mechanisms in cadmium sulphide crystals was started in an attempt to determine the nature of the defects present. The final object of the work is to determine what part, if any, these defects play in various processes not readily explained in terms of lattice vacancies

* Now at Department of Applied Physics, Science Laboratories, South Road, Durham City.

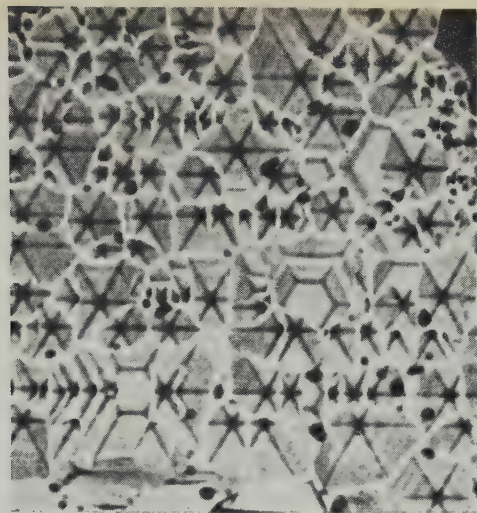


Fig. 1. Hexagonal etch pits on (0001). ($\times 220$)

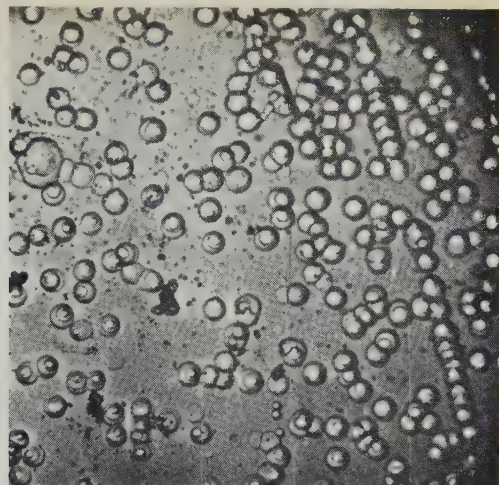


Fig. 2. Conical etch pits on (000 $\bar{1}$). ($\times 330$)

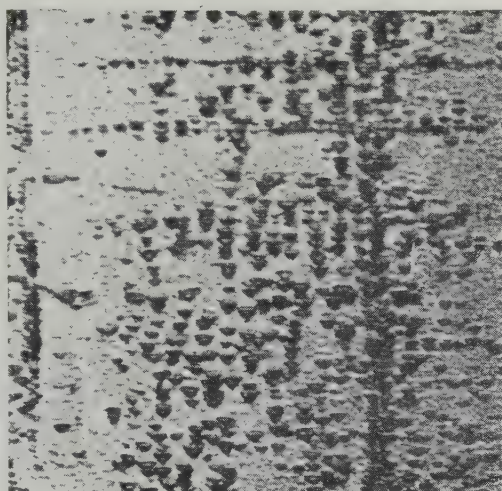


Fig. 3. Triangular etch pits on {10 $\bar{1}$ 0}. ($\times 130$)

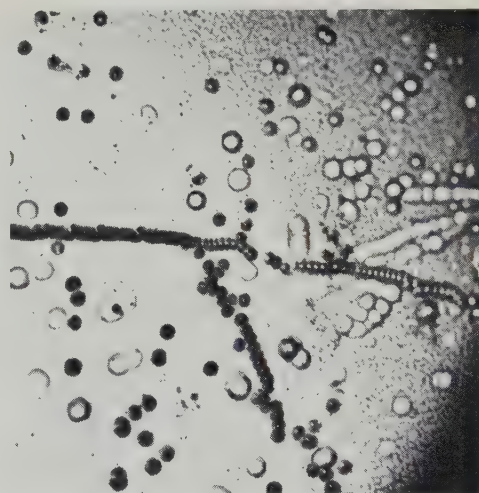


Fig. 4. Intersection of low-angled grain boundaries on (000 $\bar{1}$). ($\times 330$)

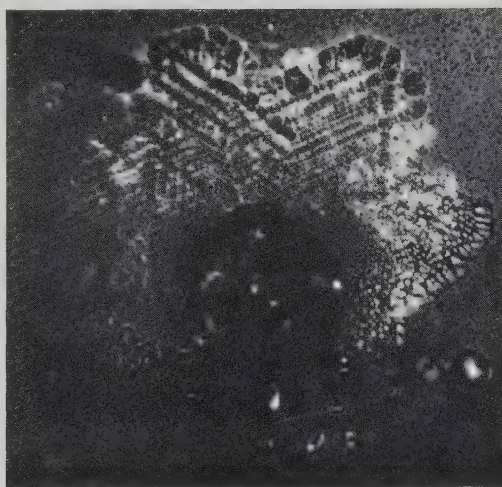


Fig. 5. Characteristic pattern of etch pits produced after indentation on (000 $\bar{1}$). ($\times 330$)

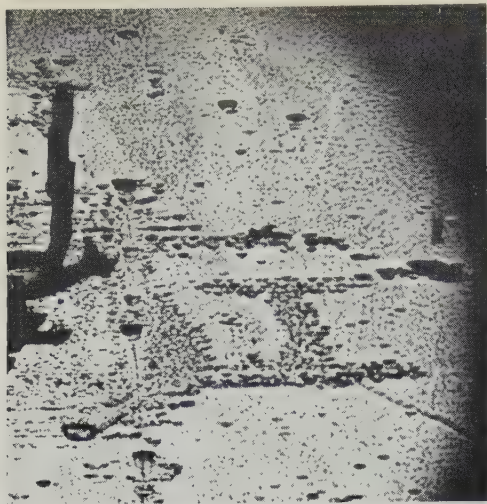


Fig. 6. Alinement of etch pits perpendicular to the c -axis after indentation on $\{10\bar{1}0\}$. ($\times 130$)

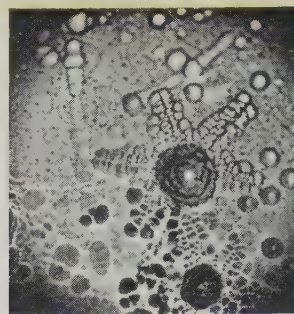


Fig. 7. Alinement of small pits around a large central pit. ($\times 330$)

Fig. 8. Hexagonal etch pits produced where decorated dislocation lines meet the (0001) surface. ($\times 330$)

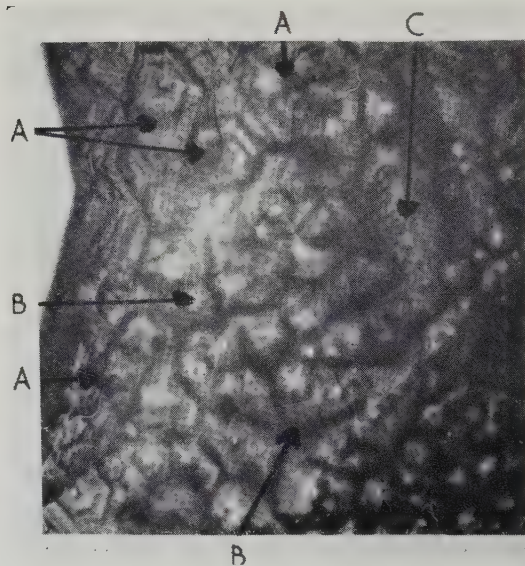


Fig. 9. Decoration of dislocations with precipitated gallium. ($\times 130$)

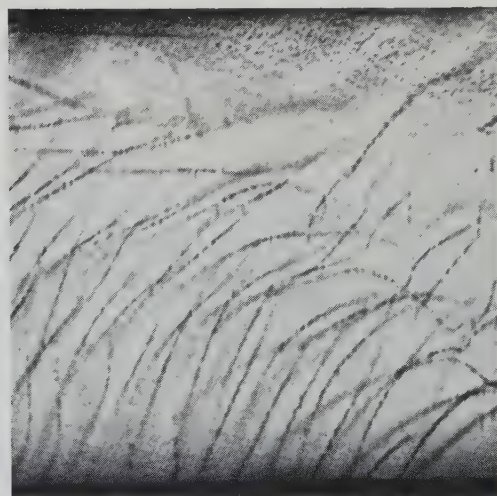


Fig. 10. Decoration of dislocations with precipitated copper. ($\times 330$)

and substitutional impurities. This paper will be mainly concerned with a description of the attempts made to identify dislocations in cadmium sulphide crystals using etching and decoration techniques, but will also include a brief account of some of the effects of dislocations on the electrical properties of crystals.

Preparation of crystals

The method of growing crystals used in this investigation has been described in detail in an earlier publication.⁽¹⁾ Briefly, it consisted of passing argon over molten cadmium to give a stream of cadmium vapour, which was reacted in a silica tube with a stream of hydrogen sulphide or argon containing sulphur vapour at 1050–1200° C. The vapour condensed to form crystals in a cooler part of the tube at 900° C. The hydrogen sulphide used was known to contain a trace of hydrogen chloride, but nevertheless the crystals prepared from it had resistivities between 10^{10} and 10^{12} Ω cm. When crystals with resistivities from 10^3 – 10^{-3} Ω cm were required, hydrogen chloride was mixed with the hydrogen sulphide, or gallium or indium vapour was added to the cadmium vapour. All the crystals prepared were of the hexagonal type. Details of crystal habit and its dependence on the growth conditions can be found in the earlier publication.⁽¹⁾

Chemical etch pits

Reynolds and Greene⁽²⁾ have recommended a procedure for producing etch pits on cadmium sulphide crystals which consists of suspending a crystal in the vapour of concentrated hydrochloric acid. It has been found with this technique that etch pits could only be produced on one of the two basal planes of the crystals, arbitrarily designated (0001). Thus this etch produced hexagonal pits on (0001), and merely roughened (000 $\bar{1}$), {10 $\bar{1}0$ } and {11 $\bar{2}0$ } faces. Similar results were obtained when crystals were immersed in dilute hydrochloric acid, a technique used by Votava.⁽³⁾ A much superior etch which will produce pits on both basal planes and on {10 $\bar{1}0$ } faces is chromic acid of the following composition: 1 g Cr₂O₃, 12.5 ml concentrated sulphuric acid H₂SO₄, 1250 ml water. After immersion in liquid of this composition and heating to 80° C for 10 minutes, the crystals were removed and washed first in water and then in methanol. Microscopic examination with vertical illumination showed that, whereas the pits on (0001) planes were hexagonal in shape (Fig. 1), those on (000 $\bar{1}$) planes were conical (Fig. 2). Triangular pits of the type shown in Fig. 3 were found on {10 $\bar{1}0$ } faces but no pits could be produced on {11 $\bar{2}0$ } faces. The pits were formed on all the types of crystal examined, with and without added impurity. Pits could also be produced on crystals into which copper and silver had been diffused subsequent to growth, provided the final concentration of impurity did not exceed 0.1%. (Copper and silver form acceptors in cadmium sulphide and are used as activators to promote high photoconductivity.) Spectrographic examination of the purest crystals, which were prepared from triply distilled, high-purity cadmium and sulphur, could detect no impurity present in concentrations greater than about 1 p.p.m. It can be concluded therefore that it is not necessary for impurities to be present for pits to be formed. X-ray analysis has shown that the sides of the hexagonal pits are always parallel to the *a*-directions. The triangular pits always have the same orientation with one side perpendicular to the *c*-axis and the apex of the triangle directed to the (000 $\bar{1}$) basal plane.

The conical pits on (000 $\bar{1}$) planes and the triangular pits on {10 $\bar{1}0$ } faces are very uniform in size. This is not the case

with the hexagonal pits on (0001) faces. Such pits show a great variety of width and depth and large numbers of flat-bottomed pits were frequently observed. Uniform pits could be produced, however, if the etch was terminated after 30 s. Under such conditions, no pits could be observed on (000 $\bar{1}$) and {10 $\bar{1}0$ } faces, but minute hexagonal pits of uniform size were found on (0001) faces. The explanation of this is that dissolution on (0001) faces proceeds much more rapidly than on the other faces and is also a function of the direction in the basal plane, so that well-defined hexagonal shapes are retained. If etching is taking place preferentially at the core of a dislocation, a pit will have a sharp apex as long as the dislocation line emerges at the surface. However, when the line suffers a change of direction, for example to lie in a basal plane, the pit develops a flat bottom. Continued etching then widens the pit and gradually reduces its height, and hence its visibility. The rate of reduction of height is much more rapid on (000 $\bar{1}$) and {10 $\bar{1}0$ } faces than on (0001) faces. The conical and triangular pits which develop flat bottoms rapidly disappear from view during continued etching, while the flat hexagonal pits remain visible. In consequence, a complicated etch pattern develops on (0001) faces, whereas the pits on (000 $\bar{1}$) and {10 $\bar{1}0$ } faces remain uniform in size and are better suited for study.

Etch pits and dislocations

The following observations suggest that the various types of pit denote the points of emergence of dislocation lines:

(1) Conical and hexagonal pits are often found alined in rows along traces of {10 $\bar{1}0$ } planes on basal planes. This suggests that here pits are formed in traces of the slip planes, slip having occurred during growth as a result of thermal strain.

(2) If a crystal plate with two large basal planes and a small *c*-dimension is etched, there is often a large but not complete degree of correlation between the hexagonal pits on one face and the conical pits on the other. In one particular crystal which contained a low-angle tilt boundary as determined by X-ray analysis, the boundary was defined by a row of conical pits on one face and a corresponding row of hexagonal pits on the other. The densities of pits in the two rows were equal.

(3) When three rows of etch pits denoting low-angle grain boundaries meet at a point, the densities of pits n_a , n_b and n_c in the three boundaries, *a*, *b* and *c* are related in the following way, if each pit corresponds to one dislocation:

$$n_a/\cos \phi_a = n_b/\cos \phi_b + n_c/\cos \phi_c \quad (1)$$

where the ϕ 's are the angles between the appropriate boundary and the nearest slip direction. The direction of slip appears to be $\langle 11\bar{2}0 \rangle$ in cadmium sulphide so that for rows of pits in basal planes, no value of ϕ can exceed 30°. Equation (1) can therefore be written:

$$n_a \simeq n_b + n_c \quad (2)$$

A number of junctions of three low-angle boundaries where equation (2) is obeyed has been observed, and a typical example is shown in Fig. 4. The difficulty with this method is to find junctions between long straight rows of pits.

(4) Experiments in which the etch pit arrays produced by plastic bending are studied were not practicable with the crystals used in this work because of the irregularity and unsuitable geometry of the majority of the samples. A further difficulty is that cadmium sulphide is brittle at room temperature and can only be deformed satisfactorily at

temperatures in excess of 700° C. However, when samples were heated to 700° C in argon and deformed by indentation with a conical point, characteristic patterns of pits were produced on subsequent etching. Identical groupings of pits were produced on both basal planes after these planes were indented. The pattern, which is similar to that produced on a {111} face of a germanium crystal grown in a $\langle 111 \rangle$ direction by the crystal-pulling method,⁽⁴⁾ is illustrated in Fig. 5. The alinement of pits into rows is along the a -directions, that is, the traces of the {10 $\bar{1}0$ } planes. Indentation on {10 $\bar{1}0$ } faces leads to production and alinement of pits in traces of the basal planes, as shown in Fig. 6.

(5) Pits are often found isolated in pairs; this is particularly easy to observe on (000 $\bar{1}$) faces. On prolonged etching, such pairs often merge and disappear, or separate before merging and disappearing. When they separate, the space between the pits is found to be occupied by a row of badly defined, rounded pits. This suggests that the pair of pointed pits defines the ends of a half-loop dislocation line. The individual pits of such pairs are rarely symmetrical, that is, the apex of a pit is not at the centre and presumably is indicative of the angle of emergence of the dislocation line at the surface.

(6) In crystals containing grown-in gallium impurity, conical pits much larger than the majority present on the same (000 $\bar{1}$) face have occasionally been observed. These large pits were often, but not always, surrounded by an array of smaller pits which lay along traces of {10 $\bar{1}0$ } planes (Fig. 7). This suggests that the central pit is caused by an aggregation of impurity, and that the misfit around the impurity has led to slip over {10 $\bar{1}0$ } planes. Similar alinements of etch pits radiating from scratches on the surfaces have also been observed.

(7) Pits characteristic of the crystal face are produced at points where decorated dislocation lines meet the surface. (The decoration of crystals is discussed in the next section.) Attempts to demonstrate photographically the coincidence of an etch pit and its decorated dislocation have not been very successful because of the difficulty of focusing the line and the pit simultaneously. Fig. 8 shows one of the best photographs obtained. The plane under examination is (0001), and the microscope was focused just below the surface of the sample which contains characteristic hexagonal etch pits. At *A*, decorated lines can be seen terminating at pointed pits. At *B*, there are some half loops with corresponding pairs of pits, and at *C* there is a low-angle boundary which would be seen to be defined by a row of pits if the crystal surface were in focus.

The observations enumerated above are all consistent with the interpretation that the pointed etch pits denote the sites of emergence of dislocation lines at the crystal surfaces. Quantitative measurements are difficult because of the high density of pitting (10^5 – 10^7 cm⁻²) and the geometry of the small samples. The results suggest that slip can occur on {10 $\bar{1}0$ } planes and on basal planes and that the slip direction is $\langle 11\bar{2}0 \rangle$. This is supported by observations of slip bands produced by plastic bending at 700° C. Slip bands on {10 $\bar{1}0$ } faces have been observed after plastic bending and lie either parallel with or perpendicular to the c -axis, depending on the orientation of the axis of bending. No visible slip bands were produced on basal planes.

The density of etch pits which can be produced depends strongly on the rate of cooling of the silica tube containing the crystals after a growth run has finished. When the furnace supply was shut off at the end of growth, the crystals were cooled initially at a rate of 200–400° C per hour. Such crystals were found to produce a high density of pits (of the

order of 10^7 cm⁻²). However, when the furnace temperature was gradually reduced after growth had finished, a much smaller density of pits was observed (10^4 – 10^5 cm⁻²). The densities of pits do not appear to be affected by the various impurities added during growth.

Decoration of dislocations with grown-in impurity

Since, at room temperature, cadmium sulphide is transparent to visible light with wavelengths greater than 5100 Å, it is a simple matter to view the interior of a crystal microscopically using transmitted light. Some gross crystalline imperfections (mainly voids and inclusions) observed in the crystals used in this study have already been described.⁽¹⁾ Apart from these obvious defects, the pure cadmium sulphide crystals and those containing grown-in chlorine impurity appear uniform throughout their volume. The majority of crystals containing grown-in gallium also appears to be uniform, but in runs where the cooling schedule after growth was slow, that is, temperature reduced by 50° C per hour, many crystals were obtained which showed that gallium had precipitated along a network of lines (presumably dislocations) in the bulk of the crystal. An example of the effect is shown in Fig. 9. In this photograph, the straight lines are perpendicular to the c -axis and lie in a {10 $\bar{1}0$ } plane. In practice it was more usual to observe an apparently random array of decorated lines with no well-defined direction, as in Fig. 10.

Grown-in copper impurity at concentrations between 0.01 and 0.1% can also be precipitated to give decoration effects if the slow cooling schedule after growth is adopted. The decoration in Fig. 10 was obtained by precipitating copper in this manner. The photograph shows a feature characteristic of decoration with copper, namely, that the lines are composed of short individual segments of precipitated impurity. These short segments always lie perpendicular to the c -axis.

Some common features of the decoration obtained with gallium and copper are:

- (1) It is most usual to encounter a random array of curved lines with many cusps, but when lines are straight and follow a well-defined direction, this direction is either parallel with or perpendicular to the c -axis.
- (2) No regular geometrical network of lines has so far been observed, regardless of the direction of observation, which was either along [0001], $\langle 10\bar{1}0 \rangle$ or $\langle 11\bar{2}0 \rangle$.
- (3) Any individual line is continuous in the crystal and only terminates if it meets the surface or meets one or more other lines within the crystal at a node.
- (4) Complete loops and half loops near a surface have been observed.
- (5) As mentioned earlier, when a decorated crystal is etched, pits develop at the points where decorated lines cut the surface. This has been observed with each of the three shapes of pit. It has not been possible to determine whether every pit is associated with a decorated line and *vice versa*.

Decoration of dislocations by diffusion

The appearance of the lines described in the previous section, and the etching effects, strongly suggest that the grown-in impurity is precipitated at dislocations during the slow cooling from the growth temperature. An obvious extension of the work was to determine whether dislocations could be decorated by diffusing in gallium or copper and precipitating the impurity using an appropriate cooling schedule. No success was obtained using gallium. Crystals

heated in gallium vapour became riddled with a network of cracks. Successful results have, however, been achieved with copper as the diffusing impurity. To decorate a crystal using copper the process is as follows. A thin layer (of the order of 0.1μ) of copper is evaporated in high vacuum on to one surface of the crystal. The crystal is then sealed into an evacuated silica tube and heated at 700°C for two hours. The cooling schedule is the critical feature, and if cooling is too rapid no decoration is observed. To obtain good decoration it is essential to cool not faster than 50°C per hour to 400°C , whereafter the cooling rate is immaterial. Greatest success can be achieved by diffusing copper into crystals containing grown-in chlorine impurity. After the diffusion such crystals are red as viewed by transmitted light and the decorated lines are clearly visible. With pure cadmium sulphide crystals, decoration is not always obtained. However, all crystals remain yellow and it is apparent that an appreciable quantity of copper remains on the surfaces of these crystals, in the metallic form. In these crystals there is therefore little indication of bulk diffusion of copper (no change in optical absorption), but when crystals are decorated they are decorated throughout their entire volume. Microscopic examination reveals not only the decorated dislocation lines but also black specks at each end of a line where it intersects the $\{10\bar{1}0\}$ surface of the crystal. The black specks are, in fact, short straight lines which lie perpendicular to the c -axis. Thus if a surface is examined using vertically incident illumination an array of short streaks is observed, each streak lying perpendicular to the c -axis. These observations suggest that with pure cadmium sulphide crystals synthesized from cadmium and sulphur vapour, the copper diffusion process takes place preferentially in the vicinity of dislocation lines. However, proper diffusion measurements are required before any conclusions can be drawn and it is proposed to extend the work in this direction.

Some effects on electrical properties

Impurities such as the halogens (chlorine) or group IIIB metals (gallium or indium) act as donors in cadmium sulphide and are completely ionized at room temperature.⁽⁵⁾ When present in concentrations of about 10^{16} cm^{-3} , they reduce the dark resistivity, ρ_0 , from about $10^{12} \Omega \text{ cm}$ for pure cadmium sulphide to $1 \Omega \text{ cm}$. To obtain high photoconductivity, it is usual to aim for a dark resistivity of the order of $10^8 \Omega \text{ cm}$ which implies a donor concentration of about 10^8 cm^{-3} . Such a low concentration is often achieved in practice by compensating a donor concentration with a nearly equal, but smaller, acceptor concentration. Copper is a common acceptor-producing impurity.

When cadmium sulphide/chlorine crystals with ρ_0 of the order of $1 \Omega \text{ cm}$ were decorated with copper, ρ_0 was found to have increased to about $10^3 \Omega \text{ cm}$. The corresponding photosensitivity was about unity [defined as $(I_{ph} - I_0)/I_0$, where I_{ph} is the photocurrent under 50 f.c. tungsten illumination and I_0 is the dark current]. However, when crystals with the same chlorine content were subjected to the same copper diffusion process, but quenched to room temperature after the heating at 700°C , ρ_0 was approximately $10^8 \Omega \text{ cm}$ and values of the photosensitivity ratio exceeded 10^4 . In a further experiment a cadmium sulphide/chlorine crystal decorated with copper, with ρ_0 equal to $5 \times 10^2 \Omega \text{ cm}$, was heated in argon at 700°C for five seconds on a strip heater. After the heating the sample was rapidly quenched to room temperature. On examination, no sign of the previous decoration was detectable, and now ρ_0 was about $10^7 \Omega \text{ cm}$,

while the photosensitivity ratio was 1.4×10^4 . The resistivity of the crystal in the decorated state shows that the quantity of copper dissolved in the lattice (that is, effective in producing acceptors) left about 10^{13} cm^{-3} donors uncompensated. On heating at 700°C for five seconds the precipitated copper was dispersed in the lattice and the rapid cooling quenched-in a supersaturated concentration of copper acceptors which led to higher values of ρ_0 and photosensitivity. Calculations based on the density of dislocation lines and the size of the discrete copper segments show that the quantity of copper segregated at dislocations would produce a concentration of about 10^{14} cm^{-3} if uniformly dispersed in the lattice. Such a concentration is of the right order of magnitude to explain the results.

Electrical effects due to plastic deformation

Preliminary results show that plastic deformation of cadmium sulphide/chlorine crystals at 700°C introduces acceptors into the crystal lattice. Some ten crystals have been successfully bent into arcs of circles with radii of curvature of about 1 cm. Measurements of resistivity before and after bending show that such treatment introduces about 10^{15} acceptors per cm^3 . Preliminary heat treatment of a sample in the bending jig without the load applied showed that the effects observed did not result from the heat treatment or take-up of impurities from the jig or the ambient argon atmosphere.

If it is assumed that each dislocation line introduces 1.5×10^7 acceptors per cm, a concentration of 10^{15} acceptors per cm^3 would require the introduction of 4×10^7 dislocation per cm^2 . The formula for the density of dislocations introduced by plastic bending is

$$N = 1/bR,$$

where R is the radius of curvature and b the Burger's vector. From it a value of b equal to $2.5 \times 10^{-8} \text{ cm}$ is obtained, which is of the order of the lattice spacing in the a -direction, that is, $4.136 \times 10^{-8} \text{ cm}$.

Discussion

This paper represents a first step in an attempt to determine whether dislocations play an important part in the photoconductive and luminescent processes in cadmium sulphide. The major part of the work so far has been concerned with attempts to identify dislocations by etch pits and by decoration. The results described here show that the uniform etch pits do denote dislocations and the decorated patterns probably indicate the actual dislocation lines. However, the question of whether or not there is a unique correlation between etch pit density and dislocation density is still unresolved. Great advantages should result from working with larger crystal samples so that specimens can be sawn to the required geometry. The problem of deforming the crystals would then be greatly simplified.

The electrical effects described briefly in the latter half of the paper show that dislocations can have important effects on some electrical properties. It remains to study these effects in detail, notably the diffusion and precipitation processes and the effects of deformation in introducing acceptors. Indications have also been obtained that dislocations may play an important part in determining the behaviour of space-charge-limited currents in insulating cadmium sulphide, and also in the photochemical and general decay effects which occur in some types of highly

photosensitive crystals. This represents a formidable programme of work which will be continued.

References

(1) WOODS, J. *Brit. J. Appl. Phys.*, **10**, p. 529 (1959).

- (2) REYNOLDS, D. C., and GREENE, L. C. *J. Appl. Phys.*, **29**, p. 559 (1958).
 (3) VOTAVA, E. *Zeits. fur Naturforsch.*, **13a**, p. 542 (1958).
 (4) BILLIG, E. *Proc. Roy. Soc. A*, **235**, p. 37 (1956).
 (5) KRÖGER, F. A., VINK, H. J., and VOLGER, J. *Philips Res. Rpts.*, **10**, p. 39 (1955).

Half-life of iridium 192

by J. W. ALLISON, B.Sc., A.G.Inst.Tech., Defence Standards Laboratories, Australian Defence Scientific Service, Department of Supply, Melbourne, Australia

[Paper received 1 March, 1960]

Abstract

Using a null method, an ionization chamber and vibrating reed electrometer were employed to compare the γ -ray activity of an ^{192}Ir source with that of a reference ^{226}Ra source over a period of 209 days. An analysis of the results by the method of least squares indicates a half-life of ^{192}Ir of 74.17 ± 0.07 days.

Introduction

SEVERAL values, ranging from 60 to 78 days, have been published in the literature for the half-life of ^{192}Ir (see Table 1). In their "Table of Isotopes" Strominger, Hollander and Seaborg⁽⁹⁾ list Chu's value (74.7 days), Sinclair and Holloway's value (74.5 days) and Kastner's value (74.37 days). Kastner's work appears to be the most precise determination available and his value is usually accepted. His work forms the basis for the rounded-off value 74.4 days quoted by the Atomic Energy Research Establishment, Harwell.^(10, 11) This value is also quoted by the American Physical Society.⁽¹²⁾

Table 1. Published values for the half-life of ^{192}Ir

Date	Author	Value (days)
1936	Fermi and Amaldi ⁽¹⁾	60
1938	Jaeckel ⁽²⁾	68
1944	Friedlander, Seren and Turkel ⁽³⁾	70 \pm 1
1947	Goodman and Pool ⁽⁴⁾	75 \pm 3
1950	Chu ⁽⁵⁾	74.7
1951	Sinclair and Holloway ⁽⁶⁾	74.5 \pm 0.7
1951	Cork, LeBlanc, Stoddard, Childs, Branyon and Martin ⁽⁷⁾	78
1951	Kastner ⁽⁸⁾	74.37 \pm 0.07 (74.70 \pm 0.22)*

* Corrected value and uncertainty, see text.

Revision of Kastner's value

Kastner obtained his value by fitting experimental results for the activity of an ^{192}Ir source, relative to a standard ^{226}Ra source, with a decay equation of the form $y = a - bt$, where $y = \log_{10}$ (relative activity) and t = the time in days. The constants a and b were determined by the well-known method of least squares which gives

$$a = (\sum t^2 \sum Y - \sum t \sum Y t) / D \quad (1)$$

and

$$b = (n \sum Y t - \sum t \sum Y) / D \quad (2)$$

where n = number of observations, $Y = \log_{10}$ (observed relative activity) and $D = n \sum t^2 - (\sum t)^2$. He obtained the values $a = 0.2626$ and $b = 0.004048$ and a corresponding half-life of 74.37 days. However, in the present work a recalculation, using his published experimental results⁽⁸⁾ and equations (1) and (2), gives $a = 0.2613$ and $b = 0.004030$. This indicates an appreciably different value for the half-life, namely $T = \log_{10} 2/b = 74.70$ days.

For the method of least squares Kastner referred to the treatment by Worthing and Geffner.⁽¹³⁾ However, the equation for the probable error p_b in b given in this reference {equation (54), p. 250} is incorrect. The correct equation may be derived as follows:

Writing $n/D = B'$ and $\sum t/D = B$ gives $b = \sum (B't - B)Y$ in which the factor $B't - B$ is a function of the precise variable t only. Hence p_b is given by

$$p_b^2 = p_Y^2 \sum (B't - B)^2 = p_Y^2 \frac{n}{D} \quad (3)$$

where $p_Y = 0.6745 \sqrt{[\sum (Y - y)^2 / (n - 2)]}$ is the probable error in Y . Using the revised values for a and b , and equation (3), the value $p_T = p_b T/b = 0.22$ days is obtained for the probable error in the half-life. This is greater than the value 0.07 obtained by Kastner.

Experimental details

For the present determination an ionization chamber and vibrating reed electrometer were employed to measure the relative γ -ray activities of an ^{192}Ir source, and a reference ^{226}Ra source, at intervals of about a week for a total period of 209 days. For each measurement the two sources were placed in turn in the simple source housing shown schematically in Fig. 1. Constant geometry was maintained throughout the experiment by permanently mounting the housing and the ionization chamber on a rigid steel framework, and by employing a stop to enable each source always to be accurately placed in the same position. In addition to being convenient, the use of constant geometry had the advantage of making it unnecessary to prevent scattered radiation from nearby walls, or the housing itself, from reaching the ionization chamber. However, the housing was lead-shielded to prevent stray radiation hazard to staff during the measurements.

A short length of brass rod was used to attenuate the radiation from the ^{192}Ir source during each measurement. The length of this rod was selected at the beginning of the experiment so that the dose-rate at the ionization chamber due to the relatively strong ^{192}Ir source (approximately

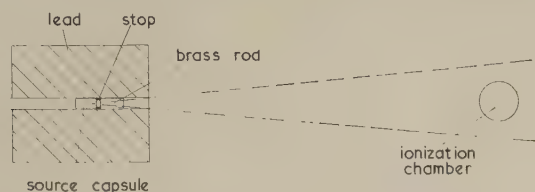


Fig. 1. Source housing and ionization chamber

1600 mc) was approximately equal to that of the ^{226}Ra source (approximately 100 mc). This procedure enabled a single electrometer range to be employed throughout the experiment and, by allowing the electrometer to run continuously, troublesome switching transients and "warm-up" effects were avoided.

By considering the activity of the ^{192}Ir relative to that of a reference source, the introduction of any errors due to possible drift of the electrometer input high resistor (nominally $10^{12} \Omega$) was avoided. The decay of the ^{226}Ra reference source itself was negligible, amounting to only about 0.025% during the entire experiment.

The ionization chamber was a sealed type, so that corrections for any pressure or temperature differences between corresponding ^{192}Ir and ^{226}Ra measurements were not required.

To obtain the maximum accuracy possible in the measurement of each source, a null method was devised in which the voltage developed across the electrometer input resistor by the ionization current was backed-off by an equal and opposite voltage, which was accurately measured by a calibrated potentiometer. To avoid disturbance of the electrometer input stage, the backing-off voltage was inserted in series with the electrometer feedback line. Sensitive indication of the null point was given by a d.c. galvanometer amplifier and recorder.

Precise adjustment of the backing-off voltage was difficult owing to the presence of random fluctuations in the galvanometer deflexion; these were due to statistical variations in the intensity of the radiation emitted by the radioactive source being measured. However, by recording these fluctuations over a suitable period of time (about 20 min), the mean galvanometer deflexion could be determined. Using the measured voltage sensitivity of the system, a correction could then be applied to the backing-off voltage for any deviation of this mean deflexion from the null. With few exceptions this correction did not exceed about 0.3%. The position of the null on the recorder chart was established each time by three checks; the first before the ^{226}Ra measurement, the second between the ^{226}Ra and the ^{192}Ir measurements, and the third after the ^{192}Ir measurement.

Results

The values obtained for $Y = \log_{10}$ (observed relative activity), and the corresponding times of observation, are given in Table 2.

Analysis of these results by the above method of least squares gives the decay equation \log_{10} (relative activity) = $0.11000 - 0.0040585 t$, and a corresponding value for the half-life of ^{192}Ir of 74.17 ± 0.07 days.

Table 2. Experimental data

Observation number	Time (days)	\log_{10} (relative activity) observed	\log_{10} (relative activity) calculated	Residual ($\times 10^4$)
1	0	+0.11059	+0.11000	+6
2	5.89	+0.08813	+0.08608	+21
3	11.78	+0.06520	+0.06221	+30
4	14.98	+0.04802	+0.04919	-12
5	18.89	+0.03221	+0.03333	-11
6	21.98	+0.02119	+0.02081	+4
7	27.97	-0.00327	-0.00353	+3
8	39.98	-0.05360	-0.05228	-13
9	46.79	-0.08181	-0.07990	-19
10	55.98	-0.11753	-0.11719	-3
11	62.98	-0.15052	-0.14562	-49
12	70.76	-0.17737	-0.17720	-2
13	84.01	-0.23144	-0.23095	-5
14	91.99	-0.26528	-0.26333	-20
15	108.99	-0.33124	-0.33233	+11
16	112.99	-0.34650	-0.34857	+21
17	115.96	-0.35932	-0.36062	+13
18	123.98	-0.39287	-0.39319	+3
19	130.00	-0.41818	-0.41761	-6
20	133.99	-0.43099	-0.43381	+28
21	140.99	-0.46142	-0.46222	+8
22	147.99	-0.48705	-0.49062	+36
23	155.00	-0.51799	-0.51906	+11
24	159.00	-0.53508	-0.53529	+2
25	161.94	-0.54868	-0.54722	-15
26	172.00	-0.58888	-0.58806	-8
27	182.98	-0.63528	-0.63263	-27
28	193.01	-0.67285	-0.67331	+4
29	200.00	-0.70201	-0.70170	-3
30	208.99	-0.73898	-0.73818	-8

The values of $y = \log_{10}$ (relative activity) obtained from the decay equation, and the corresponding residuals $y - Y$, are given in Table 2. These residuals are also shown graphically in Fig. 2, together with the residuals obtained

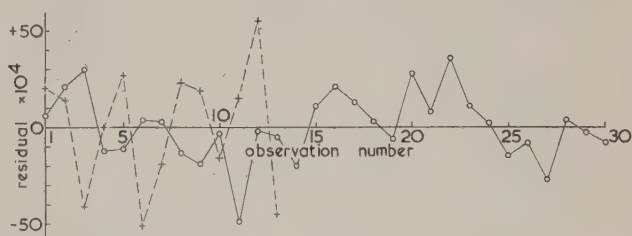


Fig. 2. Magnitude and random nature of residuals

○ = from present determination; + = from Kastner's determination (revised)

from Kastner's work using the revised values for a and b given above. Comparison of these residuals indicates that the measurements of the relative activity in the present determination are more accurate than those made by Kastner, who used a Lauritsen electroscope. As a result of this greater accuracy and the greater number of observations, the present determination is considered to be more precise.

The random nature of the residuals obtained in the present determination (see Fig. 2) shows that a linear decay equation completely describes the experimental results. This establishes the radioactive purity of both the ^{192}Ir and the ^{226}Ra sources employed.

Acknowledgements

The author wishes to thank Mr. R. G. Ackland for his assistance in the preparation of this paper. Thanks are also due to Mr. W. J. Bryant for assisting in the experimental work and calculations.

This paper is published with the permission of the Chief Scientist, Australian Defence Scientific Service, Department of Supply, Melbourne, Australia.

References

- (1) FERMI, E., and AMALDI, E. *Ricerca Sci* (II), **7** (1), p. 56 (1936).
- (2) JAECKEL, R. *Z. Physik*, **110**, p. 330 (1938).
- (3) FRIEDLANDER, H. N., SEREN, L., and TURKEL, S. H. Plutonium Project Report, CP1827 (June 1944) Reference F103 from Seaborg and Perlman. *Rev. Mod. Phys.*, **20**, p. 647 (1948).
- (4) GOODMAN, L. J., and POOL, M. L. *Phys. Rev.*, **71**, p. 288 (1947).
- (5) CHU, T. C. *Phys. Rev.*, **79**, p. 587 (1950).
- (6) SINCLAIR, W. K., and HOLLOWAY, A. F. *Nature (London)*, **167**, p. 365 (1951).
- (7) CORK, J. M., LEBLANC, J. M., STODDARD, A. E., CHILDS, W. J., BRANYAN, C. E., and MARTIN, D. W. *Bull. Amer. Phys. Soc.*, **26** (3), p. 31 (1951).
- (8) KASTNER, J. *Canad. J. Phys.*, **29**, p. 480 (1951).
- (9) STROMINGER, D., HOLLANDER, J. M., and SEABORG, G. T. *Rev. Mod. Phys.*, **30**, No. 2 (II) (1958).
- (10) A.E.R.E. Catalogue No. 4, *Radioactive Materials and Stable Isotopes*, p. 86 (January 1957).
- (11) Private communication from A.E.R.E. (November 1959).
- (12) *American Physical Society Handbook*, Section 8-124 (1957).
- (13) WORTHING, A. G., and GEFFNOR, J. *Treatment of Experimental Data*, p. 249 (New York: John Wiley and Sons Inc., 1943).

CORRESPONDENCE

Evaporated films of niobium

Niobium is one of the elements which are becoming relatively commonplace as a result of interest in its use as a possible reactor material. It is therefore of interest to explore methods of preparing thin films of niobium. The formation of niobium layers by normal plating techniques is difficult and it was therefore decided to investigate methods using vacuum evaporation. Previous attempts to use this method^(1,2) had resulted in very little success.

Schofield's⁽³⁾ determination of the melting point of niobium is probably the most reliable available. He finds that the gas content (up to 2% by weight of oxygen and nitrogen) can lower the melting point of niobium by 200°C. His final figure for the melting point, extrapolated to zero gas content and allowing for 1.9% tantalum present as impurity, is $2468 \pm 10^\circ\text{C}$. Using the data given by Dushman⁽⁴⁾ the vapour pressure and evaporation rate at the melting point are then respectively 0.42μ of mercury, and $4.5 \times 10^{-6} \text{ gm cm}^{-2} \text{ s}^{-1}$. Clearly, to obtain appreciable evaporation rates, the temperature of the niobium must be raised to at least the melting point and, preferably, higher. Therefore it is essential to use a supporting filament or crucible.

Because of the temperatures required, the choice of filament material is restricted to tungsten, tantalum or carbon. Schwarzkopf and Kiefer⁽⁵⁾ have reported that niobium reacts with carbon at 1700°C to form niobium carbide. It has also been reported⁽⁶⁾ that niobium forms a continuous series of solid solutions with tungsten and tantalum.

The choice of crucible materials is limited to the refractory oxides, borides, carbides and nitrides. However, it has been shown^(5,7) to be highly probable that niobium either reacts chemically or forms solid solutions with all of these materials. It seems inevitable, therefore, that the niobium will be contaminated with the filament or crucible material.

Accepting this position, some preliminary experiments were carried out with tungsten and tantalum filaments in a 3 in. diameter demountable tube. The filaments were made

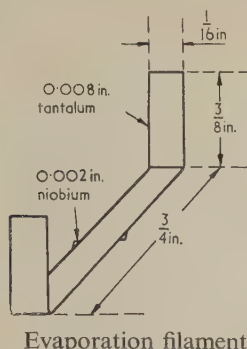
of 0.020 in. wire with the centre portion shaped into a U with a $1 \times 1 \text{ mm}$ square of 0.005 in. niobium sheet (supplied by Murex Ltd.) spot-welded to the base of the U. On heating the filament in high vacuum, the melting point of the niobium was easily visible. The brightness temperature, as determined by an optical pyrometer, was $2080 \pm 10^\circ\text{C}$. Using Whitney's⁽⁸⁾ value of 0.374 for the spectral emissivity at 0.65μ , together with a correction for reflexion losses, estimated at 2%, we calculated the true melting point of niobium to be 2410°C .

Both tungsten and tantalum filaments were wetted by the niobium as it melted. With a tungsten filament, an initial thin deposit was formed on the tube wall within a few minutes of the niobium melting, but this did not thicken. It was necessary to raise the temperature to an estimated value of 2600°C for several minutes before appreciable thickening occurred. Chemical analysis of the evaporated deposit gave its composition as 16% niobium, 84% tungsten. X-ray examination of the tungsten filament at the base of the U revealed a core of tungsten covered with a solid solution of tungsten and niobium.

With a tantalum filament, an opaque deposit with a composition 72% niobium, 28% tantalum could be obtained in a period of about one hour if the filament was heated to the melting point of niobium. Attempts to raise the filament temperature always resulted in filament failure if the temperature rise exceeded 50°C . The small difference in the lattice constants for niobium and tantalum prevented any direct information being obtained by X-ray examination on the composition of the filament at the base of the U. The grain size was large however, so that a solid solution was probable.

On the basis of these results, a practical form of evaporation source was devised. This was in the form of an 0.008 in. tantalum strip with 0.002 in. niobium sheet spot-welded to one side of the central region as shown in the figure. Such a source had an evaporating zone of $\frac{3}{4} \times \frac{1}{16} \text{ in.}$, and if maintained at the melting point of niobium, would form a

deposit at an average rate of 7×10^{-8} gm cm $^{-2}$ s $^{-1}$ at 4 cm from the filament. The composition of the deposit varied with time; after 30 min it was 69% niobium, 31% tantalum; after 2 h it was 50% niobium, 50% tantalum. Attempts to increase the quantity of niobium on a given filament showed



that failure of the filament always occurred on melting if the thickness of the niobium sheet equalled or exceeded that of the tantalum.

These films have been used to prevent the interaction of uranium and aluminium when heated in contact. At temperatures of 400–500°C, such as are attained by the fuel elements of a gas-cooled power reactor, there is a rapid reaction between uranium and aluminium. This prevents the use of aluminium as a canning material in such reactors. However, we have shown that films 0.1–0.2 μ thick, deposited as described above on the surface of the uranium, prevent the formation of uranium/aluminium inter-metallic compounds.

In conclusion, these results show that if evaporated films of uncontaminated niobium are required, high-frequency or electron-bombardment heating of a self-supporting niobium ingot is essential.

British Thomson-Houston Co. Ltd.,
Research Laboratory,
Rugby.

D. SHAW
B. N. WATTS
[2 December, 1959]

References

- (1) CALDWELL, W. C. *J. Appl. Phys.*, **12**, p. 779 (1941).
- (2) OLSEN, L. O. *J. Appl. Phys.*, **16**, p. 425 (1945).
- (3) SCHOFIELD, T. H. *J. Inst. Metals*, **85**, p. 372 (1957).
- (4) DUSHMAN, S. *Scientific foundations of vacuum technique* (London: Chapman and Hall, 1949).
- (5) SCHWARZKOPF, P., and KIEFER, R. *Refractory hard metals* (London: Macmillan, 1953).
- (6) SCHWARZKOPF, P. *Powder metallurgy* (London: Macmillan, 1947).
- (7) JOHNSON, P. D. *J. Amer. Ceramic Soc.*, **33**, p. 168 (1950).
- (8) WHITNEY, L. V. *Phys. Rev.*, **48**, p. 458 (1935).

Glow-discharge characteristics of helium–argon mixtures

The maintaining and breakdown potentials have been measured in a number of helium–argon mixtures. Simple parallel-plate diodes were employed with molybdenum-disk electrodes which could be thoroughly sputtered to eliminate contamination. The experiments were similar to those made in helium–neon mixture, which have previously been described.⁽¹⁾

The helium–argon mixture shows the well-known “Penning effect”—an increase in α , when argon is added to helium, resulting from the ionization of the argon atoms by the helium

metastables. This lowers the breakdown potential, and the results for different mixtures are seen in Fig. 1, where the Paschen curves have been plotted on logarithmic scales. The curves are similar to those obtained for neon–argon mixtures,^(2,3) with the largest drop in breakdown potential occurring in mixtures with low argon concentrations

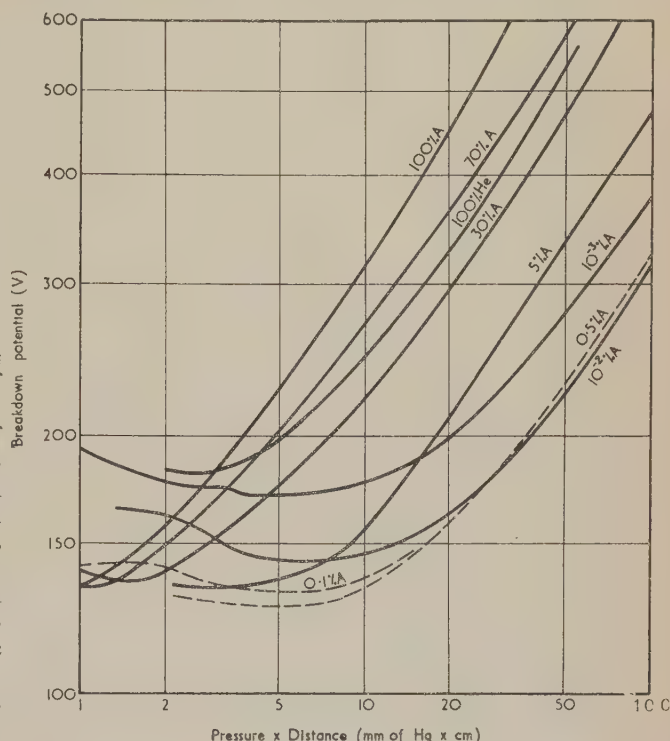


Fig. 1. Paschen curve for helium–argon mixture with molybdenum electrodes

(10 $^{-3}$ to 1%). The effect, however, is less marked than for neon–argon mixtures, as might be expected, since the collision cross-section for ionization of argon by helium metastable atoms is lower than for neon metastables.⁽⁴⁾

The normal cathode fall, V_N , for the various mixtures is given in the table. V_N shows the same trend with gas

Normal cathode fall for helium–argon mixtures and molybdenum electrodes (at 40 mm mercury pressure)

Argon in mixture (%)	V_N (V)
0	114
0.001	117
0.01	110
0.1	105.5
0.5	103
1	100
5	101
30	109
100	105

composition as the breakdown potential, but a graph of the minimum breakdown potential V_B plotted against V_N gives points which are, in the main, below the “linear relationship” previously suggested.⁽¹⁾ A closer look at helium–argon and helium–neon mixtures reveals that there are similar, although smaller, deviations from the straight line in both

systems, which are unlikely to be due to experimental errors. This is shown in Fig. 2. It is concluded, that the straight line

$$V_N = 0.58V_B + 22,$$

where V_N and V_B are in volts, is not an accurate empirical relationship for binary mixtures of the inert gases helium,

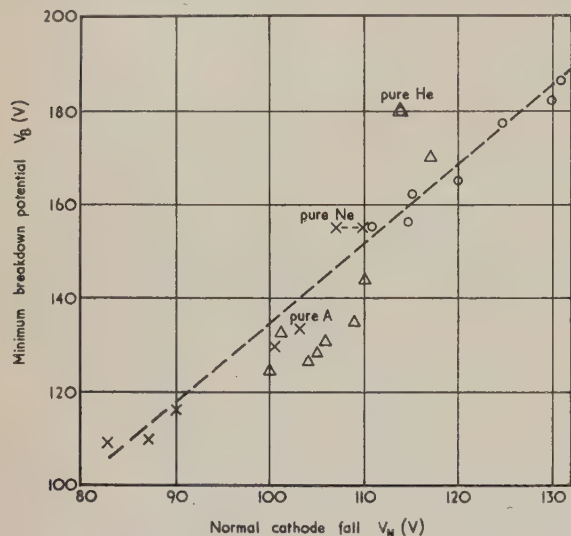


Fig. 2. Breakdown minimum plotted against normal cathode fall for inert-gas mixtures

- Helium-neon mixtures⁽¹⁾
- △ Helium-argon mixtures
- × Neon-argon mixtures (V_B according to Frouws;⁽³⁾ V_N according to Jurriaanse, Penning and Moubis⁽⁵⁾)

neon and argon, with molybdenum electrodes, but nevertheless gives a useful approximation for the design of glow-discharge tubes.

Acknowledgement is made to the Director of Mullard Research Laboratories for permission to publish this letter.

Mullard Research Laboratories,
Salfords, Surrey.

G. F. WESTON
[21 December, 1959]

References

- (1) WESTON, G. F. *Brit. J. Appl. Phys.*, **10**, p. 523 (1959).
- (2) PENNING, F. M., and ADDINK, C. C. J. *Physica*, **1**, p. 1007 (1934).
- (3) FROUWS, S. M. *Third International Conference on Ionization Phenomena in Gases, Venice, 1957*.
- (4) BIONDI, M. A. *Phys. Rev.*, **85**, p. 635 (1951).
- (5) JURRIANSE, T., PENNING, F. M., and MOUBIS, J. H. A. *Philips Res. Rep.*, **1**, p. 225 (1946).

Comments on the A.S.T.M. Powder Data File—5

The writers have now prepared a fifth booklet, bearing the above title, which contains further additions to the lists previously published and described in the Institute's Journals.* Copies of the present booklet have been distributed in the same way as were the others. Those who have not received copies of the booklets in this way may obtain them (free of charge) on request from the Institute or from us.

It is hoped that similar lists of comments will continue to be published at approximately annual intervals. Users of the Data File are urged to send to the writers any material that they feel should be included in future issues.

It would help considerably in the work of extending the File if those who are working on structures by single-crystal methods could send us the crystallographic data and sufficient of their material to permit the production of a powder pattern from it. Full acknowledgement of the source would, of course, appear on the published card.

Viriamu Jones Laboratory,
University College, Cardiff,
Great Britain.

J. W. HUGHES
ISABEL E. LEWIS
A. J. C. WILSON
[8 January, 1960]

* HUGHES, J. W., LEWIS, ISABEL E., and WILSON, A. J. C. *Brit. J. Appl. Phys.*, **10**, p. 192 (1959); *J. Sci. Instrum.*, **36**, p. 199 (1959).

Journal of Scientific Instruments

Contents of the July issue

PAPERS

- Measurement of magnetostriction within the temperature range -196 to 400°C . By R. R. Birss and E. W. Lee.
- New high-voltage multi-stage impulse generator circuit. By T. E. Broadbent.
- Magnetically operated mass-marker. By J. J. Brown, R. I. Reed and W. Simpson.
- Liquid-nitrogen cryostat for single-crystal X-ray diffraction. By A. E. Attard and L. V. AZAROFF.
- Large storage binary-to-decimal converter. By G. Dearnaley, L. G. Lawrence and H. C. Tresise.
- Growth of single crystals of anthracene. By J. N. Sherwood and S. J. Thomson.
- Wide-band detector for micro-microampere low-energy electron. By T. E. Everhart and R. F. M. Thornley.

LABORATORY AND WORKSHOP NOTES

- Modified cylindrical cell for the microelectrophoresis of suspended particles. By E. J. Ambrose and J. Ryder.
- Instruments for measuring the temperature of a running thread-line, and of a jet of viscous liquid. By M. F. Culpin and K. A. Martin.
- Bakeable bellows-type differential pressure manometer. By A. E. D. Heylen.
- Method of finding the focal curve of a photographic spectrometer. By J. F. James.
- Improved sample loading technique for solid source mass spectrometry. By R. E. Powell.
- Automatic gas-sampling device for gas chromatography. By D. W. Hill and J. R. Hook.

CORRESPONDENCE

- The theory of stresses in two-component glass to metal tube seals. From H. Rawson.
- Apparatus for the measurement of Young's modulus, between -200 and 700°C by transverse vibration in vacuum. From H. J. Stokes.

NOTES AND NEWS Notes and comments

THIS JOURNAL is produced monthly by The Institute of Physics, in London. It deals with all branches of applied physics (including theory and technique). All rights reserved. Responsibility for the statements contained herein attaches only to the writers.

EDITORIAL MATTER. Communications concerning editorial matter should be addressed to the Editor, The Institute of Physics, 47 Belgrave Square, London, S.W.1. (Telephone: Belgravia 6111.) Prospective authors are invited to prepare their scripts in accordance with the *Notes for Authors*. (Price 3s. 6d. including postage.)

REPRODUCTION. The Institute of Physics is a signatory to The Royal Society's Fair Copying Declaration. Details may be obtained upon application from The Royal Society, London, W.1.

ADVERTISEMENTS. Communications concerning advertisements should be addressed to the agents, Messrs. George Jackson (Fleet St.) Ltd., Cliffords Inn, Fleet Street, London, E.C.4. (Telephone: Holborn 3611-2.)

CLAIMS FOR MISSING JOURNALS. Claims from regular subscribers to this *Journal* for missing numbers will only be considered if received within 60 days of the date of mailing plus normal outward time of transit and time for lodging the claim. Losses attributable to failure to notify a change of address or to similar omissions will not be considered.

SUBSCRIPTION RATES. A new volume commences each January. The charge is £6 per volume (\$17 U.S.A.), including index (post paid), payable in advance. Single parts, so far as available, may be purchased at 12s. 6d. each (\$1.75 U.S.A.), post paid, cash with order. Orders should be sent to The Institute of Physics, 47 Belgrave Square, London, S.W.1, or to any bookseller.

Summarized proceedings of a conference on some aspects of magnetism, Sheffield, September 1959

Abstract

The report describes the proceedings of a conference on magnetism held at Sheffield University by The Institute of Physics in September 1959. The subjects discussed at the five sessions and reported in the article came under the headings (i) The behaviour of ferrites and some alloys; (ii) Domain effects and thin films; (iii) Domains; (iv) Neutron diffraction; (v) Permanent magnet materials.

Session 1

THE conference opened with a discussion by Dr. J. SMIT (N. V. Philips', Gloeilampenfabrieken, Eindhoven) on the form of the $(1/\chi, T)$ curve in ferrimagnetics in terms of the equation $d(1/\chi)/dT \approx -2dS/d(M^2)$. In ferromagnetic materials, short range order reduces both the entropy, S , and the change in entropy associated with a change in magnetization M . Thus there is a reduction in $d(1/\chi)/dT$ particularly near the Curie temperature, T_c , where the $(1/\chi, T)$ curve is concave upwards and lies above the line obtained by a Weiss approximation. In ferrimagnetics, however, the $(1/\chi, T)$ curve is concave downwards; this is explained by assuming that at temperatures below $2T_c$, the Weiss field is predominant and leads to an increase in anti-parallel spin ordering and hence an increased $d(1/\chi)/dT$. At high temperatures the applied field becomes comparable with the Weiss field and short range order again produces a decrease in slope. In the second part of the paper some anisotropy properties of ferrimagnetics were considered. The anisotropy is the combined effect of spin orbit interaction and the binding of the orbit to the crystal axis. For Co^{II} these quantities are of the order of 100 cm^{-1} and 1000 cm^{-1} respectively. Usually the orbital motion is quenched and low anisotropy results. When the orbit is not quenched, the

crystal anisotropy is governed by the spin-orbit coupling, and is large. In cobalt substituted materials the greater binding energy of the cobalt ion to the lattice gives rise to a rotational hysteresis. The third phenomenon discussed was the anomalous behaviour in ferromagnetic resonance of rare earth impurities in yttrium iron garnet at low temperatures.

Dr. W. MARSHALL (A.E.R.E., Harwell) then read a paper on exchange interactions in metals. He described briefly the various theories of magnetism which were based on the sign of the exchange integral, J , which required either that $J \geq 0$ or that $J < 0$. This was followed by a description of a calculation of J for a hydrogen-like atom, for which it was found that $J > 0$ for all values of the interatomic distance up to 2.5 \AA .

Dr. R. F. PEARSON (Mullard Research Laboratories, Salfords) then described measurements, by torque methods, of the first order anisotropy of cobalt substituted manganese ferrite. The contribution to the anisotropy from the cobalt ions was found to vary linearly for concentrations of cobalt up to 25% and an extrapolation of the contributions from the cobalt ions led to lower values than are observed for cobalt ferrite or cobalt substituted magnetite.

Dr. J. CRANGLE (University of Sheffield) read a paper on the magnetic properties of platinum-iron and related alloys. In the platinum-iron alloy system, a stable face-centred cubic superlattice exists over a range of compositions round Pt_3Fe . The superlattice is antiferromagnetic, and shows a characteristic maximum in the susceptibility-temperature relationship. Alloys cannot be disordered by quenching, but only by the application of cold work. Disordered alloys are strongly ferromagnetic, and the antiferromagnetic ordered state may be restored by annealing at or above about 500°C . The ferromagnetic Curie point of the disordered state seems to

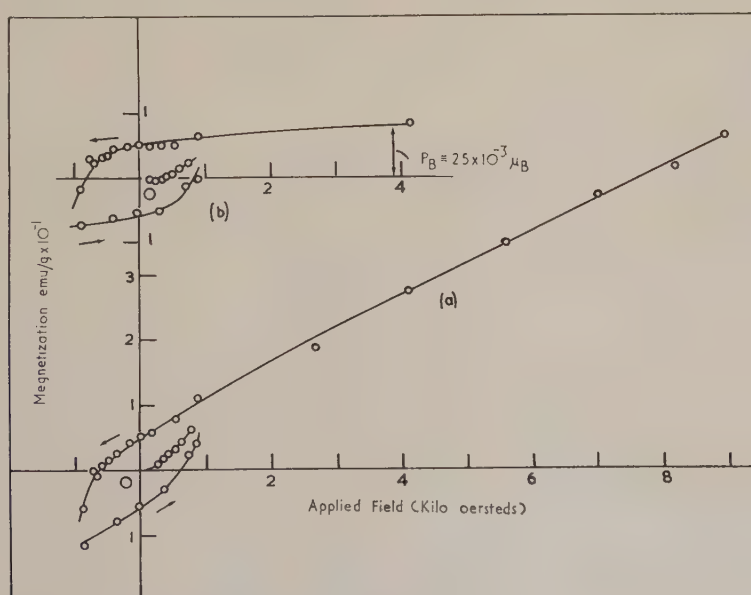


Fig. 1. Magnetization-field relation for a 28% Pt-Fe alloy

be independent of the degree of cold work, but varies with composition.

Over part, but not all, of the composition range, ordered alloys show a weak ferromagnetism superimposed on the antiferromagnetic properties. This ferromagnetism is not obviously related to the state producing the maximum in the susceptibility-temperature curve for its Curie temperature lies significantly above the observed Neel temperature, and is yet far below that for the disordered state of the same composition. Fig. 1 illustrates the form of the magnetization-field relationship for such an alloy, obtained at 77° K. It was tentatively suggested that the ferromagnetic component may arise from a defect antiferromagnetism, possibly related to antiferromagnetic domain boundaries.

The disordered Pt-Fe alloys exhibit ferromagnetism down to low concentrations of iron (Fig. 2). Their saturation

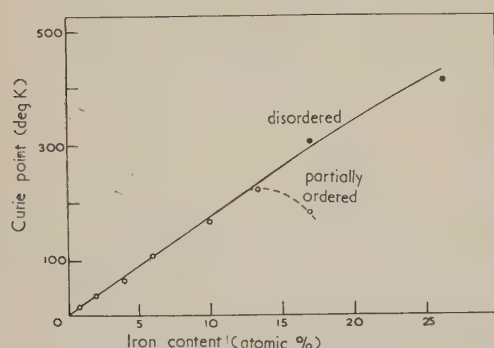


Fig. 2. Curie temperatures of Pt-Fe alloys

magnetization at the lower iron contents corresponds to a magnetic moment, if it is all located on iron atoms, of about five Bohr magnetons per iron atom. This value, although remarkably high, is just possible theoretically. The related Pd-Fe alloys show similar properties in the disordered state at low iron concentrations. But here the magnetic moment is too great to be associated only with iron atoms, and it is concluded that in this case at least part of the moment must be located on palladium atoms. It was suggested that similar behaviour seems likely in the Pt-Fe case.

The first session was concluded by discussions between Dr. A. ARROTT (Ford Motor Company, U.S.A.) and Dr. J. CRANGLE on the relevance of the theory of Sato, Arrott and Kikuchi to Fe-Pt and Fe-Pd alloys, and between Dr. J. C. SLONCZEWSKI (I.B.M., Poughkeepsie, U.S.A.), Dr. R. TEALE and Dr. J. SMIT on the anisotropy of cobalt substituted manganese ferrites, in which Dr. Slonczewski observed that Pearson's results might be interpreted as the result of a molecular exchange field H_{ex} which is smaller in cobalt substituted manganese ferrite than in cobalt substituted magnetite.

Evening discourse

The evening discourse was given by Dr. R. M. BOZORTH (Bell Telephone Laboratories Inc., U.S.A.) on the ferromagnetism of some superconducting intermetallic compounds (e.g. $GdRu_2$ and $CeRu_2$). A diagram of the hysteresis loop of an alloy of 8% $GdRu_2$ in $CeRu_2$ at 1.3° K is given in Fig. 3. This shows anomalies about the axis $H = 0$ which are due to the superconductivity of the compounds. The Curie temperature of this particular alloy was 6.2° K. Bozorth suggested the specific heat measurements might throw more light on the mechanisms involved in these mixed ferromagnetic-superconducting alloys. He then described

the magnetic properties of substituted yttrium iron garnet in relation to the theory of Gilileo, which takes account of the weakening of interactions by a reduction in the number of Fe-O-Fe bonds.

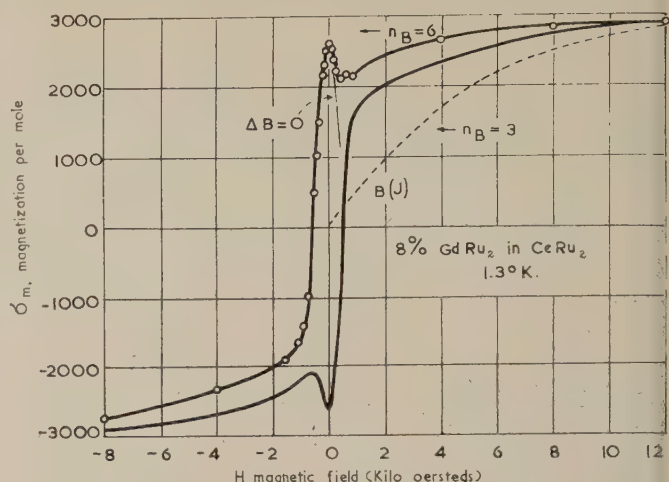


Fig. 3. Hysteresis loop of an alloy of 8% $GdRu_2$ in $CeRu_2$ at 1.3° K

Session 2

The second session was begun by Mr. M. WILLIAMS (General Electric Company Ltd., Wembley) who read a paper on the techniques of observation of magnetic domains which included colloid techniques, the Kerr and Faraday effects, and electronic techniques using flying spot scanning.

Dr. A. C. MOORE (Royal Radar Establishment, Malvern) then read a paper by himself and Mr. A. S. YOUNG on the preparation and properties of thin iron-nickel films (about 1000 Å thick) for use as storage elements in computers. Such films are required to have a uniaxial anisotropy whose direction and magnitude is sensibly constant over a suitably large plane of elements. The coercivity in the preferred direction must also be maintained constant and as large as possible consistent with a low anisotropy to encourage change in magnetization by simultaneous rotation of the elementary magnets and discourage domain wall motion. The speed of switching should be in the millimicrosecond region.

The various contributions to the anisotropy which can arise during preparation of sheets by vacuum evaporation on to a substrate were discussed under the heading of magneto-crystalline effects, magnetostriction effects, shape effects, magnetic field effects and impurity effects such as oxides. It was shown that one continuous sheet of magnetic film could be used as a many element array. Only in those parts of the film subjected to a suitable field was the magnetization changed. This was illustrated by Bitter patterns of the domain walls in a suitably treated sheet. Such a continuous sheet showed more constant characteristics (particularly preferred direction) than planes of isolated elements made by etching such a sheet or by evaporation through a perforated mask. Speeds of switching under suitable conditions were faster than 10 mμs.

Dr. H. H. SCHOLEFIELD (Telegraph Construction and Maintenance Co. Ltd., Crawley) then gave a review of the characteristics of thin rolled strip of thicknesses less than 25 μ. He described measurements of normal induction, magnetization curves, hysteresis loops, dynamic loss loops

and flux reversal times on strips of alloys such as mumetal, permendur and radiometal. It was found for mumetal that the initial permeability decreased with decreasing strip thickness and the switching time also decreased with decreasing strip thickness.

Dr. M. PRUTTON (International Computers and Tabulators Ltd., Stevenage) then described observations on the domain structure in thin nickel-iron films, made by use of the Kerr effect (see p. 335). The films were found to have hysteresis loops similar to those predicted by the Stoner-Wohlfarth theory assuming uniaxial anisotropy and it was found that, if a magnetic field were applied at an angle to the preferred axis of magnetization of the films, the domain walls occurred at angles between the direction of the applied field and the preferred axis.

A possible mechanism of formation of films of uniaxial anisotropy was described by Dr. E. P. WOHLFARTH (Imperial College of Science and Technology, London). Small regions of the film initially behave superparamagnetically and as the grains grow the magnetization in the grains tends to be stabilized in the direction of the field. Further growth will tend to form grains with the same elongation in the same direction and the grain boundaries of the final stable film will then form anisotropically, practically parallel to this direction. Reannealing in a magnetic field leads to preferred recrystallization in the direction of the field. In practice imperfections in the film modify the model although the effect of these is least in Permalloy films with the composition of zero magnetostriction. Dr. Wohlfarth suggested that measurements of the resistance and magnetoresistance of thin films might provide interesting results concerning grain boundaries since it might be expected that the effect of grain

boundaries perpendicular to the direction of current flow would be to increase the resistance.

A paper by Mr. C. E. FULLER and Dr. R. V. PEACOCK (Mullard Research Laboratories, Salfords) on switching characteristics of thin iron-nickel films was then read. The anisotropy field and switching times of a large number of films (1000 Å–3000 Å thick) in the composition range 60/40 to 95/5 nickel/iron were measured. The measurements were compared with the theoretical behaviour for a uniaxial model and Fig. 4 compares the experimental curve of anisotropy field as a function of composition, with the monotonically decreasing function predicted by Neel and the theoretical curve of Blades.

The discussion was opened by Mr. A. C. LYNCH (Post Office Research Station, Dollis Hill), who explained the advantages obtained by rolling sintered rather than melted materials to produce thin strip. This was followed by a discussion between Prof. L. F. BATES (University of Nottingham), Dr. K. HOSELTZ (Mullard Research Laboratories, Salfords) and Dr. M. MCCAIG (Permanent Magnet Association, Sheffield) on domains. Dr. W. E. PROEBSTER (I.B.M., Zurich) suggested that Dr. Prutton's results might be explained by a distribution of the uniaxial anisotropy as well as a spread of the easy direction of magnetization.

Session 3

The third session was opened by Dr. F. W. HARRISON (Mullard Research Laboratories, Salfords), who read a paper on ferrimagnetic garnet materials which have the general formula $M_3^{3+} Fe_3^{3+} O_{12}$, where M is yttrium or a rare

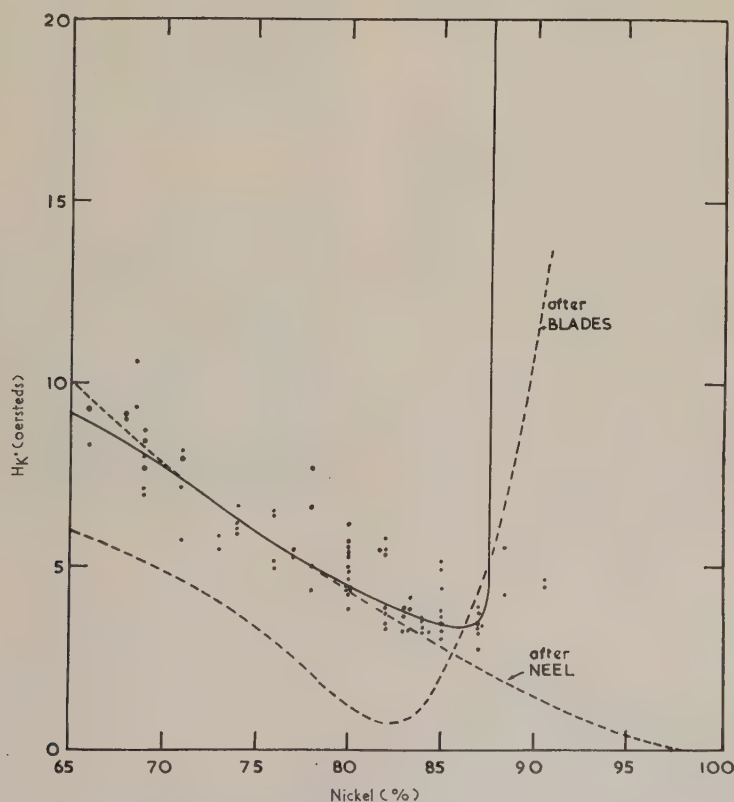


Fig. 4. Anisotropy field as a function of composition for iron-nickel thin films compared with the predictions of Neel and of Blades

earth element, the cubic space group $1a3d - O_h^{10}$ and lattice constants in the range $12.0 - 12.5 \text{ \AA}$. The unit cell contains eight formula units. Two out of the five ferric ions occupy octahedral or *a*-sites between oxygen atoms and three tetrahedral or *d*-sites. The rare earth ions occupy eight-fold or *c*-sites.

The *a* and *d* sublattice magnetic moments exhibit a strong negative interaction whilst the *c*-sublattice moment is weakly coupled negatively to the *d*-sublattice moment. Some of the materials exhibit compensation points, ranging from 290° K for gadolinium iron garnet to less than 20° K for thulium iron garnet. The Curie temperatures are relatively constant, in the range 560° K to 549° K .

The transparency of thin single crystals allows correlation of the optical and magnetic properties. Such specimens display the Faraday effect and the domain structure can be observed in polarized light.

The garnet structure allows further investigation of exchange interactions, and of the paramagnetic moments of the rare earth ions. The very narrow ferrimagnetic resonance line width of yttrium iron garnet, in contrast to the broad line widths of the rare earth garnets, makes it a very suitable material for use in ferrite microwave devices at lower frequencies. Its high resistivity, resulting from the structural requirement that all iron be trivalent, is also advantageous.

Dr. D. J. CRAIK (Boots Pure Drug Co. Ltd., Nottingham) read a paper on the domain structures of specimens of polycrystalline cobalt, nickel, and barium ferrite with differing grain sizes, which were demonstrated by the modification of the Bitter-figure technique for electron microscopy. This method permits the clear resolution of patterns on grains with diameters down to 1μ , and in the particular form used the patterns are superimposed on replicas of the grain boundaries. It was necessary to develop a new method of specimen surface preparation since electro-polishing is not possible and etching gives a rough surface.

On a single specimen of cobalt ferrite very complex and strongly defined patterns on grains about 5μ in diameter were replaced by simpler patterns, indicating a two-domain or single-domain structure, on grains about 1μ across. Nickel ferrite, with grains of average diameter of 12μ , gave three types of pattern as in Fig. 5 indicating (a) a closure structure with spacing of 0.3μ similar to structures at (100) surfaces of nickel, (b) a free-pole structure where the easy directions made a small angle with the surface, and (c) a simple structure with spacing of several microns probably representative of that of the whole grains. The walls were generally "kinked" or contorted, suggesting impedance by inhomogeneous regions, and reference was made to rapid and discontinuous movements, on magnetization, which could just be observed by optical microscopy. Specimens with progressively smaller grain size (Fig. 6) indicated the approach to the critical diameter for single-domain formation, at about 2μ .

Some earlier results on coarse-grained barium ferrite were confirmed but it was shown that specimens with $H_c = 2000$ oersteds also had a multi-domain structure (as shown in Fig. 7). The critical particle diameter was 1.2μ . It was suggested that the high coercivity should be associated with a relation between the nucleation field and the grain size, rather than with the presence of single-domain particles.

Mr. C. E. FULLER (Mullard Research Laboratories, Salford) read a paper by himself, Dr. R. W. TEALE and Dr. R. F. PEARSON on domain patterns on single crystal yttrium iron garnet.

Single crystals of yttrium iron garnet ($\text{Y}_3\text{Fe}_5\text{O}_{12}$) grown

from a lead oxide flux possess well developed (110) and (211) growth faces whose surface domain patterns were examined by the Bitter colloid technique without any preliminary polishing treatment. The patterns on the (211)

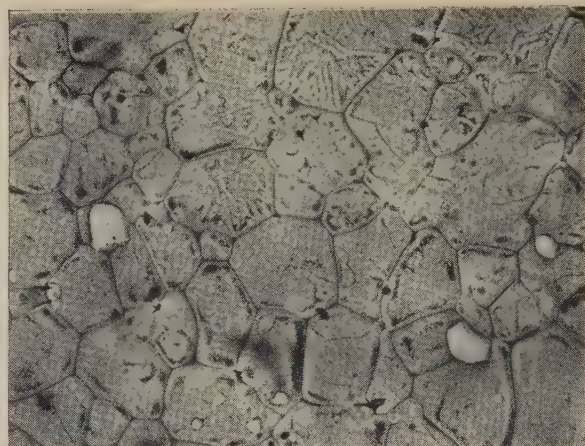


Fig. 5. Domain structure of nickel ferrite with average grain size of 12μ ($\times 1200$)

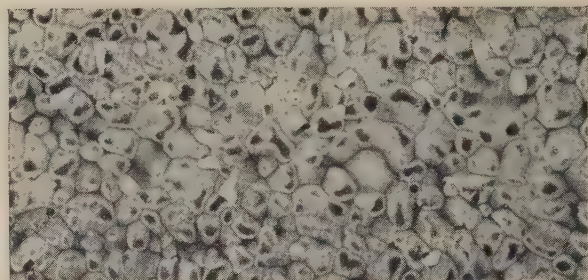


Fig. 6. Domain structure of nickel ferrite with average grain size of 3μ ($\times 2000$)



Fig. 7. Domain structure of barium ferrite, grain size 3μ , with coercivity 2000 oersteds ($\times 2000$)

faces of a large single crystal ($\sim 5 \text{ gm}$) were examined and found to be basically similar; there is evidence of subsidiary surface structures, and many new rick-rack patterns and a new type of edge-wall were found.

The changes in surface pattern on a (211) face due to mechanical polishing with 1μ diamond paste was investigated. The closely spaced parallel wall structure exhibited by the unpolished face gradually assumed a much wider spacing. The colloid deposits became fainter as the polishing proceeded until the pattern could no longer be distinguished.

Using the evidence obtained from these experiments a

unique domain magnetization model for a regular yttrium iron garnet crystal possessing only (211) faces (icositetrahedron) was proposed.

Dr. U. ENZ (N. V. Philips. Gloeilampenfabrieken, Eindhoven) then read a paper by himself and Dr. C. KOOP on the experimental and theoretical study of the domain configuration in thin layers of $\text{BaFe}_{12}\text{O}_{19}$.

Sufficiently thin crystals of barium ferrite are transparent to red light, and the domain structure of plates with surfaces parallel to the basal planes was demonstrated by the Faraday effect. Although it was necessary to observe the specimen through the bored pole-pieces of a magnet so that fields up to 5000 oersteds could be applied normal to the basal planes, the fine structures were very clearly resolved. The changes in the structure during magnetization to saturation, nucleation, and demagnetization, were shown on ciné-films.

In the demagnetized state the familiar pattern of straight lines, representing plane-sided 180° domains directly intersecting the surface, was shown. The spacing was too fine for individual measurements of the widths of the two sets of domains to be made, but application of high fields caused the double spacing to increase, indicating that the rate at which the favoured domains grew was greater than that at which those magnetized in the opposite direction decreased in width. After the latter reached a certain minimum width they were transformed to cylindrical domains as full saturation was achieved. This occurred in fields of less than $4\pi I_S$, suggesting that the resultant internal field was opposite to the magnetization. When the field was reduced from the saturating value nucleation occurred at a limited number of fixed points in the surface, which were assumed to represent regions of inhomogeneity. The nucleation fields varied from 500 to 2000 oersteds, compared with the "theoretical" value of 12000 oersteds.

Reference was made to calculations of the demagnetizing energy of the structure, in a partially magnetized specimen, from which the corresponding domain widths could be obtained by minimizing the total energy with the help of a computer. The stability of line and cylindrical domains, and the value of the saturating field, were discussed. Magnetization curves derived from the above calculations corresponded well with the observations.

There was then some discussion between Dr. Craik and Mr. J. E. KNOWLES (Mullard Research Laboratories, Salfords) on the possible square loop behaviour of a single ferrite grain and it was observed that techniques of surface preparation similar to those used by Dr. Craik had been developed by Mullard Research Laboratories.

This was followed by a description by Dr. H. W. FULLER (Laboratory for Electronics Inc., Mass., U.S.A.) on the

investigation, by electron microscopy, of domain phenomena in thin films and a ciné-film was shown of some of the domain phenomena observed.

Session 4

The fourth session was opened by Dr. G. E. BACON (A.E.R.E., Harwell) who gave a general description of the techniques of neutron diffraction applied to problems of magnetism. He then proffered an explanation of the properties of Pt_3Fe which was based on the ideas of regions of disorder in a magnetically ordered crystal and of two possible ordered spin arrangements which, within the same crystallite, were virtually exclusive.

Dr. L. M. CORLISS (Brookhaven National Laboratory, U.S.A.) read a paper on the antiferromagnetic structure of the compound CrSe . This was determined by means of neutron diffraction experiments which showed that the unit "magnetic" cell was three times as large as the structural unit cell. The planes parallel to the basal plane contain three chromium atoms whose spins form a triangular array with zero resultant moment (shown in Fig. 8). This model was shown to be similar to that proposed by Hirone and Adachi.

Dr. R. J. WEISS (Watertown Arsenal, U.S.A.), in a paper by himself, Dr. L. M. CORLISS and Dr. J. HASTINGS (Brookhaven National Laboratory, U.S.A.) discussed the antiferromagnetism observed in chromium and proposed an antiphase periodicity of the spin orientations to explain the fine structure of the peaks in the magnetic neutron reflexions.

Dr. A. ARROTT (Ford Motor Company, U.S.A.) gave an account of antiferromagnetism in metallic systems, with special reference to the Cu-Mn system, describing, *inter al.*, the hysteresis loops observed at low temperatures.

Dr. M. K. WILKINSON (Oak Ridge National Laboratory, U.S.A.) read a paper by himself, Dr. E. O. WOLLAN and Dr. W. C. KOEHLER on neutron diffraction investigations of metallic cerium and the rare earth nitrides HoN and TbN at temperatures down to that of liquid helium. The previous work on cerium which was concerned with specific heat and magnetic susceptibility can be correlated with the existence of three crystal phases. The neutron scattering experiments indicated a change in the electronic configuration of cerium when the collapsed c.c.p. phase is formed (Fig. 9) and also that there is an antiferromagnetic transition in the h.c.p. phase at about 13°K , a model of a possible magnetic ordering in hexagonal cerium is given in Fig. 10.

The investigations of the rare-earth nitrides were undertaken to determine the occurrence of possible magnetic ordering in these compounds since they have the simple rock-salt structure and might be amenable to relatively easy

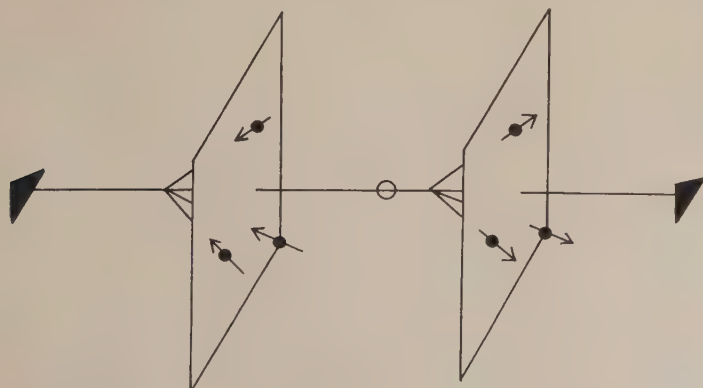


Fig. 8. Spin ordering in CrSe

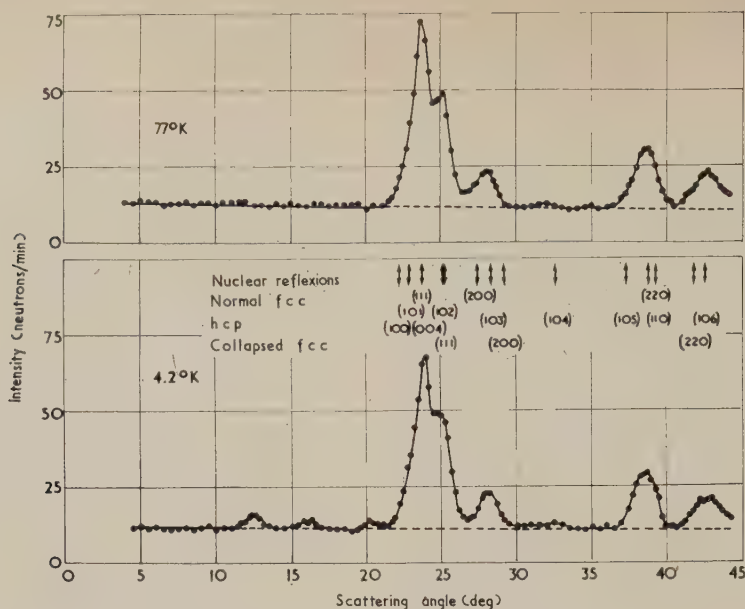


Fig. 9. Neutron diffraction patterns for cerium

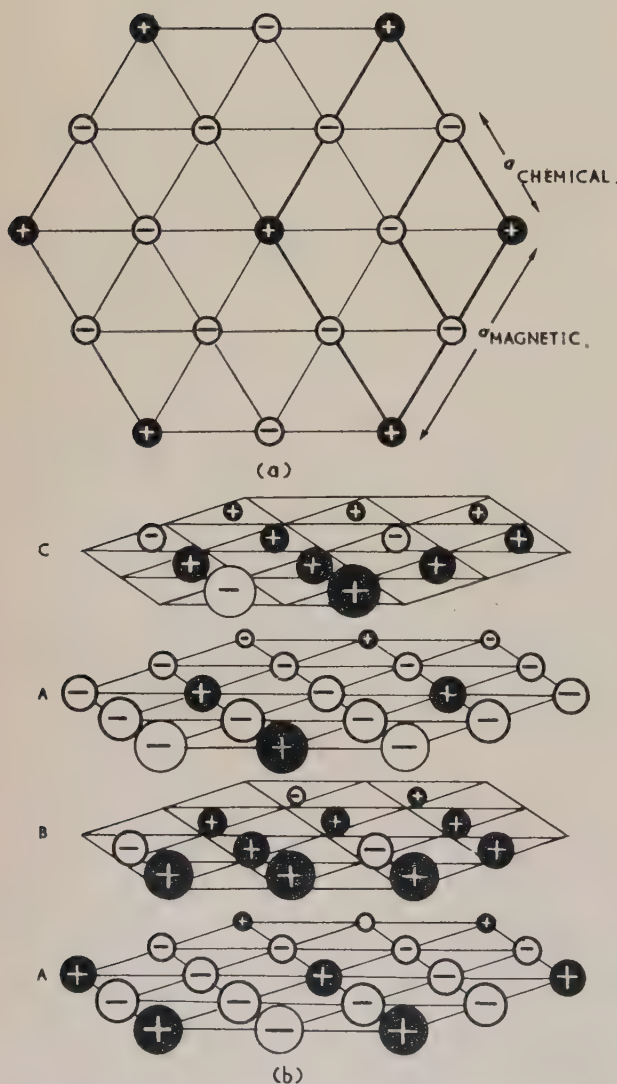


Fig. 10. Possible magnetic spin ordering in h.c.p. cerium

theoretical analysis. Both HoN and TbN become ferromagnetic with Curie temperatures of about 18° K and 42° K, respectively. Although the paramagnetic moments are consistent with those calculated for the free trivalent ions, the observed ferromagnetic moments are lower than the calculated values and indicate the effect of crystalline field interactions. Diffraction patterns at 1.3° K from both compounds (particularly HoN) show a large amount of inelastic magnetic scattering which appears to have characteristics that are different from those usually associated with critical magnetic scattering and are shown in Fig. 11.

Session 5

The fifth session was opened by Dr. T. O. PAINE (General Electric Research Laboratories, U.S.A.) who read a paper on the relation between the structure and properties of high coercivity materials. The paper gave an examination of the evidence confirming the single domain particle mechanism as a fundamental basis for high coercivity materials.

In a paper entitled "The interpretation of a.c. losses in terms of domain wall relaxation" Dr. E. W. LEE (University of Sheffield) and Mr. A. C. LYNCH (Post Office Research Station, Dollis Hill) discussed the interpretation of alternating current losses in thin ferromagnetic sheets (measured in fields so small that non-linear and hysteresis effects may safely be ignored) in terms of microeddy currents due to moving domain boundaries first suggested by Palivanov. From the measurements one can estimate a mean domain size. In the alloy 77% Fe, 14% Ni, 5% Cu, 4% Mo the mean domain size is about 30 μ for sheet of the same thickness, and this increases slightly as the sheet thickness increases. Additional measurements on an alloy of the same composition show that the mean domain size also increases with increasing grain size though not according to any simple relationship. In very thin sheets ($< 8 \mu$) there are signs that spin-relationship damping is contributing to the observed losses.

Dr. M. McCAIG (Permanent Magnet Association, Sheffield) read a paper by himself and Mr. W. WRIGHT on the variation of permanent magnet properties with crystalline orientation in columnar crystal alloys. The conclusion reached, from measurements on several samples, was that,

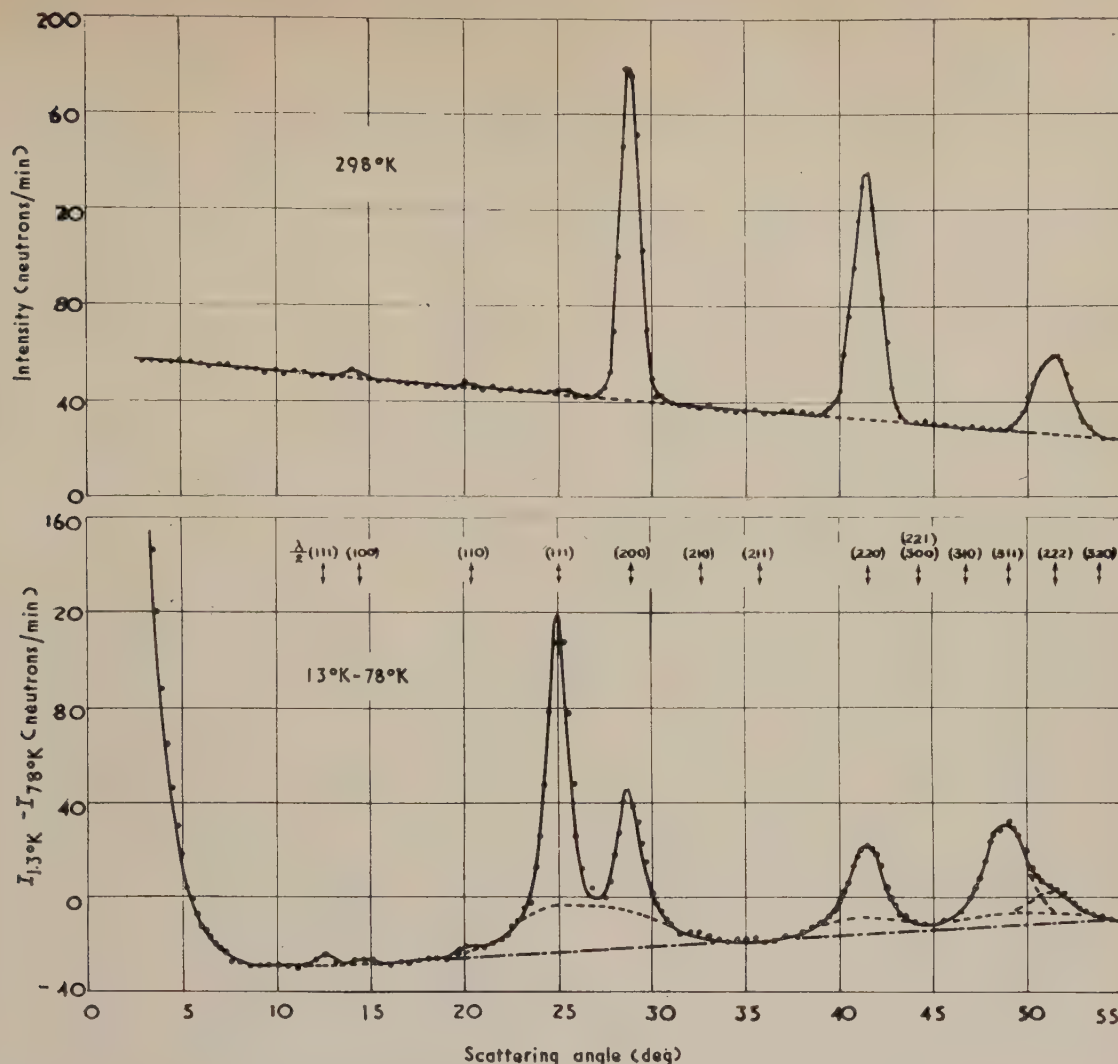


Fig. 11. Neutron diffraction patterns from HoN

although the spread of crystal axes can make significant differences to columnar properties, it does not explain all the differences observed.

Dr. J. C. BARBIER (University of Grenoble) described the investigation of thermal fluctuation fields and reptation (creeping) by measurement of differential irreversible susceptibility.

An initially demagnetized specimen acquires an intensity of magnetization J_A in an applied field H_A . An increment of field h produces an irreversible change of intensity of magnetization $J_A = S_A h$ where S_A is the differential irreversible susceptibility.

The magnetic properties at the point $A(H_A, J_A)$ of the hysteresis cycle can be strongly perturbed by fields arising from thermal fluctuations or by "creeping". Under these conditions the application of the additional field h produces

an irreversible increase of intensity of magnetization J_A which is not equal to $S_A h$ and the curve $J_A = f(h)$ is no longer a straight line of slope S_A for small values of h . Straight lines of slope S_A are observed when h is large compared to the fields of *trainage* or of "creeping".

At a given point A on the hysteresis cycle it is possible to investigate the phenomena of magnetic viscosity and "creeping" under well defined conditions, by analysis of the observed $J_A = f(h)$ curves.

Using this method it is also possible to show that the thermal fluctuation fields are distributed in all directions around that of the magnetizing field H_A .

Department of Physics,
The University,
Sheffield 10.

R. S. TEBBLE
D. E. G. WILLIAMS

Gaseous diffusion in porous media

Part 1.—A non-steady state method

by J. A. CURRIE, Ph.D., Rothamsted Experimental Station, Harpenden, Herts.

[Paper received 5 January, 1960]

Abstract

Laboratory equipment, capable of modification for use on soils in the field, was constructed to study diffusion in porous systems. A simple katharometer employs the exposed element of a thermal milliammeter to measure the instantaneous composition of hydrogen/air mixtures; the most convenient working condition is when 15 mW are dissipated in the hot wire, at which the thermocouple output changes from 0.5 mV in pure hydrogen to 2.5 mV in air. The geometry of the experimental system is simple enough to permit a standard solution of the non-steady state equation for interdiffusion of two gases to be applied, and, as a check on performance, straight tubes of slightly varying geometry were used to measure the diffusion coefficient of hydrogen into air, and its dependence on temperature. Reproducibility was very good and, within the limits of experimental error, the coefficient obtained was the same for 100% hydrogen into 100% air, and 60% air + 40% hydrogen into 100% air. Measurements at 12, 20, 28 and 36°C, fitted $D = D_0(T/273)^n$, with

$$D_0 = 0.651 \text{ cm}^2 \text{ s}^{-1} \text{ at n.t.p.}$$

$$n = 1.715$$

Standard values in the literature are $D_0 = 0.611$ (International Critical Tables⁽¹¹⁾), 0.634 and 0.661 (Smithsonian Physical Tables⁽¹³⁾). The latter reference gives $n = 1.75$.

Introduction

IN previous laboratory studies of gaseous diffusion through porous media, some methods were unsuited to the rapid handling of numerous samples and others introduced errors affecting the validity of the results. In steady state methods, Buckingham⁽¹⁾ maintained a partial pressure gradient of carbon dioxide across the sample. Penman⁽²⁾ measured the rate at which carbon disulphide and acetone vapours diffused through the sample and⁽³⁾ improved upon Buckingham's method for carbon dioxide. Van Bavel⁽⁴⁾ introduced refinements to Penman's vapour method. Non-steady state methods were used by Taylor,⁽⁵⁾ in which nitrogen was the diffusing gas; by Rust and others⁽⁶⁾ in which carbon dioxide and its radioactive isotope $^{14}\text{CO}_2$ interdiffused; and by Dye and Dallavalle,⁽⁷⁾ in which nitrogen and carbon dioxide interdiffused. These methods produced only a very general agreement which will be considered in more detail later. One of the main difficulties in transient methods is to measure rapidly changing gas compositions without interfering with the system. Strehlow⁽⁸⁾ used a hot-wire technique to measure the point concentration in binary mixtures in a Loschmidt cell, but found convection

around the wire introduced errors in a system where all gas movement ought to be by diffusion. The present method also uses a point-analysis technique, but convection effects can be ignored because the surrounding gas approximates to a well-stirred mixture.

Measurement of gaseous composition

In thermal conductivity gas analysers, the temperature of the sensitive element is usually deduced from its instantaneous resistance, whereas the present apparatus measures the potential difference across an attached thermocouple. The sensitive element is a modified Vacuo-Junction tube (manufactured by Best Products Ltd.), consisting of a 5 mm length of electrically heated wire with a chromel-constantan thermocouple sealed by an insulating compound to its midpoint, the diameter of the seal being about 0.2 mm. As manufactured, this unit is enclosed in an evacuated glass envelope, but a modified form was supplied mounted in an open-ended glass tube, approximately 1.3 mm in diameter, with the element inset about 6 mm from the open end. In a later modification, the whole of the protective glass sheath was removed.

The output of the thermocouple for a range of heating currents was measured on a portable potentiometer reading to 1 μV , and Fig. 1 shows the response in atmospheres of hydrogen, air and carbon dioxide. There is an upper limit to the useful sensitivity, governed by the lowest power dis-

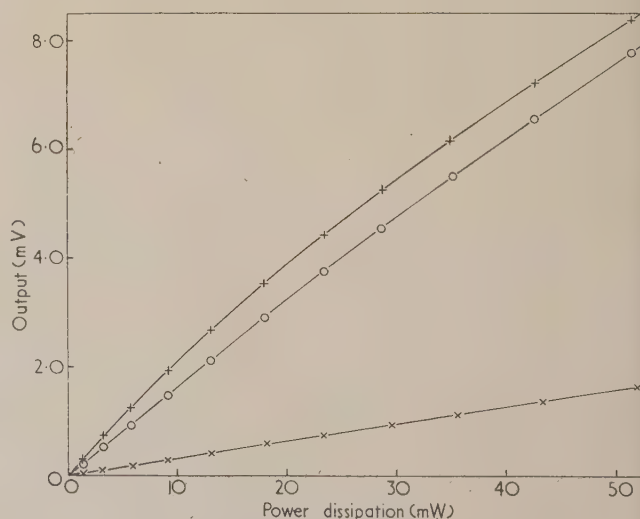


Fig. 1. Power dissipation and thermocouple response in hydrogen, air and carbon dioxide

x = hydrogen; o = air; + = carbon dioxide

sipation at which thermal drift becomes apparent. Thermal drift occurs when the excess temperature of the element is so great that both the cold junction and the surrounding gas increase slowly in temperature. An increase in cold junction temperature depresses the thermocouple output and an increase in ambient gas temperature increases the temperature of the element. Though thermal drift can be eliminated by continuously changing the sample being analysed, in the present study this was neither feasible nor desirable. When the energy dissipated was 15 mW, the sensitivity was adequate and the thermal drift of the element in air changed the thermocouple output by less than $1 \mu\text{V}/\text{min}$. In operation, a constant current is maintained in the element by frequent adjustment of the potential difference across a series resistance. The power dissipated in the element is independent of the operations required to balance the circuit and may, for practical purposes, be regarded as constant, varying only slightly with the temperature of the wire. The small thermal capacity of the wire allows a rapid response to changes in gaseous composition of the surrounding gas.

The modified Vacuo-Junction was mounted with Araldite in the centre of a Perspex disk, which was fixed at the upper end of a cylindrical brass tube of length 1 in. and diameter 2.25 in. This assembly is referred to as the "gas tube" in succeeding paragraphs. For calibration the gas tube was closed at its lower end and provision was made for the controlled admission of gases. The gas tube was initially filled with air at atmospheric pressure. A known volume of hydrogen was injected under pressure and allowed to mix thoroughly with the air in the tube. Atmospheric pressure was then restored and the thermocouple output read. Further volumes of hydrogen were added, to give a series of air/hydrogen mixtures, the compositions of which, with respect to the original gas, are given by the expression $\{V/(V+v)\}^N$ where V and v are the volumes of the gas tube and the added gas respectively and N is the number of additions. Another series of mixtures was prepared by adding successive amounts of air to hydrogen. As a check, potentiometer readings were plotted against N for the two series and from the intersection of the two lines the value of N corresponding to 50% composition was obtained. This enabled the ratio $V/(V+v)$ to be calculated and checked against the value computed from the measured volumes. Calibration was done in a constant temperature room and, because the gas sample and associated circuits were maintained at the same temperature, the resultant thermocouple readings incorporate all the effects of any temperature coefficients of the components in the circuits. Fig. 2 shows the calibration curve obtained at 20°C . The calibration was repeated at each of the four temperatures at which diffusion measurements were made. The effect of a 1°C rise in the temperature was to decrease the thermocouple output by about $1.7 \mu\text{V}$ in air and to increase it by about $0.5 \mu\text{V}$ in hydrogen.

Measurements of diffusion

Apparatus (Fig. 3). Two circular Duralumin plates with their inner faces ground flat were bolted through their centres and were both drilled to accept cylindrical brass tubes of the same diameter. The lower plate into which the sample tube was inserted was clamped horizontally and the upper plate holding the gas tube was free to rotate between two positions, in which the two tubes were completely isolated from each other (position I) or accurately aligned and interconnected (position II). Both gas and sample tubes were made to be a push fit in their recesses. When in position I, the gas tube

could be flushed out by gas admitted and discharged through two tubes fitted in the lower plate. When rotated into position II, the gases in the gas and sample tubes could interdiffuse.

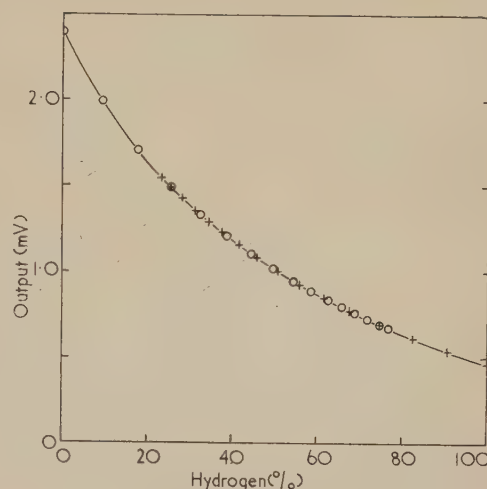


Fig. 2. Calibration curve for thermocouple in hydrogen/air mixtures at an ambient temperature of 20°C

○ = hydrogen added to air; + = air added to hydrogen

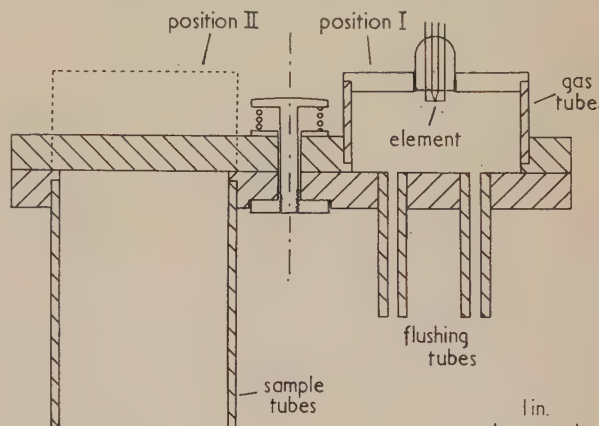


Fig. 3. Details of diffusion apparatus

In the first experiments to test the equipment, the porous material in the sample tube was a system of straight parallel tubes of known geometry. Seven Perspex tubes of nominal length 3 in. and internal diameter 0.25 in. were sealed into two circular plates of the same material, prepared so that the model could be inserted in place of the sample tube with the upper ends of the tubes either flush with the sliding plane or separated from it by the thickness of the Duralumin lip as shown in Fig. 4(a) and (b). The mean lengths and internal diameters of the tubes were measured with a travelling microscope.

Solution of diffusion equation for conditions imposed in the apparatus. Two alternative sets of boundary conditions may be imposed and a choice is needed. The first assumes that the gas in the gas tube is non-turbulent, moving only by diffusive processes so that a concentration gradient will exist between the plane containing the sensitive element and the upper end of the sample tube. Tests of the formal solution for this boundary condition on experimental data revealed consistent differences between computed and measured concentration/time curves. The second set of

boundary conditions assumes that there is always sufficient turbulence in the gas tube to eliminate any concentration gradient in it, i.e. the contents can be described as "a well-

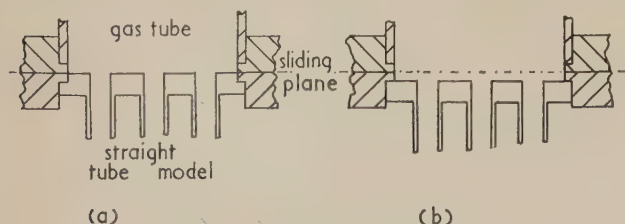


Fig. 4. The positions of the parallel tube model in relation to the sliding plane
(a) flush; (b) separate

stirred fluid". Direct and circumstantial evidence suggest that the assumption is valid. Mica dust admitted with the flushing gas and observed in a beam of light was in turbulent motion all the time until it settled out (about 5 min); and the change from position I to position II restored turbulence in a gas sample allowed to come to rest in position I. It is expected that the small heating effect of the element will maintain some degree of mixing, and a few tests showed that the response of the equipment was independent of the position of the sensing element in the gas tube. The main source of reassurance, however, is that the shapes of the concentration/time curves, and their changes with linear dimensions of the system, are in accord with expectation.

Equation of flow. Consider an element of unit area normal to the line of flow, and δx thick along the line of flow. The rate of increase of gas content is given by

$$\frac{dq}{dt} = D \frac{\partial}{\partial x} \left(\frac{\partial c}{\partial x} \right) \delta x \quad (1)$$

If the pore space is ϵ , the quantity and concentration are related by

$$q = \epsilon c \delta x \quad (2)$$

Hence the formal equation of transfer is

$$\frac{dc}{dt} = \frac{D}{\epsilon} \frac{d^2 c}{dx^2} \quad (3)$$

so that D/ϵ corresponds to the thermal diffusivity in heat transfer, and the formal solution can be written down by analogy [Carslaw and Jaeger, Ref. 9, example (iv), p. 128], as follows.

Referring to Fig. 3, the open end of the sample tube, area of cross-section A , is taken as $x = 0$, and the upper end as $x = l$, where it is in contact with the gas tube of depth a . The boundary conditions are:

- $t = 0$, in the region $0 < x < l$ there is zero concentration of the diffusing gas;
in the region $l < x < l + a$ there is concentration c_0 of the diffusing gas.
 $t > 0$ at $x = 0$, $c = 0$
 $0 < x < l$, $c = c$
 $l < x < l + a$, $c =$ the concentration at $x = l$, and is independent of x .

If the sample tube contains a porous material of porosity ϵ , then the instantaneous concentration in the region $0 < x < l$ is given by

$$c = \sum_{n=1}^{\infty} \frac{2hc_0 \exp(-D\alpha_n^2 t/\epsilon) \sin \alpha_n x}{\sin \alpha_n \{l(\alpha_n^2 + h^2) + h\}} \quad (4)$$

where $h = \epsilon/a$, and α_n , with $n = 1, 2, \dots$, are the positive roots of $\alpha \tan \alpha l = h$. At $x = l\delta$

$$\frac{c}{c_0} = \sum_{n=1}^{\infty} \frac{2h \exp(-D\alpha_n^2 t/\epsilon)}{l(\alpha_n^2 + h^2) + h} \quad (5)$$

and for $t \gg 0$ this reduces to

$$\frac{c}{c_0} = \frac{2h \exp(-D\alpha_1^2 t/\epsilon)}{l(\alpha_1^2 + h^2) + h} \quad (6)$$

A plot of $\ln c$ against t gives, after a short period, a straight line of slope $-D\alpha_1^2/\epsilon$, where α_1 depends only on the geometry of the system. As a working technique it is convenient to select from the straight part of the curve a time interval Δt such that c at t is ten times c at $t + \Delta t$; and then

$$D/\epsilon = 2.303/\alpha_1^2 \Delta t \quad (7)$$

Experimental

From the calibration graph for the sensitive element, at the appropriate ambient temperature, potential differences corresponding to a series of decreasing hydrogen concentrations were read. When the gas tube in position I had been flushed with hydrogen and the potentiometer reading indicated 100% concentration, the gas tube and porous model were brought into alignment, the stopwatch started and the first of the series of voltage readings set on the potentiometer. The time at which the potentiometer circuit became instantaneously balanced was recorded. Similar time intervals were read at successive potentiometer settings corresponding to steps of $\delta \log_{10} c = -0.05$. For $t > 60$ s a consistent linear relationship was obtained between $\log c$ and t , and the observations were maintained until c was about 5%. Mean ambient air temperature and pressure were observed during each diffusion measurement.

Three determinations were made at each of four temperatures for each of four systems of differing geometry. By varying the number of tubes from seven to six the value of ϵ was altered, and by fitting the model in the fully or partially recessed position, a was varied.

Ideally all samples should extend to the plane of sliding but, because the apparatus was to contain granular materials in later work, it was considered desirable to separate such samples from the carefully ground sliding surfaces by a small distance to prevent mechanical damage. Because the gas tube is in a well-stirred state, it is supposed that the hydrogen therein rapidly reaches an equilibrium concentration with the air in the gap, after which diffusion continues in accordance with the theoretical equation with a increased by the thickness of the Duralumin lip (a') so that c_0 is now $a/(a + a')$ instead of unity. The assumption appears to be justified by the close agreement between values of D_T obtained with and without the gap. (Table 1, compare columns A and B with C and D .)

Table 1. Coefficients of diffusion of hydrogen into air in four systems of differing geometry

Nominal temperature (°C)	$D_T = \frac{2.303 P_0}{\alpha^2 \Delta t P} \text{ cm}^2 \text{ s}^{-1}$ (Mean of three determinations)				
	A	B	System C	D	Mean
12	0.700	0.704	0.706	0.708	0.704
20	0.736	0.735	0.737	0.733	0.735
28	0.771	0.772	0.771	0.770	0.771
36	0.805	0.803	0.805	0.803	0.804

Sampling error of the mean of three samples = ± 0.0009

Results

The dependence of diffusion on pressure and temperature is usually expressed as

$$D_0 = D_{T,P}(273/T)^n \cdot P_0/P \quad (8)$$

where D_0 is the coefficient of diffusion at n.t.p.; $D_{T,P}$ is the value at T, P ; n is a constant lying between 1.5 and 2.0 and expected to be close to 1.75 for gases and 2.0 for vapours [Kennard⁽¹⁰⁾].

For a system of straight parallel tubes, the porosity ϵ is simply Ae/A , where Ae is the total cross-sectional area of the parallel tubes and A is the cross-sectional area of the gas tube. Thus for parallel tubes, D/ϵ may be rewritten as $DA/Ae = D_0$, the coefficient of diffusion through free air. As a working equation, equations (7) and (8) combine to give

$$D_0 = \frac{2 \cdot 303}{\Delta t \cdot \alpha^2} \left(\frac{273}{T} \right)^n \cdot \frac{P_0}{P} \quad (9)$$

Values of α were derived from the measured dimensions (Table 2) and the appropriate values of $h(=\epsilon/a)$. Values of D_T (corrected for pressure only) are in Table 1 and a linear regression of $\log D_T$ on $\log (273/T)$ gave

$$D_0 = 0.651 \pm 0.0003 \text{ cm}^2 \text{ s}^{-1} \\ n = 1.715 \pm 0.013$$

Table 2. Details and dimensions of straight parallel tubes

Model	A	B	C	D
No. of tubes	7	6	7	6
Position	Flush	Flush	Separated	Separated
a cm	2.544	2.544	2.826	2.826
l cm	7.566	7.566	7.566	7.566
Ae cm ²	0.1052	0.0902	0.1052	0.0902
A cm ²	22.099	22.099	22.099	22.099
$\alpha \times 10^3 \text{ cm}^{-2}$	4.940	4.294	4.492	3.902

Discussion

These small standard deviations are measures of the precision in the technique, and not necessarily measures of the accuracy of the estimates of D_0 and n . Currently quoted values for the coefficient of diffusion of hydrogen into air at 760 mm pressure and 273° K are 0.611,^(11,12) 0.634 and 0.661 cm² s⁻¹,⁽¹³⁾ and the value for n is given as 1.75. The value of D_0 obtained here comes within the range of the standard values of this so-called "constant", suggesting that the technique is adequate for its purpose, and that the explicit assumptions are valid. Two implicit assumptions were tested experimentally. First, as this is a transient method, the value of D_0 is an average over a range of hydrogen concentration decreasing from 100 to about 5%. Though the straightness of the plot of $\log c$ against t suggests no depen-

dence on concentration, five separate experiments were done with the initial concentration varied from 100 to 40%, but no significant variation in derived values of D_0 was detected.

Second, the possibility of an "end effect" was examined, for it may be that the effective plane of zero hydrogen concentration does not coincide with the open-end of the tube ($x = 0$). Directing a draught of air across the open end in an endeavour to make certain that $c = 0$ at $x = 0$ caused mass flow through the tubes, readily detected because the katharometer acted as a very sensitive anemometer. A much less drastic ventilation, produced by a rotary blade sweeping at intervals across the open end, caused no such mass flow: nor did it affect the rate of decay of hydrogen concentration, and it is presumed that the "end effect" is negligible and such sweeping is unnecessary.

Whatever the undetected error here may be, it will be trivial in the main bulk of the work on porous materials which will be subject to the same experimental conditions as the straight tubes. The parameter to be discussed is D/D_0 and any uncertainties in this ratio, arising from approximation in the theory, will be very small compared with the specification of the geometries of the porous systems themselves.

Acknowledgement

The author wishes to thank Dr. H. L. Penman for suggesting the subject for this work and for his helpful advice throughout.

References

- (1) BUCKINGHAM, E. *U.S. Dep. Agric. Bureau of Soils Bull.*, No. 25 (1904).
- (2) PENMAN, H. L. *J. Agric. Sci.*, **30**, p. 437 (1940).
- (3) PENMAN, H. L. *J. Agric. Sci.*, **30**, p. 570 (1940).
- (4) VAN BAVEL, C. H. M. *Soil Sci.*, **73**, p. 91 (1952).
- (5) TAYLOR, S. A. *Soil Sci. Soc. Amer. Proc.*, **14**, p. 55 (1949).
- (6) RUST, R. H., KLÜTE, A., and GIESEKING, J. E. *Soil Sci.*, **84**, p. 453 (1957).
- (7) DYE, R. F., and DALLAVALLE, J. M. *Industr. Engng Chem.*, **50**, p. 1195 (1958).
- (8) STREHLOW, R. A. *J. Chem. Phys.*, **21**, p. 2101 (1953).
- (9) CARSLAW, H. S., and JAEGER, J. C. *Conduction of Heat in Solids*, 2nd Ed. (Oxford: Clarendon Press, 1959).
- (10) KENNARD, E. H. *Kinetic Theory of Gases*, 1st ed. (New York: McGraw-Hill Book Co., 1938).
- (11) *International Critical Tables*, **5**, p. 62 (New York: McGraw-Hill Book Co., 1929).
- (12) *American Institute of Physics Handbook* (New York: McGraw-Hill Book Co., 1957).
- (13) *Smithsonian Physical Tables*, 9th ed. (New York: Smithsonian Institution, 1954).

Gaseous diffusion in porous media.

Part 2.—Dry granular materials

by J. A. CURRIE, Ph.D., Rothamsted Experimental Station, Harpenden, Herts.

[Paper received 5 January, 1960]

Abstract

The diffusion of hydrogen through cylindrical samples of porous granular materials, 3 in. long and 2 in. diameter, was measured by the non-steady state technique of Part I⁽¹⁹⁾, and reduced coefficients of diffusion D , referred to the value D_0 in free air, were calculated for over twenty materials with porosity ε between 0.18 and 0.98. Results are comparable with those obtained by other methods, and with those for analogous electrical properties of porous media. Replicate determinations on a given sample agree to within 1%, but larger differences, caused by variations in packing, are observed between duplicate samples of the same porosity. It is shown theoretically that $D/D_0 = (l/l_e)^2 f \varepsilon$, where f and l_e/l are factors for non-uniformity of cross-section and the increased length of the tortuous path followed by the gas, respectively. The influence on D/D_0 of not only porosity, but also particle shape, was clearly shown and there can therefore be no unique relationship for all materials, as often supposed, between diffusion rates and porosity. The equations of Burger and Bruggeman, both of which include a particle shape factor, were tested on the experimental data and neither was entirely satisfactory. An empirical equation of the form $D/D_0 = \gamma \varepsilon^\mu$ fits all materials where $\gamma (\leq 1)$ and $\mu (\geq 1)$ are constants for a specific type of granular material, and probably represent measures of pore shape. Two particle shape parameters, relative surface area and equivalent settling radius, were measured for a limited number of materials, but at best, only a general trend between these and the experimental values for the Bruggeman shape factor was observed.

Introduction

DIFFUSION in a porous medium is less rapid than in free air because of the reduced area of available cross-section and increased path length. An effective coefficient of diffusion D can be measured, and there have been many attempts to find a unique relationship between D/D_0 and the pore space ε , where D_0 is the diffusion coefficient in free air. An equation of the type $D/D_0 = \varepsilon^m$ satisfies the formal requirements at the limiting values of $\varepsilon = 0$ and $\varepsilon = 1.0$, and though Buckingham⁽¹⁾ deduced that $m = 2$ from his work on soils, later workers have sought equations of the form $D/D_0 = a\varepsilon$ or $= a\varepsilon + b$, applicable to a restricted range of porosity. Penman,⁽²⁾ using a wide variety of porous materials, gave $a = 0.66$, $b = 0$ over the range $0 < \varepsilon < 0.6$; van Bavel,⁽³⁾ from a more limited range of dry granular materials, suggested that $a = 0.58$ was more satisfactory for practical (agronomic) purposes; and Flegg,⁽⁴⁾ investigating the effect of soil aggregate size on diffusion

rate, obtained values of a between 0.53 and 0.89 working in the range $0.35 < \varepsilon < 0.99$. Dye and Dallavalle,⁽⁵⁾ using powdered potassium perchlorate, found that in the range $0.2 < \varepsilon < 0.4$, a varied between 0.73 and 0.90, whereas Rust and others,⁽⁶⁾ using mixtures of quartz sands, glass beads and silica flour, found $a = 0.60$, $b = 0.04$ for air dry materials, and $a = 0.68$, $b = 0.01$ for wetted materials. Others who have given b a value other than zero, Blake and Page,⁽⁷⁾ making measurements on two soils *in situ*, gave $a = 0.71$, $b = 0.01$, and $a = 1.3$, $b = -0.13$. Taylor⁽⁸⁾ calculated $a = 0.97$, $b = -0.09$; $a = 0.78$, $b = -0.08$; and $a = 0.67$, $b = 0.00$ for quartz sand, powdered glass and soil respectively. Though Raney⁽⁹⁾ has measured diffusion rates in field soils, values of a or b cannot be inferred from his data.

Theoretical studies have been by analogy. De Vries⁽¹⁰⁾ used the formula derived by Burger⁽¹¹⁾ for the electrical conductivity of an alloy of one metal having inclusions of elliptical particles of another, setting

$$D/D_0 = \varepsilon / \{1 + (k - 1)(1 - \varepsilon)\}$$

where k is a shape factor. He showed that, for $k = 1.5$ (the value attributed to spherical particles by Burger), and where porosity is adjusted for a percentage of blocked pores, a relationship is given which is in good agreement with Penman's experimental results for soils. There is, however, no theoretical justification for his assumption that the blocked pore space is given by $\beta(1 - \varepsilon)\varepsilon$ where β has been assigned the value 0.4. De Vries⁽¹²⁾ considers in greater detail the applicability of several formulae to the analogous flow of heat through porous media. Of these, that of Burger, already mentioned, and another from Bruggeman,⁽¹³⁾ are most nearly in accord with experimental data for heat flow. For gaseous diffusion, the Bruggeman equation becomes $D/D_0 = \varepsilon^m$, where m is a shape factor, and though it can be shown that Burger's equation is a special case of the Bruggeman equation, with $m \simeq k$, the range of porosity over which they are equivalent is limited. Both formulae indicate that diffusion rate depends not only on porosity, but also on particle shape. This dependence on particle shape has been ignored in many attempts to find a unique relationship for all diffusion data, though it has been noted that certain specific materials gave results somewhat removed from the general trend in others. Penman⁽²⁾ attributed such differences in glass spheres and mica to the variations in diffusion path length with particle shape and also, in mica, to anisotropy of structure. Flegg⁽⁴⁾ pointed out that the low values of D/D_0 for vermiculite were obtained because "such materials with a plate-like structure are not to be expected to behave in the same way as more granular materials". De Vries,⁽¹⁰⁾ though he introduced the concept of shape factor into gaseous

diffusion studies, did not exploit it in his analysis of Penman's results, preferring to use a constant value of $k = 1.5$ (for spherical particles), and explained deviations from the theoretical in terms of non-continuous air space or "blocked pores". A re-examination of Penman's results shows that—as examples—the behaviour of glass spheres, sand and salt can fit the Burger equation if k is given the values 1.43, 1.81 and 2.16 respectively.

Marshall^(14, 15, 16) has adapted a theoretical treatment of viscous flow of liquid in a porous system⁽¹⁴⁾ to give $D/D_0 = \varepsilon^{3/2}$ for gaseous diffusion⁽¹⁵⁾ and got approximate agreement⁽¹⁶⁾ with the data of Taylor⁽⁸⁾ for wetted materials. A modification of the original theory by Millington and Quirk⁽¹⁷⁾ leads to $D/D_0 = \varepsilon^{7/6}$. Millington⁽¹⁸⁾ has since proposed that $D/D_0 = \varepsilon^{4/3}$.

Theoretical

Steady state flux. Consider unit partial pressure difference maintained across a porous solid of length l , and cross-section A . The flux can be written in terms of an effective diffusion coefficient D , as DA/l . If now the porous solid is regarded as made up of a system of tortuous tubes of average length l_e ($l_e > l$), and of total cross-section, normal to the length, A_e ($A_e < A$), then the flux may also be written as $D_0 A_e / l_e$. It seems reasonable to set the porosity as

$$\varepsilon = A_e l_e / Al$$

from which

$$D/D_0 = (l/l_e)^2 \varepsilon \quad (1)$$

Non-steady state flux. If a volume Aa of a gas, initially at concentration c_0 , is allowed to diffuse through a porous solid of volume Al and length l in which the initial concentration of the same gas is zero, then the rate of change of concentration at the common interface is given by equation (6) of Part I⁽¹⁹⁾ as

$$\partial \ln c / \partial t = -D\alpha_1^2 / \varepsilon \quad (2)$$

where α_1 is the first positive root of

$$\alpha \tan \alpha l = \varepsilon / a \quad \text{or} \quad \alpha_1 l \tan \alpha_1 l = \varepsilon l / a.$$

For the equivalent set of parallel tubes, length l_e , the decay equation is

$$\partial \ln c / \partial t = -D_0 \alpha_0^2 \quad (3)$$

where α_0 is the first positive root of

$$\alpha \tan \alpha l_e = (1/a)(A_e/A) \quad \text{or} \quad \alpha_0 l_e \tan \alpha_0 l_e = A_e l_e / aA \quad (4)$$

But $A_e l_e = \varepsilon Al$ and hence the last equation becomes

$$\alpha_0 l_e \tan \alpha_0 l_e = \varepsilon l / a \quad (5)$$

Hence

$$\alpha_0 l_e = \alpha_1 l$$

Also

$$\alpha_0^2 D_0 = \alpha_1^2 D / \varepsilon$$

i.e.

$$D/D_0 = \varepsilon (l/l_e)^2 \quad (6)$$

Equation (6), derived for both steady and non-steady state flow, is applicable only to the ideal porous material in which all the pores are of uniform cross-section throughout their length.

Diffusion through tubes of non-uniform cross-section. The

total effective cross-section may be reduced as a result of constrictions along the length of the tube from A_e to A_e' , where $A_e'/A_e = f$. The diffusion equation is therefore more correctly derived in the form

$$D/D_0 = (l/l_e)^2 f \varepsilon \quad (7)$$

The value of f is considered in the Appendix, for one of the simplest possible cases, a sinusoidal form. $D_0 \varepsilon / D$ is frequently referred to as the tortuosity factor, but it can be clearly seen that, as Carman⁽²⁰⁾ suggested, this is no longer justifiable.

Determination of D/D_0

For a system of fixed geometry (known l and a), α_1 is uniquely determined when ε is known; and hence α_1^2 / ε {equation (2)} is simply a function of ε , say $\phi(\varepsilon)$. For a tenfold change in concentration in time Δt , then

$$D = 2.303 / \Delta t \phi(\varepsilon) \quad (8)$$

A graph of $2.303 / \phi(\varepsilon)$ against ε was prepared (it is indistinguishable from a straight line) and with ε known and Δt measured, D is easily determined and corrected for temperature and pressure.

The technique for measuring Δt is identical with that described in Part I for the straight tube model. For diffusion measurements on granular materials, the sample was packed into a brass tube where it was supported by a gauze at the lower end. The tube was then inserted into the recess in the fixed lower plate of the apparatus. Porosities were calculated from the internal dimensions of the tube, the weight of the sample and the true particle density where

$$\varepsilon = 1 - \frac{\text{weight of sample}}{\text{volume of tube} \times \text{true density}} \quad (9)$$

The supporting gauze offers a resistance to diffusion proportional to its thickness and inversely proportional to its free cross-sectional area. By the choice of suitable material, this resistance was kept to a minimum. Nylon mesh having a total thickness of 0.1 mm and a free cross-sectional area of about 90% was used whenever possible. For coarse materials, a 1.5 mm hexagonal mesh was used and, for fine powders, a portion of nylon stocking. The resistance of these materials can be shown by calculation to be less than 0.1% of the resistance of a typical sample. For more dense materials, the greater rigidity of a woven wire mesh was preferred and, by calculation, its resistance decreased the value of D/D_0 by 0.25%.

Whenever possible, samples were carefully packed to avoid compression and consequent distortion of particles. Variations in porosity about the expected mean for random packing were achieved by lightly tapping the brass tube. Excessive variations in packing were avoided in the more compressible materials, to prevent orientation of particles and consequent anisotropic structure, but the experimental evidence suggests that this was not always successful. Care was taken to ensure that the sample surface was level with the top of the tube to avoid errors in the values taken for a , l and ε .

The value of D_0 used to calculate the ratio D/D_0 was $0.651 \text{ cm}^2 \text{ s}^{-1}$, as determined in Part I with the same apparatus. Errors in the original measurements are in the same sense as those occurring in the measurements of D , and will tend to be minimized in the final expression of the results in the form D/D_0 .

Experimental results

Fig. 1 shows the values for D/D_0 (Table 1) plotted against the corresponding values of ε . At first sight these results seem to fit the equation $D/D_0 = 0.60\varepsilon$ for $0 < \varepsilon < 0.8$. The data for materials having $\varepsilon > 0.8$ do not conform to the above relationship and cannot be interpreted satisfactorily without reference to the probable effects of particle shape.

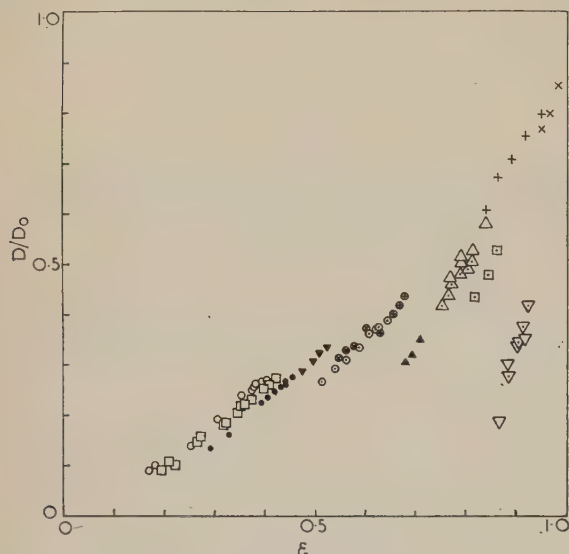


Fig. 1. Dependence of coefficient of diffusion on porosity. D/D_0 and ε

- | | |
|-------------------------|---------------------------|
| ○ Glass spheres | △ Kaolin (Suprex) |
| □ Sand | △ Kaolin (Peerless No. 2) |
| ● Carborundum | + Celite |
| ▼ Sodium chloride | × Steel wool |
| ⊗ Barnfield soil crumbs | □ Perspex flakes |
| ○ Woburn soil crumbs | ▽ Vermiculite |
| ⊕ Highfield soil crumbs | ▽ Mica |
| ▲ Pumice | |

Burger and Bruggeman equations. Fig. 2, where $D/D_0\varepsilon$ was plotted against ε , shows that within the group of points for each type of particle, $D/D_0\varepsilon$ is not constant, but is itself a function of porosity as the equations of Burger and Bruggeman predict. It should be borne in mind that these formulae were derived for ellipsoidal particles. Comparison of the diffusion data obtained by experiment with the theoretical values from these equations should therefore be restricted to the glass beads, but on the assumption that all other particles have an equivalent ellipsoidal form, it has been extended to them too. Values for k and m , the Burger and Bruggeman shape factors, were computed for all the experimental points where $k = \{\varepsilon/(1 - \varepsilon)\}\{(D_0/D) - 1\}$ and

$$m = \log(D/D_0)/\log \varepsilon.$$

Table 1 shows the variability of both factors. Each type of material gives a range of values for k and m . Materials which give a "rigid" packing over a limited range of porosities, e.g. glass spheres, sands, carborundum and soil crumbs, show a smaller variability than those giving "soft" packings over a much larger range of porosities, e.g. mica, kaolin and celite (a diatomaceous silica). Because of their rigidity of packing, materials of the first type can exhibit only minor variations in pore geometry, whereas those of the second type are prone to compression and particle orientation giving anisotropic structure, and have therefore a much more variable pore

geometry. It must be remembered that k and m are particle shape factors, whereas diffusion depends directly on pore shape. When a porous material is packed in such a way

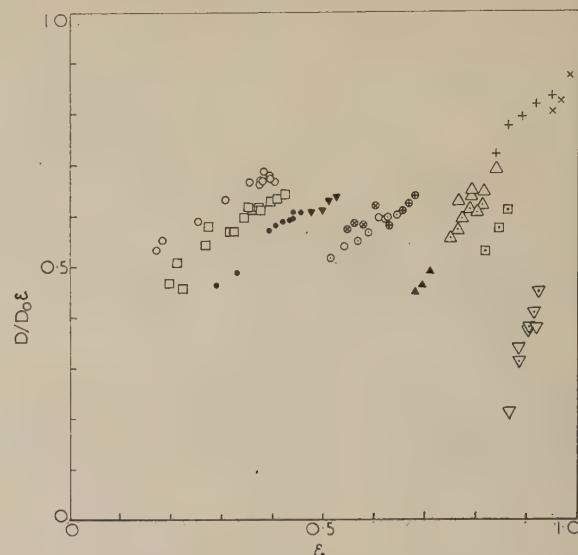


Fig. 2. Dependence of coefficient of diffusion on porosity. $D/D_0\varepsilon$ and ε

- | | |
|-------------------------|---------------------------|
| ○ Glass spheres | △ Kaolin (Suprex) |
| □ Sand | △ Kaolin (Peerless No. 2) |
| ● Carborundum | + Celite |
| ▼ Sodium chloride | × Steel wool |
| ⊗ Barnfield soil crumbs | □ Perspex flakes |
| ○ Woburn soil crumbs | ▽ Vermiculite |
| ⊕ Highfield soil crumbs | ▽ Mica |
| ▲ Pumice | |

that the shape of the particles no longer confers a characteristic shape on the pores, a particle shape factor cannot be expected to account for much of the variance in experimental results.

For spheres, sand and carborundum powder, the value of k is constant for packings of uniform size, but is bigger for packings of mixed sizes; and the value of m is constant whether the particles are uniform or mixed. The expected value for spheres is $k = m = 1.5$, but the values found (Table 1) are $k = 1.80$, $m = 1.41$, agreeing well with values that can be deduced from data given by Carman⁽²⁰⁾ for which $k = 1.73$, $m = 1.39$, or by Wooding⁽²¹⁾ (working on the stability of diffusing liquids), from which $k = 1.88$, $m = 1.45$. Pearce,⁽²²⁾ working on the analogous problem of the electrical properties of oil/water emulsions, showed that an equation, identical with that of Burger, when applied to gaseous diffusion in spherical particles, is excellent for the ordered distributions of spheres and cylinders for which it was produced, but is not adequate for random distributions; and De Vries⁽¹²⁾ found the Burger equation to be of limited value in predicting the thermal conductivity of a granular system. The difference between the theoretical value of $k (= 1.5)$ and the observed value (1.80) may be partly because of the randomness in the packing of the spheres.

The Bruggeman equation was derived for a random distribution of spheres, and though the agreement between theory ($m = 1.5$) and observation ($m = 1.41$) is much better than for the k values, there is a consistent difference yet to be accounted for. It is unlikely to arise from particle size distribution, as suggested by Pearce, because for spheres, m changes very little over a range of mixtures having the ratios of maximum to minimum diameter of 10 : 1, and there-

Table 1. *Values for ε , D/D_0 , k and m*

[Figures in first column are particle diameters (in mm)]

Material	ε	D/D_0	k	m	Material	ε	D/D_0	k	m
Spheres					Highfield soil crumbs				
0.75–0.80	0.405	0.271	1.83	1.44	1–2	0.680	0.436	2.75	2.15
0.75–0.80	0.396	0.267	1.80	1.42		0.669	0.419	2.80	2.16
0.75–0.80	0.381	0.256	1.79	1.41		0.656	0.401	2.85	2.17
0.38	0.395	0.269	1.77	1.41		0.630	0.367	2.93	2.17
0.38	0.383	0.263	1.74	1.39	Talc (powdered)	0.768	0.473	3.67	2.84
5–6	0.375	0.249	1.80	1.42		0.747	0.420	4.08	2.97
5–6	0.376	0.252	1.79	1.41		0.727	0.399	4.01	2.88
Mixtures	0.255	0.150	1.94	1.39		0.708	0.404	3.56	2.62
Mixtures	0.355	0.240	1.74	1.38	Kaolin: Suprex	0.813	0.506	4.07	3.28
Mixtures	0.183	0.101	1.99	1.35		0.804	0.490	4.27	3.27
Mixtures	0.307	0.194	1.84	1.38		0.788	0.483	3.98	3.05
Sand						0.773	0.461	3.98	3.01
0.25–0.50	0.424	0.274	1.95	1.51		0.765	0.438	4.18	3.08
0.25–0.50	0.402	0.254	1.97	1.50		0.752	0.419	4.19	3.05
0.25–0.50	0.375	0.231	1.99	1.50	Peerless 2	0.839	0.582	3.74	3.09
0.25–0.50	0.355	0.221	1.94	1.46		0.813	0.527	3.91	3.09
2–3	0.411	0.262	1.97	1.50		0.791	0.503	3.74	2.93
1–2	0.361	0.222	1.98	1.48		0.790	0.513	3.58	2.83
$\frac{1}{2}$ –1	0.399	0.253	1.97	1.50		0.767	0.482	3.53	2.75
$\frac{1}{2}$ –1	0.377	0.231	2.01	1.50	Celite	0.950	0.795	4.88	4.47
Mixtures	0.321	0.182	2.12	1.50		0.945	0.784	4.73	4.30
Mixtures	0.269	0.147	2.14	1.46		0.940	0.786	4.26	3.88
Mixtures	0.346	0.207	2.03	1.48		0.918	0.753	3.67	3.22
Mixtures	0.325	0.186	2.11	1.50		0.891	0.708	3.37	2.99
Mixtures	0.274	0.159	2.00	1.47		0.864	0.672	3.10	2.72
Mixtures	0.223	0.103	2.51	1.51		0.840	0.607	3.40	3.00
Mixtures	0.197	0.092	2.42	1.56	Vermiculite				
Mixtures	0.212	0.108	2.22	1.43	(< 2)	0.924	0.419	16.79	10.98
Spheres/sand						0.915	0.377	17.79	11.06
Mixtures	0.171	0.091	2.06	1.44		0.905	0.346	18.00	10.85
Carborundum	0.442	0.269	2.15	1.61		0.886	0.278	20.18	10.57
	0.442	0.263	2.22	1.64	Mica				
	0.434	0.257	2.22	1.63	(powdered)	0.919	0.351	20.98	12.38
	0.421	0.248	2.21	1.61		0.904	0.341	18.20	10.67
	0.407	0.237	2.21	1.60		0.885	0.302	17.79	9.79
	0.456	0.269	2.27	1.67		0.867	0.186	28.53	11.78
	0.456	0.285	2.10	1.59	Pumice				
Mixtures	0.394	0.226	2.23	1.60	2	0.710	0.350	4.55	3.07
	0.330	0.162	2.55	1.64		0.695	0.323	4.77	3.11
	0.293	0.135	2.66	1.63		0.681	0.308	4.80	3.07
Sodium chloride	0.527	0.336	2.20	1.70	Perspex flakes				
(irregular crystals)	0.512	0.323	2.21	1.69	1–2	0.863	0.528	5.63	4.33
	0.499	0.308	2.24	1.69		0.846	0.480	5.95	4.39
	0.476	0.289	2.23	1.69		0.819	0.436	5.86	4.16
Sodium metasilicate	0.530	0.339	2.20	1.70		0.802	0.435	5.26	3.77
(fragmented material)	0.502	0.314	2.20	1.68	Steel wool				
	0.470	0.292	2.15	1.63	Domestic	0.984	0.853	10.57	9.87
	0.463	0.281	2.21	1.65		0.967	0.798	7.42	6.53
Woburn soil crumbs	0.645	0.389	2.85	2.15		0.951	0.767	5.90	5.28
2–3	0.623	0.371	2.80	2.10	Plaster of Paris	0.492	0.230	3.24	2.07
	0.609	0.364	2.72	2.04	Polyurethane plastic foam	0.974	0.662	19.13	15.71
0.2–0.5	0.627	0.375	2.80	2.10	Brass turnings	0.691	0.457	2.66	2.12
0–2.0	0.589	0.335	2.84	2.07	Ceramic beads	0.535	0.304	2.63	1.90
	0.563	0.310	2.87	2.04	Hypo*			1.88	1.47
	0.541	0.293	2.84	2.00	Magnesium sulphate*			2.23	1.65
	0.515	0.267	2.91	1.99	Sucrose*			1.91	1.51
Barnfield soil crumbs					Sodium citrate*			1.90	1.49
1–2	0.603	0.374	2.54	1.94	Sulphate of ammonia*			2.12	1.57
	0.578	0.338	2.59	1.98					
	0.562	0.330	2.60	1.92					
	0.548	0.315	2.64	1.92					

* Mean of ten determinations at different ε values.

is even less variation in m for carborundum powder mixtures in which the diameter ratio changed from 100 to 1.

Empirical relation

When $\log D/D_0$ is plotted against $\log \epsilon$ (Fig. 3), the set of points for a given material lie on a straight line. A general

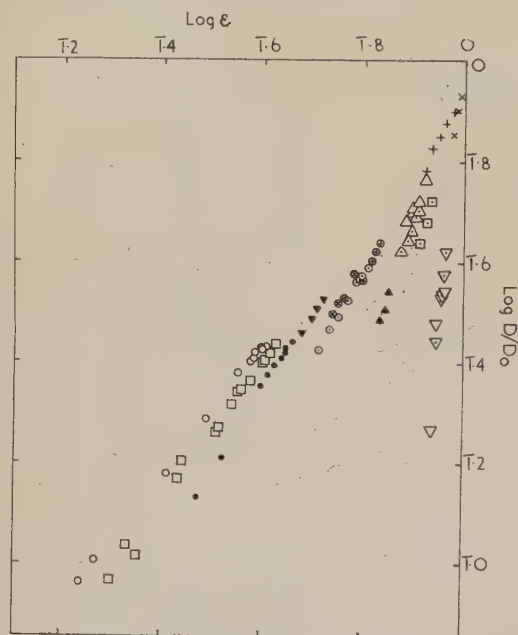


Fig. 3. Dependence of coefficient of diffusion on porosity. $\log(D/D_0)$ and $\log \epsilon$

- | | |
|-------------------------|---------------------------|
| ○ Glass spheres | △ Kaolin (Suprex) |
| □ Sand | △ Kaolin (Peerless No. 2) |
| ● Carborundum | + Celite |
| ▼ Sodium chloride | × Steel wool |
| ⊗ Barnfield soil crumbs | □ Perspex flakes |
| ○ Woburn soil crumbs | ▽ Vermiculite |
| ⊕ Highfield soil crumbs | ▽ Mica |
| ▲ Pumice | |

equation of the form $D/D_0 = \gamma \epsilon^\mu$ fits all the materials tested, with $\gamma = 1$, $\mu = m$, as limiting values. The values of γ lie between 1.0 and 0.8, and μ is always less than m . Very roughly, γ increases with the mean porosity for each type of material, and though errors in the measurement of either D/D_0 or ϵ might cause deviations from $\gamma = 1$ there is no known or suspected source of experimental error important enough to account for the magnitude of the deviations. Further, Wyllie and Gregory⁽²³⁾ working with unconsolidated media, gave data fitted by the equation $D/D_0 = \gamma \epsilon^\mu$ with $\gamma < 1$; and all the data summarized by Carman⁽²⁰⁾ for glass spheres can be fitted with $\gamma = 0.81$, though they come from different workers using different techniques.

The shape factor

The value of μ is probably a measure of pore shape, and in the hope that this might be related to particle shape, two attempts were made to define and measure a particle shape factor. Using regularly shaped crystals, a *relative surface area* (S_r) was calculated from measured dimensions, defined as the ratio of the surface area to that of a sphere of the same volume. From diffusion measurements on these materials values of m were determined and in Fig. 4, m is plotted against S_r . On the same diagram are the theoretical Bruggeman curves for ellipsoids having relative semi-axes $1 : 1 : n$, with $n > 1$ and $n < 1$; though the wide divergence of these curves clearly indicates that surface area is not an adequate index to shape, the six sets of experimental data plotted do show a clear trend of m increasing with relative surface area.

The second factor tested was the *relative "Stokes" radius*, and measurement was restricted to those particles big enough for their volumes to be estimated accurately. The settling velocity of the materials was measured in a 160 cm column of mineral oil, and the equivalent radius calculated from

$$r = V(\rho - \sigma)g/6\pi\eta v \quad (10)$$

where V and ρ are the volume and density of a particle settling with velocity v in a liquid of density σ and viscosity η .

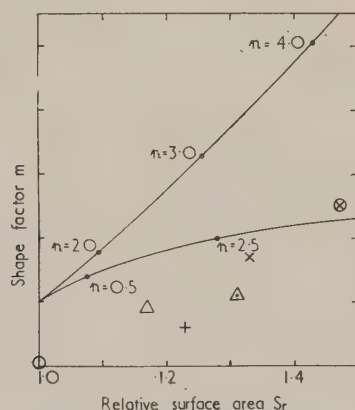


Fig. 4. Relationship between the Bruggeman shape factor m and the relative surface area of the particles. Theoretical curves are shown for ellipsoids having relative half axes $1 : 1 : n$

- | |
|----------------------|
| ○ Spheres |
| △ Sodium citrate |
| + Hypo |
| × Ammonium sulphate |
| ⊗ Magnesium sulphate |
| △ Sucrose |

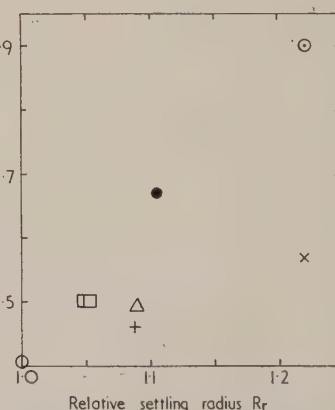


Fig. 5. Relationship between the Bruggeman shape factor m and the relative particle settling radius

- | |
|-----------------------|
| ○ Spheres |
| △ Sodium citrate |
| + Hypo |
| □ Sand |
| × Ammonium sulphate |
| ● Sodium metasilicate |
| ○ Insulating beads |

The relative Stokes radius R_v was calculated as r/r_s where r_s is the radius of a sphere having the same volume as the settling particle. The result of plotting m against R_v (Fig. 5) shows a trend, but no unique relationship, and the points for the rod-like materials lie below those for the more compact materials.

Conclusions

The coefficient of diffusion through a porous medium is clearly a function of both internal geometry and porosity. Neither of the theoretical equations considered is satisfactory for predicting diffusion rates through porous materials. Both the equations of Burger and of Bruggeman include only a single shape factor, that for particle shape. An equation having two shape factors is required because a single shape factor cannot satisfactorily define both particle shape and the spacial distribution of the particles. An empirical equation of the type $D/D_0 = \gamma e^{\mu}$ appears to be satisfactory for all the granular materials investigated, γ and μ being functions of the material. The equation is not expected to apply to wetted materials in which the geometry of the gas-filled pores will be appreciably altered by the liquid phase.

Acknowledgement

The author wishes to thank Dr. H. L. Penman for his interest and encouragement and for valuable discussion in the course of this work.

References

- (1) BUCKINGHAM, E. *U.S. Dept. Agric. Bureau of Soils Bull.* No. 25 (1904).
- (2) PENMAN, H. L. *J. Agric. Sci.*, **30**, p. 437 (1940).
- (3) VAN BAVEL, C. H. M. *Soil Sci.*, **73**, p. 91 (1952).
- (4) FLEGG, P. B. *J. Sci. Food Agric.*, **4**, p. 104 (1953).
- (5) DYE, R. F., and DALLAVALLE, J. M. *Industr. Engng Chem.*, **50**, p. 1195 (1958).
- (6) RUST, R. H., KLUTE, A., and GIESEKING, J. E. *Soil Sci.*, **84**, p. 453 (1957).
- (7) BLAKE, G. R., and PAGE, J. B. *Soil Sci. Soc. Amer. Proc.*, **13**, p. 37 (1948).
- (8) TAYLOR, S. A. *Soil Sci. Soc. Amer. Proc.*, **14**, p. 55 (1949).
- (9) RANEY, W. A. *Soil Sci. Soc. Amer. Proc.*, **14**, p. 61 (1949).
- (10) DE VRIES, D. A. *Trans Fourth Int. Congr. Soil Sci.*, Vol. II, p. 41 (1950).
- (11) BURGER, H. C. *Phys. Zs.*, **20**, p. 73 (1919).
- (12) DE VRIES, D. A. *Meded. Landbouwhooges.*, **52**, p. 1 (1952).
- (13) BRUGGEMAN, D. A. G. *Ann. Phys. (Leipzig)*, **24**, p. 636 (1935).
- (14) MARSHALL, T. J. *J. Soil Sci.*, **9**, p. 1 (1958).
- (15) MARSHALL, T. J. *J. Soil Sci.*, **10**, p. 79 (1959).
- (16) MARSHALL, T. J. *Commonwealth Bureau of Soils, Technical Communication No. 50* (1959).
- (17) MILLINGTON, R. J., and QUIRK, J. P. *Nature (London)*, **183**, p. 387 (1959).
- (18) MILLINGTON, R. J. *Science*, **130**, p. 100 (1959).
- (19) CURRIE, J. A. *Brit. J. Appl. Phys.*, **11**, p. 314 (1960).
- (20) CARMAN, P. C. *Flow of gases through porous media*, p. 48 (London: Butterworths Scientific Publications, 1956).
- (21) WOODING, R. A. *Proc. Roy. Soc. A*, **252**, p. 120 (1959).
- (22) PEARCE, C. A. R. *Brit. J. Appl. Phys.*, **6**, p. 113 (1955).
- (23) WYLLIE, M. R. J., and GREGORY, A. R. *Trans Amer. Inst. Min. Eng.*, **198**, p. 103 (1953).

Appendix

Diffusion through tubes of non-uniform cross-section. The value of f , the factor for tubes of non-uniform cross-section, is derived for a porous medium consisting of tubes of sinusoidal form, ignoring the shape of streamlines.

Set the area as

$$A' = p + q \sin \theta \quad (11)$$

The length of unit cell l is from $\theta = -\pi$ to $\theta = +\pi$.

$$x/l = \theta/2\pi \quad \text{and} \quad dx = (l/2\pi)d\theta$$

The impedance of unit pore

$$I = \int_0^l \frac{dx}{A'} = \frac{l}{(p^2 - q^2)^{1/2}} \quad (12)$$

and the volume of unit pore

$$V = \int_0^l A' dx = lp \quad (13)$$

$(p^2 - q^2)^{1/2}$ represents the effective free cross-section of the tube available for diffusion ($=\Delta A_e'$).

For a straight tube $q = 0$

whence $I = l/p$

and $V = lp$

p therefore represents the cross-section of the straight tube of equal volume, that is of equal porosity ($=\Delta A_e$).

But by definition

$$f = A_e'/A_e = \frac{\Sigma(p^2 - q^2)^{1/2}/\Sigma p}{\text{mean cross-section}} = \frac{(\text{maximum} \times \text{minimum cross-section})^{1/2}}{\text{mean cross-section}} \quad (14)$$

Table 2. Range of values of f for different ratios of area

Maximum/Minimum cross-sectional area	f
1.0	1.0
2.0	0.944
3.0	0.867
4.0	0.800
5.0	0.746
6.0	0.701
7.0	0.662
8.0	0.629
9.0	0.600
10.0	0.575
100.0	0.218

Table 3. Comparison between values for D/D_0 for spherical particles

	Closest packing	Cubic packing
Porosity ε	0.26	0.48
$(l/l_e)^{2*}$	0.66	1.00
f^*	0.87	0.76
D/D_0		
Equation (7)	0.149	0.365
Burger ($k = 1.5$)	0.190	0.381
Burger ($k = 1.8$)	0.163	0.339
Bruggeman ($m = 1.5$)	0.133	0.333
Bruggeman ($m = 1.4$)	0.151	0.358

* Calculated from the geometry of the system.

Table 2 shows the range of values of f for different ratios of maximum to minimum cross-sectional area.

It is of interest to make the following comparison (Table 3) between values for D/D_0 for spherical particles obtained using equation (7) and from the Burger and Bruggeman equations using theoretical and experimental shape factors.

For both cubic and hexagonal packing, the value for D/D_0 given by equation (7) lies between the theoretical values given by the equations of Burger and Bruggeman, where $k = m = 1.5$. The best agreement is observed in both systems between the values given by equation (7) and the Bruggeman equation, where $m = 1.4$, the experimental value.

Contact electrification of semiconductors

by W. R. HARPER, Ph.D., F.Inst.P., 67 Burton Court, London, S.W.3

[Paper first received 13 October, 1959, and in final form 20 April, 1960]

Abstract

Recently published experimental findings on the electrification of rutile powder by sliding down a metal chute can be explained by an extension of the present author's theory of the separation electrification of metals. The mechanism of the electrification of insulators must, in most cases, be quite different.

Introduction

THE mutual electrification of metals resulting from light contact without rubbing, followed by separation, has received a quantitative explanation based on the quantum-mechanical theory of electron levels in metals.⁽¹⁾ Different procedures for the investigation of the electrification of insulators used by Peterson,⁽²⁾ Wagner⁽³⁾ and by the present author,^(4, 5) have led to differing experimental results. The significance of these results has been discussed by Loeb,⁽⁶⁾ and by the author.⁽⁷⁾ Experiments on semiconductors by Cooke⁽⁸⁾ and Jewell-Thomas⁽⁹⁾ have recently been reported by Donald.⁽¹⁰⁾ These experiments led to a remarkable empirical law, that applied also to insulators, the significance of which was not understood at the time. The purpose of the present paper is to show that the quantum-mechanical theory of semiconductors predicts the law for semiconductor/metal contact, but makes it difficult to understand how it comes about that the law has been found to apply to insulator/metal contact as well, and difficult also to reconcile the findings of Cooke and Jewell-Thomas with those of Peterson and Wagner.

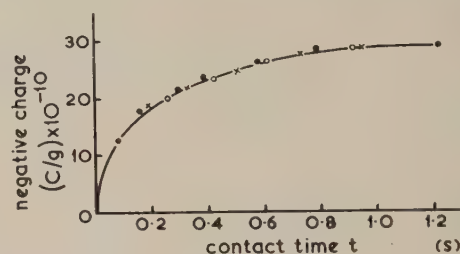
The law found by Cooke and Jewell-Thomas for particles sliding down a chute refers to the dependence of the charge acquired by given particles sliding down a given chute when the chute length and inclination are varied. The charge was found to depend only on the time it took the particles to descend the chute, different combinations of chute length and inclination that gave the same time of descent giving the same charge. That this was so for the semiconductor rutile may be seen from Fig. 1, taken from Donald's paper, in which charge is plotted against time of descent for different chute lengths and inclinations. The form of dependence of charge on time is established by Fig. 2, also taken from Donald's paper, in which $\log \{C_m/(C_m - C)\}$ is plotted against t , C_m being the maximum charge attained for $t = \infty$, and C the

charge at time t . It is seen that $\log \{C_m/(C_m - C)\}$ is proportional to t , from which it follows that

$$C = C_m \{1 - \exp(-t/T)\} \quad (1)$$

where T is a relaxation time.

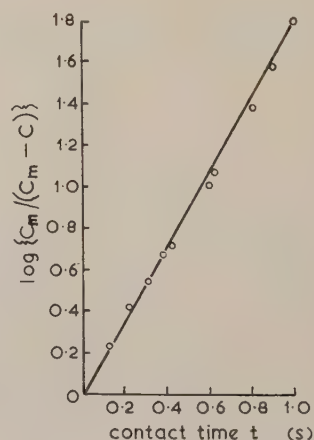
The law is the same as the law of the charging of a capacitor to which a potential is suddenly applied through a resistance.



[Reproduced by permission of Research]

Fig. 1. Charging of rutile for different chute lengths and inclinations

○ = 40° × = 35° ● = 30°



[Reproduced by permission of Research]

Fig. 2. Graph of function $\log \{C_m/(C_m - C)\}$ against contact time t for rutile 100/120 mesh on nickel chute, $R = 0.074$ in. ($C_m = 29.0 \times 10^{-10}$ C/g)

Cooke⁽⁸⁾ and Jewell-Thomas⁽⁹⁾ interpreted it somewhat differently, supposing there to be a steady transfer of charge to a capacitor, accompanied by a leakage current which balances the transfer when the maximum charge has been attained. The questions arise of whether charge is moved by mechanical transfer or because of the presence of a potential difference, what capacitor is being charged and what resistance is involved. By mechanical transfer is meant the movement of charge by forces that are not electrical, so that the movement is against the potential difference that is being built up, as in an electrostatic belt generator, in contradistinction to a current caused by a potential difference, which is in the direction of the potential difference. The situation is more complicated when the contact point moves about during the charging, and when varying potentials are introduced by the mechanical movement of charges. In discussing what mechanisms of charging may be involved in a particular experimental procedure, it is important to be clear about how each mechanism is supposed to work. In fact, there has been a muddling of models in the published literature.

Contact topography

Even when experiments are performed with optically polished surfaces, it is only an approximation to regard the surfaces as smooth. On the other hand, contact in which spiky protuberances on the one surface dig into the opposing surface must be uncommon in experiments on triboelectrification; asperities tend to be broken off or crushed. Contact "points" are likely to be rounded. Contact between spheres is a better mathematical approximation to typical contact between actual surfaces, than is contact between cone and plane. This consideration at once introduces a difficulty. If the surfaces become charged because of the existence of a potential difference between them, then the magnitude of the charge is proportional to the capacitance between the relevant parts of the surfaces at the instant of breaking contact. Classical electrical theory makes the capacitance infinite for the approximation of two spheres separating. It is therefore essential that any model that makes the charging dependent on a contact potential should be explicit about how this infinity is avoided. The author's theory⁽¹⁾ of the separation charging of metals avoided the infinity by allowing for the passage of electrons, across a small but finite gap between the surfaces, by tunneling through the potential barrier, as allowed by quantum mechanics. In consequence of this effect, electrical contact is not broken until the spheres have separated to a distance of the order of 10 \AA .* The capacitance is therefore finite. Moreover, though the gap is very small, the capacitance is not very large, because the infinity in question is a logarithmic one.

The problem of the infinity does not arise if the charge transfer is by ions which are moved by forces other than electrical ones, e.g. by diffusion, or if the charge is carried by the movement of matter in bulk, on however small a scale. When the charging is brought about by a potential difference, several factors must be considered which may operate to eliminate the infinity. Let us consider the possibilities.

(i) That it is wrong to use the approximation of two spheres; that the proper approximation is a cone on a plane. If this were so for the typical contact "point", it would

nevertheless be certain that contacts of the other sort would occur from time to time. If they did, they would give rise to occasional infinite charges, or at any rate occasional spuriously large charges. This has never been observed. We therefore continue to use the approximation of two spheres.

(ii) That the final stabilization of charge occurs when there is a finite gap between the spheres. This will always be the case when electrons take part, because they can tunnel through distances of an order of magnitude greater than molecular dimensions. It will also be the case if the potential difference causing charge separation is electrolytic in origin, and arises in a layer of adsorbed water. This is likely to happen at high humidities, but other considerations such as (iii) may be more important. The ability of an electron to penetrate a potential barrier is consequent on its small mass; a proton has the same chance of penetrating a barrier only if the barrier is $\sqrt{1837} = 42.86$ times thinner—since it is the root of the mass that is involved—and a heavier ion will penetrate only if the barrier is thinner still. Tunneling such as we are interested in is only possible for ions if the gap is a fraction of an Ångström unit. This, of course, also follows from the fact that an ionic crystal behaves as a solid, not as a fluid. We see that, as soon as the separation of the spheres is appreciable on the molecular scale, the tunneling of ions is negligible.

(iii) There will be a limit to the number of electrons or ions available to constitute the charge, and a limit to the number of states that they can occupy. In principle, these limitations are always present, but will be cared for if we use a model based on the quantum-mechanical theory of the solid state. In the case of metals, the consideration is over-ridden by the effect of tunneling, but it will clearly be important in the case of semiconductors. The author⁽⁷⁾ has given reasons for supposing that there are no empty levels on the surface of insulators, and that this is the reason why "electrophobic" insulators do not charge as a result of light contact with metals.⁽⁴⁾ The enormous charging of some "electrophilic" insulators found by the author,⁽⁵⁾ estimated at $8.7 \times 10^3 \text{ e.s.u./cm}^2$ for one set of experiments, should then be attributed to the transfer of positive ions.

(iv) Not only is there a limitation on the number of electrons that can be accommodated per unit surface area, there is a corresponding limitation on the charge per unit volume. A so-called surface charge is really a surface layer of charge of finite thickness. In the case of a metal the thickness is of molecular magnitude,⁽¹¹⁾ but for a poorly conducting semiconductor it will be very much greater.⁽¹²⁾ In this case, the classical conception of a sphere with a surface charge must be replaced by a sphere carrying a volume charge, the density of which falls off rapidly inwards from the surface. If the thickness of the layer of charge is small compared with the radius, such a sphere will behave like a somewhat smaller sphere carrying a true surface charge, and the capacitance of two semiconducting spheres in actual contact will be equal to that for two slightly smaller mathematical spheres with a small gap between them (with due allowance for the dielectric constant of the semiconductor). The capacitance will therefore be finite.

It is apparent that, to avoid getting into difficulties over contact topography, any proposed model should take some cognisance of whether the charge is represented by ions or electrons, what energy levels are available for them, and where the levels are localized. If this is done, the contact of spheres will be a reasonable representation of actual conditions.

* It is necessary to mention that the critical gap depends on the work function of the metals, since the author has been misquoted in this respect.

Hot spots

Two so-called flat surfaces in seeming contact actually touch at a few contact "points". When rubbed together, the work of friction appears as heat at these "points". Bowden and Tabor⁽¹³⁾ have shown that, with sufficiently vigorous rubbing, the resulting hot spots can attain a very high temperature. Donald⁽¹⁰⁾ is of the opinion that the results of Cooke and Jewell-Thomas that we are discussing have to do with the formation of hot spots, and the macroscopic transfer of material that is associated with the phenomenon. Loeb,⁽⁶⁾ however, is of the opinion that the generation of heat by friction is seldom involved in the transfer of charge. Frenkel⁽¹⁴⁾ has proposed an explanation of the triboelectrification of insulators which depends on the insulator becoming an intrinsic semiconductor where hot spots are formed. There is, in principle, a contact potential between an insulator and a metal, or between two insulators, but the contact potential is not established until a double layer of charge has been set up at the interface, to provide the potential discontinuity. In an insulator at room temperature, electrons available from the valency band cannot get into the empty levels in the conduction band, because they have insufficient energy to do so, and the double layer cannot form. The increase of temperature at the hot spots enables this to occur, and a charge transfer takes place to establish the contact potential. When the hot spot cools off, the charge is frozen in.

Frenkel uses the equation of heat conduction to derive an approximate formula for the temperature rise ΔT in the hot spot, when its lifetime is t and an amount of heat Q per unit area of hot spot is liberated during its life. Defining the specific heat per unit volume as c and the thermal conductivity as λ , his formula is

$$\Delta T = Q/\sqrt{(2c\lambda t)} \quad (2)$$

Frenkel then takes reasonable values for the numerical quantities occurring in the formula in order to demonstrate that a temperature rise of 1000° C can easily occur. In doing so, however, he substitutes the assumed value for the rate of generation of heat per unit area of hot spot for Q , whereas the formula requires the amount of heat generated during the assumed lifetime of 10^{-4} s. Correcting Frenkel's mistake makes the rise in temperature 10° C, which is negligible. This weakens the case for the theory so much that any applicability it may have must be confined to extremely vigorous rubbing.

It would seem unlikely that hot spots are formed when a powder flows down a chute, and indeed, Cooke,⁽⁸⁾ using the theory given by Bowden and Tabor,⁽¹³⁾ estimated the temperature rise for such a case to be a few thousandths of a degree if true metal to insulator contact is involved, or perhaps a tenth of a degree if the insulator makes contact with a less thermally conducting oxide film on the metal. In view of this estimate, and the numerical error in Frenkel's paper, we must reject the idea that hot spots play a significant part in the charging experiments that led to the empirical law that charge depends on time of descent only.

Contact potentials

The contact potential between two metals is the difference between their work functions; when it has become established, the tops of the filled energy levels in the two metals are adjusted to the same height, as shown in Fig. 3(a). Frenkel does not commit himself about what is levelled up in the

case of insulators, and it is difficult to decide from the writings on triboelectricity of other authors whether they suppose it to be the bottom of the conduction band as in Fig. 3(b), or the top of the valency band as in Fig. 3(c). It does not seem to be widely known that it should be the middle of the forbidden band that is levelled up, as in

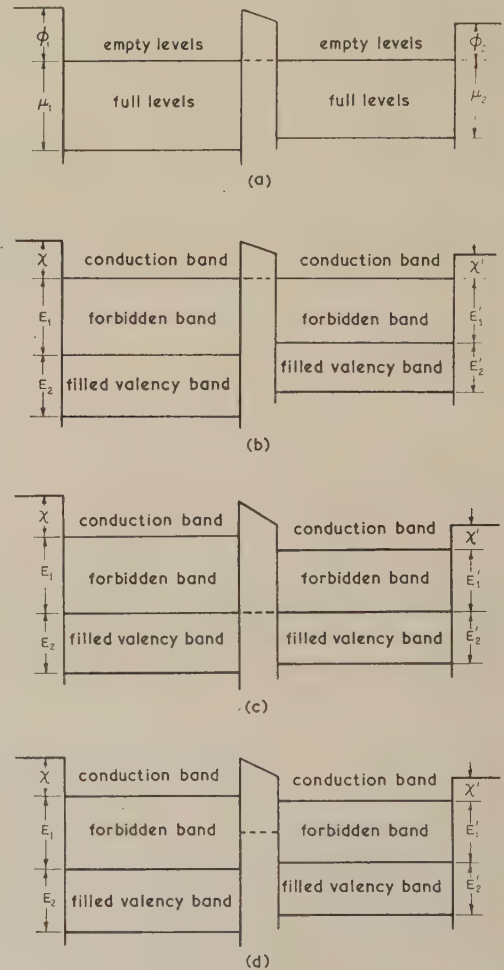


Fig. 3. Equilibrium conditions for contact

- (a) Metal/metal (correct)
- (b) Insulator/insulator (incorrect)
- (c) Insulator/insulator (incorrect)
- (d) Insulator/insulator (correct)

Fig. 3(d), though this was pointed out by Fowler⁽¹⁵⁾ in 1933. Fig. 3(a) represents two metals in equilibrium, and Fig. 3(d) two insulators in equilibrium. The contact potentials are therefore $\phi_2 - \phi_1$ and $(\chi' + \frac{1}{2}E_1') - (\chi + \frac{1}{2}E_1)$ respectively. But we have seen that the contact potential between insulators cannot establish itself under normal conditions of simple contact. As pointed out by Frenkel, the double layer giving rise to the potential discontinuity would take too long to form, and require too great a thickness of material to contain it, because the maximum permitted charge density in an insulator is vanishingly small.

A semiconductor is an intermediate case. If it is an intrinsic semiconductor, it is like an insulator in which the contact potential *can* become established. If it is an excess-semiconductor, with localized donor levels just below the conduction band, then a level halfway between the donor levels

and the bottom of the conduction band will become adjusted to the appropriate (Fermi) level in the other material. The contact between a metal and an excess-semiconductor is shown in Fig. 4(a). It is seen that the contact potential is slightly less than $\phi - \chi$, and the semiconductor behaves very like the insulators in Fig. 3(b). A deficit-semiconductor, with acceptor levels just above the valency band, will have

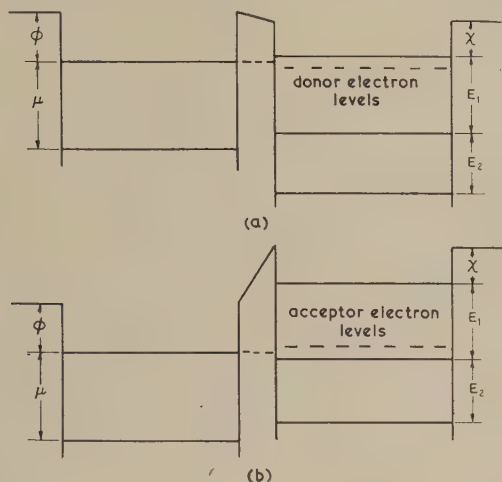


Fig. 4. Equilibrium conditions for contact

- (a) Metal/excess semiconductor (correct)
(b) Metal/deficit semiconductor (correct)

a contact potential slightly less than $\chi + E_1 - \phi$, behave rather like the insulators in Fig. 3(c) and adjust itself, when in contact with a metal, to the condition shown in Fig. 4(b).

In all cases where equilibrium has been established, a double layer must have formed which adjusts the potentials of the two materials so that the Fermi levels are the same in both. The Fermi level is such that lower levels are more likely to be filled than not, and higher levels less likely to be filled than not. The Fermi level is a hypothetical level when it occurs in a forbidden band, defined by the mathematical form of the distribution function.

Figs. 3 and 4 take no account of the effects that arise (above the absolute zero) when the density of conduction electrons is different in the two materials—the Seebeck effect in the case of metals. As the Seebeck potential for metals is small compared with the contact potential, it could be ignored in the author's theory of the charging of metals,⁽¹⁾ but this is not necessarily permissible for semiconductors, for which thermoelectric effects can be much greater than for metals. The readjustment of energy levels that occurs when a semiconductor is brought into contact with another semiconductor or a metal will be modified by secondary effects, owing to the difference in density of conduction electrons in the two materials causing a relative displacement of the Fermi levels; the secondary effects may be important if the rubbing is vigorous, so that the readjustment of energy levels occurs in a hot spot. When a protuberance on one surface is moved over a relatively smooth part of an opposing surface, it is the protuberance that gets really hot: the hot spot is on one surface only. The resulting temperature difference between the two surfaces will give rise to a potential difference which can result in a charge redistribution, even when the two surfaces are of the same material. What is a secondary effect with dissimilar materials then becomes the main effect with like materials, and moreover, if the two surfaces are strictly equivalent apart from the mechanics of

the rubbing process, it is the only electronic effect, as far as one can see, that could operate. This process may well be responsible for the charging observed by Henry⁽¹⁶⁾ in the asymmetric rubbing of synthetic polymers, since the rubbing was vigorous. It is a particular case of the more general explanation proposed by Henry^(17, 18) himself, which, however, was classical rather than quantum-mechanical in form.

Further complications arise if the electronic states on the surface are different from those in the interior. Just what effect these complications have on the simple picture of the formation of a double layer on contact will depend on the particular materials in question, and can only be determined by experiment on the materials used in the charging measurements. Unfortunately, such information is not available for the semiconductor rutile (titanium dioxide). We can assume, however, that when rutile makes contact with a metal, the relative position of the Fermi level in the metal is shifted to correspond to somewhere in the forbidden zone of the rutile considered as an insulator. The shift is likely to be of the order of magnitude of one volt.

Rutile

We are now in a position to give an explanation of the charging of rutile observed by Jewell-Thomas^(9, 10) as being due to the contact potential between semiconductor and metal. The rutile particle is rather like one electrode of a capacitor the other being the metal chute and the capacitance is charged by the contact potential as in the author's theory of the charging of metals⁽¹⁾ though there are important differences between the two cases. Of necessity the comparison between theory and experiment will be rough, accurate data not being available, but in principle no adjustable constants are involved, so an order of magnitude comparison is significant.

Rutile (titanium dioxide) has a specific gravity of 4.25, and assuming the particles used in the experiments of Cooke and Jewell-Thomas to have been spherical, they had a mean radius of 7.0×10^{-3} cm and a mass of 6.08×10^{-6} g so that there were 1.65×10^5 particles per gramme of powder. We may estimate the area of contact between the rutile particle and the nickel chute from the theory of the elastic deformation of a sphere against a plane, given by Hertz. In the form used by Bowden and Tabor,⁽¹³⁾ the formula for the radius of contact is

$$a = 1.1 \left\{ \frac{Fr}{2} \left(\frac{1}{E_1} + \frac{1}{E_2} \right) \right\}^{1/3} \quad (3)$$

in which F is the normal force, r the radius of the sphere, E_1 and E_2 the Young's moduli of the sphere and plane, and all are expressed in c.g.s. units. Taking Young's modulus for rutile to be 5.1×10^{12} dyn/cm² and for nickel 5.4×10^{12} dyn/cm², the radius of contact comes out to be 2.2×10^{-6} cm.

The radius of contact is small compared with the size of the particle. An electrical current flowing from the chute into the particle is therefore severely constricted at the contact, and the electrical resistance of the contact will determine the magnitude of the current. Since the resistivity of the rutile is many orders of magnitude greater than that of a metal, the contact resistance is that of a circular electrode of radius a , feeding current into a semi-infinite medium, the resistivity of which will be called ρ . This resistance is well known to be $\rho/4a$. When the particle first makes contact with the chute, the current flowing into the particle is equal

to the contact potential divided by the resistance, because no back voltage has yet been built up. A contact potential of one volt would therefore give an initial charging current of $4a/\rho$ amperes per particle. If the contact "point" changes, the current will still be $4a/\rho$ amperes until a back voltage develops. The initial charging rate found by Jewell-Thomas was 1.1×10^{-8} A/g, which is 6.7×10^{-14} amperes per particle. Using the value of a just calculated, the resistivity works out to be $1.3 \times 10^8 \Omega \text{ cm}$. If the particles were inhomogeneous, this would be an average value.

The resistivity of rutile was investigated by Cooke,⁽⁸⁾ who measured the resistance of the compressed powder in a tube. He found that the apparent resistivity varied with the compression, and concluded that the resistance he measured was that of the contact points between particles. Unfortunately he did not measure the compression, but one can easily see that the true resistivity must have been very much less than the apparent. If the compression was, for example, 1 kg/cm^2 , the formula already used predicts a radius of contact of almost exactly one hundredth of the radius of the particle. Compare now the resistance of a column of particles, strung like beads on the axis of an enveloping cylinder, with the resistance of the solid cylinder. If the radius of the particle is R , there will be $1/2R$ particles per unit length. There will also be this number of contacts per unit length, and each contact has a resistance of $\rho/4a$ each side of the contact. The resistance per unit length is therefore $\rho/4aR$. The resistance of the solid cylinder is $\rho/\pi R^2$. The apparent resistivity of the powder is therefore $\pi R/4a$ times the value for the solid. At 1 kg/cm^2 this ratio is $100\pi/4$. The apparent resistivity measured by Cooke was $2.4 \times 10^{10} \Omega \text{ cm}$. At 1 kg/cm^2 the true resistivity would have been $3 \times 10^8 \Omega \text{ cm}$. Since a is proportional to the cube root of the assumed compression, the value assumed is not very critical.

The resistivity required by the theory of the charging of spheres was $1.3 \times 10^8 \Omega \text{ cm}$, so the order of magnitude is in agreement, but the numerical value is wrong by a factor of just over two. There is good reason for not expecting the agreement to be exact, apart from not knowing the value of the compression in Cooke's experiment. The observed initial charging current is greater than the calculated; this would be explained if the actual contact area was greater than that calculated for the idealized case of sphere/plane contact, as, indeed, is to be expected. The initial charging current is therefore satisfactorily accounted for by the theory.

The semiconducting properties of rutile have been investigated by Breckenridge and Hosler,⁽¹⁹⁾ but the rutile they used was much more conducting than that used by Cooke and Jewell-Thomas. However, the mechanism of conduction was presumably not very different. Rutile is an excess (n-type) semiconductor, current being carried by electrons in the conduction band that have reached it from the donor levels by thermal excitation [see Fig. 4(a)]. The number of vacant donor levels is, of course, equal to the number of electrons that have been excited into the conduction band, N per cm^3 . It is reasonable to assume that the difference in conductivity between the rutile of Jewell-Thomas and that of Breckenridge and Hosler was due to a difference in N , the mobility of the charge carriers being the same. The mobility μ measured by Breckenridge and Hosler was about $1.0 \text{ cm}^2/\text{V s}$ for crystalline rutile, and $0.1 \text{ cm}^2/\text{V s}$ for rutile in ceramic form. The latter is probably more applicable to the rutile used in the charging experiments. Since the resistivity is given by $\rho = 1/Ne\mu$ where e is the electronic charge, one finds, from the value deduced for ρ , that $N = 4.8 \times 10^{11}$.

If the rutile had been positively charged by the metal, the space charge would have been carried by the ionized donor levels, the conduction band being denuded of electrons, in which case the space charge would be limited by the concentration of donor levels N . The resulting surface layer is then well known to have a thickness given by $\sqrt{(VK/2\pi Ne)}$, where V is the contact potential and K the dielectric constant. The dielectric constant of rutile has been measured by Schmidt,^(20, 21) and is very high. For rutile powder it is 114. From the assumed figures one finds that the thickness of a surface layer of (positive) charge is $1.6 \times 10^{-2} \text{ cm}$. This is rather greater than the diameter of a particle ($1.4 \times 10^{-2} \text{ cm}$). If the rutile had charged positively, then the particles would have been too small to accommodate the "surface layer".

In fact, the rutile charged negatively. The charge would therefore be carried by electrons in the conduction band. There are many more levels at the bottom of the conduction band to accommodate electrons than there are donor levels, though fewer than in a metal in which the vacant levels come half-way up a band. There will be a limitation on charge density for negative charging, but not nearly as severe as for positive charging. The thickness of the layer of surface charge will be between that for a metal and that for positive charging. The thickness depends on factors for which it is difficult to allow; rough calculations make it reasonable to assume that it will be between 10 and 100 Å, but, fortunately, the value is not critical.

The charge redistribution relaxation time in the semiconductor is $K\rho/4\pi$, which, for the present case, is just over a millisecond. This is short on the time scale of the charging experiments. It follows that the space charge will build up simultaneously over different parts of the surface, and the potential drop during charging will be confined to the neighbourhood of the current constriction at the point of contact. Furthermore, if the latter moves about, the surface charge can redistribute itself quickly enough to follow the movement. Such movement can, therefore, be ignored, and the particle will charge like a capacitor across which a potential is suddenly applied, and conform to the charging law found experimentally.

The saturation charge depends on the effective capacitance. We allow for the finite thickness of the "surface charge" by taking the equivalent sphere to be smaller than the actual particle; this has a negligible effect on the assumed radius, but introduces a gap between sphere and plane. The appropriate value for the gap is half the thickness of the charge layer; this is taken to be between 5 and 50 Å. There is also the effect of the dielectric constant to be allowed for. If we assume the effective depth of the charge layer below the true surface to be K times less than the above values, we shall overestimate the effect of the dielectric constant. It will be sufficient to take $5/114 \text{ Å}$ as a lower limit for the effective gap, and 50 Å as an upper limit. Choosing the same expression for the capacitance as was used in the author's theory for metals, we have, for a gap x between a plane and a sphere of radius R , a capacitance

$$R\{\gamma + \frac{1}{2} \log_e (2R/x)\} \quad (4)$$

in which $\gamma = \text{Euler's constant} = 0.5772$, and all lengths are in centimetres. Substitution of numerical values gives $6.4 \times 10^{-2} \text{ cm}$ and $4.0 \times 10^{-2} \text{ cm}$ as the upper and lower limits for the capacitance. It is, perhaps, surprising that these limits are so close together; mathematically, this comes from the gap occurring logarithmically in the formula for capacitance, and physically because the contribution to the

capacitance from the region of surface close to the contact is less important than one might think. It may be concluded that a mean value of 5×10^{-2} cm cannot be far from the true value.

Jewell-Thomas gives the saturation charge for rutile as 3.0×10^{-9} C/g, which works out at 5.5×10^{-5} e.s.u. per particle. For a contact potential of 1 V, the capacitance would be 1.7×10^{-2} cm. For a smaller assumed contact potential the capacitance would be greater. The estimated theoretical value is three times greater. It is, however, unnecessary to account for the discrepancy entirely in terms of a smaller contact potential. We have assumed perfectly maintained contact between sphere and plane to represent the actual contact conditions as the particles slide down the chute. This, obviously, is idealized: the particles will execute a jumping motion for at least part of the time. As a result, the effective capacitance will be reduced. In any case, one cannot expect precise numerical agreement, and it is clear that the discrepancy is no more than one would expect from an approximate treatment. This treatment has explained the initial charging current, the saturation charge and the form of the charging curve for rutile. The time constant is not an independent quantity.

The charging of semiconductors

Let us compare the explanation we have given for the charging of rutile with that for the charging of metals by light contact. Both arise from a flow of electrons setting up the contact potential by the formation of a double layer astride the interface. In the case of metals the double layer is established almost instantaneously and its thickness is of molecular dimensions, but in a semiconductor the thickness may be comparable with the size of the particle charged, and the time required comparable with the duration of an experiment. Current can pass between the two surfaces by quantum-mechanical tunnel effect if the surfaces are separated by less than a certain critical gap. In consequence, two metals separated by less than the critical gap, or in contact, at once adjust the double layer so that the potential difference between them is equal to the contact potential. When separated to more than the critical gap, their charges remain constant if they are insulated, instead of their potential difference. If, however, one half of a double layer resides in a semiconductor, it is necessary for electrons to flow into a thickness of semiconductor comparable with the now considerable thickness of the "surface" charge, before the double layer can become partly, or fully, established. This process is relatively slow, and prevents appreciable transfer of charge by tunnel effect during the short time this is operative if the surfaces are brought into contact and then quickly separated. For a semiconductor to become charged by electron transfer, relatively long contact is required. When contact is broken, tunnel effect is operative for too short a time for there to be any appreciable loss of charge. This is because the charge is not resident on the surface. In the case of metals, the surface charge adjusts itself adiabatically, so long as tunnel effect permits it to do so, and the final charge is that at tunnel cut-off when the critical gap is reached during separation. For this reason, the author called the form of charging that occurs with metals "separation charging". By contrast, semiconductor charging is *contact* charging.

It is of interest to calculate what the charge on the particles in Jewell-Thomas's experiment would have been if the particle had been metallic instead of semiconducting, and

the contact potential 1 V. The author's theory⁽¹⁾ gives the charge in e.s.u. as

$$\frac{(\phi_1 - \phi_2)R_1R_2}{300(R_1 + R_2)} \left\{ 1.151 \log_{10} \frac{R_1R_2}{R_1 + R_2} + \zeta \left(\phi, \frac{\eta\sqrt{a}}{M} \right) \right\} \quad (5)$$

in which the contact potential is the difference between the work functions ϕ_1 and ϕ_2 , R_1 and R_2 are the radii of the two contacting spheres in centimetres, and ζ is a function plotted in Fig. 8 of Ref. 1. For $\phi = 5$, which will refer to metals with an oxide surface film, and for laboratory conditions, $\zeta \simeq 9$. We also have $R_1 = 7.0 \times 10^{-3}$ and $R_2 = \infty$. Substituting these values gives the separation charge as 1.5×10^{-4} e.s.u. This is nearly three times the observed value of 5.5×10^{-5} e.s.u. for rutile. A greater charge for metals than for semiconductors is to be expected, because the critical gap for $\phi = 5$ works out at 12.7 \AA , which is smaller than the thickness of the "surface" charges one expects with semiconductors. The capacitance at cut-off with metals is therefore greater than any effective capacitance for a "surface" charge on a semiconductor.

Insulators

Consider now what the model of the charging of a semiconductor predicts as the conductivity becomes less, in other words as the semiconductor behaves more like an insulator. The initial charging current will be proportionately less. The resistivity of the rutile we have been considering was $10^8 \Omega \text{ cm}$, whereas the resistivity of a good insulator⁽²²⁾ is in excess of $10^{16} \Omega \text{ cm}$. If the greater resistivity is entirely due to a lower electron density, this is at least 10^8 times smaller in the insulator than in rutile. An initial charging current 10^8 times less than for rutile, for which the contact charging relaxation time was 0.26 s , would necessitate an impossibly long time for the saturation charge (or a charge comparable with that found on rutile) to be reached. Furthermore, insulators cannot, in general, accommodate a negative space-charge in the conduction band as we suppose happens in the case of rutile; the charge density is therefore limited to a value comparable with the density of conduction electrons. In the case of rutile, we saw that such a limitation would have made it hardly possible to fit the "surface" layer into the rutile particle; for a charge density 10^8 times less, the layer would be 10^4 times thicker and, for this reason also, could not form, there being far too little room for it. The saturation charge would therefore become less as a semiconductor became more like an insulator, even if it had time to build up, which it has not. The model expands in time and space when the semiconductor becomes less conducting than rutile, so that it puts itself "out of court" as far as good insulators are concerned. Frenkel⁽¹⁴⁾ was the first to point this out.

All this makes it surprising that Cooke and Jewell-Thomas found the initial charging current for the insulator zircon to be of the same order of magnitude as for the semiconductor rutile, and the charges for short times to be comparable, with the charge on zircon continuing to increase when that on rutile had already reached a saturation value. The explanation we have given for the charging of rutile makes it quite clear that we must look for a different explanation for zircon, but the explanation must still give the same form of dependence of charge on time, as well as charging rates of the same order of magnitude. There is such an alternative.

Good insulators, other than synthetic polymers and a few

others, normally have a surface conductivity which, though small, greatly exceeds their volume conductivity and makes the latter difficult to measure.⁽²²⁾ The surface conductivity appears to be associated with the presence of moisture, though not very dependent on the relative humidity when this is below 40%, as it was in the experiments of Cooke and Jewell-Thomas. For reasonably clean surfaces, the meagre information available covers surface resistivities ranging between 10^{13} and $10^{15} \Omega$. If the surface resistivity is represented by σ , we assume the resistance across a rectangle of length l , and breadth b , to be $\sigma l/b$. The resistance between the inner and outer perimeters of an annulus of internal and external radii r_1 and r_2 respectively is

$$\int_{r_1}^{r_2} \frac{\sigma dr}{2\pi r} = \frac{\sigma}{2\pi} \log_e \frac{r_2}{r_1} \quad (6)$$

The contact resistance for a circle of radius a feeding current into a semi-infinite volume was inversely proportional to a , but when it is feeding current into a surface we see that the resistance depends logarithmically on a , so the value of a is not very critical, nor is that of the distance to the boundary to which the current is going. For an order of magnitude calculation let us put $r_2 = 7.0 \times 10^{-3}$ cm (the radius of the rutile particles), $r_1 = 2.2 \times 10^{-6}$ cm (the radius of contact for rutile), and $\sigma = 10^{13} \Omega$. The resistance proves to be $1.3 \times 10^{13} \Omega$, so 1 V would give an initial charging current of the order of magnitude of 10^{-13} A, which is the order of magnitude we are looking for. We see now that, if we replace a volume resistivity of $10^8 \Omega \text{ cm}$ for rutile, by a surface resistivity of $10^{13} \Omega$ for zircon, but otherwise retain the model, we predict initial charging currents of the same order of magnitude in both cases.

We still predict that there will be no charging if the surface resistivity is very high, as is the case for synthetic polymers such as polystyrene. This is in accordance with the author's discovery that hydrophobic insulators are electrophobic, giving no charge from light contact with metals,⁽⁴⁾ but indicates that we must look for a quite different explanation of the charging of clean electrophilic insulators. In the meantime let us continue with the assumption that there was a significant electrolytic layer present on the insulators that behaved like rutile.

We have invoked a form of electrolytic conduction to account for the charging current being able to flow, so it is logical to assume that the potential driving it was also electrolytic in origin—and, indeed, there seems to be no alternative to this.* Without being precise about the possible sources of an electrolytic potential at a metal/insulator interface in the presence of an electrolyte, it may be taken for granted that there is no difficulty in accounting for a potential of the order of 1 V in this way.

There remains the question of just what capacitance is charged by the charging current. This, it would seem, should be the capacitance between the surface of the particle and the chute. How, then, do we eliminate the unwanted infinity? Almost certainly, a severely limiting factor would be the diffusion of ions away from the contact "point", so preventing a large charge from building up there. But if, subject to some limitation of this kind, the charge *can* be carried by electrolytic ions, then it is to be presumed as a

first approximation that the particle will be charged like a capacitor, of capacitance comparable with its radius, through a resistance, and in consequence that the charge will increase with time in the way it does with a semiconductor. It is therefore possible that the experiments on zircon are to be explained by such a model, but other experiments of Cooke on small glass spheres prepared according to different procedures cannot be so explained, because two specimens which had the same initial charging rate were found to have surface resistivities differing by three orders of magnitude. The glass spheres, however, did not conform to the law of charge being a function of time of descent only.

Charge densities on insulators

The observed charge density on rutile reached a maximum of 9×10^{-2} e.s.u./cm². A metal with the same contact potential would have charged about three times as much. Zircon was not very different from rutile. These charge densities are low; the particles could have carried a far greater charge without losing it by corona discharge. Medley⁽²³⁾ has obtained a charge density of 500 e.s.u./cm² on polythene, the charge being stabilized by proximity to an earthed conductor. The author⁽⁵⁾ estimated the local charge density at single "point" contact in experiments on clean quartz to be in the region of 10^4 e.s.u./cm², and pointed out that there would be no stray ions in the small region of high field to start a gas discharge.

Now whereas the rutile required a time of the order of a second to become charged, the transfer of charge in the author's experiments on quartz was, by comparison, instantaneous. It was not a case of waiting for a capacitance to become slowly charged, as with the rutile, though the charge did spread over the surfaces after they had been separated. It must be supposed that with the two surfaces in juxtaposition, the electric fields tending to spread the charge were relatively low, and the surface behaved as an insulator, but that when the opposing charges were separated, the fields became so much higher that conduction along the surfaces occurred. This behaviour is quite different from that which we have seen to account for the charging of a semiconductor. It seems⁽⁷⁾ that it should be attributed to the mechanical transfer of loosely bound positive ions. This form of charging will not, however, account for the behaviour of zircon. If the transfer of charge is instantaneous, and proportional to the number of contact "points" that have been made and broken, but the accumulation of charge is limited by back discharge, then we should expect the forward transfer to be proportional to the length of the chute and the loss of charge to be dependent on the time of descent, being greater for a slower descent. This would mean the resulting charge would decrease with increasing time of descent for a given chute length, whereas for zircon, as for a semiconductor, it increased. In general, we would expect an increase in speed to favour charging by mechanical transfer of ions, but to reduce charging due to currents from contact potentials, other things being equal.

The charging characteristics to be expected from mechanical transfer have been found by Peterson⁽²⁾ and Wagner,⁽³⁾ in experiments on the rolling of insulating spheres on metal surfaces. The experimental results were explained in terms of a model as follows. As the sphere rolls, contact is continuously made and broken. There is a mechanical transfer of charge proportional to the area that has made contact for the first time. This assumption is not quite the same as that made in the last paragraph, but leads to the same shape of

* The alternative of a hot spot permitting the establishment of the contact potential, suggested by the author in a lecture to the Non-destructive Testing Group of The Institute of Physics on 22 May, 1959, must now be withdrawn, in view of the mistake in Frenkel's paper.

charging curve with different constants. As the charged area moves away from the metal surface, relatively large voltages are developed due to a decrease of capacitance. This gives rise to a return current to the metal, opposing the charging. As more of the surface becomes charged, more current returns to the metal, ultimately balancing the charge transfer which is getting less, and a saturation charge is reached. It should be noted that this model postulates an actual charge transfer which decreases with time, from which must be subtracted an actual return current which is proportional to the charge already transferred, the former resulting from the movement of the ball and the latter from surface conduction. Neither would occur with pure sliding: only the contact "point" would become charged. In this respect the model is quite different from the model for semiconductors. Nevertheless, it gives the same form of dependence of charge on time for a given speed, but, unlike the semiconductor model, makes the current proportional to the speed; that is, to the distance covered in a given time. The experiments of Cooke and Jewell-Thomas are therefore incompatible with this model. The charge transfer obtained by Wagner, estimated on the same basis as for the author's experiments on quartz, was of the order of 10 e.s.u./cm^2 . This compares with 10^4 e.s.u./cm^2 in the author's experiments, and $10^{-1} \text{ e.s.u./cm}^2$ in those of Cooke and Jewell-Thomas.

Discussion

The orders of magnitude just quoted come from different insulators tested in different ways, but, even so, the extent of the difference is remarkable. In all cases the surfaces were clean, at least on ordinary laboratory standards. Additionally, the author used the refinements of solvent cleaning, and Wagner the refinements of high-vacuum technique. Cooke and Jewell-Thomas were concerned with reproducibility, rather than with cleaning the natural minerals in which they were interested. It should be realized that "cleaning" is often a misnomer. Baking in a high vacuum serves the purpose of removing volatile and decomposable contaminants, but refractory contamination is baked on. A suitable choice of solvents may dissolve all the original contamination, but, when the last solvent is water, hydroxyl groups may become attached to the surface and a monomolecular layer of water be left which is firmly attached. "Cleaning" a surface should be thought of as *preparing* it in a particular way. It would seem that different ways of preparing a surface can give widely differing charging properties, without contamination in the ordinary sense being necessarily present.

Loeb⁽⁶⁾ has criticized the author's experiments on quartz, on the grounds that the surfaces were patchy, but without admitting that no other experimenter has used sufficiently fine discrimination to reveal whether such patches were present or not, since their methods carried out a continuous averaging. In any case, the enormous charging found by the author only appeared after scrupulous cleaning, and disappeared if the surfaces became contaminated with a monomolecular layer of grease, so it must have been the clean, not the dirty patches that gave the large charging observed. The

amount of charging observed by Peterson and Wagner was, by comparison, so small that the author would have said in his own experiments that the charging had disappeared! Since this did happen when the quartz was accidentally contaminated, it may be that the surfaces used by Peterson and Wagner were similarly contaminated. Loeb confesses that trouble was experienced by Peterson from contamination due to sputtering, but it is difficult to assess how clean the method of preparation used by Wagner would leave the surfaces. What, then, is to be said about Cooke and Jewell-Thomas's charging, that Peterson and Wagner would have considered negligible, but which is still sufficiently large to form the basis of an industrial method of mineral separation? We do not yet know enough about insulators to answer such questions at this time.

Acknowledgement

I am indebted to Mr. D. F. Gibbs for pointing out several features of these charging problems that I had not fully appreciated, and for help in elucidating the implications.

References

- (1) HARPER, W. R. *Proc. Roy. Soc. A*, **205**, p. 83 (1951).
- (2) PETERSON, J. W. *J. Appl. Phys.*, **25**, p. 907 (1954).
- (3) WAGNER, P. E. *J. Appl. Phys.*, **27**, p. 1301 (1956).
- (4) HARPER, W. R. *Proc. Roy. Soc. A*, **218**, p. 111 (1953).
- (5) HARPER, W. R. *Proc. Roy. Soc. A*, **231**, p. 388 (1955).
- (6) LOEB, L. B. *Static Electrification* (Berlin: Springer, 1958).
- (7) HARPER, W. R. *Phil. Mag. Suppl.*, **6**, p. 365 (1957).
- (8) COOKE, B. A. Ph.D. Thesis (University of London, 1954).
- (9) JEWELL-THOMAS, S. R. C. Ph.D. Thesis (University of London, 1957).
- (10) DONALD, M. B. *Research*, **11**, p. 19 (1958).
- (11) MROWKA, B., and RECKNAGEL, A. *Phys. Z.*, **38**, p. 758 (1937).
- (12) DARROW, K. K. *Research*, **7**, p. 46 (1954).
- (13) BOWDEN, F. P., and TABOR, D. *The Friction and Lubrication of Solids* (Oxford: University Press, 1950).
- (14) FRENKEL, J. *J. Phys. U.S.S.R.*, **5**, p. 25 (1941).
- (15) FOWLER, R. H. *Proc. Roy. Soc. A*, **141**, p. 56 (1933).
- (16) HENRY, P. S. H. *Brit. J. Appl. Phys., Suppl. 2*, **4**, p. 31 (1953).
- (17) HENRY, P. S. H. *Brit. J. Appl. Phys., Suppl. 2*, **4**, p. 6 (1953).
- (18) HENRY, P. S. H. *J. Text. Inst.*, **48**, p. P5 (1957).
- (19) BRECKENRIDGE, R. G., and HOSLER, W. R. *Phys. Rev.*, **91**, p. 793 (1953).
- (20) SCHMIDT, W. *Ann. Phys. (Leipzig)*, **9**, p. 919 (1902).
- (21) SCHMIDT, W. *Ann. Phys. (Leipzig)*, **11**, p. 114 (1903).
- (22) CURTIS, H. L. *Bureau of Standards Bulletin*, **2**, paper S. 234 (1914).
- (23) MEDLEY, J. A. *Brit. J. Appl. Phys., Suppl. 2*, **4**, p. 28 (1953).

Rolling-sphere viscometer for structured liquids

by G. W. SCOTT BLAIR, M.A., D.Sc., F.R.I.C., F.Inst.P., and J. C. OOSTHUIZEN, B.Sc.,* National Institute for Research in Dairying, University of Reading

[Paper received 18 February, 1960]

Abstract

In the apparatus described, since the sphere is very small compared with the cylindrical tube containing the sample, fresh channels can be found for quite large numbers of tests. In this way measurements are made on hitherto unsheared material, and this is important in studying thixotropic or otherwise structured systems. The instrument may be used even when inertia effects are considerable since, over a wide range of experimental conditions, a very simple correction of the Oseen type is found to apply.

Relative viscosities of glycerine-water mixtures and of fat-free milks determined in the sphere viscometer agree adequately with those from an Ostwald or other capillary viscometer; but the structure of renneted milk, even before rigidity sets in, is damaged by the drastic shearing and, for such systems, the rolling-sphere viscometer gives a more reliable picture of viscosity changes.

Introduction

IN studying slightly thixotropic, or otherwise structured systems, it is often advantageous to use a method for measuring viscosity or apparent viscosity in which the force-flow relation can be frequently determined on material which has not already been sheared. In all the usual viscometers, either the greater part of the material is continually sheared or, as in the case of a rolling sphere which almost fills the cross-section of a cylindrical tube, only a single shear can be given on hitherto unsheared material. This type of viscometer will not be considered in the present paper.

The falling-sphere viscometer is inconvenient because, to meet the above requirements, the spheres must be dropped in a series of carefully separated positions, and this is not easy to do.

The changes which take place in the viscosity of milk or of casein solutions under the influence of rennin and similar enzymes before any rigidity appears, have been determined by a number of workers (Bendixen,⁽¹⁾ Tapernoux and Vuillaume,⁽²⁾ Söhngen, Wieringen and Pasveer,⁽³⁾ Tewes,⁽⁴⁾ Christensen⁽⁵⁾, Tsugo and Yamauchi⁽⁶⁾). These authors variously report progressive increases, progressive decreases and decreases followed by increases in viscosity; a situation which is unsatisfactory in view of the potential usefulness of viscosity studies in investigating the nature of the action of enzymes on casein. (This aspect of the subject will be discussed elsewhere.) However, they all used drastic methods for measuring viscosity: capillary, concentric cylinder or "sinker" viscometers, which, by continuously shearing the whole or most of the sample, would be expected to interfere seriously with processes involving any association of protein molecules which may precede gelation.

The best method would appear to be to measure the speed of rolling of a sphere down an inclined cylindrical tube, having a diameter much larger than that of the sphere, and to rotate the tube through a small angle between the runs so that fresh material is used for each test, or at least quite long periods for recovery are allowed. The tube, diameter 1.8 cm, is enclosed in a jacket through which water is circulated at the required temperature (32° C for these experiments).

Very little has been published on the theory or use of viscometers of this kind. Block,⁽⁷⁾ using a ratio of tube to sphere diameters of 1 : 32, explains some very complex data by assuming a slippage between the surface of the sphere and the liquid. He is criticized by Burwell,⁽⁸⁾ who does not believe that this slippage is possible and accuses Block of failing to allow for inertia effects. Block,⁽⁹⁾ in his reply, quotes a large number of papers on the use of the rolling-ball viscometer for studying the effects of pressure on viscosity of liquids, but claims that only three of them, those of Flowers,⁽¹⁰⁾ Hersey⁽¹¹⁾ and Höppler,⁽¹²⁾ study the behaviour of the instrument itself. He claims that, in using Oseen's modification of Stokes's original treatment, he "takes into (partial) account the effect of the inertia of the liquid, which Stokes neglected". No further relevant work would seem to have been published since that of Block.

Reviewing briefly the papers quoted by Block, the usefulness of the rolling-sphere viscometer was first pointed out by Flowers, but for rather viscous liquids in which metal balls could be used. Flowers deplored the prevalent use of orifice viscometers such as were and still are common for testing oils, and he concluded: "The use of present flow-type viscometers should be discontinued. The sphere and tube type of viscometer may be used for comparisons of absolute viscosity over a wide range with a moderate error." Flowers used a sphere with a diameter about half that of the tube. Hersey gave a dimensional analysis of such a viscometer but, from our own experimental results we conclude that for our problems, his treatment is needlessly complicated. Moreover, he was mainly concerned with experiments under high pressures.

Höppler showed that the maximum speeds were reached when the ratio of diameters of tube to sphere is about 1 : 73; but in the viscometer which he described, the ratio is much nearer to unity and he was generally concerned with liquids of rather high viscosity. Our own experiments, therefore, follow closely on those of Flowers, except that for all but the highest viscosities, we have used Nylon (obtainable from Insley Industrial Supply Co., London) and not metal spheres.

The difference in density between the sphere and the sample is sometimes very small, and care must be taken to ensure that it does not become so slight as to lead to serious errors. In such cases, stainless steel spheres are used, the relative viscosities being determined by comparison with a

* Permanent address: Glen College of Agriculture, Orange Free State, Union of South Africa.

glycerine-water mixture, the viscosity of which is known, since steel balls do not give reliable data for water, the difference in density being too large.

Following the earlier work of Coulomb, Flowers developed a simple equation to relate the force of resistance to the ball (F) to the velocity (v). The manner in which he wrote this equation was slightly confusing and we have therefore modified it to read:

$$F = A\eta v + B\rho_1 v^2 \quad (1)$$

where ρ_1 is the density of the liquid, η is viscosity, A is a constant with dimensions (L), and B is a constant with dimensions (L^2). This equation implies a curvilinear relation between v and $\sin \theta$ where θ is the angle of tilt. But, if we know the value of B , the viscous resistance F_η , which is $A\eta v$, will be given by the total resistance minus the inertia term.

$$F_\eta = \frac{4}{3}\pi r^3(\rho_b - \rho_1)g \sin \theta - B\rho_1 v^2 \quad (2)$$

where r is the radius and ρ_b is the density of the sphere.

Flowers did not make any attempt to evaluate his inertia term and tried to work at velocities at which it was negligible. The constant B must have the dimensions of an area. Though analogous to Oseen's inertia correction for the freely falling sphere, it is unlikely to bear the same relation to the radius of the sphere. Since it seemed likely that B would be at least of the same order of magnitude as $\frac{1}{2}\pi r^2$, we first tried equating it to this value. Provided that the difference in density between sphere and liquid is not unreasonable, and the velocities are not too high (equal to or less than 3 cm/s), this gives remarkably good results. At higher velocities, B becomes greater than $\frac{1}{2}\pi r^2$.

Experimental results

Fig. 1 shows curves plotting F_η versus v for a series of mixtures of glycerol and water, and Fig. 2 shows similar curves for fat-free milk and water mixtures.

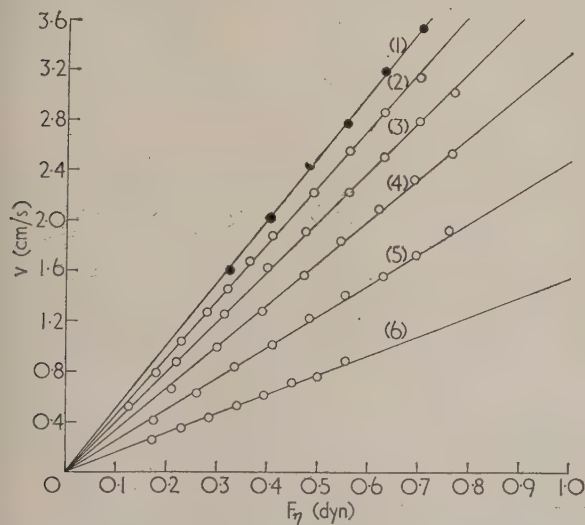


Fig. 1. Velocity against viscous resistance for glycerine-water mixtures

● = steel sphere, diameter = 0.100 cm, $\rho = 7.64 \text{ g/cm}^3$
○ = Nylon sphere, diameter = 0.3175 cm, $\rho = 1.1618 \text{ g/cm}^3$
Curve 1, 30% glycerol in water; curve 2, water; curve 3, 5% glycerol in water; curve 4, 10% glycerol in water; curve 5, 20% glycerol in water; curve 6, 30% glycerol in water

For the more viscous samples, the inertia correction becomes very small and not very accurate.

By comparing the slopes of the F_η versus v curves for the sample and for water, a relative viscosity can be immediately

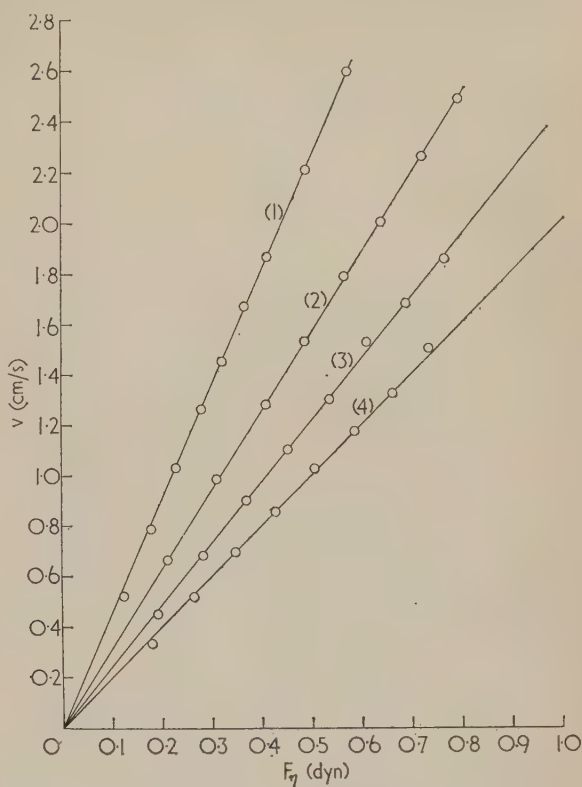


Fig. 2. Velocity against viscous resistance for a series of reconstituted fat-free milk samples

Curve 1, water, $\rho = 0.9951 \text{ g/cm}^3$; curve 2, reconstituted milk, $\rho = 1.0212 \text{ g/cm}^3$; curve 3, reconstituted milk, $\rho = 1.0394 \text{ g/cm}^3$; curve 4, reconstituted milk, $\rho = 1.0501 \text{ g/cm}^3$

obtained without having to make any assumptions about the magnitude of the constant A in equation (1). These relative viscosities can then be compared with those derived from an Ostwald viscometer or better, since some of the more concentrated samples are not quite Newtonian, from the U-tube capillary viscometer described by one of us (Scott Blair⁽¹³⁾). In this viscometer, a horizontal capillary tube is sealed on to wider tubes at each end and these are bent upwards into a vertical position. The liquid is sucked up one of the arms and then allowed to fall, the meniscus being followed on a scale. Negative logarithmic head is plotted against time and straight lines passing through the origin indicate Newtonian behaviour. The viscosity is calculated from their slopes. Small deviations from Newtonian behaviour can often be expressed in terms of the exponent of a log-log plot of these curves.

Fig. 3 shows a typical curve for fat-free milk, which is seen to be virtually a true fluid, and another curve for whole milk, which shows slight non-Newtonian behaviour.

Concentrated fat-free milk was diluted so as to give a series of samples having a range of relative viscosities both greater and less than that of natural fat-free milk (approximately 1.6). The relative viscosities calculated from the rolling sphere after correcting for the B term are plotted, in Fig. 4, against the corresponding values from the Ostwald viscometer. It is evident that, correcting for inertia losses

on the assumption that $B \simeq \frac{1}{2}\pi r^2$, the slopes of the F_η versus v curves give reliable and reasonably accurate values for relative viscosity. This makes it justifiable to assume

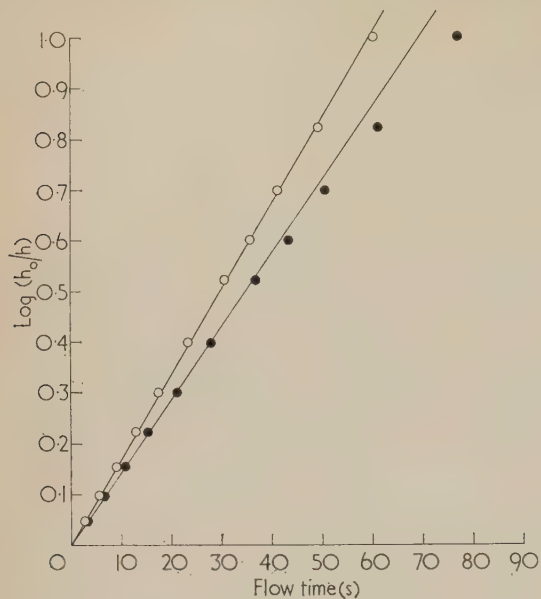


Fig. 3. Milk samples in Scott Blair U-tube viscometer

○ = fat-free milk
● = whole milk

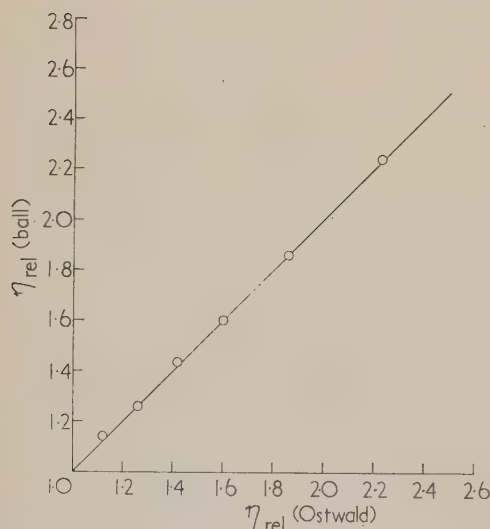


Fig. 4. Comparison of relative viscosities with Ostwald viscometer and sphere viscometer for fat-free samples of reconstituted milk at various concentrations

that, for renneted milk, when capillary viscometer data may not be reliable, relative viscosities determined in the rolling-sphere viscometer truly represent changes which take place when the system is undisturbed by shearing. Data on milk containing fat are less satisfactory.

Data showing the changes in viscosity with time, after addition of rennet, are shown in Fig. 5 and it is clear that there is at first a well-defined fall in viscosity, followed by an increase before the onset of rigidity stops the sphere altogether. In this particular experiment, the effect of shearing in an Ostwald viscometer is to diminish the viscosity

during the later stages when viscosity is rising. In some other experiments, where the structure is even weaker, the initial fall is over-emphasized by the shearing. It is possible to vary the composition of the mixture of rennet and milk in such a way as to maximize or minimize these effects. Further data on renneted milk will be published elsewhere.

It is felt that the method may well prove useful for viscosity measurements in other liquids of low viscosity, which may have a sensitive structure liable to be destroyed temporarily (thixotropy) or permanently by shearing.

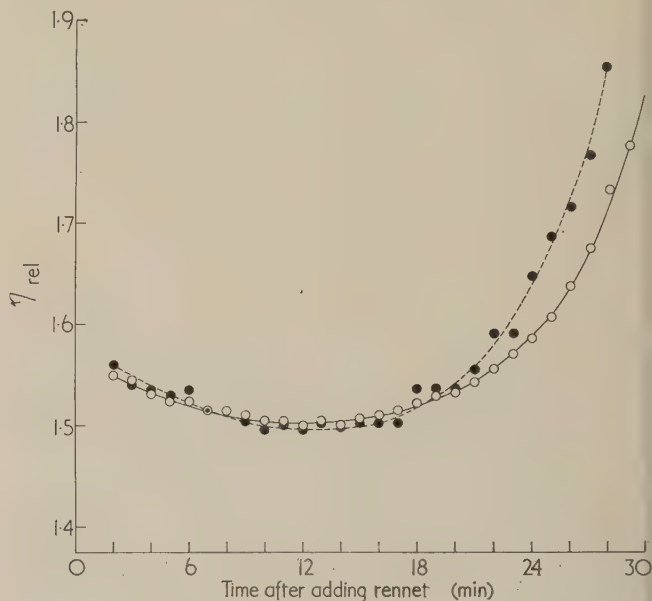


Fig. 5. Relative viscosity of renneted milk before onset of rigidity

● = rolling sphere viscometer
○ = Ostwald capillary viscometer

Acknowledgements

We are grateful to Dr. G. H. Lean of the Hydraulics Research Station and to Prof. J. M. Burgers for helpful discussions and correspondence. One of us (J. C. O.) is indebted to the South African Department of Agricultural Technical Services for a grant.

References

- (1) BENDIXEN, H. A. *Proc. 20th Ann. Meeting W. Divn. Amer. Dairy Sci. Assocn.*, p. 72 (1934).
- (2) TAPERNOUX, A., and VUILLAUME, R. *Lait*, **14**, p. 449 (1934).
- (3) SÖHNGEN, N. L., WIERINGEN, K. T., and PASVEER, A. *Receuil Trav. Chim. Pays-bas.*, **56**, p. 280 (1937).
- (4) TEWES, G. *Biochem. Z.*, **323**, p. 119 (1952).
- (5) CHRISTENSEN, L. R. *Arch. Biochem. Biophys.*, **53**, p. 128 (1954).
- (6) TSUGO, T., and YAMAUCHI, K. *Proc. 14th Intern. Dairy Congr. (Rome)*, **2**, p. 588 (1956).
- (7) BLOCK, R. B. *J. Appl. Phys.*, **11**, p. 635 (1940).
- (8) BURWELL, J. T. *J. Appl. Phys.*, **12**, p. 257 (1941).
- (9) BLOCK, R. B. *J. Appl. Phys.*, **13**, p. 56 (1942).
- (10) FLOWERS, A. E. *Proc. Amer. Soc. Test. Mater.*, **14**, p. 565 (1914).
- (11) HERSEY, M. D. *J. Washington Acad. Sci.*, **6**, p. 525 (1916).
- (12) HÖPLER, F. *Z. Tech. Phys.*, **14**, p. 165 (1933).
- (13) SCOTT BLAIR, G. W. *Biochem. J.*, **35**, p. 267 (1941).

Observations of the magnetization reversal process in thin films of nickel-iron, using the Kerr magneto-optic effect*

by M. PRUTTON, Ph.D., Research and Design Division, International Computers and Tabulators Ltd., Stevenage, Herts.

[Paper first received 21 January, and in final form 27 April, 1960]

Abstract

Observations of the magnetization reversal process in uniaxial thin films of nickel-iron about 1500 Å thick are reported. The experimental techniques used involve the comparison of measurements made in a Kerr magneto-optic apparatus, with the 400 c/s hysteresis loops taken with the pick-up loop both along and at right angles to the applied field. The results suggest that the magnetization reversal process in a film orientated with its easy axis at an oblique angle to the applied field occurs in three stages:

- (i) *coherent rotation until the angle is reached where a discontinuous jump in the orientation of the magnetization is expected to start;*
- (ii) *domain nucleation and growth from this angle to the angle where the jump should finish;*
- (iii) *coherent rotation until the magnetization lays along the field. The way in which some actual films differ from this model is discussed.*

Introduction

THE colloidal suspension technique is well established as a method of revealing the domain boundaries in the surfaces of ferromagnetic materials, but it has several distinct disadvantages if used alone in the study of the magnetization reversal process in thin ferromagnetic films:

- (i) it gives little information about the direction of the magnetization within the domains themselves;
- (ii) in the case of new types of domain boundary which are not associated with surface distributions of magnetic poles (such as the Néel wall), the powder may not indicate the presence of a boundary at all;
- (iii) it is difficult to use in dynamic experiments where domain walls are made to move;
- (iv) there is a possibility that there may be an interaction between the colloid particles and the film in such a way as to modify the domain structure in the film.

Use of the Kerr magneto-optic effect overcomes most of these disadvantages in that it is an inertialess method, which gives the direction of magnetization within a domain, and the existing domain pattern is not altered because of the interaction between the polarized light and the material.

Unfortunately, the effect is so small that contrast between adjacent domains is low, and high magnifications cannot be used. Therefore, the Kerr magneto-optic effect is most useful when employed in conjunction with the powder

technique, the latter to give detailed knowledge of the boundary regions and the former to give information about the direction of magnetization within a domain.

This paper is concerned with the use of the Kerr effect to investigate the magnetization reversal process in thin films of nickel-iron, as the first part of such a general study of the reversal process in thin films.

The problem

The films discussed in this paper were prepared by evaporation from an ingot of 81.19 nickel-iron on to glass substrates heated to 350°C.⁽¹⁾ They were deposited in the presence of a uniform magnetic field of 80 oersteds until they were about 1500 Å thick. When cooled to room temperature such films showed hysteresis loops that were very nearly characteristic of a rotating magnetization reversal with a uniaxial anisotropy, as described by Stoner and Wohlfarth.⁽²⁾ A detailed comparison between Stoner and Wohlfarth's model and the practical films has been made by Bradley and Prutton,⁽³⁾ in which the principal differences between the simple model and a real film prepared as described above were shown to be:

- (i) the coercivity along the anisotropy axis (the easy direction) is always less than the anisotropy field H_k , and not equal to it as required by the simple theory.

The anisotropy field is related to the anisotropy energy K and the magnetization M through the equation

$$H_k = 2K/M$$

and is measured from the hysteresis loop at right angles to the anisotropy axis ("hard direction");

- (ii) the hard direction $B-H$ plot is never a straight line but has a small finite coercivity H_{ch} and a slight constriction at $B=0$;

(iii) there is no coherent magnetization rotation when fields are applied exactly in either the hard or the easy direction, and at most orientations only part of the total flux appears to be rotating;

- (iv) there is always a finite slope in the sides of the hysteresis loop greater than that to be expected from the effects of the demagnetizing field alone.

It has been suggested by Humphrey⁽⁴⁾ that the magnetization reversal in these films can be associated with what he describes as a non-coherent rotation process, and these experiments were undertaken in order to learn some of the details of such a process.

Method

The use of the reflexion of plane polarized light at the surface of a magnetic material to reveal the domain structure was

* Based on a paper read at the conference on "Some aspects of magnetism" held by The Institute of Physics in Sheffield, September 1959.

first described in a series of papers by Fowler, Fryer, and others.⁽⁵⁻⁷⁾ Kranz and Drechsel⁽⁸⁾ have shown that by means of a layer of transparent dielectric of suitable thickness deposited on to the magnetic surface, the Kerr effect can be enhanced and the contrast between adjacent domains considerably improved.

The apparatus used by the author has been described elsewhere,⁽⁹⁾ along with a description of further improvements in contrast that can be obtained by the insertion of a quarter-wave plate in the system.

Results

The results described here were taken on four films typical of those produced, which are very close approximations to the simple model of rotational magnetization reversal. They all had easy direction coercivities H_c of between 3.0 and 3.2 oersteds, anisotropy fields H_k between 3.4 and 4.7 oersteds and were about 1500 Å thick.

Observations of the reversal with fields applied along the easy axis revealed that the process is one of nucleation and wall motion, with no coherent rotation at all. This is clear both from direct magneto-optic experiments, and from hysteresis loop studies using a pick-up coil arranged so as to detect flux changes at right angles to the applied field.⁽³⁾ The nucleation field, i.e. the field required to produce small reverse nuclei (generally at the edge of the film), was usually of the order of half the coercivity H_c . The wall motion, occurring as the applied field was increased, was always irreversible as the field could be removed at any stage during the reversal and the domain pattern was unchanged. A typical domain pattern during an easy-direction reversal is shown in Fig. 1.

The behaviour of the films when a field was applied at right angles to the easy direction⁽⁹⁾ depended upon their history. Taking a film which was initially a single domain, increasing the field in the hard direction resulted in coherent rotation until the whole magnetization was lying along the

direction of the field. On decreasing the field the magnetization was observed to split into a fine anti-parallel domain structure (Fig. 2), presumably because it experienced no torque towards either easy direction. Subsequent increase in the applied field caused the magnetization within these

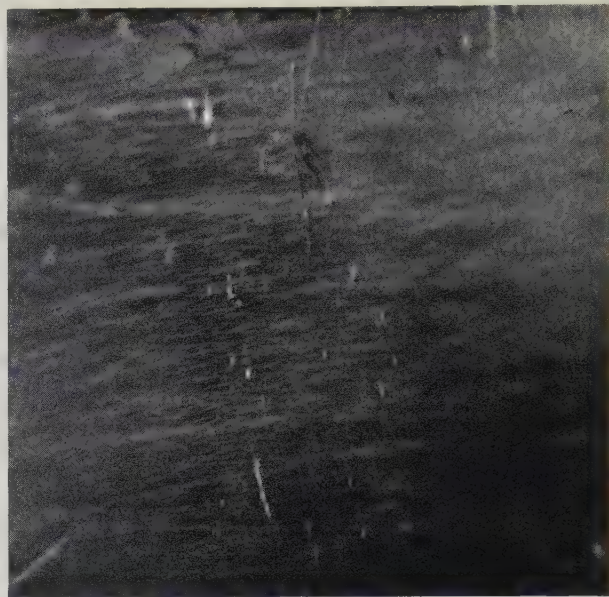


Fig. 2. A network of complex domain structure observed by removing the field from a good uniaxial film previously saturated in its hard direction

domains to rotate towards the field direction, without any movement of the domain boundaries, until the film was saturated in the hard direction. The finite coercivity exhibited in the hard direction by these films may well be associated with the energy required to create these domain boundaries.

The reversal processes observed when the field was applied at other angles to the anisotropy axis were always associated



Fig. 1. Typical domain structure in a film partially reversed by a field along its easy axis. Walls are observed to lie both along the easy axis and at an angle of about 20° to the easy axis

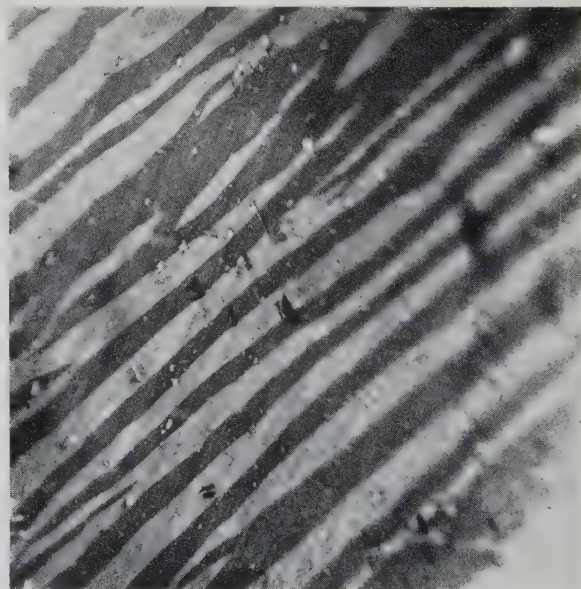


Fig. 3. A typical domain structure observed in a good uniaxial film with a field applied at 45° to its easy axis

with domain growth, the reverse domains tending increasingly to straight edged bars as the angle α between the field and the easy axis was increased. A photograph of a typical domain structure observed for $\alpha = 45^\circ$ is shown in Fig. 3. Information about this reversal process was derived from the following two sets of experiments.

(1) *Measurement of the nucleation field.* Photographs of the hysteresis loops of each sample were taken at 15° intervals in α between 0° and 90° using both crossed and aligned pick-up loop arrangements. The scales on these photographs were normalized, using the total flux in the easy direction as unity for the ordinate and $H_k = 1$ for the abscissa. The same samples were put in the Kerr apparatus, and for each value of α the nucleation field H_n and the field H_s required just to saturate the film were measured. After correction to the normalized values h_n and h_s , these fields were marked on the hysteresis loop. The points on the loop corresponding to these events were then compared with the end-points of the Stoner-Wohlfarth discontinuity⁽²⁾ which occurs at a field h_c , and is bounded by the cosines of the angles ϕ_0 and ϕ'_0 that the magnetization makes with the applied field when it passes through the discontinuous jump predicted by this

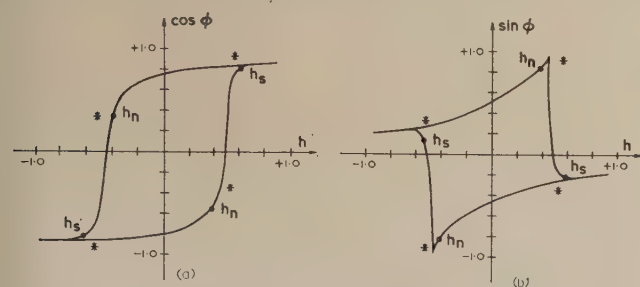


Fig. 4. The comparison of nucleation field and theoretical commencement of a discontinuous magnetization jump in a hysteresis loop taken with $\alpha = 30^\circ$ for both (a) aligned and (b) crossed pick-up loops

● = observation; * = terminating points of theoretical discontinuity

theory of coherent rotation. Fig. 4 shows these points marked on two hysteresis loops for $\alpha = 30^\circ$.

(a) It is clear that some coherent rotation does occur before the nucleation field is reached because:

- (i) some flux appears in the crossed pick-up loop before nucleation occurs; and
- (ii) a uniform change in reflected light intensity is observed in the Kerr apparatus before the reversed nuclei are seen.

(b) The nucleation field can be seen to correspond quite well with the beginning of the expected discontinuity at $(h_c, \cos \phi_0)$. It was observed that h_n was generally less than h_c , this difference increasing as the p ratio ($p = H_c/H_k$) of the sample decreased.

(c) Although the saturation field h_s is not generally near to the end of the expected discontinuity at $(h_c, \cos \phi'_0)$ it is near the point where the two branches of the loop join again.

(d) It was observed that further coherent rotation towards the direction of the applied field occurred once the domain reversal was over.

(2) *Measurement of the wall angles.* Study of the half-reversed films in cases like that shown in Fig. 3 revealed two points.

(a) During the growth of the domains the field could be removed and the domain boundaries did not change their

positions. However, the contrast between adjacent domains increased, indicating that during the reversal process (with the field always present) the directions of the magnetization were not simple anti-parallel arrangements as they appeared to be in the easy direction switching process.

(b) The angle θ_w between the boundaries of the strip domains and the applied field changed as the angle α between the easy axis and the field was varied. Three of the samples studied had $p = 0.7$ and the variation of θ_w with α for these samples is shown in Fig. 5.

This variation in θ_w with orientation α was such that θ_w was always about 60° away from the angle ϕ_0 , where a discontinuous magnetization jump should occur.

The fourth sample had $p = 0.91$ and in this case θ_w was less than 60° away from ϕ_0 , its variation with α also being shown in Fig. 5.

Measurements of θ_w were only possible between $\alpha = 15^\circ$ and $\alpha = 75^\circ$, as for lower values of α the domain walls

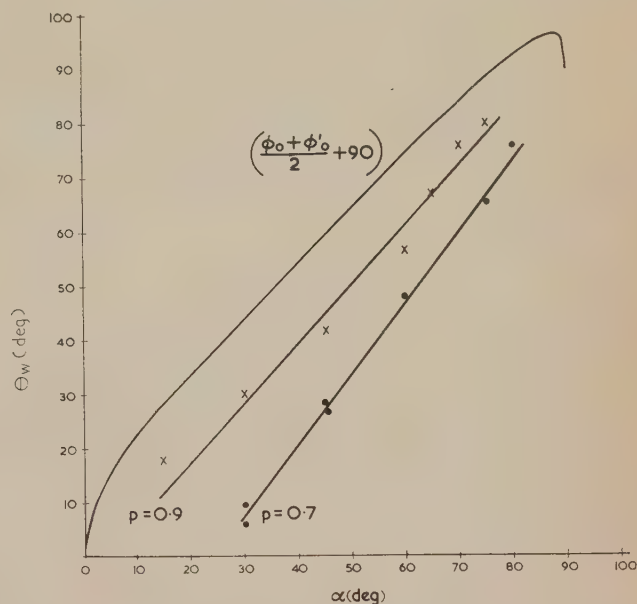


Fig. 5. The variation of wall angle θ_w as a function of the orientation α of the sample

were very irregular although tending to lie along the easy axis, and for higher values of α the contrast between adjacent domains became too low to discern the boundaries.

Similar experiments on films prepared in such a way so as to show little anisotropy (in that the hysteresis loops did not change shape as the orientation of the samples in the field was changed), revealed that:

- (i) no coherent rotation occurred before domains were nucleated;
- (ii) little or no change in the contrast between domains could be observed when the field was removed from a half-reversed sample;
- (iii) the domain walls did not tend to form in straight lines as in the anisotropic samples.

Conclusions and discussions

By the very special techniques of preparation described above, thin films of nickel-iron alloys near 80% nickel in composition can be prepared which show magnetic hysteresis very near to that described by Stoner and Wohlfarth for a

system with coherently rotating magnetization and simple uniaxial anisotropy. When an increasing field is applied to one of these films at an oblique angle to the easy axis, the reversal process occurs in three distinct steps:

(i) the whole magnetization rotates coherently until it is near the angle where a discontinuous jump in orientation should occur;

(ii) nucleation of domains then occurs and the reversal process appears to proceed by domain wall motion. The magnetization within these domains are not anti-parallel. As the angle α increases so the domains become increasingly bar-like in structure with their walls lying at angle θ_w to the applied field such that $(\phi_0 - \theta_w) \simeq 60^\circ$ for films with $p = 0.7$;

(iii) when the domain growth is complete, further coherent rotation occurs until the magnetization lies along the direction of the field.

The second stage of nucleation and domain growth might be expected to occur if the films were inhomogeneous. In this case the critical angle ϕ_0 would be reached by some parts of a film before others and incoherent rotation would occur. However, if such inhomogeneities were the cause of nucleation it would be expected that the reversed nuclei would occur at the same place in the film at each switching operation. This does not appear to be the case, as a different domain pattern is observed every time a film is partially reversed.

Consider the reversal process in which the magnetization rotates to the critical angle ϕ_0 , and then some parts of the film pass through the discontinuity to the angle ϕ'_0 , others remaining at ϕ_0 . The wall between the two orientations will have minimum energy if it arranges itself so that $\text{div } M = 0$ across the boundary, which will be achieved if the wall bisects the angle between the two directions of magnetization.

In Fig. 5 Stoner and Wohlfarth's data has been used to include a plot of the bisector of the angles ϕ_0 and ϕ'_0 versus α . It is clear that the values of θ_w for the sample with $p = 0.91$

are much nearer this bisector than are the values of θ_w for the samples with lower p ratios. Thus it would appear that as $p \rightarrow 1$ so the directions of magnetization within one set of domains during this reversal process tend to ϕ_0 , while the remaining domains are magnetized along ϕ'_0 .

When fields are applied in either of the directions where "zero-torque" situations can arise, the reversal process is quite different. The easy direction reversal process is entirely one of nucleation, and wall motion and the hard direction process is associated with the formation of a complex network of very small domains.

Acknowledgements

The author would like to thank Mr. A. J. Wells for his assistance with the observations on the films, and the Directors of International Computers and Tabulators Ltd. for their permission to publish this paper.

References

- (1) PRUTTON, M., and BRADLEY, E. M. *Proc. Phys. Soc.*, **75**, p. 557 (1960).
- (2) STONER, E. C., and WOHLFARTH, E. P. *Proc. Roy. Soc. A*, **240**, p. 74 (1948).
- (3) BRADLEY, E. M., and PRUTTON, M. *J. Electronics Control*, **6**, p. 81 (1959).
- (4) HUMPHREY, F. B. *J. Appl. Phys.*, **29**, p. 284 (1958).
- (5) FOWLER, C. A., JR., and FRYER, E. M. *Phys. Rev.*, **100**, p. 746 (1955).
- (6) FOWLER, C. A., JR., FRYER, E. M., and STEVENS, J. R. *Phys. Rev.*, **104**, p. 645 (1956).
- (7) FOWLER, C. A., JR., and FRYER, E. M. *Phys. Rev.*, **104**, p. 552 (1956).
- (8) KRANZ, J., and DRECHSEL, W. *Z. Phys.*, **150**, p. 632 (1958).
- (9) PRUTTON, M. *Phil. Mag.*, **4**, p. 1063 (1959).

Skeleton strength and critical porosity in set sulphate plasters

by K. K. SCHILLER, Ph.D., F.Inst.P., The British Plaster Board (Holdings) Ltd., Research and Development Department, East Leake, Leicestershire

[Paper first received 4 February, and in final form 1 April, 1960]

Abstract

A theory dealing with the strength of porous brittle bodies which has been shown previously to apply to neat plasters is extended to cover sand bearing plasters. The sand grains have to be regarded as solid pores. The strength of sanded plasters is equal to that of the plaster matrix cementing the sand grains together. In spite of the increase of the characteristic parameters with sand content plasters are in practice the weaker the more sand they bear. This is because more water has to be added with respect to the plaster to obtain the desired consistency. The results are derived graphically from a special representation of the experimental results. Griffith's crack

theory of brittle strength is shown to apply to the quality factor.

THE strength of mortars, concretes, plasters and similar materials is of considerable practical importance either in its own right or as an indirect indication for the suitability of some other property such as resistance to wear, etc. It depends on the relative proportions of aggregate and bonding agent and the strength of the latter. This, in turn, is determined by its origin, purity and manufacturing method and also by the amount of water used when preparing the mix.

It has previously been shown^(1,2) that the strength of neat hemihydrate plasters is essentially determined by its porosity and the intrinsic strength of the crystals making up the skeleton of the set mass. In the case of neat and pure plaster the porosity is given almost entirely by the quantity of water in the mix which is in excess of that required for hydrating the hemihydrate in accordance with the equation:



This excess water dries out and leaves behind in the set mass interconnecting voids or pores. These pores have an exceedingly complicated shape, the geometry of which is quite beyond any useful mathematical description. By comparison of two widely differing simplified models, it was, nevertheless, found possible to generalize the common features of the resulting formulas. The surprisingly simple result is that, as a first approximation, the strength of set materials (without aggregate) as a function of porosity is given by the formulae:

$$S = q \log \frac{p_{cr}}{p}, \quad (2a)$$

or:

$$S = q \log \frac{w + 0.36}{w - 0.15} + q \log p_{cr}, \quad (2b)$$

where S is the strength, p the porosity (i.e. the pore volume per cc) and w the water ratio (i.e. the number of millilitres of water mixed with 100 g of plaster). The terms q and p_{cr} are the two parameters characteristic for a given type of plaster. As the derivation of these formulas shows, they can be interpreted physically: q , which is referred to as the quality factor, is a measure of the skeleton strength, and p_{cr} , the critical porosity at which the strength becomes negligible. If higher approximations are introduced, more characteristic constants appear, but it does not seem necessary at this stage to make use of them. There are, however, experimental indications here and there that a two-parameter equation may not always be sufficient.

The quality factor depends on the type of test, so that tensile, transverse and compressive tests will lead to different values of q because brittle materials fail in general at different stresses under different types of loading. The critical porosity which only characterizes the pore system is the same for every type of test. As an example, Fig. 1 shows the compressive, transverse and tensile strengths plotted against the logarithm

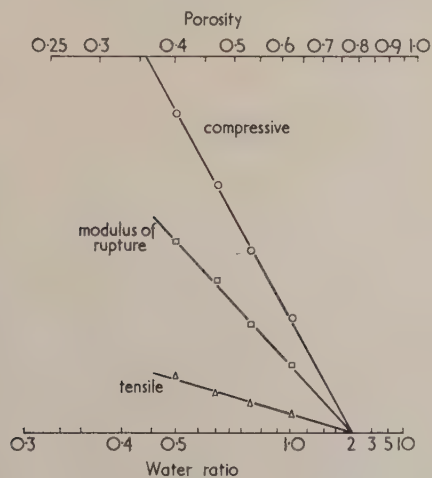


Fig. 1. Compressive, transverse and tensile strength plotted against logarithm of porosity

of the porosity obtained by testing samples gauged with different quantities of water. The practical usefulness of these two parameters occurs because they characterize the strength of the set plaster without reference to the amount of water used. This is of importance because two types of plaster which appear to differ in strength may do so only on account of a difference in the water needed for a specified consistency of the mix (the so-called water demand).

The purpose of this paper is to report on the results of experiments which we have done recently dealing with plasters of varying fineness of grind to which sand has been added as an aggregate. To make progress at all, it was unavoidably necessary to relax somewhat the desirable rigour of experimentation. This is the more acceptable as the fundamental equations (2) dealing with neat plaster have been definitely established by experiments performed under strict conditions.

Investigated were two types of plaster, four degrees of fineness, three proportions of aggregate and four water ratios. For each combination, twelve samples were prepared six of which were tested in tension and six in compression; this is the very minimum to obtain statistically significant results.

The results were plotted in a manner described below, and the points show a linear relation. In one or two cases, the quality factor and the critical porosity were determined by the method of least squares. To make the expression:

$$\sum_i \left(S_i - q \log \frac{p_{cr}}{p_i} \right)^2 \quad (3)$$

a minimum with respect to both q and p_{cr} (where S_i is the measured strength value of a sample of porosity p_i) it can easily be shown that:

$$q = \frac{1}{N} \sum S_i \cdot \sum \log \left(\frac{1}{p_i} \right) - \sum S_i \log \frac{1}{p_i} \quad (4)$$

and:

$$\log \frac{1}{p_{cr}} = \frac{\sum \log \frac{1}{p_i} \cdot \sum S_i \log \frac{1}{p_i} - \sum S_i \left(\log \frac{1}{p_i} \right)^2}{N \sum S_i \log \frac{1}{p_i} - \sum S_i \cdot \sum \log \frac{1}{p_i}} \quad (5)$$

It should be noted that tests with at least two porosities (or water ratios) have to be performed, since otherwise equations (4) and (5) give the indeterminate form 0/0; at least two points are, of course, required to define the straight line of best fit.

In the early stages of experimentation, the measured strength values were plotted against the porosity of the set plaster matrix holding the aggregate sand grains together (standard sand 18/25 mesh). The results clearly showed that this is a mistake [Fig. 2(a)]. Although straight lines are obtained, they do not intersect with the abscissa at the same point. The straight lines behave themselves, however, if the sand grains are regarded as "solid pores", i.e. the total porosity is regarded as being made up of the sum of the void volume and the sand volume, per unit bulk volume. Fig. 2(b) gives the results plotted against total porosity.

That the sand grains may reasonably be regarded as solid pores is suggested by the fact that the mechanical effect of the empty pores is to act as stress raisers; the stress in the neighbourhood of a pore in a body under load is higher than it would be if the pore were not there. Stresses are similarly raised in the neighbourhood of an inclusion with elastic

constants differing from those of the surrounding material. Indeed, an empty pore may be regarded as an inclusion with vanishingly small elastic constants.

Figs. 3 and 4 show, as examples, curves obtained for an open-pan calcined plaster, mixed with standard sand in

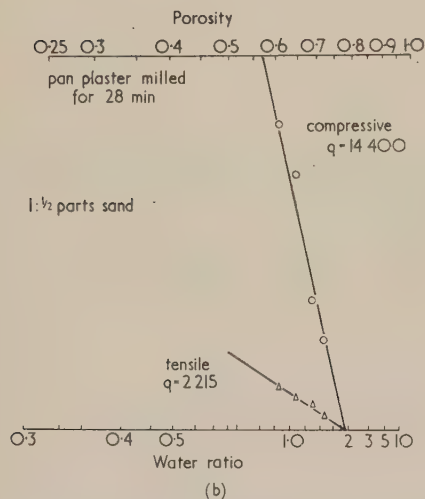
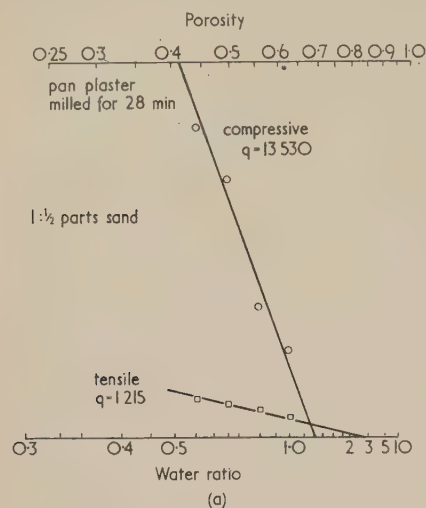


Fig. 2. (a) Strength plotted against porosity of set plaster matrix. (b) Strength plotted against total porosity

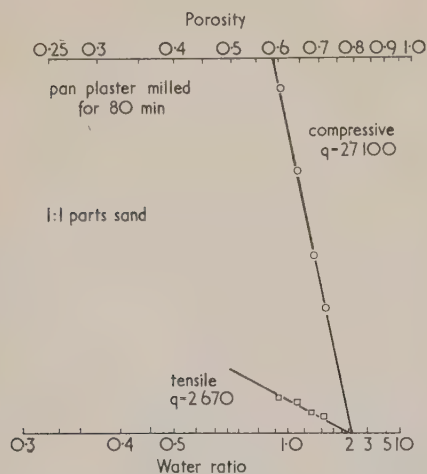


Fig. 3. Curve obtained for open-pan calcined plaster

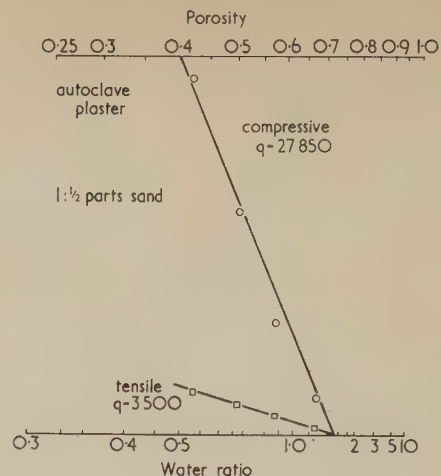


Fig. 4. Curve obtained for autoclave plaster

the ratio of one part of plaster to one part of sand by weight, and an autoclave plaster mixed in the ratio of one part of plaster to half a part of sand by weight. The tests with the pan plaster were repeated after subjecting the plaster to different degrees of ball milling with porcelain balls but the differences in the results were somewhat erratic and not statistically significant.

Fig. 5 shows the effect of adding sand to the plaster on the quality factor for compression tests. The relationship is

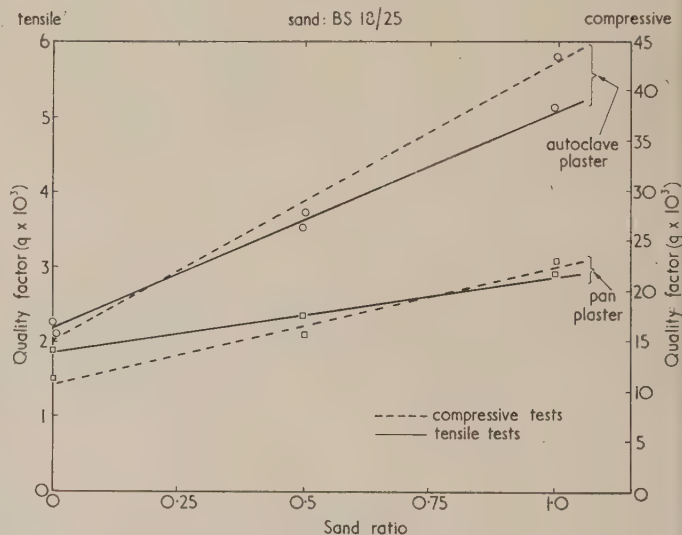


Fig. 5. Effect on quality factor of adding sand to plaster

practically linear although there is a faint suggestion that the curves are slightly concave upwards. The same may be said for Fig. 5 which shows the quality factors for tensile tests. The skeleton strength of the autoclave plaster is both greater and more sensitive to the quantity of aggregate than the pan plaster. Fig. 6 shows the way in which the critical porosity depends on the quantity of aggregate. The trend is for the critical porosity to increase with the proportion of sand added but the total change is rather small. It should be noted that q and p_{cr} are given by the position of the straight lines in the graph and that they are determined by the four experimental points each of which is itself the average of six tests.

They have, therefore, considerably stronger experimental support than the individual points.

The increase of the quality factor with sand content indicates that the strength of the set plaster skeleton increases. Nevertheless, it is a well-known fact that plasters containing

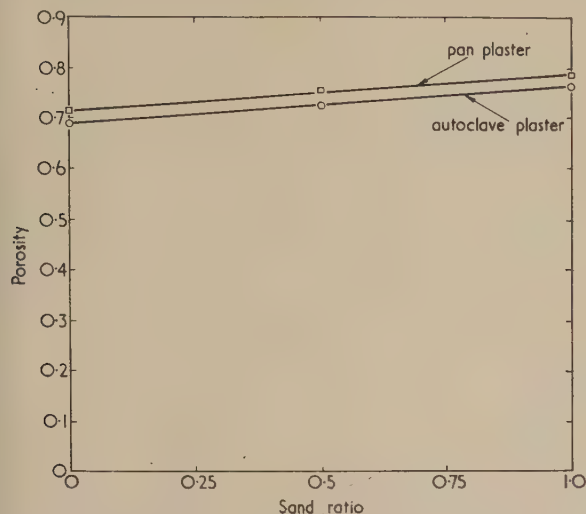


Fig. 6. Dependence of critical porosity on quantity of aggregate

sand are weaker than neat plasters because, for a given consistency, a sanded plaster has a greater water demand with respect to the plaster component than a neat one. A sanded plaster has, therefore, a larger total porosity both because there is more excess water to evaporate and there are the "solid pores" of the sand.

These relationships are best discussed by means of Figs. 7 and 8 which refer to the pan plaster and autoclave plaster respectively. The top graphs show the compressive and

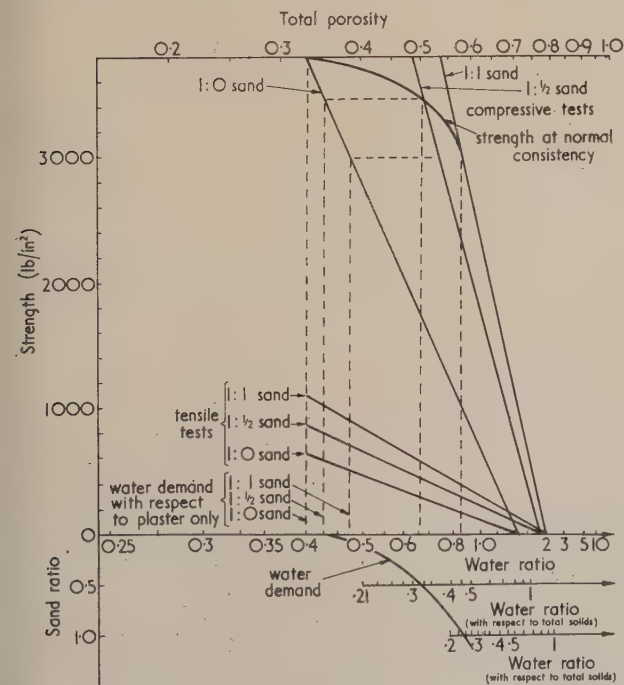


Fig. 7. Effect of sand and water ratio on strength of pan plaster

tensile strength curves. As both compressive and tensile strengths are plotted as positive ordinates, the negative ordinate is used to carry a sand ratio scale. The horizontal top edge of the graph carries a graduation of the abscissa in total porosity whilst its graduation in terms of water ratio

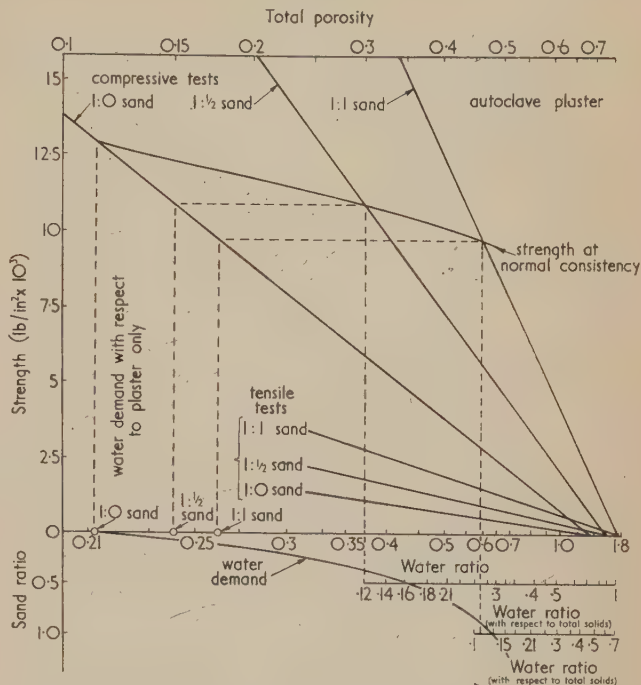


Fig. 8. Effect of sand and water ratio on strength of autoclave plaster

with reference to solids is presented at the horizontal lines going through 0, $\frac{1}{2}$ and 1 sand ratio (the ratios at which tests were performed).

In the bottom portion of the two graphs, the curve is drawn which shows how the quantity of water required for a given consistency (measured by the dropping ball method according to B.S. 1191) depends on the quantity of sand in the plaster. This quantity is called the water demand. The strengths of the set plaster corresponding to different sand proportions is obtained by drawing a vertical line (shown dashed) at the point of the water demand curve corresponding to the required sand ratio and intersecting it on the appropriate strength curve in the upper portion of the graph. The curve connecting the compressive strengths corresponding to the normal consistency at different sand ratios is shown at the top of the figure. It will be seen that in spite of the fact that the skeleton strengths are the greater and the critical porosities the higher, the more sand there is in the plaster (the straight lines get steeper and move to the right) the strengths at normal consistency drop with increasing sand content. This occurs because, although the quantity of water required with respect to the total solids (i.e. plaster and sand together) drops, it increases with respect to the quantity of plaster present. For the pan plaster, the water demand figures with respect to the plaster component only are:

- 1 part plaster to 0 part sand, 40.5%
- 1 part plaster to $\frac{1}{2}$ part sand, 43.0%
- 1 part plaster to 1 part sand, 47.5%

The graph now further shows that the strength of sanded plaster is exactly the same as that of a neat plaster made at

the same water ratio. This has already previously been shown to be the case by H. Andrews.⁽³⁾ (This relationship is clearly shown by the dashed lines.) The strength of the neat plaster at the water ratio of 43% is exactly the same as that of a sanded plaster with a sand ratio $\frac{1}{2}$ at a standard consistency. The same relation holds between neat plaster at 47% water ratio and plaster with a sand ratio 1. The same relations are shown in Fig. 8 which refers to the autoclave plaster. Whether this relation is true for all types of plaster and sand it would be premature to deduce at this stage but it does not seem unlikely.

The apparent similarity of the curve representing the plaster strength at normal consistency S_d and water content at different sand contents suggests a simple relation between sand and strength. Thus, whichever scale one uses for the abscissa, say x , the slope of the strength curve may be expected to be proportional to the slope of the water content curve, that is, $-dS_d/dx = kds/dx$ (where k is a proportionality constant). The minus sign is introduced because the s -curve increases downwards and the S -curve upwards. The solution of this equation is a linear relation between the strength at normal consistency and the sand content, namely $S_d = S_{od} - ks$ where S_{od} is the strength of the neat plaster ($s = 0$). This result depends on the degree to which the similarity between the two curves as expressed in the former equation is true; comparison with experimental values show that it can only be regarded as a moderate approximation. In any case, that it cannot be entirely true is easily seen by the fact that according to this formula the strength would become negative for a sufficiently large sand ratio.

The quality factor q is a measure of the skeleton strength of the plaster. To this one might expect Griffith's crack theory of strength to apply.⁽⁴⁾ One consequence of this theory is that the tensile strength should be $\frac{1}{8}$ of the compressive one, and this should hold for every water ratio. This implies that the lines corresponding to the tensile and compressive strengths should meet at the same point on the

abscissa; this holds, as was shown, for the point corresponding to the critical porosity. The curves for compression and tension in Fig. 7 corresponding to the 1 to 1 and 1 to $\frac{1}{2}$ sand mixes show a ratio of 8.0 to 1 and those corresponding to the neat plaster show a ratio of 6.2 to 1. In Fig. 8 these numbers are 8.5 to 1, 8.0 to 1 and 6.9 to 1 respectively. This is, on the whole, in good agreement with Griffith's prediction.

The plasters used so far have been rather pure and the sand chosen fell into a rather narrow sieving range. Care is therefore required before applying the results to plasters with impurities, different sizes and graduations of sand or plasters obtained by different methods of grinding. There are indications that some at least of the parameters describing the elastic and rheological properties of set plasters are related to its strength and may thus fit into the scheme proposed.

At this stage, however, the main conclusion to be drawn from the work described is the further confirmation of the correctness, usefulness and heuristic value of the present approach.

Thanks are due for many helpful discussions to Dr. H. G. Howell, Mr. H. Andrews and Dr. J. B. Taylor; also to Mr. G. W. Cafferata whose comments based on long experience in the gypsum industry were very welcome.

This work forms part of the fundamental research programme at the British Plaster Board (Holdings) Ltd.

References

- (1) SCHILLER, K. *Nature*, **180**, p. 862 (1957).
- (2) SCHILLER, K. *Mechanical Properties of Non-Metallic Brittle Materials*. Edited by W. H. Walton (London: Butterworths Scientific Publications, 1958).
- (3) ANDREWS, H. Private communication.
- (4) GRIFFITH, A. A. *First Int. Congr. Appl. Mech. (Delft)*, p. 55 (1924).

Calibration of manganese and gold foils for relative neutron flux measurements

by K. G. STEPHENS, B.Sc., Ph.D., A.Inst.P., and W. M. COOPER, B.Sc., Grad.Inst.P., Research Laboratory, Associated Electrical Industries Ltd., Aldermaston, Berks

[Paper first received 10 March, and in final form 8 April, 1960]

Abstract

The usual method of intercalibrating foils for relative flux measurements, made by comparing the β^- activities of the foils after exposure to the same neutron flux, is compared with a method dependent on weighing the foils.

The mass intercalibrations agree to within $\pm 1\%$ of the activity intercalibrations for gold and manganese foils in the range 90 to 100 mg/cm² thick, if a theoretical correction estimating the β^- absorption in the foil is applied to the measured mass values.

Introduction

ACTIVATION of foils is a standard method of measuring relative neutron flux distributions. Before irradiating the foils for such measurements they must be intercalibrated. Intercalibration of foils is usually done by choosing one foil as a standard and relating the response of the other foils to this standard. This ratio will be known as the radiation ratio R in the remainder of the paper. The result of the calibration is a correction or normalizing factor for each foil. The usual procedure of irradiating the foils

in the same neutron flux, in a spectrum similar to that in which the foils are to be used, and then counting them with a standard Geiger counter arrangement, is relatively time consuming and expensive.

By comparing, for each foil, the correction factor deduced from this method with the ratio of the mass of the foil to the mass of the standard foil (defined as the mass ratio M), an attempt has been made to find the conditions which must obtain to ensure that by simply weighing foils, calibration factors can be deduced which are sufficiently accurate for relative flux measurements to be made to within $\pm 1\%$.

Description of the foils

Four sets of ten circular foils were used in the experiment. Two sets were made of a manganese-nickel alloy containing 11% nickel, and the other two sets were made of 99.99% pure gold. These foils were selected from several hundred foils produced to specification by Johnson Matthey and Co. Ltd. The foils were distinguished by numbers engraved lightly upon them. The mass of each foil was found by means of a chemical balance accurate to 0.1 mg. In no case did the standard error of the mean of four weighings exceed 0.1 mg. Mean diameters of the foils were found from three measurements with a microscope. The two sets of gold foils had mean diameters of 1.1313 and 1.1311 cm and the two sets of manganese foils had mean diameters of 1.1306 and 1.1316 cm. In each set the standard error of the mean was less than 0.0005 cm.

A few manganese foils were examined for uniformity of thickness using a β -gauge and the variations of thickness across a foil were found to be less than $\frac{1}{4}\%$. This is to be expected, since the foils were produced by rolling and variations across a foil should be small.

Thus, the areas of the foils vary by only about 0.1% and the spread in the masses of the foils is due mainly to variation in mean thickness. For both the manganese and gold foils the foil thickness was of the order of 90 mg/cm², which is equivalent to 50 μ (0.002 in.) for gold and 125 μ (0.005 in.) for manganese.

The determination of the radiation ratio

The activation of the foils. One set of gold foils and one set of manganese foils were activated on a graphite block at the end of a long pole which was inserted into a beam tube of the Harwell reactor Gleep. The manganese foils were irradiated for 3 min in a nominal flux of 2×10^7 n/cm²s. During the irradiation the pole was rotated continuously to ensure uniform irradiation of each foil.

The other two sets of foils were irradiated in the oscillator boat of Gleep. These foils were placed about 1 in. apart in fluxes similar to those indicated above. The flux along the length of the boat was estimated to be constant to within $\frac{1}{2}\%$. One gold foil was irradiated separately with a 0.020 in. thick cadmium cover, under identical conditions to the other nine foils. The cadmium ratio as measured with this gold foil was 4.5.

In the neutron irradiation the gold, manganese and nickel isotopes underwent (n, γ) reactions to form β -active isotopes. Table 1 gives the data⁽¹⁾ for the gold, manganese and nickel reactions.

The contribution of the active nickel isotopes ⁵⁹Ni, ⁶³Ni and ⁶⁵Ni, to the total activity of the manganese nickel foil is negligible compared with the ⁵⁶Mn activity. The isotope ⁶⁵Ni, which has a half-life of 2.57 hours, similar to that of ⁵⁶Mn, is produced from ⁶⁴Ni which occurs to the extent of

approximately 0.1% in the manganese-nickel alloy, and has a cross-section approximately one-sixth that of the ⁵⁵Mn isotope which forms 89% of the foil material. Thus the contribution of the ⁵⁶Mn to the total disintegration rate after irradiation was greater than that of ⁶⁵Ni by a factor of about 10^4 . The isotopes ⁵⁹Ni and ⁶³Ni have half-lives of 8×10^4

Table 1. Data for gold and manganese (n, γ) reactions

Isotope	Abundance (%)	Cross-section (barns)	Isotope produced	β -Decay E_{max} (MeV)	Branching ratio (%)	Half-life
¹⁹⁷ Au	100	98	¹⁹⁸ Au	0.96	98.6	2.69 d
				0.29	1.4	
⁵⁵ Mn	100	13.3	⁵⁶ Mn	2.81	50	2.57 h
				1.04	30	
				0.65	20	
⁵⁸ Ni	67.76	4.6	⁵⁹ Ni (not β -active)			
⁶² Ni	3.66	15	⁶³ Ni	0.067		125 yr
⁶⁴ Ni	1.16	2	⁶⁵ Ni	2.10	57	2.6 h
				1.01	14	
				0.60	29	

years and 125 years respectively. Therefore, the activity produced by them after a three-minute exposure can be neglected in comparison with the ⁵⁶Mn activity.

Measurement of foil activities. Four pairs of Geiger-Müller counters were used to measure the foil activities allowing four foils to be counted simultaneously. One of the foils in each set of ten was chosen as the standard or monitor foil. Each foil was compared with this monitor foil in each pair of counters. A cyclic system of counting was used which ensured that in one complete cycle each foil was counted relative to the monitor foil six times. The counting rates used were such that the statistical error in any one ratio was less than 1%. Corrections were applied for background, decay of foil activity and the counter dead time.

Results

Inspection of Fig. 1 shows that for the gold foils there are differences between R and M of up to 0.06. Also $R-M$ is always opposite in sign to $M-1$ and the magnitude $|R-1|$

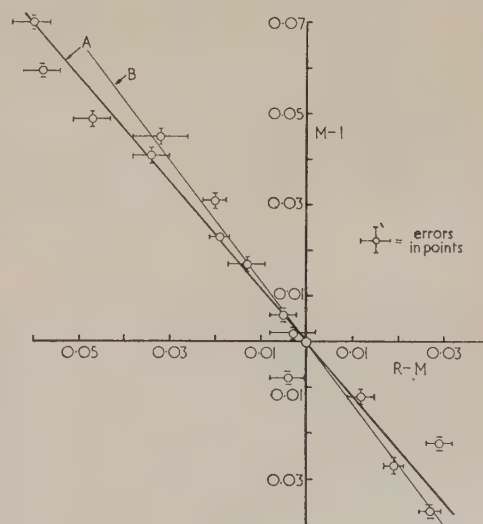


Fig. 1. The difference between the radiation ratio R and the mass ratio M plotted against $M-1$ for gold. Curve A, least squares fit through experimental points; curve B, theoretical line, $\mu = 0.025$ cm²/mg

increases with the magnitude $|M-1|$. This general trend is also observed for the manganese foils, but in two cases $R-M$ is the same in sign as $M-1$. This may be due to the smaller difference of R and M for manganese, resulting in relatively large experimental errors in $R-M$.

Discussion of results. The differences between R and M could be due to neutron flux depression around the foil, neutron self-shielding of the inside of the foil by its outer layers or β -ray self-absorption in the foil material. These effects are discussed below.

Neutron flux depression and neutron self-shielding of the foils. During foil irradiations in a reactor, there will be neutron flux depression in the region of a foil and neutron self-shielding within a foil. The magnitude of these effects will be a function of the thickness of the foils. The change in magnitude of these effects was estimated for the second set of gold foils where the thickness varied from 92.87 to 101.35 mg/cm². These estimates were based on the theory of Bothe⁽²⁾ as modified and corrected by various authors.^(3,4)

The flux depression correction factor was 1.0035 and only varied by three units in the last figure over the above thickness range. Self-shielding correction factors were larger and varied from 1.064 for the thinnest foil (92.87 mg/cm²) to 1.070 for the thickest foil (101.35 mg/cm²). For manganese foils these factors were 1.0180 for a foil 82.59 mg/cm² thick and 1.0185 for a foil 94.3 mg/cm² thick.

It is clear, especially for gold, that these effects alone cannot account for the differences between R and M .

β -ray self-absorption in the foils. The difference in values of R and M may result from the varying amount of β -ray self-absorption with foil thickness. A probable explanation of the results follows.

Consider two foils of equal diameters having a mass ratio m_1/m_2 greater than unity, so that $M-1$ is positive. The self-absorption of emitted β^- particles in the heavier, or thicker, foil will be more than in the lighter foil. If S_1 and S_2 are the corresponding activities per unit thickness, S_1 will be less than S_2 and the measured radiation ratio R which is given by $m_1 S_1 / m_2 S_2$ will be less than the corresponding mass ratio m_1/m_2 , making $R-M$ negative. It follows from the above that $|R-M|$ should increase with $|M-1|$.

From an experimental self-absorption curve⁽⁵⁾ for the β -rays from ¹⁹⁸Au, values of the self-absorption correction for a gold foil 92.87 mg/cm² thick is 0.48 and for a foil 101.35 mg/cm² thick 0.455, a difference of approximately 5%. These differences are of the right order of magnitude to account for the differences in R and M .

For ⁵⁶Mn β -rays, since the self-absorption of the higher energy particles (see Table 1) is less, the difference in self-absorption factors for the same thickness range is between 2 and 3%.

Calibration correction of mass ratios

It was decided to apply to the mass ratio for each foil a correction factor based on the value of the self-absorption for each foil relative to that for the monitor foil. Thus, if k is the ratio of the measured activity to the true activity for a given foil, then k_1/k_2 is the factor by which the mass ratio m_1/m_2 is to be multiplied to give a theoretical value of the radiation ratio (R_T).

The value of k may be expressed by⁽⁶⁾

$$k = 1 - \exp(-\mu l) / \mu l \quad (1)$$

where μ cm²/mg is the mass absorption coefficient of the β -rays and l mg/cm² is the foil thickness. The curve obtained

from this expression is similar in shape to the experimental curve (Fig. 2). Values of μ were obtained from the experimental results of Meister.⁽⁷⁾ For gold, a value of 0.025 cm²/mg was used and for manganese a value of 0.006 cm²/mg.

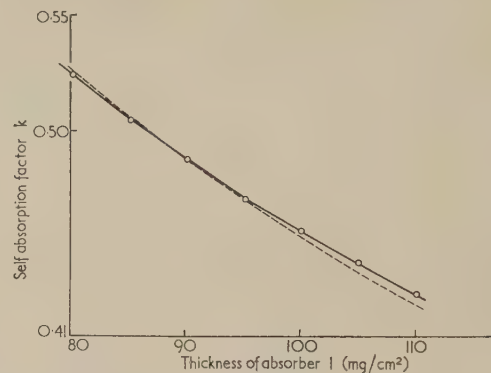


Fig. 2. Comparison of theoretical correction curve for gold with the experimental self-absorption curve. The two curves are normalized at 90 mg/cm²

--- = experimental curve — = theoretical curve

Correction factors thus calculated were applied to all foils and the values of R_T for gold and manganese foils are compared with R and M in Tables 2 and 3 respectively. The values of R_T and R shown in Table 2 for gold all agree to

Table 2. Values of R_T , R and M for gold

Foil number	Correction factor	Mass ratio (M) [$\pm 0.001(5)$]	Calculated radiation ratio (R_T)	Measured radiation ratio (R)
121	0.967	1.045	1.011	1.013 \pm 0.006
123	0.950	1.070	1.016	1.010 \pm 0.004
124	0.965	1.049	1.012	1.002 \pm 0.004
125	0.987	1.017	1.004	1.004 \pm 0.004
126	1.020	0.973	0.992	0.992 \pm 0.004
127	0.959	1.057	1.014	0.999 \pm 0.004
129	0.998	1.002	1.000	0.999 \pm 0.005
984	1.036	0.954	0.988	0.2245 (cadmium covered)
981	1.029	0.963	0.991	0.990 \pm 0.002
986	1.021	0.973	0.993	0.992 \pm 0.002
985	1.017	0.978	0.995	1.007 \pm 0.003
974	1.009	0.988	0.997	1.000 \pm 0.003
971	0.995	1.006	1.000	1.001 \pm 0.003
1001	0.982	1.023	1.004	1.004 \pm 0.002
987	0.977	1.031	1.007	1.011 \pm 0.002
980	0.969	1.041	1.009	1.007 \pm 0.004

within 1.5% and, for all but three foils, R_T and R agree to within 0.6%. In Table 3 all values of R_T and R for manganese agree to within 1.5% and, for all but one foil, to within 1%.

By assuming the correction factor to be exact, an expression relating $R-M$ to $M-1$ can be found as a function of the monitor foil thickness and the absorption coefficient μ . This shows that for small $(M-1)$, i.e. less than 0.1,

$$(M-1) = -(R-M) / \{1 - \mu l_2 / \exp(\mu l_2) - 1\} \quad (2)$$

where l_2 is the monitor foil thickness.

Thus the relationship is linear with a slope of

$$-1 / \{1 - \mu l_2 / \exp(\mu l_2) - 1\} \quad (3)$$

Table 3. Values of R_T , R and M for manganese

Conclusions

Foil number	Correction factor	Mass ratio (M) [$\pm 0.001(5)$]	Calculated radiation ratio (R_T)	Measured radiation ratio (R)
341	1.008	0.968	0.976	0.983 ± 0.004
342	1.007	0.971	0.978	0.974 ± 0.004
343	0.996	1.016	1.012	1.010 ± 0.007
344	1.011	0.958	0.968	0.965 ± 0.005
345	1.011	0.955	0.965	0.964 ± 0.005
346	1.012	0.947	0.958	0.951 ± 0.004
347	1.010	0.959	0.969	0.967 ± 0.003
348	1.015	0.939	0.953	0.957 ± 0.003
349	1.012	0.952	0.963	0.959 ± 0.004
331	1.014	0.940	0.953	0.945 ± 0.002
330	1.009	0.963	0.972	0.964 ± 0.004
327	1.005	0.979	0.984	0.975 ± 0.003
338	1.002	0.991	0.993	0.985 ± 0.002
369	0.995	1.019	1.014	1.005 ± 0.002
351	0.992	1.033	1.025	1.025 ± 0.004
368	0.990	1.042	1.032	1.041 ± 0.005
352	0.987	1.054	1.040	1.043 ± 0.004
360	0.983	1.071	1.053	1.068 ± 0.003

For the two monitor foils used in the two gold sets, the slope of this line is virtually constant, varying only from 1.35 to 1.30. The mean of these slopes, 1.32(5), agrees well with the slope of 1.18 of the best least squares fit through the experimental points. Both lines are shown in Fig. 1.

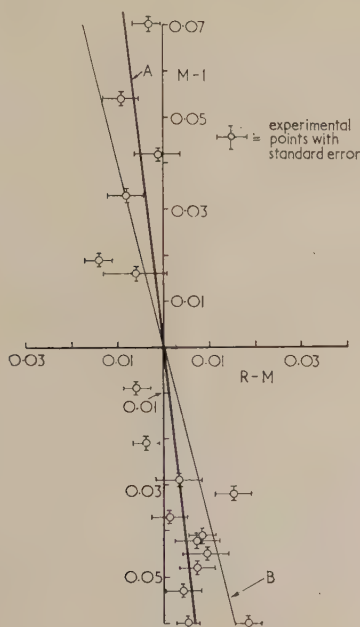


Fig. 3. The difference between the radiation ratio R and the mass ratio M plotted against $M-1$ for manganese. Curve A, least squares fit to experimental data; curve B, theoretical line.

A similar calculation of slope for manganese foils gives a value of -4 , which is to be compared with -9 as obtained from the experimental line (Fig. 3).

The masses of a selection of gold and manganese foils, of nominal thickness 0.002 and 0.005 in. respectively, were in the range 88 to 101 mg for gold and 82 to 95 mg for manganese. These variations result from variations in thickness.

Direct intercalibration of the gold foils for use in relative flux measurements cannot be performed to an accuracy of 1% by only correcting for mass differences. Neutron flux depression, neutron self-shielding and β -ray self-absorption are functions of foil thickness. It has been shown for the gold foils that, although neutron flux depression and self-shielding may be neglected for relative measurements, in order to get foil intercalibration to within 1% a correction for β -ray self-absorption must be applied to the mass ratios. A theoretical expression for this correction factor has been applied to the mass ratios, and the resulting ratios were shown to be in good agreement with the ratios obtained from the experimental data. In all cases (fifteen) the agreement was better than 1.4% and, in all but three cases, the agreement was better than 0.6%.

The β -ray self-absorption correction factors for the manganese-nickel foils are smaller than those for gold and, without making the corrections, values of the mass ratios agree with the measured radiation ratios to within 1%, in all but three cases out of eighteen. The maximum difference in these cases is 2%. After making the corrections, the maximum difference in one case only is 1.5%, and in all other cases is better than 1%.

The experiment suggests that in order to get the required 1% accuracy from measurements using these gold and manganese foils, the foils should be sorted into sets, such that the thickness variation within sets is only ± 0.5 and ± 1.0 mg/cm² for gold and manganese respectively. By comparing the monitor foils of each set, intercalibration of sets may be performed to $\pm 1\%$ by applying the theoretical correction where necessary. This is a useful method of intercalibration when facilities for uniform irradiation of foils are limited.

Acknowledgements

We would like to thank the staff of the Gleep reactor at the Atomic Energy Research Establishment for irradiating the foils, and also Dr. J. Shaw and Mr. P. Solari of the Nuclear Power Group, Knutsford, for their help in arranging one of the irradiations. We would also like to thank Dr. A. J. Salmon and Dr. K. Firth for their advice and Mr. G. Woolford, Mrs. M. Stephens, Miss A. Smith and Mr. C. Waters for their assistance in counting and computing. The authors are indebted to Dr. T. E. Allibone for permission to publish this paper.

References

- (1) STROMINGER, D., HOLLANDER, J. M., and SEABORG, G. T. *Rev. Mod. Phys.*, **30** (2), Part II, p. 585 (1958).
- (2) BOTHE, W. *Z. Phys.*, **120**, p. 437 (1943).
- (3) GALLAGHER, T. L. *Nuclear Sci. Engng*, **3**, p. 110 (1958).
- (4) TITTLE, C. *Nucleonics*, **9**, p. 60 (1951).
- (5) YOUNG, J. D. Private communication (M.Sc. Thesis, University of Birmingham).
- (6) ATEN, A. H. W. *Nucleonics*, **6**, p. 68 (1950).
- (7) MEISTER, H. *Z. Naturforsch*, **13a**, p. 722 (1958).

Interpretation of γ -ray scintillation spectra from fission-product mixtures

by D. H. PEIRSON, B.Sc., F.Inst.P., Atomic Energy Research Establishment, Harwell

[Paper first received 1 December, 1959, and in final form 16 February, 1960]

Abstract

γ -ray scintillation spectra are calculated for the products of simultaneous slow neutron fission of uranium 235. These theoretical spectra serve as a basis for comparison with practical measurement of fission-product mixtures. The variation with time, from 1 to 28 days, of the photoelectric peak height is shown for the prominent fission product activities. A rapid method of half-life analysis is described for use when peaks are inadequately resolved in energy. The effect of spectrometer resolution is discussed.

Introduction

THE determination of the yield of a radio-nuclide after fission involves the separation of one radioactive isotope from a mixture of many others. Standard radiochemical techniques have been developed⁽¹⁾ for the separation of fission products and these are applied to samples of fissile material after irradiation in a reactor or particle accelerator, and to samples of fall-out from nuclear explosions.

Alternatively, since most (but not all) fission products emit γ -radiation, the mixture may be analysed with a scintillation spectrometer. Such analyses have been made previously by the author using samples after irradiation in a reactor⁽²⁾ and samples of nuclear-weapon debris.

From the gross γ -ray spectra of a mixture of fission products, individual radio-nuclides of high yield may be identified qualitatively by measurement of the energy and the half-life of decay of the γ -ray peaks arising from photoelectric conversion in the scintillation crystal. Quantitative interpretation of the spectra requires a knowledge of:

- the variation of scintillation-counter efficiency with energy in order to convert the γ -ray peak height (or area) into γ -ray or X-ray intensity; and
- the decay scheme of the radio-nuclide in order to convert γ -ray or X-ray intensity into disintegration rate. The analysis may be further extended by relating observed disintegration rate to fission yield of the radio-nuclide.

It is the purpose of this paper to collect the data required for these calculations and to derive γ -ray scintillation spectra for a standard condition of fission. Differences in any practical measurement of mixed fission-product spectra from this standard case may then be readily related to differences in fission product yield or disintegration rate.

Method

The activities and abundances of fission products after simultaneous slow neutron fission of uranium 235 have been

calculated by Hunter and Ballou.⁽³⁾ (This has since appeared in a revised edition by Bolles and Ballou.⁽⁴⁾) In their calculation, a yield and half-life are assigned to each fission-product radio-nuclide. Then the disintegration rates of each member of each decay chain are computed for various times after fission. It remains to convert the disintegration rates (per 10^4 fissions) as calculated by Hunter and Ballou into γ -ray scintillation spectra.

Decay-scheme data have been collected from Hollander *et al.*⁽⁵⁾ and from the Nuclear Science Abstracts. Where uncertainty exists, it has been necessary to make confirmatory measurements of γ -ray spectra from separated activities. From this data a factor (≤ 1) may be extracted to represent the abundance of γ -rays or X-rays per disintegration.

An efficiency factor for a sodium-iodide crystal of standard dimensions 1 in. by 1.5 in. diameter, is derived from an existing laboratory calibration for this common size of crystal. For convenience in dealing with complicated spectra, this calibration has been derived in terms of the height (rather than the area) of the plot of photoelectric peak against energy. Thus if it is assumed⁽²⁾ that the photoelectric peak follows a Gaussian distribution and that the scintillation process is linear, then:

$$\begin{aligned}\text{peak height} &\propto \frac{(\text{peak area}) \times (\text{channel width})}{\text{peak width}} \\ &\propto \frac{(\text{peak area}) \times (\text{channel width})}{(\text{energy})^{1/2}}\end{aligned}$$

Therefore, in terms of relative efficiencies:

- peak-height efficiency is given by the *ratio* of the peak-area efficiency and the square root of energy for the case where the amplitude analysis of the scintillation pulse uses a *constant* channel width; and
- peak height efficiency is given by the *product* of the peak-area efficiency and the square root of energy where a channel width *proportional* to energy⁽⁶⁾ is used.

A "peak-height factor", equal to the product of the γ -ray (or X-ray) abundance factor and the peak-height efficiency, may be derived from the combination of decay scheme and crystal-efficiency data. If the disintegration rates calculated by Hunter and Ballou⁽³⁾ are multiplied by the "peak-height factor" for each γ -ray, curves of scintillation peak-height against time may be obtained.

Scintillation spectra are derived for fission-product activities that are prominent from 1 day to 28 days. For convenience of graphical representation, the "peak-height factor" used in this paper refers to use of a channel width *proportional* to energy. From the peak-height/peak-area relation quoted

Table 1. *Decay scheme and crystal efficiency*

Fission product	Half-life	γ energy (MeV)	Branching ratio	Internal conversion $1/(1+\frac{e}{\gamma})$	Crystal peak height efficiency	Peak height factor	
						Arbitrary	Relative to La^{140} 1.6 MeV
$\text{Cs}^{135\text{m}}$	$9.2\text{h} + 10^{-10}\text{s}$	0.25	1	1/1.05	0.38	0.36	5.6
$\text{Nb}^{97\text{m}}$	17h + 60s	0.75	1	1/1.015	0.125	0.12	1.9
Nb^{97}	17h + 60s + 72m	0.67	1	1/1.0015	0.14	0.14	2.2
I^{133}	21h	0.53	0.94	1	0.185	0.17	2.65
Ce^{143}	33h	0.29	~ 0.4	1	0.35	0.14	2.2
Pm^{149}	54h	0.29	1	1	0.35	0.35	5.5
Mo^{99}	68h	0.74	0.1	1	0.13	0.013	0.2
		0.78	0.04	1	0.12	0.005	0.08
$\text{Tc}^{99\text{m}}$	68h + 6h	0.14	1.0	1	0.37	0.37	5.8
Te^{132}	78h	0.23	1	1	0.39	0.39	6.1
I^{132}	78h + 2.3h	0.53	0.25	1	0.185	0.046	0.72
		0.67	1.0	1	0.14	0.14	2.2
		0.78	0.75	1	0.125	0.086	1.3
		0.96	0.2	1	0.1	0.02	0.31
		1.16	0.08	1	0.082	0.006	0.09
		1.40	0.11	1	0.07	0.008	0.12
Xe^{133}	5.3d	0.08	1	1/2.8	0.28	0.1	1.56
I^{131}	8.1d	0.36	0.8	1/1.018	0.28	0.24	3.8
Nd^{147}	11.3d	0.092	0.6	1/1.8	0.3	0.1	1.56
		0.32	0.15	1	0.32	0.05	0.78
		0.53	0.25	1	0.185	0.05	0.78
Ba^{140}	12.8d	0.54	0.14	1	0.18	0.025	0.39
La^{140}	12.8d + 40h	0.33	0.1	1	0.31	0.03	0.47
		0.49	0.40	1	0.2	0.08	1.25
		0.82	0.24	1	0.115	0.03	0.47
		1.60	1.0	1	0.064	0.064	1.0
Ce^{141}	33d	0.145	0.67	1/1.4	0.38	0.18	2.8
Ru^{103}	42d	0.50	1	1	0.2	0.2	3.1
Zr^{95}	65d	0.72	~ 0.5	1	0.13	0.065	1.02
		0.756	~ 0.5	1	0.125	0.063	0.98
Nb^{95}	65d + 35d	0.77	1	1	0.12	0.12	1.87
Ce^{144}	290d	0.08	~ 0.04	$\sim 1/2.2$	0.28	0.005	0.08
		0.134	~ 0.08	$\sim 1/1.7$	0.37	0.017	0.27
Rh^{106}	1y + 30s	0.51	0.21	1	0.19	0.04	0.62
		0.62	0.10	1	0.15	0.015	0.23
$\text{Ba}^{137\text{m}}$	33y + 2.6m	0.66	0.92	1/1.1	0.14	0.12	1.9
Np^{239}	2.3d	0.104	0.6		0.33	0.20	3.1
		0.225	0.11		0.39	0.043	0.68
		0.28	0.106		0.35	0.037	0.58
U^{237}	6.7d	0.062	0.42		0.24	0.101	1.54
		0.103	0.53		0.33	0.174	2.7
		0.205	0.19		0.39	0.074	1.16

Table 2. *Fission product activity and scintillation peak height*

(Figures in brackets denote number of zeros after decimal point)

Energy range (MeV)	Fission Product	γ Energy (MeV)	Peak Height Factor	(a) Activity dpm per 10^4 fissions (ref. (3))										Cumulative fission yields: ref. (3) (atoms per 10^4 fissions)
				(b) Peak height rel. to La^{140} 1.6 MeV										
				1h	3.5h	12h	1d	2d	4d	7d	14d	28d	105d	
<0.1	Xe^{133}	0.08	1.56	(4)5 (4)78	(2)30 (2)47	(1)12 (1)19	(1)21 (1)33	(1)29 (1)45	(1)29 (1)45	(1)22 (1)34	(2)87 (1)14	(2)14 (2)22	(7)59 (7)92	470
	Ce^{144}	0.08	0.08	(3)89 (4)72	(3)89 (4)72	(3)89 (4)72	(3)89 (4)72	(3)89 (4)72	(3)88 (4)70	(3)88 (4)70	(3)86 (4)69	(3)83 (4)67	(3)69 (4)55	510
	Nd^{147}	0.09	1.56	(1)11 (1)17	(1)11 (1)17	(1)11 (1)17	(1)11 (1)17	(1)10 (1)16	(2)88 (1)14	(2)73 (1)11	(2)47 (2)73	(2)19 (2)30	(4)15 (4)23	260
0.1-0.2	Ce^{144}	0.134	0.27	(3)89 (3)24	(3)89 (3)24	(3)89 (3)24	(3)89 (3)24	(3)89 (3)24	(3)88 (3)24	(3)88 (3)24	(3)86 (3)23	(3)83 (3)22	(3)69 (3)19	510
	Te^{99m}	0.14	5.8	- -	- -	- -	(1)76 0.44	(1)59 0.34	(1)36 0.21	(1)17 (1)985	(2)295 (1)17	(4)91 (3)53	(12)43 (11)25	590
	Ce^{141}	0.145	2.8	(3)87 (2)24	(2)44 (1)12	(2)88 (1)25	(2)97 (1)27	(2)96 (1)27	(2)92 (1)26	(2)85 (1)24	(2)71 (1)20	(2)50 (1)14	(3)75 (2)21	590
0.2-0.3	Te^{132}	0.23	6.1	(1)56 0.34	(1)55 0.34	(1)51 0.31	(1)45 0.275	(1)37 0.225	(1)24 0.15	(1)12 (1)73	(2)27 (1)165	(3)13 (3)79	(11)80 (10)49	380
	Cs^{135m}	0.25	5.6	(1)96 0.54	0.22 1.23	0.32 1.8	0.22 1.23	(1)54 0.30	(2)18 (1)10	(5)88 (4)49	- -	- -	- -	590
	Ce^{143}	0.29	2.2	0.17 0.375	0.18 0.395	0.15 0.33	0.12 0.264	(1)70 0.154	(1)25 (1)55	(2)56 (1)122	(3)17 (3)375	(6)14 (5)31	- -	540
	Pm^{149}	0.29	5.5	(1)12 (1)66	(1)25 0.14	(1)30 0.165	(1)25 0.14	(1)18 (1)99	(2)87 (1)48	(2)30 (1)165	(3)25 (2)14	(5)18 (5)99	- -	140
0.3-0.4	Nd^{147}	0.32	0.78	(1)11 (2)86	(1)11 (2)86	(1)11 (2)86	(1)11 (2)86	(1)10 (2)78	(2)88 (2)69	(2)73 (2)57	(2)47 (2)366	(2)19 (2)148	(4)15 (4)117	260
	La^{140}	0.33	0.47	(3)39 (3)18	(2)14 (3)67	(2)48 (2)225	(2)76 (2)356	(1)12 (2)56	(1)16 (2)75	(1)17 (2)80	(1)12 (2)56	(2)58 (2)27	(4)90 (4)42	610
	I^{131}	0.36	3.8	(1)14 (1)53	(1)15 (1)57	(1)17 (1)64	(1)17 (1)64	(1)16 (1)61	(1)14 (1)53	(1)11 (1)42	(2)61 (1)23	(2)18 (2)68	(5)23 (5)87	330
0.4-0.6	La^{140}	0.49	1.25	(3)39 (3)49	(2)14 (2)175	(2)48 (2)60	(2)76 (2)95	(1)12 (1)15	(1)16 (1)20	(1)17 (1)21	(1)12 (1)15	(2)58 (2)725	(4)90 (3)112	610
	Ru^{103}	0.50	3.1	(2)39 (1)121	(2)39 (1)121	(2)39 (1)121	(2)38 (1)118	(2)38 (1)118	(2)36 (1)112	(2)35 (1)109	(2)31 (2)96	(2)25 (2)78	(3)69 (2)215	340
	Rh^{106}	0.51	0.62	(4)66 (4)41	(4)66 (4)41	(4)66 (4)41	(4)66 (4)41	(4)66 (4)41	(4)66 (4)41	(4)65 (4)40	(4)64 (4)395	(4)63 (4)39	(4)54 (4)335	50
	I^{133}	0.53	2.65	0.14 0.37	0.22 0.58	0.18 0.48	0.13 0.345	(1)59 0.156	(1)13 (1)345	(2)14 (2)37	(5)66 (4)175	(9)17 (9)45	- -	490

Table 2 (continued). Fission product activity and scintillation peak height

(Figures in brackets denote number of zeros after decimal point)

Energy range (MeV)	Fission Product	γ Energy (MeV)	Peak Height Factor	(a) Activity dpm per 10^4 fissions (ref. (3)) (b) Peak height rel. to La^{140} 1.6 MeV										Cumulative fission yields: ref. (3) (atoms per 10^4 fissions)
				1h	3.5h	12h	1d	2d	4d	7d	14d	28d	105d	
0.4-0.6 (Cont'd)	I^{132}	0.53	0.72	(1)26 (1)19	(1)41 (1)295	(1)51 (1)366	(1)47 (1)34	(1)38 (1)274	(1)25 (1)18	(1)13 (2)93	(2)28 (2)20	(3)14 (3)10	(11)82 (11)58	380
	Nd^{147}	0.53	0.78	(1)11 (2)86	(1)11 (2)86	(1)11 (2)86	(1)11 (2)86	(1)10 (2)78	(2)88 (2)69	(2)73 (2)57	(2)47 (2)37	(2)19 (2)15	(4)15 (4)12	260
	Ba^{140}	0.54	0.39	(1)23 (2)90	(1)23 (2)90	(1)22 (2)86	(1)22 (2)86	(1)21 (2)82	(1)18 (2)70	(1)16 (2)60	(1)11 (2)43	(2)50 (2)196	(4)78 (4)30	610
0.6-0.7	Rh^{106}	0.62	0.23	(4)66 (4)15	(4)66 (4)15	(4)66 (4)15	(4)66 (4)15	(4)66 (4)15	(4)66 (4)15	(4)65 (4)15	(4)64 (4)148	(4)63 (4)145	(4)54 (4)124	50
	Ba^{137m}	0.66	1.9	(4)21 (4)40	(4)21 (4)40	(4)21 (4)40	(4)21 (4)40	(4)21 (4)40	(4)21 (4)40	(4)21 (4)40	(4)21 (4)40	(4)21 (4)40	(4)20 (4)38	620
	Nb^{97}	0.67	2.2	0.25 0.55	0.34 0.75	0.29 0.64	0.17 0.375	(1)63 0.138	(2)89 (1)196	(3)48 (2)106	(6)50 (5)11	- -	- -	620
	I^{132}	0.67	2.2	(1)26 (1)57	(1)41 (1)90	(1)51 0.112	(1)47 0.104	(1)38 (1)84	(1)25 (1)55	(1)13 (1)285	(2)28 (2)62	(3)14 (3)31	(11)82 (10)18	380
0.7-0.8	Zr^{95}	0.72	1.02	(2)35 (2)355	(2)46 (2)47	(2)46 (2)47	(2)46 (2)47	(2)46 (2)47	(2)45 (2)46	(2)43 (2)435	(2)40 (2)408	(2)35 (2)355	(2)15 (2)15	630
	Mo^{99}	0.74	0.2	0.1 (1)20	(1)98 (1)196	(1)90 (1)18	(1)80 (1)16	(1)62 (1)134	(1)38 (2)76	(1)18 (2)36	(2)31 (3)62	(4)96 (4)192	(12)45 (13)90	590
	Nb^{97m}	0.75	1.9	0.39 0.74	0.36 0.685	0.27 0.51	0.16 0.305	(1)58 0.11	(2)83 (1)158	(3)44 (3)84	(6)47 (6)89	- -	- -	620
	Zr^{95}	0.756	0.98	(2)35 (2)345	(2)46 (2)45	(2)46 (2)45	(2)46 (2)45	(2)46 (2)45	(2)45 (2)44	(2)43 (2)425	(2)40 (2)395	(2)35 (2)345	(2)15 (2)15	630
	Nb^{95}	0.77	1.87	(4)20 (4)375	(4)40 (4)75	(4)60 (3)112	(3)10 (3)187	(3)19 (3)355	(3)36 (3)675	(3)57 (2)107	(2)10 (2)187	(2)17 (2)32	(2)20 (2)375	630
	I^{132}	0.78	1.3	(1)26 (1)34	(1)41 (1)53	(1)51 (1)66	(1)47 (1)61	(1)38 (1)49	(1)25 (1)325	(1)13 (1)17	(2)28 (2)365	(3)14 (3)18	(11)82 (10)106	380
	Mo^{99}	0.78	0.08	0.1 (2)80	(1)98 (2)78	(1)90 (2)72	(1)80 (2)64	(1)62 (2)495	(1)38 (2)30	(1)18 (2)14	(2)31 (3)25	(4)96 (5)77	(12)45 (13)36	590
0.8-0.9	La^{140}	0.82	0.47	(3)39 (3)18	(2)14 (3)66	(2)48 (2)225	(2)76 (2)36	(1)12 (2)56	(1)16 (2)75	(1)17 (2)80	(1)12 (2)56	(2)58 (2)27	(4)90 (4)42	610
0.9-1.0	I^{132}	0.96	0.31	(1)26 (2)81	(1)41 (1)127	(1)51 (1)158	(1)47 (1)146	(1)38 (1)118	(1)25 (2)77	(1)13 (2)40	(2)28 (3)87	(3)14 (4)43	(11)82 (11)25	380

[Continued on next page]

Table 2 (continued). Fission product activity and scintillation peak height

(Figures in brackets denote number of zeros after decimal point)

Energy range (MeV)	Fission Product	γ Energy (MeV)	Peak Height Factor	(a) Activity dpm per 10^4 fissions (ref. (3)) (b) Peak height rel. to La^{140} 1.6 MeV										Cumulative fission yields: ref. (3) (atoms per 10^4 fissions)
				1h	3.5h	12h	1d	2d	4d	7d	14d	28d	105d	
1.0-1.2	I^{132}	1.16	0.09	(1)26 (2)235	(1)41 (2)37	(1)51 (2)46	(1)47 (2)425	(1)38 (2)34	(1)25 (2)225	(1)13 (2)117	(2)28 (3)25	(3)14 (4)126	(11)82 (12)74	380
1.4-1.6	I^{132}	1.40	0.12	(1)26 (2)31	(1)41 (2)49	(1)51 (2)61	(1)47 (2)56	(1)38 (2)46	(1)25 (2)30	(1)13 (2)156	(2)28 (3)34	(3)14 (4)17	(11)82 (12)98	380
1.6-1.8	La^{140}	1.60	1	(3)39 (3)39	(2)14 (2)14	(2)48 (2)48	(2)76 (2)76	(1)12 (1)12	(1)16 (1)16	(1)17 (1)17	(1)12 (1)12	(2)58 (2)58	(4)90 (4)90	610
Activation products (N.B. activity dpm per 10^3 atoms of U^{239} and U^{237} at $t = 0$)	Np^{239}	0.104	3.1	- -	- -	0.177 0.55	0.153 0.475	0.113 0.35	(1)62 0.192	(1)26 (1)805	(2)35 (1)108	- -	- -	
		0.225	0.68	- -	- -	0.177 0.12	0.153 0.104	0.113 (1)77	(1)62 (1)42	(1)26 (1)177	(2)35 (2)238	- -	- -	
		0.28	0.58	- -	- -	0.177 0.102	0.153 (1)89	0.113 (1)655	(1)62 (1)36	(1)26 (1)15	(2)35 (2)203	- -	- -	
	U^{237}	0.062	1.54	(1)72 0.111	- -	(1)69 0.108	(1)66 0.102	(1)59 (1)91	(1)48 (1)74	(1)35 (1)54	(1)17 (1)26	(2)39 (2)60	- -	
		0.103	2.7	(1)72 0.194	- -	(1)69 0.186	(1)66 0.178	(1)59 0.16	(1)48 0.23	(1)35 (1)95	(1)17 (1)46	(2)39 (1)106	- -	
		0.205	1.16	(1)72 (1)83	- -	(1)69 (1)80	(1)66 (1)764	(1)59 (1)683	(1)48 (1)558	(1)35 (1)405	(1)17 (1)197	(2)39 (2)45	- -	

above, it follows that the "peak-height factor" may be converted to the case of constant channel width by dividing it by γ -ray energy.

Calculated γ -ray scintillation spectra

The decay-scheme and crystal-efficiency data are collected together in Table 1. The fission products are listed in order of increasing half-life. The branching ratio is the fraction of disintegrations that emit a certain γ -ray. The internal conversion term is calculated from $1/\{1 + (e/\gamma)\}$, where e/γ is the ratio of the number of conversion electrons to the number of unconverted γ -rays. Peak-height factors are obtained from the product of the γ -ray (or X-ray) abundance factor (that is, branching ratio multiplied by internal conversion) and the arbitrary peak-height efficiency. In the final column, the peak-height factor is normalized against a value of unity for the La^{140} peak at 1.6 MeV. Included in Table 1 with the fission products of uranium 235 are two neutron activation products of uranium 238.

In Table 2, the fission products are regrouped according to energy of γ -ray. The fission-product activities (in dpm per 10^4 fissions) according to Hunter and Ballou⁽³⁾ are presented at suitable intervals and multiplied by the appropriate peak-height factors to give the variation of scintillation peak height with time. In view of the method of normalization of the

peak-height factors, the peak height for the 1.6 MeV γ -ray of La^{140} retains its equivalence to activity per 10^4 fissions of this fission product.

The calculated peak heights of Table 2 were plotted in Figs. 1-7. These calculated curves represent the γ -ray scintillation spectra that would be observed, between 12 and

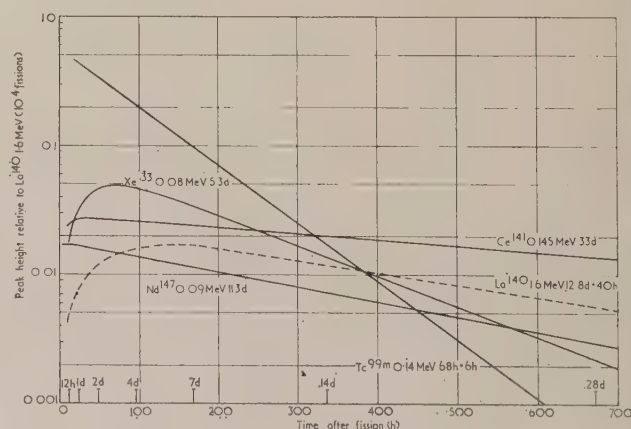


Fig. 1. Variation with time of peak height Peaks < 0.2 MeV

700 h, from the idealized case of simultaneous slow neutron fission of uranium 235. Relative fission-product activities may be calculated by a comparison at any time of peak heights in a practical example of fission with this standard case. Furthermore, by reference to the fission yields (Table 2) used by Hunter and Ballou,⁽³⁾ the relative activities may, if

required, be stated in terms of relative yield. The accuracy of the fission yield and activity data presented by Hunter and Ballou does not affect the present application. It is sufficient that the data should represent a basis to which an experimental determination of relative yield or activity may be referred.

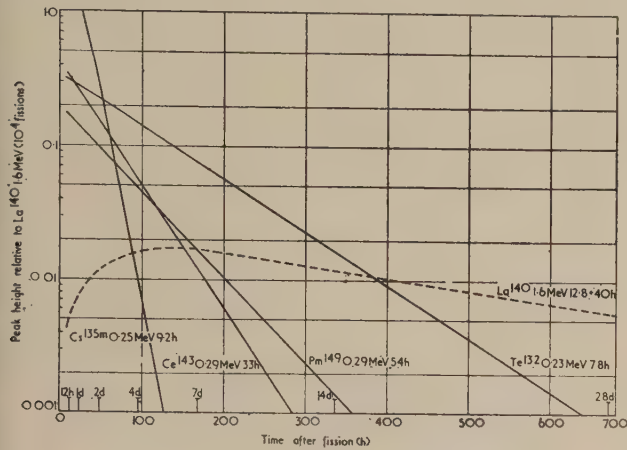


Fig. 2. Variation with time of peak height Peaks, 0.2 - 0.3 MeV

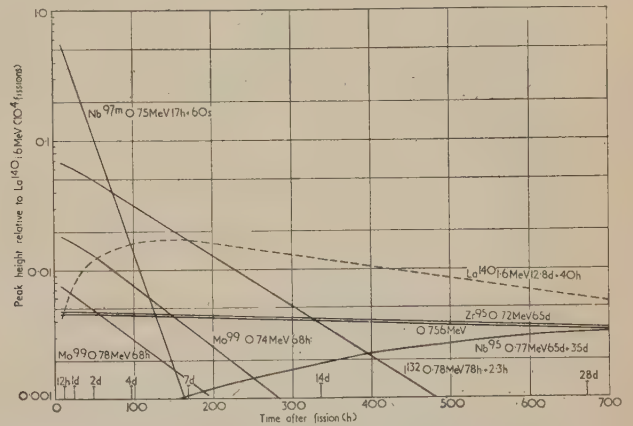


Fig. 5. Variation with time of peak height Peaks, 0.7 - 0.8 MeV

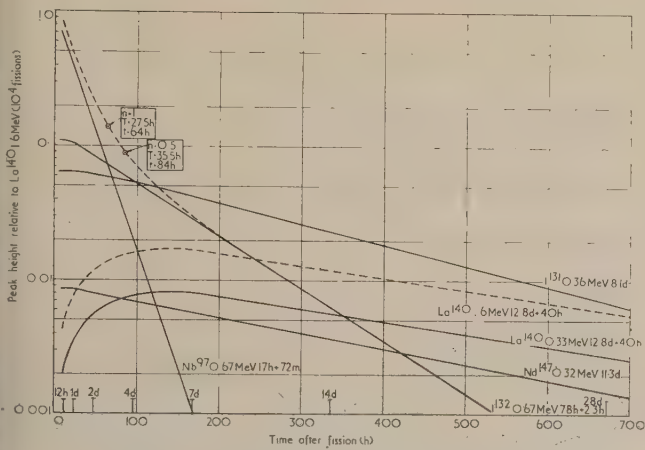


Fig. 3. Variation with time of peak height Peaks, 0.3 - 0.4 MeV and 0.6 - 0.7 MeV

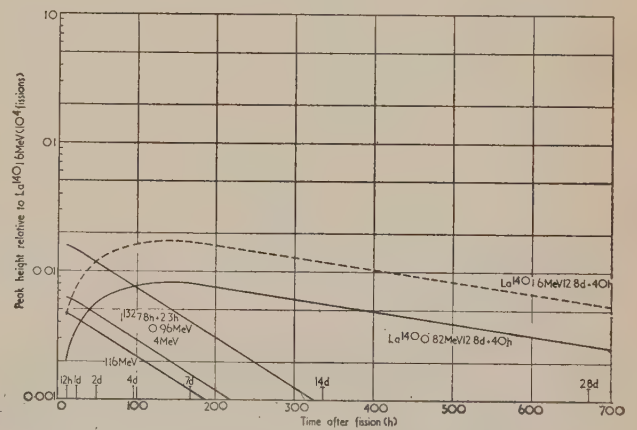


Fig. 6. Variation with time of peak height Peaks, 0.8 - 1.4 MeV

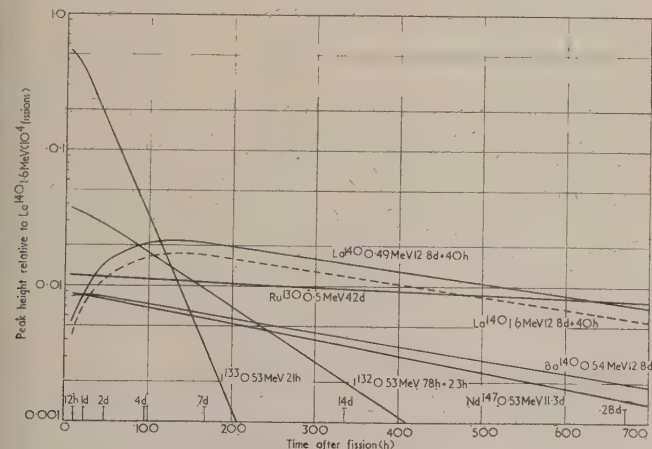


Fig. 4. Variation with time of peak height Peaks, 0.4 - 0.6 MeV

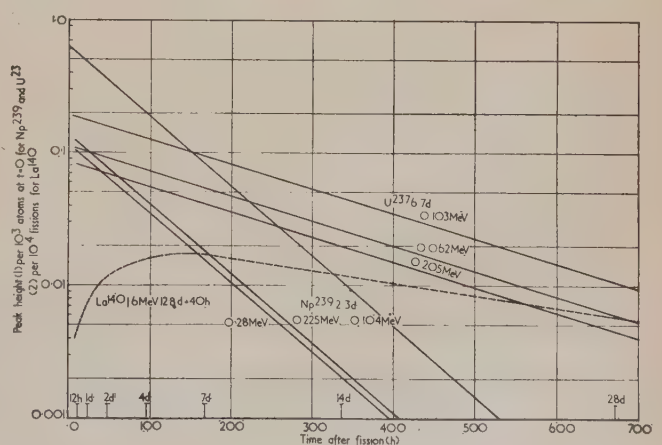


Fig. 7. Variation with time of peak height of activation products Np²³⁹ and U²³⁷

Spectrometer resolution

Separation of peaks with similar energies is limited by the practical resolving power obtained with the spectrometer. Resolving power, or resolution, is usually measured by the full width of the peak (at half maximum height) due to Cs^{137} at 0.661 MeV. A typical resolution measured with a sodium-iodide crystal of 1 in. by 1.5 in. diameter is 0.053 MeV or 8% of the total energy. By virtue of the assumed linearity of the scintillation process (see Method, above) the peak width varies as the square root of the energy. Conventionally, neighbouring peaks may be said to be resolved when separated by more than a full width of the peak.

Work by Engelkemeir⁽⁷⁾ has shown an apparent departure from linearity in the scintillation process. Kelley *et al.*⁽⁸⁾ have discovered that peak width is not directly related to the square root of energy. Iredale⁽⁹⁾ has confirmed both anomalous effects, and has obtained an empirical relationship between peak width and energy. Thus for one sodium-iodide crystal of the standard dimensions, peak width varies substantially in the predicted manner above 0.661 MeV. At 0.145 MeV (Ce^{141}), the peak width is reduced by about 30%, although the product of peak width and peak height remains proportional to peak area.

The reasons for the departure from normal statistical behaviour have not yet been discovered. Meanwhile, it would seem necessary to allow for this anomaly by correcting the standard peak-height efficiency (see Method, above) by an empirical relationship determined for the scintillation crystal used for spectrometric measurement.

Analysis of half-life

When the photoelectric peaks due to the γ -rays from fission products are identical in energy (that is, beyond the resolving power of the spectrometer), it is necessary to attempt differentiation by half-life as well as by energy. In the practical case, this is achieved by observing the rate of decay of a composite peak.

It can be seen from Figs. 1–7 that such composite peaks often reduce to a combination of two components, the half-lives of which will be known. In such a case, one customary method of separation of the two components is by graphical subtraction of the long-lived component obtained after the short-lived component has died out. Greater precision for a shorter period of observation is possible by simple manipulation⁽¹⁰⁾ of the expression for the combined peak height:

$$A = a \exp(-\lambda_a t) + b \exp(-\lambda_b t),$$

where a , b are the component peak heights at time $t = 0$, and λ_a , λ_b are the component decay constants ($\lambda_a > \lambda_b$). Multiplication by $\exp(\lambda_b t)$ gives:

$$A \exp(\lambda_b t) = a \exp\{-(\lambda_a - \lambda_b)t\} + b.$$

With $A \exp(\lambda_b t)$ and $\exp\{-(\lambda_a - \lambda_b)t\}$ as variables, this is the equation to a straight line having slope a and intercept b . This method gives satisfactory results when applied to two-component decay, but requires considerable computation.

Greater rapidity is possible using a method that calculates the slope of the composite decay curve at a time corresponding to a selected ratio of the separately decaying components. The slope, on a log-linear scale, is expressed (Appendix 1) as the effective half-life T corresponding to the ratio n :

$$\frac{T}{T_b} = \frac{n+1}{n(T_b/T_a) + 1},$$

where T_a , T_b are the component half-lives ($T_b > T_a$), and:

$$n = \frac{a}{b} \exp\{-(\lambda_a - \lambda_b)t\}.$$

The application of this method may be demonstrated by reference to Fig. 3 in which the composite peak-height decay curve, such as would be measured in a practical experiment, has been computed by the addition of the separate peak heights due to Nb^{97} (17 h) and I^{132} (78 h). For convenience n is chosen as 1. The ratio of half-lives T_b/T_a for these two activities is 4.6 so that T/T_b is 0.35 and T is 27.5 h. Inspection of the composite curve shows that the slope (or effective half-life) has this value when t is 64 h. This (for n equal to 1) is the time when the peak heights of the two components are equal, as may be confirmed immediately from the component curves. A similar exercise is carried out for n equal to 0.5. The expression for T/T_b for n equal to 0.1–5 is drawn in Fig. 8. Choice of n is guided by the range

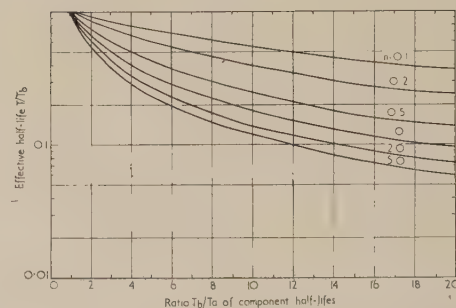


Fig. 8. Variation of effective half-life with ratio of component half-lives

$$\begin{aligned} T_a, T_b &= \text{half-lives of components } a \text{ and } b (T_b > T_a) \\ n &= \text{ratio of peak heights of components } a \text{ and } b \\ T &= \text{effective half-life corresponding to } n \\ \frac{T}{T_b} &= \frac{n+1}{n(T_b/T_a) + 1} \end{aligned}$$

of the experimental measurements: thus in Fig. 3 for t greater than 200 h, n tends to 0 and hence T equals T_b .

Where, as in Fig. 4, peak heights of identical or similar energies are not immediately reducible to two-component decays, it is possible to use estimates of peak height derived from determinations at other energies. Thus the peak height for I^{132} at 0.53 MeV may be calculated using the data of Table I from the straight-forward determination of I^{132} at 0.67 MeV in Fig. 3. If the peak height at 1.6 MeV for La^{140} is given, the contributions in Fig. 4 due to La^{140} at 0.49 MeV and to Ba^{140} at 0.54 MeV may be derived in a similar manner. After subtraction of the components due to I^{132} , Ba^{140} and La^{140} , the residual curve contains peak height contributions due to I^{133} , Nd^{147} and Ru^{103} . The peak heights due to Nd^{147} and Ru^{103} may be separated after a time t of 250 h when the I^{133} activity has effectively disappeared.

A similar approach may be made to the energy range covered by Fig. 5. In this range, and in that covered by Fig. 4, successful separation of the various activities is particularly dependent upon the precision of the spectrometer measurements.

References

- (1) CORYELL, C. D., and SUGARMAN, N. *National Nuclear Energy Series*, 4-9 (New York: McGraw-Hill, 1951).
- (2) PEIRSON, D. H. *Brit. J. Appl. Phys.*, 6, p. 444 (1955).
- (3) HUNTER, H. F., and BALLOU, N. E. *U.S.N.R.D.L.*, Report ADC-65 (1949).

- (4) BOLLES, R. C., and BALLOU, N. E. *U.S.N.R.D.L.*, Report 456 (1956).
- (5) HOLLANDER, J. M., PERLMAN, I., and SEABORG, G. T. *Rev. Mod. Phys.*, **25**, p. 469 (1953).
- (6) PEIRSON, D. H., and IREDALE, P. *Brit. J. Appl. Phys.*, **8**, p. 422 (1957).
- (7) ENGELKEMEIR, D. *Rev. Sci. Inst.*, **27**, p. 589 (1956).
- (8) KELLEY, G. G., BELL, P. R., DAVIS, R. C., and LAZAR, N. H. *I.R.E. Transactions—Scintillator Counter Symposium NS3*, No. 4, p. 57 (1956).
- (9) IREDALE, P. (A.E.R.E. Harwell). Private communications.
- (10) FREILING, E. C., and BURNEY, L. R. *Nucleonics*, **14**, No. 9, p. 112 (1956).

Appendix 1

Effective half-life of a complex decay curve

If an activity A consisting of two components a and b having exponential decay constants λ_a and λ_b ($\lambda_a > \lambda_b$) is considered, then:

$$A = a \exp(-\lambda_a t) + b \exp(-\lambda_b t).$$

On differentiation:

$$\frac{dA}{dt} = -\lambda_a a \exp(-\lambda_a t) - \lambda_b b \exp(-\lambda_b t).$$

The slope of the expression for A plotted on the usual log-linear scale is:

$$\frac{d(\log A)}{dt} = \frac{1}{A} \cdot \frac{dA}{dt}$$

That is:

$$\frac{d(\log A)}{dt} = -\frac{\lambda_a \exp(-\lambda_a t) + \lambda_b \exp(-\lambda_b t)}{a \exp(-\lambda_a t) + b \exp(-\lambda_b t)},$$

or, after division by $b \exp(-\lambda_b t)$:

$$\frac{d(\log A)}{dt} = -\frac{(a/b)\lambda_a \exp\{-(\lambda_a - \lambda_b)t\} + \lambda_b}{(a/b) \exp\{-(\lambda_a - \lambda_b)t\} + 1}.$$

If the ratio $(a/b) \exp\{-(\lambda_a - \lambda_b)t\}$ of component activities is at any time equal to n , then:

$$\frac{d(\log A)}{dt} = -\frac{n\lambda_a + \lambda_b}{n + 1},$$

which becomes:

$$\frac{d(\log A)}{dt} = -\frac{0.693}{n + 1} \left(\frac{n}{T_a} + \frac{1}{T_b} \right),$$

where T_a and T_b are half-lives corresponding to λ_a and λ_b . This reduces to $-0.693/T$, where T is the slope, measured as an effective half-life at this time.

Hence:

$$\frac{T}{T_b} = \frac{n + 1}{n(T_b/T_a) + 1}.$$

The ratio n may represent activities or, as in the present case, scintillation peak heights. The quantity T/T_b is plotted against T_b/T_a for various n in Fig. 8.

Measurement of crystallinity in drawn polyethylene terephthalate fibres by X-ray diffraction

by G. FARROW, Ph.D., B.Sc.(Tech.), and D. PRESTON, Research Department, Fibres Division, Imperial Chemical Industries Ltd., Harrogate, Yorkshire

[Paper received 14 March, 1960]

Abstract

A method has been devised for the measurement of crystallinity in drawn fibres of polyethylene terephthalate fibre by an X-ray technique. Strictly monochromatic X-ray radiation is used and the X-ray camera is evacuated. This enables the photographic film, which is used to record the X-ray reflexion, to be free of "white" radiation and parasitic X-ray radiation normally termed "air scatter". The results show that the crystallinity in drawn yarns is much lower than expected and that no correlation exists between the crystallinity so measured and the density of the yarns.

The X-ray photographic method that has been developed is now comparable in speed with the alternative method

of recording the X-ray diffraction pattern by means of a Geiger-Müller counter.

Introduction

As part of the characterization of polyethylene terephthalate fibres, a knowledge of the degree of crystallinity is important. Crystallinities inferred from density and infra-red measurements suffer from theoretical disadvantages⁽¹⁾ particularly if applied to oriented structures such as polyethylene terephthalate fibres. The implications of this are enlarged upon elsewhere.⁽²⁾

Broadly speaking, there are two different methods of measuring crystallinity in polymers by X-ray diffraction. In the method of Goppel,⁽³⁾ the absolute intensity of the non-crystalline background at a point where no crystalline reflexion occurs is compared with the intensity at the same point for a wholly non-crystalline sample. The method requires absolute corrections for air scatter and incoherent scatter and the use of a standard sample to eliminate errors due to absorption. On the other hand, the method of Matthews *et al.*,⁽⁴⁾ by which the integrated intensity of the crystalline reflexions is compared with the integrated intensity of the amorphous background has the advantage that only relative intensities are required. We have followed the latter method, our X-ray intensities being recorded on a photographic film which was then scanned by a microdensitometer.

Measurements of crystallinity on unoriented samples of polyethylene terephthalate, by X-ray techniques, were already known.^(5,6) The difficulty in this particular case lay in the production of a randomized sample of polyethylene terephthalate drawn fibres which was suitable for X-ray diffraction and which gave, on exposure to the X-ray beam, a photograph equivalent to that obtained from an undrawn, randomly oriented specimen of polyethylene terephthalate. If the sample is insufficiently randomized, then the relative intensities of the crystalline reflexions will not be present in their correct proportions. Certain planes in the crystal will be preferentially oriented to the X-ray beam at the expense of others and the resultant photograph will not be equivalent to that obtained from a crystalline, unoriented specimen of polyethylene terephthalate.

There were three possible ways of producing a randomized sample:

- (a) by a mechanical device which would rotate the sample in a number of different directions, simultaneously, during its exposure to the X-ray beam;
- (b) by chopping or folding the fibres in such a way that the sample was randomized before being placed in the X-ray beam;
- (c) by a combination of (a) and (b).

A mechanical device as mentioned in (a) was constructed but was difficult to use with a focusing X-ray camera, to be described later. Efforts were concentrated on (b) and suitable samples were produced in cylindrical form (Fig. 1) by a method similar to that of Hermans and Weidinger.⁽⁷⁾

Experimental

(i) *Sample preparation.* The material used for this work was polyethylene terephthalate film, chip and yarn both amorphous and crystalline. In the production of polyester yarn, the molten polymer is first extruded and collected as amorphous filaments with slight orientation (melt spun yarn) and then stretched by drawing continuously. The second drawing stage is carried out either over a heated cylindrical pin alone or with such a pin followed by a heated plate. In the drawn material used in these experiments, the pin temperature was maintained at 90° C and the plate when used at 180° C. The yarn was drawn to different draw ratios and the method of sample preparation was also applied to yarns with different filament diameters. Heat crystallization of yarns was carried out in a silicone oil bath before the manufacture of the samples. They were either held freely or under tension in the oil and brought up to the required temperature slowly to avoid sudden shrinkage and then held at the required temperature for half an hour.

After cooling, the samples were washed with carbon tetrachloride to remove any oil adhering to the surface, and dried.

The fibres were chopped (with a new razor blade on a polythene pad) so as to contain a range of sizes from fractions

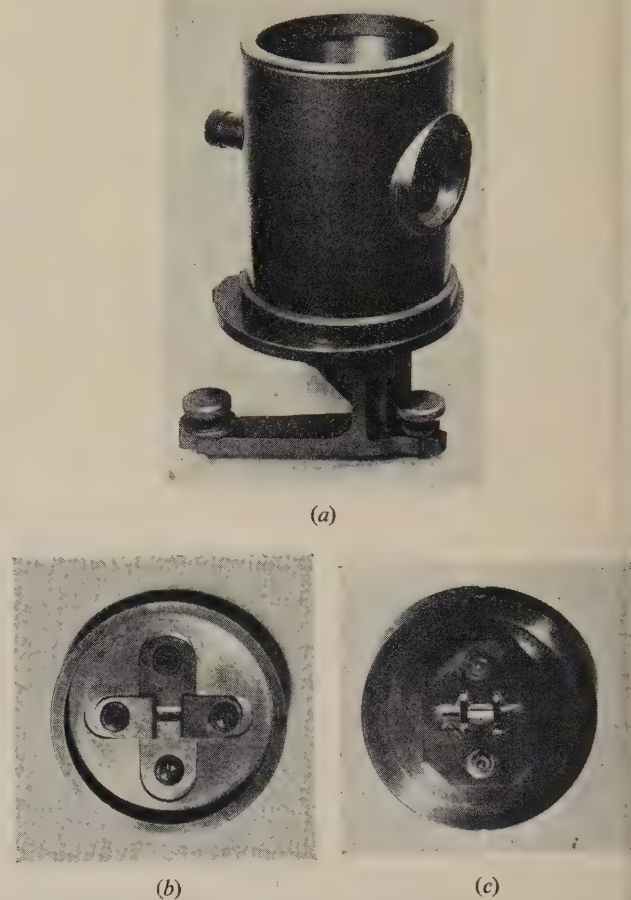


Fig. 1. (a) 9 cm focusing camera
(b) Brass disk sample holder which fits on to circumference of camera. Slits stop secondary X-ray radiation reaching film
(c) Reverse side of sample holder showing randomized sample in position

of a millimetre in length to lengths of 2–3 mm. The chopped fragments were wetted with a few drops of water containing a small amount of wetting agent, Lissapol N, and were mixed thoroughly into spherical shape with a dissecting needle. Small spherical pellets were then removed from this mass and introduced into a stainless-steel cylindrical mould (internal dimensions approximately 1 mm diameter \times 5 mm height) and pressure applied with a shaped steel rod. The water was expelled, mopped up with filter paper and the sample was dried for fifteen minutes in an oven at 40° C. This produced a sample which was compact but fragile, held together by the folding-in of the fibres during the pelleting process.

(ii) *Randomness of sample.* To be certain that the method of sample preparation was reasonable it was necessary to check on their degree of randomness. If samples are not properly randomly oriented, then the ratio of intensities of specific reflexions will not be the same as the ratio of the intensities of the same reflexions derived from randomly

Table 1. *Ratios of intensities*

	Height (cm)		Ratio 01̄1/1̄10	Height (cm)		Ratio 01̄1/100
	01̄1	1̄10		01̄1	100	
<i>Randomly oriented film 20 thou. thick</i>						
½ h at 150° C	6.5	7.5	0.87	6.5	8.5	0.76
½ h at 212° C	7.5	8.8	0.89	7.5	11.0	0.69
½ h at 230° C	5.6	6.1	0.92	5.6	7.4	0.76
<i>Spun yarn low orientation</i>						
½ h at 120° C	6.9	8.3	0.83	6.9	9.4	0.73
½ h at 150° C	5.7	6.5	0.88	5.7	7.0	0.81
½ h at 230° C	8.5	9.5	0.89	8.5	12.0	0.71
<i>Spun yarn high orientation</i>						
½ h at 120° C	4.5	5.1	0.88	4.5	5.8	0.77
½ h. at 150° C	5.9	6.9	0.86	5.9	8.5	0.69
½ h at 230° C	9.5	10.4	0.88	9.5	12.8	0.73
<i>Drawn yarn heat treated ½ h at 210° C</i>						
D.R. 3.6 free	5.7	6.3	0.89	5.7	8.2	0.70
D.R. 3.6 tension	6.7	7.2	0.92	7.2	9.6	0.70
D.R. 4.8 free	5.0	5.4	0.92	5.1	6.7	0.75
D.R. 4.8 tension	5.2	5.5	0.94	5.2	6.8	0.77

oriented heat crystallized chip, film or spun yarn. These ratios have been checked and examples are given in Table 1 below. Fig. 2 illustrates the intensities and indices referred to in the table. It can be seen from Table 1 that the variation of intensity is on the whole no greater than that of the undrawn specimens. Ideally, only samples of the same crystallinity should be compared.

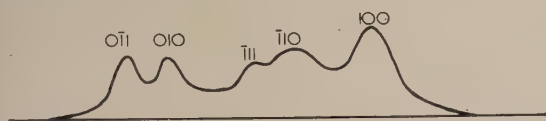


Fig. 2. Profile across equator of X-ray photograph of crystalline polyethylene terephthalate film

It is also possible to check the degree of randomization in the samples by a second method. If a sample is insufficiently randomized because of the method of packing, the majority of the fibres will tend to lie in horizontal planes perpendicular to the length of the sample. Since the sample, when mounted on the X-ray camera, lies with its length perpendicular to the X-ray beam, an incompletely randomized sample would give an X-ray photograph in which the intensity of the reflexions along the meridian would be different from those around the equator. This cannot be readily seen in the normal photograph used for crystallinity purposes, taken on a cylindrical camera; but by using a flat plate camera, where the cone of X-ray reflexions is meeting a flat surface normal to the cone, such intensity variations may be readily discerned.

Sets of reflecting planes which are completely random will give circles of equal intensity on the flat plate camera. If such a photograph is then scanned by the microdensitometer across the meridian and equator, respectively, then the two profiles should be identical, or the areas underneath the respective curves should be the same. Table 2 illustrates this for a few samples.

It can be seen that the values for total areas beneath the microdensitometer traces do not differ by more than 3%

for each respective, equatorial and meridional scan except for the last one where the sample is poorly randomized.

(iii) *X-ray camera.* In previous work on unoriented samples of polyethylene terephthalate, long exposure times had been necessary to obtain a suitable X-ray photograph. To reduce

Table 2. *Comparison of areas*

Sample Draw ratio	Total area (cm ²)	
	Equator	Meridan
4.5	164	161
3.0	190	192
4.0	89	92
5.0	77	100

this, a microfocus X-ray tube, 100 micron model (by Messrs. Hilger and Watts) which delivers a much more powerful X-ray beam than that from a conventional sealed-off tube, was used. The design is based on that of Ehrenberg and Spear⁽⁸⁾ and gives a beam of X-rays either as a fine spot or in the shape of a line.

The line focus of the microfocus X-ray tube was particularly suited for use with a focusing monochromator (focusing crystal). The use of focused monochromatic radiation offered two advantages. First, background fogging of the film was greatly reduced because "white" radiation was removed and second, when used in conjunction with a focusing camera the monochromator gave increased resolution and increased intensity to the X-ray reflexions. These facts also contributed to a decrease in exposure times with an increase in accuracy of determination of X-ray crystallinities. Further improvement in the clarity of the X-ray photograph was obtained by eliminating, by evacuation of the X-ray camera, parasitic X-ray scatter produced by the X-ray beam striking molecules of air.

The type of focusing monochromator used, a quartz crystal asymmetrically ground and elastically bent has already been described by Guinier.⁽⁹⁾ The distance from the target of the X-ray tube to the centre of the crystal plate was 80 mm

and from the centre of the plate to the focus was 140 mm, that is, the monochromatic beam came to a focus 140 mm from the centre of the quartz crystal. If used in conjunction with a focusing camera, then to satisfy the geometrical requirement for perfect focusing of the diffracted beams, the furthest point on the camera wall had to be placed exactly here. The path taken by the beam is illustrated by a diagram (Fig. 3.) Now, because all angles subtended at the circum-

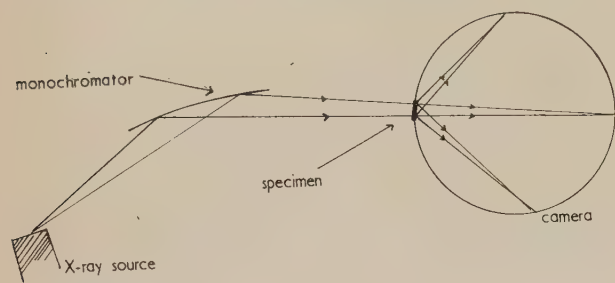


Fig. 3. Focusing effect of ground and bent crystal sample on wall of camera

ference of a circle by a given arc are equal, the diffracted beams from the specimen, lying in the equatorial plane, will come to a focus on the circumference of the vertically held camera.

A simple cylindrical X-ray camera (Fig. 1) of 9 cm diameter was used. The maximum diameter of camera that could be used was determined by the allowed distance between camera and focusing crystal which in itself was fixed by the wavelength of the X-ray radiation. The diameter of the camera chosen was also a compromise between length of exposure time and the best possible separation of the X-ray reflexions (thicker in the case of oriented samples) to give maximum resolution. The specimen and the film were both placed on the circumference of the camera. To facilitate easy loading of the specimen, the front portion of the camera, in the form of a 2 in diameter brass disk (Fig. 1), was made detachable. Into the back of the camera was cut a rectangular slot for the exit of the line-shaped primary beam diametrically opposite the specimen. The X-ray film normally used, Ilford G (12.5×17.5 mm) was of high speed and moderate fog level. Before being placed in the camera a rectangular hole was punched in the centre of the film to correspond to the exit slot for the main beam on the camera to prevent fogging of the film. The film was held in position around the inside circumference of the camera by circular retaining rings top and bottom and located by a hollow rectangular plug fitted into the exit hole for the main beam.

The camera rested on a small stand (Fig. 1) and was located in position by two small pins. This stand, with three adjustable legs, was located on the broad base of another stand containing an O-ring for a vacuum seal and the entry and exit ports for evacuating the camera. The three legs of this base were also adjustable in height and slide in the triangular grooves of a locating plate on the body of the X-ray unit. The whole assembly can be moved backwards and forwards along the grooves, facilitating removal of the bell jar. The exact position of the camera was determined by an adjustable stop along one of the grooves, for as already stated the camera must be at a precise distance (within ± 2 mm) from the crystal for focusing to be achieved. A bell jar was placed over the whole camera assembly and was evacuated to approximately 1 mm of mercury pressure. The bell jar was fitted with a beryllium window at the appropriate level

to allow the X-ray beam to enter the camera with negligible absorption.

Exposure times required for randomized samples were of the order of one hour. After development, the X-ray films were washed, dried and scanned by a microdensitometer (by Joyce, Loebl and Company Ltd.).

(iv) *Measurement of crystallinity.* On the X-ray photographs of polyethylene terephthalate the crystalline and amorphous reflections overlap (Fig. 4) and it is therefore,

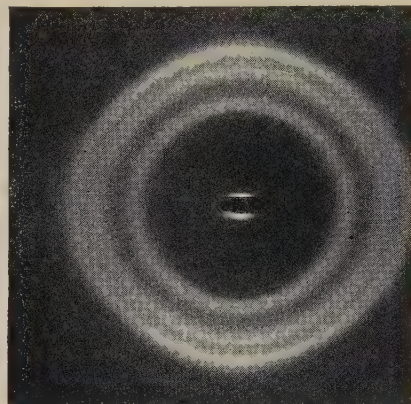


Fig. 4. X-ray photograph of polyethylene terephthalate

necessary to reconstruct the amorphous curve underneath the crystalline scatter. It has been assumed that the scattering efficiencies to X-rays of the crystalline and amorphous regions are the same⁽⁴⁾ and that, also, the amorphous material in partially crystalline drawn fibres of polyethylene terephthalate gives rise to the same X-ray reflexion contour, but reduced in proportion, as that in a truly amorphous sample. Some experimental justification for this latter assumption can be found from examination of traces of randomized samples of moderately oriented material (low draw-ratio yarn) which show very little or no crystallinity, and comparing the contours of the X-ray traces with those obtained from unoriented amorphous samples. For example, Fig. 5, illustrates a contour from a yarn of draw ratio 2.0

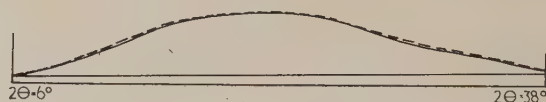


Fig. 5. Continuous line: undrawn amorphous specimen of polyethylene terephthalate (density = 1.335 g/ml.)
Broken line: low draw-ratio (2.0) specimen of polyethylene terephthalate randomized
($\Delta = 94 \times 10^{-3}$; density = 1.348 g/ml.)

birefringence 95×10^{-3} superimposed on that from an undrawn amorphous sample. The contours are almost identical. Similar results were obtained from other samples of low draw-ratio yarn. It was, therefore, concluded that the distribution of van der Waal's distances in the "amorphous" regions of the oriented samples was similar to that found in the non-oriented state. By eliminating air scatter from the X-ray film, an additional fitting point *B*, Fig. 6, normally obscured, is available at low angles enabling any abnormalities to be more readily seen in the reconstructed amorphous curve. The rise in the background of the trace, Fig. 6, is due to X-ray incoherent scatter and was

assumed to be linear. Experimental verification of this was adduced from a similar rise in background found in the wholly crystalline compound known as the "linear trimer".
 $\text{MeO} \left[\text{OC} - \text{C}_6\text{H}_4 - \text{CO}_2 - (\text{CH}_2)_2 - \text{O} \right]_2 \cdot \text{OC} - \text{C}_6\text{H}_4 - \text{CO}_2 \text{Me}$
 first reported by Zahn *et al.*⁽¹⁰⁾ which gives an X-ray powder



Fig. 6.—Trace of crystalline polyethylene terephthalate with reconstructed amorphous curve

New fitting point *B* (no air scatter). *A* reference point for calculation of amorphous background; rise in background, incoherent scatter

pattern almost identical with that from a heat-crystallized sample of polyethylene terephthalate.

Now the apparent percentage crystallinity (C_a) of a sample is equal to:

$$\frac{\text{area of the crystalline fraction}}{\text{area of crystalline fraction} + \text{area of the amorphous fraction } (A_a)} \times 100.$$

The total value of the denominator is easily computed by measuring the total area of the trace obtained by scanning the X-ray film with a microdensitometer. This quantity is actually determined automatically by an integrating device coupled to the microdensitometer (to be described elsewhere).¹¹

The area of the amorphous curve is obtained by reducing the whole of the amorphous contour obtained from an amorphous specimen of polyethylene terephthalate in proportion to the height of the background at point *A* (Fig. 4) on the trace, where the amorphous background at this point is resolved from the adjacent crystalline reflexions. We have also found it satisfactory to obtain the area of the amorphous fraction by reading off the background height at point *A* from a graph which plots various background heights at this point against the total area of an equivalent amorphous contour for the particular expansion ratio in use on the microdensitometer. This saves the reconstruction of the whole amorphous curve; a check was made for abnormalities by superimposing a template of amorphous curves of different areas on the trace which was being measured.

To convert C_a to a true crystallinity C , it is necessary to correct for the non-coincidence of the centres of gravity of the amorphous and crystalline reflexions.⁽⁴⁾ A factor of 0.98 was obtained for polyethylene terephthalate with the present focusing camera, the crystalline reflexions being measured over the range $2\theta = 6^\circ$ to $2\theta = 38^\circ$. The formula for the calculation of true crystallinity is then:

$$C = \frac{C_a}{C_a + 0.98A_a}.$$

Results

Results are given in Table 3 where X-ray crystallinities and those found by density are given for a number of different types of yarn under a variety of conditions.

Table 3. Crystallinities

Pin drawn and *pin and plate yarns

Yarns D.R.	Density (g/l)	% Cryst. density	X-ray, two results % Cryst.		Density (g/l) oriented non-cryst.	Mean X-ray
3.6	1.368	27.6	7.9	7.7	1.359	8.0
4.4	1.374	32.6	12.4	13.8	1.358	13.0
4.8	1.369	28.3	16.0	17.3	1.349	17.0
*3.6	1.389	45.0	27.8	27.9	1.355	28.0
*4.4	1.387	44.0	28.0	30.6	1.352	29.0
*4.8	1.387	44.0	23.8	24.2	1.359	24.0

Heat crystallized yarns $\frac{1}{2}$ h at 145°C and $\frac{1}{2}$ h at 210°C

Free and under tension. Pin drawn and *pin and plate

D.R.	Temp. (°C)	Condition	Density (g/l)	% Cryst. density	X-ray, two results % Cryst.		Density (g/l) oriented non-cryst.	Mean X-ray
3.6	145	Free	1.389	45	29.7	33.4	1.351	32.0
4.8	145	Free	1.384	41	36.9	34.3	1.341	36.0
3.6	145	Tension	1.388	44	37.6	34.6	1.346	35.0
4.8	145	Tension	1.387	43	28.4	30.6	1.351	29.0
3.6	210	Free	1.415	67	43.0	42.0	1.363	42.0
4.8	210	Free	1.416	68	40.8	40.4	1.367	40.0
3.6	210	Tension	1.415	67	41.0	40.0	1.367	40.0
4.8	210	Tension	1.409	62	40.8	42.5	1.359	42.0
*3.6	145	Free	1.389	45	35.0	37.7	1.346	36.0
*4.8	145	Free	1.388	44	36.6	34.0	1.346	35.0
*3.6	145	Tension	1.396	51	35.6	35.7	1.352	36.0
*4.8	145	Tension	1.391	47	36.4	32.4	1.351	34.0
*3.6	210	Free	1.409	62	41.4	40.3	1.360	41.0
*4.8	210	Free	1.411	63	43.0	42.4	1.359	44.0
*3.6	210	Tension	1.410	63	40.2	43.0	1.360	42.0
*4.8	210	Tension	1.412	64	42.4	43.4	1.360	43.0

The following comments may be made on these results:

- (1) The X-ray crystallinities of pin drawn yarns are shown to be extremely low but dependent on draw ratio.
- (2) The pin and plate treated yarns give crystallinities which are practically independent of draw ratios.
- (3) Crystallinities calculated from density for drawn yarns are found to be much higher than those observed by the X-ray method, but they do follow the same trend, for example almost constant values for the pin and plate yarns.
- (4) If the X-ray measure of crystallinity is taken as the yardstick and if this figure is subtracted from that obtained by density, the density of the non-crystalline regions in drawn fibres can be calculated (Table 3). An average value of 1.355 g/ml. is found for most types of yarn.
- (5) Yarns heated in a silicone oil bath at 210° C show abnormally high mean densities and rather higher densities for the non-crystalline regions.
- (6) No special experiments have been done to work out a standard deviation for the measurement of X-ray crystallinity, but some guidance may be obtained from an examination of Table 3. Two determinations were done on each yarn, that is, two different samples were made and exposed to the X-ray beam for a different length of time. Now the heat-treated yarns at a particular temperature give approximately the same figure for crystallinity irrespective of draw ratio, so if these yarns are considered as representing a single population of crystallinities then a standard deviation can be worked out.

For

- (a) pin-drawn yarns heated treated at 145° C where there seems to be a maximum variation:
Standard deviation = 3.24
Coefficient of variation = 9.8%;
- (b) Pin and plate yarns heated treated at 210° C:
Standard deviation = 1.22
Coefficient of variation = 3%.

These values, 9.8% and 3%, represent the range of the coefficient of variation.

Conclusions

An X-ray method, suitable for the measurement of crystallinity in drawn polyethylene terephthalate fibres has been devised. It is comparable in speed with the alternative method of recording an X-ray diffraction pattern by means of a Geiger-Müller counter which would take about one hour or more to produce a trace suitable for crystallinity measurements. The additional step of having the X-ray film scanned by a microdensitometer is partially off-set by X-raying another sample while this is taking place. There is no correlation between the crystallinity so determined and that calculated from the density of the yarn.

Acknowledgement

The authors would like to acknowledge the help given by many colleagues in Research Department for helping with the construction of apparatus, the supply of yarns and helpful criticisms of the manuscript.

References

- (1) GRIME, D., and WARD, I. M. *Trans Faraday Soc.*, **54**, p. 959 (1958).
- (2) FARROW, G., and WARD, I. M.: *Polymer* (in press).
- (3) GOPPEL, J. M. *Appl. Sci. Res. A*, **1**, pp. 3, 18 (1947).
- (4) MATTHEWS, J. L., PEISER, H. J., and RICHARDS, R. B. *Acta Cryst.*, **2**, p. 85 (1949).
- (5) HOWELLS, E. R. Imperial Chemical Industries (Plastics Division). Unpublished work.
- (6) MARTEN, L., and WARD, I. M. Imperial Chemical Industries (Fibres Division). Unpublished work.
- (7) HERMANS, P. H., and WEIDINGER, A. *J. Appl. Phys.*, **19**, p. 491 (1948).
- (8) EHERENBERG, W., and SPEAR, W. E. *Proc. Phys. Soc. B*, **64**, p. 67 (1951).
- (9) GUINIER, A. *X-ray Crystallographic Technology*, Ch.6 (London: Hilger and Watts Ltd., 1952).
- (10) ZAHN, H., *et al.* *Angew. Chem.*, **68**, p. 229 (1956).
- (11) FARROW, G., and PRESTON, D. *J. Sci. Instrum.* (in press).

Variable ultrasonic water delay line

by G. W. WILLIAMS, Ph.D., Defence Research Telecommunications Establishment, Ottawa, Canada

[Paper first received 4 February, and in final form 6 April, 1960]

Abstract

A variable delay line that uses ultrasonic propagation in water has been constructed. The delay, variable from 200 to 2600 μ s, is controlled by an input voltage, and is variable at a rate of 40 μ s/s. A bandwidth of 800 kc/s is achieved at the carrier frequency of 7 Mc/s. The delay is stable to better than 0.05% over the normal range of room temperatures. Automatic gain control holds the change in level of the output pulse to better than ± 1 dB.

Introduction

THIS unit resulted from a request for a variable delay line for use either in a target simulator or in radar correlation studies. The requirements were determined largely by the proposed simulator, and were stated as follows:

- (a) Delay—variable 150 to 2500 μ s;
- (b) Minimum bandwidth—500 kc/s;
- (c) Tracking speed—40 μ s/s minimum;
- (d) Delay proportion to input voltage—accurate to 0.1%;

(e) Change in delay due to room-temperature fluctuations—less than 5 μ s/h.

A literature survey indicated that the most practicable scheme would be ultrasonic propagation in a liquid. The only other approach considered was propagation along a wire, but information available indicated that success with this method would be doubtful.

Ultrasonic liquid delay lines

Background. Delay lines that employed ultrasonic propagation in liquids were used to some extent during World War II. These fell into two classes: lines for trigger delays that required a steep wavefront but not a wide frequency response, and lines for m.t.i. (moving-target indication) cancellation that had to reproduce faithfully the input pulse. Generally, the transmitting medium used was water in the former and mercury in the latter. The Radiation Laboratory of the Massachusetts Institute of Technology developed a number of such delay lines⁽¹⁾ using both mercury and water, but there is no record that any of these covered a wide range of delays with reasonable bandwidth.

It is known that a variable water delay line was made at the Royal Aircraft Establishment (Farnborough), but information on the amount of variation and the bandwidth was not available to the writer. A water line with a delay variable from 50 to 1400 μ s, an overall bandwidth (including amplifier) of 300 kc/s, and a carrier frequency of 5.5 Mc/s was constructed at Columbia University.⁽²⁾ In this case, a rather high attenuation (about 4 dB/ft) was reported.

Transducer characteristics. The bandwidth of an ultrasonic delay line can be discussed in terms of acoustic theory and the electromechanical properties of the transducers. The present discussion is restricted to the case of quartz transducers driven at thickness resonance, which appears to be the most practicable in the megacycle-per-second region. Under these conditions, a useful amount of power is transmitted to the liquid and the internal losses of the quartz may be neglected. The bandwidth can then be shown to depend on the relationship between the propagation constants of the quartz and of the surrounding media. The complete treatment has been given by Huntington, Emslie and Hughes.⁽³⁾

The symbols to be used are defined as follows:

- d = transducer thickness (cm)
- $\omega/2\pi$ = applied frequency (c/s)
- v = velocity of sound (cm/s)
- K = dielectric constant of quartz
- $= 4.58$
- h = piezoelectric coefficient of quartz
- $= 14.3 \times 10^4$ C.G.S. e.s.u.
- S = active transducer area (cm²)
- ρ = density (g/ml)
- β = propagation constant
- $= \omega/v$
- Y = appropriate modulus of elasticity.

Subscripts 0, 1, 2 refer to quartz, medium 1 and medium 2. With reference to Fig. 1, propagation takes place in

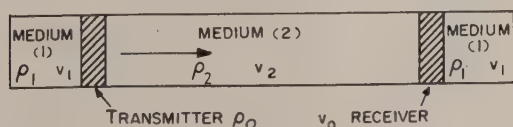


Fig. 1. Schematic representation of delay line

medium 2 and the crystals are backed by medium 1. The electrical impedance of the transducers can be shown to be:

$$\frac{V}{I} = \frac{4\pi d}{j\omega KS} + \frac{h^2}{\omega S} F(\beta d), \quad (1)$$

where:

$$F(\beta d) =$$

$$\frac{2\beta Y(\cos \beta d - 1) + j(Y_1\beta_1 + Y_2\beta_2) \sin \beta d}{\beta Y(\beta_1 Y_1 + \beta_2 Y_2) \cos \beta d + j(\beta^2 Y^2 + \beta_1 Y_1 \beta_2 Y_2) \sin \beta d}$$

The first impedance term is always much the larger when the crystal is damped by a liquid or solid medium, so the crystal admittance may be written to a good approximation as:

$$\frac{I}{V} = j\omega C + (Z)^{-1} \quad (2)$$

where C is the electrostatic capacity of the crystal and:

$$Z = \frac{16\pi^2 d^2}{h^2 K^2 \omega S F(\beta d)}$$

At the resonant frequencies of the crystal, βd equals $n\pi$ (n odd), at which point F reduces to $4(\beta_1 Y_1 + \beta_2 Y_2)^{-1}$. Since Y equals $v^2 \rho$, Z at resonance becomes:

$$Z(n\pi) = \frac{1}{4(Z_1 + Z_2)} \quad (3)$$

where:

$$\begin{aligned} Z_1 &= k\rho_1 v_1, \\ Z_2 &= k\rho_2 v_2, \\ k &= \left(\frac{4\pi d}{hK}\right)^2 \frac{1}{S}. \end{aligned}$$

The term k is the proportionality factor between the transformed impedance Z and the acoustical impedance ρv . The crystal admittance at resonance is then:

$$j\omega C + \frac{4}{Z_1 + Z_2} \quad (4)$$

The crystal current is seen to consist of a charging current into the electrostatic capacity of the crystal, and a conduction current through two series elements representing the loading on the two crystal faces.

The frequency dependence of the crystal impedance may be simplified by finding the curvature of the impedance curve in the neighbourhood of resonance. The Q -factor is then defined as that of a simple series resonant circuit which varies with frequency in the same way as the crystal impedance, and this suffices to determine the bandwidth of the system. The simplified equation for Q -factor becomes:

$$Q = \frac{n\pi}{4} \left\{ \frac{4(Z_1 Z_2 + Z_0^2)^2 - (Z_1 + Z_2)^2 (Z_2^2 + 2Z_0^2)}{Z_0^2 (Z_1 + Z_2)^2} \right\}^{1/2} \quad (5)$$

For operation at the fundamental, with $Z_1 = Z_2$ (crystal transmitting into and backed by the same medium):

$$Q = \frac{\pi Z_0}{4Z_1}, \quad (6)$$

and with $Z_1 = 0$ (approximately true for air backing):

$$Q = \frac{\pi}{4Z_2} \{2(Z_2^2 - Z_0^2)\}^{1/2}. \quad (7)$$

This effective Q is for the conductance portion of the admittance. The large capacitive susceptance must be tuned by the driving circuit and shunted by a resistance low enough to give a bandwidth greater than that of the crystal. This effectively makes the driver a constant voltage source.

Attenuation. The attenuation in a delay line is a significant factor, since the signal-to-noise ratio will limit the usable delay. The total attenuation arises from several factors:

- (1) mismatch at the transducers,
- (2) power loss in the crystal backing,
- (3) beam spreading at long path lengths,
- (4) attenuation of the ultrasound in the liquid,
- (5) losses at reflectors.

The ratio of the receiving crystal output voltage to the driving voltage is given by Huntington as

$$\frac{\text{output voltage}}{\text{input voltage}} = \frac{8Z_2R_r}{(Z_1 + Z_2)^2} \quad (8)$$

where R_r is the resistance shunted across the receiver in order to give the required electrical bandwidth. This assumes that, in the usual case, R_r is small compared with Z_1 and Z_2 . This voltage loss is not a true attenuation, since the crystals are essentially lossless, but is due to mismatching at transmitter and receiver. However, of this loss, 3 dB is accounted for at each transducer by the power lost into the backing medium.

Beam spreading is of interest, not only because of the loss of signal over long path lengths (long delays), but also because it gives an indication of the mechanical tolerances necessary in the system to prevent additional losses through misalignment. A detailed analysis of the sound field in front of a piston radiator in an infinite baffle is precisely the same as that for a plane wave front after it passes through a circular aperture in a thin wall. Fresnel interference occurs close to the radiator, and this produces a fine structure of maxima and minima. Fraunhofer diffraction occurs at a greater distance and results in the familiar pattern of a central lobe surrounded by cones of diminishing intensity. The half angle of the first minimum is $\sin^{-1}(1.22\lambda/d)$ where d is the diameter of the transducer.

Since, in the usual practical case, the receiving crystal is the same diameter as the transmitting crystal, and the signal is due to the average intensity over the crystal face, Fresnel diffraction is not observed. Huntington has calculated the total force on the receiving crystal in the Fraunhofer region and shown that it approaches the hyperbolic form:

$$F = \frac{PS^2}{\lambda d}, \quad (9)$$

where:

- F = total force on the receiving crystal,
- P = pressure at the transmitter,
- S = area of each transducer,
- d = distance from transmitter to receiver,
- λ = acoustic wavelength in the medium.

In any liquid, absorption results in an exponential decrease in sound intensity with distance from the source. This can be calculated as the sum of two terms that involve the shear viscosity and the thermal conductivity of the medium. Both terms give rise to an attenuation which is proportional to the square of the frequency.

In acoustic delay lines of over a few hundred microseconds delay, reflectors are usually used to reduce the physical size

of the tank. To prevent sound transmission into the reflector material, the material and incident angle are chosen to give total reflexion. For a corner reflector (incident angle 45°), a material capable of transmitting sound with a velocity greater than about 2100 m/s is required, and this criterion is met by all the normal constructional materials (steel, brass, aluminium, etc.). A large attenuation has been observed⁽¹⁾ for some reflectors in contact with mercury, but this has been attributed to the phase shift at reflexion from air bubbles trapped in surface irregularities at the mercury-metal interface. Neither a very smooth surface nor a rough-ground surface will show this effect. It is to be expected that air trapped at a water-metal interface would be absorbed by the water and would not contribute to the reflexion loss.

Construction of delay line

Choice of life parameters. The liquids suitable for use in long delay lines are restricted to water and mercury because of attenuation. Mercury has a much lower attenuation and a much higher acoustic impedance, hence a greater bandwidth than water. A variable line requires a greater volume of liquid than does a fixed line and is most easily designed with a free liquid surface. Under these conditions, because of the weight, cost and toxicity of mercury, it is advantageous to use water if at all possible.

The acoustic impedance of water is 1.5×10^5 g cm/s compared with 15×10^5 g cm/s for quartz. The transducers will then have an effective Q of 15.7 and 7.85 with water on one and two faces, respectively. A carrier frequency of 7.5 Mc/s was chosen as a compromise between bandwidth and attenuation. At this frequency, a back-loaded transducer should have a bandwidth of 950 kc/s. At 20° C and 7.5 Mc/s, the absorption is 12.4 dB/m or 3.78 dB/ft. For a transducer diameter of 1 in. and a load of 2000 Ω , the transducer loss is 13.5 dB. The major part of this loss is the power absorbed in the back loading and the unavoidable mismatch dictated by bandwidth consideration. This amounts to 12 dB. The loss through beam spreading will be about 7 dB for a total delay of 2600 μ s. The maximum attenuation will then be approximately 70 dB, with a change of 50 dB as the delay is increased from 200 to 2600 μ s. This variation will be absorbed by a.g.c. action in the receiver amplifier.

Crystals and mounting. Silver plated X-cut quartz crystals, 1 in. in diameter and resonant at 7.5 Mc/s, were obtained. In preliminary experiments it was found that the resonant frequency shifted to 7 Mc/s when the crystal was cemented into the holder. This loading effect is not mentioned by other workers. However, it does not appear to degrade the operation of the crystal as a transducer.

The transmitter and receiver crystals were mounted in a single machined aluminium block (Fig. 2) in order to eliminate the need for alinement adjustments. The crystals were cemented into the block with a thermosetting adhesive⁽⁴⁾ and the resulting active area was $\frac{7}{8}$ in. in diameter. An air-drying silver paint was used to ensure electrical contact between the block and the front face of the crystals. A No. 38 copper wire was soldered to the rear face to make connexion to a coaxial connector. The space behind the crystals was filled with transformer oil, which provides the same degree of damping as water. A sponge-rubber washer in this space absorbs the power radiated from the rear crystal face and reduces multiple reflexions that occur between the transducers at short delays. The oil space was also vented to the atmosphere to prevent any build-up of pressure. The slot cut in the block between the transducers serves to reduce

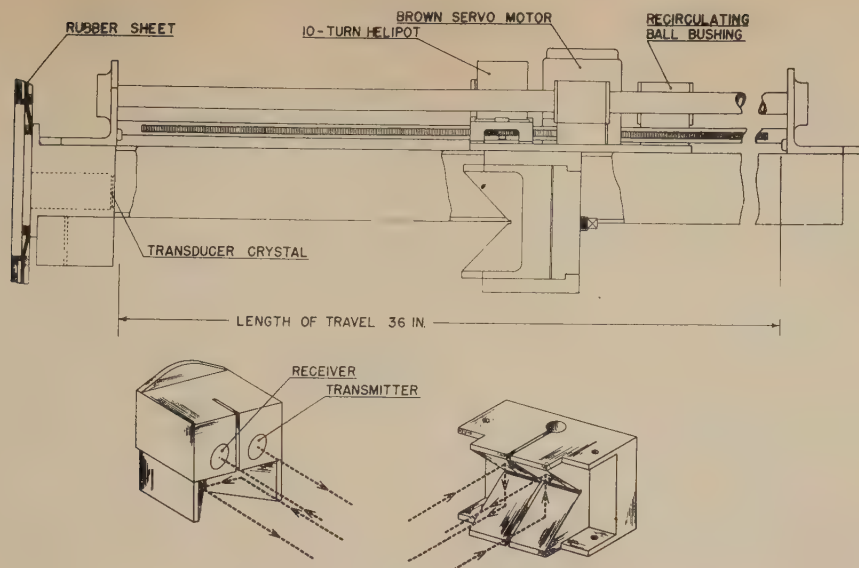


Fig. 2. Construction of delay line

acoustic feed-through from transmitter to receiver. Before installation, this slot was filled with a sheet of sponge rubber. A flange on the rear of the block was bolted to a rubber sheet in the end of the water tank. Hence the transducer connectors are available externally.

Reflector system and tank. To obtain the required delay in a tank of reasonable dimensions the sound wave travels the length of the tank four times. The system includes movable and fixed reflectors and is illustrated in Fig. 2. The supporting elements for the movable reflector are $\frac{3}{4}$ in. diameter stainless-steel rods, supported on a rigid aluminium channel framework with provision for adjustment to make the rods parallel. The reflector platform rides on the stainless-steel rods by means of three recirculating ball bushings, and the reflector is attached to the platform with provision for adjustment about a vertical axis. This platform also carries the driving servo-motor geared to a rack on the frame, and a linear 10-turn potentiometer also geared to the rack. There are also two microswitches that switch off the motor at each end of the track.

The second reflector is fastened to the underside of the crystal mounting block and rubber washers are inserted between the reflector and block to allow adjustment of the reflector angle about a horizontal axis perpendicular to the main axis of the line. This single adjustment on each set of reflectors is sufficient. The right-angle reflectors themselves are machined out of solid aluminium.

The water tank (12 × 12 × 50 in.) is formed of sheet aluminium, and the aforementioned rubber sheet seals the crystal block through the tank wall. A lid is provided with a lengthwise slot to pass the cable to the moving reflector.

Amplifiers. The driver amplifier accepts a 2.5 V (r.m.s.) pulse-modulated 7.0 Mc/s carrier, and delivers a signal of at least 35 V (r.m.s.) to the transducer. The output stage consists of push-pull cathode followers, coupled to a 2200 Ω cable. The far end of the cable then feeds the transducer through a matching transformer with the secondary winding shunted by a 1000 Ω resistor. In this way, the cable is matched and the bandwidth is made sufficiently large.

The receiving crystal, shunted with a coil in order to tune out its capacitance, is connected through a matched 2200 Ω cable to the amplifier. The use of a matched cable eliminates the need for a preamplifier, since it adds little extra capaci-

tance to the crystal. The receiving amplifier has four single-tuned stages with a high-gain a.g.c. loop to hold the output at about 10 V (r.m.s.). The received signal varies by 40 to 50 dB as the delay is changed, but the output is held constant to within ± 1 dB.

Servo-system. The elements of the servo-system are shown schematically in Fig. 3. The sensing element is the 10-turn

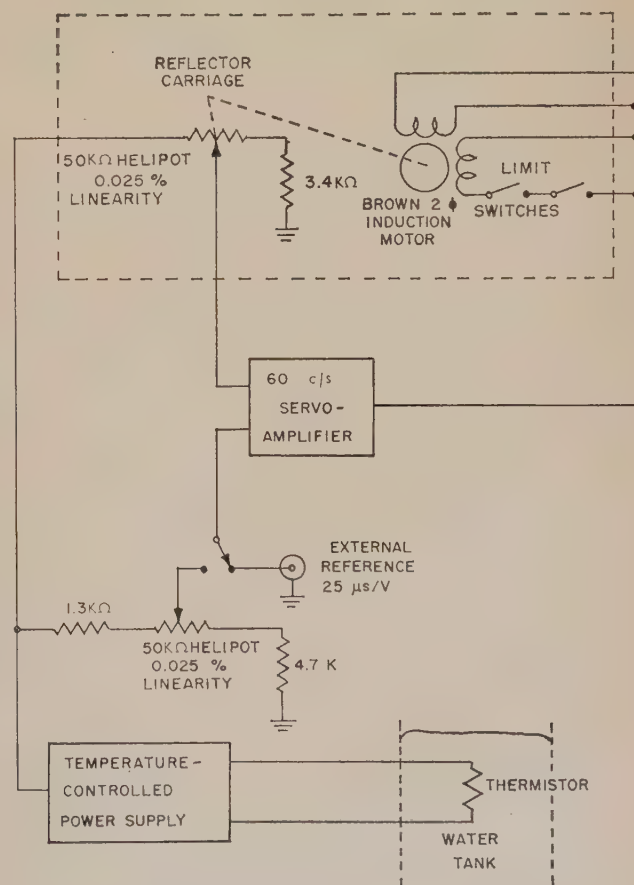


Fig. 3. Servo-system schematic

potentiometer mounted on the reflector carriage. 100 V (d.c.) is impressed on it, and the voltage on the potentiometer arm is compared with the input voltage to provide the error voltage to the servo-amplifier. The error voltage is then chopped at 60 c/s, amplified, and used to drive the two-phase servo-motor on the reflector carriage. The plate current of the output stage flows through the motor winding and provides the damping required to make the system stable.

The comparison voltage for the system is either supplied externally as some function of time, or is derived from an internal 10-turn potentiometer for use at fixed delays. The external voltage required is 1 V for each 25 μ s.

The stability of the voltage supply for the sensing potentiometer has a direct effect on the stability of the delay line. However, the major source of delay variation is the temperature coefficient of sound velocity in water. At room temperature this variation is $+2.4$ m/s deg C⁽⁵⁾ which corresponds to a delay change of -0.16% per deg C. Rather than control the water temperature or raise it to 75° C where the coefficient becomes zero, the variation was compensated electrically. A thermistor immersed in the water produced an equal negative temperature coefficient in the regulated reference supply. The servo-system then moves the reflector to compensate for the changing sound velocity. The panel-mounted potentiometer is operated from the same supply, so the delay is not temperature compensated when set manually.

Measured line characteristics

Attenuation and spurious signals. The attenuation curve shown in Fig. 4 was obtained at 23° C with constant input to the transmitter. An oscilloscope and preamplifier were used to measure the received pulse. If a change in calibration that occurred when the amplifier gain was changed is neg-

lected, the attenuation curve has a uniform slope of 3.5 dB/ft. The extrapolated loss at zero delay is 22 dB, of which 6 dB is accounted for by loss into the back loading of the crystals. The remaining 16 dB cannot be entirely accounted for by mismatch to the transducer. The measurement was not sufficiently precise to distinguish the loss caused by beam spreading from that due to pure attenuation.

Pinkerton⁽⁶⁾ measured the attenuation as 3.3 dB/ft at 20° C and 2.5 dB/ft at 30° C. The higher attenuation observed in the present case is certainly due in part to beam spreading. It is also worth noting that the attenuation rises rapidly as the temperature decreases and reaches 7.4 dB/ft at 0° C. The signal-to-noise ratio is thus a function of temperature, and operation at maximum delay is satisfactory only at temperatures above 20° C.

The level of the spurious signals is also shown in Fig. 4. The first multiple reflexion (three times the delay of the primary signal) is about 32 dB down at a delay of 200 μ s, and since it is attenuated at three times the rate of the primary signal, it quickly becomes insignificant. A signal at one-half the primary delay arises from simple reflexions from the reflector carriage. It is about 98 dB below the transmitted signal, so it is not objectionable. Feed-through from transmitter to receiver is observed to be 95 dB below the transmitter level. This appears to be electrical feed-through, which occurs in spite of decoupling in the power supply leads and double shielding on the transducer cables. A larger acoustic feed-through (distinguishable by the delay involved) was eliminated by the sheet of sponge rubber in the slot between the two transducers.

Bandwidth. The waveforms of the transmitted and received pulse are shown in Fig. 5. The rise and decay times

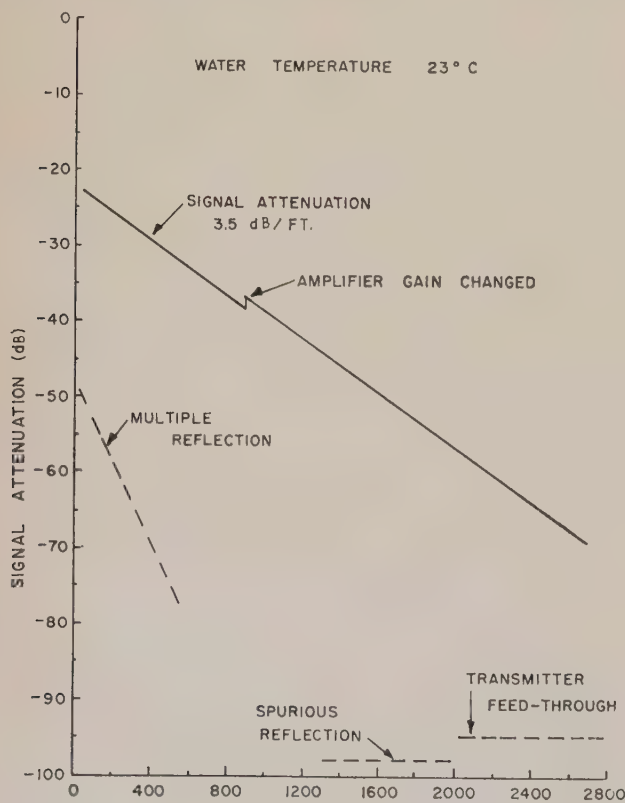


Fig. 4. Line attenuation at 7.0 Mc/s

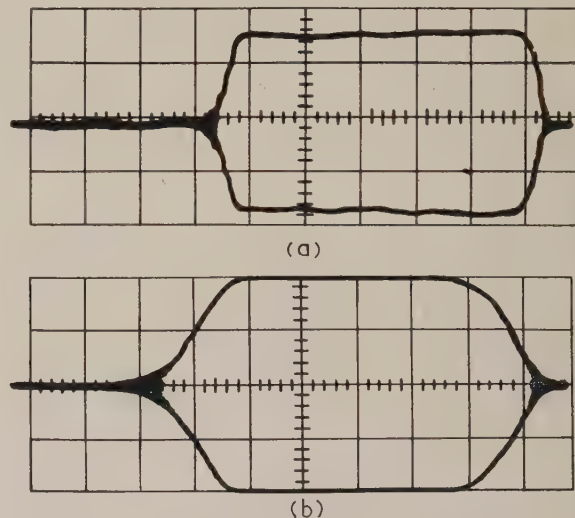


Fig. 5. (a) Transmitted, and (b) received pulse (time scale 1 μ s/cm)

of the transmitted pulse are fast enough to be ignored. The rise time of the received pulse is nearly 1 μ s, corresponding to a bandwidth of about 800 kc/s.

A greater bandwidth can be obtained by raising the carrier frequency, since they are proportional. 10 Mc/s transducers were installed in the line and the bandwidth increased by the expected amount. However, the f^2 -increase in attenuation limited the useful delay to 1600 μ s. If a wider bandwidth were required, some other changes could be investigated. The transducers could be backed with a higher impedance material at the expense of higher losses since most of the

power is then radiated into the backing. Methylene iodide, which has twice the acoustic impedance of water, would produce a 50% increase in bandwidth. Any major increase in bandwidth calls for the use of mercury as a backing material and, if the losses are then prohibitive, for its use as a transmitting medium.

Temperature coefficient. Immersion heaters were used to change the water temperature by 6°C and the delay was then measured by triggering the pulse generator with the received pulse. A single pulse was injected and circulated with a repetition rate determined by the delay. A frequency-interval counter was then used to measure the delay change to within 0.1 μ s. At a delay of 2500 μ s the observed change was +1.2 μ s which corresponded to a temperature coefficient of +0.008% per deg C. The uncompensated delay, using the panel-mounted potentiometer, changed by 33 μ s at an initial delay of 2600 μ s. This corresponds to a temperature coefficient of -0.21% per deg C which differs from the published value of -0.16% per deg C.⁽⁸⁾

Servo-system. The maximum travel speed of the reflector corresponded to a rate of change of delay of 80 μ s/s. As the maximum rate of change required is half of this figure, the system should track well. Moving and resetting the panel-mounted potentiometer showed that the reflector returned to its original position with a delay change of less than 0.2 μ s. As the setting accuracy is limited by the potentiometer linearity (0.025%) to 0.6 μ s, the servo-system is adequate for the application.

Summary of delay line characteristics

- (1) Delay—min. 200 μ s.
max. 2600 μ s.

- (2) Control—Internal helipot, 2.6 μ s/div.
External voltages, 25 μ s/V.
- (3) Temperature coefficient—Internal control, -0.21% per deg C.
External control, +0.01% per deg C.
- (4) Bandwidth—Approx. 800 kc/s (pulse rise time 1 μ s).
- (5) Tracking speed—40 μ s/s.
- (6) Input 2.5 V (r.m.s.) pulse-modulated 7 Mc/s carrier.
- (7) Output 10 V (r.m.s.) \pm 1 dB over total range.
- (8) Spurious signals 28 dB down over total range.
- (9) Size 56 in. long \times 40 in. high \times 20 in. deep.

Acknowledgements

This work was under Defence Research project D48-55-03-07. The author is indebted to Mr. F. W. Simpson for many discussions on ultrasonic theory and techniques. The author also acknowledges the help of Mr. N. A. Harrison on the mechanical design and of Mr. H. C. Frayn and Mr. D. F. Way-Nee in the construction and measurements.

References

- (1) BLACKBURN. *Components Handbook*, pp. 218-242 (New York: McGraw-Hill, 1949).
- (2) GITLIN, S. A. *Electronics*, **29**, p. 143 (1956).
- (3) HUNTINGTON, I., *et al.* *J. Frank. Inst.*, **245**, p. 1 (1948).
- (4) Araldite 502, Ciba Co. Ltd., Montreal.
- (5) MASON, W. P. *Piezoelectric Crystals and their Application to Ultrasonics*, p. 335 (London: Van Nostrand, 1950).
- (6) PINKERTON, J. *Nature (London)*, **160**, p. 128 (1947).

Wall effect in the flow of lubricating greases in plunger viscometers*

by A. D. BRAMHALL, B.Sc., and J. F. HUTTON, B.Sc., A.Inst.P., Shell Research Ltd., Thornton Research Centre, Chester

[Paper first received 15 February; and in final form 4 April, 1960]

Abstract

In the plunger viscometer, grease is sheared between the surface of a long piston, or plunger, and the inner wall of a coaxial cylinder, the motion of the plunger being along the long axis of the cylinder. For some greases the flow curves depend on the width of the gap between the plunger and the cylinder, whilst for others the flow curves are independent of the gap width.

The results are best explained by postulating the existence of layers of softer grease adjacent to the viscometer walls with unmodified grease in between. For a given grease the layer thickness is independent of gap width. An analysis is presented which agrees with experimental results and permits the correction of the results to give a unique flow curve for the unmodified bulk grease.

* Paper presented at the Spring Meeting of the British Society of Rheology, 7-9 April, 1960, at Manchester.

The magnitude of the correction shows a tendency to decrease with increasing roughness of the walls, with increasing viscosity of the base oil and with decreasing size of crystalline soap-fibre aggregates in the grease.

Introduction

THE flow curves of lubricating greases are usually determined in our laboratory with a plunger viscometer. This instrument, developed by Blott, has been briefly described elsewhere.⁽¹⁾ In the plunger viscometer (see Fig. 1), the grease is sheared in the narrow annular gap between the inner wall of a cylinder, closed at one end, and the outer wall of a piston (or plunger) which is forced by an applied load into the grease contained in the cylinder. For each of a series of loads, the mean velocity of the plunger is

measured over a short distance. An outline of the theory leading to expressions for determining the shear stress at the wall and the apparent rate of shear is given in Appendix 1.

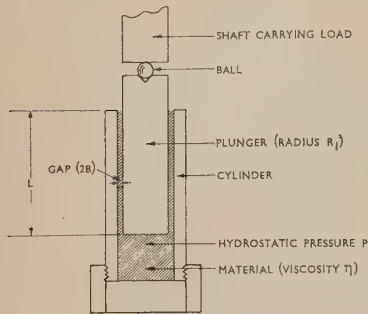


Fig. 1. The plunger viscometer

If the logarithm of apparent viscosity is plotted against the logarithm of apparent rate of shear (that is, $\log \eta / \log D$), the curve obtained is usually of the form shown by the solid line in Fig. 2. The curve has sometimes been drawn to show

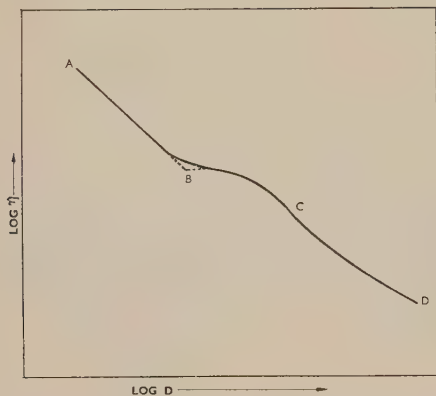


Fig. 2. Typical $\log \eta / \log D$ curve for greases

a discontinuity in slope at *B* as shown by the broken line; the scatter of the experimental points is such that the precise form of the curve cannot be determined. The position and magnitude of the large kink *BC* varies from grease to grease. With a few greases there is no kink in the range of rates of shear usually measured, that is from about 10^{-2} to 10^4 s^{-1} .

To make measurements over a large range of shear stresses and rates of shear, we have a set of plunger viscometers with annular gap widths ranging from 0.0042–0.062 cm. However, there is a wide range of rate of shear common to all the viscometers. If $\log \eta / \log D$ curves of a given grease are determined using the whole set of viscometers it is found

that they are not always coincident. Fig. 3, for Grease *A*, is an example of a set of curves which, within experimental error, are independent of gap width. On the other hand, Fig. 4 for Grease *B* and Fig. 5 for Grease *C*, illustrate sets of divergent curves. Many commercial greases based on calcium, sodium and lithium soaps also give divergent curves. Comparison of the curves in Fig. 4 shows that the divergencies due to the gap-width effect are greater than the reproducibility. The magnitude of the divergencies can be considerable. For instance, with Grease *C*, Fig. 5, the value of the apparent viscosity at a rate of shear of 100 s^{-1} measured in viscometer 3*B* is only one-quarter of that measured in viscometer 8*B*. When these effects occur, it means that the plunger viscometer cannot be used for accurate work at rates of shear which are often encountered in practice.

Results from the plunger viscometer are required for studies of the pumpability of greases through pipes. Some recent work reported by Summers-Smith⁽²⁾ concerns an introductory attempt to predict grease pumpability from flow data determined in the laboratory. At higher rates of shear, the plunger viscometer proved to be superior to a capillary viscometer in that it gave results more in agreement with data obtained from flow in a pipeline. However, at a shear rate below about 10 s^{-1} the plunger viscometer results showed a marked divergence from the pipe-line data and the capillary results in this range were the more reliable. It is interesting to note that 10 s^{-1} is in the range where viscometer gap-width effects are noticeable in Figs. 4 and 5. Thus the sudden failure of the plunger viscometer to conform with other instruments may be linked with these effects.

In this paper we aim to find the cause of the discrepancies between viscometers of different dimensions and a method for eliminating them.

Theoretical

1. Possible reasons for the observed discrepancies in the flow curves

There are three features of the gap-width effect which are important:

- (i) By comparison of a number of sets of flow curves, it has been observed that all the sets showing a dependence on viscometer gap width have a "kinked" shape, whilst all the sets showing no gap-width dependence are smooth curves.
- (ii) It can be seen from Figs. 4 and 5 that throughout the rate-of-shear range where there are divergencies, the values of the apparent viscosity, at a given apparent rate of shear, are smaller the narrower the gap used.

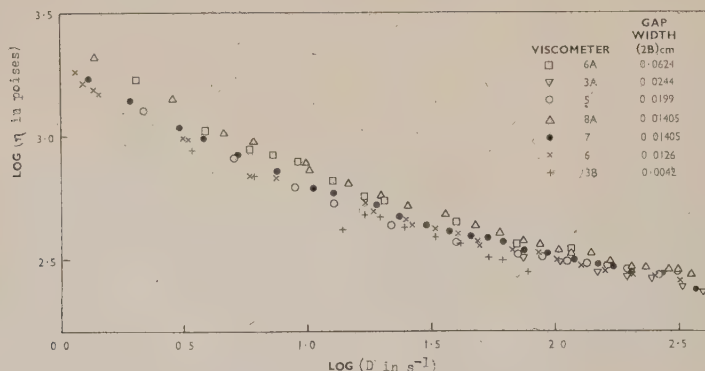


Fig. 3. $\log \eta / \log D$ curves for Grease *A* (Aluminium soap in a high-viscosity base oil). Temperature 25°C

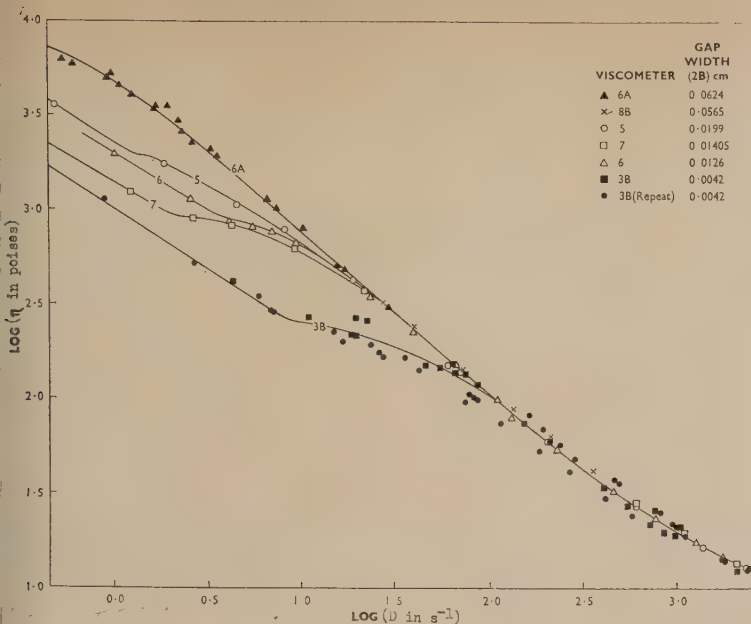
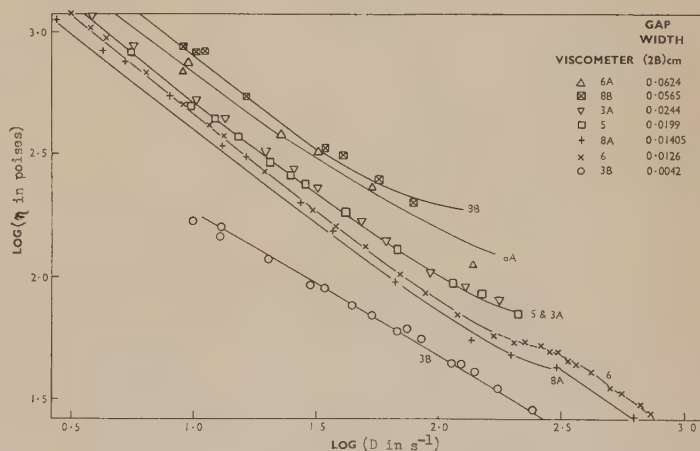


Fig. 4. Log $\eta/\log D$ curves for Grease B (Calcium soap in a medium-viscosity oil). Temperature 25°C

Fig. 5. Log $\eta/\log D$ curves for Grease C (Lithium soaps in a low-viscosity synthetic ester oil). Temperature 25°C



- (iii) Because the range of rates of shear at which the kink region starts and finishes is displaced to higher values of rate of shear, with decreasing gap width, the kink region does not reflect a bulk property of the grease, but it must be an effect of the viscometer used.

With these facts known, the following theories were considered as feasible explanations of the observed discrepancies.

(a) *A soap-filtration effect.* The gap may act as a filter for the larger soap particles in the grease. The filtering effect would be larger, for a given grease, the smaller the gap width. Should filtration occur, the gap would contain material with a lower soap content than that of the bulk grease. Hence the apparent viscosity will be lower. This argument would fit the fact that the apparent viscosity is lower the narrower the annular gap. This explanation, however, is unsatisfactory because, when the plunger is nearing the bottom of the cylinder, the viscosity should become abnormally high because of the increased concentration of soap particles in the remaining grease. But it is always observed that the plunger goes to the end of the cylinder without showing this effect.

(b) *Effect of pressure on the viscosity.* Since the hydrostatic pressure exerted on the grease sample in the viscometer varies throughout an experiment and also varies from

viscometer to viscometer for a given shear stress, it is possible that the effect of pressure on viscosity is involved in some way. An increase in viscosity would be expected with an increase in pressure. To test this point, an experiment was performed in which the flow curves were determined at a constant load (that is, constant hydrostatic pressure). Because of the changing annulus length while the plunger descended, quite a large range of rates of shear could be covered in this way. The results of several such experiments, each at a different load, made on Grease B are plotted in Fig. 6. It can be seen that there is no displacement of the flow curves with increasing load and hence the effect of pressure on viscosity has no significance in the problem.

(c) *A thixotropic effect.* With some materials, the viscosity at a constant rate of shear decreases with the amount of shear to which it has been subjected. This effect, if it is reversible, is known as thixotropy and is a characteristic of many greases. When viscometers having different dimensions are used it was thought that thixotropy might well produce discrepancies between the curves so obtained. The results from the above-mentioned experiment, which was made to find the pressure effects on the flow curve, show that thixotropy is an unsatisfactory explanation of the gap-width effect. In these experiments, the conditions were such that at the lower loads a given value of rate of shear was obtained with

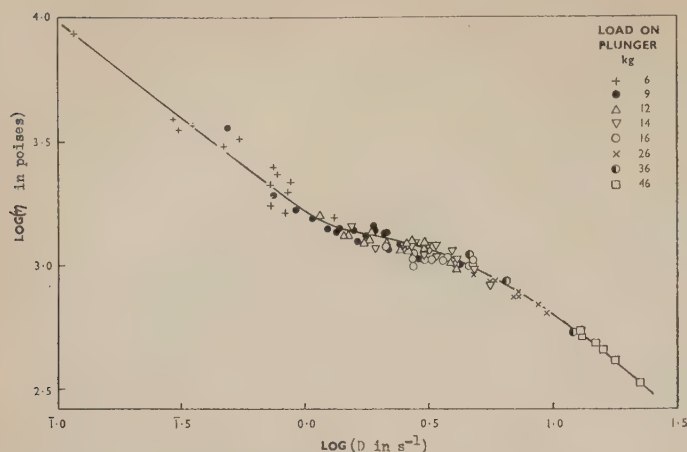


Fig. 6. $\log \eta / \log D$ curves for Grease B. Determined at constant pressures. Viscometer 8A. Temperature 25°C

a short annulus length whilst at higher loads the same rate of shear was obtained with a long annulus. The amount of shear, at a given rate of shear, increases with increase in annulus length. Thus, at a given rate of shear, thixotropy would be revealed by a lower value of apparent viscosity the higher the applied load. Fig. 6 for Grease B, a grease which produces a large gap-width effect, shows that the viscosity at any given rate of shear is independent of load.

(d) *The effect of slip at the viscometer walls.* Effects due to slip at the walls of capillary tubes have been found for greases by Blott and Bonnor.⁽³⁾ Blott and Bonnor have also shown, by a torsion-ring experiment, that the surface slip effect is not confined to capillary tubes. Further Amner, Blott, and Dawtre⁽⁴⁾ concluded that the straight portion AB of the "kinked" curve, Fig. 2, obtained using a plunger viscometer, is due to a slip effect, the grease sliding on a thin film of oil at the viscometer walls. However, the last-mentioned workers did not develop this idea in any detail. Schofield and Scott Blair⁽⁵⁾ studied the slip of aqueous suspensions in capillaries and calculated the thickness of the layer of water on which slip occurred. More recently the phenomenon has been considered by Vand⁽⁶⁾ and Maude and Whitmore⁽⁷⁾ for aqueous suspensions of uniformly-sized spheres. These workers concluded that slip is caused by a reduced concentration of the suspension near the wall, which arises from the purely geometrical consideration that the centres of the particles must be displaced from the wall by an amount at least equal to their radii.

A grease is a suspension in oil of soap aggregates of various sizes. Therefore, it seems probable that when a grease enters the gap of a viscometer, the aggregates of soap will be displaced away from the walls. The larger aggregates in the grease will be displaced farther than the small ones. Therefore, near the wall there will be formed a layer in which the soap concentration will increase gradually from a low value at the wall to that of the bulk grease at a distance related to the size of larger soap aggregates. The postulate of a low concentration at the wall permits us to ascribe a yield stress to the wall layer. There will be a tendency for the grease to slip on this layer at stresses well below the yield stress of the bulk grease. Therefore, an analysis was developed with the assumption that a wall layer exists.

2. Analysis of the problem of flow in the plunger viscometer with slip on a wall layer

(a) *The model chosen.* Firstly, although the physical picture given in section 1(d) is of a layer of variable soap

concentration and hence variable properties, for ease of calculation we consider an equivalent average layer in which the properties are constant throughout. Secondly, this average layer is assumed to obey the Bingham equation:

$$\tau - \tau_s = \eta_s D,$$

where τ is the shear stress, τ_s is the yield stress of the layer, η_s is the plastic viscosity of the layer and D is the rate of shear. Thirdly, the layer is assumed to have the same thickness d and properties η_s and τ_s independent of the viscometer through which the grease flows.

(b) *Sketch of the analysis.* A full analysis is given in Appendix 2. Using the model chosen, we find that a plug of the bulk grease will slide on the wall layer at a velocity v given by:

$$v = (d/\eta_s)(\tau - \tau_s), \quad (1)$$

where the shear stress τ is given by $P(2B)/2L$. The quantity P is the pressure drop, $2B$ is the viscometer gap width and L is the length of annulus.

This is a slip velocity which must be added to the velocity acquired by the bulk grease due to its own deformation. When this is done, a new expression for the rate of flow is obtainable and this leads to the expression:

$$D_{\text{obs.}} = D_b + D_s \quad (2)$$

where $D_{\text{obs.}}$ is the rate of shear calculated from the dimensions of the viscometer and the observed rate of descent of the plunger, using the normal equation [equation (14), Appendix 1]; D_b is the rate of shear due to the flow of the bulk grease; and D_s is a rate of shear due to slip. Therefore, to calculate the value D_b we must subtract from the observed value the contribution D_s due to slip. When the shear stress is less than the yield stress of the bulk grease D_b will be zero and D_s is therefore equal to $D_{\text{obs.}}$. In the theory, we derive the following equation for D_s :

$$D_s = \frac{6d}{2B\eta_s}(\tau - \tau_s). \quad (3)$$

This equation shows that D_s is a linear function of the shear stress τ . Therefore, there will be a range of shear stresses up to the yield stress of the bulk grease where the graph of $D_{\text{obs.}}$ against τ will be linear. This linear part will have an intercept τ_s and a slope M ,

$$M = 6d/2B\eta_s. \quad (4)$$

Experimental test of the slip theory

The concept of a slip layer as described in Section 2(a) will be confirmed if (i) the observed D/τ curve has a linear part at low shear stresses and (ii) for a given grease the value $M(2B)/6$ (equal to d/η_s) is independent of the viscometer gap width $2B$.

A number of greases have been tested and they all show that these conditions apply. Examples are given in Fig. 7 for Grease B and Fig. 8 for Grease C. In each curve there is a linear region at the lower shear stresses. At higher shear stresses, the bulk grease starts to deform and the curves start

is drawn and extrapolated to the highest measured shear stress. At various values of the abscissa τ , the ordinates D_s of this line are subtracted from the ordinates of the observed D/τ curve. Then for each shear stress, the difference is the rate of shear D_b . The apparent viscosity η of the bulk grease is the ratio of τ to D_b . In Fig. 9 the true $\log \eta/\log D$ plot is shown for Grease B. It can be seen that:

- all the points lie on the same curve regardless of the viscometer gap size.
- the characteristic kink which was previously found in the $\log \eta/\log D$ curve has now completely disappeared.

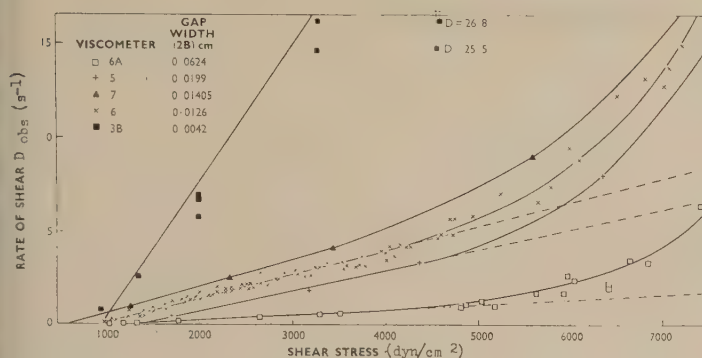


Fig. 7. Curves of observed rate of shear against shear stress measured in different viscometers. Grease B. Temperature 25°C

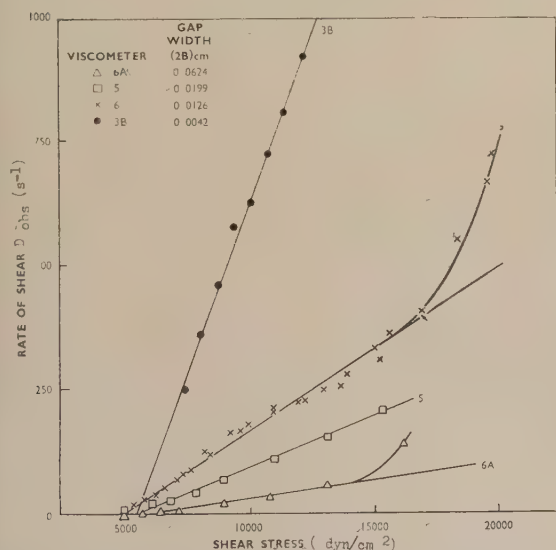


Fig. 8. Curves of observed rate of shear against shear stress measured in different viscometers. Grease C. Temperature 25°C

to deviate from linearity. To check the second condition, the slopes M were found for different gap widths for the various greases. From these the values of d/η_s were calculated. Table 1 gives the results obtained for Greases B and C and for two additional greases, D and E (made by different processes from lithium soap and a medium-viscosity mineral oil). It can be seen that the values of d/η_s for each grease are fairly constant. Certainly there is no relationship between these values and the plunger gap size. Hence these results give strong support to the slip theory.

Correction of observed flow curves

The flow curves can be corrected to give the true $\log \eta/\log D$ curve of the bulk grease by applying equations (2) and (3) as follows. The straight portion of the observed D/τ curve

- the effect of the slip correction is negligible at higher rates of shear (above 100 s^{-1}). This is because the correction due to the slip effect D_s , is insignificant compared with the large rates of shear due to the deformation of the bulk grease, D_b .

Nature of the slip layer

The linear part of the D/τ curves at low shear stresses confirms that, within the sensitivity of the plunger viscometer experiments, the wall layer has a well-defined yield stress. This result implies that either there is no layer of pure oil adjacent to the wall or that any such layer is penetrated by surface asperities. Our experiments do not enable us to eliminate either of these possibilities.

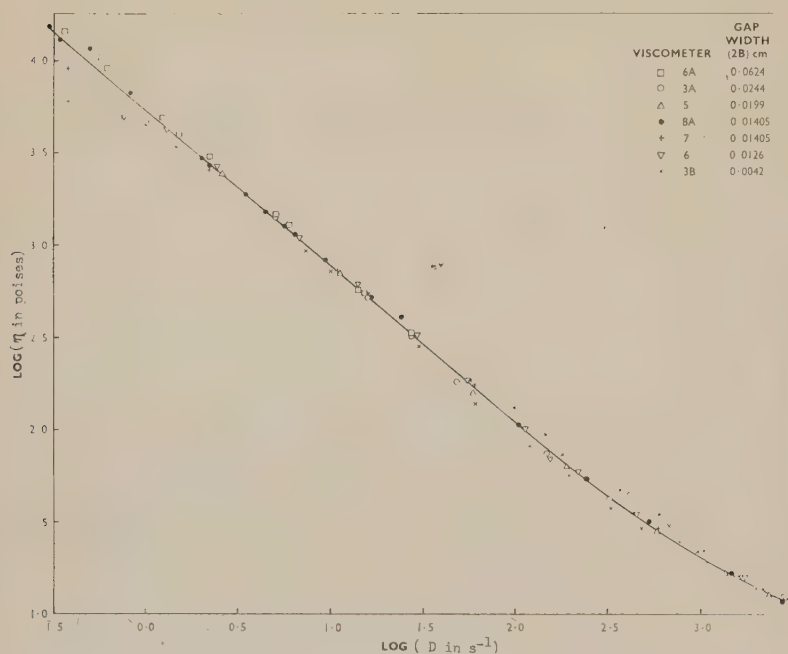
The scatter of values of d/η_s given in Table 1 is not random. There seems to be a relationship between the value of d/η_s and the material from which the viscometer cylinder was constructed. This can be seen by comparing columns 3 and 4 of Table 2 in which the results for Grease B are rearranged.

It is surprising that the relationship is almost uninfluenced by the material of the plunger. The reason for this is not known. It was thought that the correlation between d/η_s and viscometer material might be due to surface finish. Therefore Talysurf measurements were made of the surface roughness of the plungers and cylinders. The values of the centre-line average roughness (c.l.a.) so obtained are also given in Table 2. The relationship between the values of d/η_s and c.l.a. is not good, but there is a trend towards higher values of d/η_s for the smoother cylinders. Similarly for Grease C; in a glass-lined cylinder, d/η_s is $9.6 \times 10^{-6} \text{ cm/P}$, and in the metal cylinders d/η_s is about $7.0 \times 10^{-6} \text{ cm/P}$. The reason for the poor relationship may be that c.l.a. is considerably influenced by surface waviness of relatively large wavelength; the roughness which has most influence on the value of d/η_s is probably of very small wavelength and not separately measurable with the Talysurf equipment.

A comparison of the rheological properties of the slip layers for different greases shows interesting relationships. The relevant data are summarized in Table 3 (for convenience,

Table 1. Values of d/η_s for various greases at 25° C, with viscometers of different gap widths

Viscometer	Gap width (2B) (cm)	d/η_s (10 ⁶ cm/P)			
		Grease B (calcium base)	Grease C (lithium base)	Grease D (lithium base)	Grease E (lithium base)
3B	0.0042	5.45	95.6	—	—
6	0.0126	2.71	68.5	3.54	145
7	0.01405	3.30	—	—	—
8A	0.01405	3.67	—	—	—
5	0.0199	3.60	68.0	2.14	153
3A	0.0244	5.15	—	—	—
6A	0.0624	2.33	75.5	1.98	113
Mean values		3.6	77	2.6	140

Fig. 9. The corrected $\log \eta / \log D$ curve for Grease B. Temperature 25° CTable 2. Relationship between magnitude of d/η_s and the material of the viscometer cylinder for Grease B

Viscometer	Material of:		d/η_s (cm/P)	C.L.A.* (μ in.)	
	Plunger	Cylinder		Plunger	Cylinder
6	steel	steel	2.71×10^{-6}	6.8	12.0
6A	brass	steel	2.33×10^{-6}	7.8	12.0
7	brass	brass	3.30×10^{-6}	4.8	16.0
5	brass	brass	3.60×10^{-6}	3.0	5.9
8A	brass	brass	3.67×10^{-6}	5.0	14.0
3B	steel	glass	5.45×10^{-6}	5.5	4.0
3A	brass	glass	5.15×10^{-6}	9.2	4.0

* Centre-line average roughness.

Table 3. Rheological data of the slip layer and bulk grease for different greases at 25° C

	Grease A (aluminium base)	Grease B (calcium base)	Grease C (lithium base)	Grease D (lithium base)	Grease E (lithium base)
Mean value of d/η_s (Å/P)	~0	375	7690	255	13700
τ_s yield stress of layer (dyn/cm ²)	—	1300	5000	3000	9000
τ_0 yield stress of bulk grease (dyn/cm ²)	—	4800	16000	11000	26000
τ_0/τ_s	—	3.7	3.2	3.7	2.9
Viscosity of base oil (P)	65	1.20	0.090	1.75	1.75
Minimum value of d (Å)	~0	450	690	450	24000
Texture of grease	very smooth	smooth	smooth	smooth	very coarse

d is expressed in Ångström units). The yield stress of the slip layer is a virtually constant fraction of the yield stress of the bulk grease. On the other hand, the mean value of d/η_s varies considerably from grease to grease.

One cannot derive separately values for d and η_s . However, calculation shows that at quite low shearing stresses, the rate of shear in the layer is of the order of 10^4 s^{-1} . At such high rates of shear, the viscosity of a grease is approaching that of the base oil. Therefore there is some justification in replacing η_s by the base-oil viscosity. When this is done, the value obtained for d is the smallest possible. This minimum value of d has been calculated for different greases and is given in Table 3. It can be seen that for the coarse-textured grease, the minimum value of d is very much higher than for the smooth-textured greases. This result agrees well with the idea that the layer arises because the larger soap aggregates must be displaced away from the walls of the viscometer. Clearly the very large aggregates in a coarse-textured grease will suffer a greater displacement than the small particles in a smooth grease. The boundary between the bulk grease structure and the softer layer structure will therefore be farther from the wall for coarse textures.

Discussion

The lack of coincidence of $\log \eta/\log D$ curves for a given grease when measured in plunger viscometers of different gap widths can be explained by postulating a thin layer at the walls of the viscometer comprising, on average, a softer grease than the bulk grease. In addition, the equations developed on the basis of this postulate give a simple method of obtaining, from the plunger-viscometer measurements, the flow curve of the bulk grease. This curve is independent of the viscometer gap width.

The immediate practical value of these results is that with a knowledge of the true flow curves of greases valid comparisons can now be made of their flow properties at low rates of shear as well as at high rates of shear. Summers-Smith⁽²⁾ has calculated that the low range of rates of shear from less than 0.1 s^{-1} to 100 s^{-1} is important in grease pumping through pipes. This is the range where slip effects are important in the plunger viscometer. Therefore, calculations of pumping rates from plunger viscometer data, can now be carried out with greater accuracy than was hitherto possible.

Since slip has been found to be so important in the plunger viscometer, the question arises: will slip be important in the pipes used in dispensing systems and capillary viscometers? Calculation of the effect of slip in a pipe leads to the following equation analogous to equation (4), for the plunger viscometer:

$$M = 4d/a\eta_s \quad (5)$$

where a is the pipe radius. For greases of average texture, slip will be negligible in a plunger viscometer when $2B \geq 0.1 \text{ cm}$, and from equations (4) and (5) negligible in a pipe when $a \geq 0.067 \text{ cm}$. Now most pipes in a dispensing system exceed this radius so slip, although present, will not be important. The corrected flow curve obtained with the plunger viscometer, for example, the curve shown in Fig. 9, can therefore be applied, without further modification, to the dispensing problem.

The results of this investigation have shown that the phenomenon of slip at a wall may have a valuable application in the quantitative measurement of grease texture. Grease texture, assessed by a light microscope,⁽⁸⁾ has been shown to be important in relation to the performance of certain types of greases in ball and roller bearings. However, the

microscope method has disadvantages in that the comparisons of texture are subjective and require much skill. Further, it is impossible with the method to compare textures of two different types of grease, say, lime-base with lithium-base greases. Although the present work has not shown conclusively that textures of different types of grease can be properly compared quantitatively, the results given in Table 3 indicate that the new approach is most promising.

Following the completion of this work, we had the opportunity of discussing the results with Prof. G. V. Vinogradov of the Academy of Sciences, Moscow, during the Third International Congress on Rheology (1958). In a number of papers, Sinitsyn and Vinogradov⁽⁹⁻¹¹⁾ have described their studies of slip effects in grease flow down capillaries and have obtained results similar to those described in the present paper. Empirically, they obtained equation (2) with D_s equal to σ/a , where a is the capillary radius, and σ equal to $k(\tau - \tau_s)$, with k a constant. Comparison with our equations (3), (4) and (5) shows that k equals $4d/\eta_s$. Whilst Prof. Vinogradov agrees that our view of the formation of the slip layer is plausible he considers that there may be other explanations, for example, an orientation of the elongated soap fibres in the strong shear field near the viscometer wall. Studies of orientation in grease flow⁽⁸⁾ show that of our five test greases, B is most easily orientated and, of the two similar lithium-base greases, D is more easily orientated than E . Thus, the evidence so far obtained is in favour of a displacement of fibre aggregates rather than an orientation of fibres.

Acknowledgements

The authors express their thanks to the Directors of Shell Research Ltd., for their permission to publish this paper, and to Mr. T. V. Jones for his assistance in the experimental work.

References

- (1) AMNER, J. W., and BLOTT, J. F. T. *Principles of Rheological Measurement*, p. 25 (Edinburgh: Thomas Nelson and Sons Ltd., 1949).
- (2) SUMMERS-SMITH, D. *Proceedings of the Conference on Lubrication and Wear*, p. 519 (London: Institution of Mechanical Engineers, 1957).
- (3) BLOTT, J. F. T., and BONNER, W. B. *Proceedings of the (First) International Congress on Rheology, Part II* p. 265 (Amsterdam: North Holland Publishing Co., 1948).
- (4) AMNER, J. W., BLOTT, J. F. T., and DAWTREY, S. *N.L.G.I. Spokesman*, **14**, Part 8, p. 7 (1950).
- (5) SCHOFIELD, R. K., and SCOTT BLAIR, G. W. *J. Phys. Chem.*, **34**, p. 248 (1930); **34**, p. 1505 (1930); **35**, p. 1212 (1931); **39**, p. 973 (1935); **43**, p. 853 (1939).
- (6) VAND, V. *J. Phys. Colloid Chem.*, **52**, p. 277 (1948).
- (7) MAUDE, A. D., and WHITMORE, R. L. *Brit. J. Appl. Phys.*, **7**, p. 98 (1956).
- (8) HUTTON, J. F., MATTHEWS, J. B., and SCARLETT, N. A. *J. Inst. Petroleum*, **41**, p. 163 (1955).
- (9) SINITSYN, V. V., and VINOGRADOV, G. V. *Doklady, Akad. Nauk. (U.S.S.R.)*, **91**, p. 323 (1953).
- (10) SINITSYN, V. V., and VINOGRADOV, G. V. *Kolloid Zhur. (U.S.S.R.)*, **17**, p. 233 (1955).
- (11) SINITSYN, V. V. *Trudy Tret'ei Vsesoyuznoi Konferentsii po Kolloidnoi Khimii*, p. 127 (Akad. Nauk. U.S.S.R., 1956).
- (12) SMITH, G. S. *J. Inst. Petroleum*, **43**, p. 227 (1957).

Appendix 1

An outline of Blott's theory of the plunger viscometer

With reference to the sketch of the viscometer in Fig. 1, the gap $2B$ is very small compared with the radius of the plunger R_1 and the average velocity of flow of material in the annulus is very large compared with the velocity of the plunger. Thus, the flow may be regarded as flow between two stationary parallel plates of width $2\pi R_1$ and length L . Smith⁽¹²⁾ has carried out the calculation without this simplification and obtains the same expression for rate of shear. The effect of the simplification is to give values of viscosity high by $100B/(R_1 + 2B)\%$. Since R_1 is about 1 cm for all the viscometers, the greatest error, for viscometer 6A, is less than 3%.

It is assumed that b , Fig. 10, is the distance of any pair

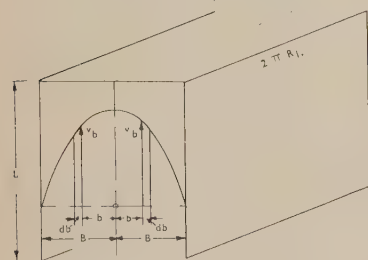


Fig. 10. Representation of flow in a plunger viscometer

of planes from the centre of the annulus, τ is the shearing stress on these planes and v_b is the velocity. The shear stress on the planes at distance b from the centre of the gap due to the pressure difference P is obtained by equating forces on the two symmetrically disposed planes. Then:

$$\tau = Pb/L. \quad (6)$$

For a Newtonian liquid

$$\tau = \eta D = -\eta \frac{dv}{db},$$

so from equation (6):

$$v_b = \int_B^b -\frac{Pb}{\eta L} db = \frac{P(B^2 - b^2)}{2\eta L}. \quad (7)$$

The total rate of flow is given by:

$$Q = \int_0^B 2\pi R_1 \cdot 2v_b db, \quad (8)$$

which, in the viscometer, is equal to the volume rate of displacement of the plunger, namely:

$$Q = \pi R_1^2 \frac{dL}{dt}. \quad (9)$$

Substitution for v_b from equation (7) into equation (8), integration, and elimination of Q from equations (8) and (9) give:

$$\frac{dL}{dt} = \frac{P(2B)^3}{6\eta R_1 L}, \quad (10)$$

For equilibrium of the plunger, the force due to the shearing stresses on the wall plus the force due to the hydrostatic pressure on the bottom must equal the total load. This equality leads to:

$$P = \frac{Mg}{\{\pi R_1(R_1 + 2B)\}}. \quad (11)$$

Hence the shear stress at the wall is:

$$\tau = \frac{P(2B)}{2L} = \frac{Mg(2B)}{\{2\pi LR_1(R_1 + 2B)\}}. \quad (12)$$

From equations (10) and (11) it follows that:

$$\eta = \frac{Mg(2B)^3}{\{6\pi R_1^2 L(R_1 + 2B)(dL/dt)\}}. \quad (13)$$

The apparent rate of shear at the wall is:

$$D = \frac{3R_1(dL/dt)}{(2B)^2}. \quad (14)$$

Appendix 2

The theory of the plunger viscometer modified to include the effect of slip on a layer at the walls

In addition to the symbols already defined, it is assumed that the surface layer has a thickness d . This layer is assumed to be a soft grease and to obey the Bingham equation:

$$\tau - \tau_s = \eta_s D, \quad (\tau > \tau_s), \quad (15)$$

where τ_s is the yield stress and η_s the plastic viscosity of the soft grease. It is necessary to find the velocity v of the boundary between this layer and the bulk grease, that is, the velocity in the plane at $b = (B - d)$, in Fig. 10. For a plane in the slip layer, equations (15) and (6) give:

$$D = -\frac{dv}{db} = \frac{Pb}{L\eta_s} - \frac{\tau_s}{\eta_s}.$$

Then, at $b = (B - d)$:

$$v = -\int_B^{B-d} \left(\frac{Pb}{L\eta_s} - \frac{\tau_s}{\eta_s} \right) db = \frac{d}{\eta_s} \left(\frac{P(2B)}{2L} - \tau_s \right), \quad (16)$$

neglecting second-order terms in d .

For the calculation of total flow, the slip velocity must be added to the velocity acquired by the bulk grease due to its own deformation. Then equation (7) of Appendix 1 becomes:

$$v_b = \frac{P(B^2 - b^2)}{2\eta L} + \frac{d(\tau - \tau_s)}{\eta_s}, \quad (17)$$

and the total rate of flow Q is, in parallel with equation (8):

$$Q = 4\pi R_1 \int_0^{(B-d)} \frac{P(B^2 - b^2)}{2\eta L} db + 4\pi R_1 \int_0^B \frac{d}{\eta_s} (\tau - \tau_s) db.$$

By integration and the neglecting of second and third order terms in d :

$$Q = \frac{\pi R_1 P(2B)^3}{6\eta L} + \frac{2\pi R_1 (2B)d}{\eta_s} (\tau - \tau_s). \quad (18)$$

Substitution for Q and P from equations (9) and (12) gives:

$$\frac{dL}{dt} = \frac{\tau(2B)^2}{3R_1\eta} + \frac{2d(2B)}{R_1\eta_s} (\tau - \tau_s). \quad (19)$$

Now in calculating the observed apparent rate of shear in

experiments such as those illustrated in Fig. 3 we use equation (14) of Appendix 1. Therefore:

$$D_{obs.} = \frac{3R_1(dL/dt)}{(2B)^2} \quad (20)$$

Substitution between equations (19) and (20) gives:

$$D_{obs.} = \frac{\tau}{\eta} + \frac{6d}{(2B)\eta_s}(\tau - \tau_s).$$

But τ/η equals D_b where D_b is the apparent rate of shear for the bulk grease. So we can write:

$$D_{obs.} = D_b + D_s,$$

where:

$$D_s = \frac{6d}{(2B)\eta_s}(\tau - \tau_s)$$

is the increase in measured rate of shear due to slip.

Application of photoelectric densitometry to the assessment of respirable dust samples

by A. R. BUGDEN, B.Sc., A.Inst.P., R. J. HAMILTON, B.Sc., A.Inst.P., and G. H. S. JONES, M.A., B.Sc.,*
Mining Research Establishment, Isleworth, Middlesex

[Paper received 9 February, 1960]

Abstract

A technique has been developed for rapid assessment of the samples of respirable mine dusts obtained with the long-running thermal precipitator (NCB/MRE dust sampler type 101). The size segregation of particles in these dust samples enables the optical density of a thin strip across the deposit to be converted to the number of particles in that strip, the relationship being a function of mean particle size. The addition of a specially shaped weighting mask in the light beam enables a single measurement of the optical density of the whole deposit to be converted to the total number of particles, independently of the size distribution of the dust.

A densitometer has been devised and laboratory and field trials have established appropriate conversion factors from optical density to number of particles. The loss of light caused by the sample is measured over a small angle in order to reduce the difference between coal and the more transparent rock particles. For routine mine samples, which consist in general of mixed coal and rock, use of mean conversion factors is recommended.

Operation of the apparatus is simple and rapid, with accuracy and consistency comparable with microscope counting, and it is believed that a high proportion of the routine dust samples can be evaluated in this way. Further advantages of the technique are that it can be adapted, in conjunction with incineration, to the compositional analysis of dust samples and, by using appropriate conversion factors or weighting masks, to the measurement of the mass of dust in the samples.

Introduction

FOR the assessment of the health hazard of airborne dust it is necessary to measure the concentration of particles having a falling speed such that they can penetrate the nose and be collected in the lungs. The collection of dust by thermal precipitator, followed by microscopical counting and sizing of particles, provides a convenient method of

estimating the concentration of the fine respirable particles in the presence of the larger ones, and the thermal precipitator has the advantage of being self-contained and portable. As a result of the Medical Research Council's recommendation⁽¹⁾ the technique was adopted as standard in this country for the sampling of respirable dust in coal mines, and the agreements between the various branches of the coal industry as to approved dust levels are based upon its use. Unfortunately the microscopical counting is a laborious and time-consuming procedure, and imposes a limit to the extent that the method can be exploited. Experience has also disclosed that visual counting is subject to a number of errors, in particular those connected with the personal bias of the microscopist. In order to reduce the effort required to evaluate the large number of airborne dust samples, obtained in the course of the National Coal Board's routine dust-sampling programme, a technique of rapid evaluation using a photoelectric densitometer has been devised for use with the dust samples obtained with the long-running thermal precipitator,⁽²⁾ an instrument which itself enables considerable reductions to be made in the effort needed to obtain a given routine sampling coverage.

Measurement of the optical density of a dust deposit in place of microscope counting has the advantages of speed, simplicity and objectivity, but there have in the past been difficulties in relating optical density to the number of particles in the deposit. The main difficulty has been that particles covering a wide range of size are normally collected together, and since the optical density of such a deposit is primarily related to the total projected area of the particles, changes in size distribution of the sample can result in considerable change in the relationship between optical density and particle number. This disadvantage can be reduced by incorporating a size selector⁽³⁾ in the dust-sampling instrument so that only the respirable dust particles are collected, but since even then the projected areas of the particles cover a very large range, correspondingly wide variations will still occur in the relationship between optical density and particle number.

The long-running thermal precipitator (l.r.t.p.) employs gravity settlement and thermal precipitation successively,

* Now at Suffield Experimental Station, Ralston, Alberta, Canada.

giving a much greater degree of size segregation than most other dust samplers. Following removal of non-respirable dust in a size selector, the respirable dust falls out on a horizontal glass slide, gradually eliminating the largest (fastest-falling) particles, until below the thermal precipitation element only those finer than about 3μ remain and are precipitated together. Fig. 1 shows the size segregation of

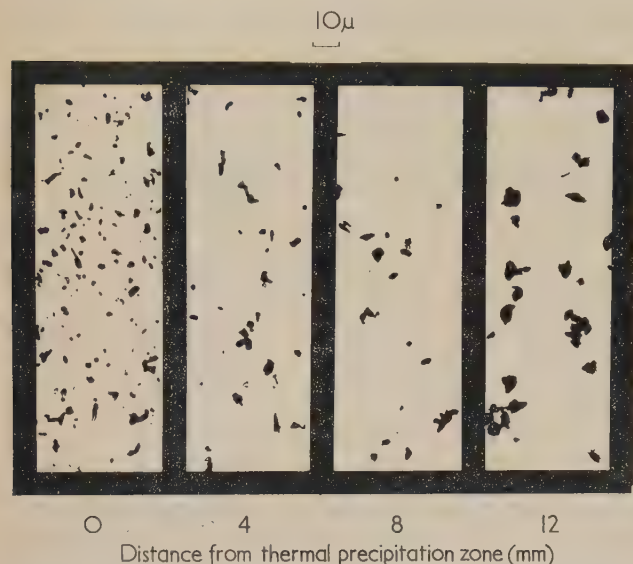


Fig. 1. Photomicrograph of dust at different positions on long-running thermal precipitator slide, showing size segregation

particles on a typical long-running thermal precipitator slide, obtained in a coal mine. The size segregation, although not perfect, does permit selection of zones in which the mean size of particles can be assumed constant, so that measurements of optical density of such zones can be related to numbers of particles.

A technique has been developed in which the optical density of the dust deposit is measured in twelve successive narrow strips across the slide at right angles to the direction of airflow. The optical density measurements in the strips are converted to numbers of particles by the application of calibration factors. These factors have been determined experimentally by comparison with microscopical counts in the narrow strips. This technique has been further developed to permit a single overall density measurement to be converted to the total number of particles in the dust deposit, independently of size distribution, by interposing a specially shaped weighting mask between light source and dust slide.

Theoretical considerations

(1) Optical

The loss of light caused by a dust particle is dependent on its size, shape and optical properties. For a large opaque particle (greater than 100μ diameter) the loss is directly proportional to the geometrical projected area, but for smaller particles it is modified by scattering and varies non-linearly with geometrical area, and depends moreover on the solid angle in which the light loss is measured. Equations for the light scattered by spherical particles were derived by Mie⁽⁴⁾ as solutions of Maxwell's electromagnetic equations. These scattering equations are extremely complex, and numerical solution is laborious, and possible only for spherical particles (Sinclair).⁽⁵⁾

The light loss can be considered as directly proportional to the scattering area, which is the geometrical area multiplied by a parameter sometimes known as the total scattering coefficient. This coefficient is a complex function of the ratio of particle size to wavelength of the light, of the refractive index and absorption of the particle and of the solid angle in which the light loss is measured instrumentally (the acceptance angle).

When the light loss is measured over a very narrow forward angle (less than 1°), the scattering coefficient is oscillatory with respect to relative particle size or refractive index, reaching maximum values of about 4 and tending asymptotically to a value 2 at the larger particle sizes. The value of the scattering coefficient is then very sensitive to light acceptance angle, but less so at wider acceptance angles, where the value of the scattering coefficient decreases and approaches unity. For particles with a high absorption, the oscillations are reduced and reach their limiting value at smaller values of particle diameter.

In the present application the particles are irregularly shaped with diameters within the range 0.2 to 10μ , and lie on a thin glass plate in air. The wavelength of the effective illumination is determined by the source emission and the sensitivity of the detector, and has a spread of about 0.5μ with a peak at 0.8μ . The routine mine samples consist of mixtures of coal particles and rock particles, so that there is a spread of both refractive index and absorption.

It has been pointed out by Walton,⁽⁶⁾ by Van de Hulst⁽⁷⁾ and by others, that an approximate picture of the scattering behaviour can be obtained if the forward light scattering is considered as the sum of two components, one due to diffraction and the other to refraction and reflexion. Experimental work by Ellison⁽⁸⁾ has confirmed this approximation for some industrial dusts. The diffraction scattering is confined to a very narrow forward angle, and the scattering by refraction and reflexion to a rather wider angle, both being sensitive to the shape of the particles. The diffraction component depends on particle size only, and is therefore the same for transparent and opaque particles (e.g. rock and coal). If the loss of light could be measured over a very narrow forward angle (less than 1°) the two types of particle would have nearly equal scattering coefficients, but the coefficients would remain very sensitive to measurement conditions and also to particle size. If the loss of light is measured over a wider angle, more of the light scattered by refraction and reflexion from the transparent particles will be accepted so that the scattering coefficient will be lower for transparent particles than for opaque particles. However, there is the advantage that the actual values are less sensitive to changes in acceptance angle and particle size, and approach unity.

In the densitometer constructed for the present application a compromise is made between restricting the light aperture, in order to minimize the apparent difference between rock and coal particles, and providing a simple instrument which does not require critical initial adjustment. Measurements of the loss of light from rock dust and coal dust slides, at various line aperture, between 15° and 2° , showed that between 10° and 2° there is no appreciable increase in the optical density of rock dust slides relative to coal dust slides, but that matching of the incident and acceptance light apertures becomes more critical as the angle is decreased. In practice, the solid angle of illumination used is that subtended by a rectangular aperture 1.6×0.4 cm at a distance of 11.4 cm ($8^\circ \times 2^\circ$); this gives scattering coefficients close to unity for both rock and coal dust on l.r.t.p. slides. These apparent

scattering coefficients were determined from the apparent scattering areas calculated from the calibration factors, together with the real geometrical areas determined from size distribution measurements by visual microscopy. Except for the first 2 mm at the coarse end of the deposit, where the mean geometrical area is very variable, the apparent scattering coefficients lie between 0.9 and 1.1, and there is no marked correlation with mean size or optical properties of the particles. (However, the difference in density between rock and coal, 2.5 g/cm³ and 1.4 g/cm³, causes the mean geometrical diameter in a given zone of deposition to be greater for coal than for rock, and results in differences in calibration factors for the two materials.) This relative invariance of scattering coefficient with particle size means that no additional errors are introduced from this cause by touching or overlapping of particles.

(2) Derivation of calibration factors

Under the conditions defined at the end of the last section, the loss of light from that incident on a narrow zone of the dust slide is proportional to the total projected area of the dust deposited in the zone, which, because of overlap of particles, will in general be less than the aggregate of the projected areas of the individual particles. If the overlap of projected areas is random, as in the case of particles in suspension, the loss of light will be related logarithmically to the number of particles according to a modified form of the Lambert-Beer law:

$$\begin{aligned} I &= I_0 \exp(-\tfrac{1}{4} \pi d^2 n k) \\ \log_e I_0/I &= \tfrac{1}{4} \pi n d^2 k \\ \text{optical density } D &= \log_{10} (I_0/I) \\ &= \tfrac{1}{4} \pi d^2 n k \log_{10} e \\ D &= F d^2 n \end{aligned} \quad (1)$$

where I_0 = incident light intensity, I = transmitted light intensity, n = number of particles per unit area, d = diameter of particles, k = scattering coefficient, and F is a constant.

Number assessment. The original method involved making measurements of optical density, within a defined acceptance angle, of twelve successive zones, each 1 mm wide and 1 cm high, at distances x along the dust deposit. By the application of previously determined calibration factors f_x for each zone, the optical densities were converted to the number n_x of particles greater than 1 μ per unit area,

$$n_x = f_x D_x \quad (2)$$

and for a dust deposit of length t , height h and area $S(=ht)$, the total number of particles N is

$$N = h \int_0^t f_x D_x dx \quad (3)$$

so that, by zonal assessment,

$$N = S \overline{(f_x D_x)} \quad (4)$$

When the dust concentration on the slide is low, there is an approximately linear relationship between optical density D equal to $(-\log_{10} I/I_0)$ and absorption factor A equal to $(1 - I/I_0)$, namely, $D = A \log_{10} e$. This condition holds for most l.r.t.p. mine samples, and makes possible the introduction of a simplified technique of integral assessment, in which the twelve zonal density measurements are replaced by a single reading, from which the total number of particles N can be obtained directly.

Using a special illumination system in which the height of

the dust deposit illuminated at any distance x is proportional to the calibration factor f_x , under conditions of uniform illumination across the field, the light flux at a distance x along the trace is proportional to f_x and a weighted transmission is obtained for the whole deposit. The total area illuminated is then $\int_0^t f_x dx$, and the absorption factor A can be expressed as

$$\begin{aligned} A &= \left\{ \int_0^t f_x dx - \int_0^t f_x (1 - A_x) dx \right\} / \int_0^t f_x dx \\ &= \int_0^t f_x A_x dx / \int_0^t f_x dx \end{aligned} \quad (5)$$

but $A = D/\log_{10} e$ and $A_x = D_x/\log_{10} e$ so that D and D_x can be substituted for A and A_x , giving

$$\begin{aligned} D &= \int_0^t f_x D_x dx / \int_0^t f_x dx \\ &= N/ht f_x \end{aligned} \quad (6)$$

so that, by integral assessment,

$$N = S D f_x \quad (7)$$

A similar result could be obtained by making the intensity of illumination at x proportional to f_x instead of varying the height of deposit illuminated under constant intensity illumination.

Mass assessment. It is possible to use the densitometer to estimate the mass of dust in an l.r.t.p. deposit. The calibration factors cannot be determined directly, but can be derived from the number calibration factors to the inverse square roots of which they are proportional, as shown below.

If the average particle diameter at a distance x along the slide is d_x , then the mass m_x of particles (of density ρ and shape factor γ) in unit area is

$$m_x = n_x d_x^3 \rho \gamma \pi / 6 \quad (8)$$

but from equation (1)

$$d_x = \sqrt{(D_x / F n_x)}$$

and from equation (2)

$$n_x = f_x D_x$$

and inserting these expressions and combining the numerical and constant factors $\pi \rho \gamma F$, the expression (8) for m_x reduces to

$$m_x = E D_x / \sqrt{f_x}$$

where E is a constant. Then the total mass M on the slide is

$$\text{by zonal assessment, } M = C \overline{(D_x / \sqrt{f_x})} \quad (9)$$

$$\text{by integral assessment } M = C D \overline{(1 / \sqrt{f_x})} \quad (10)$$

where C is a constant factor for a particular material.

The densitometer

The requirements of the densitometer for this work are (i) the ability to measure optical densities in the range 0.002 to 0.1 with an accuracy of ± 0.0005 , and (ii) an optical system which ensures that (in the absence of the weighting mask) there is uniform illumination at a constant solid angle at any point on a 12 mm square field on the dust slide, and

that the detector similarly collects light from any point of the dust deposit over a fixed solid angle only.

The design of the densitometer here described is only one of several types which would fulfil these requirements, and was developed in the absence of any suitable commercial instrument. The necessary sensitivity is achieved by using a split light beam system with twin photocells in a null balance circuit (Figs. 2 and 3). The dust slide is placed in one light beam and a calibrated density wedge in the other. The wedge is adjusted to equalize the light falling on the two photocells, as shown by zero reading in the indicator system. The density wedge is an annular disk covering a density range of 0.4, and a fine movement enables densities to be read at

intervals of 0.0002. The light source is a 12 V, 48 W, tungsten lamp with axial coiled filament, fed from a constant voltage transformer. Vacuum photoemissive cells (Mullard type 90 CV) are used; these have low dark currents, are free from hysteresis and show stability and linearity over a wide range of illumination, with peak sensitivity for radiation of wavelength 0.8μ .

The signals from the two photocells are fed into a voltage stabilized d.c. amplifier bridge circuit (Fig. 2), which is initially balanced with the photocells dark. Optical density measurements are then made in terms of the wedge setting required to equate the signals from the two photocells, and so restore the bridge circuit to balance. The net density of the dust deposit is obtained by subtracting the density of the clear slide.

The optical system is shown in Figs. 3 and 4. The light source L is imaged (I in Fig. 4) by a condenser C on the

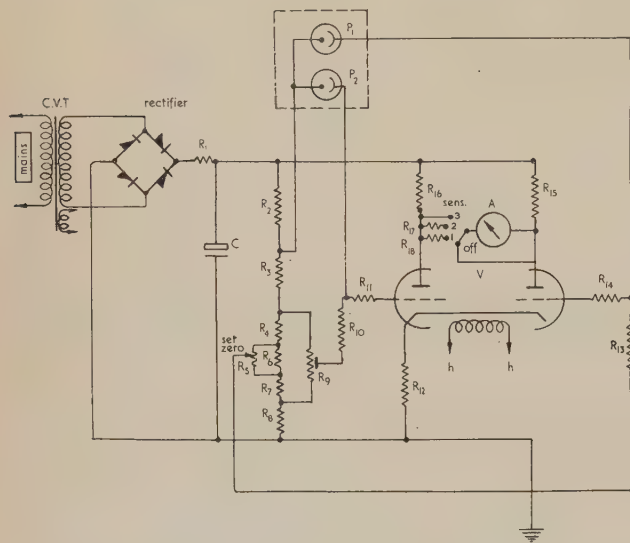


Fig. 2. Electrical circuit of densitometer

$R_1 = 4.7 \text{ k}\Omega$	$R_{13} = 4.7 \text{ M}\Omega$
$R_2 = 47 \text{ k}\Omega$	$R_{14} = 470 \Omega$
$R_3 = 22 \text{ k}\Omega$	$R_{15} - R_{17} = 47 \text{ k}\Omega$
$R_4 = 100 \Omega$	$R_{18} = 470 \text{ k}\Omega$
$R_5 = 1 \text{ k}\Omega$	$C = 4 \mu\text{F}$
$R_6 = 200 \Omega$	$V = \text{ECC91}$
$R_7 = 100 \Omega$	$P_1, P_2 = 90\text{CV}$
$R_8 = 33 \text{ k}\Omega$	$A = 50.0 - 50.0 \mu\text{A}$
$R_9 = 2.5 \text{ k}\Omega$	$C.V.T. = \text{Advance, Type MT. 161A.}$
$R_{10} = 4.7 \text{ M}\Omega$	
$R_{11} = 470 \Omega$	
$R_{12} = 47 \text{ k}\Omega$	

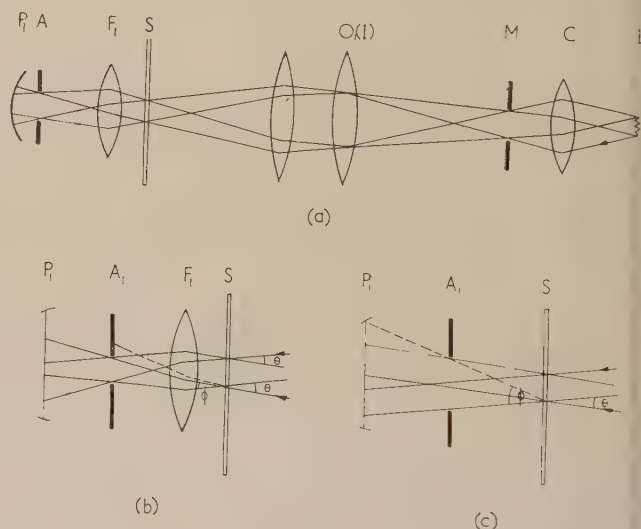


Fig. 4. Optical system: detail

(a) Optical diagram of direct light beam through dust sample arm. (b) Definition of beam from dust slide by aperture at A_1 , $\phi = \theta$. (c) Lack of definition of beam in absence of F_1 , $\phi > \theta$

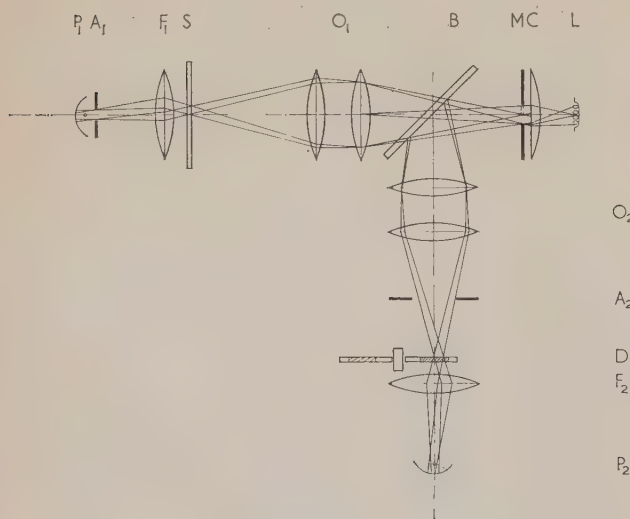


Fig. 3. Optical system of densitometer

front lens of each of two objectives O_1, O_2 , one in each light beam, a half-silvered mirror B set at 45° acting as a beam splitter. The field aperture M is placed close to the back surface of the condenser, at the common focus of the two objectives: a system of "Maxwellian view" which provides uniform illumination of the aperture. Aperture M is imaged at unit magnification by the objective lenses on the dust slide S in one arm and on the density wedge D in the other, and the transmitted beams are converged by lenses F_1, F_2 on the cathodes of the respective photocells, P_1, P_2 . In the density wedge arm an adjustable aperture A_2 provides for initial photometric balance of the two light beams. The field of illumination at S is defined by the field aperture M , and the angle of illumination θ at any point on S is defined by the size of the image I on the lens O_1 . The purpose of the lens F_1 between dust slide S and the detector P_1 is to ensure that the angle of acceptance ϕ of scattered light at P_1 is the same for all points on the dust deposit. Lens F_1 forms an image of I at A_1 [Fig. 4(b)] so that an aperture at A_1 can be adjusted to transmit a constant angle ϕ equal to the incident angle θ . In the absence of F_1 this is not possible [Fig. 4(c)].

The field aperture M is either (i) a $1 \text{ mm} \times 1 \text{ cm}$ slit, or

(ii) a 12 mm square with the weighting mask superimposed. This weighting mask (Fig. 5) has effectively twelve 1 mm apertures across its width, the heights of which are in proportion to the zone calibration factors; that is, the area of each zone and thus the light flux is proportional to f_x . (It

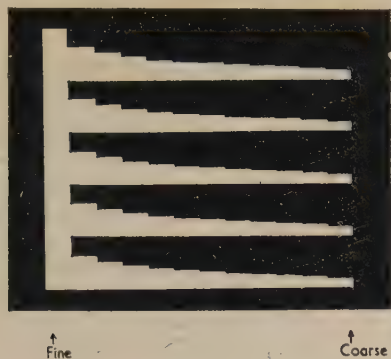


Fig. 5. Weighting mask

is in practice more convenient to control the total illumination of a zone by area than by intensity.) The largest of these apertures is 1 cm in height, and the smaller ones are each divided up so as to cover the full height of the dust deposit. The dust slide holder has adjustments to enable the dust deposit to be precisely aligned with respect to the image of this weighting mask.

Experimental

Dust samples were obtained in the laboratory with the long-running thermal precipitator of four typical mining materials: soft coal, anthracite, mudstone and white sandstone. Microscope counts of particles greater than 1μ diameter were made in such a way that the number of particles could be obtained in each of twelve zones of 1 mm width. These counts were compared with twelve zone density measurements, and average calibration factors for each zone derived. The shapes of the calibration curve were similar for the four materials, but the actual values of the calibration factors for the extreme materials (sandstone and soft coal) differed by 30%. In practice, the typical colliery dust cloud consists of a mixture of coal and stone dust particles, and it was decided that a set of mean calibration factors would be adequate for all mine dust samples. This set (Fig. 6) was used to determine total number of

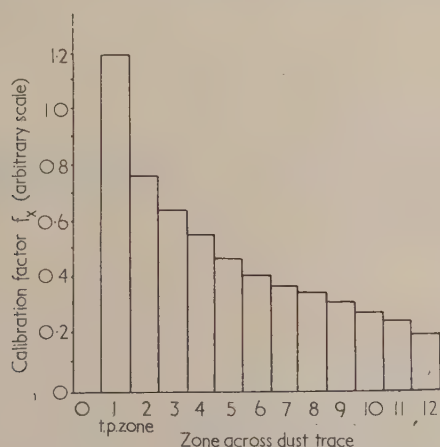


Fig. 6. Number calibration factors

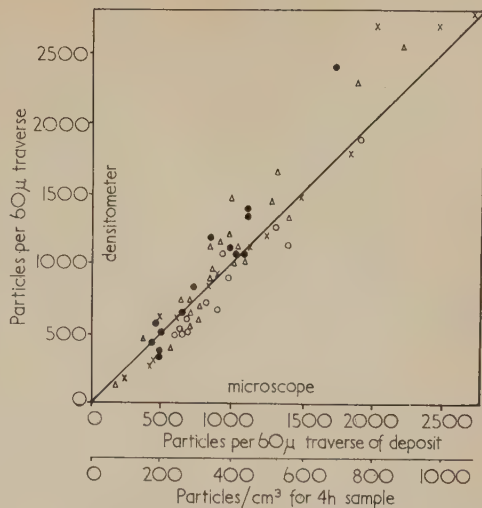


Fig. 7. Relationship between microscope counts and densitometer counts. Laboratory calibration samples. Zonal assessment

● = soft coal; Δ = anthracite; × = mudstone; ○ = sandstone

particles, and the individual values were compared with microscope assessment (Fig. 7). From this set of mean calibration factors the weighting mask was designed, permitting a single density measurement to be used. This reduced the time for assessment to two minutes per sample, enabling one hundred samples to be assessed in a day.

A large number of routine mine samples were evaluated in this way and results compared with microscope assessment (Fig. 8). The standard deviation is about 25%. This scatter

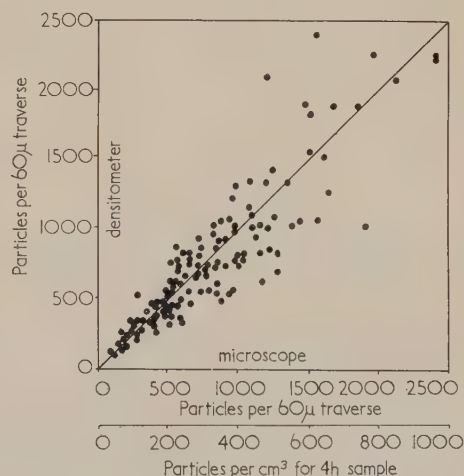


Fig. 8. Relationship between microscope counts and densitometer counts. Routine mine samples. Integral assessment

of results is greater than with the laboratory-prepared samples, probably due to contamination of the slides. (When the requirements for densitometric evaluation were better appreciated by the field laboratory personnel there was better agreement between the two methods.) It must be remembered also that a proportion of the scatter in the results can be attributed to known inconsistencies of microscope counting.⁽⁹⁾

Some experiments were carried out to examine the correlation between the mass of dust on an l.r.t.p. slide, calculated from larger weighed samples collected concurrently on a paper filter, and a value obtained from zonal density measurements weighted by calibration factors determined as above. Dust-laden air from a windswept tumble mill was collected on a paper filter after being drawn through a long horizontal duct, in which was placed a stacked horizontal elutriator which gives the standard respirable dust cut-off at the flow rate of $2.7 \text{ ft}_3/\text{min}$. (The standard cut-off for respirable dust involves the removal from the sampled cloud of all particles with falling speeds greater than that of a $7.1 (5\sqrt{2}) \mu$ unit density sphere and of 50% of those particles with falling speed equal to that of a 5μ unit density sphere.) In the duct beyond the elutriator, and just in front of the filter, was placed a long-running thermal precipitator sampling head with its own size-selector removed. Seventy pairs of samples on filter paper and on l.r.t.p. slides were obtained in this way, covering fourteen coal types.

The ratios of densitometric evaluation of mass ($\overline{D_x/\sqrt{f_x}}$) to mass M obtained from filter paper weighings gave a mean value for C which was used to convert all density measurements to mass values. These are plotted against the individual masses determined experimentally by filter paper weighings

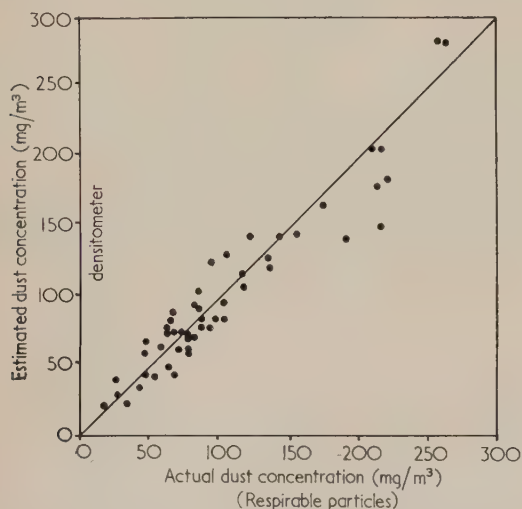


Fig. 9. Relationship between mass concentration and densitometer estimation. Coal samples. Zonal assessment

in Fig. 9. The standard deviation is about 20% (i.e. comparable with the agreement on number assessment).

Since mass is not at present an accepted standard for evaluation of respirable mine dusts, these experiments were not pursued very far, but it is apparent that acceptable correlation between mass and optical density can be obtained on l.r.t.p. samples.

Application to discrimination between coal and non-coal particles

The technique can be adapted to the measurement of the relative proportions of coal and non-coal particles in l.r.t.p. samples. This adaptation has been described previously by Donato⁽¹⁰⁾ and consists in measuring the optical density of the dust deposits both before and after incineration at 550°C .

When coal particles are heated they burn, leaving behind small residual "ash" particles, which, in the course of normal

microscope counting, cannot be distinguished from the unaffected rock dust particles in the deposit. However, since the ash residues are invariably considerably smaller than the coal particles from which they came, their effect on the densitometer "count" of the sample is negligible, so that the "count" obtained after incineration represents the non-coal particles only.

Discussion and conclusions

Calibration factors have been determined in this work for mine dust samples, covering a limited range of particle shape and density. The method is applicable to other dusts, for which the calibration factors would have to be determined experimentally. For the present application calibration factors have been determined for particles greater than 1μ diameter, although the present number assessment (by microscopical technique) for rock is in terms of particles greater than 0.5μ diameter. It does not appear practicable to extend the calibration down to 0.5μ diameter, because these very fine particles are nearly all collected in the thermal deposition area of the long-running thermal precipitator samples, and owing to the very wide variations in size distribution in this region there would be great difficulty in establishing reliable factors.

At low densities of particle deposition, where there is negligible overlapping of particles, the number obtained from microscopical examination will be in agreement with that from densitometric assessment, zonal or integral. At higher densities, due to overlap and association of particles, microscopical counting will underestimate the number⁽¹¹⁾ but densitometric measurements are relatively free from such errors.

The agreement between densitometer and microscopical estimations is similar in magnitude to that obtained between microscopists. The required standard of cleanliness of slide is higher than for routine microscopical evaluation, but there are compensating advantages in that much higher densities of the sample can be accurately assessed, and the whole of the deposit is used. The method has the general advantages over microscopy of lower skill requirements and higher speed and consistency.

Acknowledgements

The authors are grateful to Mr. W. H. Walton for many helpful suggestions during the course of the work. A number of people in the N.C.B. Scientific Control organization, particularly Mr. J. M. N. Thornton of Durham Division and Mr. E. White of North-Eastern Division, have helped in field testing the instrument, as has also Mr. J. R. Hodgkinson of the Safety in Mines Research Establishment. Miss P. M. T. Miles and Mrs. M. M. Sutcliffe carried out much of the experimental work in this laboratory.

The work described in this paper was carried out as part of the research programme of the Scientific Department of the National Coal Board and is published by permission of the Director-General of Research.

References

- (1) BEDFORD, T., and WARNER, C. G. *Medical Research Council, Spec. Rep. Ser. No. 244* (London: H.M. Stationery Office, 1943).
- (2) HAMILTON, R. J. *J. Sci. Instrum.*, **33**, p. 395 (1956).
- (3) WALTON, W. H. *Brit. J. Appl. Phys., Suppl. 3*, p. S. 29 (1954).

- (4) MIE, G. *Ann. Phys. (Leipzig)*, **25**, p. 377 (1908).
 (5) SINCLAIR, D. *J. Opt. Soc. Amer.*, **37**, p. 475 (1947).
 (6) WALTON, W. H. *Suppl. to Trans Instn Chem. Eng.*, **25**, p. 141 (1947).
 (7) VAN DE HULST, H. C. *Light Scattering by Small Particles* (New York: John Wiley and Sons, Inc., 1957).
 (8) ELLISON, J. MCK. *Proc. Phys. Soc. (London) B*, **70**, p. 102 (1957).
 (9) HOLDSWORTH, J. F., PRICE, H. F., and TOMLINSON, R. C. *Brit. J. Appl. Phys. Suppl.* 3, p. S. 96 (1954).
 (10) DONATO, R. J. *Annals of Hygiene*, **1**, p. 280 (1960).
 (11) ROACH, S. A. *Brit. J. Ind. Med.*, **15**, p. 250 (1958).

Photoelectric method for the analysis of fluctuation records and its application to electrical noise*

by J. SCOTT, M.Sc., The Nuclear Power Group, Radbroke Hall, Knutsford, Cheshire

[Paper first received 2 March, and in final form 31 March, 1960]

Abstract

A photoelectric method is described for obtaining the after-effect function for a stationary-fluctuation process from a record in the form of a graph or oscillogram. The method is applied to the statistical analysis of some records of electric noise from various sources. Future possible developments of the method are indicated.

Introduction

THE analysis of a stationary-fluctuation process may be directed towards the information available on the spectrum of the process, or alternatively, towards more direct information on the constituent events underlying the process. The approach is, to some extent, governed by the method of observation. If the response of the measuring apparatus modifies significantly the characteristics of the fluctuation record, then the spectral approach will be the more fruitful. However, if the characteristics of the measuring apparatus allow the observation of individual events, then the spectral approach is of doubtful value and, in fact, the concept of a spectrum under these conditions must be examined carefully.⁽²⁾

For a stationary and ergodic stochastic process $f(t)$, the autocorrelation function is defined, if $\overline{f(t)} = 0$, as:

$$\rho_\tau = \frac{\int_{-\infty}^{+\infty} f(t+\tau)f(t) \cdot dt}{\int_{-\infty}^{+\infty} \{f(t)\}^2 \cdot dt} \quad (1)$$

The autocorrelation function ρ_τ is related to the spectrum of the fluctuations by the following two relationships which form the well-known Wiener-Khinchine theorem:

$$\rho_\tau = \int_0^\infty I_n(v) \cos 2\pi v\tau \cdot dv, \quad (2)$$

$$I_n(v) = \int_0^\infty \rho_\tau \cos 2\pi v\tau \cdot d\tau. \quad (3)$$

Here $I_n(v)$ is the normalized spectral-density function.

* Substance of part of the author's M.Sc. Thesis.⁽¹⁾

Two types of after-effect functions for the process $f(t)$ are defined by the following equations^(3, 4):

$$\Delta_\tau^2 = \lim_{T \rightarrow \infty} \frac{1}{T} \int_{-T/2}^{+T/2} \{f(t+\tau) - f(t)\}^2 dt, \quad (4)$$

$$\Delta'_\tau = \lim_{T \rightarrow \infty} \frac{1}{T} \int_{-T/2}^{+T/2} |f(t+\tau) - f(t)| dt \quad (5)$$

These functions may be normalized to form the "reduced after-effect functions":

$$\delta_\tau^2 = \frac{\Delta_\tau^2}{\Delta_\infty^2} = \frac{\Delta'_\tau}{2\sigma^2}, \quad (6)$$

where the variance σ^2 of $f(t)$ is given by:

$$\sigma^2 = \overline{\{f(t)\}^2}, \quad (7)$$

and:

$$\delta'_\tau = \frac{\Delta'_\tau}{\Delta_\infty}. \quad (8)$$

It is easily shown from equations (1) and (4) that:

$$\Delta_\tau^2 = 2\sigma^2(1 - \rho_\tau), \quad (9)$$

and it follows from equations (9) and (6) that:

$$\delta^2 = (1 - \rho_\tau). \quad (10)$$

It is not possible to establish a similar relationship for Δ'_τ , but it follows from the definition of the variance that:

$$\sigma^2 \overline{|f(t+\tau) - f(t)|^2} > \Delta_\tau^2 - (\Delta'_\tau)^2. \quad (11)$$

Thus the difference between the functions Δ_τ^2 and $(\Delta'_\tau)^2$ is itself a function of τ ; it is zero for $\tau = 0$, and has a maximum value for $\tau = \infty$, when no correlation exists between $f(t+\tau)$ and $f(t)$. Because of this, Δ_τ^2 will always be greater than $(\Delta'_\tau)^2$.

The after-effect functions provide perhaps the most direct picture of the statistical features of stationary fluctuation processes; in particular those of "quasi-periodic" character. A theoretical study of these problems is to be found in the Ph.D. Thesis of T. Lukes (1960) (to be published elsewhere).

A photoelectric method for the measurement of Δ'_τ

Briggs and Phillips⁽⁵⁾ comment that a measurement of Δ'_τ can be obtained from the area enclosed between an infinite length of record $f(t)$, displaced by a time τ with respect to itself and superposed upon itself. The planimetric method of measurement of this area used by these authors is, however, rather cumbersome and not very accurate. A simple photoelectric method was therefore devised instead. It can be used for the analysis of fairly long records of stationary time series in the form of graphs which must be simple enough to enable them to be converted into opaque complementary profiles.

In the work described, the records were "single-shot" oscillograms of electrical noise on 35 mm film. The production of the profile was then quite simple. The films were enlarged and printed on extra-contrast bromide paper. With 10×8 in. prints it was then an easier matter to cut out the complex shapes. One of these was then reversed and photographed on a black background using process photographic plates. The photographic plate, size $3\frac{1}{4} \times 3\frac{1}{4}$ in. was copied in turn by contact printing with a lantern slide plate which provided an exactly complementary profile, which differed slightly in opacity. Later, it will be shown that this difference in opacity, if small, does not matter. A schematic diagram of the apparatus used is shown in Fig. 1.

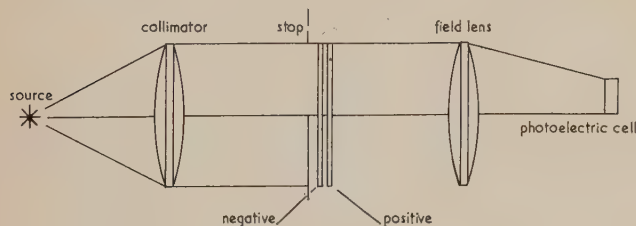


Fig. 1. Schematic form of optical components

The two profile plates were mounted, emulsion to emulsion, 1 mm apart, in two plate holders which could be displaced against each other by two micrometer screws with an accuracy of about 0.1 mm. A collimated light beam from the light source (a 100 W projector lamp) after passing through the plates, was condensed upon a barrier-layer photocell. The current from the photocell was measured using a microammeter, which had a full-scale reading of 500 μ A. A description of the apparatus together with details of precautions will be found in the author's thesis.⁽¹⁾

It is convenient to label the plates "negative" and "positive" to simplify description of the experimental procedure. In a typical experiment the negative was first moved relative to the positive and the photocell current recorded as a function of displacement. The procedure was then repeated with the positive and the sum of the currents for equal relative displacements plotted as a function of time. Time and displacement were related by using a time trace on the oscillogram. From each pair of plates two independent curves can be obtained, each covering half the length of the record. This is done by placing the aperture stop first in front of one half of the plates and then in front of the other half. One of these positions of the stop is shown in Fig. 1.

It will be shown that the sum of the photocell currents for a particular displacement is a linear function of Δ'_τ . The two displacements shown in Fig. 2 are considered. The transmissions P_1 and P_2 of the two plates represent the fractions of the incident radiation passing through the blackened parts of them. Consequently, in the areas where

the profiles overlap, the fraction of energy transmitted is P_1P_2 . It is assumed that the sum of the unshaded areas in Fig. 2(a) is ϵ_1 and of the doubled-cross-hatched areas is

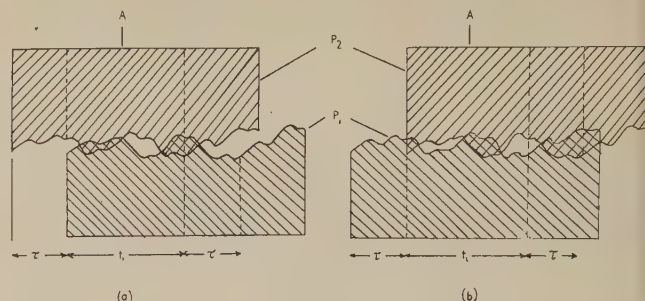


Fig. 2. Complementary profile positions

ϵ_2^* . If it is also assumed that unit flux is incident upon the plates, then the flux transmitted is:

$$F_{(a)} = \left[A - \left\{ \int_{\tau}^{t_1+\tau} f(t) dt + \epsilon_2' \right\} \right] P_2 + \left[\int_0^{t_1} f(t) dt - \epsilon_2 \right] P_1 + \epsilon_2 P_1 P_2 + \epsilon_1, \quad (12a)$$

where A is the area of the aperture stop and t_1 is the time range of the record within the stop. Similarly, from Fig. 2(b):

$$F_{(b)} = \left[A - \left\{ \int_0^{t_1} f(t) dt + \epsilon_1 \right\} \right] P_2 + \left[\int_{\tau}^{t_1+\tau} f(t) dt - \epsilon_1 \right] P_1 + \epsilon_1 P_1 P_2 + \epsilon_2. \quad (12b)$$

Thus, from equations (12a) and (12b):

$$F_{(a)} + F_{(b)} = (\epsilon_1 + \epsilon_2) (1 + P_1 P_2 - P_2 - P_1) + 2AP_2 + \left\{ \int_0^{t_1} f(t) dt + \int_{\tau}^{t_1+\tau} f(t) dt \right\} (P_1 - P_2). \quad (13)$$

If P_1 and P_2 and also $(P_1 - P_2)/P_1$ are small compared with unity (say, of the order of 1%), the terms containing $P_1 P_2$ and $P_1 - P_2$ in equation (13) can be neglected in comparison with the term $2AP_2$, and therefore:

$$F_{(a)} + F_{(b)} \approx \epsilon_1 + \epsilon_2 + 2AP_2. \quad (14)$$

It follows from the definition of Δ'_τ given by equation (5) that:

$$\Delta'_\tau = \frac{\epsilon_1 + \epsilon_2}{t_1}, \quad (15)$$

and as the photocell currents are proportional to $F_{(a)}$ and $F_{(b)}$ respectively, the sum $I(\tau)$ of these currents is indeed a linear function of Δ'_τ .

A feature of the barrier-layer photocell used was that it required "ageing" and before each experiment it was illuminated until the cell current reached a minimum. A series of tests taken over intervals of a few days showed that the method was capable of reproducing results on a sample of nine oscillograms to within 5% and the main features,

* The unshaded areas in Fig. 2(b) are, of course, the same as the cross-hatched areas in Fig. 2(a), and vice versa.

despite this difference, were reproduced faithfully. In addition to this test of the long-term stability of the method, the results were compared with direct numerical computation from the records. The comparison between the photoelectric method and the numerical method is illustrated in Fig. 3 for three different samples of electrical noise.

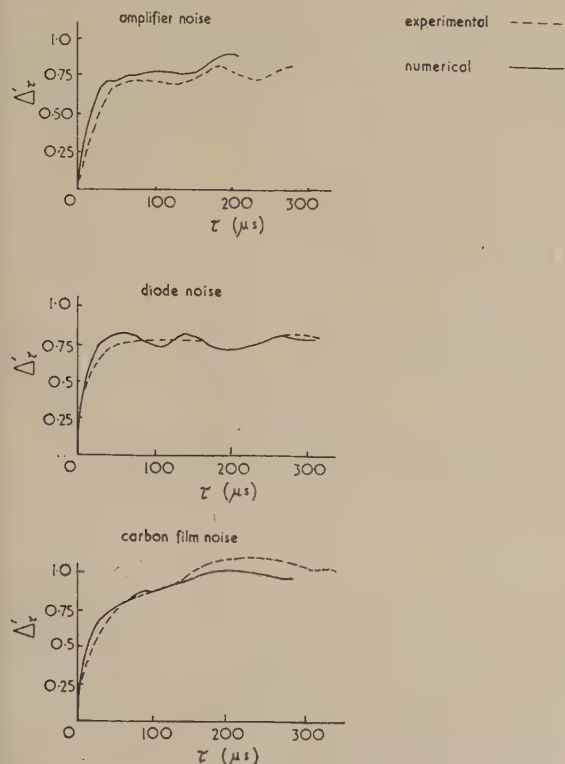


Fig. 3. Comparison of experimental and numerical results

Application of the method to the analysis of valve and semiconductor noise

To demonstrate the usefulness of the new method for the statistical analysis of stationary fluctuation records it was applied to the computation of the after-effect function Δ'_t of records of various types of electrical noise. The records consisted of oscillograms on 35 mm film, each obtained by a single sweep of approximately 1.5 ms duration, kindly put at our disposal by Dr. D. A. Bell of the Department of Electrical Engineering of the University of Birmingham.

The after-effect functions obtained from these records are exhibited in Figs. 3, 4 and 5, each of the curves representing averages from a number of different records. The Germanium diode 1 was described as having appreciable storage of "holes", the Germanium diode 2 as having negligible storage of "holes".

It can be seen from Figs. 3, 4 and 5 that the curves bear a significant similarity to one another. The fundamental mechanisms which give rise to these fluctuations are different enough to lead to the suspicion that the similarity is imposed by the characteristics of the amplifying circuits. If this were not so, it would be reasonable to expect the curves to show maxima and minima appropriate to the transit time of the carriers.

In first approximation, the beginnings of the curves may be represented by after-effect functions of the form:

$$\delta_t^2 = 1 - \exp(-\beta\tau) = \beta\tau - \frac{1}{2}\beta^2\tau^2 + \dots, \quad (16)$$

which hold for fluctuation processes with a single characteristic "relaxation time" θ equal to $1/\beta$ (see, for example, reference 4). The values of θ obtained from Figs. 3, 4 and 5 are shown in the table.

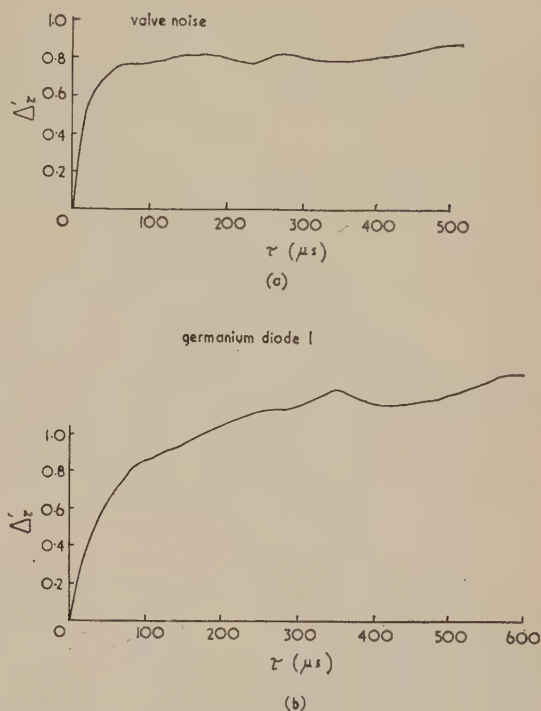


Fig. 4. Experimental results

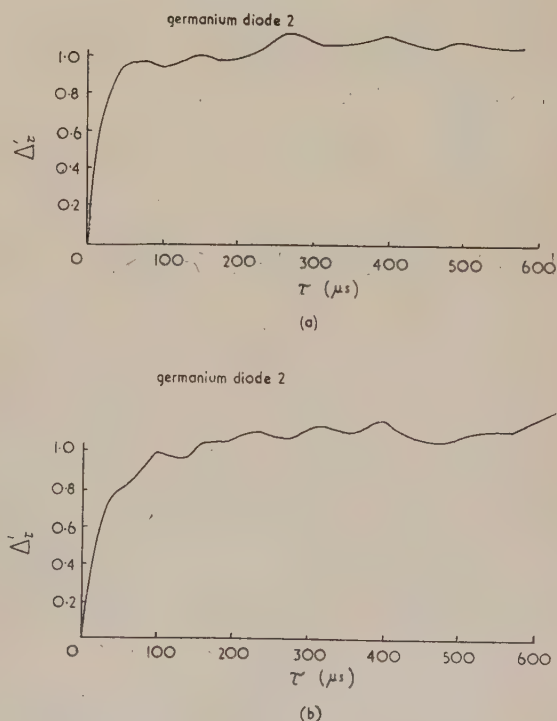


Fig. 5. Experimental results

Table of values of θ

Type of noise	Fig. No.	$\theta(\mu\text{s})$	$(a/b) \times 10^4$
Amplifier noise	3a	70	1.11
Diode noise	3b	45	3.46
Carbon film noise	3c	100	-0.38
Valve noise	4a	70	1.79
Germanium diode 1	4b	300	-0.62
Germanium diode 2	5a	55	1.53
Germanium diode 2	5b	170	0.04

To discuss the significance of these figures, it is necessary to consider the frequency response of the amplifier used to obtain the records, which is shown in Fig. 6. The restricted

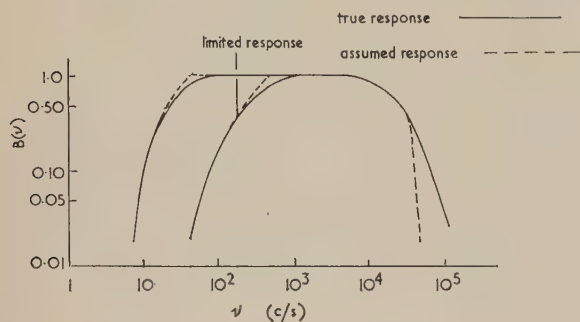


Fig. 6. Amplifier frequency response

response was used for the results of Fig. 3 and the more extended one for Figs. 4 and 5.

The upper frequency limit of the amplifier is approximately 4.2×10^4 c/s which would preclude relaxation times of the order of less than $25 \mu\text{s}$. It seems that the relaxation times for the noise produced by valves, Figs. 3(a), 3(b) and 4(a), have nothing to do with the primary noise mechanisms but are produced by the finite response of the amplifier. On the other hand, the relaxation time for the germanium diode 1 is considerably greater and well within the resolving capacity of the amplifier circuit. The same is true of the relaxation times of the germanium diode 2 and the carbon film, Figs 3(c) and 5(b), although they are only half as large.

This result is not unexpected, as it is generally recognized that the electrical noise produced by semiconductors is characterized by a wide range of relaxation times, in contrast to metallic conductors and electronic valves, where the relaxation times are of a very much smaller order of magnitude. The particularly large value of θ for the germanium diode 1 most probably results from the fact that this diode had an appreciable storage of holes, as mentioned before.

To account for the complete shape of the after-effect functions, use can be made of the nature of the spectrum of the fluctuations. For if the spectrum of the primary fluctuations is known, and also the characteristics of the amplifier, then the after-effect function can be computed using the Wiener-Khinchine theorem and equation (9). It seems reasonable to assume a simplified spectrum for the primary fluctuations consisting of a linear combination of the two most frequently occurring spectra, that is, the "white" and the inverse-frequency or " $1/\nu$ " spectrum. The existence of the latter is well known.^(6, 7, 8, 9) The spectral density is then of the form:

$$I(\nu) = a + (b/\nu). \quad (17)$$

The actual response curve of the amplifier (Fig. 6) was further replaced by a trapezoidal curve consisting of two

inclined and one horizontal straight line, as shown in Fig. 6. The autocorrelation functions ρ_τ , corresponding to a "white" and a " $1/\nu$ " spectrum modified by the restricted amplifier response, can be computed easily from equation (2), and from these, the reduced after-effect function δ_τ by means of equation (10).

The δ_τ curves are shown for the two spectra and responses in Fig. 7. The difference between curves for "white" noise for the two responses was negligible and only one result is shown. A series of maxima appear at integer multiples of the reciprocal of the amplifier cut-off frequency and these are

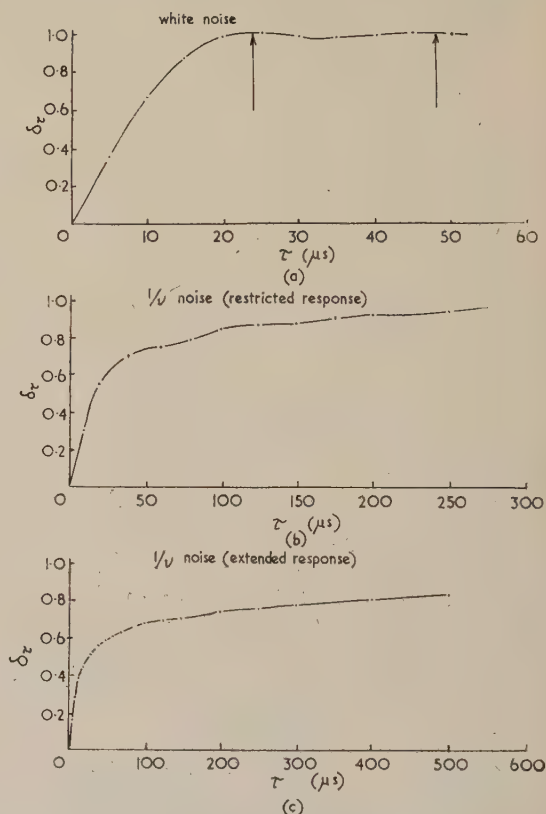


Fig. 7. Theoretical curves

indicated by arrows in Fig. 7. The distinctive feature of this curve is the rapidity with which δ_τ reaches the first maximum.

The two amplifier responses provide two different results for the variations of δ_τ with τ . The results have only been computed over the same range of τ as the experimental results. The main feature of these curves is the slow approach to a maximum value of δ_τ for some large value of τ . The rate is more rapid in the case of the restricted response, which indicates a suppression of the longer relaxation times.

From this brief examination of the results produced by pure spectra, two main points emerge: first, the shape of the after-effect function for "white" noise depends solely on the upper limit to the frequency response; and second, the after-effect function for a " $1/\nu$ " spectrum is predetermined largely by the lower limit to the frequency response.

For the mixed spectrum of equation (17), the autocorrelation function may be written in the form:

$$\rho_\tau(M) = \frac{a'}{a' + b'} \rho_\tau(W) + \frac{b'}{a' + b'} \rho_\tau\left(\frac{1}{\nu}\right), \quad (18)$$

$$\text{where: } a' = a \int_0^{\infty} B(\nu) d\nu, \quad (19a)$$

$$b' = b \int_0^{\infty} \frac{B(\nu)}{\nu} d\nu, \quad (19b)$$

and $B(\nu)$ is the frequency-response function of the amplifier.

It is seen from Fig. 7 that $\rho_{\tau}(W)$ is approximately equal to zero for τ greater than $25 \mu\text{s}$. It therefore follows from equation (9) that for $\tau > 25 \mu\text{s}$:

$$\Delta_{\tau}^2(M) = \Delta_{\infty}^2(M) - \frac{\Delta_{\infty}^2(M)\rho_{\tau}(1/\nu)}{\{1 + (a'/b')\}}. \quad (20)$$

If one identifies, as a first approximation, $(\Delta_{\tau})^2$ and Δ_{τ}^2 , it is possible to obtain values of Δ_{∞}^2 and a'/b' from equation (20) by plotting $(\Delta_{\tau})^2$ against $\rho_{\tau}(1/\nu)$. The method of least squares was used to obtain best values of the gradient and the intercept of the straight line, and from these the values of a'/b' . The corresponding values of a/b was then obtained from equations (19) and are exhibited in the above table.

In actual fact, according to equation (11), Δ_{τ}^2 is greater than $(\Delta_{\tau})^2$, and hence the real values of a/b must be larger than those shown in the table. This accounts for the fact that some of these figures are negative, which, of course, would be physically meaningless; it is to be assumed that in these cases the real values of a/b would be positive and much smaller than the rest.

With the exception of Fig. 5(a), all the semiconductor noise records are characterized by high relaxation-time values and low values of a/b , indicating a large ratio of "1/ ν "-to-"white" noise. On the other hand, the comparatively large values of a/b for the noise curves in Figs. 3(a), 3(b) and 4(a) indicate a higher proportion of "white" noise, which is in keeping with their origin in amplifier and valve noise.

Concluding remarks on the photoelectric method

The results obtained with the help of the new method described in the previous section show that the method is indeed capable of analysing fluctuation records and drawing definite conclusions from them as to the statistical character of the fluctuation phenomena. It would probably be necessary to extend the upper and lower frequency limits of the amplifier circuits used for obtaining the records in order to obtain better information on the primary mechanism of the fluctuation.

The apparatus used to obtain these results was rather simple and it would be advantageous to improve it in some respects and make it automatic in operation. If records are to encompass longer time scales, the resolution of the optical components becomes important and attention must be paid to the collimation of the light beam. Considerable effort would be saved if the complementary displacements could be achieved simultaneously by using two pairs of plates and combining the photocell currents so that the output would be directly proportional to Δ_{τ}^2 .

Acknowledgements

I am indebted to Dr. D. A. Bell of the Department of Electrical Engineering in the University of Birmingham for providing the noise oscillograms and the frequency response of the amplifier used for obtaining them. My thanks are also due to Prof. J. D. Bernal for his permission to carry out this work in the laboratories of the Physics Department of Birkbeck College and to Dr. R. Furth, who suggested this line of research and acted as supervisor for my work for the M.Sc. degree at London University.

References

- (1) SCOTT, J. M.Sc. Thesis (University of London, 1959).
- (2) FURTH, R. *Proc. Roy. Soc. A*, **192**, p. 593 (1948).
- (3) SMOLUCHOWSKI, M. V. *Abhandlungen uber die Brownsche Bewegung und verwandte Erscheinungen* (Leipzig). Ostwald's Klassiker der exakten Naturwissenschaften, p. 207 (1923).
- (4) FURTH, R. *Geophysical bulletin V. Dublin Inst. for Adv. Studies* (1952).
- (5) BRIGGS, B. H., and PHILLIPS, G. J. *Proc. Phys. Soc. B*, **63**, p. 907 (1950).
- (6) MONTGOMERY, H. C. *Bell System Tech. J.*, **31**, p. 950 (1952).
- (7) BAKER, D. K. *J. Appl. Phys.*, **25**, p. 922 (1954).
- (8) *Photoconductivity Conference* (New York: J. Wiley and Sons Inc., 1954).
- (9) MONTGOMERY, H. C., and SHOCKLEY, W. *Phys. Rev.*, **78**, p. 646 (1950).

Effects of oil vapour contamination on the adhesion of zinc sulphide films to glass and silica

by L. HOLLAND, F.Inst.P., and S. K. BATEMAN, Vacuum Deposition Research Division, Edwards High Vacuum Ltd., Crawley, Sussex

[Paper first received 3 February, and in final form 6 May, 1960]

Abstract

An investigation has been made of the effect of adsorbed oil molecules from diffusion pump fluids on the adhesion of zinc sulphide films to glass and evaporated silica substrates. Zinc sulphide films evaporated on to fresh coatings of silica in a silicone oil diffusion pump system readily peeled in a humid atmosphere, because the silica was contaminated by chemisorbed silicone molecules; silicones were not chemisorbed by glass covered by adsorbed water. Tests were made to find the time taken to cover a substrate surface with sorbed layers of different types of pump oil and thereby destroy the zinc sulphide film adhesion. A test oil was held in a water-cooled tray in the coating vessel and the specimen exposed to the non-saturated oil vapour for different periods before zinc sulphide deposition. Silica coatings held at 50° C could be exposed to Silicone 703 for 1 min, and Silicone 704 for 4 min, before the adhesion of the superimposed zinc sulphide deposit was badly impaired. Adsorbed molecules of Apiezon "C" did not unduly affect the adhesion of zinc sulphide films. With a silica layer at 230° C the formation time for a chemisorbed film of silicones was 75 min. Raising the temperature of the silica surface reduces the period for which silicone molecules linger and orientate themselves on the substrate. When glass is heated in silicone vapours in vacuum it gradually becomes covered with chemisorbed molecules as the OH-groups are removed, leaving the surface unshielded.

Introduction

It is generally accepted that the adhesion of evaporated metal and dielectric films to glass substrates is adversely affected by the adsorption of contaminants from the vacuum atmosphere, but there has been no detailed study of this aspect of vacuum deposition. The atmosphere in a kinetic vacuum plant is mainly composed of water vapour, released from the walls of the system, and organic vapour, released by rubber seals and pump fluids. Adsorption of hydrocarbon molecules by a clean substrate surface will undoubtedly prevent an evaporated layer coming within the range of the surface attractive forces, and during the early use of oil diffusion pumps, trouble was often experienced because oil vapour *back streamed* directly on to the substrate surface. For many years adherent evaporated films have been obtained with oil diffusion pumps fitted with water-cooled baffles, which prevent the pressure of the oil vapour reaching a saturated value in the coating vessel. However, the vapour pressure of most pump fluids in equilibrium with a baffle at 15° C is such that the substrate surface would be covered with a mono-molecular layer in a minute or so if every molecule striking the surface was sorbed.

Generally one finds that adherent films can be evaporated on to glass surfaces which have been glow-discharge cleaned, so that if oil sorption does occur the contaminants must be only weakly bonded. However, the authors have recently observed that diffusion pump oil can be strongly adsorbed by fresh silica surfaces prepared in vacuum.

Evaporated zinc sulphide films are reasonably adherent to clean glass, but zinc sulphide films deposited on freshly evaporated silica layers may completely lack adhesion to the silica surface when the coatings are prepared in an apparatus with a silicone oil diffusion pump. Thus when part of a glass slide was coated with silica, by slowly evaporating silicon monoxide, and zinc sulphide was then deposited on both the treated and untreated surfaces, the zinc sulphide film on the silica broke up into minute fragments and peeled immediately it was exposed to air, whereas the film on the untreated glass was stable and could be burnished without being removed. The experiment was repeated several times with the same result. Some zinc sulphide films on silica substrates did not immediately disintegrate on exposure to air, but these only had to be breathed on for them to spontaneously break up and emit a strong smell of hydrogen sulphide.

If the zinc sulphide was evaporated on to the silica surface immediately after the silicon monoxide evaporation ceased, then the zinc sulphide film did not disintegrate when subsequently exposed in air at high humidities. On the other hand, if the fresh silica surface was exposed in the vacuum for several minutes before evaporating the zinc sulphide, then the superimposed layer subsequently peeled. Silica films which were exposed to the atmosphere immediately after deposition, and then returned to the vacuum chamber and glow-discharge cleaned, could then be left for many minutes in vacuum and adherent zinc sulphide films could still be obtained.

The adverse effect of the vacuum exposure on the zinc sulphide adhesion was attributed to silicone molecules from the diffusion pump being chemisorbed by the nascent silica. It is known that silicone molecules can be chemisorbed to glass by using dimethyl silicon chloride, which chemically reacts with the adsorbed water and removes it from the surface, and Holland⁽¹⁾ has found that silicone molecules are directly adsorbed to freshly evaporated silica films in vacuum. Chemisorbed silicone molecules are oriented with their polar groups adjacent to the glass and their non-polar groups, i.e. methyl groups, outermost. Presumably the methyl groups of the oriented silicone molecules have no attraction for zinc sulphide, which merely lays on the surface until reaction with water vapour in the atmosphere liberates hydrogen sulphide and strains the film so that the poor interface bond is broken. When the fresh silica surface is rapidly exposed to the atmosphere a chemisorbed water layer is formed which prevents the subsequent chemisorption of

silicones at normal temperature.⁽¹⁾ Glow-discharge cleaning of a glass before coating may remove the hydroxyl groups which cover the surface, but there is usually ample water in the atmosphere of a glow discharge in a kinetic system for the OH-groups to be replaced. The presence of hydroxyl groups on a cleaned glass apparently does not prevent the production of adherent zinc sulphide films. Regnault⁽²⁾ found that water and zinc sulphide reacted to form hydrogen sulphide and zinc oxide at very high temperatures, and a similar reaction could occur when zinc sulphide vapour is deposited on glass covered with water molecules.

Arising from the foregoing observations, a series of experiments were made to compare the effects of different diffusion pump fluids on the durability of zinc sulphide films deposited on glass and silica substrates.

Experimental apparatus

The experimental work was carried out in an evaporation plant with an 18 in. diameter metal chamber evacuated by an oil diffusion pump (Edwards type 903B) charged with Apiezon "C" oil. The latter oil was used because of the low ultimate pressure (approximately 10^{-7} mm of mercury ionization gauge reading) obtained with a blanked-off pump when fitted with a water-cooled baffle. The lead-in electrodes were sealed with rubber O-rings and the chamber sealed with an L-shaped rubber gasket to a metal base plate. The evaporation plant was typical of that currently used for the deposition of thin films. For evaporation purposes the chamber could be exhausted to an ultimate pressure of 5×10^{-5} mm of mercury (Penning gauge reading).

A spiral filament and a radiation-heated vapour source were used for evaporating the silicon monoxide and zinc sulphide respectively. The vapour sources were mounted under the specimen glass as shown in Fig. 1. The experimental glass was covered by a shutter which could be rotated by a vacuum-sealed shaft to expose progressively the glass surface to the vapour source. The high tension cleaning system was fitted with shielded cathode electrodes as described by Holland.⁽¹⁾ Measurement of the coefficient of

friction of an ion-bombarded glass showed that the surface had been freed from organic layers remaining after chemical cleaning with iso-propyl alcohol. The glass specimen could be mounted on a copper block fitted with a thermocouple and the evaporation rate adjusted so that the substrate temperature did not rise unduly. The specimen could also be heated to about 230° C by a radiant heater mounted at the top of the vessel.

A tray of diffusion pump oil, some 20 cm² in area, was mounted in the chamber facing the specimen glass, as shown in Fig. 1. The tray was water-cooled to keep it at 15° C which was the same temperature as that of the water-cooled baffle over the diffusion pump. Oil vapour from the tray in the vessel could thus evaporate directly on to the specimen surface, but it could not condense as a fluid layer because the specimen temperature was always above 15° C. Thus vapour molecules could only be adsorbed to the substrate surface. A large part of the desorbed gas in a kinetic system is water vapour and phosphorus pentoxide was placed in the vacuum chamber to lower its partial pressure. When silicon monoxide is evaporated the water vapour is temporarily gettered and this, together with the drying agent, tends to raise the ratio of oil-to-water molecules impinging on the substrate.

Experimental procedure and results

Low-temperature substrate. Each glass was glow-discharge cleaned for 10 min and then coated with a $\lambda/4$ -film of silicon monoxide evaporated at 0.1 μ of mercury pressure for 10 min. Immediately the evaporation ceased the shutter was moved to cover the test glass whilst the zinc sulphide was raised to the evaporation temperature. After one minute the evaporation had become rapid and the shutter was moved at minute intervals to expose progressively the glass to the zinc sulphide vapour and produce a stepped deposit as shown in Fig. 2. The silicon monoxide base layer was exposed to the

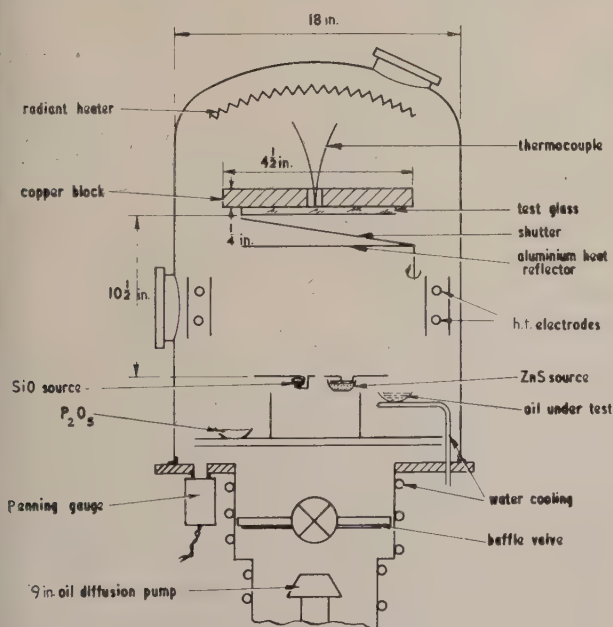


Fig. 1. Apparatus used for determining the effect of oil vapours on the adhesion of zinc sulphide films

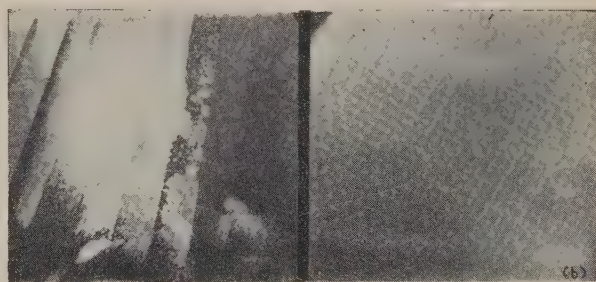


Fig. 2. The appearance of zinc sulphide films deposited on silica exposed to Silicone 704 vapour in one-minute steps. (a) substrate 50° C; (b) substrate 230° C

residual gas in the vacuum chamber for periods between 1 to 10 min before top coating. The zinc sulphide evaporation rate was about 10 Å/s so that a $\lambda/4$ -film was deposited every minute. The support temperature did not rise above 50° C during evaporation. An initial test was made with a silica-coated glass exposed to the residual gases emitted by the components in the vacuum system, subsequent tests were made with different vacuum oils in the vacuum chamber, namely, Apiezon "C" and Silicones D.C. 703 and 704.

Tests were also made of evaporating zinc sulphide on to glass specimens which had been glow-discharge cleaned for some 10 min, but not silica-coated. The zinc sulphide was raised to the evaporation temperature with the clean glass

covered by the shutter and the procedure outlined above then followed. The specimens used in these tests are referred to as "aged" glass to differentiate them from the fresh silica coatings.

After preparation under the above conditions, the zinc sulphide films were exposed to a humid atmosphere immediately they were removed from the vessel to find if they would peel, and the results are given in Table 1. The table

and the time noted for peeling to occur. The temperatures of the humidity bath rose and fell between 32 to 40°C over half-hour periods, with the saturated vapour pressure of the water following the temperature change. The results obtained, given in Table 1, show that Apiezon "C" gives the most durable deposit. It is possible that heating even "aged" glasses in silicone vapours for long periods will permit the formation of a chemisorbed silicone layer because the chemical bonds

Table 1. Resistance of zinc sulphide films to peeling in a humid atmosphere after exposing the substrate at different temperatures to oil vapours in vacuum

Test oil* (10 min max. exposure)	Substrate temperature 50° C		Substrate temperature 230° C		Time in humidity bath (h)
	Silica base coating	Aged glass	Silica base coating	Aged glass	
None	Stable films	Stable films	Stable films	Stable films	16
Apiezon "C"	Peeled after several weeks	Stable films	Stable films	Stable films	8-10
Silicone 704	Unstable after 3-5 min oil exposure	Stable films	Stable films†	Stable films†	6
Silicone 703	Unstable after 1 min oil exposure	Films became hazy after several weeks	Stable films†	Stable films†	2

* Diffusion pump charged with Apiezon "C".

† Zinc sulphide films finally peel if the base is exposed to silicone vapours at high temperature for 1½ h.

shows that Apiezon "C" does not immediately affect the stability of the zinc sulphide film, whereas the silicone oils can produce weakly adherent films with fresh silica substrates. It could be contended that the stepwise variation in the thickness of the zinc sulphide films could have influenced their durability on contaminated substrates. Thus the films affected by silicones in Table 1 after 3-5 min were of the order of a wavelength thick. However, similar results have been obtained after the same exposure periods when producing uniform $\lambda/4$ -films.

High-temperature substrate. The copper block used for cooling the specimen in the previous experiments was removed and tests were made with the glass heated to a high temperature. After glow-discharge cleaning for 10 min the substrate was heated to 230°C in 15 min, and maintained at this temperature during the tests for oil contamination. Experiments were made with silica-coated and uncoated glass exposed to different oil vapours as before. The silica deposits were prepared on the heated substrates and the zinc sulphide evaporated as previously described. Generally three samples were prepared.

The results given in Table 1 show that zinc sulphide films deposited on glass and fresh silica at 230°C did not peel when exposed in a humid atmosphere, irrespective of the nature of the oil vapour in the coating vessel. The results suggest that the oil molecules striking the hot specimen were mainly re-evaporated. Such a result is understandable with non-polar oils such as the Apiezon type, but it is difficult to see why the silicone oils which form chemisorbed layers on silica were re-evaporated. Further tests were therefore made baking silica-coated glass specimens in the vapour of Silicone 704 for ½, 1, 1½ and 1¾ h periods before deposition of the zinc sulphide. Zinc sulphide films deposited on silica-coated glass after heating for 1½ h at 230°C readily peeled from the substrate when exposed to air. Silica-coated glasses baked under these conditions became strongly hydrophobic.

Zinc sulphide films deposited on "aged" glass that had been heated to 230°C for a short period (10 min) and exposed to different oil vapours were much more durable than normal temperature films and could be tested in a humidity bath

of the OH-groups shielding the surface are broken at the high temperature. Thus it is known that hydrophobic films can be formed by heating glass in a kiln with silicone vapours. Glass specimens were therefore heated in vacuum with silicone vapour for a long period at 230°C and it was found that the surface became hydrophobic.

Preparation of hard zinc sulphide films. When glass specimens which have been cleaned in a glow discharge are baked, there is a period during the baking when the glass can be recontaminated by adsorbed molecules. This may affect the adhesion of subsequently deposited films, and the following films were made to determine the best method of preparing the substrate. All tests were made with Apiezon "C" in the evaporation chamber.

(a) The glass specimen was baked to 230°C for 15 min and afterwards glow-discharge cleaned for 10 min. Zinc sulphide, after being pre-heated to the evaporation temperature for 1 min, was then evaporated over the complete glass for 12 min to form a $7/4 \lambda$ thick film.

(b) The glass specimen was glow-discharge cleaned for 10 min then heated to 230°C over a period of 15 min. A silicon monoxide film about a quarter of a wavelength thick was then deposited. The zinc sulphide was finally evaporated as in (a).

(c) The glass specimen was glow-discharge cleaned for 10 min before baking at 230°C for 15 min. The zinc sulphide was then evaporated as in (a).

Three samples were prepared in each of the above groups and the time taken at which each of the samples showed signs of peeling when in the humidity bath. Half of each test glass was burnished before humidity testing to see if this influenced the durability. The humidity bath was controlled as described in the previous section.

The results given in Table 2 show that the most water-resistant films are those in group (a) and the least resistant are in group (c). A set of specimens were prepared and their scratch resistance tested with a sclerometer. The loads required on a steel pin to produce a visual scratch on the various groups were $a = 150$ g; $b = 20$ g; $c = 6$ g, which gives the same order of durability as that found with the

humidity bath. Burnishing did not improve the humidity resistance of the coatings, but the burnished zones were less easily scratched.

Table 2. Humidity resistance of zinc sulphide films on silica and glass substrates treated in different ways

Test	Time in humid bath (h)			
	Sample 1	Sample 2	Sample 3	Average
a	27	24	21	24
b	18	16	17	17
c	9½	8½	6	8

The tests were made with Apiezon "C" in the vacuum chamber.

General discussion

It has been shown that the durability of zinc sulphide films deposited in a kinetic vacuum system on glass or silica critically depends upon the nature of the residual oil molecules, the temperature of the substrate and the degree to which the substrate has been previously covered by adsorbed molecules, such as those of water. Silicone molecules are chemisorbed by glass or silica surfaces, providing these are not shielded by OH-groups, and zinc sulphide films are weakly adherent to silicone-covered surfaces. Apiezon fluids have least adverse effect on the adhesion of zinc sulphide films because their non-polar molecules are only weakly bonded to the base, and if the substrate temperature rises during the initial stages of film deposition this is sufficient for them to re-evaporate. The manner in which silicone molecules are chemisorbed by silica or glass surfaces in vacuum is worthy of consideration. Silicone 704 consists of molecules with a constant molecular weight of 484 and a diameter of about 10 Å, so that some 10^{14} molecules per square centimetre are required to cover a surface. The vapour pressure of Silicone 704 has been reported as 5×10^{-9} mm of mercury at 15°C by Huntress and others⁽³⁾ who extrapolated a curve determined at high vapour pressures. Using these values one obtains a

time for a monolayer to form of about 3–4 min if the coefficient of sorption is one. This agrees with the measured time of 3–5 min for the adhesion of a fresh silica base to zinc sulphide to be completely destroyed by a chemisorbed layer at a substrate temperature of 50°C. When the temperature of a fresh silica coating is raised to 230°C it takes 75 min for chemisorption to lower the adhesive forces of the surface, from which it can be deduced that only six out of every hundred molecules are chemisorbed on first impact.

The silicone molecules will strike the substrate by either their polar or non-polar terminals and the chemisorbed layer must be formed as follows. At normal temperature, silicone molecules which strike the substrate by non-polar terminals must be physically adsorbed and linger on the surface for a sufficient time to orientate themselves in the chemisorbed state, because the sorption coefficient is known to approach one. When the substrate temperature is raised, the period for which physically adsorbed molecules linger on the surface decreases so that the formation of a chemisorbed layer increasingly depends on the oil molecules striking the surface by their polar terminals.

It is fortuitous that chemisorbed oil films do not readily form on "aged" glass surfaces, but they can form on "aged" glass during baking in vacuum. It is current practice to glow-discharge clean glass before baking, but it has been shown here that the hardest zinc sulphide films are produced on surfaces which are first baked and then glow-discharge cleaned.

References

- (1) HOLLAND, L. *Brit. J. Appl. Phys.*, **9**, p. 410 (1958).
- (2) MELLOR, J. W. *A Comprehensive Treatise on Inorganic and Theoretical Chemistry*, Vol. 4, p. 594 (London: Longmans, Green and Co., 1923).
- (3) HUNTRESS, A. R., SMITH, A. L., POWER, B. D., and DENNIS, N. T. M. *Symposium on Vacuum Technology*, p. 104 (London: Pergamon Press, 1957).

Explanation of the enhanced arc velocity on magnetic electrodes

by P. E. SECKER, B.Sc., Ph.D., Queen Mary College, University of London, London, E.1

Paper first received 7 March, and in final form 9 May, 1960]

Abstract

When an arc moves between parallel horizontal metal electrodes, under the influence of the transverse magnetic field set up by current flow in the electrodes, the velocity/current characteristic is found to depend on the cathode material. The characteristics may be separated into two groups, one comprising the magnetic and the other the non-magnetic materials. Calculations indicate that the enhanced velocity of the former group is due to a high-frequency skin effect near the rapidly moving cathode spot, such that the current paths are forced to the outer regions of the electrode, so increasing the

transverse magnetic flux density in the critical region just outside the cathode.

Introduction

WHEN an arc is established between parallel metal electrodes and fed with current at one end only of these, movement of the arc will be induced by the self-magnetic field of the current in the electrodes. At atmospheric pressure the movement is in the Amperian

direction and the velocity is found to be dependent on the arc current, the electrode material and its surface condition, and to a lesser extent, on the electrode spacing.

Guile and Mehta,⁽¹⁾ using an electrode system of two parallel cylindrical rods mounted horizontally with one vertically above the other, and with a current feed to the electrodes at one end only, measured the arc velocity as a function of current. They found that the arc velocity increased with current and was dependent on the nature of the electrode materials. The characteristics could be separated into two groups according to whether the material was magnetic or non-magnetic. Representative curves for mild steel and extruded brass are reproduced in Fig. 1. It is the aim of this paper to show that the greater velocity on the

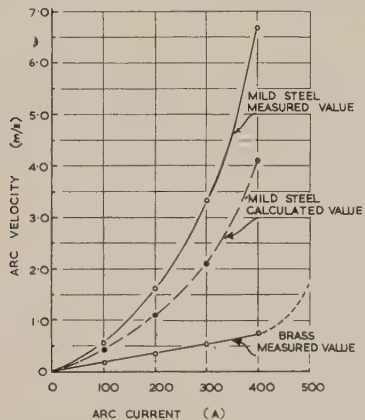


Fig. 1. Arc velocity as a function of current for typical magnetic and non-magnetic electrodes. Inter-electrode spacing 3.2 cm, electrode diameter 9.5 mm

— = experimental curves
 - - - - - = extrapolation of experimental curve to region of high scatter
 - - - - - = calculated curve for mild steel

magnetic steel electrode may be accounted for by the increased transverse magnetic field set up by a skin effect at the rapidly-moving cathode spot.

From the work of Guile, Lewis and Mehta⁽²⁾ and from experiments described elsewhere,⁽³⁾ it is known that the regular movement of the arc depends on the behaviour of the cathode spot, and that the arc velocity is directly proportional to the transverse magnetic flux density in the cathode fall region and independent of the magnitude of the arc current, provided the latter exceeds approximately 40 A.

In the arrangement which yielded the results shown in Fig. 1, the transverse magnetic field in the cathode fall just outside the electrode was provided solely by the current in the electrodes. The self-field set up by the current in the arc itself exerted only a "pinch" force to constrict the arc diameter, but could not effect movement of the arc column or cathode spot.

Skin effects due to arc root movement

The cathode spot is made up of a number of emitting regions or sites, and the movement of each is thought to occur by a series of small but discrete jumps.⁽⁴⁾ An existing site is believed to become gradually less efficient as an emitter, and a new site forward of the arc is simultaneously conditioned to take over the main arc current. Smith⁽⁵⁾ has suggested that, since the current paths to consecutive emitting sites must change very rapidly within the electrodes, a skin

effect should be present near the cathode spot. It was thought that this skin effect, which would be more noticeable in magnetic electrodes, might be the factor causing the increased velocity found with these electrodes.

It is possible to derive a formula relating the "skin depth" to the properties of the conducting medium and the rate of change of current at the cathode spot.

$$\text{Skin depth } \Delta = 5033 \sqrt{(\rho/\mu f)} \quad (1)$$

where ρ is the resistivity in ohm-centimetres, μ is the relative permeability and f is the effective skin frequency. In this case it is somewhat difficult to assign values to f , since it is a measure of the rate at which current paths in the cathode near the emitting spot are changing. An increase in the arc velocity V would be expected to increase the frequency, and a reduction of the skin depth should have a similar effect, as the current paths would then be restricted to a thinner outer conducting shell in the electrode, so that a given movement of the cathode spot would result in greater disturbance of the current paths. Thus the period in which the arc moves a distance comparable with the skin depth may be adopted as a criterion for the effective frequency, i.e. $f = V/\Delta$. Substituting for f in equation (1) and solving for Δ yields:

$$\Delta = (5033)^2 (\rho/\mu V) \quad (2)$$

In calculating the depth of the conducting shell, values of ρ were taken as 6.2×10^{-6} and $10^{-5} \Omega \text{ cm}$ for the extruded brass (55% copper, 43.5% zinc and 0.37% lead) and mild steel respectively. The value of μ for brass was taken as 1, but for the mild steel it was not reasonable to assign a single value to the relative permeability, as at the higher currents employed the magnetic flux density inside the electrodes would have approached the saturation level.

In order to estimate the value of μ corresponding to each current value, it was necessary to calculate the approximate value of magnetic field strength corresponding to each value of arc velocity on mild steel. It was assumed that the greater arc velocity on the mild steel, as compared with brass, was due to an increased transverse magnetic flux density outside the cathode of the former. The transverse magnetic field strength outside the brass cathode could easily be evaluated for any value of current, assuming a uniform current distribution in the electrode. The magnetic field strength outside the mild steel cathode was then taken to be equal to that outside the brass electrode, increased by the ratio of the velocities on steel and brass for that particular current. Thus the value of H at the surface of the steel electrode corresponding to each value of arc current could be found, and from published data for the steel in question, this yielded the equivalent steady-state value of μ . However, for any particular element of the electrode, the magnetic field increases rapidly from zero to a maximum as the cathode spot passes over it, and then decreases to a much lower value corresponding to the steady-state flow of current at points distant from the moving cathode spot. A mean value of μ , therefore, has to be used in each case and the latter was found from the appropriate $\mu - H$ graph. For a given peak value of field strength H_p , the mean value of μ was taken as $\left(\int_0^{H_p} \mu dH \right) / H_p$, although it is possible that a value of μ weighted more in favour of the higher values of H would have been more appropriate. Table 1 shows the skin depth for both brass and steel, together with the calculated values of μ for the latter.

Table 1. Skin depth as a function of arc current

Arc current (A)	Brass		Mild steel		Skin depth (mm)
	Velocity (m/s)	Skin depth (mm)	Velocity (m/s)	Mean μ	
100	0.174	90.4	0.55	500	0.0922
200	0.329	47.8	1.63	252	0.0619
300	0.517	34.5	3.33	159	0.0478
400	0.790	19.9	6.66	105	0.0361

To estimate the increase of transverse magnetic field at the cathode spot due to the skin effect in the steel, it is first necessary to calculate the flow pattern of the current in the conducting outer shell of the electrode near the cathode spot. If second-order interaction effects between different current flow lines are neglected and the skin depth is small, then the flow pattern in the conducting cylindrical shell [Fig. 2(a)] will be the same as that in the conducting sheet of Fig. 2(b), where the cylinder has been cut along the line of symmetry.

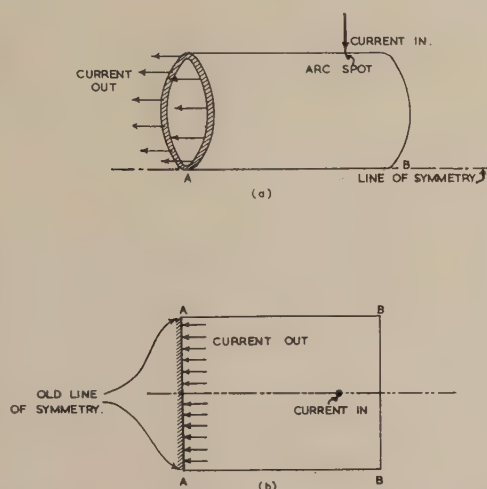


Fig. 2. (a) Current flow path in electrode near cathode spot due to skin effect

(b) Conducting sheet representing current flow conditions in cathode near arc spot

As the current flow paths are altering only in the immediate vicinity of the cathode spot, the skin effect will only be operative in this same region, and hence the model flow pattern defined by Fig. 2(b) will have certain limits. In experiments carried out by Guile,⁽⁶⁾ photomicrographs of the cathode arc track showed that the distance between adjacent emitting sites was approximately 0.10 cm. This distance has been taken to be approximately valid for the data shown in Fig. 1 and it has been assumed, somewhat arbitrarily, that the skin effect extends back from the cathode spot a distance equal to 1.5 times the distance between adjacent emitting sites. (In fact, the skin effect can only extend back from the cathode spot for a very limited distance, and it is seen from Fig. 3 that the main changes in the current paths occur near the cathode itself, not near the boundary of the influence of the skin effect. The factor of 1.5 was chosen for convenience in calculation.) This defines the end boundary of the cylindrical shell {giving also the end boundary conditions of the conducting sheet [Fig. 2(b)]} which is assumed to be an equipotential, an assumption which will be approximately satisfied in most cases. Using a relaxation method it is possible to plot the current flow in the conducting sheet. Fig. 3 shows half the flow pattern, which must be symmetrical about the centre axis. It will be noted that the current is mainly restricted to that half of the conducting sheet near

the line of symmetry passing through the arc spot. Utilizing the rather gross simplification that, in fact, the current flows uniformly down a semi-cylindrical shell [i.e. the top half of the cylinder in Fig. 2(a)] until it reaches the plane of the arc spot, where the flow lines turn through 90° and follow the

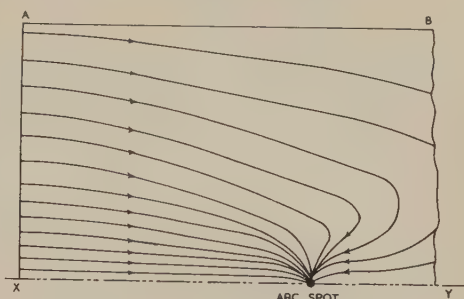


Fig. 3. Current flow pattern for one-half of the conducting sheet

cylinder surface until they terminate in the arc spot, it is possible to evaluate the transverse magnetic field at the cathode spot. Details of this calculation are given in the Appendix, and the values of the field strength are shown in Table 2. In addition to the "skin effect" magnetic field, there

Table 2. Total magnetic flux density at cathode spot

Arc current (A)	Brass		Mild steel		Total (Wb/m ²)	Ratio of flux density, mild steel-brass
	Normal component and total (Wb/m ²)	Flux density (Wb/m ²) Normal component (Wb/m ²)	Flux density (Wb/m ²) Skin component (Wb/m ²)	Flux density (Wb/m ²) Skin component (Wb/m ²)		
100	0.00238	0.00146	0.00470	0.00616	2.59	
200	0.00476	0.00292	0.01330	0.01625	3.41	
300	0.00714	0.00438	0.02514	0.02952	4.14	
400	0.00914	0.00584	0.04324	0.04908	5.38	

will be a transverse magnetic field due to the normal uniform current flow along the electrodes from the input leads to the shell boundary. For the electrode configuration from which the results shown in Fig. 1 were obtained, this steady-state field gives a magnetic flux density just outside the cathode of 0.0146×10^{-4} Wb/m². The total magnetic flux density for any particular arc current is then the sum of these two components as shown in Table 2.

The last column in Table 2 gives the ratio of the transverse fields at the cathode root for brass and steel electrodes with the same arc current in each case. Thus from the values of velocity for the brass electrodes, the velocities for mild steel can be predicted as in Fig. 1. It will be seen that although the magnitudes of the predicted and measured velocities differ, the characteristic shape of the velocity/current plot for mild steel is, in fact, exhibited in the theoretical curve. It must be remembered that no account has been taken of the effect on arc velocity of the differences due to other properties such as boiling point, thermal conductivity, surface condition, etc. Further, the assumption that the current flowed uniformly in a semi-cylindrical shell would give a magnetic field strength at the cathode considerably less than that actually produced by the tightly bunched flow-lines near the cathode spot.

Conclusions

From the comparison of the measured and calculated arc velocities on mild steel electrodes, it would seem reasonable to infer that the enhanced velocity observed on these

electrodes fed with current from one end is largely due to a skin effect. This effect may also be invoked to explain the rapid increase in arc velocity for brass, Dural and aluminium, noted by Guile and Mehta⁽¹⁾ at high currents. Until a certain critical velocity is attained, the skin depth is so great that there is no appreciable distortion of the current flow pattern in the cathode electrode. At the critical velocity, however, the reduced skin depth perturbs the current flow pattern and thus causes an increase in the transverse magnetic field just outside the cathode. This in turn increases the arc velocity so further enhancing the skin effect. Such a mechanism would be expected to give rise to a discontinuity in the velocity/current characteristic of the type actually observed for many non-magnetic materials, although it would be necessary to adopt a different criterion for the effective skin frequency to that used here, as this latter leads one to expect a complete absence of a skin effect in non-magnetic materials (see Table 1). On steel, however, even for very low currents, the velocity is well above the threshold value.

Acknowledgements

The author wishes to thank Prof. M. W. Humphrey Davies for his encouragement, Dr. T. J. Lewis for his advice and constructive criticism during the preparation of this paper, and Dr. C. G. Smith for making the original suggestion which prompted these calculations. This work was carried out during the tenure of a D.S.I.R. maintenance allowance, and the recent award of an I.M.E.A. Scholarship by the Institution of Electrical Engineers is gratefully acknowledged.

References

- (1) GUILLE, A. E., and MEHTA, S. F. *Proc. Instn Elect. Engrs*, **104** A, p. 533 (1957).
- (2) GUILLE, A. E., LEWIS, T. J., and MEHTA, S. F. *Brit. J. Appl. Phys.*, **8**, p. 444 (1957).
- (3) SECKER, P. E., and GUILLE, A. E. *Proc. Instn Elect. Engrs*, **106** A, p. 311 (1959).
- (4) LEWIS, T. J., and SECKER, P. E. *Nature (London)*, **186**, p. 30 (1960).
- (5) SMITH, C. G. Private communication.
- (6) GUILLE, A. E. *E.R.A. Tech. Report*, O/T19 (Leatherhead: Electrical Research Association, 1956).

Appendix

Calculation of magnetic field due to current flowing in a cylindrical half-shell

To simplify calculations it will be assumed that the current flows entirely in an infinitesimally thin sheet midway between the two boundary walls of the shell caused by skin effect, i.e. $\Delta/2$ from each edge (see Fig. 4). Consider an element of

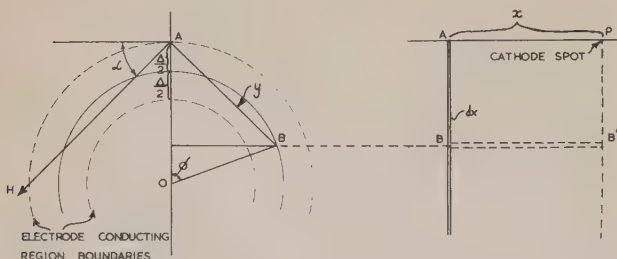


Fig. 4. End and side view of conducting half-shell

the shell distance x from the arc spot. At atmospheric pressure the cathode fall distance is approximately 10^{-5} cm and hence may be neglected in comparison with the shell thickness. It is required to evaluate the magnetic field at the point P (cathode spot) on the shell surface. Suppose a current i is flowing through a point such as B on the shell element. Let the line BP have length r , and let BP make an angle θ with AP .

Transverse field at P , due to current at B flowing distance x towards P , equals

$$dH = (idx \sin \theta / 4\pi r^2) \cos \alpha \quad (3)$$

Putting $r = y \operatorname{cosec} \theta$ and $x = y \cot \theta$ (Fig. 4), then

$$dH = i \sin \theta \cos \alpha d\theta / 4\pi y \quad (4)$$

If j is the average current density in the shell, then

$$i = jsd\phi \Delta \quad (5)$$

and if I is the total current,

$$j = I / \pi S \Delta \quad (6)$$

$$i = Id\phi / \pi \quad (7)$$

and

$$dH = I \sin \theta \cos \alpha d\theta d\phi / \pi 4\pi y \quad (8)$$

It is now necessary to obtain $\cos \alpha$ in terms of ϕ . From Fig. 4 it can be seen that $\cos \alpha = AD/AB = AD/y$ and since

$$AD = AO - OD = OF + AF - OD = s + \frac{1}{2}\Delta - s \cos \phi$$

then

$$dH = I \sin \theta AD d\theta d\phi / \pi 4\pi y^2 \quad (9)$$

Now

$$y^2 = AD^2 + BD^2 = 2s^2 + \frac{1}{4}\Delta^2 + s\Delta - 2s(s + \frac{1}{2}\Delta) \cos \phi \quad (10)$$

Integration along a current element from B to B' will give the field at P due to the current $Id\phi/\pi$ acting along the line BB' i.e.

$$H_{BB'} = (IADd\phi / 4\pi y^2) (\cos \theta)_{\theta=\pi/2}^{\theta=\max} \quad (11)$$

where $\theta_{\max} = \cos^{-1}(x/r) = \cos^{-1}\{x/\sqrt{(x^2 + y^2)}\}$.

The net magnetic field at P is thus obtained by summing all the components similar to $H_{BB'}$.

Total transverse magnetic flux density at

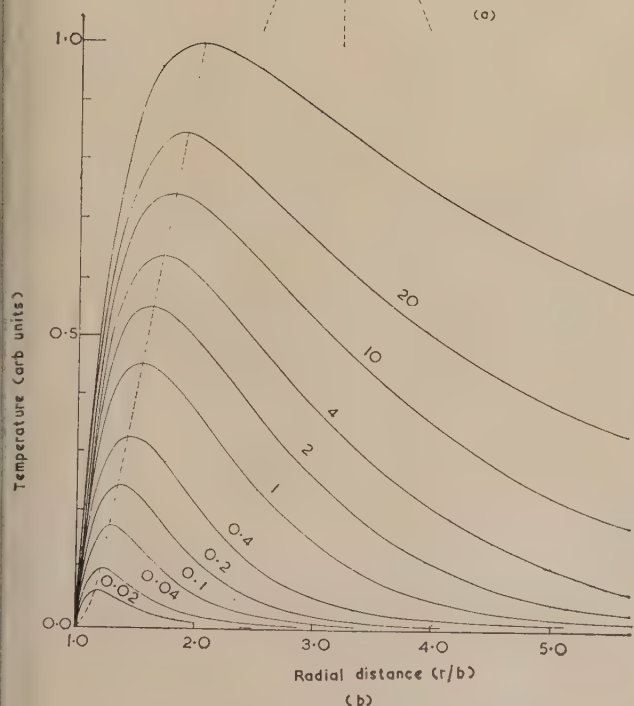
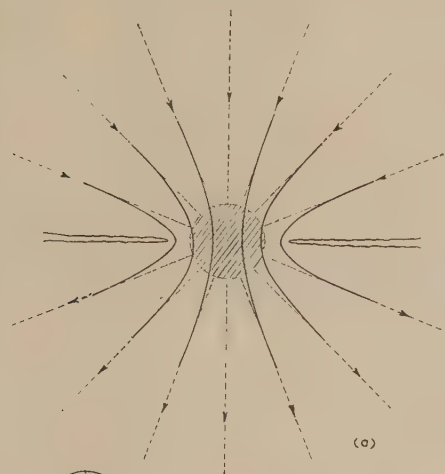
$$\begin{aligned} P &= 4\pi \times 10^{-7} \frac{I}{4\pi} 2 \sum_{\phi=-\pi/2}^{\phi=\pi/2} \frac{AD x}{y^2 \sqrt{(x^2 + y^2)}} \text{ Wb/m}^2 \\ &= \frac{I \times 10^{-7}}{\pi} 2 \sum_{\phi=0}^{\phi=\pi/2} \frac{\left(s + \frac{\Delta}{2} - s \cos \phi\right) x}{\left(2s^2 + \frac{\Delta^2}{4} + s\Delta\right) - s(2s + \Delta \cos \phi)} d\phi \\ &\quad \frac{1}{\sqrt{\left\{x^2 + 2s^2 + \frac{\Delta^2}{4} + s\Delta - s(s + \Delta \cos \phi)\right\}}} \text{ Wb/m}^2 \quad (12) \end{aligned}$$

This expression has been evaluated by approximate integration techniques for the different values of Δ and s given by Table 1, and the evaluated flux densities are shown in Table 2.

Thermal transients in graphite-copper contacts

We should like to comment on two points in the recent article under the above title by Dr. W. Davies (10, p. 516, 1959).

(1) There seems to be some confusion between the equations $\nabla^2\psi = 0$ and $\nabla^2\psi + k\psi = 0$. The solutions of the second equation are, of course, solutions of the first only in the



Temperature growth in a graphite/copper contact

(a) The real geometry and the lines of flow are shown as bold lines, and the geometry and lines of flow in the model considered are shown as faint and dashed lines. (b) The numbers against the curves are the values of kt/b^2 , where k is the thermal diffusivity, and b the radius of the sphere. The unlabelled curve is the equilibrium distribution

trivial case when $k = 0$, which in the present context means an equilibrium. Consequently the author's conclusion that equipotentials are isotherms is also true only in equilibrium. That it is so then is well known, even without the author's

restriction that the thermal and electrical conductivities are constant (Kohlrausch 1900⁽¹⁾ and many later workers, e.g. Greenwood and Williamson⁽²⁾). But it is certainly not true in general under transient conditions. Consider, for example, a circular contact between two similar semi-infinite solids [see Fig. (a)]. The current through the contact is well known to be distributed in the same way as the electrostatic charge on a disk, i.e. it is concentrated round the periphery of the contact area. Accordingly the rate of heat production is very large on the periphery, and at the beginning of the heating, the temperature will be greatest there. Thus the contact area, although by symmetry an equipotential, is certainly not an isotherm (see Greenwood and Williamson⁽²⁾).

There are, of course, simple cases where it is true that equipotentials are isotherms even in transient conditions. This must clearly hold in problems with a single space variable, for if this variable is r , then the surfaces $r = \text{const.}$ are both equipotentials and isotherms. The cases considered in detail by Dr. Davies are all of this type.

(2) In his discussion of the temperature growth in a graphite contact, the author claims that the position of the warmest section is independent of time. This clearly cannot be true. In the model considered, the maximum temperature under equilibrium conditions occurs at $r = 2b$ but since the rate of heat production is greatest near the graphite/copper interface, then initially the greatest temperature must be close to this interface.

We are at present engaged in a study of the transient temperature changes which occur in the region of contact between similar and dissimilar metals, and were fortunate in having available a programme for a digital computer which could easily be modified to calculate the temperature distribution in the case considered by Dr. Davies. The figure shows the initial growth of the temperature profile. It can be seen, for example, that when the maximum temperature is a quarter of the final maximum temperature it is located at the section $r = 1.4b$: at that instant the section $r = 2b$ has reached only one-eighth of the final maximum temperature.

This means that the author's conclusions regarding the temperature of sliding contacts must be modified. For the case when the final maximum temperature is 500°C , at the instant $kt = 0.33$ the section $r = 2b$ will have reached 50°C as quoted, but the greatest temperature at that time will in fact be 100°C at $r = 1.3b$.

Tube Investments Research
Laboratories,
Cambridge.

J. A. GREENWOOD
J. B. P. WILLIAMSON
[10 March, 1960]

REFERENCES

- (1) KOHLRAUSCH, F. *Ann. Phys. Leipzig*, **1**, p. 132 (1900).
- (2) GREENWOOD, J. A., and WILLIAMSON, J. B. P. *Proc. Roy. Soc. A*, **246**, p. 1 (1958).

I agree entirely with the remarks made by Greenwood and Williamson in their letter and I am most grateful to them for pointing out my errors. I can only apologize for, and I certainly have no excuse for making such an elementary error as to assume that in the general case the solution of $\nabla^2\psi + k\psi = 0$, is the same as that of $\nabla^2\psi = 0$ —it is not so,

of course, as they point out, except for thermal equilibrium. This means that in the general case equipotential surfaces are not isothermal surfaces except in thermal equilibrium; however, I reduced my problem to one involving only one space variable, and clearly in such a case the electrical potential and the temperature are functions of r and t only and the equipotential surfaces *are* isothermals even under transient conditions and my analysis is valid.

As for their second point, which concerns the location of the region of maximum temperature for finite values of t , I can only apologize again for making a rash conclusion. Actually the drift of the region of maximum temperature from the vicinity of $r = b$ to the final position $r = 2b$, is fairly obvious from an examination of my expression for the temperature θ , equation (9), p. 519. It is readily seen that under steady state conditions the region of maximum temperature is that of $r = 2b$, that is to say

$$(\partial\theta/\partial r)_{r=2b} = 0 \text{ when } t \rightarrow \infty$$

For finite values of t , however, $(\partial\theta/\partial r)_{r=2b}$ is not zero, in fact it has a negative value which decreases in magnitude as t increases. This indicates quite clearly that the region of maximum temperature lies at any instant somewhere between $r = b$, and $r = 2b$, and that it is gradually drifting towards the region $r = 2b$. Thus the warmest section to which I referred on p. 519 is in fact that section which is hottest ultimately.

University College of South
Wales and Monmouthshire,
University College,
Cardiff.

W. DAVIES
[26 March, 1960]

Measurement of coupling coefficient and Q of low- Q piezoelectric ceramics

A piezoelectric element may be represented⁽¹⁾ by the equivalent circuit shown in Fig. 1(a). If the parameters C_0 , R , C and L are known, the coupling coefficient and motional quality factor Q may be calculated:

$$k^2 = \frac{C}{C_0 + C}, \quad (1)$$

$$Q = \frac{1}{R} \sqrt{\left(\frac{L}{C}\right)}. \quad (2)$$

C_0 is the capacitance of the disk at frequencies well removed from resonance, and is easily measured. The values of R , C and L must, however, be calculated from the frequency dependence of the equivalent shunt capacitance C_ω and resistance R_ω , or impedance.

The values of k and Q are normally obtained⁽²⁻⁴⁾ from the frequencies and impedances at resonance and anti-resonance, by means of approximate relationships. These approximations hold good when the materials have a high Q , such as possessed by barium titanate and lead zirconate titanate, but become inaccurate for values of Q much less than 100. More exact equations have been developed⁽⁵⁾ for low- Q materials, but these still require measurements at both resonance and anti-resonance. It has been shown⁽²⁾ that when the figure of merit, defined as the quotient of the motional quality factor Q and the capacitance ratio C_0/C , falls below 2, a piezoelectric element exhibits no anti-resonance, so that the existing methods cannot be used. Ceramics with a low motional Q are required for use in

pulse transducers. A new method, based only on the resonance and involving no approximations, has therefore been developed.

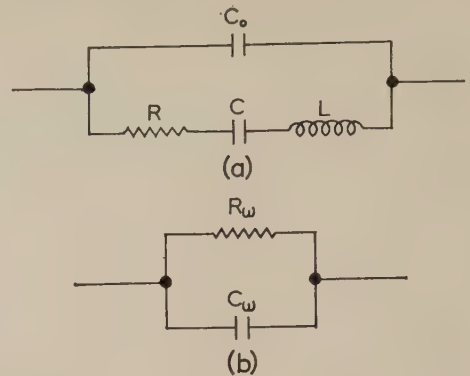


Fig. 1. Diagrams of (a) the equivalent circuit of a piezoelectric element, and (b) parameters as measured

Equating the real and imaginary parts of the admittances of the circuits shown in Figs. 1(a) and (b) we have:

$$Y'_\omega = \frac{1}{R_\omega} = \frac{R}{R^2 + \left(\omega L - \frac{1}{\omega C}\right)^2}, \quad (3)$$

and:

$$Y'_\omega = \omega C_\omega = \omega C_0 - \frac{\left(\omega L - \frac{1}{\omega C}\right)}{R^2 + \left(\omega L - \frac{1}{\omega C}\right)^2}. \quad (4)$$

At resonance, where $\omega_0 = 1/\sqrt{LC}$, equations (3) and (4) give respectively:

$$R_{\omega_0} = R; \quad C_{\omega_0} = C_0 \quad (5)$$

Rewriting equation (4) and substituting for R from equation (5), we have:

$$C_\omega = C_0 - \frac{C\left(\frac{\omega^2}{\omega_0^2} - 1\right)}{\left\{\frac{\omega^2}{\omega_0^2 Q^2} + \left(\frac{\omega^2}{\omega_0^2} - 1\right)\right\}}, \quad (6)$$

since $R\omega_0 C$ is equal to $1/Q$.

Differentiating equation (6) with respect to ω and equating the resulting expression to zero, we obtain a quadratic in ω^2 :

$$Q^2 \omega^4 - 2\omega_0^2 Q^2 \omega^2 + (Q^2 - 1)\omega_0^4 = 0, \quad (7)$$

with roots:

$$\omega^2 = \omega_0^2 (1 \pm 1/Q). \quad (8)$$

Thus, when C_ω is maximum and minimum, we have:

$$\omega_{\max}^2 = \omega_0^2 (1 - 1/Q), \quad (9a)$$

and:

$$\omega_{\min}^2 = \omega_0^2 (1 + 1/Q). \quad (9b)$$

Thus:

$$Q = \frac{\omega_{\min}^2 + \omega_{\max}^2}{\omega_{\min}^2 - \omega_{\max}^2}, \quad (10)$$

while from equation (2):

$$C = \frac{1}{R\omega_0 Q} \quad (11)$$

Thus equations (10) and (11) may be used to obtain the values of Q and series capacitance C from the frequencies at which C_ω is maximum and minimum, and the value of R_ω at resonance. The values obtained are exact, while the accuracy improves as Q falls, since the difference $(\omega_{\min}^2 - \omega_{\max}^2)$ becomes larger and can be measured more accurately.

Fig. 2 shows an example of the resonance curves obtained from a lead-niobate ceramic disk vibrating in thickness mode.

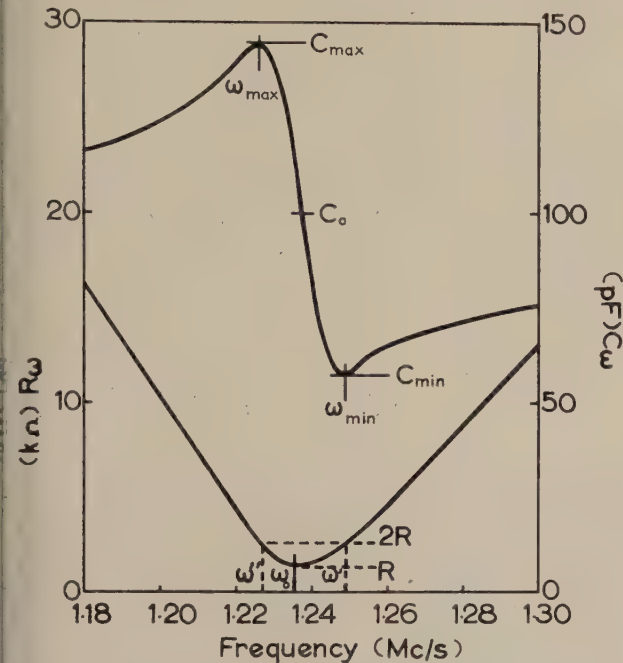


Fig. 2. Resonance curves of lead niobate disk vibrating in thickness mode.

This has a motional Q of 56 and coupling coefficient k_{33} of 0.13, giving a figure of merit of 0.95. The measurements were made with a transformer-coupled h.f. bridge (by Wayne-Kerr, type B601) together with a r.f. signal generator as source and Communications Receiver R1155 as detector.

An alternative method due to Farren⁽⁶⁾ may be used to determine Q when the piezoelectric activity is low and the maxima and minima of C are ill-defined. This is based purely on the R_ω curve, and is also exact.

Let the frequencies at which R_ω is equal to $2R$ be ω' and ω'' . Substituting $R_\omega = 2R$ in equation (3), we obtain a quadratic in ω^2 :

$$\omega^4 L^2 C^2 - \omega^2 (2LC + R^2 C^2) + 1 = 0. \quad (12)$$

Now:

$$(\omega' - \omega'')^2 = (\omega'^2 + \omega''^2) - 2\omega'\omega'' \quad (13)$$

so that:

$$(\omega' - \omega'')^2 = \frac{2L + R^2 C}{L^2 C} - \frac{2}{L^2 C^2} = \frac{R^2}{L^2} \quad (14)$$

Therefore:

$$Q = \frac{\omega_0 L}{R} = \frac{\omega_0}{\omega' - \omega''} \quad (15)$$

Employing this method on the example given in Fig. 2, we obtain a Q of 52, in good agreement with the first method.

While modified lead-niobate ceramics may have values of motional Q and coupling coefficient considerably in excess of these figures, such materials have figures of merit well in excess of 2, and conventional methods may be employed. Under certain circumstances C_{\min} may become negative, in which case a mica capacitor is placed in parallel with the element to keep the total C' positive.

The thickness mode resonance curves are sometimes complicated by spurious resonances,⁽⁷⁾ although this effect is least serious with low- Q ceramics. In these cases, the true-thickness mode curves may usually be sketched in to obtain both ω_{\max} and ω_{\min} with sufficient accuracy. Alternatively measurements may be confined to the radial mode.

REFERENCES

- (1) VAN DYKE, K. S. *Proc. Inst. Radio Engrs*, **16**, p. 742 (1928).
- (2) MASON, W. P., and FAIR, I. E. *Proc. Inst. Radio Engrs*, **30**, p. 464 (1942).
- (3) BURSTEIN, E. *Rev. Sci. Instrum.*, **18**, p. 317 (1947).
- (4) MASON, W. P., and JAFFE, H. *Proc. Inst. Radio Engrs*, **42**, p. 921 (1954).
- (5) MARTIN, G. E. *J. Acoust. Soc. Amer.*, **26**, p. 413 (1954).
- (6) FARREN, L. I. Private Communication from the Research Laboratories of the General Electric Co.
- (7) SHAW, E. *J. Acoust. Soc. Amer.*, **28**, p. 38 (1956).

G.V. Planer Ltd.,
Sunbury-on-Thames,
Middlesex.

R. M. GLAISTER
[10 May, 1960]

Notes and comments

The amalgamation of The Institute of Physics and The Physical Society

The incorporation of a new body on 17 May, 1960, under the name of "The Institute of Physics and The Physical Society" marks the fulfilment of the desire expressed by the overwhelming majority of the members of the Institute and Society that the "necessary action" should be taken to implement the scheme for amalgamation prepared by a Joint Committee. The originating bodies have now been formally wound up and their assets handed over to the new one.

The first President of the amalgamated body is Sir John Cockcroft and the four Vice-Presidents are Dr. J. Topping, Dr. W. H. Taylor, Professor R. W. Ditchburn and Mr. A. J. Philpot, each responsible to the Council for a defined area of the many activities taken over by the new organization from its predecessors. The Presidents of the predecessors (Sir George Thomson and Mr. J. A. Ratcliffe) are also members of the new Council. The other Officers are Dr. J. Taylor (Honorary Treasurer) and Dr. C. G. Wynne (Honorary Secretary).

The Physical Society of London, as it was then called, was founded in 1874 and on the initiative of that Society's Council The Institute of Physics was founded 45 years later. The original scheme envisaged a kind of federation of societies interested in physics, to provide among other objects, rooms for meetings, a library, and a common secretariat. In fact, the Institute's offices were in the Society's present rooms in South Kensington from 1927 to 1949 and the Institute provided the secretariat for The Physical Society and The Optical Society which themselves amalgamated in 1931.

At the time of its establishment no one could have foreseen the spectacular growth and influence of physics in the modern world. Broadly speaking, before the war the scientific meetings and publications of the Institute were confined to applied physics while those of the Society were concerned more with pure physics. As, however, the boundary between these two aspects became less definite there has been increasing overlap in the activities of the two bodies and in their membership. It is not, therefore, surprising that during the past 20 years proposals for the amalgamation of the two bodies have been made repeatedly and from time to time detailed proposals examined, until eventually a satisfactory solution was worked out.

The qualification for the award of Fellow of The Institute of Physics, Associate of The Institute of Physics, and Graduate of The Institute of Physics will remain unchanged and members of the new body holding these diplomas will also be Fellows of The Physical Society. Besides the three Institute of Physics' grades of membership of the new body

there will also be the grade to be known as "Fellow of The Physical Society". All the Fellows of the old Society will be automatically transferred to this new grade, but new candidates for election to the grade will be required to possess a degree or diploma in physics recognized by the Council, or to satisfy the Council that they have a sufficient knowledge of physics.

Provision has been made for other scientists and engineers to participate in the scientific and educational work of the new body. Activities relating to the practice of the profession as such, will be strictly confined to those possessing one of the Institute's diplomas.

The executive Officers of the new body are *Secretary*: Dr. H. R. Lang; *Editor and Deputy Secretary*: Dr. A. C. Stickland; and *Deputy Secretary*: Mr. N. Clarke. The registered offices and headquarters are at 47 Belgrave Square, London, S.W.1, and for the present, offices will also be retained at 1 Lowther Gardens, South Kensington, London, S.W.7.

Journal of Scientific Instruments

Contents of the August issue

PAPERS

- Tomograph for industrial radiography. By D. Charles.
A 450J spark discharge for shadowgraph photography. By L. Whitlow.
Moiré fringe reading head for use with a fine grating. By D. A. Palmer.
Production of islands and dice in semi-conductor slices with an ultrasonic drill. By R. D. Knight.
Single tube sedimentation apparatus for the measurement of particle size distribution. By J. Kobak and D. J. Loveridge.
Multipoint digital temperature recorder with punched tape output. By T. S. Holden.
High vacuum high temperature X-ray camera. By B. A. Hatt, P. J. C. Kenton and G. I. Williams.
Sensitive and simple integrator. By J. P. Funk.
Accurate measurements of phase differences with the Babinet compensator. P. Hariharan and D. Sen.
Some modifications to an oscilloscope camera, and the construction of a control unit. M. H. Evans and G. Pierson.
Temperature regulator for close temperature control. By E. N. Herzberg.
Time analyser using a crystal-controlled trochotron tube. By T. Dobrowolski and J. Walker.
The torsionmeter—an instrument for the study of gels considered as elastic solid. By W. A. Southorn.
Portable electrometer voltmeter. By W. E. K. Gibbs.
Novel displacement detector and its application in a recording thermobalance. By J. C. Van Der Breggen and H. J. Wouterlood.
Ratiometer phase angle indicator. By K. L. Morphey.

LABORATORY AND WORKSHOP NOTES

- Transistor operation of electromechanical registers. By J. C. Barton.
Cut-off for the vacuum manipulation of chlorine. By M. Green and K. H. Maxwell.
Test tube adaptor for use in optical density measurements. By J. B. Dawson.
Simple high temperature X-ray camera. By G. Farrow and D. Preston.
Stabilized high-intensity light source. By C. M. Hurd.
Simple detector for small leaks using a thoriated tungsten emitter with oxygen as probe gas. R. N. Bloomer and W. C. Brook.

CORRESPONDENCE

- Foam viscometer. From R. J. French.

NOTES AND NEWS

- New instruments, material and tools Notes and comments

THIS JOURNAL is produced monthly by The Institute of Physics and the Physical Society, in London. It deals with all branches of applied physics (including theory and technique). All rights reserved. Responsibility for the statements contained herein attaches only to the writers.
EDITORIAL MATTER. Communications concerning editorial matter should be addressed to the Editor, The Institute of Physics and The Physical Society, 47 Belgrave Square, London, S.W.1. (Telephone: Belgravia 6111.) Prospective authors are invited to prepare their scripts in accordance with the *Notes for Authors*. (Price 3s. 6d. including postage.)

REPRODUCTION. The Institute of Physics and The Physical Society is a signatory to The Royal Society's Fair Copying Declaration. Details may be obtained upon application from The Royal Society, London, W.1.

ADVERTISEMENTS. Communications concerning advertisements should be addressed to the agents, Messrs. George Jackson (Fleet St.) Ltd., Cliffords Inn, Fleet Street, London, E.C.4. (Telephone: Holborn 3611-2.)

CLAIMS FOR MISSING JOURNALS. Claims from regular subscribers to this *Journal* for missing numbers will only be considered if received within 60 days of the date of mailing plus normal outward time of transit and time for lodging the claim. Losses attributable to failure to notify a change of address or to similar omissions will not be considered.

SUBSCRIPTION RATES. A new volume commences each January. The charge is £6 per volume (\$17 U.S.A.), including index (post paid), payable in advance. Single parts, so far as available, may be purchased at 12s. 6d. each (\$1.75 U.S.A.), post paid, cash with order. Orders should be sent to The Institute of Physics and The Physical Society, 47 Belgrave Square, London, S.W.1, or to any bookseller.

Summarized proceedings of a conference on X-ray analysis London, November 1959

The Autumn Conference of the X-ray Analysis Group of The Institute of Physics was held at The Institution of Civil Engineers, London, on 13 and 14 November, 1959. The topics under discussion were "Structure analysis" and "Apparatus and experimental techniques".

First and second sessions: Structure analysis

DR. C. W. BUNN (Imperial Chemical Industries Ltd., Plastics Division, Welwyn Garden City) opened the Conference and took the Chair for the first session. Dr. C. A. BEEVERS and Dr. H. W. EHRLICH (University of Edinburgh) discussed the interpretation of the Patterson synthesis for organic crystal structures in which all atoms are of approximately equal weight. Here the Patterson function is not dominated by heavy-atom vectors and so the highest peaks correspond to coincidences of vectors. These coincidences may be exact, giving sharp peaks, as in molecules containing symmetrical groups of atoms such as zigzag chains or regular rings, or they may be imperfect, giving diffuse peaks, where the symmetrical groups are distorted or slightly misaligned. Using as an example the planar molecule 2:13-benzfluoranthene (Fig. 1), the authors

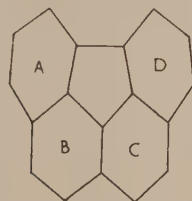


Fig. 1. Planar molecule 2 : 13-benzfluoranthene

showed how a study of the disposition of sharp and diffuse peaks due to vectors between rings could enable the molecular orientation and position to be deduced. In this molecule there are (i) three naphthalene nuclei AB, BC and CD which give sharp six-fold vectors, (ii) pairs of rings A and C, B and D which are slightly misaligned and give diffuse peaks, and (iii) the pairs A and D, considerably out of alignment, giving a very diffuse peak. All these peaks could be identified in the Patterson synthesis. The position of the molecule was found by considering the sharp and diffuse peaks corresponding to vectors between two centrosymmetrically related molecules.

This approach can be extended to five- and seven-membered rings: pyrazole and glucurone containing planar pentagons are structures which were solved entirely by this method. Dr. Beevers and Dr. Ehrlich urged the study of the highest peaks in the Patterson function in the light of knowledge of molecular shape, contesting Buerger's statement⁽¹⁾ that the commonest error in the interpretation of complex Patterson projections is to assume that the prominent peaks are the significant ones.

In reply to a question from Dr. H. P. STADLER (King's College, Newcastle-upon-Tyne), Dr. Ehrlich said that in the Patterson syntheses discussed the peaks had been sharpened

but the origin peak had not been removed. Mr. E. N. MASLEN (Chemical Crystallography Laboratory, Oxford) pointed out that in more complex cases, where the system of known shape is only a small part of the whole molecule, the expected pattern in the Patterson function may be obscured by other features; this can be overcome by choosing a modification function which enhances the expected vectors. He quoted cephalosporin C as a structure solved by using a modification function having a maximum at about 1.5 Å. The consequent enhancement of 1.5 Å vectors enabled a six-membered ring occurring twice in an asymmetric unit of sixty-three atoms to be recognized.

In the second paper, Dr. H. J. MILLEDGE (University College, London) spoke about refinements of crystal structures made using the programme she has written for the Ferranti Pegasus computer. She explained that her programme is confined to strictly diagonal refinement for atomic co-ordinates, anisotropic temperature factors, overall scale and overall temperature factor. The neglect of cross terms and the limitation of the number of specified thermal ellipsoid orientations to only seven were necessitated by the small size of Pegasus compared with some other computers. Speed had been sacrificed to versatility, a decision which she had not regretted. Dr. Milledge said that refinement by diagonal least squares would converge rapidly, provided one made a judicious choice of the fractional shifts to be applied and provided the observed data were good. Of the structures investigated at University College it was usually found that for those which would not refine there was some inherent fault in the observed intensities, e.g. poor reproducibility of intensities for pentaerythritol, $R > 15\%$. One may compare this example with graphite and anthracene (Dr. D. C. Phillips's data) which had been refined until R was less than 5%. Weighting schemes were not used; a "bad" reflexion was omitted completely and all other reflexions were given equal weight. Dr. Milledge concluded by saying that attempts at solving structures, by using the programme to calculate changes in positions of molecules by least squares, had failed. It would be necessary to provide criteria for the acceptance or rejection of new structures proposed by the refinement.

In discussion, Miss DIANA PILLING (University of Leeds) made three comments: (1) Pegasus is not too small to include off-diagonal terms in refinement. In Cruickshank's programme a 6×6 matrix is used for anisotropic temperature parameters for twenty-five atoms and a 3×3 matrix for co-ordinates; (2) a definite improvement is obtained by using weighting schemes, that of Hughes usually being preferred; (3) there is usually an 80% correlation between overall scale and isotropic temperature factor refinement, so that cross terms between them are important. Dr. Milledge agreed with the last point and admitted that Pegasus is large enough to include some cross terms, but she did not concede the advantage of weighting schemes other than the alternative of acceptance or complete exclusion of a reflexion.

On behalf of herself and Dr. H. J. MILLEDGE, Dame KATHLEEN LONSDALE (University College, London) described

some X-ray studies of borazon. Borazon, cubic BN with a zinc-blende type structure, $a = 3.615 \text{ \AA}$, B-N 1.565 \AA ,⁽²⁾ was synthesized in the General Electric Research Laboratories, New York, at high pressures and temperatures. No changes in interplanar spacings or in intensities were observed in passing from room to low temperatures. Of the specimens, provided by Dr. Wentorf, some are black, some yellow, most are twins. There is reported to be considerable impurity and some deficiency in N.⁽²⁾

Borazon was heated in a vacuum in a graphite holder. No change was observed at 1500°C ($\pm 20^\circ$) after five minutes. Three minutes heating at 1650°C caused partial conversion with some preferred orientation; one minute at 1800°C and at higher temperatures caused complete conversion to a hexagonal form of a graphitic type with co-ordinates:

$$\text{N: } 0, 0, 0 \text{ and } \frac{2}{3}, \frac{1}{3}, \frac{1}{2}; \quad \text{B: } 0, 0, \frac{1}{2} \text{ and } \frac{1}{3}, \frac{2}{3}, 0.$$

The normal form of hexagonal BN is white with atoms in positions

$$\text{N: } 0, 0, 0 \text{ and } \frac{1}{3}, \frac{2}{3}, \frac{1}{2}; \quad \text{B: } 0, 0, \frac{1}{2} \text{ and } \frac{1}{3}, \frac{2}{3}, 0.$$

The bond lengths are identical in the two hexagonal forms, viz. B-N 1.446 \AA , B . . . N 3.331 \AA . The strong bond is longer and the weak bond shorter than the corresponding C-C bonds in graphite. The consequent differences in interplanar spacings make it easy to demonstrate the absence of any marked graphite contamination of the BN by the holder. Heated specimens retained their shape but yellow borazon crystals turned black.

It seems that the mechanism of the conversion of cubic to hexagonal BN is favourable to a graphitic rather than to a normal hexagonal form. It follows that a direct conversion, by a simple process of compression and heating, from normal hexagonal BN to borazon, is rather improbable.

Replying to a question from Prof. J. D. BERNAL (Birkbeck College, London), Dame Kathleen said that there was no evidence for the existence of a wurtzite form of BN. There is macro-twinning on $[111]$ like diamond but no micro-twinning. Dr. E. G. STEWARD (G.E.C. Research Laboratories, Wembley) asked whether the anomalies observed in the diffraction patterns of borazon heated above the inversion temperature were other than those normally associated with a graphite-type structure which is not fully ordered. Rather than produce the ideal structure one would expect this transformation to result in stacking disorder (turbostratic) effects and give, for example, only partially modulated 10 and 11 bands. Dame Kathleen replied that the stacking disorder found in the "graphitized" BN and in graphitized diamond are similar, but there is no evidence that this is different from stacking disorder as frequently found in terrestrial graphite. The point was that the disorder is invariably found, even in meteoritic graphite.

Dr. H. LYNTON (Fulmer Research Institute Ltd., Stoke Poges) presented a paper by himself and Miss JOAN E. FLEMING on the structure of low tridymite. Interest in this structure had been occasioned by a programme of work on the fundamental nature of glass. Cartz⁽³⁾ had approached the latter problem by postulating structural models for glass and calculating their X-ray diffraction patterns for comparison with the observed pattern. The models for this method, which was thought to be more sensitive than analysis of the radial distribution function, were based on cristobalite and tridymite, the high-temperature crystalline forms stable in the glass-forming region. Structures have been proposed for cristobalite by Wyckoff,⁽⁴⁾ Barth,⁽⁵⁾ and Nieuwenkamp,⁽⁶⁾ but for tridymite, of which seven forms have been reported,

a complete structure analysis has been made for only one form (Gibbs⁽⁷⁾).

Crystals of low tridymite had been extracted from a silica brick which had been heated in a gas retort for 1900 working days at about 1380°C . Only one single crystal had so far been found, others being aggregates; it is hexagonal or pseudo-hexagonal with $a = 30.08 \text{ \AA}$, $c = 49.08 \text{ \AA}$ and 864 SiO_2 groups in the unit cell. All X-ray photographs show hexagonal positional symmetry, but there are small random variations in intensities of equivalent reflexions, at first thought to be caused by absorption in the irregularly shaped crystal. Oscillation photographs taken about the c axis show outstandingly strong layer lines for $l = 0, 6, 12 \dots$, which define a small unit cell with $a = 5.01 \text{ \AA}$, $c = 8.18 \text{ \AA}$; this is nearly the same as that of high tridymite,⁽⁷⁾ $a = 5.03 \text{ \AA}$, $c = 8.22 \text{ \AA}$.

The strong pattern was examined first, modifying the structure of high tridymite to give the gross structure of the sub-cell. The $(hk \cdot 0)$ zone contains only strong reflexions, showing that in the $[00.1]$ direction the structure is projected as thirty-six identical sub-cells. From the $[00.1]$ Fourier projection and by trial and error, the positions of silicon and oxygen atoms were adjusted to give agreement of observed and calculated intensities, agreement indices $R = 0.20$ for $(hk \cdot 0)$, $(hk \cdot 6)$, $(hk \cdot 18)$ and 0.13 for $(hk \cdot 12)$ (large cell). This structure gives Si-O bond lengths: 1.80 \AA with linear Si-O-Si in the $[00.1]$ direction and 1.51 \AA with an Si-O-Si angle of 145° close to the (00.1) plane (see also 1.53 and 1.55 \AA for the same bonds in high tridymite).

Examination of the rectangular projection on (01.0) , corresponding to which $(h0 \cdot l)$ reflexions are present only for even indices (giving $a = 15.04 \text{ \AA}$, $c = 24.54 \text{ \AA}$) also led to modification of the high tridymite structure, but in a different way from that discussed above. In particular, a split of the oxygen into two "half" atoms, both with $z = 0.25$ but different x co-ordinates, was indicated. The bond lengths are now 1.69 \AA with Si-O-Si angle 128° in the $[00.1]$ direction and 1.78 \AA (118°), 1.54 \AA (105°), 1.56 \AA (142°) close to (00.1) . It may be concluded that the linear Si-O-Si bonds in high tridymite become bent in low tridymite as in other silica structures. A possible reason for the different results obtained from different projections of the structure may be divergence from hexagonal symmetry. For $(hk \cdot 0)$, $(hk \cdot 6)$, $(hk \cdot 12)$, $(hk \cdot 18)$ data hexagonal symmetry was assumed and intensities of equivalent reflexions averaged. $(h0 \cdot l)$ data which were not averaged with $(0k \cdot l)$ and $(\bar{h}\bar{k} \cdot l)$ free to show non-hexagonal tendencies.

Dr. H. D. MEGAW (Girton College, Cambridge) commented that this is an example of a phenomenon now appearing in many silicate structures as they are studied in more detail, viz. the occurrence of large unit cells made up of integral numbers of nearly identical sub-cells. Another example is anorthite which has only four sub-cells. The explanation of this phenomenon must be that the bond angles at oxygen and at silicon lie in a limited range for stability and this does not allow the construction of a perfectly repeating unit. The scatter in the Si-O bond lengths discussed in the paper, though large, is no greater than that found at first for anorthite and other feldspars where subsequent refinement gave uniform Si-O bond lengths.

Prof. J. D. BERNAL suggested that the authors should follow the thermal transformation cycle to see which oxygen atom moves off the Si-Si line (this had originally been done by Gibbs). He mentioned that with carborundum, some crystals showed every sixth layer line strong while others showed every fifth layer strong, and that this might possibly

be the case also with tridymite. Prof. H. LIPSON (Manchester College of Science and Technology) added to this the case of klockmannite, CuSe , which is hexagonal with thirteen-fold multiplication in the a direction, and 2000 atoms in the unit cell. Even computers are not equal to this problem which is best tackled by optical methods.

Following this was a paper on the structure of cinnabar by Dr. S. CHANDRASEKHAR and Dr. H. J. MILLEDGE (University College, London). This crystal structure was elucidated by Aurivillius⁽⁸⁾ in 1950. As a large number of data are available relative to the number of parameters (two co-ordinates and the temperature factors for mercury and sulphur atoms), this crystal can be used to study the dispersion correction applicable to mercury and the extent to which accurate refinement can be expected in heavy atom structures. Because the absorption coefficient for $\text{CuK}\alpha$ radiation is large (1500 cm^{-1}), attempts were made to grind the crystal to a sphere, but the crystal split and became quasi-ellipsoidal elongated along $[00.1]$ and to a lesser extent along one $[10.0]$ direction. With a specimen so shaped, for a study of anomalous dispersion effects, it is necessary to apply absorption corrections; this was done by applying an ellipsoidal distortion to the reciprocal lattice and then using a spherical correction. The $[00.1]$ projection is almost centrosymmetric so that anomalous dispersion effects are not important and symmetrically related reflexions should have equal intensities. Good agreement between intensities of such reflexions was obtained after applying absorption corrections in the way described. The structure has been studied at room temperature and at liquid nitrogen temperature, and thermal expansion coefficients obtained. The structure proposed by Aurivillius, although based on intensities collected using a large crystal and $\text{CuK}\alpha$ radiation without application of absorption corrections, has been found substantially correct.

The first session was concluded with a paper by Dr. R. S. CALDER (Cavendish Laboratory, Cambridge) on the electron distribution in lithium hydroxide monohydrate. The structure of $\text{LiOH} \cdot \text{H}_2\text{O}$, space group C2/m with four molecules in the unit cell, contains lithium atoms tetrahedrally co-ordinated by oxygen, pairs of tetrahedra sharing an edge (Pepinsky⁽⁹⁾). There are $\text{O} \cdots \text{O}$ distances of 2.68 \AA , taken by Pepinsky as indicating the presence of hydrogen bonds linking tetrahedra. The present work had been undertaken (a) to locate the hydrogen atoms on these bonds, (b) to show whether the H_2O unit actually exists in the crystal and (c) to study the nature of the $\text{Li}-(\text{OH})$ bond which might be predominantly ionic or covalent.

The relative intensities of the X-ray reflexions were measured to a high accuracy using a scintillation counter diffractometer with unfiltered $\text{MoK}\alpha$ radiation. A few measurements were made with silver radiation to check for extinction. The intensities of all the equivalent reflexions were measured and a disagreement of more than 2% within a set was considered as indicating misalignment of the instrument. The maximum error in F_o , estimated from the experimental measurements only, was 0.2 ($F_{000} = 88$) with an average standard deviation of 1.5%. Small crystals were used to reduce extinction errors; absorption was negligible.

Co-ordinates and anisotropic temperature parameters for oxygen and lithium atoms were determined using the difference Fourier technique with the McWeeny spherical neutral atom scattering factors.⁽¹⁰⁾ To eliminate uncertainties in atomic shape caused by bonding and to remove the hydrogen atoms, only terms with $\sin \theta/\lambda$ greater than 0.4 were used. The

structure was refined to $R = 4\%$ and the hydrogen atoms then appeared on the difference maps as peaks of density $0.2 \text{ e.}\text{\AA}^{-2}$. It was realized that the omission of low-order terms had caused an "inverse series termination effect". The co-ordinates of the hydrogen atoms were found by calculating a difference synthesis with all terms (Fig. 2). The

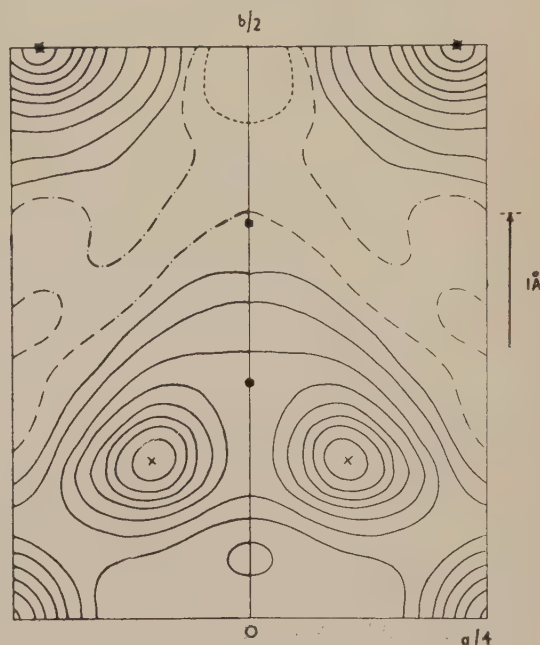


Fig. 2. $\text{LiOH} \cdot \text{H}_2\text{O}$, difference Fourier synthesis showing hydrogen atoms (c-projection)

● = oxygen ■ = lithium x = hydrogen
Contour interval $0.1 \text{ e.}\text{\AA}^{-2}$

final discrepancy factors R were 1.5% for $(h0l)$ and 2.1% for $(hk0)$ reflexions (with $\sin \theta/\lambda$ greater than 0.4). The value of R rises to 2.5% when all terms are included. The accuracy of co-ordinates was: oxygen 0.001 \AA , lithium 0.002 \AA , hydrogen 0.02 \AA ; that of anisotropic temperature factors: oxygen 2%, lithium 5%. Scaling was done by comparing F_o and F_c peak heights. The very small amount of negative electron density (minimum $-0.1 \text{ e.}\text{\AA}^{-2}$) in the F_o synthesis attests its accuracy.

The results show that two hydrogen atoms are definitely associated with the oxygen atom on the diad axis, with an O-H distance 0.94 \AA , $\text{O} \cdots \text{O}$ 2.68 \AA . Thus the H-O-H grouping exists in the crystal with dimensions close to those of the free water molecule and to previously studied molecules of water of crystallization. The third hydrogen atom is 0.93 \AA away from the other oxygen atom, so that the hydroxyl group is also localized. The hydrogen bonds are very nearly straight. There is no excess or deficiency of electronic charge around either lithium or hydroxyl oxygen. This supports chemical theory which predicts a predominantly covalent Li-O bond. Removal of all atoms from a difference synthesis leaves no significant density except a peak of $0.2 \text{ e.}\text{\AA}^{-2}$ between the water oxygen and lithium, which may represent some effect of a covalent bond between these atoms. The water-lithium distance is longer than the hydroxyl-lithium, indicating a weaker bond. The water oxygen is tetrahedrally co-ordinated by two hydrogen and two lithium atoms.

Dr. J. C. SPEAKMAN (University of Glasgow) commented that the small peak between the water oxygen and lithium

may represent the first direct evidence for the co-ordinate link. He asked what is meant by an interatomic distance when, as here, it has been quoted to within one or two thousandths of an Ångström unit. Dr. Calder replied that the distances given are simply those between the centres of atomic peaks in the Fourier syntheses. In reply to a question from Dr. H. J. MILLEDGE, he said that the final co-ordinates were not obtained from Fourier maps but were those used to calculate the structure factors which gave the good agreement quoted.

For the second session, Prof. H. LIPSON (Manchester College of Science and Technology) took the chair. The session commenced with a paper by Prof. J. M. ROBERTSON and Mr. D. G. WATSON (University of Glasgow) on the crystal structure of azulene. Work had been started on this crystal in the hope of obtaining accurate information about the molecular geometry and the electron density distribution, with a view to explaining properties, such as the dipole moment of 1D, not in accordance with the two Kekulé formulae. The results were, from this point of view, disappointing but were of interest in another direction. Preliminary examination by Robertson and Shearer⁽¹¹⁾ showed the unit cell of azulene to be similar to that of naphthalene. Systematic absences of X-ray reflexions indicated the space group $P2_1/a$. Since there are two molecules in the unit cell this would normally be taken as indicating a centrosymmetrical molecule, which is at variance with the accepted chemical formula. An $N(z)$ test on $(h0l)$ intensities indicated that the projection on (010) was non-centrosymmetric, so that the space group would be Pa , the $(0k0)$ reflexions being accidentally halved. A structure based on these conclusions was refined (two-dimensional data) to give $R = 11.1\%$ for $(h0l)$ and 17.2% for $(0kl)$. However, it was found impossible to refine three-dimensional data beyond $R = 22\%$. The possibility of a disordered structure in $P2_1/a$ was considered. Disorder was not evident in the X-ray photographs, but Günthard⁽¹²⁾ had found the entropy of solid azulene to be substantially higher than that of naphthalene. It was concluded that the statistical tests of $(h0l)$ intensities were invalid because of the small number (fifty) of terms available. A variance test of all the three-dimensional data indicated centrosymmetry; this was confirmed by the test due to Sim.⁽¹³⁾

A trial structure with superposition of two molecules related by a symmetry centre corresponding to random reversal of direction of azulene molecules in the crystal was refined as far as $R = 6.5\%$. For the final stages, full matrix least squares refinement with anisotropic temperature factors was used. The cross terms between atoms will be important in azulene where there is much overlap. However, at the end of the refinement the shifts in co-ordinates were still about 0.02 Å and the lengths of the bonds, excluding the transannular bond, range from 1.34 to 1.46 Å . Average lengths for chemically equivalent bonds range from 1.38 to 1.41 Å , as in benzene. The length of the transannular bond is 1.483 Å with the smallest standard deviation (0.004 Å) of any of the bonds. This bond is thus distinctly longer than the others, as would be expected if the molecule is represented by 2 Kekulé type formulae, and its length agrees with Dewar's prediction $1.47 \pm 0.01 \text{ Å}$ for a bond between two sp^2 -hybridized carbon atoms. Evidently the results of this examination are not completely satisfactory, even though the agreement between observed and calculated intensities is very good; further possibilities such as unequal occupation of molecular sites must be examined.

The next paper, by Mr. H. N. SHRIVASTAVA and Dr. J. C.

SPEAKMAN (University of Glasgow), read by the former, dealt with the crystal structure of and hydrogen bonding in potassium hydrogen di-*p*-nitrobenzoate. This compound-like potassium hydrogen disalicylate has been found to be of the type $M^+X^- \cdot HX$ in which the anion and free acid molecule are crystallographically distinguishable. In contrast, most acid salts MHX_2 so far examined have proved to be of the type $M^+X-\bar{H}-X$, where the X residues are linked across a crystallographic symmetry element (e.g. a centre) by an apparently symmetrical hydrogen bond. Hadži had predicted the unsymmetrical structure of potassium hydrogen di-*p*-nitrobenzoate from its infra-red absorption spectrum, which may be considered as a superposition of the spectra of the free acid and of its neutral potassium salt. The spectrum of potassium hydrogen di-*o*-nitrobenzoate, shown by Speakman and Mills to be a symmetrical type compound, is quite different and, like the spectra of other symmetrical acid salts, does not include features characteristic of the free acid.

The compound studied here is triclinic with $a = 11.44 \text{ Å}$, $b = 4.05 \text{ Å}$, $c = 17.20 \text{ Å}$, $\alpha = 93.8^\circ$, $\beta = 104.1^\circ$, $\gamma = 90.5^\circ$, two molecules per unit cell. Statistical tests of intensities indicated space group $P\bar{1}$. The high symmetry of the *p*-nitrobenzoate residues complicated the Patterson function and made recognition of the "heavy atom" vectors difficult. Attempts to prepare isomorphous rubidium or ammonium salts failed; presumably the structure depends for its stability on the precise size of the cation. The structure was ultimately solved by a combination of two methods applied to the sharpened Patterson projection on (010) , viz. the Burger minimum function and a systematic search for the vector sets of the two independent pairs of centrosymmetrically related *p*-nitrobenzoate residues. Using electron density and difference syntheses the structure has been refined to $R = 13\%$. The difference maps indicate considerable thermal anisotropy, but so far only isotropic temperature factors have been used. The anion residue makes closer contacts with the potassium ion than does the acid molecule. There is a hydrogen bond between the acid molecule and the anion. Its length, between 2.5 and 2.8 Å , has not been determined accurately because the y -co-ordinates are only approximate. Attempts are being made to improve them by the use of generalized projections.

In the ensuing discussion, Dr. P. J. WHEATLEY (Monsanto Research S.A., Zürich) asked whether the NO_2 and CO_2 groups are coplanar with the benzene ring or if there is twisting about the C-C and C-N bonds. Mr. Shrivastava replied that the acid molecule certainly appears to be planar. For the anion there may be small deviations from planarity but one cannot be certain until the y -co-ordinates are known. In reply to Mr. S. F. DARLOW (Manchester College of Science and Technology), who asked if there is six-fold co-ordination of K^+ by O, Mr. Shrivastava said that the potassium ion makes eight contacts with oxygen, four short, two medium and two long. Again, the final answer depends on the y -co-ordinates.

Mr. E. J. McIVER (University of Cambridge) reported on the structure of bultfonteinite, a hydrated calcium silicate containing some fluorine, with the composition $\text{Ca}_4\text{Si}_2\text{O}_{10}\text{F}_2\text{H}_2$. The unit cell has dimensions $a = 10.992 \text{ Å}$, $b = 8.182 \text{ Å}$, $c = 5.671 \text{ Å}$, $\alpha = 93^\circ 57'$, $\beta = 91^\circ 19'$ and $\gamma = 89^\circ 51'$. Piezoelectric tests were inconclusive but there were systematic weaknesses indicating a pseudo-monoclinic space group $P2_1/c$. Patterson projections were interpreted by analogy with CaF_2 and corresponding electron density projections constructed and refined to $R_{h00} = 11.4\%$, $R_{h0l} = 9.5\%$, $R_{0kl} = 8.7\%$.

There are isolated $[\text{SiO}_4]^{4-}$ (neso-) groups and having located the oxygen atoms and decided where the fluorine atoms were, the various kinds of hydrogen bonds could be identified. There are three short hydrogen bonds (2.48 \AA) with hydrogen in the centre; four long bonds (2.73 \AA) with hydrogen nearer one of the oxygen atoms. The only feature of the structure which prevents it from assuming monoclinic symmetry is the absence of one hydrogen atom from the glide plane. The mineral is twinned on (100) and the twinning could be removed by heating, giving a monoclinic phase. The transformation takes place only between 395 and 400°C . The monoclinic phase has the space group $P2_1/c$ and the hydrogen atom probably occupies the two related sites statistically. Some suggestions as to the mechanism of the transformation were made.

Dr. E. SÁNDOR (University of Cambridge) then described an investigation which he had made with Dr. W. A. WOOSTER on diffuse streaks in the diffraction pattern of vanadium single crystals.⁽¹⁴⁾

Diffuse streaks observed in the diffraction pattern of 99.6% pure vanadium single crystals have been identified as the diffraction pattern of a separate hexagonal phase, which consists of vanadium atoms in hexagonal close packing with nitrogen atoms in octahedral holes. The hexagonal lattice parameters are:

$$a = 2.88 \pm 0.01 \text{ \AA}, c = 4.55_5 \pm 0.01 \text{ \AA}, \\ \text{and } c/a = 1.58 \pm 0.01.$$

In most specimens the hexagonal phase has twelve equally probable different orientations relative to the b.c.c. vanadium matrix. The lattice relations of the two phases can be described as follows:

$$(00.1)_{cph} || \{110\}_{bcc} \text{ and } [10.0]_{cph} || [111]_{bcc}$$

i.e. the most densely populated planes of the two phases and one of their most densely populated rows coincide. One particular vanadium single crystal has been found, in which the hexagonal lattice has twenty-four different orientations. Possible explanations of the observed lattice relations were then discussed.

The last paper of this session was a single-crystal reaction under irradiation: photo-oxide of anthracene to anthraquinone, by Mr. J. S. STEPHENS and Dame KATHLEEN MONSDALE (University College, London). The photo-oxide of anthracene ($\text{C}_{14}\text{H}_{10}\text{O}_2$) crystallizes in $P2_1/a$ with $a = 6.10 \text{ \AA}$, $b = 5.86 \text{ \AA}$, $c = 11.42 \text{ \AA}$, $\beta = 107^\circ$, four molecules in the unit cell. When left for some time it decomposes into anthraquinone, the process taking about six months under ordinary conditions. The reaction is accelerated on irradiation by X-rays, and arrested by cooling in a refrigerator. While X-ray photographs for structure determination were being taken it was noticed that the pattern was becoming less intense and that a new, apparently single, crystal pattern was appearing. The latter increased in intensity steadily until practically none of the original was left. In oscillation photographs taken about the a axis, alternate layer lines weaken and the final pattern is restricted to low orders. With the a axis vertical, the layer-line separation of the new structure (which was identified as anthraquinone) is nearly $1\frac{1}{2}$ times that of the original.

The orientation of the molecules in the photo-oxide has been found to be approximately the same as that of the molecules in anthraquinone. The similarity of the unit cells is shown by the following reciprocal lattice dimensions:

$$\text{photo-oxide, } a^* = 6.49 \times 10^{-2}; b^* = 17.06 \times 10^{-2}; \\ c^* = 9.15 \times 10^{-2}; \beta^* = 73^\circ$$

$$\text{anthraquinone, } a^* = 6.53 \times 10^{-2}; b^* = 25.37 \times 10^{-2}; \\ c^* = 13.04 \times 10^{-2}; \beta^* = 77.3^\circ$$

The two compounds have the same space group, but anthraquinone has only two molecules in the unit cell. On decomposition, the molecules of the photo-oxide turn slightly, the b and c axes close up while the a axis remains the same length.

A von Eller optical Fourier synthesis of the photo-oxide based on intensities collected at room temperature shows elongated peaks for the atoms of the HC-O-O-CH bridge, indicating considerable thermal vibration of those atoms in a direction perpendicular to the long axis of the molecule. An optical synthesis constructed from low-temperature data shows much sharper peaks. The photo-oxide molecules are bent with a pseudo-symmetry plane through the central bridge; they are linked together by weak $\text{C-H} \dots \text{O}$ bonds along the direction of the b axis. As the molecules of anthraquinone are planar the transformation must involve considerable local disturbance of the structure, but must take place initially in such a way that chains of the old kind of molecules are embedded in the new structure. Early Laue photographs with the incident beam along [101], which is the axis exactly common in direction to both initial and final structures, shows the development of a single sharp, but continuous, circle, typical of a fibrous intermediate stage in which only one precise identity period exists. This is superimposed upon a sharp Laue pattern of the original material. The final rotation and Laue patterns are those of a structure with considerable rotational disorder about [101], although the other layer-line patterns can be obtained without difficulty.

The keen interest shown in this paper is evidenced by the considerable discussion which followed. Dr. P. J. WHEATLEY asked if the reaction is brought about by radiation of any other wavelength such as visible light. Dame Kathleen replied that the effect of visible light had not been tried, but the reaction takes place at room temperature even without irradiation. Dr. J. S. ROLLETT (The University Computing Laboratory, Oxford) suggested that the anisotropy of the oxygen atoms in this structure might be explained in terms of the anisotropic scattering factor curves of McWeeny rather than by thermal vibration. Dame Kathleen said that the absence of such anisotropy in the low-temperature Fourier synthesis suggested that thermal vibration was the cause; related compounds also show such thermal vibrations. Dr. J. ADAM (Atomic Energy Research Establishment, Harwell) commented that radiation-induced phase transformations appear to be possible only if the new phase can also be produced and retained at the given temperature by thermal treatment. The present work seems to support this generalization. The question by Mr. S. F. DARLOW as to the energy involved in breaking the $\text{C-H} \dots \text{O}$ bonds was answered by Dr. H. J. MILLEDGE, who said that one can only estimate the change in Debye factor with amount of radiation supplied, and herself questioned whether this can be interpreted. Dr. P. P. EWALD (Polytechnic Institute of Brooklyn, U.S.A.) suggested that one might distinguish between thermal motion and deformation of the atomic state by vibrations by conducting parallel studies with X-ray and neutron diffraction on the same substance. Dame Kathleen replied that this should be possible theoretically but seems not to work in practice.

Dr. Milledge added that more work is needed on simple structures and that agreement between the results from X-ray and neutron diffraction is not as good as it should be. Disputing this, Dr. W. COCHRAN (Cavendish Laboratory,

Cambridge) mentioned the good agreement obtained in the case of lithium hydride, and Dr. G. E. BACON (Atomic Energy Research Establishment, Harwell) said that it is too soon to draw conclusions about discrepancies. Apart from cases where significantly different things, such as nuclear position and centre of gravity of electron density, are being measured, there is no evidence that X-ray measurements do not agree with those from neutron diffraction. He quoted a recent case where very good agreement was obtained, 4:4'-dichlorodiphenyl sulphone.⁽¹⁵⁾

Third session: Apparatus and experimental techniques

Mr. G. HARBURN and Dr. C. A. TAYLOR (Manchester College of Science and Technology) opened the final session by reporting on the latest development in their special field of optical diffractometry. It has now been shown to be possible to produce optical transforms corresponding to non-central sections of the reciprocal lattice. The structure factor equation can be written as

$$F_{hkl} = \sum f_n \exp 2\pi i(hx_n + ky_n) \exp i\phi, \text{ where } \phi = 2\pi lz.$$

Two-dimensional optical transforms are obtained by punching holes at points corresponding to the x - and y -co-ordinates and this corresponds to giving ϕ the value 0. In optical terms this means that the phases of the beams of light passing through all the holes are the same. If a method can be found of changing the relative phases it would be possible to represent the z -co-ordinates and to obtain transforms corresponding to non-zero values of l . For example, if $\phi = 2\pi z$ the equation would then give F_{hk1} . It is necessary for ϕ to be continuously variable from 0 to 2π . So far the experimental work has been done on the large diffractometer (15 in. diameter lenses of focal lengths 30 ft), but in principle the method could be applied to smaller ones. The condenser system has been modified and now incorporates a Polaroid filter and a suitably oriented quarter-wave plate of mica, so that a circularly polarized beam is produced. If half-wave plates of mica are now placed in the plane of the mask, the relative phases of the light passing through them can be varied by changing their orientations in the beam. The phase difference between beams passing through two plates is twice the angle between their fast directions, thus the rotation of 180° of one piece of mica relative to another gives a phase change of 360° . The device is linear and the amplitude transmitted remains constant and independent of the azimuthal orientation. The masks have been made of Bakelite drilled with holes at the positions representing the x - and y -co-ordinates of the structure under examination. Quarter-inch diameter brass plugs fitted to these holes carry the half-wave plates. A simple instrument has been devised enabling the plugs to be rotated quickly to any given azimuth while the plate is outside the diffractometer.

The phase-changing principle has been tested and found to work satisfactorily, but so far attention has been confined to trying out the ideas on known structures. A complete three-dimensional optical transform of pentaerythritol has been prepared and can be studied in two ways. If the various sections are prepared on glass plates they can all be mounted together to give a "solid" representation of the transform, or the separate sections can be compared directly with the corresponding sections of the weighted reciprocal lattice.

Starting with the mask and the necessary data it took three to four hours to obtain a set of prints corresponding to all the nine layers. There are three ways in which three-dimensional transforms may be useful. First, it is hoped

to gain experience of the nature and appearance of three-dimensional transforms which should help in the interpretation of three-dimensional weighted reciprocal lattices. Secondly, the method can be used section by section as a test of a set of co-ordinates and may be expected to bear the same kind of relationship to the three-dimensional structure factor work that two-dimensional transforms bear to the determination of projections. Thirdly, it may be possible to derive the third co-ordinate when one projection has been determined by purely optical considerations. Experiments have already been made which suggest that this process is a distinct possibility, and it is hoped to try out the ideas on an unknown structure in the near future.

In reply to questions Mr. Harburn explained the relationship of his device to Buerger's X-ray microscope where the phase-changing was accomplished by tilting mica plates. The transform as recorded did not appear to be sensitive to small (5°) changes in the phase of one point. The method was expected to be useful, nevertheless, for locating molecules in the z -direction and the phase settings could be made to about 1° .

Dr. J. W. JEFFERY and Mr. K. M. ROSE (Birkbeck College, London) then gave an account of their most recent work on the practical problems involved in the accurate measurement of relative intensities of X-ray reflexions by photographic means.

Photometry of the spots on an integrating Weissenberg film has been chosen, after trials of other methods, as the best photographic method of measuring intensities.

With considerable care it is possible to confine the sources of error effectively to absorption in the crystal, to the film and its development and to non-uniformity of film background. The latter is mainly caused by variation along the Laue streak for low-angle reflexions. For this reason $\text{CuK}\alpha$ radiation was chosen as more suitable than $\text{MoK}\alpha$ for measuring intensities photographically. Up to a maximum density of 1.2 the standard deviation of errors due to the film and its development can be reduced below 1% of the maximum. To minimize absorption errors, spherical crystals of Whitlockite [$\text{Ca}_3(\text{PO}_4)_2$ with $\mu = 274 \text{ cm}^{-1}$ for $\text{CuK}\alpha$ and $\text{Co}[\text{Hg}(\text{CNS})_4$] ($\mu = 480$) were ground to a diameter of about 0.2 mm. The exact size and a measure of the imperfections were obtained by photomicrography.

Both crystals were of high symmetry, so that a satisfactory test of the accuracy achieved was obtained by comparison of symmetry equivalent reflexions. Whitlockite ($R\bar{3}c$) gave ten sets of sixteen equivalent reflexions on the same film and $\text{Co}[\text{Hg}(\text{CNS})_4]$ (14) a larger number of sets of five or six reflexions.

Errors due to small irregularities of shape were shown theoretically to be proportional to the intensity of reflexion and the absorption coefficient. The results for the two spherical crystals were in agreement with the theory and, by extrapolation, showed that for a similar near-spherical crystal of $\mu = 10$, crystal errors should be negligible compared with film errors. For such a crystal, the standard deviation of symmetry equivalent reflexions should be less than 1% of the maximum intensity measured. Highly symmetrical organic crystals are being used to check this conclusion and the results will be reported to the Congress of the International Union of Crystallography in Cambridge. The main paper will be submitted to *Acta Crystallographica* and a description of the photometer and its performance will be submitted to the *Journal of Scientific Instruments*.

Dr. S. CHANDRASEKHAR queried the statement, that the only convenient method of correcting for extinction is by

comparing single crystal and powder data, saying that he had, in work using polarized X-rays, shown it to be possible to correct for both primary and secondary extinction fairly accurately in a single crystal of any shape. Powder photographs might be difficult to index reliably. Dr. Jeffery replied that low-angle powder photographs, with powders of less than $1\ \mu$ grain size produced by a micronizer air-blast mill, nevertheless gave the corrections experimentally and not inconveniently. The powder pictures could be obtained free of the preferred orientation which Dr. H. J. MILLEDGE had pointed out might occur with regularly-shaped crystal fragments.

Dr. U. W. ARNDT reported that the single-crystal X-ray diffractometer which he and Dr. D. C. PHILLIPS (Royal Institution, London) have developed and which was first described at the X-ray Analysis Group conference in April, 1958,⁽¹⁶⁾ has been made fully automatic. It will now produce a complete record of the intensities of all reflexions within the range $2\theta = 0$ to 60° , one reciprocal lattice level at a time. The measurements are corrected for background and are presented both as a plain language record and on punched tape in a form suitable for further processing by means of an electronic digital computer. Amplifying his remarks in reply to questions by Dr. W. A. WOOSTER, Dr. R. W. H. SMALL (University of Birmingham) and Mr. R. S. CALDER, Dr. Arndt explained that the design involved, of course, a compromise between various features such as counter resolution, aperture and range, but that the counter aperture was made large enough to admit the whole of any reflexion. Although Dr. JEFFERY had pointed out that the background near a spot should be measured along a Laue streak, the diffractometer did not do this, but the proportional counter with pulse-height discrimination used in the instrument secured a large measure of monochromatization, and therefore the Laue streaks were not a serious problem. The half-peak width of the distribution for $\text{CuK}\alpha$ radiation is about 14%.

Mr. B. R. BUTCHER here interpolated an account of the Schulz diffractometer for preferred orientation work which he had designed at the Atomic Energy Research Establishment, Harwell, and which had been realized by Seaton Creaghe Engineering Ltd. The machine was demonstrated and was available for inspection in the exhibition of apparatus (Fig. 3). The principle of its operation is due to Schulz⁽¹⁷⁾ and has the great advantage that the absorption of the specimen is constant, for any particular reflexion, for all angles of tilt. The performance of the final instrument had been checked and evaluated. Defocusing was the major difficulty.

Mr. C. WAINWRIGHT then described an X-ray powder diffraction camera which he and Dr. C. GRIFFITHS had produced some time ago at the National Physical Laboratory, Teddington.

This apparatus was built to fulfil a need for a solid-specimen camera which would permit a reasonable precision in positioning the specimen and film, and in measuring up the patterns; and robust enough to handle, if necessary, specimens of considerably larger bulk than can be easily introduced into most conventional cameras. Vertical and cross-movements allow accurate positioning of the specimen, or of any portion of it. The camera has proved very suitable for the speedy mounting and examination of solid samples for a variety of purposes, and has allowed more refined equipment to be reserved for investigations which call for the higher levels of precision.

Dr. E. ARUJA (Building Research Station, Garston, Herts.) said he was describing his high-temperature camera because

it did in fact work. It is based on a very successful high-temperature microscope stage,⁽¹⁸⁾ developed at the Building Research Station.

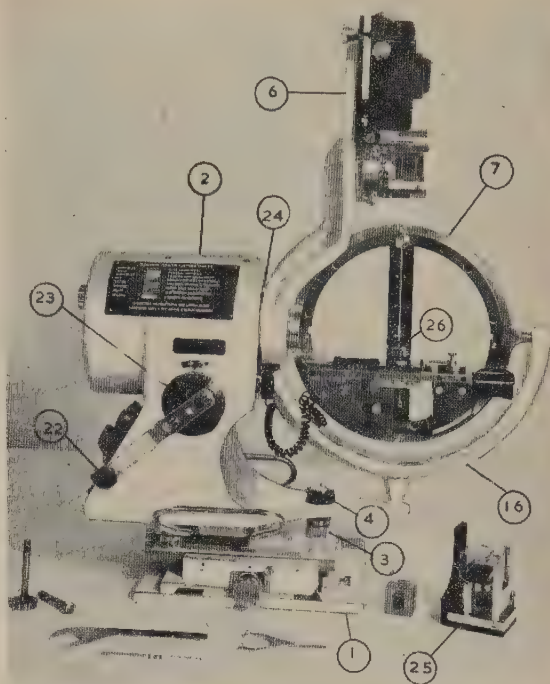


Fig. 3. Schulz diffractometer for preferred orientation studies

The essential feature of the camera is the use of a thermocouple to serve the triple function of mounting, heating and temperature measurement of the specimen. The device is simple, compact and inexpensive and has proved very reliable. It has been used at temperatures up to 1850°C , and there are possibilities of further development. Most of the work so far has been on an improvised model in the 1000 – 1600°C range, but as the specimen is mounted without admixtures and is exposed (i.e. not in a capillary) it has proved useful in dehydration experiments even below 200°C .

Mr. A. M. ADAMS (Central Electricity Research Laboratories, Leatherhead) described the modification of a 9 cm diameter Unicam powder camera by the fitting of an equatorial septum which enables two photographs to be taken at once. For example, specimens of Fe_3O_4 and $\gamma\text{-Fe}_2\text{O}_3$, in the same capillary tube but separated by a rod of quartz, could be examined simultaneously. An account has already been published. Dr. ARUJA added in replying to questions that his heater could be used for single crystals but with limitations on the range of reflexions. He said he used Durofix to glue his specimens of metal filings to the heater. Dr. H. J. MILLEDGE stressed the desirability of having photographs of the unknown substance and a reference material on the same film.

Mr. J. R. STANSFIELD (Hilger and Watts Ltd., London) then presented an account of the latest versions of the X-ray generator made by Messrs. Hilger and Watts Ltd. In this continuously evacuated generator, the tube itself is a small capsule on the top of its pumping tube. The focus is only 19 mm from the outer tube wall and apparatus can be brought close to the focus. Both cathode and anode assemblies can be changed. A microfocus gun giving a circular focal spot of diameter 0.04 mm , which, with a copper target can be

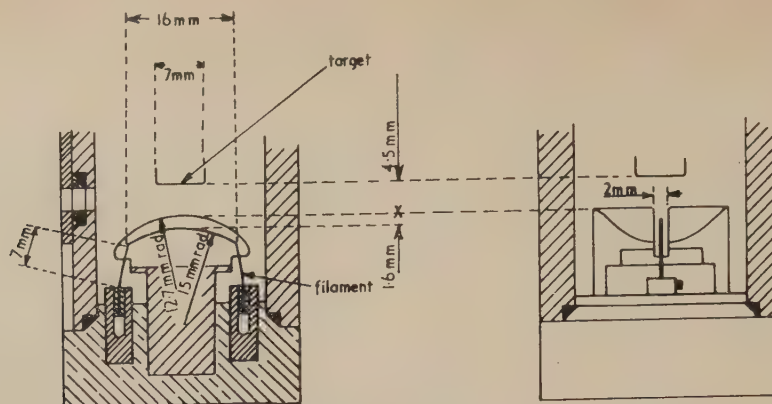


Fig. 4. Cathode assembly for high-power semi-microfocus X-ray tube

operated at 25 W (15 kW/mm^2) and a gun giving a line focus $0.1 \times 1.4 \text{ mm}$ operating at 150 W (1.1 kW/mm^2) can be fitted. A new cathode assembly has now been developed (Fig. 4) which gives a larger focus of $0.1 \times 5 \text{ mm}$ and operates at 450 W (0.9 kW/mm^2). The width of the focal strip can be adjusted by altering the bias. For the lower power versions of the tube, interchangeable target tips detachable from the main rod are used, but for the highest power the anode must be without such a gap and the whole anode has to be changed. The tube is thus suitable for ordinary uses as well as for micro-diffraction.

Dr. F. YOEELL (The University of Leeds) supplemented this paper by demonstrating two modifications to an earlier version of the Ehrenberg and Spear fine-focus tube as manufactured by Hilger and Watts Ltd. He showed a solid copper anode rod with air-cooling fins which would operate at $\frac{1}{2} \text{ mA}$. It had a screwed-on replaceable tip. The electron optics of the system could also be improved by making the tip hemispherical with a flattened end instead of flat.

Dr. R. W. H. SMALL asked whether a large-focus tube might not be useful for examining stationary crystals, and Dr. H. J. MILLEDGE commented that Zachariasen had used this method for integrating intensities.

The distinguished visitor's address in the evening of 13 November was given by Prof. P. P. EWALD (Polytechnic Institute of Brooklyn, U.S.A.), who spoke of the early days of X-ray analysis from a personal point of view.

G. J. BULLEN
A. L. MACKAY

References

- (1) BUERGER, M. J. *Vector space*, p. 126 (New York: John Wiley and Sons, 1959).
- (2) WENTORF, R. H., jun., *J. Chem. Phys.*, **26**, p. 956 (1957).
- (3) HARGREAVES, A., and STANLEY, E. *Brit. J. Appl. Phys.*, **10**, p. 117 (1959).
- (4) WYCKOFF, R. W. G. *Z. Krist.*, **62**, p. 189 (1925).
- (5) BARTH, T. F. W. *Amer. J. Sci.*, **23**, p. 350 (1932).
- (6) NIEUWENKAMP, W. *Z. Krist. A*, **96**, p. 454 (1937).
- (7) GIBBS, R. E. *Proc. Roy. Soc. A*, **113**, p. 351 (1926).
- (8) AURIVILLIUS, K. L. *Acta Chem. Scand.*, **4**, p. 1413 (1950).
- (9) PEPINSKY, R. *Z. Krist. A*, **102**, p. 119 (1939).
- (10) McWEENY, R. *Acta Cryst.*, **4**, p. 513 (1951).
- (11) ROBERTSON, J. M., and SHEARER, H. M. M. *Nature (London)*, **177**, p. 885 (1956).
- (12) GÜNTARD, H. H. Thesis, Zürich (1949).
- (13) SIM, G. A. *Acta Cryst.*, **11**, p. 123 (1958).
- (14) SÁNDOR, E., and WOOSTER, W. A. *Acta Cryst.*, **13**, p. 339 (1960).
- (15) BACON, G. E., and CURRY, N. A. *Acta Cryst.*, **13**, p. 10 (1960).
- (16) SIME, J. G., and ABRAHAMS, S. C. *Acta Cryst.*, **13**, p. 11 (1960).
- (17) HARGREAVES, A., and STANLEY, E. *Brit. J. Appl. Phys.*, **10**, p. 121 (1959).
- (18) SCHULZ, L. G. *J. Appl. Phys.*, **20**, p. 1030 (1949).
- (19) ARUJA, E., WELCH, J. H., and GUTT, W. *J. Sci. Instrum.*, **36**, p. 16 (1959).

Pumping characteristics of a titanium droplet getter-ion pump

by L. HOLLAND F.Inst.P., and L. LAURENSEN, Vacuum Deposition Research Division, Edwards High Vacuum Limited, Crawley, Sussex

Paper received 17 March, 1960]

Abstract

The performance has been studied of a 12 in. diameter titanium getter-ion pump with an evaporated-getter area of 3400 cm². The titanium was evaporated from an electron-bombarded molten bead suspended via a frozen zone from a cooled anode; a triode electrode system was used for ionization pumping. The sorption rates of a number of gases were measured in the pressure range 10⁻⁴–10⁻⁸ mm of mercury. The pumping speed for nitrogen was enhanced by operating the ionization source during evaporation. The h.t. voltage used with the vapour source influenced the form of the titanium bead, and at low voltages (approximately 800 V) and high power inputs (approximately 465 W) large metal droplets were obtained giving the highest evaporation and sorption rates. Sorption rates were greatly increased if a diffusion pump was in operation during gettering, because impurity gases slowly sorbed by the getter-ion pump were more effectively removed. Pumping speeds in l./s at 10⁻⁶ mm of mercury for the getter-ion pump with a diffusion pump (10 l./s) in operation and a titanium evaporation rate of 40 mg/min were as follows: oxygen₂—2450; nitrogen₂—4500; hydrogen₂—1600; air—600; argon—2.5; Calor gas—90. The low pumping speed of air was due to the low sorption rate of the argon component. Hydrocarbon gases were slowly sorbed and when mixed with active gases greatly reduced their pumping speed. The pump-down characteristics of the getter-ion pump were examined and it was found that the ultimate pressure was only slowly regained after exhausting oxygen. The sorption efficiency can be found from the equation: $S_m = \alpha S_0$, where S_m is the measured sorption rate per unit getter area (l./s cm²), S_0 is the ideal sorption rate and α the sorption coefficient. Values of α measured at 10⁻⁶ mm of mercury were as follows: oxygen₂—0.068; nitrogen₂—0.12; hydrogen₂—0.012; possible reasons for the low value of α for hydrogen are considered.

Introduction

IN recent years, interest has been growing in the use of getter-ion pumps, both for maintaining the vacuum in the sealed envelopes of electronic tubes and for providing the vacuum in particle accelerators; an extensive review of these pumping techniques has been made by Holland.⁽¹⁾ Interest in the use of getter-ion pumps for exhausting particle accelerators of large capacity was stimulated by the hope that such devices would neither give rise to hydrocarbon contamination nor require cold traps, as are necessary with either oil or mercury diffusion pumps. The "Evapor-ion" pump developed by Herb^(2, 3) and others⁽⁴⁾ in America, promised to have a pumping performance comparable with a conventional diffusion pump and therefore to be suitable

for exhausting large-capacity vessels. The Herb pump operates by evaporating a titanium getter from an electron-bombarded post, but this device only gives limited service because titanium reacts with all available types of refractory used for the heated post. Holland, Laurenson and Holden⁽⁵⁾ have described a titanium getter pump in which the evaporation-support reaction is overcome by feeding a titanium wire along a cooled electrode into an electron stream where it forms a molten globule which becomes suspended from the electrode via a frozen zone.

Getter-ion pumps made with the frozen-zone droplet have proved to possess several advantages other than freedom from support deterioration, these are:

- (i) The evaporation conditions are extremely stable because the titanium globule hanging from its cooled support is held in a stable position with respect to the electron bombarding stream, whereas when a molten globule is formed on the end of a free wire it tends to melt back out of the beam, as shown elsewhere by Holland and Laurenson.⁽⁶⁾
- (ii) The ratio of the heat radiated by the droplet source to the vapour emitted is the lowest possible because only the titanium to be evaporated attains a high temperature; this relationship is important if the apparatus is not to become overheated and degas during evaporation.
- (iii) Thoroughly degassed metal can be used for evaporation by initially rapidly feeding the titanium wire to form a large droplet which is degassed at the melting point before subsequently raising the temperature for rapid evaporation; this has overcome the problem of obtaining gas-free metal.

The stability of the titanium evaporation in the getter-ion pump under discussion has permitted repeatable and reliable measurement of pumping performance. The practical design of such a pump has been recently described by Holland and Laurenson⁽⁷⁾ and the present report is mainly concerned with its pumping performance particularly in combination with conventional pumps.

Design and operation of titanium droplet pump

The apparatus used in the experiments on pumping performance is briefly described below.

Pump design. The getter pump shown in Fig. 1 is 24 in. long by 12 in. diameter with a side port of 9 in. diameter for connexion to a vacuum system. The pump contains the evaporation source, facilities for ionization and a hot filament for degassing the pump by electron bombardment. Stainless steel is used for the pump body with water-cooling coils brazed to the outside. The stainless-steel shell is argon arc-welded with internal welds or, where this is not possible,

with external welds with complete penetration of the wall to eliminate gas pockets. All of the vacuum seals are made with aluminium wire gaskets⁽⁸⁾ which are bakeable and the electrical lead-in electrodes are of the glass/metal or ceramic/metal type.

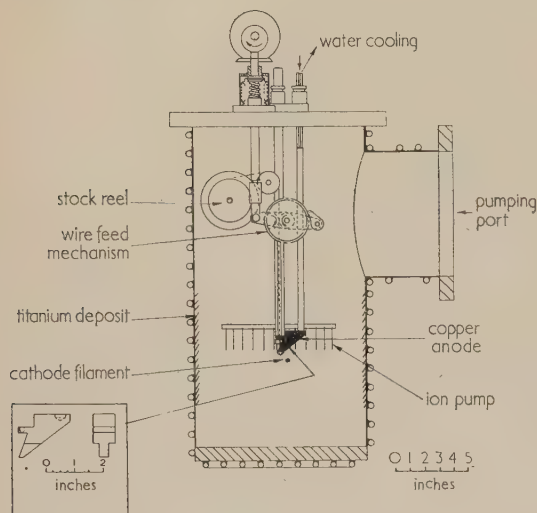


Fig. 1. Titanium droplet getter-ion pump

The evaporation source consists of a water-cooled copper anode, from which titanium is evaporated by electron bombardment. The electron emitter is made from 1 mm diameter tungsten wire bent into an arc so that it partly surrounds the protruding titanium wire. Titanium wire is fed down the side of the copper anode and into the electron stream by two knurled wheels driven through a metal bellows seal. The ionization electrodes surround the vapour source and consist of two concentric stainless-steel bands from which tungsten wires hang vertically. Both of the electrodes are positive with respect to the vapour source cathode which also supplies the electron stream for ionizing the residual gas. Positive ions formed in the residual gas can be trapped in the pump wall which serves as a negative electrode. The degassing filament is made of 1 mm diameter tungsten wire and is suspended below the ionization grids from separate lead-in electrodes.

One of the two cathode filaments is heated as desired using a 6 V, 80 A transformer with its secondary winding insulated for 14 kV from earth; this permits the cathode to be insulated from or connected to earth, as desired. Power for evaporation and degassing is obtained from a rectified h.t. supply giving a maximum output of 3 kV at 0.5 A; either the positive or negative side of this supply can be earthed. The output voltages of both the l.t. and h.t. supplies are controlled by Variac transformers in the mains input. The full h.t. power is used for degassing the pump by electron bombardment before titanium evaporation is commenced. High rates of evaporation up to 500 mg/min have been obtained with the droplet source, but a much lower evaporation rate of 50 mg/min with a power input of 450 W (applied potential of 800–1200 V) has been found to be the most which can be used in a 12 in. diameter pump. This is because the pump walls and components cannot be adequately cooled at high evaporation rates and therefore degas badly.

The getter pump is pre-pumped by a silicone oil diffusion pump (50 l/s) fitted with a liquid-air trap made of stainless steel and a high-vacuum isolation valve with a Fluon seating.

The pumping speed available at the getter-pump after baffling is 10 l/s. The pre-pumping system is capable of a blanked-off ultimate pressure of 10^{-8} mm of mercury and less than 10^{-7} mm of mercury when pumping the getter-ion pump after baking to degas.

Operation of the getter pump. The getter-ion pump is operated as follows. The pump shell is first connected to the positive side of the h.t. supply and electron-bombarded so that it reaches a temperature of about 400°C in three hours. After degassing, the liquid-air trap is filled and the getter pump is water-cooled. Titanium evaporation is commenced and continued until the desired pressure is reached. The vacuum can then be maintained by alternately evaporating the getter and operating the ionization source alone. In the experiments to be described, the effects of operating the ion source and vapour sources together and separately are considered.

Pressure and pumping-speed measurements. The gas pressure was measured with an Alpert-type ionization gauge connected to the blank-off plate on the pumping port. Pumping speeds were generally measured by determining the time for a fixed volume of gas at atmospheric pressure to pass into the pump with the pump pressure held constant. Low sorption rates such as those for ion pumping were determined from pressure/pumping-time curves.

Pumping performance

The pumping characteristics of a getter-ion pump are dependent on many factors, such as the rate of renewing the getter film, the nature of gas to be sorbed, etc., and these are related in a complex manner. The individual effects of a number of these operational conditions on the pumping mechanism and performance of the titanium pump have been investigated and are discussed below.

Metal droplet size and filament position

The relative position of the filament and copper anode determine the form assumed by the molten titanium bead and therefore in turn the rate of evaporation of the getter. The filament must be carefully positioned below and to one side of the copper anode as shown in Fig. 1 so that the feed wire is bombarded and becomes molten as it moves past the lower edge of the anode. If the filament is too near the edge of the anode where the feed wire appears, then the titanium wire may be bombarded and melted on the inclined plane of the anode and a satisfactory bead not obtained. Also, if the filament is too low under the anode the titanium bead on the end of the wire is mainly bombarded on its underside and the top of the droplet is insufficiently heated for the metal to flow onto the anode. Some of the possible forms assumed by the titanium droplet with different bombarding voltages are shown in Fig. 2.

Thermal radiation from the titanium droplet and positive ions from the metal vapour strike the cathode so that thermal emission of electrons may still occur when the low-tension

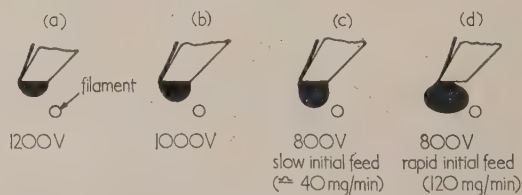


Fig. 2. Bead position at different voltages, and dependence of shape on feed rate (titanium wire 20 s.w.g.)

current to the filament is reduced. Also the negative space charge between the electrodes is partially neutralized by positive ions. The foregoing conditions can give rise to a self-sustained arc discharge unless the current output of the h.t. supply is limited. The power supply used here was fitted with a high-reactance transformer which limited the current flowing when the load impedance fell. With this system the applied voltage and electron current cannot be individually controlled by varying the supply voltage or the cathode emission temperature as in a thermionic diode, because the emission does not reach a saturated value. The applied voltage could, however, be adjusted independently of the current flowing by varying the size of the titanium droplet to change the gap between the anode and cathode filament.

When the titanium bead is near to the filament with a low applied voltage (about 800 V) the l.t. supply can be switched off once evaporation has commenced, but this is not done because movement of the bead by the feed wire causes the filament to cool.

If the titanium wire is fed slowly into the electron stream the metal globule produced gradually wets and spreads over the underside of the anode as shown in Fig. 2. The final size of the roughly hemispherical droplet is controlled by the bombarding voltage required. The lower the voltage, the larger the droplet and evaporation rate which can be obtained. When the titanium is fed slowly and the feed occasionally stopped and restarted, there is a tendency for the wire to shift laterally along the anode and this aids the wetting of the anode by the molten titanium. In fact, in the early stages of droplet growth, several small titanium beads sometimes become suspended from the anode. If the titanium feed rate is initially rapid, then a single bead tends to be formed on the wire which, because of absence of lateral movement, is anchored to the anode over a small area. This type of bead formation is unstable and usually occurs at low voltages as shown in Fig. 2(d).

Effect of power input on pumping speed for nitrogen

Electron bombardment potential. Tests have been made to study the effect of the vapour-source bombarding potential on the pumping speed. Comparative pumping-speed curves for nitrogen at 1200, 1000 and 800 V are given with the grid electrodes of the ionization system connected to and disconnected from the positive terminal of the h.t. supply. The pumping speeds have been plotted in terms of l/s which is the usual method with diffusion-type pumps and therefore permits a direct comparison of performance to be made.

It can be seen from Fig. 3 that the pumping speed varies inversely with the applied voltage whether the grids of the ionization system are at a positive or floating potential; the pumping speed is, however, always greater when the grid electrodes are at a positive potential. The increase in the pumping speed as the bombarding potential is reduced is due to the evaporation rate of the getter rising, as discussed above. The enhancement of the sorption rate of a getter when the gas is ionized by an electron stream has been the subject of much conjecture. Thus Gale⁽⁹⁾ observed that the sorption rate of a titanium film for active gases was increased by the ionizing effect of a Penning gauge and Holland and Harte⁽¹⁰⁾ found that the gas sorption rate was raised even though the getter surface repelled positive ions. Holland⁽¹¹⁾ has advanced the theory that the electron stream atomizes gas molecules which more readily diffuse between the grain boundaries of the film.

Although high pumping speeds can be obtained with a low bombarding potential it has been found that, with the

ionization grids connected, the pumping action falls off more rapidly as the pressure is increased than when a high potential is used. This is attributed to an increased proportion of the

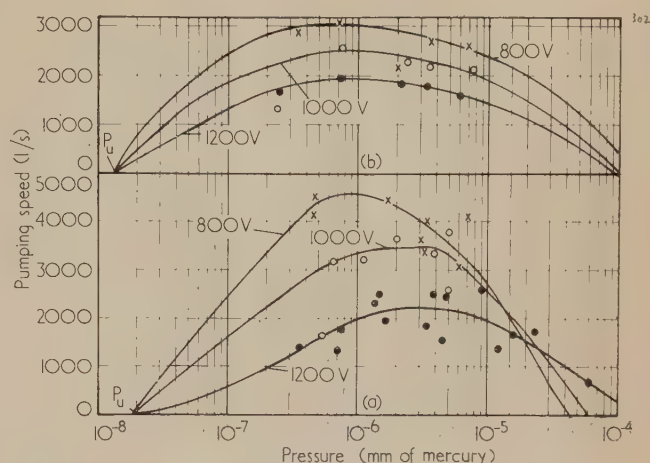


Fig. 3. Pumping speed of getter pump at different voltages for nitrogen with diffusion pump in operation (a) with (b) without ionization system

(P_u is the ultimate pressure obtained during continuous evaporation)

electron stream travelling to the ionization grids at the higher pressure (about 10^{-5} mm of mercury) which reduces the bombardment of the titanium bead and decreases the evaporation rate; the negative space charge between the filament and grids is more effectively neutralized at high pressure by positive ions. Even at a low pressure (less than 10^{-6} mm of mercury) 200 mA of the total bombarding current (500 mA at 800 V) flows to the ionization grids. When using low h.t. voltages the titanium bead becomes cold as the pressure rises above 10^{-5} mm of mercury. If the ionization grids are disconnected from the power supply the bead can be heated and pumping continued up to a pressure of 10^{-4} mm of mercury. Above the latter pressure, the bombardment again becomes unstable if the pump wall is negative because of the formation of a cold-cathode discharge. However, when used with the pump wall at a positive potential to avoid unstable discharges, the pumping speeds are low at pressures above 5×10^{-5} mm of mercury because the condensing metal film is rapidly saturated with gas.

H.T. power input. Tests were made to find how the power input to the evaporation source affected the sorption rate with the bombarding potential held as constant as was practical. The tests were done with the ionization grids connected to and disconnected from the h.t. supply. The curves in Fig. 4 show that raising the power input increases the pumping speed, presumably because the evaporation rate of the getter is greater. When the ionization system is in operation, it can be seen from Fig. 4(b) that the sorption rate is increased for each power input to the vapour source; some 200 W of the power input flowed to the ionization grids in each of these tests. Fig. 4(b) also shows that, when the power input is varied with a constant h.t. voltage of 800 V, the sorption rate is greater than for equivalent power inputs at 900 V, and this is in agreement with the results discussed in the previous section.

Pumping speeds for gases and mixtures of gases

Sorption rates were measured for a number of gases and gas mixtures with the getter-ion pump connected to and

isolated from the diffusion pump. The comparative sorption rates were obtained by opening the needle valve to admit a measured flow of gas and then observing the pressure readings

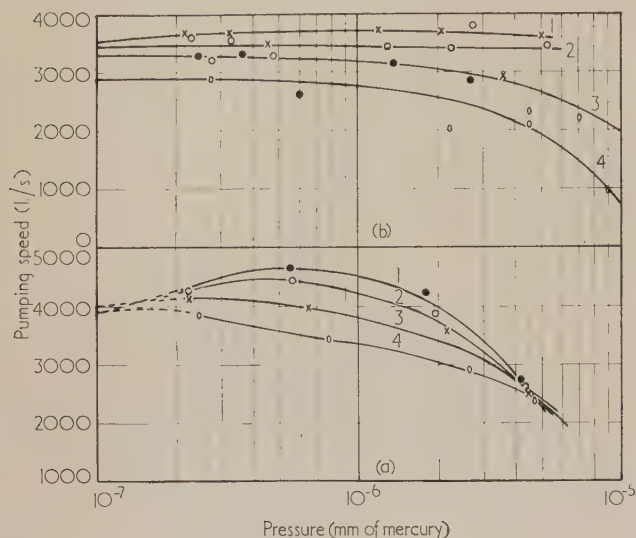


Fig. 4. Pumping speed of getter pump for nitrogen at fixed voltages and different power inputs (a) with (b) without ionization system

(Diffusion pump always in operation)

with the isolation valve both open and shut. This procedure avoided any slight variations of bead size, evaporation rate and condition of the getter film between two readings.

Fig. 5 gives the pumping speeds obtained for oxygen, nitrogen and hydrogen with a power input to the evaporation source of about 400 W (800 V, 500 mA). The upper curve for each gas was with the small oil diffusion pump in operation and the lower curve with the getter-pump isolated; the ionization system was used throughout. The curves in Fig. 5 show that, for each gas tested, the diffusion pump

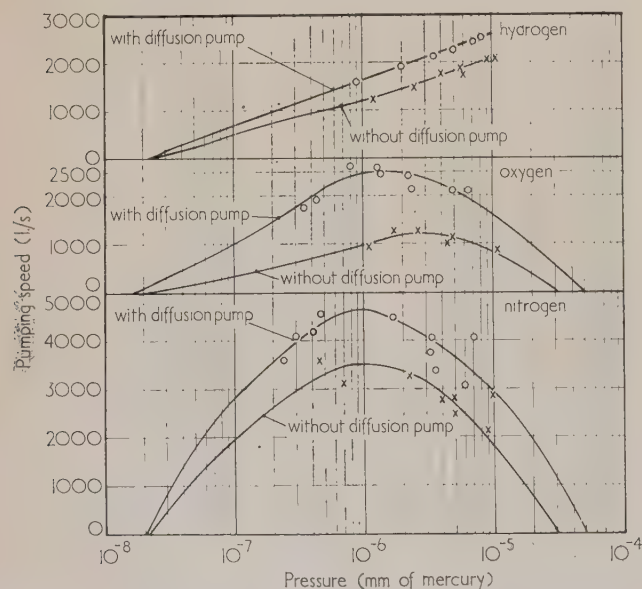


Fig. 5. Pumping speed curves for O_2 , N_2 and H_2 at an applied potential of 800 V both with and without the diffusion pump in operation

(All measured values corrected for ionization gauge sensitivity factors)

raised the pumping speed of the getter ion-pump out of proportion to its own baffled pumping speed (10 l/s). This effect has already been observed by the writers⁽⁷⁾ when measuring pumping speeds over a more restricted pressure region than that considered here. It is believed that the enhancement of the pumping speed arises from the diffusion pump removing certain gases from the getter-ion pump. The effect and nature of these gases is as follows:

- (1) Certain gases, such as the inert type, are slowly sorbed so that when present in gas mixtures or as impurities in other gases their equilibrium pressure in the pump can be very high compared with their partial pressure in the gas being admitted. This produces the overall effect of a low pumping speed for the gas being admitted.
- (2) It has been shown that hydrocarbon vapours tend to be formed in getter-ion pumps by reaction between hydrogen and carbon present in the metal being evaporated. Such hydrocarbons would become unsaturated by bombardment of the electron stream and strongly chemisorbed to the getter surface where they could hinder the sorption of other gases.

Pumping speed for air. The pumping speed of the getter-ion pump for air is shown in Fig. 6. These pumping speeds

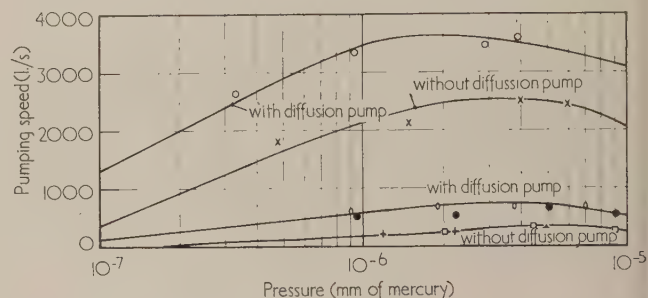


Fig. 6. Pumping speed curves for mixtures of: 80% N_2 , 20% O_2 ($= O, X$); 1% A, 99% N_2 ($= O, \square$) and air ($= \bullet, +$) at an applied potential of 800 V

are low compared with those obtained for pure oxygen and nitrogen. To find the reason for this, a mixture of oxygen and nitrogen in the proportions present in air was prepared, and the pumping speeds measured for the mixture. It can be seen from Fig. 6 that the curve for the pumping speed of the mixture is the mean of the pumping speed curves given in Fig. 5 for pure oxygen and nitrogen. Atmospheric air is exhausted at only a fraction of the speed of the nitrogen/oxygen mixture, presumably because of the presence of inert gases which comprise 0.933% of the total composition. Most of the inert gas is argon (0.93% of total air composition) and so a mixture of 1% argon in nitrogen was prepared and the pumping speeds again measured. The results obtained with this mixture were identical with those obtained for atmospheric air. From this it can be inferred that the partial pressure of argon in the pump was high because of its low sorption rate and this lowered the apparent pumping speed of air. The difference between the pumping speeds measured for air with the getter pump being exhausted and isolated from the diffusion pump has already been attributed by the writers⁽⁷⁾ to the partial pressure of argon in the getter-ion pump being reduced by the diffusion pump.

The effect of the poorly sorbed inert gas on the measured pumping speed is as follows. The volumetric pumping speed

is expressed as: $S = (M_X + M_I)/P_m$, where M_X and M_I are the respective rates in terms of $1 \mu/s$ at which the active and inert components flow into the pump and P_m is the total apparent pressure—measured by the ion gauge. If the gauge sensitivity factors for the gas components are similar and can be ignored then $P_m = P_X + P_I$, where P_X and P_I are the partial pressures of the components. For equilibrium in the pump: $M_X = S_X P_X$, and $M_I = S_I P_I$.

If, for example, the conditions in the isolated getter-ion pump when exhausting air are considered, the pumping speed for the oxygen/nitrogen components of the air is $S_X = 2500 \text{ l./s}$ and for argon a mean speed of $S_I = 2.3 \text{ l./s}$. Now air contains 0.93% of argon so that the apparent pumping speed S is $\frac{99.07 + 0.93}{(99.07/1500) + (0.93/2.3)}$, or 212 l./s , which is in fair agreement with the measured speed for air of 180 l./s .

If the pumping speed is now increased by a diffusion pump by only a small amount, this can have a pronounced effect on the apparent pumping performance of the getter-ion pump. Thus, in the example considered here, the diffusion pump raises the pumping speed of the nitrogen/oxygen mixture to 3600 l./s presumably because of the removal of unknown impurities, whereas the speed for argon with both the ion and diffusion pumps operating was 4.4 l./s . The new value for S would then be $\frac{99.07 + 0.93}{(99.07/3600) + (0.93/4.4)}$, or 403 l./s .

Thus, if the rate of pumping an inert gas is increased by only a small amount by, for example, raising the ion-pumping speed or using an auxiliary diffusion pump, then the apparent pumping performance for air is greatly improved.*

Pumping performance of Calor-gas/nitrogen mixtures

The effect of hydrocarbon gases on the pumping performance of the getter-ion pump was examined using Calor gas and mixtures of Calor gas and nitrogen. Calor gas is a mixture of butane (78–84%), propane (15–20%) and butine (1–2%). Nitrogen was chosen as the second component of the mixture because it had a high pumping speed and the influence of the hydrocarbon gas would be more easily measured. Fig. 7 shows the pumping-speed curves obtained for pure Calor gas and gas mixtures containing 5%, 10% and 50% Calor gas in nitrogen. Measurements were made with the getter-ion pump isolated and connected to the diffusion pump. The pumping speed of the getter-ion pump for pure Calor gas was exceedingly low and not greatly increased when the diffusion pump was in operation. The values plotted in Fig. 7 for the gas mixtures are based on ionization-gauge readings corresponding to equivalent nitrogen values. The inset curve for pure Calor gas has been derived from corrected ionization-gauge readings; the gauge sensitivity for Calor gas was determined and found to give an ion current 3.7 times that for nitrogen at the same pressure.⁽¹²⁾

It is difficult to decide conclusively from Fig. 7 whether the reduction in the pumping speed for nitrogen occurs because the gettering rate has been reduced by adsorbed

hydrocarbons or because the Calor gas component has a high partial pressure in the pump resulting from its low rate of removal. Unfortunately, the pumping-speed curves

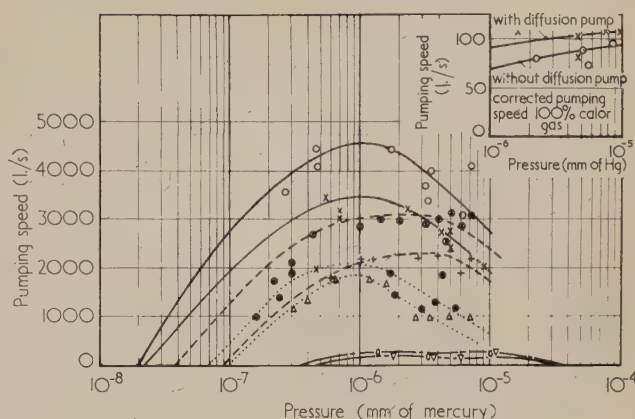


Fig. 7. Effect of the presence of Calor gas on the pumping speed of nitrogen with getter-ion pump operated at 800 V (Pressure and pumping speeds are based on nitrogen equivalent values. Inset graph: corrected speeds for 100% Calor gas)

— = pure N_2 ; \circ = with diffusion pump; \times = isolated; — — — = 5% Calor gas, 95% N_2 ; \otimes = with pump; + = isolated; . . . = 10% Calor gas, 90% N_2 ; \bullet = with pump; \triangle = isolated; - - - - - = 50% Calor gas, 50% N_2 ; \circ = with pump; ∇ = isolated

cannot be so easily analysed as those for argon/nitrogen mixtures discussed in the previous section. This is because the composition of the gas mixture in the getter pump not only differs from that of the inlet gas as a result of selective pumping of the components, but also undergoes changes as the hydrocarbon molecules are dissociated by electron bombardment. In fact, it became extremely difficult to obtain consistent results as the concentration of Calor gas was increased. The pumping performance obtained under these conditions is probably influenced by the degree to which the pump has been contaminated by decomposed hydrocarbon layers which are deposited on the electrodes of the ionization system. However, it is reasonable to suppose that hydrocarbon impurities, unlike inert-gas impurities, will effect the gettering rate of chemically active gases. Thus Stow⁽¹³⁾ has recently reported that an evaporated titanium film has a reduced sorption rate if contaminated by diffusion pump oil vapour.

Pump down curves for nitrogen and oxygen

Pump-down curves for nitrogen and oxygen with the getter-ion pump isolated from the diffusion pump were taken after repeatedly admitting gas to raise the pressure, as shown in Figs. 8 and 9. These results were obtained by quickly admitting gas to obtain the required starting pressure and then shutting the inlet valve and observing the pump-down cycle. During the pressure rise and fall the pump was operated at 800 V and 500 mA so that the getter was being evaporated. When the pressure had fallen to an asymptotic value, the evaporation was discontinued by reducing the power input to 500 V at 180 mA so that only the ionization system was in operation.

It can be seen that for nitrogen the initial pressure has little effect on the rate at which the ultimate pressure is re-attained, but for oxygen the higher the initial pressure the lower is the rate at which the pressure is subsequently reduced. One would expect oxygen to be pumped as readily by the

* Since this was printed Kumagai *et al.* (*Advances in Vacuum Science and Technology*, Vol. I, p. 433, London: Pergamon Press, 1960) have reported that they found that a diffusion pump greatly increased the pumping speed of a titanium pump for tank oxygen and assumed that this was due to inert gas impurities in the tank gas. The tank gases (O_2 , H_2 , N_2) used by us were free from inert gases but organic gas impurities would be generated within the pump.

freshly condensing metal as nitrogen. It is believed that the apparently slow pumping rate arises from oxygen combining with the titanium to form a lower oxide which poorly sorbs

assumed that the pumping speed of argon is independent of pressure, which is normally the case for ionization pumping of inert gases, then the sorption rate can be found from the pressure-time curves in Fig. 10 using the expression:

$$S = \frac{C}{t_2 - t_1} \log_e \frac{P_1 - P_s}{P_2 - P_s}$$

where S is the pumping speed; C the volume of the getter-ion pump chamber; P_s the ultimate pressure; and $(t_2 - t_1)$ the

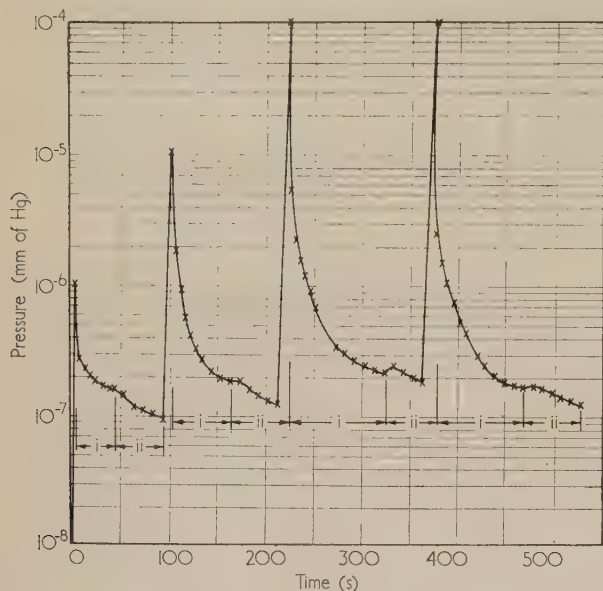


Fig. 8. Nitrogen pump-down curves from successively higher pressures
(Diffusion pump not in operation)

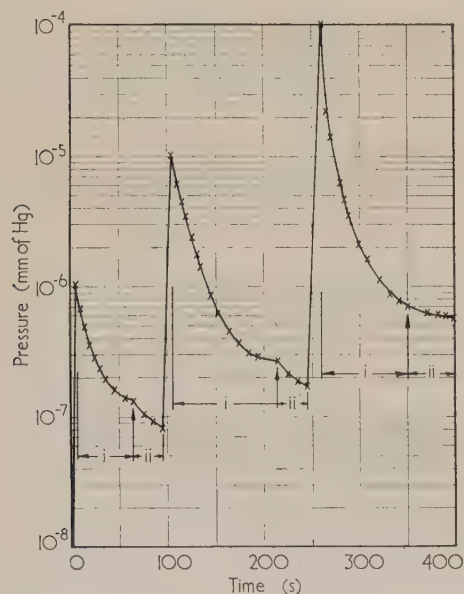


Fig. 9. Oxygen pump-down curves from successively higher pressures
(Diffusion pump not in operation)

impurity gases such as the hydrogen liberated from the molten titanium and metal fittings.

Ion-pumping argon

Pump-down curves were measured for argon with and without the diffusion pump open to the getter-ion pump. The power input to the getter-ion pump was 1 kV at 500 mA so that titanium was evaporated during the tests. If it is

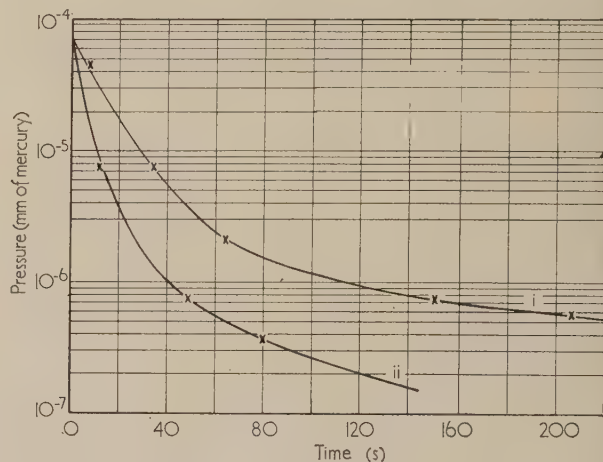


Fig. 10. Pump-down curves for argon with continuous evaporation (a) with (b) without diffusion pump

time for the pressure to change by the amount $(P_1 - P_2)$. Pumping speeds obtained for argon by this method are shown in Table 1.

Table 1. *Pumping speeds for argon*

Pressure 10^{-3} mm (of Hg)	Ti-evap. + ion pump (l./s)	Ti-evap. + ion pump + diffusion pump (l./s)
0.04 - 0.06	3.2	10.0
0.01 - 0.02	2.5	7.5
0.004 - 0.006	2.3	4.3
0.001 - 0.002	0.92	2.5

This method of determining pumping speeds could not be used with the active gases because they were pumped at high rates and the pressure measurements were influenced by the gauge tabulation.

General discussion

The getter-ion pump described here gives an ultimate pressure of 10^{-8} and 5×10^{-9} mm of mercury when used with the small diffusion pump fitted with a liquid-nitrogen trap. This performance is obtained when evaporating from a large droplet of titanium which has been thoroughly degassed by pre-heating. Thus it is improbable that hydrogen evolution from the commercially obtained titanium wire is responsible for the ultimate gas pressure. It is believed that the ultimate pressure is at present limited by degassing from the feeder mechanism of the vapour source which cannot be baked sufficiently to outgas the components completely. Further work on the getter-ion pump is directed towards lowering the degassing rate of the vapour source by mounting the feeder mechanism in a separately exhausted cell.

In Table 2, the performance of the getter-ion pump is shown for a range of gases expressed in terms of pumping

speed per unit area of titanium condensate. The rate of evaporation was 40 mg/min from a titanium bead of about 1.4 g weight and the condensate area 3400 cm², so that the film had a growth rate of about 4 Å/s. Also given in the table is the sorption coefficient α which is related to the measured pumping speed per unit area (S_m) by $S_m = \alpha S_0$, where S_0 is the volumetric rate at which gas impinges on unit area of the getter. It has been shown that the sorption rate of the continuously forming getter for nitrogen is enhanced by the ionization (atomization) of the gas molecules. The degree to which the gas molecules had been activated or dissociated by the ionizing stream was not known, and it is possible that a more efficient ionization system, for example, a Penning type, would further raise the sorption coefficient. Hydrogen was found to have a low sorption coefficient in the getter-ion pump although experiments on static evaporated titanium films showed it had a similar sorption rate to nitrogen and oxygen.⁽¹⁰⁾ Values of α derived from the results of Holland and Harte for titanium films activated with a Penning system are given in Table 2. These values are low compared with those for continuous evaporation because the static deposit was partially saturated by gas when the measurement was taken (one minute after preparation).

Table 2. *Pumping speed of getter-ion pump for active gases* (measured with a titanium condensation rate of 0.2 $\mu\text{g cm}^{-2} \text{s}^{-1}$)

Gas*	Continuous evaporation		Static film ⁽¹⁰⁾	
	S_m^\dagger ($\text{l. s}^{-1} \text{cm}^{-2}$) ($P = 10^{-6} \text{ mm of Hg}$)	Sorption coefficient α	S_m ($\text{l. s}^{-1} \text{cm}^{-2}$) ($P = 10^{-5} \text{ mm of Hg}$)	Sorption coefficient α
Oxygen	0.72	0.068 (0.10)‡	0.059	0.0056
Nitrogen	1.35	0.12 (0.12)‡	0.065	0.0057
Hydrogen	0.49	0.012 (0.037)‡	0.053	0.004
Calor	0.27	—	—	—

* All pressure readings corrected for gauge sensitivity factor.

† Auxiliary diffusion pump in operation.

‡ Values calculated from results of Davis and Divatia.⁽⁴⁾

There are several possible explanations for the low sorption coefficient of hydrogen and the following are under consideration:

- (i) The low sorption coefficient may arise from the condensing metal atoms momentarily producing a high temperature at the outer film surface which inhibits the hydrogen adsorption (that is, the initial stage before diffusion in the film) of the impinging hydrogen molecules; the metal atoms arrive at about twice the rate of hydrogen molecules at 10^{-6} mm of mercury gas pressure. The oxygen and nitrogen would not be affected in this way because they tend to form stable chemical compounds with the titanium film.
- (ii) The sorption coefficient of nitrogen was found to be increased by operation of the ionization system, but a similar test has not yet been made with hydrogen. However, the degree to which hydrogen is ionized at

a given pressure by an electron stream is less than that for oxygen or nitrogen (the positive ion current for hydrogen compared with nitrogen under similar conditions is in the ratio 1 : 2.5). Thus, although at a given pressure many more hydrogen than nitrogen molecules impinge on the getter surface per unit time, a smaller percentage of the hydrogen molecules are activated by the ionization system.

- (iii) The titanium evaporant contained a small quantity of carbon (less than 0.1%) and this could have combined with the inflowing hydrogen to form methane which was poorly sorbed by the film. Klopfer and Ermrich⁽¹⁴⁾ found that methane was produced in a small titanium pump from the hydrogen and carbon in the evaporant. The writers could degas and remove hydrogen from their titanium but the carbon impurity only evaporated at the evaporation temperature of the titanium. At the evaporation rate used here the amount of carbon volatilized would be sufficient to produce one litre-micron/second of methane if all of the carbon reacted with hydrogen.

References

- (1) HOLLAND, L. *J. Sci. Instrum.*, **36**, p. 105 (1959).
- (2) HERB, R. G., DAVIS, R. H., DIVATIA, A. S., and SAXON, D. *Phys. Rev.*, **89**, p. 897 (1953).
- (3) HERB, R. G. *Vacuum*, **9**, p. 97 (1959).
- (4) DAVIS, R. H., and DIVATIA, A. S. *Rev. Sci. Instrum.*, **25**, p. 1193 (1954).
- (5) HOLLAND, L., LAURENSEN, L., and HOLDEN, J. T. *Nature*, **182**, p. 851 (1958).
- (6) HOLLAND, L., and LAURENSEN, L. *Symp. Electron Bombardment Heating*, 1959 (Services Electronics Research Laboratory, to be published).
- (7) HOLLAND, L., and LAURENSEN, L. *Le Vide*, **81**, p. 141 (1959).
- (8) HOLDEN, J. T., HOLLAND, L., and LAURENSEN, L. *J. Sci. Instrum.*, **36**, p. 281 (1959).
- (9) GALE, A. J. *C.V.T. Vacuum Symposium Trans.*, p. 12 (London: Pergamon Press, 1956).
- (10) HOLLAND, L., and HARTE, A. *Intern. Symp. Residual Gases in Electron Tubes and Related High Vacuum Systems, Como September 1959* (London: Pergamon Press, to be published).
- (11) HOLLAND, L. *Intern. Symp. Residual Gases in Electron Tubes and Related High Vacuum Systems, Como September 1959* (London: Pergamon Press, to be published).
- (12) ELSWORTH, L. *Vacuum*, to be published.
- (13) STOW, R. L. *Nature*, **184**, p. 542 (1959).
- (14) KLOPFER, A., and ERMIRICH, W. *Advances in Vacuum Science and Technology*, Vol. 1, p. 427 (London: Pergamon Press, 1960).

Numerical investigation of a range of unipotential electron lenses

by J. VINE, M.Sc., Associated Electrical Industries (Woolwich) Ltd., Harlow Research Laboratories, Harlow, Essex

[Paper first received 6 April, and in final form 17 May, 1960]

Abstract

An electronic digital computer has been applied to the computation of focal lengths and spherical aberration constants of unipotential lenses, utilizing field data obtained from a resistance network analogue.

Results obtained are presented in graphical form and shown to be in good agreement with published experimental results, but not, in the case of spherical aberration constants, with results based on analytical approximation to the axial potential distributions.

The sources of error in the computations are discussed, and the accuracy of the results estimated.

Introduction

THE three-aperture electron lens, of which the unipotential lens is a special case, finds application in microscopes and cathode-ray tubes. Its properties have been studied both experimentally, for example, by Liebmann,⁽¹⁾ and by Lippert and Pohlitz,⁽²⁾ and by the use of theoretical approximations to its potential distribution, as by Regenstreif⁽³⁾ and Archard,⁽⁴⁾ but no systematic investigation has been made by numerical ray tracing, as has been done for magnetic lenses by Liebmann and Grad⁽⁵⁾ and Liebmann.⁽⁶⁾ The tediousness of such ray tracing has now been considerably reduced by the application of an electronic digital computer, and this paper presents results which have been obtained for a range of unipotential lenses, and compares them with results obtained by other methods.

To confine the present investigation the simple electrode geometry shown in Fig. 1 was chosen, and consideration given to variation of the two geometrical parameters S/D , T/D . A similar arrangement has been used by Archard, and by

Lippert and Pohlitz, and its choice therefore provides the added interest of comparison with their theoretical and experimental results.

Field measurements and trajectory computation

The axial field distributions of the chosen range of lenses were investigated by means of a resistance network, the equipment used being essentially that described by Liebmann,⁽⁷⁾ modified by the incorporation of a "reflecting plane" near the right-hand edge of the fine-mesh region whose z dimension is thereby effectively nearly doubled when applied to r, z problems having additional symmetry about a plane perpendicular to the axis. Such a plane of symmetry, parallel to one of the co-ordinate axes, can be introduced into any Laplacian network of orthodox rectangular meshes by simply doubling all resistor values lying along the line in which the plane is to intersect the network, and disconnecting resistors perpendicular to this line on the unwanted side of it.

Fig. 2 illustrates the method adopted to enable the r, z

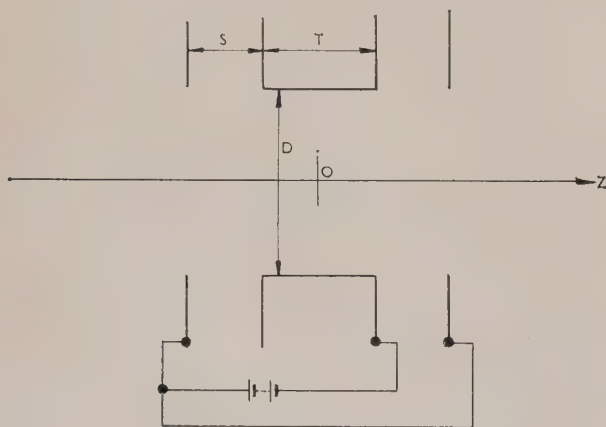


Fig. 1. Unipotential lens
Geometry symmetrical about $z = 0$

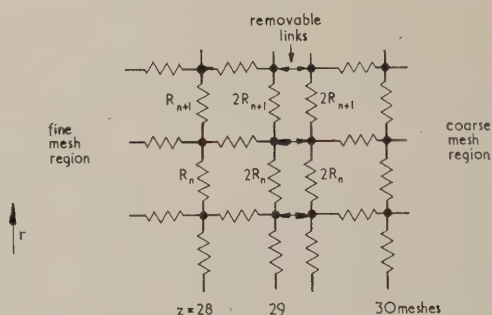


Fig. 2. Introduction of a reflecting plane into an r, z network
Links in: normal operation

$z = 30$ is boundary between fine and coarse mesh regions
Links out: operation in fine mesh region with plane of symmetry at $z = 29$

network in question to be used either in its normal condition (links inserted) with a fine mesh region extending over $z = \pm 30$ or, as in the present application (links removed) with the reflecting plane at $z = +29$, providing, effectively, 118 unit meshes in the z direction. In either case, the coarse surround increases the total z dimension by 120 units. The system of removable links ensures reliable connexions and allows rapid conversion from one condition to the other.

The lens models were set up on the network with a radius R of 10 meshes, and axial potential values ϕ were read to five decimal places, over the region from lens centre (reflecting plane) to the point where the value 0.98 was exceeded (relative to 1.0 on the outer electrodes and zero on the centre electrode). About 35 to 40 measurements were

involved for each lens. The limit $\phi < 0.98$ is arbitrary, and its likely effect on the derived lens constants is discussed later.

To detect network faults or mistakes in measurements third-order differences were calculated for each potential distribution. Any gross irregularities shown up by this process were investigated and the necessary corrections made.

Trajectories were computed by integration of the ray equation using the method of Liebmann,⁽⁸⁾ adapted for application of an electronic computer.⁽⁹⁾ For a given set of initial conditions, namely the radial co-ordinate r_1 and the direction r'_1 of the electron at a specified position z_1 , the method provides the paraxial solution r, r' and also the small deviations from this $\Delta r, \Delta r'$, arising from third-order aberrations. Two independent rays were computed for each lens, ray 1 starting parallel to the axis and a small distance from it, and ray 2 starting on and at a small angle to the axis. Starting and finishing points of the computation were symmetrically disposed ($\mp z_1$) about lens centre, and close to the edges of the chosen field region.

Results

Paraxial properties. The focal length of interest is that relevant to the application of the lens as an electron-microscope projector. If a ray starting at $z = -z_1$, parallel to the axis, reaches $z = z_2$ with slope r'_2 , this focal length f is given by

$$f = r_1/r'_2 \quad (1)$$

provided z_1 and z_2 are both large, so that practically the entire lens field is included.

In the present work, $z_2 = z_1$ to maintain symmetry. The results for ray 1 have been used to give f directly from equation (1), and the principal plane co-ordinate z_p from

$$-z_p = z_1 + \frac{r_1 - r_2}{r'_2} \quad (2)$$

The geometry of equations (1) and (2) is illustrated in Fig. 3.

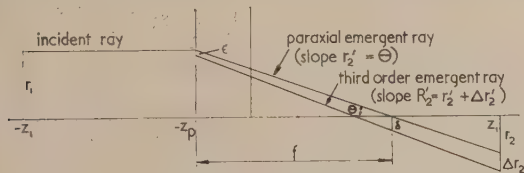


Fig. 3. Derivation of lens constants from results for ray 1

Because of the symmetry of the lens about the plane $z = 0$, its paraxial properties are completely determined by computation of one ray. The results for ray 2 can therefore also be used to calculate f and z_p , as a check on accuracy. This was done, and corresponding values of f were found to agree to within 0.1%.

The results for f and z_p are summarized in Figs. 4 and 5 respectively, where curves of f/D and z_p/D against T/D are plotted for three values of S/D . The focal-length curves are similar in form to those given by Archard⁽¹⁰⁾ and show as do his a minimum focal length of about $0.9D$. For closer comparison, Fig. 6 reproduces a graph given by Archard⁽¹¹⁾ comparing his results with experimental values obtained by Lippert and Pohlitz. This shows contours of constant h/f against co-ordinates $T/h, D/h$, where $h = 2S + T$. The present results for those lenses falling within the range of the graph have been plotted as isolated points, the positions of which are seen to be reasonably consistent with the contours.

Spherical aberration. The definition of the spherical aberration constant C_s is illustrated in Fig. 3. If δ is the radial displacement from the paraxial focus, of a ray incident parallel to the axis, and θ is the angular aperture at the paraxial focus, then

$$\delta = C_s \theta^3 \quad (3)$$

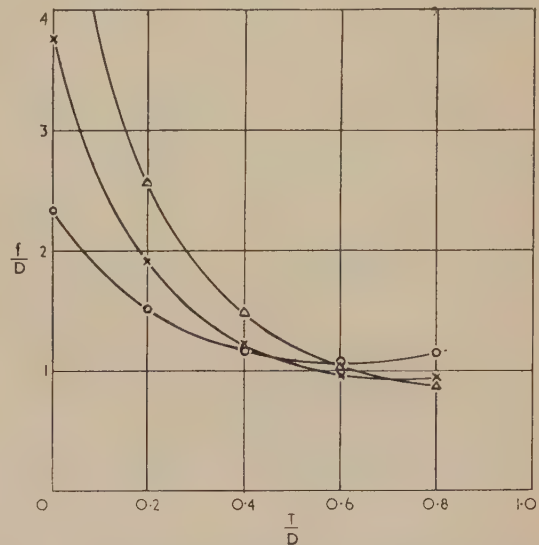


Fig. 4. Curves for focal length as a function of lens parameters

- Δ $S/D = 0.4$
- \times $S/D = 0.6$
- \circ $S/D = 1.0$

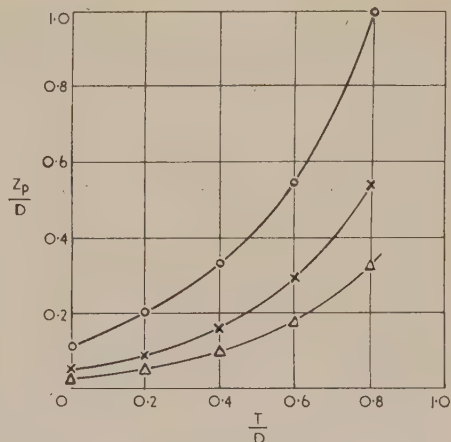


Fig. 5. Position of principal plane z_p/D as function of lens parameters

- Δ $S/D = 0.4$
- \times $S/D = 0.6$
- \circ $S/D = 1.0$

In terms of the results for ray 1, δ is given by

$$\delta = \Delta r_2 - \frac{r_2}{r'_2} \Delta r'_2 \quad (4)$$

where $\Delta r_2, \Delta r'_2$ are the third-order deviations from the paraxial solution r_2, r'_2 at $z = +z_1$. The constant C_s may thus be obtained from equation (3) where $\theta = r'_2$. The results of ray 2 do not provide a check on accuracy in this

case because the constant C_s is restricted to the particular lens conjugates implied in its definition.*

The results for special aberration are given in Figs. 7(a) and 7(b), the former showing curves of C_s/D against T/D

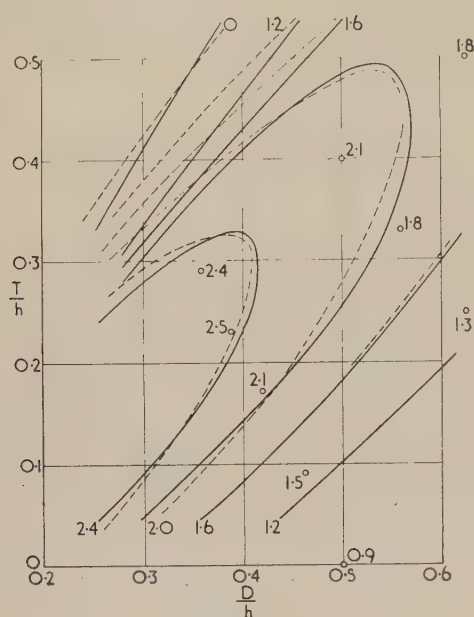


Fig. 6. Contours of h/f

Comparison of results with theoretical values of Archard (broken contours) and experimental values of Lippert and Pohlit (full contours)

$$h = 2S + T$$

and the latter C_s/f against T/D , for different values of S/D . Comparison with Fig. 6 shows that, for each value of S/D , minimum aberration occurs at the value of T/D giving also minimum focal length. Figs. 7(a) and 7(b) also show for the cases $S/D = 0.6$ and 1.0 , curves calculated by Archard⁽¹⁰⁾ from the theoretical treatment of Regenstreif. There is agreement on the form of the curves and the position of the minima, but a discrepancy factor of 2-3 is apparent in respect of actual values at any point, Archard's curves suggesting lower aberrations than are indicated by the numerical computation. On the other hand, there is again good agreement with experimental results. Fig. 8 shows the numerically derived values plotted against Lippert and Pohlit's contours of constant C_s/h . If allowance is made for the slow variation of C_s/h in the region where the curves loop back, discrepancies between the two sets of results appear to be only about 25%, which is very satisfactory.

Consideration of errors

To provide an indication of the accuracy of the results presented above it is appropriate to describe, and discuss briefly, the possible sources of error.

Truncation errors in the field determination. The effects of mesh size, and of sharp corners on the electrodes, were considered by Liebmann and Grad in their study of magnetic lenses. By carrying out computations with three model sizes, $R = 5, 10$ and 20 meshes for the same lens, they showed

* Ray 2 in fact supplies additional information and may be used in conjunction with ray 1 to determine completely the third-order aberration properties of the lens for non-skew rays. This is possible because of the symmetry about $z = 0$, without which it would be necessary to compute four independent rays.

that truncation errors were negligible for the case $R = 10$. It has been assumed that this applies also to the unipotential lenses, and no direct check was considered necessary.

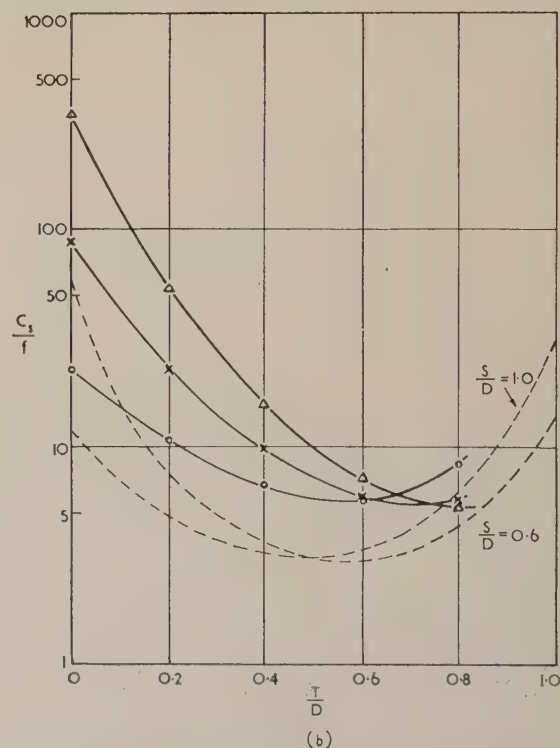
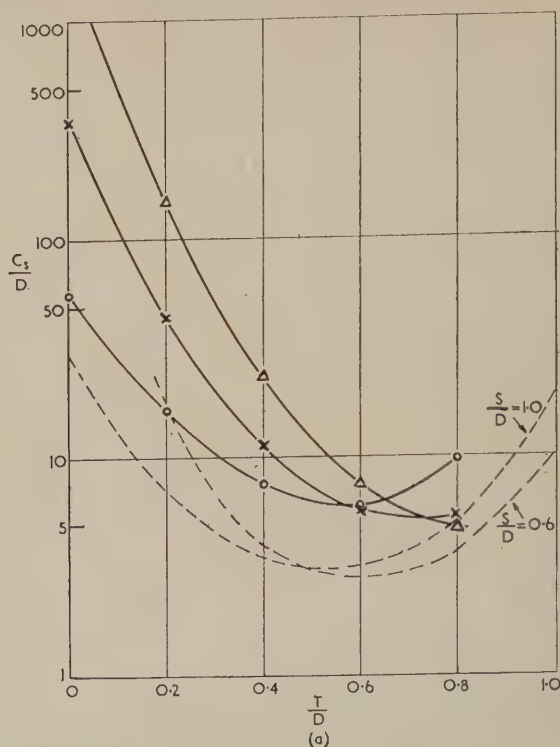
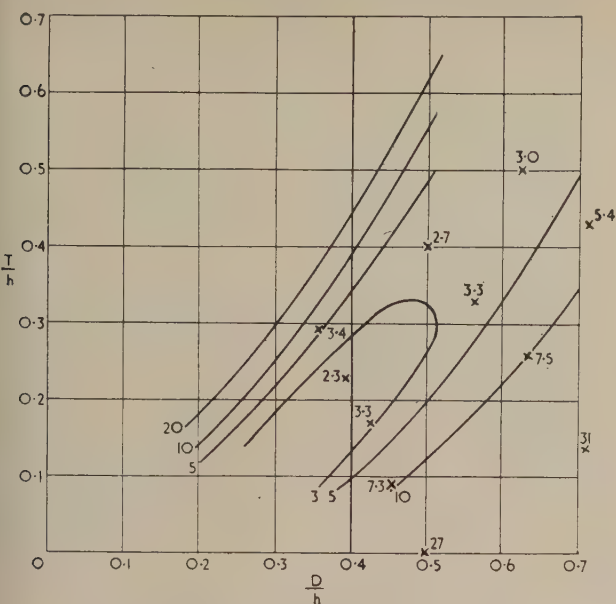


Fig. 7. Spherical aberration as a function of lens parameters

(a) C_s/D (b) C_s/f
 Δ $S/D = 0.4$
 \times $S/D = 0.6$
 \circ $S/D = 1.0$

(broken lines are theoretical curves given by Archard)



Comparison of results with experimental curves of Lippert and Pohlit

$$h = 2S + T$$

distribution, because resistance values drifted with age outside their tolerance limits. These errors produce irregularities in the third-order differences: to ascertain the effect of these, the distribution for the lens $S/D = 0.6$, $T/D = 0.6$, was smoothed, and complete computations were carried out using both the smoothed and the unsmoothed values. The results obtained are shown in Table 1.

	f	C_s
Unsmoothed potentials	0.99200	5.8219
Smoothed potentials	0.99204	5.8223

In view of the similarity of the two sets of results, not altogether expected in the case of C_s , where third- and fourth-order differences form quite important terms, it appears that preliminary smoothing, before ray-tracing, is unnecessary.

Effect of the field in the region $\phi > 0.98$. For the purpose of ray tracing, only the central portion of the lens field, where $\phi \leq 0.98$ was used, the end regions $\phi > 0.98$ being ignored. To ascertain the effect of these end regions on the derived lens constants, three separate computations were carried out for the lens $S/D = 0.6$, $T/D = 0.2$, using field regions of differing extent, defined by the limiting values for ϕ of 0.95, 0.98 and 0.99. The results are summarized in Table 2.

Field region	$z_{\overline{p}}$	f	C_s
$\phi \leq 0.95$	0.113	1.803	33.7
$\phi \leq 0.98$	0.085	1.860	43.3
$\phi \leq 0.99$	0.073	1.868	45.9
$\phi \leq 1.00$	0.06	1.88	48.0

(by extrapolation)

The inclusion of a greater extent of field is seen to lead to an increased focal length, a marked decrease in lens thickness as measured by the principal-plane separation, and an increased spherical-aberration constant. The last line in the table represents results for the infinite-field region, obtained by extrapolation, and it appears that the errors introduced by considering only the field region $\phi \leq 0.98$ are likely to be of the order of 1% for focal length, and 10% for C_s . This, however, is an academic consideration, since the infinite-field region could never be used in practice.

Accuracy of the trajectory computation. To ensure correctness of the computer programming, and to assess the accuracy of the computational method, use was made of the analytical solution of the ray equation given by Regenstreif.⁽³⁾ The lens constants were computed for a parabolic potential distribution, approximating to the central region of a moderately strong unipotential lens, and compared with values obtained analytically from the Regenstreif theory. The numerical work was carried through with two different step lengths h , and the results are shown in Table 3.

	Numerical		
	$h = 0.05$ (24 steps)	$h = 0.025$ (48 steps)	Analytical
f	1.08173	1.08169	1.08168
C_s	1.55	1.59	1.63

For the larger value of h , which corresponds most closely to the step length used in computing the majority of the results presented in this paper, the error in C_s is about 5% while the discrepancy in focal length is negligible.

Conclusions

The most important factor affecting the accuracy of results is the omission of the end regions of the field. There would appear to be no point in attempting, by refinement of network or computational techniques, to obtain results of greater accuracy, except perhaps in connexion with a particular application when the extent of the lens field to be utilized could first be precisely defined. For general purposes the accuracy of the results presented here is adequate, the probable errors being of the order of 1% for focal length and 10% for spherical aberration constant.

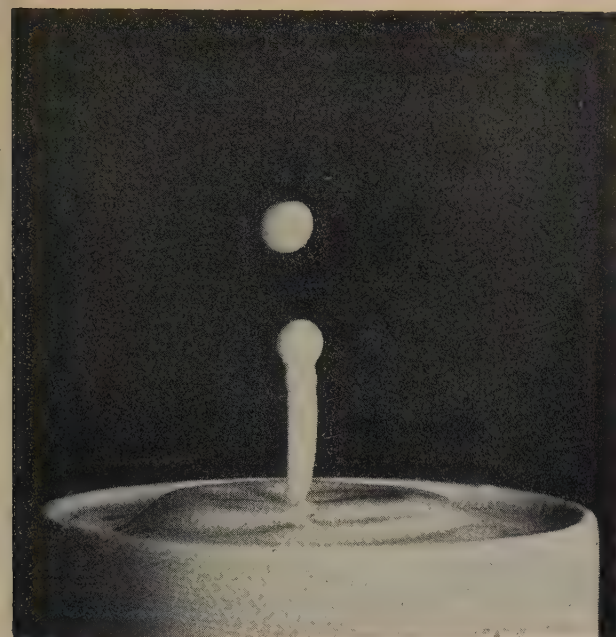
References

- (1) LIEBMANN, G. *Proc. Phys. Soc. B*, **62**, p. 213 (1949).
- (2) LIPPERT, W., and POHLIT, W. *Optik.*, **9**, p. 456 (1952); **10**, p. 447 (1953); **11**, p. 181 (1954).
- (3) REGENSTREIF, E. *Ann. Radioelect.*, **6**, p. 51 and p. 114 (1951).
- (4) ARCHARD, G. D. *Brit. J. Appl. Phys.*, **7**, p. 330 (1956).
- (5) LIEBMANN, G., and GRAD, E. M. *Proc. Phys. Soc. B*, **64**, p. 956 (1951).
- (6) LIEBMANN, G. *Proc. Phys. Soc. B*, **65**, p. 94 (1952).
- (7) LIEBMANN, G. *Journées Internationales du Calcul Analogique, Proceedings*, p. 346, Fig. 22 (Brussels: Presse Académie Européenne, 1956).
- (8) LIEBMANN, G. *Proc. Phys. Soc. B*, **62**, p. 753 (1949).
- (9) VINE, J. *The Computer Journal*, **2**, p. 134 (1959).
- (10) ARCHARD, G. D. *Assoc. Elec. Ind., Research Report A752*, Figs. 10 and 27.
- (11) ARCHARD, G. D. *Assoc. Elec. Ind., Research Report A462*, Fig. 2.

Contents

	PAGE		PAGE
<i>Aerodynamics, propulsion systems, flow and mechanics</i>		<i>Nuclear and cosmic-ray physics, apparatus, techniques and data (continued)</i>	
Advanced propulsion systems	413	Unprocessed and processed radio-isotope preparations and special radiation sources	422
Deformation, strain and flow: An elementary introduction to rheology	413	Nuclear reactor materials	422
High-speed aerodynamics and jet propulsion. Vol. 5. Turbulent flows and heat transfer	414	Penetration of charged particles in matter	423
Hypersonic flow	414	Physikalische Kernchemie	423
Non-Newtonian fluids	414	Plasma physics and thermonuclear research. Vol. I	423
Progress in solid mechanics. Vol. I	414	Radiation hygiene handbook	423
Rheology. Theory and applications. Vol. III	415	Uranium production technology	424
<i>Chemistry and the properties of materials</i>		<i>Photography</i>	
Beryllium	415	Electronic flash photography	424
Einführung in die Physik der Leiterwerkstoffe	415	<i>Reference books and miscellaneous</i>	
Problems of metallography and the physics of metals	416	Acta Imeko 1958: Proceedings of the International Measurements Conference, Budapest, 24-30 November, 1958. Vols. 1-5	424
Progress in non-destructive testing. Vol. 2	416	Analysts pocket book	425
Structure reports for 1952. Vol. 16	416	Chemical engineering practice. Vol. 11. Works design, etc.	425
Werkstoffkunde der Hochvakuumtechnik. Band I. Metalle und metallisch leitende Werkstoffe	416	Classification and indexing in science	425
<i>Heat, thermometry, low and high temperature physics</i>		Evaporation and droplet growth in gaseous media	425
Advances in cryogenic engineering. Vol. 5	417	Friction in textiles	425
Flames: Their structure, radiation, and temperature	417	Gas chromatography abstracts 1958	426
Formation and trapping of free radicals	417	Moisture in textiles	426
Guide de thermométrie: Méthodes—réalisations des mesures	417	Structural damping	426
Handbuch der Kältetechnik. Vol. III	417	<i>Solid state physics and crystallography</i>	
Progress in cryogenics. Vol. 2	418	Methods of experimental physics. Vol. 6. Solid state physics. Part A	426
<i>Magnetic, electrical and electronic devices and properties</i>		Solid state physics. Advances in research and applications. Vol. 9	427
Basic data of plasma physics	418	Solid state physics in electronics and telecommunications. Vol. 1. Semiconductors. Part I	427
Beam and wave electronics in microwave tubes	418	Solid state physics. Advances in research and applications. Vol. 10	427
Der transistor	418	Crystal chemistry of simple compounds of uranium, thorium, plutonium, neptunium	427
Electrical impedance plethysmography	418	<i>Theoretical physics, mathematical techniques, computers and control systems</i>	
Electrical noise: Fundamentals and physical mechanism	419	Encyclopedia of physics. Vol. VIII/I: Fluid dynamics. 1	427
Ionization phenomena in gases. Vols. 1 and 2	419	Lectures on Fourier integrals. Annals of mathematics studies No. 42	428
The many body problem	419	Non-linear wave mechanics	428
Millimicrosecond pulse techniques	419	Organization et fonctionnement des machines arithmétiques	428
Optics of thin films	420	Reciprocals of the integers from 1000 to 9999	428
Progress in dielectrics. Vol. 2	420	Regression analysis	428
The scattering and diffraction of waves	420	The theory of thin shells	429
Structure and properties of thin films	420	Wärme-und Stoffaustausch in Arbeitsdiagrammen auf projektiver Grundlage	429
Telemetry systems	421	Wave propagation and group velocity	429
<i>Nuclear and cosmic-ray physics, apparatus, techniques and data</i>			
Atomic radiation and polymers	421		
Directory of nuclear reactors. Vol. 11: Research, test, and experimental reactors	421		
Glossaria interpretum: Nuclear physics and atomic energy. Terms of nuclear physics and nuclear technology in English, French, German, and Russian	421		
Glossary of atomic terms	422		

New books section



These two photographs appear in *Electronic flash photography* published by Temple Press Ltd. and reviewed on p. 424. The photograph on the left shows a stage in the formation of a milk drop. On the right is a night aerial flash photograph of Boston, U.S.A., taken at 2000 feet.

Aerodynamics, propulsion systems, flow and mechanics

Advanced propulsion systems. Edited by M. ALPERIN and G. P. SUTTON. (Oxford: Pergamon Press Ltd., 1959.) Pp. 278. Price 45s.

This volume contains the published proceedings of a symposium held in Los Angeles, California, in December 1957. The symposium was sponsored by the Directorate of Advanced Studies, Air Force Office of Scientific Research, and Rocketdyne, and was designed to bring together American scientists and engineers concerned with the principles of propulsion for space vehicles. This volume contains eighteen papers dealing with ion propulsion systems; the ion rocket engine; experimental studies on the thrust from a plasma jet; comparison of propulsion systems; thrust from plasma; potential aircraft applications of closed gas cycle nuclear power plants; speculation about future trends in lightweight electric equipment; direct power conversion; electrostatic and magnetohydrodynamic generators; propulsive devices; liquid propellant *status quo*; ozone—fluorine; use of metals and metal hydrides in rocket and jet propulsion; human hazards of space flight; stabilized free radicals; research on free radicals as rocket propellants; system considerations affecting new propulsion applications.

Deformation, strain and flow: An elementary introduction to rheology. 2nd ed. By M. REINER. (London: H. K. Lewis and Co. Ltd., 1960.) Pp. xiv + 347. Price 63s.

The subject dealt with in this volume, which is a second edition of *Deformation and flow*, is concerned with the general principles of rheology and with their application to a wide variety of materials having complex rheological properties. After dealing with the more straightforward subjects, viscosity, elasticity, plasticity, strength, etc., the author discusses more complex behaviour, which is classified

under headings such as Plastico-Dynamics or the Bingham-body, Elastico-Viscosity and Firmo-Viscosity, More Complex Bodies, Creep, etc.,. A chapter on Volume Rheology draws attention to the importance of this rather neglected subject. Other chapters deal with Structural Viscosity, Work Hardening, and the so-called Second-order Phenomena, that is, effects depending on the *square* of the strain, and with mathematical forms of representation and analysis of flow properties.

Professor Reiner approaches his subject with a wide background of knowledge and a deep historical and philosophical interest, and a book by him cannot fail to be stimulating. His book will on this account be read with interest and profit by those, whether physicists or engineers, whose work brings them into contact with rheological problems. Nevertheless, certain warnings should be given. It may be impossible for any single author to comprehend and assimilate the whole broad field of rheology as it exists to-day. Some limitation of the field is therefore almost inevitable. The limitation which Professor Reiner has consciously accepted is to confine himself to macroscopic behaviour, and not to attempt any interpretation of properties in terms of molecular concepts. As a result the whole field of polymers, in which so many of the recent practical and theoretical rheological developments have occurred, is necessarily excluded. While this must be accepted, the restriction unfortunately leads the author to neglect by far the most helpful way of understanding certain properties of rubber solutions, which are discussed from a less illuminating mathematical standpoint. As an example, on the question of normal pressures in shear flow (Weissenberg effects) he states "The explanation of Weissenberg effects, both on the macroscopic, phenomenological and the microscopic, structural level, is therefore *an open question*" (p. 314, author's *italics*). This is not strictly true, for a well-established molecular theory for these phenomena exists. The model actually introduced (p. 319) to represent these effects can only be described as bordering on the fantastic. (Incidentally,

the discovery of the elongation of a metal wire under torsion by Poynting, which Professor Reiner claims (p. 318) to have rescued from oblivion in 1954, was in fact noted by Rivlin (*Philos. Trans A*, **242**, p. 173, 1949) in connexion with his own observations of a similar effect in rubber). The claim to have established phenomena due to normal stresses in air (p. 319) does not mention the serious criticisms brought against these observations by G. I. Taylor and P. G. Saffman (*J. Aeronaut. Sci.*, **24**, p. 553, 1957).

Even on more classical ground the author is sometimes misleading. Thus in criticizing Trouton's analysis of his experiment on the flow of bitumen under a tensile stress, in which the stress is decomposed into two shear stresses and a hydrostatic tension, he remarks (p. 80): "Trouton is wrong in stating that the two shears are 'at right angles to each other . . . the planes in which the shears act make an angle which is necessarily greater than 90°', and adds in a footnote: "It is exactly 120°". Reference to the first edition shows the corresponding footnote there (p. 178) to read: "It is approximately = 118½°.", suggesting that the author may himself be a little uncertain. In the reviewer's opinion, Trouton's statement, though somewhat imprecisely expressed, is (taken in its context) substantially correct, while Professor Reiner's "correction" (though one can see his point) is confusing rather than helpful.

A number of small errors and misprints were noticed, the most serious being on p. 158, where the calculated viscosity of glass is given as 6.3×10^{-18} poises. This should be $4.6 \times 10^{+20}$. This section also has a mistake in the Rayleigh reference, and mis-spells the word *sagitta*.

These examples are symptomatic of a certain lack of reliability which must be set against the genuine merits of the book as a spirited exposition of a fascinating subject.

L. R. G. TRELOAR

High-speed aerodynamics and jet propulsion. Vol. 5. Turbulent flows and heat transfer. Edited by C. C. LIN. (U.S.A.: Princeton University Press; London: Oxford University Press Ltd., 1959.) Pp. xv + 549. Price £5 5s.

This is the fifth of a series of books prepared under the general editorship of von Karman surveying all the fundamental science behind aircraft and rocket propulsion and flight. Each of the books has a special editor, and the special editor of this one is C. C. Lin, who is also the author of the section dealing with Statistical Theories of Turbulence. In effect, the book is in two quite distinct halves, the first half dealing with the transition from laminar to turbulent flow, the theory and experimental nature of turbulent flow, and statistical theories of turbulence, while the second half is a treatise on heat transfer dealing with the conduction of heat, convection, and friction in flowing liquids, convective heat transfer in gases, the cooling by protective fluid films, the physical basis of thermal radiation, and engineering calculations of radiant heat exchange.

As each of these main sections has a separate author, it tends to be a complete treatise on this part of the subject in itself, but nevertheless, there is comparatively little overlapping. At first sight it is a little odd to find a chapter on laminar flow in a book with the title of this one, but this is because it is concerned with laminar flow in convective heat transfer.

It is fair to say that all the authors use mathematics in the way that physicists use it, namely for each equation there is a good discussion explaining what it means and its experi-

mental basis. The diagrams are excellent representing a convenient generalization of all the experimental work in each case, and the book can be recommended as an almost encyclopaedic survey of its subject. M. W. THRING

Hypersonic flow. Edited by A. R. COLLAR and J. TINKLER. (London: Butterworths Scientific Publications, 1960.) Pp. xv + 432. Price 70s.

This book represents the proceedings of the Eleventh Symposium of the Colston Research Society held in the University of Bristol in 1959. The symposium was international in character and was intended to appeal to the physicist, the mathematician and the engineer. The book is divided into six parts corresponding to the six sessions of the conference and the scope of the papers comprises surveys and details of the experimental facilities, techniques for simulating hypersonic flight conditions in the laboratory, experimental results, investigation of the properties of gases at elevated temperatures, theoretical solutions of particular flow problems including unsteady flow, and applied research in the form of studies of configuration, propulsion, and kinetic heating of vehicles designed for hypersonic flight. The discussions on the papers are included as well as a preface by A. R. Collar.

Non-Newtonian fluids. By W. L. WILKINSON. (Oxford: Pergamon Press Ltd., 1960.) Pp. xiv + 138. Price 37s. 6d.

The main theme of this book, which is one of a series of monographs on chemical engineering, is the formulation of the principles governing the flow of non-Newtonian fluids through tubes. The subject is introduced by a consideration of the equations which define the rheological properties of the main classes of non-Newtonian fluid, and the methods by which these properties may be determined. This is followed by the derivation of equations for both laminar and turbulent flow of these fluids in a variety of practical systems. Other problems considered are heat transfer in laminar and turbulent flow, and the mixing characteristics of non-Newtonian fluids.

Though the treatment is necessarily condensed, a great deal of thought must have gone into the preparation and arrangement of the material in this monograph. Its value is enhanced by the skilful presentation of results in terms of dimensionless quantities whenever possible so as to facilitate their practical application. The book will be warmly welcomed by engineers and physicists concerned with these applications of rheology.

L. R. G. TRELOAR

Progress in solid mechanics. Vol. 1. Edited by I. N. SNEDDON and R. HILL. (Amsterdam: North-Holland Publishing Co., 1960.) Pp. xii + 448. Price £5.

The subject of solid mechanics is one which borders on a number of different scientific disciplines. Papers describing recent advances in this field are consequently scattered in journals devoted to physics, applied mathematics, metallurgy and engineering and it is becoming increasingly difficult to follow the quite rapid progress which is taking place in plasticity, elasticity and viscoelasticity both from a mathematical and a physical point of view. The appearance of this series of volumes under the editorship of Professors Sneddon and Hill is thus extremely welcome. This first volume contains eight articles which cover a wide range of topics. The titles of these articles are: "Viscoelastic waves", by S. C.

Hunter; "Matrices of transmission in beam problems", by K. Marguerre; "Dynamic expansion of spherical cavities in metals", by H. G. Hopkins; "General theorems for elastic-plastic solids", by W. T. Koiter; "Dispersion relations for elastic waves in bars", by W. A. Green; "Thermoelasticity. The dynamical theory", by P. Chadwick; "Continuous distributions of dislocations", by B. A. Bilby; "Asymmetric problems of the theory of elasticity for a semi-infinite solid and a thick plate", by R. Muki.

The articles are well written and are by authors who are actively engaged in the fields they review and the volume can be unhesitatingly recommended to all interested in solid mechanics. One can only regret that the high price of this volume may prevent it from achieving as wide a circulation as it undoubtedly deserves.

H. KOLSKY

Rheology. Theory and applications. Vol. III. By F. R. EIRICH. (New York: Academic Press Inc.; London: Academic Books Ltd., 1960.) Pp. xvi + 680. Price £7 10s.

In contrast to the first two volumes of this series, the present volume is primarily concerned with the rheology of materials of industrial interest. Individual chapters discuss suspensions of electrified particles and polyelectrolytes, rubber latices, printing inks, pastes and paints, sand-water and clay-water mixtures, inorganic glasses, concrete, crystalline and cross-linked polymers, lubrication, adhesion, moulding (of plastics), spinning (of fibres), and screw extruders. The remaining chapters deal with more general topics, namely "The normal co-ordinate method for polymer chains in dilute solution" (B. H. Zimm), "The principles of rheometry" (S. Oka) and "The viscosity and elasticity of interfaces" (D. W. Criddle).

The present work is characterized by a freshness and originality which will make it a very valuable reference book for those wishing to familiarize themselves with the present state of development of rheology in their own special fields. The series of three volumes, taken together, provides impressive evidence that rheology is at last shaking off its adolescent self-consciousness and beginning to acquire the characteristics of a vigorous and mature science.

L. R. G. TRELOAR

Chemistry and the properties of materials

Beryllium. By G. E. DARWIN and J. H. BUDDERY. (London: Butterworths Scientific Publications Ltd., 1960.) Pp. ix + 392. Price 70s.

In this book the authors have followed the general pattern of the earlier publications in the series "Metallurgy of the rarer metals". In the first part there are chapters on extraction of beryllium from its minerals, on the preparation of the pure metal and of the oxide and on methods of fabrication. This is followed by sections giving the physical, mechanical and chemical properties of the metal and two chapters on alloys and compounds. The book concludes with two short chapters devoted respectively to nuclear properties and the health hazards involved in handling certain beryllium compounds.

Although beryllium has been used for many years, mainly as an alloying element to confer improved mechanical properties on metals such as copper and nickel, it has become important recently because of its possible applications in nuclear reactors and, if its ductility can be improved, as a structural material.

The authors have summarized the very large amount of literature that has appeared, mainly during the past 10-15 years, and have included a very full bibliography. Nothing appears to have been left out; and this is perhaps one of the main criticisms of the book. They state in the preface "It is perhaps inevitable in this stage of development that many results are contradictory". They do not, however, appear to have been discriminating in their choice of material or to have attempted a critical assessment of much of the evidence presented, and these are the things that the reader is entitled to expect of a book written by those with expert knowledge of the subject. A second criticism is the inclusion in a book devoted to a single metal of so much technology which is common to metals in general and which has already been published. The description of much of this technology is so sketchy and vague as to be almost valueless. The paragraph on p. 46 on the cold pressing and sintering of beryllia is typical of many examples that may be cited; to the reader who is familiar with powder metallurgy, many of the statements will appear to be obvious, whereas to the reader who is not familiar with these techniques the amount of useful information conveyed is negligible. And what is one to make of the following paragraph, on p. 57, referring to the thermal conductivity of beryllia? "In Figure 3.6. the data of various workers are collected, and extrapolated to zero porosity using this relationship. The curves are not strictly comparable since the shape, size and orientation of the pores and the grain size of the beryllia vary with the raw material and mode of preparation. A minimum is shown at 1600°C, mainly by analogy with more pronounced minima observed in alumina and magnesia specimens; it is believed to be due to increased heat transfer at high temperatures by radiation in the translucent beryllia".

In spite of the above serious criticisms the book contains much information that will be useful to a limited number of workers; but all that is valuable could have been put in a publication of half the length.

G. W. WARREN

Einführung in die Physik der Leiterwerkstoffe. By K. M. KOCH and R. REINBACH. (Vienna: Verlag Franz Deuticke, 1960.) Pp. vii + 255. Price öst.S.222.

Nearly one-third of this book consists of a survey of the technically important physical properties of materials used in various branches of electrical engineering. The materials are classified under the headings of conducting materials, resistance materials, heating elements, materials for resistance thermometry, and thermo-elements. In addition to this technical data, the authors have thought it desirable to give the practising electrical engineer some knowledge of the physics governing these properties and the rest of the book consists of an exposition, at an elementary level, of some of the main features of the physics of solids, with emphasis on the electrical properties.

I think that it will be generally admitted that many of the materials which are used in practice have been developed largely on an empirical basis and that physics is often unable to explain why certain technical processes are so desirable. This is evident in the present book, where there is little direct connexion between the technical sections and the remaining parts. Thus, the main point at issue in commenting on a book of this kind is the extent to which a limited knowledge of the physics of the electrical properties of materials is of value to the practical electrical engineer. This question has to be left here to be answered on an individual basis. For those

who feel that such knowledge is desirable, this book should provide a useful starting point.

J. R. DRABBLE

Problems of metallography and the physics of metals. Edited by B. YA LYUBOV. Translated from the Russian. (New York: Consultants Bureau, Inc.; London: Chapman and Hall Ltd., 1960.) Pp. 476. Price 76s.

The Metallography and the Physics of Metals Institute of the Central Scientific Research Institute of Ferrous Metallurgy published in 1955 a symposium on the results of its work during the years 1951–53, and this publication has now been translated into English. It is essentially a collection of research papers on a variety of topics in ferrous metallurgy. Although these papers have been grouped together under some main headings there has been no attempt to present a general unified view of the subject. The book will thus be valuable mainly to the specialist in providing him in a conveniently collected form some of the most important of the U.S.S.R. research papers issued on the physical metallurgy of steel during the period considered. After an affectionate obituary notice of V. I. Danilov (1902–1954), who worked on the structure of liquids, some sixty research papers are presented. The most important of these is a group on the formation, structure, and properties, of martensite, including several in which G. Kurdjumov is an author. His views on the X-ray line broadening and hardness of martensite, as being due to fine submicroscopic irregularities of structure are particularly interesting and have now been largely confirmed by very recent electron microscopic studies of martensite. The other papers in the symposium cover a wide variety of topics on diffusion, alloy carbides, coercivity of steel, and various aspects of process metallurgy. There is one paper on lattice vacancies, but nothing on dislocations.

A. H. COTTRELL

Progress in non-destructive testing. Vol. 2. Edited by E. G. STANFORD and J. H. FEARON. (London: Heywood and Co. Ltd., 1960.) Pp. viii + 250. Price 55s.

The aim of the series is "to publish reports on the progress made in relating the properties of materials to each other and to the structural factors which produce them, as well as to survey the six principle methods of flaw detection". This second volume contains seven articles. The first treats radiology with high-energy X-rays. This is followed by an article on the mechanical testing of high polymers. The third article deals with the application of electrical methods for the detection of flaws and for the study of metal structure. Following this is an article covering the uses of radioactive isotopes in non-destructive testing and an article dealing with defect assessment using ultra-sonic waves. The last two articles treat studies of ageing and precipitation in metals using anelastic damping measurements and the application of paramagnetic resonance to non-destructive testing. The series is international in character and contributors to this volume are R. Halmshaw and C. G. Pollitt, H. Kolsky, I. Vigness, J. F. Cameron, D. G. W. Claydon, K. M. Entwistle and J. W. Orton.

Structure reports for 1952. Vol. 16. Edited by A. J. C. WILSON. (Utrecht: N.V.A. Oosthoek's Uitgevers MIJ; on behalf of the International Union of Crystallography, 1959.) Pp. viii + 651. Price £11 6s.

Little need be said about the latest volume of *Structure reports*. It maintains the high standards of the earlier

volumes, and is an essential reference work for all researchers concerned with crystalline materials. In a brief search for errors, the reviewer detected on p. 3 (reference 1) G. J. Finch instead of G. I. Finch; noted on p. 82 disfiguring blurs from the type holders; and was (mildly) disconcerted by peculiar punctuation in the legend to Fig. 1 on p. 200, repeated beneath Fig. 1 on p. 203.

A footnote to the advertisement sheet inserted in the volume forestalls the reviewer's intention to urge (again) the maximum acceleration in producing further volumes: for Vols. 17 and 18 are "in an advanced state of preparation".

W. H. TAYLOR

Werkstoffkunde der Hochvakuumtechnik. Band 1. Metalle und metallisch leitende Werkstoffe. By W. ESPE. (Berlin: VEB Deutscher Verlag der Wissenschaften, 1959.) Pp. xii + 916. Price DM145.

In the construction of high vacuum apparatus of all kinds the selection and fabrication of materials requires special consideration. This is particularly important when materials are to be used in the construction of sealed-off equipment in which a very low pressure is to be maintained for long periods, such as electronic tubes and related devices.

One of the first books entirely devoted to this subject was published in 1936 with the title *Werkstoffkunde der Hochvakuumtechnik* (materials technology of high vacuum technique) by W. Espe and M. Knoll. This was soon universally acclaimed as an important contribution to the subject and invaluable to anyone concerned with the construction and manufacture of electronic and other high vacuum equipment. It was selected as one of a number of "classical" German books to be reproduced by special licence in the U.S.A. in 1943. The present book by W. Espe is based on a series of lectures on vacuum technology at the universities of Prague and Bratislava and in effect is the first part of a considerably enlarged edition. Volume I deals only with metals and metallic conductors while further volumes have been promised covering siliceous materials (glass, quartz ceramics, etc.) ancillary vacuum materials, metal to glass and metal to ceramic sealing techniques, getter materials, etc., and some of these have already appeared in the Slovakian language. Thus, in nearly one thousand pages, metallic materials, their properties and fabrication as required for high vacuum applications, are described with considerable technical details were necessary. The book is well produced and richly illustrated with a large number of instructive diagrams and tables. An idea of its scope may be gauged from the fact that this subject was dealt with in 157 pages in the 1936 edition.

A short metallographical introduction is followed by a consideration of the properties of different metals and alloys in independent sections following the general scheme of the original book. These sections treat topics such as the origin of the metal, concentration and refining from the ore, fabrication, mechanical and thermal properties, chemical properties, technical applications, etc., being followed in each case by an extensive bibliography. A useful chapter on processing techniques deals particularly with topics such as degassing, joining of metals and surface treatments. An appendix contains useful general comparisons and tables. No doubt this book will be of considerable interest to all who are concerned with high vacuum technology. The title may be slightly misleading in that there is a definite bias to electronic applications of high vacuum. Thus, the treatment of stainless steels seems neglected (8 pages) because "these materials are

not considered so important" (note that Fe-alloys in general occupy about 70 pages). On the other hand there is a great amount of information on industrial processes and many reports of useful practical observations are included which must be of the very widest interest. W. STECKELMACHER

Heat, thermometry, low and high temperature physics

Advances in cryogenic engineering. Vol. 5. Edited by K. D. TIMMERHAUS. (New York: Plenum Press Inc., 1960.) Pp. viii + 584. Price \$13.50.

The fifth volume of the proceedings of the Fifth National Conference, held at the University of California in Berkeley, September, 1959, and sponsored by the National Bureau of Standards—Atomic Energy Commission Cryogenic Engineering Laboratory in Boulder, Colorado, is divided into eleven sections. These are: applications and techniques; missile technology; insulation; superinsulation; heat transfer; design and application; liquefaction and refrigeration; mechanical properties; fluid phenomena; processes and data. The last section consists of two additional papers on an improved d.c. power regulator and vacuum gaskets for use at 20° K.

Flames: Their structure, radiation, and temperature. 2nd. ed. By A. G. GAYDON and H. G. WOLFARD. (London: Chapman and Hall Ltd., 1960.) Pp. xiii + 383. Price 70s.

It is seldom that your reviewer receives a book with such pleasure as this one because Gaydon and Wolfhard have very successfully done what they attempted to do, namely to provide a simple and yet fundamental study of the physics and chemistry of small laboratory type flames, while leaving the field of industrial flames in furnaces to another book by the same publishers. This new edition consists of a revision and bringing up to date of the main chapters of the first edition, together with a new chapter on combustion processes of rocket-type fuels, which carries the work somewhat beyond the small laboratory flames, although the interest is still mainly in the information which can be obtained by spectroscopic methods. The final chapter is also rewritten and called "Recent progress on some flame problems", and mentions new techniques, such as Weinberg's inclined slit technique for flame temperature, and the use of shock tubes in which the authors themselves have been closely concerned.

The appearance of this book in a second edition emphasizes the need for realizing that the approach of the physicist, the chemist and the engineer to flames, whether laboratory or industrial, are entirely different. The chemist is mainly concerned with qualitative effects, such as whether the reaction proceeds by this mechanism or that one, and even when he uses physical techniques such as spectroscopy, his interests remain primarily qualitative. The physicist, on the other hand, is concerned primarily with the quantitative differential equations describing the heat release rate, the temperature, and the mixing rate in flames. Finally, the engineer is only concerned with the best way in which he can put the fuel and oxidant into the flame in order to obtain a flame giving the required overall output of hot combustion gases and radiant heat transfer. It is obviously very important that these three viewpoints should come closer together and certainly Gaydon and Wolfhard's book is a great step in the direction of bringing the viewpoint of the chemist and the viewpoint of the physicist closer together, but I think it is fair to say that they leave to

others the problem of bringing the viewpoint of the physicist and that of the engineer closer together.

In revising the book, the authors have taken account of the Fifth, Sixth, and Seventh International Combustion Symposia, which cover about three hundred papers, and they have added references to over two hundred new papers to the book. The book can therefore be fully recommended as a completely up-to-date survey of this very interesting field where chemistry and physics overlap. M. W. THRING

Formation and trapping of free radicals. Edited by A. M. BASS and H. P. BROIDA. (New York: Academic Press Inc.; London: Academic Books Ltd., 1960.) Pp. xvi + 522. Price £5 14s. 6d.

In recent years, new techniques have allowed free radicals (including atoms and simple inorganic species as well as more complex organic radicals) to be produced and trapped in significant concentrations in solid phases, especially at low temperatures; their properties may be investigated by old methods or by new ones such as electron spin resonance spectrometry.

Much of the work described in this book seems to have been motivated by the rather visionary prospect of obtaining materials with a high enough free radical concentration to give rocket fuels with hitherto unattainably high specific impulses, and a chapter is devoted to rocket propulsion; but the results of this work have considerably wider implications.

This book should interest anyone concerned with free radicals in condensed phases who needs an up-to-date general survey of the field; the literature is covered up to late 1959 by the authors of most chapters. P. A. SMALL

Guide de thermométrie: Méthodes—réalisations des mesures. By C. GOUX. (Paris: Editions Eyrolles and Gauthier-Villars, 1959.) Pp. 232. Price 2,600 fr.

This book, of some 80,000 words, is divided into four parts: Principal methods of measurement, Temperature scales, Choice of method of measurement and Making of measurements. This plan makes it rather difficult to use the book as a "guide". For example, information about optical pyrometry occurs in at least eight places (only one of which appears in the index) and when we have referred to them all, we have still not been told what a disappearing-filament pyrometer is, only that there is such an instrument. Some sources of error are mentioned, but there is no indication of their magnitudes or how these may be calculated.

Treatment of resistance thermometry is very superficial. There is no reference to the special bridges used for this work, while methods for the elimination of lead resistance are vaguely referred to in two separate chapters, but without any detail. There is a bibliography with 13 entries, but there are no references in the text. J. A. HALL

Handbuch der Kältetechnik. Vol. III. Edited by R. PLANK. (Berlin: Springer-Verlag, 1959.) Pp. viii + 511. Price DM84.

The third volume of this great compendium of low-temperature technique deals with the methods of cryogenics and with the basic problems of heat transfer. The first section, written by Professor R. Plank himself, the editor of the series, presents an excellent survey of the principles underlying the production

of low temperatures. Since the methods based on changes of state—called here “thermodynamic methods”—are treated in more detail in other volumes of the series, he devotes a rather more generous portion of space to the electrical and magnetic methods. These are not generally known to the engineers, for whom the book will be mainly of value, and they will welcome this clear and concise account.

The next two sections, dealing with heat transport by conduction and by mass transport, are written by Professor Baehr and Dr. Hoffmann. The basic, but also the engineering, problems are treated in considerable detail, and a large amount of valuable data is included. The volume closes with a section on thermal radiation by Professor Baehr which, like Section 1, deals mainly with the basic principles.

K. MENDELSSOHN

Progress in cryogenics. Vol. 2. Edited by K. MENDELSSOHN. (London: Heywood and Company Ltd., 1960.) Pp. vii + 280. Price 63s.

This volume is one of a series, international in character, designed to provide critical and up-to-date information in the various branches of cryogenics, and to acquaint workers in one field of low-temperature research with techniques being developed in others. It contains eight articles, the first dealing with the storage and handling of cryogenic liquids, the second with the gas refrigerating machine and its position in cryogenic technique, the third with the separation of deuterium on an industrial scale by low-temperature distillation, and the fourth with low-temperature bubble chambers; the fifth article consists of the 1958 scale of temperatures for the liquid helium-4 region and a discussion thereon, while the last three cover resistance thermometers for low temperatures, the three level solid state maser, and the methods of nuclear orientation.

Magnetic, electrical and electronic devices and properties

Basic data of plasma physics. By S. C. BROWN. (Massachusetts: Technology Press of the Massachusetts Institute of Technology; New York: John Wiley and Sons Inc.; London: Chapman and Hall Ltd., 1959.) Pp. viii + 336. Price 52s.

This book which represents the lecture notes of a course given by the author at the M.I.T., covers the fundamental physical processes controlling the conduction of electricity through gases at moderate temperatures and pressures. It also deals with the mechanism of the chief discharge processes including the arc, glow discharge and corona. The strength, and indeed the bulk, of the book is in the very numerous illustrations, mostly in the form of graphs showing experimental results. These make it a very useful book of reference. Unfortunately the coverage is by no means complete, for example there is no reference to the work of Llewellyn Jones and the Swansea school, though it should be said that the preface claims only that the book deals with those parts of the subject of interest to the M.I.T. workers.

The text covers the most important points and is commendably free of clutter, in a few places a little more explanation would have removed obscurities. This is apt to happen in a book derived from lecture notes, which no doubt would have been amplified when they were delivered.

G. P. THOMSON

Beam and wave electronics in microwave tubes. By R. G. E. HUTTER and SHIRLEY W. HARRISON. (London: D. Van Nostrand Co. Ltd., 1960.) Pp. xii + 378. Price 73s. 6d.

During the past twenty years or so there have been introduced many electronic devices like the klystron, magnetron, and other travelling-wave tubes. In this book the author attempts to describe the essential features and to analyse the operation of such devices. The theory is limited to small signals and to those approaches which have had some success in explaining performance. There is no mention of the dynamical theory of bunching, the analysis being in terms of space charge waves. Older readers will be surprised to find that such names as Webster and Kompfner do not appear in the lengthy author index.

After three introductory chapters which provide general background, there is established the essential field and circuit theory of wave guides and resonators, followed by sections on the interaction between fields and electron beams in gaps, drift spaces, and slow-wave structures. The remainder of the book deals with the application of the basic principles to various types of tube, with a final chapter on noise. The treatment is essentially and deliberately mathematical with no attempt to give any physical pictures. Within these limitations the book is successful and it can be recommended to those who like the mathematical approach. Others will find the book useful as an up-to-date reference to the theory of travelling-wave tubes.

M. R. GAVIN

Der transistor. By J. DOSSE. (München: R. Oldenbourg, 1959) Pp. 274. Price DM26.

This is the third and enlarged edition of the book originally published in 1955. The treatment of the subject is descriptive rather than mathematical, and includes a brief historical introduction and discussion of the conduction processes in semi-conductors. The mode of action of transistors is then explained and the various types that have been investigated are described. The present state of development is outlined, but no mention of mesa structures or alloy-diffused types is made. Multilayer (P.N.P.N.) devices with negative resistance switching characteristics, various kinds of transistor, dualism of valves and transistors, noise considerations, d.c. operation and stabilization of working point are all discussed fairly fully. About one-quarter of the book is devoted to the circuit applications of various transistors.

The treatment is simple, direct and authoritative, and very few errors or misprints were noted. There is an extensive bibliography for further reading, and a good index. While the book does not offer anything which cannot be found in English language texts, it provides a useful, concise introduction to the subject and indeed would form an excellent reading text for engineers and physicists wishing to improve their knowledge of the German language. The production and diagrams (several coloured) are excellent.

C. A. HOGARTH

Electrical impedance plethysmography. By J. NYBOER. (Springfield, Illinois: Charles C. Thomas; Oxford: Blackwell Scientific Publications Ltd., 1959.) Pp. xvii + 243. Price 60s.

A plethysmograph is an instrument which records changes in volume of a given organ or part of the body; in an impedance plethysmograph, this is done on the basis of recordings of changes in electrical impedance of the tissues concerned to medium- or high-frequency alternating current.

It is used clinically to investigate problems connected with blood flow and the effects of external influences on it. Some readers may already know Dr. Nyboer's article on this subject in Glasser's *Medical Physics*. Dr. Nyboer has been working in this field, in which he is an acknowledged expert, for over twenty years, and the present monograph enables him to set out his work in extended form. Physicists will find the physics in the early chapters rather elementary, and the subsequent jump to quite complicated applications somewhat sudden; but if they read through the later clinical chapters, they will find much of interest and may well be surprised at the uses to which Ohm's law and a Wheatstone bridge can be put. Medical research workers use plethysmography as a tool and are sure to find this account of it stimulating.

C. B. ALLSOPP

Electrical noise: Fundamentals and physical mechanism. By D. A. BELL. (London: D. Van Nostrand Co. Ltd., 1960.) Pp. x + 342. Price 50s.

The many electronic devices now available are limited in their applications by fluctuations of a fundamental character grouped under the general heading of "Noise". It is remarkable how the noise characteristics of many differing devices are similar. For example: the flicker noise of thermionic tubes is similar in characteristic to the excess noise of $p-n$ junction devices. Much theoretical and experimental work on noise has taken place over the last few years and the author has made several notable contributions. His original work in the field plus his experience of teaching the subject to advanced students has equipped him well for writing this book.

After introductory and formal theoretical chapters the main electronic devices are taken in turn and their noise characteristics are described and analysed. These devices include diodes, grid-controlled valves, photomultipliers, beam amplifiers, masers, parametric amplifiers, radiation detectors, metal films, rectifiers, and transistors. The book concludes with a chapter on noise standards and measuring techniques.

The treatment is simple yet authoritative and the book can safely be recommended for honours students and research workers. The bibliography is full and up to date and by present standards the price is reasonable for the large amount of information presented.

C. A. HOGARTH

Ionization phenomena in gases. Vols. 1 and 2. Edited by N. ROBERT NILSSON. (Amsterdam: North-Holland Publishing Company, 1960.) Pp. 1210. Price £12 6s. set.

The Fourth International Conference on Ionization Phenomena in Gases took place at Uppsala in August 1959. The published proceedings represent the exchange of information among 600 scientists from 25 different countries. The programme includes sections on plasma physics, on fundamental processes and electric discharges. The papers are divided into four sections corresponding to the four parallel sessions at the conference. The first deals with fundamental processes in gas discharges. The second covers different types of discharges and applications. This is followed by a section treating theoretical and experimental studies in plasma physics, and the last section deals with production, confinement and heating of plasmas. The first section is subdivided into four parts, the first treating collision processes, the second, ionization in an electric field, the third,

radiation processes, and the fourth covering surface gas interaction. The second section is subdivided into five parts: glow discharges, arc-discharges, spark discharges, applications, and new methods of measurement. The second volume contains the last two sections, which are in turn subdivided, the third section into four parts and the fourth section into five parts. The third section covers transport phenomena and stability problems, velocity distribution of electrons in a plasma and interaction between a plasma and a beam of charged particles, waves in plasma, and, finally, spectra from plasmas. The last section deals with the longitudinal pinch, mirror machines, the azimuthal pinch, shock waves, and further methods of production, confinement and heating.

The many body problem. (New York: John Wiley and Sons, Inc.; Paris: Dunod; London: Methuen and Co. Ltd., 1959.) Pp. xv + 675. Price £5.

This publication contains the lectures presented at the Summer School for Theoretical Physics organized by the University of Grenoble at Les Houches in 1958. It covers much of the important work done on the Quantum Mechanics of many-particle systems up to the date of the School.

One of the interesting advances in this field has been the calculation of the effects of interparticle interactions by perturbation theory. In a long contribution, K. A. Brueckner discusses a perturbation expansion of the ground-state energy of many-particle systems and applies the theory to the atomic nucleus, the electron gas and the liquids He^3 and He^4 . N. M. Hugenholtz treats mathematical aspects of the perturbation expansion, while C. Bloch and C. de Dominicis and also K. Huang give the results of investigations on perturbation expansions of the partition function.

Collective motions in many-particle systems constitute another topic presented in the lectures. D. Pines discusses the theory of Plasma Oscillations in an electron gas, while D. Bohm and H. J. Lipkin treat the problem of introducing co-ordinates to describe the collective motions. K. A. Brueckner touches on the calculation of collective effects by perturbation theory in the electron gas and in liquid He^4 .

The theory of superconductivity has for many years provided a baffling theoretical problem. It appears that the electron-electron interaction that produces the effect cannot be treated by perturbation theory in any simple way. J. R. Schrieffer discusses the approximate solution to the problem by a canonical transformation. The condition required for the appearance of superconducting states is the existence of an attractive force between electrons which tends to produce electron pairs. Nuclear forces have a similar property. B. R. Mottelson and S. T. Beliaev apply methods developed for the theory of superconductivity to the nuclear structure problem with very interesting and important results.

This collection of articles will be a valuable reference for anybody concerned with the quantum mechanics of many-particle systems. It provides a useful guide through the mass of literature on the subject.

D. M. BRINK

Millimicrosecond pulse techniques. 2nd ed. By I. A. D. LEWIS and F. H. WELLS. (Oxford: Pergamon Press Ltd., 1959.) Pp. xviii + 417. Price 50s.

The new edition of this monograph follows the general lines of the original. The overall size has increased by about one-third, but no new sections have been found necessary. The main chapter headings are Transmission Lines, Transformers,

Pulse Generators, Amplifiers, Oscilloscopes, Nuclear Applications and Miscellaneous Applications. The new material is distributed over all the sections, including the list of references (now exceeding 700 in number). One of the main developments since the first edition is the introduction of solid state diodes and transistors for switching. A few basic high-speed transistors, diodes and associated circuits are described briefly and, somewhat surprisingly, at the end of the section on miscellaneous applications. However, all in all, this new edition will be welcomed as an authoritative and up-to-date account of an important and rapidly developing field.

M. R. GAVIN

Optics of thin films. By A. VAŠIČEK. (Amsterdam: North-Holland Publishing Co., 1960.) Pp. xiii + 403. Price 80s.

This book covers most of the theory of thin films, starting from Maxwell's equations, and progressing by way of transmission and reflexion at a single dielectric boundary, through single layer films, to the more interesting problems which can be solved with multi-layer stacks.

In this reviewer's opinion too much time and space are devoted to the first stages of this progression. Extensive comparisons are made between theories expounded by the author and those published by other workers, while some of the questions on multi-layer stacks, not so readily answered experimentally, such as dependence of their properties on angle of incidence or state and degree of polarization, are barely mentioned.

Nevertheless, this book collects together most of the theoretical work on thin films by the author, an undoubtedly valuable contributor to this field; at the same time providing a review of some of the theories put forward by other writers, some of which, coming from Eastern Europe, might be new to workers in this country. In this context a Russian alternative to the Maxwell Garnett theory for very thin metallic films is mentioned.

In his preface the author promises a second book on the measurement and practical applications of thin films which, in conjunction with the present volume, should provide a comprehensive survey of this branch of physics.

E. J. TRETHEWEY

Progress in dielectrics. Vol. 2. Edited by J. B. BIRKS and J. H. SCHULMAN. (London: Heywood and Co. Ltd., 1960.) Pp. viii + 225. Price 55s.

This is the second volume in an annual series which aims at reviewing the present state of knowledge in the field of dielectrics.

With the exception of the chapter dealing with irradiated polymers, most of the volume is devoted to a review of dielectric phenomena occurring at low field strengths. As such it forms a useful complement to Volume 1 which dealt primarily with the electrical breakdown of dielectrics.

It is doubtful whether Chapter I dealing with polarization and absorption achieves the object, stated in the preface, of providing sufficient background for the appreciation of weak field phenomena. In some cases the derivation of mathematical expressions for certain physical concepts of polarization and absorption has, for reasons of space, been so condensed that it would have been better merely to have quoted the result and the reference. However, subsequent chapters are to a large extent complete in themselves. They cover the effects of composition and structure on the dielectric properties of polymeric and inorganic materials. In particular

the chapter dealing with the dielectric properties of polymeric systems is logically developed to deal with a wide range of polymers. The chapter dealing with the dielectric properties of glass is written in a way which will appeal to the technologist and the scientist. Here again sufficient basic theory is given to make the whole of the chapter readily understood. High permittivity ceramics are dealt with in another chapter which is concerned primarily with the basic properties of these materials and the specialized techniques involved in their manufacture. The last chapter is concerned with the theory of arrays of conducting and insulating elements having dielectric properties at microwave frequencies.

The absence of an index neglects the opportunity for cross-reference on topics which are common to several chapters.

After the frustration of finding the first sentence of the first section of Chapter I to be without a predicate, the rest of the volume is found to be reasonably free of errors. As in the case of the first volume the layout of the book is pleasing and it is well illustrated.

N. PARKMAN

The scattering and diffraction of waves. By R. W. P. KING and TAI TSUN WU. (Massachusetts: Harvard University Press; London: Oxford University Press Ltd., 1959.) Pp. xvii + 218. Price 32s. 6d.

This volume is the seventh in a series of monographs issued by the Harvard University Press describing the results of research activities carried out at Harvard. The book takes the form of an extended research report and is accordingly somewhat specialized in its contents, and will be mainly of interest to those working in the same field of research—namely on the scattering and diffraction of electromagnetic waves by various objects. Extensive work of this kind has been carried out for some years in a number of laboratories mainly in connexion with the determination of radar echoing areas by the use of models.

In order to understand the fundamental principles, investigators have been driven to study first of all the simpler geometrical shapes such as cylinders, spheres, disks, cones, etc. A considerable part of the book deals with the theory of scattering and diffraction by bodies having such shapes and with the methods used for making measurements in order to compare theory and experiment. The authors confine themselves mainly to a discussion of the work carried out at Harvard and although some references are given to other work they are by no means complete and no mention is made of a good deal of related work carried out elsewhere. Most of the material has already been issued as Cruft Laboratory reports, but those engaged in similar work will welcome this integrated account of the Harvard research.

The book is well produced, contains a great many diagrams and figures to illustrate the text, and the modest price makes it good value for money. Anyone interested in electromagnetic wave theory will find some interesting reading, but the book is essentially one for the specialist.

R. A. SMITH

Structure and properties of thin films. Edited by C. A. NEUGEBAUR, J. B. NEWKIRK and D. A. VERMILYA. (New York: John Wiley and Sons, Inc.; London: Chapman and Hall Ltd., 1959.) Pp. xiv + 561. Price 120s.

An international conference was held in New York in September 1959, the complete proceedings of which are contained in this volume. The conference was sponsored by

the U.S. Air Force Office of Scientific Research, Air Research and Development Command, and the Research Laboratory of The General Electrical Company. The volume contains many papers on the research that is being made on the use of thin films to obtain information about the bulk properties of matter, and these include studies of phase transformations, chemical reactivity, superconductivity, electrical resistance, the Hall effect, magnetic properties and magnetoresistance. The volume is divided into five sections with an introduction by J. W. Mitchell. The first two sections contain papers on the formation and mechanical properties of thin films. The third and fourth sections deal with the electrical and magnetic properties of thin films and the fifth section covers chemical interactions at surfaces. Finally there is a panel discussion on the theory of surfaces.

Telemetering systems. By P. A. Borden and W. J. Mayo-Wells. (New York: Reinhold Publishing Corporation; London: Chapman and Hall Ltd., 1959.) Pp. vii + 349. Price 68s.

This book is concerned solely with electrical telemetering systems, and no mention is made of any other systems. A comprehensive survey of transducers and systems is presented and the whole book is copiously illustrated. The treatment is marred, however, by lack of appraisal of the various methods listed and this results in the book being of little use to anyone not intimately connected with the field of telemetry. The illustrations too are of doubtful value, since they are for a large part reproductions from manufacturers' manuals.

There is a good chapter on mobile systems, particularly those used in missile work. A much needed chapter on reliability is also included.

This book is a useful catalogue and contains numerous references, but it is not recommended to those who wish to become more closely acquainted with telemetry systems.

M. W. SAGE

Nuclear and cosmic-ray physics, apparatus, techniques and data

Atomic radiation and polymers. By A. Charlesby. (Oxford: Pergamon Press Ltd., 1960.) Pp. xiii + 556. Price £5 10s.

The author of this book, who is internationally famous in this field, has ably summarized the wealth of data gathered over the past ten years in a subject which is not only of fundamental and technological interest, but has also applications to the biological sciences. Introductory chapters on the physical background and on sources of ionizing radiation are followed by accounts of the behaviour of individual polymers; among these the chapters on polyethylene may particularly be mentioned as a detailed presentation of a complex and at times confusing field. A number of topics of general relevance to polymer chemistry and to radiation chemistry are also described.

Scientifically and technically the exposition is excellent, and the bibliographies (up to 1959) most valuable; indexing is good. However, the brevity of style and economy of words lead at times to statements which may confuse the non-specialist reader. The reviewer would like to have seen more space devoted to calorimetry as an absolute method of pile dosimetry, while the statement on p. 90 does scant

justice to the merits of the medium-energy cyclotron for radiation damage work. Similarly, the statements on pp. 463 and 464 may be taken to mean that the Van de Graaff beam is naturally pulsed, whereas it is in fact continuous but may be pulsed externally.

There is a disturbingly large number of misprints and minor inaccuracies, and in many cases a better layout of tables could have been achieved. More noticeable errors are the use of old values for the half-lives of ^{137}Cs and ^{90}Sr , the lack of charge balance in the seventh equation on p. 185, disagreement between text and caption to Fig. 22.5, and the peculiar inversion of the metallic salts of acrylic acid in Table 22.7. A strong plea should also be made for adoption in British texts of the Royal Society recommendation regarding the location of mass numbers in formulae.

These criticisms should not be allowed to detract from the merits of the book, and it is hoped that their causes will be eradicated in the second edition which we may confidently expect.

C. B. AMPHLETT

Directory of nuclear reactors. Vol. II: Research, test and experimental reactors. (Vienna: The International Atomic Energy Agency, 1959.) Pp. 348. Price 21s.

The aim of the publishers is "to accelerate and enlarge the contribution of atomic energy to peace, health and prosperity through our world". This is a reference book intended to provide information for those interested in the atomic field either at technical or management level. A third volume is to be issued shortly to cover reactors not mentioned in this one for various reasons. It is proposed to issue supplements in order to keep this volume directory complete. Minor differences in construction or physical parameters are not given. The directory is divided into seven sections dealing with: light-water-moderated, pool-type research reactors; light-water-moderated, tank-type research reactors; liquid-homogeneous-research reactors; solid-homogeneous-research reactors; heavy-water-moderated research reactors; graphite-moderated research reactors; organic-moderated research reactors. The book also includes an alphabetical index, conversion tables, and a list of abbreviations.

Glossaria interpretum: Nuclear physics and atomic energy. Terms of nuclear physics and nuclear technology in English, French, German and Russian. By G. J. BÉNÉ, R. BEELER and M. GOLUB. (Amsterdam: Elsevier Publishing Company, 1960.) Pp. viii + 213. Price 16 guilders.

At first sight, this second volume in the *Glossaria interpretum* series makes a favourable impression. The arrangement is one which has rightly become almost invariable in such dictionaries: a main section, in which some 2000 entries are arranged in English alphabetical order and numbered, with cross-lines guiding the eye to the corresponding French, German and Russian equivalents, is followed by indexes in the other three languages, the same numbers being used to refer to the appropriate entry in the main section.

On closer examination, the work does not fulfil expectations. One expects some way of dealing with cross-references, and some way of dealing with synonyms. What system there is may be illustrated from the introductory paragraph on "Abbreviations and symbols" (the misspelling is by no means the only one): "The numbers in brackets after terms in the first column (English) refer to other phrases

containing the same word". That is, some English terms are followed by parentheses enclosing the reference numbers of the terms entered elsewhere which involve the first word in the entry concerned. For example, "absorption curve (555, 741, 1150, 2059)" signifies that the four terms corresponding to those numbers involve the word *absorption*. But would it not have been far more useful, even if a little longer, to give the actual terms? It is in any case obvious where, for example, *absorption edge* is to be sought, if not under *absorption*, and the user could then see forthwith whether any term sought appears in the dictionary at all. The cross-referencing is, furthermore, incomplete (*self-absorption* is not one of the four terms enumerated at *absorption*) and inexact (because if the dictionary contains no entry under the desired reference word—for example, *curve*—the reference appears under a related word, in this case *curvature*, or not at all).

"In order to reduce the number of entries, expressions comprising a noun and an adjective" (are given) "at the place resulting from the alphabetical order of the adjective, and only a cross-reference will be found under the noun; in cases however where the noun and adjective form an indivisible expression the term will be found under the noun." This subtle criterion seems to have baffled the compilers themselves: many expressions appear under both components, usually with somewhat different renderings in the other languages; and it seems that *low power reactor* and *scintillation detector* form "indivisible expressions", while *low flux reactor* and *scintillation counter* do not.

"A comma between two terms in the first column (English) means that their order is to be reversed. The comma in the other columns separate two or more synonyms." In reality, the comma in the other columns is sometimes either redundant or used to separate synonymous parts (for example, "physique pure, générale, fondamentale"), and that in the first column is sometimes used to separate synonyms. English synonyms are either treated in this inconsistent way or entered quite separately, with no clue to their synonymy except the identity of their foreign equivalents.

Nothing is said about the sources of the renderings, no definitions and no genders are given, and most of the abbreviations used are unexplained.

The repertoire of terms, though notable for the inclusion of some semi-colloquial terms like *shimming*, which offer great difficulty to translators, gives no evidence of systematic collection. The reviewer looked in vain for *neutron*, *proton*, *uranium*, *plutonium*, *diffusion*, *capture*, *energy*, *lethargy*, *ionization chamber*, *coincidence*, *fuel rod* and many other simple expressions (though some compounds of them are given), but on the other hand, he would have been successful had he turned to this dictionary in search of *even number*, *sodium hydroxide* or *subterranean steam*. He found *pions* but not *muons*, *real part* but not *imaginary part*, *polar vector* but not *axial vector*. The equivalents given are generally correct, but include some wordy periphrases (the German for *shimming* occupies seven lines). Many German compounds are printed as two words instead of one (in the main vocabulary, but not in the German index), and sympathy will be felt for the translator who trustingly renders *sol particles* as "particules élémentaires venant du soleil" or the equivalent German or Russian phrase. The various renderings are not always the same part of speech (*tritiate* is rendered by a French noun phrase, a German adjective phrase and a Russian verb phrase), nor do they always cover the same range of meanings of the English term. In short, *Nuclear Physics and Atomic Energy* is excellent in conception and lamentable in execution.

J. B. SYKES

Glossary of atomic terms. (London: United Kingdom Atomic Energy Authority, 1960.) Pp. 54. Price 3s. 6d. from H.M. Stationery Office.

Although this little book has evidently not been as carefully checked as it might have by technical experts in the Authority, and the selection of terms seems somewhat arbitrary, it should prove useful to non-specialist writers.

International directory of radio-isotopes. Vol. 1: Unprocessed and processed radio-isotope preparations and special radiation sources. (Vienna: The International Atomic Energy Agency, 1959.) Pp. 264. Price 21s.

The use of radio-isotopes is now so widespread, and the number of organizations producing them so large, that a user may have very great difficulty in finding the most suitable source of supply. This is particularly true in the so-called under-developed countries, where it may be difficult to make personal contact with other scientists, or to find libraries containing complete ranges of catalogues.

The International Atomic Energy Agency has therefore performed a very useful service in preparing this International Directory of Radio-isotopes. It lists the products and gives the addresses of about fifty institutions and firms in about a dozen countries, ranging from large primary producers which give a very comprehensive service, to firms which specialize, for instance, in therapeutic and radiographic sources or labelled chemical and pharmaceutical products.

The catalogue includes nearly two hundred isotopes or mixtures of isotopes. Enough information on nuclear properties is given to save constant reference to other tables. Details are given of unprocessed sources, processed sources, such as chemically stabilized solutions, special sources, and standardized sources. Prices are given in the currency of the country of origin, and also in U.S. dollar equivalents.

This is to be followed by a second volume dealing with labelled compounds. Together they will make an extremely useful work of reference.

W. J. WHITEHOUSE

Nuclear engineering monographs: No. 7. Nuclear reactor materials. By B. R. T. FROST and M. B. WALDRON. (London: Temple Press Ltd., 1959.) Pp. vii + 79. Price 12s. 6d.

This booklet condenses into seventy-three pages of text a sweeping survey of nuclear materials which will be appreciated by metallurgists because of its breadth and authority, as well as by the engineers for whom it was published. After twenty-six pages of background theoretical metallurgy, are chapters dealing with structural materials, fuel materials, liquid metals, ceramic reactor materials and corrosion. The extraction and preparation of nuclear materials, their properties and problems associated with the uses of them are all dealt with. It is not to be expected that a book into which so much is compressed that crystal structure, from the basic types of unit cell to Miller indices and Bragg's law, is explained in three and a half pages and chemical thermodynamic properties in one and a half pages, will be quickly or lightly read. Indeed, the only serious criticism is that a little too much has perhaps been introduced; the account of the phase rule goes into such detail as explanation of monotectic and syntectic which is more detail than in fact called for. Syntectic, the explanation of which appears to be in error, is a term not in familiar use even among physical metallurgists!

This little book should be of value and interest to those

who want a safe introduction to an important unfamiliar subject and to many who will appreciate so authoritative a survey of whole wide fields with parts of which they are very familiar.

G. A. GEACH

Penetration of charged particles in matter. (Nuclear Science Series No. 29.) Edited by E. A. UEHLING. (Washington: National Academy of Sciences—National Research Council, Publication 752, 1960.) Pp. x + 174. Price \$2.

This volume contains the proceedings of the informal conference held at Gatlinburg, U.S.A., in September 1958. The conference was sponsored by the Atomic Energy Commission, National Science Foundation, and the Air Force Office of Scientific Research in order to explore the possibilities of a new synthesis of experimental and theoretical information. The book is divided into six parts with an appendix of comments on the "Collective" effects in atoms and in extended media. The work covers stopping power and ranges, recent developments in the theory of stopping power, charge changing collisions, atomic and molecular scattering, ionization in gases by high-energy particles, and microscopic and macroscopic energy loss distributions.

Physikalische Kernchemie. By U. SCHINDEWOLF. (Braunschweig: Friedr. Vieweg and Sohn, 1959.) Pp. viii + 194. Price DM19.80.

The scope of this attractive book is that of the lectures in Nuclear Chemistry offered at the Massachusetts Institute of Technology. It is certainly well within the capabilities of those who have taken an honours degree in chemistry.

Without unnecessary preamble, it begins by dealing with the characteristics of the various ways in which the nucleus may suffer transformation. After a discussion of nuclear systematics and models of the nucleus comes a consideration of theories of radioactive disintegration. Nuclear reactions are introduced by a description of Rutherford's early work. It is typical of the book that the work of the pioneers in this field fits in comfortably with the author's treatment of his subject. The neutron and its reactions are given a whole chapter which is followed by one on fission. In slightly different vein, there are chapters on the genesis and abundance of the elements and on nuclear geochemistry. Chemical topics are dealt with in a chapter on methods of handling trace quantities of radioactivity and one on radiochemical aspects of analysis.

This book is not a practical manual, nor does it set out to be, but it provides an excellent background of nuclear physics without going deeply into the subject. Lucidly and concisely written, it is easy and pleasant to read. Inside the back cover is a removable chart of the nuclides.

J. D. M. MCCONNELL

Progress in nuclear energy. Series XI. Plasma physics and thermonuclear research, Vol. 1. Edited by C. LONGMIRE, J. L. TUCK and W. B. THOMPSON. (Oxford: Pergamon Press Ltd., 1959.) Pp. vii + 612. Price £5 5s.

This is the eleventh volume of a series devoted to publishing the principal papers given at the 1958 Conference at Geneva on the peaceful uses of atomic energy. Since up till this time the subject had been the victim of considerable security restrictions, the papers in this volume were in many cases the first public announcement of the important work which they

describe, work carried out at great expense chiefly in U.S.A., Britain and U.S.S.R.

These papers taken together form an excellent textbook of the subject as known in the summer of 1958. There has been something of a lull since as far as published work is concerned, and little of first-rate importance would need to be added now. The selection of papers is on the whole good, though the reviewer must record with regret the absence of any account of the work on pinch discharge at the A.E.I. Laboratory at Aldermaston. This subject is a fascinating combination of theory, experimental physics and large-scale engineering. The physics of gaseous discharges has attracted and fascinated experimenters since the early eighteenth century, it led to the discovery of the electron, of the proton and of isotopes, but its complexity and difficulty is such that the behaviour of plasma even under fairly simple conditions still cannot be predicted with certainty. Great advances have been made, we know a great deal more than we did, but not enough yet to provide the engineers with a firm basis for design. In many respects the subject much resembles aerodynamics, of which indeed it is an example with the ordinary difficulties complicated by electromagnetic forces. As in aerodynamics it is reasonable to select out of the infinite number of possible problems those which represent idealized forms of possible devices, for example aerofoils in the one case and the pinch discharge in the other. One needs to apportion the effort over a wide spectrum between "basic" and "applied" research. But in designing "basic" experiments one should keep in mind the possible applications of the principles, while at the "applied" end of the spectrum one must be careful that each stage towards a device for producing energy is so designed that something fundamental can be learned, even if the results are disappointing.

G. P. THOMSON

Radiation hygiene handbook. Edited by H. BLATZ. (London: McGraw-Hill Publishing Co. Ltd., 1959.) Pp. xi + 922. Price £10 13s. 6d.

In lapidary inscriptions (Dr. Johnson advised) a man is not upon oath. The same dispensation is freely used by those inconspicuous members of the publishing profession who write the words on book jackets. Here, for once, is a book to which the blurb does not do justice. "With this helpful handbook", the reader is told, "you have at your fingertips the answers to virtually any question that may come up about the safe and healthful use of radioactive materials." This description is misleading in two ways. Firstly, the book deals with many radiation hazards other than those produced by radioactive materials; secondly, it is much more than a catechism of questions and answers.

Mr. Blatz has assembled a large and useful compendium with three main ingredients. To begin with, there are mathematical tables, glossaries, isotope catalogues, X-ray absorption figures and suchlike basic data. The largest part of the book deals with the generation, measurement and absorption of various kinds of radiation and sub-atomic particles. Finally, all of this information is used in discussing the problem of maintaining radiation safety, both for people occupationally exposed and for the general public. Here the published recommendations of the National Bureau of Standards are quoted extensively.

Some of the more controversial issues (such as the hazards of fall-out and of diagnostic radiology) are mentioned but not elaborated. On the other hand, the sections dealing with

the handling and disposal of radioactive material in large quantities are particularly well done. Most of the 23 chapters appear to have been written no later than 1957; consequently the recommendations that they contain are not always up to date.

These and other small defects, including a number of inconsistencies and misprints, do not greatly detract from the merits of this splendid book which offers a rich fund of useful guidance and information for those concerned with radiation protection in universities, industrial laboratories or atomic energy establishments.

J. M. A. LENIHAN

Uranium production technology. Edited by C. D. HARRINGTON and A. E. RUEHLE. (London: D. Van Nostrand Co. Ltd., 1959.) Pp. xii + 579. Price £6 11s. 6d.

This is an excellent book describing in detail the extensive developments involved in the production of large tonnages of high purity uranium metal in the U.S.A.; the growth of the technology is covered from the gram scale of the Manhattan project in 1942 to the present production scale of 3300 lb ingots of metal. The U.S. Atomic Energy Commission are to be congratulated on their making possible the publication of the significant features of the technology and there is no doubt that this volume will be welcomed not only by workers in atomic energy but also by chemists, chemical engineers and metallurgists generally. The basic chemistry and metallurgy underlying the processes are dealt with in outline but the major part of the book is devoted to the technology of the purification process, the production of UO_2 , UF_4 and uranium metal and the techniques used for metal fabrication.

The first commercial purification processes, both batch and continuous, were based on the ether extraction method of Peligot; later tributyl phosphate was developed as the solvent with either kerosene or hexane as the diluent because of safety and lower capital and operating costs and the processes operated at the Fernald, Ohio and Weldon Spring, Missouri plants including outline flowsheets, operating conditions and costs are described in detail. The processes involved in the production of the intermediate products UO_2 and UF_4 and the reduction of UF_4 with magnesium or calcium followed by vacuum melting and casting are also treated in a similar detailed way. Of especial mention is the more recent trend towards the development of fluidized bed processes for the intermediate products. The work on the production of uranium direct ingot (dingot) suitable for fabrication without remelting and casting is also of special interest to the metallurgist.

The writing of this book was a co-operative effort by the staff of the Uranium Division of Mallinckrodt Chemical Works. The style is uniform and concise and the book, although expensive, is attractively presented. P. MURRAY

Photography

Electronic flash photography. By R. ASPDEN. (London: Temple Press Ltd., 1959.) Pp. xvi + 192. Price 37s. 6d.

He would be a remarkable man who could write a "balanced work of high technical merit", which is what the publishers claim this book to be, covering all the aspects which are suggested by the titles of the chapters in it. He would need

to be expert in some branches at least of such diverse subjects as the theory of electrical discharges in gases, electronics, photography, X-rays, optics and illumination engineering, and have a wide knowledge of the various techniques and applications of the electronic flash. Considering that the author intended his book to be a condensed survey—it amounts to about 50,000 words plus illustrations (see p. 413)—taking up two-fifths of the space—the descriptions of electronic circuits, X-rays and the techniques and applications are adequate. So also is the chapter on commercial flash equipment. For these aspects the book is worth while. But the treatment of the theory of electrical discharges in gases is extremely elementary, of the illumination engineering (that is to say, the way in which to get the right amount of light on the subject) so meagre as to be almost non-existent and of photography partly irrelevant and partly wrong. What shall we think of the author who gets wrong the formula which ought to tell us what exposure will be produced on a film by a given arrangement of tube and camera, and indeed does not explain what the "guide-number" is that he is writing about? It is things like the latter which lead here and there to a curious air of *non sequitur*, a simpler example of which is: "Krypton was largely used as a filling in the early days, because xenon, which has a higher luminous efficiency, was difficult to procure. An increased supply of this gas was made available during the war, however, and in this period British lamp manufacturers and government establishments developed a great variety of specialized tubes for research purposes. One of the most important of these was the 'Arditron', an argon-filled, ultra-high-speed tube. . . ." This air of *non sequitur* is most noticeable in the more theoretical sections. If his book reaches a second edition, the author would do well to omit the theory and use the space made available to show readers new to electronic flash photography how to set about different kinds of job. His experience suggests that he is well qualified to do this. And please may we have something more useful about photography? E. W. H. SELWYN

Reference books and miscellaneous

Acta Imeko 1958: Proceedings of the International Measurements Conference, Budapest 24-30 November, 1958. Vol. 1: Pp. 443. Vol. 2: Pp. 444. Vol. 3: Pp. 372. Vol. 4: Pp. 460. Vol. 5: Pp. 419. (Budapest: Hungarian Scientific Society for Measurement and Automation, 1959.)

The published proceedings of the 1958 International Measurements Conference, organized by scientific societies in Hungary, Poland and the U.S.S.R., provide Western readers with a convenient means of reviewing the present state and development of metrology and instrument technology in these and other countries of Eastern Europe. Of the 127 papers published no less than 113 originate from the three organizing countries with the German Democratic Republic and Czechoslovakia. As summaries in English are provided with 121 of the papers printed in languages other than English (or French), it is possible for readers of English to gain a reasonable first impression of the contents of practically all the papers without recourse to translation. At the end of each volume is reproduced in English (as well as in the other three official languages) a list of titles and authors of the papers appearing therein.

The conference was organized into three main sections dealing with the following topics: I. Contributions of general interest (10 papers, mainly of review type); II. (comprising 9 sub-sections) Geometric quantities; Mechanical quantities; Optical measurements; Temperature, flow and humidity; Electric quantities; Magnetic quantities; Electric and electronic measuring techniques; Chemistry, physical chemistry and structure analysis; Measurement and application of the ionizing radiations (102 papers in all); III. Organization, economy, technology and education (15 papers).

This collection of papers, taken on the whole, is worthy of notice by all those interested in present-day trends of metrology and instrument technology. H. BARRELL

Analysts pocket book. By J. R. MAJER. (London: Butterworths Scientific Publications, 1959.) Pp. 100. Price 17s. 6d.

Though intended for chemical analysts, many of the tables in this book will be useful to physicists: atomic weights, solubilities, densities, conversion tables, logarithms, anti-logarithms, etc. This little book hardly differs from many of its predecessors, and the price seems rather high, even though tables are expensive to print. The method of binding makes it possible both to carry the book in an overall pocket, or to place it open on the bench with the required pages lying flat.

G. W. SCOTT BLAIR

Chemical engineering practice. Vol. 11. Works design, etc. Edited by H. W. CREMER. (London: Butterworths Scientific Publications, 1959.) Pp. vi + 390. Price 95s.

The eleventh volume of *Chemical engineering practice* fulfils a valuable purpose in that it deals with broader aspects of the subject, which the chemical engineer is more likely to encounter in his professional career rather than in his formal training.

The volume opens with a chapter on works design, layout and execution, while this chapter deals with specialized problems in plant design and construction which normally become the responsibility of the civil and constructional engineer, its inclusion is timely in that the chemical engineer should be familiar with the general procedure involved in this field.

There follows a chapter on works administration wherein is set out a succinct presentation of the many aspects of chemical plant management. Its author has succeeded in covering a wide field with precision and clarity, and provides the reader with a sound background to modern views on plant management. This chapter is a notable contribution to the whole work.

A chapter on the Factories Acts and other legislation includes sections on factory legislation and the alkali, etc., Works Regulation Act, 1906, Works Orders 1928 to 1958. Here again the reader will find useful information on the legal background of plant operation. There follows a chapter on works safety in which the many details so necessary to safe operation are discussed.

Equally valuable is the concluding chapter on patents, which provides the chemical engineer with sufficient knowledge for his effective purpose. These four chapters together therefore provide considerable breadth to the whole work and will significantly enhance its value as a reference work.

The volume as a whole maintains the high standard achieved in the previous published volumes. H. THOMAS

Classification and indexing in science. 2nd ed. By B. C. VICKERY. (London: Butterworths Scientific Publications, 1959.) Pp. xix + 235. Price 30s.

In his preface, the author states that his book did not set out to be a manual, but primarily a study of method. It is certain, however, that it will be read and used in both manners. It must be gratifying that a second, enlarged edition has been called for within the space of a year and it has been amplified so that it may better serve the purpose of helping those who have to construct systems of information retrieval.

With the output from scientific work continually increasing, it is essential to devise means of classifying and recording data on the subject-matter so that a subsequent user shall be able to find all such records. It is this ability to be able to find the information again that makes the problem of subject indexing of such importance. Any scheme devised must take into account that the user may refer to an index at a different starting point from the one who prepared it.

This book is to be commended to all involved in classification, indexing and the use of recorded information. The author deals with many systems and outlines their advantages and disadvantages. Into this second edition he has brought developments discussed at an international conference less than a year prior to publication, so the work is fully up to date. A. J. MADDOCK

Evaporation and droplet growth in gaseous media. By N. A. FUCHS. Translated from the Russian by J. M. PRATT. Edited by R. S. BRADLEY. (Oxford: Pergamon Press Ltd., 1959.) Pp. 72. Price 30s.

This monograph by N. A. Fuchs, doyen of the Soviet school of aerosol physics, is most welcome as a comprehensive and detailed survey of existing knowledge, both theoretical and experimental, of the subject of the evaporation and growth of droplets of pure liquids in gases. Modern theory stems, on the one hand, from the classic paper by Fuchs himself published in 1934 on the evaporation of a stationary droplet in a still atmosphere and, on the other, from the notable work of Frössling in 1938 relating to the moving droplet. Since then refinements have been introduced especially by Bradley and his co-workers whose elegant experiments completely verified Fuchs's theoretical treatment.

Derivation of the basic theory is of importance in cloud physics, in many processes in chemical industry and in the combustion of engine fuels, and the author is to be congratulated on a contribution which will prove invaluable over such a wide range of disciplines. Maybe, in a second edition, he will undertake the formidable task of extending the scope of the monograph to solutions.

The translation by J. M. Pratt, under the authoritative editorship of R. S. Bradley, is admirable. Production is clear, but photographic reproduction from the typescript has rendered some of the subscript symbols almost microscopic in size. The house and date of publication of the original, which in point of fact was 1958, are not stated.

H. L. GREEN

Friction in textiles. By H. G. HOWELL, K. W. MIESZKIS and D. TABOR. (London: Butterworths Scientific Publications, 1959.) Pp. xii + 263. Price 42s.

Friction testing and, more particularly, its tricky offshoot, abrasion testing, have acquired in some textile circles a reputation for the exasperation they produce: no two experimenters come to the same conclusions. I can think of another

branch of textile studies which is just as bad in this respect, and both have this in common that they are much affected by small changes in the surface condition of the fibres and of the materials that they rub against. It is my only serious complaint against this book that, in the textile sections, too little emphasis is laid on the state of the surfaces (see, for instance, the tables at the end). Perhaps the fault is not so much the authors' as the experimenters', but the former could have protested more. This having been said, it must be acknowledged that the three authors have made a most painstaking and praiseworthy account of a difficult subject. The book is divided into three parts dealing respectively with the mechanism of friction in general, with the effects of friction on textile processing, and with the measurement of friction, tension, and abrasion. The style is generally clear and readable, though not always grammatical (I was sorry to meet the old ambiguous phrase " x decreases with y " meaning, as usual, the opposite of what it says). The book will be a mine of references to anybody interested in its subject, and its thoroughness is shown by the description of some fifty different methods of measuring textile friction that have been published. The authors wisely refrain from attempting the same feat with abrasion testing.

P. S. H. HENRY

Gas chromatography abstracts 1958. Edited by C. E. H. KNAPMAN and C. G. SCOTT. (London: Butterworths Scientific Publications, 1960.) Pp. vii + 262. Price 42s.

This collection of abstracts, covering the period to the end of 1958 and sponsored by the Gas Chromatography Discussion Group, was drawn from three individual bibliographies composed by members of the Group. It is intended as a preliminary volume of *Gas chromatography abstracts*, the first volume of which should be ready this year. It contains 1462 references and a substantial subject index.

Moisture in textiles. Edited by J. W. S. HEARLE and R. H. PETERS. (Manchester: The Textile Institute; London: Butterworths Scientific Publications, 1960.) Pp. ix + 203. Price 40s.

Hygroscopicity is an important property of the traditional textile fibres, and its study has always been one of the major physico-chemical research activities in the field of fibre science. In this country this work has been carried out most intensively by the Research Associations of the cotton and the wool industries, and it is not surprising, therefore, that most of the contributors to this collection of essays, based on a series of lectures at Manchester, have been closely associated with these institutions. Within their self-imposed limits the authors have produced a readable and authoritative outline of the principal effects of moisture absorption. The limits referred to seem to eschew any detailed consideration of structural questions, so that we find it accepted as quite normal that important adsorption theories "consider the water molecules to be adsorbed on internal surfaces or sites . . . , and apart from supplying these sites the textile is considered to play little part in the process". However, for a physicist who might be more interested in the comfort of his clothing than in the reason why his wife's clothes-line shortens when it gets wet, there is here much worth reading; if it were not for its price, it could also be recommended for students in the more advanced courses of textile technology.

H. J. WOODS

Structural damping. Edited by J. E. RUZICKA. (Oxford: Pergamon Press Ltd., 1960.) Pp. 165. Price 30s.

The aim of this book is to collect information on structural damping that is useful in engineering design into one reference. The work represents a selection of papers presented at a colloquium on structural damping held at the annual meeting of the American Society of Mechanical Engineers (ASME), in Atlantic City, New Jersey, in 1959. The colloquium was sponsored by the Shock and Vibration Committee of the Applied Mechanics Division of the ASME. The book is divided into seven sections. The first deals with the engineering significance of structural damping with particular emphasis placed on material damping and the second section presents a review of progress in the analysis of interfacial slip damping. The third section discusses the damping of plate flexural vibrations by means of viscoelastic laminae, with particular emphasis placed on such practical damping configurations as automotive undercoat, damping tape, and sandwich plates with dissipative cores. Following is a section on the vibrational energy dissipation at structural support junctions and the fifth section describes the details of structural damping measurement methods. The sixth section considers the material design for resonant members, proper selection of a structural material being made by use of a fatigue strength-damping criterion which is applied to many practical machine member designs. The final section is a selected bibliography on structural damping containing over a hundred references.

Solid state physics and crystallography

Methods of experimental physics. Vol. 6. Solid state physics.

Part A. Edited by K. LARK-HOROVITZ and V. A. JOHNSON. (New York: Academic Press Inc.; London: Academic Books Ltd., 1959.) Pp. xvi + 466. Price 86s.

This volume opens with a tribute to the late Professor Karl Lark-Horovitz from his fellow editor.

Professor Lark-Horovitz was among the few with the necessary breadth of grasp to plan and edit a volume of this nature. The volume is in two parts, the first of which is noted here. The material is organized in the order—how to prepare your crystal; how to verify that it is what you hoped it would be, what to do with it when you've got it. Preparation and structure determination occupy half this book, followed by mechanical properties, thermal properties, and high pressure studies. Diffusion is drawn under mechanical properties, presumably because of its role in micro-creep and mechanical damping. Electromagnetic and optical measurements at normal and low pressures fall into the second part.

The plan of the book is sensible, with a minimum of overlap (perhaps, indeed, rather too little) between the different sections. The amount of theoretical material quoted by various authors varies enormously, but is largely only where, as in dislocation theory, the matter is both novel and important. No book of this sort can replace a proper literature search, but it can save a great deal of trouble at the start of a search. References are freely given, though there seem to be far too few from the Soviet literature. The second part of the volume is of equal quality.

G. WYLLIE

Solid state physics. Advances in research and application.

Vol. 9. Edited by F. SEITZ and D. TURNBULL. (New York: Academic Press Inc.; London: Academic Books Ltd., 1959.) Pp. xv + 548. Price £5 3s. 6d.

This series continues to be useful and valuable. A pleasing feature is the contents list for preceding volumes with the list of planned articles for future volumes, which constitutes a broad summary of the state of the art.

The present volume contains three fairly closely related articles on crystal spectroscopy, with four others on diverse topics. H. C. Wolf surveys present experimental knowledge of the spectra of aromatic molecular crystals and adds a short account of the present theory, due largely to Davydov, which provides a framework for the experimental results. Further work on the temperature dependence of line shapes and intensities is required at many points. The reader may find it useful to refer back to D. S. McClure's article on spectra of molecular crystals in Volume 8 of the series: McClure adds a long and lucid article on the spectra of ions in crystals in this volume. E. Heer and T. B. Novey discuss the effect of intra-crystalline fields in inducing precession of a radio-active nucleus between two successive decays, and so changing the angular correlation of the product particles. The new very fast counting techniques make such measurements useful both for nuclear and for solid state physics. The nature of the information obtained is much the same as can be had from nuclear magnetic and quadrupole resonance techniques, but in a new region of the parameters.

A. Guinier contributes an authoritative article on the study of heterogeneities in solid solutions of metals by small-angle X-ray diffraction. W. W. Scanlon, under the over-general title of "Polar semiconductors", gives a clear review of the semi-conducting behaviour and electronic properties of the PbS, PbSe, PbTe group of crystals. D. J. Montgomery reviews the complex of experimental information and misinformation, and of theoretical speculation, which obscures the static electrification of solids, and ends with an optimistic prospect of future investigation. A. H. Kalin and H. P. R. Frederikse discuss the oscillatory behaviour of susceptibility and conductivity of metals and semiconductors with increasing magnetic fields, which arises from the great statistical weight of the nearly flat electron orbits in the presence of the field. The experimental results essentially plot the area of the sections of the Fermi surface normal to the field and give a very useful guide to mapping the surface—they only determine it if it is of a rather simple type. The amplitude of the effect is in poor agreement with the theory. G. WYLLIE

Solid state physics in electronics and telecommunications.

Vol. I. Semiconductors. Part 1. Edited by M. DÉSIKANT and J. L. MICHIELS. (London: Academic Press, 1960.) Pp. xxiii + 638. Price £6 8s. 6d.

The proceedings of an International conference held in Brussels, June 1958, have been published with the aim of establishing an area of common understanding between scientists and engineers of all nations in the field of solid state physics. The book is divided into six sections, with an additional general article by Dr. W. Shockley on crystals, electronics, and man's conquest of nature. The remaining sections deal with preparations of semiconductors and applied problems, properties of semiconductors, solid state theory, the effects of intense electric fields in semiconductors, noise in semiconductors and surface phenomena.

Solid state physics. Advances in research and applications.

Vol. 10. Edited by F. SEITZ and D. TURNBULL. (London: Academic Press, 1960.) Pp. xv + 516. Price £5 3s. 6d.

During the editing of this volume the editors learned of the sudden death of M. R. Schafroth, one of the contributors, and the final article, therefore, represents this author's last written comments on the field of superconductivity. Five articles, in all, are presented in this book. The first describes how positron annihilation studies can yield information about certain solid state problems. Following this is an article dealing with intermetallic diffusion phenomena. The third article deals with wave functions for electron-excess colour centres in alkali halide crystals, while the fourth article treats the continuum theory of stationary dislocations. The fifth article is written by the late Professor Schafroth and deals with the theoretical aspects of superconductivity, covering both the phenomenological and the microscopic theories. The other contributors are Philip R. Wallace, David Lazarus, B. S. Gouray, F. J. Adrian, and Roland de Wit.

Crystal chemistry of simple compounds of uranium, thorium,

plutonium, neptunium. By E. S. MAKAROV. Translated from the Russian by E. B. UVAROV. (New York: Consultants Bureau, Inc.; London: Chapman and Hall, Ltd.; 1959.) Pp. iii + 145. Price 42s.

This is a very valuable and comprehensive summary of the subject. About two-thirds of the book is devoted to factual data on the structures of the polymorphic modifications of Th, U, Np and Pu, and on the structures of the compounds of these elements. The last chapter is a stimulating discussion on the duality of their chemical nature. There is a rather elementary introductory chapter on general crystal chemistry which some readers may find unnecessary. The translation is good and the production satisfactory. Very few misprints were noted. There is a bibliography running to 117 references, but it is a pity that no index is included. J. THEWLIS

Theoretical physics, mathematical techniques, computers and control systems**Encyclopedia of physics. Vol. VIII/I: Fluid dynamics. 1.**

Edited by S. FLUGGE and C. TRUESDELL. (Berlin: Springer-Verlag., 1959.) Pp. vi + 471. Price DM132.

This volume contains the following four contributions: (a) Physical foundations of fluid dynamics (in German), by K. Oswatitsch; (b) Mathematical principles of classical fluid mechanics (in English), by J. Serrin; (c) Laminar boundary layers (in English), by L. Howarth; (d) Transition to turbulence (in German), by H. Schlichting.

These four articles naturally reflect the diverse interests and points of view of the authors. For example, Professor Serrin treats the foundations within the framework of Rational Mechanics: and his article, which is novel and original, contains a larger injection of mathematical rigour than is customary, since most applied mathematicians are motivated by a more physical point of view. In strong contrast, Professor Schlichting's article on transition leans heavily on the experimental facts and the interpretation of them, and it is clear that the nature of subject-matter dictates such an approach. The other two articles fall between the two extremes described above; however, a glance at them

shows at least one difference, namely that Professor Oswatitsch does refer in a little detail to experiment, whereas Professor Howarth confines himself more strictly to theory.

The present reviewer believes that each of these four articles is of value both for reference and for detailed study. It is to be hoped that further articles on fluid dynamics, in other parts of Volume VIII, will maintain the standard of those in this volume.

J. T. STUART

Lectures on Fourier integrals. *Annals of mathematics studies* No. 42. By S. BÖCHNER. Translated from the original by M. TENENBAUM and H. POLLARD. (New Jersey: Princeton University Press; London: Oxford University Press, 1959.) Pp. 333. Price 40s.

The present publication is a translation of Böchner's *Vorlesungen über Fouriersche Integrale* (Leipzig, 1932) and of his *Monotone Funktionen, Stieltjessche Integrale und Harmonische Analyse* [*Math. Ann.*, **108**, pp. 378–410 (1933)]. Böchner's book has long been recognized, with Titchmarsh's *Introduction to the Theory of Fourier Integrals*, as the main treatise on the theory of Fourier integrals. It contains, in addition to the "classical" results concerning Fourier integrals, the theory of positive definite functions, of the generalized Fourier integral, and theorems concerning the reciprocal of Fourier transforms. In addition to making this classic work available to English-speaking graduate students beginning the study of the theory of integral transforms, the publication of this translation at the present time will remind workers on the theory of groups and of distributions of much pioneer work done in these disciplines by Böchner in this book.

The book itself, and this translation of it, can warmly be recommended to anyone beginning to study the theory of Fourier analysis; anyone interested only in applications to physics of Fourier integrals is advised to try something easier.

I. N. SNEDDON

Non-linear wave mechanics. By L. DE BROGLIE. (London: D. Van Nostrand Co. Ltd., 1960.) Pp. xi + 304. Price 57s.

This is a fascinating monograph written by one of the pioneers of modern physics. The title of the English translation is somewhat misleading; the original title *Une tentative d'interprétation causale et non linéaire de la mécanique ondulatoire* covers more truly the contents. The author's objective was to give a full and comprehensive account of his investigations concerning the theory of "double solution" which would make it possible to render a strictly causal and complete interpretation of quantum mechanics as opposed to the orthodox probabilistic interpretation. It is well known that de Broglie's theory consists essentially in finding such solutions u of the wave equation which have a mobile region of singularity embedded, so to speak, in a continuous wave. The conventional probability wave ψ would be proportional to the u -wave outside the singular region. In order to avoid various difficulties it appears that the wave equation must contain some non-linear correction terms.

It would be, of course, completely out of bounds either to discuss the theory in detail or to give a criticism within the framework of a book review. This important task must be undertaken by future scientific research works. What we certainly may say here, however, is that the book gives an extremely clear, self-consistent and candid presentation, not only of the topic itself, but also of the intellectual

development of these ideas by the distinguished author in the course of the last 35 years. To many physicists who are interested in the way in which physical ideas are conceived, developed, partly rejected at a stage, then taken up again from a slightly different angle, modified once again and so forth, this monograph will provide enlightening reading material. It should also be mentioned that the first 85 pages give a very thorough and fascinating exposition of the conventional framework of quantum mechanics, the study of which could be recommended to any student of modern theoretical physics.

P. ROMAN

Organisation et fonctionnement des machines arithmétiques. By H. BOUCHER. (Paris: Masson et Cie, Éditeurs, 1960.) Pp. 427. Price 70 NF.

The author has written this book in order to fill what he regards as a deplorable gap in French technical literature. He realizes that the subject is already well covered by British and American books and so, although this is a competently written volume, it will have no special appeal except to those who prefer to read their computation in French. The usual aspects of high-speed computers are considered in reasonable detail including, in Part I, basic electronics, memory devices and circuit design. Part II is concerned with programming. Fifteen pages are devoted to the digital differential analyser. With the book are three loose leaves giving details of available computers for commercial and scientific work and of machines working in real time. These lists are remarkably up-to-date and contain a considerable amount of useful information.

The bibliography contains references to eighty-nine books and articles. The text is illustrated by a large number of diagrams.

J. CRANK

Reciprocals of the integers from 1000 to 9999. By T. H. REDDING. (London: Taylor and Francis Ltd., 1960.) Pp. v + 43. Price 18s. 6d.

These tables list the reciprocals multiplied by 10^6 of the integers 1000 to 9999. The entries are direct reading and are claimed to be correct to three decimal places. With mechanical calculating machines of the "barrel-setting type" and certain types of adding and listing machines the process of division is most conveniently regarded as one of multiplication by a reciprocal. The main purpose of the tables is to facilitate the evaluation of quotients and compound fractions in this way. They are, of course, also suitable for general use. In a twenty-two page Appendix, a discussion of the tables is prefaced by a description of barrel-setting machines and their operation, illustrated by worked examples. The tables are clearly printed on good-quality paper and are well bound.

J. CRANK

Regression analysis. E. J. WILLIAMS. (New York: John Wiley and Sons, Inc.; London: Chapman and Hall Ltd., 1959.) Pp. ix + 214. Price 60s.

A great deal of laboratory experiment is devoted to the finding of relationships between physical quantities. In the great majority of cases, some would say all, the practical uses to which these findings are ultimately put involve the prediction of the expected value of one of the quantities corresponding to a stated value of the other. Inevitably,

variability of unknown or unexplored cause is present thus introducing a problem of estimation; the parameters of the relation are not known with certainty because they have to be estimated from a sample of variable observations. In this book are collected the methods of estimation appropriate to various situations including the case of the functional relationship which needs special treatment.

The author has performed a useful service in collecting together these results which are only briefly dealt with in most texts on statistical methods. The fact that the (worked) examples are drawn from the author's experience as a consultant in the fields of forestry, agriculture, biology and chemistry should deter no one from using this book since it is addressed to all practitioners of the experimental sciences and the text is in general, though mathematically expressed, terms.

Derivations of the many formulae are not given but instead there are references to the original papers and some other books. The great advantages of matrix methods of calculation are obtained without imposing too much on the reader unfamiliar with them. One chapter is devoted to the allied subject of discriminant functions.

Altogether this is a book for reference which fills a need; its contents are the concern of every experimenter.

E. D. VAN REST

The theory of thin shells. By V. V. NOVOZHILOV. Translated from the Russian by P. G. LOWE. Edited by J. R. M. RADOK. (Groningen: P. Noordhoff Ltd., 1959.) Pp. xvi + 376. Price \$9.50.

The book deals with the theory of thin shells based on the Kichhoff hypothesis that straight lines perpendicular to the middle surface remain straight and perpendicular to it after deformation, and that direct stresses perpendicular to the middle surface may be neglected. It is divided into four chapters: (1) the general theory of thin shells; (2) the moment-less or "membrane" theory; (3) cylindrical shells, and (4) shells of revolution. The dependence upon Kichhoff's hypothesis limits the theory to an approximate one which cannot be developed into a more accurate theory. Nevertheless, the work may be safely described as the technical theory of thin shells. The author regards thin shells as those for which the ratio of thickness of shell to maximum radius of curvature of the mid-surface is less than $1/20$. The strains are expanded in power series of z (the variable across the thickness of the shell) as far as the quadratic term, and then only the linear terms, are retained. Considering the carefulness with which this strain theory has been set forth, the treatment accorded to the equivalent mid-surface loading wrench in para. 7, Chap. 1, seems rather inadequate. A cursory examination resting on the statement that the applied forces on the surfaces of the shell "will in all practical cases act normal to the middle surface" is not in keeping with the rigorous treatment accorded to the strains. The statement is not true in the case of snow-loading, for example. Among the various treatments of the transformations of the equations of thin shell theory, the author's own contribution to the subject is the reduction of the equations from six to three by exploiting the symmetry of the equations by the use of complex combinations of stresses. There is

no complex-variable theory involved, but he makes considerable use of the idea resulting in a very compact treatment, although separation into real and imaginary parts is necessary before he can apply his boundary conditions.

The translation reads well and the book is excellently produced though a first perusal led to the mis-spellings "auther" in the translator's preface, "appearance" on p. 84, "canonical" on p. 95, and "oft" (for "of") on p. 255. The work is certainly a welcome and useful addition to the works in the English language on the subject.

C. SNELL.

Wärme-und Stoffaustausch in Arbeitsdiagrammen auf projektiver Grundlage. By W. MATZ. (Berlin: Springer-Verlag, 1960.) Pp. viii + 142. Price DM24.

It is difficult to review a book like this briefly because it is essentially based on an idea which is quite new to the reviewer, namely, the application of the concepts of projective geometry and harmonic points to the thermodynamic working diagrams, and to such things as temperature, exchanger area diagrams for counterflow heat exchangers. Other physical and chemical systems treated by projective geometry include the three-component diagram in extraction processes, rectification and concentration processes, and indeed it would appear that the author has worked out most of the consequences of his title.

How far these elaborate diagrams making use of two-, three- and even four-dimensional projective geometry, are in fact useful in Applied Physics, is as yet an open question, although it is certainly true that such diagrams are used already in the form of nomograms such as the Ellingham Diagram for chemical reaction equilibria. If it does prove to be of real value, then the author can claim to have done for the purely mathematical techniques of projective geometry what Einstein did for tensor calculus when he introduced the general theory of relativity.

M. W. THRING

Wave propagation and group velocity. By L. BRILLOUIN. (New York: Academic Press Inc.; London: Academic Books Ltd., 1960.) Pp. xi + 154. Price 48s.

This volume is a collection of papers written by Professor Brillouin (one by Sommerfeld) between 1914 and 1933. The topics treated in the papers arose originally from the apparent discrepancy between the result of special relativity that no signal can travel with a velocity in excess of c and the fact that in dispersive media the group velocity of light can exceed c . The introductory chapter is an excellent summary of the results, drawing attention to the need to distinguish between the group, energy-transfer and signal velocities. This chapter will be of considerable interest to many physicists, and to honours degree students. The remainder of the book is devoted to a mathematical development of the subject (using contour integrals) and the application of the general results to the Lorentz-Lorenz electron model of dielectrics. The book does not claim to do more than provide physicists with easy access to the original papers. Nonetheless it is somewhat surprising that in such a book, recommended to radio engineers, there is no mention of the work of the last twenty years, and that the ionosphere is called the Heaviside layers.

M. I. LARGE

Emission of negative ions of oxygen during the activation of oxide-coated cathodes

by N. A. SURPLICE, B.Sc., Ph.D., A.Inst.P., Physics Department, University College of North Staffordshire, Keele

[Paper first received 7 April, and in final form 13 May, 1960]

Abstract

Oxide-coated cathodes have been used as ion sources in a simple mass spectrometer and have been found to emit atomic negative ions of oxygen during their activation at high temperatures (1150–1275° K). A retarding potential at the collector was used to separate the ions emitted by the cathode from the ions formed in the residual gas. Most of the oxygen ions from the cathode arrived at the collector with more energy than they could have obtained from the potential difference across the electron gun, and their number increased as the cathode became more active. The evidence suggests that the ions were formed by dissociation of the oxide coating, then diffused to the surface and were removed by positive ion bombardment. Such a process would leave oxygen vacancies in the oxide which would act as electron donors and increase its electron emission.

Introduction

A NEWLY formed oxide-coated cathode has to undergo a process known as activation before it gives a sufficiently high and stable emission current of electrons, and this is usually accomplished by keeping the cathode at its operating temperature (about 1100° K) and drawing electron current from it for several hours. During this treatment it might be expected that partial dissociation of the oxide lattice would lead to the emission of oxygen in the form of negative atomic ions. Although these ions have not previously been detected during activation,^(1,6,7) some recent indirect evidence has favoured their formation⁽⁵⁾ and there has been considerable evidence that they accompany the normal cathode emission of electrons.^(1–4)

Apparatus

The cathodes were made of O-nickel buttons which had been cleaned by heating in hydrogen and then sprayed with a commercial carbonate suspension. They were 0.5 cm² in area and their coating was about 0.01 cm thick. Six cathodes were studied: one was prepared of each of the single carbonates of barium, strontium and calcium, and three were prepared from the double carbonate suspension that the author had used in previous experiments on poisoning.⁽⁸⁾ Four of the cathodes had commercial heaters embedded in alumina, but two of the mixed-oxide cathodes had homemade heaters of tungsten covered with ceramic beads.

Each cathode in turn was made the ion source of a small mass spectrometer which could distinguish negative ions of masses up to 45 with a resolving power of about a hundred. The negative ions emitted from the cathode were accelerated by the modulator and the anode of a simple electron gun,

then were selected by a magnetic analyser and detected by a d.c. amplifier at the collector. This arrangement was simple but inefficient. Under typical operating conditions only 2×10^{-3} of the electron current reached the anode and only 2×10^{-7} of it reached the collector. However, a greater proportion of the negative-ion current would reach the collector because it would be less affected by the fringing field of the electromagnet, which is shown in Fig. 1.

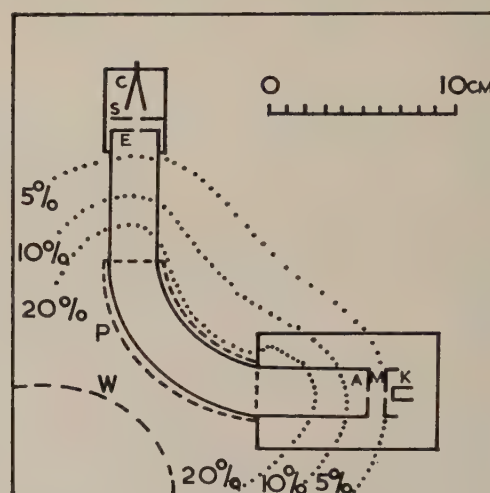


Fig. 1. Block diagram of mass spectrometer, showing fringing field of magnet

K, cathode; M, modulator; A, anode; E, exit slit; S, screen; C, collector; P, mild-steel pole piece; W, winding on yoke of magnet

Dotted lines show fringing field as a percentage of the field strength between the centres of the pole pieces

The glass envelope of the mass spectrometer was cracked open and cleaned chemically before each cathode was inserted with its new electron gun, and the envelope resealed. Further particulars have been given in a previous paper.⁽⁸⁾ The instrument was evacuated by a mercury diffusion pump, through a liquid-air trap. It was baked for an hour to drive off water vapour and then the alkaline-earth carbonates were converted to oxides by gradually increasing the cathode temperature from 350° C to 950° C over three hours. The whole instrument was baked at 390° C for a further eighteen hours. Finally the cathode was kept at 950° C while the other electrodes were eddy-current heated to redness, and afterwards the pumping tube was sealed off and barium getters were fired. Throughout these operations the pressure was too low to be recorded by a Penning gauge, so may be assumed to have been well below 10^{-5} mm of mercury during breakdown and probably better than 10^{-6} mm of

mercury when the tube was sealed off; the mass spectrum never included any CO_2^- and only once showed any trace of CO^- .

Experimental results

Emission of oxygen as negative ions. Each cathode was activated by drawing electron current from it to the modulator, which was at 250 V positive with respect to the cathode and had a hole in it of 0.1 cm diameter. The modulator collected 99.8% of the electron current and screened the cathode so effectively from the anode that it made little apparent difference to the activation process whether the anode voltage of 950 V was on or off. During the entire activation process each cathode was observed to be emitting the atomic negative ion of oxygen $^{16}\text{O}^-$, but not the molecular ion $^{32}\text{O}^-$. The initial current of negative ions of oxygen to the collector at cathode potential was about 10^{-14} A from the mixed oxide cathodes and generally increased to 10^{-13} A after a few hours, though for one cathode it reached 3×10^{-12} A. The height of the oxygen ion peak was found to be proportional to its area, and so it gave a satisfactory measure of the ion current.

Energy distribution of the oxygen ions. The energy distribution of the oxygen ions emitted from cathodes made with mixed oxides was found by measuring their ion current to the collector against a retarding potential. Each plotting of an energy distribution curve took about ten minutes, and there were apparently no changes in the energy distribution during this short time. The steady ion current was measured at each retarding potential after slightly increasing the magnetic field to compensate for the higher momentum of the ions. It was not practicable to measure energy distributions of the much smaller ion currents emitted by cathodes made with single oxides. The contact potential difference between the collector and the cathode (usually 2 V) was found by reducing the magnetic field and measuring the electron current to the collector over a range of retarding potentials.

The integral energy distribution curves for the oxygen ions from all the mixed-oxide cathodes were qualitatively similar, and those for cathode 9F are shown in Fig. 2 for various stages of its life. The curves may be considered in three parts, of which the first two include all ions emitted directly from the cathode. Ions in part A had more energy than they could have obtained from the electron gun alone and had presumably gained the difference from positive ions which bombarded the cathode,⁽⁴⁻⁹⁾ whereas ions in part B could have been evaporated from the pores of the cathode. The ions in part C had not been emitted from the cathode but had been formed in the space between it and the modulator. The variation of the curves with time is typical of all three cathodes and shows that, as time went on, proportionately fewer ions were formed in the space near the cathode but that no permanent change was detected in the energy distribution of high-energy ions. The curves do not show the tiny part of the ion current which had excess energy of up to 50 V.

Variation of oxygen ion emission with time. A particular study was made of the variation with time of the current of oxygen ions that was emitted directly from the cathode. For two mixed-oxide cathodes (8E and 8F), the oxygen ion currents were studied in detail during activation and were found to increase irregularly until the electron current became fairly steady, and then to decrease again. The results are shown in Fig. 3. The long-term variations of the high-energy part of the oxygen-ion current were studied for cathode 9F and

were found to be fairly smooth. The ion current rose to a maximum in four hours and then decreased again while the electron emission continued to rise for a further two hours. Fig. 4 shows the different variation of the ion and electron currents for the first 100 hours of cathode life. After 120

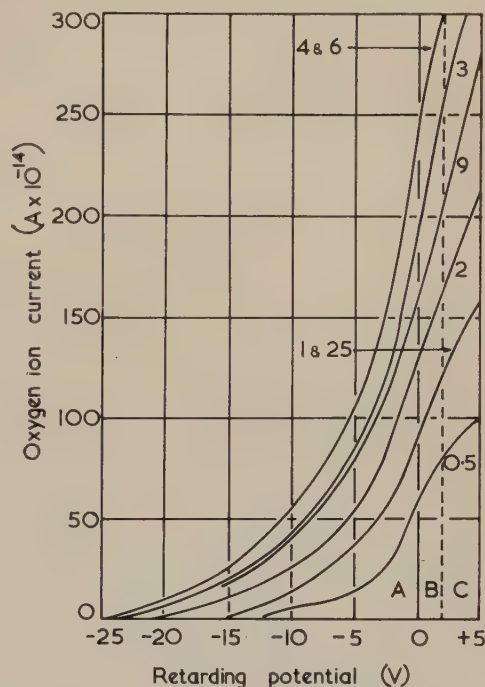


Fig. 2. Variation with time of energy distribution of oxygen ions emitted during activation of cathode 9F at 1150°K . Numbers on curves show time in hours from beginning of activation process

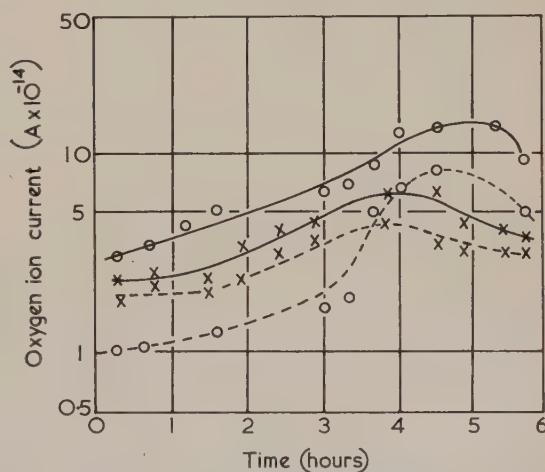


Fig. 3. Variation with time of current of oxygen ions emitted directly from cathodes during their activation
— cathode 8E at 1200°K ○ ○ ○ = part A of the ion current
--- cathode 8F at 1150°K × × × = part B of the ion current

hours the oxygen ion current rose irregularly for the remainder of the useful life of the cathode, and it varied more nearly in proportion to the electron current when the cathode temperature or anode voltage was changed. This change of behaviour was probably caused by the dissociation of barium oxide which had evaporated on to the modulator and anode

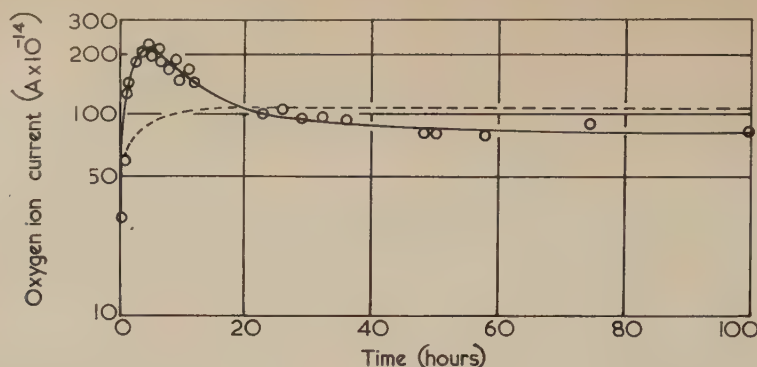


Fig. 4. Variation with time of currents of oxygen ions and of electrons from cathode 9F
 — oxygen-ion current - - - electron current

and had formed a noticeable film there by the end of the life of the cathode.

Both the oxygen-ion currents and the steady electron currents which could be drawn from the cathodes made with single oxides of barium, strontium and calcium were much smaller than those from the cathodes made with mixed oxides. From the barium-oxide cathode, the high-energy part of the oxygen-ion current varied similarly to the curve shown in Fig. 4, but its maximum was only 10^{-13} A at 1275° K, and from the strontium- and calcium-oxide cathodes it was only of the order of 10^{-14} A at 1350° K.

Discussion

In the present experiments, the cathode coating contained about fifty times more oxide and the electrometer was ten times more sensitive than in the experiment of Grattidge and Shepherd,⁽¹⁾ who had not been able to detect any emission of negative ions of oxygen when a small cathode was activated by heating it briefly to a high temperature. However, a few percent dissociation of their cathode would have yielded about 10^{-9} A of oxygen ions which had to pass through a deflexion chamber and slits of similar dimensions to the ones in the author's instrument, and therefore only about 10^{-14} A would have reached the collector and it would have remained undetected. The author's observation of atomic negative ions of oxygen, rather than molecular ones, agrees with all experiments in which modern vacuum techniques have been used to study the ions that accompany a cathode's normal emission of electrons.⁽¹⁻⁴⁾

The currents of oxygen ions were collected against a retarding potential which selected the ions emitted by the cathodes and rejected the ions formed in the residual gas. Some of the ions (part B in Fig. 2) could have evaporated from a chemisorbed layer of gas on the cathodes but the majority (part A of Fig. 2) had extra energy which they had presumably obtained from positive ions which bombarded the cathodes, and their current did not vary like the one from an adsorbed layer of gas. It has previously been found that such an adsorbed layer does form when a cathode is poisoned by oxygen, and during its recovery the cathode emits a current of oxygen ions which decreases as its electron emission increases.⁽⁸⁾ However, during the present experiments on activation, the cathodes were found to emit increasing currents of oxygen ions as their electron emission increased. During the activation of a cathode there is evidence that negative oxygen ions are formed by the dissociation of its alkaline earth oxides,⁽⁵⁾ and this seems to be the most probable source of the ions observed in the present experiments. It is suggested that they diffuse to the surfaces

of the crystals, or the top surface of the cathode, and are removed by positive-ion bombardment. The oxygen vacancies thus left in the crystal lattice would act as electron donors and increase the electron emission. The rapid initial rise of both ion and electron currents would be explained by a rapid diffusion of negative ions to the surface and thus a rapid increase of the number of electron donors in the oxide coating. The subsequent decrease of ion current would occur if a concentration gradient of negative ions built up near the surface and retarded their diffusion, and then the electron current would rise less rapidly than before. The ion current would become steady when equilibrium had been reached between the rate of arrival of ions at the surface and their rate of removal from it. When the electron current had become steady the rates of emission of oxygen and barium ions would also be expected to be equal. If the transmission factor of the mass spectrometer for negative ions is assumed to be of the order of 10^{-5} , then the electron emission from these cathodes had reached a steady value by the time that a few percent of the oxygen in their coatings had been evolved. There did not appear to be any correlation between the amount of oxygen emitted by the three mixed-oxide cathodes and their ability to emit electrons, but this is not particularly significant because the amount of barium emitted is not known. Some recent evidence suggests that the electron emission of a cathode does not primarily depend on the whole of its oxide coating, but on a thin layer of barium oxide at its base,⁽¹⁰⁾ and so its work function would be independent of the amount of oxygen emitted by its coating.

Acknowledgements

The author thanks Prof. F. A. Vick and Prof. D. J. E. Ingram for laboratory facilities during 1959 and 1960 respectively, Mr. C. H. B. Mee for discussions, Mr. H. Stuart and Mr. L. Robertson for blowing the glass envelopes for the mass spectrometers, and Siemens-Edison-Swan Ltd. for the gift of valve stems.

References

- (1) GRATTIDGE, W., and SHEPHERD, A. A. *Proc. Phys. Soc. (London) B*, **67**, p. 177 (1954).
- (2) BACHMAN, C. H., and CARNAHAN, D. W. *Proc. Inst. Rad. Engrs (New York)*, **26**, p. 529 (1938).
- (3) BROADWAY, L. F., and PEARCE, A. F. *Proc. Phys. Soc. (London)*, **51**, p. 335 (1939).
- (4) SLOANE, R. H., and WATT, C. S. *Proc. Phys. Soc. (London)*, **61**, p. 217 (1948).

- (5) METSON, G. H. *Proc. Inst. Elect. Engrs (London)*, Monograph 243 R (1958).
 (6) BECKER, J. A. *Phys. Rev.*, **34**, p. 1323 (1929).
 (7) ISENSEE, H. *Z. Phys. Chem. (Leipzig) B* **35**, p. 309 (1937).
 (8) SURPLICE, N. A. *Brit. J. Appl. Phys.*, **10**, p. 359 (1959).
 (9) ARNOT, F. L., and BECKETT, C. *Proc. Roy. Soc. A* **168**, p. 103 (1938).
 (10) METSON, G. H. *Proc. Inst. Elect. Engrs (London)*, Monograph 289 R (1958).

Sorption and desorption of gas in a hot-cathode ionization gauge

by F. A. BAKER, M.Sc., Grad.Inst.P.,* The Polytechnic, Regent Street, London, W.1, and
 T. A. GIORGI, M.Sc., Grad.Inst.P., S.A.E.S. Getters, Via Gallarate 215, Milan, Italy

[Paper first received 1 March, and in final form 8 June, 1960]

Abstract

An omegatron has been used to analyse continuously the gases present during sorption/desorption experiments with a hot-cathode ionization gauge. It is shown that the most abundant residual gas at the termination of ion sorption pumping is carbon monoxide.

Ten per cent or less of the total gas originally sorbed is readily recovered at an exponential rate, indicating that this fraction of the gas is held at solid surfaces rather than within the solids themselves. It is also found that the fraction of gas that is readily recovered diminishes with successive pumping and recovery according to the relation $(i_+)_{\max}^2 \propto 1/t$, where t is the time recorded from initial operation of the experimental gauge and $(i_+)_{\max}$ is the positive ion current corresponding to the maximum pressure attained during recovery.

that are likely to be involved are dependent upon the nature of the gas under consideration. In practice a mixture of gases is invariably present, and it is not necessarily sufficient to know what part each of the constituents would play if alone present to a high degree of purity; i.e. it is important to investigate the various phenomena, both in a series of pure gases and in known mixtures of gases.

In the present study a method has been developed to examine the sorption and desorption of gas in a hot-cathode ionization gauge. A mixture of gases was present throughout these investigations and this mixture was analysed by means of an omegatron. An important feature of these experiments has been the way in which the atomic mass range was continuously scanned⁽⁴⁾ in order to give a continuous record of the manner in which the gas constitution changed with time during sorption/desorption.

Introduction

VACUUM technologists have recently devoted considerable effort to the development of getter-ion pumps capable of producing so-called "dry" vacua of the order of 1×10^{-9} torr or less. Much of this effort is concentrated on scaling-up small pumps in order to achieve the high speed/capacity requirements of very large systems.

These developments are, to some extent, based on work by Schwarz⁽¹⁾ and Alpert⁽²⁾ concerning certain properties of the hot-cathode ionization gauge. Although these two workers did much towards determining the reliability and accuracy of gas pressure measurements made with the gauge, very little work has been directed at the determination of the physical bases of the observed gas clean-up mechanism.

In making an attempt to determine such physical bases one must be quite clear of the phenomena, or particular aspects of a phenomenon, that require explanation.⁽³⁾ Also it is very important to recognize that most of the phenomena

Experimental apparatus

It was decided to use an omegatron of relatively simple construction in order to minimize the number of variables that would have to be dealt with during use. The omegatron actually used was of the type already described by Reich and Nöller.⁽⁵⁾ All the electrodes were of platinum and a relatively rigid construction was achieved by mounting one of the r.f. plates on the grounded shield screening the lead carrying the resonating ion current.

The necessary r.f. potential was obtained from a video oscillator (type TF 885A/I by Marconi Instruments Ltd.). The stability of this instrument was checked, using a crystal-controlled frequency meter, and found to be perfectly satisfactory after an initial warming-up period. Resonating ion currents from 1×10^{-7} to 1×10^{-14} A were measured by means of a vibrating reed electrometer (type M572 by Ekco Ltd.) and continuously registered on a potentiometer-type pen recorder (by Cambridge Instrument Co. Ltd.). The latter instrument was provided with a supplementary pen which enabled a frequency record to be made, thus facilitating the identification of peaks.

Alcomax III alloy energizing blocks were used in the

* Now at Transistor Division, Standard Telephones and Cables Ltd., Footscray, Sidcup, Kent.

construction of the permanent magnet (by W. Jessop and Son Ltd.) which provided a field of approximately 2600 oersted. The pole-pieces were shaped so as to provide a relatively uniform flux density in the interaction volume of the omegatron.

Continuous scanning of the atomic mass range was accomplished with the aid of a reversible d.c. motor coupled to the r.f. oscillator capacitor drive.

The Bayard-Alpert pattern hot-cathode ionization gauge was normally operated by means of a standard stabilized electron emission unit (type 1075 B by Atomic Energy Research Establishment, Harwell). Positive ion currents from 4×10^{-4} to 4×10^{-10} A were measured by means of an electrometer valve unit of the type described by Allenden⁽⁶⁾ and continuously registered on a small pen recorder.

Electrical apparatus and the all-borosilicate glass vacuum system are illustrated in Fig. 1. The gauges were evacuated,

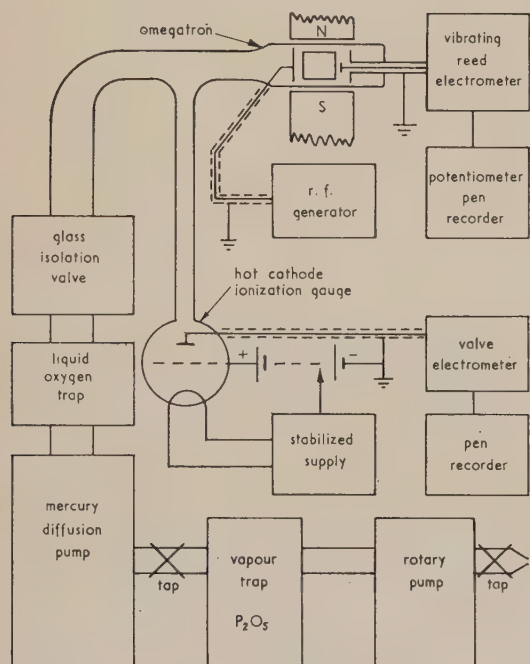


Fig. 1. The pumping system and electrical control units

through a 20 mm diameter greaseless ground-glass isolation valve, by means of a two-stage mercury diffusion pump. The isolation valve could be opened or closed at will by means of a small permanent magnet. A liquid oxygen trap was used to minimize the influence of mercury and other vapours on the pump ultimate.

Experimental procedure

No experiment was conducted before the system was thoroughly degassed. This was accomplished by first baking for a few hours at from 400 to 450° C, and secondly by degassing the metal gauge structures for approximately one hour. The latter was achieved primarily by means of electron bombardment in the hot-cathode ion gauge and by radio-frequency heating of the omegatron. This procedure was usually repeated two or three times, after which there was no difficulty either in maintaining a pressure in the range from 1×10^{-7} to 8×10^{-10} torr, with the glass valve closed, or with the consistency of results.

The speed at which the mass range was scanned was

adjusted so as to provide adequate resolution coupled with sufficient speed to allow changes in gas constitution to be followed. On average the range from 70 to 450 kc/s or 60 to 10 a.m.u. was covered in 100 s.

Experiments were conducted by analysing residual gases present at the diffusion pump ultimate, through degassing the hot-cathode ion gauge, during a period of ion sorption pumping with the gauges isolated from the diffusion pump, and, finally, with the ion gauge electron accelerating potential switched off. It is important to note here that any desorption data, obtained where ion-sorption pumping is terminated by removing the filament supply, is unreliable. Accordingly, in these experiments ion pumping was always terminated by removing the electron accelerating potential.

The possibility of the omegatron removing gas by ion-sorption was also taken into account. The theoretical pumping speed, for normal operating conditions ($5 \mu\text{A}$ electron current; 1.0 V r.m.s.; 0.3 V trapping), is approximately 1×10^{-5} litre/s at maximum. This figure is negligible compared to a possible 1×10^{-1} litre/s for the hot-cathode ion gauge and was never observed in practice.

Experimental results

Results of these experiments are presented in two ways:

(a) composite mass spectra illustrate the gas constitution before and after some specific operation;

(b) partial pressure indications, of the more abundant residuals, are plotted against time in order to illustrate the manner in which changes shown in (a) have occurred.

Thus, Fig. 2 illustrates composite spectra of gases present

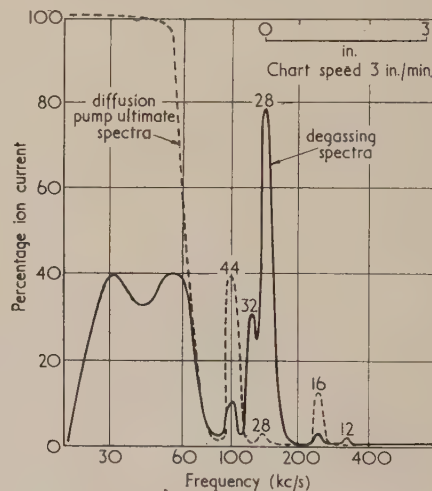


Fig. 2. Diffusion pump ultimate ($100\% \equiv 1 \times 10^{-12}$ A) and degassing spectra ($100\% \equiv 3 \times 10^{-13}$ A) i. = $4 \mu\text{A}$; trapping = 0.1 V; r.f. = 2.0 V r.m.s.

at the diffusion pump ultimate and gas constitution during degassing of the electrodes of the ion gauge, i.e. the changes brought about by initiating degassing are illustrated. The most striking point here is the evolution of 28 and 32 a.m.u. Clearly, masses greater than about 44 a.m.u. are not resolved, although their presence is to be observed. The precise form of these unresolved masses, at the diffusion pump ultimate, was found to vary in detail from experiment to experiment. These variations were attributed to slight variations in charging the liquid oxygen trap and are therefore possibly due to mercury vapour.

Fig. 3 illustrates the variation in gas constitution with time

during degassing of the ion gauge electrode structure. The evolution of 28 a.m.u. was thought to be due to the complex reaction between carbon, on the hot tungsten filament, and oxygen, from water vapour, to form carbon monoxide.⁽⁷⁾

At the start of ion pumping (Fig. 4) 28, 32 and some masses in excess of 44 a.m.u. are the most abundant. Pumping appears to remove the larger mass numbers more rapidly; in fact the rate of removal was too rapid to allow a record to

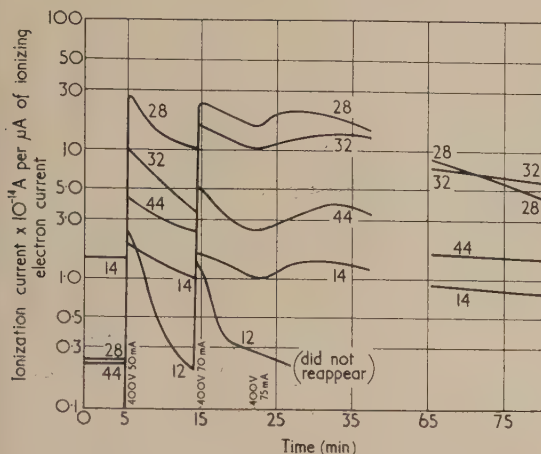


Fig. 3. Partial pressure indications against time during ion gauge degassing

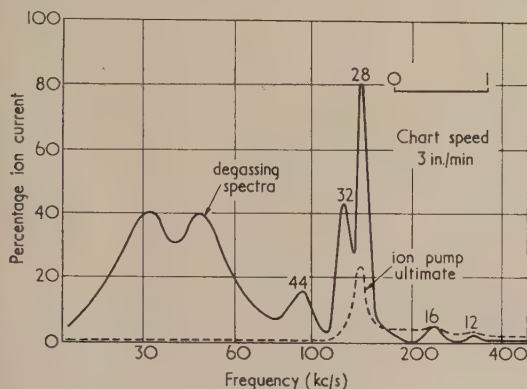


Fig. 4. Ion gauge degassing ($100\% \equiv 1 \times 10^{-12}$ A) and ultimate pressure spectra ($100\% \equiv 1 \times 10^{-13}$ A) $i = 4 \mu\text{A}$; trapping = 0.1 V; r.f. = 2.0 V r.m.s. (Scale = 1 in.)

be taken. Accordingly (Fig. 5), only the time variation of 28 a.m.u. and total gas pressure are illustrated during pumping, whilst the desorption, or recovery, curves were obtained individually. Here it is important to consider the ionization collision cross-sections of the various masses for electrons; i.e. the illustrated variations of positive ion currents with time are individually directly proportional to the variation of partial gas pressure with time but, relative to one another, may give a misleading impression.

At the termination of ion-sorption pumping (Fig. 6) the 28 a.m.u. peak is the only one of any consequence and recovery of gas under these conditions is primarily 28 a.m.u. A careful analysis of the cracking pattern obtained shows that this is almost entirely due to carbon monoxide rather than nitrogen.

Finally, by alternately applying and removing the hot-cathode ion gauge electron accelerating potential, a series of pumping and recovery curves was obtained (Fig. 7). In each

case recovery was initiated from the same total gas pressure. It was observed that the total amount of gas recovered in this manner diminished with successive switching, i.e. each

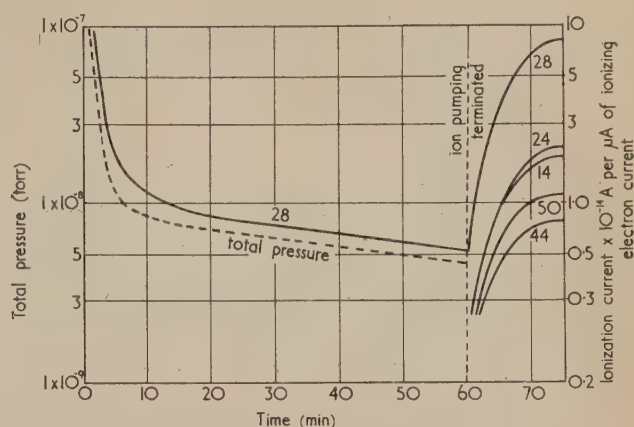


Fig. 5. Ion gauge pumping and recovery curves. Initial total pressure $\approx 8 \times 10^{-7}$ torr

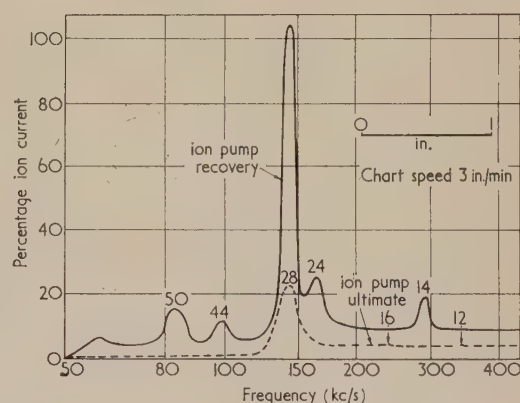


Fig. 6. Ion gauge ultimate pressure ($100\% \equiv 1 \times 10^{-13}$ A) and recovery spectra ($100\% \equiv 3 \times 10^{-13}$ A)

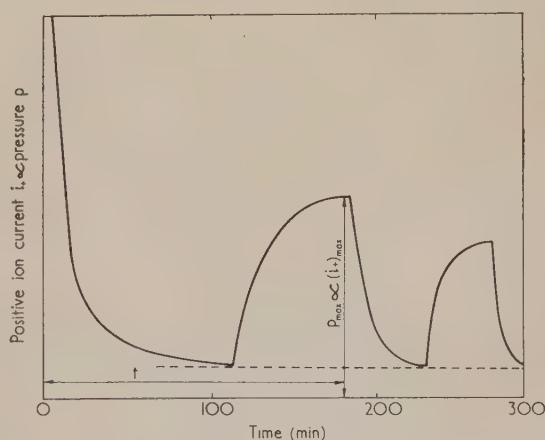


Fig. 7. Successive pumping and recovery with ion gauge

recovery curve rose to a maximum quasi-static pressure p_{\max} which assumed successively smaller values with each switching and was recorded as a positive ion current $(i+)_{\max}$.

The time variation of positive ion current during recovery

was approximately exponential for a particular gas, and the maximum pressure p_{max} was related to time t by the equation

$$p_{max}^2 \propto (i_+)^2_{max} \propto a(1/t) - b \quad (1)$$

where a and b are positive constants and time t is recorded from the instant that the gauge was originally switched on. Typical values for a and b are as follows:

	$a(\text{m}\mu\text{A})^2\text{s}$	$b(\text{m}\mu\text{A})^2$
28 a.m.u.	6.2×10^4	13.5
18 a.m.u.	4.5×10^4	21.7

It was always found that the maximum quantity of gas recovered in this manner, i.e. the first recovery after initial pump-down, was 10% or less of the total quantity of gas that had been pumped. Thus if initial pumping resulted in a fall of pressure from 1×10^{-7} to 1×10^{-9} torr, the first recovery of gas might be expected to lead to a maximum pressure p_{max} of 1×10^{-8} torr or less.

Critique

Varnerin and Carmichael⁽⁸⁾ have pointed out that opinion as to whether positive ions are removed *at* solid surfaces or *penetrate* those surfaces is divided. These workers have described an experiment devised to test which possibility occurs in practice. The test depends upon the fact that gas removed at a solid surface is likely to be recovered at an exponential rate; whilst the rate-determining process in the case of gas that had penetrated the surface may be diffusion.

The present study clearly overcomes difficulties experienced by the above workers, and provides a continuous record of gas pressures for as long as desired from the instant that the experimental gauge is switched off. It is evident from the results that illustrate a near exponential variation of pressure with time, that some gas is recovered at a rate which indicates that it was held at the solid surfaces. However, this is never more than a small fraction of the total gas that is removed and is observed to diminish with increasing time. Thus, either a number of vacant sites, of larger binding energy, for which there is a small probability of filling, are slowly being filled or diffusion from a surface concentration *into* the body of the material is slowly taking place.

Binding energies Q for the fractions of gases held on the solid surfaces can be estimated by calculating the number of gas molecules, of a particular type, readily recovered, and by using the equation⁽⁹⁾

$$(\text{average time of stay of molecule}) = \tau = \tau_0 \times \exp \{Q/(k \times T)\} \quad (2)$$

where τ_0 is the period of vibration about the equilibrium position perpendicular to the surface, k is Boltzmann's constant and T the absolute temperature.

The form of this equation is such that quite a large variation in time τ results in a relatively small variation in the magnitude of Q . The best approach is to estimate the range of times τ , in which the greater part of the gas in question is recovered, and the wall temperature T .

For a time range from 1 to 600 s (Fig. 6) and a wall temperature of 350° K the binding energy Q lies in the range

$$25 \text{ kcal/mol.} \leq Q \leq 30 \text{ kcal/mol.} \quad (3)$$

i.e. the binding energy for the gas that is not readily recovered is larger than 30 kcal/mol. at 350° K.

If the diminution is taken to be due to a diffusion mechanism it is certain that relatively small depths may be considered in a cylindrical geometry, i.e. a reasonably accurate solution to Fick's equation should be given by considering a plane geometry. In such a case the surface concentration C is given by the equation

$$C \propto t^{-1/2} \times \exp \{-A/(D \times t)\} \quad (4)$$

where t equals time, A is a constant and D is the diffusion coefficient. It is clear that for sufficiently long times the equation approximates to $C \propto t^{-1/2}$. In the above experiments times of the order of 10^4 s were not uncommon and although results illustrate a $C^2 \propto 1/t$ dependence they do not give a $C \propto 1/t^{1/2}$ dependence. Accordingly, it is supposed that both of the suggested phenomena occur simultaneously. The possible existence of more active sites seems particularly likely when considering that glass was employed as the gauge envelope.

Conclusion

To test the latter findings further, an experimental gauge which contains the electrical discharge within metal surfaces has been devised. A series of experiments using the pure gas technique as opposed to the gas mixture/omegatron techniques described here, is being conducted by one of us (F. A. B.) in the inert gases. Since no rare gas is supposed to permeate any metal⁽¹⁰⁾ this should provide a critical test on the above findings.

Finally, it should be made quite clear that such small distances are involved that it is by no means certain that Fick's law should be applied, even to give an approximate solution. Also considerable care is necessary, since the diffusion coefficient is exponentially related to temperature, and is known in some cases to vary with concentration by a factor of 10^3 .

Acknowledgement

We wish to thank Dr. N. W. Robinson and Mr. J. Yarwood for useful discussions and encouragement. Thanks are also due to Mr. F. Y. Poynton for facilities to conduct this work at Northampton College of Advanced Technology, London.

References

- (1) SCHWARZ, H. *Z. Phys.*, **122**, p. 437 (1944).
- (2) ALPERT, D. *J. Appl. Phys.*, **24**, p. 860 (1953).
- (3) BAKER, F. A., and YARWOOD, J. *Vakuum Technik*, **6**, p. 186 (1957).
- (4) BAKER, F. A., and GIORGI, T. A. Paper read at International Vacuum Symposium, Como, Italy (23–25 September, 1959).
- (5) REICH, G., and NÖLLER, G. H. *Z. Phys. Nukl.*, **9**, p. 617 (1957).
- (6) ALLENDEN, D. *Elect. Engng*, p. 31 (January 1958).
- (7) BLEARS, J. *J. Sci. Instrum. (Suppl. 1)*, **28**, p. 36 (1951).
- (8) VARNERIN, L. J., and CARMICHAEL, J. H. *J. Appl. Phys.*, **26**, p. 913 (1957).
- (9) FRENKEL, J. *Z. Phys.*, **26**, p. 117 (1924).
- (10) NORTON, F. J. *J. Appl. Phys.*, **28**, p. 34 (1957).

Solution of ladder networks containing non-linear resistances

by T. KOVATTANA, M.Sc., and J. R. BARKER, Ph.D., F.Inst.P., Imperial College of Science and Technology, London

[Paper received 13 May, 1960]

Abstract

A graphical method of solving network problems involving non-linear and/or negative resistances is described and fully developed for the case of ladder networks. Such networks have been used for the solution of non-linear differential equations, using an analogy based on finite differences, and the examples given in this paper are of this application.

Introduction

IN 1951, Cherry⁽¹⁾ gave a description of a planar electrical resistance network which, in a single diagram, showed the network topology, the V - I characteristics of each resistance, Kirchhoff's circuit laws and the power relationships. The present paper uses Cherry's diagram to solve problems involving resistance networks and shows that it is particularly useful when some or all of the resistances are non-linear. It is also applied to networks containing negative resistances. A resistance network can be the analogue of the finite-difference form of a non-linear differential equation and, as many papers on this analogy have appeared in this Journal, our illustrative examples will be taken from this field. The new method of solution is of special interest because it can be used for those cases where the iterative analogue techniques described by Liebmann and Bailey,⁽²⁾ Karplus⁽³⁾ and Hutcheon⁽⁴⁾ fail to converge.

Ladder network of positive resistances

To introduce the method, the ladder network of Fig. 1 is considered. In this, all the series elements are linear

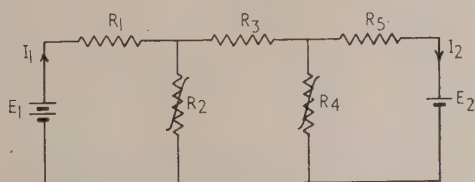


Fig. 1. Ladder network with non-linear shunt elements

resistors, the shunt resistors are non-linear resistors and e.m.f.'s E_1 and E_2 ($E_1 > E_2$) are applied at the ends. The voltages at the two intermediate nodes have to be found. However, for the moment, suppose that the problem has already been solved so that the final diagram can be exhibited, as in Fig. 2. Within an area defined by the two rectangles of sides $E_1 \times I_1$ and $E_2 \times I_2$ the following appear:

- Portions of the V - I characteristics of the resistors 1, 3 and 5 which have slopes R_1 , R_3 and R_5 respectively;
- Portions of the non-linear V - I characteristics of the

shunt resistors 2 and 4, starting at zero potential and continuing up to their actual operating points;

- All these V - I characteristics appear, diagonally, inside minor rectangles which are fitted together in a way which

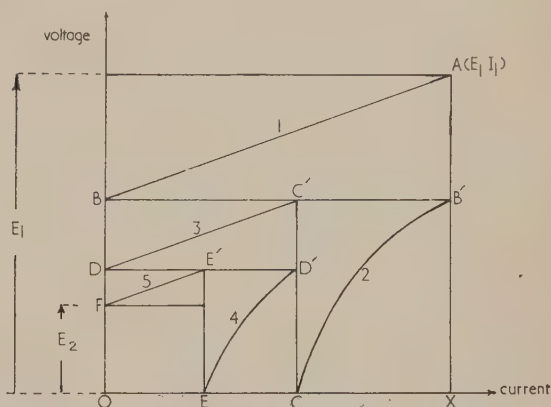


Fig. 2. Rectangle diagram for network of Fig. 1
 $OX = I_1$, $OE = I_2$ and $XA = E_1$

satisfies both of Kirchhoff's Laws. For example, the sum of the voltage drops across 1, 3 and 5 should be $E_1 - E_2$, and this relationship is satisfied by the voltages represented along the left-hand edge of the main rectangle (on which all the node potentials appear). Next, taking horizontal distances in Fig. 2, the current in 1, which is I_1 , can be seen to equal the sum of the currents in 2 and 3; similarly, the sum of the currents in 4 and 5 is the current in 3.

(d) Finally, the area of each minor rectangle represents the power dissipated in a resistance, and the total area of these minor rectangles 1-5 is $E_1 I_1 - E_2 I_2$, which is the power supplied by the two sources, so that the law of conservation of energy is satisfied.

The method of solving the problem when only E_1 and E_2 are given is very simple. After estimating I_1 , an attempt is made to draw the diagram, to scale, using the V - I characteristics in the following order: 1, 2, 3, 4 and 5. (Templates will be needed for the non-linear V - I characteristics, and, if not many cases are to be solved, these can be cut out of graph paper of the same kind as is used for the rectangle diagram. If a lot of work is to be done, it is worth making metal templates for the characteristics.) The drawing is made as follows. On Fig. 2, A is the point (E_1, I_1) ; AB is drawn of slope R_1 , whence AB' is $I_1 R_1$, leaving voltage $XB' = OB$ for the rest of the network. The current traversing the non-linear resistor R_2 is found by sliding its V - I characteristic to the position 2 (it passes through B' and has its origin at C) whence current CX flows through it and OC remains to traverse R_3 . $C'D$ of slope R_3 is drawn next, from C' which is vertically above C , and OD will be the

voltage across R_4 . The current in R_4 is obtained by sliding its V - I characteristic to the position 4. E/F is drawn of slope R_5 and, if I_1 were correctly chosen, OF would be equal to E_2 . On completion of the drawing, the distance OF on Fig. 2 is unlikely to be equal to E_2 , but it will be obvious in what sense to adjust I_1 in order to improve it, and a second attempt can then be made. We have been surprised by the speed with which this trial and error process leads to the correct solution, especially when a little intelligent interpolation is applied.

If the ladder network is long and highly attenuating and $E_2 = 0$, the voltages remote from the source E_1 cannot be found accurately unless a very large drawing is used. In this case, it is better to improve I_1 , in the latter stages only, by numerical calculation. If OA is calculated for two values of I_1 , preferably one larger and one smaller than the true value, improvement by interpolation is rapid because of the good start given by the graphical method. (The calculations are simple: starting with E_1 and I_1 , the voltage drops and currents can be found as the ladder is traversed from left to right.)

Example 1

The first example is taken from Hutcheon and Spalding's paper⁽⁵⁾ on steady-state heat flow, with convective losses, in uniform bars. The differential equation to be solved is:

$$\frac{d^2\theta}{dy^2} = k\theta^{5/4} \quad (1)$$

in which θ represents temperature at a distance y along the bar. The numerical value of k is 12.5 and the boundary values are $\theta = 1$ at $y = 0$ and $d\theta/dy = 0$ at $y = 1$, for the example presented here.

It is not necessary in this Journal to repeat the derivation of the finite-difference analogue network. It is sufficient to say that the node potentials V on the ladder network of Fig. 3

Hutcheon and Spalding's values are obtained from their Fig. 7a, bottom graph, and are, of course, similar.

Ladder network containing negative resistances

Negative resistances appear in finite-difference analogue networks as shunt elements when, if

$$\nabla^2\phi = f(\phi, x, y, z) \quad (2)$$

is being solved, $f(\phi, x, y, z)$ is negative. (In passing, it should be mentioned that constant-current sources are often used in place of the shunt resistors, in analogue equipment, particularly if the resistances are negative.)

If the solution ϕ is wave-like along the ladder, the normal iterative analogue computers fail to converge to a solution under conditions given by Fisher,⁽⁶⁾ although Korthals Altes⁽⁷⁾ has suggested a tedious practical method of double iteration which does give convergence. No such troubles beset the graphical method of this paper.

Example 2

A case for which the analogue computers will encounter convergence difficulties is taken as the next example. Consider:

$$\frac{d^2\phi}{dx^2} + k^2\phi = 0 \quad (3)$$

with $k^2 = 1$, $\phi = 10$ at $x = 0$ and $\phi = 0$ at $x = 3\pi/2$, for which the exact solution is $\phi = 10 \cos x$. The analogue network is shown in Fig. 4 for a finite difference interval of $\pi/4$. Its solution by means of the rectangle diagram is carried out as already described but it is slightly complicated by the fact that the component rectangles will trespass outside the main rectangle $E_1 \times I_1$. There is however a simple rule to enable the diagrams to be drawn quickly, a rule which applies also to the ladder network of positive resistances.

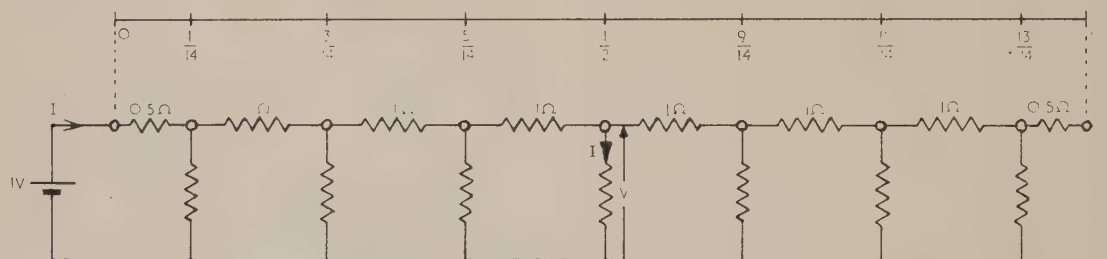


Fig. 3. Finite-difference analogue network for heat-flow problem

For all shunt elements:

$$I = \frac{12.5}{49} V^{5/4},$$

where V is in volts and I in amperes

should be numerically equal to the temperatures θ in the bar at the values of y indicated. (Any discrepancy between the values of θ satisfying equation (1) and the node potentials will be due to the coarseness of the finite-difference approximation used.)

For the network of Fig. 3, I_1 was estimated to be 0.40 A. Foolsap graph paper was used and a paper template cut out for the non-linear V - I characteristic. On successive drawings it was found that $I_1 = 0.40$ A was too small, 0.50 A was too much, 0.45 A was too small, 0.46 A was too big and 0.458 A seemed very close. The node voltages were then, reading from left to right on Fig. 3:

1.0, 0.77, 0.50, 0.33, 0.22, 0.15, 0.11, 0.09 V.

Rule

- The V - I characteristics are used in the order 1, 2, 3, 4, ... as labelled on Fig. 4.
- Each V - I characteristic lies diagonally inside a rectangle.
- Each successive V - I curve has its operating point at that corner of the previous rectangle which is not occupied by the previous V - I curve and which is not on either the V - or I -axis of the diagram.
- If a series element is being dealt with, the V - I curve has its origin on the V -axis and if a shunt element, it is on the I -axis.

Applying this to the network of Fig. 4, an initial estimate of I_1 is made and this determines the starting point A

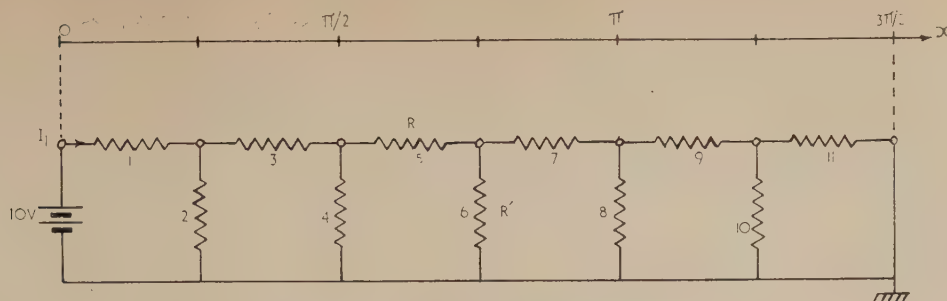
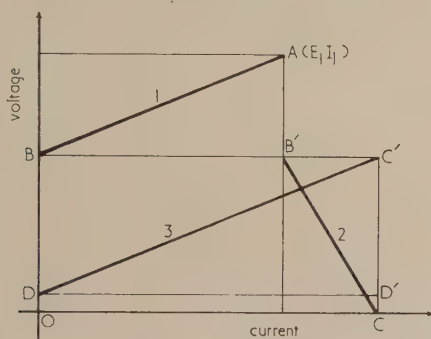


Fig. 4. Network for vibration problem.

All shunt elements $R = 1 \Omega$ All shunt elements $R' = -1.621 \Omega$

co-ordinates: 10V, I_1 A) on the diagram shown in Fig. 5. A line of slope 1Ω is drawn from A to intersect the voltage axis at B. This defines the first rectangle, for resistor 1, of which B' is the corner which satisfies the rule. From B', a line of slope -1.621Ω is drawn to intersect the current axis at C. This line is the diagonal of the second rectangle,

Fig. 5. V - I diagram for the first three elements of the network in Fig. 4The node potentials are E_1 , OB and OD

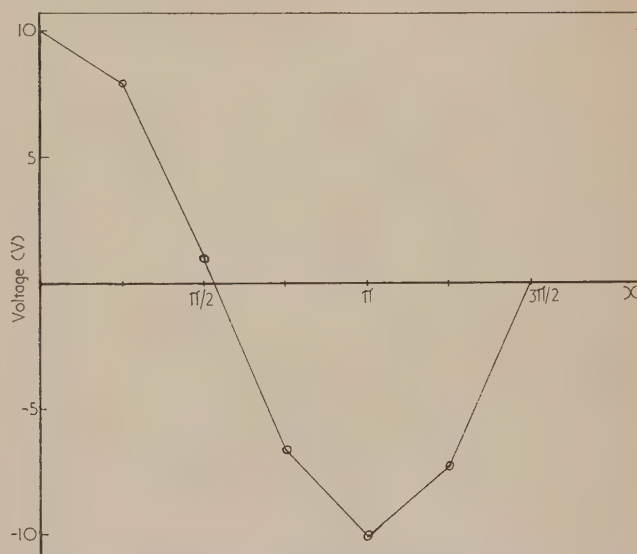
For resistance 2, whose corner C' is the starting point for the next V - I line. Close examination of Fig. 5 shows that Kirchhoff's laws will be satisfied on the diagram. When the diagram is completed, the value of I_1 can be assessed and another trial made. In the example, the correct value of I_1 is 2.13 A and Fig. 6 shows a graph of the node voltages along the network. These depart slightly from $10 \cos x$, but the error is due to finite differencing and is not relevant to the network-solving; errors in the network solution cannot be detected in Fig. 6.

Other applications

It seems likely that the solution of some two-dimensional problems involving the equation

$$\frac{\partial^2 \phi}{\partial x^2} + \frac{\partial^2 \phi}{\partial y^2} = f(\phi, x, y),$$

and the solution of one-dimensional elastic problems, involving a fourth-order differential equation, can be carried out by extensions of the graphical method. We are already tackling eigenvalue problems. However, the application of non-linear resistance networks is not restricted to the single group of circuits considered so far. For example, for mine-ventilation networks⁽⁸⁾ and gas and water-distribution systems, useful preliminary investigations might well be carried out graphically. Bridge networks containing tungsten filament

Fig. 6. Node potentials on network of Fig. 4 approximate to $10 \cos x$

lamps and d.c. amplifier networks might provide other useful applications.

This paper has described a method of solving non-linear resistance networks. It should, however, be possible to interpret it as a graphical method of solving the finite difference approximation to a differential equation without mentioning the resistance network analogy at all.

Acknowledgement

The authors' thanks are due to Mr. B. J. Prigmore for his helpful criticisms of the first manuscript.

References

- (1) CHERRY, E. C., *Phil. Mag.*, **42**, p. 1161 (1951).
- (2) LIEBMANN, G., and BAILEY, R. *Brit. J. Appl. Phys.*, **5**, p. 32 (1954).
- (3) KARPLUS, W. J. *Brit. J. Appl. Phys.*, **6**, p. 356 (1955).
- (4) HUTCHEON, I. C. *Brit. J. Appl. Phys.*, **8**, p. 370 (1957).
- (5) HUTCHEON, I. C., and SPALDING, D. B. *Brit. J. Appl. Phys.*, **9**, p. 185 (1958).
- (6) FISHER, M. E. *Brit. J. Appl. Phys.*, **9**, p. 288 (1958).
- (7) J. PH. KORTHALS ALTES. *Brit. J. Appl. Phys.*, **10**, p. 176 (1959).
- (8) SCOTT, D. R., and HUDSON, R. F. *J. Sci. Instrum.*, **30**, p. 185 (1953).

Passage of current through the glass envelope of a receiving-type valve

by H. N. DAGLISH, B.Sc., Ph.D., A.Inst.P., Post Office Engineering Department, Research Station, Dollis Hill, London, N.W.2

[Paper first received 17 May, and in final form 23 June, 1960]

Abstract

In normal operation of receiving-type valves, with soda glass envelopes, a small current may flow through the glass to an external coating. Part of this current consists of positive ions generated by the flow of electrons through the atmosphere inside the envelope. As the pressure inside the valve falls during operation, the value of the ratio of the current through the envelope to the anode current flowing in the valve also falls, eventually reaching a stable value which is independent of pressure. This residual value is due to the emission of photoelectrons from the inside of the glass, when bombarded by X-rays generated at the anode. It therefore depends upon the nature of the anode surface and upon the anode potential.

The continuous passage of this photoelectric current through the glass may generate small quantities of gas by electrolysis, and so affect the behaviour of the valve. Experimental evidence suggests that the risk of permanent damage to the cathode emission is very small.

1. Introduction

IN normal operation of a thermionic valve, small positive currents flow to those electrodes which are at a potential equal to, or more negative than, that of the cathode. These currents include the positive ions generated by the passage of electrons through the residual gas inside the envelope. The magnitudes of these currents fall very rapidly during the first few hours of the life of the valve, eventually reaching fairly stable values.⁽¹⁾ An example of this, for the envelope of a receiving-type pentode, is shown in Fig. 1. It has been shown⁽²⁾ that this decay corresponds to a rapid fall in pressure, but that when the positive currents have

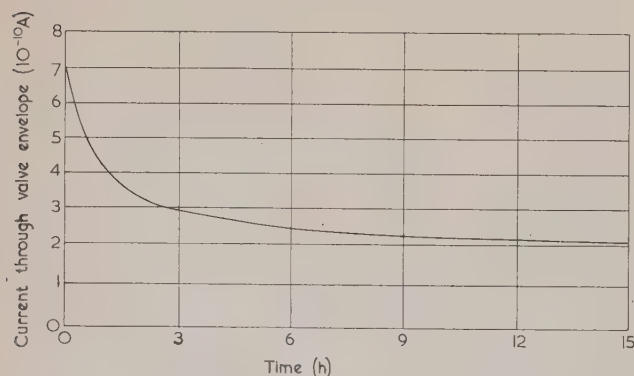


Fig. 1. Decay of current through the envelope of a newly pumped type 10P1 valve
(Measured at $V_a = 60$ V, $i_a = 3$ mA)

reached stable values, the pressure continues to decrease. The stable values of the positive currents are then independent of the ultimate gas pressure in the valve and are, in fact, due to the emission of photoelectrons, rather than the collection of positive ions.

The continuous bombardment of the anode by electrons causes the generation of soft X-rays. The photons of this X-radiation eject photoelectrons from the various electrodes and from the inner surface of the glass envelope. These currents which result are independent of pressure, but depend upon the potential of the anode and also upon the nature of the material from which the anode is made. This phenomenon is also responsible for the failure of conventional ionization vacuum gauges to measure pressures less than about 10^{-8} torr, as described by Nottingham,⁽³⁾ Lander,⁽⁴⁾ Bayard and Alpert⁽⁵⁾ and Metson.⁽²⁾

The positive currents flowing to the control grid and suppressor grid of a pentode may be measured directly, but that to the envelope is obtained by measuring the current flowing through the glass to an external collector. The majority of receiving-type valves have envelopes of soda glass with a relatively high electrical conductivity. The leakage path of least resistance from the inside of the envelope is therefore through the glass to the outer collector. In normal operation of such a valve, with a coating on the outside of the glass at cathode potential, the photoelectric currents due to the bombardment of the envelope by soft X-rays will flow continuously through the glass throughout the operational life of the valve.

The electrical conductivity of glass is primarily due to the presence of mobile positive ions, and the continued flow of current may cause electrolytic decomposition of the glass. Experiments have therefore been carried out to determine the magnitude of this effect, and the consequences of the release of any products of this electrolysis into the evacuated envelope.

2. Experimental arrangements

The tubes used for these experiments were similar in most respects to the standard type 10P1 pentode, developed for use in Post Office submarine telephone repeaters. This valve has already been described in detail.⁽⁶⁾ The envelopes of the experimental tubes were made of a soda glass. The sketch in Fig. 2 shows a cross-section through the electrode structure, and it is clear that the soft X-rays which are generated at the inner surfaces of the simple plate anodes will bombard a considerable area of the inner surface of the glass envelope.

A conducting band of colloidal graphite was painted round the outside of the envelopes, to collect the current

caused by bombardment of the envelope by soft X-rays. The position of this band is indicated in Fig. 3. The X-ray induced currents were measured with a sensitive vibrating condenser electrometer, with the valves enclosed in an earthed copper screening box. A conventional autobias circuit was

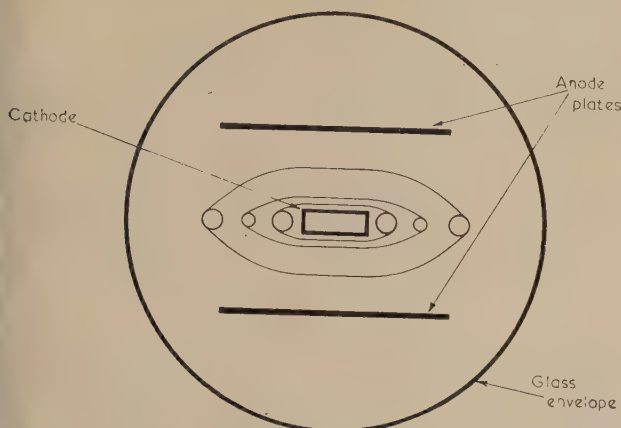


Fig. 2. Cross-section of the experimental valve, showing the extent to which the envelope is exposed to soft X-rays generated at the inner surface of the anode plates

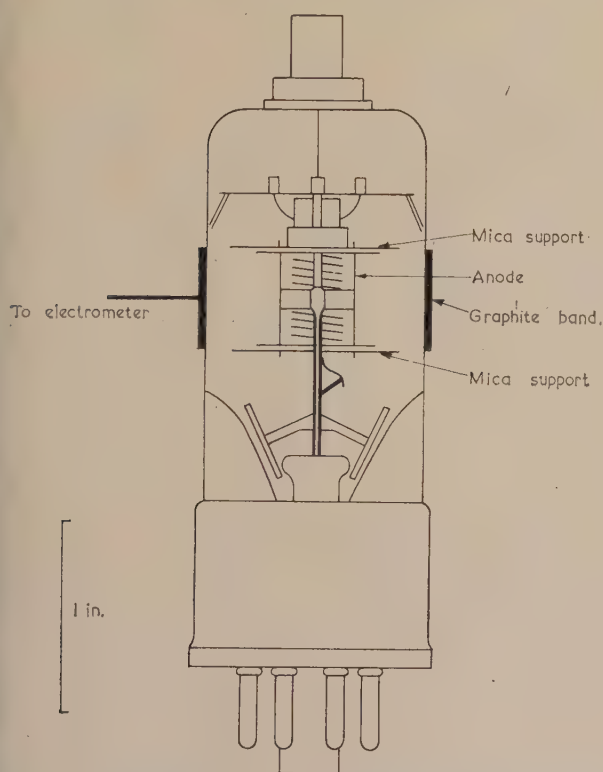


Fig. 3. Experimental valve, showing the position of the graphite band on the outside of the envelope

used to operate the valves, with normal operating conditions. ($V_a = V_{g2} = 70V$, $I_a = 10$ mA.)

In all the measurements described below a small correction has been made to account for the X-ray currents corresponding to the screen-grid current. In order to reduce this correction, the screen-grid potential was reduced to 30 V during measurements.

3. Magnitude of the current through the envelope of the experimental pentodes

3.1 *The current as a function of the anode current.* In all the experiments, the current through the envelope was found to be proportional to the anode current flowing through the valve. This is illustrated for one valve in Fig. 4. In the

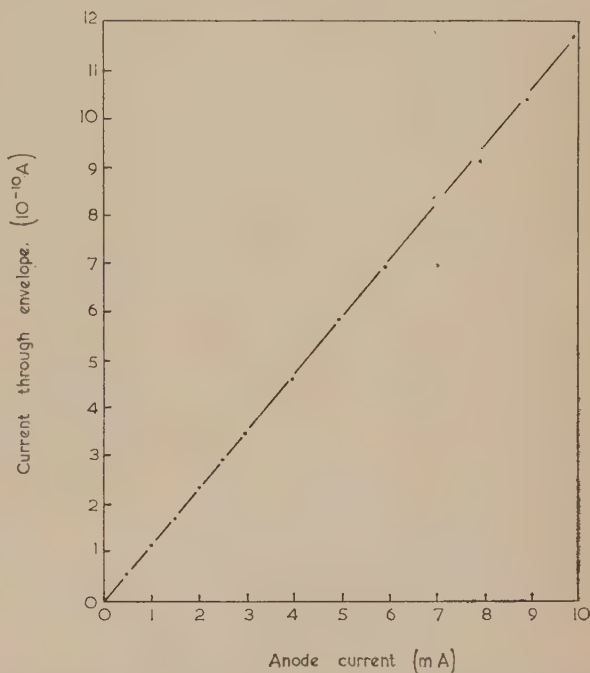


Fig. 4. Current through the glass as a function of anode current

remainder of this paper it will therefore be convenient to refer to the ratio (i^+/i_a) of the current through the envelope to the anode current, rather than to the actual values of the currents.

3.2 *The current as a function of anode voltage.* At relatively low anode potentials the current through the glass increases linearly with anode potential. Extending the measurements to higher voltages shows that the linearity continues, but with a series of sharp changes of slope. Examples are shown in Figs. 5 and 6. (These measurements were made at a reduced anode current (1 mA) to avoid overheating the anodes.)

3.3 *The current as a function of time.* Although Fig. 1 suggests that stable values of the positive currents are attained in a few hours as the gas pressure falls, more detailed examination reveals a further slow change in the X-ray current. Thus, Table 1 gives values measured under normal operating conditions after various intervals, for a valve with anodes of pure nickel.

Table 1. Decay of current through the envelope of a pentode

Time (h)	i^+/i_a
19	7.9×10^{-8}
200	6.2
700	5.6
1500	5.3
2300	4.8
3000	4.4

This decay is attributed to the decomposition of a thin film of barium and strontium oxide on the inner surfaces of

the anode. This film is deposited during processing of the oxide cathode,⁽⁷⁾ and is slowly decomposed and dispersed by electron bombardment. As the oxide layer becomes thinner, so its influence on the emission of soft X-rays diminishes.

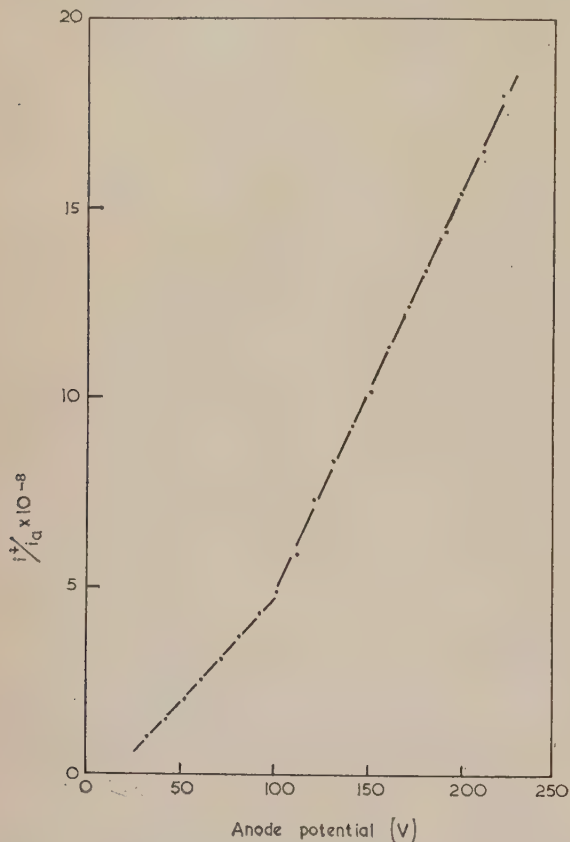


Fig. 5. The ratio i^+/i_a for the envelope as a function of the anode voltage

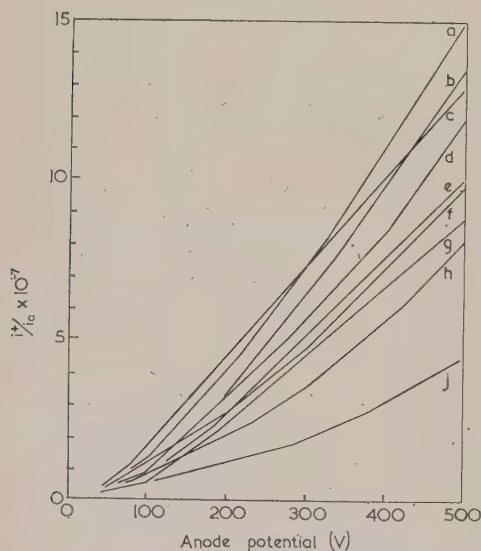


Fig. 6. The ratio i^+/i_a for various anode materials, as a function of anode voltage

Curve *a*, molybdenum; curve *b*, aluminium; curve *c*, titanium; curve *d*, zirconium; curve *e*, palladium; curve *f*, tantalum; curve *g*, nickel; curve *h*, platinum; curve *j*, carbon

The level of the X-ray current is virtually constant only after some thousands of hours of operation.

3.4 *The current as a function of anode material.* Special valves were made with anodes of a number of different materials, as listed in Table 2. The carbon was in the form of colloidal graphite on a molybdenum or platinum substrate.

Table 2. Experimental anode materials

Anode material	Atomic number
Carbon	6
Aluminium	13
Titanium	22
Nickel	28
Zirconium	40
Molybdenum	42
Palladium	46
Tantalum	73
Platinum	78

The results for the various elements are illustrated in Fig. 6, which shows the variation of i^+/i_a with anode voltage, after 3000 hours operation under standard conditions. As well as pure nickel, anodes of various nickel alloys were examined. Little difference was noted in the behaviour of valves with anodes of nickel alloys containing 4% tungsten, 0.25% silicon and 0.1% of magnesium respectively. The behaviour of valves with anodes of "O"-nickel (which contains about 0.3% silicon, 0.7% magnesium and 0.1-0.4% of carbon) was rather different, and is considered separately in Section 3.5.

It is possible to compare these results with earlier published data on the relative efficiency of production of soft X-rays. Richardson and Robertson⁽⁸⁾ measured this for a number of materials, in a continuously pumped apparatus using special electrostatic traps to eliminate residual ion-currents. Data from the present experiments and from the paper of Richardson and Robertson are compared in Fig. 7. The ratio of X-ray current to electron current is plotted against the atomic number of the anode material. (Different scales are, of course, used for the two sets of values, as the geometries of the two systems are quite different.)

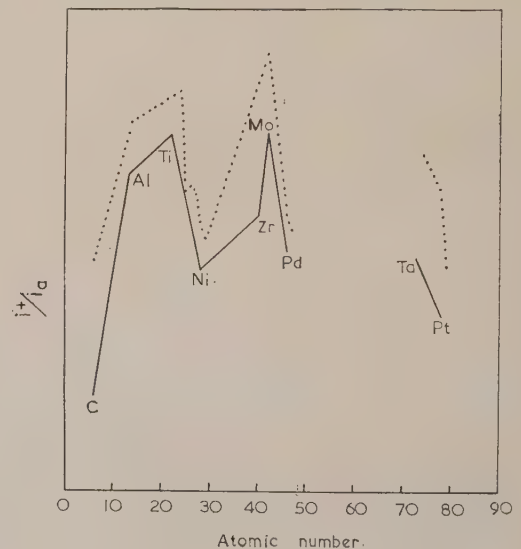


Fig. 7. The ratio i^+/i_a as a function of the atomic number of the anode material (at 300 V)

..... = data from Richardson and Robertson⁽⁸⁾
 — = present measurements

The general similarity between the two sets of data is further evidence that the current through the envelope is, in fact, determined by the magnitude of the X-radiation from the anode of the valve.

The comparisons in this section have been made on the assumption that the photoelectric efficiency of the glass envelope is the same in each valve, and remains constant.

3.5 Behaviour of "active" nickel anodes. The behaviour of valves with anodes of "O"-nickel depends upon the pre-processing of the anode material. If the material is processed by heating in wet hydrogen, the X-ray level produced in the valve is the same as for other nickel alloys, discussed above. If, however, the anodes are processed by etching and vacuum out-gassing in order to retain the chemical activity of the reducing agents (carbon, magnesium and silicon) in the alloy, the behaviour is quite different. As shown in Fig. 8,

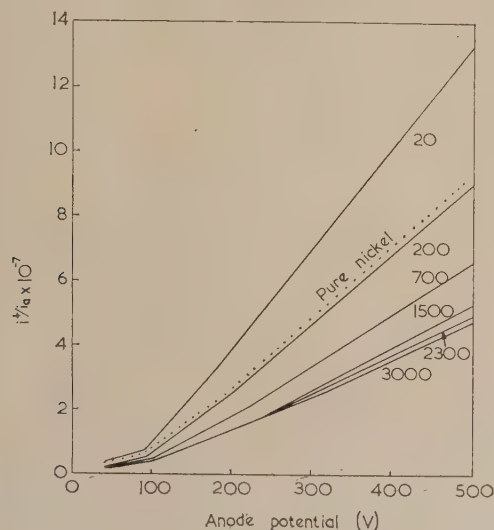


Fig. 8. The decay of i^+/i_a for the envelope of valves with active "O"-nickel anodes

(Marked with time of operation in hours. The dotted line is for valves with pure nickel anodes, after 3000 h.)

the value of i^+/i_a falls much more rapidly than for the other valves with nickel anodes. The final value of this ratio is also much lower (2.60×10^{-7} instead of 4.60×10^{-7} at 300 V).

The other anodes giving very low values of i^+/i_a are those deliberately coated with a thin layer of carbon, and it is suggested that the anomalous behaviour of the active "O"-nickel anodes is due to the formation of a very thin carbon skin. Experiments have been described, by Farnsworth and others,⁽⁹⁾ in which electron diffraction measurements revealed the formation of a carbon layer on nickel heated in a vacuum. Reynolds and others⁽¹⁰⁾ have reported the liberation of free carbon in receiving-type valves with active nickel anodes. The carbon originates in the nickel alloy, being removed by stoving in wet hydrogen; "O"-nickel treated in this way therefore cannot grow a carbon surface film, and consequently gives the same X-radiation intensity as pure nickel.

4. The conductivity of the glass envelope

The X-ray induced currents described above all pass through the soda glass envelope to an external collector. In normal operation the whole envelope is usually covered with an earthed conductive coating, and it is therefore desirable

to know the possible consequences of the continuous passage of current through the glass.

It has been demonstrated⁽¹¹⁾ that the current is carried almost entirely by positive sodium ions which can move easily through the open lattice structure of the glass. The mobility of the ions increases as the temperature is raised. The electrical conductivity of glass is therefore greater at higher temperatures.

Burt⁽¹¹⁾ and Hull showed that sodium could be released into a soda glass electric lamp bulb, by using the filament as a thermionic emitter. A bath of molten sodium nitrate served both as the anode and as a reservoir of sodium. Kirby⁽¹²⁾ used the same method to determine the electrochemical equivalent of sodium, obtaining a value within $\frac{1}{2}\%$ of the accepted value.

In all such experiments an external reservoir of sodium was provided. If no reservoir is provided, sodium is removed from the glass, causing polarization. Fig. 9 shows the rapid

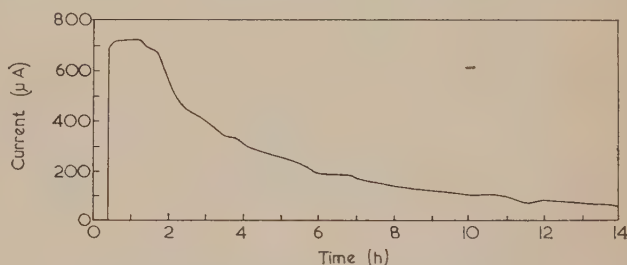


Fig. 9. Polarization of soda glass during electrolysis (Temperature 110°C , applied voltage, 360 V)

decay of current which is obtained. Even under these polarizing conditions the transport of sodium follows Faraday's law. If such a curve as Fig. 9 is integrated, the amount of sodium liberated can be calculated. This may then be compared with a direct determination of the sodium. Such a comparison has been made in a series of experiments, with the results shown in Table 3. The experimental tubes consisted of an evacuated envelope of soda glass, with an axial filament of tungsten. This filament was heated, and current drawn to an anode of graphite on the outside of the glass. The glass was heated to increase the mobility of the ions, and the current allowed to flow until the cooler parts of the interior of the envelope were covered by a shining mirror of metallic sodium. This sodium was measured by opening the tubes under distilled water, and then titrating the resulting alkaline solution.

Table 3. Electrolytic generation of sodium from soda glass

Glass temperature ($^\circ\text{C}$)	Amount of sodium (mg)	
	Chemical determination	Faradaic calculation
113	3.46	3.57
150	2.10	2.16
208	3.75	3.86

The agreement is consistent with the accuracy to be expected of such a simple experiment. One possible source of error is loss of sodium redissolved in the glass. In preliminary experiments in which the tungsten filament was mounted on a lead glass pinch, almost half of the sodium attacked the lead glass and was lost. The measurements in Table 3 were made on tubes entirely of soda glass, the tungsten emitter being mounted on platinum wires sealed directly through the soda glass.

When polarization occurs, the glass becomes depleted of sodium. Kirby⁽¹²⁾ demonstrated that this damage to the glass structure was accompanied by the evolution of gas, by passing a heavy current between two wires embedded in a bead of hot glass. Small bubbles were produced inside the glass.

The X-ray current through the envelope of a receiving-type valve is so small, less than 10^{-9} A, that it is difficult to demonstrate the evolution of any gas at all. However, if a much larger current is passed through the glass, between graphite electrodes on both the inside and outside surfaces, then some gas evolution can be measured. Fig. 10 shows

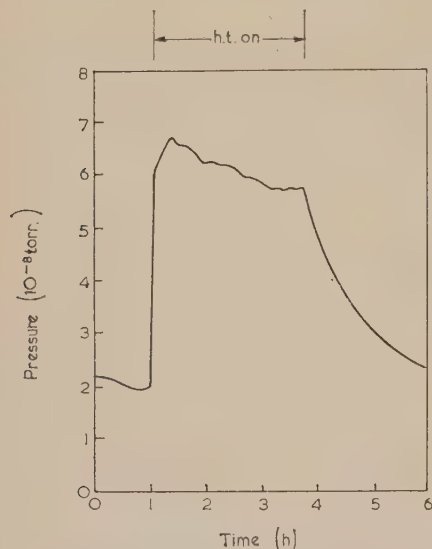


Fig. 10. Evolution of gas during the electrolysis of soda glass
(Temperature 92° C, applied voltage 300 V)

the pressure inside a sealed tube of soda glass, measured by a Bayard/Alpert ionization gauge.⁽⁵⁾ The conductivity of the glass was increased by warming to 92° C. A current of 0.5 mA was then passed through the glass by connecting a 300 V battery between the two graphite electrodes (the outer negative, the inner earthed). The evolution of gas is measurable under these circumstances but is small when compared with the amount of sodium transferred through the glass.

A similar experiment was performed, in which the envelope contained an operating type 10P1 pentode valve (with 4% tungsten-nickel cathode core) as well as a Bayard/Alpert gauge. The "working point" of the pentode is a convenient parameter to indicate changes in the emission level of the oxide-cathode. The "working point" is defined as the potential difference applied between the control grid and the cathode in order to maintain the required constant anode current. The behaviour of the valve, and the changes in pressure are shown in Fig. 11.

The envelope was warmed to 85° C to increase the conductivity of the glass and the pentode allowed to become stable. When a 180 V battery was connected between the two graphite electrodes (the outer negative, the inner earthed) the initial current through the glass was 166 μ A.

After 51 min, the working point of the valve had fallen to zero from a stable initial value of -2.9 V. During this time the current through the glass had decayed to 105 μ A, whilst the pressure inside the envelope had risen from

5×10^{-10} to 9×10^{-9} torr. The valve was left on test with current flowing through the glass. As polarization took place this current diminished to a few microamperes, and the valve began to recover. After 150 hours, the working point had recovered to about -1.2 V, and eventually recovered completely.

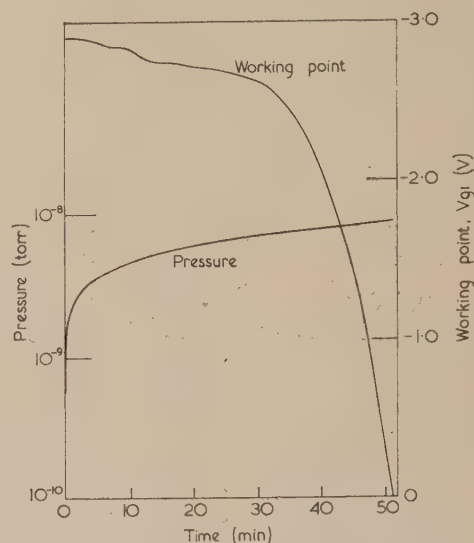


Fig. 11. Effect on a type 10P1 pentode of gas evolved electrolytically from soda glass

If an attempt is made to extrapolate the results of this experiment to a normally operating valve, where the current through the glass is very much smaller, it is clear that the normal recovery processes in a fully active oxide cathode so far exceed the rate of evolution of gas, that the consequences of the glass electrolysis on the behaviour of an adequately processed valve are probably negligible.

If the magnitude of the current through the glass is increased by increasing the anode potential or anode current, and particularly if the anode is of molybdenum, or titanium (the characteristic level of X-ray generation of which is greater than the other metals examined) the risk of damage is greater. However, the electrolysis may be prevented by providing an earthed coating on the inside of the envelope, or by using a high resistance lead glass. If the former alternative is adopted, it is important that the coating inside the envelope should be at the same potential as the outside surface. Otherwise the resultant flow of electrolytic current may be much greater than the original photoelectric current, resulting in either cathode poisoning by gas attack, or damage to the glassware due to the release of sodium vapour inside the envelope.

Conclusions

In normal operation of receiving-type valves, with soda glass envelopes, a small current may flow continuously through the envelope. This current depends upon the generation of soft X-rays at the anode, and is therefore a function of the anode potential and anode current. Because the electrons incident on the anode are relatively slow, their penetrating power is poor. Consequently, the level of the soft X-radiation may depend on the nature of any surface films as well as that of the anode material itself.

The passage of this current through the glass may cause

the release of gas into the valve. Although this release of gas may be increased by passing large currents through the glass, the rate of evolution under normal operating conditions is very small, so that the phenomenon is likely to have a negligible effect on the operation of the valve, as long as the cathode possesses reasonable reserves of activation.

Acknowledgement

Acknowledgement is made to the Engineer-in-Chief of the Post Office for permission to make use of the information contained in the paper.

References

- (1) METSON, G. H. *Brit. J. Appl. Phys.*, **1**, p. 73 (1950).
- (2) METSON, G. H. *Brit. J. Appl. Phys.*, **2**, p. 46 (1951).

- (3) NOTTINGHAM, W. B. See DUSHMAN, S. *Vacuum Techniques*, p. 359 (New York: John Wiley and Sons, Inc., 1949).
- (4) LANDER, J. J. *Rev. Sci. Instrum.*, **21**, p. 672 (1950).
- (5) BAYARD, R. T., and ALPERT, D. *Rev. Sci. Instrum.*, **21**, p. 571 (1950).
- (6) HOLMES, M. F., and REYNOLDS, F. H. *Proc. Instn Elect. Engrs*, **107 B**, p. 165 (1960).
- (7) DAGLISH, H. N. *Proc. Instn Elect. Engrs*, **107 B**, p. 481 (1960).
- (8) RICHARDSON, O. W., and ROBERTSON, F. S. *Proc. Roy. Soc. A*, **115**, p. 280 (1927).
- (9) FARNSWORTH, H. E., SCHLIER, R. E., GEORGE, T. H., and BURGER, R. M. *J. Appl. Phys.*, **29**, p. 1150 (1958).
- (10) REYNOLDS, F. H., JOHNSON, C. B., and ROGERS, M. W. *Proc. Instn Elect. Engrs*, **104 B**, p. 487 (1947).
- (11) BURT, R. C. *J. Opt. Soc. Amer.*, **11**, p. 87 (1925).
- (12) KIRBY, P. L. *Science Progr.*, **38**, p. 257 (1950).

Temperatures reached in a bimetallic brake drum

by T. P. NEWCOMB, M.Sc., A.Inst.P., Ferodo Ltd., Chapel-en-le-Frith, Stockport, Cheshire

[Paper received 20 April, 1960]

Abstract

A solution is given to permit the determination of the temperature attained at the friction surface of a bimetallic brake drum during a single brake application. No assumptions are made concerning the manner in which heat is shared between the drum and lining. This solution is then compared with those obtained when all the heat generated is assumed to enter the drum, and when the amount of heat entering the drum is dependent on the thermal properties of the cast iron and brake lining material only.

cerns the solution to the linear flow of heat through a composite body consisting of three infinite slabs between parallel boundaries, in which at one interface (between lining and drum) there is a thermal flux which decreases linearly with time, whilst at the other interface (between the two metals of the drum) there is continuity of thermal flux and temperature and at the outer boundaries there is no flow of heat (i.e. cooling is ignored). This solution is compared with that obtained when all the heat is assumed to flow into the drum, and that obtained when it is assumed that the heat sharing ratio is dependent on the thermal properties of the cast iron and brake linings alone.

Introduction

IN a previous paper* a solution was presented enabling the temperature to be determined at the interface of a lining and bimetallic drum (composed of an inner layer of cast iron and an outer layer of aluminium) during a single brake application to bring a vehicle to rest. This solution was based on the assumption that all the heat generated enters the drum, which does not cause a serious error when brake applications are of short duration (e.g. 5 s) or when brake linings are made of material having very low thermal constants. However, many brake applications are of long duration (high-speed stops) and also brake linings vary considerably in thermal properties, and it is of interest to determine whether the above assumption causes appreciable error in the friction surface temperature at long brake applications. This is the problem examined here and con-

Heat problem and application of its solution

Consider the linear flow of heat in a composite solid consisting of three parallel-faced infinite slabs, the complete body being initially at zero temperature. The first medium (lining) lies in the region $-d_3 < x < 0$ and has physical properties $K_3, \rho_3, c_3, k_3, v_3$, whilst $0 < x < d_1$ denotes the second medium (cast iron layer) and $d_1 < x < d_2$ represents the third medium (aluminium layer), the physical properties of each being $K_1, \rho_1, c_1, k_1, v_1$ and $K_2, \rho_2, c_2, k_2, v_2$ respectively. The quantities K, ρ, c, k, v , with suffixes for whichever body is considered, refer respectively to the thermal conductivity, density, specific heat, thermal diffusivity and the temperature rise at any point x in the medium concerned. At the surface of contact $x = 0$ there exists a total thermal flux Q ($1 - at$), uniformly distributed over the plane, whilst at the two outer plane boundaries $x = -d_3$ and $x = d_2$ there is no flow of heat. At the surface of separation $x = d_1$ between medium one and medium two, it is assumed that

* NEWCOMB, T. P. *Engineering (London)*, **187**, p. 709 (1959).

there is no contact resistance and that continuity of heat flux and temperature exists across the boundary. Fig. 1 shows a diagrammatic sketch of the arrangement.

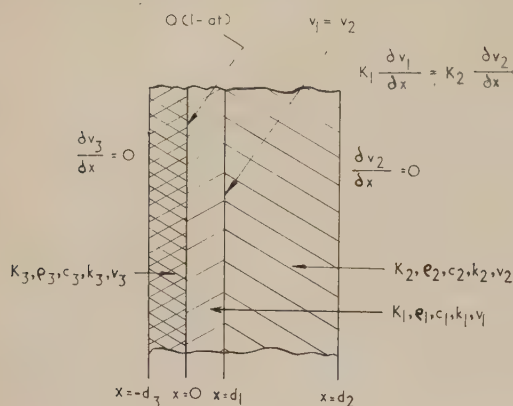


Fig. 1. Diagrammatic sketch of a cross-section of a lining in contact with a bimetallic brake drum together with boundary conditions for the heat problem

The partial differential equations to be solved are

$$\frac{\partial^2 v_1}{\partial x^2} - \frac{1}{k_1} \frac{\partial v_1}{\partial t} = 0 \quad 0 < x < d_1, t > 0 \quad (1)$$

$$\frac{\partial^2 v_2}{\partial x^2} - \frac{1}{k_2} \frac{\partial v_2}{\partial t} = 0 \quad d_2 > x > d_1, t > 0 \quad (2)$$

$$\frac{\partial^2 v_3}{\partial x^2} - \frac{1}{k_3} \frac{\partial v_3}{\partial t} = 0 \quad -d_3 < x < 0 \quad (3)$$

subject to the boundary conditions

$$v_1 = v_3 \text{ and } K_3(\partial v_3/\partial x) - K_1(\partial v_1/\partial x) = Q(1 - at) \text{ at } x = 0 \quad (4)$$

$$\partial v_3/\partial x = 0 \text{ at } x = -d_3 \quad (5)$$

$$v_1 = v_2 \text{ and } K_1(\partial v_1/\partial x) = K_2(\partial v_2/\partial x) \text{ at } x = d_1 \quad (6)$$

$$\partial v_2/\partial x = 0 \text{ at } x = d_2 \quad (7)$$

Using the Laplace transform and solving in the usual manner as outlined previously by the author,* it can be shown that at the interface of drum and lining the equation for the temperature rise v takes the form

$$v = \frac{k_1^{\frac{1}{2}} Q}{K_1(y + \sigma w + \beta z)} \left[t \left(1 - \frac{at}{2} \right) + C(1 - at) - aD + \frac{1}{(y + \sigma w + \beta z)} \{ aA(t + C) + aB - A \} - \frac{aA^2}{(y + \sigma w + \beta z)^2} \right] - \frac{2k_1^{\frac{1}{2}} Q}{K_1} \sum_{m=1}^{\infty} \left(\frac{1}{\delta_m^2} + \frac{a}{\delta_m^4} \right) \frac{(1 - \sigma \tan \delta_m y \tan \delta_m w) \exp(-\delta_m^2 t)}{(y + \beta z + \sigma w) - (y \sigma + \sigma \beta z + w) \tan \delta_m y \tan \delta_m w - (\beta y + z + \sigma \beta w) \tan \delta_m z \tan \delta_m y - (\sigma \beta y + \sigma z + \beta w) \tan \delta_m z \tan \delta_m w} \quad (8)$$

where

$$A = \frac{1}{6} \{ \beta z(3y^2 + 3w^2 + z^2 + 6\sigma wy) + y^3 + \sigma w^3 + 3yw(w + \sigma y) + 3z^2(y + \sigma w) \}$$

$$B = (\beta z/120) \{ 5y^4 + 5w^4 + z^4 + 30y^2w^2 + 10z^2y^2 + 10z^2w^2 + 20\sigma wy(w^2 + y^2 + z^2) \}$$

$$+ \frac{1}{120} \{ y^5 + \sigma w^5 + 10(y^3w^2 + \sigma y^2w^3 + z^2y^3 + \sigma w^3z^2) + 5(yw^4 + \sigma y^4w + 6yw^2z^2 + 6\sigma wy^2z^2 + z^4y + \sigma z^4w) \}$$

$$C = \frac{1}{2} (y^2 + w^2 + z^2 + 2\sigma wy)$$

$$D = \frac{1}{24} \{ y^4 + z^4 + w^4 + 6(y^2w^2 + y^2z^2 + z^2w^2) + 4\sigma wy(w^2 + y^2 + 3\sigma z^2) \}$$

$$w = \frac{d_2 - d_1}{k_2^{\frac{1}{2}}}, \quad y = \frac{d_1}{k_1^{\frac{1}{2}}}, \quad z = \frac{d_3}{k_3^{\frac{1}{2}}}, \quad \sigma = \frac{K_2(k_1^{\frac{1}{2}})}{K_1(k_2^{\frac{1}{2}})}, \quad \beta = \frac{K_3(k_1^{\frac{1}{2}})}{K_1(k_3^{\frac{1}{2}})}$$

and $\pm \delta_m, m = 1, 2, 3 \dots$ are the roots of the equation

$$\beta \tan \delta z (1 - \sigma \tan \delta y \tan \delta w) + (\tan \delta y + \sigma \tan \delta w) = 0$$

* NEWCOMB, T. P. *Brit. J. Appl. Phys.*, **10**, p. 204 (1959).

From equation (8) values of v/Q (proportional to temperature rise) have been calculated at the interface of drum and lining during a 5, 10 and 16 second brake application when $d_1 = 0.3$ cm, $d_2 = 1.5$ cm and $d_3 = 0.4763$ cm. The drum and lining have physical properties $K_1 = 0.12$ cal cm⁻¹ s⁻¹ deg. C⁻¹, $k_1 = 0.12$ cm² s⁻¹, $K_2 = 0.48$ cal cm⁻¹ s⁻¹ deg. C⁻¹, $k_2 = 0.86$ cm² s⁻¹, $K_3 = 1.8 \times 10^{-3}$ cal cm⁻¹ s⁻¹ deg. C⁻¹ and $k_3 = 3.3 \times 10^{-3}$ cm² s⁻¹. The values v/Q are shown graphically in Fig. 2, together with values obtained when all the heat is assumed to flow into the drum. If at the friction surface the heat generated is shared between drum and lining depending on the thermal properties of the cast iron and brake linings alone, then the amount λQ entering the drum is given by

$$\lambda Q = Q / \left\{ 1 + \frac{A_3 (K_3 \rho_3 C_3)^{\frac{1}{2}}}{A_1 (K_1 \rho_1 C_1)^{\frac{1}{2}}} \right\}$$

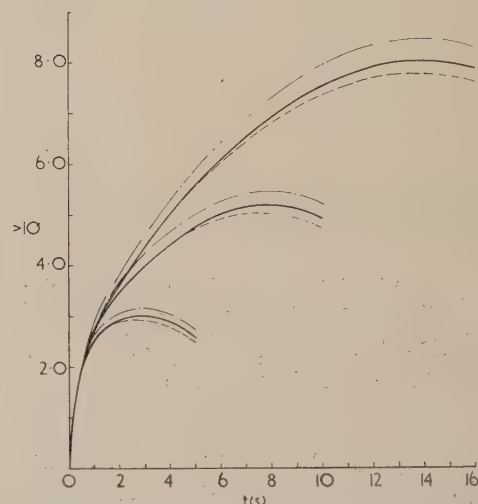


Fig. 2. Variation of v/Q at the interface of drum and lining at any instant during a 5, 10 and 16 s brake application using a bimetallic drum ($d_1 = 0.3$ cm, $d_2 = 1.5$ cm)

— based on the assumption that all the heat generated entered the drum
 --- based on the assumption that 95% of the heat generated enters the drum
 exact solution

where A_1 is the area of rubbing path and A_3 is the area of friction material in one drum. With typical friction materials, sliding on cast iron $\lambda = 1/\{1 + 0.09(A_3/A_1)\}$ and for a 90° and 120° arc of lining, $\lambda = 0.957$ and 0.943 respectively. Thus for drum brakes where the angle of arc generally lies between 90 and 120° , λ changes little from 0.95 . When λ takes this value the temperature rise during the application is also shown in Fig. 2.

These curves show that only a small error is introduced

by assuming that the heat sharing ratio is dependent only on the thermal properties of the cast iron and brake linings alone.

Acknowledgements

The author wishes to thank Dr. R. T. Spurr and Mr. A. J. Stinton of the Research Division of Ferodo Ltd. for assistance and criticism, and the Directors of Ferodo Ltd. for permission to publish this paper.

NOTES AND NEWS

Notes and comments

Elections to The Institute of Physics

The following elections were made by the Board of The Institute of Physics:

Fellows: W. Ashhurst, V. Balashov, G. A. Bell, J. G. Campbell, J. H. Coupland, D. E. Davies, L. W. Davies, M. Davis, R. Jones, R. D. Lowde, G. B. F. Niblett, D. W. Pashley, W. G. H. Schwietzke, S. P. Thong, H. Tunley.

Associates: J. E. Allen, D. W. Ballentyne, G. G. Bowman, E. A. Braun, A. F. C. Brown, L. D. Brown, J. R. Butler, R. W. Cotterhill, J. Daley, R. R. Davis, G. E. H. Deadman, M. E. Delany, N. Gerald, M. J. Goodman, W. A. Heslop, H. Hofer, A. Hood, R. Hughes, F. W. E. Jackson, G. J. Johnson, K. V. Krishna Rao, A. G. Little, H. Lockett, M. C. Lovell, N. A. Lynch, A. F. McFarlane, M. H. McTaggart, G. A. Manning, I. F. Mayer, J. I. Missen, A. O'Connor, N. J. Peacock, R. Phillips, M. R. Piggott, B. Pounder, R. R. Preston, J. B. Rich, G. W. Rowe, M. C. Sexton, D. Shaw, G. R. Sothorn, R. C. Spragg, F. S. Ward, P. G. Williams, J. A. Woodward.

Thirty-five Graduates, twenty-six Students and four Subscribers were elected.

Annual Report of The Institute of Physics, 1959

The annual report of The Institute of Physics for 1959 which was adopted at the final meeting of the Institute before its amalgamation with The Physical Society shows that at the end of the year the total membership in all grades was 6,754, an increase of 445 on the previous year. The number of applications for membership continued to increase and reached a new record of 933 during the year. The Report records that at a General Meeting on 1 December, the Scheme for amalgamation was unanimously adopted and the Board was requested to take the necessary action to implement the proposals.

The number of candidates entering for the Graduateship examination of the Institute continued to increase at a very satisfactory rate; 119 candidates took papers compared with 80 the previous year. Only 39 candidates were successful and of these 13 held university degrees and 26 the Higher National Certificate in applied physics.

The Report again records the expanding activities in many fields including education, scientific publications, conferences

and symposia and meetings arranged by the Branches and specialist subject Groups.

During the year the Institute's Benevolent Fund gave assistance to ten cases where members of the Institute or their dependents had met with misfortune.

Solid-state electronics

We have received the first issue of a new bi-monthly periodical entitled *Solid-state electronics*. The publishers state that "It is the function of this *Journal* to bring together in one publication outstanding papers reporting original work in various areas of applied solid-state physics, including transistor technology in all its aspects, transistor theory and design, crystal growing and handling, preparation of junctions, and transistor process technology. Also of interest are applications of intermetallic and other binary and ternary semiconductors, applications of ferrites and ferroelectrics, the design and performance of galvanomagnetic devices, thermoelectric properties and their applications, electroluminescent and related devices, photoconductors, and photovoltaic cells and solid-state batteries. The *Journal* will also consider problems of packaging, stability, reliability, and device life. Papers covering novel topics extending the frontiers of existing solid-state technology are, of course, invited. Review papers covering important topics in the field of solid-state electronics will be presented at intervals."

The Editor-in-Chief is Dr. W. Crawford Dunlap, Jr., of the Raytheon Company, Waltham, Mass., U.S.A. The publishers are Pergamon Press Ltd., of Oxford.

Contemporary physics

In announcing this new periodical the publishers say "This new *Journal* has been established to publish review articles on various aspects of physics of a standard suitable for teachers in schools and in technical colleges, scientists in industry, and others striving to keep in touch with modern developments. It is hoped to maintain the highest level of scientific content, and at the same time to interpret this content in a way that the ordinary graduate can understand. The Editorial Board has in mind the kind of treatment given in lectures at refresher courses organized by the Universities, and indeed the real object of the *Journal* is of comparable intent".

The *Journal* will appear six times a year. The main features

will be: Major articles of about 6000 words which will be descriptive surveys of advances in physics, relatively elementary interpretations of theoretical matters, and papers on the historical, philosophical, and educational aspects of the subject; articles of about 2000 words, which will deal with individual topics in greater detail; essay reviews which will interpret the contents of outstanding publications, either books or original papers; book reviews, for which reviewers, as well as commenting by their own specialist standards, will try to assess a book's usefulness to the ordinary reader of the *Journal*.

The Editor is Mr. G. R. Noakes, and he is supported by an Editorial Board of five distinguished physicists. The first issue of eighty pages contained the following contributions: "Molecular beams", by O. R. Frisch; "Nuclear structure", by R. J. Blin-Stoyle; "Alexander von Humboldt and the beginnings of geophysical research", by C. Kellner; "The selection of experiments for the Cavendish Laboratory alternating-current course", by E. V. Beck; "Skidding friction", by B. Sabey, and "Atomic light sources," by E. J. Wilson and J. D. H. Hughes. In addition there are three essay reviews and seven other book reviews.

The price of single parts is 5s. (75 cents) excluding postage. There are to be six parts to the volume. The subscription price per volume is £1 7s. (\$4.00), including postage. The publishers are Taylor and Francis Ltd., Red Lion Court, Fleet Street, London, E.C.4.

TIM: a brushless generating magnetometer

Referring to the paper by Dr. McCutchen published in our November 1959 issue under the above title, the Compagnie Française Thomson Houston of 6, Rue Marion-Nikis, Paris (XV^e) inform us that they designed and built an apparatus working on the same principle in 1954. It was shown at the 1955 exhibition of the Société Française de Physique and a brief description of it appeared in the catalogue of that exhibition. Industrial forms of the apparatus have been built and successfully operated. They will be glad to supply further information to any readers who may be interested.

Errata

In the paper entitled "Measurement of atomic differential scattering cross-sections" which appeared on p. 259 of the June 1960 issue of this *Journal* an error occurred in the second line of the section headed "Theory". For ρ/NA read $\rho N/A$.

In the paper by Farrow and Preston entitled "Measurement of crystallinity in drawn polyethylene terephthalate fibres by X-ray diffraction", published in the August issue of this *Journal*, Figs. 1(b) and (c) and Fig. 4, should be turned through a right-angle.

British Standards Institution

We have recently received the following new publications of the British Standards Institution:

British Standards Yearbook 1960. This contains information about the Institution and the services it offers. It lists the British Standards current at 1 January, 1960, and gives a brief description of each. Price 15s.

British Standards Institution Annual Report 1959-1960. The report covers all the Institution's activities from 1 April 1959, to 31 March, 1960. Price 7s. 6d.

New Standards are: B.S. 3238: Part 1: 1960—*Graphical symbols for components of servo-mechanisms. Part 1. Transducers and magnetic amplifiers*. Price 4s. 6d. B.S. 1568: 1960—*Magnetic tape sound recording and reproduction*. Price 4s. 6d. B.S. 3231: 1960—*Specification for thermographs (bimetallic type)*. Price 3s. B.S. 1780: 1960—*Specification for bourdon tube pressure and vacuum gauges*. Price 15s. B.S. 1041: Part 3: 1960—*Code for temperature measurement. Part 3. Industrial electrical resistance thermometers*. Price 5s. B.S. 3202: 1959—*Recommendations on laboratory and furniture fittings*. Price 25s.

All these publications may be obtained from British Standards House, 2 Park Street, London, W.1.

Journal of Scientific Instruments

Contents of the September issue

PAPERS

- Error of rectifier-type milliammeters in low-resistance circuits. By J. Wilbur-Hamm and W. E. K. Gibbs.
Daylight factor meter. By D. P. Turner.
Time-sorter for use in the nanosecond range. By G. Jones.
Isotopic analysis of boron in boron trifluoride by mass spectrometry, and measurement of natural boron 10 concentration. By P. G. Bentley.
Ratiometer for low-current mass spectrometry. By F. D. S. Butement and N. P. Finkelstein.
Measurement of space density of charge in flowing liquids. By A. Schuringa and C. Luttik.
Reduction of dead-time in halogen-quenched Geiger counters. By B. B. Trotter.
Apparatus for the measurement of gas velocity in furnaces and models. By A. E. Pengelly.
Simple continuous chart and integrating device for a Joyce-Loebl microdensitometer Mk. I. By G. Farrow and D. Preston.
Measurement of thermal diffusivity of semiconductors by Ångström's method. By A. Green and L. E. J. Cowles.
Heavy-water electrolysis unit for generation of deuterium gas provided with automatic switch-off and safety devices. By P. K. Dutt.
Temperature-controlled permanent magnet for high-resolution nuclear magnetic resonance. By B. A. Evans and R. E. Richards.
Improved design for an auto-focus range-finder. By H. Asher, L. Dodin and H. P. Mulholland.

LABORATORY AND WORKSHOP NOTES

- Vernier scale arrangement for the measurement of peak heights on mass spectrometer charts. By J. R. Richards.
Insulated terminals for high-vacuum systems using demountable glass-metal seals. By R. S. Nelson.
Cosine correction of a weatherproofed photovoltaic cell. By E. T. Weston and D. Paix.
Automatic silver concentration control for nuclear emulsion fixing baths. By E. Dahl-Jensen.
Robust and sensitive spoon gauge. By B. J. Aylett.

NOTES AND NEWS

New instruments, materials and tools New books Notes and comments

THIS JOURNAL is produced monthly by The Institute of Physics and The Physical Society, in London. It deals with all branches of applied physics (including theory and technique). All rights reserved. Responsibility for the statements contained herein attaches only to the writers.

EDITORIAL MATTER. Communications concerning editorial matter should be addressed to the Editor, The Institute of Physics and The Physical Society, 47 Belgrave Square, London, S.W.1. (Telephone: Belgravia 6111.) Prospective authors are invited to prepare their scripts in accordance with the *Notes for Authors*. (Price 3s. 6d. including postage.)

REPRODUCTION. The Institute of Physics and The Physical Society is a signatory to The Royal Society's Fair Copying Declaration. Details may be obtained upon application from The Royal Society, London, W.1.

ADVERTISEMENTS. Communications concerning advertisements should be addressed to the agents, Messrs. George Jackson (Fleet St.) Ltd., Cliffords Inn, Fleet Street, London, E.C.4. (Telephone: Holborn 3611-2.)

CLAIMS FOR MISSING JOURNALS. Claims from regular subscribers to this *Journal* for missing numbers will only be considered if received within 60 days of the date of mailing plus normal outward time of transit and time for lodging the claim. Losses attributable to failure to notify a change of address or to similar omissions will not be considered.

SUBSCRIPTION RATES. A new volume commences each January. The charge is £6 per volume (\$17 U.S.A.), including index (post paid), payable in advance. Single parts, so far as available, may be purchased at 12s. 6d. each (\$1.75 U.S.A.), post paid, cash with order. Orders should be sent to The Institute of Physics and The Physical Society, 47 Belgrave Square, London, S.W.1, or to any bookseller.

Summarized proceedings of a symposium on the generation of temperatures below 1° K—London, December, 1959

A one-day symposium on the methods of generating temperatures below 1° K was held by the Low-Temperature group of The Physical Society on 11 December, 1959. Six papers of a review nature were read and discussed. Attention focused primarily on the techniques of adiabatic demagnetization and on the use of ^3He ; nevertheless some of the more difficult techniques were reviewed with the more recently discovered properties of ^3He .

Introduction

THE papers read at the symposium were: "The use of ^4He " by Mr. G. Davey (Clarendon Laboratory, Oxford); "The use of ^3He " by Mr. M. Hobden (Clarendon Laboratory, Oxford); "Adiabatic demagnetization" by Dr. E. Mendoza (University of Manchester); "Nuclear cooling" by Dr. N. Kurti (Clarendon Laboratory, Oxford); "Dilution of ^3He by ^4He " by Dr. H. London (A.E.R.E., Harwell); and "Some properties of solid ^3He and ^4He below 1° K" by Dr. H. Brewer (Clarendon Laboratory, Oxford).

In the last few years it has become much easier, technically, to produce temperatures well below 1° K because ^3He , the light isotope of helium, has become available in quantities sufficient for cryogenic purposes. This has extended the directly accessible liquid helium range down to about 0.3° K, a very favourable platform from which to begin adiabatic demagnetizations; ^3He therefore figures prominently in this report. In the first section ^4He and ^3He are compared as cryogenic liquids, the second section deals with demagnetization techniques, and the third section with other methods of getting below 1° K and in so doing refers to some of the properties of solid ^3He . Where possible the references given are to review articles with good bibliographies, rather than to specialized original papers.

^4He and ^3He as cryogenic liquids

Liquid ^4He and ^3He have marked differences in their properties which are attributable to the differences in atomic mass and nuclear spin. The way in which these differences depend on the fundamental parameters of the atoms is of great interest, and has been recently reviewed in a number of articles.⁽¹⁻⁴⁾ For the present purposes the most important difference lies in their vapour pressure curves which are shown in Fig. 1. At the same pressure a bath of liquid ^3He will yield much lower temperatures than one of ^4He . However, ^3He is still very expensive (1000\$ per litre of gas at n.t.p.) and its use has been very restricted. On the other hand the properties of ^4He below the λ -point transition at 2.18° K, i.e. the helium II region, introduce certain difficulties.⁽⁵⁾

The properties of liquid helium II can be understood in terms of the two-fluid model,⁽⁶⁾ in which liquid helium consists of two interpenetrating fluids. One behaves more or less as a normal liquid, the other behaves as a "super-

fluid" being capable of frictionless motion, and there is presumed to be virtually no interchange of momentum between the two liquids. In a vessel containing liquid helium II the surfaces above the liquid are covered by a film of helium about 100 atoms thick. The superfluid

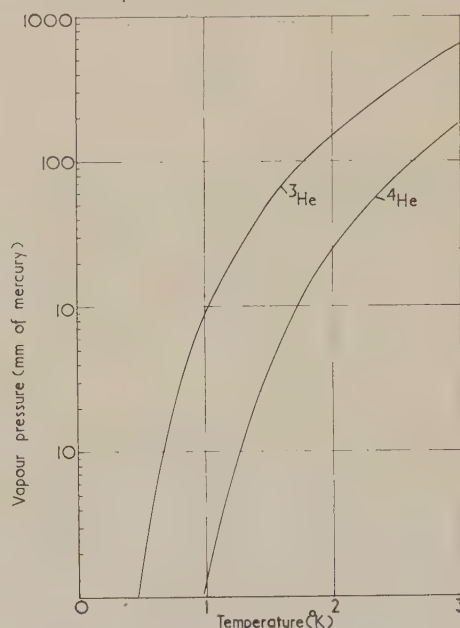


Fig. 1. Vapour pressures of ^3He and ^4He

component of the liquid flows through this film at a rate which is proportional to the circumference of the vessel out of which it is flowing. If a constriction exists the flow is proportional to the perimeter of the constriction; it is also approximately independent of the length of the film. The rate of flow is dependent on the nature of the surface over which it is flowing, the rougher and dirtier the surface the greater the flow. This can reduce the efficiency of a cryostat as it gets older.

These effects have been demonstrated in numerous experiments (see a review by Atkins⁽⁷⁾) and they must be taken into account in attempting to generate temperatures below 1° K by pumping ^4He . In a simple parallel-sided Dewar vessel containing liquid helium II, the helium film will creep up the walls to those regions where the temperature corresponds to the λ -point, and evaporation will take place from the film surface as well as from the liquid surface.

The precise pressure distribution in the evaporated gas above the liquid will depend upon the geometry, but there is always the possibility of warmer gas from near the top of the film recondensing at the liquid surface, so giving an extra thermal leak beyond that due to the film and other normal causes. Keesom⁽⁸⁾ generated temperatures of about 0.73° K in a well protected, but open, bath containing 1.5 cm³ of liquid and using a pumping speed of approximately 675 litre/s.

However, a restriction such as a narrow tube, or a pin-hole in a diaphragm immediately above the helium bath, reduces the film flow so that the pumping speed, to yield end temperatures of approximately 0.75° K, need only be about 10 litre/s.^(9, 10) These restrictions can be a disadvantage, compared with an open bath, for many experimental arrangements. Modern booster pumps of high speed are comparatively compact and, with a suitably designed pumping line, approximately 0.75° K is obtainable in an open Dewar vessel. A typical arrangement, designed by Edwards and Brewer and used by Mr. G. Davey at the Clarendon Laboratory, Oxford, is shown in Fig. 2. The helium II is confined to the tail of a Dewar flask, so that the film flow

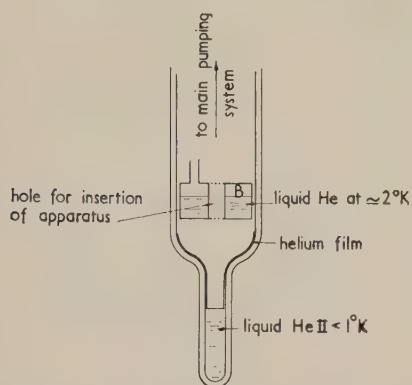


Fig. 2. Schematic arrangement of cryostat for use with ^4He to generate very low temperatures

corresponds to the diameter of the tail. The vessel *B* contains liquid helium at approximately 2° K serving as a radiation shield, and also ensuring that the helium film creeps up the walls of the Dewar flask to the widest part near *B*, where it may evaporate in a region where the pumping speed is high. Whatever the arrangements used it seems that the practical limit to the temperatures attainable using ^4He in this way is approximately 0.74° K.

In comparison with the difficulties involved with ^4He , the use of ^3He seems to offer many advantages. Liquid ^3He is not superfluid, certainly above 0.1° K, and at 1° K its vapour pressure is approximately 10 mm of mercury or about seventy times that of ^4He (see Fig. 1), while at approximately 0.5° K the ratio is as high as about 10^4 . However, owing to the high cost only small quantities of ^3He are available at present, e.g. hundreds of cubic centimetres, or at most 2 to 3 litres of gas, and in addition complete arrangements for conserving the gas must be provided.

The critical temperature and pressure are 3.3° K and 875 mm of mercury respectively. The specific heat of the liquid can be taken as about 10^6 erg/cm³ of liquid between 1 and 0.3° K and the latent heat of evaporation is approximately 10^7 erg/cm³. Thus in pumping the liquid from 1° K to approximately 0.3° K in a bath, about 10% of the liquid will be evaporated. The proportion of ^4He present in the liquid must be kept below about 5%, otherwise separation into two phases will occur bringing all the λ -point troubles of liquid ^4He at the lower temperatures.

In view of the critical point data, ^3He has only been liquefied in small quantities by condensation in contact with baths of liquid ^4He boiling at reduced pressure. A small quantity of gas can be condensed into a suitably designed and thermally-protected small chamber of about 1 or 2 cm³

capacity, from which it can then be pumped. Thus with only about 150 cm³ of gas yielding approximately 0.25 cm³ of liquid, Kurti and Hobden, Clarendon Laboratory, Oxford, have generated temperatures of approximately 0.35° K which can be held for about ten hours, while with bigger quantities, e.g. approximately 4 cm³ of liquid, theoretical durations of about fifty hours are feasible in an apparatus developed by Seidel and Keesom.⁽¹¹⁾ Peshkov, Zinov'eva and Filiminof⁽¹²⁾ used an apparatus shown schematically in Fig. 3 and from which the function of the Dewar system is obvious; *C* is a small bore stainless steel tube through which ^3He can pass and *D* is a valve admitting the condensed liquid into the

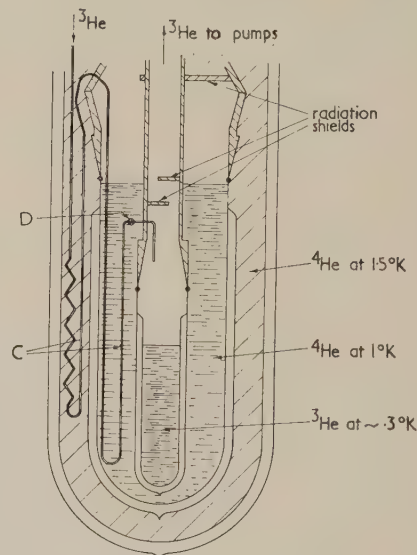


Fig. 3. ^3He cryostat, after Peshkov, Zinov'eva and Filiminof

innermost Dewar vessel, where it can be pumped away using a pumping system capable of 30 litre/s. With this apparatus temperatures of about 0.3° K have been generated. The same quantity of ^3He can be repeatedly recondensed in shots as long as the ^4He lasts. One can equally well devise a cryostat in which the ^3He is continually circulated and so have a large refrigerating capacity. Garwin and Reich⁽¹³⁾ have used this system to generate temperatures near 0.5° K. With all such apparatus the auxiliary pumping systems for ^3He must be perfectly gas tight and so arranged that the ^3He can be pumped away into safe storage. Moreover, the volumes of the condensation lines and pumping lines must be designed taking into account the temperature distribution along them, so that only the minimum quantity of ^3He is used as gas to fill them at the working pressures, thus giving the maximum quantity of liquid. Peshkov and Zinov'eva⁽¹⁴⁾ have given a thorough review of the work on ^3He recently, in which a number of ^3He cryostats have been described. In addition to that of Kurti and Hobden, Wilks and Harding, also at the Clarendon Laboratory, Oxford, have devised a successful cryostat using ^3He well below 1° K.

With both ^3He and ^4He there is a boundary heat resistance between a solid body and the liquid surface. Thus, whenever heat is to be dissipated in an experiment immersed in liquid helium, the corresponding temperature discontinuity across the solid liquid surface should be taken into account. For ^3He the boundary resistance ($^{\circ}\text{K cm}^2 \text{W}^{-1}$) is approximately $130/T^2$ while for ^4He it is approximately $45/T^2$.

Adiabatic demagnetization techniques

The techniques involved in the use of adiabatic demagnetization of paramagnetic materials to generate very low temperatures are well established.^(15,16) Many paramagnetic salts have magnetic susceptibilities χ , which follow a Curie-Weiss law over wide ranges of temperature, i.e. $\chi = C/(T - \theta)$ for $T > \theta$, where C is Curie's constant and θ is the Weiss constant. If the material can be cooled through the temperature $T = \theta$, χ should tend to infinity; in practice some sort of magnetic ordering occurs near $T = \theta$. Typical materials are the hydrated salts of the rare-earth and transition metals, the alums, ruby and garnet.

For the present purposes it is convenient to think of the paramagnetic ions in the crystal as being elementary magnets, the moments being made up from orbital and electron spin contributions according to the nature of the ion and of the spin-orbit coupling. Constant θ is a measure of the strength of the interactions between the elementary magnets and between them and electric fields in the crystal; at low enough temperatures these interactions can cause the moments to line up in a particular way, i.e. some degree of ordering takes place.

The entropy, which can be taken as a measure of the degree of disorder, changes considerably in such a process, as shown in curve *A* of Fig. 4. The specific heat C_p reflects this change, for $C_p = dQ/dT = TdS/dT$, so that at a tempera-

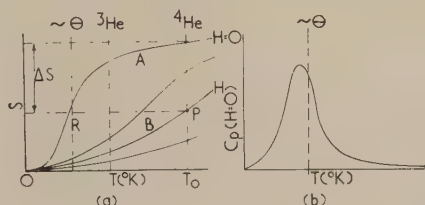


Fig. 4. (a) Entropy temperature curve for paramagnetic ion near 0° K
(b) Specific heat curve in zero magnetic field

ture comparable with θ , the specific heat will go through a pronounced maximum. At a temperature well above θ , a sufficiently powerful imposed external magnetic field H will also induce order and the entropy will correspondingly fall by, say, ΔS to a value such as at *P* in curve *B*, Fig. 4. If T_0 is to remain constant during this magnetization a quantity of heat $Q = \Delta S.T_0$ must be evolved and conducted away from the system. If now the system can be thermally isolated, on removal of the external magnetic field (adiabatic demagnetization) the temperature must fall to correspond to some point such as *R* on curve *A*, Fig. 4. A schematic arrangement by which this sequence of operations can be realized is shown in Fig. 5; *E* is a specimen of paramagnetic salt enclosed in a vacuum case *F* which is surrounded by a bath of liquid helium *G*. Bath *G* may be pumped to approximately 1° K while exchange gas is left in *F* and the magnetic field applied, so that the heat of magnetization is conducted through the exchange gas to the helium bath. When equilibrium is achieved the exchange gas can be removed by pumping, so insulating the salt thermally. Now on removal of the magnetic field the temperature of the salt will fall. Any residual helium exchange gas left in *F* will be adsorbed on the surface of *E*.

There are many practical snags: radiation must be excluded; vibration of the system (e.g. due to pumps) can create heat leaks of a few ergs per second; as warming-up proceeds,

helium adsorbed on *D* will be desorbed and the high vacuum in *E* will break down to some extent. If the specimen is used to cool another material, reasonable thermal contact may be difficult to achieve. To overcome this arrangements

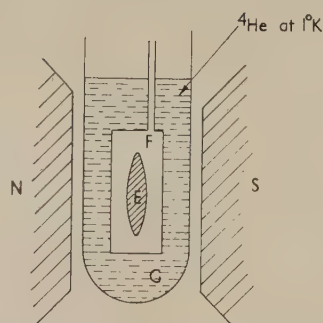


Fig. 5. Schematic arrangement for adiabatic demagnetization

of copper fins and wires, embedded in the specimen and attached to the object to be cooled, have been used with some success and are probably satisfactory down to 10^{-2} ° K. Owing to the poor thermal conductivity in the paramagnetic salts used themselves, temperature equilibrium may be difficult to establish. On the other hand from Fig. 4 demagnetization from a strong magnetic field will automatically bring the salt into that region of temperature where the specific heat is high, so the initial warm-up rate will be slow. Fig. 4 also shows the advantage of using a ^3He bath for initial cooling, a given low temperature can be realized with a much smaller magnetic field. To obtain the lowest temperatures by this method it is necessary to demagnetize a material in which θ is very small, and hence one in which the interactions between the paramagnetic ions are small; θ may be reduced by separating the ions as much as possible as in the hydrated alums, e.g. ferric ammonium alum, $\text{Fe}_2(\text{SO}_4)_3(\text{NH}_4)_2\text{SO}_4 \cdot 24\text{H}_2\text{O}$.

The magnetic susceptibility of a typical salt follows the Curie-Weiss law quite accurately at temperatures well above θ , which is usually less than 0.1° K. The values of C and θ can then be determined by measuring the susceptibility χ in the liquid ^4He range between 1 and 4° K. Values of χ measured below 1° K can be used to measure the temperature, assuming that the Curie-Weiss law is followed accurately; temperatures on such an extrapolated scale are referred to as T^* .

The susceptibility of the salts has been used as a measure of temperature in most experiments but the resistance of the usual carbon resistors can equally well be used. In either case calibration on the absolute (as opposed to T^*) scale is a tedious business.^(15,17)

When measuring χ at the lowest temperature, owing to the powerful paramagnetism exhibited in the specimen, correction must be made for the demagnetizing effect of the free poles and hence the shape of the specimen has to be mathematically simple (a sphere or ellipsoid of revolution); even so the errors in estimating this correction can be considerable.⁽¹⁸⁾

For many purposes it is desirable to stabilize the very low temperatures generated, or alternatively deal with a rather high heat influx. To this end a number of attempts have been made to devise heat pumps. The most successful was that of Daunt who originated the A.D. Little magnetic refrigerator. In this machine a large specimen of paramagnetic salt is used as the working substance and is taken

through a "Carnot cycle" by applying and removing alternately a magnetic field. Contact with the heat sink (liquid helium at 1° K) and the cooled reservoir (a salt with a high heat capacity at the low temperature) is controlled through heat switches. These are strips of lead used as the usual superconductive switches. In the normal state their thermal conductivity is much higher than in the superconductive state, the state being controlled by magnetic fields from auxiliary solenoids. With machines of this type temperatures of about 0.3° K can be reached and held with small fluctuations each cycle. An easier system is to demagnetize from a fairly high field to a low field of a few hundred gauss, then to continue the demagnetization slowly so that the further cooling effect can just balance the heat influx. Such a system can be servo-controlled and will produce very steady temperatures for limited periods.⁽¹⁷⁾

Other heat switches have been tried, including the simple idea of mechanical contact. An ingenious one is to use a vertical tube filled with liquid ³He. When heat is applied at the bottom it is quickly convected to the top through the liquid, while heat applied at the top can only travel by conduction through the walls of the tube and through the liquid; however, the admittance ratio is rather poor.

It is difficult to generate temperatures below approximately 0.01° K in a single demagnetization as fields higher than about 25 kilo-oersteds would be required. However, by using two stages in which one salt at about 0.1° K acts as the thermal sink for the magnetization of a second salt, temperatures as low as 0.001° K have been generated with only about 9 kilo-oersteds. Darby and others⁽²⁰⁾ used iron alum as the first stage and chrome alum as the second; thermal contact was achieved by embedding many fine copper wires in each specimen and joining them with a lead wire used as a superconductive switch.

To achieve even lower temperatures, it appears at first sight that the magnetic ions have simply to be separated further to reduce θ . There is a limit to the dilution feasible, for the number of ions per cubic centimetre of salt becomes too small to give a useful change in total entropy. However, use can be made of the nuclear paramagnetism (nuclear spins) to carry the temperature scale downwards. Because the moments are so much smaller than those of the electrons, fields of the order of 50 kilo-oersteds at about 0.01° K are necessary as the starting conditions. This means that the nuclear paramagnetic must be cooled with an "electron" paramagnetic material previously demagnetized to near zero field. The technical difficulties involved were first overcome by Kurti and others.⁽¹⁹⁾ The electron paramagnetic was chrome potassium alum mixed to a slurry with glycerol and water and enclosed in a Perspex container. A very large number of fine (40 s.w.g.) copper wires were embedded evenly in the slurry, so providing a very large surface for thermal contact. At the lower ends the copper wires were folded over several times to form the nuclear specimen, which was in fact the metallic copper itself; the wires, of course, also provided the thermal link. Metallic copper was chosen because the nuclei have large moments and because the nuclear spin-lattice relaxation time was likely to be of the order of minutes, as opposed to many hours in the case of dielectric materials at the very low temperatures. The use of wires also cut eddy-current heating effects to the minimum. By surrounding the specimens and thermal link with a shield cooled by demagnetizing manganos ammonium sulphate at the same time as the chrome alum, heat leaks were cut to about 1 erg/min. The final temperature of the nuclear system was estimated from susceptibility measurements to

be near 20×10^{-6} ° K. More recently, Kurti and Hobden have repeated this experiment under more favourable conditions. A shield cooled with ³He was held at 0.3° K; the nuclear spins were demagnetized from approximately 0.012° K and 30 kilo-oersteds. An a.c. bridge, which produced very small fields in the specimen, was used for nuclear susceptibility measurements. The lowest temperature of the nuclear system was estimated to be 1.3×10^{-6} ° K.

Other techniques for generating temperatures below 1° K

A number of other techniques have been discussed for generating temperatures below 1° K. First there is the adiabatic magnetization of a superconductor. Below the transition temperature in zero field the entropy of the metal in the superconducting state is smaller than that of the normal state, as shown in Fig. 6. If a magnetic field is applied adiabatically and is of sufficient strength to destroy

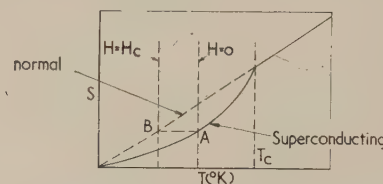


Fig. 6. Entropy temperature curves for a superconductor

the superconductivity the temperature must fall, e.g. from A to B in Fig. 6. This magneto-caloric effect has been demonstrated by Mendelssohn and his collaborators. More recently they have been able to use it in generating temperatures of about 0.5° K.

It has recently been shown that the melting curve of ³He⁽²¹⁾ has a minimum at about 0.5° K, which is in accord with the theory of Pomeranchuk. Below this temperature, from the Clausius equation

$$(dp_m/dT) = (S_{liq} - S_{sol})/(V_{liq} - V_{sol}) < 0$$

where the symbols are obvious. At the minimum, $S_{liq} = S_{sol}$, but below it, S_{sol} must be greater than S_{liq} . According to Pomeranchuk⁽²²⁾ this is due to the much larger effect of exchange interactions in the liquid. Working below the minimum it should be possible to generate very low temperatures using the adiabatic solidification of ³He by compression. According to Pomeranchuk's theory a final temperature of approximately 10^{-6} ° K is possible, while that of Primakoff⁽²³⁾ suggests about 10^{-3} ° K.

In the recent studies of liquid ³He it has also been shown⁽²⁵⁾ that the entropy of the liquid increases with increasing pressure in a range from the vapour pressure to 22 atm. Adiabatic compression of liquid ³He produces a cooling effect. This has been measured but is, unfortunately, not enough to make an effective method of reaching low temperatures ($\Delta T \sim 0.05$ ° K at 0.3° K).

When two liquids are mixed the entropy of the mixture should be greater than that of the two separate components. If the mixing can be carried out adiabatically a cooling should result. The heat of mixing liquid ³He and ⁴He has been estimated at approximately 2 cal/mol ³He; Dr. H. London⁽²⁵⁾ has been developing a technique using this idea, in which liquid ³He is diluted with ⁴He through a superleak. Con-

tinuously operating cycles are feasible, but the method is fraught with considerable difficulty. Nevertheless end temperatures of about 0.1° K should be possible.

D. H. PARKINSON

References

- (1) FEYNMAN, R. P. *Progr. Low Temp. Phys.*, **1**, p. 17 (1955).
- (2) HAMMEL, E. F. *Progr. Low Temp. Phys.*, **1**, p. 78 (1955).
- (3) WILKS, J. *Rep. Progr. Phys.*, **20**, p. 38 (1957).
- (4) ABRIKOSOV, A. A., and KHALATNIKOV, J. M. *Rep. Progr. Phys.*, **22**, p. 329 (1959).
- (5) AMBLER, E., and KURTI, N. *Phil. Mag.*, **43**, p. 1307 (1952).
- (6) GORTER, C. J. *Progr. Low Temp. Phys.*, **1**, p. 1 (1955).
- (7) ATKINS, K. R. *Progr. Low Temp. Phys.*, **2**, p. 105 (1957).
- (8) KEESOM, W. H. *Proc. Roy. Acad., Amsterdam*, **35**, p. 136 (1932).
- (9) BLAISSE, B. S., COOKE, A. H., and HULL, R. A. *Physica 's-Grav.*, **6**, p. 231 (1939).
- (10) COOKE, A. H., and HULL, R. A. *Nature (London)*, **143**, p. 799 (1939).
- (11) SEIDEL, G., and KEESOM, P. H. *Rev. Sci. Instrum.*, **29**, p. 606 (1958).
- (12) PESHKOV, V. P., ZINOV'EVA, K. N., and FILIMINOF, A. I. *J. Exp. Theor. Phys., U.S.S.R.*, **36** (9), p. 734 (1959).
- (13) GARWIN, R. L., and REICH, H. A. *Rev. Sci. Instrum.*, **30**, p. 7 (1959).
- (14) PESHKOV, V. P., and ZINOV'EVA, K. N. *Rep. Progr. Phys.*, **22**, p. 504 (1959).
- (15) AMBLER, E., and HUDSON, R. P. *Rep. Progr. Phys.*, **18**, p. 251 (1955).
- (16) GARRETT, C. G. B. *Magnetic Cooling* (Harvard University Press, 1954).
- (17) KURTI, N. *Supplemento del Nuovo Cimento*, **6**, p. 1101 (1957).
- (18) KURTI, N., and SIMON, F. E. *Phil. Mag.*, **26**, p. 849 (1938).
- (19) KURTI, N., ROBINSON, F. H. N., SIMON, F. E., and SPOHER, D. A. *Nature (London)*, **178**, p. 450 (1956).
- (20) DARBY, J., HATTON, J., ROLLIN, B. V., SEYMOUR, E. F. W., and SILSBEE, H. B. *Proc. Phys. Soc. (London), A*, **64**, p. 861 (1957).
- (21) BAUM, J. L., BREWER, D. F., DAUNT, J. G., and EDWARDS, D. O. *Phys. Rev., Letters* **3**, No. 3, p. 127 (1959).
- (22) POMERANCHUK, I. YA. *J. Exp. Theor. Phys. U.S.S.R.*, **20**, p. 919 (1950).
- (23) PRIMAKOFF, H. *Bull. Amer. Phys. Soc.*, **2**, p. 63 (1957).
- (24) BREWER, D. F., and DAUNT, J. G. *Phys. Rev.*, **115**, p. 843 (1959).
- (25) LONDON, H., CLARKE, G. R., and MENDOZA, E. *Kamerlingh Onnes Conference, Leiden. Physica*, **24**, Supplement, p. 135 (1958).

Pre-breakdown conduction in continuously-pumped vacuum systems

by W. K. MANSFIELD, B.Sc., Ph.D., A.Inst.P., Nuclear Engineering Laboratory, Queen Mary College, London

[Paper first received 18 May, and in final form 20 June, 1960]

Abstract

Measurements have been made under impulse conditions of the coefficients A' , the number of H^+ ions emitted per 250 keV H^- ion, and B' , the number of H^- ions emitted per 250 keV H^+ ion, for metal surfaces covered with the contaminating layers likely to be formed in continuously-pumped high-voltage apparatus. The values obtained for A' were 1.0, 1.1 and 0.54, and for B' 0.43, 0.24 and 0.44 for copper, aluminium and steel targets respectively. The product of these coefficients is such as to make very probable the hypothesis that pulse discharge conduction in these systems is due to the regenerative exchange of positive and negative ions of hydrogen. The transient nature of this form of conduction is thought to be due to the charging up of the insulating contaminant.

Introduction

AN account⁽¹⁾ has been given of the investigations carried out in this laboratory upon "electron loading" in the accelerator tubes of electrostatic generators. These investigations have shown that the phenomenon is due to the passage of pulses of current of millisecond duration which will be referred to as "pulse discharge conduction". The characteristics of pulse discharge conduction were described, and it was postulated that the conduction was due to the regenerative exchange of positive and negative ions of hydrogen, originating from contaminants upon the electrode surfaces.

Reference was made in this account to the preliminary measurements of A' , the number of H^+ ions emitted by impact of a H^- ion on the positive electrode, and B' , the number of H^- ions emitted by a H^+ ion. This report gives the results of the more sophisticated measurements which have now been made.

Experimental observations

Fig. 1 shows the pressurized electrostatic generator (1 MV), the accelerator tube and the associated measuring apparatus. The accelerator tube, which is of a sandwich construction, was made by the General Electric Co. Ltd. It is 15 in. long and has an aperture of 4 in. diameter. For these measurements the high-voltage end was blanked off with a copper plate and the other end had a system of offset, insulated baffles with a central $\frac{1}{2}$ in. diameter aperture. It was found, on running the generator, that pulses of current to the insulated baffles could be detected when a voltage of about 150 kV was applied to the tube. These pulses were of 100 μ A peak magnitude and some few milliseconds in duration.

With the passage of a few pulses the tube "conditioned-up" to such an extent that continuous pulsing occurred at about

one per second with a voltage of 250 kV. Thereafter a more long-term conditioning process was observed; the voltage necessary to produce a pulse rate of one per second (V_{th}), referred to as the "pulse threshold voltage", increased at about 10 kV per hour.

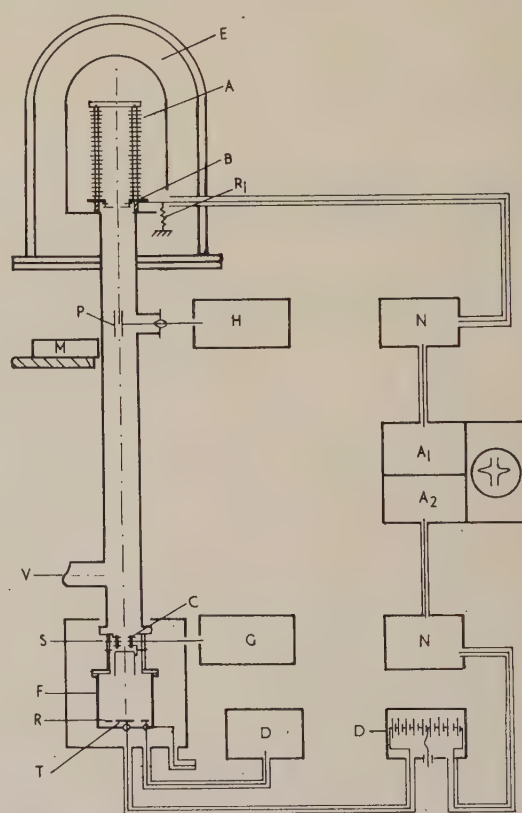


Fig. 1.—Accelerator tube, electrostatic generator and measuring apparatus

A , accelerator tube; A_1 and A_2 oscilloscope amplifiers; B , insulated baffle-plates; C , collimating aperture; D , battery boxes; E , electrostatic generator; F , Faraday chamber; G , electron trap supply voltage, 0 to -2 kV; H , deflector plate supply 0–10 kV; M , permanent magnet; N , pre-amplifiers; P , electrostatic deflector plates; R , ring collector electrode; R_1 , baffle-plate current monitoring resistance, 10 k Ω ; S , electron trap electrode; T , target electrode

Mass analysis of the particles emerging from the aperture in the base of the accelerator tube revealed electrons, negative ions of mass number 1 and to a much less extent 12, and energetic neutral particles when the generator gave a negative potential. Positive ions of mass numbers 1, 2 and 12, and

energetic neutrals were detected when running with a positive polarity.⁽²⁾ Further it was found that both beams are virtually mono-energetic, the charged particles possessing the energy which could be acquired by falling through the total potential applied to the tube.

The magnitude of the primary negative beam currents, i.e. those due to the negative ion and electron components, were determined by paralleling all the electrodes in the Faraday chamber to the insulated Faraday chamber, F and measuring the total current with and without magnetic deflexion. The pulses of current were amplified and displayed on a cathode ray oscilloscope. It was found that the amplitudes of these pulses were not uniform; however, by recording simultaneously the pulses of current flowing to the insulated baffle plate B , at the base of the accelerator tube, it was possible to normalize the pulse heights with respect to the baffle-plate pulses since a strictly linear relationship existed between the two pulses. Thus all currents measured were referred to an arbitrary pulse of $100 \mu\text{A}$ amplitude in the baffle-plate circuit.

The entry into the chamber of secondary electrons produced by collisions of the primary beam with the edges of the collimating aperture, C ($\frac{3}{4}$ in. diameter), was prevented by the inclusion of the electron trap electrode, S , biased at -2 kV .

The negative ion component, I_p^- , was found to be

$$I_p^- = -0.96 \pm 0.05 \times 10^{-8} \text{ A} \quad (1)$$

and the electron component, I_p^e , was

$$I_p^e = -24.5 \pm 1.1 \times 10^{-8} \text{ A} \quad (2)$$

By means of electrostatic and magnetic deflexion, the negative beam could be split so that (1) only neutral particles (electrostatic deflexion), (2) neutral particles and heavy negative ions (weak magnetic deflexion), or (3) the whole negative beam continued undeflected on to the target, T . The current flowing in the target circuit was measured for bias voltages on the target of $+360$ to -360 V with respect to the earthy Faraday chamber, F . Again the heights of the pulses observed were normalized with respect to a $100 \mu\text{A}$ pulse to the accelerator tube baffle-plate.

Fig. 2 shows the results obtained for these measurements from which the following tentative deductions may be made.

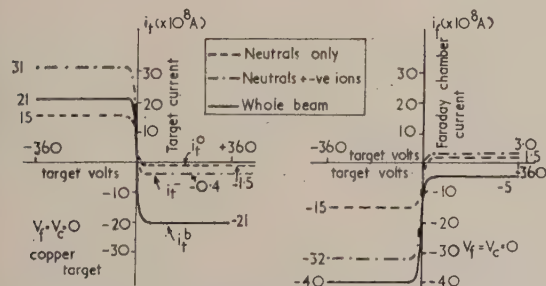


Fig. 2. Variation of target and Faraday chamber currents with target voltage

With the target positive and the neutral beam incident on it, the current $i_t^o = -1.5 \times 10^{-8} \text{ A}$, (a negative current will indicate the collection of negative charge by an electrode). This current could be due to charge stripping of the incident neutrals releasing positive ions from the target, or to the collection of secondary electrons produced by high-speed, reflected neutrals striking the Faraday chamber. In the

former case the neutral beam releases I_o^+ positive ions where

$$I_o^+ = 1.5 \times 10^{-8} \text{ A} \quad (3)$$

With the target negative and with the neutral beam the target current is $15.0 \times 10^{-8} \text{ A}$. Whence the current of electrons, I_o^e (and possibly negative ions) emitted by the neutral beam is given by

$$I_o^e = 15 \times 10^{-8} \text{ A} \quad (4)$$

With magnetic deflexion, neutrals and negative ions strike the target and when this is positive the measured current $i_t^n = -4.0 \times 10^{-8} \text{ A}$. This current is assumed, for the moment, to consist of three components, the incident negative ions, I_p^- together with the secondary positive ions emitted by the neutrals, I_o^+ and the negative ions I_{\pm}^- therefore

$$i_t^n = I_p^- + I_o^+ + I_{\pm}^-$$

Using equations (1) and (3), it follows that the number of positive ions released by the negative ions is given by

$$I_{\pm}^+ = -1.54 \times 10^{-8} \text{ A} \quad (5)$$

As before this is likely to be in error since the secondary electrons ejected from the chamber walls by reflected high-speed neutrals and negative ions have been ignored. However a first estimate of A' may be made

$$A' = \frac{\text{Number of positive ions released}}{\text{Number of incident negative ions}} = I_{\pm}^+/I_p^- = 1.54/0.96 = 1.6 \quad (6)$$

With the target negative the target current $i_t^n = 31 \times 10^{-8} \text{ A}$. Since this current also has three components, the primary negative ion current, I_p^- , and the secondary electron current released by neutrals, I_o^e and negative ions I_{\pm}^- , it is possible to determine I_{\pm}^- , the number of electrons released by the negative ion beam

$$I_{\pm}^- = 17 \times 10^{-8} \text{ A} \quad (7)$$

Small errors may arise if fast reflected particles make multiple collisions within the chamber.

For the undeflected beam of electrons, negative ions and neutrals the measured current $i_t^b = 21 \times 10^{-8} \text{ A}$ (when the target is negative). This has five components, the primary electron and negative ion currents, I_p^e and I_p^- , together with the secondary electron currents due to electrons I_o^e , neutrals I_o^+ and negative ions I_{\pm}^- . Whence, using equations (1), (2), (4) and (7), the secondary electron current due to electrons is given by

$$I_o^e = 14.5 \times 10^{-8} \text{ A} \quad (8)$$

Thus the secondary emission coefficient, δ_e for 250 keV electrons is found to be

$$\delta_e = I_o^e/I_p^e = 14.5/24.5 = 0.59 \quad (9)$$

However, no great reliance can be placed on this value for reasons given below.

With the target positively biased to prevent the escape of secondary electrons and with electrons, negative ions and neutrals striking the target, the target current, $i_t^b = -21 \times 10^{-8} \text{ A}$. Assuming only the emission of positive ions, this current is due to the negative beam current, $I_p^- + I_p^e$, plus the secondary positive ion currents due to electrons, I_{\pm}^+ , neutrals I_o^+ and negative ions I_{\pm}^+ . Using equations (1), (2), (3) and (5), the current of positive ions emitted by electrons I_{\pm}^+ is found to be

$$I_{\pm}^+ = +7.5 \times 10^{-8} \text{ A} \quad (10)$$

The current for these positive ions, however, is of the wrong sign, since the emission of positive ions should give a negative current to the target. The explanation of this result is that about one third of the incoming electrons are reflected as high-speed electrons which are not held at the target by the bias voltage. The magnitude of the current of reflected electrons plus the tertiary electrons emitted from the chamber walls is many times greater than the current of secondary positive ions produced by the primary electrons, and in consequence the positive ion current I_e^+ is completely masked.

It is the presence of these high-speed reflected electrons which make the value of δ_e given in equation (9) unreliable. For the same reason many of the published values of the secondary emission coefficient of high-speed electrons are of dubious validity.

It is clear that the measurement of A' by this technique is liable also to be in error if tertiary electrons are emitted from the chamber walls by high-speed reflected neutrals and negative ions. In an attempt to overcome this defect a ring collector electrode, R , was placed around the target electrode but slightly below the plane of the target. By biasing the target 48 V positive to prevent the escape of low-speed secondary electrons, the collector negatively, and earthing the Faraday chamber, it was hoped that the collector would collect only the positive ions emitted by the target.

Fig. 3 shows the variation of collector current with collector bias voltage when the target was irradiated with the

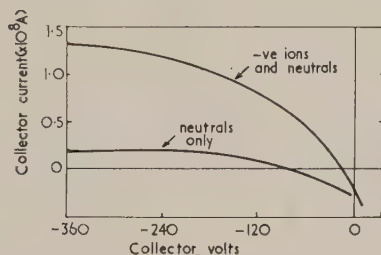


Fig. 3. Variation of collector current with collector bias for neutral and neutral plus negative ion beam

neutral and neutral plus negative ion beams. Assuming a limiting value of 0.2×10^{-8} A and 1.3×10^{-8} A for the collector current in each case, the value of the positive ion current emitted by the neutrals, I_e^+ becomes 0.2×10^{-8} A and by the negative ions, I_e^+ , 1.1×10^{-8} A. This gives a revised value for A' .

$$A' = I_e^+/I_p^- = 1.1/0.96 = 1.15 \quad (6a)$$

In another experiment a grid was mounted on the outer collector electrode shown in Fig. 1, and biased negatively with respect to the Faraday chamber, thus suppressing the emission of tertiary electrons from the chamber.

Table 1. Target currents for gridded chamber

Electrode potentials			Target current ($\times 10^{-8}$ A)		
V_t	V_f	V_g	Electrons, -ve ions and neutrals	-ve ions and neutrals	Neutrals only
-312	+120	0	22.4	30.9	14.4
+312	+120	0	-19.9	-2.17	-0.14

Table 1 gives the results obtained for the target current when biased positively and negatively and irradiated with the three types of beam. Analysing these results in the manner

described above, a new value of the secondary emission coefficient A' is obtained

$$A' = 1.07/0.96 = 1.1 \quad (6b)$$

The assumption has been made that the reflexion coefficient for high-speed negative ions is negligible. Should this not be the case this value of A' would be an underestimate.

By assuming that a fraction δ_e^r of the incident electrons are reflected (or inelastically scattered) whilst retaining sufficient energy to escape from the target ($E > 312$ eV) it is possible to calculate both the true secondary emission coefficient δ_e and the "reflexion" coefficient δ_e^r .

The following values are obtained for the 250 keV electrons here considered

$$\delta_e = 0.37 \quad (11)$$

$$\delta_e^r = 0.28 \quad (12)$$

The polarity of the generator was reversed and the voltage across the accelerator tube raised until pulsing occurred. The pulse threshold voltage was 230 kV, i.e. not significantly different from that on negative polarity.

By connecting together all the electrodes to the Faraday cage, the total positive ion beam current was determined as before for a 100 μ A pulse to the baffle-plate.

$$I_p^+ = 2.01 \pm 0.04 \times 10^{-8} \text{ A} \quad (13)$$

With the grid biased negative with respect to the Faraday chamber and with positive or negative potentials of 312 V on the target, the values of the target current were determined, both with and without electrostatic deflexion. The results are given in Table 2.

Table 2. Target currents for gridded chamber, positive beam

Electrode voltages (V)			Target current ($\times 10^{-8}$ A)	
V_t	V_f	V_g	Positive ions and neutrals	Neutrals only
+312	0	-120	2.2	0
-312	0	-120	33.0	7.0

It is seen that with neutrals incident on a negative target, the current I_e^+ of secondary electrons and negative ions is given by

$$I_e^+ = 7.0 \times 10^{-8} \text{ A} \quad (14)$$

The intensity of the neutral beam accompanying the positive ion beam is seen to be less than that with the negative beam. A possible explanation of this is that the source of these neutrals is the charge-exchange process for which the cross-section is greater for negative than for positive ions.⁽³⁾

The current of secondary negative particles emitted by the positive ions I_{+}^b is found to be

$$I_{+}^b = 33.0 - 7.0 - 2.01 = 24 \times 10^{-8} \text{ A} \quad (15)$$

Assuming that the negative ion to electron ratio is the same as that in the negative beam, i.e. $0.96/24.5$, the current of secondary negative ions I_{+}^- is given by

$$I_{+}^- = 24 \times (0.96/24.5) = 0.94 \times 10^{-8} \text{ A} \quad (16)$$

Whence the ratio of secondary negative ions to incident positive ions, B' can be determined from equations (15) and (16).

$$B' = I_{+}^-/I_p^+ = 0.94/2.07 = 0.47 \quad (17)$$

and the ratio of secondary electrons to incident positive ions, B is given by

$$B = (24 - 0.94)/(2.01) = 11.5 \quad (18)$$

The assumption has been made in deriving equations (16) to (18) that the negative ion to electron ratio equals that in the negative beam. To verify this assumption it was decided to magnetically analyse the secondary particles ejected by the positive beam and measure the electrons and negative ion secondaries separately.

Fig. 4 shows the apparatus devised to perform this separation. Since it had been found that the secondary particles

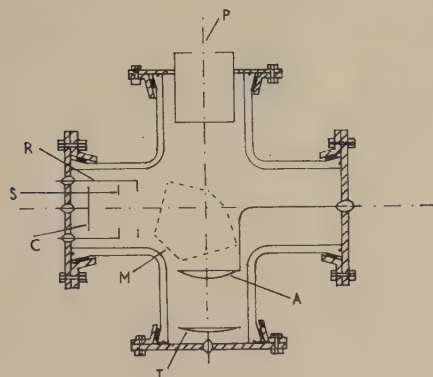


Fig. 4. Magnetic analysis chamber

A, accelerator electrode, 0.875 in. diam. aperture, ± 360 V; C, collector electrode connected to pre-amplifier, 0V; M, magnet pole-piece, 10–390 gauss; P, primary beam enters here; R, collimator or shield electrode; S, electron trap electrode, -120 V; T, target, ± 120 V

produced at the target had energies less than 50 eV, they were accelerated through a potential of 500 V so that their mean spread in energy was less than 5%. The target and accelerator electrodes had the form of a Pierce gun⁽⁴⁾ with the incident primaries entering through an aperture, 0.875 in. diameter in the accelerator electrode. Targets of copper, aluminium and mild steel were spun to give a radius of curvature of 14 cm. The copper accelerator electrode had a radius of curvature of 7 cm and was mounted 7 cm vertically above the target.

The secondary particles from the target were focused into a beam by the accelerator and bent through 90° by means of an electromagnet into a divergent beam of 0.5 in. diameter at the collector electrode. In front of the collector were mounted a secondary electron suppressor and a collimating electrode. An electrostatic screen surrounded the collector electrode assembly consisting of the Aquadag coating on the inner surface of the glass vessel together with an aluminium spinning surrounding the outside of the assembly. Partial magnetic screening of the region between the accelerator and the target was obtained by surrounding the lower arm of the vessel with a soft iron box.

Fig. 5 shows the variation of collector current with electromagnet current when the target was bombarded by the positive beam. Definite identification of the negative ions of hydrogen was confirmed.

Table 3 gives the results of the measurements with the positive beam. It is seen that the assumption that the

negative ion to electron ratio for the secondary particles is indeed about 1 : 25. However the magnitude of the secondary electron current from the copper target is considerably smaller than that obtained with the gridded Faraday chamber

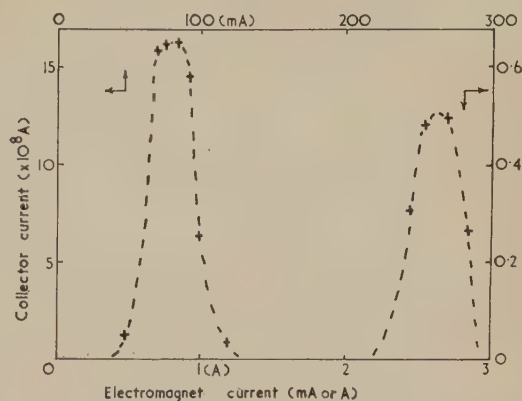


Fig. 5. Variation of collector current with electromagnet current

measurement. If it is assumed that this is due to the partial interception by the accelerator electrode of both the primary and secondary beams it is possible to correct for this reduction when determining the secondary emission coefficient B' .

When measurements were made with the negative beam a complication arose because it was found that the magnetic field necessary to turn the secondary positive ions round onto the collector was of the right sign and magnitude to bend the primary (250 keV) electrons also into the collector region. In consequence it was necessary to sweep out the electrons from the negative beam by applying at all times a weak magnetic field at M, Fig. 1. It was not possible therefore to measure the number of positive ions ejected by electrons.

Table 4 gives the results of the measurements with the negative ion and neutral beams. By applying the same correction factor as that used in the positive beam measurement it is possible to deduce the secondary emission coefficient A' for copper, aluminium and steel.

Table 5 summarizes the values of the coefficients A' , B' and the product $A'B'$ obtained using the three experimental arrangements. The standard deviations quoted make no allowance for systematic errors.

It should be noted that the values of A' and B' derived from the plain and gridded Faraday chamber measurements are strictly the ratio of the number of positive and negative ions of all kinds emitted by the mixture of negative and positive ions found in the beams respectively, whereas the values obtained with the magnetic analysis technique refer to the numbers of H^+ and H^- ions emitted by the mixture of negative and positive ions respectively. The difference between these two types of measurements is expected to be small, however, since as has been observed by other workers^(2, 5) it is the hydrogen ions which are by far the most abundant.

Table 3. Magnetic analysis of secondaries produced by the positive beam on copper, aluminium and steel targets

Target material	Copper		Aluminium		Steel	
	Electromagnet current		Electromagnet current		Electromagnet current	
Collector current ($\times 10^8$ A)	70 mA	2.8 A	70 mA	2.8 A	70 mA	2.8 A
Positive ions + neutrals	-15.7	0.53 ₅	-12.1	-0.29	-16.8	-0.52
Neutrals only	-3.0 ₅	-0.06	-4.8	-0.02	-4.9	-0.04

Table 4. *Magnetic analysis of positive H ions produced by negative ions and neutrals on copper, aluminium and steel targets*

Target material	Copper	Aluminium	Steel
Magnet current (A)	2.8	2.8	2.8
-ve ions and neutrals ($\times 10^8$ A)	+0.75	+0.79	+0.41
Neutrals only ($\times 10^8$ A)	+0.20	+0.22	+0.12

Table 5. *Summary of the values obtained for the secondary emission coefficient A' and B' and the product $A'B'$ together with the standard deviations*

Material	Copper		Aluminium		Steel
Method of measurement	Plain Faraday chamber	Gridded Faraday chamber	Magnetic analysis		
A'	1.15 ± 0.08	1.1 ± 0.11	1.02 $\pm 0.08_5$	1.05 ± 0.09	0.54 ± 0.05
B'		0.46 ± 0.04	0.43 ± 0.03	0.24 ± 0.03	0.44 ± 0.04
$A' B'$		0.51 ± 0.08	0.44 ± 0.06	0.25 ± 0.04	0.24 ± 0.03

Discussion

The values of A' and B' given in Table 5 appear just insufficient to prove the hypothesis that pulse conduction is due to the regenerative exchange of positive and negative ions of hydrogen. However, it is significant that the product $A'B'$ approaches unity more nearly than does the product AB as defined by van Atta and his co-workers.⁽⁶⁾

A number of reasons can be offered to substantiate the hypothesis despite the fact that $A'B' < 1$.

The current of negative ions emitted by the combined action of the neutrals and positive ions is 0.95×10^{-8} A (revised figure from Table 3) which should be compared with the total negative ion beam current of 0.96×10^{-8} A (equation 1). Clearly the combined action of the positive ions and neutrals is just sufficient to maintain the required number of negative ions. However, the negative ions and neutrals only release 1.33×10^{-8} A positive ions (revised figure from Table 4) instead of 2.01×10^{-8} A (equation 13) and the discrepancy between $A'B'$ and unity is probably due to an error in this measurement. Thus, from the total beam current measurements, it is to be expected that a current of 0.96×10^{-8} A of negative ions and their associated neutrals should release a current of 2.01×10^{-8} A of positive ions.

Possible sources of error are:

(1) Some of the negative ions, on their way to the target, undergo charge exchange reactions resulting in a loss in the number of high-speed particles arriving at the target. Assuming a charge exchange cross-section of 10^{-16} cm²⁽³⁾ for 250 keV H^- in H_2 , a pressure of 2×10^{-5} mm Hg and a path length of 2 m, 1.5% of the negative ions undergo charge exchange. A few of the high-speed neutrals formed will be deflected sufficiently to prevent them reaching the target.

(2) In addition to this loss it is possible that those high-speed neutrals which do reach the target may not be so effective in producing positive ions as the negative ions from which they originated. No data is available to correct for this effect.

(3) Finally, it is also possible that the A' coefficient is sensitive to the field existing at the target surface. Harris⁽²⁾ has reported an interesting effect on the accelerator tube used. He found that shorting out sections of the accelerator

tube starting from the anode end increased the threshold voltage for pulse conduction, whereas shorting from the cathode end had little effect. (It should be noticed that in both cases a higher mean field across the tube was maintained.) The important parameters were apparently the total voltage and the field at the anode electrode since the effect of shorting out the tube in the vicinity of anode was to reduce the field at the anode.

Effects due to (1) and (2) are unlikely to introduce an error in A' exceeding a few per cent and therefore it is postulated that the A' coefficient is field sensitive.

It is impossible to compare the values obtained for A' and B' with other published work because no measurements under identical conditions have been reported. With a copper target bombarded by 300 keV protons, Mitropan⁽⁷⁾ has found no emission of negative ions immediately after heat treatment of the target at 900° K. A value of 5×10^{-4} was, however, obtained for B' some 90 minutes later. He stated that the dependence of B' upon time may be related to the formation of a surface layer of atoms adsorbed onto the target. Such a layer could be due to adsorption from the surrounding gas medium or diffusion of gas from the body of the target. The vacuum conditions pertaining in his apparatus differ considerably from those used in this investigation, i.e. metal parts were baked at high temperatures and the vacuum pressure was less than 10^{-8} mm Hg. In consequence the conditions at the surfaces of the targets are unlikely to be the same. Since it is clear that the source of the negative ions must lie in the surface layer no direct comparison of results is possible although it is probable that the thicker layers of contamination upon the surfaces used in this investigation will give rise to higher values of B' .

Theoretical estimate of A' and B' . In view of the lack of supporting experimental evidence it is desirable to justify theoretically the high values obtained for A' and B' . To do this it is necessary to consider the state of the metal electrode surfaces in the vacuum system.

For a continuously-pumped vacuum system the metal surface will be covered with a layer of adsorbed gas or vapour molecules.

For the vacuum system used the pump oil vapour pressure at room temperature should be about 10^{-7} mm Hg.⁽⁸⁾ But Blears⁽⁹⁾ has shown that partial pressures of up to 10^{-5} mm Hg of various hydrocarbons persist for at least 25 minutes after pumping down a metal vacuum system.

Ennos⁽¹⁰⁾ has calculated that the maximum possible rate of growth of a hydrocarbon layer is as much as 60 Å/s for unbaked metal systems, this assumes unity density for the layer. The use of a liquid nitrogen trap will greatly reduce the rate of formation. However, oil vapour from the two pumps will diffuse into the high-vacuum region when the liquid nitrogen in the trap is exhausted and this oil will be pumped back out of the surface only slowly when the cold trap is refilled. In consequence a monolayer of contamination is likely to reform on a metal surface in a matter of seconds or minutes.

Furthermore, once exposed to a high field these contaminating layers will be bombarded by high energy particles. Ennos⁽¹⁰⁾ has shown that bombardment by electrons with energies of a few thousand electron volts led to the growth of a contaminating layer to thicknesses exceeding 1000 Å. The actual contamination compound formed is extremely resistant to chemical solvents and is most probably a hydrocarbon polymer. Continued irradiation may lead to the carbonization of the underlying polymer compounds with the release of hydrogen. Carbonization is also likely to

occur due to the catalytic reduction of the hydrocarbon at the metal interface.⁽¹¹⁾

The picture of the metal surface that emerges from these considerations is therefore of a monolayer of freshly condensed oil vapour upon a hydrocarbon polymer of the order of 100 Å thickness. Under irradiation the oil vapour is polymerized and the hydrocarbon layer grows in thickness. Equilibrium under these conditions is obtained when the rate of conversion of oil vapour molecules to the polymerized state equals the rate of supply of fresh molecules.

An explanation of the large magnitude of the coefficients A' and B' is now possible. The density of the hydrocarbon assumed to be $(\text{CH}_2)_n$ will be approximately 1, so that the number of hydrogen atoms per cubic centimetre will be

$$\frac{6 \times 10^{23}}{14} \times 2$$

which is equivalent to

4.3×10^{22} hydrogen molecules per cubic centimetre.

The ionization cross-section for 250 keV protons in $(\text{CH}_2)_n$ is not known but is likely to be of the order of that in hydrogen. Taking the value obtained by Keene,⁽¹²⁾ 0.16 cm^2 for the ionization cross-section in hydrogen, the number of primary ionizing collisions per proton in a layer of 100 Å thickness is 4.3. Some of the "knock-on" protons formed may also have sufficient energy to cause further ionization as can be inferred from the results of Lorentz and Zimmerman⁽¹³⁾ on the range of protons in polythene. For 250 keV protons, the rate of energy loss is 0.75 keV $\mu\text{g}/\text{cm}^2$. A 100 Å layer of $(\text{CH}_2)_n$ would therefore involve the loss of 0.75 keV. Assuming the absorption of 35 eV per ion pair created, such a loss would yield 21 ion pairs. It is not surprising, therefore, that the number of secondary electrons released per 250 keV proton should equal 11.5.

It is difficult to estimate the number of negative ions that will be released. Most of the work that has been published on negative ion formation by protons refers to the charge-exchange process in which fast negative ions are produced. It is possible that small numbers of these will be reflected back through the layer by collisions; however, the negative ions of interest here had energies of less than 50 eV.

The radiative capture cross-section of electrons by hydrogen atoms has been calculated⁽¹⁴⁾ to be $3 \times 10^{-22} \text{ cm}^2$ so that only an insignificant number of H^- ions can be created in the hydrocarbon layer by direct attachment of electrons to the atomic hydrogen present.

Similarly Schulz⁽¹⁵⁾ has shown that the cross-section for H^- ion formation by electrons in molecular hydrogen is less than $3.5 \times 10^{-20} \text{ cm}^2$ for electron energies up to 20 eV.

No quantitative measurements have been made on H^- formation in polymerized hydrocarbons although Bailey and his co-workers⁽¹⁶⁾ have observed H^- ions produced by electron bombardment of gaseous CH_4 and C_2H_6 .

The great density of hydrogen in the layer does, however, make probable three-body collisions for which considerably high cross-sections might be expected if resonance energy transfer is involved.

It is seen that due to the lack of experimental evidence it is not possible to prove either that sufficient negative ions will be produced in the layer or that a sufficient number will be able to escape from the layer.

On the reverse polarity it is to be expected that the negative ions will be equally effective as the protons in producing ionization but the escape of the larger H^+ ions created will be more difficult than for the electrons. It does not seem

unreasonable to suppose that about one in ten of those formed escape ($A' = 2$) or that the field in the layer will be of importance in determining the number that do escape.

It is seen from the foregoing arguments that the values of A' and B' can be plausibly explained on the basis of collisions within a contaminating layer alone. It is pertinent, therefore, to question whether the underlying metal will play any significant role in determining the value of A' or B' .

The experiments of Ennos suggest that the base metal is of little importance in determining the thickness of the layer built up. The results of Arnal do in fact show little dependence of V_{th} upon the metal used as electrodes once steady pulsing is established, thus with a 3 mm gap he obtained $V_{th} \approx 60 \text{ kV}$ for copper, tantalum and magnesium and $V_{th} \approx 55 \text{ kV}$ for stainless steel. In the experiments with tantalum, magnesium and stainless steel it appeared to be necessary for a spark to occur before steady pulsing would occur. This could possibly be due to the necessity of puncturing an oxide layer before the normal growth of the contaminating layer could ensue.

Electrostatic charging of the contaminating layer. The contaminating layer will affect not only the criterion for pulse discharges but also the growth of such discharges since the layer will be but a poor conductor of electricity. As a result, the surface of the contaminant will hold, albeit only momentarily, a net charge which will modify the local field.

The range of the incident 250 keV particles in the layer is as follows:

(a) electrons $60 \text{ mgm}/\text{cm}^2 \sim 0.06 \text{ cm}$,⁽¹⁷⁾ and

(b) protons (and negative hydrogen ions) $0.5 \text{ cm air} \sim 0.005 \text{ cm}$,⁽¹⁸⁾ assuming a $(\text{CH}_2)_n$ composition with unity density. It follows therefore that most of the charge incident on the layer is buried in the metal base. However, most of the charge escaping is drawn from the layer which is left with a net charge opposite to that on the underlying metal (see Fig. 6).

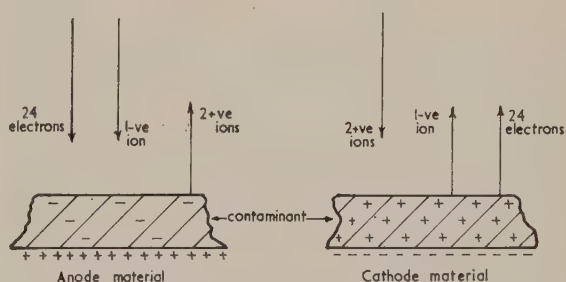


Fig. 6. The charging effects in the contaminating layer

For the accelerator tube used the surface area of the end plates is $3.14 \times (10/2)^2 \text{ cm}^2$, the peak current leaving the anode and cathode are 8 and $100 \mu\text{A}$ respectively and the pulse lasts for approximately 5 ms. The average net area charge density left in the layers are up to 5.1×10^{-10} and $6.4 \times 10^{-9} \text{ C}/\text{cm}^2$ at anode and cathode electrodes respectively. These charge densities could result in electric fields of up to 2.9×10^3 and $3.5 \times 10^4 \text{ V}/\text{cm}$. (A dielectric constant of 2 has been assumed for the hydrocarbon layer.) The applied field is $4.3 \times 10^3 \text{ V}/\text{cm}$ at both electrodes and it is seen that whereas the field at the cathode is determined mainly by the space charge that at the anode is still sensitive to the applied field.

Similar results can be deduced from the measurements of Arnal when his pulse discharge was not quenched by the fall in the applied voltage. Thus, with a low-impedance

voltage source, pulses of $50 \mu\text{A}$ amplitude lasting for 0.1 s were observed with a 3 mm gap and a threshold voltage of 60 kV . The cathode layer field in this case could rise to $4 \times 10^6 \text{ V/cm}$ as compared with the applied field of $2 \times 10^5 \text{ V/cm}$.

Space charge fields of these magnitudes will profoundly affect the exchange process, forcing the discharge to spread outwards from the initiatory region and leading to the observed diffuse discharge with an approximately uniform current density (i.e. that current that gives a specific space charge density on the contaminating layer).

Of course these fields will not persist and the charge created in the layer will leak away to the metal at a rate governed by the conductivity of the layer. Once the charge has leaked away the stage will be set for further discharges.

Conclusions

In view of the justification of the experimentally determined coefficients A' and B' it is proposed that a regenerative exchange of positive and negative ions of hydrogen is indeed the cause of pulse conduction, the electrons playing only a minor role. It is seen that the source of these ions is a contaminating layer of hydrocarbon and further that the charge built up on this layer leads naturally to the transient nature of the discharge and to the diffuse discharge column with its uniform current density.

Insufficient experimental evidence is available to predict the variation of A' and B' with applied voltage. If, however, it is established that A' is proportional to the product of the energy of the incident ions and the anode field intensity to the first order of approximation, and further that B' is proportional to the energy of the positive ions alone, it will follow that the product $A'B'$ is proportional to (V^3/d) for uniform field gaps of separation d . With these assumptions, the discharge criterion $A'B' = 1$ leads to the experimentally determined law (Arnal⁽⁵⁾) that $V_{th} \propto d^{1/3}$ ($40 \text{ kV} < V_{th} < 100 \text{ kV}$). However the results of Lorentz⁽¹³⁾ would suggest that although the rate of energy loss of protons, dE/dx , is an increasing function of E up to 150 keV , thereafter it decreases, so that less ionization occurs in the layer than for lower energies. To attain the criterion $A'B' = 1$ at voltages exceeding 150 kV the extracting mechanisms might be expected to require enhancement by the application of higher fields at the surfaces than those necessary for lower voltages.

The fact that pulse conduction ceases when the electrodes are heated to 200°C ⁽¹⁹⁾ is directly attributable to the removal of the layer of contamination at these temperatures. Ennos also reports that contaminating layers will not grow on electrodes at temperatures above 200°C .

The conditioning effects observed are probably due to the changes in nature of the contaminating layer. Thus, initially, the surfaces will be contaminated with a layer of oil vapour several molecules thick which under bombardment has both its thickness reduced by a type of sputtering action and its composition changed by radiation-induced polymerization and carbonization. The increase in voltage necessary to sustain pulse conduction as the surface "conditions" is then due to this decrease in thickness of the layer and to the reduction in hydrogen concentration in the layer as a result of the carbonization.

The "fully-conditioned" state represents an equilibrium state for which the growth of the outer surface by the radiation-induced bonding of incident oil-vapour molecules just counter balances the effect of the radiation-induced carbonization of the inner surface. Super-conditioning occurs when the rate of growth of the outer surface is limited by the

rate of arrival of fresh molecules whilst the carbonization process meets no such limitation. Under these conditions a higher voltage will be necessary to maintain pulse conduction. However, provided that the bombardment of the surface is reduced (i.e. the voltage lowered), the surface of the system will revert to the equilibrium condition with a time constant governed by the rate of arrival of fresh oil vapour molecules on the surface.

The hydrogen released as a result of carbonization and sputtering of the contaminating layer will give the observed pressure rise consequent upon pulse conduction.

As suggested in the earlier report⁽¹⁾ the effect of gas pressure upon the threshold potential is due to the scattering of the positive and negative ions of hydrogen by the gas molecules in the tube. Due to the much smaller cross-section for electrons no such effect would occur if the electrons were of primary importance.

Consequences of pulse conduction. The deleterious effects of pulse conduction upon the performance of accelerator tubes and electron microscopes has already been commented upon.⁽¹⁾ All continuously-pumped high-voltage apparatus is liable likewise to exhibit pulse conduction. Even in sealed-off systems pulse conduction can occur if sufficient contaminating material is left within the system.

The possibility of pulse conduction leading to vacuum breakdown should also be commented upon. If the pulse rate is sufficiently great the pressure rise in the system may be such that a normal low pressure discharge may be struck. Similarly if the build up of the contamination is allowed to continue indefinitely, ultimately the electrostatic forces in the layer (possibly in the form of whiskers) will be sufficient to detach a portion of it giving rise to vacuum breakdown via the "clump mechanism".⁽²⁰⁾

Both eventualities are minimized when first commissioning high-voltage equipment by adopting the "conditioning technique" whereby the voltage is raised slowly in steps.

Suppression of pulse conduction. Pulse conduction can be suppressed by preventing hydrocarbon contamination of the electrodes. In sealed-off systems this can be achieved by baking the system at temperatures in excess of 200°C for a few hours before sealing-off.

The problem is not so simple with continuously-pumped systems. Ennos has shown that the major contribution towards contamination in a typical demountable vacuum system comes from the pump oil vapour, the vacuum grease and certain types of rubber employed as gaskets. In addition metal, unless cleaned (by the chemical removal of a layer of the surface), can provide hydrocarbon contamination.

To prevent recontamination it is necessary firstly to provide a cold trap which is perpetually maintained at a low temperature to exclude backing-pump and diffusion-pump oil from the high-voltage region and secondly to eliminate all high-vacuum grease and rubber gaskets except those of black neoprene type.

A possible alternative in some cases is to run at an elevated temperature ($\sim 200^\circ \text{C}$) those parts of the systems likely to give rise to pulse conduction.

If it proves impossible to prevent the contamination of the surfaces a final remedy is to use transverse magnetic or reversed electrostatic fields at the cathode and anode electrodes thus preventing the charged ions from leaving the electrodes from which they originate. For accelerator tubes this remedy has limitations since it makes the extraction and focusing of the ion beam very difficult. However, improvement in performance is obtained if it is used at one end of the tube only.

References

- (1) MANSFIELD, W. K., and FORTESCUE, R. L. *Brit. J. Appl. Phys.*, **8**, p. 73 (1957).
- (2) HARRIS, D. J. Ph.D. Thesis, University of London (1953).
- (3) ALLISON, S. K. *Rev. Mod. Phys.*, **30**, p. 1137 (1958).
- (4) PIERCE, J. R. *Theory and Design of Electron Beams* (New York: D. van Nostrand, 1949.)
- (5) ARNAL, R. D.ès Sci. Thesis, Paris (1955).
- (6) VAN ATTA, L. C., NORTHROP, D. L., and VAN DE GRAAFF, R. J. *Phys. Rev.*, **49**, p. 761 (1936).
- (7) MITROPAN, I. M., and GUMENIUK, V. S. *Sov. Phys. J.E.T.P.*, **5**, p.157 (1957).
- (8) ELLIS, S. E. Paper read to Amer.E.M.Soc., Washington (1951).
- (9) BLEARS, J. *J. Sci. Instrum., Supplement No. 1. Vacuum Physics*, p. 36 (1951).
- (10) ENNOS, A. E. *Brit. J. Appl. Phys.*, **4**, p. 101 (1953).
- (11) ASHMORE, P. G., WRIGHT, P. G., KEMBALL, C. *Proc. 2nd Int. Cong. on Surface Activity*, **2**, p. 317 (London: Academic Press, 1957).
- (12) KEENE, J. P. *Phil. Mag.*, **40**, p. 369 (1949).
- (13) LORENTZ, D. C., and ZIMMERMAN, E. J. *Phys. Rev.*, **113**, p. 1199 (1959).
- (14) MASSEY, H. S. W. *Negative Ions*, 2nd ed. (London: Cambridge University Press, 1950).
- (15) SCHULZ, G. J. *Phys. Rev.*, **113**, p. 816 (1959).
- (16) BAILEY, T. L., MCGUIRE, J. M., and MUSCHLITZ, E. E. *J. Chem. Phys.*, **22**, p. 2088 (1954).
- (17) GLENDENIN, L. E. *Nucleonics*, **2**, p. 12 (1948).
- (18) BETHE, H. A., and LONGMUIRE, C. *Phys. Rev.*, **75**, p. 306 (1949).
- (19) STEVENSON, D. G. Ph.D. Thesis, University of London (1954).
- (20) CRANBERG, L. *J. Appl. Phys.*, **23**, p. 518 (1952).

Use of an electrical analogue for the solution of a variety of torsion problems*

by S. C. REDSHAW, D.Sc., Ph.D., Department of Civil Engineering, University of Birmingham

[Paper first received 23 May, and in final form 23 June, 1960]

Abstract

A brief review of Saint-Venant torsion theory is given and the advantages and disadvantages of the various forms in which the equations can be expressed are discussed in relation to electrical analogue computation. It is shown how, by the use of a simple passive resistance network, solutions can easily be obtained both for simply connected regions as well as for the analytically difficult problem of multiply connected regions. Examples of the application of the electrical-analogue method to the problems of plastic torsion, the torsion of compound bars, thick hollow sections and thin-walled sections filled with a dissimilar material, are given.

Introduction

THE use of electrical analogies for the solution of sundry partial differential field equations occurring in mathematical physics, is now reasonably well known. Briefly, the analogy is made between the flow of electricity in a conducting medium and the flow of a gas, for example, or the lines defining a stress function or some other characteristic of the physical system. Once the analogy is accepted, either an analogue involving the use of a continuous conducting sheet, whether solid or fluid, or a network analyser can be used. In the first case, a direct analogy to the differential equation in question is provided, whereas a network analyser can only provide an analogy to the required equation when expressed in finite difference form; in consequence, the truncation errors introduced by the approximate finite-

difference equations usually have to be reduced by the use of a fine network mesh. In this respect, the network analyser is the experimental counterpart of the relaxation technique.

Although the torsion problem may be solved by either the conducting sheet or network techniques, the boundary conditions, and often the required conditions within the region, are such that for an accurate solution the conducting sheet analogy is at a disadvantage. The use of an electrical potential analyser of the network type for the solution of elastic torsion problems concerning simply connected isotropic regions has been described by Redshaw⁽¹⁾ and subsequently Palmer⁽²⁾ has reported the results of a refinement of the method to the analysis of several hundred sections. It is the object of the present paper to describe the application of the network method to other torsion problems involving plasticity, composite sections of dissimilar material, thick-walled tubes and other multiply connected regions.

General torsion theory

There are several alternative ways of formulating torsion theory and as it is important, particularly from the point of view of the electrical analogue, to select the most appropriate method for the problem under consideration, the following review of torsion theory is given.

Simply connected regions

Torsion function. The solution of the problem of torsion of prismatical bars of constant cross-section by couples applied at the unrestrained ends was given by Saint-Venant,⁽³⁾ who proposed the semi-inverse method by which he assumed only

* Paper presented at The Institute of Physics Stress Analysis Group Conference, September, 1959.

some of the features of the displacements and of the forces. He then determined the remaining features of those quantities so as to satisfy all the equations of elasticity. Using the notation of Fig. 1 for non-circular shafts, Saint-Venant assumed that warping of the cross-sections would occur

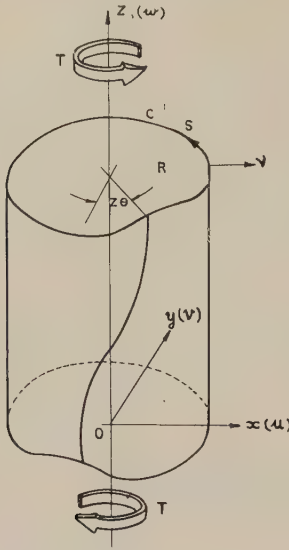


Fig. 1. Notation

and that it would be the same for all cross-sections, so that the displacement w would be independent of z . The analysis led to the result that the warping function ϕ had to satisfy the Laplace equation

$$\frac{\partial^2 \phi}{\partial x^2} + \frac{\partial^2 \phi}{\partial y^2} = 0 \quad (1)$$

in the domain occupied by the material, with the boundary condition

$$\frac{d\phi}{dv} = y \cos(xv) - x \cos(yv). \quad (2)$$

Then the problem of determining the torsion, or warping, function ϕ is a special case of the secondary-boundary value problem of Potential Theory. This problem is of the Neumann type, consisting of the determination of a function which is harmonic in a given region with a prescribed normal derivative on the boundary.

Conjugate function. Since the torsion function ϕ is harmonic in the region of the cross-section, it is possible to construct the analytic function $\phi + i\psi$ where ψ is the conjugate harmonic function related to ϕ by the Cauchy-Riemann equations, thus

$$\frac{\partial \phi}{\partial x} = \frac{\partial \psi}{\partial y}, \quad \frac{\partial \phi}{\partial y} = -\frac{\partial \psi}{\partial x}. \quad (3)$$

If the region R is simply connected, the function ψ will be single-valued.

Framing the problem in terms of the conjugate function leads to the determination of a function ψ that satisfies the Laplace equation

$$\frac{\partial^2 \psi}{\partial x^2} + \frac{\partial^2 \psi}{\partial y^2} = 0 \quad (4)$$

in the region R , and satisfies the boundary condition

$$\psi = \frac{1}{2}(x^2 + y^2). \quad (5)$$

The solution of this problem, well known as the Dirichlet problem, is unique.

Shearing stress function. Again, the torsion problem may be formulated in terms of a function Ψ , which may be defined as

$$\Psi = \psi - \frac{1}{2}(x^2 + y^2). \quad (6)$$

The stress function Ψ satisfies Poisson's equation

$$\frac{\partial^2 \Psi}{\partial x^2} + \frac{\partial^2 \Psi}{\partial y^2} = -2 \quad (7)$$

in the region, and assumes the value

$$\Psi = \text{constant} \quad (8)$$

on the boundary. Finally, if Prandtl's⁽⁴⁾ stress function χ is used, the Poisson equation

$$\frac{\partial^2 \chi}{\partial x^2} + \frac{\partial^2 \chi}{\partial y^2} = -2G\theta \quad (9)$$

is obtained with the boundary condition

$$\chi = \text{constant}. \quad (10)$$

Multiply connected regions

The torsion problem of hollow shafts has been concisely summarized by Sokolnikoff.⁽⁵⁾ If a shaft has several longitudinal cavities the surfaces of which, together with the exterior longitudinal surfaces, are free from loads, then the boundary condition of equation (2) will apply for all longitudinal surfaces. Also, the function ψ conjugate to ϕ , satisfies on each contour the condition

$$\frac{d\psi}{ds} = \frac{d}{ds} \left\{ \frac{1}{2}(x^2 + y^2) \right\}, \quad (11)$$

or

$$\psi = \frac{1}{2}(x^2 + y^2) + k_i. \quad (12)$$

The constants k_i will in general, have different values on the various contours. The function ϕ is determined by the boundary conditions to within an arbitrary constant and, therefore, its conjugate function ψ must also be determined within an arbitrary constant. Thus only one of the arbitrary constants k_i can be assigned freely, the remaining constants must be so determined as to make the function ψ single valued in the region.

For multiply connected regions, the boundary condition imposed on the shearing-stress function Ψ is often more convenient than that imposed on ψ .

Because Ψ is defined by equation (6) and it also satisfies equation (7) in the region occupied by the material, it follows, as a consequence of the definition of Ψ , that on the contours C_i , the function satisfies the conditions

$$\Psi = k_i, \quad (i = 1, 2, \dots, n) \quad (13)$$

where the value of only one of the constants k_i may be assigned arbitrarily. Usually, for convenience, the value of the constant on the outer boundary is chosen such that $k_0 = 0$. At an internal boundary, the value of Ψ is determined by the further requirement that ϕ (the plane harmonic function which is conjugate to ψ) must, since it measures the axial displacement due to twisting, be single valued at every point on the section. Therefore, the integral

$$\oint \frac{\partial \phi}{\partial s} ds = \oint \frac{\partial \psi}{\partial v} dv \quad (14)$$

taken around any one boundary must be zero.*

* The contour integration may be carried out on any closed contour, either within the region or coinciding with the boundary providing the chosen contour encloses that boundary and none other.

It follows from equation (6) that

$$\oint \frac{\partial \Psi}{\partial \nu} ds = -\frac{1}{2} \oint \frac{\partial}{\partial \nu} (x^2 + y^2) ds = -2A \quad (15)$$

by Green's transformation, A denoting the area contained within that boundary. The expression for the twisting moment is

$$T = 2G\theta \left(\iint_R \Psi dx dy + \sum_{i=1}^n k_i A_i \right). \quad (16)$$

The foregoing basic theory covers all cases of elastic torsion. The application of the theory to particular cases will be considered in detail in later sections.

Selection of appropriate electrical analogy

As there are several ways of formulating the torsion problem, the actual function selected for a particular case will depend on the type of electrical analogue available and the information, such as shearing stresses or torsion constant, which is required. The characteristics of the various functions discussed in the previous section have been summarized for simply connected regions in the accompanying table. An examination of the table shows that either a Laplace or a Poisson equation has to be solved, the boundary conditions being such that either a Neumann or a Dirichlet problem is involved. For ease of computing shearing-stress components,

Summary of formulation of torsion problem for simply connected regions

Function	Shearing stress components		Torsional couple	Equation to be solved in domain	Boundary condition
Saint-Venant's torsion function ϕ	$G\theta \left(\frac{\partial \phi}{\partial x} - y \right)$	$G\theta \left(\frac{\partial \phi}{\partial y} + x \right)$	$G\theta \iint_R \left(x^2 + y^2 + x \frac{\partial \phi}{\partial y} - y \frac{\partial \phi}{\partial x} \right) dx dy$	Laplace $\nabla^2 \phi = 0$	Neumann $\frac{d\phi}{d\nu} = y \cos(x, \nu) - x \cos(y, \nu)$
Conjugate function ψ	$G\theta \left(\frac{\partial \psi}{\partial y} - y \right)$	$-G\theta \left(\frac{\partial \psi}{\partial x} - x \right)$	$G\theta \iint_R \left(x^2 + y^2 - x \frac{\partial \psi}{\partial x} - y \frac{\partial \psi}{\partial y} \right) dx dy$	Laplace $\nabla^2 \psi = 0$	Dirichlet $\psi = \frac{1}{2}(x^2 + y^2)$
Shearing stress function Ψ	$G\theta \frac{\partial \Psi}{\partial y}$	$-G\theta \frac{\partial \Psi}{\partial x}$	$2G\theta \iint_R \Psi dx dy$	Poisson $\nabla^2 \Psi = -2$	Dirichlet $\Psi = \text{constant}$
Prandtl's shearing stress function χ	$\frac{\partial \chi}{\partial y}$	$-\frac{\partial \chi}{\partial x}$	$2 \iint_R \chi dx dy$	Poisson $\nabla^2 \chi = -2G\theta$	Dirichlet $\chi = \text{constant}$

the torsional couple or the torsion constant from the experimental results, it is preferable to work in terms of either the function Ψ or χ but, experimentally, there may be disadvantages, as a Poisson type equation is involved. The use of the warping function ϕ not only adds to the difficulty of subsequent computation but requires a rather awkward boundary condition, whereas the use of the function ψ has great advantages experimentally, providing a network analogue is used, at the expense of computational difficulty.

A rheoelectric analogue, such as an electrolytic tank or conducting paper, is useful in cases where irregular or curved boundary shapes are required, but with these analogues it is difficult to apply electrical potentials at a large number of points within the field and along the boundary, particularly when a steep potential gradient around the boundary is

involved. On the other hand, it is quite easy to apply potentials which may vary rapidly from point to point, both internally and on the boundary, to a large number of nodes on a network analogue. The difficulty of awkward boundary shapes can be overcome by the use of a fine mesh separation, graded nets⁽⁶⁾ or even modifying the network at appropriate boundary positions. The use of a fine mesh also reduces the truncation errors introduced by the approximate form of the finite-difference equation which replaces the appropriate partial-differential equation.

In connection with the network method it is important to realize that, at the outset, an approximation is introduced by the use of a finite-difference equation. The error in the case of the Laplace equation can be reduced to negligible proportions by the use of a fine mesh, but for the Poisson equation, although the truncation error for the finite-difference expression is reduced by the use of a fine mesh, errors are introduced by the actual analogue network. This error will be discussed in the next section.

If a network analogue is selected, it will usually be found advantageous after weighing the foregoing advantages and disadvantages, to work in terms of the function Ψ , or χ which is virtually the same thing, particularly for work which involves a large number of somewhat similar sections. However, on occasions, there are very real advantages in working in terms of the function ψ . For problems involving multiply connected regions it is usually preferable to work in terms of the shearing stress function Ψ .

The network analogue

The method whereby certain partial-differential equations may be solved by means of a passive resistance network is well known and has been described fully elsewhere.^(1, 7) Briefly, the equation is expressed in finite-difference form and, on the basis of Ohm's and Kirchhoff's laws, the network will provide a solution to the equation at a number of discrete nodal points. Although square, rectangular, triangular, hexagonal and polar networks can be constructed, it is usually found that the use of a square mesh is most convenient.

The Laplace equation in finite-difference form is written

$$\sum_{n=1}^4 \phi_n - 4\phi_0 = 0, \quad (17)$$

and this equation is represented analogously by a square mesh of equal-valued resistances.

The Poisson-type equation, as occurring in the torsion problem, can be expressed in finite-difference form as

$$\sum_{n=1}^4 \Psi_n - 4\Psi_0 + 2a^2 = 0, \quad (18)$$

where a is the mesh interval,

The analogous network of resistances r , representing this equation requires a resistance R to be connected to each node of the network used for the solution of the Laplace network, the other ends of the R resistances being connected to a common base. In the analogy, if V represents the electrical potential at a node, the network provides a solution to the equation

$$\sum_{n=1}^4 V_n - 4V_0 + \frac{r}{R}(E - V_0) = 0, \quad (19)$$

where E is the potential applied to the network (see Fig. 2). It will be seen that equation (19) is analogous to equation (18) providing $V_0 \ll E$, in which case the term Er/R will be

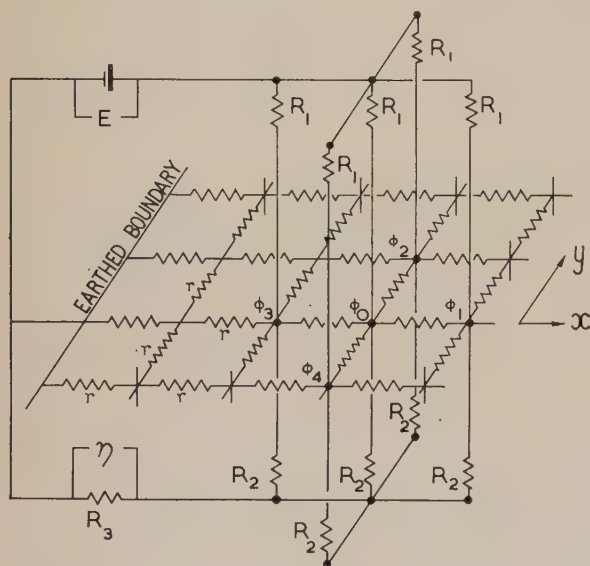


Fig. 2. Circuit diagram of potential analyser
 r , mesh resistors; R_1 , base resistors;
 R_2 , integrating resistors; R_3 , measuring resistor

constant. Herein lies the difficulty mentioned in the last section which is encountered when this approximation to the Poisson equation is made because, although the ratio r/R may be chosen to be very small, nevertheless when a large number of resistors R are placed in parallel, which occurs when a fine mesh is used, then V_0 will not be negligible in comparison with E , and to preserve accuracy either a compromise has to be struck between using a coarser net with larger finite-difference truncation errors, or correcting currents must be fed into the network. Alternatively, a more complicated network which will provide a better finite difference approximation with a coarser mesh, as proposed by Persico,⁽⁸⁾ may be used.

The method of using the networks is extremely simple, the boundary shape of the cross-section is either set out on the board by short-circuiting appropriate points, or prescribed potentials are applied to the boundary points, according to

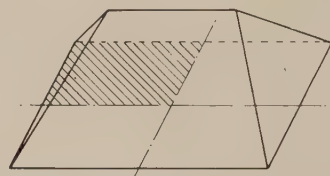
which analogy is being used. The network is energized from a low-voltage battery and potentials at nodal points measured with a voltage dividing resistance box, using a galvanometer as a null circuit-indicating device. In circumstances where only the torsion constant is required it is advantageous to use a simple integrating circuit, as described by Palmer,⁽²⁾ for summing the potentials over the cross-section, thus enabling the torsion constant to be obtained from a single measurement.

Variations in technique will best be exemplified by the consideration of a number of typical cases.

Simply connected regions

Elastic torsion. For simply connected regions it will usually be found preferable to work in terms of the shearing-stress function Ψ ; a Poisson network is required and the simple boundary condition $\Psi = \text{constant}$, usually taken as zero for convenience, holds. The electrical circuit, including the integrating circuit for the evaluation of the torsion constant is shown in Fig. 2. The torsion constant is proportional to the potential η across the resistor R_3 . Where it has been possible to compare the results of this method with analytical results, it has been found that there is only one or two per cent difference. The results from the analogue have been found, as would be expected, to be in excellent agreement with results obtained from the use of the relaxation method, using the same size of mesh.

Plastic torsion. The method of analysing the twisting of a shaft under conditions which cause plastic yielding of a portion of the section have been described by a number of



NADAI ROOF, SURFACE MAXIMUM GRADIENT.

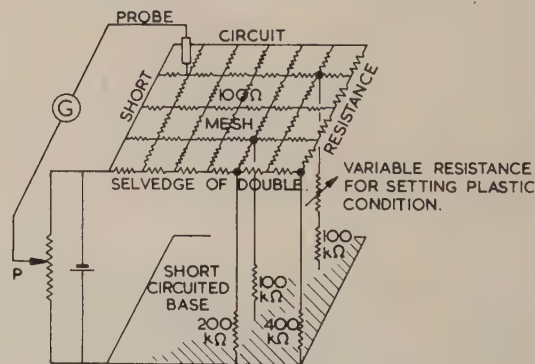
[illegible]

Fig. 3. Plastic torsion of rectangular bar

investigators including Allen⁽⁹⁾ who gives a clear description of the application of the Relaxation method to this problem. The approach to the problem, when the network analogue is used, follows that of the relaxation method. A Poisson net may be used and the values of the required function is measured at all nodal points. At nodes where these potentials exceed those prescribed by considerations of the "Nadai roof," rheostats are inserted in series with the base resistors and so adjusted that the potentials at those points shall be set to the prescribed value. The field is then re-scanned and the potential values appropriate to the plastic condition recorded. Subsequent correction to the extent of the plastic region can be made without re-scanning the whole field. The electrical circuit is shown in Fig. 3.

Composite bar. The torsion problem of a composite bar, in the form of a simply connected region may be readily solved by means of the shearing-stress function Ψ or χ . As before, a Poisson equation has to be solved, and the only difficulty lies in the fact that the resistances of the networks representing the dissimilar materials must be in the ratio of the shear moduli. The value of the required function may again be set to zero around the boundary, and the condition at the interface of the dissimilar materials is that the value of the function at corresponding points shall be the same. The tangential strain must be continuous across the interface and this condition is satisfied, in the case of two or more materials, by

$$\frac{1}{G_1} \frac{\partial \Psi_1}{\partial \nu} = \frac{1}{G_2} \frac{\partial \Psi_2}{\partial \nu} = \dots = \frac{1}{G_n} \frac{\partial \Psi_n}{\partial \nu} \quad (20)$$

where the subscripts refer to various materials joined together.

The interface boundary condition is automatically satisfied in the network by electrically connecting corresponding points along the interface. A circuit diagram and the results for the

torsion of a rectangular bar composed of two materials the moduli of rigidity of which are in the ratio 3 : 1, corresponding to a composite bar of steel and aluminium alloy, is shown in Fig. 4.

Multiply connected regions

Composite bars. Consider a long cylindrical bar composed of several isotropic materials in which one material surrounds the others, the materials being joined together, without slipping, at their interfaces. For torsion with free warping, the stresses, given in terms of Prandtl's stress function χ , are

$$\tau_{xz} = \frac{\partial \chi_i}{\partial y}; \quad \tau_{yz} = -\frac{\partial \chi_i}{\partial x}, \quad (21)$$

where $i = 1, 2 \dots n$. Each function χ_i must satisfy the Poisson type equation

$$\nabla^2 \chi_i = -2G_i \theta \quad (22)$$

in its corresponding region R_i . The boundary conditions can be expressed in terms of the stress function by consideration of the components of shearing stress normal and tangential to a curve in the cross-section. These components are, respectively,

$$\tau_{\nu z} = -\frac{\partial \chi_i}{\partial s}; \quad \tau_{sz} = \frac{\partial \chi_i}{\partial \nu}. \quad (23)$$

Referring to Fig. 5, the condition that the external boundary of the cross-section must be free of stress is obtained by integrating the first of equations (23) along C_1 :

$$\chi_1|_{C_1} = K_1, \quad (24)$$

where K_1 is a constant.

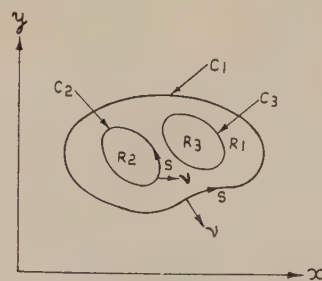


Fig. 5. Cross-section of composite bar

At an interface such as C_2 , the tangential strain must be continuous across C_2 . In terms of the stress function this condition is

$$\frac{1}{G_1} \frac{\partial \chi_1}{\partial \nu} \Big|_{C_2} = \frac{1}{G_2} \frac{\partial \chi_2}{\partial \nu} \Big|_{C_2} \quad (25)$$

Also, the shearing stress component normal to C_2 must be continuous across C_2 . Hence

$$\frac{\partial \chi_2}{\partial s} \Big|_{C_2} = \frac{\partial \chi_1}{\partial s} \Big|_{C_2} \quad (26)$$

When the last equation is integrated, the following equation results

$$\chi_2|_{C_2} = \chi_1|_{C_2} + K_2, \quad (27)$$

where K_2 is a constant.

The problem is to find the shearing stress functions χ_1 and χ_2 which satisfy equation (22) in their respective domains,

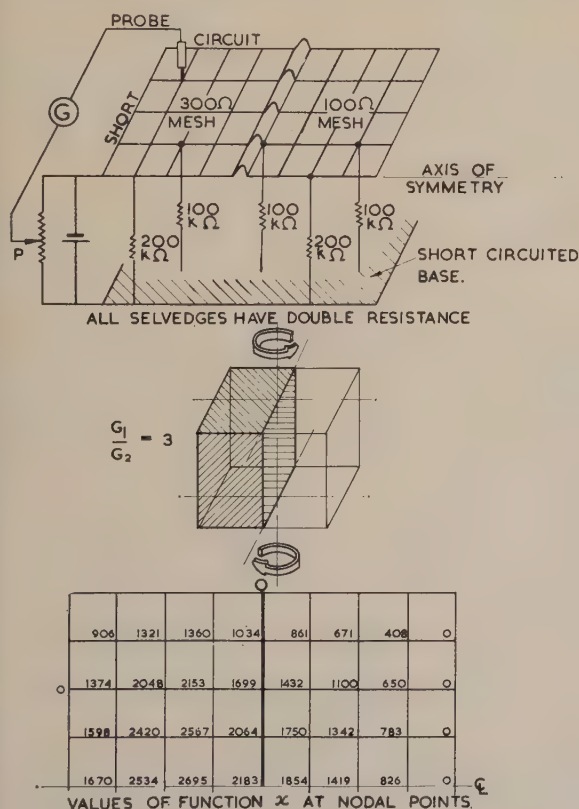


Fig. 4. Torsion of composite bar

and the boundary conditions given by equations (24), (25) and (27). The torsional couple on the cross-section is

$$T = - \sum_{i=1}^2 \iint \left(x \frac{\partial \chi_i}{\partial x} + y \frac{\partial \chi_i}{\partial y} \right) dx dy. \quad (28)$$

Integrating by parts and making use of equations (24) and (27) gives

$$T = \sum_{i=1}^2 K_i \int_{C_i} (-x dy + y dx) + \sum_{i=1}^2 \iint_{R_i} 2 \chi_i dR_i. \quad (29)$$

The stresses and couple on the cross-section are independent of the constants K_i . Therefore these constants may be chosen arbitrarily. For convenience, all the constants K_i are taken to be zero so that the expression for the couple is analogous to that for the torsion of a uniform cross-section, that is to say, the couple equals twice the volume under the stress-function surface.

In the electrical analogue, two or more networks will be required such that the ratio of their unit resistances equals the ratio of the torsional rigidities of the various materials. The shape of the appropriate domains are set up on the networks and corresponding nodes are connected at all interfaces. As Poisson-type equations have to be solved, base resistors have to be connected to all nodal points. The free ends of the base resistors are short-circuited, and an electrical potential is applied between the base and the short-circuited outer boundary. It is important to note that the boundary conditions at the interfaces are automatically satisfied. The electrical circuit, therefore, is essentially the same as that described for the torsion of a simply connected composite bar.

Hollow thick-walled bar. The torsion of a hollow bar will be recognized as a special case of the multiply connected composite bar. The electrical circuit of the analogue is shown in Fig. 6. Working in terms of the shearing stress function χ ,

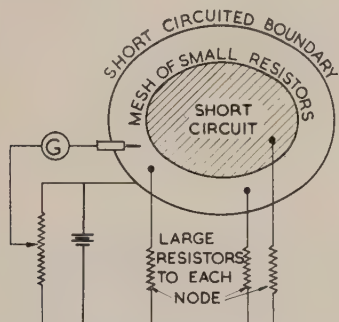


Fig. 6. Electrical analogy for torsion of thick hollow bar (Poisson approach)

the region corresponding to the hole must be short-circuited. The condition that the axial displacement due to twisting shall be single valued at every point on the section, see equation (15), is

$$\oint \frac{\partial \chi}{\partial v} ds = -2A_2,$$

where A_2 is the area of region R_2 . When the circuit is energized, it will be seen that this condition is automatically satisfied.

The great advantage of this method is that the network does not have to be cut in order to set out the shape of the hole. Weiner⁽¹⁰⁾ has described a network for this problem which requires a "cut" network in which the interior boundary

condition is not automatically satisfied but may be determined experimentally.

An interesting comparison between the electrical analogy and Prandtl's membrane analogy for the same case will be noted. In the membrane analogy, a membrane is stretched between the boundary shape and the edge of a weightless rigid lamina, representing the hole, situated horizontally above the base and maintained there by pressure, the pressure on the underside of the lamina being balanced by the tension in the membrane at its inner boundary. For equilibrium

$$\iint_A p dx dy + T \oint \frac{dw}{dv} ds = 0, \quad (30)$$

where p = pressure on membrane,
 T = membrane tension per unit length,
 w = membrane deflection,
 A = area of hole.

If equation (30) is divided by T , then

$$\oint \frac{dw}{dv} ds = - \frac{p}{T} \iint_A dx dy, \quad (31)$$

and it will be seen that this equation is analogous to equation (15).

An alternative method of solving this problem is to work in terms of conjugate function ψ , in which case a Laplace equation has to be solved in the domain with a Dirichlet boundary condition. External boundary values are calculated in accordance with the equation

$$\psi|_{C_1} = \frac{1}{2}(x^2 + y^2), \quad (32)$$

and internal boundary values by means of the equation

$$\psi|_{C_2} = \frac{1}{2}(x^2 + y^2) + K. \quad (33)$$

On the network, potentials are applied to the nodal points on the external boundary from one potential divider in accordance with equation (32), and potentials are set, from a second potential divider having its own battery, on the internal boundary, as dictated by the expression

$$\psi|_{C_2} = \frac{1}{2}(x^2 + y^2).$$

When the network is energized, the condition

$$\oint_{C_2} \frac{\partial \psi}{\partial v} ds = 0, \quad (34)$$

will be automatically satisfied, ψ taking the value on the interior boundary as prescribed by equation (33). The appropriate circuit diagram is shown in Fig. 7. As a Laplace equation has to be solved, base resistors are not required.

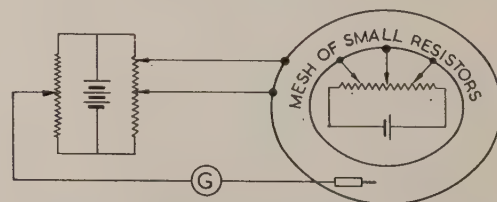


Fig. 7. Electrical analogy for torsion of thick hollow bar (Laplace approach)

Potentials are measured at the nodes of the section, the stresses and the torsion constant being calculated in the normal manner.

Synge and Cahill⁽¹¹⁾ have obtained an approximate solution to the torsion problem for a hollow square by using the hypercircle method, carrying out the computation with a Standards Eastern Automatic Computer. The problem which was considered by them was that of a hollow square bounded externally by a square the side of which was twice the length of the internal square. Calculations were made for mesh separations of $\frac{1}{8}$, $\frac{1}{16}$, $\frac{1}{32}$ and $\frac{1}{64}$ the length of the external side. The $\frac{1}{8}$ mesh separation represented the closest approximation possible on S.E.A.C. without resorting to tape storage. This particular problem has been solved in terms of both the conjugate function ψ and the shearing stress function Ψ on the electrical analogue potential analyser, but using the much finer mesh separation of $\frac{1}{64}$. Although readings were taken at each node for both of the electrical analogue experiments, the results, in terms of ψ , have been compared in Fig. 8 with the calculated results obtained by Synge and Cahill at coincident points on a mesh separation of $\frac{1}{16}$. Remembering that the S.E.A.C. results were obtained for a mesh separation of $\frac{1}{48}$, the agreement with the electrical analogue readings is very good.

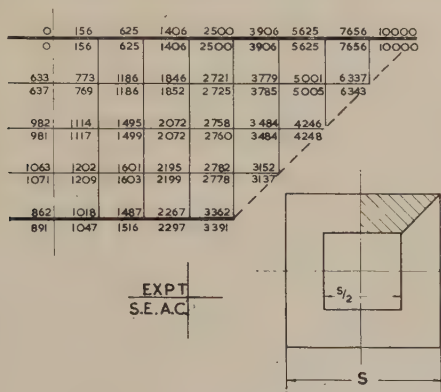


Fig. 8. Torsion of hollow square shaft

Comparison of values of ψ obtained from electrical analogue experiment and S.E.A.C. computation

As far as the electrical analogue is concerned, the experimental methods, working either in terms of the conjugate function ψ or the shearing stress function Ψ are very rapid although, for ease in computing the torsion constant,* it is preferable to work in terms of the shearing stress function. In both methods, the necessity for a two-stage analysis, which is necessary if the relaxation method is used,⁽¹²⁾ is avoided.

Thin-walled shell filled with dissimilar material. In aircraft design, there are numerous examples of thin-walled metal cylinders, such as control surfaces and propeller blades, which have been stabilized and stiffened by filling the interior with a low-density foamed-plastic material which adheres to the inner wall of the cylinder. Recognizing the importance of this problem, McComb⁽¹³⁾ has described a theoretical method for determining the torsional stiffness of thin-walled shells filled with a dissimilar material. In his solution, an approximate boundary-value problem was formulated on assumptions similar to those stipulated in the Bredt torsion theory of thin-walled shells. McComb solved this boundary-value problem exactly for a rectangular cross-section, and

* The expressions for the torsional couple, when either the function ϕ or ψ is used, are identical to those listed in the table for simply connected regions. In terms of the shearing stress function Ψ , the torsional couple is as given by equation (16); it is implicit in this equation that $k_0 = 0$.

approximately for slender triangular and diamond cross-sections. Unfortunately, the computational labour involved in the exercise of this method is severe and therefore an electrical analogue was sought which would be capable of obtaining solutions of acceptable accuracy easily and speedily. The development of a suitable analogue has already been described in detail⁽¹⁴⁾ and it will be sufficient here to give a brief description of the method.

The equations of elasticity for the torsion of a composite bar, with free warping, may be particularized for the case of a cylinder consisting of a thin-walled shell of one material filled with a core of another. If the thickness of the shell skin is small compared with the overall dimensions of the cross-section, the stress in the wall may be assumed to be uniformly distributed over the thickness. This stress is equal to the normal derivative of the stress function.

To solve the problem it is necessary to find a function χ which satisfies the Poisson equation

$$\nabla^2 \chi = -2G_2 \theta, \quad (35)$$

in the region R bounded by the contour C , see Fig. 9. In addition, the equation

$$\frac{\partial \chi}{\partial \nu} \Big|_C = -\frac{G_2}{G_1 t} \chi \Big|_C \quad (36)$$

must be satisfied along the boundary C . Then the torsional couple on the bar is equal to twice the volume under the stress function surface, that is to say

$$T = 2 \iint_R \chi dx dy. \quad (37)$$

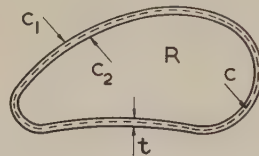


Fig. 9. Cross-section of thin-walled composite cylindrical bar

As far as the electrical analogy is concerned, the torsional problem of the foam-filled shell presents two important differences from the torsion problem of solid homogeneous bars. The first difference lies in the boundary condition which, for the foam-filled shell, as has been seen, is that the normal derivative of the function at the boundary shall be proportional to the function at that point. This will be recognized as a Fourier boundary condition whereas for the solid bar, a Dirichlet or Neumann condition holds. The second difference between the two problems is a practical one because, for the solid bar, the shape of the boundary of the cross-section can be set up anywhere within a continuous net, the particular Dirichlet condition calling for all points on the boundary to be set at some constant potential whereas, for the present case, the Fourier boundary condition requires the net to terminate actually at the boundary.

The electrical circuit representing the analogy is shown in Fig. 10. It should be observed that the boundary resistors are of constant value, this resistance being made proportional to the parameter $G_1 t / G_2$ in order to satisfy equation (36). The necessity for ensuring that the net actually terminates at the boundary may be satisfied by using a form of construction for the network which will enable appropriate resistors to be removed, thus allowing the shape of the cross-section under investigation to be "cut out" on the network. Results for

rectangular-, triangular- and diamond-shaped sections have been reported by Redshaw⁽¹⁴⁾ and, where comparison with theoretical solutions is possible, the agreement is good.

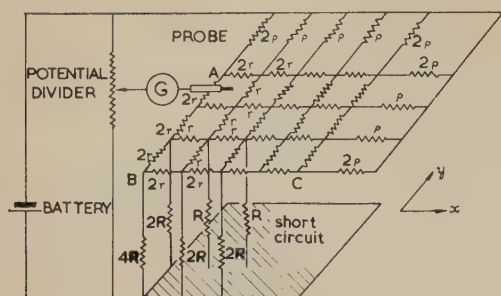


Fig. 10. Circuit diagram

Note: AB and BC are axes of symmetry

In many cases of interest, the sections are extremely slender and a serious experimental difficulty arises. This difficulty lies in the fact that the boundary of the section does not necessarily coincide with nodal points of the net. Because of the slenderness of the section, the device of using a very fine net and taking the actual boundary point to the node nearest to the correct boundary contour, is not satisfactory. The alternative of using irregular mesh lengths near the boundary by suitable adjustment of the resistances of the mesh resistors will also be found to be tedious and unsatisfactory for slender sections. However, the difficulty can be overcome if the section is transformed by means of an affine transformation from a slender triangle to an isosceles right-angled triangle.

In effect, a rectangular mesh is used and the electrical analogue then solves the equation

$$\frac{\partial^2 \chi}{\partial X^2} + \frac{1}{k^2} \frac{\partial^2 \chi}{\partial Y^2} = -2G_2\theta \quad (38)$$

Then, using the linear transformation

$$x = X, y = kY, \quad (39)$$

a right-angled triangle, for example, is changed to an isosceles right-angled triangle. In this manner the difficulty of a boundary not intersecting nodal points is avoided as a right-

angled triangle can be set out on a square mesh without trouble.

Conclusions

In conclusion, although the solution of individual cases of the torsion of bars with free warping has been described, nevertheless the electrical analogue method is so powerful that the solution of a complicated problem such as the torsion of composite bar with hollow regions, and twisted into the plastic range, could be investigated without undue difficulty. The experimental accuracy is sufficient for all engineering purposes.

References

- (1) REDSHAW, S. C. *Proc. Inst. Mech. Engrs*, **159**, 55, p. 52 (1948).
- (2) PALMER, P. J. *Aluminium Development Association Research Report No. 22* (1953).
- (3) SAINT-VENANT, B. DE. *Extrait du Tome XIV des Mémoires Présentés par divers Savants à l'Académie des Sciences* (1855).
- (4) PRANDTL, L. VON. *Physikalische Zeitschrift*, **IV**, p. 758 (1903).
- (5) SOKOLNIKOFF, I. S. *Mathematical Theory of Elasticity*. 2nd Ed., p. 169 (London: McGraw-Hill Publishing Co. Ltd., 1956).
- (6) PALMER, P. J., and REDSHAW, S. C. *J. Sci. Instrum.*, **34**, p. 407 (1957).
- (7) LIEBMANN, G. *Actes des Journées Internationales de Calcul Analogique*, Bruxelles, p. 346 (1956).
- (8) PERSICO, E. *Nuovo Cimento*, **9**, p. 74 (1952).
- (9) ALLEN, D. N. DE G. *Relaxation Methods*, p. 212 (London: McGraw-Hill Publishing Co. Ltd., 1954).
- (10) WEINER, J. H. *J. Appl. Mech.*, **20**, p. 562 (1953).
- (11) SYNGE, J. L., and CAHILL, W. F. *Quarterly of Applied Mathematics*, **XV**, No. 3, p. 217 (1957).
- (12) SHAW, F. S. *Commonwealth of Australia, Council for Scientific and Industrial Research Division of Aeronautics Report*, SM 36 (1944).
- (13) MCCOMB, JR., and HARVEY, G. *National Advisory Committee for Aeronautics Report 1316* (1957).
- (14) REDSHAW, S. C. *Actes des 2es Journées Internationales de Calcul Analogique*, Strasbourg, p. 328 (1959).

Importance of insulating inclusions in arc initiation

by R. HANCOX, B.Sc.(Eng.), Ph.D., A.M.I.E.E., Controlled Thermonuclear Reactions Division, Atomic Energy Research Establishment; Harwell, Berkshire

[Paper first received 11 May, 1960]

Abstract

The initiation of arcs on a metal surface in contact with a plasma (ion density about 10^{14} ion/cm³) has been studied with metal specimens known to contain microscopic alumina inclusions. The specimens were biased negatively with respect to the plasma, and for voltages above 300 V the time lag before arcing occurred was inversely proportional to the positive ion current drawn by the specimen from the plasma, but independent of voltage. At lower voltages the time lag increased rapidly with decreasing voltage. Arcing was also independent of the nature of the ions and the pressure of neutral gas in the

plasma. These results are consistent with the initiation of the arcs by dielectric charging and breakdown of the inclusions.

1. Introduction

IN a review of materials used for the construction of discharge tubes for C.T.R. devices,^(1, 2) it has been shown that metals possess marked superiority over ceramics or other insulating materials in their thermal properties and ease of fabrication. The principal disadvantage of metals, however,

is their tendency to form arc spots when exposed to a hot plasma, and this has been the main cause of plasma contamination in existing devices. Even when the wall of the discharge tube approximates to an equipotential surface, as with the continuous resistive liner in a toroidal tube,⁽³⁾ arcing still occurs. The formation of these arcs has been studied, therefore, with a view to constructing a metal discharge tube which is free from arcing.

The problem of arc formation on a metal surface in contact with a plasma is similar in several respects to that of low-pressure glow-to-arc transitions. Work in this field has emphasized the importance of the condition of the metal surface, and such transitions are found to be assisted by oxide layers,⁽⁴⁾ films of low work function material, or microscopic inclusions of insulating material.⁽⁵⁾ Previous work⁽²⁾ with high-current discharge tubes also suggests that these factors, and particularly the presence of inclusions, are of importance in the initiation of arcs on the metal walls of such tubes. The experiments described in this paper were therefore undertaken to demonstrate the conditions under which arcing would occur on a metal surface which was known to contain inclusions when in contact with a plasma.

Experimental procedure

The experimental arrangement is similar to that used in the earlier experiments,^(1,2) in which specimens in the form of a probe were inserted into a toroidal discharge tube and biased at a potential of a few hundred volts negative with respect to the plasma potential by means of an external circuit and second electrode in the plasma. Under these conditions the specimen drew a positive ion current of about 1 A/cm² from the plasma. In all previous experiments a d.c. voltage has been applied to the specimen, but it has been shown⁽⁶⁾ that the considerable statistical fluctuations observed in the results were inherent in such a system because the arcing behaviour of the specimens is a function of the positive ion current which it draws from the plasma as well as the applied voltage and that this was not sufficiently controlled in the experiments. The experimental technique has been improved, therefore, by the use of pulsed voltages of only a few micro-seconds duration applied to the specimen such that the current drawn from the plasma is approximately constant during the time of the test. This method has two further advantages. Firstly, the energy associated with the voltage supply to the specimen can be greatly reduced, thus reducing the damage to the specimens when arcing occurs and also reducing the conditioning effect (that is, a progressive variation in results during the course of each test). Secondly, the time lag between the instant of application of the voltage pulse and the initiation of the arc can be measured, thus yielding more information than was available in the previous experiments.

The specimens, which were of aluminium, were first polished to obtain a scratch-free surface, and then lightly rubbed in alumina powder of 1 μ particle size. This final treatment left a uniform mat surface with a considerable number of alumina particles embedded in it. The specimens were then mounted in the electrode assembly, placed in the vacuum system, and tested.

The electrodes for the arcing tests formed a coaxial line, with the specially prepared specimen as the end of the inner conductor. A glass tube, which formed the insulation between the electrodes, was fitted with a thin glass shield at the open end which restricted arcing to the central portion of the specimen. The whole electrode assembly was inserted

by means of a vacuum seal into a side arm of the torus so that it projected into the discharge.

The tests were performed in a four-inch bore glass torus in which a 1500 A discharge of 100 μ s duration was induced. The energy store for the discharge was a 1 μ F capacitor charged to 10 kV, and was discharged by means of an ignitron through the 16-turn primary winding of a pulse transformer of which the torus formed the single secondary turn. The torus formed part of a vacuum system, of base pressure 2×10^{-6} mm of mercury, into which various gases could be admitted to give working pressures in the range 5 to 50×10^{-3} mm of mercury with a continuous flow of gas.

Voltage pulses of up to 2 kV and of 5 μ s duration were applied to the specimen by discharging a 75 Ω line through a coaxially mounted thyatron. The saturated positive-ion current drawn from the plasma by the specimen was independent of the voltage but could be varied either by varying the conditions of the discharge (that is, current or pressure) or, more conveniently, by varying the instant during the main discharge when the voltage was applied to the specimen. The current was measured by means of a low resistance in series with the electrodes and displayed on a c.r.o., thus giving a simultaneous measure of both the specimen current and the time lag before arcing occurred.

Experimental results

In previous work on arc initiation under similar conditions, difficulty has been experienced in obtaining consistent results because of variations of both the surface conditions of the specimens and the test conditions from one discharge to another, and it has been necessary to take the mean of many measurements. In the present experiments, however, these effects have been greatly reduced, such that each individual time lag measurement was consistently repeatable. The distribution of time lags for a given condition was approximately Gaussian about a mean value with a standard deviation of 10% of the mean value, thus showing that the time lag is mainly formative rather than statistical. Variations from one specimen to another were also of the order of 10%. Each arc left a separate pit of about 20 μ diameter on the specimen.

If the current drawn by the specimen from the plasma was varied, the time lag was found in all cases to be inversely proportional to the current. The results from measurements on two specimens in a nitrogen discharge are shown in Fig. 1, where each point is an individual measurement.

Series of curves, such as that of Fig. 1, taken in hydrogen and nitrogen discharges with various voltages applied to the specimen between 750 and 2000 V showed only a slight dependence of the time lag on voltage, the time lag increasing with increasing voltage for a given current to the specimen. The effect was more marked in a helium discharge, and results are given in Fig. 2 for two voltages. The fact that the effect is most noticeable in helium suggested that the measured current to the specimen contained an appreciable contribution of electron current due to secondary electron emission from the specimen. This was checked by measuring the variation of specimen current with voltage, and the resulting values of the secondary electron emission coefficients are plotted in Fig. 3. Although little information is available on secondary emission by positive-ion bombardment, these figures agree well with values obtained elsewhere.⁽⁷⁾ Attempts were also made to detect any current resulting from photo-emission by withdrawing the specimen into the side arm of the torus where it was still illuminated by the discharge, but the ion density was low. No such currents were detected

however. If correction is made for the secondary electron current, then the time lags are found to be independent of voltage for a given positive-ion current, for voltages in the range 750 to 2000 V.

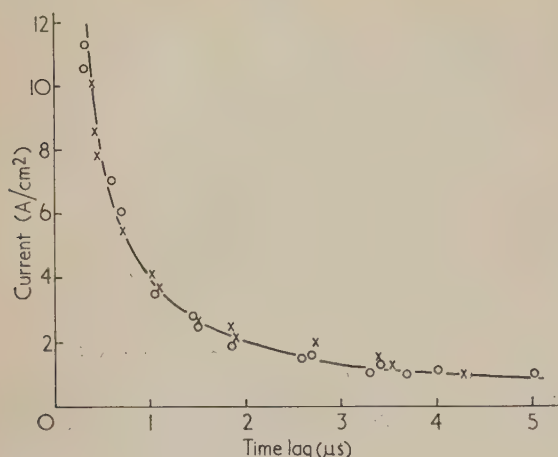


Fig. 1. Variation of time lag with current to the specimen. Discharge in Nitrogen at 25×10^{-3} mm of mercury pressure. Specimen voltage 750 V. (Results for two similar specimens are shown.)

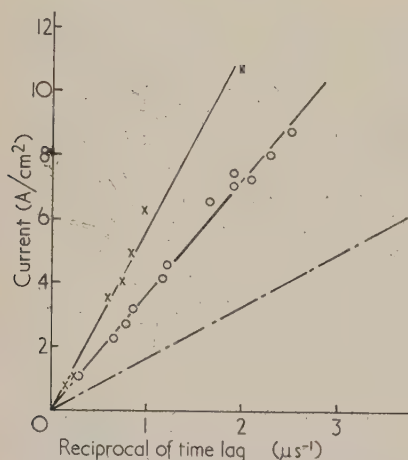


Fig. 2. Variation of time lag (plotted as a reciprocal) with current to the specimen at two voltages

Discharge in Helium at 25×10^{-3} mm of mercury pressure

○ Specimen voltage 750 V

× Specimen voltage 1500 V

--- Both curves corrected for secondary electron emission

Measurements were also made at low voltages in order to find the limit at which the results ceased to be independent of voltage. The results for a nitrogen discharge are shown in Fig. 4, and it is seen that the time lag is constant down to voltages of 300 V, after which there is a rapid increase of time lag with reduction of voltage.

Measurements were made with discharges in four different gases—hydrogen, helium, nitrogen, and argon—thus giving a range of 1 to 40 for the mass of the positive ions drawn by the specimen from the plasma. After correction had been made for the secondary electron current, no dependence on the gas of the main discharge was observed. The pressure of neutral gas in the discharge was also varied by varying the gas pressure in the torus over the range 5 to 50×10^{-3} mm of mercury. Two sets of results for an argon discharge are shown in Fig. 5, and it is seen that there is no effect.

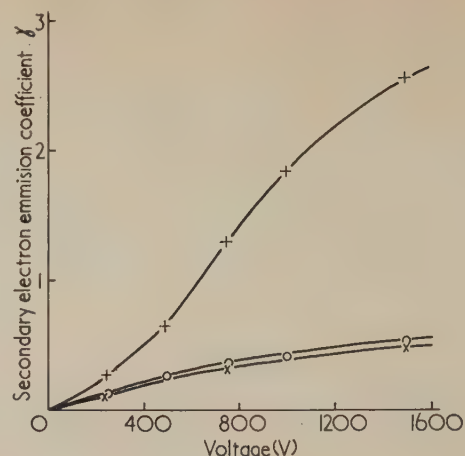


Fig. 3. Measured values of the secondary electron emission coefficient

× Hydrogen ions ○ Nitrogen ions + Helium ions

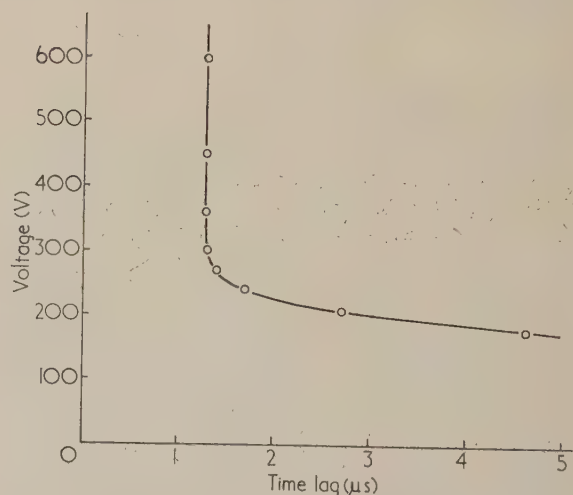


Fig. 4. Variation of time lag with voltage on specimen for a positive-ion current of 3 A/cm^2

Discharge in Nitrogen at 25×10^{-3} mm of mercury pressure. (Each point is the mean of six measurements.)

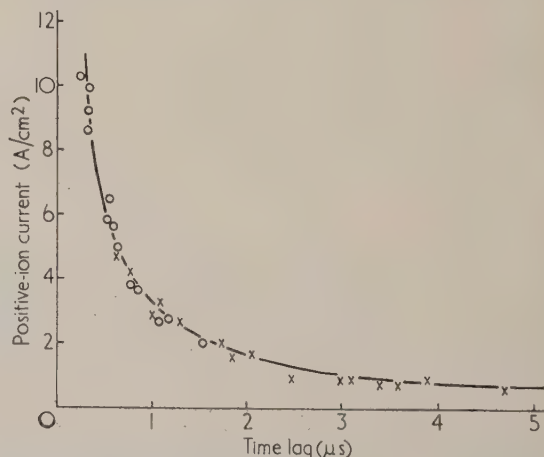


Fig. 5. Variation of time lag with current to the specimen, for a discharge in Argon at two different pressures

Voltage on specimen 1000 V

× 10×10^{-3} mm of mercury pressure

○ 50×10^{-3} mm of mercury pressure

Discussion

The current drawn by the specimen in the tests was space-charge limited. Under these conditions, a positive-ion sheath forms over the surface of the specimen of about 10^{-2} cm thickness, and the electric field near the specimen is limited to this region thus being of the order 10^5 V/cm at the surface of the metal. Hence the initiation of an arc might be caused by one of two basically different mechanisms.

Arc initiation could result from the field emission of electrons caused by the high field in the space-charge sheath. This might cause ohmic heating of small points as in vacuum breakdown, or lead to the formation of an electron avalanche by ionization of neutral gas, as proposed for glow-to-arc transitions.⁽⁸⁾ In either case, however, the process would be very dependent on the electric field. Under the conditions of the present experiments, the field at the surface of the specimen would be a function of both the applied voltage and the mass of the positive ions. Since arcing was independent of these parameters, it could not be due to field emission of electrons caused by the space-charge field.

An alternative mechanism of arc initiation involves the dielectric charging, and subsequent breakdown, of an insulating layer or particles on the surface. Such a mechanism would give a time lag which was inversely proportional to the current to the specimen as observed in the experiments. The possibility that arcing was influenced by the natural oxide layer on the specimen has been eliminated by experiments in which a fresh aluminium surface was evaporated on to a specimen and allowed to oxidize and then tested. After a few initial arcs, the specimen ceased arcing even under the most severe test conditions. It seems most likely, therefore, that the arcing was in fact initiated by the dielectric charging and breakdown of the inclusions, as expected.

This conclusion is supported by the fact that specimens prepared in a similar manner but without the intentional addition of inclusions did not arc either as easily or so consistently as the specially prepared specimens. The experimental results also agree quantitatively with this conclusion. If it is assumed that the dielectric breakdown of the inclusions follows the mechanism proposed by Fröhlich,⁽⁹⁾ breakdown of an alumina particle of $1\ \mu$ size would be expected to occur at fields of the order of 3×10^6 V/cm. This corresponds to a product of positive-ion current density and time lag of 2.4×10^{-6} A s/cm², which is close to the experi-

mental value of 3.2×10^{-6} A s/cm². Furthermore, the rate of charging of the inclusions should be independent of the applied voltage provided this is greater than the change in surface potential required for breakdown. For a breakdown field of 3×10^6 V/cm and a $1\ \mu$ particle size, this potential would be 300 V, which agrees well with the measured lower limit for the independence of arcing on voltage.

Conclusions

The initiation of arcs on a metal surface in contact with a plasma has been studied with specimens known to contain microscopic insulating inclusions. The results obtained suggest that, under these conditions, arcing was initiated by the dielectric charging and subsequent breakdown of these inclusions. With alumina inclusions of $1\ \mu$ size, the time lag before arcing occurred was inversely proportional to the positive-ion current to the specimen. For applied voltages above 300 V the time lag was independent of voltage for any given positive-ion current. Arcing was also independent of the nature and pressure of the gas in the main discharge.

Acknowledgement

The author wishes to acknowledge the valuable assistance of Mr. C. H. Walker in making the experimental measurements reported in this paper.

References

- (1) CRASTON, J. L., HANCOX, R., *et al.* *Proc. 2nd UN. Int. Conf. on the Peaceful Uses of Atomic Energy, Geneva*, **32**, p. 414 (1958).
- (2) ROBSON, A. E., and HANCOX, R. *Proc. Instn Elect. Eng.*, **106** (A2), p. 47 (1959).
- (3) MITCHELL, J. T. D., WHITTLE, H. R., *et al.* *Proc. Instn Elect. Eng.*, **106** (A2), p. 74 (1959).
- (4) JENKIN, J., and JONES, T. B. *J. Appl. Phys.*, **28**, p. 663 (1957).
- (5) PEIL, P. C. L., and GRIFFITHS, L. B. *Nature (London)*, **183**, p. 1481 (1959).
- (6) WALKER, C. H. *Proc. Instn Elect. Eng.*, **106**, (A2), p. 82 (1959).
- (7) VON ENGEL, A. *Ionized Gases*, p. 81 (Clarendon Press, Oxford, England, 1955).
- (8) BOYLE, W. S., and HAWORTH, F. E. *Phys. Rev.*, **101**, p. 935 (1956).
- (9) FRÖHLICH, H. *Proc. Roy. Soc.*, **160** A, p. 230 (1937).

Measurement of convective heat transfer by means of the Reynolds analogy

by R. A. GRANVILLE, B.Sc., A.Inst.P*, and GENEFER BOXALL, B.Sc., British Iron and Steel Research Association, 140 Battersea Park Road, London, S.W.11

[Paper received 8 June, 1960]

Abstract

Preston's method for measuring skin friction in pipes has been extended to include non-uniform flow, with and without pressure gradients, over flat surfaces. By means of a modified form of the Reynolds analogy, the local convective heat transfer coefficient can be related to the skin friction, and it is proposed that the method be used in aerodynamic models of furnaces and in heat transfer plant of simple geometry. More investigations are required of

the effects of fluid turbulence, surface roughness and surface curvature on convective heat transfer and skin friction.

List of symbols

C_f = local skin friction coefficient = $\tau_0/\frac{1}{2}\rho U_m^2$.
 C_p = specific heat of fluid at constant pressure.
 d = external diameter of Pitot tube.

* Now with the Esso Petroleum Company

- H = shape parameter = δ^*/θ .
 h = local heat transfer coefficient.
 K = thermal diffusivity = $k/\rho C_p$.
 K_s = Stanton number = $q/(\rho U_m C_p (T_f - T_w)) = h/\rho U_m C_p$.
 k = thermal conductivity of fluid.
 P = total pressure recorded by a Preston probe.
 p_0 = static pressure at the surface.
 P_r = Prandtl number of fluid = ν/K .
 dp/dx = pressure gradient at the surface at position x , in the direction of the x axis.
 q = rate of heat transfer at wall.
 R_θ = a Reynolds number = $U_m \theta/\nu$.
 S = "correction term."
 T_f = absolute temperature of fluid outside the boundary layer at x .
 T_w = absolute temperature of wall surface at x .
 U_m = fluid velocity outside the boundary layer at position x , in the direction of the x axis.
 u = fluid velocity inside the boundary layer at position x , in the direction of the x axis.
 x = distance measured along the wall in the direction of flow.
 y = normal distance from the test plate surface.
 δ^* = boundary layer displacement thickness.
 ν = kinematic viscosity of fluid.
 ρ = density of fluid.
 θ = boundary layer momentum thickness.
 τ_0 = shearing stress at wall (skin friction).

Introduction

UNDER conditions of laminar fluid flow it is often possible to calculate the convective heat transfer between the fluid and a body immersed in it. Spalding⁽¹⁾ and Sparrow⁽²⁾ provide recent examples of developments in this field. In most circumstances associated with industrial heat transfer equipment, the flow is turbulent and, because it is not yet possible to solve such problems analytically, the heat transfer must be estimated from empirical relationships or directly measured. Unfortunately, direct measurement is difficult and often impossible, but it has been found possible to relate the local convective heat transfer coefficient to the local coefficient of skin friction under some conditions of turbulent flow.⁽³⁾ Preston⁽⁴⁾ has described a simple method for determining the local skin friction from the measured pressure difference between a total head tube, lying in contact with the surface, and the local static pressure. This method was successfully employed by Sigalla⁽³⁾ to determine the heat transfer from a wall jet, and some developments of the technique and plans for its extended use have been published by Granville and Sigalla.⁽⁵⁾ Recently, the method has been developed to the point where it may be put to more practical use, and in the succeeding sections of this paper the work is briefly described, together with those aspects which require further examination.

The Reynolds analogy

Any fluid, at temperatures and pressures likely to be encountered in industrial heat transfer plant, which passes over a stationary surface has a region in which the velocity decreases from its "free stream" value to zero at the surface. The region of decreasing velocity is termed the boundary layer, in which the flow may be laminar, or turbulent. A

fully developed turbulent boundary layer may be divided into three main zones:

- fully turbulent, near to the free stream;
- a "buffer" zone, in the central position of the boundary layer;
- a laminar sub-layer, very close to the boundary surface.

Through the boundary layer diffuse molecules of the fluid, from the free stream to the surface, where they give up excess heat and momentum. This diffusion manifests itself as convective heat transfer and skin friction. Provided the diffusion mechanisms are similar, there exists an exact similarity between the two phenomena and this is the basis of the Reynolds analogy, which may be written non-dimensionally as:

$$C_f/2 = K_s \quad (1)$$

Thus from a measurement of the shearing stress at the wall τ_0 , the convective heat transfer coefficient h can be calculated. In fact, heat may also be transferred by conduction which makes a virtual increase to the rate of heat diffusion, and for gases, the ratio of momentum diffusion to heat diffusion (the Prandtl number P_r) is approximately 0.72.

Thus the modified Reynolds' analogy can be written as,

$$K_s = S(C_f/2) \quad (2)$$

where S , the "correction term," is a function of the Prandtl number. Various expressions have been obtained for S , but for a Prandtl number of 0.72 and for values of C_f from 4×10^{-3} to 6×10^{-3} , S is nearly constant and equal to 1.2. For more accurate assessment of S , it is recommended that the formula proposed by Rubesin⁽⁶⁾ be used,

$$S = \frac{1 + 11.5 C_f/2 \cdot (T_w/T_f)}{P_r^{1/3} + 11.5 C_f/2 \cdot (T_w/T_f)} \quad (3)$$

Thus, for practical application, τ_0 , U_m , T_f and T_w are measured, and assuming ρ and C_p are known, h can be calculated.

The course of the authors' experiments has been to verify and extend the use of Preston's method, for measuring τ_0 .

Preston's method for "pipe flow" and flat plates with zero pressure gradient

Preston⁽⁴⁾ used dimensional arguments to show that there is a region within all turbulent boundary layers where the velocity profiles are similar, and that they depend on τ_0 and the physical properties of the fluid. He also demonstrated that τ_0 can be measured by placing a cylindrical total head tube, facing the main flow direction, in contact with the surface. The difference between the static pressure at the surface and that measured by the probe is then uniquely related to τ_0 and the dimensions of the total head tube. Preston's experiments were performed in a pipe in which the inside diameter/outside diameter ratio of the total head tubes was accurately maintained at 0.600, and a calibration (equation 4) was obtained for various sizes of tube where the outside diameter was d .

$$\log_{10} \frac{\tau_0 d^2}{4\rho\nu^2} = 0.875 \log_{10} \frac{(P-p_0)d^2}{4\rho\nu^2} - 1.396 \quad (4)$$

In these experiments d was always less than one-tenth of the velocity boundary layer thickness, which is the normal

distance from the boundary surface at which the fluid attains (within 1 or 2%) a velocity equal to that of the main stream. Furthermore, the calibration did not hold for

$$\log_{10} \left\{ \frac{(P - p_0)d^2}{4\rho v^2} \right\} < 5.0 \quad (5)$$

This calibration was confirmed by Sigalla and Painz⁽⁷⁾ who also found that the inside diameter/outside diameter ratio of the total head tube (Preston probe) was not critical between 0.60 and 0.70. This discovery increases the usefulness of Preston's method because such tubing is readily available for making probes.

Other laboratories, with facilities for making independent measurements of the skin friction coefficients, studied the use of Preston probes on flat plates with zero pressure gradients and concluded that the calibration obtained by Preston (equation 4) for pipe flow gave results approximately 12% too low. The revised calibration for flow over flat surfaces given by Bradshaw and Gregory⁽⁸⁾ (equation 6), can also represent experimental data obtained by Smith and Walker.⁽⁹⁾

$$\log_{10} \frac{\tau_0 d^2}{4\rho v^2} = 0.875 \log_{10} \frac{(P - p_0)d^2}{4\rho v^2} - 1.350 \quad (6)$$

Despite the significant difference between equations (4) and (6), the reasons for it are not properly explained. Nevertheless, equation (6) is a useful representation of all data obtained on flat surfaces presently known to or determined by the authors, and is sufficiently accurate for estimating the convective heat transfer to flat surfaces.

The effect of misalignment between the probe and the direction of flow was determined⁽¹⁰⁾ in the B.I.S.R.A. 4 × 8 in. wind tunnel. Correct alignment is obtained when the pressure at the probe is a maximum and, provided the misalignment is less than 5°, the resulting error is less than 2%. Fig. 1 illustrates the response of a Preston probe when misaligned to the flow direction and, for purposes of comparison, the response of a total head tube in a free stream is also shown.

Other experiments showed that for a turbulent boundary layer on a flat plate, with zero pressure gradient along the direction of flow, the outside diameter of the Preston probe can be as large as one-fifth of the velocity boundary layer thickness. The work was then extended⁽³⁾ to include those

flows in which the free stream velocity was not uniform, because this circumstance is frequently encountered in practice. A two-dimensional wall jet was formed (a long

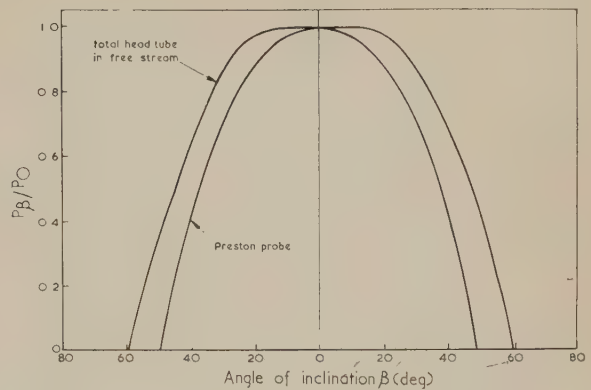


Fig. 1. Effect of yaw on Preston probe pressure

narrow slot, through which air was discharged, with the lower wall continued as a flat plate) to provide a turbulent boundary layer. The local maximum velocity at the limit of this boundary layer decreased along the direction of flow. This system is illustrated in Fig. 2. Two important conclusions were drawn from these studies.

- (i) The skin friction coefficient can be defined in terms of the local maximum stream velocity.
- (ii) Skin friction coefficients measured by Preston's technique when used with the modified Reynolds analogy (equation 2) predict heat transfer coefficients which are in good agreement with direct measurements made elsewhere on a similar apparatus.

Preston's method for flat plates with pressure gradients

In general, because of changes in the cross-section of the system through which the fluid is flowing, pressure gradients will be generated along the boundary walls. A negative or favourable gradient, measured along the direction of flow, is produced if the flow cross-section is reduced, and a positive

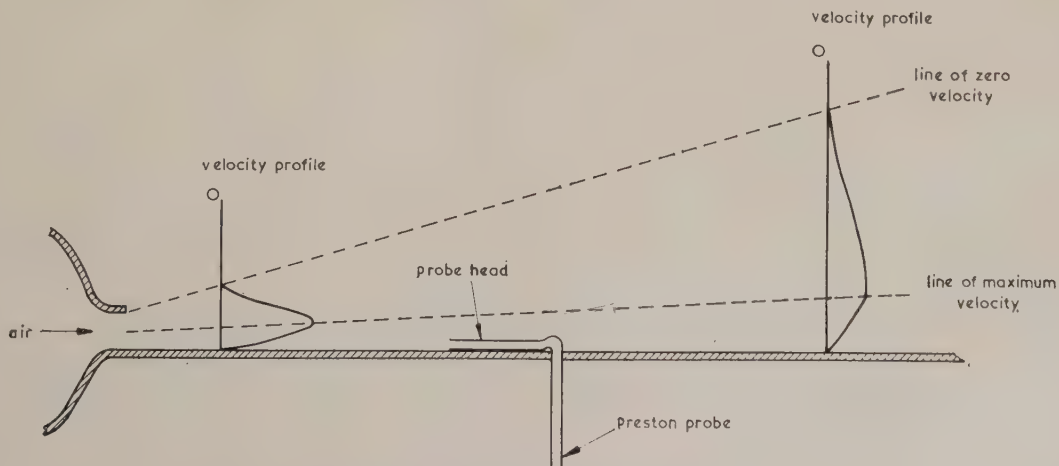


Fig. 2. Wall jet with Preston probe

or adverse gradient if the cross-section is enlarged and the flow velocity is thereby reduced.

It is known that pressure gradients alter the profiles of boundary layers, and this distortion might penetrate sufficiently near to the wall to upset the calibration of the Preston probe. Ultimately, when the flow separates from the wall, the profile is flat and in this circumstance Preston's method must be expected to fail. A brief description of some measurements in boundary layers with pressure gradients and the conclusions to be drawn from them is given below.

A negative pressure gradient was created along the surface of a flat plate by placing opposite to it a baffle, so that the flow was accelerated as it passed from the leading to the trailing edge of the flat test plate. Over a length of 16 in. the cross-section, through which the airstream passed, was approximately halved by a baffle inclination of about 8°.

Pressure gradients, expressed as $(dp/dx) \cdot (2/\rho U_m^2)$, up to 1.7 ft^{-1} were generated.

Independent estimates of the skin friction coefficients were made using a formula proposed by Ludweig and Tillman,⁽¹¹⁾ equation (7) below

$$\tau_0/\rho U_m^2 = 0.123 \times 10^{-0.678H} \times R_\theta^{-0.268} \quad (7)$$

Where

$$H = \delta^*/\theta$$

$$\delta^* = \int_0^\infty \left(1 - \frac{u}{U_m}\right) dy$$

$$\theta = \int_0^\infty \frac{u}{U_m} \left(1 - \frac{u}{U_m}\right) dy$$

$$R_\theta = U_m \theta / \nu$$

It was found that the Preston probe results, used in conjunction with equation (6) give results consistent with the Ludweig and Tillman formula (equation 7) and the authors conclude that Preston's method is applicable for measuring τ_0 on flat plates with negative pressure gradients, at least as large as those obtained during these experiments.

Positive or adverse pressure gradients up to 0.75 ft^{-1} were similarly generated along a flat plate about 36 in. long. At the leading edge the baffle was 1.5 in. from the surface of the test plate, and when inclined at an angle of more than 9° the boundary layer began to separate at about 30 in. from the leading edge. It was found that, at or near to the region of flow separation, the pressure difference between the Preston probe and the wall static pressure tapping ($P - p_0$), was almost independent of the outside diameter of the probe. Thus, it may be seen from equation (6) that this lack of sensitivity sets a practical limitation to the method at or near regions of flow separation.

Throughout these two sets of experiments the ratio of probe outside diameter to the velocity boundary layer thickness was varied. In the favourable pressure gradients it was found that this ratio could be as large as 0.3 without affecting the consistency of the results. In the adverse pressure gradients the rapid growth of the boundary layer made it impracticable to search for an acceptable upper limit of probe diameter, but ratios less than 0.10 gave consistent results.

Recommendations for the construction and use of Preston probes

It cannot yet be claimed that Preston's method is proved to be suitable and general in application, but it is developed

to the stage where it can be usefully employed in aerodynamic models of furnaces and in heat transfer plant, such as a metal recuperator, provided the geometry is simple. In order to assist further experimentation, the methods of selecting and using a probe; based on the experiences obtained in the authors' laboratory, are given below.

Tubing with an inside diameter/outside diameter ratio of about 0.60, but between 0.55 and 0.70, should be used to make the probe and the tip should be finished square and smooth. The head portion, i.e. that lying at right angles to the stem, and facing into the flow along the surface at which τ_0 is to be measured (Fig. 2), should be at least $10d$ long, where d is the outside diameter of the tubing. Static pressure measuring holes in the surface should be located between $3d$ and $5d$, one on either side of the probe head on a line at right angles to the probe direction and passing through the tip of the probe.

An estimate of the velocity boundary layer thickness can be made by moving the probe away from the surface, into the free stream, until the pressure difference between the probe tip and the wall static pressure reaches a maximum. If this distance is less than $10d$ a smaller probe should be used, but if this is impracticable a slightly larger tube can be tried; if this gives the same value of τ_0 the original probe may be safely used.

The free stream velocity U_m is measured by using the probe as an ordinary Pitot tube, and obtaining the difference in pressure between it and the wall static pressure when

$$P - p_0 = \frac{1}{2} \rho U_m^2 \quad (8)$$

To measure τ_0 , replace the probe on the surface and use equation (6) to interpret the pressure signal. The skin friction coefficient, C_f , can then be calculated

$$C_f = \tau_0 / \frac{1}{2} \rho U_m^2 \quad (9)$$

In all cases $\log_{10} \{(P - p_0)d^2/4\rho\nu^2\}$ must be greater than 5.0. The procedure for calculating the convective heat transfer coefficient h has already been described earlier in this paper.

Sources of error

There are three factors of considerable importance to this work which require further investigation. A higher level of turbulence in the free stream increases the values of h and τ_0 above those values determined in the low turbulence flows normally found in a wind tunnel. The effect of surface roughness, provided the irregularities are not sufficient to promote local areas of flow separation, is to increase τ_0 and to a lesser extent, h . However, there are grounds for believing that the interior surfaces of some industrial furnaces are aerodynamically smooth, and consequently the use of Perspex models, which is now firmly established as a means for studying and improving furnace design, is a useful and valid means for employing and extending Preston's method.

The studies reported by Kestin and Maeder,⁽¹²⁾ Sugawara and others⁽¹³⁾ and Smith and Epstein,⁽¹⁴⁾ amongst others, constitute a useful start to the establishment of relationships between free stream turbulence and surface roughness, and skin friction and heat transfer, but they are technically difficult fields to pursue. Unfortunately, much of the available data does not distinguish between local and average values of h and τ_0 , and there also exists the recurrent problem of providing an adequate definition of surface roughness.

With the exception of the original calibration studies^(4, 6)

on the interior surfaces of pipes, all succeeding studies have been made at flat surfaces. Provided the radius of curvature of a surface is large compared with the probe diameter, say 500 to 1000 d , the authors would not expect great difficulty in taking and interpreting measurements. However, it would be useful to pursue some studies of flow over singly curved surfaces to determine how far the present work, which has been confined to two-dimensional flows, can be applied.

Conclusions

(i) Present knowledge and experience of the Reynolds analogy combined with the extended calibration of Preston's method for measuring skin friction, provide a practical, if limited, means for determining local coefficients of convective heat transfer.

(ii) This technique is particularly appropriate for use in Perspex models of industrial furnaces and heat transfer equipment of simple geometry.

(iii) More studies are required of the effects of free stream turbulence, surface roughness and surface curvature on the processes of heat and momentum transfer between a fluid stream and its bounding surface.

References

- (1) SPALDING, D. B. *J. Fluid Mechanics*, **4**, pp. 22-32 (1958).
- (2) SPARROW, E. M. *J. Fluid Mechanics*, **4**, pp. 321-9 (1958).
- (3) SIGALLA, A. *Aircraft Engng*, **30**, pp. 131-4 (1958).
- (4) PRESTON, J. H. *J. Royal Aero. Soc.*, **58**, pp. 109-21 (1954).
- (5) GRANVILLE, R. A., and SIGALLA, A. *Research*, **11**, pp. 326-8 (1958).
- (6) RUBESIN, M. W. *N.A.C.A., T.N.*, p. 2917 (1953).
- (7) SIGALLA, A., and PAINZ, W. *B.I.S.R.A. Report P/5/57*. Unpublished.
- (8) BRADSHAW, P., and GREGORY, N. *A.R.C.*, **20**, 199 *F.M.*, 2684 (1958).
- (9) SMITH, P. W., and WALKER, J. H. *N.A.C.A., T.N.*, 4321 (1958).
- (10) SIGALLA, A. *B.I.S.R.A. Report P/2/58*. Unpublished.
- (11) LUDWEIG, H., and TILLMAN, W. *N.A.C.A., T.M.*, 1285.
- (12) KESTIN, J., and MAEDER, P. F. *N.A.C.A., T.N.*, 4018 (1957).
- (13) SUGAWARA, SATO, KOMATSU, and OSAKA., *N.A.C.A., T.M.*, p. 1441 (1958).
- (14) SMITH, J. W., and EPSTEIN, N. *J.A.I.Ch.E.*, pp. 242-8, June (1957).

Determination of preferred orientation in polycrystalline metal foils using a sputtering technique

by R. S. NELSON, B.Sc., Metallurgy Division, A.E.R.E., Harwell, Berkshire

[Paper first received 4 May, and in final form 23 June, 1960]

Abstract

The preferred crystal orientation of metal foils has been qualitatively analysed by observing the pattern produced when atoms sputtered from the surface in a gas discharge are collected on a plate.

WHEN polycrystalline metal specimens with random grain orientation are subjected to positive-ion bombardment in a gas discharge, atoms are sputtered from the surface in random directions. It has been observed by Wehner* that the sputtered deposits from single crystals show definite symmetrical patterns. These patterns are due to the preferential ejection of atoms in the direction of the close-packed lines, for example in a face-centred cubic structure, ejection occurs along the [110] directions of the crystal. This preferential ejection has been used for the determination of preferred crystal orientation in polycrystalline metal foils. A diagram of the apparatus is shown in Fig. 1.

* WEHNER, G. K. *Phys. Rev.*, **102**, p. 690 (1956).

An electrical discharge was passed in argon in such a way that the specimen under investigation was bombarded with

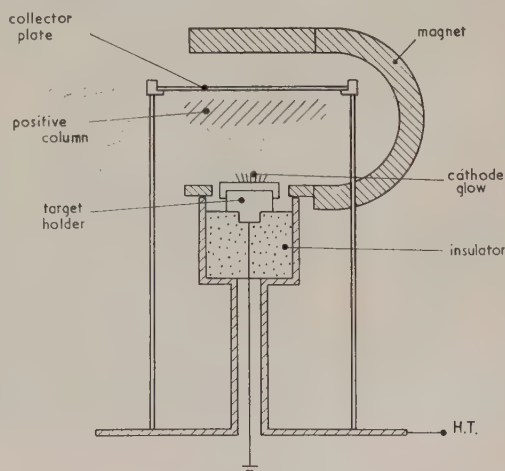


Fig. 1. Apparatus

positive ions. The specimen was mounted in a Dural target holder of $\frac{1}{2}$ in. diameter which acted as the cathode. Dural, which is not readily sputtered, was chosen in order that the deposit sputtered from the target would not be obscured by that from the holder. A 2-in. diameter disk of white glazed card held at a distance of 1 in. from the target was used to collect the sputtered deposit. This was easily discernible against the white background. For meaningful deposits, it was necessary that the mean free path of the sputtered atoms should be greater than the separation between target and collector. This condition required a pressure of a few microns and in order to maintain a discharge at this pressure a magnetic field was used to increase the ion density (Penning and Moubis.)* A permanent magnet, acting as an anode and

with pole pieces cut away as shown, produced this field in the target region. The localized magnetic field together with the geometrical arrangement of anode and cathode confined the discharge to the target region, thus reducing the h.t. power consumption. With this arrangement it was possible to maintain a 2 kV discharge in argon at pressures as low as 1μ with ion currents of about $500 \mu\text{A}$.

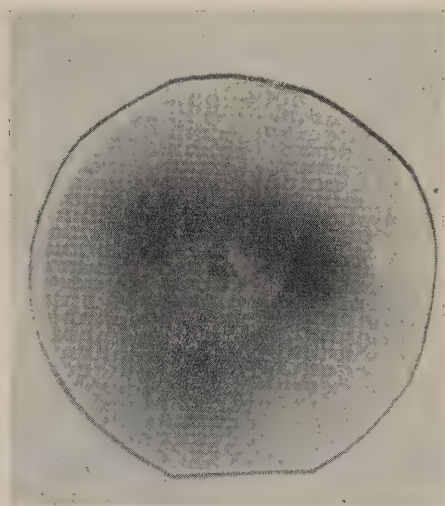
The method has so far been applied to the following metals silver, gold, copper, palladium and rhodium. These have a wide range of sputtering rates in argon, and clear visible deposits were observed after the times indicated in the table

Approximate sputtering times for a visible deposit in an argon discharge of about $500 \mu\text{A}$

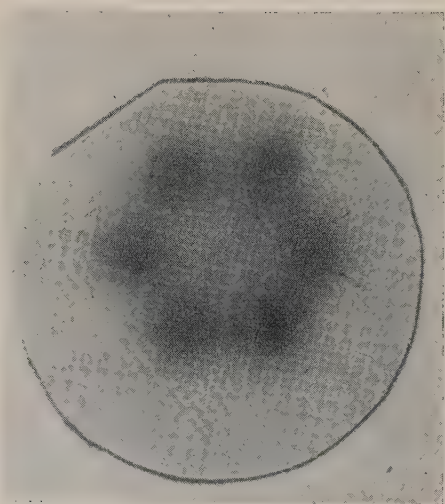
Metal	Time for visible deposit (min)
Ag	1
Au	3
Cu	5
Pd	25
Rh	40

Fig. 2 shows the sputtered deposits from gold foils prepared by evaporation on lithium-fluoride crystal substrates at a temperature of 550°C . Laue X-ray diffraction patterns indicated that such foils were composed of small crystals or crystallites which had strongly preferred orientation. Fig. 2(a) shows the pattern of three spots obtained from a foil which had a pole figure corresponding to the $\{111\}$ planes lying in the surface. Fig. 2(b) shows a deposit in which the six symmetrically arranged spots now correspond to a mixture of two preferred orientations, such that the gold was deposited with the $\{111\}$ planes in contact with the substrate and the $[101]$ directions in the two orientations making an angle of 180° with each other. Characteristic patterns were obtained for other preferred orientations, for example, an orthogonal pattern of four spots was given by a crystal having $\{100\}$ planes in the surface. A specimen with no preferred orientation produced a deposit with maximum intensity at the centre and falling off symmetrically towards the edges.

Fig. 3 shows the sputtered pattern of a textured gold foil which was prepared by rolling, with subsequent annealing at 850°C for three hours. This resulted in a preferred orienta-



(a)



(b)

Fig. 2. Sputtered deposits from gold foil prepared by evaporation. (a) Three spots; (b) Six symmetrically arranged spots

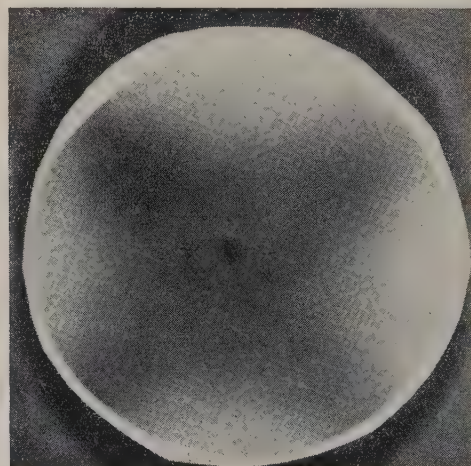


Fig. 3. Sputtered pattern of a textured gold foil prepared by rolling and subsequent annealing

* PENNING, F. M., and MOUBIS, J. H. A. *Koninkl. Ned. Akad. Wetenschap. Proc.*, **43**, p. 41 (1940).

ion with the $\{100\}$ planes in the surface and the $[001]$ direction in the rolling direction. The pattern, which takes the form of a diffuse cross, indicates this orientation together with a random background corresponding to the unoriented grains of the foil.

Though this method of determining preferred orientations

lacks the precision of X-ray or electron diffraction techniques, it has the advantages of being both simple and rapid.

Acknowledgement

The author wishes to thank Mr. M. W. Thompson for many useful discussions concerning the work.

CORRESPONDENCE

On the nature of whiskers

During his investigations in 1953 on the growth of mercury whiskers from the vapour phase, G. W. Sears⁽¹⁾ came to the conclusion that whiskers are monocrystals containing a single axial screw-dislocation. He eventually developed⁽²⁾ a theory of the growth of whiskers from the vapour phase; his theory was in qualitative agreement with the experimental result.

Screw dislocations determine both the usual habit of whiskers and the mechanism of their growth. Experimental attempts to prove the existence of axial screw-dislocations have been rather unsuccessful, however, and the problem needs further investigation. In many cases X-ray experiments and decoration techniques have not revealed single axial screw-dislocations in whiskers.

Observations on whiskers in the field emission microscope^(3, 4) have revealed effects connected with the existence of axial screw-dislocations in only a few per cent of the number of whiskers investigated. "Eshelby twist" i.e. the rotation of the field emission pattern after partial pull-off of the whiskers, however, has been observed in some instances^(4, 5); this effect had not been observed in the earlier experiments.⁽³⁾

The best method suitable for the investigation of the structure of whiskers is field ion microscopy^(6, 7). Etch

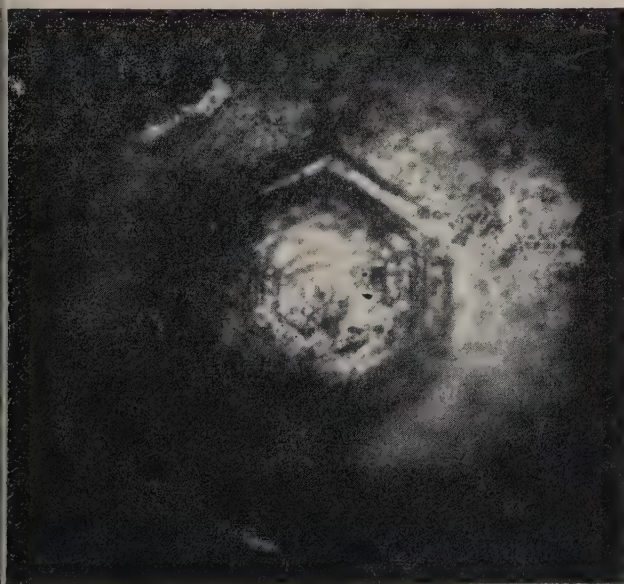


Fig. 1. Etch-figure in the centre of the section of an $80\ \mu$ whisker of Si with single axial screw dislocation. Magn. $\times 900$

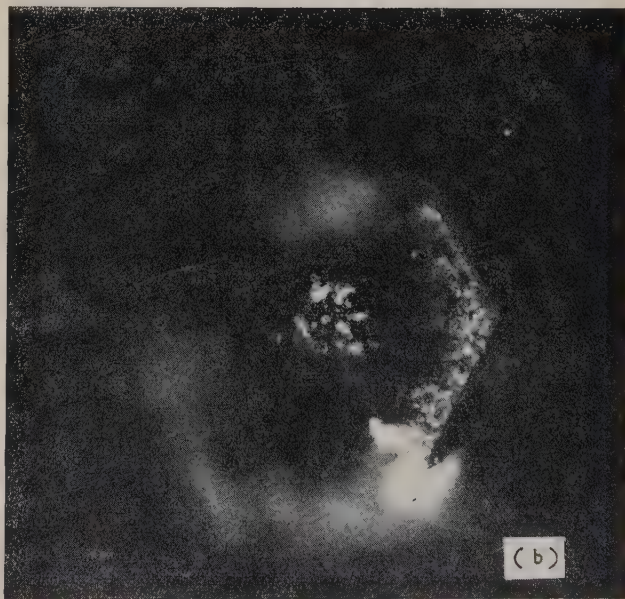
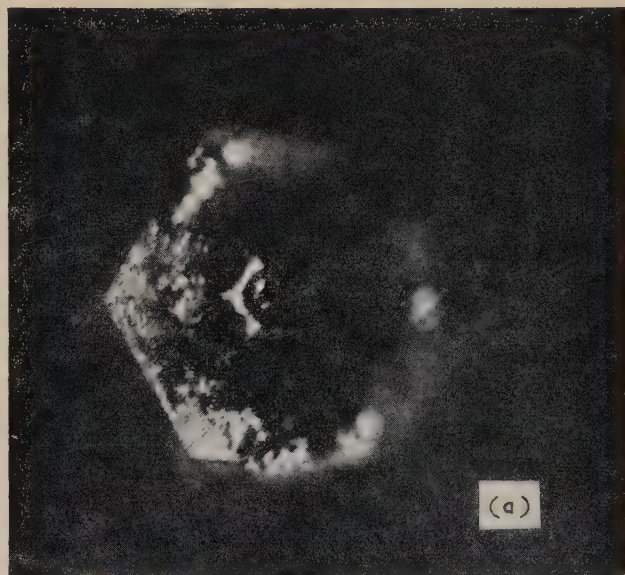


Fig. 2. Etch-figures of $80\ \mu$ Si whiskers shown in (a) and (b) with repeating structures of concentric cores. Magn. $\times 200$

methods permit investigation of the transverse section of the whiskers and provide new facts concerning the structure of whiskers and the mechanism of their growth. R. V. Coleman⁽⁸⁾ has applied these to reveal axial screw-dislocations in metal whiskers.

A special technique for the polishing and etching of the transverse-section of whiskers has been developed in our laboratory. Fig. 1 shows the transverse section of Si whiskers after treatment with the Dash etch.⁽⁹⁾ The radial dimensions of the whiskers are about $80\ \mu$ and they were obtained by reduction of SiCl_4 with zinc⁽¹⁰⁾. The typical etch-pattern in the centre of the section proves the existence of a single screw dislocation in the whisker under investigation. This fact serves also to indicate that analogous etch-figures often observed on the surface of macro-crystals are true images of screw dislocations.

Figs 2(a) and 2(b) represent the etch-pattern of other Si whiskers with similar radial dimensions, i.e. about $80\ \mu$. It is rather difficult to interpret these patterns on the basis of the existing theory of whisker growth. The hexagonal transverse sections of the whiskers in question, similar to the section in Fig. 1, before etching, have not revealed the expected single screw-dislocation even after 12 h etching, but a concentric core structure is observed. Fig. 3 shows the longitudinal section of the structure of such a core after partial etching away of the outer parts of the whisker.

Further investigations are in progress.



Fig. 3. Structure of the inner core of one of the whiskers after partial etching away of the outer layers. Longitudinal section. Magn. $\times 200$

The authors are grateful to Professor J. Mazur for his encouragement and to R. Bernadzikowski and J. Rafalowicz for their assistance in preparation of the whiskers.

Low-Temperature Laboratory,
Polish Academy of Sciences,
Wroclaw,
Poland.

A. GROHMAN
J. KRYLOW
[25 May, 1960]

REFERENCES

- (1) SEARS, G. W. *Acta Met.*, **1**, p. 457 (1953).
- (2) SEARS, G. W. *Acta Met.*, **3**, p. 361 (1955),
Acta Met., **3**, p. 367 (1955).
- (3) GOMER, R. J. *Chem. Phys.*, **28**, p. 457 (1958).
- (4) SIROTIENKO, J. G., SPIWAK, G. B. and GROHMAN, A. (in the press).
- (5) ESHELBY, J. D. *J. Appl. Phys.*, **24**, p. 176 (1953).
- (6) MULLER, E. W. *J. Appl. Phys.*, **24**, p. 176 (1959).
- (7) NIKLIBORC, J., GROHMAN, A., LENKOW, W. and WORKOWSKI, G. (to be published).
- (8) COLEMAN, R. V. *J. Appl. Phys.*, **29**, p. 1487 (1958).
- (9) DASH, W. C. *J. Appl. Phys.*, **30**, p. 459 (1959).
- (10) LYON, D. W., OLSON, C. M., and LEWIS, E. D. *Trans. Electrochem. Soc.*, **96**, p. 359 (1949).

Dynamic measurement of elasticity using resonance methods

The use of dynamic methods for measuring elasticity has much to recommend it,⁽¹⁾ for the specimens may be very small, weighing only a small fraction of a gram, and the frequencies used, often of the order of 100 kc/s, can be measured by counting techniques to an accuracy of one part in a million. Many of the resonance techniques employed in the past have, however, been unduly complicated; for instance, the composite resonator technique⁽²⁻⁵⁾ requires the cementing of the specimen to the electromechanical transducer, often of quartz, though barium titanate and piezomagnetic materials have been employed. Except in rare and fortunate circumstances, or when low accuracy is tolerable, this join, even though prepared with great care, needs to be made near a stress node, and therefore the length of the specimen must be accurately related to that of the transducer, a requirement causing much additional labour and one not met when conditions, for example, temperature, are varied widely.

These considerations have been surveyed⁽⁶⁾ by the writer and the purpose of the present communication is to draw attention to the alternative system of exciting and detecting resonance by means of tenuous magnetostrictive transducers, a system often shown at these Laboratories during the last ten years, but still not in very widespread use. Adapted from an early T.R.E. magnetostrictive⁽⁷⁾ device, Stanford^(8,9) about 1950 (as a result of discussion with the writer, Mr. D. O. Sproule and others) adopted this system for longitudinal resonance, and about the same time the writer⁽¹⁰⁾ modified it for torsional resonance.⁽¹¹⁾

The early methods which we employed up to 1953,^(12,13) shown at *A* and *B* of the figure, gave valuable information on the longitudinal and torsional elasticity of brittle iron in the temperature range -240 to $+1000^\circ\text{C}$, for this was a material on which a simple spot-welding technique for fixing the wires was adequate. But the welding or cementing of the magnetostrictive tube or wire was troublesome and methods such as *C* and *G* were therefore evolved. These have since been used up to temperatures exceeding 1000°C to test such materials as pure iron, sintered alumina, nimonic titanium and fused quartz.

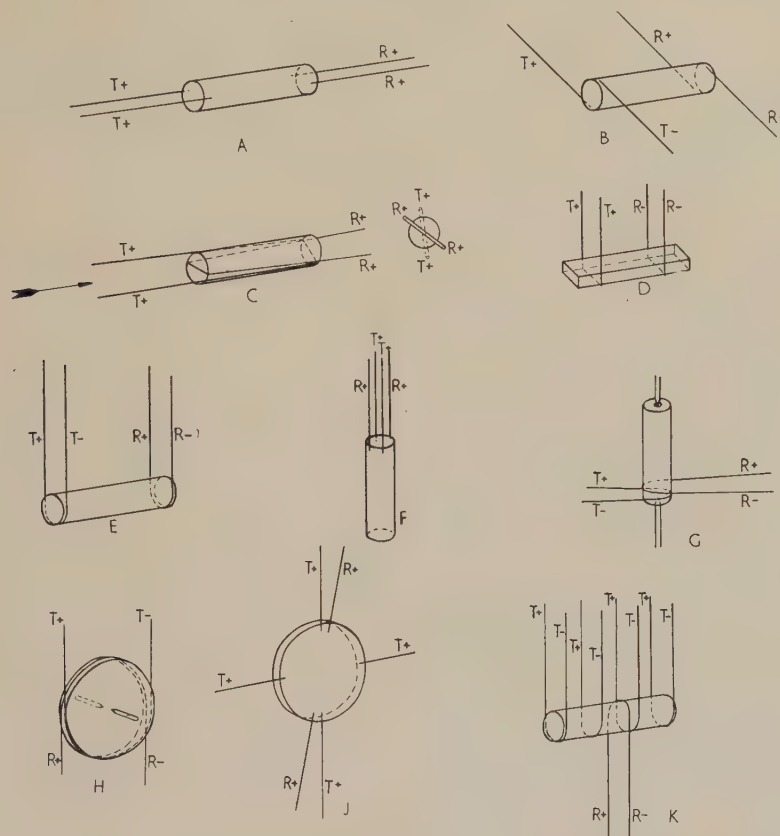
E and *F* are simple variants of *G* and *D*, the former being much used here for highly accurate torsional resonance testing, while *D* has been used for resonance tests in bending; it has points of similarity with the so-called "jiggling" methods of various investigators⁽¹⁴⁻¹⁷⁾ using, for example, asbestos string, though our method, by acoustically matching the terminations of the threads, avoids the errors which can arise from the standing waves. Method *J* enables the modulus $E/(1 - \sigma^2)$ to be measured with the disk in radial resonance,⁽¹⁸⁾ and *H* can excite disks into tangential resonance both for isotropic materials and also for anisotropic materials where, in the latter case, the elasticity has circular symmetry.

about the axis of the specimen; method *K* could be similarly employed for rods.

Apart from the great advantage which these methods possess of avoiding the trouble of welding or cementing to the specimen, they also have the additional advantage that the transducers can be located at room temperature outside the high- or low-temperature region in which the specimens

atmosphere, these modifications should enable measurements of elasticity to be carried out at temperatures well over 2000° C.

These tenuous magnetostrictive transducers have been employed for elasticity measurements at pressures up to 1500 atmospheres, the torsionally resonating specimens and the transducers being immersed in the pressure liquid. The



Methods of using tenuous magnetostrictive transducers to measure elasticity dynamically

The magnetostrictive wires or tubes are marked T_+T_+ and R_+R_+ for transmitters and receivers respectively where the pair is in phase and T_+T_- and R_+R_- when the pair is out of phase. *A*, *C* and *F* are for measuring Young's modulus (*E*) or $(1/s_{33})$. (Wires in *F* can be looped under specimen and splayed as in *C*). *B*, *E* and *G* are for measuring modulus of rigidity (*G*) or $(1/s_{44})$. *H* and *K* are for measuring *G* or $(1/s_{66})$.

J is for measuring $E/(1 - \sigma^2)$, where σ is Poisson's ratio

are situated; temperature-resistant wires like nichrome can be welded to the magnetostrictive wires to take the vibrations into and from the specimen.

One other advantage is noteworthy: the wide frequency range of these transducers. The type already illustrated in 1954 (Fig. 10, Ref. 19) operates reasonably well from 30 kc/s to over 300 kc/s. Because of this we only require three or four equipments for testing by resonance specimens as diverse as concrete or rock bars a few feet long (at a few kilocycles), specimens of coal or plastic and specimens a few millimeters long (at about a megacycle⁽²⁰⁾).

More complicated arrangements using directional couplers and alternatively an electromechanical bridge⁽¹³⁾ have been employed to enable a single thread to be used not only to support the specimen but also to act both for transmitting and receiving the vibrations; if the extension wire of nichrome be replaced by tungsten surrounded by a neutral or reducing

increase in the damping observed suggests that the device could be used for measuring the viscosity of liquids at high pressures.

The work described in this letter is part of the research programme of the National Physical Laboratory and is published by permission of the Director.

G. BRADFIELD

(Submitted in June 1957 and accepted in revised form July 1960)

National Physical Laboratory
Teddington
Middlesex.

REFERENCES

- (1) BRADFIELD, G. *Proc. Third International Congress on Acoustics, Stuttgart* (1959); *Elsevier* (Amsterdam) (1960).

- (2) QUIMBY, S. L. *Phys. Rev.*, **25**, p. 558 (1925).
- (3) BALAMUTH, L. *Phys. Rev.*, **45**, p. 715 (1934).
- (4) NOWICK, A. S. *Phys. Rev.*, **80**, p. 249 (1950).
- (5) SUTTON, P. M. *Phys. Rev.*, **91**, p. 816 (1953).
- (6) BRADFIELD, G. *The Physical Examination of Metals*, Edited by Chalmers and Quarrell, Chap. XI, Arnold (London, 1960).
- (7) BRADFIELD, G. *Electronic Engng*, **20**, p. 74 (1948).
- (8) STANFORD, E. G. *Nuovo Cimento*, **7**, Suppl. 2, Ser. 9, p. 332 (1950).
- (9) STANFORD, E. G. *Research*, **6**, p. 21 (1953).
- (10) BRADFIELD, G. *Second Interim Memorandum Concerning Elastic Constants of Dilute Copper Alloys (with elements of B sub-group)*, National Physical Laboratory Memorandum No. PHYS/UE (1951).
- (11) LOCKSPEISER, SIR B. *Engineer*, **191**, p. 318 (1951).
- (12) Contribution by National Physical Laboratory, *Nature*, **170**, p. 527 (1952).
- (13) BRADFIELD, G. *Measurement of Elastic Constants*, National Physical Laboratory Memorandum, PHYS/U.8 (1952).
- (14) FÖRSTER, F. *Zeits. f Metallkunde*, **29**, p. 109 (1937).
- (15) KÖSTER, W. *Zeits. f Metallkunde*, **35**, pp. 57, 194 (1943).
- (16) ROBERTS, M. H., and NORTCLIFFE, J. *J. Brit. Iron and Steel Inst.*, **157**, p. 345 (1947).
- (17) ANDREWS, C. W. *Metal Progress*, **58**, p. 85 (1950).
- (18) LOVE, A. E. H. *Mathematical Theory of Elasticity*, 4th Ed., p. 498 (New York: Dover Publications, 1944).
- (19) BRADFIELD, G. *Acustica*, **4**, p. 171 (1954).
- (20) BRADFIELD, G. *Proc. Instn Elect. Engrs*, **104** Pt. B, Suppl. 7, p. 558 (1957).

NOTES AND NEWS

Notes and comments

The Royal Society's Fair Copying Declaration

The Institute and Society, in common with more than 70 other scientific and learned societies, has subscribed to the Royal Society's Declaration on Fair Copying which reads as follows:—

We will regard it as fair dealing for the purpose of private study or research when a non-profit-making organization, such as a library, archives office, museum or information service, owning or handling scientific or technical periodicals published by us makes and delivers a single reproduction of a part of an issue thereof to a person or his agent representing in writing that he desires such reproduction in lieu of a loan or manual transcription and that he requires it solely for the purpose of private study, research criticism or review, and that he undertakes not to sell or reproduce for publication the copy supplied, provided:

1. The recipient of the copy is given notice that he is liable for infringement of copyright by misuse of the copy, and that it is illegal to use the copy for any further reproduction.
2. The organization making and furnishing the copy does so without profit to itself.
3. Proper acknowledgement is given to the publication from which the copy is made.
4. Not more than one copy of any one excerpt shall be furnished to any one person.

The exemption from liability of the library, archives office, museum or information service herein provided shall extend to every officer, agent or employee of such organization in the making and delivery of such reproduction when acting within the scope of his authority of employment. This

exemption for the organization itself carries with it responsibility to see that employees caution those receiving copies against the misuse of material reproduced.

We reserve the right to take action against any person or organization copying or misusing for any purpose whatever the whole or part of a work published by us without abiding by the conditions laid down herein unless the person or organization has our special permission in respect of the item to be copied.

We reserve the right to withdraw this declaration.

Journal of Scientific Instruments

Contents of the October issue

PAPERS

- Magnetic probes of high frequency response. By S. E. Segre and J. E. Allen.
 Transistorized frequency stabilization for reflex klystrons used in magnetic resonance. P. Jung.
 Cyclic shearing interferometer. By P. Hariharan and D. Sen.
 Automatic range-changing of a linear ratemeter. By S. Lovett.
 Production of a pulsed magnetic field using an electrolytic capacitor bank. By D. G. Bate and R. F. Saxe.
 Transformer bridges for use with resistance strain gauges and similar transducers. By L. N. Clarke.
 Production of millimicrosecond current pulses using a pressurized spark gap. By J. H. Adlam and L. S. Holmes.
 Electronic apparatus for the study of X-rays with proportional counter. By N. Patla.
 An X-ray fluorescence method for determination of the transition-metal content in very small specimens of alloys. By P. J. Brown.

LABORATORY AND WORKSHOP NOTES

- Pyrolytic coating of quartz and ceramic vessels used for zone melting. By R. Beels and W. De Sutter.
 Furnace for the uniform heating and mixing of powders in controlled atmospheres. By H. Monk and F. F. Kierys.
 Frequency stabilization of klystrons. By M. J. A. Smith.
 Oscillating flat-specimen holder for an X-ray powder camera. By J. D. Wilkinson and L. D. Calvert.

THIS JOURNAL is produced monthly by The Institute of Physics and the Physical Society, in London. It deals with all branches of applied physics (including theory and technique). All rights reserved. Responsibility for the statements contained herein attaches only to the writers.

EDITORIAL MATTER. Communications concerning editorial matter should be addressed to the Editor, The Institute of Physics and The Physical Society, 1 Lowther Gardens, Prince Consort Road, London, S.W.7. (Telephone: Kensington 0048.) Prospective authors are invited to prepare their scripts in accordance with the *Notes for Authors*.

REPRODUCTION. The Institute of Physics and The Physical Society is a signatory to The Royal Society's Fair Copying Declaration. Details may be obtained upon application from The Royal Society, London, W.1.

ADVERTISEMENTS. Communications concerning advertisements should be addressed to the agents, Messrs. George Jackson (Fleet St.) Ltd., Cliffords Inn, Fleet Street, London, E.C.4. (Telephone: Holborn 3611-2.)

SUBSCRIPTION RATES. A new volume commences each January. The charge is £6 per volume (\$17 U.S.A.), including index (post paid), payable in advance. Single parts, so far as available, may be purchased at 12s. 6d. each (\$1.75 U.S.A.), post paid, cash with order. Orders should be sent to The Institute of Physics and The Physical Society, 47 Belgrave Square, London, S.W.1, or to any bookseller.

CLAIMS FOR MISSING JOURNALS. Claims from regular subscribers to this *Journal* for missing numbers will only be considered if received within 60 days of the date of mailing plus normal outward time of transit and time for lodging the claim. Losses attributable to failure to notify a change of address or to similar omissions will not be considered.

Summarized proceedings of a conference on the borders of X-ray analysis—Reading, April, 1960

The Annual Spring Conference of the X-ray Analysis Group of The Institute of Physics was held at the University of Reading, on 8 and 9 April, 1960. The papers and discussions ranged over a number of subjects including neutron and electron diffraction, X-ray emission spectroscopy and X-ray micro-analysis.

THE conference was opened under the chairmanship of Dr. C. W. BUNN (Imperial Chemical Industries Ltd., Welwyn Garden City). Dr. W. COCHRAN (University of Cambridge) read the first paper on neutron spectroscopy and the lattice dynamics of crystals. The inelastic scattering of thermal neutrons (λ in the range 1 to 4 Å) is closely analogous to X-ray diffuse scattering. The most important difference between the two types of scattering is that for X-rays the fractional change in frequency is extremely small (of the order of 10^{-5}), whereas in the neutron case, with the energy of a neutron comparable with a quantum of lattice vibrational energy, the change in frequency may be quite large. By measuring the intensity of the scattered neutron beam as a function of both frequency and angle, it is possible to derive the dispersion relationship between the frequency and wave number of the normal modes of vibration of the crystal and hence, in principle, to deduce the force constants between the atoms.

Experiments have been carried out by Brockhouse's group^(1, 2) at Chalk River, Canada, on a number of cubic crystals using the experimental arrangement shown in Fig. 1.

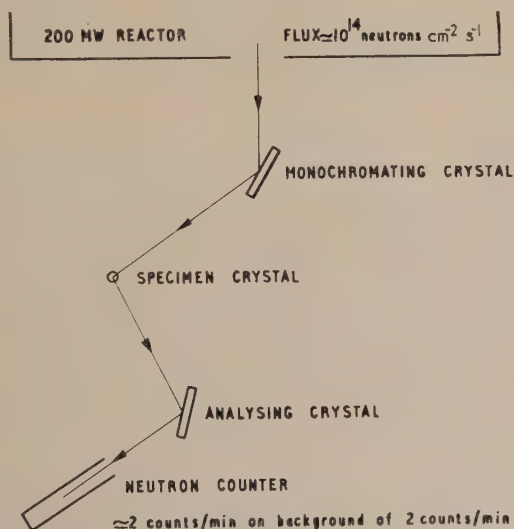


Fig. 1. Schematic layout of arrangement at Chalk River for neutron inelastic scattering experiments

In interpreting the results for sodium iodide the forces taken into account were (a) the Coulomb interaction between ions, (b) the repulsion of nearest neighbours due to the overlap of closed electron shells, and (c) forces arising from the polarization of the iodine atoms. The dispersion curve

calculated on this model was in good agreement with that observed.

In reply to a question by Dr. R. W. CAHN (University of Birmingham), Dr. Cochran stated that work had been confined to cubic crystals and so no anisotropic Debye-Waller factors had yet been derived. Dr. BUNN commented that in solution-grown crystals of some polymers the chain molecules are folded at regular intervals of about 100 Å. He asked whether the method of neutron inelastic scattering could be used to investigate the suggestion that the folding was due to the increase of the amplitude of vibration with chain length, leading to structural instability at a critical length. Dr. Cochran replied that the method could be used in principle, but would be difficult to apply because of the high incoherent scattering from hydrogen.

The next paper dealt with the magnetic scattering of neutrons^(3, 4) and was read by Mr. R. D. LOWDE (Atomic Energy Research Establishment, Harwell). The neutron possesses a magnetic moment and will be scattered by the spatial distribution of unpaired spins in the atoms of a magnetic material. In this way a selected portion of the electron density distribution can be studied. The magnetic contribution to the scattering can be isolated from the nuclear part by studying either the spatial dependence of the intensity, the magnetization dependence or the temperature dependence. A further method is to use a polarized neutron beam to study the difference in total scattering for the two spin states of the neutron.

A number of different magnetic phenomena have been investigated. Direct evidence has been obtained for a spiral arrangement of the unpaired spins in MnAu_2 .⁽⁵⁾ Critical scattering at the Curie temperature has been observed in a number of ferromagnetic materials.⁽⁶⁾ Experiments on the diffuse scattering from 3d-transition-element alloys have shown that, in a wide range of materials, a magnetic atom placed in the lattice of another magnetic element tends to retain its own characteristic magnetic moment.⁽⁷⁾ This has stimulated theoretical work, seeking to explain the magnetic properties of 3d transition elements on the basis of localized ionic 3d wave functions. There has also been much interest in the measurement of magnetic form factors, which are related to the spatial distribution of electron spins on an atom.

Given a sufficient degree of localization of the unpaired electrons, a spin system will sustain a type of excitation known as a spin wave, which is a periodic disturbance of the spins analogous to a sound wave. Spin waves have been observed in an antiferromagnetic material,⁽⁸⁾ a ferrite⁽⁹⁾ and in a metallic ferromagnet.⁽¹⁰⁾ The exchange integral, describing the magnetic coupling between atoms, can be derived from measurements of the intensity of neutrons scattered by these spin waves.

In the next contribution Dr. T. B. RYMER (University of Reading) discussed the measurement of intensities of electron diffraction patterns. Photographic measurements were made of the integrated intensities of diffraction rings from specimens of gold, aluminium and lithium fluoride prepared by vacuum deposition. The intensity of the undiffracted central beam

was also measured. Because of the great difference in intensity of the central and the diffracted beams, it was found necessary to make a double exposure. An exposure of about 10 s served to record the diffraction rings. A second exposure of 10 ms was then made on the same plate; during this exposure the whole trace was moved across the plate in a sinusoidal curve by means of electrostatic deflexion. The diffraction rings had negligible photographic effect during the second exposure, but the central spot produced a trace suitable for microphotometry.

According to the kinematical theory, the integrated intensity of a diffraction ring is proportional to $\mu\phi^2d$, where ϕ is the Fourier potential coefficient, μ the multiplicity factor and d the interplanar spacing. The dynamical theory gives an intensity proportional to $\mu\phi d$. It was found that gold, which has large potential coefficients, satisfies the dynamical theory; lithium fluoride, with very small coefficients, satisfies the kinematic theory; and aluminium, with medium coefficients, gives results intermediate between those of the two theories. Further measurements of the diffraction patterns from gold showed that the intensities of the diffraction rings were proportional to the specimen thickness and attained the values predicted by the dynamical theory for specimen thicknesses of about 3000 Å. This showed that the average number of crystals in the thickness of the film was unity and that there must have been a considerable quantity of amorphous material in the film.

If the crystallites in a specimen have a fibre axis normal to the specimen plane, the diffraction ring intensity I is a function of $Z = \sin \alpha \cos \phi$, where ϕ is the azimuth of a point on the diffraction pattern measured from the projection of the specimen normal to the photographic plate and α is the angle between the electron beam and the normal to the specimen. If the experimental $I = f(z)$ curve is extrapolated to cover the range of z from -1 to $+1$, the area under it is twice the intensity for a randomly oriented specimen, and in this way intensity measurements can be made on oriented samples.

The last paper in the session, by Prof. M. BLACKMAN and Dr. A. E. CURZON (Imperial College of Science and Technology, London), was read by Dr. Curzon and dealt with the effect of size on the melting point of small crystals. Takagi⁽¹¹⁾ has studied this effect for crystals (radii 100 Å) of bismuth, lead and tin by an electron diffraction method. In his experiments no information was obtained on the distribution of crystallite radii, although this is important in the interpretation of the results.

In the experiments conducted by the authors^(12, 13) the crystallites were obtained by condensing tin on to a carbon film, which was then mounted in a furnace inside an electron diffraction camera. The apparatus was designed to enable the transmission diffraction pattern to be studied as the specimen was heated. All the tin had melted at 212°C, although the melting point of bulk tin is 232°C. The melting point was not sharp but could be determined to $\pm 3^\circ\text{C}$. The distribution of crystallite radii, measured with an electron microscope, was found to be roughly Gaussian. Since the number of irregularly shaped crystallites increased as the average diameter increased beyond 100 Å, the diameter of the crystallites was restricted to an average value of 40–100 Å by altering the amount of material evaporated.

As the temperature increased during the experiment the smaller crystallites melted first and a diffraction pattern was formed, consisting of diffuse haloes superimposed on the sharp diffraction rings of the solid. Let T_m be the temperature at which the diffuse scattering completely masks the sharp

rings, and r_m the maximum radius of particle melted at this temperature. It was assumed that 80% of the particles had radii $r \leq r_m$; the interpretation was not radically altered if 70 or 90% was selected instead of 80%.

On the basis of the simple theory given by Takagi it can be shown that

$$\frac{T_\infty - T_m}{T_\infty} = \frac{1}{\rho_1 L_{12}} \cdot \frac{2\sigma}{r_m} \quad (1)$$

where T_∞ = melting point in °K of bulk tin

T_m = melting point of the tin particle

ρ_1 = density of solid tin

L_{12} = latent heat of tin

σ = surface free energy per square centimetre of the interface between solid and liquid tin

r_m = radius of the tin particle.

Several assumptions which were not strictly valid for the crystallites were used in deriving equation (1). Nevertheless it should give a semi-quantitative description of the experiments and, in fact, a plot of T_m versus $1/r_m$ was a straight line. From the slope, a value of $\sigma = 73 \pm 7 \text{ erg/cm}^2$ was derived. The value obtained from Takagi's experiments was $\sigma = 66 \text{ erg/cm}^2$. These two results do not agree with the values obtained from supercooling experiments on tin by Vonnegut,⁽¹⁴⁾ $\sigma = 54.5 \text{ erg/cm}^2$, and by Pound and La Mer,⁽¹⁵⁾ $\sigma = 58.5 \text{ erg/cm}^2$, the discrepancies probably being due to simplifications in both the theory of size dependence and the nucleation theory of solidification.

Next a group of four papers was read on the subjects of X-ray microscopy and X-ray microanalysis. Dr. W. C. NIXON (University of Cambridge) described the design of an apparatus. If the principles of electron optics are applied to the design of microfocus X-ray tubes, a loading approach of 100 kW/mm² can be achieved for a 1–2 μ X-ray source. This high X-ray output per unit target area can be used for contact microscopy or for microscopy by projection, with fluorescent screen viewing and photographic recording. Absorption analysis can be carried out by measuring the density of the photographic negative, or by direct detection of the incident and partially absorbed beams with an X-ray counter.

When the electron beam strikes the specimen itself, rather than an intervening target, the emitted X-rays can be analysed with a crystal spectrometer to give the composition of the specimen. An instrument based on these lines was first designed by Castaing and Guinier.⁽¹⁶⁾ Subsequent improvements have included the development of scanning techniques, which allow the direct formation of images of selected small areas. The wavelength of the characteristic X-rays increases as the atomic number of the emitting element falls; owing to the difficulty of working at long wavelengths, elements with atomic numbers less than twelve cannot be analysed at present, but attempts are being made to overcome this limitation.

Dr. P. DUNCUMB (Tube Investments Ltd., Hinxton Hall) described some metallurgical applications of X-ray microscopy. The contact method of microradiography has been extensively used to give information on the microstructures and chemical composition of metal specimens. In the projection method highly divergent beams of X-rays from a projection microscope have been used in two distinct ways: (1) to study the internal structure of a metal sample by absorption contrast, and (2) to determine the lattice parameters and the degree of perfection of the crystal from the diffraction pattern of excess and deficient cones of X-rays.

Both these features have been of value in the study of beryllium.⁽¹⁷⁾

Quantitative measurements of the X-ray absorption in a thin specimen can be related to the composition of regions down to $1\ \mu$ in diameter.⁽¹⁸⁾ However, in metallographical work greater importance attaches to the emission method in which the electron beam, $1\ \mu$ in diameter, excites characteristic emission from the specimen itself, thus permitting direct chemical analysis of a selected point in the surface. A relative accuracy of 1% in the measurement of high concentrations is often obtainable, and the minimum detectable concentration is 0.1% or lower. By scanning the electron beam over the surface and selecting the appropriate X-ray emission line, an image can be formed on a cathode-ray tube of the surface distribution of a given element.⁽¹⁹⁻²²⁾ At the same time, a similar image can be produced from back-scattered electrons giving information about the surface topography, which can be easily correlated with the optical image. Instruments are being developed to extend the range of elements which can be analysed to include carbon, nitrogen and oxygen—elements of particular importance to the metallurgist. Graphite flakes in cast iron have been detected by a scanning microanalyser using a thin-window proportional counter with single-channel pulse-height analysis (Fig. 2). With more refined methods of pulse analysis, such as the matrix method,⁽²³⁾ it is hoped to extend the technique to give sufficient quantitative accuracy for practical problems.

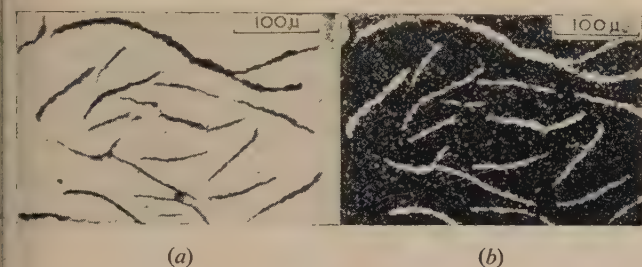


Fig. 2. Graphite flakes in cast iron shown up in X-ray scanning microanalyser by selection of 44 Å carbon K radiation

(a) optical (b) carbon K radiation

Mineralogical applications of X-ray microanalysis were described by Dr. J. V. P. LONG (University of Cambridge). The solution of petrological problems frequently depends on a knowledge of the composition of co-existing mineral phases in a rock, or of the variation of composition with rock type. Polished thin sections of rock have been examined by both absorption and emission methods of X-ray microanalysis. In mineralogical work the physical properties and the ranges of composition differ considerably from those encountered in metals and alloys. These differences influence the experimental techniques; for example, anomalous absorption effects can arise from imperfect polishing of the specimen and it is preferable to collect the emitted X-rays at as large an angle as possible to the surface. For emission microanalysis it is important to use an optical microscope to view the specimen in transmitted light during exposure to the electron beam. The visible fluorescence produced in transparent minerals by electron bombardment allows the point of contact of the probe to be located, and, since the colour of the emitted light varies for different elements, it is sometimes possible to identify the mineral grains and to delineate the grain boundaries.

Mr. T. MULVEY (Associated Electrical Industries Ltd., Aldermaston) read the last paper on X-ray microanalysis. For quantitative analysis certain corrections for absorption and fluorescence must be made, and these corrections become more serious as the analysis is extended to lighter elements. A possible method of reducing these effects is to make the beam strike the specimen at normal incidence, by bending the electron beam through a right-angle with the aid of an anastigmatic electron prism. Deposition of carbon on the specimen can be caused by the breakdown of hydrocarbon vapour by the electron beam; a method of controlling this contamination is to introduce oxygen, which combines with the carbon to form carbon monoxide or carbon dioxide. For the analysis of light elements the electron accelerating voltage must be reduced, thereby reducing the current density in the probe. The aperture of the last lens cannot be opened up to increase the probe current because of spherical aberration in the lens. However, it is possible that this aberration can be corrected using quadrupole and octupole units. Experiments by Dolby⁽²⁴⁾ indicate that under controlled conditions light elements should give an appreciable spectral intensity: the difficulties of analysing these elements, although formidable, appear to be technical rather than fundamental.⁽²⁵⁾

In commenting on the papers on microanalysis, Mr. R. C. STANLEY (Central Electricity Research Laboratories, Leatherhead) emphasized that pulse-height discrimination is essential for the analysis of light elements. He quoted as an example a sample containing 0.1% sulphur by weight, which gave peak-to-background ratios of 1.3 : 1 without, and 6 : 1 with pulse-height discrimination. The microanalyser in use at the Smithsonian Astrophysical Observatory, U.S.A., was described briefly by Dr. A. R. LANG (University of Bristol). This instrument has three unusual features: a high take-off angle (55 deg) from the specimen, reducing sensitivity to specimen contour; observation of the specimen in air, so that large specimens can be examined; and a simple mechanism for moving the specimen from the optical microscope to the electron probe. Mr. N. SWINDELLS (Associated Electrical Industries Ltd., Aldermaston) referred to the use of microanalysis for alloy constitutional studies of refractory metals. The characteristic radiation is $L\alpha$ and, because the absorption coefficients of $L\alpha$ radiation are not known, they must be interpolated from the adjacent values for $K\alpha$ wavelengths. Dr. A. FRANKS (National Physical Laboratory, Teddington) announced that, if the accuracy of quantitative measurements in microanalysis could be improved by using standard homogeneous metallurgical specimens, consideration would be given at the N.P.L. to producing such standards.

Dr. A. R. LANG next read a paper by himself and Dr. N. KATO (University of Bristol) on some X-ray diffraction effects of individual dislocations. The X-ray method of studying dislocations exploits the much greater X-ray reflecting power of an "ideally imperfect" crystal compared with an "ideally perfect" one. In good quality crystals of low dislocation density, the core of a dislocation can be regarded as the centre of a cylindrical region of relatively imperfect crystal embedded in a matrix of more perfect crystal. By employing high-resolution photographic techniques, these imperfect regions can be shown up in the images of Bragg reflexions: their extra reflected intensity gives strong contrast in both transmission through the crystal and reflexion from the surface of the crystal. Dislocation configurations in the interior of large single crystals can be studied by the method of "projection topographs".^(26, 27) The direction of the Burgers vector of individual dislocations can be determined

from the variation of the dislocation contrast with the orientation of the reflecting plane. In this way dislocation combinations at nodes and dislocation reactions, such as the Lomer reaction, can be analysed.

"Pendellösung" fringes were described and a tentative explanation of them was given. These fringes run parallel to the bevelled edges of wedge-shaped crystals; they have no connexion with dislocations and, in fact, are associated with highly perfect regions of the crystal. In the discussion Dr. P. B. HIRSCH (University of Cambridge) maintained that the kinematical theory of X-ray diffraction can explain the appearance of Pendellösung fringes and also the splitting into two lines of the images of dislocations. Dr. Lang contested these statements and suggested that the kinematical theory may explain unusual contrast effects in electron microscopy but not in X-ray diffraction, where the wavelength and angular width of the diffraction peak are so different.

Dr. A. KELLY (University of Cambridge) remarked that, although the electron microscope method of revealing dislocations had previously been applied to metals only, he had recently succeeded in observing dislocations in a typical ceramic, magnesium oxide. The specimen was made thin enough for transmission electron microscopy by cleaving and chemical dissolution.

The Evening Discourse was given by Prof. E. G. COX (University of Leeds) under the title of "Professorial reflexions". This lively and interesting talk was in the nature of a farewell to the X-ray Analysis Group of the Institute, in which Prof. Cox has been prominent for many years.

For the last session the chair was taken by Prof. H. LIPSON (Manchester College of Science and Technology) and the opening paper on X-ray spectroscopy of some transition and noble metals was read by Prof. Y. CAUCHOIS (University of Paris). Measurement of the X-ray emission band gives information about the density curve for the filled levels in the conduction band, whereas the absorption band gives information about the density curve for the levels which are normally empty. The density curve relates the density function $N(E)$, to the energy E , where $N(E)dE$ is the number of levels between E and $E + dE$. Emission and absorption edges in metals occur at the same wavelength and are related to breaks in the density curve. In deriving the density curve from the experimental intensity distribution the effects of three factors must be taken into account: the width of the deep level of high energy which is associated in the transition with the lower energy band, the probability of transition, and the instrumental factor which involves the "diffraction pattern" of the analysing crystal in the spectrograph.

An account was given of the results, obtained recently at the Laboratoire de Chimie Physique de la Faculté des Sciences de Paris, for the noble metals, silver, palladium, platinum, gold, and the transition metals, iron, cobalt, nickel, copper.

Mr. MULVEY asked whether the discrepancies in the K and L fine structures found by different authors could be ascribed to the penetration of electrons into the specimen. Prof. Cauchois replied that this was quite likely: at a wavelength of 15 Å correction for penetration is impossible, because of the Auger effect and the low fluorescence yield. Other difficulties are the temperature effect (local heating produced by the electron beam), surface contamination, and a possible perturbation of the surface distribution of states. Prof. Lipson inquired whether the method could be used to explore the shape of the Fermi surface in single crystals. In reply, Prof. Cauchois pointed out that it is not possible

to examine a particular direction in momentum space, as the electrons constantly change their direction within the metal: in germanium no difference was detected in emission between the single crystal and the polycrystal.

Methods and applications of X-ray spectroscopic analysis were described by Dr. J. L. de VRIES (Philips, Eindhoven). X-ray spectroscopy has been used as a research technique for some time, but its application as a tool for routine chemical analysis only started comparatively recently. In the X-ray emission method the elements are excited by electrons (e.g. from radioisotopes) or, more commonly, by primary X-rays. The specimen can be a metal, powder or liquid, and the use of a vacuum path allows the analysis of lighter elements and of the L -lines of heavier elements. For quantitative analysis a monochromator crystal selects a particular emission line and the measured intensity is compared with that given by chemically analysed standards. In general, the K -lines give higher intensity, but the L -lines sometimes give a better peak-to-background ratio. In the analysis of uranium for molybdenum and zirconium the K -lines of molybdenum and zirconium are masked by weak L -lines of uranium; the $Zr\text{-}L\alpha$ line at 6 Å and $Mo\text{-}L\alpha$ line at 5.4 Å are therefore used and are detectable down to 0.1% composition. For maximum intensity one needs about 100 mg with flat crystals, and under these conditions the limit of detection has been reported as 10^{-9} g . The lightest element which can be detected with commercial equipment is sodium, and the normal range of sensitivity of the emission method is 10^{-4} – $10^{-1}\%$, depending on the element and its matrix. The relative precision can be 1% or less. The method is especially suitable for routine analyses, and instruments have been developed which can determine many elements automatically.

The absorption method of analysis is restricted to the analysis of thin layers and to relatively simple solutions. The thickness of a layer can often be measured by observing the absorption of the characteristic lines of the base material by the layer. The absorption coefficients of chromium for $FeK\alpha$ and $FeK\beta$ radiations are sufficiently different to enable the thickness of the chromium layer on steel to be measured directly in the 0 – $20\text{ }\mu$ range.

In reply to a question from Dr. U. W. ARNDT (The Royal Institution, London) about the relative advantages of electron and X-ray excitation, Dr. de Vries said that the intensity is much higher for electron beam excitation, but the peak-to-background ratio is lower. Changes in the sample itself can be caused by the electron beam. Radioisotopes provide a stable and convenient source for electron excitation, but the intensity is low.

The next paper was delivered by Dr. K. W. ANDREWS (United Steel Co. Ltd., Rotherham) who reviewed the subject of X-ray fluorescent analysis in relation to metallurgical research and control. Instruments for X-ray fluorescent analysis can be used for analytical control. In the metallurgical industry the aim is to provide rapid analytical control of (a) raw materials, (b) materials occurring during processes (e.g. slags), and (c) products. At present the techniques for examining slags are the least advanced.

Some basic problems arise in connexion with fluorescent analysis. The amount of a particular element in a sample can be measured by calibration against standard samples. The calibration curves can only be used if there are no wide variations in the quantities of other elements. Alloys of different base compositions can be analysed using different calibration curves or by the use of a single curve with an appropriate correction factor.

When fluorescent X-rays are produced at a certain depth in a thick sample they may be absorbed before emerging from the surface or they may cause further fluorescence in other elements. These factors affect the analysis in two ways. First, for a single element in a constant matrix a non-linear relationship may arise between concentration and intensity, and second, the intensity of an element will depend not only on its own concentration, but also on that of the other elements. It is necessary to calculate these effects and to establish an absolute relationship between the chemical composition and the X-ray intensity. This problem is very complicated as the primary radiation is not monochromatic and each element emits more than one wavelength.

The final paper of the conference, by Dr. P. T. DAVIES and Mr. J. L. KENDALL ("Shell" Research Centre, Thornton), dealt with the X-ray fluorescent analysis of aqueous solutions by a double dilution method.

As stated in the previous paper, the aim in X-ray fluorescent analysis is to relate X-ray intensity to chemical composition, and inter-element effects lead to complications which are not easily overcome. The method of analysis used by the authors was designed to determine the concentration of an element in an unknown matrix. They applied a method used by J. Sherman⁽²⁸⁾ to the analysis of aqueous solutions, and allowance was made for the interaction of other elements in the sample by carrying out X-ray intensity measurements at two different dilutions of the sample. The theoretical basis of the method assumes that the incident beam is monochromatic and that mutual fluorescence in the sample can be neglected. Then if I_1 is the intensity of a spectral line of element 1 at a concentration c_1 in a light matrix, one has

$$\frac{A}{I_1} = (1 - B) + \left(B + \sum_{i=2}^{i=n} k_i c_i \right) / c_1 \quad (2)$$

where $(n-1)$ interfering elements are present at concentrations $c_i (2 \leq i \leq n)$ and A , B and k_i are all constants. The elements of the light diluent do not appear explicitly. It can be shown that, if a sample containing several detectable elements is diluted with a light diluent and, for a particular element, a graph is drawn relating reciprocal intensity and reciprocal concentration, then a straight line will be obtained, the slope of which has the same value G as for the element alone in the diluent.

An analysis is conducted by measuring the intensities of a spectral line at two different dilutions, D_1 and D_2 , in the diluent. Dilution is defined as the weight of diluted mixture containing unit weight of the sample. If t_1 and t_2 are the corresponding reciprocal intensities, the concentration c of the element in the sample is given by

$$c = G(D_2 - D_1) / (t_2 - t_1) \quad (3)$$

The single calibration constant G must be determined for each element to be analysed. Test analyses on known solutions show that good results can be obtained for single elements in aqueous solutions or for the heavier elements in mixtures. In mixtures mutual fluorescence causes errors in the results for the lighter elements.

Normally concentrations down to 0.2 g/100 ml. of an element can be determined on a 5 ml. sample. The time for the determination of each element is approximately $\frac{1}{2}$ h and standardization for a particular element can be completed in a day. Provided the detector and crystal are not changed, standardization should be permanent.

In the discussion Dr. H. HUGHES (United Steel Co. Ltd., Rotherham) commented that his laboratory had developed

a method whereby 0.1 g of a sample is fused, the mixture dissolved in acid and the intensity measured. Comparison with standard solutions showed that reliable analyses could only be carried out if the solutions were made up with the same acid.

R. P. FERRIER
B. T. M. WILLIS

References

- (1) BROCKHOUSE, B. N., and IYENGAR, P. K. *Phys. Rev.*, **111**, p. 747 (1958).
- (2) BROCKHOUSE, B. N., COCHRAN, W., and WOODS, A. D. B. To be published.
- (3) EGELSTAFF, P. A. *Brit. J. Appl. Phys.*, **10**, p. 1 (1959).
- (4) BACON, G. E., LOWDE, R. D., and DYER, R. F. *Atomic Energy Res. Establ. (Harwell) Rep. M/R 2857* (1959).
- (5) HERPIN, A., MERIEL, P., and VILLAIN, J. *C.R. Acad. Sci. (Paris)*, **15**, p. 249 (1959).
- (6) LOWDE, R. D. *Rev. Mod. Phys.*, **30**, p. 69 (1958).
- (7) SHULL, C. G., and WILKINSON, M. K. *Phys. Rev.*, **97**, p. 304 (1955).
- (8) GOEDKOOP, J. A., and RISTE, T. *Nature (London)*, **185**, p. 450 (1960).
- (9) RISTE, T., BLINOWSKI, K., and JANIK, J. *J. Phys. Chem. Solids*, **9**, p. 153 (1959).
- (10) LOWDE, R. D., and UMAKANATHA, N. *Phys. Rev. Letters*, **4**, p. 524 (1960).
- (11) TAKAGI, M. *J. Phys. Soc. Japan*, **9**, p. 359 (1954).
- (12) BLACKMAN, M., and CURZON, A. E. *Structure and Properties of Thin Films* (New York: John Wiley and Sons, 1959).
- (13) CURZON, A. E. Ph.D. Thesis, London (1959).
- (14) VONNEGUT, B. *J. Colloid, Sci.*, **3**, p. 563 (1948).
- (15) POUND, C. M., and LA MER, V. K. *J. Amer. Chem. Soc.*, **74**, p. 2323 (1952).
- (16) CASTAING, R., and GUINIER, A. *Proceedings of a Conference on Electron Microscopy at Delft* (1949).
- (17) SAWKILL, J., and SCHWARZENBERGER, D. R. *Tube Investments Report No. 92* (1959).
- (18) LONG, J. V. P. *J. Sci. Instrum.*, **35**, p. 323 (1958).
- (19) COSSLETT, V. E., and DUNCUMB, P. *Nature (London)*, **177**, p. 1172 (1956).
- (20) DUNCUMB, P. *Brit. J. Appl. Phys.*, **10**, p. 420 (1959).
- (21) MELFORD, D. A., and DUNCUMB, P. *Metallurgia, Manchr.*, **57**, p. 159 (1958).
- (22) MELFORD, D. A. *New Scientist*, **6**, p. 746 (1959).
- (23) DOLBY, R. M. *Proc. Phys. Soc. (London)*, **73**, p. 81 (1959).
- (24) DOLBY, R. M. *Brit. J. Appl. Phys.*, **11**, p. 64 (1960).
- (25) ARCHARD, G. D. *Proceedings of an International Symposium on X-ray Microanalysis at Stockholm* (1959).
- (26) LANG, A. R. *Acta Cryst.*, **12**, p. 249 (1959).
- (27) LANG, A. R. *J. Appl. Phys.*, **30**, p. 1748 (1959).
- (28) SHERMAN, J. *6th Annual Conference on Industrial Applications of X-ray Analysis, Denver* (August, 1957).

Contrast of electron micrographs

by J. S. HALLIDAY, Ph.D., F.Inst.P., and T. F. J. QUINN, B.Sc., Grad.Inst.P., * Research Laboratory, Associated Electrical Industries Ltd., Aldermaston, Berks.

[Paper first received 21 April, and in final form 8 August, 1960]

Abstract

The variations of contrast in electron micrographs of amorphous films, with film thickness, electron accelerating voltage and objective aperture angle, are discussed; elastic and inelastic electron scattering and the possibility of plural scattering are taken into account. Experimental results, obtained with vacuum-evaporated iron films, confirm a formula of the type first proposed by Hall.⁽¹⁾ However, the contrast is about four times smaller than predicted, using scattering cross-sections based on Lenz's⁽²⁾ data. Results for other materials, obtained by previous workers, indicate similar discrepancies. At present, the likeliest explanation appears to be a theoretical under-estimation of the scattering into angles smaller than 10^{-3} rad. The limitations of contrast measurements for assessing specimen thickness or constitution are discussed, and a new criterion for replica and shadowing materials suggested.

Introduction

THE ultimate limit of contrast perception, for detail near or below the limit of resolving power of the electron microscope, has been considered in a previous paper from this Laboratory.⁽³⁾ In this paper the contrast differences between areas that are large, compared with the resolving power, are considered. In principle, it should be possible to determine the thickness of films examined in the electron microscope from absolute measurements of the contrast of their images. Ohh and Carroll⁽⁴⁾ have recently used this method to deduce the thickness of oxide films formed during the electrolytic thinning of stainless steel foils. Similarly, if an inhomogeneous film of known thickness is examined, for example a microtomed section of biological tissue, it should be possible to determine the variations of specimen density, and hence their composition, from the contrast variations in the electron micrograph. At normal working voltages, 50 kV or more, the contrast variations obtained with biological specimens are poor, owing to the small density variations from one component to another. Nixon⁽⁵⁾ has shown that a considerable improvement can be gained by operating at 6 kV but, as yet, the resolving power of such low-voltage microscopes is relatively poor.

Zeitler and Bahr⁽⁶⁾ have related the contrast variations in electron micrographs to variations in the mass thickness of the corresponding points in the specimen, and their analysis is based on the following assumptions: (1) that the maximum mass thickness is small enough for plural scattering to be ignored; (2) that only elastic electron scattering occurs in the

specimens; and (3) that the resolved images are formed by transmitted (unscattered) electrons and electrons scattered through angles smaller than the objective aperture angle. As far as practical considerations are concerned, the first assumption is very restrictive. If it is arbitrarily stipulated that the proportion of the scattered electrons that are plurally scattered must be less than 25% for plural scattering to be ignored, as assumed by Zeitler and Bahr,⁽⁶⁾ then theoretically the specimen thickness must be less than 0.5 times the electron mean free path in the specimen. Assuming elastic scattering, the corresponding film thicknesses for 50 kV electrons are 240, 68, 51 and 28 Å for carbon, iron, silver and gold respectively. The second assumption raises a more fundamental objection, since inelastic electron scattering occurs in all materials. Thus, Lenz⁽²⁾ has shown theoretically that the total cross-section for the inelastic scattering, due to collisions causing ionization, decreases monotonically from about 20 to 0.3 times the elastic scattering cross-section as the specimen atomic number increases from 1 to 100. Taking both elastic and inelastic scattering into account, Zeitler and Bahr's theory would appear to be restricted to films no thicker than 45, 32, 33 and 20 Å in the instances of carbon, iron, silver and gold respectively.

Hall⁽¹⁾ had correlated contrast and specimen thickness some years earlier but, unlike Zeitler and Bahr,⁽⁶⁾ did not relate all the equation constants to the atomic scattering cross-sections. He did, however, consider both elastic and inelastic scattering and the effects of plural scattering. Hall showed that the variations of the contrast produced by silicon monoxide films, examined at 65 kV, substantiated his formula. The variations of the contrast of polystyrene latex particles with aperture angle and accelerating voltage have since been described by Hall and Inoue⁽⁷⁾; these were also in accord with Hall's theory.

In this paper an exact form of the Hall⁽¹⁾ relation between contrast and specimen thickness is derived; this should be obeyed at normal aperture angles over a reasonably extensive range of specimen thickness and operating voltage. It is shown that a relation similar to that proposed by Zeitler and Bahr⁽⁶⁾ would be expected if exceedingly small apertures of about 10^{-5} rad, were used. Experimental measurements of the contrast of electron micrographs, obtained at several voltages in the range 33 to 175 kV, with specimens of iron are described. The variations of contrast with specimen thickness, operating voltage and objective aperture angle are in qualitative agreement with the exact Hall relation, but the magnitude of the contrast is much less than predicted. Finally, the accuracy with which relative thickness measurements can be made, and the possible use of contrast measurements for specimen analysis, are discussed.

* Now at Brunel College of Technology, Acton, London.

Theory

Let $\sigma(\theta)$ be the atomic cross-section for elastic and inelastic scattering of electrons through all angles between 0 and θ ; the total scattering cross-section is $\sigma = \sigma(\pi)$. The fraction of the electrons scattered by an atom into the solid cone of semi-apex angle θ is $p(\theta) = \sigma(\theta)/\sigma$. The variations of $p(\theta)$ and $p_e(\theta)$ with θ , where $p_e(\theta) = \sigma_e(\theta)/\sigma$ and $\sigma_e(\theta)$ is the cross-section for elastic scattering only, have been calculated for the iron atom, using the theoretical expressions for the differential scattering cross-sections given by Lenz⁽²⁾ (see Fig. 1). The variations for 50 and 100 kV electrons have been plotted, and it will be noted that both $p(\theta)$ and $p_e(\theta)$ are relatively insensitive to this variation in voltage.

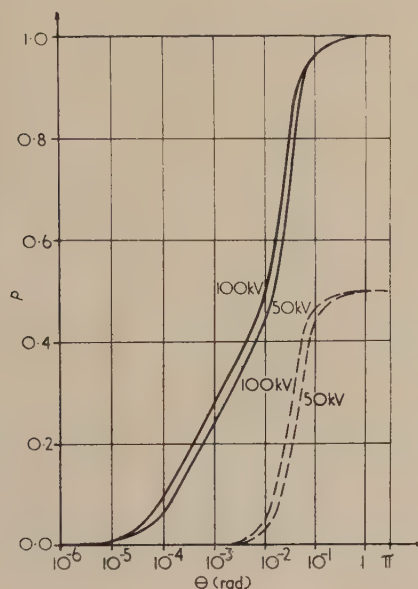


Fig. 1. The variation of the fraction of the scattered electrons scattered into a solid cone, semi-angle θ , iron atoms

— $p(\theta)$ — — $p_e(\theta)$

The contrast C of a given area of specimen is taken to be $\ln(I_0/I_c)$, where I_0 is the intensity of electrons incident on the specimen and I_c is the intensity which passes through this area and through the microscope objective lens into the resolved image. The intensity of unscattered electrons which arrives at a depth x in a specimen, is $I_0 \exp(-x/\lambda_T)$ where λ_T , the mean free path of the electrons in the specimen, is $1/N\sigma$, N being the number of atoms per cubic centimetre. The intensity, which is singly scattered into a solid cone semi-apex angle θ after passing through a lamina, thickness δx , at this depth is

$$\delta I_s = p(\theta) I_0 (\delta x / \lambda_T) \exp(-x/\lambda_T) \quad (1)$$

In order to calculate the proportion of this intensity, which traverses the remainder of the specimen thickness $t - x$, and passes through the objective aperture angle α , all scatter paths between the lamina and exit face of the specimen should be considered. This calculation is simple when α is much smaller than the most probable angle of scatter θ_p . In such conditions it is extremely unlikely that any plurally-scattered electrons would pass through the objective aperture and one may write $p(\alpha)$ for $p(\theta)$ in equation (1). It also follows that the intensity scattered at the lamina, which

emerges from the specimen and passes through the objective aperture, is

$$\delta I_s \cdot \exp\{-(t-x)/\lambda_T\}$$

If all of these scattered electrons enter the resolved image, then integration and addition to the unscattered intensity, $I_0 \exp(-t/\lambda_T)$, gives

$$I_c = I_0 \{1 + p(\alpha)(t/\lambda_T)\} \exp(-t/\lambda_T) \quad (2)$$

If the inelastically scattered electrons do not enter the resolved image, but form a general background over the whole image field, then $p(\alpha)$ in equation (2) must be replaced by $p_e(\alpha)$; if the possibility of inelastic scattering is completely ignored, then equation (2) becomes identical with that proposed by Zeitler and Bahr.⁽⁶⁾

The variations of C with t/λ_T predicted by equation (2), assuming that $p(\alpha)$ equals 0 and 0.8, are shown in Fig. 2, curves 1 and 2 respectively. Theoretically, $p(\alpha)$ should not be as large as 0.8 when $\alpha \leq \theta_p$, but this value has been selected for the diagram to emphasize the features of equation (2), and because large values of $p(\alpha)$ have been found experimentally. Curve 1 would apply if an infinitesimally small aperture were used, or if the unscattered

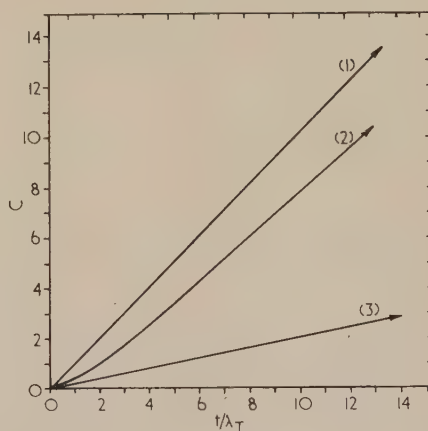


Fig. 2. The variation of contrast C with the ratio t/λ_T (schematic)

Curve (1), no scattered electrons in the image, $p(\alpha) = 0$; curve (2), no plurally scattered electrons in the image, equation (2), $p(\alpha) = 0.8$; curve (3), plurally scattered electrons in the image, equation (4), $p(\alpha) = 0.8$

electrons alone entered the resolved image. The initial slope of curve 2 is $\{1 - p(\alpha)\}$ but this increases rapidly towards a slope of unity; it is already 0.9 when t/λ_T is 5.0. Whilst these curves imply that results obtained at all voltages will fall on a single curve for a given aperture, this is not strictly true since $p(\alpha)$ is a function of voltage. However, as previously pointed out, these variations are relatively small.

When the accelerating voltage and the specimen thickness are such that the majority of the scattered electrons are singly scattered, equation (2) reduces to

$$I_c = I_0 [1 - (t/\lambda_T)\{1 - p(\alpha)\}] \quad (3)$$

and this equation holds for all values of α . The maximum value of t/λ_T , for which equation (3) may be expected to apply, is indicated by the fact that 90% of the scattered electrons will be singly scattered, if t/λ_T is about 0.2, and only 75% when t/λ_T is about 0.5.

From Lenz's⁽²⁾ expressions for the differential cross-sections, it can be shown that, at 100 kV, equation (2) should be obeyed for iron specimens, when α is much smaller than 3×10^{-5} rad, if all the singly-scattered electrons enter the image; α must be much smaller than 2×10^{-2} rad if the inelastically-scattered electrons do not enter the image. In practice, the aperture angle is usually about 10^{-2} rad, and therefore some plurally-scattered electrons are very likely to pass through the objective aperture. Equation (2) will still be satisfied, provided that these electrons do not enter the resolved image. However, if the plurally-scattered electrons do go into the image, the rate of increase of contrast with increasing values of t/λ_T will not be so rapid as that predicted by equation (2). At relatively small values of t/λ_T , the variation of contrast with t/λ_T will tend to be linear, curve 3, Fig. 2, and the equation for this line must be

$$I_c = I_0 \exp [-\{1 - p(\alpha)\}(t/\lambda_T)] \quad (4)$$

in order that equation (3) shall be satisfied at the origin. At larger values of t/λ_T the contrast will increase more rapidly and eventually the slope of the contrast *versus* (t/λ_T) curve will reach unity. Equation (4) has the same form as that originally proposed by Hall.⁽¹⁾

As a first approximation, it might be supposed that the maximum value of t/λ_T for which equation (4) will apply is given by α/θ_p . On this basis, equation (4) should be obeyed for t/λ_T values up to about thirty with iron specimens and an objective aperture of 10^{-3} rad. However, many electrons are singly scattered through angles that are large compared with θ_p , and therefore this estimate of the t/λ_T range will probably be too large. Also, it is reasonable to suppose that a diminishing proportion of the plurally-scattered electrons which pass through the aperture will enter the resolved image as t/λ_T increases, since the mean energy loss caused by inelastic scattering will increase and cause correspondingly larger chromatic aberrations. This factor will also reduce the effective t/λ_T range of equation (4).

When equation (4) is obeyed, the contrast C is simply $\{1 - p(\alpha)\}t/\lambda_T$. If inelastic scattering did not occur, the contrast C_e would be given by $\{1 - p'(\alpha)\}t/\lambda_e$, where $p'(\alpha)$ is $\sigma_e(\alpha)/\sigma_e$ and λ_e is $1/N\sigma_e$. Now λ_e/λ_T is $(1 + n)$, where n is the ratio of the inelastic to the elastic total scattering cross-sections, and therefore,

$$\frac{C}{C_e} = (1 + n) \left\{ \frac{1 - p(\alpha)}{1 - p'(\alpha)} \right\} \quad (5)$$

With iron specimens and an objective aperture of 10^{-3} rad, n is about 1.1 (Lenz⁽²⁾), $p(\alpha)$ is about 0.25, $p'(\alpha)$ is zero and so C/C_e is about 1.6. Thus the film thickness deduced from contrast measurements would be wrong by this factor if inelastic scattering were ignored. The error is least with specimens of high atomic number, when n is small, but, as Lippert⁽⁸⁾ has shown, may be large with specimens composed of very light elements.

Experimental

The iron specimens were prepared by vacuum evaporation on to glass slides, which had each been partially covered with a very thin film of Teepol, and then arranged at various distances from the source. The iron films on the Teepol-coated areas were removed, by dipping the slides into water, and then mounted on copper electron microscope grids. The advantage of this method of specimen preparation is that

supporting films, which would cause unwanted electron scattering, are avoided. The thickness of the films remaining on the Teepol-free areas of the microscope slides were determined by multiple beam interferometry (Tolansky⁽⁹⁾).

Ilford thin-film half-tone plates were used to record the micrographs and, in order that the density of photographic blackening could be related to relative electron intensity, two electron diffraction patterns were recorded on each plate using different exposure times, all other conditions being kept constant.

Results

The variation of contrast with specimen thickness and accelerating voltage. Two specimens of thickness $448 \pm 25 \text{ \AA}$ and $754 \pm 36 \text{ \AA}$ were examined at 50, 70 and 100 kV in the experimental E.M.6 electron microscope (Haine and Page⁽¹⁰⁾). During experiments the current to the condenser lenses was switched off and a 2 mil aperture was inserted about 1 cm above the specimen, so that overheating and any consequent recrystallization or evaporation of the specimen was prevented. No physical aperture was used in the objective lens, but a second grid of finer mesh size was placed about 0.01 in. below the specimen. This practice was first used by Hall⁽¹⁾ in an attempt to measure directly the intensity of unscattered electrons. In every experiment two micrographs were recorded, the first showing an area of film and the second a hole in the specimen, and both showing an out-of-focus image of a bar of the second grid.

The density in the region of these grid bars was always greater when an area of film was imaged, due to poor imaging of electrons scattered through large angles in the specimen (Hall⁽¹⁾). After subtracting these local background intensities, the ratio I_0/I_c could be determined from the two micrographs. The values of C derived from these experiments are plotted against t/λ_T in Fig. 3. It is clear that all values lie

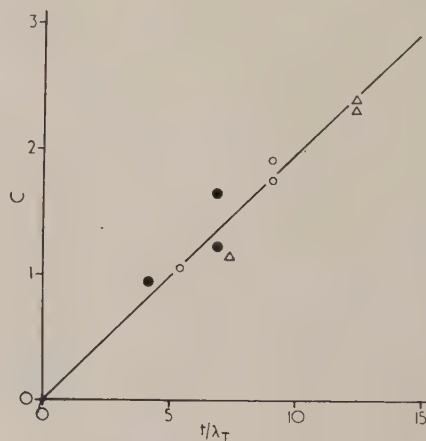


Fig. 3. The variation of the contrast C with t/λ_T ; results obtained with iron films in the experimental E.M. 6 electron microscope

● = 100 kV ○ = 70 kV △ = 50 kV

reasonably close to a straight line, of slope 0.19, which passes through the origin. It can be concluded that equation (4) is satisfied within the limits of experimental error for $0 < t/\lambda_T < 13$ and that the experimental value of $p(\alpha)$ is about 0.81 for voltages between 50 kV and 100 kV.

it is obvious that the use of a second grid does not lead to determinations of the unscattered electron intensities.

Low-magnification point-projection micrographs of large areas of each specimen were also obtained in a single-lens diffraction camera, when the electron source was focused a few millimetres behind the specimen. Five specimens, with thicknesses ranging from 355 to 1413 Å, were examined at voltages from 33 to 175 kV; the contrast values are shown in Fig. 4. Again a straight line which passes through the

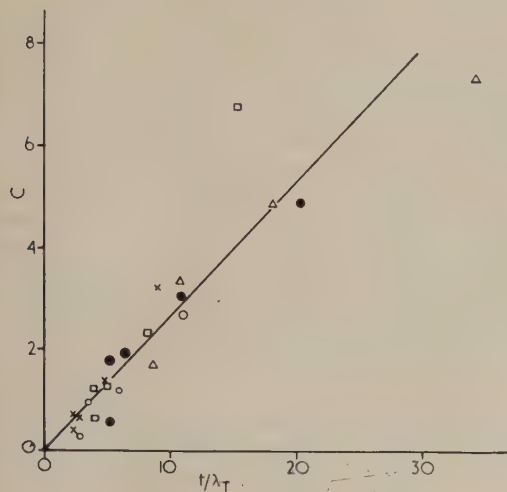


Fig. 4. The variation of the contrast C with t/λ_T ; results obtained with iron films in a high-voltage electron diffraction camera

× = 175 kV ○ = 128 kV □ = 80 kV ● = 59 kV
Δ = 33 kV

origin provides a reasonable fit, at least for $0 < t/\lambda_T < 20$; the experimental value of $p(\alpha)$ is 0.73.

The variation of contrast with objective aperture angle. In this series of experiments a single specimen, about 1080 Å

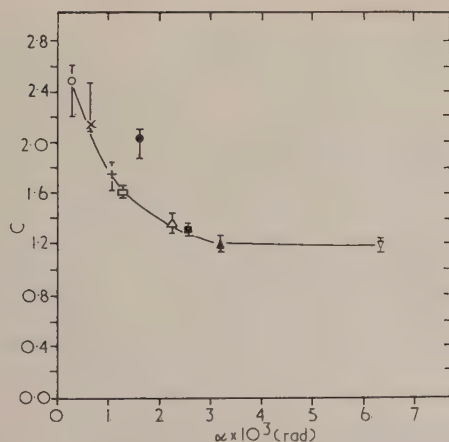


Fig. 5. The variation of contrast C with objective aperture angle α . (Iron specimen, 1080 Å thick, 100 kV)

Key: The first number after the symbol is the objective aperture diameter (in mils) and the second is the distance between the specimen and the aperture disk (in mm)

○ = 0.5, 24; × = 0.5, 10; + = 2.0, 24; □ = 1.0, 10;
● = 0.5, 4; Δ = 2.0, 11.3 (both specimen and aperture disk well above the objective lens); ■ = 2.0, 10; ▲ = 1.0, 4;
▽ = 2.0, 4

thick, was examined at 100 kV in the E.M.6 electron microscope. No second grid was employed, but various effective aperture angles were obtained by changing the distance between the specimen and the objective lens, and by inserting 0.5, 1.0 and 2.0 mil apertures in the plane of the lens. In some of the experiments it was arranged that approximately equal angular apertures were obtained with different distances from specimen to lens, in order to determine whether or not the first pole-piece of the objective exerted any appreciable condenser action. This was further checked by an experiment in which both the specimen and the aperture were situated well above the objective lens.

All but one of the experimental results fall on a single curve when C is plotted against α (see Fig. 5), and therefore it is concluded that the objective lens was not significantly affecting the predetermined aperture angles. Fig. 6 shows

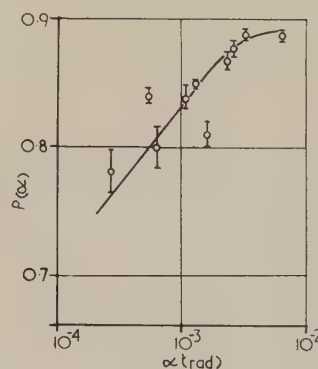


Fig. 6. The experimental variation of $p(\alpha)$ with aperture angle α . (Iron specimen examined at 100 kV)

the corresponding variation of $p(\alpha)$ with α , it being assumed on the basis of the previous results that equation (4) was always satisfied; as expected, $p(\alpha)$ increases as α increases. However, the experimental $p(\alpha)$ values are about three times greater than those predicted (see Fig. 1). It is considered that the slow rate of increase of $p(\alpha)$ with α , observed at the largest aperture angles, was due to the limiting effective aperture angle set by spherical aberration effects in the objective lens.

Discussion

It can be concluded from the present results that the contrast of electron micrographs of amorphous specimens and those composed of very small crystallites is given by a relation of the form proposed by Hall,⁽¹⁾ for all specimen thicknesses and operating conditions that are likely to be used. The Zeidler and Bahr⁽⁶⁾ relation, suitably modified to allow for inelastic scattering, is not obeyed. However, it has been shown that this relation would only be expected if the plurally-scattered electrons that pass through the objective aperture did not contribute to the resolved images.

There will be deviations from the Hall type of relation when phase contrast effects are apparent at the edges of holes or isolated particles photographed at high magnification. Deviations will also occur when the size of the crystallite images on the photographic plate becomes comparable with the effective size of the microphotometer slit. Differences in the contrast of individual crystallites, due to diffraction by those in suitable orientations, will then become apparent. For most materials the angles of deviation of

diffracted electrons are greater than the objective aperture angle, and so a diffracting crystallite will usually appear to be thicker than a non-diffracting one. Such effects will be more noticeable when the average number of crystallites in the film thickness is small. The contrast of a single crystal diffracting film will vary with film thickness, being proportional to $A \sin^2(Bt)$ where A and B depend upon the accelerating voltage and the Bragg reflexions operating (see Whelan⁽¹¹⁾ for a recent review of the theory), and will be influenced by dynamical effects. These arise even with the thinnest films, which are less than a hundred Ångströms thick with many metals (Blackman,⁽¹²⁾ Halliday⁽¹³⁾).

Quantitative comparison of the exact form of the Hall relation, equation (4), with the experimental results, show that the contrast achieved in practice is much poorer than that predicted. By means of equation (4) it is now possible to deduce from Hall's results⁽¹⁾ the values of $p(\alpha)$ for several other elements (see Table 1). Other $p(\alpha)$ values have been calculated from unpublished experimental data obtained by Haine and Agar, in the course of their measurements of

Table 1. *Experimental values of $p(\alpha)$*

From data published by C. E. Hall⁽¹⁾

Element	Be	Cr	Ge	Pd	Pt	Ur	SiO
Atomic No.	4	24	32	36	78	92	11
							(mean)
p	0.90	0.57	0.56	0.70	0.79	0.76	0.86

From unpublished data obtained by M. E. Haine and A. W. Agar

Element	C	Al	Cu	Ag	Au
Atomic No.	6	13	29	47	79
p	0.95	0.89	0.67	0.83	0.85

differential scattering cross-sections⁽¹⁴⁾ and have been included in Table 1. All the values are large, ranging from 0.56 for germanium to 0.95 for carbon. It is unfortunate that no physical objective apertures were used by these other workers, and therefore exact comparison with theory is impossible. However, the experimental $p(\alpha)$ values for carbon, chromium and gold would have been expected theoretically for aperture angles of 0.05, 0.03 and 0.14 rad respectively. From the spread of these angles and their magnitude, it is clear that the discrepancy between theory and experiment is fairly widespread. Coupland⁽¹⁵⁾ has reported that the contrast of electron micrographs of Formvar films, obtained at 150 kV with known aperture angles, is less than that predicted for carbon films; however, he had used the Molière⁽¹⁶⁾ expression for elastic scattering and the Koppe⁽¹⁷⁾ expression for inelastic scattering, both of which have been shown to be inadequate by the experimental work of Leonhard.⁽¹⁸⁾ Ohh and Carroll⁽⁴⁾ used the Lenz⁽²⁾ expressions to calculate theoretical values for $p(\alpha)$, and therefore it is likely that the estimates of the thickness of their oxide films are too small, probably by a factor of two; if so, this would bring their results into closer agreement with previous thickness measurements made by more conventional methods.

Two factors may have caused the discrepancy, namely diffraction effects and an error in the theoretical differential scattering cross-sections. Diffraction could only affect the mean contrast of a large area of micro-crystalline material by changing the intensity of the undeviated electrons that enter the image; the intensity of elastically-scattered electrons

that pass through the aperture is negligible, whether or not the specimen is crystalline, unless one of the unit cell dimensions of the crystallites is very large. However, recent measurements of the contrast of diffraction patterns obtained in predominantly single-scattering conditions have shown that vacuum-evaporated iron films are, in fact, largely amorphous (Halliday⁽¹³⁾). It is not unlikely that several of the specimens prepared by Hall⁽¹⁾ and by Haine and Agar⁽¹⁴⁾ also had a large amorphous content, and this is certainly true of carbon and silicon monoxide. Therefore it is concluded that diffraction effects are probably not the cause of the discrepancy. The theoretical $p(\alpha)$ values would be too small if the theoretical differential scattering cross-sections were underestimated at angles less than 10^{-3} rad. The latter deficiency has already been suggested by Halliday,⁽¹⁹⁾ in view of discrepancies between the intensity distributions of electrons scattered by relatively thick carbon films into angles between 10^{-3} and 10^{-2} rad, as measured by Haine and Agar,⁽¹⁴⁾ and those distributions predicted for such specimens by Lenz.⁽²⁾

From an experimental standpoint, the thickness of films can be determined provided that a calibration curve is obtained with films of known thickness. From the points in Fig. 3, the following relation is obtained:

$$t/\lambda_T = (5.20 \pm 0.39)C \pm 1.05 \quad (6)$$

The percentage errors to be expected in the thickness of iron films examined at 100, 50 and 25 kV are given in Table 2.

Table 2. *The percentage errors to be expected in the thicknesses of iron films of varying thickness, determined from the contrast of micrographs obtained at different accelerating voltages*

$t(A) \backslash$ Voltage (kV)	100	50	25
100	120	70	40
500	30	20	15
1000	20	15	10

Almost identical errors would be expected from measurements of point-projection micrographs obtained in the electron diffraction camera. The least inaccuracy is expected when t is large and the voltage low, but the practical limitations in these respects are that the measurement of very high contrasts from photographic images is difficult, and that the lowest operating voltage of most commercial electron microscopes is 50 kV. The spread of the points in Figs. 3 and 4 is somewhat large and may be due to some unevenness in the thickness of each specimen. The spread of Hall's⁽¹⁾ experimental results obtained with silicon oxide films at 65 kV is smaller but, after statistical analysis, it has been found that the percentage errors involved in determining the thickness of a silicon oxide film from its contrast is the same as that for an iron film of the same thickness.

Hall⁽¹⁾ has indicated that small abrupt changes in film thickness should be detectable; this is true even though film thicknesses cannot be determined very accurately. Generalizing equation (6), one obtains

$$\frac{t}{\lambda_T} = \frac{(1 \pm \epsilon)}{\{1 - p(\alpha)\}} \cdot C \pm \delta \quad (7)$$

When the photographic plates are exposed, so that the density D is proportional to the electron intensity ($D \leq 1.0$)

it is simple to show that a small change in thickness Δt is given by

$$\Delta t = \frac{(1 \pm \epsilon)}{\{1 - p(\alpha)\}} \cdot \frac{\log_{10} e}{D_t} \cdot \frac{\Delta \mathcal{I}}{\mathcal{I}} \quad (8)$$

where D_t is the density corresponding to a specimen thickness t and $\Delta \mathcal{I}/\mathcal{I}$ is the fractional change in the light transmitted when the image of the film thickness change is microphotometered. As Hall⁽¹⁾ stated, the minimum detectable value of $\Delta \mathcal{I}/\mathcal{I}$ is about 10^{-2} when D_t is 1.0. This for iron specimens examined at 100, 50 and 25 kV, Δt is 2.5, 1.4 and 0.7 Å respectively.

An assessment of the possible use of the electron microscope for the analysis of specimen composition can be gained from an examination of values of the contrast per unit thickness of different materials. From equation (4) it can easily be shown that

$$C/t = [\rho(1 + n)\{1 - p(\alpha)\}]/L_e \quad (9)$$

where $L_e = \rho\lambda_e$ and ρ is the specimen density; L_e is a function of voltage but can be regarded as independent of specimen material. Relative values of (C/t) have been calculated from the values of $p(\alpha)$ in Table 1 and with the values of n given by Lenz⁽²⁾ (see Table 3). Clearly, it would not be possible to differentiate between the elements chromium, palladium and platinum, and difficult to distinguish these from uranium and copper, because their C/t values are so similar. If a specimen were composed of two elements having widely different values of C/t , for example, aluminium and copper, an approximate analysis should be possible.

Table 3. Relative values of the contrast per unit thickness of specimen material, C/t

Element	Be	C	Al	Cr	Fe	Cu
C/t	1.3	0.5	0.9	6.5	3.3	5.9
Element	Ge	Pd	Ag	Pt	Au	U
C/t	4.6	6.6	2.9	6.3	4.0	6.0
Material	SiO					
C/t	0.7					

The contrast per unit thickness is obviously one of the criteria for judging the value of a material for replicating and shadowing purposes. A high value of C/t is required for a good shadowing material, to avoid geometrical distortion by "pile-up" effects, and a low value of C/t is needed for a good replica material, in order that the shadowing shall have the most effect. For example, with the aid of equation (9) it can be shown that the minimum thickness of a partial layer of platinum that should be detectable on a carbon film at 50 kV is 0.6 Å, whereas 9 Å of carbon would be required on a platinum film. It is interesting to note that the values of C/t in Table 3 substantiate what has been found in practice;

the smallest values are 0.5 for carbon and 0.7 for silicon monoxide, whilst the values for the well-known shadowing materials, chromium, palladium and platinum, are about ten times greater.

Acknowledgements

The authors wish to thank Mr. G. Rickards for his assistance in the experimental work. They also thank Dr. T. E. Allibone, Director of the Laboratory, for permission to publish this paper.

References

- (1) HALL, C. E. *J. Appl. Phys.*, **22**, p. 655 (1951).
- (2) LENZ, F. *Z. Naturforsch.*, **9a**, p. 185 (1954).
- (3) HAINE, M. E. *J. Sci. Instrum.*, **34**, p. 9 (1957).
- (4) OHM, S., and CARROLL, K. G. *J. Appl. Phys.*, **30**, p. 1620 (1959).
- (5) NIXON, W. C. *Proceedings of the 4th International Conference on Electron Microscopy, Berlin*, paper No. 26.08 (1958).
- (6) ZEITLER, E., and BAHR, G. F. *Exp. Cell Res.*, **12**, p. 44 (1957).
- (7) HALL, C. E., and INOUE, T. *J. Appl. Phys.*, **28**, p. 1346 (1957).
- (8) LIPPERT, W. *Z. Naturforsch.*, **13a**, p. 274 (1958).
- (9) TOLANSKY, S. *Multiple Beam Interferometry of Surfaces and Films* (Oxford: Clarendon Press, 1948).
- (10) HAINE, M. E., and PAGE, R. S. *Proceedings of the 1st Regional Conference on Electron Microscopy in Europe, Stockholm*, p. 32 (1956).
- (11) WHELAN, M. J., *J. Inst. Metals*, **87**, p. 392 (1958-59).
- (12) BLACKMAN, M. *Proc. Roy. Soc. A*, **173**, p. 68 (1939).
- (13) HALLIDAY, J. S. *Proc. Roy. Soc. A*, **254**, p. 30 (1960).
- (14) HAINE, M. E., and AGAR, A. W. *Brit. J. Appl. Phys.*, **10**, p. 341 (1959).
- (15) COUPLAND, J. H. *Proc. Phys. Soc. (London) B*, **69**, p. 642 (1956).
- (16) MOLIÈRE, G. *Z. Naturforsch.*, **2a**, p. 133 (1947).
- (17) KOPPE, H. *Z. Phys.*, **124**, p. 658 (1948).
- (18) LEONHARD, F. *Z. Naturforsch.*, **9a**, pp. 727, 1019 (1954).
- (19) HALLIDAY, J. S. *Brit. J. Appl. Phys.*, **11**, p. 259 (1960).

Production of resonance radiation in discharge tubes of non-circular cross-section

by M. A. CAYLESS, B.Sc., A.R.C.S., A.Inst.P., Research Laboratory, Associated Electrical Industries (Rugby) Ltd., Rugby

[Paper received 7 July, 1960]

Abstract

The theory of d.c. low-pressure metal-vapour rare-gas discharges is developed, for the cases of simple one-stage and simple two-stage ionization, in a manner which enables the performance of a discharge in a tube of any given cross-sectional shape to be derived from that of an "equivalent" discharge in an "equivalent" tube of circular cross-section. The latter can be obtained from a more detailed investigation of the discharge in a circular tube.

It is shown that the discharges are capable of producing substantially more resonance radiation per unit length at a given efficiency in tubes of a "flattened" cross-sectional shape, than in tubes of a circular cross-sectional shape, particularly when there is a narrow, or waisted, middle section. Multi-stage ionization ultimately restricts the extent to which this improvement can be carried to aspect ratios of about 3 : 1.

1. Introduction

RECENT developments in low-pressure, gas-discharge lamps have shown that considerable advantages can be gained by using tubes of non-circular cross-section.⁽¹⁾ In particular, higher efficiencies or higher output of resonance radiation per unit length of tube can be obtained in this way for both fluorescent and sodium lamps. It is the purpose of this paper to explain this and to deduce the principles governing the choice of the most advantageous shape of cross-section.

The theory is developed primarily for the mercury rare-gas discharge, of the type used in fluorescent lamps, namely at a rare-gas pressure of between about 0.1 and 10 mm and a mercury vapour pressure of a few microns. Some modifications would be necessary before it could be applied directly to a discharge of the sodium lamp type. Only the positive column is considered, the regions near the electrodes producing but a small fraction of the radiation.

The ideal objective would be to deduce the characteristics (output, efficiency, field, etc.) of the positive column of any given discharge from its specifying parameters (size, shape, current, gas pressure, etc.) and the basic physical properties of its constituents (collision cross-sections, life-times, etc.). It will be shown that it is possible to divide this problem into two parts, such that the general theory is first worked out for discharges in tubes of circular cross-section, these then being extended to give the characteristics in comparable discharges in tubes of non-circular cross-section. This is a much more tractable proposition. The present paper is concerned only with the second part of the procedure: the comparison of the characteristics of discharges in tubes of non-circular cross-section with those of discharges in tubes of circular cross-section. The detailed theory of the circular discharge will be

given elsewhere. (A brief account of this procedure is given in Ref. 2.)

2. Assumptions

A uniform steady d.c. positive column is assumed, without striations or time variation, in a tube containing a metal vapour (specifically, but not necessarily, mercury) and a rare gas. Apart from secondary considerations, such as longitudinal cataphoresis, there is little observed difference between d.c. and 50 c/s a.c. operation, and such discharges often show neither stationary nor running striations nor oscillations, except at low currents, and the average outward characteristics (output, field, etc.) are little different when these are present. It is assumed that only the metal vapour is excited and ionized, and that the rare gas serves only to ensure diffusive conditions for all the particles involved; this will be so, in the case of mercury in argon, neon or helium, if the gas pressure and vapour pressure are greater than about 100 μ and 1 μ respectively.

The concentrations of the unexcited atoms and the gas temperature are assumed constant throughout the tube. (This is nearly true in a fluorescent lamp, but not in a sodium lamp.) The positive column is assumed to be an electrically neutral plasma, in which excitation and ionization occurs by electron impact and by the emission and absorption of resonance radiation. The tube is assumed to have electrically insulating walls, so that the electrons and ions move under conditions of ambipolar diffusion, as treated by Schottky.^(3, 4)

In the mercury discharge there are a large number of different transitions between the different states of excitation and ionization.^(2, 5) All these must be taken into account in the detailed theory of the production of resonance-radiation in the circular discharge.⁽²⁾ However, it is possible to compare discharges in tubes of different cross-sectional shape by considering only the two simplified schemes illustrated in Fig. 1. In Fig. 1(a) excitation to the resonance level and

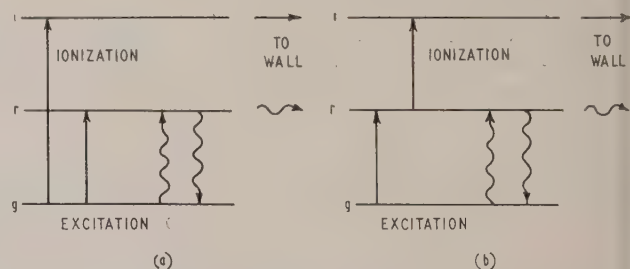


Fig. 1. (a) and (b) show the one- and two-stage ionization processes respectively; g , r and i indicate the energy levels of the ground state, the resonance state and the ions respectively. The wavy lines show the resonance absorption process and the horizontal arrows represent diffusion to the walls

ionization are assumed to occur directly from the ground state. In Fig. 1(b) ionization is assumed to occur only by electron collision with atoms already excited to the resonance level. These will be called the "one-stage" and "two-stage" cases respectively: the former is just that considered by Schottky⁽³⁾ in his theory of the circular discharge; the latter is considered because it is known that much of the ionization in the mercury discharge occurs *via* the excited 6^3P states.^(6, 7) (Spence⁽⁸⁾ has considered the case of two-stage ionization in circular tubes, but he assumes that the electrons and excited atoms are similarly distributed over the cross-section, which is not the case as the present results show.)

Because some of the ionization will occur *via* the metastable levels 6^3P_2 and 6^3P_0 , as well as the resonance level 6^3P_1 , and because of the influence of collisions of the second kind, which are ignored here, actual discharges may be expected to behave in a manner somewhere between those predicted for the one- and two-stage cases, which thus represent two limits for the expected behaviour of real discharges.

Transport of the atoms excited to the resonance level is mainly by emission and re-absorption of resonance photons. It is assumed that this process can be described by an effective diffusion constant which can be calculated from resonance-radiation transport theory.^(9, 10) Although Holstein⁽¹⁰⁾ shows that it is not strictly correct to regard the process as one of diffusion in this way, it is nevertheless quite easy to calculate an effective diffusion constant from his results which allows reasonably accurate deductions to be made from them, probably as accurately as his assumptions permit (see, for example, Ref. (11), especially pp. 217 and 226). It is not necessary to know the exact value of the constant for the present purpose.

The electron energy distribution is taken to be constant throughout the positive column. Careful probe measurements⁽¹²⁾ show that in this type of discharge the distribution is almost Maxwellian, with perhaps a slight deficiency at high energies. It is therefore assumed that it is fully described by an electron temperature, although this is not essential to the theory: any single parameter determining the energy distribution would suffice.

3. Theory

The concentration of any species α is denoted by n_α , and $z_{\alpha\beta}$ denotes the number of transitions per unit volume by electron collision from state α to state β per unit concentration of state α per unit electron concentration. The quantities $z_{\alpha\beta}$ are readily calculated by integrating the cross-sections over the electron energy distribution.⁽¹³⁾ V_α denotes the energy of level α above the ground state, and $V_{\alpha\beta} = V_\beta - V_\alpha$. Subscripts g, r, i, e and a refer to the ground state, the resonance state, ions, electrons and rare gas atoms respectively (except for D_a), and D_a and D_r denote the ambipolar diffusion constant and the effective diffusion constant for the resonance state (defined in Section 2) respectively. Subscripts 1 and 2 are used, when necessary, to distinguish parallel quantities in the one- and two-stage cases respectively; usually they will be used only when the quantity obeys different analytical relations in the two cases, and is not merely numerically different. They will also be omitted in statements applying to both cases. Δ denotes the Laplacian operator throughout.

The number of particles of species α diffusing out of an elementary volume δV , with a surface σ , is

$$Q\delta V = - \int_\sigma D_\alpha \text{grad } n_\alpha \cdot d\sigma \quad (1)$$

Hence the number diffusing outwards at any point per unit volume is

$$Q = - \lim_{\delta V \rightarrow 0} \frac{1}{\delta V} \int_\sigma D_\alpha \text{grad } n_\alpha \cdot d\sigma = - \text{div } D_\alpha \text{grad } n_\alpha \quad (2)$$

Hence if D_α is constant, as implied in the assumptions,

$$Q = - D_\alpha \text{div grad } n_\alpha = - D_\alpha \Delta n_\alpha \quad (3)$$

The general equations are obtained by equating this to the net number of transitions into each level in the steady state.

For boundary conditions it is assumed that the concentrations are negligible at the walls, compared with those in the body of the discharge, and n_i, n_r are thus put equal to zero at the boundary. This is satisfactory for rare gas pressures of 1 mm and over, and mercury vapour pressures of more than a micron or two (see Appendix 1).

The two cases may be developed in a parallel manner, as follows.

(a) *One-stage ionization.* Referring to Fig. 1(a), the conservation equations for this case are, remembering that $n_e = n_i$ in a neutral plasma,

$$D_a \Delta n_i + z_{gi} n_g n_i = 0 \quad (4)$$

$$\text{and} \quad D_r \Delta n_r + z_{gr} n_g n_i = 0 \quad (5)$$

$$\text{Defining} \quad x = n_i/n_{i0} \quad (6)$$

where n_{i0} is the maximum value of n_i ,

$$\text{and} \quad \Lambda_1^2 = D_a/z_{gi} n_g \quad (7)$$

these both reduce to

$$\Lambda_1^2 \Delta x + x = 0 \quad (8)$$

$$\text{if} \quad n_r = (D_a z_{gr}/D_r z_{gi}) n_i \quad (9)$$

Thus equation (8) provides the solution to both equations (4) and (5) provided n_r and n_i are similarly related at the boundary. The solution of equation (8) is discussed in Section (4) and Appendix 2; note that it also determines Λ_1 as an eigenvalue, which determines T_e through equation (7).

The resonance radiation output per unit length is

$$W_r = \int e V_{gr} z_{gr} n_g n_i dS \quad (10)$$

where dS is the element of the cross-sectional area S . By defining two dimensionless factors

$$j = \frac{1}{S} \int x dS \quad (11)$$

$$\text{and} \quad k = S/\Lambda_1^2 \quad (12)$$

and using equations (6) and (7), equation (10) can be written

$$W_r = j k \eta_1 \quad (13)$$

$$\text{where} \quad \eta_1 = e V_{gr} D_a z_{gr} n_{i0}/z_{gi} \quad (14)$$

The energy balance equates the total power input to the electron cloud to that lost in collisions thus:

$$Ei = \int (n_i (z_{gr} n_g e V_{gr} + z_{gi} n_g e V_{gi}^1 + z_e n_a) dS \quad (15)$$

where $V_{gi}^1 = V_{gi} + \frac{5}{2} k T_e$, the second term representing the kinetic energy carried by the electrons to the walls, n_a is the concentration of rare gas atoms, z_e is the rate of loss of energy by the electrons in elastic collisions with the rare gas atoms per unit electron and rare-gas atom concentration, E

is the longitudinal electric field and i the current through the discharge.

Using equations (11), (12) and (14), equation (15) reduces to

$$Ei = jk\eta_1(1 + \delta_1 + \epsilon) \quad (16)$$

$$\text{where } \delta_1 = z_{gi}V_{gi}^1/z_{gr}V_{gr} \quad (17)$$

$$\text{and } \epsilon = z_e n_a / z_{gr} n_g e V_{gr} \quad (18)$$

two dimensionless quantities representing the proportion of energy lost to the walls and to heating the rare-gas atoms respectively. The efficiency of resonance radiation production is

$$e = W_r/Ei = 1/(1 + \delta_1 + \epsilon) \quad (19)$$

The mobility equation is

$$\frac{i}{E} = e\mu_e \int n_e dS = jk\nu_1 \quad (20)$$

$$\text{where } \nu_1 = e\mu_e \Lambda_1^2 n_{i0} = \frac{e\mu_e D_a n_{i0}}{z_{gi} n_g} \quad (21)$$

Combination of equations (16) and (20) yields

$$E^2 = (\eta_1/\nu_1)(1 + \delta_1 + \epsilon) \quad (22)$$

$$\text{and } i = jk\{\eta_1\nu_1(1 + \delta_1 + \epsilon)\}^{1/2} \quad (23)$$

Note that, in this case, $i \propto n_{i0}$ {from equations (14) and (21)} whilst E is independent of n_{i0} . As a result of this, E is independent of i , since all the other Greek-letter factors are determined solely by T_e , which is determined by equation (7).

(b) *Two-stage ionization.* The conservation equations for this case {Fig. 1(b)} are

$$D_a \Delta n_i + z_{ri} n_r n_i = 0 \quad (24)$$

$$D_r \Delta n_r + z_{gr} n_g n_i - z_{ri} n_r n_i = 0 \quad (25)$$

Defining $x = n_i/n_{i0}$ as in equation (6)

$$y = \phi n_r \quad (26)$$

$$\text{and } \Lambda_2^4 = D_a D_r / z_{ri} z_{gr} n_g n_{i0} \quad (27)$$

$$\text{where } \phi = \frac{D_r}{\Lambda_2^2 z_{gr} n_g n_{i0}} = \left(\frac{D_r z_{ri}}{D_a z_{gr} n_g n_{i0}} \right)^{1/2} \quad (28)$$

and ignoring the last term of equation (25), which is always negligible, equations (24) and (25) become

$$\Lambda_2^2 \Delta x + xy = 0 \quad (29)$$

$$\Lambda_2^2 \Delta y + x = 0 \quad (30)$$

which are equations for x , y and the eigenvalue Λ_2 .

The solution of equations (29) and (30), giving the functions x and y , together with the eigenvalue Λ_2 , is discussed in Section 4 and Appendix 2.

$$\text{Defining } j_{xy} = \frac{1}{S} \int xy dS \quad (31)$$

$$\text{and } f = j_{xy}/j \quad (32)$$

where j is defined by equation (11), together with

$$k = S/\Lambda_2^2 \quad (33)$$

as in equation (12), then the resonance radiation per unit length in this case becomes

$$W_r = eV_{gr} \int n_i(z_{gr} n_g - z_{ri} n_r) dS$$

$$\text{that is, } W_r = jk\eta_2(1 - \psi f), \quad (34)$$

$$\text{where } \eta_2 = eV_{gr}(z_{gr} D_a D_r n_g n_{i0}/z_{ri})^{1/2} \quad (35)$$

$$\text{and } \psi = (D_a z_{ri} n_{i0}/D_r z_{gr} n_g)^{1/2} \quad (36)$$

The energy balance is

$$Ei = \int n_i(z_{gr} n_g e V_{gr} + z_{ri} n_r e V_{ri}^1 + z_e n_a) dS \quad (37)$$

which becomes, after some manipulation,

$$Ei = jk\eta_2(1 + \delta_2 f + \epsilon) \quad (38)$$

$$\text{where } \delta_2 = \psi V_{ri}^1/V_{gr} \quad (39)$$

and ϵ is defined by equation (18).

The efficiency of resonance radiation production is

$$e = \frac{W_r}{Ei} = \frac{1 - \psi f}{1 + \delta_2 f + \epsilon} \quad (40)$$

and the mobility equation (20) becomes, in this case,

$$i/E = jk\nu_2 \quad (41)$$

$$\text{where } \nu_2 = e\mu_e \Lambda_2^2 n_{i0} = e\mu_e \left(\frac{D_a D_r n_{i0}}{z_{ri} z_{gr} n_g} \right)^{1/2} \quad (42)$$

Equations (38) and (41) combined give

$$E^2 = (\eta_2/\nu_2)(1 + \delta_2 f + \epsilon) \quad (43)$$

$$i = jk\{\eta_2\nu_2(1 + \delta_2 f + \epsilon)\}^{1/2} \quad (44)$$

Note that in this case η_2 and ν_2 both contain n_{i0} implicitly, as well as as a factor, since its occurrence in equation (27) influences the electron temperature. Thus i is only approximately proportional to, and E only approximately independent of, n_{i0} . The dimensionless factor f arises as a result of the distribution functions n_i and n_r being different. In fact, f varies only slightly with the shape ($f = 0.7 \pm 0.04$ for all the shapes examined) and δ_2 is always small, so its effect on the relative performance of different shapes is negligible.

4. Equivalent tubes and discharges

The dimensionless equations (8) or (23) and (24) may be solved for any shape of tube by numerical methods. A Pegasus digital computer was used for the present calculations, the method being outlined in Appendix 2. In a few simple cases, equation (8) possesses analytical solutions, which agree well with the numerical solutions (better than 1%).

The computer is programmed to calculate directly all the dimensionless quantities denoted by Roman letters in Section 3, viz. x , y , j , k , j_{xy} and f . The virtue of the treatment given in Section 3 is that these quantities, which are conveniently referred to as the *geometrical factors*, depend only on the cross-sectional shape of the discharge tube, and not on its size, or on the physical properties of the discharge.

On the other hand, the characteristic diffusion lengths Λ , obtained from equations (12) or (33), depend on the size; also, through the area S . For any particular discharge, the electron temperature T_e may be obtained from Λ by equations (7) or (27), since all the quantities involved are functions of T_e , and from T_e all the other quantities denoted by Greek letters (η , ν , δ , etc.), in the equations of Section 3, may be calculated. These quantities are therefore all functions of the physical properties of the discharge, but depend on the size and shape of the tube only through Λ : they are conveniently referred to as the *physical factors*.

A set of discharge tubes, of different cross-sectional shapes, all of which yield the same value of Λ (in either the one- or two-stage cases) may be called "*equivalent tubes*". This is

a simple geometrical definition, quite independent of any particular discharge which may be run in the tubes.

If a set of equivalent tubes is filled with the same gases, at the same pressures, and operated at the same temperatures and at such currents that the maximum ion concentration is the same in each, then, from the preceding theory, the electron temperature T_e , and hence all the physical factors, are the same in each. These may be called "equivalent discharges".

In each case (one-stage or two-stage) the current necessary to run equivalent discharges is proportional to the geometrical factor

$$l = jk \quad (45)$$

by equations (23) and (44), and the output of resonance radiation from equivalent discharges is also proportional to the same factor, by equations (13) and (34), since the physical factors are the same. The longitudinal field E_z and the efficiency e , are the same for all equivalent discharges in the one-stage case, and very nearly so for the two-stage case, since the only geometrical factor involved is f which, as pointed out in Section 3, has only a very small effect.

Thus the geometrical factor l is a measure of the amount of resonance radiation per unit length, attainable at a given efficiency, from discharges in a tube of a given shape.

It is usually more convenient to express the output from tubes of various shapes relatively to that from equivalent discharges in equivalent circular tubes. This is done by writing

$$J = j/j_c, \quad K = k/k_c \quad \text{and} \quad L = l/l_c \quad (46)$$

$$\text{together with} \quad H = \eta l_c = \eta_c l_c \quad (47)$$

where the suffix c denotes the appropriate quantity for the equivalent discharge in the equivalent circular tube. The output of resonance radiation per unit length is

$$W_r = \eta j k = H J K = H L \quad (48)$$

and the output relative to the equivalent circular tube is

$$W_r/W_{rc} = J K = L \quad (49)$$

The separate factors J and K are retained in these formulae because of their simple physical significance: K is proportional to the relative cross-sectional area of the equivalent tubes, and J is a measure of the degree to which this area is filled by the plasma.

Note that what is compared is the relative output at the same efficiency. It is not possible to compare quantitatively, in so simple and general a manner, the relative efficiencies for the same output, although since efficiency decreases as output increases (provided the vapour-pressure is kept constant), it is clear qualitatively that shapes with high outputs at given efficiencies will also give high efficiencies at given outputs.

The advantage of this treatment is that it separates, to a reasonable degree of approximation, the purely geometrical factors involved in different shapes, from the physical factors (gas, pressure, temperature, etc.). These latter may be studied in detail for one shape, say the circular, and the results used to provide a reasonable estimate of the performance of other shapes, by means of the appropriate factors.

5. Results

The one-stage and (in most cases) the two-stage theories have been evaluated for tubes of the cross-sectional shapes defined by Fig. 2 and Table 1. The relative sizes of the

Table 1. Cross-sectional shapes of biconcave tubes

Shape	B1	B2	B3	B4	B5	B6	B7
B/A	$\frac{1}{2}$	$\frac{1}{2}$	$\frac{1}{2}$	$\frac{1}{2}$	$\frac{1}{3}$	$\frac{1}{3}$	$\frac{1}{3}$
C/A	0.25	0.25	0.35	0.4	0.222	0.25	0.267
r/A	0.813	0.183	1.288	1.90	2.03	2.69	3.35

A = maximum major width = diameter of convex surfaces

B = maximum minor width

C = minor width at centre

r = radius of concave surfaces

equivalent tubes obtained for each of these shapes, together with the geometrical factors J , K and L , are given in Table 2.

Table 2. Geometrical factors for tubes, of the shapes shown in Fig. 2, "equivalent" to a circular tube of unit diameter

Shape (Fig. 2)	Aspect ratio $A:B$	One-stage					Two-stage				
		A	B	J	K	L	A	B	J	K	L
C1	1:1	1.00	1.00	1.01†	1.00†	1.01†	1.00	1.00	1.00	1.00	1.00
E1	2:1	1.57	0.78	0.93	1.24	1.13	1.58	0.79	0.86	1.26	1.08
E2	3:1	2.20	0.73	0.85	1.60	1.36					
R1	2:1	1.46	0.73	0.94	1.36	1.28	1.48	0.74	0.84	1.39	1.17
R2	3:1	2.06	0.69	0.94	1.81	1.70	2.12	0.71	0.70	1.92	1.34
R3	15:4	2.54	0.68	0.94	2.18	2.05	2.64	0.71	0.58	2.38	1.39
B1	2:1	2.29	1.14	1.04	2.22	2.31**	2.31	1.16	0.97	2.27	2.20**
B2	2:1	2.08	1.04	1.09	1.95	2.12*	2.12	1.06	0.85	2.06	1.75
B3	2:1	1.87	0.93	1.03	1.72	1.77	1.91	0.96	0.81	1.80	1.47
B4	2:1	1.70	0.85	0.97	1.55	1.50					
B5	3:1	2.76	0.92	1.08	2.54	2.75**					
B6	3:1	2.56	0.85	1.12	2.31	2.58*	2.70	0.90	0.62	2.59	1.61
B7	3:1	2.44	0.82	1.05	2.21	2.32	2.57	0.86	0.63	2.46	1.48

A , B are the relative axial dimensions; K is the relative cross-sectional area; J is the relative degree to which the tube is filled by the discharge {see equations (11) and (46)}; $L = JK$ is the relative amount of resonance radiation per unit length produced by "equivalent" discharges

** Discharge unstable

* Discharge probably unstable

† Numerical value/Analytical value

The analytical values are shown for the one-stage rectangular cases

The relative sizes of the shapes shown in Fig. 2 are the equivalent sizes calculated for the one-stage case. In the two-stage case the non-circular tubes are slightly larger, as Table 2 shows, but this would only just be apparent in a drawing.

Figs. 3 to 6 show the function $x (= n_i/n_{i0})$ along the major axis and, in conjunction with Table 2, show graphically how the factor J represents the degree to which the plasma fills

the tube. In several cases this function does not reach its maximum at the centre of the tube; in such cases the discharge would be unstable and pass along one side only, rendering these calculations inapplicable. Those cases when this will certainly happen are marked ** in Table 2, and those in which it will probably happen are marked *. The normalized function y is shown in some cases: it always lies rather above x , the excited atoms being rather more widely distributed than the electrons and ions.

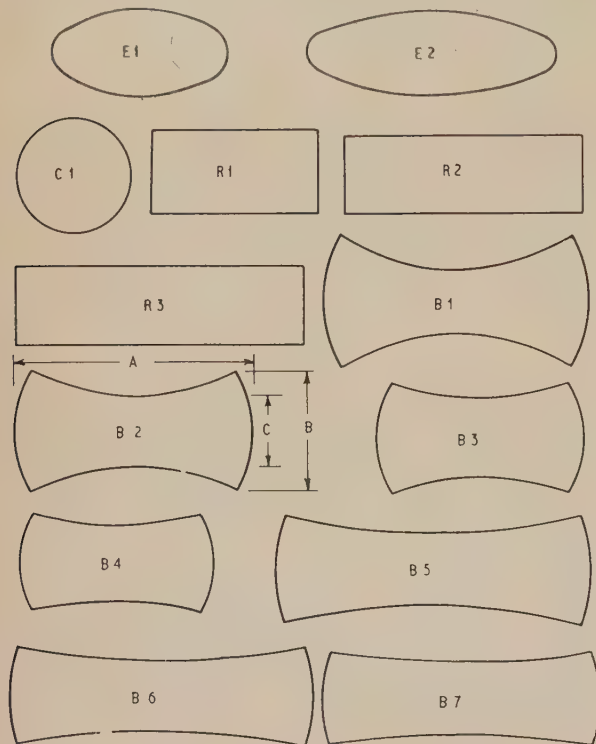


Fig. 2. The relative sizes of equivalent tubes of different cross-sectional shapes, in the case of one-stage ionization

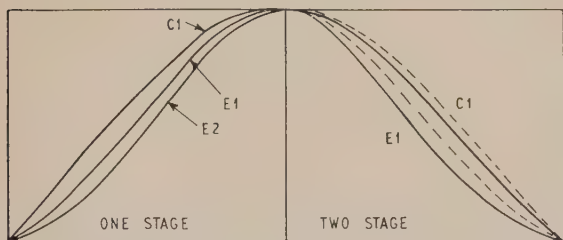


Fig. 3. Normalized plasma density distributions across circular tubes and across major axes of elliptical tubes. Full lines x ; broken lines y (two-stage only)

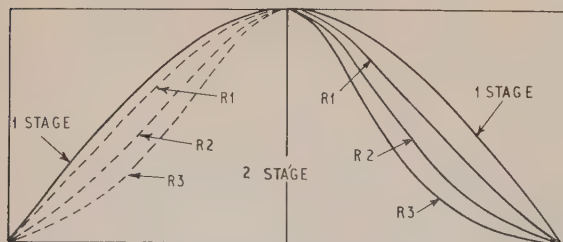


Fig. 4. Normalized plasma density distributions across major axes of rectangular tubes. Full lines x ; broken lines y (two-stage only)

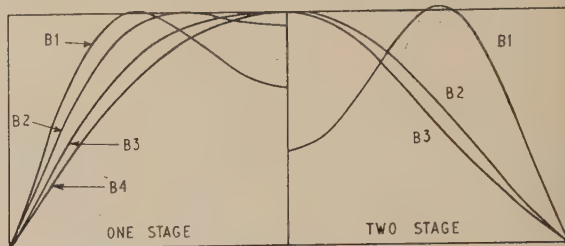


Fig. 5. Normalized plasma density distributions, x , across major axes of biconcave-shaped tubes of 2:1 aspect ratio

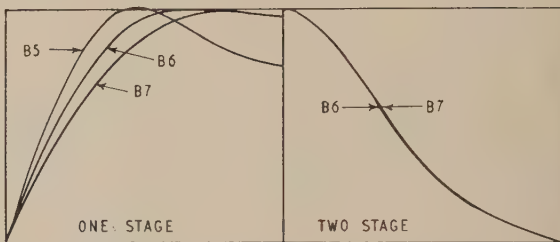


Fig. 6. Normalized plasma density distributions, x , across major axes of biconcave-shaped tubes of 3:1 aspect ratio

6. Discussion

It is clear that the "flatter" the tube (i.e. the greater the aspect ratio $A:B$) the more resonance radiation is emitted per unit length by equivalent discharges. For a given type of shape (e.g. a set of shapes obtained by rectilinear projection, such as a series of ellipses or rectangles) this is entirely due to the increase in K , i.e. the cross-sectional area. This is partially offset by the decrease in the "filling factor" J , particularly in the two-stage cases.

For rectangular tubes with purely one-stage ionization, the output per unit length could be increased indefinitely by increasing A/B , since J is constant, the tube being always filled to the same extent by the plasma; but with two-stage ionization, constriction becomes so marked for ratios greater than about 3:1 that there is little to be gained by further flattening. Actual mercury discharges always contain a substantial proportion of two-stage ionization at high currents, as pointed out in Section 2, and thus approximate closely to this condition at large aspect ratios.

Even with purely one-stage ionization, the discharge has difficulty in filling elliptical cross-sections. This trend is reversed in "dumb-bell" or "bone-shaped" cross-sections, of which the "biconcave" shapes B1 to B7 (Fig. 2) are the best of those examined. These therefore have high values of J as well as of K (which is high because the narrow middle section ensures a relatively high electron temperature), and thus have outstandingly high values of L . The process is limited by the obvious fact that if the waist is too narrow, the discharge will simply pass along one side alone, as in

B1 and B5, and the calculations for these cases are invalid. Note that this occurs gradually in the one-stage case, and suddenly in the two-stage case, as observed in practice. Another limitation is illustrated by comparing B6 and B7. At high aspect ratios the biconcave shapes are almost rectangular over their middle section, and the spreading effect of the biconcave shape is thus largely offset by the constricting effect which occurs with rectangular tubes in the two-stage case, giving an almost identical plasma density distribution. Thus for the biconcave shapes also, there is little to be gained from aspect ratios greater than about 3:1.

Acknowledgements

The author would like to thank his colleagues at the Research Laboratory of A.E.I. (Rugby) Ltd., for their interest and support, and especially Mrs. M. L. Read, of the Engineering Mathematics Department, who carried out most of the digital computer programming and operation.

Appendix 1

Boundary conditions

It is not difficult to show that the boundary condition $n_x = 0$ is satisfactory, provided the mean free path of the diffusive process is much smaller than the cross-sectional dimensions of the tube. The details of the proof differ for each type of diffusion, but this paper is concerned only with two species, the ions (with their associated electrons) and the atoms excited to the resonance level.

In the case of the ions and electrons, diffusing under ambipolar conditions, the electron free path is the controlling factor. This is a rather indeterminate quantity, because of the Ramsauer effect, but is generally of the order of 1 mm at a pressure of 1 mm of mercury of a rare gas, and the approximation is therefore justified at this and higher pressures.

In the case of the resonance atoms, the diffusion is principally due to the resonance photons, and the mean free path of these {suitably defined: see Ref. (9)} is determined by the mercury vapour pressure. Kenty⁽⁷⁾ finds that the effective mean free path in a fluorescent lamp of 1.8 cm radius at 40° C is 0.15 cm and, in general, it is found that the approximation is justified for tubes of a few centimetres cross-section if the vapour pressure does not fall much below a few microns (i.e. the wall temperature much below about 30° C).

More exact calculations, using more precise boundary conditions, have shown that little error is introduced, even when these conditions are only just satisfied; this is because the edges of the discharge make only a small contribution to the total output of resonance radiation.

Appendix 2

Method of obtaining the solutions

Equations (8), (29) and (30) were solved for the various shapes by using finite difference approximations in which the cross-sectional area is divided into a mesh of rectangular grid points (usually Δ was expressed in Cartesians, but occasionally cylindrical polars were used). In most cases the semi-major width was divided into twelve sections and the semi-minor width into six. The differential equations

(8), (29) and (30) were thus replaced by algebraic equations of the form

$$AX + \lambda_1 X = 0 \quad (50)$$

and

$$\frac{1}{Y}AX + \lambda_2 X = 0 \quad (51)$$

$$AY + X = 0 \quad (52)$$

where X and Y are vectors related to the functions x and y , λ_1 and λ_2 are constants related to Λ_1 and Λ_2 and A is a square matrix representing Δ for the appropriate boundary conditions. The method of solution depends on the fact that A can be arranged to be of "quasi-diagonal" form, i.e. such that all its elements, except those within a certain distance of the principal diagonal, are zero. A digital computer method has been devised⁽¹⁴⁾ for solving equations of the form equation (50) when A is of this form, and this was used to find the smallest latent root λ_1 and the corresponding vector X , using a Pegasus computer. The vectors corresponding to the other latent roots contain negative elements, and thus have no physical significance.

Equations (51) and (52) were solved by an extension of this method. A guess was made for the vector Y ; the matrix A was divided by this, and equation (51) solved for λ_2 and X , as was equation (50). A new value of Y was then obtained by solving equation (52), using the same computational procedure.⁽¹⁴⁾ The process, which was written as a self-contained Pegasus programme, converges in four to seven iterations.

For most of the shapes, solution of equation (50) took 10–15 min, and of equations (51) and (52), 50–90 min. The matrices each take an hour or two to write out and check.

The dimensionless quantities j , j_{xy} and f are obtained by integrating x and y , which are directly related to X and Y , in accordance with equations (11), (31) and (32), a two-dimensional form of Simpson's rule being used for this purpose. The value of K is given by $S\lambda_1$ and $S\lambda_1^{1/2}$ in the two cases, S being the area in the same units as those used in forming the matrix. The complete calculations were written as self-contained computer programmes.

To find the relative sizes of a set of equivalent tubes, their areas are determined from the values of K and their common value of Λ by equations (12) or (33). If the tubes are to be equivalent to a circular tube of radius R , the value of Λ is given by equations (12) or (33) and the values of K for a circular tube. These are 18.2 and 22.0 for the cases of one- and two-stage ionization respectively, and give therefore

$$\Lambda_{1c} = (\pi R^2/18.2)^{1/2} = R/2.405 \quad (53)$$

$$\text{and} \quad \Lambda_{2c} = (\pi R^2/22.0)^{1/2} = R/2.65 \quad (54)$$

References

- (1) AICHER, J. O., and LEMMERS, E. *Illum. Engng*, **52**, p. 579 (1957); **55**, p. 39 (1960).
- (2) CAYLESS, M. A. *Proceedings of the Fourth International Conference on Ionization Phenomena in Gases, Uppsala*, 1959, Vol. 1 (Amsterdam: North Holland Publishing Co., 1960).
- (3) SCHOTTKY, W. *Z. Phys.*, **25**, pp. 342, 635 (1924); see also Ref. (4), p. 236 *et seq.*
- (4) FRANCIS, G. *Handb. Phys.*, **22**, p. 53 (Berlin: Springer-Verlag, 1956).
- (5) KENTY, C. *J. Appl. Phys.*, **21**, p. 1309 (1950).
- (6) KLARFELD, B. *Z. Tekh. Fiz. USSR*, **5**, p. 913 (1938).

- (7) KENTY, C. *Phys. Rev.*, **80**, p. 95 (1950).
 (8) SPENKE, E. *Z. Phys.*, **127**, p. 221 (1950); see also Ref. (4), p. 128.
 (9) KENTY, C. *Phys. Rev.*, **42**, p. 823 (1932).
 (10) HOLSTEIN, T. *Phys. Rev.*, **72**, p. 1212 (1947); **83**, p. 416 (1951).
 (11) FOWLER, R. G. *Handb. Phys.*, **22**, p. 209 (Berlin: Springer-Verlag, 1956).
 (12) EASELY, M. A. *J. Appl. Phys.*, **22**, p. 590 (1951).
 (13) CAYLESS, M. A. *Brit. J. Appl. Phys.*, **10**, p. 186 (1959).
 (14) CAYLESS, M. A. *The Computer Journal*. To be published.

X-ray microscopy of beryllium

by J. SAWKILL, M. Met., Ph.D., and D. R. SCHWARZENBERGER, B.A., Tube Investments Research Laboratories, Hinxton Hall, Cambridge

[Paper received 6 July, 1960]

Abstract

The point-projection X-ray microscope has been used to study a variety of beryllium specimens, ranging from single crystals to finely-polycrystalline metal containing inclusions. The highly divergent beam of X-rays from a source $1\ \mu$ in diameter gives, on the same photograph, a microradiograph of the specimen with a resolution of $1\ \mu$ and a divergent beam diffraction pattern. Together these can give information about the distribution of heavier elements or cracks in the beryllium, the variation in perfection of the crystal lattice and, with a single crystal, the orientation and lattice parameters of the specimen.

Introduction

THE point-projection X-ray microscope⁽¹⁾ provides a highly divergent beam of X-rays from a source about $1\ \mu$ in diameter, suitable for both microradiography and divergent beam X-ray diffraction. A diagram of the experimental arrangement is given in Fig. 1. The electron beam is focused on to a metal foil about $1\ \mu$ thick, which

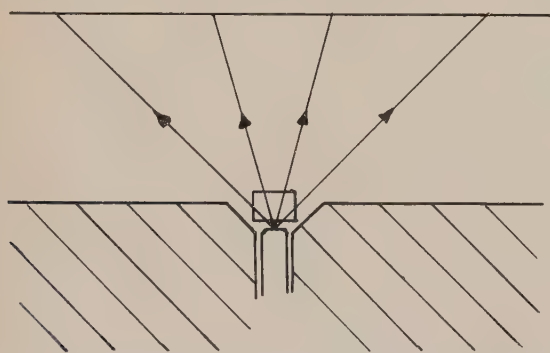


Fig. 1. Experimental arrangement of the X-ray microscope

acts as a transmission target. The specimen is placed in air immediately above the target, giving a shadow on the fluorescent screen or photographic plate placed in the path of the transmitted beam. The magnification is given by the ratio of the distance between the target and screen, to the distance between the target and specimen. The high primary magnification allows visual inspection of larger inclusions and the location of areas of particular interest. As the source

of X-rays is very small, the depth of focus is large, so that the specimen may be at any position between the target and plate according to the magnification required; a thick specimen of any shape can be observed, although the magnification then varies considerably throughout the specimen thickness. Normally no special preparation of the specimen is required.

If the accelerating voltage, which may be varied between 15 and 50 kV, is above the excitation voltage for the characteristic X-rays of the particular target in use, a transmission divergent beam diffraction pattern may be recorded from a crystalline specimen, in addition to the shadow microradiograph. Published work describing the use of the point-projection X-ray microscope for the examination of metallurgical specimens concentrates almost entirely on the microradiograph [see, for example, the articles in Ref. (2)], while the diffraction effects occurring in a divergent beam have generally been used for observations on the perfection and lattice parameters of good single crystals only [e.g. as in Ref. (3)]. Many metallurgical specimens, including most of the beryllium specimens studied, give rise to both types of contrast so that a transmission divergent beam diffraction pattern is superimposed on the microradiograph. Consideration of the two together often gives additional information about the microstructure of a specimen. Contact microradiographs of some thin beryllium specimens have been given by Udy,⁽⁴⁾ but this arrangement shows no diffraction contrast.

Beryllium is particularly suitable for microradiographic examination because of its low absorption coefficient for X-rays; the presence of most heavier elements is shown up by a large decrease in the transmitted intensity. The exposures for beryllium specimens up to 1 cm in thickness were about fifteen seconds with the photographic plate 4 cm above the X-ray source, using Ilford Special Lantern Contrasty Emulsion.

Absorption contrast

As the absorption coefficients of most other elements are much greater than that of beryllium, small amounts of other elements in solution may be expected to decrease the transmitted X-ray intensity considerably. For example, for a beryllium specimen 0.6 cm in thickness, the addition of 0.1% by weight of iron decreases the transmitted X-ray intensity to 73% of its original value (calculated for $\text{CuK}\alpha$ radiation,

neglecting fluorescence). In addition, most elements have a very small solid solubility in beryllium, so that even small amounts of impurity or alloying elements are likely to be present as a second phase, giving an even greater contrast against the beryllium matrix than if dispersed in a solid solution.

Figs. 2 to 5 are photographs of specimens of beryllium with a heavier second phase present, giving good contrast by the difference in absorption coefficient. Figs. 2 and 3 are microradiographs of extruded beryllium with heavier included material; the specimen was in the form of a cylinder, 1 cm in diameter and 0.5 cm in length parallel to the extrusion direction. The length was placed normal to the photographic plate for Fig. 2 and parallel to it for Fig. 3. The magnification on the print varies between about ten times for the part nearest the X-ray source to five times for the furthest part of the specimen. With the arrangement as in Fig. 1, vertical features in the specimen appear radial on the photograph as well as the truly radial features. These can be distinguished by taking stereoscopic pairs of photographs, or two photographs at right angles, as in Figs. 2 and 3. Comparison of these photographs shows that the large inclusions are, in fact, aligned parallel to the extrusion direction. The grain size in a transverse section was about 0.002 cm, which is too small for any distinct diffraction contrast to be seen. [See paragraph (iii) under Diffraction contrast.]

Fig. 4 is a microradiograph of a sintered alloy of beryllium with 5% ruthenium. In the region shown, the specimen thickness is two or three times the grain diameter. The ruthenium rich phase is present in a needle-like structure, apparently in grain boundary regions, and the same structure was observed in an optical examination. Fig. 5 is a microradiograph of a rolled sheet, 0.01 cm thick, of an alloy of beryllium with 1.8% silicon. The silicon rich phase is in particles which appear to be distributed at random in the matrix, but observations on stereoscopic pairs of photographs showed that the particles were in strings parallel to the rolling direction. Several other alloys of beryllium with small amounts of other materials were examined; the heavier the alloying element, the greater the contrast. In general, the second phase was continuous in grain boundary regions in the sintered alloys, but broken up into discrete particles in the rolled sheet alloys.

Diffraction contrast

(i) *Single crystal.* When a highly divergent beam of X-rays is transmitted through a single crystal, diffraction leads to a pattern of cones of deficient and excess intensity (Fig. 6); (hkl) planes of spacing d give rise to a deficient cone of angular radius $\cos^{-1}(\lambda/2d)$, and axis $[hkl]$. The expected pattern of deficiency cones can thus be calculated for a given X-ray wavelength and crystal structure, and drawn (e.g. on a stereographic projection) for comparison with the conic sections recorded on the photographic plate. This allows the deficiency cones to be indexed and the approximate orientation of the crystal to be seen. It was found that for a beryllium single crystal, giving sufficient contrast for the deficiency cones to be visible on a fluorescent screen, the orientation could be seen directly when a prominent crystallographic axis was approximately normal to the screen [e.g. $[10\bar{1}0]$ as in Fig. 7]. The pattern of excess cones depends on the relative positions of the specimen, source and plate, in addition to the crystal structure and the X-ray wavelength, while the deficiency line pattern is independent of the exact experimental arrangement.

Observations on the deficiency line pattern may allow the lattice parameters to be calculated in terms of the wavelength only. An intersection of three or more conics at a single point may arise from the symmetry of the lattice and be independent of the wavelength; for example, in any cubic crystal the deficiency conics from (200) and (020) planes always intersect on the conic from the (220) planes. Other multiple intersections, however, may depend on the relation between the X-ray wavelength and the lattice parameters of the crystal. Then, under favourable circumstances, calculations from such exact or near coincidences may allow the lattice parameters to be determined accurately for crystals of high symmetry. Calculations from two such coincidences, exact for $\text{CuK}\alpha_2$ radiation, on a photograph of a beryllium crystal taken on the point-projection X-ray microscope, gave

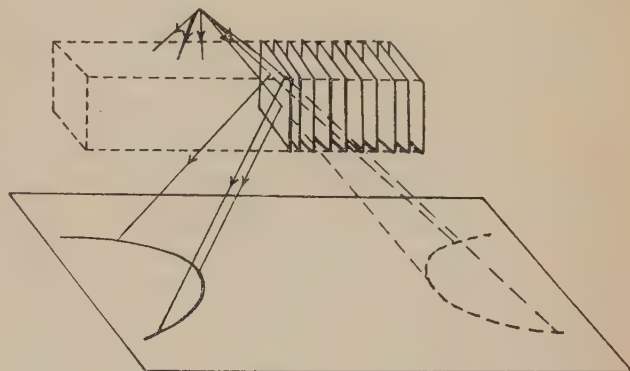


Fig. 6. Diagrammatic representation of the formation of deficiency and reflexion cones

the following values for the lattice parameters: $a = 2.2866 \pm 0.0006 \text{ \AA}$, $c = 3.5833 \pm 0.0009 \text{ \AA}$, $c/a = 1.5671$, at 22°C .⁽⁵⁾ With cubic crystals of greater perfection, lattice parameters have been determined with an accuracy of $\pm 0.002\%$,⁽³⁾ compared with $\pm 0.026\%$ for the beryllium values quoted here.

(ii) *Imperfections.* If the crystal is perfect, the deficiency lines are very narrow and may be difficult to record on a photograph, whereas with a less perfect or strained crystal, the lines are broadened. When there is a continuous variation in orientation within a single crystal the lines may be very wavy, and the presence of subgrains gives rise to deficiency cones with several distinct components. The angular orientation differences present in the crystal may be estimated by comparison of the distances on the photographic plate, between the components of a conic arising from the substructure, and from the known $\text{K}\alpha$ doublet separation for the particular radiation and set of reflecting planes. For example, the (0002) lattice spacing of beryllium is 1.79 \AA , the $\text{CuK}\alpha_1$ and α_2 wavelengths are approximately 1.540 and 1.544 \AA , giving a difference in the angular radius of the (0002) deficiency cone of $4'$ of arc. Then, if the components arising from differently oriented regions within the crystal are sharp lines, angular differences down to about $2'$ of arc may be detected. The direction in which the lattice is rotated, in passing across a low-angle boundary, may be estimated by a comparison of the extent and direction of the splitting of different conics. This may not detect all subgrains in the crystal, as the whole volume of the crystal is not observed at once, but only those parts which are on the surfaces of the cones from which diffraction occurs.

(iii) *Polycrystalline specimens.* With a polycrystalline specimen, short lengths of deficiency lines are recorded and

not a complete pattern of conics (compare Figs. 7 and 9), as directions deficient in X-rays can occur only within the projection of the grain in which they arise. In general, indices cannot be assigned to the lines, and only a qualitative estimate of the substructure and perfection can be made. For a grain of diameter D and magnification on the plate M , the maximum length of a section of a deficiency conic recorded on the plate is DM ; the length s of the recorded section of a deficiency conic is usually less than this, as the line does not necessarily coincide with the grain diameter; indeed, the orientation of some grains may prevent entirely the occurrence of deficiency lines in their projected area. If the grains are very small, the sections of deficiency conics may be so short and close together that they cannot easily be distinguished. To estimate the minimum grain diameter required for the deficiency lines to be visible, the effective width w of a deficiency line may be taken as approximately the $K\alpha$ doublet separation in the plane of the plate, and the line assumed to be distinguishable if $s > 4w$; i.e. for a single layer of grains $D > 4w$. For n layers of grains, one above another, the patterns overlap; if the grains are approximately spherical, and the deficiency lines are assumed to be visible if they occupy the same proportion of total area as for a single layer, the minimum grain diameter is $4nw$. The specimen thickness $t = nD$, giving the minimum grain diameter at which some diffraction contrast is recognizable as $4wt$. This estimate is probably rather low, and should be increased to allow for the sections of deficiency lines not always coinciding with the maximum diameter of a grain. It should also be increased if the lines are broadened by the crystal imperfections, or if the lattice parameters are large, compared with the wavelength of the radiation, so that even for a single crystal there are many reflexions. Using this criterion, the calculated minimum grain diameter at which the deficiency lines may be distinguished, for a specimen of beryllium 0.1 cm thick at 0.5 cm above a copper target, is about 0.001 cm, taking an average value of w for all possible reflexions. There is, however, an additional factor to consider: a single crystal or an individual grain in a polycrystalline specimen must be of a suitable thickness in the direction of the incident X-ray beam for deficiency conics of reasonable contrast to occur. For beryllium, with such a low absorption coefficient for X-rays, the minimum thickness is as great as 0.02 cm, so that this criterion, rather than length and overlapping of deficiency line sections, governs the minimum grain diameter for observation of diffraction contrast.

Combined microradiograph and diffraction pattern

Microradiographs of beryllium specimens with large variations in X-ray absorption, but no appreciable diffraction contrast, and the deficiency line pattern arising from diffraction in a specimen of uniform absorption coefficient, have been considered in the previous sections. Most specimens are intermediate between these two extremes, and a deficiency line pattern is recorded simultaneously with the microradiograph.

There are several advantages in considering these two types of information together. The deficiency line pattern is of value in revealing the grain-size of the specimen when the microradiograph shows inclusions in the material, showing whether they are concentrated at the grain boundaries or within the grains. Similarly, transgranular and intergranular cracking can be distinguished. In the deformation and recrystallization of a specimen, as described in more detail in paragraph (ii) below, the changing perfection of the grains

can be followed and correlated with the development of cracks or the positions of inclusions, as seen by absorption contrast. The short exposure time is an added advantage, allowing continuous changes, for example during the recrystallization of a specimen, to be followed by a series of photographs at short intervals of time. Precipitation effects in an alloy might similarly be followed by differences in absorption in the microradiograph, while any change in lattice parameter or perfection could be detected at the same time.

Two beryllium specimens giving a deficiency line pattern with the microradiograph have been studied in detail.

(i) Photographs have been taken at intervals along a zone-refined single-crystal rod of beryllium, about 25 cm in length and 0.6 cm in diameter, with the impurities concentrated towards one end by the zone refining process. At the pure end, Fig. 7, the pattern of deficiency conics is sharp, with no subgrains in the crystal, and no absorption contrast from the presence of heavier elements. By comparison with a stereographic projection of the expected pattern of conics, the orientation can be seen to be $[10\bar{1}0]$ normal to the photograph, with $[11\bar{2}0]$ approximately along the length of the rod, from left to right on the photograph, i.e. basal planes are parallel to the length of the rod. After this highly perfect region, about 1 cm in length, the conics become split into several sharp components; among most of the crystal there are three main components, corresponding to a total range of orientation of just under 1° . The directions of the orientation differences indicate that the subgrains are columnar, parallel to the length of the rod. At 18 cm from the pure end, precipitated impurity particles are first seen. The impurity appears to be concentrated in bands, rather than increasing smoothly from a low concentration at one end to a high concentration at the other. Fig. 8 shows such a discontinuity in the concentration of impurity, probably arising from a decrease in the volume of the molten zone during refining. The rod remains essentially a single crystal with fairly sharp deficiency conics and a range of orientation not greater than about 1° , even where the concentration of impurity is very high. Two photographs gave sufficiently clear deficiency line patterns, with suitable multiple inter-sections in $\text{CuK}\alpha_2$ radiation, to allow the lattice parameters to be determined in terms of the wavelength. In a fairly clear region, at about 20 cm from the pure end of the crystal the coincidences appeared exact, giving the values of a and c quoted in the section on Diffraction contrast. At the pure end, Fig. 7, the radii of the conics are slightly smaller, indicating a decrease of 0.02% in a and c , assuming c/a , and hence the absolute values of a and c separately could not be determined. This indicates that impurities expand the lattice slightly.

Thus a single series of photographs taken at intervals along the rod gives information about the variation in perfection, the variation in lattice parameters and the distribution of impurities in the crystal.

(ii) The deformation and recrystallization of a polycrystalline specimen of cast beryllium has been followed by divergent beam X-ray photography. The specimen was a cylinder 1 cm in diameter and 0.5 cm in thickness, with a grain size of about 0.1 cm. In the as-cast state, Fig. 9(a), the pattern consists of short sections of deficiency conics, with overlapping from the presence of several grains in the thickness of the specimen; the presence of subgrains gives rise to lines split into several components, and strains broaden the lines so that the $K\alpha$ doublet is not resolved in all the grains.

After 2% compression of the specimen at room temperature

the lines are broader and more wavy from distortions in the crystal lattice, Fig. 9(b). With further compression this effect increases and cracks develop, until after 10% compression, as in Fig. 9(c), the deficiency lines can scarcely be distinguished and extensive cracking is observed. After recrystallization of the specimen at 950° C for two hours, Fig. 9(d) shows that the cracks are still present, although a sharp deficiency line pattern has returned. The lines are now split solely from the $K\alpha$ doublet separation, indicating the absence of subgrains, and are slightly shorter, showing that the grain size has decreased. Porosity and cracking are difficult to observe in beryllium purely by absorption contrast, as the absorption coefficient of beryllium does not differ greatly from that of air. This is, however, partially offset by the occurrence of total external reflexion of X-rays incident at a glancing angle on an internal air-beryllium surface, outlining cracks with bright and dark lines. The refractive index for $FeK\alpha$ radiation in beryllium is $1 - 5 \times 10^{-6}$, giving a critical glancing angle of 10' of arc up to which total external reflexion can occur. Thus the reflected X-rays suffer a deviation of a few minutes of arc only, and the resulting crack outline is only slightly displaced or distorted compared with the microradiograph. Total external reflexion of X-rays is particularly noticeable for specimens of low X-ray absorption.

Acknowledgements

The single-crystal specimens of beryllium were kindly provided by the Atomic Weapons Research Establishment, Aldermaston, and the alloys by the Atomic Energy Research Establishment, Harwell, and the Brush Beryllium Co. We should like to thank Dr. J. W. Menter for valuable discussions, and the Chairman of Tube Investments Ltd. for permission to publish this work.

References

- (1) COSSLETT, V. E., and NIXON, W. C. *Proc. Roy. Soc. B*, **140**, p. 422 (1952).
- (2) COSSLETT, V. E., ENGSTRÖM, A., and PATTEE, H. H. *X-ray Microscopy and Microradiography* (New York: Academic Press Inc., 1957).
- (3) LONSDALE, K. *Phil. Trans Roy. Soc.*, **240**, p. 219 (1947).
- (4) UDY, M. C. *The Metal Beryllium*, Chapter 8, p. 515 (Cleveland: American Society of Metals, 1955).
- (5) SCHWARZENBERGER, D. R. *Phil. Mag.*, **4**, p. 1242 (1959).

X-ray microscopy of beryllium microradiographs, Figs. 2-5, 7-9

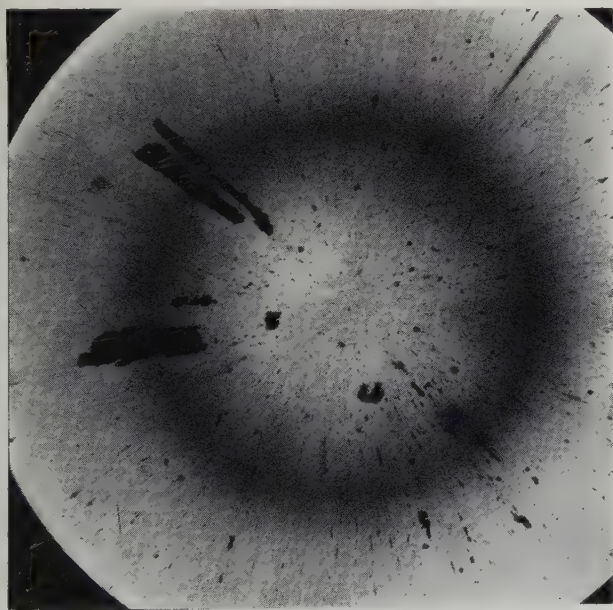


Fig. 2. Extruded beryllium with heavy included material. Copper radiation. Magnification $\times 5$ to $\times 10$

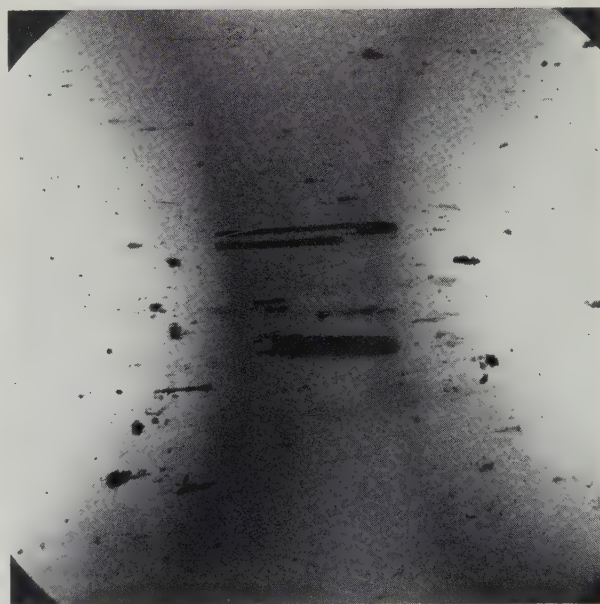


Fig. 3. Extruded beryllium with heavy included material. Copper radiation. Magnification $\times 1\frac{1}{2}$ to $\times 10$

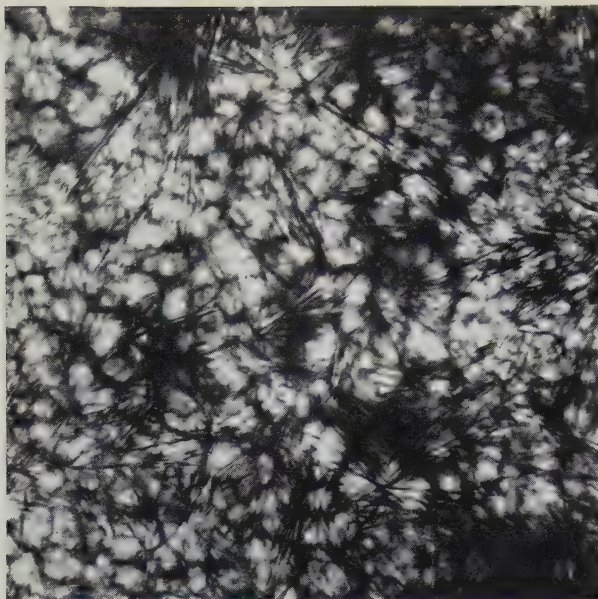


Fig. 4. Sintered alloy beryllium 5% ruthenium. Copper radiation. Magnification $\times 75$

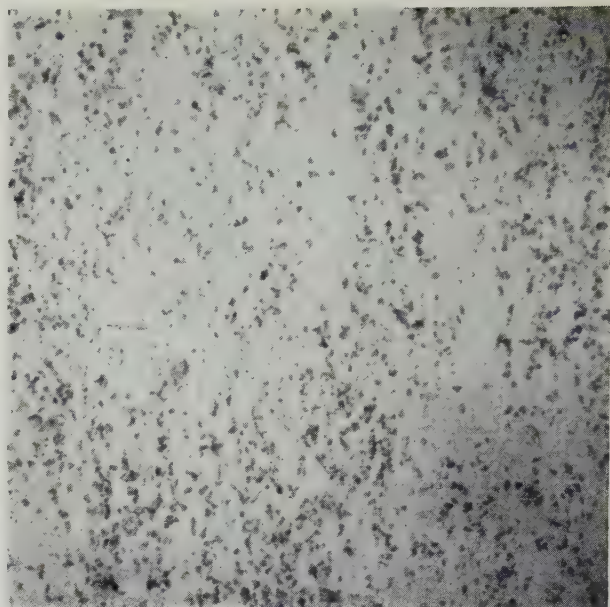


Fig. 5. Rolled alloy sheet beryllium 1.8% silicon. Copper radiation. Magnification $\times 75$

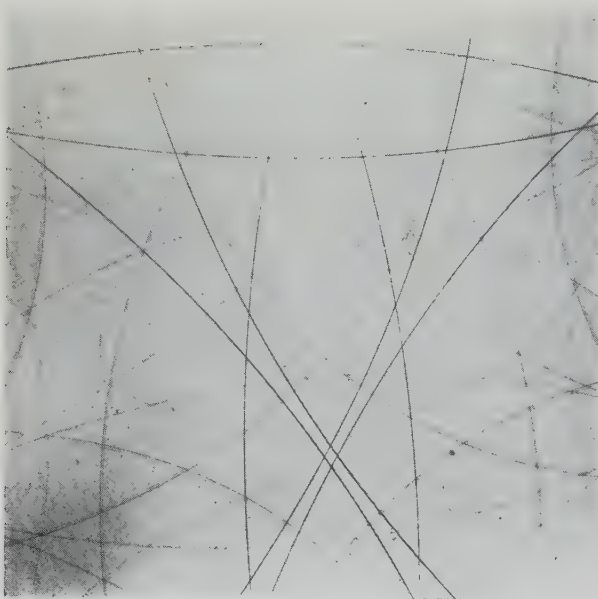


Fig. 7. Pure end of a zone-refined crystal of beryllium. Copper radiation. Magnification $\times 20$



Fig. 8. Impure end of a zone-refined crystal of beryllium. Copper radiation. Magnification $\times 20$

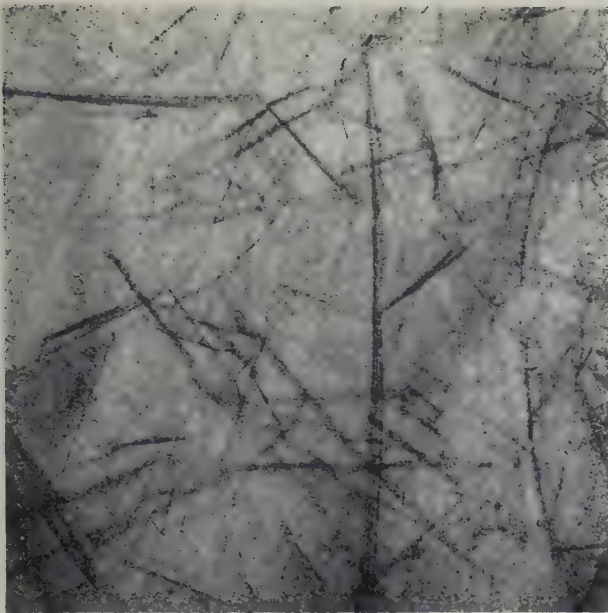


Fig. 9(a). Polycrystalline beryllium as cast. Iron radiation.
Magnification $\times 10$ to $\times 25$

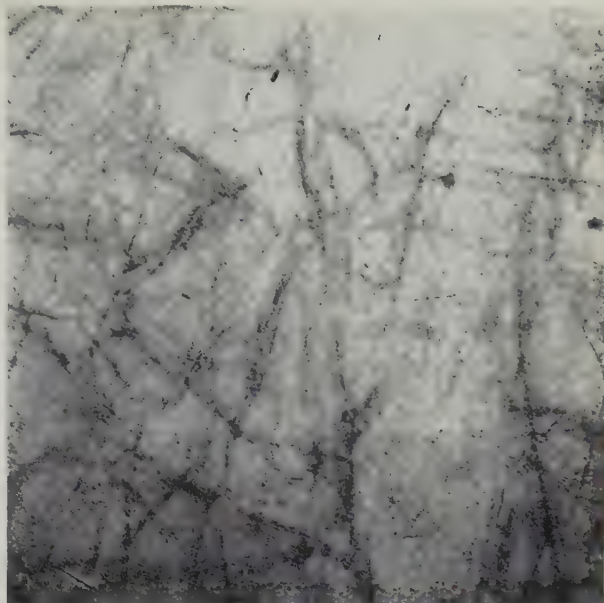


Fig. 9(b). Polycrystalline beryllium after 2% compression

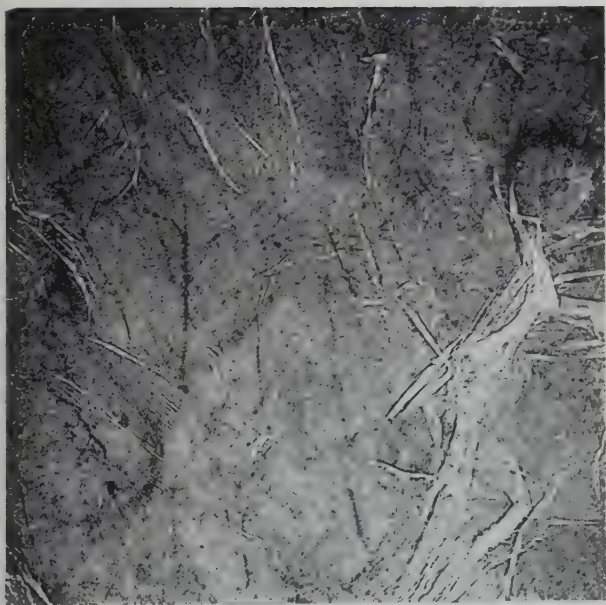


Fig. 9(c). Polycrystalline beryllium after 10% compression

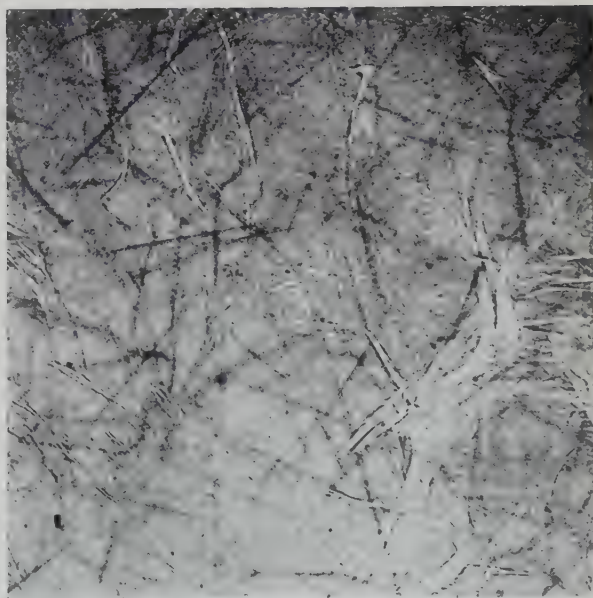


Fig. 9(d). Polycrystalline beryllium recrystallized

Selected-area diffraction in the electron microscope

by R. PHILLIPS, B.Sc., A.Inst.P., Aeon Laboratories, Egham, Surrey

[Paper received 14 July, 1960]

Abstract

A direct demonstration is given of the error in the area contributing to the recorded diffraction pattern, which arises from use of the incorrect objective focal length in microdiffraction experiments in the electron microscope. The effect of errors in the final intermediate lens setting is also discussed, and reproducibility of the camera constant λL in selected area diffraction is investigated.

Agar* has emphasized that a certain operational procedure has to be closely followed, if a selected area diffraction pattern in a three-stage electron microscope is to come solely from the area defined by the selector aperture under magnified image conditions. It is the purpose of this paper to demonstrate directly the contributions which may occur from an annulus outside the image of the aperture, due to incorrect excitation of the objective lens, and to comment on another important aspect of selected area diffraction—the reproducibility of λL .

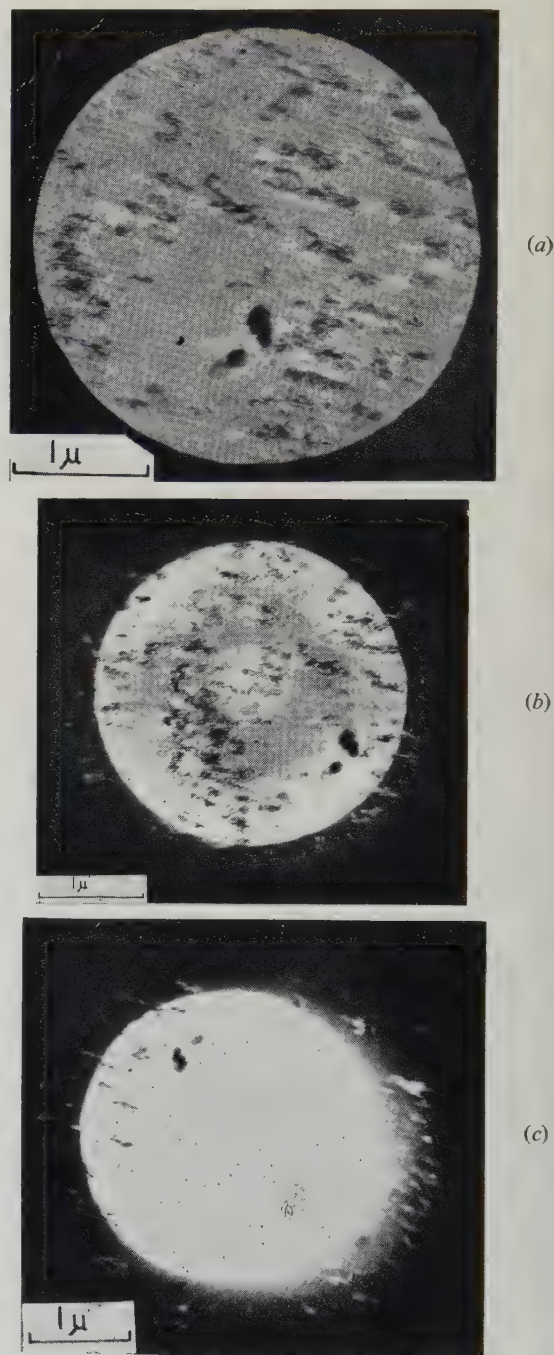
The correspondence of the area contributing to the diffraction pattern to that defined by the selector aperture

A SECTION of aluminium cut with an ultra-microtome was used as a specimen to investigate the true area contributing to its diffraction pattern. The specimen was photographed without an objective aperture, but with a $50\ \mu$ selector aperture above the intermediate lens. Fig. 1(a) was obtained by strict adherence to the correct procedure, i.e. the image of the selector aperture was focused on the final screen using the intermediate lens and then the final image of the object was focused with the objective lens. Two other photographs were obtained at objective lens excitations which one might easily be tempted to use in the course of microscope operation if the correct procedure were ignored.

Fig. 1(b) was taken with the intermediate lens set for a magnification of $\times 12\ 500$ (the correct procedure gave a magnification of $\times 17\ 000$), the image then being focused with the objective.

Fig. 1(c) was obtained with the intermediate lens set to give a magnification of $\times 27\ 500$, the image being focused with the objective. The magnification quoted for the figures defines the objective focal length which would be operating if a diffraction pattern were next obtained by reducing the total magnification to zero with the intermediate lens.

In each of the figures the bright field image is sharply defined, but in Figs. 1(c) and (b) it is surrounded by a dark field image of diffraction maxima. Thus, when a diffraction pattern is formed with the objective focal length used in Figs. 1(c) and (b), the orders involved in forming the diffraction contrast in the image will receive contributions from the dark field image region. If there are higher



Selected area micrograph

(a) Correct magnification. (b) Magnification too low.
(c) Magnification too high

* AGAR, A. W. *Brit. J. Appl. Phys.*, **11**, pp. 185-189 (1960).

diffraction orders produced by the specimen which do not give rise to diffraction maxima in its image, then contributions to those orders of the diffraction pattern may come from regions outside the dark field image. The extent of the region outside the bright field which contributes to some of the diffraction pattern is, in fact, limited by the maximum divergence of the beams produced by the specimen and accepted by the instrument. A simple ray diagram confirms the above discussion and further shows that some of the diffracted beams from the bright field regions are excluded by the selector aperture under the conditions of Figs. 1(c) and (b), as is mentioned in the instruction manual of the Siemens Elmiskop I.

In the work described by Agar,* the finite size of the crystal was a limitation on the accuracy which could be obtained in correlation of experimental measurements of the area outside the image of the aperture contributing to the diffraction pattern with electron optical theory. The method outlined above overcomes this difficulty, but is tedious to apply in detail because the dark field images have to be indexed.

The setting of the intermediate lens

It is easier to judge the correct setting of the intermediate lens in obtaining a selected area pattern if stages 3 and 4 of the procedure, as described by Agar, are reversed. That is, if the condenser lens is defocused before the final adjustment is made to the intermediate lens. For maximum resolution it is necessary to survey the centre spot of the pattern with a telescope during final adjustment of the intermediate lens and, since a small round spot is required on the plate, the condition is judged on the inclined screen as a small ellipse with its major axis normal to the axis of tilting of the screen.

When the intermediate lens is underfocused from the smallest round transmitted spot condition, the centre spot is extremely elongated in one direction; when it is overfocused, the spot is elongated in a direction at right angles. This is due to astigmatism in the intermediate lens which causes the lens to image the centre spot of the pattern in the back focal plane of the objective in a range of positions, according to the angular orientation of the beams concerned around the optic axis. The extremes of these positions may be called v_1 and v_2 , the position of the least distorted image being near $(v_1 + v_2)/2$. When $(v_1 + v_2)/2$ is located at the object plane of the projector, the image on the final screen is small and round. When $(v_1 + v_2)/2$ is below this plane, the transmitted spot is elongated along the direction of the rays imaged at v_2 and *vice versa*.

Thus, the small round spot condition corresponds to a definite setting of the intermediate lens, and the one which gives maximum resolving power in the diffraction pattern.

The same distortions will be applied to the diffracted spots as to the centre spot when the intermediate lens is incorrectly set, and this accounts for the general change in spot shapes in the sequence recorded in Agar's Fig. 8. This effect, together with the impossibility of focusing the spots all in the same way as explained by Agar, means that great care is required in operation and interpretation if the detailed shapes of diffraction maxima obtained in the electron microscope are to be seriously used in specimen analysis.

The camera constant for selected-area diffraction

There are a number of applications of selected-area diffraction in which it is more advantageous to maintain an

accurately known λL -value, than good correlation between the selected area and that actually contributing to diffraction. The identification of small crystals and the deduction of difficult orientations are examples of such applications. It is therefore important to consider the accuracy which may be expected in λL and how it might be improved.

It is readily shown that the effective camera length L of selected-area diffraction patterns is given by:

$$L = f_0 m M \quad (1)$$

where f_0 is the focal length of the objective, m is the magnification of the intermediate lens, and M is that of the projector.

Thus:

$$\Delta L/L = \Delta f_0/f_0 + \Delta m/m + \Delta M/M \quad (2)$$

where $\Delta L/L$ is the percentage error in L , etc. Consider the three components of the percentage error in turn. In most instruments, the projector is always maintained at minimum focal length, and $\Delta M/M$ is negligible; in the Siemens Elmiskop I, however, $\Delta M/M$ may be considered as the error in fitting the illuminated circle to the 9-cm circle scribed on the final screen. This can be eliminated by always operating the projector at maximum current for recording diffraction patterns; $\Delta m/m$ is the error in resetting the zero order spot to the small round condition. With careful operation this error is small.

The error $\Delta f_0/f_0$ is the error which arises from not exactly adjusting the magnification at which the image is focused before taking the pattern (thus defining f_0), together with the error in focusing the image and the error which arises from the different levels at which different specimens sit in the instrument, which necessitates changes in f_0 to get each specimen in focus. By changing the objective lens current deliberately, without altering the other setting, it has been shown that changes of 9 mA in a total current of 500 mA (i.e. 2%) give rise to variations in λL of about 3%. A change of 9 mA is quite large in objective lens current, but errors of 1 to 2% can readily arise from the $\Delta f_0/f_0$ component.

With the facilities currently supplied on microscopes, the procedure described by Agar must be followed if a reasonably constant λL value is to be obtained from selected-area diffraction, and even then an error of about 3% may be expected. Furthermore, if specimens sit at different heights in the instrument due to using different specimen holders, the procedure itself results in variations in λL , other than those due to random errors of judgement. This incidentally emphasizes that the calibrating grid should be mounted in the same holder as had been used for the specimen undergoing identification. It would seem feasible to make an arrangement so that the alteration of a switch adjusts the objective and intermediate lens currents to appropriate values for diffraction. In order to overcome hysteresis effects in the lenses, it may be necessary to incorporate some device for demagnetizing the lenses in the circuit. Such a procedure should standardize λL and make it independent of specimen level, but variations in specimen level and accelerating voltage will give errors in the area selected. These errors are not a severe drawback for some types of investigation, and can be calibrated and allowed for if necessary.

Finally, it may be mentioned that careful measurement of a calibration pattern shows that the product rd , where r is the radius of the ring and d is the spacing of the planes producing it, varies slightly but significantly with r ; $rd = \lambda L$ is only an approximate expression, and the full expression shows that rd decreases slightly with increasing values of r .

* AGAR, A. W. *Brit. J. Appl. Phys.*, **11**, pp. 185-189 (1960).

Furthermore, the spherical aberration of the objective causes f_0 to be smaller for larger values of θ , again causing rd to decrease as r increases. The variation in background intensity has a very small effect in the opposite direction. The determination of the d -values of an unknown material will best be accomplished by applying the formula:

$$(rd)_{\text{unknown}} = (rd)_{\text{calibration}} \quad (3)$$

when r_{unknown} and $r_{\text{calibration}}$ are similar values. This method

incorporates most of the accuracy obtained by simultaneous diffraction methods without involving the complicated experimentation associated with the latter.

Acknowledgements

The author wishes to thank Mr. A. W. Agar, Head of the Aeon Laboratories, for helpful discussions and for permission to publish this note.

Study of background structure in platinum/carbon shadowing deposits

by D. E. BRADLEY, Research Laboratory, Associated Electrical Industries Ltd., Aldermaston, Berks

[Paper received 30 June, 1960]

Abstract

The aggregation of metal shadowing deposits into small crystallites causes a background structure well known to electron microscopists. A different structure has been found to occur with amorphous shadowing materials. The paper describes the form of the structure and it is shown that the main cause is the hydrocarbon deposit formed on surfaces in the evaporating unit. The effect of the statistical distribution of the shadowing atoms on the ultimate resolution obtainable is discussed.

Introduction

THE background structure of evaporated metals used in shadow-casting for the electron microscope is caused by the aggregation of the shadowing layer into discrete crystallites. The size of the crystallites limits the resolution obtainable. Amorphous films which are stable under electron bombardment would obviously be more satisfactory, but those which can be easily deposited by vacuum evaporation usually have insufficient electron scattering power to permit their successful use for shadowing. However, the recent development of a method for the simultaneous evaporation of platinum and carbon⁽¹⁾ has enabled amorphous films of high electron scattering power to be produced, and the deposits do not aggregate under electron bombardment. The application of this technique to various problems has indicated that electron micrographs of very high resolution can be obtained. However, very fine background structures have been found in platinum/carbon films, and this paper discusses possible causes of these structures and how they can be reduced.

Coarse background structure

The method of evaporation is identical to that used for carbon⁽²⁾ save that the rod electrodes consist of a mixture of platinum and carbon. When a smooth surface is shadowed, a very coarse 100 Å structure is visible in the electron microscope. It is thought that this is caused by carbon scattered from adjacent apparatus into the deposit. If this carbon is prevented from reaching the specimen, by interposing a large screen fitted with a 2 mm aperture between

the source and target, the background structure is greatly reduced.

Fine background structure

Two types of background structure differing in appearance have been observed on using the aperture. The first, which occurred on smooth surfaces shadowed at angles greater than 45°, is shown in Fig. 1. The second, much coarser structure was found when a similar surface was shadowed at angles below 45° and is shown in Fig. 3. Fig. 2 shows a surface shadowed at 45° with an intermediate structure: Mica, which according to electron diffraction evidence



Fig. 1. A platinum/carbon film deposited normally on to freshly cleaved mica

is atomically smooth, was used in these examples. Surfaces of other cleaved crystals, such as magnesium oxide and lithium fluoride, which are also perfectly smooth, gave the same results, so that it is certain that the structure is due to the process of shadow-casting rather than the specimen.

The finer of the two structures (Figs. 1 and 2) has an appearance suggesting that the contrast changes are caused by a variation in the thickness of the film normal to the direction of the electron beam. The contrast is very low, and the dimensions of the structure are of the order of 20 Å. It is interesting to note that the structure becomes slightly coarser and more contrasty when the angle of deposition is changed from normal to 45°. It is likely that the uneven

ness in the film is beginning to be shown up by shadowing effects, as is clearly the case when the angle is further reduced to 26° (Fig. 3). Here, the film shows definite raised regions casting shadows. The maximum height of these small asperities as deduced from the shadow lengths is

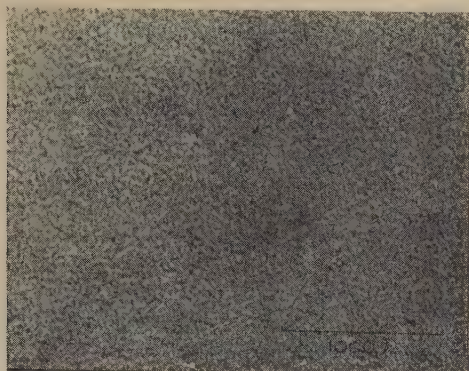


Fig. 2. A platinum/carbon film deposited at 45° on to freshly cleaved mica



Fig. 3. A platinum/carbon film deposited at 26° on to freshly cleaved mica

about 20 \AA , but they cover an area about 50 \AA across. Their angle of slope must be less than 45° , since they are not properly shadowed at this angle of deposition.

Though the appearance of the two structures is different, it is possible that they could be due to the same cause. The 20 \AA thickness difference in the film could well produce the contrast variations shown in the normally deposited film.

The causes of fine background structure

The most likely cause of the background structure in evaporated amorphous deposits is some contaminating layer from the atmosphere or the evaporating unit. It was found that atmospheric deposits were not the cause of the structure, since it appeared on mica and other surfaces, heated to several hundred degrees C prior to insertion in the plant, which was evacuated before the specimens were cool. This procedure would have removed deposits from the atmosphere but not from the plant, since the specimens were cold when the shadowing film was deposited.

It is known that a layer of contaminating molecules containing hydrocarbons is present on all surfaces in demountable vacuum systems, and this has been studied with particular reference to contamination in the electron microscope by Ennos.⁽³⁾ He only provides indirect evidence of its presence and gives no estimate of its thickness, a

factor of importance in the present investigation. It has been possible to study this film directly in the electron microscope by depositing a film of carbon against a vertical step (in a carbon film) about 500 \AA in height. The step is viewed in the electron microscope with its face parallel to the direction of the electron beam. An electron micrograph, such as that shown in Fig. 4, provides an "end-on" view of the contaminating deposit sandwiched between layers of carbon. In this case several bursts were used in the carbon evaporation, so that the layer produced after different time intervals could be studied in an electron micrograph. This procedure is described in detail elsewhere,⁽⁴⁾ but the result is of importance here in that it is possible to estimate the thickness of the layer.



[Reproduced from *Nature*]

Fig. 4. An "end-on" view of a contaminant layer deposited from a vacuum system (see text)

The first interesting point arising from Fig. 4 is the striking contrast difference between the carbon and contaminant layer. The high transparency of the layer suggests that it must contain large numbers of atoms with an atomic number less than carbon, in this case presumably hydrogen. This would be expected if the layer consisted of hydrocarbon molecules together with, possibly, some water molecules. In Fig. 4, the layer marked *A* represents the contaminant deposited after the plant was pumped down from atmosphere and subsequently evacuated with the diffusion pump for 30 min, as is the case with surfaces to be shadowed. Its thickness is about 25 \AA , and such a layer could easily give rise to the structure in Fig. 3. The remainder of the layers in Fig. 4 were formed during different time intervals between bursts of carbon, and show that the layer is not due to material deposited at atmospheric pressure. A further experiment has indicated that the layer is damaged by energy absorption from the stream of impinging shadowing atoms. This was carried out as follows. A thick contaminant layer was represented by a film of Apiezon B oil deposited on glass from a solution in benzene. This was then shadowed with platinum/carbon. On attempting to remove the resultant film by immersing the glass in benzene, it was found that the central part of the shadowed area, which had presumably received more energy than the surrounding region, remained firmly attached. This showed that the oil substrate was no longer soluble in benzene and had therefore undergone some form of chemical change. This phenomenon had also been observed on occasions on a mica substrate when no Apiezon oil film was present. Such chemical decomposition would almost certainly involve physical change, so that there is little doubt that this process plays a large part in the formation of background structure.

Attempts to reduce the magnitude of the background by subjecting the substrate to weak electron bombardment during the deposition of the shadowing material produced no conclusive effect. However, this procedure did cause the shadowing film to adhere so strongly to the mica that it was only removable by chemical attack. The contaminating layer was decomposed by electron bombardment⁽³⁾ and its bonding to the mica strengthened.

It is clear that the nature of the contaminating layer will vary from one pumping plant to another, so that the magnitude and appearance of the background structure will also vary.

Attempts to prevent the formation of the layer by depositing the shadowing material on to a surface at 250°C were impracticable, since it was found that platinum/carbon films granulate at this temperature. If a method could be devised to remove the hydrocarbons without damaging the specimen or the shadowing film, the background would be considerably reduced, but further considerations given below suggest that some structure would always be present.

The statistical distribution of atoms in a shadowing film

It is clear that no evaporated amorphous film can be perfectly smooth because of the statistical variations in its thickness. Their possible effect on the background structure of shadowing films is discussed here. These variations will also depend on the angle of deposition, therefore their mechanism of formation under conditions of normal evaporation are considered first, with reference to Fig. 5(a). It is assumed that no surface migration takes place.

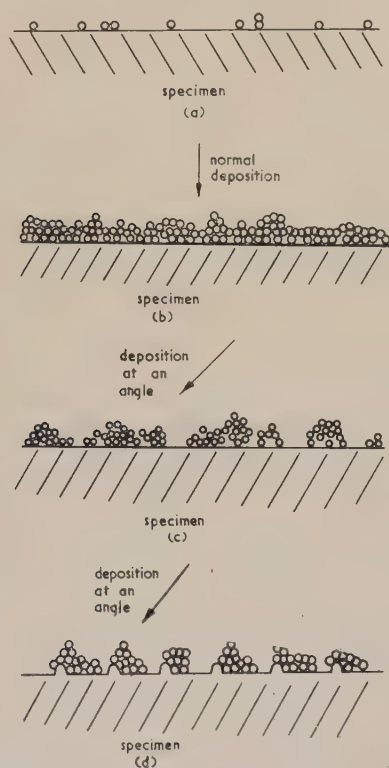


Fig. 5. (a) The random distribution of the first few atoms of an evaporated amorphous material to reach a smooth surface. (b) The suggested random distribution of a layer of amorphous atoms evaporated normally on to a smooth surface. (c) The suggested distribution of a layer of amorphous atoms evaporated at an angle on to a smooth surface. (d) The suggested distribution of a layer of amorphous atoms evaporated at an angle on to a surface possessing a very fine structure

Atoms deposited normally on to a smooth surface will be randomly distributed, and the first few atoms to arrive could be arranged as shown in Fig. 5(a). As the film becomes thicker, the variations will resemble those shown in Fig. 5(b). In a film 25 Å thick, the mean deviation will be ± 5 Å, a thickness difference which will probably be detectable in the electron microscope with a film of high electron scattering power.

When a film is deposited at an angle, the first few atoms to arrive will be distributed in a similar manner to normal deposition as in Fig. 5(a). As the film thickness increases, the randomly distributed single atoms will prevent the new arrivals from reaching areas on the surface immediately behind them with respect to the source, causing small groups of atoms, larger than those occurring with normal deposition, to form as shown in Fig. 5(c). These groups will increase in size causing greater thickness variations than in normally deposited films, and contrast from these variations will be increased by any shadowing effects.

The statistical effect described will influence the ultimate efficiency of the shadow-casting method and will probably represent a severe limitation when examining atomically smooth surfaces, but it would not necessarily prevent the detection of very fine structures. It can be seen from Fig. 5(d) that such structures are likely to provide the pile-up sites instead of the first few evaporated atoms; the shadows cast would therefore correspond to the surface topography. In order to test this theory, a specimen with a very fine recognizable surface structure would be needed. It seems certain that the arrays of molecules in the majority of high molecular weight crystalline materials would be too closely packed to provide adequate surface contouring, though there is a chance that some protein crystals may possess the desired characteristics.

Conclusions

It is clear that the main limitation to the resolution obtainable by shadow-casting with platinum/carbon is due to the contaminant film produced by the evaporating unit. If demountable vacuum systems can be improved, so that there is no contaminating layer, it is likely that a further limitation will be imposed by statistical effects.

In the case of metal shadowing materials it is possible that the removal of the layer will also improve the results. If this is achieved, it is likely that statistical effects will again affect the ultimate efficiency by influencing the size of the crystallites. The fact that the angle of deposition, which influences statistical distribution, affects the size of the crystallites⁽⁵⁾ supports this view.

It is difficult to compare the relative merits of crystalline and amorphous shadowing materials since specimens suitable for such a comparison are rare. However, it must be remembered that the contrast variations in crystalline materials are influenced by diffraction effects. Because of this, amorphous shadowing materials provide a slightly higher resolution, and certainly a less confusing electron micrograph. The overall quality and the sharpness of the shadows obtained with amorphous materials is definitely superior.

One of the objectives in using a high resolution shadowing material is to make use of the "magnification" produced by forming a shadow several times longer than the height of the original object. In this way, one might expect to detect changes in surface elevation beyond the limit of resolution of the electron microscope. Unfortunately, the effect of contaminant layers limits the lateral resolution available to about 20 Å.

It is not possible to give an exact figure for the resolving power of platinum/carbon shadowing since this will depend on the nature of the specimen and other factors already discussed. It has been found, however, that steps 10 \AA in height can be resolved at shadowing angles of $\tan^{-1} \frac{1}{2}$ (26°). For minimum background, a rather higher angle is desirable (about 45°).

In practice, the relationships between the angle of deposition and the size of the background structure with both crystalline and amorphous materials will conform to the same general rule, namely that the background increases as the angle decreases (i.e. approaches grazing incidence).

Acknowledgements

The author would like to thank Dr. J. S. Halliday, Mr. D. P. R. Petrie and Mr. T. Mulvey for their valuable discussions and help, and Dr. T. E. Allibone, Director of the Laboratory, for permission to publish this paper.

References

- (1) BRADLEY, D. E. *Brit. J. Appl. Phys.*, **10**, p. 198 (1959).
- (2) BRADLEY, D. E. *Brit. J. Appl. Phys.*, **5**, p. 65 (1954).
- (3) ENNOS, A. E. *Brit. J. Appl. Phys.*, **4**, p. 101 (1953).
- (4) BRADLEY, D. E. *Nature (London)*, **187**, p. 227 (1960).
- (5) HOLLAND, L. *J. Opt. Soc. Amer.*, **43**, p. 376 (1953).

Smoke density integrator

by R. M. STOREY, B.Sc., Grad.Inst.P., Humber Laboratory, Department of Scientific and Industrial Research, Hull

[Paper received 8 July, 1960]

Abstract

A simple instrument is described which both indicates and integrates the optical density of smoke in the range 0 to 1.0 optical density per foot. It consists of a detector unit exposed to the smoke and a remote control unit containing the indicator and integrator. A barrier-layer photocell, mounted within the detector unit, is loaded to give a logarithmic light intensity-voltage characteristic, so that a smoke obeying the Beer-Lambert law gives rise to a linear decrease in cell voltage with increasing optical density. Integration is achieved by means of a capacitor charged by the out-of-balance current of a self-rectifying a.c. bridge, in which the impedance of one arm is controlled by the photocell output. The overall stability over twenty-four hours is of the order of $\pm 6\%$.

Introduction

IT has long been known that exposing foodstuffs to wood smoke enhances their flavour and colour, and effects their preservation. The smoke-curing of fish has been studied in recent years with a view to discovering methods by which the process may be controlled. The instrument to be described was designed as one of the means by which this could be achieved. Although hitherto used for the measurement of wood smoke, its use could well be extended to other smokes. Whilst the particulate phase of wood smoke is mainly responsible for the attenuation of light passing through it,⁽¹⁾ it is now believed that the particles themselves play only a minor part in deposition on fish.⁽²⁾ However, it has been shown that the amount of smoke deposited can be predicted within practical limits from observations of the optical density of the smoke to which fish is subjected.⁽³⁾ The amount of smoke deposited is dependent on, amongst other factors, the density of the smoke and the period during which smoke of a given density is passed over the fish. For the purpose of process control, therefore, a sufficiently good index of the amount of smoke deposited is the integral of the product of smoke density and time.

During the course of this work, two instruments were designed specifically for measuring the optical density of wood smoke. The first is a recording smoke-density meter,⁽⁴⁾ which is suitable for measurements in mechanical smoking kilns.⁽⁵⁾ The second is a much simpler, portable instrument⁽⁶⁾ based on a single selenium barrier-layer photocell and calibrated microammeter, designed initially for observations in traditional smoke-curing houses. The integrator has been developed from this simple instrument.

A detailed study⁽¹⁾ of the attenuation of white light by wood smoke has shown that within the limits of normal practice, the relation between the mass concentration of the smoke and the optical density is in agreement with the Beer-Lambert law, for the tungsten filament lamp and barrier-layer photocell system employed in the simple smoke-density meter, referred to above. This study shows that since at any point in the beam of light passing through the smoke the angle subtended by the photocell is finite, a small amount of scattered light is collected by the photocell and gives rise to an observed optical density, which is less than the true value. This source of error is discussed later.

After the initial development of the integrator it was discovered that a similar technique had been used to integrate auroral light.⁽⁷⁾ Light quantity meters are available commercially. These are either designed for photographic exposure control (the Quantex light quantity meter by the Baldwin Instrument Co. Ltd.) or the integration of the intensity of daylight [by Photoelectronics (M.O.M.) Ltd.].

Description of instrument

The voltage produced across a selenium barrier layer photocell of the type used (type M.1, by Evans Electro-selenium Ltd.), suitably loaded and under suitable conditions of illumination, is

$$E = K \log_{10} I \quad (1)$$

where K is a constant and I is the intensity of light falling on the photocell.

If a parallel beam of light of initial intensity I_0 passes through a smoke obeying the Beer-Lambert law, then

$$E_0 - E = K \log_{10} (I_0/I) \quad (2)$$

where E_0 is the voltage produced in the absence of smoke; $\log_{10} (I_0/I)$ is defined as the optical density D of an absorbing medium so that the smoke can be characterized by the optical density per unit length D/L , where L is the length of the light path in the smoke.

The instrument consists of a detector unit, which is placed entirely in the smoke, and a remotely situated indicating and integrating unit. The detector unit consists of a single-beam arrangement which, for simplicity, is to be preferred to a double-beam, null-balancing method which is more difficult to indicate remotely, even though the single-beam technique is inherently less stable. However, this latter method can be made sufficiently stable for the present purposes over periods of the order of 24 h, provided that certain precautions are taken. To achieve this it is necessary to supply the lamp from a constant voltage transformer and to maintain the

Araldite to the outer case G , which is a $3\frac{1}{2}$ in. inner diameter aluminium tube, 20 in. long. Smoke is allowed to pass through the light beam by means of ports on either side of the tube. The light path through the smoke is defined by Pyrex glass windows K cemented on Tufnol disks F which are cemented to the tube with Araldite. Smoke is prevented from condensing on to the windows by heating them by passing an electric current through a transparent conducting layer deposited on the glass. The windows were coated in the laboratory by spraying a concentrated solution of stannic chloride over them while they were maintained at a dull red heat. This method produces a conducting film, which is resistant to abrasion and which has a resistance of 30 to 100 Ω per square. Conducting glass can be obtained commercially (from Megatron Ltd.), but is generally of higher resistance. Electrical contact is made to the windows by spring contacts E (Fig. 1).

The error in optical density measurement due to the forward scattering of light by the smoke particles, which is inherent in all absorption methods, may be reduced by

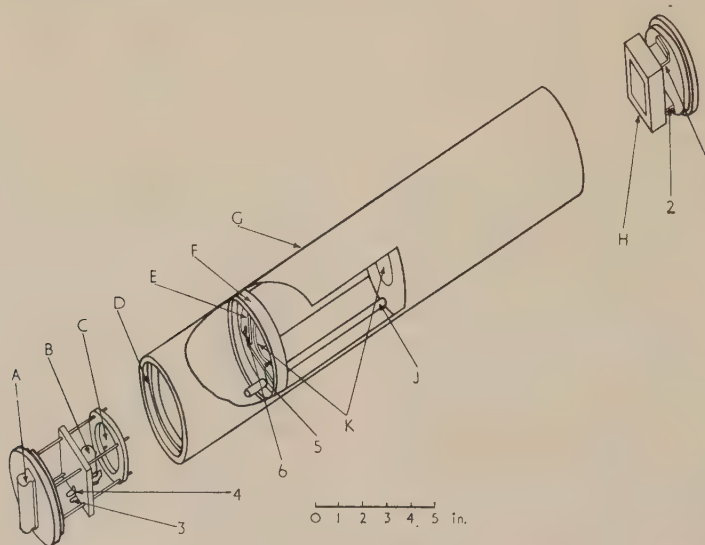


Fig. 1. Diagram of detector unit

photocell at a constant temperature. In the simple instrument mentioned above⁽⁶⁾ it was found necessary, in field work, to pre-fatigue the photocell by short-circuiting it under normal illumination for a short period, so that the instrument was sufficiently stable for use within about five minutes. Since the initial warming-up period of the integrator is about half an hour, and since it is used continuously in one situation, although portable, it has been found unnecessary to pre-fatigue the photocell.

Details of the detector unit are shown in Fig. 1. Light from a 6 V, 1 A, class G4 projector lamp B (Fig. 1) is focused by means of a $1\frac{1}{2}$ in. focal length lens C so that photocell H is fully illuminated. The photocell comprises twenty small selenium barrier-layer photocells connected in series, and has a sufficiently high impedance to enable the output to be fed directly to the grid of a thermionic valve. The value of the grid resistor of this valve is so chosen that the output voltage of the photocell varies logarithmically with light intensity.

The photocell and optical system are mounted in line on removable Tufnol endpieces A (Fig. 1) which are a smoke-tight fit in Tufnol rings D . These rings are sealed with

arranging for the maximum angle subtended by the photocell at any point in the smoke to be as small as possible. In the present instrument, the distance between the photocell and the window defining the smoke path at the end remote from the light source has been extended, in relation to the earlier instrument,⁽⁶⁾ so that this angle does not exceed 12° . The error is estimated to be about 2.5% of the indicated density but could, of course, be further reduced by increasing the overall length of the detector unit.

The temperature of the photocell is maintained at approximately $38 \pm 2^\circ \text{C}$ by means of a 15 W heater and a small thermostat (type PQLX, by Electrothermal Engineering Ltd.) connected across the supply leads to the heated windows, which are not shown in Fig. 1. Electrical connexion is made between the detector unit and the integrating unit by means of seven-way screened cable. The length of the cable is limited only by the voltage drop introduced in the conductors carrying current to the lamp, the heated windows and the photocell heater. In practice, this length can be at least 30 ft, allowing the detector unit to be readily placed in a convenient position within the smoke. The numbering of the electrical connexions 1-6 in Fig. 1 corresponds with the numbered

terminations in Fig. 2. The seventh wire is connected to a lamp in the indicator unit and to the thermostat switch in the detector unit, thus enabling a check to be made on the satisfactory operation of the thermostat.

The circuit diagram of the indicating and integrating unit is shown in Fig. 2. Pentodes V_1 and V_2 and the centre-tapped winding L_1 on transformer TR_2 form the four arms of a self-rectifying a.c. bridge. The primary of TR_2 is fed from a constant-voltage transformer TR_1 . For conditions of no smoke, the bridge is balanced by adjusting the anode current of V_2 , so that the milliammeter M_1 indicates zero current. An integrating capacitor C_1 , in series with meter M_1 , is charged by the constant out-of-balance current produced

to be set at a predetermined value for a given value of optical density indicated by M_1 .

A Smidt double-triode trigger circuit,⁽⁸⁾ in addition to V_3 , would improve the stability of the counting rate at the expense of simplicity.

Calibration

The integrator is switched on and allowed to stabilize for a period of about half an hour. The balanced condition for unattenuated light, as shown by zero indication on meter M_1 is achieved by adjustment of RV_4 (coarse) and RV_5 (fine) (Fig. 2).

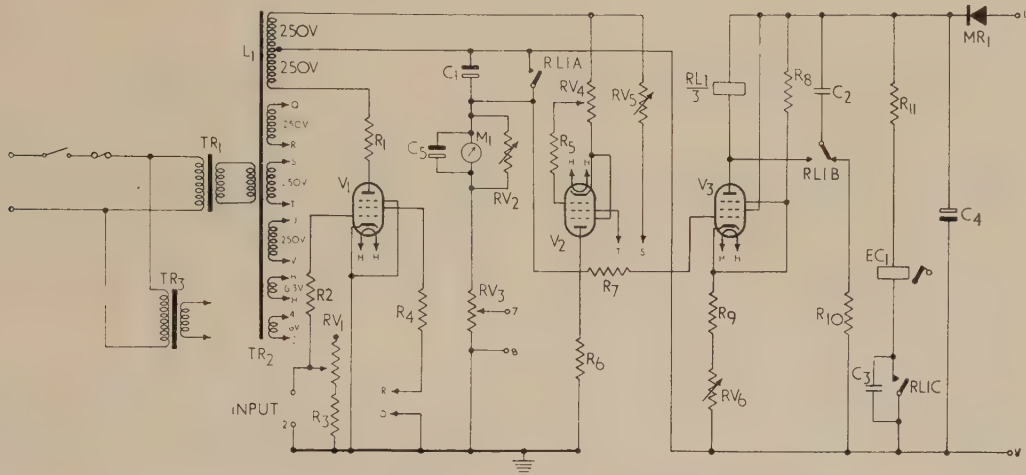


Fig. 2. Circuit diagram of indicating and integrating unit

$R_1 = 25 \text{ k}\Omega$
 $R_2 = 1 \text{ M}\Omega$
 $R_3 = 2.7 \text{ M}\Omega$
 $R_4 = 47 \text{ k}\Omega$
 $R_5 = 1 \text{ M}\Omega$
 $R_6 = 25 \text{ k}\Omega$
 $R_7 = 1 \text{ M}\Omega$
 $R_8 = 10 \text{ k}\Omega$
 $R_9 = 700 \Omega$
 $R_{10} = 10 \text{ k}\Omega$
 $R_{11} = 5 \text{ k}\Omega$

$RV_1 = 2 \text{ M}\Omega$ linear
 $RV_2 = 250 \Omega$ w.w.
 $RV_3^* = 10 \Omega$ w.w.
 $RV_4 = 5 \text{ k}\Omega$ w.w.
 $RV_5 = 50 \text{ k}\Omega$ w.w.
 $RV_6 = 500 \Omega$ w.w.
 $C_1 = 2000 \mu\text{F}$, 6 V, electrolytic
 $C_2, C_3 = 0.1 \mu\text{F}$
 $C_4 = 32 \mu\text{F}$, 350 V, electrolytic
 $C_5 = 6000 \mu\text{F}$, 6 V, electrolytic

* Provides 0–10 mV output for potentiometer-recorder via terminals 7 and 8

All carbon resistors $1 \text{ W} \pm 10\%$ except R_{11} (3 W w.w.)

$V_1, V_2, V_3 = \text{CV138}$

$MR_1 = \text{half-wave rectifier } 250 \text{ V}, 50 \text{ mA}$

$M_1 = \text{milliammeter } 0.1 \text{ mA}, \text{ resistance } 55 \Omega$

$TR_1 = \text{constant-voltage transformer type M.T. 161A. Advance Components Ltd.}$

$TR_2 = \text{ specially wound transformer. Input } 230 \text{ V, Output } L_1 \text{ } 250\text{--}0\text{--}250 \text{ V, } 20 \text{ mA QR } 250 \text{ V, } 2 \text{ mA. ST } 250 \text{ V, } 2 \text{ mA. UV } 250 \text{ V, } 40 \text{ mA. HH } 6.3 \text{ V, } 1 \text{ A } 4, 3.6\text{--}0 \text{ V, } 1 \text{ A.}$

$TR_3 = \text{transformer input } 230 \text{ V, output } 24 \text{ V, } 2 \text{ A}$

$EC_1 = \text{electromagnetic counter, Sodco type TCZ4E, } 5.8 \text{ k}\Omega, 120 \text{ V, 4-digit with manual reset}$

when the anode current of V_1 is increased, by a reduction in the grid bias, when the output of the photocell falls due to the presence of smoke. To maintain linearity in the characteristics of V_1 and V_2 it was found necessary to supply their screen grids from separate windings on TR_2 , connected so that the potentials were suitably in phase with the corresponding anodes. Pentode V_3 is biased-off by means of resistors R_9 and RV_6 so that the anode current is below the operating current of relay RL_1 . As the charge on C_1 increases V_3 becomes more conducting, until RL_1 operates. Contacts RL_{1A} then discharge C_1 ready for the next cycle. During the non-conducting period of V_3 , capacitor C_2 is charged from the h.t. supply via changeover contacts RL_{1B} . When RL_1 operates, C_2 is discharged through RL_1 , causing it to "hold on" for a short period after V_3 has become non-conducting again. This allows C_1 to discharge fully, and at the same time contacts RL_{1C} are closed for a sufficiently long period to operate the electromagnetic counter EC_1 . The bias applied to the control grid of V_3 is adjusted so that the counting circuit is triggered when C_1 has been charged to an appropriate amount. This allows the rate of counting

A scale reading in optical density per foot printed on the chart of meter M_1 , is subdivided linearly in the range 0–1, so that in calibrating with standard filters allowance must be made for the path length of the light, which in this instrument is 6 in. Neutral density filters (by Ilford Ltd.) of 1% accuracy have been used for this purposes. The procedure for adjustment is as follows.

A neutral density filter of optical density approaching 0.5 is inserted in the light path and the meter shunt RV_2 adjusted until a scale reading equal to twice the filter density is obtained. The first filter is then replaced by a second of lower density, approximately 0.1 optical density, and the scale reading observed. If this does not correspond to twice the density of the filter the photocell load resistor RV_1 is adjusted, and the procedure is repeated until correct readings are obtained at each of the calibration points and at zero optical density. This method ensures both that the photocell is operating on a logarithmic characteristic and that M_1 is reading correctly.

The integrator is then calibrated by placing a neutral density filter in the light path and adjusting RV_6 until the

hourly count on the counter EC_1 is numerically 1000 times the density indicated on M_1 . The register will then indicate the value $\int (D/L)dt$ in intervals of $10^{-3} \text{ ft}^{-1} \text{ h}$, when the detector unit is exposed to smoke of varying density.

Performance

A neutral density filter of 0.15 optical density was selected in order to simulate smoke of density 0.3 ft^{-1} typically encountered in controlled fish-smoking kilns. The counter was then made to record at a rate of 300 counts per hour as described above. The table shows the number of counts registered in one hour when neutral density filters of various other values were inserted in the light path of the detector unit.

Comparison of indicated and correct integrated smoke density over period of one hour

Density of neutral filter	Reading on meter M_1	No. of counts on counter per hour [$\approx 1000 \int (D/L)dt$] (mean value)	Correct value of $\int (D/L)dt$ ($\text{ft}^{-1} \text{ h}$)	Error of mean values (%)
0.05	0.10	103 ± 4 -7	0.1	+3.0
0.10	0.20	202 ± 2 -4	0.2	+1.0
0.15	0.30	300 ± 3	0.3	0.0
0.20	0.40	395 ± 2 -5	0.4	-1.3
0.25	0.50	496 ± 3	0.5	-1.0
0.40	0.80	788 ± 4 -5	0.8	-1.5
0.50	1.00	977 ± 3 -4	1.0	-2.6

As can be seen from the table, the integrator is not perfectly linear, but is sufficiently so for the present purposes. Greater accuracy could be achieved by calibrating the integrator at the expected mean density. The figures quoted in the table include any instability in the lamp and photocell, and they indicate the overall accuracy of the instrument.

The zero drift and optical density calibration drift were each found to be within $\pm 2\%$ of full-scale reading over each twenty-four hour period. The drift in the rate of counting was also found to be approximately $\pm 2\%$ of the correct value for a given density over each twenty-four hour period. Thus, to obtain results which are accurate to better than $\pm 6\%$, it is essential to check the calibration of the integrator

and make any necessary adjustments every twenty-four hours. The effect of mains voltage fluctuation in the range 200–250 V was found to be negligible.

The integrated values of smoke density over a normal curing period of four hours were compared with calculated values based on a graphical plot of instantaneous smoke densities and time. The calculated integrals were found to agree to within $\pm 0.5\%$ of the indicated values for densities observed at two-minute intervals, whereas the agreement was only within $\pm 5.0\%$ for observations at ten-minute intervals due to unavoidable random fluctuations of the smoke density between observations.

Although the accuracy and stability of the integrator are not great enough for its use as a precision instrument, they are adequate for the purpose for which it was designed.

Acknowledgements

The work described in this paper was carried out as part of the programme of the Department of Scientific and Industrial Research. Dr. A. C. Jason of Torry Research Station, Aberdeen, gave advice and encouragement during the development of the instrument. Mr. H. Bruce prepared the heated windows and assisted in the construction of the instrument and Mr. A. Lees prepared the drawings. Crown copyright is reserved.

References

- (1) FOSTER, W. W. *Brit. J. Appl. Phys.*, **10**, p. 416 (1959).
- (2) Department of Scientific and Industrial Research. *Torry Research*, 1958, p. 14 (London: H.M. Stationery Office, 1959).
- (3) Department of Scientific and Industrial Research. *Report of the Food Investigation Board for the year 1954*, p. 30 (London: H.M. Stationery Office, 1954).
- (4) JASON, A. C. *Process Control and Automation*, **3**, p. 6 (1956).
- (5) CUTTING, C. L. *Dept. Sci. Ind. Res., Lond., Food Investigation Leaflet No. 10* (London: H.M. Stationery Office, 1951).
- (6) STOREY, R. M. *Chemical Processing*, **3**, p. 25 (1957).
- (7) VALLANCE JONES, A., and GUSH, H. *Rev. Sci. Instrum.*, **25**, p. 928 (1954).
- (8) COLLINGE, B., and TAI, C. T. *J. Sci. Instrum.*, **28**, p. 5 (1951).

Some electrical and surface properties of sintered nickel matrix cathodes

by R. W. FANE, M.Sc., Ph.D., A.Inst.P., Baddow Research Laboratories, Marconi's Wireless Telegraph Co. Ltd., Great Baddow, Essex

[Paper first received 5 July, and in final form 18 August, 1960]

Abstract

Measurements of the work function of nickel matrix cathodes yield values in the region of 1 eV. Schottky plots are found to agree with theory provided the cathode surface is polished. Deviations from the image law at low field strengths may be explained using patch theory with suitably chosen parameters. The results of surface field determinations indicate a very small degree of coverage of the nickel grains by alkaline earth metals or oxides.

Introduction

IN a previous paper⁽¹⁾ the preparation and metallurgy of a sintered nickel cathode was described. It was suggested that emission took place from alkaline earth oxide grains within a nickel matrix. Results have been obtained which indicate more clearly the state of the activated surface, and it is this aspect which is the main subject of the present paper.

Work function measurements

The electron emission from a semiconductor is given by the Fowler equation,

$$j_0 = GA(1-r)N_0^{1/2} \frac{h^{3/2}}{(2\pi mk)^{3/4}} T^{5/4} \exp\left(-\frac{X-R/2}{kT}\right) \quad (1)$$

where j_0 is the current density (A/cm²) under zero field conditions, N_0 is the donor centre density, R is the energy gap between the donor centres and the bottom of the conduction band, X is the electron affinity, r is the reflexion coefficient, $A = 2\pi me k^2/h^3$ and G depends on the nature of the donors and will equal unity for F centres and two for centres containing paired electrons.

This equation is based on the impurity semiconductor model and depends on there being a uniform density of donor states in the immediate neighbourhood of the emitting surface. The electrons in the conduction band are assumed to arise because of thermal excitation from the donor levels; the fractional transfer of electrons in such a process is, however, assumed to be small. In addition, the donor states are considered to be several units of kT below the conduction band energy level.

The expression $(X - R/2)$ is largely independent of temperature, and a plot of $\log(j_0/T^{5/4})$ against $1/T$ results in a slope which is a measure of the true work function at 0° K.

If, however, the semiconductor levels are referred to the Fermi level of the metal with which it is in contact, the more familiar T^2 law results,

$$j_0 = A_0(1-r)T^2 \exp\left\{-\frac{(X-\mu)}{kT}\right\} \quad (2)$$

where $A_0 = 4\pi me k^2/h^3$ and μ is the depth of the Fermi level below the conduction band.

The work function obtained from equation (2) is an empirical constant determined by linear extrapolation of the temperature dependent work function curve to 0° K. The temperature coefficient of the work function depends upon the donor concentration. The slope of the Richardson line using equation (2), differs by only a few per cent from that given by the $T^{5/4}$ law, but the intercept value will differ considerably, as has been shown by Wright.⁽²⁾ Since only the work function is considered here and the T^2 law has most generally been used by other workers, it will be applied in the present case.

Effects of patches on the thermionic emission in accelerating fields

Microphotographs have shown that the cathode surface consists of oxide grains within a nickel matrix. The present investigations have been directed towards a determination of the state of the surface under operating conditions and, in particular, the degree of coverage of the nickel grains by barium. The method of approach has been to use the Schottky plot as a means of investigating the surface field resulting from the sum of the image and patch fields.

The patch theory, first proposed by Langmuir,⁽³⁾ has been considered in detail in a review by Herring and Nichols.⁽⁴⁾ In the present case, at high anode voltages, the applied field is large compared with the patch field and, under such conditions, the normal Schottky theory will apply and the emission from each patch will be independent of neighbouring patches. The total current per unit area will then be given by,

$$j_0 = A_0 T^2 \sum_i f_i (1 - \bar{r}_i) \exp(-e\phi_i/kT) \exp\{e(eE)^{1/2}/kT\} \quad (3)$$

where f_i is the fraction of the surface occupied by the i 'th patch with average reflexion coefficient \bar{r}_i . The Schottky plot will, under these conditions, give a straight line of the same slope as that for a uniform surface.

If the surface consists of only two values of work function, ϕ_M and ϕ_m , and the appropriate fractions of the surface are f_M and f_m respectively then, under zero field conditions and neglecting the reflexion coefficients

$$\bar{\phi} - \phi_m = -kT/e \ln[f_m + f_M \exp\{-e(\phi_M - \phi_m)/kT\}] \quad (4)$$

where $\bar{\phi}$ is the emissive mean work function defined by

$$\bar{\phi} = \frac{kT}{e} \ln \left\{ \frac{1}{\int \int f_i \exp\left(\frac{-e\phi_i}{kT}\right)} \right\} \quad (5)$$

Using the work functions of nickel and alkaline earth oxides

for ϕ_M and ϕ_m respectively, $\phi_M - \phi_m \approx 4.0$ eV and with $f_m = 0.5$ one has $\bar{\phi} - \phi_m = 0.06$ eV.

Thus the Richardson plot of a surface consisting of patches with two different values of work function yields the zero field emissive mean value of work function at 0° K, this emissive mean value approximating closely to the minimum work function of the surface.

Method of measurement

The thermionic emission is dependent upon the number and nature of the donor centres. Nergaard⁽⁵⁾ and Frost⁽⁶⁾ explain long-term emission decay in terms of a mobile donor hypothesis. Donors are assumed to move away from the cathode-vacuum interface under the action of the externally applied field. This makes the validity of d.c. measurements questionable. Measurements made with reduced cathode temperature to avoid dissipation and anode poisoning effects are also open to criticism, since the mechanism of conduction through the coating is thought to change from semiconduction to conduction *via* the pores of the coating at about 800° K.

Pulses of about 2 μ s duration and 250 p.r.f., variable in amplitude up to about 1.5 kV, have been used in these investigations, permitting measurements to be made at normal operating temperatures. The overall accuracy of the readings was estimated at better than $\pm 5\%$.

The temperature of the cathode in one valve (No. 482) was measured to an accuracy of ± 1 deg C by means of a thermocouple, the hot junction of which consisted of a fine molybdenum wire welded to the nickel rim of the cathode. The temperature measured with an optical pyrometer agreed within ± 5 deg C after correction for emissivity and glass adsorption, and this latter method was used in the other cases.

Experimental results

The table shows typical values found for Schottky plots and the curves for valve No. 475 are shown in Fig. 1. For

two of these valves (Nos. 475 and 482) the cathodes were polished. The resulting Schottky slopes approximate closely to those expected from theory. This compares with the normal sintered unpolished cathode (No. 294) where slopes are larger than the theoretical results, but less than is generally observed with oxide-coated cathodes.

Typical values found for Schottky plots

Valve No.	Temperature (°K)	Practical slope ($\times 10^2$)	Theoretical slope ($\times 10^2$)	Practical slope / Theoretical slope
475	1085	1.77	1.31	1.30
	1180	1.11	1.20	0.926
	1195	1.10	1.19	0.928
	1206	1.19	1.18	1.01
	1258	1.05	1.13	0.934
482	1020	0.802	1.05	0.763
	1086	0.906	1.00	0.906
	1135	1.50	0.96	1.56
	1166	0.94	0.93	1.01
294	1081	1.90	1.00	1.90
	1103	1.89	0.961	1.97
	1125	1.88	0.965	1.95
	1146	1.90	0.949	2.00
	1158	1.93	0.939	2.08

Since the slopes approximate closely to the theoretical results, the use of the extrapolated Schottky lines to give a zero field emission is justified. The values of the work function for these particular valves, determined from the Richardson plots, are 0.73, 1.23 and 1.07 eV respectively. Very few measurements of the work function of this type of cathode have been published. Mesnard and Uzan⁽⁷⁾ give 0.85 to 1.6 eV for cathodes prepared by a similar technique, although, by comparison, emission levels are low, probably due to a different A constant. Richardson⁽⁸⁾ gives 1.7–1.8 eV, in agreement with the earlier paper of Beck and others.⁽⁹⁾ These latter authors did, however, prepare cathodes by a slightly different technique. In a later paper, Beck⁽¹⁰⁾ gives 1.31 eV as the slope of a Richardson plot. Similar results have been obtained by Balas, Dempsey and Rexer,⁽¹¹⁾ who found a range 1–1.25 eV for their impregnated nickel matrix cathodes.

Determination of the surface field from Schottky plots

For positive anode voltages a diode characteristic may be considered in three sections. These are: the space-charge-limited section, the Schottky line where the anode field is large compared with the cathode patch field and the portion just below the Schottky line where both patch field and anode field are operating. It is this latter section of the characteristic which is now being considered.

Using Schottky image theory for the reduction in work function due to collector field, it may be shown that

$$d(\log_{10} j)/dF_c = ez_0/2.3kT \quad (6)$$

where F_c is the collector field and z_0 is the distance from the emitter where this field neutralizes the surface field, resulting from image and patch field.

The curves of Fig. 1 are plotted as $\log j$ against \sqrt{V} , where V is the anode voltage. The slope of the Schottky curve

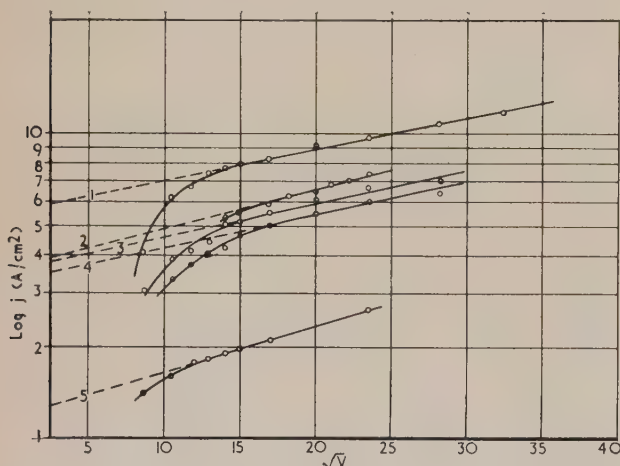


Fig. 1. Schottky plots for a polished cathode. Valve No. 475

Curve	Temperature (°K)	Zero field emission (A/cm²)
1	1258	5.4
2	1206	3.78
3	1195	3.60
4	1180	3.32
5	1085	1.17

Anode-cathode; 0.0178 cm

$\{d(\log j)/d\sqrt{V}$ is related to the quantities in equation (6) as follows,

$$\frac{d(\log j)}{dF_c} = \frac{d(\log j)}{d\sqrt{V}} \frac{D}{2\sqrt{V}} \quad (7)$$

where D is the anode-cathode spacing.

From the slope of the Schottky curves the value of z_0 may therefore be found for various values of \sqrt{V} or F_c . Since at distance z_0 , $F_c = E_s$, the surface field E_s is determined.

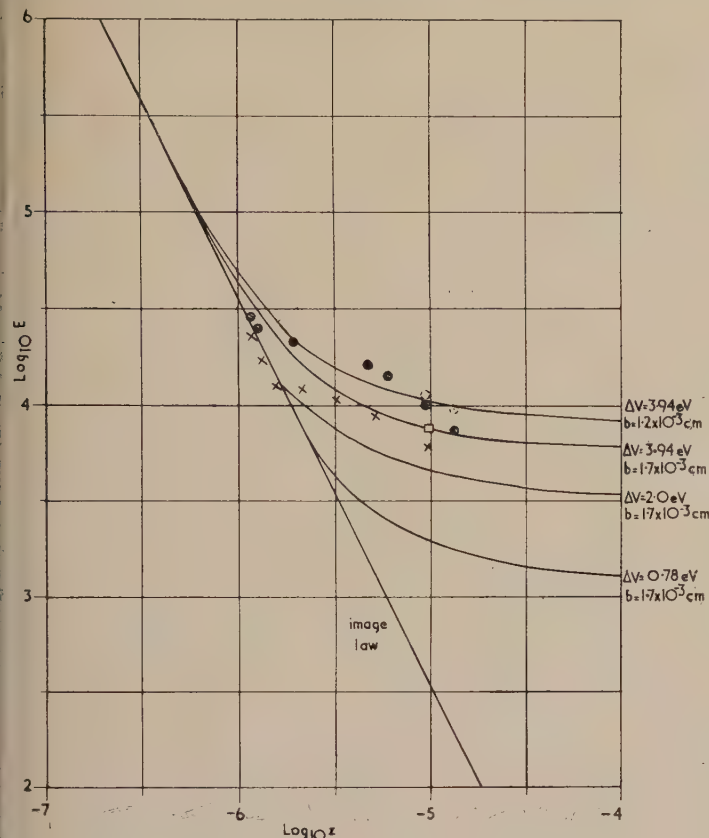


Fig. 2. Surface held as a function of distance from the cathode

- = Valve No. 482
- × = Valve No. 475
- = Corrected points, valve No. 482
- = Corrected point; valve No. 475

Taking the slope of the Schottky plots at various points where they deviate from the straight line [curve (1) for No. 475 and similarly for another valve] has given the values of z and E shown in Fig. 2.

The surface field may also be calculated from patch theory. Using the "checkerboard" patch theory proposed by Compton and Langmuir⁽¹²⁾ the field acting on an electron near the surface is, according to Linford,⁽¹³⁾

$$E_s = E_p + E_i = \{8\sqrt{(2)\Delta V/\pi b}\} \exp. \{-\sqrt{(2)\pi z/b}\} + e/4z^2 \quad (8)$$

where E_p and E_i are the patch and image fields respectively and ΔV is the difference in work function between square patches of side b cm.

Microphotographs of the surfaces of the cathodes used indicated an average patch dimension of approximately 1.7×10^{-3} cm. Using the value 4.9 eV for the work

function of nickel⁽¹⁴⁾ and 1.02 eV as the average slope value of four Richardson plots gives $\Delta V = 3.94$ eV. For bariated nickel the work function would be about 1.8 eV, giving $\Delta V = 0.78$ eV. Curves based on these various values are also shown in Fig. 2, E_s having been calculated from equation (8). The shift in the curves for a change in b to 1.2×10^{-3} cm, with $\Delta V = 3.94$ eV, shows the effect of a change in the patch dimensions.

The falling-off of the low field points may be due to space charge effects. A method of correcting for this has been given by Ivey.⁽¹⁵⁾ The correction depends on the value of current calculated from the $3/2$ power law and, where curves have not been asymptotic to this law, figures have been estimated by extrapolation of the space-charge-limited characteristic. The corrected points are indicated in Fig. 2 and are seen to be close to the theoretical curves.

Degree of surface coverage

No studies have been made of the work function of nickel as a function of the degree of coverage by barium, and values for the coverage can only be estimated in the present case by comparison with the analogous case of barium on tungsten.

Moore and Allison⁽¹⁶⁾ studied the thermionic emission *versus* coverage of barium oxide on various metals, the coverage being determined by a radioactive tracer technique. For tungsten, molybdenum and tantalum the behaviour was almost identical, the work function for $1/10$ th monolayer being approximately the same as for a conventional sprayed oxide coating.

Moore and Allison⁽¹⁷⁾ also studied the adsorption of barium and strontium on tungsten. As for the alkaline earth oxides on tungsten, they found that the major change in work function occurred for the first 0.2 of a monolayer. Their data shows that at a fractional coverage of 0.2 the work function is reduced to about 2.9 eV.

Considering the above $\log E$ *versus* $\log z$ curves, it can be seen that when ΔV reaches about 2 eV, i.e. when the work function of the nickel patches has fallen to 3.0 eV, the theoretical curve would be considerably below the experimental points. It therefore seems likely that the coverage in the present case is less than 0.2 and possibly less than 0.1 of a monolayer, provided alkaline earth metals and oxides show similar characteristics on nickel and tungsten.

Electron emission images of the cathode surface have also shown that non-uniformities exist with a well-activated cathode, and are in qualitative agreement with the above conclusions.

Discussion and conclusion

Richardson lines, using values of saturated emission determined by Schottky plots, indicate a work function for the present nickel matrix cathodes in the region of 1 eV. An analysis of the patch effect applicable to this case shows that the work function, measured by this method, yields the minimum work function of the surface and is consistent with the value accepted for activated alkaline earth oxides.

The variation in electron emission with field follows closely the Schottky law. Lack of conformity with theory, observed in some cases, seems to be a result of surface roughness. Results for well-polished cathodes can be

explained by image theory, the departures from the image line at low field intensities being attributable to the patchy nature of the surface.

Determinations of the cathode surface field suggest that an active cathode consists of a nickel matrix with emitting oxides in the pores. The nickel grains do not appear to be covered to any great extent with barium or barium oxide. Beck⁽¹⁰⁾ now accepts such a model but does not establish the state of the surface, while in an earlier paper by Beck and others,⁽⁹⁾ the mechanism was considered to be that of an atomic film emitter. It must be noted in this connexion, however, that the techniques used in the preparation of the cathodes differs from those described here, particularly in the details of the sintering process. Richardson⁽⁸⁾ also used a technique similar to that employed by Beck, and concluded from radioactive tracer measurements that the barium coverage of the nickel is small.

There is some evidence to suggest that barium does not migrate on nickel.^(18, 19) Possibly this is due to the extreme tenacity of the oxide layer almost certainly present on the nickel. Even if the oxygen layer is removed during the hydrogen sintering and does not re-form during subsequent exposure to the atmosphere, it is known that oxygen is evolved from oxide cathodes⁽²⁰⁾ and also from similar nickel matrix cathodes.⁽²¹⁾ It is suggested that barium diffusing over a nickel grain forms a layer of barium-on-oxygen-on-nickel or barium oxide-on-nickel round the perimeter of the grain and prevents further diffusion over the surface. If the conditions for complete coverage could be determined and established, a more uniform and efficient emitter would result.

Since the emission is predominantly from the oxide grains, the Schottky plots could be expected to show the characteristics displayed by conventional oxide-coated cathodes, i.e. a slope of $2\frac{1}{2}$ –3 times the theoretical value. The cathodes not given a high polish show larger slopes than polished ones, but still less than usually observed with oxide cathodes. Such cathodes would, however, have a smoother surface than a wet-sprayed oxide cathode. Morgulis⁽²²⁾ attempted to explain the field-dependent decrease in work function by assuming that the field partly penetrates the semiconductor, due to the limited concentration of free electrons. In the present case a polycrystalline solid is involved having a large area of contact with the nickel grains; highly active oxide grains could, therefore, result. If the density of donors is high the decrease in work function, due to the depression of energy bands near the surface, would then be small.

Nergaard⁽⁵⁾ suggested the use of an alternative emission equation based on a mobile donor hypothesis. Such a mechanism would also result in emission decay. Limited observations using long pulses (of the order of 100 μ s) show that decay does not occur in all valves using matrix cathodes. Since it is likely that one type of donor is active in all cases, the decay process sometimes observed might be attributable to influences external to the cathode. Beck⁽¹⁰⁾ finds that when decay is observed, the observations fit the law proposed by Dejardin, Mesnard and Uzan,⁽²³⁾ based on a semiconductor model. The law deduced by Sproul,⁽²⁴⁾ which would apply to a barium or barium oxide monolayer, does not give such close agreement, thus supporting the view that

the cathodes are not essentially of the barium-on-nickel dispenser type.

Acknowledgement

The author wishes to express his thanks to the Engineer-in-Chief, Marconi's Wireless Telegraph Co. Ltd., for permission to publish this paper. The results presented are an abridged version of part of a thesis approved for the Ph.D. degree in the University of London.

References

- (1) FANE, R. W. *Brit. J. Appl. Phys.*, **9**, p. 149 (1958).
- (2) WRIGHT, D. A. *Proc. Instn Elect. Engrs*, **100** (III), p. 125 (1952).
- (3) LANGMUIR, I. *Gen. Elect. Rev.*, **23**, p. 504 (1920).
- (4) HERRING, C., and NICHOLS, M. H. *Rev. Mod. Phys.*, **21**, p. 185 (1949).
- (5) NERGAARD, L. S. *R.C.A. Rev.*, **13**, p. 464 (1952); *Halbleiter Probleme*, Vol. 3, p. 154 (Braunschweig: Friedr. Vieweg and Son, 1956).
- (6) FROST, H. B. Thesis, *Transient Changes in Oxide Cathodes* (Massachusetts Institute of Technology, 1954).
- (7) MESNARD, G., and UZAN, R. *Vide*, **9**, p. 1492 (1954).
- (8) RICHARDSON, J. F. *Brit. J. Appl. Phys.*, **8**, p. 361 (1957); Ph.D. Thesis (University of Birmingham, 1959).
- (9) BECK, A. H. W., CUTTING, A. B., BRISBANE, A. D., and KING, G. *Vide*, **9**, p. 302 (1954).
- (10) BECK, A. H. W. *Proc. Instn Elect. Engrs*, **106** (B), p. 372 (1959).
- (11) BALAS, W.; DEMPSEY, J., and REXER, E. F. *J. Appl. Phys.*, **26**, p. 1163 (1955).
- (12) COMPTON, K. T., and LANGMUIR, I. *Rev. Mod. Phys.*, **2**, p. 123 (1930).
- (13) LINFORD, L. B. *Rev. Mod. Phys.*, **5**, p. 34 (1933).
- (14) HERRMANN, G., and WAGENER, S. *The Oxide-coated Cathode* (London: Chapman and Hall Ltd., 1951).
- (15) IVEY, H. F. *Phys. Rev.*, **76**, p. 554 (1949).
- (16) MOORE, G. E., and ALLISON, H. W. *Phys. Rev.*, **77**, p. 246 (1950).
- (17) MOORE, G. E., and ALLISON, H. W. *J. Chem. Phys.*, **23**, p. 1609 (1955).
- (18) French Patent, 903976, see Ref. 10.
- (19) BENJAMIN, M., and JENKINS, R. O. *Phil. Mag.*, **26**, p. 1049 (1938).
- (20) PLUMLEE, R. H. *R.C.A. Rev.*, **17**, pp. 190 and 231 (1956).
- (21) SURPLICE, N. A. Private communication.
- (22) MORGULIS, N. *J. Phys. U.S.S.R.*, **11**, p. 67 (1947).
- (23) DEJARDIN, G., MESNARD, G., and UZAN, R. *Cahiers de Phys.*, **10**, p. 1 (1956).
- (24) SPROUL, R. L. *Phys. Rev.*, **67**, p. 166 (1945).

Wear of the hard and soft phases in cobalt-bonded tungsten carbide

by J. GOLDEN, B.Sc., Ph.D., and G. W. ROWE, M.A., Ph.D., A.Inst.P., Tube Investments Research Laboratories, Hinxton Hall, Cambridge

[Paper first received 26 May, and in final form 20 July, 1960]

Abstract

It has previously been widely accepted that the normal wear pattern of cobalt-bonded tungsten carbide is a steady attrition of the soft matrix, leading to occasional loosening of hard carbide grains. This hypothesis seems to have been based on visual examination of autoradiographs of copper wire drawn through radioactive tungsten carbide dies.

The present experiments show that autoradiographs of this type, having a steady general level of blackening with local dense spots superimposed, are obtained if the copper surface is not sufficiently well prepared. On smooth surfaces uniform autoradiographic density is observed. Detailed measurements of the former type of autoradiograph have been made, showing first the short-lived tungsten activity and finally the long-lived cobalt activity. These refute the suggestion that the spots are carbide grains and that the general level is cobalt. The composition of the wear deposit in both is the same, and corresponds closely to the initial composition of the bonded carbide. The revised picture of steady continuous wear of both phases concurrently, accords with other experimental evidence quoted.

1. Introduction

IN an earlier paper⁽³⁾ it has been shown that when tungsten carbide and copper surfaces are well prepared, the transfer of tungsten carbide to the copper in the unlubricated condition is smooth and steady. However, where defects or chemical inhomogeneities occur in the copper surface, there can be sudden increases in the wear. Autoradiographs then show a steady background with discrete spots of high intensity superimposed upon it. Results of this type were first obtained by Button, Davies and Tourret⁽¹⁾ who tentatively suggested that the smooth background was predominantly cobalt and the local spots predominantly tungsten carbide grains. Similar results have been obtained by Dahl and Lueg,⁽²⁾ and other workers, and the explanation has become widely accepted.

The original hypothesis was, however, qualitative and somewhat tentatively advanced. More detailed quantitative experiments, described in this report, show that when the fragmentary type of wear occurs on copper, the proportions of cobalt and tungsten in the large fragments and in the background wear are practically identical. This proportion, moreover, corresponds very closely to the original composition of the material.

2. Apparatus and technique

A simple apparatus was used in which short straight tracks were made by a radioactive tungsten carbide slider, of radius

4 mm, on copper blocks, under a load of 2 kg. The blocks were prepared on 0000 paper under benzene, and the tungsten carbide slider was lapped on a soft stone under distilled water before use. This produced a reasonable representation of a worn carbide surface. The bonded carbide contained 92% WC, 6% Co and 2% TaC, the average grain size being 1–2 μ . It was irradiated in a neutron flux of 10^{12} neutrons/cm² for two days. The major part of the activity produced was due to short-lived ¹⁸⁷W, but appreciable quantities of the longer-lived isotopes were also produced. Autoradiographs were obtained by exposing the tracks to a photographic film (Ilford Industrial B X-ray film) under a pressure of about $\frac{1}{2}$ lb/in.² This gives good definition. The first exposure was quite short, three days, to register the strong short-lived ¹⁸⁷W activity. Further autoradiographs were obtained at subsequent intervals until finally after more than 400 days the activity was almost entirely due to the longest-lived isotope, ⁶⁰Co. The exposure time was then very much longer, fifty days in all, but a good detailed autoradiograph was obtained. All the autoradiographs were then assessed by an automatic recording and integrating microdensitometer. The areas under the microdensitometer trace represent the intensities of activity and hence the weights of material in a given region. Thus the first autoradiograph, when calibrated, gives the amount of tungsten, and the last autoradiograph the amount of cobalt, in a particular position. The blackening powers of the isotopes differ one from another, so, to calibrate the autoradiographs for each isotope, solutions were made of known activities of ¹⁸⁷W, ¹⁸⁵W, ¹⁸²Ta and ⁶⁰Co. Cotton threads were soaked in these solutions and exposed to autoradiograph film as described elsewhere.⁽⁵⁾ The blackening density produced by given activity of the various isotopes was then determined by the microdensitometer. Expressed in integrated microdensitometer units per 10^8 disintegrations the results were:

$$^{187}\text{W} = 26.0; \quad ^{185}\text{W} = 3.9; \quad ^{182}\text{Ta} = 21.5; \quad ^{60}\text{Co} = 6.34.$$

It is clear, therefore, that any comparison of autoradiographs which neglects these correction factors is meaningless.

3. Results

Calculations of the decay of activity and of film blackening of the nuclides, based on activation data. From the data published in the Harwell catalogue it is possible, knowing the length and intensity of the activation, to calculate the intensity and decay of each nuclide separately. We shall consider first the initial composition of the material. The bonded tungsten carbide slider contained 92% WC, 6% Co and 2% TaC. The proportions of the elements are W = 86.4, Ta = 1.9, Co = 6%, residue C. Fig. 1 shows the composite decay curve for the hard phase (¹⁸⁷W, ¹⁸⁵W and ¹⁸²Ta) and

for the soft phase (^{60}Co) from pile exit onwards. The periods occupied by the first two autoradiographs are indicated on the curve. The integral of the curve during each period gives the total activity to which the appropriate

carbide during the first autoradiograph, for example, is 79.9×10^{12} ; while that due to ^{60}Co in the last autoradiograph is 41.5×10^{12} . In order to compare the autoradiographs obtained by exposure to different isotopes we need to take into account the blackening power of the individual nuclides as determined above. Table 1(b) gives the film blackening to be expected on each autoradiograph as a result

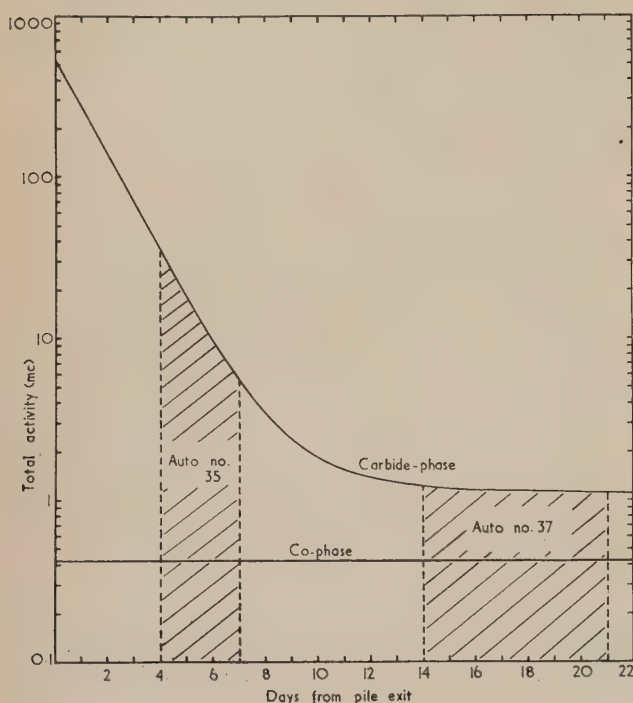


Fig. 1. A logarithmic plot of the theoretical decay of activity of the original material, calculated from the data for individual nuclides. The periods occupied by two of the autoradiographs are shown

autoradiograph was exposed. These exposure data, expressed in millicurie-days per gram (mc d/g) of the original bonded carbide, are shown for each nuclide in Table 1(a).

Table 1. Theoretical autoradiograph blackening due to the hard and soft phases in one gram of the original cobalt-bonded tungsten carbide, calculated from activation data and the blackening powers of the nuclides

(a) Radiation exposure due to each nuclide (mc d)

Autoradiograph no.	Hard carbide phase				Matrix	
	^{187}W	^{185}W	^{182}Ta	Total	Soft Co phase	^{60}Co
35	25.2	2.36	1.14	28.7	1.11	
37	0.03	5.6	2.8	8.4	2.95	
48	—	5.0	2.7	7.7	3.43	
102	—	0.44	0.93	1.37	13.1	

(b) Film blackening due to each nuclide (10^4 integrated microdensitometer units)

Autoradiograph no.	Hard carbide phase				Soft matrix phase ^{60}Co (both phases)		Original material (both phases)
	^{187}W	^{185}W	^{182}Ta	Total			
35	2080	29.2	77.6	2187	22.2		2209
37	2.2	69.0	191	262	59.1		321
48	—	61.6	183	245	69.0		314
102	—	5.5	62.7	68	263		331

Since one mc d corresponds to 3.17×10^{12} disintegrations, the number of disintegrations due to $^{187}\text{W/g}$ of bonded

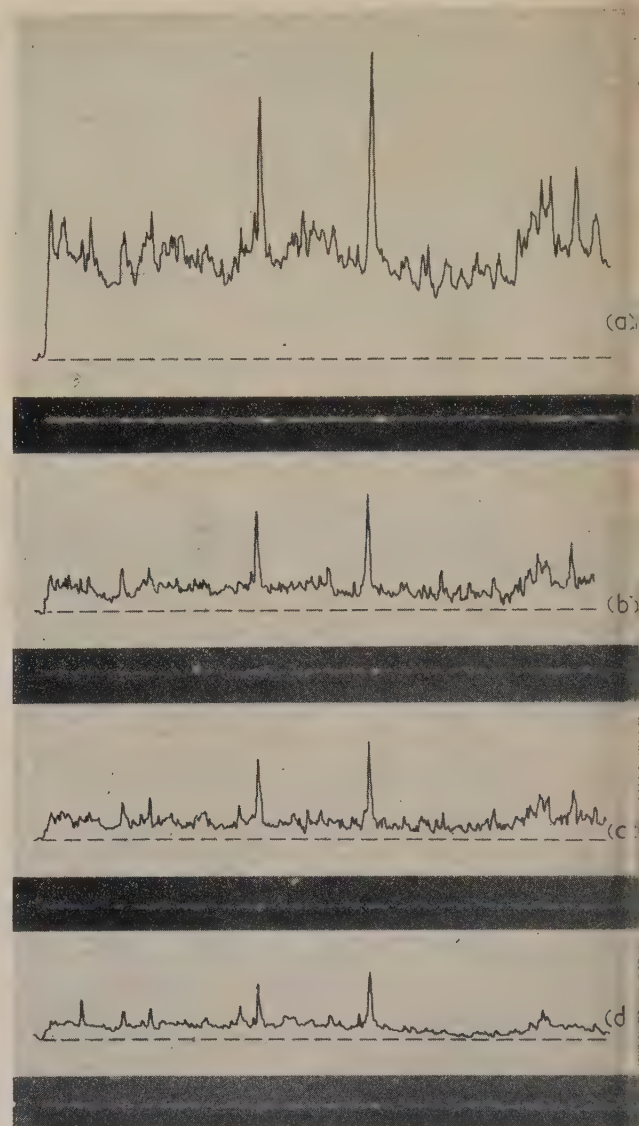


Fig. 2. Prints and microdensitometer traces obtained from autoradiographs of the sliding track 4 on block C55. The films were exposed for suitable times at four sequential intervals to register first the ^{187}W activity and finally the ^{60}Co activity

(a) Auto. 35 (b) Auto. 37
(c) Auto. 48 (d) Auto. 102

of the individual nuclides present in one gram of the original material.

Now the experiment is intended to distinguish, if possible, between the wear of the hard phase and that of the soft cobalt-rich matrix. The film blackening due to the sum of the ^{187}W , ^{185}W and ^{182}Ta nuclides during the first autoradiograph is 2187, compared with 22.2 due to the soft phase. The ratio is 98.6, compared with 0.26 on the fourth

autoradiograph. There is thus a change in the ratio of the blackening powers of the two phases by a factor of about 400 over the period concerned. This should, of course, be clearly detectable on the autoradiographs if certain parts are pure tungsten carbide and other parts pure cobalt.

Autoradiograph records. Fig. 2 shows prints of the sequence of autoradiographs obtained from block C55, track 4, at intervals from a week to two years, together with the microdensitometer traces. It can be seen that, despite the change in the ratio of the film blackening due to the two phases by a factor of 400, the general shape of the microdensitometer records remains the same. The major peaks remain visible on the last autoradiograph.

Table 2 gives detailed measurement of the total blackening of this film in the peak regions and in the general levels. The latter is assessed by drawing a median line and measuring the height of this line above the background in the region of the peak concerned.

Table 2. Experimental measurements of total autoradiograph blackening in the peak areas of high local intensity and in the general level of more uniform intensity

Autoradiograph no.	Peak A	Peak B	General level A	General level B
35	133	206	5.0	4.6
37	46	73	1.1	0.9
48	44	59	0.7	0.75
102	24	44	0.6	0.6

Fig. 3 shows the autoradiograph prints and microdensitometer traces obtained from sequential autoradiographs of track 3 on block C51X using increased linear magnification of the instrument.

Comparison of observed results with calculated data. For this comparison it is convenient to express the results as ratios of the blackening on the earlier films to that on the last film.

Table 3(a). Ratios derived from Table 1(b), showing the theoretical blackening on the earlier autoradiographs relative to that on the last one, for the two phases and for the original mixture

Autoradiograph no.	Hard carbide phase	Soft matrix phase	Original mixture
35	32.1	0.085	6.68
37	3.84	0.224	0.97
48	3.6	0.261	0.95
102	1	1	1

(b) Ratios derived from Table 2 and other tracks on the same autoradiographs, showing the experimental blackening of the earlier autoradiographs relative to that of the last one, for comparison with Table 3(a)

Autoradiograph no.	Peak areas	General levels
35	6.1 ± 1.8	6.9 ± 2
37	2.0	1.7
48	1.6	1.2
102	1	1

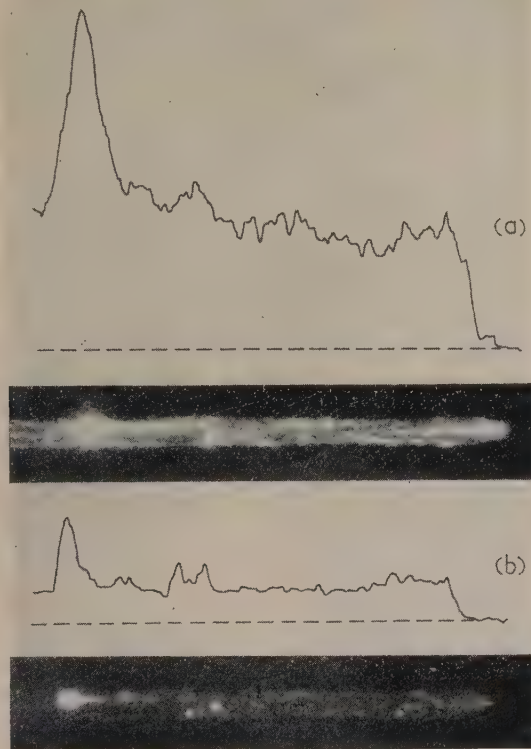


Fig. 3. Prints and microdensitometer traces obtained from sequential autoradiographs of track 3 on block C51X, with increased linear magnification of the instrument. Autoradiograph 35 shows predominantly tungsten, and autoradiograph 102 predominantly cobalt

(a) Auto. 35

(b) Auto. 102

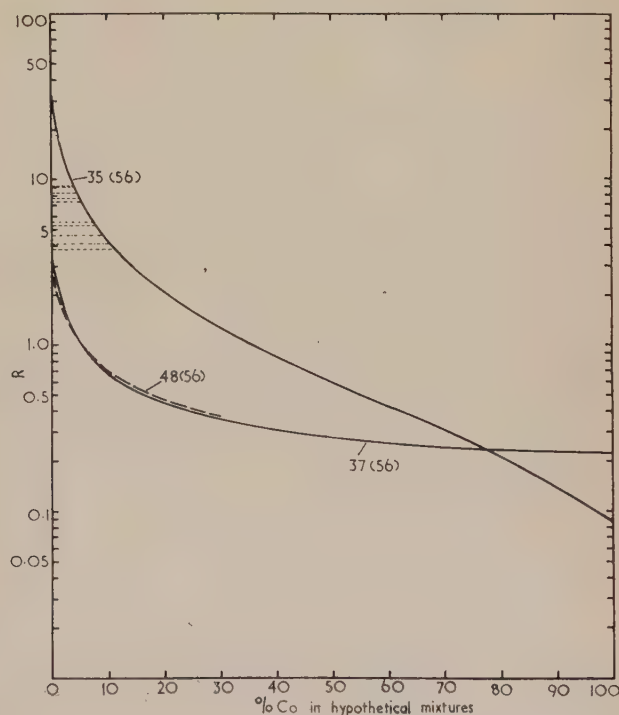


Fig. 4. The ratio R of the blackening of earlier autoradiographs relative to the final autoradiograph 102, predicted on the basis of isotope data and empirical blackening powers of the nuclides, for hypothetical materials of various cobalt contents but constant proportions of tungsten and tantalum. The broken horizontal lines indicate the ratios found from experimental measurements of film blackening

Table 3(a) gives the theoretical ratios, deduced from the calculated data of Table 1(b) for the hard phase, the soft matrix, and the original material (both phases).

Table 3(b) gives the experimental results from measurements on the actual autoradiographs.

It will be seen that the latter do not differ significantly from each other in the peak areas and in the general levels. Both agree much more closely with the calculations based on the original composition than with those based on either carbide phase or cobalt phase alone.

Estimation of composition of the worn material. The composition of the worn material can be estimated from Fig. 4. This shows again the ratio of the blackening on the earlier autoradiographs to that on the last autoradiograph, calculated from Table 1(b) as a function of percentage cobalt content in hypothetical mixtures. The full curve of Fig. 4 is thus obtained from the combination of activation data, decay curves, and an empirical determination of nuclide blackening power. The experimental measurements of the film blackening ratios are shown on the ordinate scale of Fig. 4. From the intersections it is found, using the data from autoradiographs 35 and 102, that the average composition of the material producing both peaks and general level is $6.5 \pm 2\%$ Co. If we include the results from autoradiographs 37 and 48, which depend more on the ^{182}Ta contribution, the overall accuracy is less but the average cobalt content deduced is then $5.8 \pm 3\%$. All the autoradiographs thus suggest that both the peaks and the background are close in composition to the original material.

4. Conclusion

The commonly accepted view of the wear process of cobalt-bonded tungsten carbide appears to be based on a number of general observations, and in particular on experiments in copper wire drawing by Button, Davies and Tourret.⁽¹⁾ Their suggestion that cobalt wears away steadily until eventually tungsten carbide grains are pulled out is not valid for the experiments reported here. It is also obvious from experiments with well-prepared copper or steel surfaces^(3,4) that the wear deposit is uniform, within the resolution limits of autoradiographs. Examination by optical and electron microscopy also reveals no wear fragments as large as the original grains (1 to 2 μ across). Furthermore, when a large single crystal of tungsten carbide is used as the slider, the wear is steady on a well-prepared copper plate (Fig. 5), showing that it is false to assume that hard tungsten carbide is unable to wear uniformly on a soft material.

These results suggest that with a cobalt-bonded tungsten carbide, both the soft matrix and the hard grains wear steadily away together during dry sliding.

5. Acknowledgements

We thank the chairman of Tube Investments Limited for permission to publish these results, and Mrs. B. J. Francis and Mr. T. A. Nunn for producing and measuring the autoradiographs.

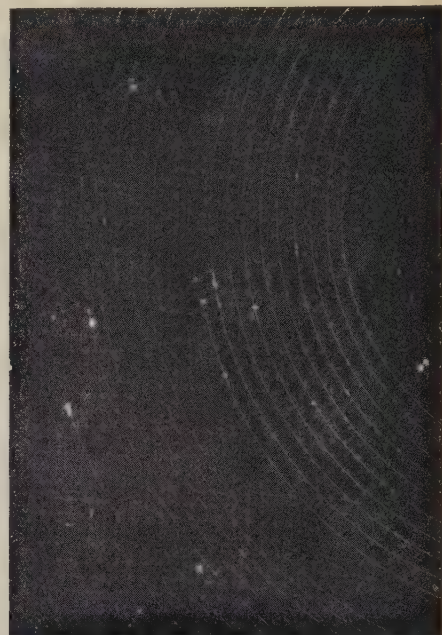


Fig. 5. An autoradiograph print showing the wear of a single crystal of tungsten carbide running in a spiral track on copper, under 30 g load. For the outer circuits the crystal plate was transverse, and for the inner circuits along the sliding direction

References

- (1) BUTTON, J. C. E., DAVIES, A. J., and TOURRET, R. *Nucleonics*, **9**, p. 34 (1951).
- (2) DAHL, W., and LUEG, W. *Stahl und Eisen*, **76**, p. 257 (1956).
- (3) GOLDEN, J., and ROWE, G. W. *Brit. J. Appl. Phys.*, **9**, p. 120 (1958).
- (4) GOLDEN, J., and ROWE, G. W. *Radioisotopes in Scientific Research*, **1**, p. 343 (Oxford: Pergamon Press Ltd 1957).
- (5) GOLDEN, J., and ROWE, G. W. *Wear*, **1**, p. 49 (1958).

Fifth order spherical aberration of magnetic lenses

by G. D. ARCHARD, Associated Electrical Industries Ltd., Aldermaston, Berks.

[Paper first received 10 June, and in final form 30 June, 1960]

Abstract

Knowledge of the fifth order spherical aberration of magnetic lenses is required in order to show how much error is left when third order aberration is corrected. This is found theoretically for lenses of the bell-shaped field type. It is found that, for lenses of moderate strength, third and fifth order coefficients are numerically very similar.

IN discussing the spherical aberration of electron lenses attention is usually restricted to third order terms. Knowledge of the fifth order aberration would be useful for two reasons: (1) to confirm that it is small in comparison with the third order aberration, and (2) to show how much error remains when third order aberration has been corrected.

The general ray equation is

$$2\phi r'' = (\partial\phi/\partial r - r'\partial\phi/\partial z)(1 + r'^2) \quad (1)$$

For magnetic lenses, ϕ becomes

$$\phi = \Phi - (e/2m)/A^2 \quad (2)$$

(Φ = accelerating voltage, A = magnetic vector potential) where

$$A = \frac{r}{2}B - \frac{r^3}{16}B'' + \frac{r^5}{384}B^{IV} \dots \quad (3)$$

(B = axial field strength.)

Equation (1) may be written in the form

$$r'' + \frac{1}{4}EB^2r = f_3 + f_5 \quad (4)$$

where $E = e/2m\Phi$ and f_3 and f_5 contain r , r' to the third and fifth orders respectively, terms of higher order being neglected.

The paraxial ray equation is obtained by neglecting f_3 and f_5 ; a ray starting from a point on the axis may then be described by

$$r = \alpha h_1 \quad (5)$$

h_1 being the solution of the paraxial equation with the initial conditions

$$h_{10} = 0; h_{10}' = 1 \quad (6)$$

The third order equation is obtained by neglecting f_5 ; solution by the method of the variation of parameters then gives

$$r = \alpha h_1 + h_1 \int_0^z \bar{h}_1 f_3 dz - \bar{h}_1 \int_0^z h_1 f_3 dz \quad (7)$$

the integrals in which can be represented accurately enough on replacing r in the expansion of f_3 by αh_1 . In this, \bar{h}_1 is the solution of the paraxial equation with initial conditions

$$\bar{h}_{10} = 1; \bar{h}_{10}' = 0 \quad (8)$$

As is well known, this gives the third order aberration in the image plane as

$$\delta r = r - \alpha h_1 = M \int_0^1 h_1 f_3 dz \quad (9)$$

(M = magnification, integration extends from object to image), this being proportional to α^3 since f_3 contains αh_1 to third order. The third order spherical aberration constant is then given by

$$C_3 \alpha^3 = \int_0^1 h_1 f_3 dz \quad (10)$$

The fifth order equation is obtained by taking equation (4) as it stands; solution by the method of the variation of parameters then gives

$$r = \alpha h_1 + h_1 \int_0^z \bar{h}_1 (f_3 + f_5) dz - \bar{h}_1 \int_0^z h_1 (f_3 + f_5) dz \quad (11)$$

Terms in α^5 arise in two ways, (1) on replacing the r 's in f_5 by αh_1 , and (2) on replacing the r 's in f_3 by

$$r = \alpha h_1 + h_1 \int_0^z \bar{h}_1 f_3 dz - \bar{h}_1 \int_0^z h_1 f_3 dz \quad (12)$$

In the latter case the terms in α^3 considered earlier also appear; the α^5 terms arise because $\int \bar{h}_1 f_3 dz$ contains terms in α^3 so that a second approximation to r is

$$r = \alpha h_1 + \alpha^3 h_3 \quad (13)$$

and cubing this gives a term in α^5 .

The fifth order spherical aberration constant is then given by

$$C_5 \alpha^5 = \int_0^1 h_1 (f_{35} + f_5) dz \quad (14)$$

where f_{35} comprises the α^5 terms in f_3 , these being found from

$$h_3 = h_1 \int_0^z \bar{h}_1 f_{33} dz - \bar{h}_1 \int_0^z h_1 f_{33} dz \quad (15)$$

in which f_{33} is the earlier approximation for f_3 , produced by setting $r = \alpha h_1$.

In full, the aberration terms are thus

$$\begin{aligned} \int_0^1 h_1 f_5 dz = & \int_0^1 \left\{ E \left(-\frac{1}{128} BB^{IV} h_1^6 - \frac{3}{256} B''^2 h_1^6 - \right. \right. \\ & - \frac{1}{32} BB''' h_1^5 h_1' - \frac{1}{32} B' B'' h_1^5 h_1' + \\ & + \frac{1}{8} BB'' h_1^4 h_1'^2 + \frac{1}{4} BB' h_1^3 h_1'^3 \Big) + \\ & + E^2 \left(\frac{3}{64} B^3 B'' h_1^6 + \frac{1}{16} B^3 B' h_1^5 h_1' - \frac{1}{16} B^4 h_1^4 h_1'^2 + \right. \\ & \left. \left. + E^3 \left(-\frac{1}{64} h_1^6 B^6 \right) \right\} dz \quad (16) \end{aligned}$$

and

$$\int_0^1 h_1 f_{35} dz = \int_0^1 h_1 \left[E \left\{ \frac{3}{8} BB'' h_1^2 h_3 + \frac{1}{4} BB' (h_1^2 h_3' + 2h_1 h_3 h_1') - \frac{1}{4} B^2 (h_3 h_1'^2 + 2h_1 h_1' h_3') \right\} - \frac{3}{16} E^2 B^4 h_1^2 h_3 \right] dz \quad (17)$$

where h_3 is given by equation (15) and

$$f_{33} = E \left(\frac{1}{8} BB'' h_1^3 + \frac{1}{4} BB' h_1^2 h_1' - \frac{1}{4} B^2 h_1 h_1'^2 \right) - \frac{1}{16} E^2 B^4 h_1^3 \quad (18)$$

In general the field distribution of magnetic lenses would have to be measured to a very high degree of accuracy in order to determine the derivatives of B required for these equations. Many practical lenses however have field distributions of the same general shape as Glaser's⁽¹⁾ bell-shaped field, for which h_1 , h_1' and B are known analytically. It is convenient therefore to work out aberrations for lenses of this form, which are characterized by

$$\left. \begin{aligned} B &= B_0 \sin^2 \phi \\ z &= d \cot \phi \\ k^2 &= EB_0^2/4 \end{aligned} \right\} \quad (19)$$

(where d is the half-width of the bell), in which k^2 corresponds in practical lenses to Liebmann's⁽²⁾ k^2 , R being the pole-piece

$$k^2 = 0.022 B_0^2 R^2 / \Phi \quad (20)$$

bore radius.

For large magnifications the values of ϕ at object and image are $\phi_1 = 0$ and $\phi_0 = \pi/\sqrt{(1+k^2)}$. As analytical

integration would be tedious and not very useful, the integration has been done step by step using a digital computer, the Ferranti Mercury taking only five minutes to work out C_5 for ten values of k^2 . The results appear in the following table, Glaser's third order coefficients and focal lengths being attached for comparison.

Aberration coefficients

k^2	C_3/d	C_5/d	f/d
0.2	15.02	104.3	3.81
0.4	3.308	7.740	2.14
0.6	1.571	2.301	1.63
0.8	0.999	1.081	1.39
1.0	0.735	0.622	1.25
1.2	0.591	0.397	1.17
1.4	0.502	0.269	1.155
1.6	0.442	0.189	1.078
1.8	0.401	0.135	1.050
2.0	0.370	0.096	1.031

Acknowledgements

The author wishes to thank Mr. D. P. R. Petrie for helpful criticism and Dr. T. E. Allibone, Director of the Laboratory, for permission to publish this note.

References

- (1) GLASER, W. *Grundlagen der Elektronenoptik* (Vienna: Springer-Verlag, 1952).
- (2) LIEBMANN, G. *Proc. Phys. Soc. B*, **68**, p. 727 (1955).
- (3) SCHERZER, O. *Optik*, **2**, p. 114 (1947).

CORRESPONDENCE

Static and dynamic elastic constants

In a paper entitled "Microcracks and the static and dynamic constants of annealed and heavily cold-worked metals", by Bristow, which appeared in the February 1960 issue of this *Journal*, attention was drawn to the difference between the static and dynamic bulk modulus and Poisson's ratio for aluminium, copper and nickel determined from measured values for Young's modulus and the shear modulus. A difference was observed also in the Poisson's ratios measured directly.

Observations on ice* show a similar difference between the static and dynamic values of Young's modulus and Poisson's ratio. It was observed also that in the temperature range of 0 to -40°C , the static-value for Young's modulus perpendicular to the C axis of the single crystal is only slightly temperature dependent, whereas the Young's modulus for stresses perpendicular to the grain boundaries of columnar multigrained ice is markedly temperature dependent. The sonic value for Young's modulus lies between 9.0 and 10.0×10^{10} dyn/cm², depending on the frequency of the stress used in the determination. The static value for the

single crystal was found to be about 8.34×10^{10} dyn/cm² and for the multigrained ice, $(5.69 - 6.48 \times 10^{-2}T) \times 10^{10}$ dyn/cm², where T is the temperature in deg. C.

Poisson's ratio obtained from sonic measurements is found to be about 0.32. This compares with 0.42 found from static measurements on the single crystal. The Poisson's ratio obtained from the static measurements on multigrained ice was found to be temperature dependent.

The longitudinal strains, calculated for a given stress from the sonic and static observations on multigrained and single-crystal ice and from sonic observations reported in the literature, were plotted against the corresponding transverse strains. The least-squares fit to the plotted points had a correlation coefficient of 0.92 and could be expressed by

$$e_t = 0.30 \frac{S}{E_S} + 0.88 \left[\frac{S}{E_T} - \frac{S}{E_S} \right], \quad (1)$$

where e_t is the transverse strain; S is the applied stress; E_S is the Young's modulus obtained from the velocity of an ultrasonic pulse ($= 10 \times 10^{10}$ dyn/cm²), E_T is the Young's modulus at temperature T or determined sonically.

Equation (1) indicates that two processes appear to be involved in the deformation of the ice. One process, with a

* GOLD, L. W. *Can. J. Phys.*, **36**, p. 1265 (1959).

Poisson's ratio of about 0.30, was attributed to the elastic deformation of the grains. The second process or processes, with an effective Poisson's ratio of about 0.88, is considered to result in the relaxation of stresses along preferred planes, particularly those stresses associated with the constraints imposed by the grain boundaries. A Poisson's ratio of 0.88 could occur for the multigrained ice because of the symmetry involved. Movement caused by relaxation of stresses associated with the grain boundaries would occur primarily in the direction normal to the long axis of the columnar grains. The reason why the observations on the single crystals should satisfy equation (1) also is not known, but it may be associated with the relaxation of stresses along preferred planes.

Bristow expressed the opinion that the relaxation phenomenon is probably not responsible for the differences that were reported for the metals. The experiments on the ice indicate that relaxation phenomena probably play a major role in determining the differences which were observed. It is perhaps not valid to compare too closely the results obtained with ice with those obtained with metals since ice is a non-metal, and the observations were conducted at temperatures within 40° C of the melting point. Furthermore, the multigrained ice was columnar in structure and metals are normally granular. Even if the mechanisms involved are different, the conclusion still remains that the usual relationships between the elastic moduli may not be valid under all conditions of stressing, particularly for a material such as ice where two deformation processes appear to be active.

Snow and Ice Section,
Division of Building Research,
National Research Council,
Canada.

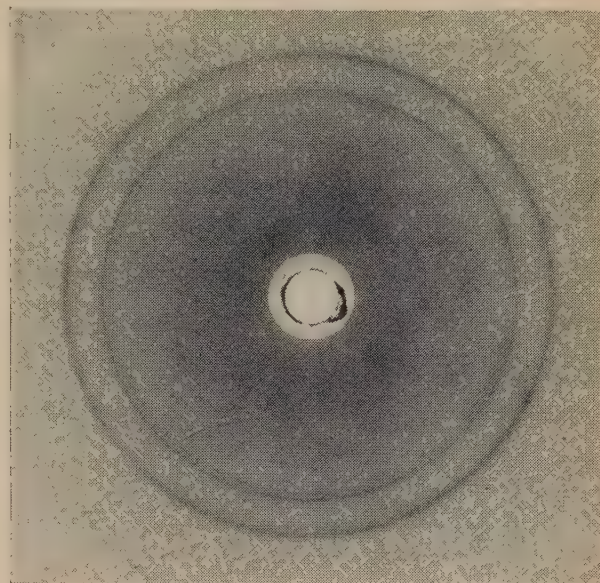
L. GOLD
[3 May, 1960]

X-ray stress determination in austenitic steel

In a recent paper by Moore published on pp. 242-4 of the June 1960 issue of this *Journal*, the author has described the application of the multi-exposure X-ray back-reflexion method to the determination of macro-stress in the surface of austenitic steel. One of the main difficulties in dealing with austenite lies in the selection of a suitable radiation, the object being to produce diffraction lines from the austenite and from a specimen-to-film distance calibrating material at as high angles as possible. With all X-ray stress measurements, the difficulty of reading the position of an unresolved K_α doublet is a source of considerable error.

The purpose of this note is to call attention to the use of

unfiltered chromium K radiation for back-reflexion work on austenite. A suitable calibrating material is then stress-free silver, prepared as described by Frommer and Lloyd.* The lines produced on the film are the chromium K_β reflexion from the 311 planes of austenite, at a Bragg angle of about 74½ deg, and the sharply resolved chromium K_α doublet from the 222 planes of silver, at about 76° 35' for the α_1 component.



X-ray back-reflexion photograph (unfiltered CrK radiation showing 311 K_β line of austenite and 222 K_α doublet of silver) (approximately full size)

The advantage of recording the diffraction of a single characteristic wavelength by a strained lattice is seen in the accompanying photograph; in this particular case complete rotation of the specimen in its own plane was necessary owing to large grain size. Air scattering generally leads to fairly high background density with chromium radiation, but great improvement in contrast is obtained by somewhat over-exposing and using a photographic reducer after fixing.

Stewarts and Lloyds Ltd.,
Corby,
Northants.

J. H. S. NEILSON
[9 August, 1960]

* FROMMER, L., and LLOYD, E. H. *J. Inst. Metals*, 70, p. 102 (1944).

Notes and comments

Elections to The Institute of Physics

The following elections were made at its final meeting by the Board of The Institute of Physics on 22 June, 1960.

Fellows: J. Dutton, J. Dyson, A. Franks, R. J. Hamilton, E. W. Jones, C. A. Ramm, W. Steckelmacher, S. G. Tomlin, F. Tyler, G. I. Williams.

Associates: W. E. Armstrong, T. H. Baker, D. D. Bayes, C. Birch, H. C. Buckingham, A. Bowling, G. Bullock, D. M. Burns, E. W. Burdett, G. W. Canning, D. G. Christie, M. D. Clark, E. Coen, R. Collins, T. K. Dean, R. H. de Vere, J. G. Forrest, J. B. Forsyth, H. G. Frost, F. Gardner, H. I. Glass, G. L. Gooberman, A. Green, W. Haddock, N. J. Hidden, G. S. Holister, A. R. Joy, D. W. Lewin, G. D. Lill, R. E. Loughhead, V. E. Miller, T. P. Moorhead, K. A. Morley, J. L. Parmee, T. I. Putner, R. M. Rees, E. A. Richards, P. E. Richmond, P. O. Rogers, W. Salter, D. M. Schlapp, E. Shuttlesworth, D. A. Silverston, J. R. Thompson, F. R. Tipping, S. Turner, A. L. Wallis, J. A. Warburton, G. M. Ward, E. J. Wheeler, K. B. Whiting, W. T. Wilkinson, P. R. Williams, R. V. Williams.

Thirty-four Graduates, twenty-four Students and four Subscribers were also elected.

Conference on irreversibility and statistical mechanics

The Institute of Physics and The Physical Society announces that it is arranging a conference on statistical mechanics (with special reference to irreversibility). It will be held at Queen Mary College, London, on Monday and Tuesday, 19 and 20 December, 1960.

A full programme has already been arranged. The topics include the general theory of irreversibility, random processes, liquids (theory and experiment) and irreversibility in gases and in plasma.

Further information and preliminary programmes can be obtained from The Secretary, The Institute of Physics and The Physical Society, 47 Belgrave Square, London, S.W.1.

Isotope Information Bureau

The United Kingdom Atomic Energy Authority has recently opened an Isotope Information Bureau at its London Office in Charles II Street, S.W.1. This bureau has been established to provide industry with a convenient central point of enquiry when seeking information on the production and uses of radioisotopes. A display in the bureau outlines developments in the industrial applications of radioisotope and informative catalogues and other literature provide a more detailed account of the work which is, and has been, proceeding in the field.

A qualified staff in constant attendance can provide visitors with a basic introduction to the industrial uses of radioisotopes and can specify reference works for study by those with further interests. Enquirers can be placed in touch with the appropriate departments of the Authority in those cases where detailed information is sought.

Information and advice is provided by the Bureau free of charge.

Polymer

Polymer was founded to provide an international medium for the publication of original papers on the chemistry, physics and application of polymer research, and on other disciplines which contribute to the development of polymer science. The research effort now devoted to this field together with the number of papers written on the subject was considered large enough to justify the publication of this specialized journal. A feature of the journal is the publication of short communications dealing with work which merits publicity before a full paper can be prepared and published. These communications, like the papers, are refereed and edited.

Polymer appears quarterly and commenced January 1960. It contains about 500 pages per volume; the price is £5 per volume, and subscriptions should be placed with Butterworths Scientific Publications, 4 & 5 Bell Yard, London, W.C.2.

Journal of Scientific Instruments

Contents of the November issue

PAPERS

- Apparatus for measurement of sorption of reactive, condensable vapours up to 350° C. By R. M. Barrer and S. Wasilewski.
- Lens mass-spectrometer leak detector. By D. Cosutta and W. Steckelmacher.
- Apparatus for the floating-zone refining of gallium arsenide. By F. A. Cunneen and R. Wickham.
- Rapid counter for small particles in suspension. By J. B. Cornwall and R. M. Davison.
- Measurement of the optical thickness of absorbing specimens with the three-beam interferometer. By P. Hariharan and D. Sen.
- Digito-analogue computer for solving linear simultaneous equations and related problems. By E. V. Krishnamurthy.
- Inexpensive graph plotter for five-track paper tape. By L. Molyneux and E. H. Schneider.
- Low-compliance diaphragm-capacitance gauge for measurement of liquid pressures of the order of 1 in. water. By A. S. Lodge.
- Instrument for the measurement of specular reflectivity of bright metal surfaces. By B. A. Scott.

LABORATORY AND WORKSHOP NOTES

- Simple method for stopping a radiation chopper in a preferred position. By M. F. Kimmitt.
- Flap-valve for long narrow apertures. By G. W. King.
- Hot tube nylon cord cutter for balloon flights. By J. A. Phillips.
- Film carrier for the analysis of oscillograms by means of a travelling microscope. By T. M. Parnell.

NOTES AND NEWS

New instruments, materials and tools. New books. Notes and comments.

THIS JOURNAL is produced monthly by The Institute of Physics and The Physical Society, in London. It deals with all branches of applied physics (including theory and technique). All rights reserved. Responsibility for the statements contained herein attaches only to the writers.

EDITORIAL MATTER. Communications concerning editorial matter should be addressed to the Editor, The Institute of Physics and The Physical Society, 1 Lowther Gardens, Prince Consort Road, London, S.W.7. (Telephone: Kensington 0048.) Prospective authors are invited to prepare their scripts in accordance with the *Notes for Authors*.

REPRODUCTION. The Institute of Physics and The Physical Society is a signatory to The Royal Society's Fair Copying Declaration. Details may be obtained upon application from The Royal Society, London, W.1.

ADVERTISEMENTS. Communications concerning advertisements should be addressed to the agents, Messrs. George Jackson (Fleet St.) Ltd., Cliffords Inn, Fleet Street, London, E.C.4. (Telephone: Holborn 3611-2.)

SUBSCRIPTION RATES. A new volume commences each January. The charge is £6 per volume (\$17 U.S.A.), including index (post paid), payable in advance. Single parts, so far as available, may be purchased at 12s. 6d. each (\$1.75 U.S.A.), post paid, cash with order. Orders should be sent to The Institute of Physics and The Physical Society, 47 Belgrave Square, London, S.W.1, or to any bookseller.

CLAIMS FOR MISSING JOURNALS. Claims from regular subscribers to this *Journal* for missing numbers will only be considered if received within 60 days of the date of mailing plus normal outward time of transit and time for lodging the claim. Losses attributable to failure to notify a change of address or to similar omissions will not be considered.

Summarized proceedings of a conference on applied spectroscopy—Seascale, June 1960

The Summer Conference of the Applied Spectroscopy Group of The Institute of Physics was held at the Wind-scale Club, Seascale, near the United Kingdom Atomic Energy Authority Works, on 16 and 17 June, 1960. About fifty members of the group assembled at this conference, and the papers presented, together with the ensuing discussion, are summarized below. Among the topics discussed were the Mössbauer effect, the chemical and isotopic analyses of radioactive materials by spectroscopic and radioactivation techniques, the use of spectroscopy in determination of discharge temperatures and the development of monitoring systems for beryllium determination.

THE first talk was given by Dr. W. M. LOMER, Atomic Energy Research Establishment, Harwell, under the title "Atomic physics in a nuclear age". Dr. Lomer criticized the title (which had been suggested for him) on the grounds that physics should be considered as a general subject rather than split into certain aspects. He contrasted the training of physicists in Britain with those in the United States. In the former country the graduate learnt his post-graduate physics by overcoming difficulties in his research, whereas in the United States greater emphasis was placed on formal training during his research career.

Mössbauer effect

The main topic of Dr. Lomer's talk concerned implications of the Mössbauer effect. A crystal of an iron compound, containing radioactive ^{57}Co in some of the sites normally occupied by iron, is prepared. There is a slow decay of the ^{57}Co to ^{57}Fe which is in an excited state; this emits a low energy γ -ray of 14 000 eV (corresponding to approximately 1 Å wavelength). The important feature is that the natural width is very small—of the order of 10^{-8} eV. The ratio of the natural line width to line energy (denoted by $\Delta E/E$) is of the order of 10^{-12} , and possible broadening due to Doppler effect does not appear because the recoil momentum is given to the crystal as a whole. The relatively long wavelength of the γ -ray meant that vibrations of the atoms in the crystal had very little broadening effect. (The natural width for visible light is of the order of 10^{-7} eV and the energy in the yellow region corresponds to 2.1 eV; the ratio of line width to energy is thus 10^{-7}). Because the emitting system is the small nucleus relatively isolated in the crystal, pressure and electric fields do not materially affect it.

Natural iron contains about 2% of the isotope ^{57}Fe . Thus irradiation of iron with this characteristic 14 keV γ -ray will give rise to resonance absorption.

This effect can be used to measure relative velocities between a source of these rays and absorbing material containing ^{57}Fe . If the absorber is moved relative to the source (as shown in Fig. 1) then there will be a slight shift in the

frequency due to this motion and, at low velocities of a few tenths of a millimetre per second, an absorption line can be seen.

The most publicized application of the Mössbauer effect has been the measurement of the gravitational red shift. Dr. Lomer emphasized that this was not a "proof" of Einstein's theory of relativity, but merely a terrestrial experiment testing the applicability to electromagnetic photons of the principles of equivalence of gravitational fields and

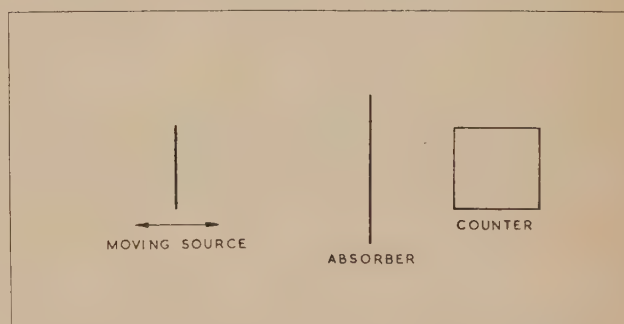


Fig. 1. An illustration of the experimental system for observing spectra in the studies of crystals using the Mössbauer effect

acceleration. If the absorbing material is placed some 40 ft below the source, the photons gain energy from the gravitational field, with the result that there is a shift of the order of $\frac{1}{400}$ of the line width. Recent experiments, both at Harwell and in the United States, in which this line is observed by a counting technique have shown that shifts of this magnitude are present. However, experiments under more finely controlled conditions are necessary to confirm such an application of the Mössbauer effect. Moreover, in answer to a later question, Dr. Lomer stated that the effect of temperature had not originally been fully taken into account, and that a difference of about 1°C between the source and absorber would also account for a shift of this magnitude. (It was interesting to note that this effect of temperature had been pointed out by a Cambridge undergraduate, Mr. Josephson.)

The second application of the Mössbauer effect could give information on the states which electrons in crystals can take. The new effect allows an investigation of the splitting of the ground and excited states of the nucleus due to hyperfine interaction. A type of Zeeman pattern is studied, in which the field acting on the nucleus is provided by the electrons. Some preliminary results from such an investigation are shown in Fig. 2.

It has been found that a source and absorber prepared as different chemical compounds may not be in resonance with one another, since the different electron densities give rise to a small difference in the nuclear levels. This may be

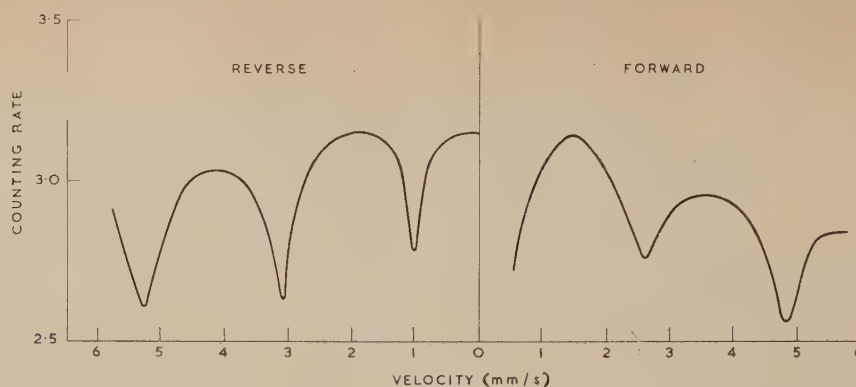


Fig. 2. Results obtained in a Mössbauer γ -ray absorption measurement of the hyperfine field splitting of nuclear levels in ferromagnetic iron. The source was iron (containing ^{57}Fe) dissolved in copper, the absorber was iron (enriched with ^{57}Fe) and a relative motion of 1 mm/s produces an energy shift of 4.8×10^{-8} eV (this curve is published by courtesy of Dr. C. E. Johnston and Mr. J. Ridlout)

caused by small variations in the electron density acting on the nucleus, so that information about the nucleus could possibly be observed by an application of the Mössbauer effect.

Dr. Lomer finally emphasized that interest in atoms rather than nuclei may be slightly old fashioned, but, nevertheless, an understanding and appreciation of this new spectroscopy, just as for conventional spectroscopy, called for a knowledge of physics as a whole.

The analysis of radioactive materials

The second paper was read by Mr. F. J. WOODMAN (United Kingdom Atomic Energy Authority, Windscale), on this topic, with particular reference to the use of spectroscopic and other instrumental methods. He emphasized that the success of the atomic energy programme depends very largely upon the analytical services, which must be kept flexible and up-to-date within reasonable limits of costs. Included in the wide range of interests of the analyst are the examination of the raw materials, the course of the various extraction processes, the composition, purity, and isotopic abundance of the reactor fuels, the analysis of the many other materials that go into the building of a reactor, the stages in the processing of the radioactive fuel after use in reactors and, finally, problems connected with safety and biological considerations.

Increasing demands are made on the analyst by the growth of atomic energy projects and it is, therefore, essential to investigate both time- and cost-saving techniques in the laboratory and in the factory. The use of instrumentation in analysis is particularly promising for plant applications. Use is made of semi-skilled labour for routine operations where possible, since it enables the analyst to devote his skill and attention to the more complex analyses. Conventional analytical methods can be applied after suitable modification to enable the radioactivity to be dealt with safely. Protection must be given to both the operator and the expensive equipment whilst interference effects, e.g. γ -ray interference on X-ray measurements, must be eliminated. There are two different problems involved, namely containment against ingestion of α -active materials and shielding against β , γ activity. The magnitude of the problem is seen when the maximum permissible concentration of plutonium in air is compared with that of the more usual industrial hazards (see Table 1).

Table 1. Maximum permissible concentration of toxic materials (mg/m^3)

Arsenic	0.5
Lead	0.15
Mercury	0.1
Beryllium	0.002
Plutonium	0.000 000 03

Because shielding renders servicing of equipment difficult it is preferable to restrict the sample to the smallest shielded volume and keep most of the equipment outside this shielding.

Two instrumental methods were then discussed in greater detail; these were emission spectroscopy and γ -ray spectrometry.

Emission spectroscopy was used very early in the development of the atomic energy project. Emission spectra are obtained as soon as there is sufficient of a new element to do so and analytical applications are subsequently worked out. Various designs of container were evolved in attempts to meet the conflicting requirements of arc and spark excitation of α , β and γ emitting compounds. Those described were the rather elaborate stainless steel cassette developed by Feldman (at Oak Ridge, U.S.A.), the throw-away plastic cassette used at Harwell and the Windscale silica tube cassette—as shown in Fig. 3—which may be cleaned and re-used. Separation methods such as solvent extraction and ion exchange are used to remove the plutonium from the impurities before the spectrographic examination, but a small quantity of plutonium invariably remains and containment is still necessary. The glove box work is speeded up by providing a switch (operated from within the box) that both starts the spark discharge and racks the plate on automatically, thereby eliminating the need for the operator to get out of the gloves after loading each sample. A typical glove box arrangement is illustrated in Fig. 4.

Much simpler shielding can be used if most of the activity is removed; for example 1 c of γ -active caesium can be removed almost completely by ion exchange from sodium and rubidium impurities, which are then measured using the Lundegardh flame method. Feldman, on the other hand, used a cell that was heavily shielded with three feet of concrete for the analysis of highly active corrosion products from the homogeneous reactor experiment at Oak Ridge. The light from the excitation source was brought out to a Jarrell-Ash

Ebert spectrograph by a lens system that included a 90 deg. bend as a trap for the γ -radiation.

Significant advances have been made during the last eight



Fig. 3. Photograph of the cassette used at Windscale to restrict radioactive contamination when active materials are being spectroscopically examined

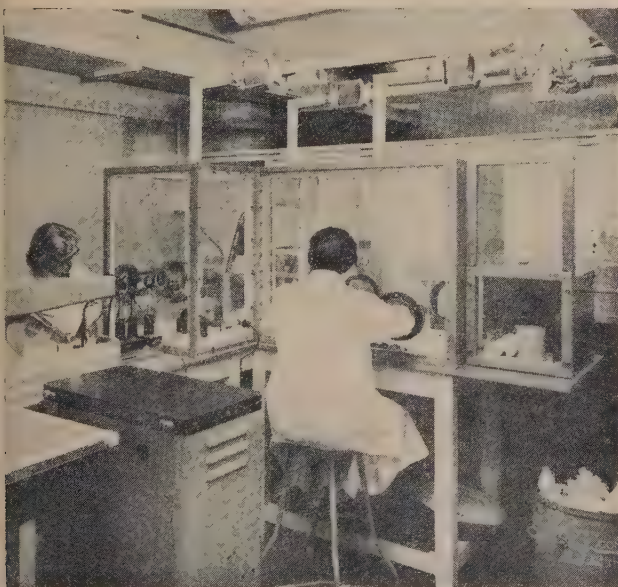


Fig. 4. A general view of a glove box attached to a spectrograph

years by the use of γ -spectrometry as an analytical method. A thallium-activated sodium iodide crystal, usually not smaller than $1 \times 1\frac{1}{2}$ in., is the detector and the signal from

an attached photomultiplier tube is amplified and fed to an analyser unit. The photoelectric peak height, or more strictly the area enclosed by the peak, is a measure of the quantity of a particular nuclide present in the sample. Interaction of the γ -photons with the crystal produces (a) photoelectrons, (b) Compton continuum, (c) pair production, depending on the energy of the photons and the atomic number of the crystal material. Anthracene, for example, gives high Compton absorption with few photoelectrons; sodium iodide, on the other hand produces, in addition to the Compton continuum, photoelectrons with discrete energies which are proportional to the incident γ energies. Pair production is obtained only when the incident γ energy is greater than 1.2 MeV.

The main advantages of γ -spectrometry are: (a) no separation or pre-treatment is necessary, (b) solids, liquids and gases can be examined, (c) sensitivity is good, for example, $0.002 \mu\text{c}$ of ^{131}I per litre can be measured, (d) it is versatile, several nuclides being determined simultaneously, and high or low activities can be measured, and (e) it is stable, a reproducibility of $\pm 5\%$ can easily be held over a week.

The lecturer then described a number of applications of the technique. Among these were the measurements, on about 5000 samples of biological interest, for ^{131}I after the Windscale incident, and the whole body counting work for which the patient is placed inside a large detection chamber. A small peak due to ^{137}Cs derived from fission product fall-out is found in all patients. A diagrammatic representation of a typical body γ -spectrum is presented in Fig. 5.

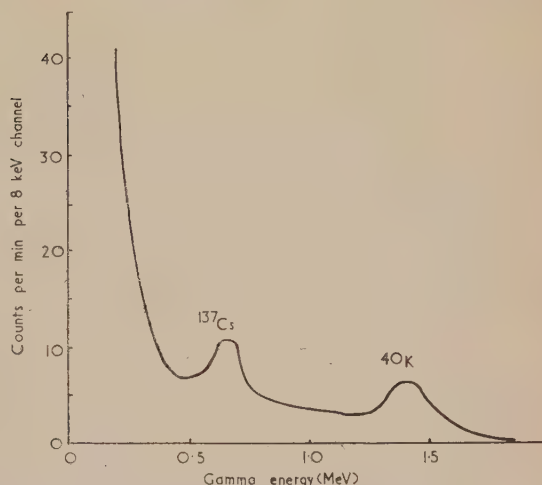


Fig. 5. A typical graph of results obtained when a whole body counter is used

A great deal of time is saved by the γ -spectrometer in the routine analysis of fission products in plant process solutions. An interesting application was the measurement of very short-lived activities induced in the carbon dioxide coolant in the Calder Hall reactors, e.g. ^{41}A (1.8 hours), ^{16}N , (7.4 seconds), ^{19}O (29 seconds). By introducing a delay line before the spectrometer, ^{16}N could be eliminated before measurements were made on ^{41}A .

In reply to a question by Dr. MENZIES (Hilger and Watts Ltd., London), Mr. Woodman confirmed that the γ -spectrometer was non-dispersive and Mr. FOREMAN (United Kingdom Atomic Energy Authority, Windscale) expressed the view that there might be advantages in the use of a dispersive system in the low energy region, but that the required quartz

crystal plates would be very expensive and the technique would, in any case, need development.

Isotopic analysis with special reference to spectroscopic methods

The final paper of the morning was read by Mr. R. P. THORNE (United Kingdom Atomic Energy Authority, Capenhurst). Mr. Thorne introduced his subject by pointing out why various isotopic ratio determinations were required in the nuclear energy programme. Abundance measurements were necessary for the control of various isotope enrichment plants (uranium, lithium, boron), the analysis of heavy water moderators, the analysis of fuel elements, nuclear cross-section measurements and for health and safety purposes.

A number of possible techniques, each dependent on some physical property, were available for the determination of isotopic concentrations. Since the first analysis by Aston, using a mass spectrometer, abundances have been determined by density, refractive index and thermal conductivity measurements, by emission, atomic absorption, infra-red absorption and nuclear magnetic resonance spectroscopy, and by the use of both natural and artificially produced radioactivity.

The mass spectroscopic determinations had advantages of high accuracy and general utility, but suffered from such factors as high capital and maintenance costs, possible confusion of ions having similar mass/charge ratios, effects where previous samples affected succeeding results and fractional isotope distillation difficulties from some types of source.

The main spectroscopic method discussed involved the determination of the ratio of $^{235}\text{U}/^{238}\text{U}$, by measurement of relative line intensities from the lines of each isotope. The difference in wavelength of certain lines from different isotopes made this method possible, and in favourable cases the separation could be a quarter of an Angström unit. Attention must be given to the widening of the ^{235}U line from the effect of magnetic hyperfine structure.

The original experimental methods involved time-consuming photographic recording techniques and the use of conventional high-resolution spectrographs, which were bulky, expensive and sometimes difficult to maintain in adjustment.

Improvements in speed and accuracy of analysis were obtained by the substitution of photoelectric for photographic recording, and some reduction in instrumental size resulted from the development of the Echelle type diffraction grating. In the U.K.A.E.A. laboratories a number of these gratings had been incorporated into high-resolution spectrographs, based either on the Littrow or Ebert system, for routine abundance measurements.

In the last few years further reduction in instrumental size and costs, coupled with increased optical efficiency, has been obtained by using a low-resolution monochromator to isolate a narrow spectral band, coupled with a Fabry-Perot étalon as the high-resolution element. Such a device involves alteration of the equivalent optical path between the two Fabry-Perot plates and, of the techniques used so far for this purpose, that of pressure scanning had been most developed and successfully used. For a change in pressure of one atmosphere, a change in wavelength coverage of about 1.2 Å at 4000 Å could be made, and this could be increased if gases of higher refractive index were used.

Many devices for the control of pressure scanning have been developed, and one having several advantages was under construction in the Development and Engineering Group at Capenhurst. A saw-toothed pressure—and hence wavelength—scan is obtained by using an electromechanical pressure controller, which enables scanning times of between 10 s and 10 min to be selected. Provision is also made to select the pressure range and for a fly-over device to eliminate unwanted wavelength regions.

As the pressure is cycled, so the fringe pattern is scanned through a small aperture in the exit focal plane, and radiation from the fringes corresponding to each isotope in turn are recorded photoelectrically. To compensate for fluctuations in source intensity, a second photomultiplier tube records part of the monochromator's output. After amplification and rectification the ratio of the two signals is recorded on a chart recorder.

The scanning generator and the general arrangement of the instrument are shown in Fig. 6 and Fig. 7 respectively. Typical scans for the uranium spectra are illustrated in Fig. 8.

Preliminary work with the Fabry-Perot instrument has indicated that the precision of measurement is better than 1% of the isotopic ratios. Although this precision is not as

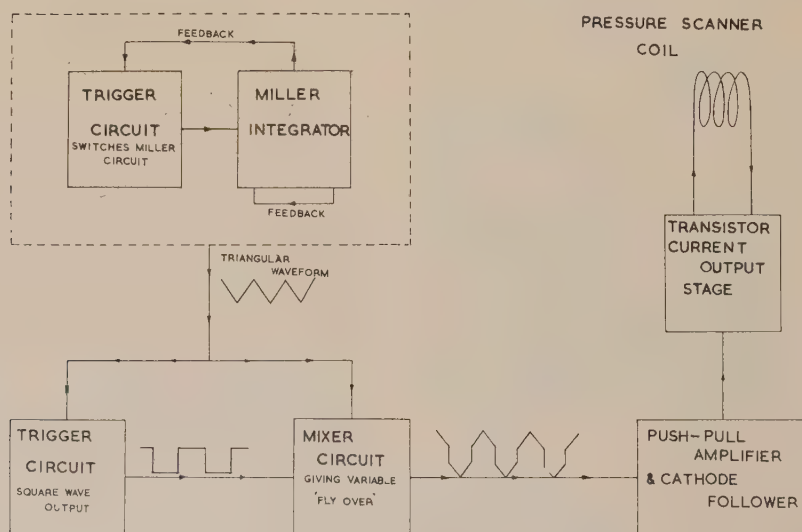


Fig. 6. Block diagram of a scanning generator

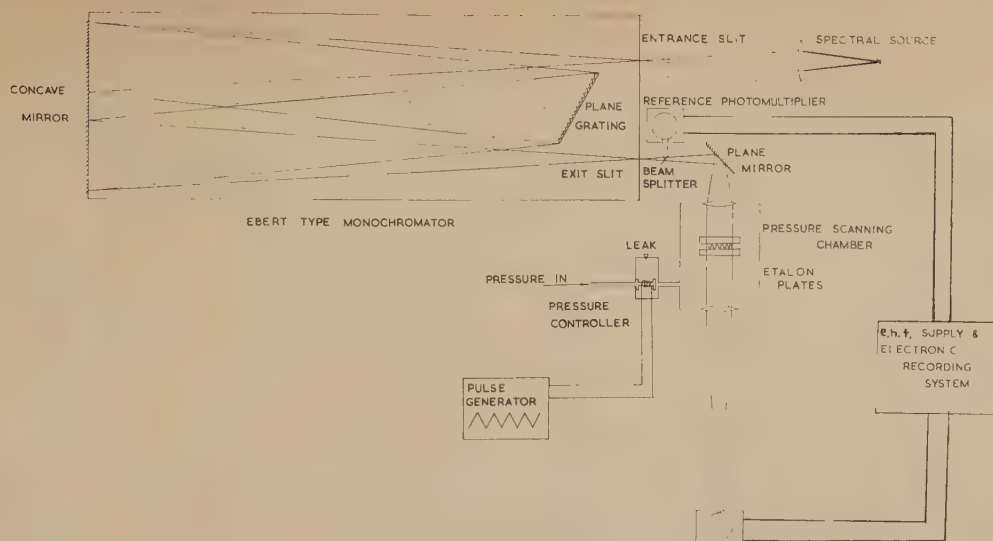


Fig. 7. A compact high resolution spectrometer for isotope analysis

good as that of a gaseous-source mass spectrometer, it is equivalent to that of the solid-source instrument and is sufficient for a large number of analytical problems. Capital

and maintenance costs of the optical instrument are lower and the high vacuum standards essential for mass spectrometers are not required.

One of the key problems associated with optical techniques is the use of a satisfactory source. High intensity, narrow line width, ease of preparation and stability were the major requirements. For work on uranium, these had been met by use of the hollow cathode source. In the form developed at Capenhurst the cathodes were not cooled and were easily interchangeable. For gaseous samples, electrodeless discharge tubes could be used, although care must be taken to avoid isotopic separation in the associated tube work.

In a short discussion Dr. MENZIES emphasized that a Fabry-Perot étalon was not always superior to an instrument involving a grating or prism. It was so in certain cases where high resolution was important, but there was a tendency at the moment to assume it was always preferable. Dr. BOVEY (Atomic Energy Research Establishment, Harwell) mentioned that, as a by-product of some work done in Prof. Jacquinot's laboratory at Bellevue with a microwave discharge tube containing plutonium, a rough estimate of the isotopic content had been made. This gave a higher reading for the ^{240}Pu isotope than that determined by a mass spectrometer, a point which surprised Mr. Thorne because he thought that the method of making such microwave tubes would rather put the ratio the other way. Dr. Bovey emphasized that this was not an investigation into isotopic determinations, but he mentioned the work because the plutonium had originally come from Windscale where the meeting was now being held.

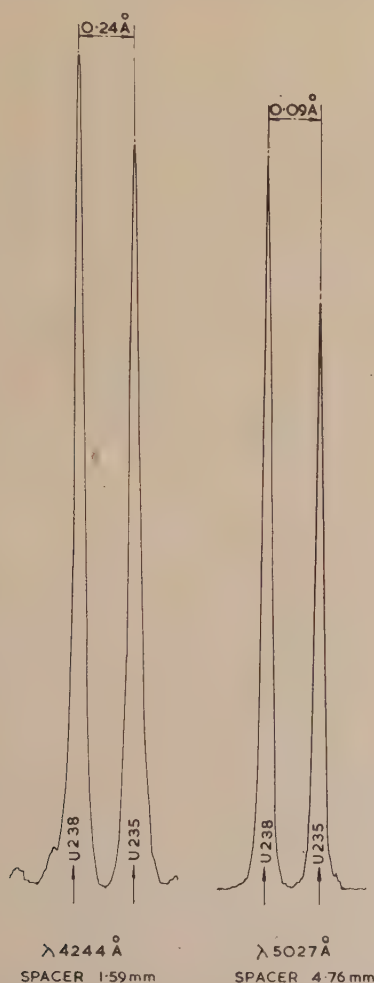


Fig. 8. Some scans of isotope shifts in two lines of uranium produced by the Fabry-Perot interferometer

Visits to Windscale Works

In the afternoon there was a visit to the Chemical Services Department and Research and Development Branch Laboratories at these Works. The Conference Members were shown a selection of the general laboratories; particular emphasis was given to emission spectrographic methods and γ -spectrometry was also seen in action. On the Research and Development side, some of the development work going on in connexion with magnox and graphite materials was seen as well as general reactor physics.

Three reactor experiments were being assembled within the former blower-house of one of the shut-down Windscale

piles. These were (a) a fine structure experiment, (b) an approach to critical assembly, and (c) an exponential experiment.

Uses of isotopes in analysis

The second session was opened by a paper on this subject by Dr. D. J. FERRETT (United Kingdom Atomic Energy Authority, Harwell). He first emphasized the value of tracer techniques to the analyst, for, whereas in most conventional analytical methods something like 10^{10} to 10^{15} atoms were required for detection, 10^5 atoms could be estimated by counting techniques; this gave a remarkable increase in sensitivity. These high sensitivities were often necessary because of the exacting demands made on new material for use in the atomic energy programme.

Recent advances that had been made in the large-scale separation of rare earths by ion exchange were largely due to radioactive tracers, the use of which enabled the course of individual rare earths to be followed. By the use of this technique the purity of these elements had been greatly improved over those separated formerly by multiple crystallizations, yet the cost was smaller. The separation of protein hydrolysates on paper chromatograms can similarly be followed by using compounds into which a ^{35}S tracer has been incorporated. If the γ -isomer of benzene hexachloride is labelled with ^{36}Cl , then this tracer can be used to locate the bulk of the isomer when separation is made from the mixture of other isomers produced during manufacture of the insecticide.

One important application of isotopes involved the dilution technique. In this, a small known quantity of a radioactive isotope of an element could be added to a mixture for which an analysis of this particular element was required. Normal chemical separation and analytical procedures could then be followed, and at the end the amount of active isotope separated could be determined by counting. The ratio of the initial to final amount of active isotope gives a correction factor for any losses incurred in the analytical procedure. In special cases there is no need for the trace element to be radioactive. If an isotope of a different mass is added, the amount finally remaining can be determined mass spectrometrically. Examples which involve this technique are the determination of uranium in sea water and the determination of lithium in granite.

Some typical results from several types of analysis are shown in Table 2.

Table 2. *Determination of uranium in sea-water by various methods*

Area	Method	Result ($\mu\text{g/l.}$)
Coastal sea-water	Mass spectrometer, type 1	3.34 ± 0.04
	Mass spectrometer, type 5	3.31 ± 0.04
Bay of Biscay	Mass spectrometry	3.31 ± 0.06
	Pulse polarography	3.41 ± 0.17
	Fluorimetry	3.25 ± 0.23

The high sensitivity of the dilution method was shown in a determination of ^{235}U in plant solutions. Most analytical techniques that determine ^{235}U are hampered by the high activity associated with the size of sample necessary to achieve the order of accuracy required, as 200 g of ^{235}U is associated with $3.6 \times 10^4 \text{ c}$ of activity. If the sample size can be reduced to 1 μg the activity is only 180 μc . This was done by using ^{233}U as the isotopic tracer and a coefficient of variation of 0.1% was achieved for the determinations.

Another technique in which isotopic properties are measured is the determination of isotope concentrations by nuclear magnetic resonance. Elements analysed by this technique include the isotopes of hydrogen, lithium, boron, sodium, fluorine, phosphorus and aluminium. A recording of a nuclear magnetic resonance investigation of ^{27}Al is shown in Fig. 9.

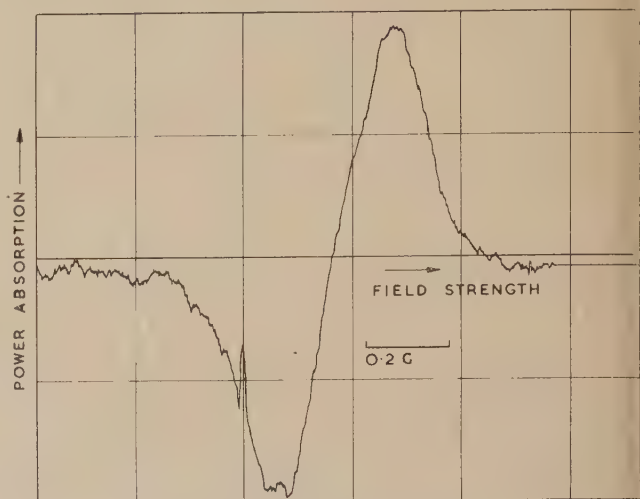


Fig. 9. A nuclear magnetic resonance study of the absorption by ^{27}Al in 3M aluminium nitrate solution

In activation analysis, samples are bombarded in a particle flux, become radioactive and the amount of radioactivity is estimated by counting. This technique has extremely low sensitivity limits. Thus arsenic can be determined to 0.002 parts per million (see Table 3) and the method was used in testing very pure silicon required for transistor manufacture.

Table 3. *Determination of arsenic, copper and antimony impurities in silicon*

Sample	Arsenic (p.p.m.)	Copper (p.p.m.)	Antimony (p.p.m.)
H	0.005	0.001	0.006
	0.005	0.003	0.002
	0.002		0.006
I	0.004	0.003	0.002
	0.003	0.003	0.002
	0.002		0.001
	0.002		0.009
J	0.004	0.009	0.003
	0.002	0.009	0.001
	0.004	0.006	0.001
	0.003	0.009	0.001

Dr. Ferrett pointed out that the precision was not good when measurements such as these were made near to the detection limits. A great advantage of the activation method in trace element determinations lies in the fact that contamination from reagent vessels, etc., is unimportant after the irradiation, since only the radioactive element is subsequently measured.

γ -spectrometry was briefly discussed as a means for analysing the products of radioactivation without any prior separation. An example was the measurement of silver

caesium and rubidium to 100, 0.1 and 5 p.p.m. respectively in a sodium/potassium alloy. An atomic pile with a neutron flux of about 10^{12} neutrons $\text{cm}^{-2} \text{s}^{-1}$ was used for most radioactivation assays, but some work can be done with small sources (flux 10^8). Irradiations are made at Harwell on behalf of outside users and even short-lived isotopes can be used, provided that the samples are flown out to their destination immediately after irradiation.

Finally, Dr. Ferrett described a simplified X-ray fluorescence analyser used at Harwell in which an X-ray emitting isotope, such as ^{55}Fe or ^{241}Am , replaced the expensive X-ray tube. Examples of analyses that could be made with this equipment were the estimation of nickel and chromium in chromium plate and of the elements present in petroleum cracking catalysts.

In the ensuing discussion, Mr. THORNE pointed out that the precision of isotope abundance measurements using counting techniques was not so high as could be obtained by optical or mass spectrometry.

In reply to Mr. GIDLEY (Imperial Chemical Industries Ltd., Birmingham), Dr. Ferrett said that the time required for these procedures was about two days for isotope dilution, a day to a week for radioactivation and about thirty minutes, depending on counting rates, for the X-ray fluorescence.

Dr. MENZIES thought that isotopic exchange of ^{36}Cl might occur between the benzene hexachloride tracer and the inactive chlorine in the other isotopes.

Use of spectroscopy in determinations of temperature

This subject was discussed by Dr. W. R. S. GARTON (Imperial College of Science and Technology, London). The speaker emphasized that this topic concerned spectroscopic techniques and interpretative methods of deriving one of the important gross parameters, defining the *physical* state of a hot gas. The question of chemical composition discussed by other speakers was only of indirect relevance.

Over the years, the astrophysicist has learned to exploit spectral line profiles and intensities to yield important information on stellar atmospheres, gas nebulae, comets, etc., and the methods used have only rather recently found great application to laboratory plasmas. The reasons for this have been twofold. The astrophysicist, having inaccessible light sources, has had to make maximum use of their spectra. Secondly, he can often reasonably assume some relatively simple form of dynamic equilibrium, e.g. thermal equilibrium over fairly large volumes. This condition is not easily achieved in the laboratory.

The assumption that there is a "temperature" of a hot gas, which can be measured, implies the existence, at least over a region large on the atomic scale, of a Maxwell-Boltzmann distribution, for at least one of the modes by which energy can be carried in the gas, e.g. translational motions of atoms or electrons, molecular vibrations or electronic excitation energy. If for all such modes the same numerical value of T is found to apply, the gas is said to be in thermal equilibrium.

The matter can be illustrated by considering one way in which this "population" or "excitation" temperature of a hot gas can be determined from relative intensity measurements on a line spectrum.

The population of the various excited states r are given in Boltzmann's law, i.e.

$$n_r = g_r \frac{ne^{-\epsilon_r/kT}}{U(T)} \quad (1)$$

where n is the total number of atoms/ cm^3 ,

$n_1, n_2 \dots n_r$ are the number of atoms in states $1, 2 \dots r$,
 $\epsilon_1, \epsilon_2 \dots \epsilon_r$, etc., are the excitation energies in each state,
 $g_1, g_2 \dots g_r$, etc., are the statistical weights of each state,
 and $U(T)$ is the partition function.

The total intensity of the transition $s \rightarrow r$ is,

$$\begin{aligned} J_{sr} &= \frac{h\nu_{sr}n_sA_{sr}}{4\pi} \\ &= \frac{h\nu_{sr}g_sne^{-\epsilon_s/kT}A_{sr}}{4\pi U(T)} \end{aligned} \quad (2)$$

whence

$$\log_e \frac{J_{sr}}{g_s\nu_{sr}A_{sr}} = \text{constant} - \epsilon_s/kT \quad (3)$$

where h is Planck's constant, ν_{sr} is the frequency, n_s is the number of atoms in state s , and A_{sr} is the coefficient of spontaneous transition from state s to state r .

Thus a plot of the left-hand side (obtained from measurement of relative intensities for a number of lines of known relative transition probabilities) *versus* ϵ_s , will, if Boltzmann's law applies, give a straight line and T can be found from its slope. If no straight line appears it is concluded that there is no thermal equilibrium, i.e., no strict meaning can be given to "temperature".

A difficulty of this method is that our knowledge of radiative transition probabilities is still rather small. In a few cases, such as that of the hydrogen atom, theoretical predictions are reliable. Another example is the extensive work of the Utrecht school, originated by Ornstein. In that work, T was determined from intensity distributions over the CN bands of a carbon arc in air, reliance being placed on theoretical formulae for the rotational line intensities. With T thus determined, the relative transition probabilities of lines of elements (e.g. aluminium) simultaneously present in the arc were found.

Work of great interest and value has been done at Kiel during the past decade, by Lochte-Holtgreven, Maecker and collaborators, on arc plasmas of quite high temperature—about 50000°K being reached at the extreme. In some of this work, the arc has been made to burn in a water-vortex,

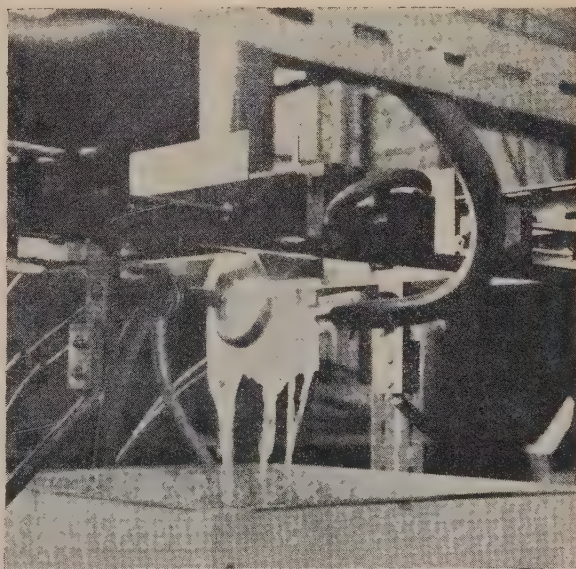


Fig. 10. A general view of a high temperature arc in which a water vortex is used

the water serving as a constricting wall. A photograph of such a water-vortex arc in action is shown in Fig. 10. From this type of arc, measurements on the intensities of lines and their profiles can be used to give information on ion density and equivalent temperatures. Examples were shown of the determination of transition probabilities for sulphur, chlorine and argon determined by this method. An early record of such spectra is given in Fig. 11 by courtesy of Mr. Foster of the University of London Observatory.

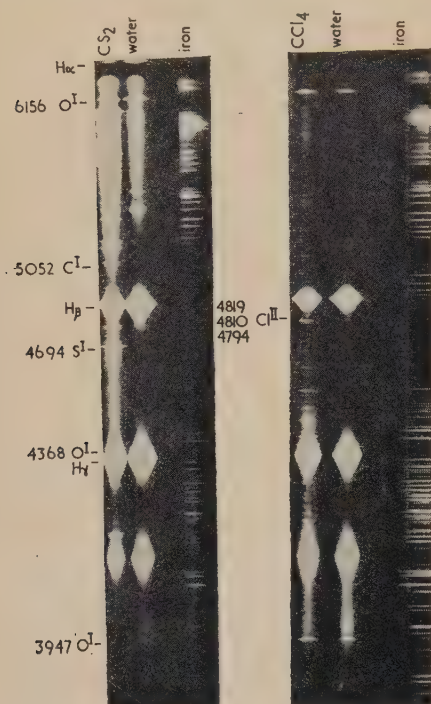


Fig. 11. Spectra given by the high temperature arc when sulphur and chlorine and argon are present (this photograph is reproduced by courtesy of Mr. E. W. Foster of London University Observatory and was taken by him several years ago during experimental trials of the apparatus)

In certain cases the difficulty of the uncertainty of the values of transition probabilities A_{sp} can be avoided by use of the "reversal temperature" technique, widely applied to flames, by Gaydon at Imperial College. In this method there must be available a light source giving a background continuum of brightness temperature higher than the population temperature of the line being used. At Imperial College, measurements have been made on arc plasma tem-

perature, by use of a flash tube as background source. One special form of transient high-brightness discharge has resulted from utilization of recently developed high-voltage capacitors of very low residual inductance. This source, in fact, yields an intense continuum down to at least 500 Å in the vacuum ultra-violet region. Because of the low inductance the discharge in such a flash tube took place within microseconds.

As a further development of this type of work, a method of measuring intensities involving a digital voltmeter and counting scaler had been added. This enabled intensities to be determined much more quickly than by normal oscilloscope methods.

In order to point out to atomic spectroscopists the limitations on present knowledge of spectra, Dr. Garton showed several examples of absorption spectra (one of which is shown in Fig. 12) taken by conventional ultra-violet techniques. These showed very marked auto-ionization phenomena and added a considerable number of previously unknown lines to the spectra of elements such as calcium, strontium and barium.

In reply to a question from Dr. LIM (University of Liverpool), he stated that these results would have an important bearing on the rate coefficients for photoionization and electron recombination in these vapours.

The detection of beryllium by spectrographic methods

The final paper was given by Mr. M. S. W. WEBB (Atomic Energy Research Establishment, Woolwich). Mr. Webb traced the course of the recognition of the toxic nature of beryllium and its compounds. The toxicity was first reported in 1933 by Weber and Engelhardt, and investigated further by Fabroni in Milan. The more widespread industrial uses during World War II made it apparent that the main hazard was from inhalation of dusts. The recommendations made in the United Kingdom in 1947 were:

- (1) the concentration of beryllium in the air of work-rooms should not exceed $2 \mu\text{g}/\text{m}^3$ as the average during an eight-hour day;
- (2) the concentration at any one time must not exceed $25 \mu\text{g}/\text{m}^3$;
- (3) the concentration in the neighbourhood of beryllium plants should not exceed $0.01 \mu\text{g}/\text{m}^3$ on the average during one month.

Ideally, monitoring should give an instantaneous record of the beryllium concentration in the atmosphere, but the early methods gave results that were delayed while the

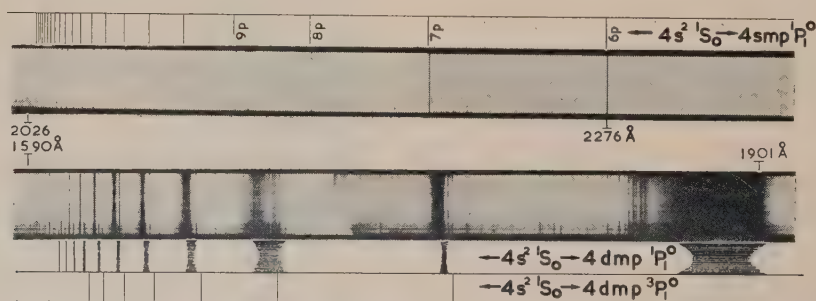


Fig. 12. The absorption spectrum of calcium. Those lines which are not lettered represent extensions of the known spectrum of calcium

beryllium that had been collected on a filter system was processed into a form suitable for final measurement. These methods cannot be used to control the condition (2) above.

Examples of filtration systems were shown which sample air at the maximum normal breathing rate of man. However, the filter medium itself must be a compromise between considerations of air flow rate and particle size retention. Particles of unit density and 0.4 to $0.8\ \mu$ radius are the most likely to be deposited in the lung alveoli, and are therefore of greatest clinical significance. Whatman 41 (by Reeve-Angel) and Fourstones A filter papers are less efficient in retaining the smallest particle sizes than glass fibre media, but all of the latter examined contained a small beryllium blank. Millipore cellulose ester filters, however, will give complete retention of particles down to $0.2\ \mu$.

The spectrographic methods used to measure the amount of beryllium on the filter pads were next discussed. These were d.c. arc on a dilution of the ashed paper in an iron oxide flux, high-voltage spark directly on the filter pad, with photomultiplier recording of the beryllium doublet at $3130\ \text{\AA}$ and an aluminium standard line at $2754\ \text{\AA}$, and spark or arc excitation after wet oxidation and solution of the paper had been carried out.

A direct-reading monitor, which was developed in 1952 by Churchill and Gillieson, was based on an Ebert grating monochromator and measured the intensity of the beryllium $3130\ \text{\AA}$ doublet produced when a sample of the air was drawn over a spark source. Serious disadvantages of this instrument were its dependence upon particle size of the beryllium and the lack of a ready means of checking the calibration.

Mr. Webb then described the direct-reading instrument that had been developed at the Woolwich Outstation of A.E.R.E. and which overcame these disadvantages. The reason for the variation of the results with particle size when a simple condensed spark was used, was shown to be the short duration and small cross-section of the spark pulses, compared with the flow of particles carried in the air stream through the spark chamber; many of the larger particles were in fact passing between the electrodes without being subjected to excitation. A triggered a.c. arc devised by Campbell and Davis at Woolwich gave a much longer time constant of the discharge and this, together with an aerodynamically designed arc chamber, excited the airborne particles much more efficiently. Since it was known that fractionation occurred in long pipes when the particle size exceeded $1\ \mu$, the air intake to the monitor is made directly at the arc chamber (shown in Fig. 13). The grating monochromator is a Czerny-Turner mount with mirrors of $27\ \text{cm}$ focal length and a $30\,000$ lines per inch grating. It is used in the third order, with an Ilford OX7 filter at the slit as an order sorter, and gives a reciprocal linear dispersion of $6\ \text{\AA}/\text{mm}$. The beryllium $3130\ \text{\AA}$ doublet and the adjacent background are detected by two photomultipliers, which charge condensers, and the integrated signals from these are recorded as line/background on a ratio recorder. An integration time of $20\ \text{s}$ for an air-flow rate of $40\ \text{litres}/\text{min}$ minimizes sampling errors. The concentration range covered by the monitor is $1\text{--}100\ \mu\text{g}/\text{m}^3$ and the accuracy obtained is $\pm 30\%$.

A simple calibrating source is built into the instrument. This consists of a condensed spark between a copper and a copper/beryllium electrode, which releases a constant amount of beryllium ($0.3\ \mu\text{g}$ beryllium/min) into a controlled flow of air, which is diverted to the arc chamber. Tests showed that none of this beryllium is precipitated in the ducts leading

to the arc. A rotating shutter admits air either directly to the monitor or through a filter to the calibrating source. The monochromator, arc chamber, trigger unit flow meter and filters are built into a portable sampling head, which is connected by a flexible hose to the main console. Single air samples may be taken or the instrument can be arranged to operate continuously during an eight-hour shift on one minute cycles of blank, calibration and sample.

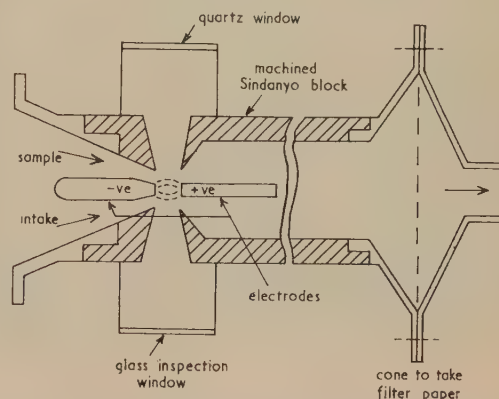


Fig. 13. A vertical section through the arc box in which the beryllium dust is excited between the electrodes

Results indicated by the monitor can be checked by collecting the particles in the exhaust air on a filter pad, which is then analysed for beryllium by the iron flux method. In this way it was shown that consistent results could be obtained from different particle sizes of beryllium metal powder and from the various beryllium compounds, beryllium hydroxide, ignited beryllia and beryllium ammonium fluoride. Field trials were also carried out in which it was shown that, although the filter pad analyses are in agreement with the averaged values from the monitor, the latter also shows the transient high concentrations of beryllium that can occur and yet remain undetected by the filter pad method, as can be seen in Table 4.

Table 4. *Instantaneous values for beryllium concentrations found by means of the spectrographic monitor**

Results produced at 1 min intervals by monitor ($\mu\text{g}/\text{m}^3$)	Mean monitor result over 20 min ($\mu\text{g}/\text{m}^3$)	Analysis of filter 20 min. sample ($\mu\text{g}/\text{m}^3$)
1.2.1.0.0.0.2.1.0.0. 0.1.2.2.0.0.1.1.0.0.	0.7	0.8
1.0.3.0.0.3.0.0.0.0. 0.0.0.0.0.1.3.0.4.21.	1.8	2.3
0.0.0.0.0.0.5.0.4.53. 4.2.10.3.2.7.3.0.2.0.	4.8	4.2

* These figures are taken from field trials carried out by co-operation between A.E.R.E. and I.C.I. Metals Division, and are reproduced with their permission. These high concentration levels were obtained near an experimental plant and all people present wore breathing apparatus.

Vanadium and titanium interfere but they are likely to be significant only if alloys with these metals were to be used in the future. Magnesium interferes by suppressing the background in the neighbourhood of the beryllium line

which gives an enhanced line to background reading; 1000 μg of magnesium gives a reading equivalent to 1 μg beryllium.

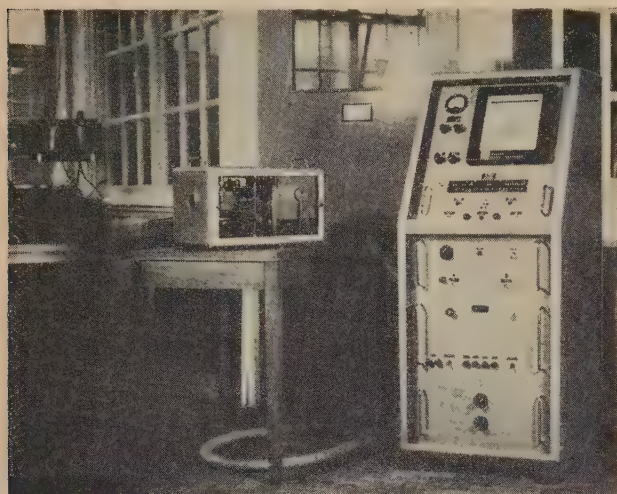


Fig. 14. A general photograph of the beryllium monitor

In the ensuing discussion Dr. MENZIES drew attention to the fact that the readings were not directly related to the number of particles of the most toxic size, since it measured

all sizes of particles that were present. In reply, Mr. Webb said that the current health physics requirement was that total beryllium should be determined.

The discussion was concluded by a practical demonstration of the beryllium monitor by Mr. R. J. Webb (A.E.R.E., Woolwich) who was responsible for its design and construction. A general photograph is given at Fig. 14.

Visit to Calder Hall

The meeting was ended by a general visit to this site. Of special interest was the burst slug detection gear which measured the solid daughter products from the Xenon fission product. Recorders showed the amount of fission product activity in every group of fuel element channels in the reactor and an automatic warning system drew attention to any increase in this activity.

Acknowledgements

The authors are grateful to the speakers for considerable help in both correcting the summaries and providing the illustrations.

A.E.R.E., Harwell,
Nr. Didcot,
Berkshire.

L. BOVEY
F. T. BIRKS

Deposition of *Lycopodium* spores upon glass slides exposed in a wind tunnel

by C. N. DAVIES, M.Sc., D.Sc., F.Inst.P., London School of Hygiene and Tropical Medicine, London, W.C.1

[Paper first received 6 July, and in final form 31 August, 1960]

Abstract

An analysis, based upon experimental data, is made of aerodynamic factors concerned in the deposition of "*Lycopodium*" spores upon glass microscope slides exposed at various angles in a wind tunnel. Gravity controls deposition on horizontal slides only at low wind speeds; with increasing speed impingement upon the leading edge of a microscope slide prevents deposition from taking place on the upper surface. At sufficiently high wind velocities deposition takes place by eddy impaction, originating from turbulence in the main air stream, upon the upper and lower surfaces. Deposition on the lee side of bluff obstacles by eddy impaction is discussed.

Introduction

IN a paper by Gregory and Stedman⁽¹⁾ a large number of experiments were described which had been carried out as a contribution to the understanding of the mechanisms by which fungal spores and other particles deposit on the surfaces of plants. The present writer studied this paper on account of his interest in fluid mechanics and the dynamics of dust particles; considering the results to be valuable and unique, a careful assessment of the aerodynamical processes involved in the wind tunnel experiments was made. Since this aspect of the data was not elaborated in the original paper, although it is of undoubted relevance to field work, both in biology and dust technology, the results of the analysis are presented here.

Experimental method and nomenclature

In the experiments of Gregory and Stedman spores of *Lycopodium* were blown down the axis of a wind tunnel and the number caught on the sticky surfaces of a microscope slide ($7.6 \times 2.5 \times 0.15 \text{ cm}^3$) was compared with the number collected by a cascade impactor, which was regarded as a perfect sampling instrument. The impactor catch was expressed as area dose, Nu_0/Q spores/cm², where N = number of spores collected, u_0 = wind speed in cm/s and Q = flow through the impactor in cm³/s.

Area dose has the advantage of being independent of the duration of emission of the spores and of fluctuations in the rate of emission, since

$$\text{Area dose} = u_0 \int_0^t c dt \text{ spores/cm}^2 \quad (1)$$

where c is the time-dependent airborne concentration (spores/cm³); it is necessary that u_0 and Q be constant.

The rate of deposition on a horizontal surface, due to gravity, is cv_s spores/cm² s where v_s is the terminal velocity

of the spores and c is the concentration just outside the surface. The total number of spores depositing on unit horizontal area due to the emission is

$$v_s \int_0^t c dt = (\text{area dose}) \times (v_s/u_0) \quad (2)$$

provided that the only mechanism at work is gravitational settling and that the area dose and the values of c are measured near enough to the surface. In the experiments these restrictions were not maintained, but the observed deposition rates were compared with the gravitational rate. The comparison was not made directly but in terms of unit area dose, thus eliminating both the absolute number of spores dispersed and the time factor. The deposition rates per unit area dose were termed "efficiencies" and expressed as percentages.

The observed efficiency of collection per unit area of slide E was compared with the efficiency of gravitational deposition E_g , where

$$E = 100 n/(Nu_0Q) \% \quad (3)$$

$$E_g = 100 v_s/u_0 \% \quad (4)$$

n being the number of spores counted per square centimetre of slide; E could be expressed as an average along the entire downwind length of the slide or given local values at successive half-centimetre zones, A to E . It will be noted that E_g is inversely proportional to the wind speed, whereas the absolute gravitational deposition rate is independent of wind speed.

The amount deposited by gravity in unit time on unit area is independent of wind speed for a cloud of infinite extent but, being proportional to the time of exposure, varies inversely as the wind speed for a small cloud with boundaries crossing the sampling place.

Deposition on horizontal slides

This followed a similar pattern to that previously described by Gregory⁽²⁾; E was nearly equal to E_g on the top surface of the slide and no deposition took place on the lower surface when u_0 was less than 50 cm/s. Increasing the wind speed resulted in a rapid fall in E , starting at the front part of the surface, that is the upwind end. For $110 < u_0 < 320 \text{ cm/s}$, E was much less than E_g at all parts of the upper surface.

Gregory and Stedman suggest that this decrease in rate of deposition is due to the bluff edge of the slide producing an up-current of air which deflects the spores away from the surface. However, the windward edge of the slide (0.13 cm thick) must act as an efficient impaction obstacle removing all spores from the approaching air which is directly in line

with it, and this is the air which then flows over the surfaces of the slide. The particles which should fall by gravity upon the upper surface of the slide would, in fact, come from the upper half of this part of the approaching air stream, which forms quite a thin surface layer as it passes over the slide.

At 110 cm/s [Ref. (1), Fig. 2, p. 656] the deposit on the trailing end of the upper surface is still nearly the same as it should be, according to the gravity formula, while the leading part of the surface is bare. Hence particles which just escaped impaction on the edge of the slide had time to fall across the layer of cleaned air before being carried beyond the slide.

Owing to skin friction the air velocity in the surface layer will be below 110 cm/s; hence only a lower limit can be calculated for the thickness of the air layer from which particles have been removed. Calling this thickness f and taking $v_s = 1.76 \text{ cm/s}^{(3)}$ we have, therefore,

$$f > 1.76 \times 2.5/110 = 0.04 \text{ cm.} \quad (5)$$

This is illustrated in Fig. 1. The thickness of the upstream zone from which impaction takes place can be obtained by

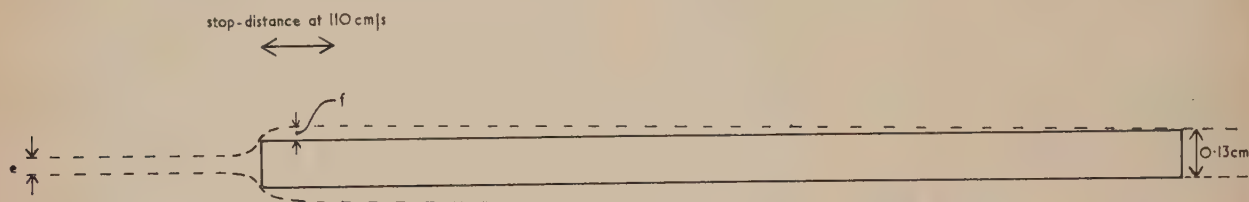


Fig. 1. The cleaned zone f from which particles have been removed by impaction on the leading edge of the slide, which they approach from zone e .

At 110 cm/s, $e \approx 0.04 \text{ cm}$, $f > 0.04 \text{ cm}$ and the speed of sedimentation (1.76 cm/s) is such that the falling particles just escape settling upon the leeward end of the upper surface

estimating the efficiency of impaction as follows. The particle parameter with reference to an obstacle of diameter $2R = 0.13 \text{ cm}$ is

$$P = v_s u_0 / gR = (1.76 \times 110) / (981 \times 0.065) = 3.03 \quad (6)$$

and the Reynolds number of the edge is

$$\text{Re} = 2u_0 R / \nu = 110 \times 0.13 / 0.15 = 95. \quad (7)$$

Referring to Davies and Peetz,⁽⁴⁾ Fig. 19, the efficiency of impaction on a cylinder for these values of P and Re is found to be about 55%. Taking 60% as appropriate to the rectangular edge of the slide gives, for the half-thickness of the approaching air stream from which all particles are impacted upon the edge of the slide, the value

$$e = 60\% \times 0.065 = 0.04 \text{ cm.} \quad (8)$$

The cleaned zone is shown to scale on Fig. 1. It does not matter whether the spores stick to the leading edge or bounce off again since, in the latter case, they will have lost all their forward motion and will therefore be unable to regain the cleaned surface air layer. The distance which a spore projected into still air, with a given velocity, travels before coming to rest is termed the stop-distance. For spores having a velocity of 110 cm/s the stop-distance is

$$d_s = PR = 3.03 \times 0.065 = 0.2 \text{ cm.} \quad (9)$$

Further increase of the wind speed to 170 and 320 cm/s results in the spores being whisked past the slide before they have time to fall through the cleaned layer f , so that gravitational deposition becomes zero over the entire surface of the slide.

The falling-off of deposition as the wind speed increases from 50 to 320 cm/s is therefore due to impaction of particles on the forward-facing, thin edge of the slide; this cleans the air of particles, leaving none in the surface layer from which particles settling upon the upper surface come. The suggestion of Gregory and Stedman that the bluff edge of the slide causes an upward current of air which deflects the particles cannot be accepted, since the stop-distance of the particles is too great for this mechanism to be effective. The present conclusion is not at variance with their observation [Fig. 5, Ref. (1)] that the deposition on horizontal razor blades agreed approximately with the gravitational figure up to the much higher wind speed of 570 cm/s.

When the wind speed increased above 170 cm/s, deposition on horizontal microscope slides recommenced on the forward part of the upper surface and spread downwind with increasing wind speed. A deposit on the lower surface, also, began to form and became equal to the upper deposit at 950 cm/s, at which speed $E = E_g$ over both surfaces. This deposition, although of the same magnitude as that due to gravity, can hardly be due to settlement. Gregory and Stedman suggest

that it results from turbulence generated by the slide itself at high wind speed.

The slide could evolve turbulence affecting the deposition of particles in two ways. First, by detachment of flow from the leading edges to give free streamlines enclosing vortices. Second, by forming a turbulent boundary layer along the surface.

At 950 cm/s the Reynolds numbers with respect to the crosswind and downwind dimensions of the slide are 825 and 16 000 respectively. The boundary layer, at the latter Reynolds number, will usually be laminar and have a thickness of about 0.13 cm. Because of the sharp leading edge the layer, as far as it exists as such, might be turbulent and thicker, but it is difficult to see how either the boundary layer, or a free streamline originating from the leading edge, could enclose a thickness exceeding 0.5 cm at the downwind end of the surface of the slide; at the leading edge, of course, the thickness is zero. These dimensions are shown to scale on Fig. 2.

On the other hand, the stop-distance for spores at 950 cm/s is

$$d_s = 1.76 \times 950 / 981 = 1.7 \text{ cm} \quad (10)$$

which is so much greater than the thickness of any conceivable region of turbulence generated by the slide that it is clear that particles entering the turbulent layer generated by the slide would hardly be affected by it, since their motion would suffice to carry them right across.

It seems clear, therefore, that the turbulent velocities which direct the spores on to the surfaces of the slide have their origin in the wind tunnel flow itself, at high speed, and are

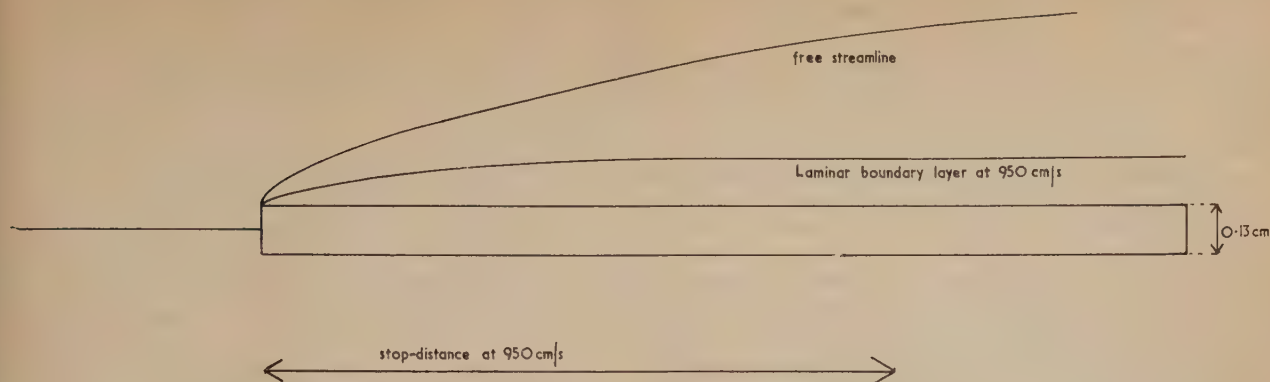


Fig. 2. A free streamline and a laminar boundary layer at 950 cm/s. These profiles represent the limits between which the zone of turbulence generated by the plate must lie

At a sufficiently high speed the profile enclosing turbulence generated by the slide would approximate to the free streamline for some distance downwind before breaking up into vortices; beyond this point a turbulent boundary layer would ultimately form

It is inconceivable that the zone of turbulence could extend outside the free streamline

not due to the presence of the slide. The deposition upon the upper and lower surfaces of the slide must therefore be regarded as an artefact of the apparatus, and would only be reproduced in the open air if turbulence of the appropriate type were existent. The rate of deposition is the same upon the upper and lower surfaces, since no gravitational deposition takes place for the reason given in the discussion about lower wind speeds. It is remarkable that the rates of deposition on the upper and lower surfaces at a wind speed of 950 cm/s should be so near to the theoretical gravitational rate; whether this is merely a coincidence or if, in fact, there is some fundamental reason for it is not yet clear to the writer.

Inclined slides

Gregory and Stedman show [Fig. 3, Ref. (1)] that deposition on slides inclined at various angles is much the same on the windward slide whether the orientation at a given angle of attack aids or opposes gravity, provided that the wind speed does not fall below 320 cm/s.

Their Fig. 2⁽¹⁾ indicates that gravitation persists at the trailing edge after impingement effects are predominant at the leading part of the surface. In these respects the behaviour of inclined slides is similar to that of horizontal ones. Impingement deposition becomes much greater than gravitational, however, when the presentation of the surface favours direct impact, independent of turbulence in the wind stream which was the essential factor for deposition at high speeds upon horizontal slides.

It seems, however, that turbulence may decrease impaction efficiency for normal incidence on narrow plates. This is suggested by Fig. 4 of Gregory and Stedman, where the efficiency for 950 cm/s is less than it is at 550 and 320 cm/s; it might have been anticipated that the efficiency would be greater at a higher wind speed, since this is certainly the case in non-turbulent air streams. A similar anomaly had previously been observed for cylinders (Davies and Peetz, pp. 294-5) and in neither case is the simple explanation that the particles were failing to adhere to the surface an acceptable one. If this is indeed an effect of turbulence in the air stream it must again be regarded as an artefact of the wind tunnel, but the reason for this behaviour is obscure.

When the results of Figs. 3 and 4 (Gregory and Stedman⁽¹⁾) for 90° presentation are plotted as E against P , the points

are low but they all fall within the band of experimental data between the two theoretical lines for cylinders illustrated by Davies and Peetz⁽⁴⁾ in their Fig. 19, with the sole exception of the point obtained at 950 cm/s with a 0.5 cm plate. For this point E is much too low as was discussed in the preceding paragraph. These curves and points are shown on Fig. 3.

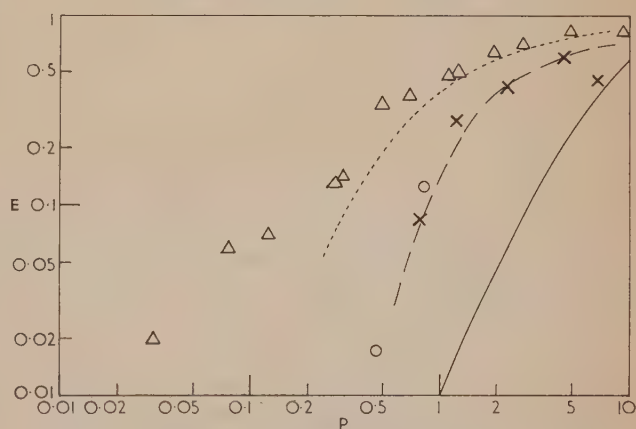


Fig. 3. Deposition on the windward side of an obstacle
Plates. Experimental. Gregory and Stedman⁽¹⁾ Fig. 3 ○
Fig. 4 ×
Theory. Brun, Demon, and Vasseur⁽⁵⁾ △
calculated for a plate with a free streamline and potential flow
Cylinders. Experimental. Amelin and Belyakov⁽⁶⁾ ———
Theory. Davies and Peetz⁽⁴⁾ ———
Ideal fluid
Re = 10

The Russian curve does not agree with the other results

When the angle of incidence is varied it is interesting to note that the maximum impaction efficiency is recorded with the plate square to the wind (90° incidence) for the maximum wind speed only. As the wind speed is reduced the maximum occurs at smaller and smaller angles, reaching 30° at 175 cm/s. The effect is less marked with the narrow plates, where the highest speed is anomalous, and at 550 cm/s the peak is at 90°, decreasing to 60° at 110 cm/s. The incidence effect is clearly due to the greater retardation of the approaching air stream when the plate is square on to the wind.

Deposition on the lee side at 90° incidence

Deposition on the lee side [Ref. (1), Table 1] was greatest at 90° incidence, except for low wind speeds at orientations giving an appreciable gravitational deposition. These results can be compared with those of Amelin and Belyakov⁽⁶⁾ and of Dawes and Slack⁽⁷⁾. The data of the latter workers were not given fully in their report and use has been made of original, unpublished material which they kindly made available.

The Russian experimenters claim that deposition on the lee side of a cylinder begins to exceed impingement on the windward side when P falls below about 0.3; their Reynolds numbers ranged from 670 to 27 000 in terms of cylinder diameter. Their results for deposition on the windward side are low, as can be seen from Fig. 3. On Fig. 4 six points due to Gregory and Stedman are shown ($0.07 < P < 1.36$, $834 < Re < 15\,800$), which are taken from their Table 1 (back of plate, 270° presentation). These points seem to be scattered around the line of the Russians for deposition on the back of a cylinder.

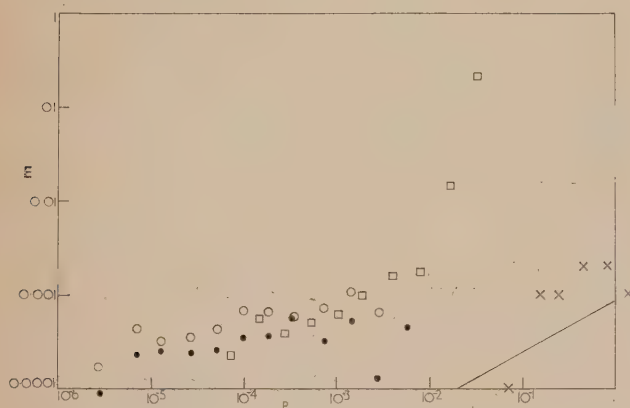


Fig. 4. Deposition on the lee side of an obstacle. (Experimental)

Amelin and Belyakov,⁽⁶⁾ Cylinders
 Gregory,⁽²⁾ *lycopodium*. Microscope slides
 Dawes and Slack,⁽⁷⁾ Coal dust. 1 in. rectangular prop in 12 in. duct
 8 in. diameter cylinder in 8 ft gallery
 High turbulence
 Low turbulence

(There was no significant difference between the deposition rates upon the windward and lee surfaces in the coal dust experiments)

On the other hand, an extensive series of points obtained with coal dust, by Dawes and Slack, extends to much lower values of P but shows a trend suggesting greater rates of lee side deposition than the Russian work. In the coal dust experiments two systems were used. A rectangular prop having a 1 in. side was set up in a 12 in. square wind tunnel and an 8 in. diameter cylinder was placed in an 8 ft mine gallery. The data obtained from the two series line up quite well when referred to the particle parameter P .

It is believed that the coal dust deposition was by the eddy impaction mechanism in extremely turbulent flows, the scale of turbulence being much greater than the stop-distance of the particles. This condition probably did not apply in the Russian work or in that of Gregory and Stedman; in these experiments the stop-distance was larger and the turbulence much less, except in the lee of the obstacle.

In two of the experiments of Dawes and Slack, in the 8 ft gallery, deposition rates were noticed to be less in places

where the walls were smooth and thus caused less turbulence. In the coal dust work there was no significant difference between the deposition rates on the front, side and rear surfaces of the obstacle.

Summing up, violent turbulence of coarse scale relative to the stop-distance of the particles caused equal deposition on all sides of the obstacle in the coal-dust experiments, the rate of deposition being related to the intensity of turbulence. Milder turbulence, of fine scale compared with the particle stop-distance, resulted in deposition on the lee side only in the experiments of the Russian workers and of Gregory and Stedman; in these, eddies induced by the obstacle played a part.

Conclusions

Deposition upon the horizontal slides was by gravity unless the wind speed was high enough to denude of particles, by impingement on the leading edge of the slide, the layer of air passing close to the surface of the slide from which settlement would otherwise have taken place.

At high speeds equal deposition upon the upper and lower surfaces was due to eddy impaction originating from turbulence in the wind tunnel.

Impingement upon the windward surface of slides facing the wind was anomalously low for the highest wind speed; possibly this can be associated with turbulence in the tunnel but no mechanism can be proposed. At smaller wind speeds the efficiencies seem to be on the low side.

In the experiments of Gregory and Stedman the stop-distance of the particles at the highest wind speed was comparable with the width of the slide. Deposition on the lee side of slides was of the same order of magnitude, in the same range of values of P , as described by Amelin and Belyakov.

The experiments of Dawes and Slack with coal dust relate to much lower values of P and of the stop-distance, and are explained by eddy impaction uniform in all directions.

The general conclusion of this analysis is that the average deposition rate of spores of *Lycopodium* over a large area can be calculated from their rate of settlement; effects due to impingement and turbulence may result in a redistribution of deposition sites but cannot affect the total rate. Such local effects will determine local deposition rates on isolated objects, but those due to turbulence depend upon the relationship of scale of turbulence to stop-distance of the particles, so that wind tunnel results may not necessarily be reproduced in the open air.

Acknowledgement

The writer is a member of the scientific staff of the Medical Research Council.

References

- (1) GREGORY, P. H., and STEDMAN, O. J. *Ann. Appl. Biol.*, **40**, pp. 651-674 (1953).
- (2) GREGORY, P. H. *Nature (London)*, **166**, p. 487 (1950).
- (3) ZELENY, J., and MCKEEHAN, L. W. *Phys. Rev.*, **30**, p. 535 (1910).
- (4) DAVIES, C. N., and PEETZ, V. *Proc. Roy. Soc., A*, **234**, pp. 269-295 (1956).
- (5) BRUN, E., DEMON, L., and VASSEUR, M. *Rech. Aéro.*, **1**, p. 55 (1948).
- (6) AMELIN, A. G., and BELYAKOV, M. I. *Dokl. Akad. Sci. USSR*, **108**, pp. 31-33 (1956).
- (7) DAWES, J. G., and SLACK, A. *Safety Mines Res. Establ. Res. Rep.*, No. 105 (1954).

Some remarks on the conduction current in insulating liquids

by K. SUGITA, Engineering Faculty, Tōhoku University, Sendai, T. SATO and Y. TORIYAMA, Musashi Institute of Technology, Tokyo, Japan

[Paper received 13 June, 1960]

Abstract

The influence of gases, absorbed in liquids and adsorbed on the surface of electrodes, upon the current conduction in insulating liquids was investigated. At field strengths up to 10^5 V/cm, the current depends upon the gases adsorbed on the electrode surfaces as well as on those absorbed in the liquid. Based upon the experimental results obtained in uniform and non-uniform fields, the hypothesis that carriers are supplied from the anode in liquids is discussed in relation to the gas-adsorbing power of the metals used as electrodes. It is believed that if the electrodes are not degassed, the conduction currents are governed not only by negative carriers from the cathode but also by positive ones formed at the anode.

Introduction

A NUMBER of investigations have been carried out to explain the processes of electrical conduction and breakdown in liquid dielectrics. Recently, measurements of high-field conduction in hexane, using a conditioning process, were presented by House,⁽¹⁾ and also careful observations of impulse breakdown of insulating liquids were reported by Hancox.⁽²⁾ The main processes of conduction suggested by these were electron emission from the cathode and electron multiplication by collision ionization, analogous to those processes in gases.

Although attention was paid to the adsorbed gases on the cathode, which have great influence on conductivity and breakdown, some basic processes involved seem to be not yet fully understood. This paper is intended to elucidate the effects of absorbed gases in liquids, and of adsorbed gas layers on the electrodes of either polarity, upon the conduction current in insulating oils. The experiments were performed with careful pretreatment of both liquid and electrodes, using uniform and non-uniform fields.

Apparatus and experimental procedure

Two commercial transformer oils (A and B), differing in their electrical conductivities, were used as the liquid. The oil was filtered through a sintered-glass filter at reduced pressure as often as required, and was admitted for tests into the closed distillation system combined with a test cell shown in Fig. 1. The distillation system was of all-glass construction, and the oil admitted could be circulated through the system in vacuum, without contamination, through a magnetically controlled stop cock.

Experiments in a uniform field were made using 25 mm diameter parallel plate electrodes of brass or 18 mm diameter ones of nickel, aluminium or copper. These were formed to a Rogowski profile and were polished mechanically to a mirror finish. Experiments in a non-uniform field were

made with a molybdenum needle (dia., 2 mm; angle of tip, 12°) and a brass plate of 25 mm diameter.

Degassing of electrodes was carried out by heating in vacuum for several hours, using a tungsten coil, or with a glow discharge in a hydrogen atmosphere, using the arrangement shown in Fig. 1.

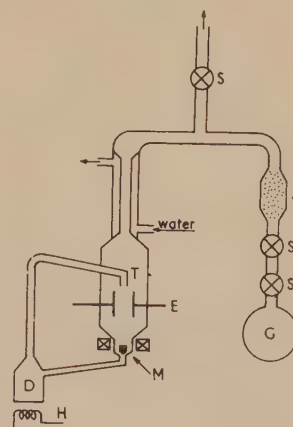


Fig. 1. Schematic diagram of distillation system with test cell A, drying agent; D, oil reservoir flask; E, electrode; G, gas reservoir flask; H, heater; M, magnetically controlled stop cock; T, test cell; S, stop cock

Presentation and discussion of experimental results

Uniform field conduction. The conductivity was measured as a function of electrode separation and field strength in oil A purified by the circulatory distillation system. The electrodes were degassed in vacuum before the oil was admitted for testing. The results are shown in Fig. 2. Fig. 3 shows three curves obtained with electrodes which had not been degassed, in the same oil A which was filtered but not distilled. Curve A in Fig. 3 was obtained in oil immediately after filtering; B corresponds to the results obtained after the filtered oil had been left open to the atmosphere for ten hours and C shows the results after the filtered oil had been pumped for 24 hours. As no significant increase of conductivity was found by exposing the oil to atmosphere for 24 hours, compared with ten hours' exposure, the latter seems to be enough to saturate the gas absorption in the oil.

It will be noted that, especially in the low-field-strength region, the currents are considerably smaller in the distilled oil with degassed electrodes (Fig. 2) than those observed in the oil filtered only, with electrodes which were not degassed (Fig. 3). Also, in Fig. 2, no increase in current dependent on the gap, which would indicate bulk ionization within the liquid, can be observed up to a stress of 2×10^5 V/cm; rather, the currents decrease with increasing electrode separa-

tion. The Schottky slopes of the curves in Fig. 2 are several times greater than those in Fig. 3, that is, the values of the slopes vary from about 2×10^{-2} to 5×10^{-3} in units of $\log_{10} I$ and $(V/cm)^{1/2}$.

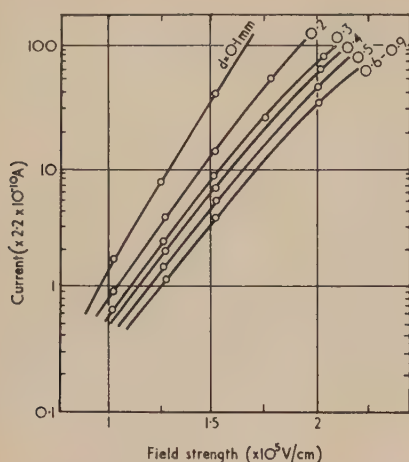


Fig. 2. Current-stress curves for distilled oil A with degassed electrodes (brass, dia. 25 mm)

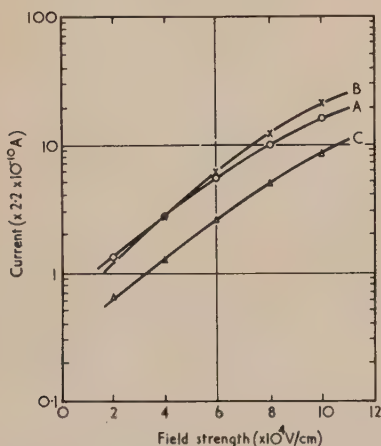


Fig. 3. Effect of gases absorbed in filtered oil A with electrodes not degassed (brass, dia. 25 mm, gap length 2 mm)

- A: Immediately after filtering
- B: After 10 hours' exposure to air
- C: After 24 hours' pumping at reduced pressure

These results suggest that in oil which is filtered only and not distilled, there exist impurities which are easily dissociated at low field strengths; and also that the reduction of the conductivity as between Fig. 3 and Fig. 2 is due not only to the purification of the oil but also to the degassing of the electrodes. The difference between the three curves in Fig. 3 could be explained as follows: the gases absorbed in the oil are responsible for the increment of curve *B* over *A*, whilst removing the gases, absorbed in the oil and adsorbed on the electrodes contributes to the decrement of curve *C* below *A*.

This explanation may be verified by the conductivity curves shown in Fig. 4, which were obtained by exchanging the gas-saturated oil for freshly filtered oil, leaving the electrode surfaces always immersed in oil. Curve *A* in the figure represents the characteristic obtained in filtered oil and with degassed electrodes, curves *B* and *C* were obtained

in oil after exposure to atmospheric pressure for four and eight hours respectively, and curve *D* was obtained after exchange for fresh oil. It would appear that gases are not adsorbed on the electrode surfaces through the liquid when the latter is exposed to the atmosphere.

Further, in order to analyse the effect of gases adsorbed on the electrode surfaces, conductivity tests were made with degassed and un-degassed electrodes of nickel and aluminium in carefully filtered oil B. The full-line curves in Fig. 5

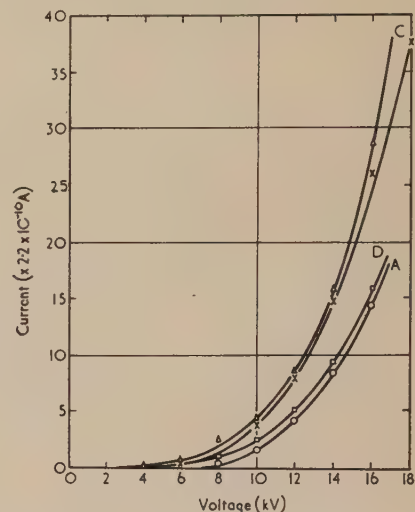


Fig. 4. Effect of gases absorbed in filtered oil B with degassed electrodes (gap length 1 mm)

- A: Original filtered oil
- B: After 4 hours' exposure to air
- C: After 8 hours' exposure to air
- D: After exchange of gas-saturated oil for fresh filtered oil

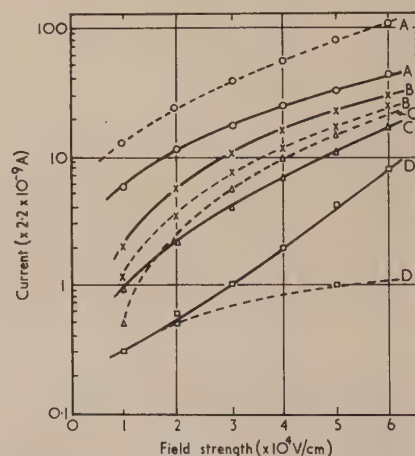


Fig. 5. Effect of degassing the electrodes in filtered oil B (gap length 4 mm), full line for nickel and broken line for aluminium

- A: Electrodes not degassed
- B: Degassed anode
- C: Degassed cathode
- D: Both electrodes degassed

show results obtained for a nickel electrode-pair and the broken lines are for aluminium. Curve *A* in each was obtained for electrodes not degassed and curves *B*, *C* and *D* correspond to degassing of anode, cathode and both electrodes respectively. It is clear that at field strengths up to 10^5 V/cm,

degassing of the anode plays an important role in reducing the conductivity, though less than that of the cathode. From these results, it may be suggested that in the case investigated the current is dependent not only on carriers from field-dependent dissociation and those supplied from the cathode, but also on those supplied from the anode, which may originate in the gas film on the surface of the electrode.

Furthermore, the appreciable difference between the results for nickel and aluminium electrodes in Fig. 5 may be attributed to the difference between the gas-adsorbing power of the materials. In this respect, it is interesting to observe the conduction current using electrodes of different materials. Results of this kind, obtained by using oil B, filtered only, and electrodes which were not degassed, are shown in Figs. 5, 7 and 8. Fig. 6 shows the results for pairs of electrodes

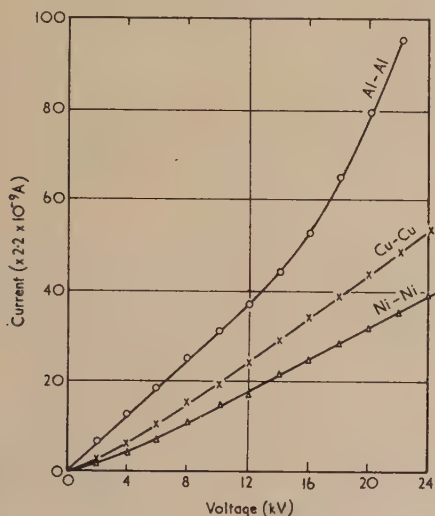


Fig. 6. The dependence on electrode materials in filtered oil B with electrodes not degassed (dia. 18 mm, gap length 4 mm)

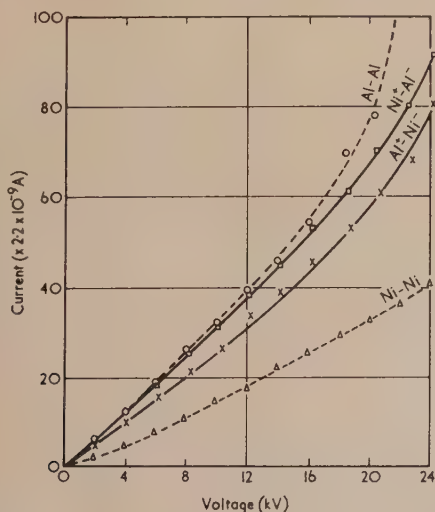


Fig. 7. Polarity-reversal test for dissimilar electrodes (not degassed) in filtered oil B (gap length 4 mm)

in comparison. It should be remarked that since the currents observed with unlike electrodes lie always between, and not coincident with, the values observed for like pairs, our suggestion that carriers are supplied from the anode is confirmed by all these results.

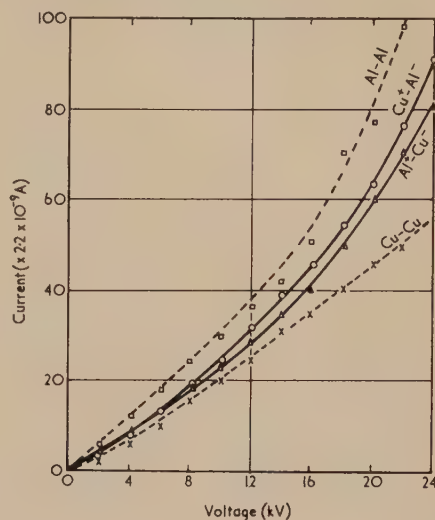


Fig. 8. Polarity-reversal test for dissimilar electrodes (not degassed) in filtered oil B (gap length 4 mm)

Non-uniform field conduction. We considered it desirable to repeat the foregoing measurements with non-uniform fields, using the needle-plane electrode system described under "Apparatus". The current-voltage characteristics shown in Fig. 9 were obtained with electrode separation as

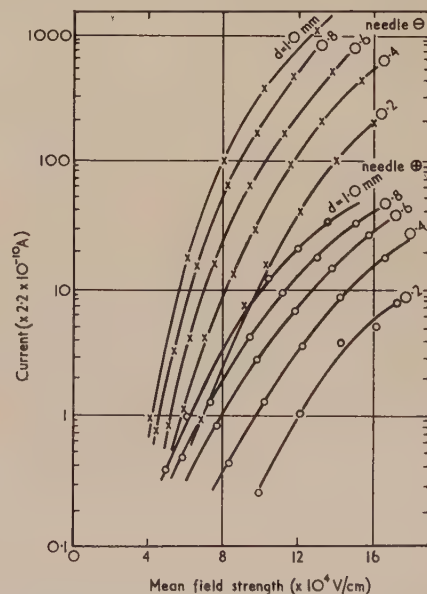


Fig. 9. Current-stress curves for distilled oil A with degassed electrodes (needle: molybdenum, dia. 2 mm, angle of tip 12°; plate: brass, dia. 25 mm)

of the same material, while Figs. 7 and 8 show results for combinations of nickel-aluminium and aluminium-copper respectively. The broken-line curves in these figures indicate the characteristics for pairs of the same material, for com-

parameter in distilled oil A, with degassed electrodes. Fig. 10 (except curve C) was obtained in the same oil, but not distilled, and with electrodes which were not degassed. Curves A in Fig. 10 (+ or - shows the polarity of the needle electrode)

correspond to the data for filtered oil; curves *B* to those obtained after exposure to air for 48 hours, and curves *C* to those obtained for distilled oil. The results show that (1) the current with a negative needle is greater than with a positive needle, excepting case *B* where the oil contains air; (2) the currents increase with increasing electrode separation for a constant mean field strength; (3) the current is less

upon the state of the anode as well as of the cathode, owing to the gases adsorbed thereon.

Conclusions

Previously, it was shown by the authors⁽⁴⁾ that at field strengths of about 10^4 V/cm, electrons introduced into transformer oil form negative ions immediately. The experimental evidence in this paper leads us to the following conclusions:

- (1) the conduction current, at field strengths up to 10^5 V/cm, depends strongly upon gas adsorbed on the surface of the electrodes as well as on that absorbed in the liquid;
- (2) when electrodes are not degassed, negative ionic carriers supplied from the cathode and positive carriers from the anode are both responsible for current;
- (3) the gas-adsorbing power of the metal used as electrode has a considerable influence on the conductivity; and
- (4) the conduction current in non-uniform fields depends not only upon the polarity of the electrode of higher field strength but also upon the gas adsorbed on its surface.

Since gas-adsorption on metal surfaces immersed in a liquid has never been adequately investigated, it is difficult to verify our assumption quantitatively. The results obtained, however, suggest that it is essential to undertake careful pre-treatment of the electrodes as well as of the liquid in any observations of pre-breakdown phenomena.

At higher field strengths near breakdown, it is reasonable to consider the process of collision ionization caused by electrons emitted from the cathode, and this process has been discussed by many workers. It is therefore necessary to extend our experiments to such higher field strengths and this work is now in progress.

Acknowledgement

The authors wish to thank Dr. S. Nagao for his encouragement and guidance.

References

- (1) HOUSE, H. *Proc. Phys. Soc. B*, **70**, p. 913 (1957).
- (2) HANCOX, R., and TROPPER, H. *Proc. Inst. Elect. Engrs. A*, **105**, p. 250 (1958).
- (3) EDLER, H. *Arch. f. Electrot.*, **25**, p. 447 (1931).
- (4) SATO, T., NAGAO, S., and TORIYAMA, Y. *Brit. J. Appl. Phys.*, **7**, p. 297 (1956).

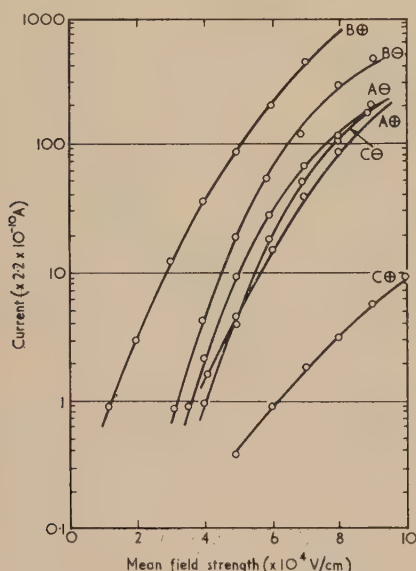


Fig. 10. Effect of gases absorbed in oil A and adsorbed on electrodes (needle-plate system similar in Fig. 9, gap length 1 mm)

A: Oil: immediately after filtering, electrodes not degassed
B: Oil: after 48 hours' exposure to air, electrodes not degassed
C: Oil: immediately after distillation, electrodes degassed

reduced by distilling the oil, especially for a negative needle, than was the case for a uniform field; and (4) the effect of absorbed gas is much more severe for a positive needle than for a negative one (this agrees with earlier findings by Edler and others⁽³⁾). In addition, if the distilled oil contained gas, we observed increased currents, but could observe no notable dependence of the conductivity on the polarity of the needle.

Although the characteristics were somewhat altered from those for a uniform field, probably due to the higher field strength which exists near the needle point, our suggestion that current carriers are supplied from the anode is still consistent with all the results. At lower field strength, the current with electrodes which were not degassed depended

Comparison of X-ray and nuclear magnetic resonance measurements of crystallinity in polyethylene terephthalate

by G. FARROW, B.Sc., Ph.D., and I. M. WARD, M.A., D.Phil., Imperial Chemical Industries Ltd.,
Fibres Division, Harrogate, Yorkshire

Paper received 7 July, 1960]

Abstract

X-ray and nuclear magnetic resonance (n.m.r.) measurements of crystallinity have been made over a wide temperature range on oriented and unoriented samples of polyethylene terephthalate. The results show that, although in general terms, no correlation exists between the two methods, above the glass transition a considerable proportion of the non-crystalline regions achieve molecular mobility. The n.m.r. method gives higher values of crystallinity than the X-ray method. This is apparently due to some of the non-crystalline material being immobilized owing to entanglements, and the presence of surrounding crystallites for this material will make a contribution to the broad component of the n.m.r. signal which is used as a measure of the crystalline fraction of the polymer.

Introduction

A COMPARISON of crystallinity measurements on polyethylene terephthalate (PET) samples of widely different degrees of crystallinity and orientation by X-ray, infra-red and density methods has already been described.⁽¹⁾ It also seemed of value to continue the work by a comparison of results obtained by X-ray diffraction and nuclear magnetic resonance (n.m.r.) measurements. This has been done in the case of polyethylene⁽²⁾ and reasonable agreement was found between the two methods for measurements made at room temperatures.

The n.m.r. absorption signal of PET at room temperature, unlike that of polythene, is not a composite one. Above the glass/rubber transition temperature (i.e. at 110° C), however, a composite signal does appear, as has been reported previously,⁽³⁾ and it is then possible to decompose the absorption into two signals of different line width.

It was concluded from the previous measurements that the narrow component of the composite signal arises from both methylene and benzene ring protons, in the amorphous regions which are undergoing considerable reorientation, and the broad component primarily from rigid benzene ring protons, presumably including those in the crystalline regions, together with the methylene group protons undergoing hindered rotations. The relative total intensities of the two components can thus be taken as the n.m.r. measure of crystallinity.

In this report, detailed X-ray and n.m.r. measurements on the same samples of PET, together with a sample of poly(tetradecuteroethylene terephthalate), have made it possible to investigate how closely the ratio of the intensities of these two components corresponds with the X-ray measure of crystallinity. In fact, in this work it is assumed that the

X-ray measure of crystallinity can be considered to be the true measure of crystallinity. This comparison then provides information concerning the nature of the non-crystalline material present in samples of varying crystallinity and orientation.

Experimental

Preparation of samples. In this comparison four polymer samples were chosen:

- (i) normal polymer chip, heat crystallized at 200° C for 1 h to give an unoriented crystalline sample;
- (ii) polymer chip; cooled slowly from 300° C to give an unoriented crystalline sample of very high crystallinity;
- (iii) polymer film, drawn by a factor of 5.75 and heat crystallized at 200° C;
- (iv) a sample of poly(tetradecuteroethylene terephthalate) heat crystallized at 200° C to give an unoriented sample of high crystallinity.

X-ray determination of crystallinity. The X-ray diffraction method has been described in detail elsewhere,⁽⁴⁾ but in order to make a valid comparison with the crystallinity values obtained by n.m.r. measurements, which, by necessity, had to be made at elevated temperatures, it was necessary to make X-ray measurements at high temperatures, for it is known that crystallinity varies with temperature. Various modifications had, therefore, to be made to apparatus to carry out these measurements. The focusing X-ray camera⁽⁴⁾ normally used for the determination of crystallinity by X-rays could not be used, as it was found impossible to place the sample on the circumference of the camera (necessary for focusing) and heat it at the same time. The specimen was held in a small furnace⁽⁵⁾ and combined with a flat plate camera which was used to record the X-ray diffraction pattern at high temperature. The apparatus is shown schematically in Fig. 1.

The distance between camera and furnace could be varied over a distance of 3 to 12 cm. The camera-to-specimen distance chosen was 5 cm. This gave a good resolution of the X-ray diffraction pattern with an exposure time of approximately two hours using CuK_α radiation. The temperature of the specimen was measured by placing a copper/constantan thermocouple immediately above it.⁽⁵⁾ The thermocouple wires entered the apparatus through the baseplate, being sealed into a rubber bung, which was then held firmly in a suitable diameter hole drilled into the baseplate. This was necessary since the whole apparatus had to be evacuated to eliminate the "air scatter" that would otherwise appear on the film, due to the primary X-ray beam striking molecules of air on its passage to the camera.

Furthermore, in order to make the measurements conform to the accuracy attained with the previous method⁽⁴⁾ of measuring crystallinity by X-ray diffraction, it was essential to use strictly monochromatic X-ray radiation. A parallel beam of X-rays was required, but rather than use a plane ground crystal monochromator, it was found more satisfactory to collimate the beam from a curved quartz crystal (G) by two slit systems (H and C, Fig. 1). Using this set-up

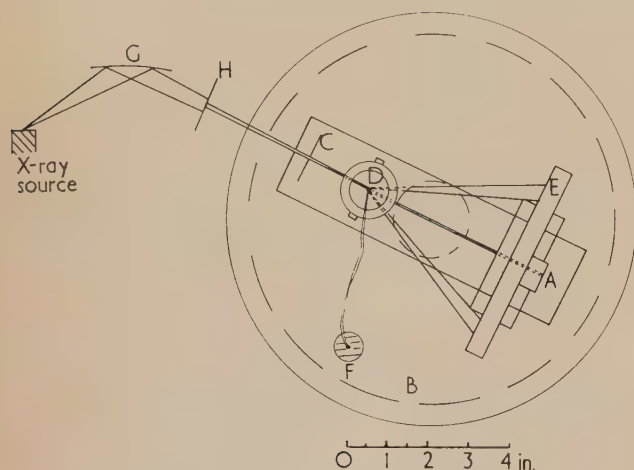


Fig. 1. Apparatus for the measurement of crystallinity of specimens of PET by X-ray diffraction at high temperatures. A, graduated track for furnace and camera; B, baseplate; C, slits for reducing X-ray beam in horizontal and vertical planes; D, furnace for heating specimens; E, X-ray camera; F, hole for entry of thermocouple wires; G, focusing quartz crystal; H, slit for reducing X-ray beam in horizontal plane. Broken line, position of bell jar for evacuation of apparatus.

a beam of greater intensity, showing less divergence than that from a plane ground lithium fluoride crystal, was obtained. The assembly was evacuated by covering it with a bell jar and pumping away the air through an exit port at the top of the bell jar. An effective seal between the bottom of the bell jar and the baseplate was obtained from a greased "O" ring let into the surface of the plate. The primary X-ray beam was admitted to the specimen through a beryllium window, set at the appropriate level in the bell jar, and then through a small hole in the side of the furnace. Temperature control of the furnace was by means of a Variac transformer. The e.m.f. developed in the thermocouple by the change in temperature was measured from a Pye Scalamp spot galvanometer which had been suitably calibrated. Once the furnace had reached a particular operating temperature it remained quite stable, owing to the fact that it was operating in a vacuum. At temperatures above 150° C, it was found necessary to protect the emulsion of the photographic film from radiant heat from the furnace by covering it with black paper coated with a thin layer of aluminium.

The X-ray film, after processing and drying, was scanned by a microdensitometer. From the resultant trace the crystallinity was determined by measuring the integrated area of the crystalline reflexions and the integrated area of the non-crystalline background, and comparing the two.⁽⁴⁾

N.M.R. determination of crystallinity. The proton resonance signals were observed using a Pound-Watkins oscillating detector at a frequency of 25 Mc/s, a narrow band amplifier and a phase-sensitive detector, applying a small 90 c/s field modulation and slowly sweeping through the resonance line, thus obtaining the derivative of the absorption signal.

Results were obtained over the required temperature range by passing a flow of pre-heated nitrogen gas over the sample and the n.m.r. coil, which were contained in a copper shielding can. This was held at the end of a German silver tube, which acted as the outer conductor of a coaxial line carrying the radio-frequency signal. The whole of the n.m.r. probe was surrounded by a Theros vacuum tube. The arrangement is shown in Fig. 2.

To obtain accurate n.m.r. signals it is necessary to ensure that the amplitude of the radio-frequency field is sufficient to saturate the resonance signal (or in the case of a composite signal, on the proton resonance signals). Quantitative measurements were

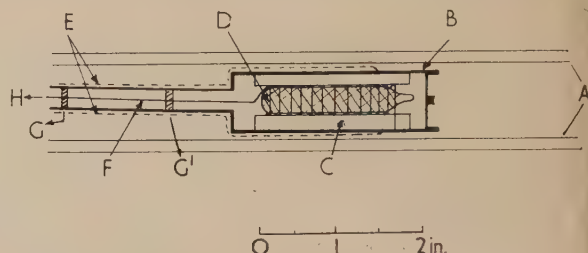


Fig. 2. Diagram of n.m.r. probe and Theros tube. A, silvered Theros flask tube; B, copper shielding can; C, pyrophilite former; D, sample; E, copper/constantan thermocouple; F, German silver tubes; G, G', PTFE spacers; H, oscillator circuit.

then made at low r.f. levels (of the order of 80 mV) when no saturation occurred. This meant a considerable reduction in signal/noise ratio compared with higher r.f. levels. In each case six measurements were made at a given temperature and the results averaged.

For the n.m.r. measurements the samples were sealed under

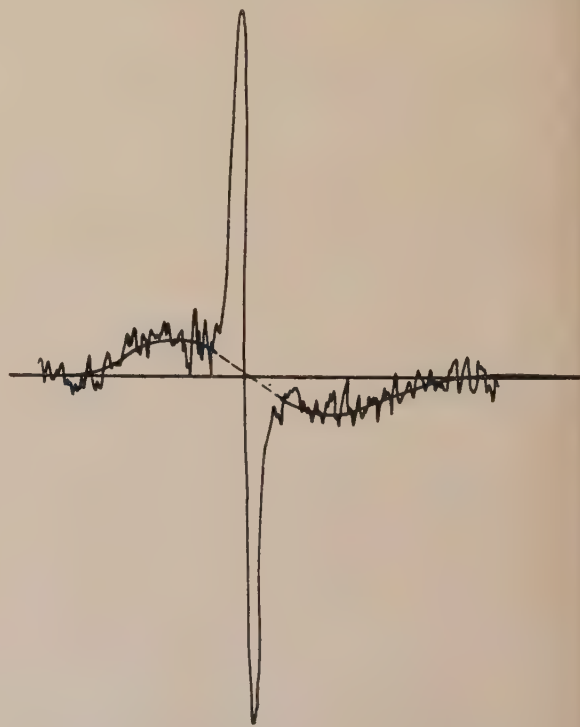


Fig. 3. Typical n.m.r. signal above glass transition showing composite nature of derivative signal from PET polymer.

vacuum into thin-walled Pyrex glass sample tubes after holding under vacuum for twenty-four hours to remove absorbed moisture. In the case of the highly oriented film two n.m.r. samples were prepared: (a) a roll of film, rolled to give an approximately randomized sample, i.e. from a long strip of film with the direction of drawing parallel to the length of the strip; (b) a pile of rectangular strips of film, each rectangle being cut so that its short edge was parallel to the direction of drawing. This sample could then be arranged so that the drawing direction was either parallel or perpendicular to the steady magnetic field H_0 .

Above the glass transition a composite derivative signal was observed. A typical n.m.r. signal is shown in Fig. 3. In each case the signal was decomposed into two signals by drawing in the broad absorption. This is clearly a somewhat arbitrary method of composition as it assumed that the narrow absorption does not possess very long "tails". However, although these tails would affect the second moments of the narrow component very considerably, they are not so important in estimating total intensity of the narrow component. The intensities of the narrow and broad component were found by calculation, the calculation giving the integral of this derivative curve.

In addition to these relative intensity measurements, the second moments of the broad component were determined for the oriented film for the two curves where the direction of orientation was respectively parallel and perpendicular to the steady magnetic field H_0 .

Results

The n.m.r. results are shown in Fig. 4 where the ratio of the intensities of the narrow to the broad components of the

n.m.r. absorptions signal are plotted against temperature. Fig. 5 shows a plot of crystallinity as measured by the X-ray method against temperature for the two samples of polymer chip, and the following tables summarize the findings from both types of measurement.

The n.m.r. values of crystallinity are only accurate to about $\pm 5\%$.

Table 1. Comparison of n.m.r. and X-ray results of crystallinity

Sample	N.M.R. (180° C) crystallinity (%)	X-ray (25° C) crystallinity (%)	X-ray (180° C) crystallinity (%)
Normal unoriented chip	72	52	46
Unoriented chip (cooled slowly)	72	62	44
Oriented film	80	53	—
Draw ratio 6 : 1			
Poly(tetradeutero-ethylene terephthalate)	74	60	—

Table 2. Comparison of second moments of broad component for H_0 parallel and perpendicular to drawing direction at an average temperature of 150° C

H_0 parallel	6.35 gauss ²
H_0 perpendicular	4.0 gauss ²

Discussion

X-ray measurements. It can be seen from Fig. 5 that one sample of heat-crystallized chip shows little decrease in crystallinity up to 200° C, whereas, in the other, the fall-off

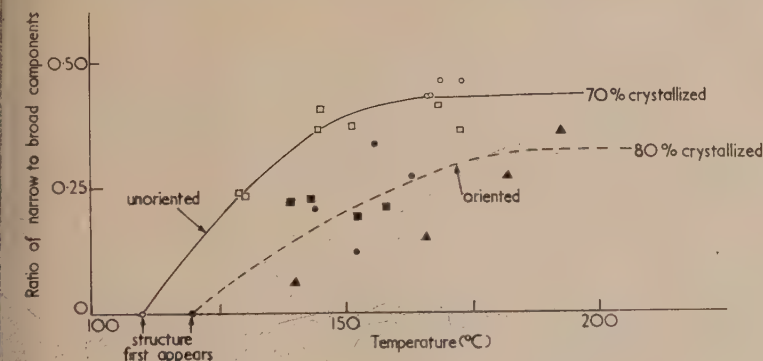
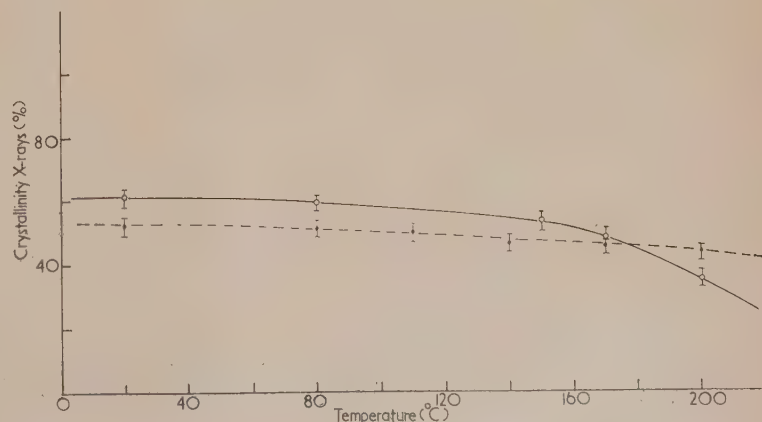


Fig. 4. Comparison of ratio of narrow to broad component for oriented PET film of high orientation and two samples of unoriented PET polymer

- = normal unoriented chip, heat crystallized up to 200° C
- = unoriented chip (cooled slowly)
- = oriented film, H_0 parallel to drawing direction
- = oriented film, H_0 perpendicular to drawing direction
- ▲ = oriented film rolled to give an approximate randomly arranged sample

Fig. 5. Crystallinity of two samples of PET polymer at different temperatures by X-ray diffraction

- = normal unoriented chip heat crystallized up to 200° C
- = unoriented chip (cooled slowly)



in crystallinity occurs at a lower temperature. In both cases, however, there is a comparatively small change in crystallinity over the temperature range considered.

It was noted with each sample that as the crystallinity fell there was a corresponding increase in the sharpness of the intensities on the X-ray diffraction photographs. This was probably due to the melting of the smaller crystallites and the edges of the larger ones, for on cooling the samples the intensities again broadened to their original shape, indicating that the smaller crystallites and dislocations had reappeared. The measurement of crystallinity on the samples of oriented film and poly(tetradeuteroethylene terephthalate) were made at room temperature, for it was concluded that over the temperature range considered, it was reasonable to assume that the crystallinity would not markedly change until at least 170°C.

With the sample of poly(tetradeuteroethylene terephthalate) there were some small changes in the ratio of the intensities of the crystalline reflexions on the X-ray diffraction pattern compared with PET, but no noticeable change in plane spacings. It was, therefore, concluded that some slight movements of atoms had occurred but not on a sufficient scale to alter the crystal structure from that found in PET.

N.M.R. measurements. As the temperature was raised above 110°C the ratio of the intensities of the narrow to the broad component of the composite n.m.r. signal increased until it achieved a constant value as seen in Fig. 4. Both samples of chip rose to approximately the same crystallinity (70%) determined by n.m.r., but the oriented film reached a higher value (80%).

The sample of poly(tetradeuteroethylene terephthalate) shows a very similar value to that of the undeuterated unoriented polymer of very nearly identical crystallinity. This suggests that at 170°C a similar proportion of the benzene rings are undergoing considerable reorientation to the proportion of chain molecules as a whole. This confirms the view that the narrow component arises from both methylene and benzene ring protons, and the broad component from rigid benzene ring protons, together with methylene groups undergoing hindered rotations.

Further confirmation of this last point, i.e. that the broad component arises partly from methylene groups undergoing hindered rotations, comes from the measurements on oriented film.

Here measurements were made with the static field H_0 parallel to the direction of orientation and with H_0 perpendicular to this direction (by rotation of the pile of film through 90 deg). It can be seen that the same ratio of narrow to broad component is found in each case. However, as would be expected on theoretical grounds,⁽⁶⁾ if the broad component consists partly of molecules undergoing hindered rotations about the axis of the molecular chains (i.e. the direction of orientation), the broad component has a larger second moment with H_0 parallel to this axis than when it is perpendicular (see Table 2).

Comparisons of X-ray and n.m.r. measurements. Examination of Table 1 shows that the n.m.r. values of crystallinity are always higher than those given by the X-ray method. This suggests that it is not correct to ascribe the broad n.m.r. signal only to crystalline material (which from the X-ray measurements at high temperatures⁽⁷⁾ is known to be substantially rigid) but that some portion of the non-crystalline material is also not mobile. The rigidity of this part of the non-crystalline material is probably due to chain entanglements. The presence of chain entanglements in the non-crystalline regions was also suggested by previous n.m.r.

measurements.⁽⁸⁾ The very large values obtained for the second moments at low temperature suggested that there were some very small inter-proton distances in the amorphous regions of the polymer.

It can also be seen from Table 1 that the oriented sample has a higher n.m.r. crystallinity value than the unoriented samples. There are two possible explanations of this. First, comparison of X-ray and density measurements on oriented samples of PET⁽¹⁾ has shown that the density of non-crystalline regions rises in such samples from the value of unoriented material, suggesting that further chain entanglement can occur.

Secondly, the mobility of the non-crystalline regions is probably further restricted simply by the spatial distribution of the crystallites. The effect of the smaller crystallites melting at high temperatures, as indicated by the X-ray measurements, is apparently too small to show up in the n.m.r. measurements.

It therefore appears that there is no correlation between the n.m.r. and X-ray measure of crystallinity in PET. This is similar to the conclusion reached by Fuschillo, Rhian and Sauer⁽⁹⁾ in the case of polyethylene. They concluded that the good agreement obtained by Collins⁽²⁾ for the crystallinity of polyethylene measured by n.m.r. and X-rays at room temperature is merely fortuitous. For, as they remark, the ratio of the narrow to broad components of the n.m.r. absorption signal in polyethylene will only be a measure of the crystalline content provided that all the protons in the non-crystalline regions are able to reorient at the critical frequency, whereas those in the crystalline regions can not. In general, this situation will not prevail and the n.m.r. measure of crystallinity will be temperature dependent. In PET, of course, an extreme situation occurs and a composite n.m.r. signal does not appear until 110°C.

Acknowledgements

The authors wish to thank Mr. D. Preston for taking the X-ray photographs and Dr. K. W. Hillier for helpful criticisms of the manuscript.

References

- (1) FARROW, G., and WARD, I. M. *Polymer*, **1**, p. 330 (1960).
- (2) COLLINS, R. L. *Bul. Amer. Phys. Soc.*, **1**, p. 216 (1956).
- (3) WARD, I. M. *Trans Faraday Soc.*, **56**, p. 548 (1960).
- (4) FARROW, G., and PRESTON, D. *Brit. J. Appl. Phys.*, **11**, p. 353 (1960).
- (5) FARROW, G., and PRESTON, D. *J. Sci. Instrum.*, **37**, p. 347 (1960).
- (6) ANDREW, E. R. *Nuclear Magnetic Resonance*, p. 18 (Cambridge: The University Press, 1955).
- (7) BATEMAN, J., RICHARDS, R. E., FARROW, G., and WARD, I. M. *Polymer*, **1**, p. 63 (1960).
- (8) LAND, R., RICHARDS, R. E., and WARD, I. M. *Trans Faraday Soc.*, **55**, p. 225 (1959).
- (9) FUSCHILLO, N., RHIAN, E., and SAUER, J. A. *J. Polymer Sci.*, **25**, p. 381 (1957).

Image formation by electron bombardment of metal targets

by E. H. HIRSCH, B.Sc., Weapons Research Establishment, Salisbury, South Australia

[Paper received 29 August, 1960]

Abstract

In a demountable vacuum system a latent image is formed of a region on a metal target which has been subjected to very weak electron bombardment. This image can be made visible by electroplating the target in a copper sulphate solution. An experimental investigation of the influence of bombarding current, electron energy and target temperature is presented. The results suggest that the effect is due to the formation of a monolayer of hydrocarbon contamination, the build-up of which is catalytically accelerated by the metal target. The effect takes place even with 5 V electrons and can be used to obtain permanent visual records of slow electron beam focal spots.

Introduction

IN the development of electron devices it is frequently desirable to have a visual record of the size and shape of an area which is being bombarded by an electron beam. In many cases such a record can be obtained by allowing the beam to impinge on a fluorescent screen, a method which is very satisfactory, but which requires an electron energy of at least several hundred volts to yield sufficient light output for direct observation or photography.

In principle, records at lower particle energy can be made by means of photographic emulsions, which are reasonably sensitive to electrons down to about 20 eV. The introduction of photographic material into the vacuum system is, however, attended by constructional complexity, and in some cases the accompanying deterioration of the vacuum conditions is undesirable. Furthermore, if the electron source is an incandescent cathode, light from the latter may produce undue fogging of the film.

In a search for a more suitable method of recording slow electrons, attention was given to the observation by Carr⁽¹⁾ that electron bombardment of a gold target results in a "latent image", which can be "developed" by exposing the target to hot mercury vapour. The bombarded area then remains unchanged, whilst the surrounding material is discoloured by amalgamation, and a permanent visual record of the focal spot results.

Experiments along the lines of Carr confirmed his findings generally, but the developing process was found difficult to control and lacked reproducibility. At this stage it was discovered that developing could be carried out very reliably by electroplating the target in an aqueous solution of copper sulphate. On sufficiently strongly bombarded areas no copper was deposited at all, whilst weaker bombardment resulted in a partial inhibition of deposition.

Details of the plating procedure such as current density, concentration and temperature of the solution were in no way critical. Also, the method is not restricted to gold targets, but was found equally effective with all target

materials used, namely nickel, platinum, silver, stainless steel, and brass.

The latent image apparently persists indefinitely, i.e. the development can be carried out at any time after bombardment, and furthermore the image is insensitive to rubbing with a cloth or to the action of strong acids or alkali.

Experimental arrangement

A more quantitative study of the dependence of image formation on factors such as electron energy, bombarding current, bombarding time, target temperature, etc., was carried out in the experimental tube shown schematically in Fig. 1.

The target, usually a nickel disk of 1 in. diameter, was mounted as shown so that it could be rotated from outside the vacuum by means of a greased metal joint. An electron gun, using a tungsten spiral as cathode, was arranged such as to bombard a rectangular strip of 1 mm width and 5 mm

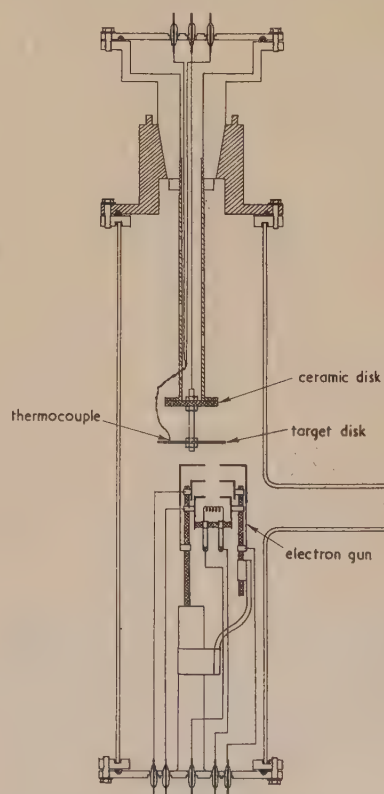


Fig. 1. Experimental tube for investigating the influence of bombarding current, electron energy and target temperature on image formation

length, slightly off the centre of the target and oriented with the longer strip dimension along a radius of the target disk. By rotating the joint, different portions of the target could in turn be bombarded, and altogether the latent images of eighteen rectangular "lines" could be produced before the vacuum had to be broken to allow developing.

For certain experiments thin thermocouple wires were spot welded to the back of the target to measure its temperature.

The system was evacuated by a type 203 oil diffusion pump (by Metropolitan-Vickers) equipped with a baffle valve, and three liquid air traps were placed in series between the pump and the experimental tube, the pressure in which was measured by an ionization gauge.

Prior to mounting in the system each target was cleaned in several rinses of acetone, and after the pressure in the system had been reduced to 5×10^{-6} mm of mercury, it was outgassed for 10 min at 900°C by induction heating, such as to ensure that, in each experimental run, the targets had as nearly as possible the same surface condition.

A target that had not been subjected to heating could at once be used to make electron records, but it was found that bombardments shortly after outgassing resulted in no record at all, or at least very weak images; in fact, only after about 45 min did the lines produced have their normal intensity. Therefore, as a standard procedure, a waiting period of one hour was allowed to elapse after outgassing before the first bombardment was made. During this time, unless otherwise stated, the pressure in the system was approximately 5×10^{-6} mm of mercury.

For a quantitative comparison of the lines produced under various conditions of bombardment, use was made of the difference in optical reflectivity of target surfaces covered in various degrees with a copper deposit.

Thus a fully "saturated" line showed the high reflectivity of a bright nickel surface, whilst a line due to less intense bombardment exhibited a reflectivity intermediate between that of clean nickel and the dull background of regions not bombarded at all, and consequently fully covered with a copper deposit.

To carry out measurement of relative reflectivity, the target disk was placed on a spectrometer table (see Fig. 2)

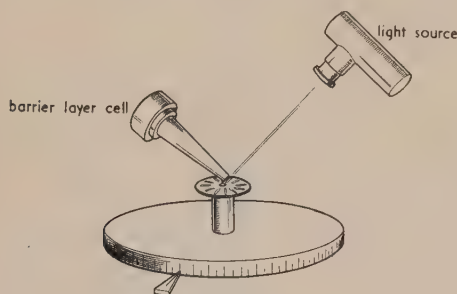


Fig. 2. Photometer arrangement

and a rectangular beam of light of approximately the same dimensions as the lines was arranged, such that as the spectrometer table was rotated the light scanned each line in turn. A barrier layer cell served to measure the relative intensity of the reflected light.

Experimental results

Typical results obtained with the photometer arrangement described above are shown in Fig. 3, where the photocurrent

is plotted against angular position of the spectrometer table. The target disk in this example represents bombardments at constant electron energy and bombarding current, the variable being the bombarding time. As Fig. 4 shows, the height h of the photocurrent peaks above the background reading increases with t , until eventually at a time T it reaches a substantially constant value, which corresponds to a target surface totally free from copper deposit. The time T at which this occurs will be referred to as the saturation time.

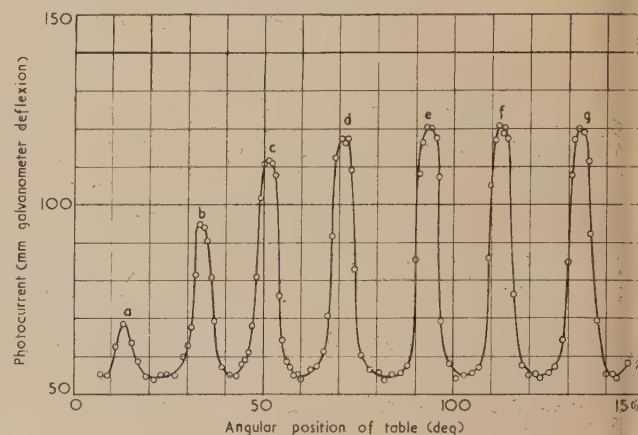


Fig. 3. Typical photometer curve

a, 75 s; b, 100 s; c, 150 s; d, 200 s; e, 225 s; f, 250 s; g, 300 s

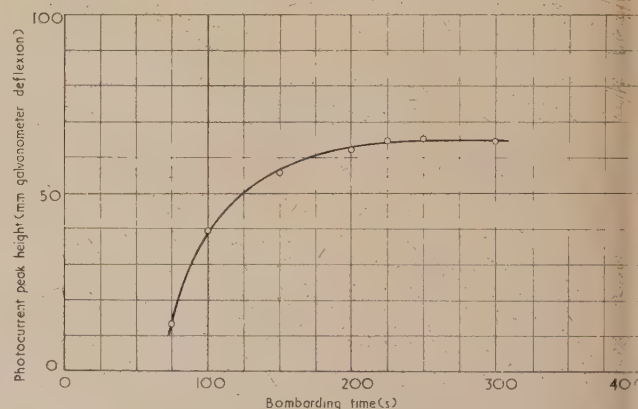


Fig. 4. Variation of photocurrent peak height with bombardment time

Experiments showed that for constant electron energy the saturation time was inversely proportional to the bombarding current, i.e. by doubling the current the saturation time could be halved.

At constant current, on the other hand, T varied with electron energy in the manner shown in Fig. 5. The experiments referred to here, covering an energy range from 25 to 500 eV, were made with a bombarding current of 1.5×10^{-7} A, corresponding to a current density of approximately 3×10^{-6} A/cm².

For electron energies above about 100 eV the saturation time is constant within experimental accuracy, but below 100 eV a rise sets in that becomes progressively steeper as lower energies are approached. Thus at 5 eV (not shown) a visible, though not saturated, image requires a bombardment for 600 s at 1.5×10^{-5} A, i.e. a current larger by two orders of magnitude than the one used in the experiment of Fig. 5.

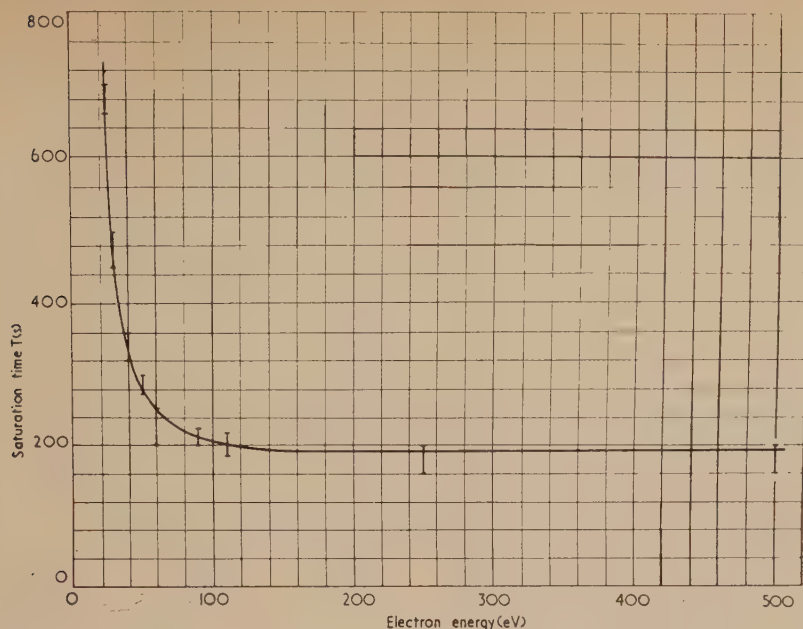


Fig. 5. Variation of saturation time with electron energy. Bombarding current density, 3×10^{-6} A/cm²

The formation of images was unaffected by exposing the targets to relatively high pressures (7 mm of mercury) of either nitrogen or hydrogen during the one-hour interval after outgassing. Likewise, carrying out the actual bombardment at a pressure of 10^{-2} mm of mercury of either of these gases had no significant effect, and it proved immaterial whether or not the system was isolated from the diffusion pump during the one-hour interval, so that decomposition products from the pump oil may be ruled out as a contributing factor in the formation of images.

On the other hand, the target temperature proved to have considerable bearing on the recording process. To investigate this effect the outgassed target, at the end of the one-hour interval when it was back at room temperature, was subjected to a second heating at a temperature T_2 . By suitably placing the induction heater coil, and by judicious intermittent operation of the heater, the target temperature could be kept substantially constant at the pre-selected value T_2 during the 10 min period of the second heating.

Immediately after switching off the heater power the first bombardment was begun, with bombarding current and voltage selected such that at room temperature a saturated line would result. It was found that even with T_2 as low as 45° C, a small but perceptible weakening of the line took place. At higher temperatures there was progressive further weakening and at $T_2 = 220^\circ$ C the image had altogether disappeared. This fairly pronounced temperature sensitivity does, of course, explain the need for a one-hour interval after outgassing, since measurements of target temperature showed that it took over half an hour for the temperature to drop from 900 to 45° C, i.e. the value at which line weakening was first noticed.

Altogether different results were obtained if a second heating was applied not before, but after the bombardment. Whilst in the former case a temperature of 220° C completely obliterated the image, the lines in the second case remained quite unaffected, even at 400° C. Weakening here was first observed at approximately 500° C, and the image was totally destroyed at 750° C.

Image formation and the electrode contamination process

It seems reasonable to associate the formation of images with the interaction of the impinging electron beam and an adsorbed layer of gas or vapour molecules, which can be removed from the target by suitable heating. In particular, the different temperature sensitivity prior and after bombardment suggests that, after the interaction, the adsorbed material is in a considerably more stable form than before. This and most of the other findings suggest a close relation between the image formation and the electrode contamination phenomenon, which is known to occur in practically all demountable vacuum systems.

In the electron microscope in particular, contamination is observed as a gradual deposition of material on the specimen whilst it is being irradiated by the electron beam.⁽²⁾ Ennos⁽³⁾ has shown that the effect is due to the interaction of the electrons with organic molecules, which, due to the use of gasket materials, vacuum grease, etc., are invariably present at low concentration in a demountable system and are condensed from the vapour phase on to the target. Both he and Poole⁽⁴⁾ found that contamination could be inhibited on surfaces raised to 250° C. This value is in good agreement with the temperature of 220° C found in the present work. Moreover, Poole showed that the contamination mechanism involved the dissociation by the electrons of the organic condensate into free radicals, and the subsequent formation by the latter of stable, chemically inert polymers on the target surface.

This dissociation process requires only very small electron energies, and as Ennos⁽³⁾ has pointed out, as long as the beam energy is large compared with the minimum energy required to effect dissociation, its influence on the dissociation rate and, therefore, on the build-up rate of contamination, should be negligible.

From direct thickness measurements of contamination layers on heavily bombarded specimens in an electron microscope, Ennos was able to deduce a constant build-up rate of about 1 Å/s for a target current density of 50 mA/cm² at beam potentials ranging from 40 to 74 kV, and in an

experimental tube run at 2 kV to avoid any target heating, the build-up rate was of the same order of magnitude.

In making a comparison with the present work, one can obviously treat the saturation time T as a measure of the build-up rate. In fact, from the definition of T it may be regarded as the time during which the target is covered with one monolayer of contaminant, and for the purposes of a rough estimate one may take the thickness of such a layer as about 3 Å.

Regarding again the saturation time curve (Fig. 5) from this point of view, it may be said that since electron recording has been observed at 5 eV, the minimum energy required for dissociation is certainly smaller than 5 eV. At about twenty times this value it is sufficiently far removed from the critical energy for the saturation time, and hence the build-up rate, to become energy independent, and in this regime one would be justified in making quantitative comparisons with Ennos' values.

Reference to Fig. 5 shows that in the constant region of the curve, T is approximately 200 s, with a current density of 3×10^{-6} A/cm², i.e. in 200 s a monolayer, which is taken to be 3 Å, is deposited. At 50 mA/cm², the current density used by Ennos, this would result in a build-up rate of about 250 Å/s, which is two orders larger than his measured rate.

This discrepancy cannot be ascribed to a higher concentration of organic contaminant, and therefore a higher contamination rate in the apparatus, since on the contrary there are strong indications that the present vacuum conditions were considerably better than those in Ennos' experiment. Thus, the latter observed after 10 min bombardment at 2 kV with 0.5 mA/cm² current density, the appearance of the characteristic light brown contamination stain. In the present arrangement, using 200 V and 0.4 mA/cm², the first faintly visible deposit was detected after approximately 9 h bombardment.

On the other hand, if the build-up rate of 250 Å/s derived from saturation-time measurements were maintained through-

out, then after 9 h a deposit of 10^{-2} mm thickness, which is very clearly discernible, would have been accumulated. This was certainly not the case.

One is thus led to conclude that the rate at which the first layer is formed, and this, of course, is all that can be derived from the saturation time, is not maintained as subsequent layers are deposited.

Most probably only the first layer is built up very quickly, for here the dissociation and subsequent polymerization takes place on a metallic surface, which, as a catalyst, may speed up the reaction very considerably. However, once the first layer is formed, any further reaction will take place not on the bare metal, but on a chemically very inert polymer, and the reaction rate will drop accordingly.

Summarizing, it may be said that there is a strong likelihood that the process involved in the electron recording effect is the formation of a first, catalytically-accelerated contamination layer. Also, it may be concluded that in a demountable high-vacuum system any clean metal target is liable to become covered with a monolayer of contaminant in a matter of a few minutes, even at bombarding rates as low as 1 μ A/cm².

Acknowledgement

The author wishes to thank Dr. W. Schwietzke for his encouragement and interest throughout the work. Publication is made with the permission of the Chief Scientist, Australian Defence Scientific Service, Department of Supply, Melbourne.

References

- (1) CARR, P. H. *Rev. Sci. Instrum.*, **1**, p. 711 (1930).
- (2) KÖNIG, H. *Naturwissenschaften*, **35**, p. 261 (1948).
- (3) ENNOS, A. E. *Brit. J. Appl. Phys.*, **4**, p. 101 (1953).
- (4) POOLE, K. M. *Proc. Phys. Soc., B*, **66**, p. 542 (1953).

Measurement of hardness at very high temperatures

by L. M. FITZGERALD, B.Sc., M.Sc., Laboratory for the Physics and Chemistry of Solids, Cavendish Laboratory, Cambridge

[Paper first received 4 July, and in final form 18 July, 1960]

Abstract

A new method of determining hardness at high temperatures has been developed and is being used, particularly, to study materials having melting-points in the region of 3000° C. The principle of the hardness measurement is the determination of the height of rebound of a spherical indenter. Tungsten-carbide balls of diameter $\frac{1}{8}$ in. are dropped on to the specimen from a height of about 22 in. The method of measurement makes use of a photomultiplier tube and an electronic timing device. A graphite-tube resistance-heated furnace is used to obtain the temperatures required. The furnace chamber and measuring apparatus is maintained at a vacuum of 0.1μ (10^{-4} mm of mercury) and is also surrounded by a water-cooling jacket. The plastic deformation of hard carbides as the temperature is increased has been measured with this apparatus. Some typical results are given.

Introduction

THE measurement of hot-hardness is a relatively simple operation when compared with other conventional types of mechanical-property test, if they are to be carried out at very high temperatures. The simple shape of specimens required for this measurement and the possibility of obtaining a number of results from a single specimen represent the main advantages of this method. The method is particularly useful for studying the behaviour of hard, brittle materials having high melting points. Such materials are the refractory carbides, borides and nitrides of the transition metals of the fourth to sixth groups of the periodic system, viz. titanium, vanadium, zirconium, niobium, tantalum and tungsten. The carbides of boron and silicon are also more readily studied by this means. With all these materials it is often very difficult to prepare complex shapes such as may be required for, say, tensile specimens. A surface suitable for hardness measurements can be obtained with comparative ease by grinding and diamond-polishing a flat face. The possibility of obtaining useful information from quite small specimens is of importance when it is not convenient, or is perhaps impossible, to use very large pieces of the material under investigation. This is a very significant point in the study of, say, diamond and also of single crystals of the materials mentioned above which are, as yet, available in quite small sizes only.

In this paper, a method of measuring the hardness at high temperatures of hard materials will be described. The principle of this hardness measurement is the determination of the height of rebound of a spherical indenter. It will be seen that this method permits the measurement of hardness at much higher temperatures than is the case for any of the hot hardness testers described in the literature. Typical

results will be given for the behaviour of the hardness as a function of increasing temperature of some of the refractory solids mentioned above.

Description of the method of hot-hardness measurement

The apparatus described here provides for the measurement of the dynamic hardness. Almost all previously described methods of hot-hardness measurement involved a static indentation-type of experiment. The highest temperature at which hardness has been measured in this way is 1500° C with equipment designed by Westbrook.⁽¹⁾ In his apparatus, a diamond indenter mounted in molybdenum was used for temperatures up to about 1000° C. Above this temperature other indenter materials have to be used. The design of the indenter and its mounting and the possibility of specimen-indenter interaction present a serious problem in all static indentation-type of hot-hardness measurements. By making use of a dynamic type of measurement, the effect of time of loading, which is important in static-type experiments, is minimized. The high rate of loading for impact-type measurements is compensated for by the proper choice of size and type of indenter and height of fall. The problem of axiality of loading, so important in tensile measurements, is eliminated altogether.

Another advantage of the equipment described below is that it gives a value of the macro-hardness of the material rather than the micro-hardness. The diameter of the indenter used here is approximately 3 mm, and the indentations produced under the particular conditions of loading are found to be approximately 0.3 mm in diameter, when measured at room temperature after cooling from the testing temperature. In static indentation experiments on hard, brittle materials, micro-indentation measurements are usually made, with diamond pyramid indenters, where the diagonal length of the impressions is of the order of a few microns. "Micro-hardness" is commonly referred to when the applied load is less than 1 kg, and it is generally a property of a single grain of the material. Since most of the materials under investigation are either sintered or hot-pressed from the powder form and have a very small grain size (of the order of 1μ), it is felt that macro-hardness measurements made at high temperatures furnish more useful information about the possible behaviour of the material when in service than would micro-hardness measurements. Furthermore, the fact that all measurements are made on the material whilst it is at the particular temperature under consideration and that, as it will be shown, hardness values can be calculated from these measurements, enhances the useful nature of the information gained by this method.

It should be pointed out that the design of this particular piece of equipment was restricted by the nature of the existing

furnace. Although hot-hardness measurement is relatively easy compared with other high-temperature mechanical-property measurements, the measurement of any property at temperatures in the region of 2000° C and higher is fraught with technical difficulties. However, it is not proposed to discuss these difficulties at length here, although some of them will be apparent from the description of the apparatus.

The furnace

The furnace associated with this equipment is similar to one used by Mordike⁽²⁾ for an investigation of the behaviour of the tensile strength of the refractory metals at temperatures in the range 800–2300° C. The furnace consists of a resistance-heated graphite tube, the main features of which can be seen in Fig. 1. The graphite tube is 22 cm long with

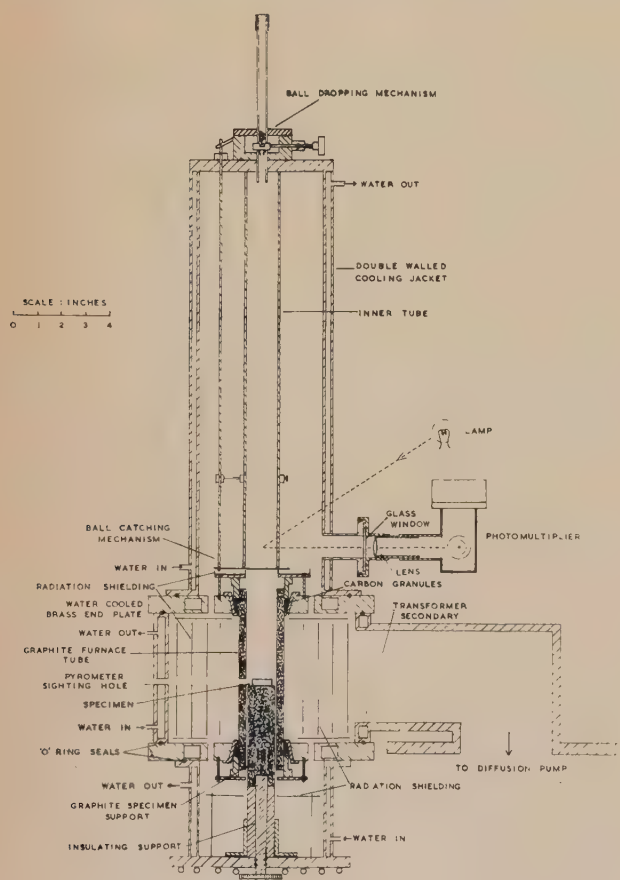


Fig. 1. Schematic sectional view of hot-hardness apparatus and furnace assembly

an external and internal diameter of 44 and 36 mm respectively. The whole furnace assembly is supported on the busbars of a 25 kVA transformer. Electrical contact is made between the water-cooled brass end-plates and the tube by means of tightly packed carbon granules. For temperatures of around 2000° C, currents of the order of 1200 A at a potential of about 9 V are required. The furnace chamber and measuring apparatus is maintained at a vacuum of 0.1μ (10^{-4} mm of mercury) by means of a 3 in. oil diffusion pump and a rotary backing pump. Temperature measurement is effected by sighting an optical pyrometer on the specimen through a small hole in the side of the furnace tube.

Hot-hardness apparatus

A schematic diagram of the complete equipment is given in Fig. 1. The specimens, which are usually in the shape of flat disks having both diameter and thickness between $\frac{1}{2}$ and 1 in., are supported on a massive graphite anvil which in turn is supported from beneath the furnace tube by means of thermally insulating material. It has been established by experiment that specimens of this size are sufficiently massive and that the indenter does not lose energy because of rocking of the specimen on its anvil support. No change in height of rebound was detected when the specimens were tightly clamped in experiments at room temperature. For materials of low density, slightly larger specimens are necessary to prevent rocking of the specimen and erratic measurements. Very small specimens may be used but they must be specially mounted. Care must be taken, in this case, that the test piece is held firmly and that it has a good seating on the massive mounting. The graphite support may be rotated from outside the vacuum chamber in order to change the area which is being subjected to measurement.

The principle of the hot-hardness measurement is the determination of the height of rebound of a spherical indenter. The fact that the whole apparatus must be maintained at a vacuum and that it must also be surrounded by a double-walled water-cooling jacket has added considerable difficulty to the determination of the height of rebound of the indenter. The method of measurement which has been incorporated makes use of a photomultiplier tube and an electronic counting device.

Tungsten-carbide indenters of diameter $\frac{1}{8}$ in. and having a mass of $\frac{1}{4}$ g are dropped on to the specimen from a height

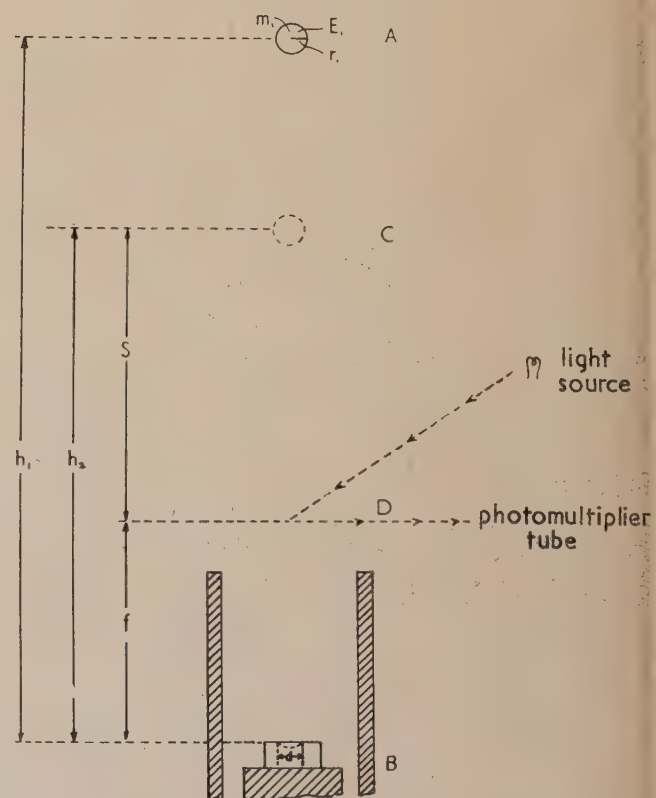


Fig. 2. Diagram representing positions of indenter before and after rebound. Optical arrangement of light source and photo-multiplier tube also shown

of about 22 in. The height of rebound is calculated by measuring the time between successive transits of the indenter past the photomultiplier after impact with the specimen. Fig. 2 shows the position of the indenter both before and after impact. The ball drops from point *A*, a height h_1 above the specimen surface *B*. The pulse obtained from the photomultiplier unit during the first passage of the ball through the point *D* is absorbed by the circuit. The second pulse, obtained as the ball rises to point *C*, a height h_2 above *B*, causes the electronic counting device to commence counting and the third pulse, obtained as the ball falls back past point *D* again, stops the counter. The time $2t$ of flight of the indenter from *D* to *C* and back to *D* enables a calculation to be made of the height *S* of *C* above *D* from the equation

$$S = \frac{1}{2}gt^2. \quad (1)$$

If the fixed height *f* of *D* above *B* is added to *S* we have the height of rebound h_2 . It is possible to plot a parabolic calibration curve giving h_2 directly in terms of the time $2t$ of the form

$$S = \frac{1}{2}gt^2 + f. \quad (2)$$

The distance *f* is made as small as possible but, of course, cannot be any smaller than at least half the length of the furnace tube since the specimen must sit in the central part of the furnace. In the present apparatus the distance *f* is 5 in. The indenter may be caught by means of a magnetically operated device which prevents it from falling back on to the specimen a second time. This device is also activated

by one of the pulses from the photomultiplier tube. It is possible to load about 50 carbide balls into the dropping mechanism and so a number of measurements may be made on a single specimen without the necessity of letting the system down to air. The physical arrangement of the apparatus can be seen in Fig. 3 which is a photograph of the equipment.

Evaluation of hardness determinations

The method of hardness measurement is the same as that used in the Shore⁽³⁾ rebound scleroscope. It has been shown by Tabor⁽⁴⁾ that the dynamic yield pressure corresponding to a velocity of impact resulting from a fall of about 25 cm is almost equal to the static yield pressure. He has derived a formula which gives a relation between the dynamic yield pressure P_d , the heights of fall and rebound h_1 and h_2 and the chordal diameter *d* of the indentation found after impact:

$$P = \frac{mg(h_1 - \frac{3}{8}h_2)}{V_a}, \quad (3)$$

where V_a is the apparent volume of the indentation which would be obtained if the indentation were considered to have the same radius of curvature as the indenter. This apparent volume is equal to $\pi a^4/4r_1$, where $2a = d =$ chordal diameter, and $r_1 =$ radius of indenter.

Tabor has derived a further relation in which *a* is eliminated and which gives *P* in terms of h_1 and h_2 . From this, and a knowledge of the elastic constants of the indenter and the specimen, hardness values can be determined from a measurement of the height of rebound only. This relation is given by the formula:

$$P^5 = \frac{h_2^4}{(h_1 - \frac{3}{8}h_2)^3} \frac{mg}{109r_1^3} \left\{ \frac{1}{f(E)} \right\}^4, \quad (4)$$

where
$$f(E) = \frac{1 - \sigma_1^2}{E_1} + \frac{1 - \sigma_2^2}{E_2}.$$

Here E_1 and E_2 are Young's moduli for the indenter and surface respectively, and σ_1, σ_2 are Poisson's ratios. If we assume that $\{1/f(E)\}^4$ does not vary greatly, we may plot *P* as a function of h_2 . In the preliminary results shown below, the height of rebound has been plotted directly as a function of temperature.

An approximate value for the time of impact in these experiments was obtained by means of piezoelectric measurements using a crystal of barium titanate mounted underneath one of the specimens. This gave a value of about 20×10^{-6} s. Tabor's equation for the time of impact for elastic collisions gave a figure of 7×10^{-6} s for the duration of impact. If we consider the impact as an instantaneous change of momentum, the mean force F_m during the impact is given by

$$F_m t = 2mv. \quad (5)$$

(With the measured value of *t* above, this gave a figure of 8.3 kg for F_m).

It has already been mentioned that the choice of indenter presents a serious problem in static-type hot-hardness measurements. The fact that the indenter is maintained at room temperature and that it passes into and out of the hot zone in such a short time means that a cemented carbide ball may be used quite satisfactorily. Except at room temperature, where the deformation is elastic, the indenter is always at a much lower temperature, and so may be

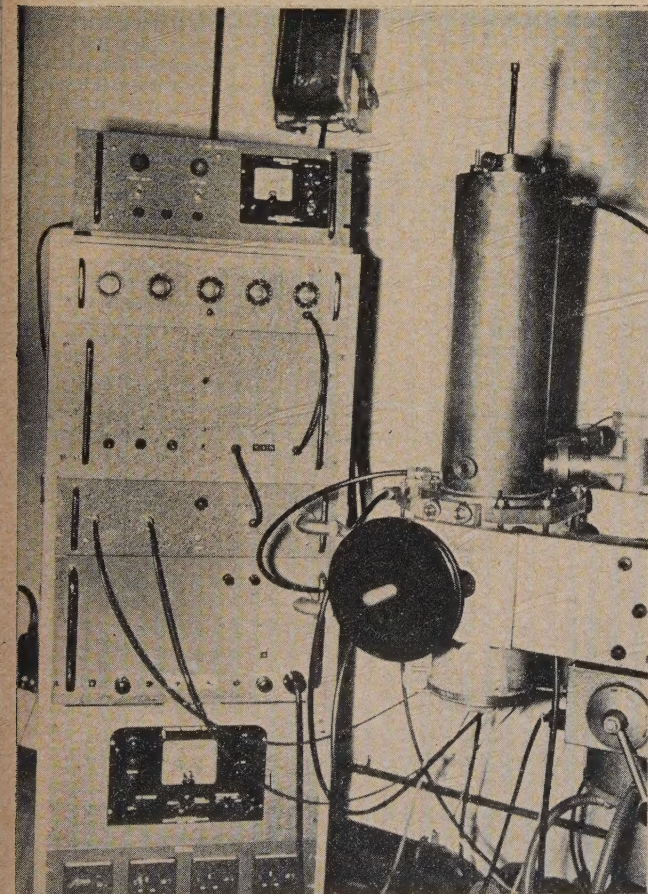


Fig. 3. Photograph of complete apparatus

expected to be harder than the test specimen. Microscopic examination of the tungsten-carbide balls did not reveal permanent deformation as a result of the impacts. The same indenters could be used repeatedly with excellent reproducibility. Sapphire balls may also be used and have the advantage of having a lower weight/size ratio, but carbide balls are used more generally because of their greater availability.

The correlation of hot-hardness data with those of other conventional high-temperature measurements has been shown by several workers.

Results for refractory carbides

Fig. 4 shows some preliminary results obtained for hardness measurements on some of the refractory carbides. For the carbides of the transition elements, there is a marked fall off in hardness with increasing temperature. In some cases, the decrease is almost linear, as with tungsten carbide, whilst

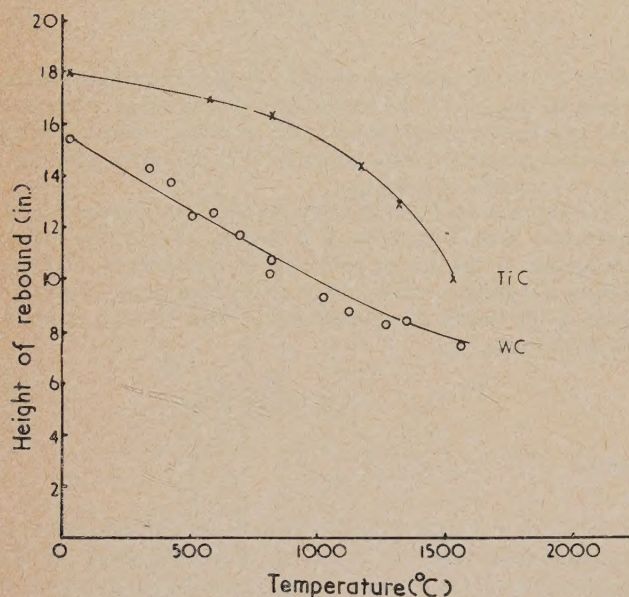


Fig. 4. Typical results for some of the refractory carbides

with others, for example, titanium carbide, there is a sharp fall at a temperature of about 1000°C. For all these materials, plastic indentations were clearly observable on cooling from even fairly low temperatures. The hardness

measured at room temperature, on cooling from the measuring temperature, has always been found to be the same as the original value.

Modification to apparatus for very high temperatures

At temperatures in excess of about 1500°C the great amount of light from the furnace tube itself caused interference with the photomultiplier tube and made it difficult to obtain accurate counts. To overcome this, a photomultiplier tube was used which had a peak response in the ultra-violet region. This tube (Mullard, type 53UVP) replaced the original R.C.A., type 931A, tube. The new tube, used in conjunction with an ultra-violet light source, allows measurements to be made at temperatures as high as the furnace can attain. It was found necessary to keep the 53UVP tube out of the magnetic field of the transformer which supplies the heating current to the furnace.

Conclusion

An apparatus has been described which permits measurements of hardness at temperatures much in excess of those obtained with any previous hot-hardness testers. The method gives the dynamic hardness as a function of increasing temperature. The operation of the apparatus has a number of technical difficulties associated with it, not the least of which is the necessity for perfect alignment of all the equipment, especially the specimen-mounting arrangement. However, the reproducibility of the results obtainable suggests the usefulness of the apparatus for studying the mechanical behaviour of materials at very high temperatures.

Acknowledgements

The author wishes to thank Dr. F. P. Bowden, F.R.S., and Dr. D. Tabor for their helpful discussions, Mr. P. W. Holmes and Mr. D. Halliday for the design and construction of the associated electronic equipment, and Miss J. Horspool for her assistance.

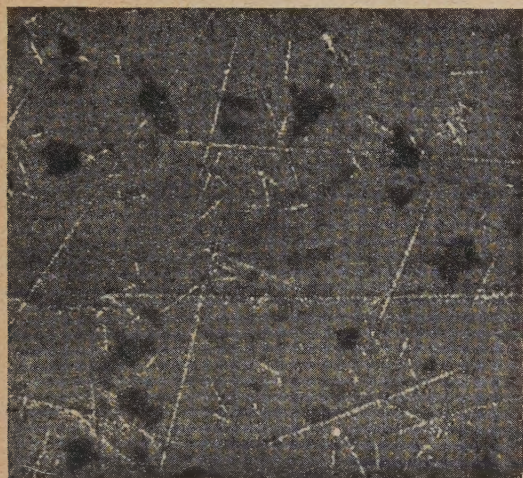
References

- (1) WESTBROOK, J. H. *Proc. Amer. Soc. Test. Mat.*, **57**, p. 873 (1957).
- (2) MORDIKE, B. L. *J. Inst. Met.*, **88**, p. 272 (1960).
- (3) SHORE, A. F. *J. Iron and Steel Inst.*, **98**, p. 59 (1918).
- (4) TABOR, D. *The Hardness of Metals*, Chap. 8, p. 11 (Oxford University Press, 1951).

New technique for the direct investigation of fission events*

A method for the electron microscopic study of individual fission events in U_{235} has been developed at this laboratory. The experimental procedure is as follows:

A film of pure aluminium (2S) is evaporated in vacuum (10^{-5} μ of mercury with helium as a residual gas) on to the surface of a sodium chloride cleavage face to a thickness of about 50 Å. On this is evaporated a film of U_{235} , calculated to be 10 Å in thickness, which is covered with an additional film of aluminium, 50 Å in thickness.



Electron micrograph of an Al- U_{235} -Al "sandwich" after thermal neutron irradiation of 2.8×10^{15} neutrons/cm² (140 000 \times)

This uranium "sandwich" is sealed in an aluminium capsule in oxygen, O_2 free argon or helium and irradiated by thermal neutrons in the Brookhaven pile to an integrated

* Under the auspices of the United States Atomic Energy Commission.

flux 2.8×10^{15} neutrons/cm². After the specimen cools to about 50 mr, it is removed from the capsule, and the metal composite is floated off the sodium chloride on distilled water and mounted on copper grids.

Upon examination in the electron microscope light track-like marks are seen in a darker matrix.

Micrographs at 140 000 \times (see the diagram) show these tracks to be 100 Å in average width, 100–20 000 Å in length, and invariably of higher electron "transparency" than the matrix. The matrix is composed of atomic aggregates (micro crystals) of aluminium, randomly oriented. Electron diffraction patterns show sharp aluminium rings, with vague traces of diffuse Al_2O_3 . No uranium rings are visible due to the small quantity of uranium atoms per unit volume. The aluminium crystallites are 50 Å in size and very uniform.

The tentative interpretation of the results of these experiments is that the tracks are produced by fission fragments. The visible effect is probably due to vaporization of aluminium atoms along the path of the fission fragment. A crude calculation of the energy transferred along such a path in 100 Å thick aluminium shows this to be quite probable. These tracks do not anneal out nor change appearance after heating 15 minutes at 250°C in a helium atmosphere nor with prolonged heating in the electron beam.

Experiments have been performed using copper, platinum and silver as the matrix, all of which show much the same appearance. A study is in progress of the structure of the evaporated metal film with respect to fission tracks. These experiments are continuing. Some of the variables to be studied are the relation between the track length, width, contrast, etc., and the crystal size, perfection, density, and thickness of the film in which the tracks appear. An attempt will be made to prove conclusively that the track is caused by the vaporization of atoms along the track. A paper is soon to be submitted which will report in detail the results of this work.

Metallurgy Division,
Brookhaven National Laboratory,
Upton, New York, U.S.A.

J. J. KELSCH
O. F. KAMMERER
P. A. BUHL
[5 August, 1960]

NOTES AND NEWS

Notes and comments

Indexes and Binding Orders

The indexes and title-pages of this volume will be dispatched with the January 1961 issue of this *Journal*.

Orders and inquiries about binding this *Journal* should be sent direct to Messrs. E. A. Weeks and Son, 168 Gower Street, London, N.W.1 (EUSton 4674), and *not* to The Institute of Physics and The Physical Society.

The charge for binding is 22s. per Volume. Binding cases can be supplied for 13s. 6d. each.

Subscriptions for 1961 can now be received. See overleaf for full details.

Elections to The Institute of Physics and The Physical Society

The following elections have been made by the Board of The Institute of Physics and The Physical Society:

Fellows: D. J. Maclean, C. G. Morgan, H. Rose, W. A. Runciman.

Associates: R. M. Absalom, D. W. Berry, L. F. Bowles, M. Braden, N. K. Bridge, P. J. Brown, I. D. Campbell, A. V. Cohen, S. M. Crawford, E. Grunbaum, M. A. R. Gunston, M. E. Harper, H. C. Harrison, J. C. Higgins, A. Hogg, C. S. Hope, A. F. Hughes, R. Innes, Z. R. Jeffrey, A. M. Jessop, D. E. N. King, J. E. Knowles, E. J. Langham, D. F. Leach, A. Levy, P. A. Mayer, E. G. Muirhead, B. Peters, J. M. Rollett, R. L. Rouse, N. H. Saunders, J. E.

Shaw, B. J. Shepstone, P. F. Smith, K. U. Snowden, P. J. Stevenson, A. V. Stockley, R. W. Strong, B. Stuttard, D. E. Swan, H. F. Symmons, H. H. Thies, R. Webster, M. J. Wheeler, B. J. Williams.

One hundred and eighteen Graduates, fifty-three Students and one Subscriber were also elected.

Annual Exhibition of Scientific Instruments and Apparatus

The 45th Annual Exhibition of Scientific Instruments and Apparatus will be the first to be organized by the recently amalgamated body of The Institute of Physics and The Physical Society. It is to be held, as usual, in the Old and New Halls of the Royal Horticultural Society from 16–20 January, 1961 (inclusive).

Entrance to the exhibition is by ticket only and these may be obtained free of charge, from the offices of the Institute and Society, 47, Belgrave Square, London, S.W.1. The Handbook of Scientific Instruments and Apparatus, published in connection with the exhibition, is also available, price 6s., by post 8s.

Symposium on Electrical Contacts

The Institute of Physics and The Physical Society announces that it is arranging a symposium on 'Electrical Contacts' in collaboration with The Institution of Electrical Engineers which will take place in the Brunel College of Technology, London, from 5th–7th April 1961.

The symposium is intended to cover recent advances in the study of the phenomena occurring at mating surfaces carrying currents used in light electrical engineering. It will include electrical erosion and material transfer, mechanical wear, and the influence of surface films and contamination and will deal with make-and-break contacts, sliding contacts, semi-permanent contacts and connections, between metallic and non-metallic materials. In view of the nature of current developments, it is considered that major interest will be focused on aspects relating to contact resistance.

The symposium is intended mainly for persons concerned with the design and improvement of contacts. There will be a small informal exhibition which will be open during the symposium to those attending the meetings. Abstracts (but not preprints) will be circulated before the symposium, the proceedings of which will not be published in full.

All communications regarding the symposium should be sent to the Secretary, The Institute of Physics and The Physical Society, 47 Belgrave Square, London, S.W.1.

Laboratory and Workshop Notes, 1956–58

Dr. Ruth Lang has compiled a fifth volume of laboratory and workshop notes from the *Journal of Scientific Instruments*, and this has been published by Edward Arnold (Publishers) Ltd., 41 Maddox Street, London, W.1. (Price 40s.)

As the royalties from this book will be donated to the

Benevolent Fund of The Institute of Physics and The Physical Society, members are specially invited to do what they can to ensure that this new volume is purchased in large numbers.

Editorial and publications sales offices

Readers are requested to note that all correspondence of an editorial nature should now be sent to the following address:

The Editor and Deputy Secretary,
The Institute of Physics and The Physical Society, 1 Lowther Gardens, Prince Consort Road, London, S.W.7 (Kensington 0048).

Correspondence concerning subscriptions, missing journals, and sales of publications should be sent to:

The Institute of Physics and The Physical Society, 47 Belgrave Square, London, S.W.1 (Belgravia 6111).

Journal of Scientific Instruments

Contents of the December issue

PAPERS

- Further experiences with aluminium wire seals for bakeable vacuum systems. By L. Elsworth, L. Holland and L. Laurenson.
- Wide-angle photoelectric integrating flashmeter. By J. Edwards, W. R. Lauder and B. R. D. Stone.
- Portable water velocity meter. By J. M. Edington and L. Molyneux.
- Swept Langmuir probe system for intense gas discharges. By H. W. Jones and P. A. H. Saunders.
- Photomultiplier soft X-ray spectrometer. By L. Jacob, R. Noble and H. Yee.
- Stability of some reactance standards. By L. H. Ford.
- Monitor for the quantitative determination of beryllium in the atmosphere. By M. S. W. Webb, R. J. Webb and P. C. Wildy.
- Vibrating reed magnetometer. By D. C. Doughty and P. Mossman.
- Geiger counter backgrounds. By B. L. Cohen.
- Temperature-control system for use with a spectrophotometer. By S. W. Thorpe.
- Viscometers having damped torsional oscillation. By B. S. Ashwin, T. Hagyard, I. C. B. Saunders and T. E. Young.

LABORATORY AND WORKSHOP NOTES

- Elimination of ghost images when using a Kerr-cell shutter. By D. W. Godwin and F. R. Brookes.
- Improved design of portable vacuum manometer. By A. T. J. Hayward.
- Simple force balance for drag measurements. By G. A. Henwood.
- Liquid-level alarm using internally reflected light. By W. E. Hood and E. Oldham.
- Improved flow-sensitive switch. By H. C. Burford.
- Method for increasing the range of a flowmeter. By C. C. Harris.

CORRESPONDENCE

- Measurement of tellurium vapour pressure using electrical discharges. From J. C. Brice.

NOTES AND NEWS

- New instruments, materials and tools. New books. Notes and comments.

THIS JOURNAL is produced monthly by The Institute of Physics and The Physical Society, in London. It deals with all branches of applied physics (including theory and technique). All rights reserved. Responsibility for the statements contained herein attaches only to the writers.

EDITORIAL MATTER. Communications concerning editorial matter should be addressed to the Editor, The Institute of Physics and The Physical Society, 1 Lowther Gardens, Prince Consort Road, London, S.W.7. (Telephone: Kensington 0048.) Prospective authors are invited to prepare their scripts in accordance with the *Notes for Authors*.

REPRODUCTION. The Institute of Physics and The Physical Society is a signatory to The Royal Society's Fair Copying Declaration. Details may be obtained upon application from The Royal Society, London, W.1.

ADVERTISEMENTS. Communications concerning advertisements should be addressed to the agents, Messrs. George Jackson (Fleet St.) Ltd., Cliffords Inn, Fleet Street, London, E.C.4. (Telephone: Holborn 3611–2.)

SUBSCRIPTION RATES. A new volume commences each January. The charge is £6 per volume (\$17 U.S.A.), including index (post paid), payable in advance. Single parts, so far as available, may be purchased at 12s. 6d. each (\$1.75 U.S.A.), post paid, cash with order. Orders should be sent to The Institute of Physics and The Physical Society, 47 Belgrave Square, London, S.W.1, or to any bookseller.

CLAIMS FOR MISSING JOURNALS. Claims from regular subscribers to this *Journal* for missing numbers will only be considered if received within 60 days of the date of mailing plus normal outward time of transit and time for lodging the claim. Losses attributable to failure to notify a change of address or to similar omissions will not be considered.